

AD-752 368

EFFECTS OF ATMOSPHERIC ACOUSTIC GRAVITY
WAVES ON ELECTROMAGNETIC WAVE PROPAGA-
TION

Advisory Group for Aerospace Research and
Development
Paris, France

October 1972

DISTRIBUTED BY:

NTIS

National Technical Information Service
U. S. DEPARTMENT OF COMMERCE
5285 Port Royal Road, Springfield Va. 22151

AD752308

AGARD-CP-115

35
AGARD-CP-115

AGARD

ADVISORY GROUP FOR AEROSPACE RESEARCH & DEVELOPMENT

7 RUE ANCELLE 92200 NEUILLY-SUR SEINE FRANCE

AGARD CONFERENCE PROCEEDINGS No. 115

on

Effects of Atmospheric Acoustic Gravity Waves on Electromagnetic Wave Propagation

DISTRIBUTION STATEMENT A

Approved for public release;

Reproduced by
NATIONAL TECHNICAL
INFORMATION SERVICE
U S Department of Commerce
Springfield VA 22151

NORTH ATLANTIC TREATY ORGANIZATION



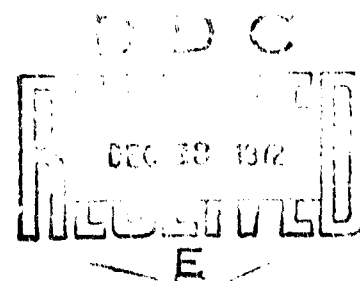
DISTRIBUTION AND AVAILABILITY
ON BACK COVER

523

NORTH ATLANTIC TREATY ORGANIZATION
ADVISORY GROUP FOR AEROSPACE RESEARCH AND DEVELOPMENT
(ORGANISATION DU TRAITE DE L'ATLANTIQUE NORD)

AGARD Conference Proceedings No.115
EFFECTS OF ATMOSPHERIC ACOUSTIC GRAVITY WAVES
ON ELECTROMAGNETIC WAVE PROPAGATION

Details of illustrations in
this document may be better
studied on microfiche.



THE MISSION OF AGARD

The mission of AGARD is to bring together the leading personalities of the NATO nations in the fields of science and technology relating to aerospace for the following purposes:

- Exchanging of scientific and technical information;
- Continuously stimulating advances in the aerospace sciences relevant to strengthening the common defence posture;
- Improving the co-operation among member nations in aerospace research and development;
- Providing scientific and technical advice and assistance to the North Atlantic Military Committee in the field of aerospace research and development;
- Rendering scientific and technical assistance, as requested, to other NATO bodies and to member nations in connection with research and development problems in the aerospace field.
- Providing assistance to member nations for the purpose of increasing their scientific and technical potential;
- Recommending effective ways for the member nations to use their research and development capabilities for the common benefit of the NATO community.

The highest authority within AGARD is the National Delegates Board consisting of officially appointed senior representatives from each Member Nation. The mission of AGARD is carried out through the Panels which are composed of experts appointed by the National Delegates, the Consultant and Exchange Program and the Aerospace Applications Studies Program. The results of AGARD work are reported to the Member Nations and the NATO Authorities through the AGARD series of publications of which this is one.

Participation in AGARD activities is by invitation only and is normally limited to citizens of the NATO nations.

The material in this publication has been reproduced directly from copy supplied by AGARD or the author.

Published October 1972

621.396

2



*Printed by Technical Editing and Reproduction Ltd
Harford House, 7-9 Charlotte St. London W1P 1HD*

THEME

The purpose of the Symposium was to convene Specialists in Physics of the atmosphere engaged in the study of energy transfers in the form of waves in a neutral medium and Specialists in Electromagnetic Wave Propagation concerned with the corresponding modifications of the electric characteristics of the medium and their effects on Electromagnetic Waves.

The contribution of radioelectric techniques to the understanding of waves excitation and propagation in a neutral medium and inversely, the known or predictable effects of such waves on the propagation of electromagnetic waves in a disturbed medium were of concern.

Acoustic gravity waves of every origin, either natural or artificial, were within the scope of the symposium. In principle, the spectrum was limited to that of gravity waves, the periods of which range from a few minutes to a few hours, and of acoustic or infra-sound waves with periods below a few minutes. Atmospheric tides and oscillations on a planetary scale were regarded as marginal.

The range of frequencies contemplated for electromagnetic waves could vary from a few kilohertz to a few gigahertz.

All the radioelectric techniques likely to provide information on the structure and dynamics of acoustics gravity waves fitted the scope of the symposium. The present status of experimental and theoretical knowledge gained owing to these techniques was reviewed.

As regards propagation, such effects as amplitude or phase variations, fluctuations in the directions of arrival, the generation of abnormal modes and focusing, were considered, and their impact on telecommunications examined.

The program has been divided in five sessions.

- SESSION I Acoustic gravity waves in the neutral terrestrial atmosphere.
 - SUBSESSION I A Natural sources and propagation.
 - SUBSESSION I B Artificial sources and propagation.
- SESSION II Coupling between the ionised atmosphere and the neutral atmosphere disturbed by acoustic gravity waves.
- SESSION III Radio electric studies on acoustic gravity waves in the neutral and ionized atmosphere.
- SESSION IV Influence of acoustic gravity waves on the propagation of electromagnetic waves.
- SESSION V Summaries recommendations and future investigations.

Program Chairmen
Collators and Coordinators

Professeur Jean Deltoue
Ecole Normale Supérieure
Laboratoire de Physique
24, rue Lhomond 75 Paris 5ème
France

Capitaine de Frégate (H) P. Halley
Ingénieur en chef au Centre National
d'Etudes des Télécommunications
38 - 40 rue du général Leclerc
92 - Issy-les-Moulineaux
France

Program Committee

Dr Lewis B. Wetzel
Superintendent Communications Science
Division, Naval Research Laboratory
Washington, D.C. 20390
USA

Professor I. Ranzi
Istituto Superiore Poste e Telecomunicazioni
Viale Trastevere, 189, Roma
Italy

Dr H. Rishbeth
Radio and Space Research Station
Ditton Park, Slough, Bucks
UK

Dr J. Klostermeyer
Max Planck Institut für Aeronomie
Institut für Ionosphären Physik
3411, Lindau/Harz
Germany

Host Nation Meeting Coordinator

Mr K. Steckel
D.G.L.R., Cologne
Germany

EPP Chairman

Dr Olav Holt
Auroral Observatory Tromsø
Norway

CONTENTS

	Page
THEME	iii
PROGRAM CHAIRMEN AND COMMITTEE	iv
PROGRAM AND SESSION CHAIRMEN	viii
TECHNICAL EVALUATION REPORT (ENGLISH AND FRENCH)	ix
Review Paper	Reference
SOME ANALOGIES BETWEEN THE PROPAGATION OF IONOSPHERIC RADIO WAVES AND ACOUSTIC-GRAVITY WAVES by K.Davies	1
 <u>SESSION I - ACOUSTIC GRAVITY WAVES IN THE NEUTRAL TERRESTRIAL ATMOSPHERE</u>	
<u>SUBSESSION I A - NATURAL SOURCES AND PROPAGATION</u>	
3D RAY TRACING FOR ACOUSTIC-GRAVITY WAVES by T.M.Georges	2
GENERATION AND PROPAGATION OF SOUND WAVES BETWEEN THE IONOSPHERE AND THE LOWER ATMOSPHERE by R.K.Cook	3
A MODEL FOR ACOUSTIC-GRAVITY WAVE EXCITATION BY BUOYANTLY RISING AND OSCILLATING AIR MASSES by A.Pierce	4
ACOUSTIC GRAVITY WAVES AND DIFFUSION EFFECTS AT THE ATMOSPHERIC BOUNDARIES by F.Warren	5
AUROLAL INFRASONIC WAVE GENERATION MECHANISM by C.R.Wilson	6
DETECTION OF 2Hz INFRASOUND PRODUCED BY MOVING AUROLAL ELECTROJETS by L.Liszka and H.Westin	7
ON WAVES GENERATED BY STATIONARY AND TRAVELING SOURCES IN AN ISOTHERMAL ATMOSPHERE UNDER GRAVITY by C.H.Liu and K.C.Yeh	8
DISCUSSIONS ON PAPERS PRESENTED IN SUBSESSION I A	I A
 <u>SUBSESSION I B - ARTIFICIAL SOURCES AND PROPAGATION</u>	
ACOUSTIC GRAVITY WAVES IN THE NEUTRAL ATMOSPHERE AND THE IONOSPHERE by N.K.Balachandran	9
MODELING OF NUCLEAR SOURCES OF ACOUSTIC-GRAVITY WAVES by B.L.Murphy and S.L.Kahalas	10
THEORIE DE LA PROPAGATION ACOUSTIQUE ATMOSPHERIQUE par Ch.Berthet et Y.Rocard	11
EXPLOSIVE EXCITATION OF LAMB'S ATMOSPHERIC EDGE MODE by J.W.Posey and A.D.Pierce	12
DISCUSSIONS ON PAPERS PRESENTED IN SUBSESSION I B	I B

SESSION II COUPLING BETWEEN THE IONIZED ATMOSPHERE AND THE NEUTRAL
ATMOSPHERE DISTURBED BY ACOUSTIC GRAVITY WAVES

JUSTIFICATION FOR THE USE OF HINES "ASYMPTOTIC RELATIONS" FOR TRAVELLING IONOSPHERIC DISTURBANCES by N.J.F.Chang	13
FULL WAVE CALCULATIONS OF ELECTRON DENSITY PERTURBATIONS CAUSED BY ATMOSPHERIC GRAVITY WAVES IN THE F2-LAYER by J.Klostermeyer	14
ATMOSPHERIC PRESSURE WAVES AT BRISBANE AND THEIR ASSOCIATION WITH CERTAIN IONOSPHERIC AND SOLAR EVENTS by G.G.Bowman	15
FURTHER REMARKS ABOUT TRAVELING IONOSPHERIC DISTURBANCES ATTRIBUTED TO JET STREAM ACTIVITY AT MID-LATITUDE by G.B.Goe	16
GENERATION OF ANOMALOUS IONOSPHERIC OSCILLATIONS BY THUNDERSTORMS by C.A.Moo and A.D.Pierce	17
A PHENOMENOLOGICAL INVESTIGATION OF AMPLITUDE AND SPECTRA OF GRAVITY WAVES by J.P.Schödel	18
COMPARISON OF COMPUTED AND OBSERVED SHOCK BEHAVIOR FROM MULTIKILOTON NEAR SURFACE NUCLEAR EXPLOSIONS by D.P.Kanellakos and R.A.Nelson	19
DISCUSSIONS ON PAPERS PRESENTED IN SESSION II	II

SESSION III RADIOELECTRIC STUDIES ON ACOUSTIC GRAVITY WAVES
IN THE NEUTRAL AND IONIZED ATMOSPHERE

FM/CW RADAR STUDIES OF PRODUCTION OF TURBULENT INSTABILITY WITHIN THERMALLY STABLE LAYERS BY INTERNAL WAVES by E.E.Gossard and J.H.Richter	20
THE DETECTION AND STUDY OF GRAVITY WAVES WITH MICROWAVE RADAR by I.Katz	21
OBSERVATIONS OF GRAVITY WAVES IN THE HEIGHT RANGE 50-70 KM by G.E.Perona	22
OBSERVATIONS D'ONDES DE GRAVITE DANS LA HAUTE ATMOSPHERE PAR DETECTION DES TRAINEES METEORIQUES par M.Glass, A.Spizzichino et I.Revah	23
NARROW-BEAM RF RADAR INVESTIGATIONS OF MID-LATITUDE IONOSPHERIC STRUCTURE AND MOTION by R.D.Hunsucker	24
AN IMPORTANT CHARACTERISTIC OF SOME TRAVELING IONOSPHERIC DISTURBANCES by L.Ranzi and P.Giorgi	25
IONOSPHERIC DISTURBANCES CAUSED BY LONG PERIOD SOUND WAVES GENERATED BY SATURN-APOLLO LAUNCHES by G.L.Rao	26
OBSERVATIONS OF TRAVELLING IONOSPHERIC DISTURBANCES AT LONDON, CANADA by J.Litva	27
THE EFFECT OF IONOSPHERIC DISTURBANCES ON THE BEARINGS OF INCOMING SKYWAVES by A.D.Morgan	28

	Reference
IONOSPHERIC TILT MEASUREMENTS NEAR THE MAGNETIC DIP EQUATOR by R.F.Trehanne	29
ON THE GENERATION AND DETECTION OF ARTIFICIAL ATMOSPHERIC WAVES by L.Liszka and S.Olsson	30
DISCUSSIONS ON PAPERS PRESENTED IN SESSION III	III

SESSION IV - INFLUENCE OF ACOUSTIC GRAVITY WAVES ON THE
PROPAGATION OF ELECTROMAGNETIC WAVES

AN APPROACH TO THE ANALYSIS OF COUPLING BETWEEN ACOUSTIC-GRAVITY WAVES AND ELECTROMAGNETIC WAVES by H.R.Raemer	31
H.F. RAY TRACING OF GRAVITY WAVE PERTURBED IONOSPHERIC PROFILES by P.L.George	32
SOME EFFECTS OF ATMOSPHERIC GRAVITY-WAVES OBSERVED ON A TRANSEQUATORIAL RADIO PATH by J.Röttger	33
PROPAGATION OF SUBMICROSECOND HF PULSES THROUGH TRAVELLING IONOSPHERIC DISTURBANCES by G.M.Lerfald, R.B.Juigens and J.A.Joselyn	34
TRAVELLING IONOSPHERIC DISTURBANCES INITIATED BY LOW ALTITUDE NUCLEAR EXPLOSIONS by W.Stoffregen	35
LA PERTURBATION IONOSPHERIQUE DUE AUX ONDES ACOUSTIQUES ET DE GRAVITE CREEES PAR UNE EXPLOSION NUCLEAIRE AU SOL DE 100 Kt A 2000 Kt OBSERVEE ENTRE 150 ET 1000 KM DU POINT DE TIR (Resumé seulement) par P.Halley	36
PROPAGATION NON-LINEAIRE ET COUPLAGE IONOSPHERIQUE DES ONDES ATMOSPHERIQUES ENGENDREES PAR UNE EXPLOSION NUCLEAIRE par P.Broche	37
NUCLEAR WEAPON EFFECTS ON THE IONOSPHERE (F REGION DISTURBANCES) by J.B.Lomax and D.L.Nielson	38
THE EFFECTS OF NUCLEAR-BURST PRODUCED ACOUSTIC-GRAVITY WAVES ON HF COMMUNICATION SYSTEMS by D.L.Nielson	39
DISCUSSIONS ON PAPERS PRESENTED IN SESSION IV	IV

SESSION V - SUMMARIES, RECOMMENDATIONS AND FUTURE INVESTIGATIONS

COMMENTS by Prof.H.Volland, Dr B.L.Murphy, Dr K.Davies, Prof.L.Ranzi, Dr H.Rishbeth, Dr H.Raemer and Dr D.Nielson	V
--	---

Program Chairmen

Professeur Jean Delloue
Ecole Normale Supérieure
Laboratoire de Physique
24, rue Lhomond - 75 - Paris 5ème
France

Capitaine de Frégate (H) P. Halley
Ingénieur en chef au Centre National
d'Etudes des Télécommunications
38 - 40, rue du général Leclerc
92 - Issy-les-Moulineaux
France

Session Chairmen

SESSION I - ACOUSTIC GRAVITY WAVES IN THE NEUTRAL TERRESTRIAL ATMOSPHERE

SUBSESSION I A - Natural sources
and propagation

Prof. H. VOLLAND
Radio - Sternwarte der Universität
53 - Bonn - Poppelsdorfer Allee 49
Germany

SUBSESSION I B - Artificial sources and
propagation

Dr J. KLOSTERMEYER
Max Planck Institut für Aeronomie
Institut für ionosphären physik
3411 - Lindau/Hartz - Germany

SESSION II - COUPLING BETWEEN THE IONIZED ATMOSPHERE AND THE NEUTRAL ATMOSPHERE DISTURBED BY ACOUSTIC GRAVITY WAVES

Prof. Jean DELLOUE
Ecole Normale Supérieure
Laboratoire de Physique
24, rue Lhomond - Paris 5ème
France

(for papers 13 to 16)

Cne Frég. (H) P. HALLEY
Ingénieur en chef au Centre National d'Etudes
des Télécommunications
38 - 40, rue du général Leclerc
92 - Issy-les-Moulineaux, France
(for papers 17 to 19)

SESSION III - RADIOELECTRIC STUDIES ON ACOUSTIC GRAVITY WAVES IN THE NEUTRAL AND IONIZED ATMOSPHERE

R. H. RISHBETH
Radio and Space Research Station
Ditton Park - Slough - Bucks
England
(for papers 20 to 25)

Prof. Ivo RANZI
Centre Radioelettrico sperimentale
"G. Marconi" viale Trastevere 189,
00100 - Rome - Italy
(for papers 26 to 30)

SESSION IV - INFLUENCE OF ACOUSTIC GRAVITY WAVES ON THE PROPAGATION OF ELECTROMAGNETIC WAVES

Dr I. WETZEL
Communication Sciences Division
NRL - Washington, D.C. 20390 - USA

SESSION V - SUMMARIES, RECOMMENDATIONS AND FUTURE INVESTIGATIONS

Prof. Jean DELLOUE
Ecole Normale Supérieure
Laboratoire de Physique
24, rue Lhomond - 75 Paris 5ème - France

TECHNICAL EVALUATION REPORT
on
AGARD SPECIALISTS' MEETING
on
EFFECTS OF ACOUSTIC GRAVITY WAVES ON ELECTROMAGNETIC WAVE PROPAGATION
by
P. HALLEY

1. Introduction

The meeting, sponsored by the AGARD Electromagnetic Wave Propagation Panel, was held at the Roter Pavillon, The Kurhaus, Wiesbaden, Federal Republic of West Germany, from 17 through 21 April 1972.

The Technical program was discussed and finalized by the Program Committee, which convened on several occasions prior to, and during the Meeting. Among the decisions made, it should be pointed out that a classified session (Session IV, classified up to the Secret level) had been planned to take place in the afternoon of 20 April, simultaneously with an unclassified Session IV on the same topic "Influence of Acoustic Gravity Waves on Electromagnetic Wave Propagation".

After discussion, the Program Committee decided to cancel the classified session and to have all the papers presented in an unclassified session, with limited or shortened oral presentations if necessary.

The purpose of this report is to provide a condensed review of the results of the meeting, and to stress the points on which light was thrown, as well as those which remained obscure or uncertain.

During Session V, entitled "Summaries, Recommendations and Future Investigations" general comments were presented on each of the first four sessions. These comments were gathered in the report on Session V by:

Prof. H. VOLLAND, for Session IA
Dr. B. L. MURPHY, for Session IB
Dr. K. DAVIES, for Session II
Prof. I. RANZI and Dr. H. RISHBETH, for Session III
Dr. H. RAEMER and Dr. D. NIELSON, for Session IV

Therefore, this report is only a supplement and a conclusion.

2. Specialists' Meeting

The purpose of this Meeting was essentially to gather atmospheric physics specialists engaged in the study of energy transfers in wave form through a neutral medium, and electromagnetic wave propagation specialists concerned with modifications in the electric characteristics of the medium. As far as this objective is concerned, the meeting may be regarded as a success, and each participant of either group was provided with an opportunity to be informed of the problems with which the other group is faced, and of possible solutions. In short, the aim in view was to pass on from the medium of characteristics such as: pressure, temperature, gas velocity, etc. to such characteristics as: electron density, ion density, number of shocks per time unit, etc. Evidently, as there is only one medium, all the characteristics involved in the various energy transfer equations are to be considered simultaneously to study disturbing acoustic gravity waves.

Electromagnetic propagation through the atmosphere involves only the electric and magnetic characteristics of the medium which are present in Maxwell equations and in associated equations necessary to the solution of a problem. This problem seems to be more simple than the general problem of atmospheric waves, and is correctly solved, as demonstrated by thousands of experimental observations.

For this reason, radioelectric techniques constitute a very important and practical means of investigating neutral wave excitation and propagation conditions. (A considerable part of our experimental knowledge on neutral waves is derived from observations based on radioelectric wave propagation).

3. Analysis of the Subject

In brief, the succession of research operations was based on the knowledge of:

- a. acoustic and gravity wave sources
- b. acoustic and gravity wave propagation, whether the process involved is linear or non-linear.
- c. the effect of acoustic or acoustic gravity waves on the electric characteristics of the medium and of the electric model of disturbed atmosphere which it is possible to schematize.
- d. radioelectric propagation through a disturbed medium.
- e. techniques for improving radio communication equipment and their use, when the atmosphere is disturbed by A. or A.G. waves. (This final and practical point being the most important).

3.1 In actual fact, many natural sources of A. and A.G. waves were identified, among which auroral discharges which heat up the atmosphere and move sometimes at supersonic speeds, carrying along associated waves. (R.C. COOK, paper 3; G.R. WILSON, paper 6)

Among the artificial sources, nuclear explosions in the atmosphere are the most important. For a low altitude explosion, the upward shock wave generates acoustic waves and, owing to a complex non-linear process, acoustic gravity waves (B.L. MURPHY and S.L. KARALAS, paper 10). A noise ring, acting as a secondary source of short period waves seems to be generated at an altitude ranging from 85 to 95 km (J. ROCARD, paper 11). Lamb's atmospheric edge mode excitation seems to make a considerable contribution to the first or first two cycles of acoustic gravity waves produced by an explosion at ground level (J.W. POSEY and A.D. PIERCE, paper 12).

Several authors reviewed the results of calculations carried out by J.S. GREENE and W.A. WHITAKER on the basis of NEWTON'S equations.

Therefore, the time and space source functions appear to be fairly well understood in the two particular cases of the auroral curtain and of low altitude energetic explosions.

3.2 Although it is very complex, the linear theory of A. and A.G. waves is now advanced enough to be applied to an isothermal or non-isothermal atmosphere. WHITHAM'S kinematic theory is a valuable complement to the classical theory, since it permits an easy calculation of trajectories.

Non-linear phenomena pose much more serious problems.

3.3 The coupling of neutral and ionized gases is expressed by coupled hydrodynamic and ionic motion equations which must be fulfilled simultaneously, without disregarding non-linear effects (J. KLOSTERMEYER, paper 14 and N.J.F. CHANG, paper 13). For the time being, it seems difficult to state which is the prevailing physical process in each case, and how its written expression can be simplified to develop a theory easier to handle.

Travelling ionospheric disturbances (TIDS) are observed and analyzed by many authors, among whom, G.B. GOE, paper 16, reports on the effect, at the F region altitude, of wind configurations associated with the jet-stream. At the altitude of the tropopause, G.A. HOO and A.D. PIERCE, paper 17, who observe and explain the oscillations of the ionosphere during periods of stormy activities. D.P. KANELLAKOS and R.A. NELSON, paper 19, who demonstrate experimentally the validity of GREENE'S and WHITAKER'S hydrodynamic calculations.

However, it must be stated that models of neutral and ionized atmospheres disturbed by A. and A.G. waves generated by the various identified sources either do not exist yet, or are far from complete.

3.4 In a disturbed atmosphere, represented by a simple model, it is possible to calculate the propagation of radio waves in the H.F. band either by ray tracing (P. GEORGE, paper 32) or by an all wave method (H. RAEMER, paper 31). Further ray tracing calculations in an ionosphere disturbed by atmospheric gravity waves provide the field amplitude at reception (taking account of periodical focusing) and the azimuth deviation (J. RÖTTGER, paper 33). It is also possible to determine experimentally the detailed structure and the motions of TIDS, by the short duration pulse technique (pulses shorter than a microsecond) (G.P. LERFELD, R.B. JURGENS, and J.A. JOSELYN, paper 34). This practical technique seems to be very promising.

I believe this particular area of research could be developed from both theoretical and experimental viewpoints.

3.5 Papers providing information on the techniques for improving radio transmissions when the atmosphere is disturbed by acoustic and acoustic gravity waves were very scarce. This gap was duly stressed by the SHAPE Technical Center representatives. However, a few data of a practical nature were presented by D. NIELSON, paper 39 and P. HALLEY, paper 36.

These data were limited to the effects of nuclear explosions on H.F. radio communications. They were of a very general character, and qualitative rather than quantitative.

We are still far from having mastered a good knowledge of the electromagnetic energy transfer function between two distant points.

4. Conclusions

The Wiesbaden technical meeting has provided new elements on the understanding of atmospheric acoustic gravity waves and their effects. Considerable advances have been made since the first coherent document which, as far as I know, was published on this subject under the title: "Acoustic Gravity Waves In The Atmosphere", Symposium Proceedings, Boulder, Colorado, July 1968.

It may be concluded that the model representing a quiet ionosphere through which winds and tidal waves are moving should be completed by the addition of natural atmospheric acoustic gravity waves which, on certain days and at certain times, modify the slopes of isoelectronic surfaces, disturb maximum electron densities, modulate absorption in lower layers and generate focussing.

All these phenomena are of interest to the user of radio communications (especially in the H.F. bandwidth), who is still far from deriving the maximum benefit from natural propagation possibilities.

Investigations on acoustic gravity waves and their consequences upon radio communications can lead to detailed short term predictions of ionospheric propagation conditions in a given geographic area.

Rapport d'évaluation technique
de
la réunion de spécialistes de l'AGARD

sur

"Les effets des ondes acoustiques et de gravité atmosphériques
sur la propagation de l'onde électromagnétique"

par

P. HALLEY

1. Introduction

La réunion organisée sous l'égide du groupe de travail "Propagation de l'onde électromagnétique de l'AGARD" a été tenue au Roter Pavillon du Kurhans de Wiesbaden, République Fédérale d'Allemagne, entre le 17 et le 21 avril 1972.

Le programme technique a été discuté et mis au point par le comité du programme, qui s'est réuni à différentes reprises avant et pendant le symposium. Parmi les décisions prises, il convient de signaler qu'une Session IV classifiée (jusqu'à Secret) avait été prévue pour le 20 avril, dans l'après-midi, en même temps qu'une Session IV non classifiée, sur le même sujet : "Influence des ondes acoustiques et de gravité sur la propagation des ondes électromagnétiques."

Après discussion, le comité du programme a décidé de supprimer la session classifiée et de présenter, en session non classifiée toutes les communications orales, si nécessaire limitées ou écourtées dans leur présentation.

Le but du présent rapport est de fournir une revue très condensée des résultats obtenus au cours de la réunion, pour signaler autant les points bien éclairés que les points restés obscurs ou incertains.

La Session V, sous le titre "Sommaires, Recommandations et Recherches futures", a permis la présentation de commentaires généraux sur chacune des quatre premières sessions. Le lecteur trouvera ces commentaires au papier V, rédigés pour

la Session I A par le Prof. H. VOLLAND,
la Session I B par le Dr B.L. MURPHY,
la Session II par le Dr K. DAVIES,
la Session III par le Prof. I. RANZI et le Dr. H. RISHBETH,
la Session IV par le Dr. RAEMER et le Dr. D. NIELSON.

Le présent rapport n'est donc qu'un complément et une conclusion.

2. La réunion de spécialistes.

Le but du symposium était, entre autres, de réunir des spécialistes de la physique de l'atmosphère engagés dans l'étude des transports d'énergie en forme d'onde dans le milieu neutre et des spécialistes de la propagation de l'onde électromagnétique que concernent les modifications des caractéristiques électriques du milieu. Sur ce point, on peut dire que le symposium a été une réussite et chacun des participants, appartenant plus particulièrement à l'un des groupes, a pu prendre connaissance de la forme des problèmes qui se posent à l'autre groupe et des solutions possibles. En bref, il s'agissait de passer en tout point du milieu des caractéristiques telles que : pression, température, vitesse du gaz, etc., aux caractéristiques telles que : densité électronique, densité ionique, nombre de chocs par unité de temps, etc.. Bien entendu, le milieu étant unique ce sont, en principe, toutes les caractéristiques qui entrent dans les différentes équations de transfert d'énergie sous toutes ses formes, qui sont à considérer simultanément pour l'étude des ondes perturbatrices "acoustiques et de gravité".

La propagation électromagnétique dans l'atmosphère n'intéresse que les caractéristiques électriques et magnétiques du milieu qui entrent dans les équations de Maxwell et dans les équations complémentaires qu'il est nécessaire d'écrire pour résoudre un problème qui apparaît comme plus simple que le problème général des ondes de l'atmosphère et qui est bien résolu comme le montrent des milliers d'observations expérimentales.

Pour cette raison, les techniques radioélectriques sont un moyen très important et commode de recherche des conditions d'excitation et de propagation des ondes neutres. (Ainsi, une grande part de nos connaissances expérimentales sur les ondes neutres provient d'observations utilisant la propagation des ondes radioélectriques).

3. L'analyse du sujet.

En somme, la succession des opérations de recherche s'effectuait sur la connaissance :

- i) - des sources des ondes acoustiques et de gravité,
- ii) - de la propagation des ondes acoustiques et de gravité en présence de processus linéaires et non-linéaires,
- iii) - de l'effet des ondes A ou A.G. sur les caractéristiques électriques du milieu et du modèle électrique d'atmosphère perturbée qu'il est possible de schématiser,
- iiii) - de la propagation radioélectrique dans le milieu perturbé,
- iiii) - des techniques destinées à l'amélioration des matériels de radiocommunication et de leur emploi, en présence d'une atmosphère agitée par des ondes A ou A.G., (Ce dernier point final et pratique étant le plus important).

3.1. En fait, de nombreuses sources naturelles d'ondes A et A.G. ont été identifiées, parmi lesquelles les décharges aurorales qui chauffent l'atmosphère et parfois se déplacent à vitesse supersonique en entraînant des ondes d'accompagnement (R.K. Cook papier 3, G.R. Wilson papier 6).

Parmi les sources artificielles il faut citer principalement les explosions nucléaires dans l'atmosphère. Pour une explosion à basse altitude, l'onde de choc ascendante produit des ondes acoustiques et par un processus non-linéaire complexe des ondes acoustiques et de gravité (B.L. Murphy et S.L. Kahalas, papier 10). Une couronne de bruit véritable source secondaire d'ondes de courte période serait créée entre 85 et 95 km d'altitude (J. Rocard, papier 11). L'excitation du mode tranchant de Lamb apporterait une contribution importante au premier ou aux deux premiers cycles des ondes acoustiques et de gravité engendrées par une explosion au niveau du sol (J.W. Posey et A.D. Pierce, papier 12).

Plusieurs auteurs sont revenus sur le résultat des calculs effectués par J.S. Greene et W.A. Whitaker à partir des équations de Newton.

Il apparaît donc que les fonctions source, temporelle et spatiale, sont approximativement saisies dans les deux cas particuliers du rideau auroral et de l'explosion énergétique à basse altitude.

3.2. La théorie linéaire des ondes A et A.G. bien que très complexe dans sa généralité est maintenant assez avancée pour être exploitable en atmosphère isotherme et non-isotherme. La théorie cinématique de Whitham vient compléter assez heureusement la théorie classique, en permettant un calcul facile de trajectoire.

Les phénomènes non-linéaires posent des problèmes beaucoup plus ardu.

3.3. Le couplage entre le gaz neutre et le gaz ionisé se traduit par l'écriture d'équations couplées hydrodynamique et ionique du mouvement, qui doivent être simultanément satisfaites, sans négliger les effets non linéaires (J. Klostermeyer, papier 14 - N.J.F. Chang, papier 13). Pour le moment, il paraît difficile de dire quel est, dans chaque cas, le processus physique dominant et comment on peut alléger l'écriture pour parvenir à une théorie plus maniable.

Les perturbations ionosphériques itinérantes (PII) sont constatées et analysées par le nombreux auteurs parmi lesquels nous citerons : G.B. Goe (papier 16) qui constate l'effet aux altitudes de la région F des configurations de vent liées au courant-jet à l'altitude de la tropopause.

G.A. Moo et A.D. Pierce (papier 17) qui constatent et expliquent des oscillations de l'ionosphère pendant les périodes d'activité orageuse.

D.P. Kanellakos et R.A. Nelson (papier 19) qui montrent par l'expérience la validité des calculs hydrodynamiques de Greene et Whitaker.

Cependant, il faut bien constater que les modèles d'atmosphère neutre et ionisée perturbée par les ondes A. et A.G. des différentes sources identifiées sont soit inexistantes soit encore très incomplets.

3.4. Dans l'atmosphère perturbée, schématisée par un modèle simple, il est possible de calculer la propagation des ondes radio dans la bande H.F. soit en trajectographie (P. George, papier 32) soit par une méthode toute onde (H. Raemer, papier 31). D'autres calculs de trajectographie dans une ionosphère perturbée par les ondes de gravité atmosphériques fournissent l'amplitude du champ à la réception (compte tenu des focalisations périodiques) et la déviation en azimut (J. Röttger, papier 33). Il est également possible de déterminer expérimentalement la structure fine et les mouvements des P.I.I. en utilisant la technique des impulsions de courte durée, inférieure à la microseconde (G.M. Lerfeld, R.B. Jurgens, J.A. Joselyn, papier 34). Cette technique pratique paraît très prometteuse.

A mon avis, ce domaine particulier de la recherche pourrait être développé tant par le calcul que par l'expérience.

3.5. Les papiers fournissant des informations sur les techniques à employer pour améliorer les radiocommunications en présence d'une atmosphère agitée par les ondes acoustiques et acoustiques et de gravité ont été très peu nombreux. Cette lacune a été dûment soulignée par les représentants du Shape Technical Center. Quelques informations pratiques ont cependant été apportées par D. Nielsen (papier 39) et P. Halley (présentation orale 36).

Ces informations étaient uniquement relatives aux conséquences des explosions nucléaires sur les radiocommunications en H.F.. Elles étaient très générales et plus qualitatives que quantitatives.

On est encore très loin d'une bonne connaissance de la fonction de transfert de l'énergie électromagnétique entre deux points distants.

4. Conclusions.

La réunion technique de Wiesbaden a apporté de nouveaux éléments sur la connaissance des ondes acoustiques et de gravité atmosphériques et de leurs effets, qui marquent un progrès important sur le premier document cohérent publié à ma connaissance sur le sujet :

"Acoustic-gravity waves in the atmosphere", symposium proceedings, Boulder Colorado juillet 1968.

Ma conclusion est que le modèle d'ionosphère calme parcourue par des vents et des ondes de marée doit être complété par la présence d'ondes acoustiques et de gravité naturelles qui, certains jours ou certaines heures, modifient les pentes des surfaces isoelectroniques, perturbent les densités électroniques maximales, modulent l'absorption dans les basses couches et provoquent des focalisations.

Tous ces phénomènes intéressent l'exploitant des moyens de radiocommunication (tout particulièrement dans la bande H.F.) qui est encore loin de tirer le parti maximum des possibilités naturelles de propagation.

L'étude des ondes acoustiques et de gravité et de leurs conséquences sur les radiocommunications peut conduire à une prévision à court terme détaillée des conditions de propagation ionosphérique dans une région géographique délimitée pour cette prévision.

**SOME ANALOGIES BETWEEN THE PROPAGATION OF IONOSPHERIC
RADIO WAVES AND ACOUSTIC-GRAVITY WAVES**

by

Kenneth Davies

Space Environment Laboratory
NOAA Environmental Research Laboratories
Boulder, Colorado 80302
USA

QUELQUES ANALOGIES ENTRE LA PROPAGATION DES ONDES RADIO DANS L'IONOSPHERE
ET DES ONDES ACOUSTIQUES ET DE GRAVITE

par

K. Davies

SOMMAIRE

La propagation des ondes radio dans l'ionosphère est semblable à celle des ondes acoustiques et de gravité dans l'atmosphère neutre. Les deux milieux sont anisotropes et dispersifs. En outre, le profil de température dans l'atmosphère rappelle dans une certaine mesure celui de la densité des électrons dans l'ionosphère. La trajectographie pour les ondes acoustiques, révèle l'existence de rayons hauts et de rayons bas de zones de silence, etc.

SOME ANALOGIES BETWEEN THE PROPAGATION OF IONOSPHERIC

RADIO WAVES AND ACOUSTIC-GRAVITY WAVES

Kenneth Davies
 Space Environment Laboratory
 NOAA Environmental Research Laboratories
 Boulder, Colorado 80302

ABSTRACT

The propagation of radio waves in the ionosphere is similar to that of acoustic gravity waves in the neutral atmosphere. Both are anisotropic and dispersive. Furthermore, the temperature structure in the atmosphere is somewhat similar to the electron density structure in the ionosphere. Ray tracing of acoustic waves exhibit high- and low- angle rays, skip zones, etc.

1. INTRODUCTION

Some participants at this meeting will be familiar with ionospheric radio propagation and not with acoustic-gravity waves whereas there are some who are more familiar with the propagation of acoustic-gravity waves than with ionospheric radio waves. This talk, is therefore, tutorial in nature and is designed to show that the two types of waves are similar in several respects.

The analogies are emphasized by defining a refractive index for acoustic-gravity waves in terms of the local speed of sound C and comparing it with the Appleton equation for the refractive index of an ionized medium (Ratcliffe, J. A., 1959). It will be shown that the acoustic cut-off frequency, ω_a , is analogous to the plasma frequency, ω_p , and that the buoyancy frequency, ω_g , (also called the Brunt-Väisälä frequency) corresponds to the electron gyrofrequency ω_c . Acoustic waves are similar to ionospheric radio waves on frequencies above the gyrofrequency whereas gravity waves are similar to whistlers (see Halliwell, R. A., 1965) which propagate on frequencies below the gyrofrequency.

2. CHARACTERISTIC FREQUENCIES AND DIRECTIONS

In a plane stratified and isothermal atmosphere the characteristic direction is that of gravity, whereas in the ionosphere it is the direction of the geomagnetic field. There are two characteristic frequencies for such an atmosphere. The first of these is the acoustic cut-off frequency ω_a , which is the natural frequency of (compressional) oscillation of the entire atmosphere about its equilibrium state. The other characteristic frequency (the buoyancy frequency, ω_g) is the frequency of oscillation of a parcel of air about its equilibrium level.

In a uniform neutral plasma containing a uniform external magnetic field, B_0 , the two corresponding characteristic frequencies are the plasma frequency ω_p and the gyrofrequency ω_c . The former is the frequency of oscillation of the electron gas when displaced from its mean position with respect to the heavy positive ions. The gyrofrequency is the frequency with which a single electron gyrates about the magnetic field.

It is clear that ω_a and ω_p depend on the bulk properties of the respective media while ω_g and ω_c refer to elements of the media.

As in ionospheric radio work we normalize the characteristic frequencies to the wave frequencies and use the symbols X and Y recommended by the International Scientific Radio Union (Ratcliffe, J. A., 1959). These symbols are defined in Table 1. The atmospheric symbolism is as follows:

- C , the speed of sound
- g , the gravitational acceleration, assumed independent of height
- H , the scale height
- γ , the ratio of specific heats at constant pressure and constant volume.

One difference between radio waves and acoustic-gravity waves is that in the former the characteristic frequencies ω_p and ω_c are independent, whereas the frequencies ω_a and ω_g are directly related thus:

$$\gamma^2 \omega_g^2 = \gamma(\gamma-1) \omega_a^2 \quad (1)$$

Insertion of the diatomic value $\gamma = 1.4$ yields

$$\omega_g^2 = 0.82 \omega_a^2 \quad (2a)$$

$$\omega_g = 0.9 \omega_a \quad (2b)$$

Thus the buoyancy frequency in an isothermal atmosphere is necessarily less than the acoustic frequency.

It is of interest to note here that in an atmosphere with a uniform height gradient of temperature the acoustic cut-off ω_a and buoyancy frequency ω_g are given by

$$\omega_a^2 = \omega_A^2 (1 + 2 H') \quad (3)$$

and

$$\omega_g^2 = \omega_g^2 \left(1 + \frac{Y}{Y-1} H'\right) \quad (4)$$

in which H' is the gradient of scale height. Under these conditions ω_a and ω_g are equal when $H' \approx 0.18$ (see Tolstoy and Lau, 1970).

3. REFRACTIVE INDICES

The refractive index μ for acoustic-gravity waves of frequency ω is defined by

$$\mu = \frac{C}{v} = \frac{Ck}{\omega} \quad (5)$$

where v is the phase velocity and k the propagation vector (see Hines C. G., 1965). The refractive index formulas are given in Table 1 in terms of the angle Y between the propagation vector k and the horizontal.

The refractive index formulas are identical for vertical propagation of acoustic-gravity waves and for transverse propagation of radio waves as are the expressions for group speed.

Refractive index curves are shown in Figure 1(a) and 1(b) for acoustic waves and HF radio waves, respectively. For $X < 1$ both families of surfaces are ellipsoids while for $X = 0$ the surfaces are spheres. For values of X near unity the μ ellipses are highly elongated. In fact, for radio waves they degenerate to a line in the direction of the geomagnetic field, whereas for acoustic waves they degenerate to a point at the origin.

On low frequencies ($Y \gg 1$) there are marked similarities between gravity waves and whistlers as shown in Table 2 and in Figures 2(a) and (b). From these figures it is seen that in both cases the refractive index is greater than unity, the refractive index surfaces are hyperboloids and that propagation is limited to certain ranges of angles and frequencies (see Figure 3). The beaming properties of gravity waves are shown in Figure 4(a) and are similar to those of whistlers sketched in Figure 4(b) (Gallet, R., 1963).

A peculiar feature of both gravity waves and whistlers is the difference between the directions of phase propagation and energy propagation (ray direction). Since the ray direction is normal to the refractive index surface, upward propagation of phase is associated with downward propagation of energy and vice versa. On the other hand, for both HF radio waves and acoustic waves the vertical components of both phase and energy propagation are in the same sense. This can be seen from the expressions for α which are positive in Table 1 and negative in Table 2.

Another interesting feature is the reversal of senses of rotation of the elements of the media. Acoustic waves produce clockwise rotation of the air parcels whereas gravity waves produce an anticlockwise motion in the plane of propagation. In the radio analogy, ordinary waves on frequencies above the gyro-frequency cause electrons to rotate in a counterclockwise fashion looking along the geomagnetic field whereas the sense of rotation is clockwise with whistlers.

4. RAY PATHS OF ATMOSPHERIC WAVES

4.1 Ray Paths of Acoustic Waves

Ray paths of acoustic waves in the earth's atmosphere illustrate some further similarities with high frequency radio waves. The U. S. 1962 Standard Atmosphere, shown in Figure 5, is temperature stratified which gives it layered properties somewhat similar to the electron layers of the ionosphere. Acoustic ray paths in the model atmosphere are shown in Figure 6 which shows that for a given wave frequency (or period) waves can penetrate the atmosphere through an iris which is reminiscent of radio waves. The ray paths of Figures 6(a) and 6(b) illustrate the dispersion effects as the wave period approaches the acoustic cut-off period. The variations of ground ranges with take-off angles with the vertical ($\varphi = 90 - Y$), see Figure 7, show the existence of skip zones - observations of which provided the first evidence of the temperature structure of the upper atmosphere (see for example Mitra, S. K., 1952, chapter III). Figure 7 also indicates the existence of high-angle and low-angle rays as in the case of radio waves (see Davies, K., 1969, section 12.3).

5. CONCLUDING REMARKS

Although there are some similarities between the propagation of acoustic-gravity waves and ionospheric radio, there are basic differences which must be borne in mind. Some of these differences are listed in Table 3.

TABLE 1

Comparison of dispersion properties of atmospheric waves in an isothermal atmosphere and ordinary radio waves in the ionosphere.

Acoustic Waves		Radio Waves	
Acoustic cut-off frequency	$\omega_a^2 = \frac{g^2}{4H^2}$	Plasma frequency	$\omega_p^2 = \frac{N e^2}{\epsilon_0 m}$
Buoyancy frequency	$\omega_g^2 = \frac{g}{H} \frac{Y-1}{Y}$	Gyrofrequency	$\omega_h = \frac{e}{m} B_0$
X	$X = \left(\frac{\omega_a}{\omega} \right)^2$	X	$X = \left(\frac{\omega_p}{\omega} \right)^2$
Y	$Y = \frac{\omega_g}{\omega}$	Y	$Y = \frac{\omega_h}{\omega}$
Frequency	$\omega > \omega_a$	Frequency	$\omega > \omega_h$
Direction	$Y \equiv$ angle with horizontal $0 < Y \leq 2\pi$	$\theta \equiv$ angle with magnetic field \underline{B}_0 $0 < \theta \leq 2\pi$	
Refractive index with gravity	$\mu^2 = \frac{1-X}{1-Y^2 \cos^2 Y}$	Refractive index with magnetic field	$\mu^2 = 1 - \frac{2X(1-X)}{2(1-X) - Y^2 \sin^2 \theta + \sqrt{Y^4 \sin^4 \theta + 4(1-X)^2 Y^2 \cos^2 \theta}}$
	$\mu < 1$		$\mu < 1$
Vertical propagation	$\mu^2 = 1 - X$	Transverse propagation	$\mu^2 = 1 - X$
Cut off	$\omega = \omega_a$	Cut off	$\omega = \omega_h$
Angle α between wave vector and ray.	$\tan \alpha = \frac{\mu^2 Y^2 \sin Y \cos Y}{1-X}$	Angle α between wave vector and ray.	$\tan \alpha = \frac{(1-\mu^2) Y^2 \sin \theta \cos \theta}{Y^4 \sin^4 \theta + 4(1-X)^2 \cos^2 \theta}$
Group and phase velocities	$u < v$		$u < v$
Group velocity (u) with vertical propagation.	$u^2 = c^2 \left[1 - \left(\frac{\omega_a}{\omega} \right)^2 \right]$	Group velocity (u) with transverse propagation.	$u^2 = c^2 \left[1 - \left(\frac{\omega_p}{\omega} \right)^2 \right]$

TABLE 2

Comparison of some formulas for gravity waves and whistlers.

Characteristic	Gravity Wave	Whistler
Frequency	$\omega < \omega_g$	$\omega < \omega_h$
Direction	$ \psi < \cos^{-1} (\omega/\omega_g)$	$ \theta < \cos^{-1} (\omega/\omega_h)$
Refractive index	$\mu^2 = \frac{X - 1}{Y^2 \cos^2 \psi - 1}$ $\mu > 1$	$\mu^2 \approx 1 + \frac{X}{Y \cos \theta - 1}$ $\mu > 1$
Angle α between wave normal and ray for very small frequencies	$\tan \alpha = - \frac{1}{\tan \psi}$	$\tan \alpha = - \frac{1}{2 \tan \theta}$
Group and phase velocities	$u > v$	$u > v$
Group velocity (u) for very small frequencies	$u = \frac{C}{\mu} = C \frac{\omega_g}{\omega} \cos \psi$	$u = \frac{2C}{\mu} = 2C \frac{\sqrt{\omega \omega_h \cos \theta }}{\omega_h}$

TABLE 3

Some differences between atmospheric waves and radio waves.

Property	AGW	Radio
1. Propagation of acoustic and HF radio waves	Atmosphere essential	Ionosphere not essential
2. Motion of medium	In plane of propagation	Mostly in plane of wave front
3. Attenuation	Increases with height	Peaks around 85 km
4. Characteristic directions	Stratification dependent on gravity	Stratification and geomagnetic field independent
5. Characteristic frequencies	Related	Independent

REFERENCES

- DAVIES, K., 1969, Ionospheric Radio Waves, Waltham, Mass., Blaisdell Publishing Company.
- GALLET, R., 1963, Whistlers, from Geophysics-The Earth's Environment, Editors C. DeWitt, J. Hieblot and A. Lebeau, pp. 553-590, New York, Gordon and Breach.
- HELLIWELL, R. A., 1965, Whistlers and Related Ionospheric Phenomena, Stanford, California, Stanford Univ. Press.
- HINES, C. O., 1965, Motions of the neutral atmosphere, chapter 6 of Physics of the Earth's Upper Atmosphere, Editors C. G. Hines, I. Paghis, T. R. Hartz and J. A. Fejer, Prentice-Hall, Inc., Englewood Cliffs, N. J.
- MITRA, S. K., 1952, The Upper Atmosphere, Calcutta, The Asiatic Society.
- RATCLIFFE, J. A., 1959, The Magneto-Ionic Theory, Cambridge, The University Press.
- TOLSTOY, I., and J. LAU, 1970, Ground level pressure fluctuations connected with ionospheric disturbances, J. Atmos. Sci. 27, 494-503.

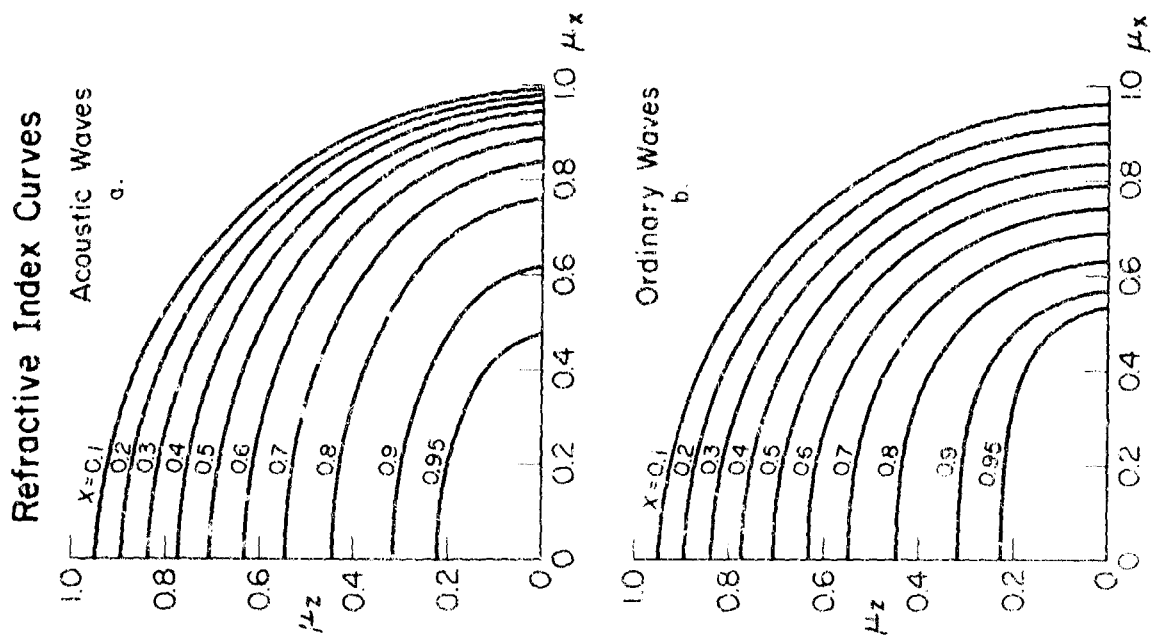


Fig. 1 Refractive index surfaces for (a) acoustic waves and (b) ordinary radio waves on frequencies above the gyrofrequency (ω_H).

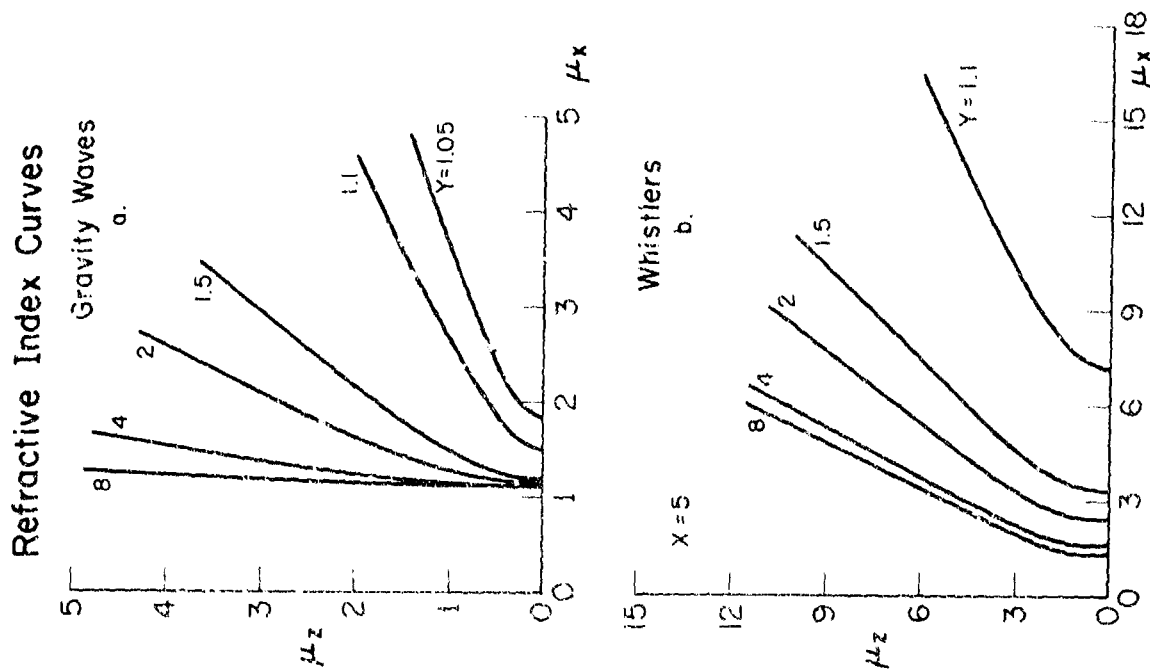


Fig. 2 Refractive index surfaces for (a) gravity waves and (b) whistlers.

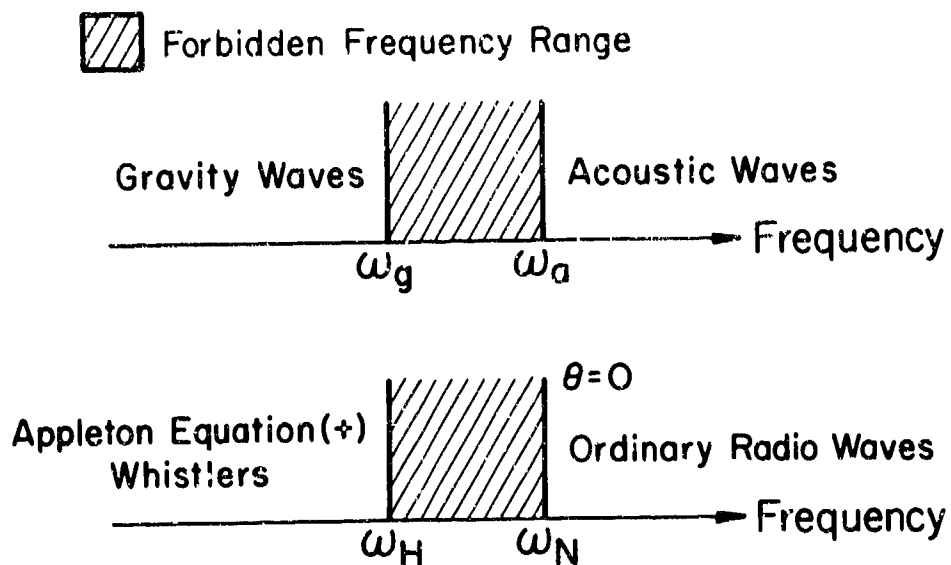
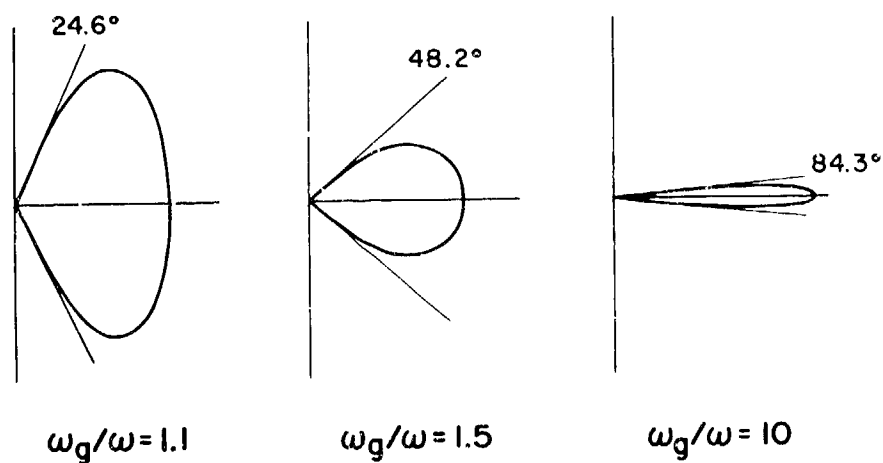
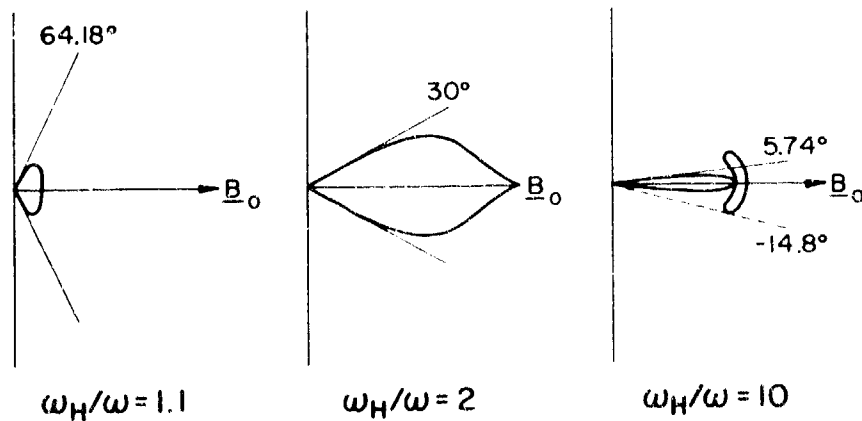


Fig.3 Allowed and forbidden regions of spectra of atmospheric waves and ionospheric radio waves.



RAY SURFACES FOR AN ATMOSPHERIC GRAVITY WAVE



RAY SURFACES FOR WHISTLERS

Fig.4 Ray surfaces for (a) gravity waves (b) whistlers to illustrate the beaming properties.

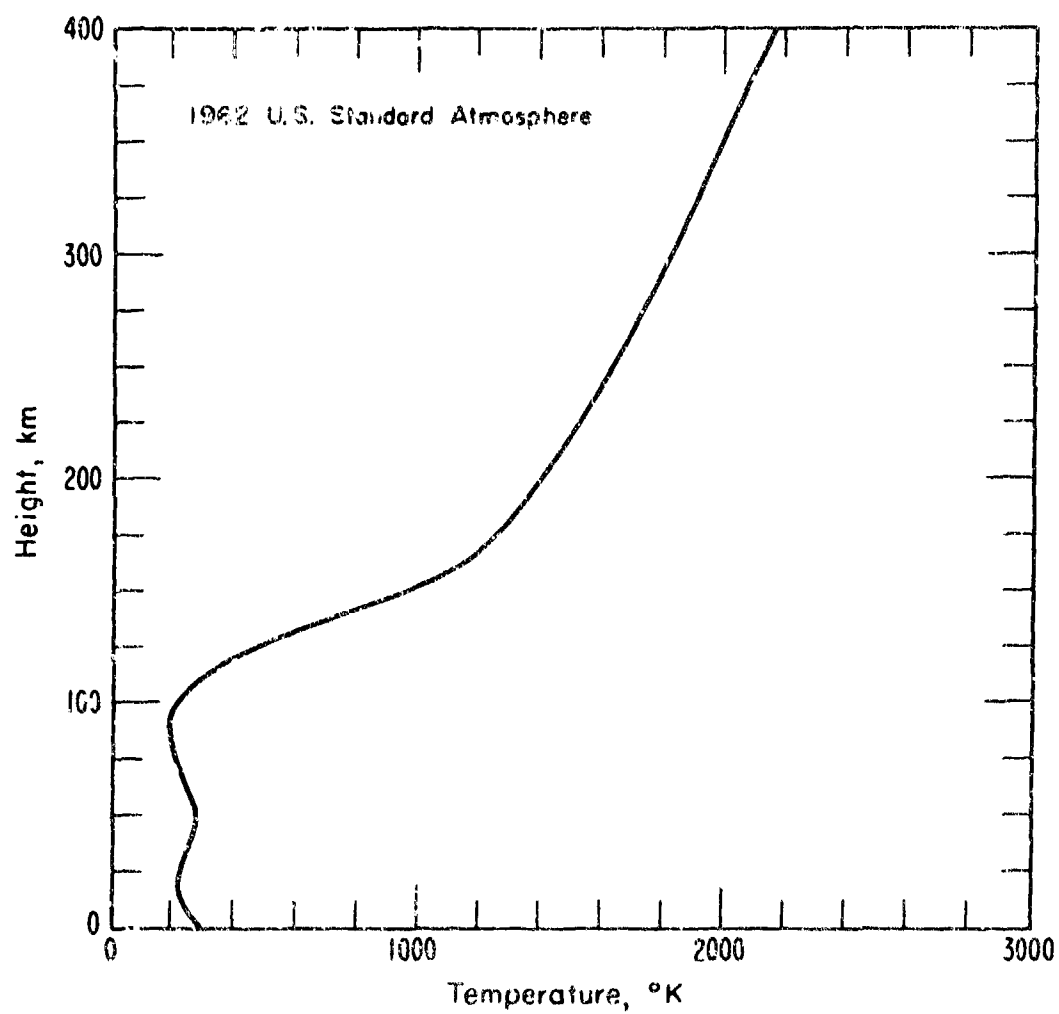


Fig.5 Temperature profile for the 1962 U.S. Standard Atmosphere.

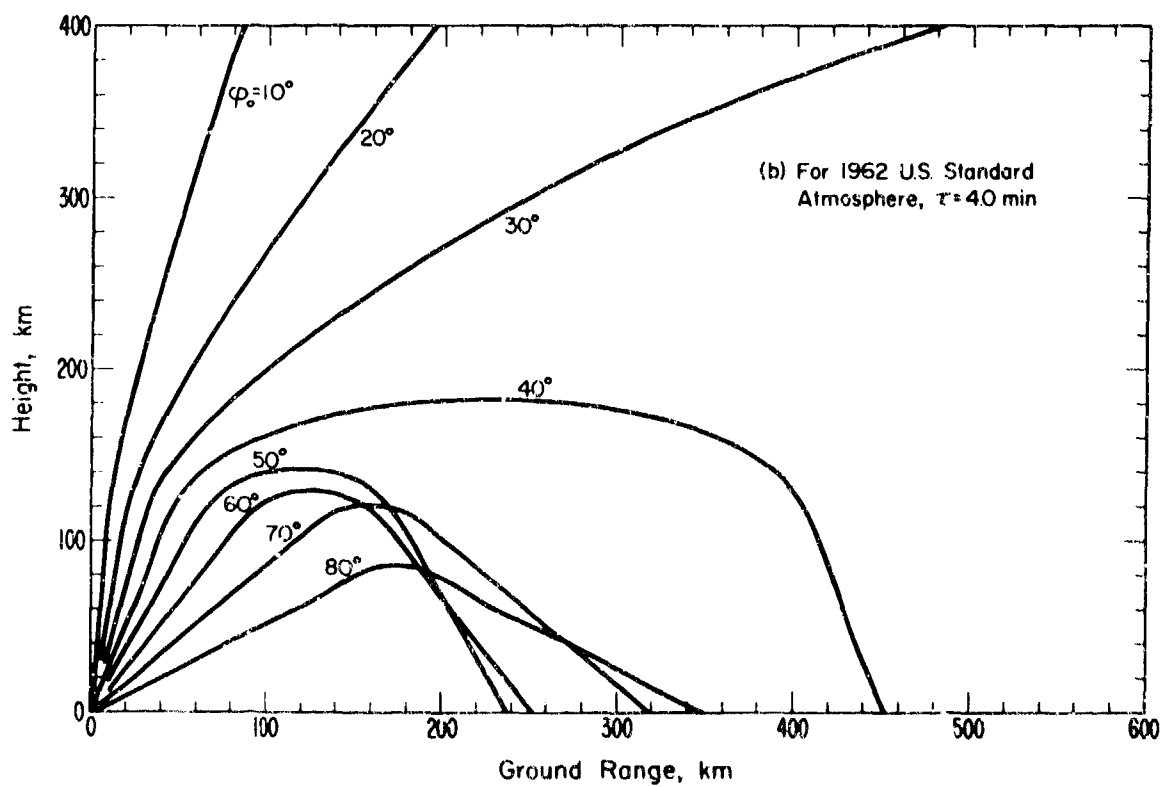
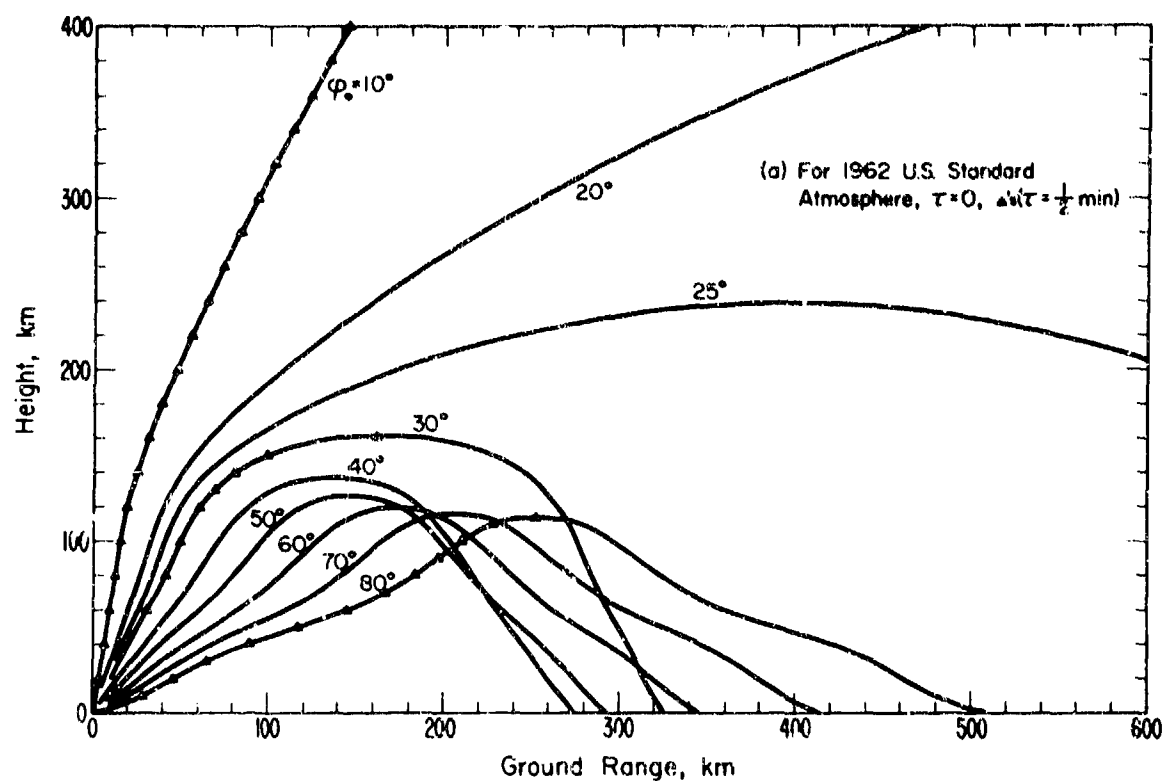


Fig.6 Acoustic ray paths in the 1962 U.S. Standard Atmosphere.

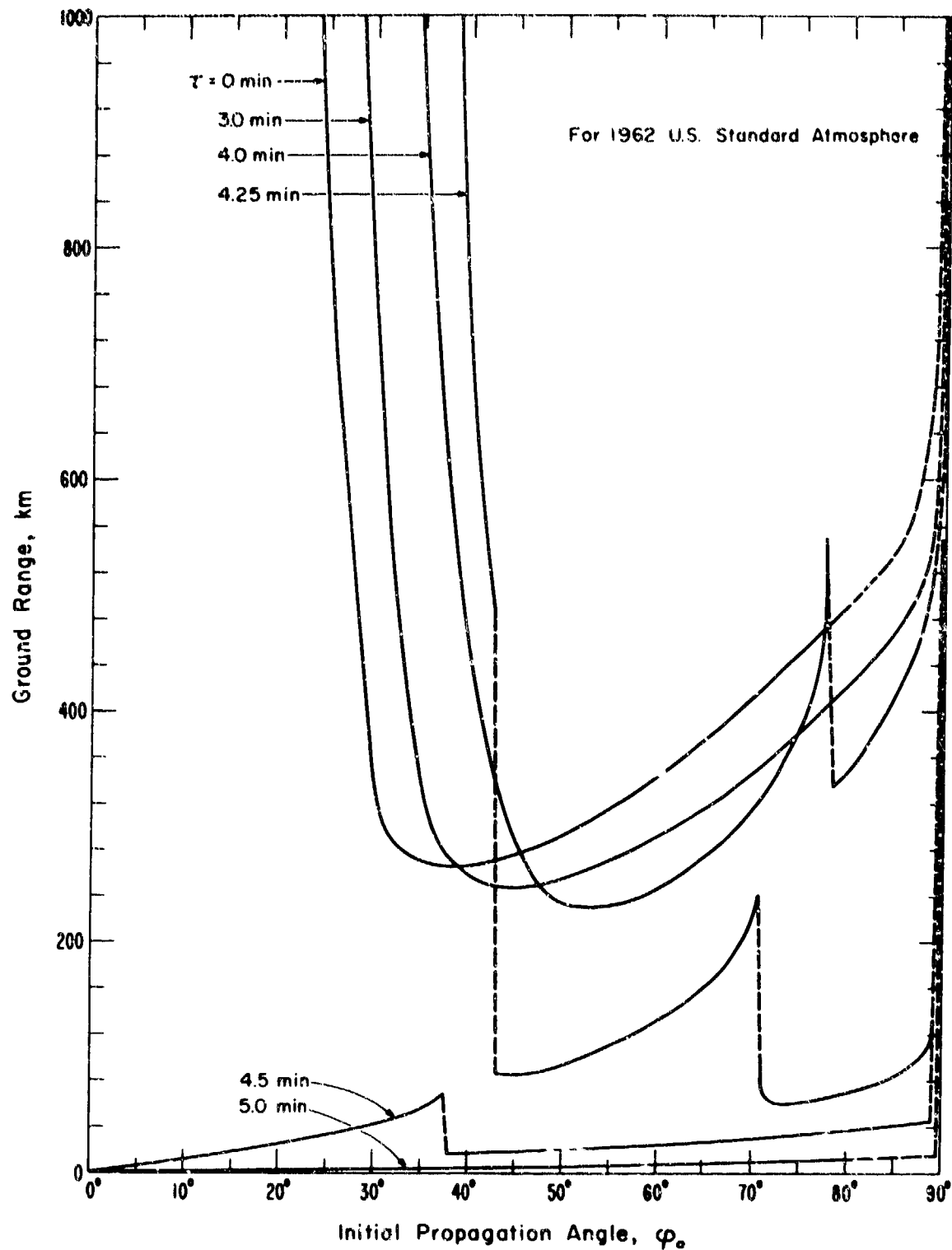


Fig.7 Variation of ground range with initial propagation angle with the vertical for acoustic waves in the 1962 U.S. Standard Atmosphere.

3D RAY TRACING FOR ACOUSTIC-GRAVITY WAVES

by

T.M.Georges

Wave Propagation Laboratory
NOAA Environmental Research Laboratories
Boulder, Colorado 80302
USA

TRAJECTOGRAPHIE A TROIS DIMENSIONS POUR LES ONDES ACOUSTIQUES ET DE GRAVITE

par

T.M. Georges

SOMMAIRE

On a mis au point un nouveau programme de trajectographie basé sur les équations canoniques de Hamilton, pour les ondes acoustiques et de gravité. Il permet de faire varier les profils de vent et de température dans l'atmosphère suivant les trois dimensions et de tenir compte de la courbure terrestre. On trouve d'intéressantes géométries de rayon, par exemple lorsque des rayons acoustiques passent dans des champs cycloniques de vent, et pour les ondes de gravité se propageant dans une atmosphère en présence de vents. Ces exemples et d'autres encore sont utilisés pour illustrer le mode d'emploi et les possibilités du programme.

3D RAY TRACING FOR ACOUSTIC-GRAVITY WAVES

T. M. Georges
Wave Propagation Laboratory
NOAA Environmental Research Laboratories
Boulder, Colorado, U.S.A. 80302

ABSTRACT

A new general-purpose ray tracing program for acoustic-gravity waves has been developed. It allows atmospheric wind and temperature to vary in all three spatial dimensions and with time and accounts for earth curvature. Ray plots show the characteristic acoustic ray patterns of a standard atmosphere but also some interesting and unexpected ray geometries in cases of more complex wind fields and for internal gravity waves.

1. RATIONALE

Ray tracing has been successfully employed to calculate the paths of wave-energy flow in inhomogeneous anisotropic media, most notably for radio waves in the ionospheric plasma, seismic waves in the earth, and for acoustic waves in the ocean and atmosphere. A few attempts have been made to extend acoustic-ray-tracing capabilities to low-frequency acoustic-gravity waves in the atmosphere (cf. PIERCE, 1966; JONES, 1969; CHANG, 1969; COWLING et al., 1971), but each scheme so far developed employs simplifying assumptions or idealized models that limit their applicability to the real atmosphere. In particular, the effects of winds are sometimes ignored or are at most constrained to be horizontal and to have only vertical gradients. Other approaches ignore either the effects of gravity or compressibility, and most neglect earth curvature and horizontal temperature gradients. Finally, no acoustic-gravity ray-tracing program of which we are aware is well documented and available in a "user-oriented" form, i.e., easy to use and readily adaptable to digital computers in common use.

The program described here is designed to overcome these limitations in the following ways:

- (a) Ray equations are derived from Hamilton's equations (rather than variations of Snell's Law) and allow three-dimensional gradients of atmospheric wind and temperature fields;
- (b) A Hamiltonian appropriate to acoustic-gravity waves in a windy atmosphere allows a single program to apply to the whole wave spectrum from pure acoustic to internal gravity waves;
- (c) Earth curvature is accounted for by writing Hamilton's equations in earth-centered spherical coordinates; and
- (d) Programming is modeled after the Jones-ITS ionospheric radio ray-tracing program, which has evolved, over several years of widespread use, into a thoroughly tested and highly user-oriented tool (JONES, 1966).

This paper briefly describes the workings and capabilities of the program. Further details and instructions for its use appear in a NOAA Technical Report (GEORGES, 1971) that can be supplied upon request.

2. THE RAY-TRACING EQUATIONS

Hamilton's equations, when applied to wave propagation, can be thought of as a differential expression of Fermat's Principle of Stationary Time. Their applications to geometrical optics and to geometrical acoustics are discussed, respectively, in the texts by KLINE and KAY (1965) and LANDAU and LIFSHITZ (1959). In their simplest vector form, they can be written

$$\dot{\mathbf{r}} = \frac{\partial H}{\partial \mathbf{K}} \quad (1a)$$

and

$$\dot{\mathbf{K}} = - \frac{\partial H}{\partial \mathbf{r}} \quad (1b)$$

where a dot indicates total time differentiation, \mathbf{K} is the wave vector, and \mathbf{r} is a point on the ray path. The Hamilton (H) is a quantity whose constancy defines the ray path, given appropriate initial conditions and a model atmosphere. For acoustic-gravity waves, H is given by the wave dispersion relation, such as that developed by HINES (1960), TOLSTOY (1963), and others for isothermal atmospheres without winds. The generalization to include winds is straightforward and is discussed by PITTEWAY and HINES (1965). The isothermal dispersion relation gives the appropriate Hamiltonian for ray tracing in nonisothermal

atmospheres because the geometrical-acoustics approximation is equivalent to assuming that the medium is locally homogeneous and is valid only when that assumption is valid. The Hamiltonian is then

$$H = \Omega^2 - \Omega^2 C^2 K^2 - \Omega^2 \omega_a^2 + C^2 k_h^2 \omega_b^2 = 0 \quad (2)$$

where Ω is the intrinsic wave frequency with respect to the air moving at a local wind velocity, γ , whose components are v_r , v_θ and v_ϕ in spherical coordinates, r , θ , ϕ . The wave frequency measured in a fixed frame is $\omega = \Omega + \gamma \cdot \mathbf{K}$, where \mathbf{K} is the wave vector (k_r , k_θ , k_ϕ). The horizontal component of \mathbf{K} is k_h . The local speed of sound is C , ω_a is the acoustic-cutoff frequency, $\gamma g/2C$, and ω_b^2 is the square of the Brunt frequency, $(\gamma-1)g^2/C^2 + g(\partial C^2/\partial z)/C^2$. In accordance with the analysis of EINAUDI and HINES (1970), a modified definition of ω_b is adopted, which accounts for the effects of vertical sound-speed (temperature) gradients on atmospheric stability. Substituting (2) into (1) and expressing in spherical coordinates (BRANDSTATTER, 1959), we get the six coupled differential ray-tracing equations:

$$\frac{dr}{dt} = C^2 k_r \Omega F + v_r \quad (3)$$

$$\frac{d\theta}{dt} = \frac{1}{r} \left\{ C^2 k_\theta (\Omega^2 - \omega_b^2) F / \Omega + v_\theta \right\} \quad (4)$$

$$\frac{d\phi}{dt} = \frac{1}{r \sin \theta} \left\{ C^2 k_\phi (\Omega^2 - \omega_b^2) F / \Omega + v_\phi \right\} \quad (5)$$

$$\frac{dk_r}{dt} = \frac{\Omega}{C} \frac{\partial C}{\partial r} (\omega_a^2 - C^2 k^2) F + (k_\theta^2 + k_\phi^2) \frac{\partial F}{2\Omega} \frac{\partial C^2}{\partial r^2} - K \cdot \frac{\partial v}{\partial r} + k_\theta \frac{dv}{dt} + k_\phi \sin \theta \frac{d\phi}{dt} \quad (6)$$

$$\frac{dk_\theta}{dt} = \frac{1}{r} \left\{ \frac{\Omega}{C} \frac{\partial C}{\partial \theta} (\omega_a^2 - C^2 k^2) F + (k_\theta^2 + k_\phi^2) \frac{\partial F}{2\Omega} \frac{\partial}{\partial \theta} \left(\frac{\partial C^2}{\partial r} \right) - K \cdot \frac{\partial v}{\partial \theta} - k_\theta \frac{dr}{dt} + r k_\phi \cos \theta \frac{d\phi}{dt} \right\} \quad (7)$$

$$\frac{dk_\phi}{dt} = \frac{1}{r \sin \theta} \left\{ \frac{\Omega}{C} \frac{\partial C}{\partial \phi} (\omega_a^2 - C^2 k^2) F + (k_\theta^2 + k_\phi^2) \frac{\partial F}{2\Omega} \frac{\partial}{\partial \phi} \left(\frac{\partial C^2}{\partial r} \right) - K \cdot \frac{\partial v}{\partial \phi} - k_\phi \sin \theta \frac{dr}{dt} - r k_\theta \cos \theta \frac{d\theta}{dt} \right\} \quad (8)$$

where

$$F = (2\Omega^2 - \omega_a^2 - C^2 k^2)^{-1}$$

These equations, though apparently complicated, are readily integrated by standard numerical methods to yield $r(t)$ and $K(t)$. The addition of a seventh equation,

$$\frac{d\omega}{dt} = K \cdot \left(\frac{\partial v}{\partial t} \right) - \frac{\Omega}{C} \frac{\partial C}{\partial t} (\omega_a^2 - C^2 k^2) F \quad (9)$$

permits integration of Doppler shift, provided the medium does not vary appreciably during ray transit.

The program described here uses a standard Adams-Moulton integration scheme with variable step length and error checking. The user specifies the maximum tolerable fractional integration error per step and thus has the option of trading computer running time for accuracy.

3. USING THE PROGRAM

The program is designed to be used, for the most part, like a "black box," that is, without much knowledge of its inner workings. Parameters that the user may wish to vary (for example, initial conditions, wave variables, and model atmosphere parameters) are input via a data deck with one such parameter per card. Sequential ray calculations, such as stepping ray launch direction, are automatically

provided for. In addition to a comprehensive printed output, automatic ray plots may be obtained on computers with cathode-ray-tube/microfilm output capabilities.

Several simple model atmospheric wind and temperature fields with variable parameters are included in the program's repertoire, and the user may readily substitute his own models. In its present form, the program accepts only continuous analytic descriptions of wind and temperature fields, but virtually any desired field may be fitted with analytic functions.

4. ILLUSTRATIONS OF APPLICATIONS - ACOUSTIC WAVES

Figure 1 displays the kind of ray plot often produced by simpler programs: that of ordinary acoustic waves in a standard-atmosphere temperature profile. Here, however, a wind blows toward the right and increases logarithmically with height. Note particularly the influence of the wind on where rays return to the ground. The wave source in this example is near the tropopause, so that pronounced ray ducting is also evident.

Figure 2 shows acoustic ray paths through an isothermal cylindrical vortex with a solid-rotating core. The ray geometry is independent of spatial scale and so is relevant to smaller vortices, such as those generated in aircraft wakes, as well as to cyclonic weather features of synoptic scale. The only variable parameter of the problem is the ratio of the maximum wind speed in the vortex to the sound speed and is indicated on the 4 panels of the figure. This maximum is attained at the dashed circles in the figure; inside the circle, wind speed varies approximately as the radius, while outside, it falls off nearly as the inverse radius. This problem is further discussed in another paper (GEORGES, 1972).

Figure 3 shows schematically how anisotropy and nonreciprocity introduced by winds affect ray propagation in acoustic sounding of the troposphere. In general, refraction alters the location of the scattering volume, the scattering angle, and the magnitude of the Doppler shift. GEORGES and CLIFFORD (1972) further analyze refractive effects in acoustic sounding.

5. ILLUSTRATIONS OF APPLICATIONS - INTERNAL GRAVITY WAVES

Because ray paths of internal gravity waves are much more difficult to develop intuitive feelings for than are acoustic waves, one tends to use a ray-tracing program much like a new experimental tool: Internal gravity ray paths, even in simple wind and temperature fields, often exhibit unexpected behavior. An example is provided by the simple case of gravity-wave propagation in a region of linear temperature gradient. Figure 4 shows two gravity-wave rays launched upward and downward in such a temperature profile. An explanation of the cusplike reflection behavior can be found by considering the direction of the normals to the constant- ω/ω_0 surfaces in the k plane (figure 4 inset), which indicate ray direction. Waves launched in a horizontally stratified medium must maintain k_x constant as they propagate; therefore, as temperature (and thus ω_0) changes, one estimates changes in ray direction by sliding up or down a vertical line through the diagram and noting the resulting changes in direction of the surface normals. For example, a ray whose phase fronts are launched downward and that propagates upward into increasing temperature (increasing ω/ω_0) experiences a gradual ray steepening until $k_z \rightarrow 0$ when ray direction abruptly reverses, executing the cusplike reflection (not a true mathematical cusp) depicted in figure 4. The level of reflection of a gravity wave depends only on the value of k_x and can be found by setting $k_z = 0$ in the dispersion relation, giving the minimum value of ω_0/ω for a given k_x :

$$\frac{\omega_b^2}{\omega^2} = \frac{n_x^2 - 1}{n_x^2 - 1.225},$$

where

$$n_x = Ck_x/\omega \quad (10)$$

Figure 5 illustrates how internal gravity waves may be ducted in a temperature minimum. Evidently the vertical propagation of internal gravity waves tends to be restrained in the presence of temperature gradients, regardless of whether temperature increases or decreases. ECKART (1960) shows ray paths that display this behavior.

Because internal-gravity-wave phase speeds are considerably slower than those of acoustic waves, gravity waves interact much more strongly with atmospheric wind fields than do acoustic waves. Gravity-wave ray paths in a linear wind profile of gradient 0.1 m/s/km serve to illustrate that nature of the interaction. Figure 6 shows five gravity-wave rays launched downwind. Each wave eventually reaches its own "critical level," i.e., where the wind speed equals the horizontal trace speed of the wave. Each wave approaches an asymptotic condition in which the wave vector tends toward vertical and phase velocity toward zero.

Gravity waves launched upwind exhibit a quite different behavior, as illustrated in figure 7. The ray is refracted upward and is eventually turned around by the wind shear. In this example, the azimuth of k is at a 45° angle with y , and lateral ray deviation also occurs, as illustrated in the plan view in figure 7.

6. CONCLUSIONS

These few examples illustrate the capabilities of the 3D ray-tracing program in simple model atmospheres and show some ray path properties that, as yet, have not apparently been appreciated.

It is expected that the program's capabilities will be refined with use and in response to user needs and suggestions. Such suggestions are, of course, welcome.

7. REFERENCES

- BRANDSTATTER, J.J., 1959, "The Theory of Propagation of Rays in an Inhomogeneous and Anisotropic Medium," Stanford Research Institute Report, Project 2241.
- CHANG, N.J.F., 1969, "Acoustic-Gravity Waves in the Ionosphere and Their Effects on High-Frequency Radio Propagation," Ph.D. Dissertation, Electrical Engineering Dept., University of Colorado, Boulder, Colorado, U.S.A.
- COWLING, D.H., H.D. WEBB, and K.C. YEH, 1971, "Group Rays of Internal Gravity Waves in a Wind-Stratified Atmosphere," J. Geophys. Res. 76, 213-220.
- ECKART, C., 1960, "Hydrodynamics of Oceans and Atmospheres," Pergamon, New York.
- EINAUDI, F., and C.O. HINES, 1970, "WKB Approximation in Application to Acoustic-Gravity Waves," Can. J. Phys. 48, 1458-1471.
- GEORGES, T.M., 1971, "A Program for Calculating Three-Dimensional Acoustic-Gravity Ray Paths in The Atmosphere," NOAA Tech. Report ERL 212-WFL 16, U.S. Govt. Printing Office, Washington, D. C.
- GEORGES, T.M., 1972, "Acoustic Ray Paths through a Model Vortex with a Viscous Core," J. Acoust. Society of America, 51, No. 1 (Part 2), 206-209.
- GEORGES, T.M., and S.F. CLIFFORD, 1972, "Acoustic Sounding in a Refracting Atmosphere," to be submitted to J. Acoust. Society of America.
- HINES, C.O., 1960, "Internal Atmospheric Gravity Waves at Ionospheric Heights," Can. J. Phys. 38, 1441-1481.
- JONES, R.M., 1966, "A Three-Dimensional Ray-Tracing Computer Program," ESSA Tech. Report IER 17-JTSA 17, U. S. Govt. Printing Office, Washington, D. C.
- JONES, W.L., 1969, "Ray Tracing for Internal Gravity Waves," J. Geophys. Res. 74, 2028-2033.
- KLINE, M., and I.W. KAY, 1965, "Electromagnetic Theory and Geometrical Optics," Wiley, New York.
- LANDAU, L.D., and E.M. LIFSHITZ, 1959, "Fluid Mechanics," Pergamon Press, Oxford, 256 ff.
- PIERCE, A.D., 1966, "Geometrical Acoustics Theory of Waves from a Point Source in a Temperature-and Wind-Stratified Atmosphere," AVCO Scientific Report, AVSSD-0135-66-CR.
- PITTEWAY, M.L.V., and C.O. HINES, 1965, "The Reflection and Ducting of Atmospheric Acoustic-Gravity Waves," Can. J. Phys. 43, 2222-2243.
- TOLSTOY, I., 1963, "The Theory of Waves in Stratified Fluids Including the Effects of Gravity and Rotation," Rev. Mod. Phys. 35, 207-230.

ACOUSTIC WAVES IN 1962 U.S. STANDARD ATMOSPHERE

$f = 300 \text{ Hz}$; Logarithmic Wind Profile: $u = 10 \text{ m/s}$ at 1 km
Elevation Angle Varies from -20° to 200° in 10° Steps

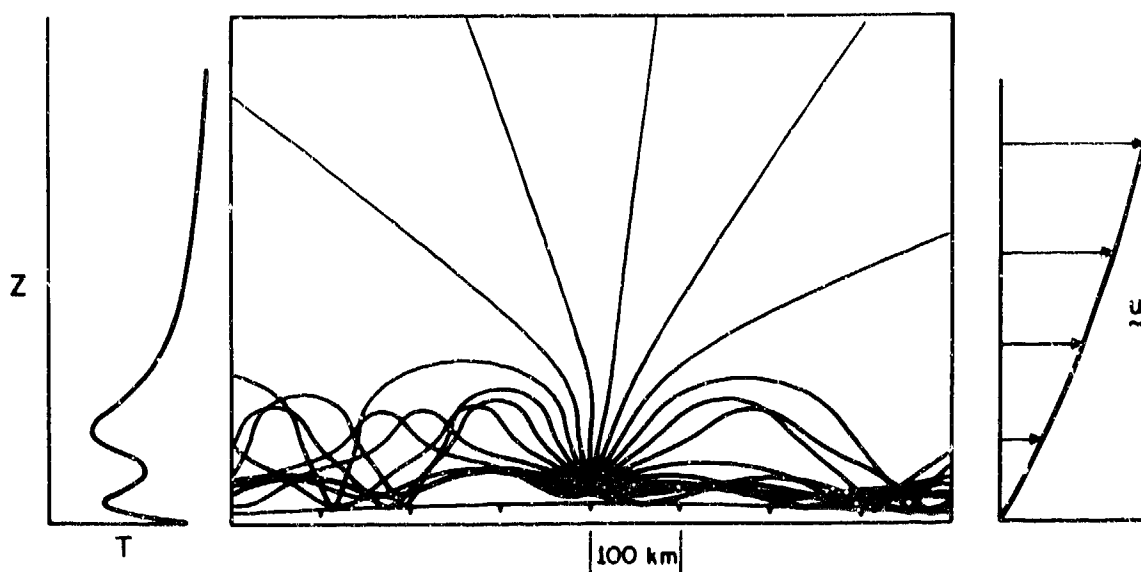


Fig.1 Acoustic waves in 1962 U.S. Standard Atmosphere temperature profile and a wind blowing to the right and increasing logarithmically with height.

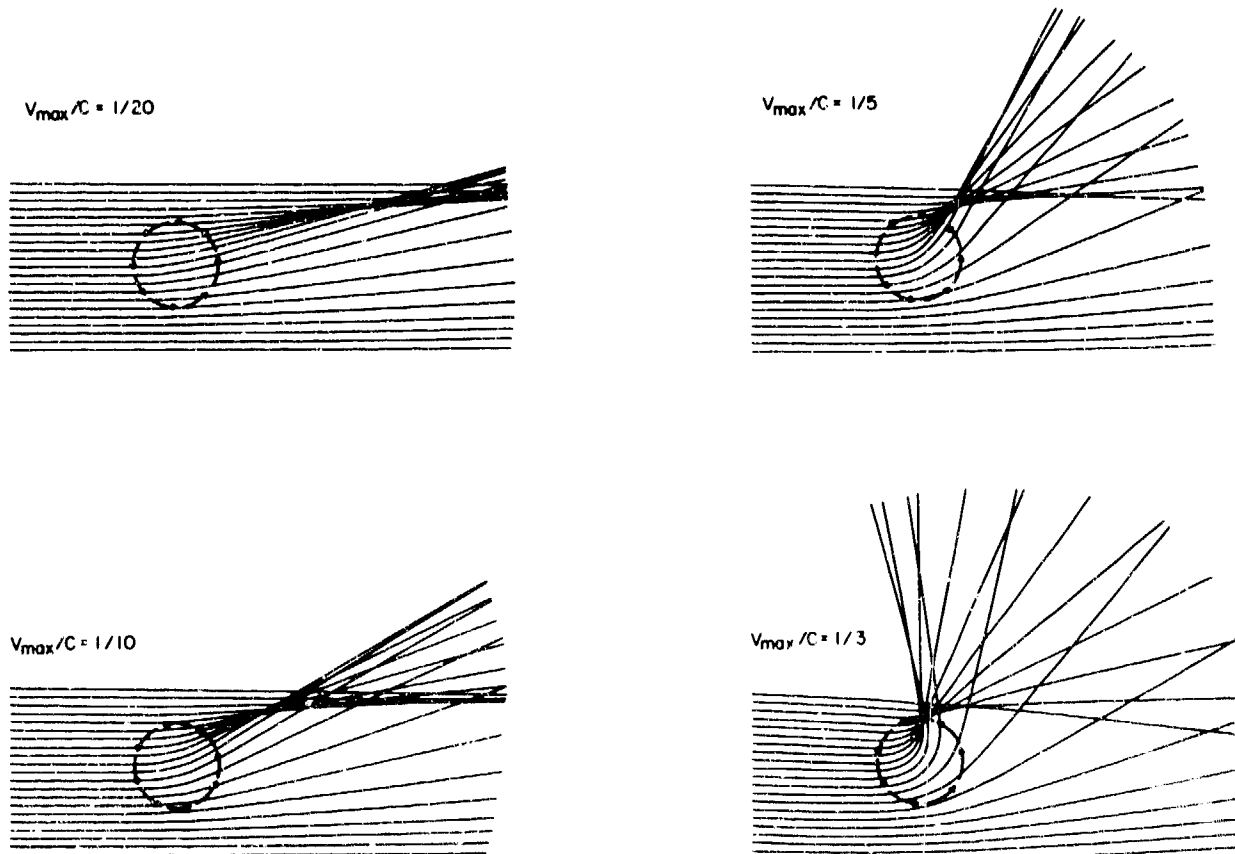


Fig.2 Acoustic ray paths through a model vortex with a viscous core. Tangential velocity maximizes along the dashed circles and has the speed indicated on each panel. (Spatial scale is arbitrary).

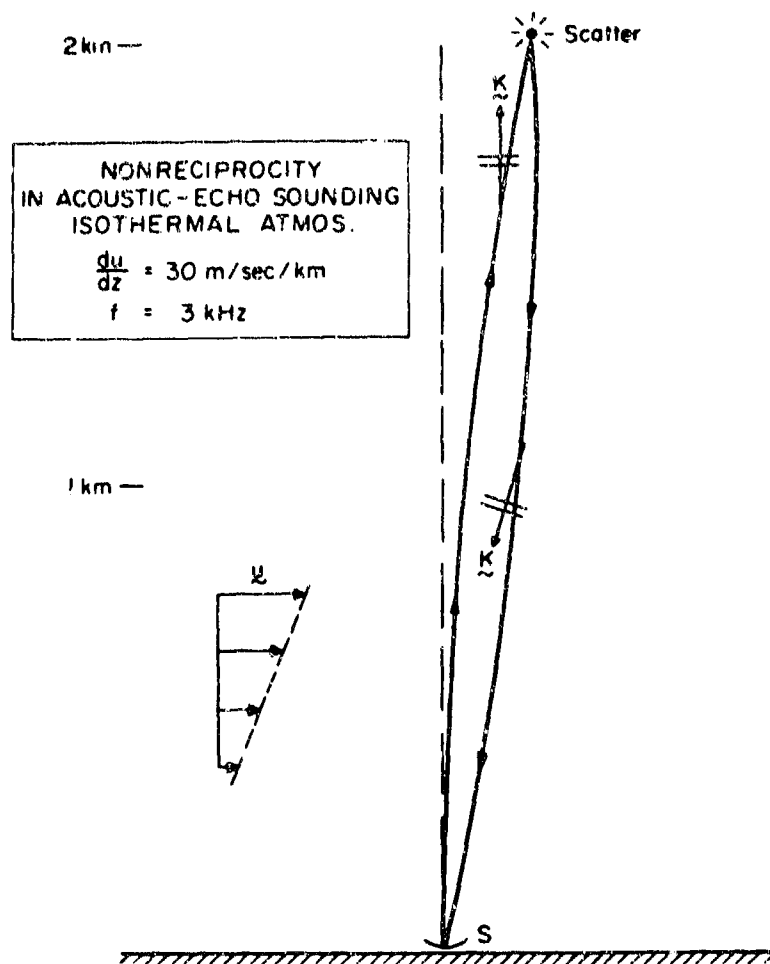


Fig.3 Acoustic ray path in an acoustic-sounding geometry illustrating nonreciprocity in the presence of wind shear.

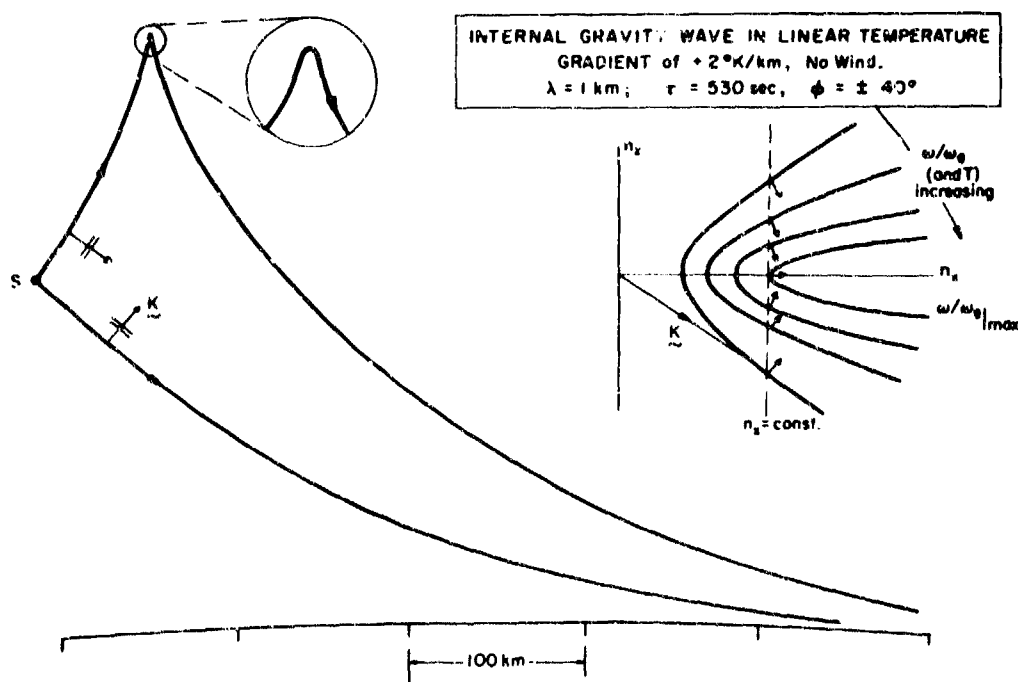


Fig.4 Internal-gravity ray paths in a positive linear temperature gradient, illustrating cusplike reflection of the upgoing ray and the asymptotic approach to horizontal of the downcoming rays.

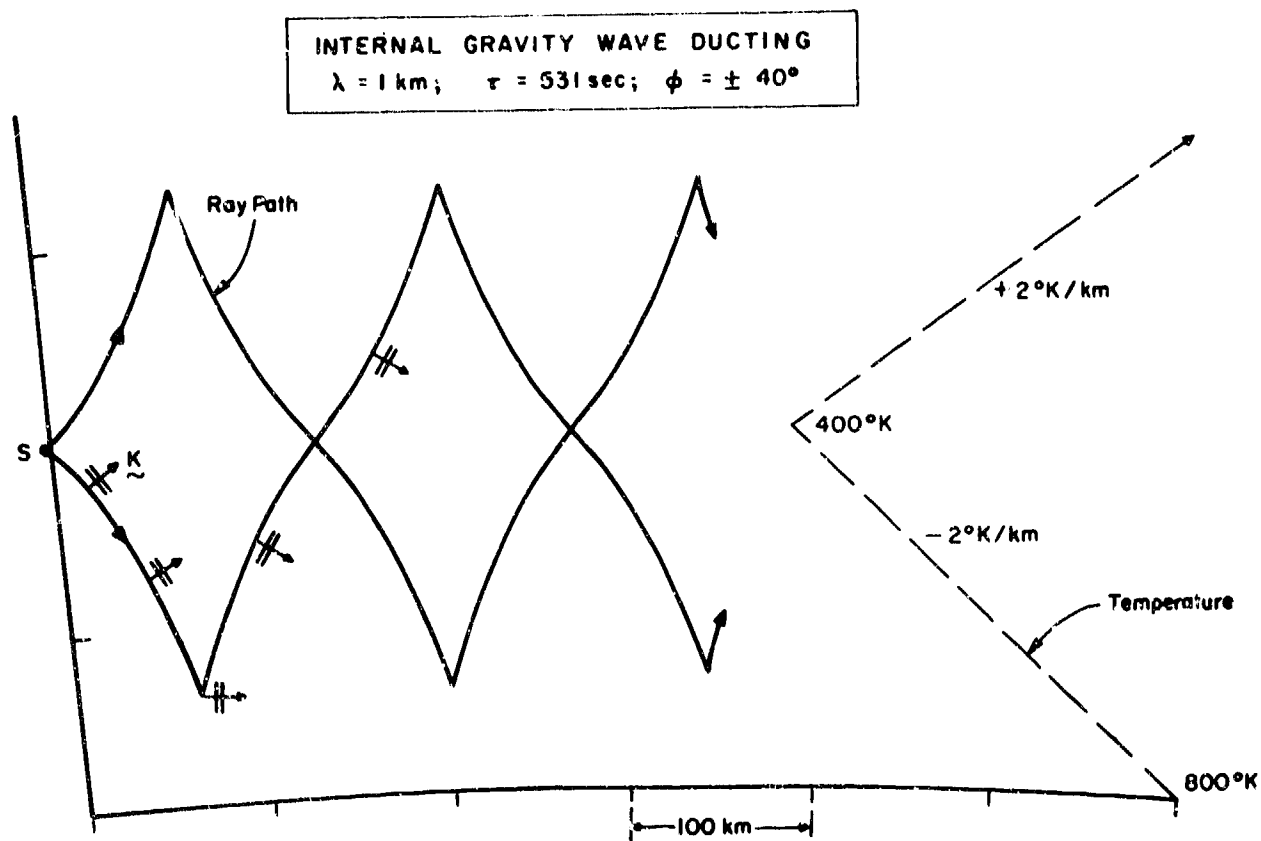


Fig.5 Internal gravity wave ducting in a piecewise linear temperature profile.

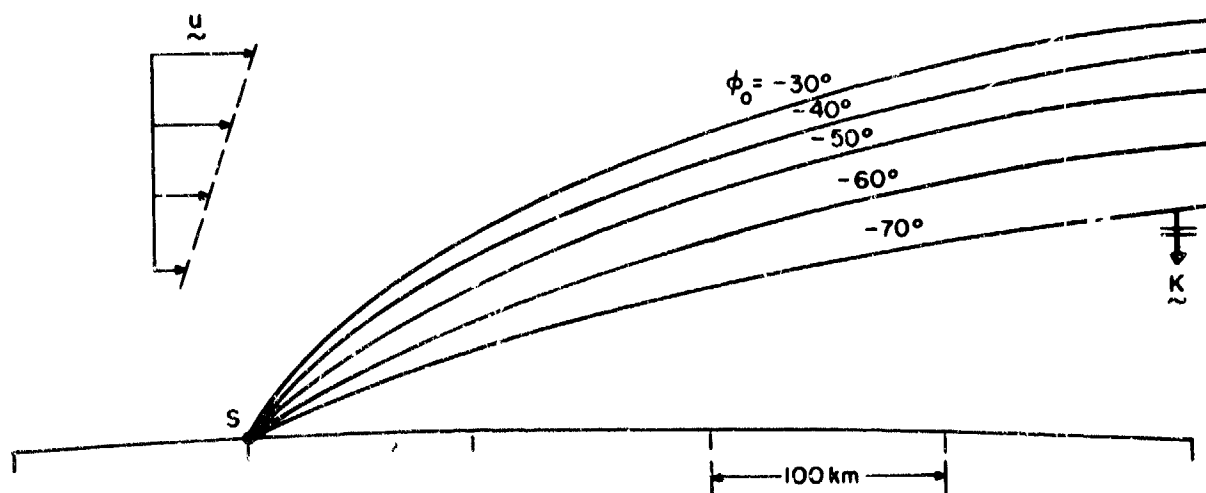
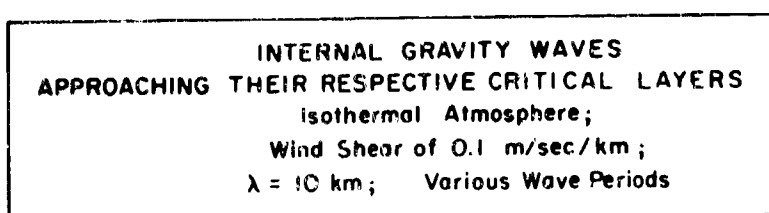


Fig.6 Internal gravity waves approaching their respective critical layers in a linearly increasing wind profile.

INTERNAL GRAVITY WAVE
 IN WIND SHEAR OF 0.1 m/sec/km
 and
 TEMPERATURE GRADIENT 0.1°K/km
 $\lambda = 10 \text{ km}$; $\tau = 475 \text{ sec}$; $\phi = -50^\circ$

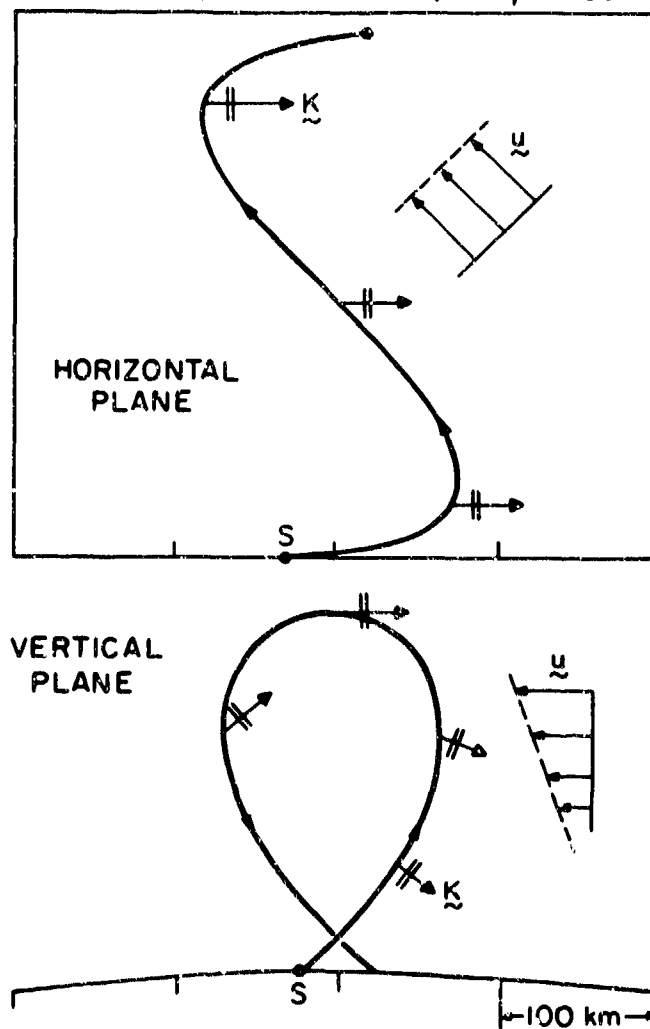


Fig.7 Three-dimensional ray path of an internal gravity wave propagating upstream in a linear wind profile.

GENERATION AND PROPAGATION OF SOUND WAVES BETWEEN
THE IONOSPHERE AND THE LOWER ATMOSPHERE

by

R.K.Cook

US Department of Commerce,
National Bureau of Standards
Washington, DC 20234
USA

CREATION ET PROPAGATION D'ONDES SONORES ENTRE L'IONOSPHERE ET LA BASSE ATMOSPHERE

par

R. K. Cook

SOMMAIRE

Différents processus physiques engendrent dans la basse atmosphère, des ondes sonores à des fréquences infrasoniques (périodes oscillatoires $> 1,0$ sec.). Parmi les sources typiques de ces ondes sonores, on peut citer les explosions volcaniques, les tremblements de terre, les gros orages, et les ondes de choc créées par des véhicules se déplaçant à des vitesses supersoniques. Dans l'ionosphère, les phénomènes créateurs d'infra-sons comprennent les décharges aurorales, ainsi que les ondes de choc provoquées par des satellites ou des météorites évoluant à des vitesses supersoniques. Nous présentons les résultats d'une analyse portant sur la production d'ondes sonores et leur propagation descendante dues aux effets d'échauffement des décharges aurorales, en particulier dans le cas des ondes se déplaçant à des vitesses supersoniques parallèlement à la surface de la terre. Les ondes "de choc" de ces décharges se propagent selon une trajectoire descendante à forte pente, leur perte d'énergie, due à l'absorption par viscosité et à la conduction de la chaleur, est très faible. On les observe fréquemment dans des stations infrasoniques situées aux latitudes élevées. Une estimation de l'échauffement auroral est tirée de la puissance des infra-sons observés à la surface de la terre.

GENERATION AND PROPAGATION OF SOUND WAVES BETWEEN THE IONOSPHERE AND THE LOWER ATMOSPHERE

Richard K. Cook
National Bureau Standards
Washington, D.C. USA

SUMMARY

Various physical processes generate sound waves at infrasonic frequencies (oscillation periods > 1.0 sec) in the lower atmosphere. Some typical sources are volcanic explosions, earthquakes, severe storms, and the shock waves from vehicles moving at supersonic speeds. In the ionosphere, sources of infrasound include auroral discharges and shock waves from satellites and meteorites moving at supersonic speeds. We present the results of an analysis for the generation of sound and propagation downwards due to the heating effects of auroral discharges, particularly those traveling at supersonic speeds in directions parallel to the earth's surface. The "shock" waves from such discharges are propagated steeply downward with very little loss of energy from absorption by viscosity and heat conduction, and are frequently observed at infrasonic stations located at high latitudes. An estimate of auroral heating is derived from the observed strengths of infrasound at the earth's surface.

1. Introduction

The aurora borealis gives rise to two types of infrasonic waves found in the atmosphere of the northern hemisphere at temperate and high latitudes. The first type is found at mid-latitudes during sufficiently strong magnetic storms even in the absence of a visible aurora at the geographical location of the infrasonic station. The second type of infrasonic wave, found near the auroral oval at high latitudes when visible sharply defined auroral forms travel overhead across the station location at supersonic speeds has directions of propagation and horizontal trace velocities very nearly the same as those of the visible auroral form. We shall develop and examine the consequences of a hypothesis that the second type of infrasound is generated by ionospheric heating caused by auroral electrical discharges.

The latter type of infrasound has been regarded as an acoustical bow wave in the ionosphere (Chimonas and Peltier, 1970). The bow wave is presumed to be generated by the electrojet line current of the auroral form, in supersonic motion perpendicular to its own length, and moving parallel to the earth's surface. The question is left open by the authors as to whether the Joule heating in the electrojet, or the Lorentz force on its moving charges, gives rise to the bow wave.

In the analysis given below we start from the rather different assumption that a thin plane sheet of the vertically descending ions forming an auroral arc generates a uniform amount of heat per unit area, causing a practically instantaneous rise in temperature T of the atmosphere, and causing as well the visible auroral discharges.

1.1 Measurement of auroral infrasound

The electroacoustical system used at an infrasonic station typically consists of an array of at least four microphones, associated electronic filter-amplifiers, and recorders. The system is designed for use as a steered array. Five characteristics of infrasonic waves passing through the station area are determined: (1) the amplitude and waveform of the incident sound pressure, (2) the direction of propagation of the wave, (3) the horizontal trace velocity c_h , (4) the distribution of sound wave energy at various frequencies of oscillation, and (5) the time of occurrence of the infrasound.

The microphones are located at ground level, approximately in the same plane, and on the average are about 8 km apart. See Figure 1 for the station at Washington D.C. Those located near the auroral zone have similar configurations. Fuller details on the measurement of infrasound have been given (Cook and Bedard, 1971), and a general summary of the observations made at several stations of an infrasonic network has been published (Cook, 1969).

1.2 Results of measurements

An extensive series of observations has been made (Wilson and his associates, summarized by him, 1971), on the infrasound associated with auroral activity. His measurement system is essentially the same as that described above. Most of the infrasonic events are wave packets which rise suddenly out of the noise and last for only a few cycles. The infrasound is apparently generated by visible sharply-defined large-scale auroral arcs traveling overhead at the infrasonic station at supersonic speeds. Many of the observations were made at the infrasonic station at College, Alaska, supplemented by data from temporary stations at Palmer, Alaska and Inuvik, Northwest Territories. A brief summary of the basic conclusions from the data is: (a) the average horizontal trace velocity is supersonic, $c_h \approx 513$ m/sec; (b) the transient pulses of sound have about the same direction of propagation and velocity as fast-moving auroral arcs overhead at Alaska, measured with an all-sky camera; (c) the dominant period of oscillation is about 20 sec; (d) peak sound pressure is typically 3 dyn/cm²; and (e) each pulse is of only a few minutes duration.

The observations of infrasound at the surface of the earth and of the visible auroral form with an all-sky camera can be explained by means of Wilson's shock wave model, in which the supersonic motion of the leading edge of an auroral arc gives rise to an acoustical shock wave (See Figure 2). The lower edge of the aurora serves as a line source (perpendicular to the plane of the paper). A particular pulse arrived at the ground station microphones 420 sec after an auroral arc passed overhead. The 420 sec delay corresponds to a source altitude of 140 km for an assumed average sound velocity $c \approx 300$ m/sec for the pulse during its passage downward through the atmosphere, and measured $c_h \approx 680$ m/sec. This altitude is to be compared with the known heights of visible auroral arcs, which in most instances have streamers extending from 110-km to 145-km altitudes.

2. Analysis for generation of auroral sound

The basic assumption we make here is that a thin plane sheet of the vertically descending ions forming an auroral arc generates a uniform amount of heat per unit area, causing a practically instantaneous rise in temperature ΔT of the atmosphere, and causing as well the visible auroral discharges. The sheet moves in a direction perpendicular to its plane at a supersonic speed M_c , where c = local speed of sound near the sheet and M = Mach number of the moving sheet, see Figure 3. The sheet ends abruptly where it has its lower edge at a height h above the surface of the earth. The density ρ of the atmosphere remains unchanged, and therefore the pressure jumps by an amount $\Delta p = \rho R \Delta T$ as the sheet passes any point in the atmosphere. In effect the heating serves as a body "force" for the generation of sound.

The temperature and pressure jumps will gradually decay with time except for jumps arising subsequently from shocks appearing at the lower edge of the sheet (to be discussed presently). But the basic features of the generation of sound can be arrived at by considering the leading plane-sheet as a heat source. Its lower edge gives rise to two shock waves. The one propagates down towards the surface of the earth, and the other proceeds towards the upper atmosphere, see Figure 3. In order to see how these are formed, we use the Fourier integral method to solve the boundary problem posed by the presence of the lower edge of the supersonically moving heated plane sheet, where there is a pressure discontinuity.

The first step is to find the downward-traveling and upward-traveling plane sinusoidal sound waves accompanying a plane wave, having a sharp lower edge, of sinusoidal variations in pressure. The latter travels at the supersonic speed M_c and has a time variation of $\exp(i\omega t)$ in the upper half of the x - z plane. Figure 3 shows the geometry of the three plane waves, whose surfaces of constant phase are parallel to the y -axis (perpendicular to the plane of the paper).

Supersonic pressure wave:

$$p = A \exp i(\omega t - k_0 x), \text{ when } z \geq 0 \\ = 0, \text{ when } z < 0$$

Downward traveling sound wave:

(1)

$$p_d = B \exp i(\omega t - k_0 x + k_z z), z < 0 \\ = 0 \text{ when } z \geq 0$$

Upward traveling sound wave:

$$p_u = C \exp i(\omega t - k_0 x - k_z z), \text{ when } z \geq 0 \\ = 0, \text{ when } z < 0$$

The magnitude of the wave number vector for both sound waves is $k = (k_0^2 + k_z^2)^{1/2} = \omega/c$. Also $k_0 = \omega/M_c$, and so $k_z = (\omega/c) (1 - 1/M^2)^{1/2}$.

The amplitudes B and C of the two sound waves are found from the following boundary conditions at the lower plane boundary $z = 0$: the sound pressure is continuous across the surface, and the perpendicular (z) component of particle velocity is continuous. The result is

$$B = A/2, \quad C = -A/2$$

(2)

The downward-traveling wave B has the same phase as the incident supersonic pressure field A and the upward traveling sound wave C differs in phase by π from A and B .

Each sinusoidal pressure component of the incident plane-sheet heat source (causing the jump increase Δp in pressure) has associated with it a sound wave traveling downward with the same phase and half the pressure amplitude. The sinusoidal components taken all together (the spectrum) make up the Fourier transform of the heat source's transient waveform. The spectrum of the sound wave is exactly the same as that of the heat source, and therefore the temporal waveform of the transient sound wave will be exactly the same as that of the incident heat source, except that its pressure will be one-half as great. Similarly the upward-traveling wave will have its waveform the same as that of the downward-traveling waveform, except that its pressure changes will be opposite in sign; see Eq. (2).

3. Pressure and temperature jumps in the ionosphere

From the observed infrasound at ground level we can make an estimate of the ionospheric heating, based on the foregoing analysis.

We recall first that the sound pressure in a plane wave traveling through the atmosphere varies as \sqrt{P} (P = local atmospheric pressure). Suppose the auroral discharge sheet has its lower edge at a geometric altitude of 110 km. The pressure there is $P = 10^{-7} \times$ (pressure at ground level); (U.S. Standard Atmosphere, 1962). The sound pressure measured at ground level is twice as great as that in the downward traveling wave, due to the almost perfect reflection of infrasound at the earth's surface. This combined with Eq. (2) leads to the net conclusion that the estimated increase in pressure Δp , behind the supersonically moving auroral discharge sheet is $\Delta p \approx 3 \times 10^{-4} \times$ (observed infrasonic pressure).

The pressure increase arises from heating due to the auroral discharge, and so we finally arrive at the following formula for the heating \dot{W} (in watts/m²) caused by the supersonically moving discharge sheet.

$$\dot{W} = (C_V/R) \Delta p M_c = \frac{5}{2} \Delta p M_c$$

(3)

in which the specific heat at constant volume C_v/R of the atmosphere, expressed in units of the gas constant R , is very nearly $5/2$.

Table 1. presents some of the data obtained at the College, Alaska infrasonic station. The data on c_h and the peak sound pressure were measured with the infrasonic system. Values of M_c were measured with an all-sky camera when an auroral arc passed overhead, except for those in parentheses. These latter values were chosen to be the same as c_h in the absence of direct visual observations on the auroral source. All of the tabulated M_c 's are greater than the speed of sound (≈ 350 m/sec) in the atmosphere at the lower edge of the auroral form, assumed to be at an altitude of 110 km. Δp was computed from $3.0 \times 10^{-4} \times$ (peak sound pressure), so as to arrive at the pressure jump at the lower edge of the auroral form. W , the heating per unit area, was computed from Eq. (3).

Table 1.

Estimated heating in supersonic auroral arcs causing infrasound

c_h , m/sec	peak sound pressure, N/m ²	M_c , m/sec	$10^4 \Delta p$, N/m ²	W , watts/m ²
671	0.56	(671)	1.7	0.29
678	0.36	1500	1.1	0.41
460	0.46	(460)	1.4	0.16
582	0.31	(582)	0.9	0.14
560	0.33	1100	1.0	0.28

4. Discussion

The visible auroral arcs are generated by energetic ions which penetrate the atmosphere down to altitudes of about 100 km. But the momentum associated with the ions is probably too small to produce directly the observed infrasound. The ionization of the atmosphere which is produced by the downcoming ions quickly decays. The atmosphere returns to thermodynamic equilibrium, particularly at the lower edge of the ionized region, in a matter of a few seconds. The heat energy which is left is very likely the source of the infrasound and the electrojet accompanying the auroral discharge.

The estimates of the heat energy per unit area tabulated above are lower than the "true" values which would be obtained if full account were taken of the propagation of strong sound waves through a gas. The pressures Δp in Table 1. are about one-hundredth of the local ambient pressure at an altitude of 110 km. Plane sound waves having such relatively strong pressures form shock waves with pressure jumps soon after generation, regardless of the waveform of the heat source. Plane shocks are propagated so that there is a balance between absorption at the pressure jump and regeneration of the jump by nonlinear actions in the mechanics of gaseous propagation. The absorption of sound is so large at an altitude of 110 km for frequencies greater than 1.0 Hz that the equilibrium thickness (at balance) of the sound pressure jump is probably several hundred meters. The net result is that a full analysis of the nonlinear and absorptive processes during propagation of the sound wave downward through the atmosphere would lead to greater estimated values of Δp than those tabulated, and hence to greater values of W .

The graphically recorded waveforms of the infrasonic pressures at any station depend on the indicial admittance of the entire electroacoustical system, from microphones through to the graphic recorders. The indicial admittance is the output recorder's response to a step-function sound pressure. To arrive at the actual sound pressure, the recorded waveform should be convolved (mathematically speaking) with the indicial admittance. In the absence of data on the actual peak sound pressures obtained through the convolution process, the values given in Table 1. were obtained from peak values on the recordings published by Wilson and his associates. The peak values were combined with the recorded waveforms produced when a known sinusoidal pressure was applied to the microphones during calibration. The actual peak sound pressures were probably greater than those tabulated, which would again lead to greater values of W .

5. References

COOK, R. K., January 1969, "Atmospheric Sound Propagation", in Atmospheric Exploration by Remote Probes, Vol. 2, pp. 633-669, published by the Committee on Atmospheric Sciences, National Academy of Sciences, National Research Council, Washington, D. C.

COOK, R. K., A. J. Bedard, Jr., 1971, "On the Measurement of Infrasound", Geophys. J. R. astr. Soc., 26, pp. 5-11

WILSON, C. R., 1971, "Auroral Infrasonic Substorms", in The Radiating Atmosphere, pp. 374-383, D. Reidel Publishing Company, Dordrecht, Holland

"U.S. Standard Atmosphere", 1962, Prepared under sponsorship of National Aeronautics and Space Administration, United States Air Force and United States Weather Bureau, and published by the U. S. Government Printing Office, Washington, D. C.

CHIMONAS, G., H. R. Peltier, 1970, "The Bow Wave Generated by an Auroral Arc in Supersonic Motion", Planet. Space Science 18, pp. 599-612

MONTGOMERY COUNTY

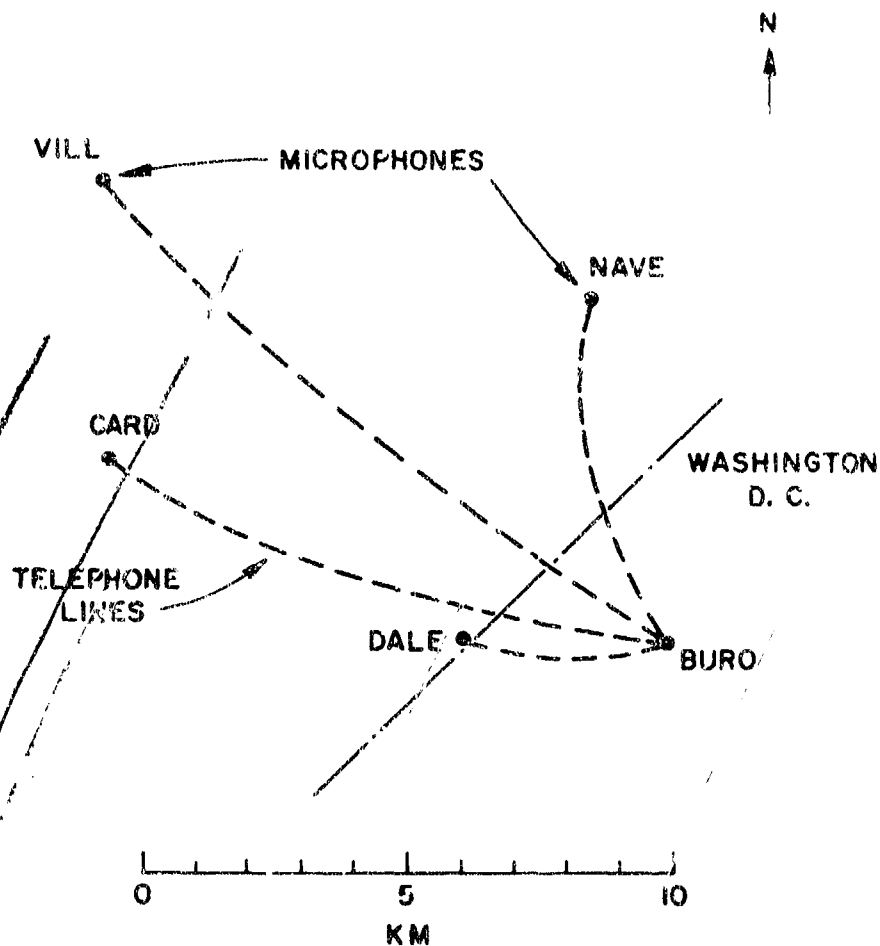


Figure 1. Location of line-microphones, all at ground level, at the infrasonics station in Washington, D. C. Recordings are made at the Buro site.

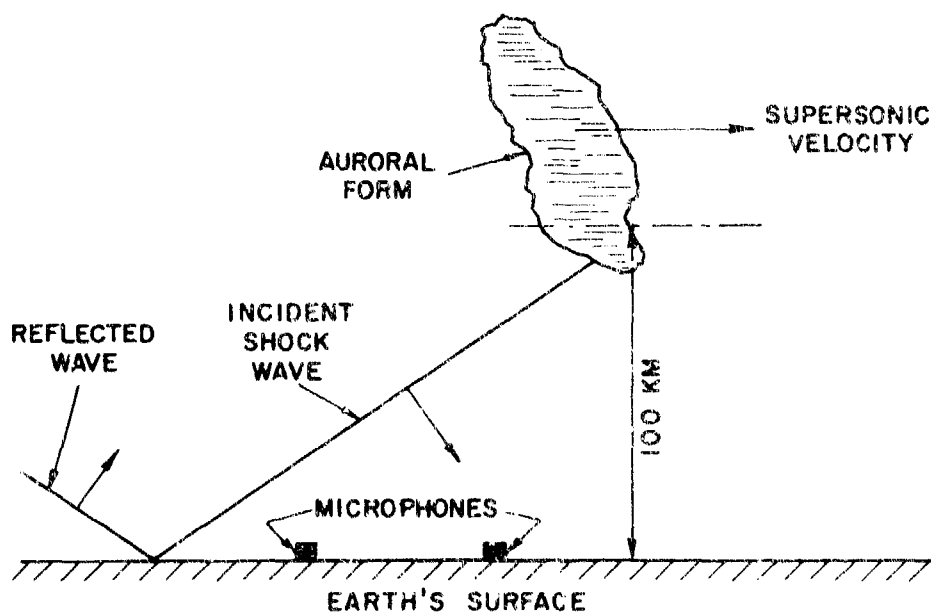


Figure 2. Acoustical shock wave caused by supersonic motion of the leading edge of an auroral form.

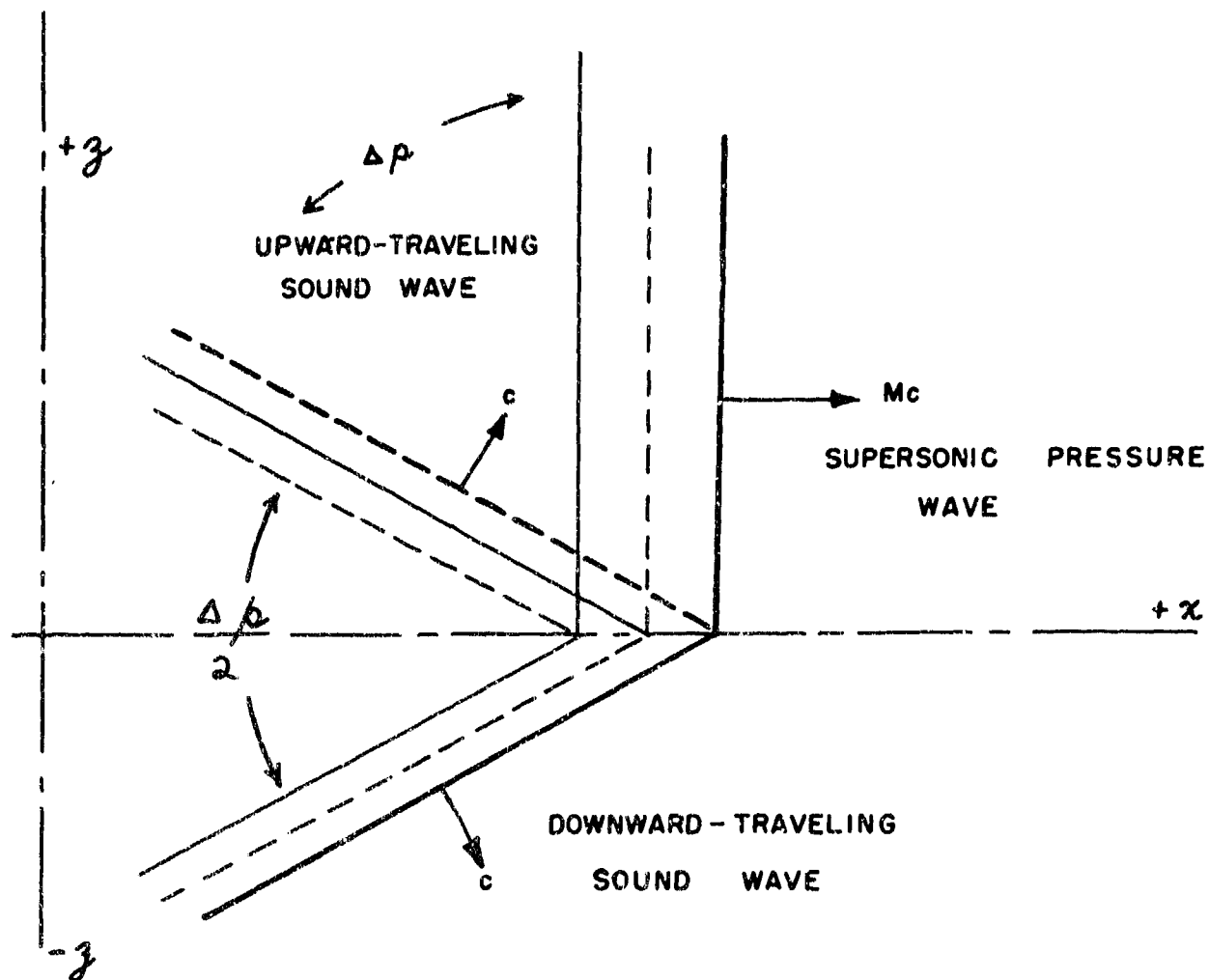


Figure 3. Upward-traveling and downward-traveling sound waves, and supersonic pressure wave, all sinusoidal. The plane waves are all perpendicular to the plane of the paper. Behind a pressure jump moving at supersonic speed, the jump pressure is (1) Δp in the upper wedge-shaped region, and (2) $\Delta p/2$ in the lower wedge-shaped region.

**A MODEL FOR ACOUSTIC-GRAVITY WAVE EXCITATION BY
BUOYANTLY RISING AND OSCILLATING AIR MASSES**

by

Allan D. Pierce

**Department of Mechanical Engineering
Massachusetts Institute of Technology
Cambridge, Massachusetts 02139
USA**

UN MODELE D'EXCITATION D'ONDES ACOUSTIQUES ET DE GRAVITE
PAR FLOTTABILITE DES MASSES D'AIR ASCENDANTES ET OSCILLANTES

par

A. Pierce

SOMMAIRE

Un modèle mathématique assez général est mis au point qui permet d'étudier l'excitation d'ondes acoustiques et de gravité par des masses d'air ascendantes et oscillantes. Les sources sont d'abord décrites par des distributions de quantités de la dynamique des fluides sur une surface fermée mobile. L'analyse montre ensuite que, en ce qui concerne la production d'ondes, ces distributions superficielles sont équivalentes à des sources ponctuelles concentrées, situées au centre du volume. Les équations d'ondes linéarisées et non homogènes, qui en résultent sont obtenues par dérivation et résolues par les fonctions de Green. Le cas d'une atmosphérique isotherme est étudié en détail.

A MODEL FOR ACOUSTIC-GRAVITY WAVE
EXCITATION BY BUOYANTLY RISING
AND OSCILLATING AIR MASSES

Allan D. Pierce
 Department of Mechanical Engineering
 Massachusetts Institute of Technology
 Cambridge, Massachusetts 02139
 U.S.A.

SUMMARY

A somewhat general mathematical model is developed for the study of the excitation of acoustic-gravity waves by rising and oscillating air masses. Sources are initially described by distributions of fluid dynamic quantities over a moving closed surface. Analysis then indicates that insofar as wave generation is concerned, such surface distributions are equivalent to concentrated point sources at the center of the volume. The resulting linearized inhomogeneous wave equations are derived and solved in terms of Green's functions. The case of an isothermal atmosphere is discussed in some detail.

1. INTRODUCTION

The purpose of this paper is to present a general mathematical framework for examination of the possible mechanisms by which buoyantly rising and oscillating air masses may excite acoustic-gravity waves. Such rising air masses may occur naturally via cumulus convection (Scorer, R.S., 1957) or as a byproduct of large man-made explosions (Sutton, O.G., 1947; Taylor, G.I., 1950). The speculation that buoyant rise may excite detectable infrasonic waves has been mentioned frequently in the literature (Pierce, A.D. and Coroniti, S.C., 1966; Jones, W.L., 1970; Tolstoy, I. and Lau, J., 1972; Warren, F.W.G., 1960) and would seem to be the most plausible explanation of the anomalous oscillations at ionosphere level observed during thunderstorm activity (Georgas, T., 1968; Davies, K. and Jones, J.E., 1970; Baker, D.M. and Davies, K., 1969; Detert, D.G., 1969). In addition, basic theoretical considerations (Tolstoy, I. and Lau, J., 1972) suggest that buoyant rise is the source of the early arriving ultra low frequency waves detected at ground level (Tolstoy, I. and Herron, T.J., 1970) following the detonation of low-yield low-altitude nuclear explosions.

The development of a theory regarding the means by which buoyant processes may excite waves is as yet in its early stages. While a considerable literature exists concerning convection and buoyant rise (see, for example, Rohringer, G., 1963; Levine, J., 1959; Lilly, D.K., 1962; Stommel, H., 1947, 1950; Richards, J.H., 1970; Malkus, J.S., 1952; Davies, R.M. and Taylor, G.I., 1950; Scorer, R.S., 1957; Morton, B.R., Taylor, G.I., and Turner, J.S., 1956; Turner, J.S., 1960, 1962a, 1962b, 1963, 1964, 1966; Scorer, R.S. and Ludlam, F.H., 1953; Slawson, P.K. and Casanady, G.T., 1971) the bulk of it does not explicitly consider the possible generation of waves. Considerable work has been done, however, on the excitation of internal waves by a rigid body moving at constant speed through a stratified fluid (Warren, F.W.G., 1960; Lighthill, M.J., 1967; Mowbray, E.D. and Rarity, B.S.H., 1967; MacKinnon, R.F., Mulley, F., and Warren, F.W.G., 1969). Some work has also been done on wave generation by rigid bodies oscillating at constant frequency (Gortler, H., 1943; Mowbray, D.E. and Rarity, B.S.H., 1967; Hurley, D.G., 1969).

The only detailed theoretical analysis of which the present author is aware, apart from numerical simulation experiments (Greene, J.S., Jr. and Whitaker, W.A., 1968), which explicitly considers acoustic-gravity wave generation by buoyant rise is that contained in the recent paper by Tolstoy and Lau (1972). In the cited paper, wave excitation by a rising nuclear fireball was modelled by a point vertical force, the point of application of which was moving vertically at constant speed through a stratified incompressible atmosphere bounded above and below by a rigid surface. The magnitude of the force was estimated from Warren's (1960) prior calculations of the wave resistance force exerted by the fluid on a rigid body moving at constant speed in an incompressible density stratified fluid.

In the present paper, some initial steps are made toward the development of a somewhat general model for study of acoustic-gravity wave excitation. In a wider sense the paper may be regarded as a sequel to a previous paper by the author (Pierce, A.D., 1968) which incorporated the presence of a source into a point source term. Here we show how one might model any, in general moving, source by a set of point source terms whose common location will in general vary with time. Although some discussion of the solution of the resulting equations is given, the application of the general model to specific problems is deferred to later publications.

2. EQUATIONS GOVERNING BUOYANT RISE AND WAVE GENERATION

The general model considered here (see Fig. 1) is that of a compressible atmosphere under the influence of gravity. The earth is taken as flat and the coordinate system is chosen such that the z axis extends vertically upwards from the earth's surface. In the absence of a disturbance the atmosphere is considered to be stratified with no ambient winds. The nature of the disturbance is presumed to be such that at all times it is axially symmetric about the z axis.

One principal assumption which we make is that there is negligible water vapor in the atmosphere. This would seem to be a reasonable idealization for the case of nuclear explosions, but it is likely to be inapplicable for the case of naturally occurring cumulus convection. In any event, one may hope some qualitative insight into the natural convection problem may be afforded by an analysis based on such an idealized model.

2.1. Conservation Laws.

In order to postpone the task of giving a precise definition to what one means by a rising bubble or a rising fireball, we consider first a hypothetical closed surface S which is moving in an arbitrary fashion through the atmosphere; the motion is presumed to be such that S is always a figure of revolution about the z axis. The net mass M , vertical momentum Π , and energy E of the mass within the volume V enclosed by S will in general change with time. One possible contribution, for example, would come from the transport of particles across the surface S . In terms of the total density ρ , pressure p , and fluid velocity \vec{u} within the volume, the total mass, vertical momentum, and energy of the volume may be considered as being defined, respectively, by the equations

$$M = \int_V \rho \, dV \quad (1a)$$

$$\Pi = \int_V \rho u_z \, dV \quad (1b)$$

$$E = \int_V \left[\frac{1}{2} \rho u^2 + p/(\gamma - 1) \right] dV \quad (1c)$$

Note that $p/(\gamma - 1)$ is the internal energy per unit volume of an ideal gas of specific heat ratio γ (1.4 for air). The so-called gravitational potential energy does not enter in Eq. (1c) since we elect here to consider gravity as an external force.

Conservation laws of compressible fluid dynamics (see, for example, Landau, L.D. and Lifshitz, E., 1959, pp 13, 186) may be used to derive expressions for the time rate of change of each of the above quantities, i.e.,

$$\frac{dM}{dt} = - \int_S \rho (\vec{u} - \vec{v}_n) \cdot \vec{n} \, dS \quad (2a)$$

$$\begin{aligned} \frac{d\Pi}{dt} + Mg = & - \int_S \rho u_z (\vec{u} - \vec{v}_n) \cdot \vec{n} \, dS \\ & - \int_S p n_z \, dS \end{aligned} \quad (2b)$$

$$\begin{aligned} \frac{dE}{dt} + g\Pi = & - \int_S \left[\frac{1}{2} \rho u^2 + \frac{p}{\gamma - 1} \right] (\vec{u} - \vec{v}_n) \cdot \vec{n} \, dS \\ & - \int_S p \vec{u} \cdot \vec{n} \, dS \end{aligned} \quad (2c)$$

Here \vec{n} is the unit normal vector pointing out of the surface, while \vec{v}_n is the surface velocity.

2.2. Effective Source Terms.

Outside the volume V , the fluid motion is governed by the aero-hydrodynamic equations, which express conservation of mass, momentum, and energy in terms of partial differential equations. The generic form of each such equation is

$$\frac{\partial \mathcal{E}}{\partial t} + \nabla \cdot \vec{I} = F \quad (3)$$

where \mathcal{E} is the density of some quantity and \vec{I} is the corresponding flux, while F is an external force or work term caused by the presence of gravity. Let V' be some volume (not necessarily the same as the V in Fig. 1) and let \vec{n}' be the unit vector pointing out of that surface S' enclosing V' . For simplicity since the value of F is immaterial in what follows, we treat the case $F = 0$. Then one may readily show from Eq. (3) that

$$\frac{\partial}{\partial t} \int_{V'} \mathcal{E} \, dV' = - \int_{S'} [\vec{I} - \mathcal{E} \vec{v}_n'] \cdot \vec{n}' \, dS \quad (4)$$

where \vec{v}_n' is the velocity of the surface S' .

In what follows, we intend to apply the various equations symbolized by Eq. (3) only to the region outside the volume V sketched in Fig. 1. However, we wish that Eq. (4) may hold for any volume V' which extends slightly into V . One way of doing this is to formally consider \mathcal{E} and \vec{I} to be identically 0 and V but with a source distributed on S such that Eq. (4) will always formally reduce to the expression corresponding to the portion of V' which is outside V (see Fig. 2). This would be the case if an additional term

$$\int_S [\vec{I} - \mathcal{E} \vec{v}_n] \cdot \vec{n} \, dS$$

or, equivalently, if

$$\int [\vec{I} - \epsilon \vec{v}_n] \cdot \vec{n} \delta(\zeta - \zeta_s) dV'$$

were added to the right side of Eq. (4) whenever V' extended partially within V . In the first expression, the prime on the integral sign means that the surface integral extends only over that portion of S which is within V' . In the second expression, the surface integral is transformed into a volume integral by the artifice of a Dirac delta function $\delta(\zeta - \zeta_s)$. Here $\zeta - \zeta_s$ is distance along any line normal to S , such that $\zeta = \zeta_s$ at S . One may note that this latter expression is identically zero whenever V' does not intersect S . Thus, if we are to take ϵ and \vec{I} as formally zero inside V , the governing equation may be put in a form which compensates for this if we add the latter expression to the right hand side of Eq. (4). The resulting equation can equivalently be put into the form

$$\int [\partial \epsilon / \partial t + \nabla \cdot \vec{I}] dV' = \int [\vec{I} - \epsilon \vec{v}_n] \cdot \vec{n} \delta(\zeta - \zeta_s) dV' . \quad (5)$$

Since this should hold for arbitrary volumes V' , the following partial differential equation may be extracted

$$\frac{\partial \epsilon}{\partial t} + \nabla \cdot \vec{I} = (\vec{I} - \epsilon \vec{v}_n) \cdot \vec{n} \delta(\zeta - \zeta_s) + F \quad (6)$$

(Note that we have here added in the term F .) This differs from Eq. (3) by the presence of a "source term" on the right hand side. The source is distributed over the surface of the "excluded" volume V .

The next step is to reduce the above distributed source term to a sum of source terms, each of which is localized at \vec{r}_c , the nominal "center" of volume V . To this purpose, we note that two expressions containing Dirac delta functions are formally equivalent if integrals over the product of each with any good function $f(\vec{r})$ give the same value (see, for example, Lighthill, M.J., 1958). Our starting point is therefore the integral

$$J = \int (\vec{I} - \epsilon \vec{v}_n) \cdot \vec{n} \delta(\zeta - \zeta_s) f(\vec{r}) dV \quad (7a)$$

$$= \int (\vec{I} - \epsilon \vec{v}_n) \cdot \vec{n} f(\vec{r}) dS \quad (7b)$$

where, in the first expression, the volume integral extends over "all space" and, in the second (equivalent) expression, the surface integral is over the surface S surrounding the excluded volume V . In Eq. (7b), we next expand $f(\vec{r})$ about $\vec{r} = \vec{r}_c$, such that

$$f(\vec{r}) = f(\vec{r}_c) + (\vec{r} - \vec{r}_c) \cdot (\nabla f)_{\vec{r}_c} + \dots \quad (8)$$

If this is inserted into Eq. (7b), we find

$$J = J_0 f(\vec{r}_c) + \sum_{i=x,y,z} J_{1i} (\partial f(\vec{r}) / \partial x_i)_{\vec{r}_c} + \dots \quad (9)$$

where

$$J_0 = \int (\vec{I} - \epsilon \vec{v}_n) \cdot \vec{n} dS \quad (10a)$$

$$J_{1i} = \int (\vec{I} - \epsilon \vec{v}_n) \cdot \vec{n} (x_i - x_{ci}) dS \quad (10b)$$

One may note also that one would get Eq. (9) if he set

$$J = \int \{ J_0 \delta(\vec{r} - \vec{r}_c) - \sum_i J_{1i} \frac{\partial}{\partial x_i} \delta(\vec{r} - \vec{r}_c) + \dots \} f(\vec{r}) dV \quad (11)$$

Thus, if we compare (11) with (7a) and recognize that $f(\vec{r})$ is arbitrary, we are at liberty to equate

$$(\vec{I} - \epsilon \vec{v}_n) \cdot \vec{n} \delta(\zeta - \zeta_s) = J_0 \delta(\vec{r} - \vec{r}_c) - \sum_i J_{1i} \frac{\partial}{\partial x_i} \delta(\vec{r} - \vec{r}_c) + \dots \quad (12)$$

Equation (6) would accordingly become

$$\frac{\partial \epsilon}{\partial t} + \nabla \cdot \vec{I} = J_0 \delta(\vec{r} - \vec{r}_c) - \sum_i J_{1i} \frac{\partial}{\partial x_i} \delta(\vec{r} - \vec{r}_c) + \dots + F \quad (13)$$

where J_0, J_{1i} are constants. With the somewhat loose application of familiar terminology, we may refer to the various terms on the right hand side of the above equation as the monopole, dipole, quadrupole, etc. terms.

Just at what point it is permissible to truncate the above source term series is difficult to

a priori state. The influence of the successive terms would appear to decrease, however, in magnitude as R/λ where R is the "radius" of V and λ is a typical wavelength. In the remainder of this paper, we assume that a truncation at the first order (dipole) term is permissible. This does not necessarily exclude the "quadrupole sources" frequently encountered in aerodynamic sound (see, for example, Lighthill, M.J., 1952) since a force dipole is formally equivalent to a mass quadrupole in the neglect of gravity.

On the basis of the preceding analysis, we here write the governing equations of compressible flow for motion outside the volume V . In each case we make appropriate identifications of \mathbf{f} , \mathbf{I} , \mathbf{J}_0 , and \mathbf{J}_{11} . The resulting equations are

$$\frac{\partial \rho}{\partial t} + \nabla \cdot (\rho \mathbf{u}) = S_M \quad (14a)$$

$$\frac{\partial (\rho \mathbf{u})}{\partial t} + \sum_1 \frac{\partial}{\partial x_1} (\rho u u_1) + \nabla p + \rho g \mathbf{e}_z = \mathbf{F}_\pi \quad (14b)$$

$$\frac{\partial}{\partial t} \left[\frac{1}{2} \rho u^2 + \frac{p}{\gamma - 1} \right] + \nabla \cdot \left(\left[\frac{1}{2} \rho u^2 + \frac{\gamma p}{\gamma - 1} \right] \mathbf{u} \right) + \rho g u_z = S_E \quad (14c)$$

where

$$S_M = S_{M0} \delta(\mathbf{r} - \mathbf{r}_c) - S_{M1} \frac{\partial}{\partial x_1} \delta(\mathbf{r} - \mathbf{r}_c) + \dots \quad (15a)$$

$$S_{M0} = \int \psi_M dS \quad (15b)$$

$$S_{M1} = \int (\psi_M)(x_1 - x_{c1}) dS \quad (15c)$$

with analogous definitions for \mathbf{F}_π and S_E . Here

$$\psi_M = \rho (\mathbf{u} - \mathbf{v}_n) \cdot \mathbf{n} \quad (16a)$$

$$\mathbf{F}_\pi = \rho \mathbf{u} (\mathbf{u} - \mathbf{v}_n) \cdot \mathbf{n} + p \mathbf{n} \quad (16b)$$

$$\psi_E = \left[\frac{1}{2} \rho u^2 + \frac{p}{\gamma - 1} \right] (\mathbf{u} - \mathbf{v}_n) \cdot \mathbf{n} + p \mathbf{u} \cdot \mathbf{n} \quad (16c)$$

On comparison with Eqs. (2) one may note that

$$S_{M0} = -dM/dt \quad (17a)$$

$$\mathbf{F}_{\pi 0} = -d\mathbf{E}/dz - M g \mathbf{e}_z \quad (17b)$$

$$S_{E0} = -dE/dt - g \mathbf{E} \cdot \mathbf{e}_z \quad (17c)$$

However, no such analogous simple identification is possible for the coefficients of the dipole source terms.

3. GENERAL SOLUTION OF ACOUSTIC-GRAVITY WAVE EQUATIONS

3.1. Linearized Equations.

In order to derive a general solution of the aero-hydrodynamic equations (14), it is convenient to restrict ourselves to low amplitude disturbances. It is hoped that the resulting solution at distances outside the volume V will not be too different from what might be found were nonlinear terms included at the outset. We let $\rho = \rho_0 + \rho_1$, $\mathbf{u} = \mathbf{u}_1$, $p = p_0 + p_1$, and discard all terms of higher order than the first in the quantities ρ_1 , u_1 , and p_1 . In this manner, we obtain

$$\frac{\partial \rho_1}{\partial t} + \nabla \cdot (\rho_0 \mathbf{u}_1) = S_M \quad (18a)$$

$$\rho_0 \partial \mathbf{u}_1 / \partial t + \nabla p_1 + g \rho_1 \mathbf{e}_z = \mathbf{F}_\pi \quad (18b)$$

$$\partial p_1 / \partial t + \gamma \nabla \cdot (\rho_0 \mathbf{u}_1) + (\gamma - 1) \rho_0 g u_{1z} = (\gamma - 1) S_E \quad (18c)$$

where the zeroth order equations require

$$dp_0/dz = -g\rho_0 \quad (19)$$

Here p_0 and ρ_0 are independent of x , y , and of time t . Note that the three source terms are all formally treated as being of first order.

To simplify the discussion, we also consider the atmosphere to be locally isothermal, i.e., that the sound speed c , where

$$c^2 = \gamma p_0 / \rho_0 \quad (20)$$

is a very slowly varying function of height. This assumption enables us to determine p_1 , ρ_1 , and \vec{u}_1 at intermediate distances from the source (i.e., our moving volume V) as though c were constant. Methods of geometrical acoustics (see, for example, Jones, W.L., 1969; Georges, T.M., 1971) could then be used to trace out the wave disturbance to larger distances.

The isothermal assumption enables us to derive a single partial differential equation for any of the various acoustical quantities (see, for example, Eckart, C., 1960). The appropriate equation for p_1 is

$$\{\mathcal{O}_{AG}\}(p_1/\sqrt{\rho_0}) = S(\vec{r}, t) \quad (21)$$

where $\{\mathcal{O}_{AG}\}$ is the well known acoustic-gravity wave operator

$$\{\mathcal{O}_{AG}\} = \frac{\partial^2}{\partial t^2} \left(\frac{\partial^2}{\partial t^2} + \omega_A^2 \right) - c^2 \left(\frac{\partial^2}{\partial t^2} + \omega_B^2 \right) \nabla_H^2 - c^2 \frac{\partial^2}{\partial t^2} \frac{\partial^2}{\partial z^2} \quad (22)$$

Here ω_A and ω_B are the so-called acoustic cutoff frequency and Brunt-Vaissala frequency, respectively, (Lamb, H., 1910; Brunt, D., 1927; Vaissala, V., 1925; Hines, C.O., 1960) with

$$\omega_A = (\gamma/2)g/c \quad (23a)$$

$$\omega_B = (\gamma - 1)^{1/2} g/c \quad (23b)$$

for the case of an isothermal atmosphere. The aggregate term $S(\vec{r}, t)$ in Eq. (21) is a somewhat complicated functional of S_M , \vec{S}_v , and S_M , i.e.,

$$\begin{aligned} \sqrt{\rho_0} S(\vec{r}, t) = & \left[\frac{\partial^2}{\partial t^2} - g \frac{\partial}{\partial z} \right] \left\{ (\gamma - 1) \left(\frac{\partial S_E}{\partial t} - g \frac{\partial S_{\pi z}}{\partial z} \right) - c^2 \frac{\partial S_M}{\partial t} \right\} \\ & - c^2 \left(\frac{\partial^2}{\partial t^2} + \omega_B^2 \right) \left[\vec{v} \cdot \vec{S}_{\pi} - \frac{\partial S_M}{\partial t} \right] \end{aligned} \quad (24)$$

Note that it is highly singular at $\vec{r} = \vec{r}_c$ and zero elsewhere. Also, one should note that the evaluation of the various time derivatives is complicated by the fact that \vec{r}_c as well as S_{M0} , S_{M1} , etc. [see Eq. (15a)] may all vary with time.

3.2. Green's Function Solution.

For simplicity, we neglect the reflection of waves from the ground and define a free space Green's function $G(\vec{r} - \vec{r}_0, t - t_0)$ for Eq. (21) which satisfies

$$\{\mathcal{O}_{AG}\} G(\vec{r} - \vec{r}_0, t - t_0) = -4\pi \delta(\vec{r} - \vec{r}_0) \delta(t - t_0) \quad (25)$$

which is zero for $t < t_0$ (causality), and which represents waves propagating away (in the sense of energy transport) from a point impulsive source. The form of this Green's function is given (Dikii, L., 1962; Pierce, A.D., 1963; Row, R.V., 1967) by

$$G(\vec{r}, t) = -\frac{1}{2\pi c^2} \int_{-\infty}^{\infty} \frac{\exp\{i[(\frac{\nu}{\mu c})R - \omega t]\} d\omega}{\zeta \mu R} \quad (26)$$

where

$$\nu = (\omega^2 - \omega_A^2)^{1/2} \quad (27a)$$

$$\mu = (\omega^2 - \omega_f^2)^{1/2} \quad (27b)$$

$$\zeta = (\omega^2 - \omega_C^2)^{1/2} \quad (27c)$$

where $\omega_C^2 = \omega_B^2(z^2/R^2)$, and $R = |\vec{r}|$. The phases of the above quantities ν , μ , and ζ are all 0 at large positive ω ; their respective branch lines may all be taken as extending vertically downwards from the appropriate branch points on the real axis. The contour of integration in Eq. (26) proceeds slightly

above the real axis (Fig. 3).

In terms of the Green' function, the solution of Eq. (21) is easily written down as a formal expression

$$\frac{p_1}{\sqrt{\rho_0}} = -\frac{1}{4\pi} \iiint G(\vec{r} - \vec{r}_0, t - t_0) S(\vec{r}_0, t_0) d^3\vec{r}_0 dt_0 \quad (28)$$

Here it is assumed the t_0 integration is from $-\infty$ up to time t_+ , such that we avoid the explicit consideration of any initial values of p_1 and its derivatives.

We may note that $S(\vec{r}, t)$ may be written in the form $\mathcal{O}_S \delta(\vec{r} - \vec{r}_0)$ where \mathcal{O}_S is a linear differential operator whose coefficients are independent of x, y and z , but which may depend on time. If one integrates each term by parts an appropriate number of times, the integrand may effectively be transformed such that

$$G \mathcal{O}_S^o \delta(\vec{r}_0 - \vec{r}_c) + (\mathcal{O}_S^{o+} G) \delta(\vec{r}_0 - \vec{r}_c)$$

where the superscript o implies operation on \vec{r}_0 and t_0 and \mathcal{O}_S^{o+} is the adjoint operator of \mathcal{O}_S^o . The spatial integrations in Eq. (28) may then be performed trivially. One may also achieve some additional simplification since $\partial G / \partial x = -\partial G / \partial x$, etc. In this manner, one derives from Eqs. (15a), (24) and (28) the following expression for p_1

$$\begin{aligned} \frac{p_1}{\sqrt{\rho_0}} = & \left[c^2 \frac{\partial}{\partial z} - (1 - \frac{\gamma}{2})g \right] \frac{\partial}{\partial t} \left[\frac{\partial \phi_{\pi z}}{\partial t} - g \phi_M \right] \\ & + c^2 \left(\frac{\partial^2}{\partial t^2} + \omega_B^2 \right) \vec{\nabla}_H \cdot \vec{\phi}_\pi \\ & - (\gamma - 1) \left[\frac{\partial^2}{\partial t^2} - g \frac{\partial}{\partial z} + \frac{\partial g^2}{2c^2} \right] \frac{\partial \phi_E}{\partial t} \end{aligned} \quad (29)$$

where

$$\begin{aligned} \phi_M = & \frac{1}{4\pi} \int_{-\infty}^t \frac{S_{M0}(t_0)}{\rho_0^{1/2}(z_c[t_0])} G(\vec{r} - \vec{r}_c[t_0], t - t_0) dt_0 \\ & - \frac{1}{4\pi} \sum_i \left(\frac{\partial}{\partial x_i} - \frac{\gamma}{2} \frac{g}{c^2} \delta_{iz} \right) \int_{-\infty}^t \frac{S_{M1}^i G}{\rho_0^{1/2}} dt_0 \end{aligned} \quad (30)$$

with similar expressions for $\vec{\phi}_\pi$ and ϕ_E . Here δ_{iz} is the Kronecker delta. The arguments of the various quantities in the integral over S_{M1} are the same as in the integral over S_{M0} . Also, $\vec{\nabla}_H$ represents the horizontal component of the gradient operator.

Equations analogous to Eq. (29) for other acoustical quantities are readily obtained by a replacement of $p_1/\sqrt{\rho_0}$ by $\sqrt{\rho_0} u_x$, $\sqrt{\rho_0} u_y$, $\sqrt{\rho_0} u_z$, $\rho_1/\sqrt{\rho_0}$, respectively, accompanied by a replacement of G in Eq. (26) by a modified Green's function

$$G \rightarrow \frac{1}{2\pi c^2} \int_{-\infty}^{\infty} \mathcal{L} \frac{\exp(i[\frac{\sqrt{\epsilon}}{\mu} R - \omega t])}{\zeta \mu R} d\omega \quad (31)$$

where the operator \mathcal{L} is taken as

$$\mathcal{L} = \frac{-1}{\omega} \frac{\partial}{\partial x} \quad \text{for } \sqrt{\rho_0} u_x \quad (32a)$$

$$\mathcal{L} = \frac{-1}{\omega} \frac{\partial}{\partial y} \quad \text{for } \sqrt{\rho_0} u_y \quad (32b)$$

$$\mathcal{L} = \frac{-1\omega}{(\omega^2 - \omega_B^2)} \left[\frac{\partial}{\partial z} + \frac{(1 - \gamma/2)g}{c^2} \right] \quad \text{for } \sqrt{\rho_0} u_z \quad (32c)$$

$$\mathcal{L} = \frac{1}{c^2(\omega^2 - \omega_B^2)} \left[\omega^2 - \frac{\gamma}{2} \omega_B^2 - (\gamma - 1)g \frac{\partial}{\partial z} \right] \quad \text{for } \rho_1/\sqrt{\rho_0} \quad (32d)$$

One may note that the equations derived here give one a formal procedure for calculating the acoustic disturbance once the various source terms are specified. While the theory holds, strictly speaking, only if the atmosphere is isothermal, the procedure outlined below should give one a method for handling nonisothermal atmospheres to a good approximation.

Briefly, in the case of the pressure fluctuations, one still retains Eqs. (29) and (30). However, the Green's function is not found from Eq. (26). Instead Eq. (25) is solved for a nonisothermal atmosphere using the guided wave representation (Pierce, A.D. and Posey, J.W., 1970) or the geometrical acoustics approximation (Pierce, A.D., 1966).

REFERENCES

- Brunt, D., 1927. The period of simple vertical oscillations in the atmosphere, *Quart. J. Roy. Meteorol. Soc.* **53**, 30-31.
- Baker, D.M. and Davies, K., 1969. F2-region acoustic waves from severe weather, *J. Atmos. Terrast. Phys.*, **31**, 1345-1352.
- Davies, K. and Jones, J.E., 1971. Ionospheric disturbances in the F2 region originating in severe thunderstorms, *J. Atmos. Sci.*, **28**, 254-262.
- Davies, R.M. and Taylor, G.I., 1950. The mechanics of large bubbles rising through extended liquids and through liquids in tubes, *Proc. Roy. Soc.*, **A200**, 375.
- Detert, D.G., February 1969. A study of the coupling of acoustic energy from the Troposphere to the ionosphere, Avco Corporation Report to Marshall SFC, NASA, on Contract NAS8-21077.
- Dikii, L., 1962. Green's function for weak disturbances in a baroclinic isothermal stratified atmosphere, *Dokl. Acad. Sci. USSR*, **143**(1), 97-100.
- Eckart, C., 1960. *Hydrodynamics of Oceans and Atmospheres*, Pergamon Press, New York.
- Georges, T.M., 1968. HF Doppler studies of traveling ionospheric disturbances, *J. Atmos. Terrast. Phys.*, **30**, 735-746.
- Georges, T.M., August 1971. A program for calculating three-dimensional acoustic-gravity ray paths in the atmosphere, NOAA Technical Report ERL 212-WPL 16, Boulder, Colorado.
- Gottler, H., 1943. *Z. Angew. Math. Mech.* **23**, 65.
- Greene, J.S., Jr. and Whitaker, W.A., 1966. Theoretical calculations of traveling ionospheric disturbances generated by low-altitude nuclear explosions, in *Acoustic-Gravity Waves in the Atmosphere* (T.M. Georges, ed.), 45-64, U.S. Gov. Printing Office.
- Hines, C.O., 1960. Internal atmospheric gravity waves at ionospheric heights, *Can. J. Phys.*, **42**, 1424-1427.
- Hurley, D.G., 1969. The emission of internal waves by vibrating cylinders, *J. Fluid Mech.* **36**, 657-672.
- Jones, W.L., 1969. Ray tracing for internal gravity waves, *J. Geophys. Res.*, **74**, 2028-2033.
- Jones, W.L., 1970. A theory for quasi-periodic oscillations observed in the ionosphere, *J. Atmos. Terrast. Phys.*, **32**, 1505-1566.
- Lamb, H., 1910. On atmospheric oscillations, *Proc. Roy. Soc.*, **A84**, 551-572.
- Landau, L.D. and Lifshitz, E., 1959. *Fluid Mechanics*, Addison-Wesley Publ. Co., Reading, Mass.
- Levine, J., 1959. Spherical vortex theory of bubble-like motion in cumulus clouds, *J. Meteor.*, **16**, 653-662.
- Lighthill, M.J., 1952. On sound generated aerodynamically: I. general theory, *Proc. Roy. Soc.*, **A211**, 564-587.
- Lighthill, M.J., 1958. *Introduction to Fourier Analysis and Generalized Functions*, Cambridge University Press, Cambridge, England.
- Lighthill, M.J., 1967. On waves generalized in dispersive systems by traveling forcing effects, with applications to the dynamics of rotating fluids, *J. Fluid Mech.*, **27**, 725-752.
- Lilly, G.K., 1962. On the numerical simulation of buoyant convection, *Tellus*, **14**, 148-172.
- Mackinnon, R.F., Mulley, F., and Warren, F.W.G., 1969. Some calculations of gravity wave resistance in an inviscid stratified fluid, *J. Fluid. Mech.*, **38**, 61-73.
- Malkus, J.S., 1952. Recent advances in the study of convective clouds and their interaction with the environment, *Tellus*, **4**, 71-87.
- Morton, B.R., Taylor, G.I., and Turner, J.S., 1956. Turbulent gravitational convection from maintained and instantaneous sources, *Proc. Roy. Soc. (London)*, **A234**, 1-23.
- Mowbray, D.E. and Rarity, B.S.H., 1967. The internal wave pattern produced by a sphere moving vertically in a density stratified liquid, *J. Fluid Mech.*, **30**, 489-495.
- Mowbray, D.E. and Rarity, B.S.H., 1967. A theoretical and experimental investigation of internal waves of small amplitude in a density stratified liquid, *J. Fluid Mech.*, **28**, 1-16.
- Pierce, A.D., 1963. Propagation of acoustic-gravity waves from a small source above the ground in an isothermal atmosphere, *J. Acoust. Soc. Amer.*, **35**, 1798-1807.
- Pierce, A.D. and Coroniti, S.C., 1966. A mechanism for the generation of acoustic-gravity waves during thunderstorm formation, *Nature*, **210**, 1209-1210.
- Pierce, A.D., 1966. Geometrical acoustics theory of waves from a point source in a temperature- and wind-stratified atmosphere, Defense Documentation Center Publ. AD-637-874, Clearinghouse for Federal Scientific and Technical Information, Washington.
- Pierce, A.D., 1968. Theoretical source models for the generation of acoustic-gravity waves by nuclear explosions, in *Acoustic-Gravity Waves in the Atmosphere* (T.M. Georges, ed.), 9-24 U.S. Gov. Printing Office.
- Pierce, A.D., and Posey, J.W., April 1970. Theoretical predictions of acoustic-gravity pressure wave-forms generated by large explosions in the atmosphere, Final Report on AFRL Contract F19628-67-C-0217, AFRL-70-1034.
- Richards, J.H., 1970. The effect of wind shear on a puff, *Quart. J. Roy. Meteor. Soc.*, **96**, 702-714.
- Rohringer, G., July 1963. Entrainment and expansion controlled fireball rise, GE TEMPO Report RM 63TMP-25, DASA Report 1409.
- Rohringer, G., July 1963. Properties of ballistic fireball rise, GE TEMPO Report RM 63TMP-26, DASA Report 1410.
- Row, K.V., 1967. Acoustic-gravity waves in the upper atmosphere due to a nuclear detonation and an earthquake, *J. Geophys. Res.*, **72**, 1559-1610.
- Scorer, R.S. and Ludlam, F.H., 1953. Bubble theory of penetrative convection, *Quart. J. Roy. Meteor. Soc.*, **79**, 94-103.

- Scorer, R.S., 1957. Experiments on convection of isolated masses of buoyant fluid, *J. Fluid Mech.*, 2, 583-594.
- Slawson, R.R. and Canady, G.T., 1971. The effect of atmospheric conditions on plume rise, *J. Fluid Mech.*, 47, 32-49.
- Stommel, H., 1947. Entrainment of air in a cumulus cloud, *J. Meteor.*, 4, 91-94 (pt. 1).
- Stommel, H., 1951. Entrainment of air in a cumulus cloud, *J. Meteor.*, 8, 127-129 (pt. 2).
- Sutton, O.G., 1947. The atom bomb trial as an experiment in convection, *Weather*, 2, 105-110.
- Taylor, G.I., 1950. The formation of a blast wave by a very intense explosion, II the atomic explosion of 1945, *Proc. Roy. Soc.*, A201, 175-186.
- Tolstoy, I. and Herron, T.J., 1970. Atmospheric gravity waves from nuclear explosions, *J. Atmos. Sci.*, 27, 55-61.
- Tolstoy, I. and Lau, J., 1972. Generation of long internal gravity waves in waveguides by rising buoyant air masses and other sources., *Geophys. J. Roy. Astron. Soc.*, (to be published).
- Turner, J.S., 1960. A comparison between buoyant vortex rings and vortex pairs, *J. Fluid Mech.*, 7, 419-432.
- Turner, J.S., 1963. The motion of buoyant elements in turbulent surroundings, *J. Fluid Mech.*, 16, 1-16.
- Turner, J.S., 1964. The dynamics of spheroidal masses of buoyant fluid, *J. Fluid Mech.*, 19, 481-490.
- Turner, J.S., 1962. The 'starting plume' in neutral surroundings, *J. Fluid Mech.*, 13, 356-368.
- Turner, J.S., 1966. The constraints imposed on tornado-like vortices by the top and bottom boundary conditions, *J. Fluid Mech.*, 25, 377-400.
- Turner, J.S., 1963. Model experiments relating to thermals with increasing buoyancy, *Quart. J. Roy. Meteor. Soc.*, 89, 62-74.
- Turner, J.S., 1964. The flow into an expanding spherical vortex, *J. Fluid Mech.*, 18, 195-208.
- Turner, J.S., 1963. The motion of buoyant elements in turbulent surroundings, *J. Fluid Mech.*, 16, 1-16.
- Vaisala, V., 1925. On the effect of wind oscillations on the pilot observations, *Soc. Scientific Fennica, Commun. Phys.-Math II*, 19, 1.
- Warren, F.W.G., 1960. Wave resistance to vertical motion in a stratified fluid, *J. Fluid Mech.*, 7, 209-229.

The research reported in this paper was supported by the Air Force Cambridge Research laboratories, Air Force Systems Command, USAF, under Contract F19628-70-C-0008.

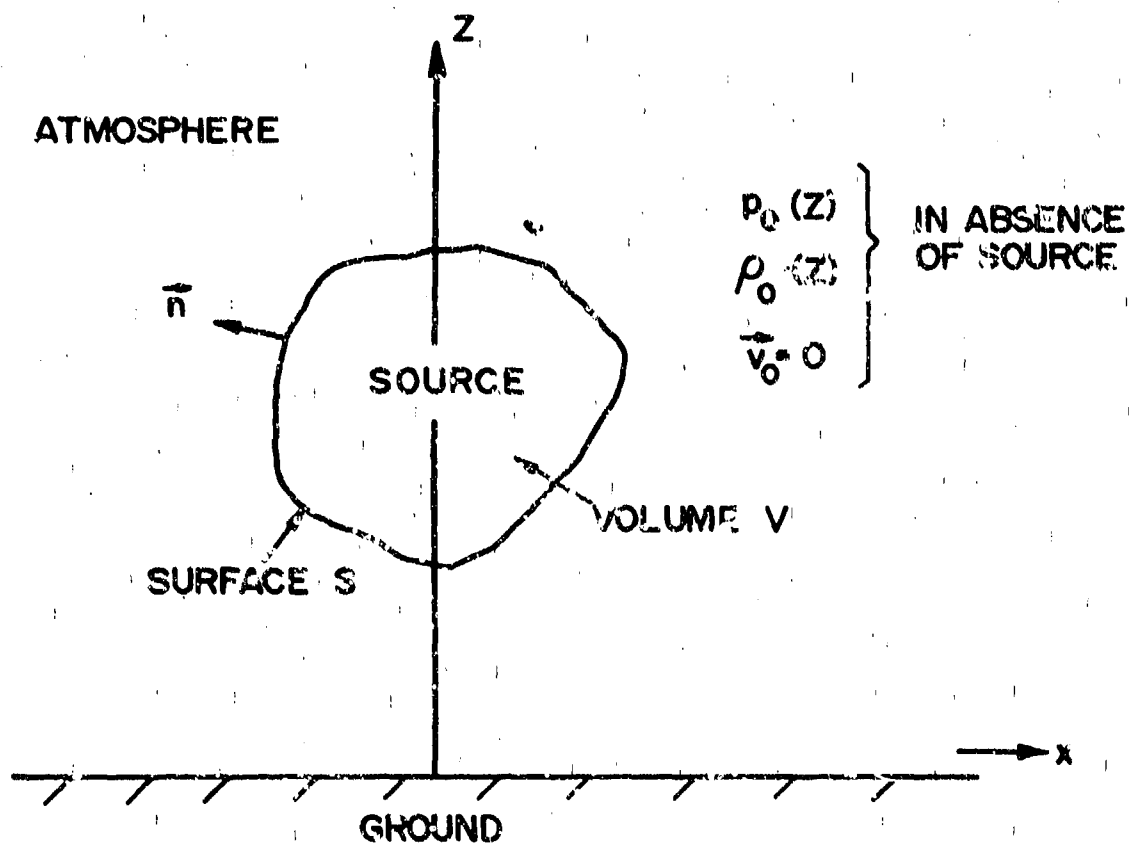


Fig.1 Sketch showing coordinate system and atmosphere model adopted in the present paper.

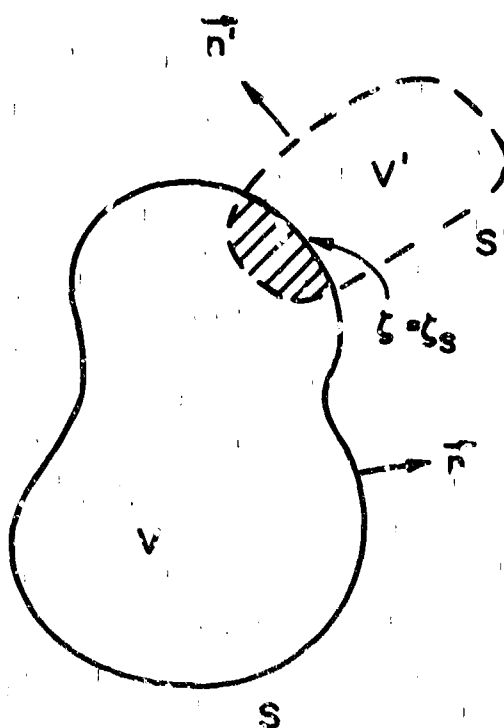


Fig.2 Sketch, illustrating the relative topologies of the two surfaces S (enclosing V) and S' (enclosing V') discussed in the text.

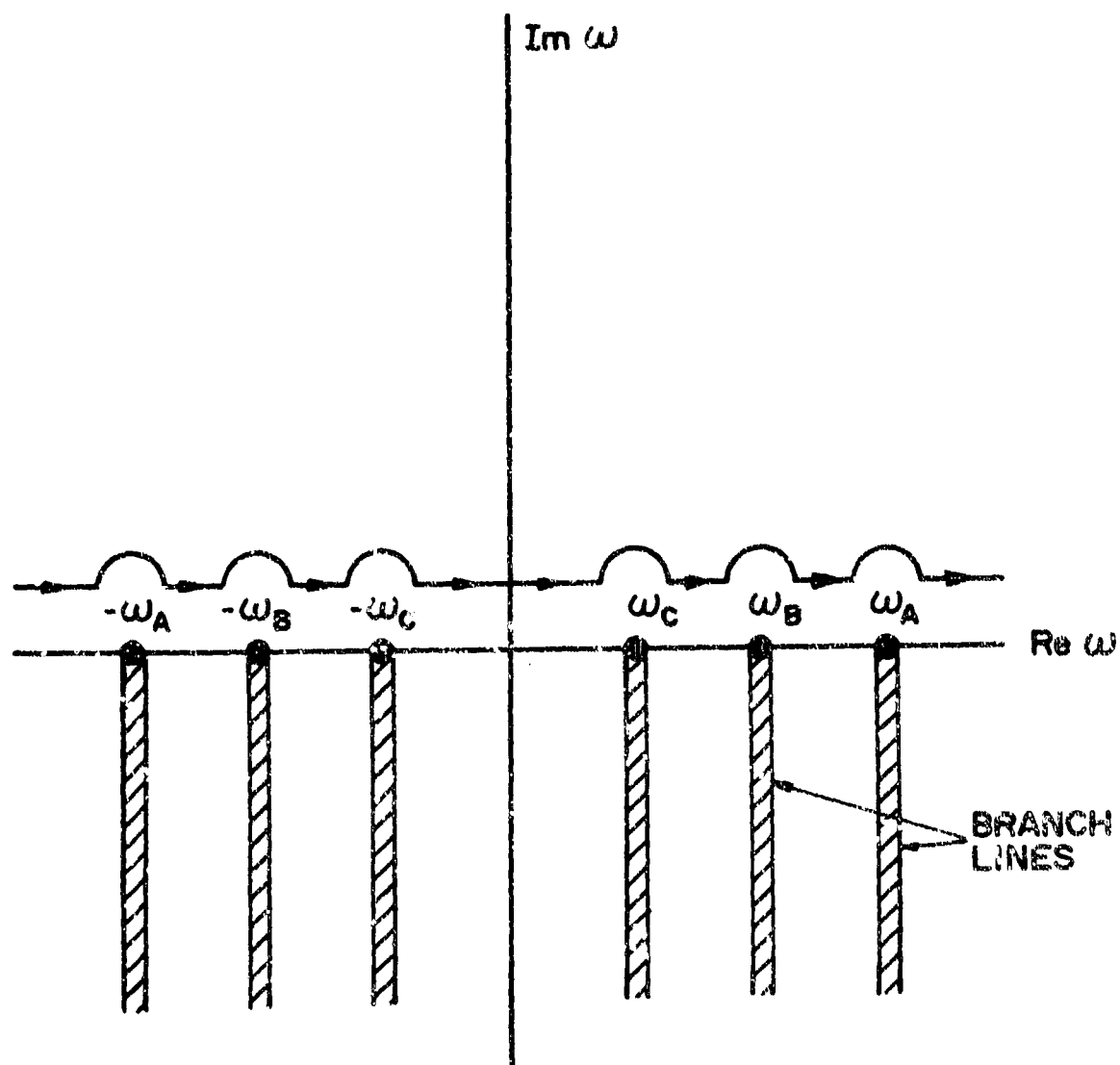


Fig.3 Sketch illustrating branch line locations and integration contour for computation of the free space Green's function.

ACOUSTIC GRAVITY WAVES AND DIFFUSION EFFECTS
AT THE ATMOSPHERIC BOUNDARIES

by

F.W.G. Warren

Imperial College
London
England

ONDES ACOUSTIQUES ET DE GRAVITE ET EFFETS DE DIFFUSION
AUX LIMITES ATMOSPHERIQUES

par

F. Warren

SOMMAIRE

Ce papier discute une hypothèse formulée au cours de précédents travaux (Warren et Arora, 1967 ; Warren et Mackinnon, 1969) relative aux conditions aux limites de la théorie linéaire des ondes acoustiques et de gravité dans l'atmosphère. Il montre que l'on peut négliger presque entièrement les effets de diffusion aux limites, à condition que le nombre d'ondes vertical ne soit pas trop petit. Les résultats obtenus pour les ondes acoustiques et de gravité concordent qualitativement avec ceux obtenus par Yanowitch (1967), mais les détails diffèrent. On obtient une limite supérieure du coefficient de réflexion pour les petits nombres d'ondes verticaux. L'auteur rappelle que ces résultats ne sont valables que si le libre parcours moyen aux altitudes élevées est petit devant la longueur d'onde horizontale.

ACOUSTIC GRAVITY WAVES AND DIFFUSION EFFECTS
AT THE ATMOSPHERIC BOUNDARIES

F.W.G. Warren
IMPERIAL COLLEGE
London
England.

ABSTRACT

This paper discusses an assumption made in some previous work (WARREN & ARORA, 1967; WARREN & MACKINNON, 1969) concerning the boundary conditions in the linear theory of acoustic gravity waves in the atmosphere. It is shown that diffusion effects at the boundaries may for the most part be ignored provided the vertical wavenumber is not too small. The results for gravity waves agree qualitatively with those obtained by Yanowitch (1967) but the details differ. An upper bound for the reflexion coefficient for small vertical wavenumbers is obtained. It is recalled that the results hold only if the mean free path at high altitudes is small compared with the horizontal wavelength.

1. INTRODUCTION

Atmospheric disturbances often excite gravity or acoustic waves which radiate energy from the source. Part of this is carried to very high altitudes while some is propagated virtually horizontally round the globe. Generally, given a local transient excitation the basic problem is to estimate the ultimate resultant mean distribution of energy throughout the depth of the atmosphere and to find the amount propagated to the highest levels. It is the fate of the latter which is a principal concern here. All the energy is finally destroyed by diffusion (perhaps turbulent) processes, of course, but at lower levels this can be protracted and so is ignored for the most part. Thus the source spectrum is supposed concentrated in those wavelengths where the diffusion effects in the lower stratosphere and troposphere are relatively feeble and in addition such that the effects of the earth's rotation (and to some extent curvature) are small. The important properties of the atmosphere which permit radiation of mechanical energy are then its elasticity and density stratification. Wind shear also plays an important rôle but more as a modifier than as a means of energy transfer.

One important aspect of this problem which will be considered in more detail here is the effect of friction and heat conduction at the very highest and lowest levels. It may be suspected that the consequences of the low level boundary layer are not very important, but this is certainly not the case for diffusion effects at great heights, say above about 200 km. Lindzen (1970) and Yanowitch (1967) and others have also considered this problem, and the present object is to make some supplementary comments upon it. For example Yanowitch ignores the effects of compressibility and thermal diffusion. On the other hand Lindzen's computations include these effects but ignore those of vertical accelerations and also of horizontal divergence at high altitudes. In particular this leaves the conclusions concerning the far field behaviour of the perturbations in some doubt. For this and other reasons it seems better to avoid these simplifications even though there is little hope of obtaining explicit closed solutions to the resulting analytical problem. For the present purpose it is sufficient to consider a two-dimensional isothermal atmosphere model and the basic equations for this are presented in the next section.

2. THE GOVERNING EQUATIONS FOR A STATIC ISOTHERMAL MODEL

At the outset a linearisation of the Navier-Stokes equations is made. Although this is a dubious process for certain types of disturbances, observations of relatively shallow waves at high altitudes is sufficient justification for this step. Influences upon the motion due to ion drag and cooling effects are ignored, because the former is relatively weak while the latter may be allowed for at a later stage by a simple modification of the wave number associated with the thermal diffusion coefficient.

The resulting momentum equations then read

$$\rho_0 \partial u / \partial t = -\partial p / \partial x + \lambda \partial / \partial x (\partial u / \partial x + \partial w / \partial z) + \mu (\partial^2 u / \partial x^2 + \partial^2 u / \partial z^2)$$

and

$$\rho_0 \partial w / \partial t = -\partial p / \partial z + \lambda \partial / \partial z (\partial u / \partial x + \partial w / \partial z) + \mu (\partial^2 w / \partial x^2 + \partial^2 w / \partial z^2) - g\rho.$$

u and w are the velocity perturbations and ρ is the density perturbation from the mean ρ_0 , this latter decaying exponentially upwards in the z -direction. This decay is defined by β (a constant) through the relation

$$(d\rho_0(z)/dz)/\rho_0(z) = -\beta = -\gamma g/a^2 = -g/c^2.$$

a and c are the adiabatic and isothermal (Newtonian) sound speeds respectively, and λ and μ are the viscosity coefficients which are assumed to be constant throughout the atmosphere. It is simpler to retain λ here, rather than make the customary substitution $\lambda = \mu/3$. The equation of continuity is $\partial \rho / \partial t + w \partial \rho_0 / \partial z + \rho_0 (\partial u / \partial x + \partial w / \partial z) = 0$, and that of compressibility, including diffusion effects arising from a temperature variation T is

$$\partial p / \partial t + w \partial p_0 / \partial z = a_0^2 (\partial \rho / \partial t + w \partial \rho_0 / \partial z) + K (\partial^2 T / \partial x^2 + \partial^2 T / \partial z^2).$$

p_0 is the mean pressure and K the coefficient appertaining to thermal conduction. This set of equations, augmented by the equation of state, form a determinate system if appropriate boundary conditions are available. As usual a wave-like solution in the horizontal x -direction is imposed for the perturbations:

$$(p, q, u, \rho, T) = (p_1(z), q_1(z), u_1(z), \rho_1(z), T_1(z)) e^{i(kx - \omega t)}$$

where the horizontal wave number k and the frequency ω are real. q is the vertical displacement of an air particle so that $w = \partial q / \partial t$. Dropping the suffix 1 this leads to a set of equations for u, u', q, q', T and T' (the prime denoting differentiation upwards) namely

$$\begin{aligned} i\bar{\omega}^{-1} du'/dz &= (1 + (\bar{\lambda} + \bar{\mu})\omega^{-1}k^2 - k^2\omega^{-2}c^2)u + (k\omega^{-1}c^{-2} - i\bar{\lambda}k)q' - k\omega^{-1}T - \beta k\omega^{-1}c^2q, \\ i\bar{\omega}^{-1} dT'/dz &= (1 + i\bar{\omega}^{-1}k^2)T - (\gamma - 1)c^2k\omega^{-1}u + (\gamma - 1)c^2q', \end{aligned}$$

and

$$(g - i(\bar{\lambda} + \bar{\mu})\omega) dq'/dz = (c^2k\omega^{-1} - i\bar{\lambda}k)u' + T' - \beta T + gq' - (\omega^2 + i\bar{\mu}\omega k^2)q.$$

This system is completed by the supplementary set $dT/dz = T'$, $dq/dz = q'$ and $du/dz = u'$. γ is the ratio of specific heats for air and

$$(\bar{K}, \bar{\lambda}, \bar{\mu}) = (K, \lambda, \mu) e^{\beta z} / \rho_0(0),$$

where $\rho_0(0)$ is the density of air at some standard level (say sea level). It should be recalled that the differential operator d/dz (which will also be represented by D) is augmented when passing through these modified forms of the diffusion coefficients e.g.

$$D(\bar{K}T) = d/dz(\bar{K}T) = \bar{K}(\beta + d/dz)T = \bar{K}(D + \beta)T.$$

So the governing system is of order six (as might be expected) which possesses six linearly independent solutions, say

$$\{u_i, u_i', q_i, q_i', T_i, T_i'\}, \quad i = 1, 2, \dots, 6.$$

The nature of these may be found in several ways but here it is convenient to proceed by a methodical elimination of all the unknowns save the temperature perturbation T . This leads to the temperature equation $\mathcal{L}T = 0$, with $\mathcal{L} = \mathcal{L}_1 - \mathcal{L}_2\mathcal{L}_3$, where

$$\begin{aligned} \mathcal{L}_1 &= \{(D - \beta)(D - 2\beta) - k^2 + \omega^2c^{-2}\}(D(D - \beta) - k^2 + \omega^2c^{-2}) \\ &\quad ((D - \beta) + (\gamma - 1)^{-1}(1 - i\omega^2c^{-2})D(1 - i\bar{K}(D^2 - k^2))), \\ \mathcal{L}_2 &= \gamma\omega^4(\gamma - 1)^{-1}g^{-1}a^{-2}\{((D - \beta)(D - 2\beta) - k^2 + \omega^2c^{-2}) \\ &\quad (1 - g\bar{\omega}^{-2}) - ((D + \beta)(D + 2\beta) - k^2 + \omega^2c^{-2})i\bar{\mu}(D^2 - k^2)\}, \end{aligned}$$

and

$$\begin{aligned} \mathcal{L}_3 &= (1 + i\bar{\lambda}k^2 - i\bar{\mu}(D^2 - k^2))(1 - i\bar{K}(D^2 - k^2)) - a^2k^2\omega^{-2}(1 - i\gamma^{-1}\bar{K}(D^2 - k^2)) \\ &\quad + (\gamma - 1)^{-1}(1 - i\omega^2c^{-2})D(1 - i\bar{K}(D^2 - k^2)). \end{aligned}$$

Once T is found, the other physical variables are given through the relations

$$\begin{aligned} \gamma[a^{-2}(1 + i\bar{\lambda}k^2 - i\bar{\mu}(D^2 - k^2))(1 - i\bar{K}(D^2 - k^2)) - k^2\omega^{-2}(1 - i\bar{K}\gamma^{-1}(D^2 - k^2))]T \\ = (\gamma - 1)[gk^2\omega^{-2} - (1 - i\bar{\mu}(D^2 - k^2)D)]q, \end{aligned}$$

giving q , and the pressure is given by

$$p = \rho_0[gq + (\gamma - 1)^{-1}(\gamma - i\bar{K}(D^2 - k^2))T],$$

while the horizontal velocity perturbation u is given by

$$\omega k^{-1}(Dq + \gamma(\gamma - 1)^{-1}a^{-2}(1 - i\bar{K}(D^2 - k^2))T).$$

Finally density changes are given by

$$\rho = \rho_0[\gamma g a^{-2}q + \gamma(\gamma - 1)a^{-2}(1 - i\bar{K}(D^2 - k^2))T].$$

These equations provide the analytical basis for the discussion. The next section considers the form of the solution at high altitudes.

3. Some properties of the solutions at large heights

An examination of the operator \mathcal{L} in the temperature equation $\mathcal{L}T = 0$ shows that it may be written in the following form:

$$\mathcal{L} = (-ice^{\beta z})^3 A \prod_{i=1}^3 (D - a_i) + (-ice^{\beta z})^2 B \prod_{i=1}^2 (D - b_i) + (-ice^{\beta z}) C \prod_{i=1}^1 (D - c_i) + \prod_{i=1}^4 (D - d_i).$$

The first product occurring here (associated with ϵ^3) equals

$$((D + 3\beta)(D + 2\beta) - k^2 + \omega^2c^{-2})((D + \gamma\beta)^2 - k^2)((D + \beta)^2 - k^2)(D^2 - k^2),$$

while the last product (free from c) equals

$$((D - \beta)(D - 2\beta) - k^2 + \omega^2 c^{-2})(D(D - \beta) - k^2 + \omega^2 a^{-2} + (\gamma - 1)g^2 k^2 \omega^{-2} a^{-2}).$$

δ is a measure (not dimensionless) of the combined effects of the various diffusion processes which occur during the shear and expansion associated with the atmospheric flow:

$$c^3 = \mu(\lambda + \mu)Ka^{-2}\omega^{-1}/(\rho_0(0))^3.$$

At sea level this is an extremely small quantity (unless of course the length scale is minute, which is not the case). The constants A , B and C are given by $A = 1$,

$$B = (\gamma K \mu)^{1/3}(\lambda + \mu)^{-2/3}(a/\gamma \omega)^{4/3},$$

and
$$C = (K/\gamma \mu)^{1/3}(K/(\lambda + \mu))^{1/3}(a/\gamma \omega)^{2/3},$$

while the a_i , b_i , c_i and d_i are known as roots of polynomials whose coefficients are determined from the χ_i , ($i = 1, 2, 3$). Thus they are functions of the frequency, wave number and Prandtl number.

The transformation

$$y = (16\delta)^{-4}(-i\epsilon)^{-3}e^{-3\delta z}, 1/6$$

is now made which throws the T-equation into the form $LT = 0$, where

$$L = A \prod_{i=1}^8 (\theta + 2a_i \beta^{-1}) + B(\delta^4/16)^{1/3} y^2 \prod_{i=1}^8 (\theta + 2b_i \beta^{-1}) + C(\delta/2)^{2/3} y^4 \prod_{i=1}^6 (\theta + 2c_i \beta^{-1}) + y^6 \prod_{i=1}^4 (\theta + 2d_i \beta^{-1}),$$

where θ denotes $y d/dy$. In this form of the equation, high altitudes correspond to small values of $|y|$, and emphasis is given to the fact that here the interaction of the diffusion processes, measured by the quantity

$$\bar{\mu}(\bar{\lambda} + \bar{\mu})\bar{K}\bar{\nu}(\bar{\lambda} + \bar{\mu})\bar{K}e^{3\delta z},$$

is more important than their individual effects which may be measured by

$$\bar{\mu} + (\bar{\lambda} + \bar{\mu})\bar{K}\bar{\nu}(K + \lambda + \mu)e^{8z}.$$

This being the case, solutions at $z = \infty$ may now be found from an examination of the behaviour near $y = 0$. Since the operator L is of the eighth order, there are eight solutions to be found, and six of these have their physical origin in the effects of interaction between the various diffusion processes. All the solutions have a regular singularity at the y -origin and in fact there are eight linearly independent Frobenius-type solutions. These are valid at heights corresponding to $|y| < 1$, that is at heights greater than z_0 , where

$$e^{3\delta z_0} = 16\omega(\rho_0(0))^3/8^4 K(\lambda + \mu)\mu a^2.$$

This is typically about 150 km. Above this level the rarefied atmosphere becomes increasingly viscous. Now the occurrence of eight solutions here shows that two spurious ones have been annexed during the process of forming the temperature equation. (This is unavoidable because of the previously mentioned 'shift-rule' property of D which comes into play during the elimination of u and q from the original sixth order set.) However they are readily exposed by a simple test. Thus the relevant indicial equation has eight roots given by

$$\sigma_i = -2a_i/\beta, \quad i = 1, 2, \dots, 8$$

and two of these may be rejected. These correspond to the factor

$$D^2 + 8\beta\omega = k^2 + \omega^2 c^{-2} + 6\beta^2.$$

Physically they represent isothermal sound waves (multiplied by an exponential function of the altitude) which could be present only in the absence of viscosity.

Of the remaining six solutions, three more may be rejected by consideration of the expressions for the viscous stresses and heat flux at large heights. These contain terms like $\lambda \partial \omega / \partial z$ and $K \partial T / \partial z$, and so if the stresses are to be bounded at high altitudes, as the physical conditions require, then the only admissible solutions are of the form $T_j(z)$, $j = 1, 2, 3$, where

$$T_1(z) = e^{-(k+2\beta)z} \sum_{n=0}^{\infty} T_{1n} e^{-\beta n z},$$

$$T_2(z) = e^{-(k+\beta)z} \sum_{n=0}^{\infty} T_{2n} e^{-\beta n z} + T_{02} \cdot z \cdot T_1(z)$$

and
$$T_3(z) = e^{-kz} \sum_{n=0}^{\infty} T_{3n} e^{-\beta n z} + T_{03} \cdot z^2 \cdot T_1(z).$$

The T_{ij} are coefficients which in principle may be determined recurrently. Corresponding solutions for q are of the form:

$$q_1(z) = e^{-kz} \sum_{n=0}^{\infty} q_{1n} e^{-\beta n z},$$

$$q_2(z) = z e^{-kz} \sum_{n=0}^{\infty} q_{2n} e^{-\beta n z} + q_{02} \cdot q_1(z),$$

$$\text{and } q_3(z) = z^2 e^{-(k+\beta)z} \sum_{n=0}^{\infty} q_{3n} e^{-\beta n z} + q_{03} \cdot q_1(z).$$

So the solutions for the vertical displacement q are characterized by the leading terms e^{-kz} , $z^2 e^{-(k+\beta)z}$ and $z e^{-kz}$. This last term is the dominant one, and coincides with one of Yanowitch's results, although his treatment omits the effect of compressibility and heat conduction. The three rejected solutions are similar to these except that $-k$ is replaced by k , and the requirement that $\lambda \partial w / \partial z$ and $K \partial T / \partial z$ be bounded precludes these. An examination of the behaviour of the corresponding pressure perturbation and other variables follows from expressions given in section 2. These too decay at sufficiently large heights.

So provided the wave amplitude at the incipient viscous level is not so large that linearization is invalid it may be concluded that the motion is negligible when $z e^{-kz}$ is sufficiently small. This altitude increases with wavelength and for very long gravity waves (~ 1000 km) this would be at heights of about 300 km. It is noted that the inclusion of a cooling effect does not substantially alter this result. Agreement with Lindzen (1970) also follows if k is set equal to zero; this is to be expected since for very long waves the horizontal divergence is negligible.

The next task is to consider the lower boundary where z -values are small and $|y|$ is large.

4. Solutions at the lowest levels

Near the earth's surface a boundary layer is to be expected. Local orographic and other features have important consequences but this is another problem and it is only necessary to consider the case of a simple plane horizontal boundary. Corresponding to large values of $|y|$, the solutions to $LT = 0$ are of two basic forms. First, there are four solutions of the Frobenius type in descending powers of y . Included among these are two whose first terms represent inviscid acoustic-gravity wave solutions - one with an upward propagation of energy, the other showing a flux downwards. The remaining Frobenius solutions have leading terms representing quasi-isothermal sound waves. These do not satisfy the original set of equations and so correspond to the two solutions introduced during the derivation of the temperature equation.

The second class of solutions are of the normal type of the form

$$T(y) = e^{\alpha y} y^{s_0} \sum_{s=0}^{\infty} T_{ns} y^{-s}.$$

Generally the series obtained here are asymptotic. There are four of these normal solutions and in terms of z the leading terms contain the dominant factors

$$\exp(\alpha_i e^{-\beta z/2}), \quad i = 1, 2, 3, 4$$

where the $\alpha_i = 2^{1/2} \gamma^{1/3} \omega^{1/2} \mu^{-1/2} \beta^{-1} \bar{\alpha}_i$, $\bar{\alpha}_i$ taking any of the four values which may be assigned to

$$(\pm \sqrt{4\gamma\beta^{-1} - 1 - i})^{1/2}$$

If here β is allowed formally to tend to zero (which is tantamount to neglecting gravity) these dominating factors are proportional to

$$\exp[\bar{\alpha}_i \cdot 2^{-1/2} \gamma^{1/3} \omega^{1/2} \mu^{-1/2} (z_0 - z)]$$

where z_0 is the datum (sea) level. The four normal type solutions therefore show two solutions with extremely rapid growth upwards and two with a fast decay. Comparison with the case in which gravity is absent ($\beta \rightarrow 0$) shows that the decaying solutions are of the boundary layer type in which the thermal and viscous layers are mixed. Now from the previous section there are three solutions available which satisfy the upper boundary condition of finite stress, and so in general there is one linear combination of these having an asymptotic expansion in which the two large growth normal solutions are absent. Moreover from the y -equation it is seen that this combination does not contain ϵ explicitly. In principle, then, the solution is determined uniquely apart from any arbitrary multiplying constant which may be found by comparison with the absolute magnitudes involved.

At low levels, the two Frobenius solutions are of the form

$$y^{\sigma+,-} \sum_{n=0}^{\infty} T_n^{(+,-)} y^{-n},$$

where the indices are given by

$$\sigma_{+,-} = -1 \pm 2(k^2 + \beta^2/4 - \omega^2 a^{-2} + (\gamma - 1)g^2 k^2 \omega^{-2} a^{-2})^{1/2} \beta^{-1}, = -1 \pm 2i\beta^{-1} m(k, \omega) \text{ say,}$$

where m is the vertical wave number. The boundary layer, of thickness $\delta = O(\mu^{1/2} \omega^{-1/2})$, virtually has no effect upon the lower boundary condition attached to the vertical displacement q , ($q_{z=0} \approx q_{z=\delta}$) and so may be ignored. The solution near sea level is then of the form

$$\mathcal{A}_+ y^{\sigma+} + \mathcal{A}_- y^{\sigma-}$$

where the $\mathcal{A}_{+,-}$ are unknown functions of all the parameters (Prandtl number, frequency, wavelength) save ϵ . In this respect the $\mathcal{A}_{+,-}$ are $O(1)$. And when m the vertical wavenumber is imaginary and equal to iM say

(so that the amplitude behaviour in the vertical direction is exponential) this approximate solution is found to be

$$A_{+e}^{1/2-M/\beta} e^{(B/2-M)z} + A_{-e}^{1/2+M/\beta} e^{(B/2+M)z} \\ = e^{1/2-M/\beta} e^{B/2z} (A_{+e}^{-Mz} + A_{-e}^{2M/\beta} e^{Mz}), \quad (M > 0)$$

in terms of the height z . Here, since $e^{2M/\beta}$ is small, the term showing the smaller growth upwards is dominant. This confirms the customary selection made in inviscid theory in the case of imaginary vertical wavenumbers.

When this wavenumber is real the choice is more difficult to substantiate. This is because of the possibility of reflexion mechanisms in the upper stratosphere and higher, arising from the ever increasing effects of diffusion. Here the tenuous gluey region above about 200 km. can act like a floating cushion which responds only to the more ponderous waves, the shorter ones being absorbed by it. In view of the analytical difficulties attached to the temperature equation, this suggests two approximations which can be made. Firstly the absorption effects may be underestimated by the omission of the ϵ and ϵ' terms. The remaining fast growing interaction term, proportional to $\epsilon^3 e^{3\beta z}$ can then be expected to over-emphasise reflexion. On the other hand the terms of smallest influence below the incipient viscous level may be dropped, and the consequent result will under-estimate reverberation because the ϵ -term retained is of smallest upward growth. Apart from some difficulties arising from the presence of the spurious isothermal wave operator, analytical solutions to the resulting approximate problems are readily obtained in terms of Meijer's G-function (Meijer, 1946). Asymptotic forms of G are given by Meijer. Thus crude but useful approximations may be obtained from

$$[ie^3 e^{3\beta z} A \prod_{i=1}^8 (D - a_i) + \prod_{i=1}^4 (D - d_i)] T = 0,$$

$$\text{and} \quad [-ie^3 e^{3\beta z} C \prod_{i=1}^6 (D - c_i) + \prod_{i=1}^4 (D - d_i)] T = 0.$$

Solutions to the first of these equations in Meijer's functions are

$$G_{48}^{mn} \left((-1)^{m+n} i e^{-3} \cdot 3^{-4} \beta^{-4} e^{-3\beta z} \left| \begin{array}{l} -a_i/3\beta \\ -d_i/3\beta \end{array} \right. \right),$$

where m and n are integers, $0 \leq m \leq 8$ and $0 \leq n \leq 4$.

If here the independent variable z is replaced by $\bar{y} = e^{-3\beta z}$, the present meaning of m and n refers to the expansion of G about $\bar{y} = 0$ and $\bar{y} = \infty$ respectively. At the \bar{y} -origin ($z = \infty$) the expansion of G contains a linear combination of m independent Frobenius solutions of the differential equation, while at infinity ($z = 0$) the asymptotic expansion of G contains n linear polynomial solutions which are dominant provided $m + n > 6$. The possible occurrence of isothermal wave solutions which were rejected from the original temperature equation now are to be admitted in the approximate solution, provided that no upward propagating type is present at low levels. This is because the same boundary conditions apply to both the original and approximate equations at these levels and in the approximate solution this allows only incoming isothermal waves. Further, the amplitude of these waves are to be small compared with the inviscid waves at low levels. In the acoustic spectrum it then follows that the appropriate solution is given by $m = 5$ and $n = 3$. This yields a low-level asymptotic

$$e^{1/2} (e^{-\pi m/6\beta} e^{imz} + e^{i\Delta} e^{-\pi m/6\beta} e^{-imz}),$$

where the complex phase shift Δ is known and has positive imaginary part. Multiplication by $e^{i(kx-\omega t)}$ now shows that the reflexion coefficient for an upward travelling acoustic wave is less than $\exp(-\pi m/3\beta)$. For gravity waves a similar argument holds, except that at high altitudes one spurious type solution showing an exponential growth upwards must be avoided. The appropriate solution is then of the form G_{48}^{3n} , which at low levels behaves like

$$e^{1/2} (e^{-\pi n/6\beta} e^{imz} + e^{i\Delta} e^{-\pi n/6\beta} e^{-imz}),$$

where here Δ has zero imaginary part. So the reflexion coefficient for gravity waves is also less than $e^{-\pi n/3\beta}$. (It is recalled that the vertical phase propagation for gravity waves is downwards.)

An exactly similar procedure may be followed through for the second type approximation, and again the spurious isothermal wave operator has to be reconsidered. If the absorption at the intermediate levels (120 km. - 180 km.) is relatively high, this approximation can be expected to yield satisfactory results. Here the reflexion coefficient is found from solutions of the form

$$G_{46}^{mn} \left((-1)^{m+n+1} i e^{-1} \beta^{-2} e^{-\beta z} \left| \begin{array}{l} -c_i/\beta \\ -d_i/\beta \end{array} \right. \right)$$

where the choice of m and n depends upon the number of coefficients c_i which have positive real part i.e. depending on the decay or growth behaviour of the approximate solution at large heights. Detailed results of this second approximation await computation. But the first gives a bound for the reflexion coefficient which is sufficient for the present purpose.

5. Conclusions

The above results confirm that reflexion may be ignored except for waves whose vertical wavelength is very large compared with the scale height β^{-1} . This implies that an inviscid model which has an isothermal upper layer can accurately simulate an atmosphere with a high altitude viscous region. For in both models all waves with a vertical exponential behaviour decay upwards without reflexion while those

whose vertical wavelength is not too large may be regarded as lost to the upper stratosphere if they can penetrate the lower temperature stratification barriers. Among other things this justifies some of the claims made in earlier papers (Warren & Arora, 1967, Warren & MacKinnon, 1969) that an inviscid temperature-stratified model can give a reasonable imitation of the effects of high level diffusion at lower levels by capping the model with an 'isosphere' i.e. by an infinite isothermal layer. Here the untrapped waves radiate freely to infinitely large heights and the resulting energy sink is not too dissimilar from diffusive dissipation.

The viscous isothermal model used here suffers from the defect in that the basic temperature gradient upwards does not vanish in reality. However the effect of this is not important for the acoustic gravity waves under discussion here because the actual temperature gradient is relatively small: most of the energy will be absorbed before the stratification reflexion mechanism can operate - except perhaps for waves with very small vertical wave numbers, $m \ll 8$. On the other hand at extremely high altitudes (say about 250 km) the continuum hypothesis begins to break down. If this is so i.e. if the mean free path is no longer very small compared with the horizontal wavelength, the motion becomes of an increasingly random nature. Viscous reflexion then can no longer be expected for organised flow no longer exists, and the estimated upper bound for the reflexion coefficient becomes misleading. This of course would enhance further the argument for the use of a model with an 'isosphere' for lower level acoustic gravity wave problems. Its position and temperature would depend upon the spectrum of the excitation. Some effects of a change of this position have been investigated numerically by MacKinnon (1970).

References

- LINDZEN, R.S. 1970. Internal gravity waves in Atmospheres with Realistic Dissipation & Temperature. Part I. Geophys. Fluid Dynamics 1, 303-355.
- MACKINNON, R.F. 1969, Can. J. Phys. 47, 707-725. Atmospheric vertical energy flux due to ground disturbance.
- MEIJER, C.S. 1946. On the G-function. Nederl. Akad. Wetensch., 49, 227-237.
- WARREN, F.W.G., & ARORA, M.K., 1967. A problem of vertical distribution of vertical distribution of mechanical wave energy in the atmosphere. Quart. J. Mech. App. Maths. 20, 315-322.
- WARREN, F.W.G., & MACKINNON, R.F., 1969. Some calculations of vertical mechanical wave energy flux in the atmosphere. Quart. J. Mech. App. Math. 22, 363-387.
- YANOWITZ, M., 1967. Effect of viscosity on gravity waves and the upper boundary condition. J. Fluid Mech. 29, 209-231.

AURORAL INFRASONIC WAVE GENERATION MECHANISM

by

Charles R. Wilson

Geophysical Institute
University of Alaska
College, Alaska

65

MECANISME DE PRODUCTION D'ONDES AURORALES INFRASONIQUES

par

Charles R. Wilson

Sommaire

La morphologie des sous-orages d'ondes infrasoniques aurorales (OIA), telle qu'on a pu la déterminer à partir d'observations infrasoniques effectuées à Inuvik ($68,4^{\circ}\text{N}$), College ($64,9^{\circ}\text{N}$) et Palmer ($60,8^{\circ}\text{N}$), le long d'un méridien magnétique passant à travers l'Alaska, révèle qu'on ne voit jamais les OIA se propager en direction du pôle, en dépit du fait que les activités aurorales observées apparaissent fréquemment au sud des stations. On a pu montrer que les OIA sont des ondes infrasoniques d'accompagnement engendrées par des mouvements supersoniques d'arcs d'électrojet auroral dirigés vers l'ouest, l'équateur ou l'est.

Des exemples particuliers d'expansions aurorales en direction du pôle, passant au zénith d'Inuvik, ont été étudiés. On a découvert que des mouvements d'arcs, avec forts électrojets, s'effectuant en direction du pôle, même à des vitesses supersoniques élevées, ne produisent pas d'ondes d'accompagnement infrasoniques. Lorsque s'effectue un renversement de la direction de l'expansion vers le pôle, et que les arcs, par suite, se déplacent en direction de l'équateur, on observe de fortes OIA à partir des arcs. Cette asymétrie dans l'apparition des OIA par rapport à la direction du mouvement d'un arc est interprétée comme une asymétrie intrinsèque du mécanisme de production à l'intérieur des arcs auroraux, et non comme un effet de propagation. On pose en postulat que l'impulsion acoustique de base à l'intérieur des arcs d'électrojet est créée par des collisions avec le gaz neutre des ions positifs entraînés par la dérive électrodynamique qui se produit dans la région E de l'arc auroral. Ainsi, la force de Lorentz est le mécanisme de couplage entre les porteurs du courant d'électrojet et le gaz neutre. Un processus d'ionisation-collision a lieu à l'intérieur des arcs auroraux, pour les arcs qui se déplacent à des vitesses supersoniques dans une direction parallèle à celle de la dérive d'ionisation par les neutres. L'augmentation de densité ionique qui en résulte pour ces arcs réduit la constante de temps pour la dérive des ions, de sorte que le couplage par la force de Lorentz a pour effet de produire une onde de choc infrasonique.

Si la translation supersonique de la nappe primaire aurorale d'électrons présente une composante de mouvement parallèle au courant électrodynamique des ions positifs, une onde de choc aurorale infrasonique se produit dans la région E de l'atmosphère et se propage vers le sol sous forme d'une onde de choc modifiée ou onde d'accompagnement. Si, par contre, le mouvement des arcs auroraux est antiparallèle à la dérive des ions positifs, il ne se produit pas d'OIA.

AURORAL INFRASONIC WAVE GENERATION MECHANISM

Charles R. Wilson
Geophysical Institute
University of Alaska
College, Alaska

SUMMARY

The morphology of auroral infrasonic wave (AIW) substorms, as determined from infrasonic observations at Inuvik (68.4°N), College (64.9°N) and Palmer (60.8°N) along a magnetic meridian through Alaska, shows that AIW are never observed propagating in a poleward direction even though auroral activity frequently occurred south of the stations. AIW have been shown to be infrasonic bow waves generated by supersonic westward, equatorward or eastward motions of auroral electrojet arcs.

Specific examples of auroral poleward expansions which cross the Inuvik zenith have been studied. It was found that even highly supersonic poleward motions of arcs with strong electrojets do not produce infrasonic bow waves. When a reversal in direction of the poleward expansion occurs and the arcs subsequently move equatorward, strong AIW are observed from the arcs. This asymmetry in the occurrence of AIW with respect to direction of motion of an arc is interpreted as an intrinsic asymmetry in the generation mechanism within the auroral arcs and not as a propagation effect. It is postulated that the basic acoustic pulse within the electrojet arcs is caused by collisions with the neutral gas of positive ions that are driven by electrodynamic drift in the E region of the auroral arc. Thus, Lorentz force is the coupling mechanism between the electrojet current carriers and the neutral gas. An ionization-collision process occurs within the auroral arcs for those arcs that are moving supersonically in a direction parallel to the direction of the neutral ionization drift. The resulting increase in ion density for such arcs reduces the time constant for ion-drag so that the Lorentz force coupling is effective in producing an infrasonic shock wave.

If the supersonic translation of the primary auroral electron sheet has a component of motion parallel to the electrodynamic drift of the positive ions, then an auroral infrasonic shock wave will be produced in the E region ionosphere and propagate to the ground as a modified shock or bow wave. If, on the other hand, the auroral arc motion is anti-parallel to the drift of the positive ions, then no AIW will be produced.

1. INTRODUCTION

Ground observations of atmospheric pressure fluctuations in the auroral zone at College, Alaska have been used to show that infrasonic waves are produced by supersonic motions of auroral arcs (Wilson and Nichiparenko, 1967; Wilson 1969a). The pressure disturbance propagates to the ground as a bow or modified shock wave. Constructive interference of the acoustic pulses generated in the E region of auroral arcs cause the formation of the bow wave as the veil of precipitating auroral electrons sweeps across the sky at supersonic speed (Wilson, 1967; Chimonas and Peltier, 1970). For the direct wave in the "front-shock" region (see Wilson, 1969c) the delay time between zenith passage of the auroral arc and reception of the auroral infrasonic wave (AIW) at the ground is six to eight minutes. For an isothermal atmosphere with no winds the horizontal trace velocity V_h of the AIW is equal in speed and direction to that of the auroral arc ($V_h = c \sec \alpha$ where c is the local speed of sound and α is the angle between the wave normal and the horizontal).

A good example of an AIW due to the zenith passage of a supersonic auroral arc at College is given in Figure 1 below the all sky camera (ASC) pictures of the aurora. The pressure versus time traces from the four infrasonic microphones have been superimposed and time shifted to show the coherent wave form of the AIW. The AIW arrived from an azimuth of 48° with $V_h = 460$ m/sec at 0720 U.T. just six minutes after the aurora arrived at the zenith. All times in the paper are in universal time. Because of the complex structure of the auroral forms and the impossibility of identifying a particular "point" on the moving aurora, at best, only an estimate can be given for the auroral speed and direction of motion. The auroral velocity normal to the arc from 0711 to 0715 was 980 m/sec with $\phi = 50^\circ$. Zenith crossing time of the supersonic arc is also shown in Figure 1 by the sudden increase in cosmic noise absorption on the College riometer at ≈ 0715 and by the reversal from minus to plus of Z , the vertical component of the surface magnetic perturbation due to the electrojet within the arc. The actual values for H and Z in Figure 1 at 0700 were -240γ and -90γ respectively due to the presence of the westward flowing auroral electrojet north of College at that time. H and Z were set equal to zero at 0700 in Figure 1, however, to show only the magnetic effect of the supersonic auroral electrojet arc shown in the all-sky photographs.

Morphological studies of AIW of the type shown in Figure 1 have demonstrated the clear association between supersonic motions that develop during the expansive phase of auroral substorms and the generation of AIW (Wilson, 1969a). Further proof of the generation of AIW by auroral electrojet arcs that are moving with supersonic speed in a direction transverse to their long axes have been obtained from a study of the rate of change of the ratio of the vertical to the horizontal component ($\frac{d}{dt} (B_z/B_h)$) of the surface magnetic

perturbation due to the electrojet Hall current along the arc (Wilson, 1969b). The variation in the direction of arrival of AIW with local time has been related to the motion of type "F" (Rathasathay and Berkey, 1965) auroral sudden cosmic noise absorption events as additional evidence connecting supersonic auroral motions taking place within the auroral oval and the generation of AIW (Wilson, 1970).

Statistical results from 139 MHz auroral-radar backscatter measurements made at Homer, Alaska by Stanford Research Institute showed that regions containing radar-aurora that were in supersonic motion

were related in time and general location to source regions of AIW's (Fremouw, 1970).

The one anomaly that arose in the study of the apparent cause-effect relation between supersonic auroral motions and the consequent generation of AIW was that poleward motions of the aurora did not seem, from the observations at College at 64.9°N (corrected geomagnetic latitude) to produce infrasonic bow waves. It was decided to establish a higher latitude infrasonic station at Inuvik N.W.T. in Canada, approximately on the magnetic meridian through College, at 71.1°N to search for AIW from poleward expansions of the auroras that cross the Inuvik zenith from south to north at supersonic speeds during most substorms.

The importance of these poleward expansion - AIW observations lies in the fact that one can discriminate between the three basic mechanisms that have been proposed for producing an acoustic pulse within the moving electrojet by comparison of AIW signal characteristics and the direction of motion of the aurora relative to the direction of the westward electrojet current J .

It is shown that the basic acoustic pulse within the electrojet arcs is caused by collisions with then neutral gas of positive ions that are driven by electrodynamic drift in the E region of the auroral arc. If the supersonic translation of the primary auroral electron sheet has a component of motion parallel to the electrodynamic drift, then an auroral infrasonic shock wave will be produced in the E region ionosphere and propagate to the ground as a modified shock or bow wave.

Statistical AIW Results

The morphology of auroral infrasonic substorms can be visualized most easily with respect to the auroral oval and not the auroral zone. Auroral arcs tend to appear most frequently along the auroral oval in a pattern that is fixed relative to the sun-earth line and eccentric with respect to the dipole pole. The auroral oval coincides with the auroral zone only in the midnight sector (Feldstein and Starkov, 1967). Although the auroral oval expands and contracts with changing geomagnetic conditions, it can be used to relate the AIW to supersonic auroral motions which take place within the auroral oval during a typical substorm (Wilson, 1969a; 1969c).

In Figure 2 the auroral oval is plotted in corrected geomagnetic latitude (ϕ_{CG}) and corrected geomagnetic local time (Whalen, 1970) for the disturbed conditions with the Feldstein parameter $Q = 5$ (Feldstein and Starkov, 1967). The geomagnetic pole (80°N , 81°W geographic) is shown at the center and the direction toward the sun is indicated by the arrow. Three circles of dots represent the locations of Palmer ($\phi_{CG} = 60.8^\circ$), College ($\phi_{CG} = 64.9^\circ$) and Inuvik ($\phi_{CG} = 71.1^\circ$) at each hour of universal time. In this diagram the locations of the three stations are fixed with respect to each other (as shown by the dashed lines at 2 U.T. and 12 U.T.) by a polar azimuthal equidistant projection map. The map and hence the three station locations rotate with changing time about the dipole pole beneath the fixed auroral oval. Midnight occurs along the magnetic meridian through College and Palmer at 1000 U.T. In this diagram the north geographic pole rotates about the center in a circle 10° in diameter. In a projection of this type one can study the variations with local time and geomagnetic latitude of the frequency of occurrence of AIW as a function of azimuth of arrival with respect to the auroral oval.

In Figure 2 the total number of AIW for the data period are plotted for 20° increments of azimuth of arrival ϕ for each hour interval of universal time at the station location for the U.T. hour at the beginning of that time interval. The number of AIW are represented by vectors pointing toward the station in the direction from which the AIW have come. The length of the vectors are proportional to the total number of AIW received at the station over the entire data period within a particular 20° interval of ϕ . The number of AIW scales are given for the vectors in the center of the oval. The scale for College is four times that for Palmer and Inuvik. The data periods and total number of AIW from all directions at all times for each station used in the construction of Figure 2 are as follows: Inuvik 16 Nov. 1969 to 31 Dec. 1970, No. AIW = 236; College 24 Dec. 1965 to 31 Dec. 1970, No. AIW = 1806; Palmer 31 Oct. 1967 to 22 Oct. 1968, No. AIW = 101.

In relating the directions of arrival and number of AIW to the location of a station with respect to the auroral oval it should be remembered that the oval shown in Figure 2 is for $Q = 5$ or disturbed conditions. When $Q = 0$ in calm conditions the oval contracts so that its equatorward boundary is everywhere poleward of 70°N and during very disturbed conditions, $Q = 8$, the oval expands to a 10° width in the midnight sector from 65° to 75° . The oval for $Q = 5$ was chosen for Figure 2 because it represents the oval for the degree of geomagnetic disturbance during which most auroral infrasonic substorms occur.

The general morphology of the auroral infrasonic substorms with reference to diagrams of the type shown in Figure 2 has been discussed in detail in earlier papers (Wilson, 1969a; 1969c; 1970). It was concluded that the AIW at College and Palmer in the evening sector 0300-0600 U.T. are due to bow waves in the "side-shock" region of westward traveling surges that are moving parallel to the oval along its northern boundary. In the midnight sector, 0900-1200 U.T., the AIW at College result from bow waves generated by equatorward motions of auroral arcs when College was in the "side-shock" region for bow waves generated by eastward traveling surges (omega bands). The time sectors from 0600 to 0900 U.T. and from 1200 to 1500 U.T. are transitional with some AIW generated by auroral motions that are parallel to the auroral oval and some by motions transverse (equatorward) to the oval. No AIW are observed in the mid-day sector from 2200 to 0200 U.T. at any of the three infrasonic stations.

At Inuvik the AIW morphology in the evening and morning sectors is similar to that at College. In the morning sector from 1600 to 2000 U.T. there are no AIW from eastward traveling surges at Inuvik when this station is poleward of the path of these surges. The bulge in the oval from 1400 to 1800 U.T. arises from the fact that the eastward traveling surges move at lower latitudes than do the westward surges in the evening sector. From the lack of AIW at Inuvik from the eastward surges, I conclude that "side-shocks" or bow waves are not radiated in the poleward direction by auroral surges. If bow waves were radiated in the poleward direction by "side-shocks" by the eastward surges, then in Figure 2 one would see AIW arriving at Inuvik from, say, 1700 to 2000 U.T. from directions parallel to or slightly to the south of the

oval center line. This is the first asymmetry that one finds in Figure 2 in the radiation of AIW by supersonic auroral motions.

The greatest asymmetry in the generation of AIW by auroral motions can be seen in Figure 2 at Inuvik and College in the time sector from 0800 to 1300 U.T. During the midnight sector auroral substorms develop within the oval with a brightening of the equatorward arcs and a very rapid motion of these arcs in the poleward direction with average speeds of 600 m/sec (Akasofu, et al., 1966a). This expansion of the auroral disturbance also takes place in the equatorward direction (Akasofu, et al., 1966b) but not nearly as dramatically as toward the pole. In Figure 2 one can see that the AIW in the midnight sector at College and Inuvik are moving from north to south or equatorward transverse to the oval. No AIW are ever observed traveling poleward in the direction of the poleward moving supersonic arcs that form the auroral bulge, which is the most conspicuous feature of the expansive phase of the auroral substorm.

During the times when the several thousand AIW plotted in Figure 2 were observed at College and Inuvik there were many hundreds of supersonic poleward expansions of the auroras which would have produced observable AIW if bow waves were generated by poleward motions in the same manner that they are generated by equatorward auroral motions.

A third asymmetry can be noticed in Figure 2. During the mid-day sector no AIW are received from across the polar cap from substorms that are occurring in the midnight sector of the oval. During some substorms the auroral bulge extends up to 80° geomagnetic latitude. If AIW were radiated poleward by the poleward expansions, then the infrasonic waves would cross the polar cap and travel the 3000 km to the Alaskan stations. Because of their high trace velocity, about 500 - 700 m/sec, AIW after reflection from the ground rise to great heights in the thermosphere where much of their energy is absorbed before being refracted back to the surface. However, observations of AIW at Washington, D.C. from the auroral substorm along the auroral oval indicate that AIW do travel at least 1000 km (Chrzanowski, et al., 1961). Thus one would expect that if AIW were radiated poleward by auroral substorms that over an observation period of five years at College, some auroral infrasonic waves would have been detected in the mid-day sector from over the polar cap traveling north to south at College. This has not been the case.

Thus the statistical evidence from several thousand AIW observed at Palmer, College and Inuvik over many years indicates that supersonic motion of an auroral electrojet arc is not, in itself, sufficient to generate AIW. In some manner the direction of motion of the arc, either poleward or equatorward, is also important in determining whether or not AIW are generated by supersonic auroral motions.

Poleward Expansions and Reversals

Examples are given of poleward expansions of auroral substorms in which bright auroral arcs move with supersonic speed across the Inuvik zenith from south to north. The poleward expansions occurred during times of sufficiently low ambient noise level so that AIW could have been detected if they were generated and propagated to the ground from the moving arcs.

All sky camera photographs from a meridian chain of stations are shown in Figure 3 to illustrate a poleward expansion on 8 January 1970. The dipole latitudes of the stations are: College 64.6°, Ft. Yukon 66.6°, Inuvik 70.2°, Sacks Harbor 75.6°. At 1015 the aurora was south of Inuvik and north of Ft. Yukon. A poleward expansion began with a brightening of the arcs at 1020 followed by rapid poleward motion crossing the Inuvik zenith at 1024 and the Sacks Harbor zenith at 1042. The speed of the poleward motion was 1030 m/sec as it crossed the Inuvik zenith. A negative bay in H of -150γ and a plus to minus change in S were recorded on the Inuvik magnetometer indicating that a westward electrojet was flowing in the poleward expanding arcs. The infrasonic records for Inuvik for 8 January 1970 are shown in Figure 4 for the period from 1011 to 1047. The noise level of \pm 1μbar during this time was quite low and yet no AIW was detected in association with the supersonic motion of this poleward expansion. If a bow wave had been radiated by the poleward moving arc, it would have arrived at Inuvik around 1030 from a direction of 200° parallel to the motion of the aurora and to the plane of ΔH , the total horizontal disturbance vector due to the electrojet in the arc.

In Figure 5 another example is given with the ASC chain of a poleward expansion that crosses the Inuvik zenith from $\phi = 210^\circ$ at a speed of 520 m/sec. The poleward expansion begins at 0446, crosses the Inuvik zenith at 0500, and comes well into the field of view of the Sacks Harbor ASC at 0507.

In the lower left hand part of Figure 6 the positions of the poleward moving arc are shown relative to Inuvik at minute intervals from 0457 to 0501. The magnetic perturbation ΔH (total horizontal disturbance vector) at 0459, when the arc is in the Inuvik zenith, and the auroral velocity vector are both shown in Figure 6. In Figure 4 one can see from the infrasonic records that no AIW were received at Inuvik within twenty minutes of the zenith crossing of the supersonic poleward expansion. There is, however, a very large AIW at 0519 coming from a direction $\phi = 51^\circ$ that is opposite to the direction of travel of the poleward expansion at 0500. The signal at 0519 was generated by the equatorward moving arc shown in Figure 5 by the ASC pictures and by the map in the lower part of the figure. This arc is moving at 1090 m/sec from $\phi = 45^\circ$ in a direction parallel to ΔH and to the auroral velocity. The delay time of about seven minutes and the parallelism of the AIW, ΔH and the auroral velocity clearly identify the equatorward moving arc as the source of the 0519 AIW.

There was a negative bay in H associated with the N to S moving arc and a minus to plus change in the Z component at 0512 as the arc crossed the zenith. Thus the electrojet of this arc which produced the 0519 AIW was directed westward. The second AIW shown in Figure 4 at 0532 on 6 December 1969 of inverted phase is probably the reflected wave associated with the direct AIW at 0519 (see Wilson, 1969c).

These examples clearly show that AIW that occur after poleward expansions are not poleward moving low waves from the poleward expansions but that they are equatorward moving AIW due to arcs that have reversed direction and are moving equatorward with supersonic speed after the poleward expansion has passed by.

The SRI auroral-radar studies at Homer, Alaska of radar-aurora motions north of College have shown that the velocities of poleward expansions during the explosive or break-up phase of auroral substorms can be measured using the Range - Time - Intensity records. Fremouw and Chang (1971) have found that even for poleward expansions with speeds as great as 2000 m/sec no AIW are radiated in the poleward direction. However, a few of the events studied with the 139 MHz radar suggested that the radar may have detected auroral-backscattering plasma moving supersonically with the source of AIW in an equatorward direction.

AIW Generation Mechanism

Before presenting a proposed generation mechanism for AIW, a summary of AIW characteristics will first be given. These following characteristics refer to an infrasonic signal from an auroral arc that has passed over the observing station. The AIW to be described is thus a direct wave (Wilson, 1969a) in the "front shock" region (Wilson, 1969c). The AIW has not been modified by propagation effects in the sound channels or by the finite collision rate of the thermosphere, or has not suffered phase inversion by reflection at the earth's surface, nor has it been split into multiple signals by multi-path propagation effects.

- 1) A single infrasonic wave packet (with a pressure vs. time profile characteristic of a shock pulse) arrives at the surface traveling in a direction parallel to the motion of the overhead supersonic auroral source with a delay time of six to eight minutes after zenith passage of the arc.
- 2) The average trace velocity of AIW is 510 m/sec giving an angle α between the wave normal and the horizontal of about 50° .
- 3) The average period (duration of the first pulse) of AIW is about 20 sec, giving a scale size, $L = TV_A$, of about 1.2 km for the source if the auroral velocity V_A is mach two.
- 4) The phase of the pressure pulse can be either positive or negative for AIW that are due to southward moving supersonic auroral arcs that contain a westward electrojet.
- 5) Supersonic auroral arcs that cause AIW have only westward electrojets which are line currents flowing along the auroral arcs.
- 6) AIW are only produced by supersonic westward and eastward propagating surges or by equatorward moving supersonic westward electrojet arcs. The source motions are thus westward in the evening, southward around midnight or eastward in the morning.
- 7) No AIW have ever been observed at Palmer, College or Inuvik from poleward moving supersonic westward electrojet auroral arcs. No AIW at these stations have ever been observed propagating south-to-north from any kind of auroral source.

A great deal of observational evidence has shown that, within the 0.5 dyne/cm^2 limit of detectability above the wind noise level, no AIW of the type described above are ever observed in association with any auroral phenomenon (when the source is within the field of view of the all sky camera) other than supersonic motion of large scale auroral forms. Thus pulsations in auroral luminosity, "flaming aurora", rapid motion of rays along an arc, or the sudden appearance of an auroral form do not produce detectable infrasound. They may however add to the general background infrasonic noise level observed during an AIW substorm. Nor do the magnetic fluctuations associated with auroral substorms, such as Pc-1 micro-pulsations, sudden impulses, sudden commencements or giant pulsations, produce detectable infrasound. The electrojet magnetic perturbation associated with arcs can be related to AIW only because of the lateral supersonic motion of the electrojets. Thus there is no detectable infrasound radiated by the "turning on and off" of a stationary electrojet arc. However, traveling ionospheric disturbances are thought to be generated by such a mechanism (Blumen and Hendl, 1969; Chimonas and Hines, 1970).

The mechanism that has the required intrinsic asymmetry with respect to direction of motion is a combination of Lorentz Force coupling (as proposed by Chimonas and Peltier (1970) and called electrodynamic drift by Martyn (1953)), and an ionization-collection process suggested by Piddington (1963, 1964) to explain the source of sporadic E ionization and ionospheric winds and waves. This generation mechanism, as explained below, is consistent with the observed AIW morphology.

In the polar ionosphere the neutral auroral ionization drifts under the influence of horizontal electric fields and the vertical geomagnetic field. In Figure 7 the electron velocity \vec{V}_e , the ion velocity \vec{V}_i and the neutral ionization velocity \vec{V}_n are shown relative to the horizontal electric field \vec{E} and the vertical magnetic field \vec{B} directed into the diagram. The three velocities are given below (Kato, 1965; Martyn, 1953).

$$\vec{V}_{e,1} = \frac{e}{m_e} \frac{\vec{E} \times \vec{B}}{B^2} - \frac{H_{e,1}}{B} \frac{\vec{B} \times \vec{E}}{B} \quad (1)$$

$$\vec{V}_n = \frac{\vec{J} \times \vec{B}}{n_e (m_e \vec{v}_e + m_i \vec{v}_i)} \quad (2)$$

$$\text{where } \vec{J} = \sigma_1 \vec{E}_1 + \sigma_2 \frac{\vec{B} \times \vec{E}}{B} + \sigma_0 \vec{E}_n \quad (3)$$

The angles in Figure 14 are given by

$$\tan \alpha_{e,1} = \omega_{e,1} / \omega_{e,1} \quad (4)$$

$$\phi_n = \frac{\pi}{2} - \alpha_n + \alpha_i \quad (5)$$

In equation (1) the Pedersen mobility $P_{e,i}$ and the Hall mobility $H_{e,i}$ are given by:

$$P_{e,i} = \frac{1}{B(\omega_{e,i}^2 + \nu_{e,i}^2)} \quad \begin{matrix} + \text{ for ions} \\ - \text{ for electrons} \end{matrix} \quad (6)$$

$$H_{e,i} = \frac{\omega_{e,i}}{B(\omega_{e,i}^2 + \nu_{e,i}^2)} \quad (7)$$

The electrons and positive ions have the same component of velocity \vec{V} in a direction perpendicular to the current vector \vec{J} and, by collisions, they exert a body force, the Lorentz Force, on the neutral gas (Martyn, 1953). The component of this neutral ionization that drifts in the direction of $\vec{E} \times \vec{B}$ is called the Hall drift, while the component in the direction of \vec{E} is called the Pedersen drift. Piddington (1963) has suggested that the southward Pedersen drift will exert a frictional force on the neutral atoms so that "a wall of neutral gas at levels ~ 100 km upward will be built up and pushed south with speeds as high as a few hundred meters per second." It is shown below that when the E region neutral gas velocity (driven by collisions with the positive ions executing electrodynamic drift) becomes as large as the supersonic velocity of translation of an auroral electrojet and is in the same direction, then a shock wave is formed which propagates to the ground as an AIW bow wave.

The problem can be treated from the point of view of ion drift or ion current with the same result. Physically the ions and electrons are moving under the influence of crossed electric and magnetic fields. However, only the ions are massive enough to transfer significant momentum to the neutral atoms. Whether one describes the ion motions as an electrodynamic drift or as a Pedersen or Hall current resulting in a Lorentz Force, we are still dealing with the same physical process, namely collisions between moving positive ions and neutral atoms.

The description of the generation mechanism in terms of electrodynamic drift rather than in terms of the resulting Lorentz Force is useful in that it relates the process to the electric fields in the auroral arcs which have been measured (Kallay, et al., 1971; Wescott, et al., 1969). The current \vec{J} in the Lorentz Force description of the coupling has not been measured directly but has only been calculated from an assumed electrojet configuration. Thus knowing the relationship between the AIW and electric fields in the arcs one can more readily compare the AIW morphology as observed to that predicted from the model and the known morphology of the ionospheric electric fields at time of substorms.

In the shock wave model for the formation of an AIW, Wilson (1967) suggested that is a pressure pulse that was of constant phase in the frame of reference of the moving auroral arc were generated by an unspecified mechanism, then by superposition of wave fronts a bow wave would be built up and would move with the aurora at the mach angle. In the first three sections of this paper we have seen that the basic process which generates the pressure pulse in the moving aurora is asymmetric with respect to north-south motion.

If electrodynamic drift of the neutral ionization is taken as the basic process in the aurora that transfers momentum to the neutral gas by collisions, then the north-south asymmetry can be explained by referring to Figure 8. Cross-sections are given in Figure 8 of the E region ionosphere translation in an equatorward direction (Case I) and in a poleward direction (Case II). The precipitation region of the primary auroral particles is moving with a horizontal velocity \vec{V}_A that is greater than the local speed of sound.

The vertical slabs of ΔX_1 and ΔX_2 of neutral E region ionization are at rest at $t = 0$. It is assumed that the neutral ionization drift velocity, \vec{V}_n , the Pedersen current and the Hall current are all zero at $t = 0$. A southward horizontal electric field \vec{E} exists in the region of the arc as shown in Figure 8 directed toward the left.

As the high conductivity region of the auroral arc (that is created by the primary auroral particles) sweeps through the E region ionosphere, the currents in the slabs of ΔX_1 , ΔX_2 of initially stationary ionosphere increase with time as:

$$\vec{J} = (\sigma_n \vec{E} + \sigma_1 \vec{E} \times \vec{B} / B) (1 - e^{-t/\tau}) \quad (8)$$

where σ_n and σ_1 are the "direct" and "transverse" conductivities respectively and τ is the collision interval between current carriers and neutrals (Ferraro and Plumpton, 1966). The current is given by:

$$\vec{J} = n_e e (\vec{V}_1 - \vec{V}_e) \quad (9)$$

so the neutral ionization velocity \vec{V}_n also increases with time as $(1 - e^{-t/\tau})$.

It is further assumed that the velocity reached by the neutral ionization \vec{V}_n at a time $T = L/V_A$ (where L is the width of the auroral arc), at the trailing edge of the arc, i.e., at $X = L$, is greater than the arc speed \vec{V}_A . Thus $\vec{V}_n > \vec{V}_A$ at $X = L$ or $T = L/V_A$. This is shown in the graph of \vec{V}_n vs. X at the bottom of Figure 8, Case I. Thus the neutral ionization drift velocity \vec{V}_n increases from zero to \vec{V}_n as the electrojet arc sweeps through any stationary slab ΔX of the E region ionosphere. For $t > T$ \vec{V}_n returns to zero. The exact shape of the curve $\vec{V}_n(t)$ in Figure 8 is not important for the model. It is only necessary that \vec{V}_n increase monotonically from $t = 0$ to T and then return to zero.

In Figure 8 for Case I where \vec{V}_A is parallel to \vec{V}_n the velocity of the neutral ionization \vec{V}_{n1} has

reached the velocity \vec{V}_1 in slab ΔX_1 has reached the velocity $\vec{V}_{n1} = \vec{V}_A$ after the arc has gone a distance X_1 past the slab. At this time ($t = X_1/V_A$) the neutral ionization in slab ΔX_1 begins to travel with the auroral arc at the speed \vec{V}_A of the arc. Now at X_2 the neutral ionization velocity in slab ΔX_2 is greater than \vec{V}_A and thus greater than \vec{V}_1 . Therefore the neutral ionization in slab ΔX_2 at X_2 tend to over-take the ionization in ΔX_1 at X_1 . Thus all the neutral ionization for $L > X > X_1$ moves toward the slab ΔX_1 to form a wall of neutral auroral ionization that moves with the auroral speed \vec{V}_A in a manner first predicted by Piddington (1963). This buildup of a wall of auroral ionization only occurs when \vec{V}_A is moving in a direction that has a positive component which is parallel to the electrodynamic drift velocity \vec{V}_n .

Referring again to Figure 8, consider Case II when \vec{V}_A is antiparallel to \vec{V}_n . This corresponds to a poleward expansion of a westward electrojet arc where \vec{E} is directed southward. The neutral ionization drift velocity \vec{V}_{n1} in slab ΔX_1 at a distance X_1 from the leading edge of the arc has a velocity $\vec{V}_{n1} = -\vec{V}_A$ and thus tends to leave the region of the supersonic arc with a relative speed of $2\vec{V}_A$. Now the neutral ionization at X_2 in slab ΔX_2 has a drift velocity $\vec{V}_{n2} > \vec{V}_{n1} = -\vec{V}_A$. Thus the neutral auroral ionization in slab ΔX_2 tends to move away from that in slab ΔX_1 with a relative speed $\vec{V}_{n2} - \vec{V}_{n1}$. Thus in Case II where \vec{V}_A is antiparallel to \vec{V}_n the neutral auroral ionization tends to be decreased in density within the arc instead of forming a wall of increasing ionization density that travels with the arc as in Case I where \vec{V}_A and \vec{V}_n are parallel.

In Case II all the ionization within the arc of thickness L is collected at the rear ($X = L$) of the arc whereas in Case I all the ionization within the path of the arc that may be $100L$ is swept up.

Barium release measurements in the ionosphere (Wescott, et al., 1970) show that \vec{V}_A is not always determined by the direction of the local electric field through $\vec{E} \times \vec{B}$ drifts. Magnetospheric convection is closely related to the auroral substorm convection in the E-W and W-E directions (Wescott et al., 1970), and thus \vec{V}_A is coupled to \vec{E} by $\vec{E} \times \vec{B}$ or Hall drifts. However, the electric field measurements by Ba cloud drifts show that ... "the poleward motion of an auroral arc does not imply any direct connection with the electric field or outward plasma drift in the magnetosphere." (Wescott et al., 1970). The Ba release measurements show that the \vec{E} field direction is southward for westward electrojets and northward for eastward electrojets. The electrojets are thus Hall currents. The total horizontal magnetic perturbation ΔH due to the Hall current electrojets will thus be in the direction of \vec{E} , the local electric field in the lower ionosphere.

Thus one can infer the direction of \vec{E} from the direction of ΔH for an auroral electrojet arc because Ba release measurements have shown that the electrojets are Hall currents in a direction $\vec{E} \times \vec{B}$. The examples given of poleward expansions show that the auroral activity \vec{V}_A is decoupled from the electric field \vec{E} for northward moving supersonic arcs; while the AIW example given in Figure 1 shows that \vec{V}_A and \vec{E} are decoupled for this equatorward moving supersonic arc. Kelley et al. (1971) using balloon-measured electric field data and all-sky auroral pictures have shown that, "the poleward surge characteristic of the auroral explosive phase is not associated with a large eastward electric field and therefore is not associated with an $\vec{E} \times \vec{B}/B^2$ drift of the auroral primaries." Therefore Cases I and II illustrated in Figure 8 do actually occur, i.e., \vec{V}_A can be parallel or antiparallel to \vec{E} because the primary auroral electron stream of precipitating particles is decoupled from $\vec{E} \times \vec{B}$ in the lower ionosphere.

When \vec{V}_A is parallel to \vec{V}_n a wall of neutral auroral ionization is built up that sweeps along with the supersonic arc. The positive ions in this wall of neutral ionization transfer momentum to the neutral gas by collisions. The frictional force between the positive ions and the neutral gas depends on the difference in the two velocities in such a way that neutral gas velocity \vec{U} changes with time as (Dougherty, 1961; Rees, 1971):

$$\frac{\partial \vec{U}}{\partial t} = \frac{n_1 m_1}{n_1 m_1 + n_n m_n} (\vec{V}_1 - \vec{U}) \quad (10)$$

Thus the neutral gas velocity would tend to \vec{V}_1 with a difference decreasing with time as $\exp(-t/\tau_n)$, where τ_n is a time scale for neutrals to reach an equilibrium velocity under the influence of ion-drag, and given by

$$\tau_n = \frac{n_n m_n}{n_1 m_1 v_1} = \frac{n_n}{n_1 v_1}$$

(Dougherty, 1961). Thus as the wall of neutral auroral ionization sweeps along the arc at a speed \vec{V}_A , collisions with the neutral gas produces a pressure pulse that, neglecting viscous terms, travels with the arc to produce the shock wave as described by Wilson (1967).

The effectiveness of the mechanism described above is illustrated in Figure 8 lies in the fact that there is a great increase in the number density n_1 of positive ions within the wall of auroral ionization traveling with the auroral arc. In addition to the increase in ionization density due to the traveling arc sweeping-up the auroral ionization as described in Figure 8, Piddington (1963) and Martyn (1953) have shown that ion drifts from higher to lower latitudes have a vertically downward drift which further increases the density of the wall of ionization built up in a supersonic auroral arc moving parallel to \vec{V}_n . An ion drift from lower to higher latitudes has a vertically upward drift which tends to decrease the E^n region auroral ionization.

If the auroral velocity \vec{V}_A is less than the speed of sound, then the build-up of a wall of neutral ionization will still take place as long as $\vec{V}_{nT} > \vec{V}_A$, however the arc moving at subsonic speed will not produce an infrasonic shock wave.

It is possible to make an estimate of the ion number density in the "wall" of neutral ionization in a supersonic auroral arc that produces an AIW. This is done by: first, calculating the neutral gas velocity perturbation u in a slab of gas dx at height z in the electrojet arc that will result in a pressure pulse $p(z)$ which when traveling with the arc at the auroral speed \vec{V}_A will produce the AIW observed at

the ground as a perturbation $p(0)$. Next the magnitude of the ion-drag time constant τ_n that is necessary in order to produce the neutral gas velocity perturbation u in the slab dx is calculated for an interaction-time $T = L/V_A$ during which the slab of neutral gas in dx is accelerated by ion-drag. This calculation of τ_n is done by use of the solution for eqs. (10) namely

$$\frac{V_1 - U}{V_1} = e^{-T/\tau_n} \quad (11)$$

when τ_n is known the number density of ions n_1 can be found from $\tau_n = n/n_1 v_1$.

Neglecting the enhancement of the AIW pressure pulse that results from superposition associated with the supersonic motion of the source and its associated bow-wave effect, the pressure perturbation $p(z)$ at a height z can be approximated by assuming a plane wave. In this case there is an exponential decrease in the pressure perturbation with height given by $p(z) = p(0) e^{-z/2H}$ where H is the scale height of the atmosphere and $p(0)$ is the observed surface perturbation. For plane waves the relation between pressure perturbation and particle velocity is given by $u = p/\rho_0 c$ where ρ_0 and c are the ambient gas density and speed of sound respectively. For an AIW of 5 dynes/cm² amplitude at the ground, values of ρ_0 and c as shown in Table I, and for a scale height H of 8 km the values of u for three different heights of the sources are as follows: $z = 100$ km $u = 675$ cm/sec; $z = 120$ km $u = 2380$ cm/sec; $z = 140$ km $u = 4380$ cm/sec.

From the model of the ionization-collection process described in Figure 8 we see that the ion velocity in the wall of neutral ionization is equal to V_A . Setting V_A in equation (11) equal to the auroral speed V_A and using the above values of u for U the ion-drag time constant τ_n and ion density n_1 can now be calculated for various widths L of the auroral arc.

The expression for the ion density can be written as:

$$n_1 = -\frac{n}{v_1} \frac{V_A}{L} \ln \left\{ 1 - \frac{p(0)}{\rho_0 c} \frac{e^{-z/2H}}{V_A} \right\} \quad (12)$$

In Table I the values of τ_n and n_1 are given for the case in which $V_A = c$ as the lower limit of auroral speed that will result in AIW production. The width of the arc L varies from 0.5 to 10 km in Table I. The values of n_1 , v_1 , c and ρ_0 used in the evaluation of n_1 from equation (12) are also shown in Table I as a function of Z .

From Table I it can be seen that the more narrow the arc width L the shorter τ_n may be in order to accelerate the neutral gas to the velocity required to produce the observed 5 dyne/cm² pressure wave at the ground. To decrease the ion-drag time constant the ion density must increase in the arc.

The values of n_1 in Table I range from 1.4×10^6 ions/cm³ for $L = 10$ km and $Z = 100$ km to 1.8×10^8 ions/cm³ for $L = 0.5$ km and $Z = 140$ km. The rapid decrease in collision frequency v_1 with increasing height results in the increase in the required n_1 with increasing height of the source for the same AIW strength signal to be observed at the ground.

The average characteristics of AIW can be used to identify the height region and average width L of the arc that are most reasonable in order to choose the most probable range of n_1 from Table I. For the simple shock wave model the auroral AIW source speed is equal to the trace velocity of the AIW observed at the ground. The average AIW trace velocity is about 510 m/sec. If the rise-time of the AIW pressure pulse observed at the ground is approximately the same as the rise-time at the source of the neutral gas velocity increase from c to u , then the interaction time $T = L/V_A$ can be set equal to the AIW rise-time. An average value of the AIW rise-time observed at College would be from 5 to 30 seconds. Thus L would vary from 2.5 to 15 km for $V_A = 510$ m/sec. The average delay time for AIW following zenith passage of a supersonic auroral arc indicates that the height of the source is between 100-120 km.

Thus a reasonable range in the n_1 from Table I would be from 10^6 to 2×10^7 ions/cm³ for supersonic auroral arc sources of AIW. These above values of ion density refer to the density in the wall of ionization moving with the arc due to the ionization-collection process and not to the basic auroral ionization due to ionization from the primary auroral particles. Recombination processes will of course limit the ion density that can be reached in the ionization-collection process.

If the auroral ionization at the 120 km level has an ambient level of $\sim 2 \times 10^5$ ions/cm³ (Francis and Karplus, 1960) and the ionization-collection process is taken to be say 50% efficient, then for a westward electrojet arc 1 km in width moving southward for say 200 km the increase in the neutral ionization density will be hundred fold to 2×10^7 particles/cm³. Unless there is an increase in the ion density within moving auroral arcs to the values indicated in Table I for $Z = 100$ to 120 km then the time scale τ_n for transferring momentum to the neutral gas by ion-drag will be too long to produce the observed infrasonic bow waves in the 10 to 100 sec period pass band.

Multiple frequency observations at 49.7, 143.5 and 226 MHz of auroral backscatter (Flood, 1965) indicate the electron densities as high as 2×10^8 electrons per cubic cm are present in the auroral E region at least part of the time and densities in excess of 2×10^7 are fairly common.

Recent observations at Chatanika, Alaska (near Fairbanks) by the Stanford Research Institute Thomson scatter radar have provided direct measurements of electron density in auroral electrojet arcs. On 9 September 1971 at 0912 U.T. electron densities of 10^6 electrons/cm³ were measured in an auroral arc in the E region by the Thomson scatter radar facility (SRI, private communication).

The north-south asymmetry in the production of AIW by supersonic auroral forms is intrinsic in the electrodynamic drift-shock wave model described above. Thus V_A must have a positive component in the direction of V_n . The mechanism will be most effective when V_A and V_n are parallel. When V_A and V_n are

antiparallel, no wall of ionization will be built up within the moving aurora and thus no large pressure pulse will travel along with the arc so bow waves can not be produced.

The magnitude and direction of \vec{V} from eqs. (2) and (5) depend on the electron and ion gyro-magnetic and collision frequencies ω_i and ν_n which undergo variations with height. The strength and direction of the current flow in the electrojet, for a given southward electric field, varies with the Pedersen conductivity σ_1 , the Hall conductivity σ_2 and the parallel conductivity σ_0 . These conductivities also vary with height in the ionosphere.

For a given model of the ionosphere parameters, n , ω_i and ν_n (Francis and Karplus, 1960), the variation with height of the directions and magnitudes of the current density \vec{J} and the neutral ionization electrodynamic drift velocity \vec{V} are given in Figure 9 looking down on the ionosphere. The electrodynamic drift \vec{V} consists of Pedersen drift (parallel to \vec{E}) around 110 km, changing in direction with increasing height to the full Hall drift around 180 km in the $\vec{E} \times \vec{B}$ direction as shown in Figure 9. The Pedersen drift attains a maximum value of $V = 0.5 E/B$ at 130 km while the Hall drift above 180 km has a constant value of $V = E/B$ (Piddington, 1963). In a study of ionospheric winds due to ion-drag in the auroral zone using rocket-borne chemical releases, Rees (1971) has found that during times of southward directed electric fields when ΔH is negative (see Rees, 1971, Figure 1) that the neutral wind is toward the southeast around 100 km (corresponding to Pedersen drag) and toward the east above 120 km (corresponding to Hall drag). This rotation in the direction of the neutral wind from south to east with an increase in height is a direct effect of the rotation of the direction of the neutral ionization drift \vec{V}_n with height as shown in Figure 9.

Above 90 km $\alpha = 90^\circ$ so \vec{V} in Figure 9 gives the direction $\phi = \pi/2 - \alpha + \alpha$ (see Figure 7) of the positive ion drift. In order for the electrodynamic drift-shock wave model to be effective, \vec{V} should be more or less parallel to \vec{V}_n . In addition to this the ion density as indicated by the calculated values in Table I must be obtainable by the ionization-collection process as limited by recombination effects. Thus at heights above 140 km the ion density as calculated for AIW production by equation (12) in Table I are too large to be obtained because of the recombination limitation. Thus in Figure 9 even though the magnitude of \vec{V} is largest at 200 km the necessary ion density n for ion-drag to be effective at these heights in the interaction-time that is available is much too large to be tenable. Thus the electrodynamic drift will not produce a pressure pulse within a supersonic arc at the greater heights. The optimum level is probably around 100-130 km for large \vec{V} and for the most effective coupling of the neutral ionization drift with the neutral gas to produce AIW in a supersonic auroral arc.

An assumption in the model was that $\vec{V}_{nT} > \vec{V}_A$. In units of E/B the maximum value of the Pedersen drift is $0.5 E/B$ (Martyn, 1953; Piddington, 1963). For an auroral speed of $V_A = 600$ m/sec and for $B = 0.543$ gauss at 100 km above College, the electric field would have to be 65 mV/m to make $\vec{V}_n = \vec{V}_A$. Barium vapor measurements of electric fields in the vicinity of auroral forms by Wescott et al., (1969) have shown that electric fields from 10 to 130 mV/m directed southward often occur. Thus it is quite reasonable to assume that $\vec{V}_n > \vec{V}_A$ in some auroral arcs translating at mach 2. From the barium release measurements by Wescott et al., (1970), the velocity of the auroral zone ionosphere has often been found to be supersonic with respect to the neutral ionosphere.

It is necessary at this point to relate the known morphology of AIW to the electrodynamic drift-shock wave model by discussing the orientation of \vec{V} as shown in Figure 9 as a function of local time along the auroral oval. Because of the increase with height of τ , the time scale for effective ion-drag, the maximum electrodynamic drift coupling will occur when the aurora is moving from a direction about $30^\circ - 40^\circ$ east of the electric field corresponding to the direction of \vec{V}_n for 120 to 130 km height. Extensive measurements of electric fields by barium vapor releases (Wescott et al., 1969; Foppl et al., 1968; Rees, 1971) show that the electrojets are Hall currents and that the electric fields are perpendicular to the electrojet Hall currents, poleward for evening conditions (ΔH positive) for the eastward electrojet and equatorward for morning conditions (ΔH negative) of a westward electrojet.

Mozar and Manka (1971) have shown using balloon-borne electric field measurements from $L = 4$ to 23 that an equatorward component of electric field that develops at the onset of a negative bay drives Hall currents that are responsible for the surface magnetic perturbation ascribed to the auroral electrojet.

For westward electrojet conditions where \vec{E} is southward, auroral motions that are toward the south-east will produce the largest AIW. The electrodynamic drift coupling with supersonic motion will vary as $\cos \theta$ where θ is the angle between \vec{V} and \vec{V}_A . Because \vec{V} in Figure 9 makes an angle of about 30° with \vec{E} , which is southward, the most effective directions for AIW to be radiated by translating westward electrojets will be from $\phi = 270^\circ$ to $\phi = 30^\circ$ inclusive for $\theta \leq 60^\circ$. By referring to Figure 2 or to the AIW morphology described by Wilson (1969a) for College, one can see that there are many AIW in the midnight and morning sectors from $\phi = 270^\circ$ to $\phi = 30^\circ$. The maximum frequency of occurrence of AIW after local midnight agrees with the fact that southward and eastward motions of the westward electrojet that prevail at this time are close to parallel to \vec{V}_n as shown in Figure 9. Thus the maximum coupling of \vec{V} with \vec{V}_A in the morning sector produces the large number of AIW seen in Figure 2 from directions that are predominantly west of north.

For eastward electrojets the \vec{V}_n diagram in Figure 9 must be rotated 180° until \vec{E} points up or northward. The Hall current will be eastward and the Pedersen drift poleward. If there were supersonic poleward motions of eastward electrojet arcs, then AIW would be expected from these arcs. However, no poleward AIW are observed in the evening sector or at any other time. Westward propagating surges are known to be strong sources of AIW (Wilson, 1969c). For the model to be effective, \vec{V}_n and \vec{V}_A must have an angle between them less than, say 60° . Westward propagating surges carry the region of negative bay westward with them. They represent the westward end of the westward electrojet region. In the transition region between eastward electrojets with poleward electric fields and westward electrojets with equatorward electric fields, the electric field must rotate from north to south. The strong AIW produced by westward propagating surges suggests that \vec{E} rotates counterclockwise (looking down on the ionosphere) so that \vec{E} is directed to the west at the head of the surge. Thus if \vec{E} is westward then \vec{V}_n max. will be directed from $\phi = 40^\circ$ so that

for \vec{V}_A moving westward and parallel to the auroral oval efficient coupling between \vec{V}_A and \vec{V}_n will take place and produce large AIW. There is a very large maximum in the number of AIW from $\phi = 40^\circ$ due to westward propagating surges at College shown in Figure 3 of Wilson (1969c) corresponding to the case where \vec{E} is probably westward.

A large body of evidence from balloon-borne electric field measurements (Moser and Manka, 1971; Kelley et al., 1971; Moser, 1971) shows that the morphology of the ionospheric electric field during substorms can be described as follows: 1) the east-west component of the ionospheric electric field becomes large and westward about an hour before the explosive phase of the substorm and remains westward throughout the substorm; 2) the north-south component of the ionospheric electric field becomes large and southward at the onset of the explosive phase of the substorm and remains so throughout the substorm. Moser (1971) has stated that in a total of 19 balloon measurements made during substorms the east-west component of electric field was westward at break-up in every case. Thus the AIW generated by westward propagating surges at break-up during the explosive surge of substorms are consistent with the needs of the model and the measured electric fields.

The lack of AIW from the south corresponds to the fact that when \vec{V}_A has a northward component during times of eastward electrojets there are no supersonic poleward motions of these arcs, and when there are poleward motions of westward electrojets the direction of \vec{V}_A is to the southeast. Supersonic auroral arc motions are associated basically with westward electrojets, thus one would expect, given the above model, that most AIW would be observed in the morning sector when \vec{V}_A is parallel to \vec{V}_n for a southward electric field, as is the case.

In summary, it is an observed fact that an infrasonic bow wave is produced if the primary auroral particle stream sweeps laterally through the neutral gas at supersonic speed in an equatorward direction. The period of the AIW is observed to be related to the width L and speed V_A of the arc by $T = L/V_A$. Because of the asymmetry in the generation of AIW by equatorward or poleward moving arcs, we know that the basic source of the traveling pressure pulse is not a mass or heat source. The source is thus a momentum source that is electromagnetic in origin and therefore it can only be collisions of positive ions with the neutral gas or ion-drag that transfers momentum to the neutral gas to produce an infrasonic wave. Thus: (1) Lorentz force coupling transfers momentum from the electrojet positive ions to the neutral gas. (2) An ionization-collection process increases the ion density in arcs that are translating parallel to \vec{V}_A to a level around 5×10^7 ions/cm³ where Lorentz force coupling can become effective. (3) The supersonic motion of the source region determines the bow wave geometry of the auroral infrasonic waves themselves.

Table I

Ion density and ion-drag time constant for various values of height Z and auroral arc width L

$Z=100$			$Z=120$			$Z=140$		
n_i #/cm ³	1.1×10^{13}		6.2×10^{11}			1.45×10^{11}		
v_n 1/sec	5.37×10^3		3.12×10^2			7.44×10^4		
c_i cm/sec	2.9×10^4		3.7×10^4			5.37×10^4		
ρ gm/cm ³	4.97×10^{-10}		2.44×10^{-11}			3.39×10^{-12}		
L (km)	τ_n (sec)	n_i #/cm ³	τ_n (sec)	n_i #/cm ³		τ_n (sec)	n_i #/cm ³	
0.5	74	2.8×10^7	20	9.7×10^7		11	1.8×10^8	
1	148	1.4×10^7	41	4.9×10^7		22	9×10^7	
2	296	6.9×10^6	82	2.4×10^6		44	4.5×10^7	
10	1482	1.4×10^6	409	4.8×10^6		217	9×10^6	

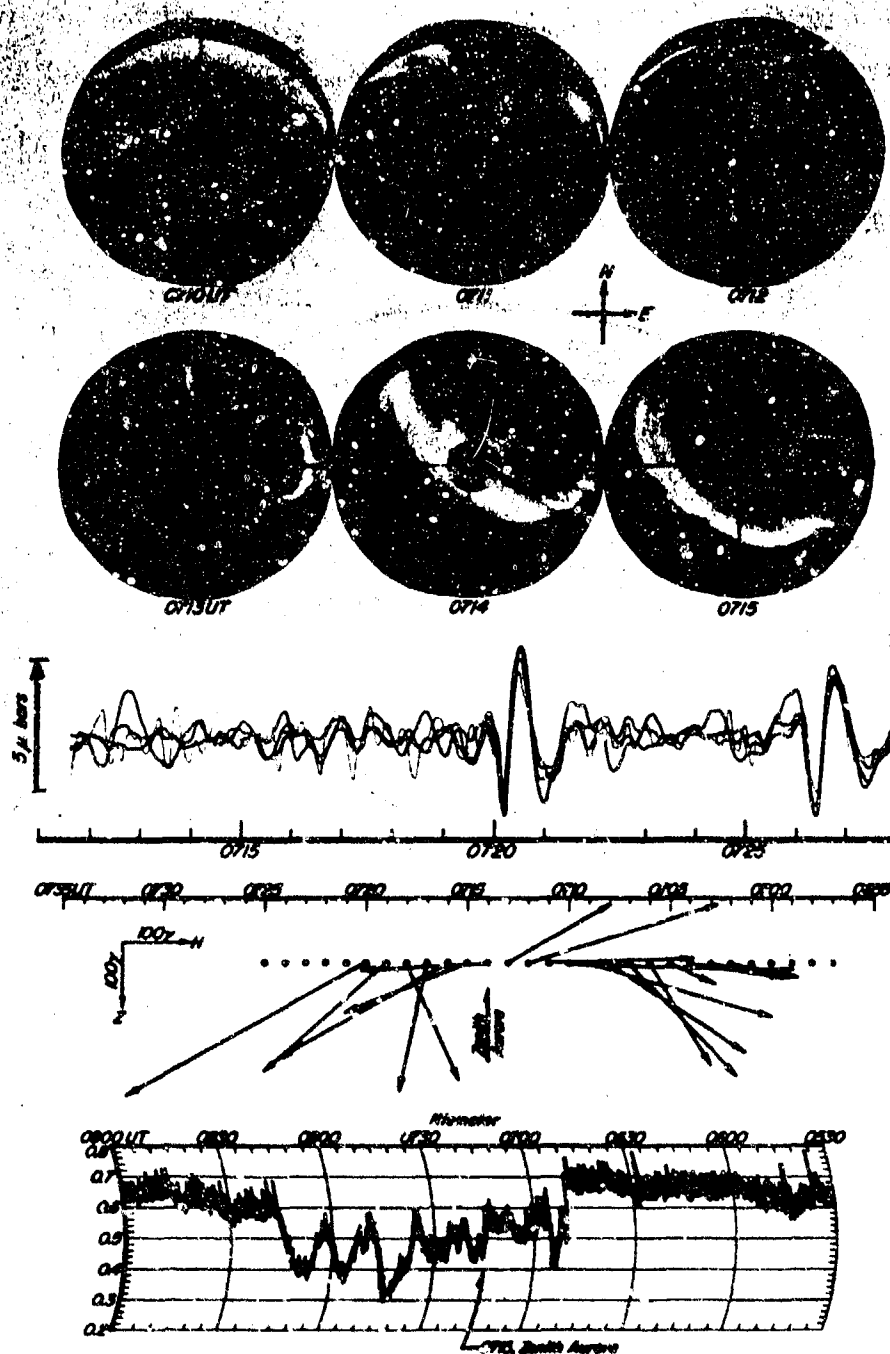
REFERENCES

- Blumer, W. and R. G. Heudl, 1969, "On the role of joule heating as a source of gravity-wave energy above 100 km," J. Atmos. Sci., 26 (2), 210-217.
- Chimonas, G. and C. O. Hines, 1970, "Atmospheric gravity waves launched by auroral currents," Planet. Space Sci., 18, 565.
- Chimonas, G. and W. R. Peltier, 1970, "The bow wave generated by an auroral arc in supersonic motion," Planet. Space Sci., 18, 599.
- Dougherty, J. P., 1961, "On the Influence of Horizontal Motion of the Neutral Air on the Diffusion Equation of the F-Region", J. Atmos. Terrest. Phys., 20, 167.
- Feldstein, Y. I. and G. V. Starkov, 1967, "Dynamics of Auroral Belt and Polar Magnetic Disturbances", Planet. Space Sci., 15, 209.
- Ferraro, V. C. A. and C. Plumpton, 1966, "Magneto-Fluid Mechanics", p. 209, Oxford University Press, Ely House, London, W. 1, England.
- Flood, Walter, A., 1965, "Some Evidence for the Occurrence of High Electron Densities in the Auroral D and E region", Final Report, Contract No. AF 19(628)-380, CAL Report No. CM-1677-P-1, 15 June 1965, Cornell Aeronautical Laboratory, Buffalo, New York, 14221.
- Foppl, H., G. Harendel, L. Haser, R. Lust, F. Melzner, B. Meyer, H. Neuss, H.-H. Robben, E. Reiger, J. Stocker, 1968, "Preliminary Results of Electric Field Measurements in the Auroral Zone", J. Geophys. Res., 73, 21.
- Francis, W. E. and R. Karplus, 1960, "Hydromagnetic Waves in the Ionosphere", J. Geophys. Res., 65, 3593.
- Fremouw, E. M., 1970, "Radar Investigations of Auroral Infrasonic Wave Sources", Annual Report, Contract F44620-69-C-0074, SRI Report 7840, Standord Research Institute, Menlo Park, California.

- Kato, S., 1965, "Theory of Movement of Irregularities in the Ionosphere", *Space Sci. Rev.*, 4, 223.
- Kelley, M. C., J. A. Starr and F. S. Moser, 1971, "Relationship Between Magnetospheric Electric Fields and the Motions of Auroral Forms", *J. Geophys. Res.*, 76, 5269-5277.
- Martyn, D. F., 1953, "Electric Currents in the Ionosphere III," *Phil. Trans. Roy. Soc. A*, 246, 306.
- Moser, F. S. and R. H. Manka, 1971, "Magnetospheric Electric Field Properties Deduced From Simultaneous Balloon Flights", *J. Geophys. Res.*, 76, 1697-1712.
- Moser, F. S., 1971, "The Origin and Effects of Electric Fields During Isolated Magnetospheric Substorms", *Space Sciences Laboratory Report, Series 12, Issue 21, University of California, Berkeley, California, 94720.*
- Parthasarathy, R. and F. T. Berkey, 1965, "Auroral Zone Studies of Sudden-Onset Radio-Wave Absorption Events Using Multiple-Station and Multiple-Frequency Data", *J. Geophys. Res.*, 70, 89.
- Piddington, J. H., 1963, "An Ionization Drift Theory of Aurora and Airglow", *Geophys. J. Roy. Astron. Soc.*, 7, 415.
- Piddington, J. H., 1964, "Geomagnetic Storms, Auroras and Associated Effects", *Space Sci. Rev.*, 3, 724.
- Rees, D., 1971, "Ionospheric Winds in the Auroral Zone", *Journal of the British Interplanetary Society*, Vol. 24, pp. 233-246.
- Wescott, E. M., J. D. Stolarik and J. P. Heppner, 1969, "Electric Fields in the Vicinity of Auroral Forms From Motions of Barium Vapor Releases", *J. Geophys. Res.*, 74, 3469.
- Wescott, E. M., J. D. Stolarik, and J. P. Heppner, 1970, "Auroral and Polar Cap Electric Fields From Barium Releases", *Particles and Fields in the Magnetosphere*, ed. by B. H. McCormac, D. Reidel Publishing Co., Dordrecht, Holland.
- Whalen, J. A., 1970, *Environmental Research Papers No. 327, 27 July 1970, AFCRL-70-0422, Air Force Cambridge Research Laboratories, L. G. Hanscom Field, Bedford, Massachusetts, U.S.A.*
- Wilson, C. R., 1967, "Infrasonic Pressure Waves from the Aurora: a Shock Wave Model", *Nature*, 216, No. 5111, 131-133.
- Wilson, C. R. and S. Nichparenko, 1967, "Infrasonic Waves and Auroral Activity", *Nature*, 214, 5095, 1299-1302.
- Wilson, C. R., 1969a, "Auroral Infrasonic Waves", *J. Geophys. Res.*, 74, 1812-1836.
- Wilson, C. R., 1969b, "Infrasonic Waves from Moving Auroral Electrojets", *J. of Planet. and Space Physics*, 17, 1107.
- Wilson, C. R., 1969c, "Two-Station Auroral Infrasonic Wave Observations", *Planet. and Space Sci.*, 17, 1107.
- Wilson, C. R., 1970, "Auroral Infrasonic and Ionospheric Absorption Substorms", *J. Atmos. Terrest. Phys.*, 74, 4511-4522.
- Wilson, C. R., 1971 (in press), "Auroral Infrasonic Waves and Poleward Expansions of Auroral Substorms at Inuvik, N.W.T.", *Canada, Geophys. J. of Roy. Ast. Soc.*

ACKNOWLEDGEMENTS

Research supported by the Atmospheric Sciences Section, National Science Foundation, NSF Grant GA-16821 and by the Advanced Research Projects Agency, in cooperation with the U.S. Dept. of Commerce, NOAA Geoacoustics group. I would like to thank the Inuvik Research Laboratory for operating the infrasonic equipment at Inuvik.



COLLEGE, 8 SEPTEMBER 1969

Fig.1 ASC photographs of supersonic auroral arc that produced AIW shown at 0720 as superposed pressure vs. time traces time shifted to show coherent wave. The plus to minus change in the Z component is shown in the H-Z plane diagram of the magnetic perturbation due to the arc. The sudden increase in cosmic noise absorption at 0715 is shown on the College riometer.

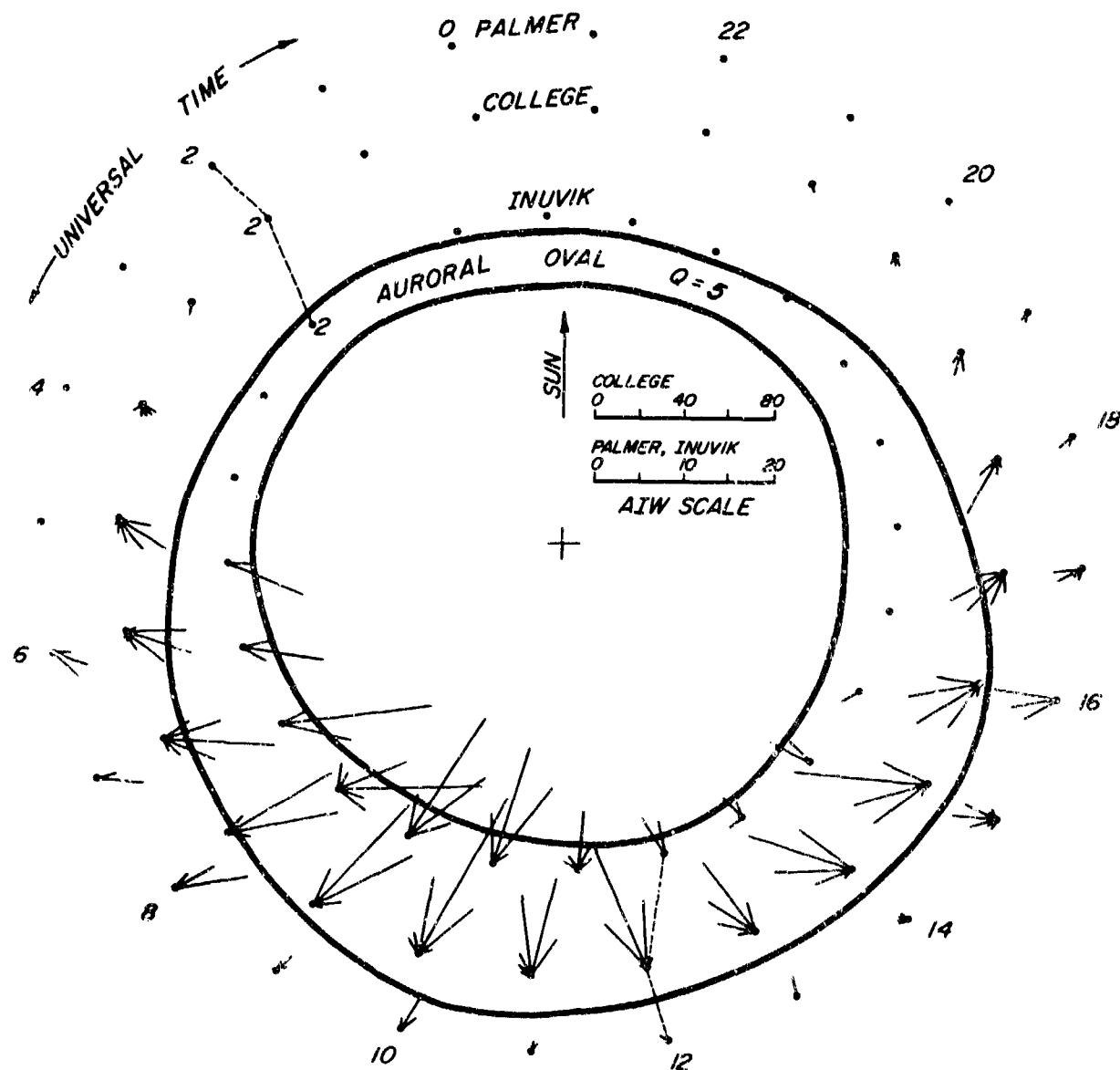


Fig.2 Number of AIW as a function of ϕ , plotted at the locations of Inuvik, College or Palmer with respect to the auroral oval for each hour (U.T.) and each 20° of ϕ . The scale for the number of AIW is given in the oval for each station. The vectors point toward the origin in the direction from which the AIW came.

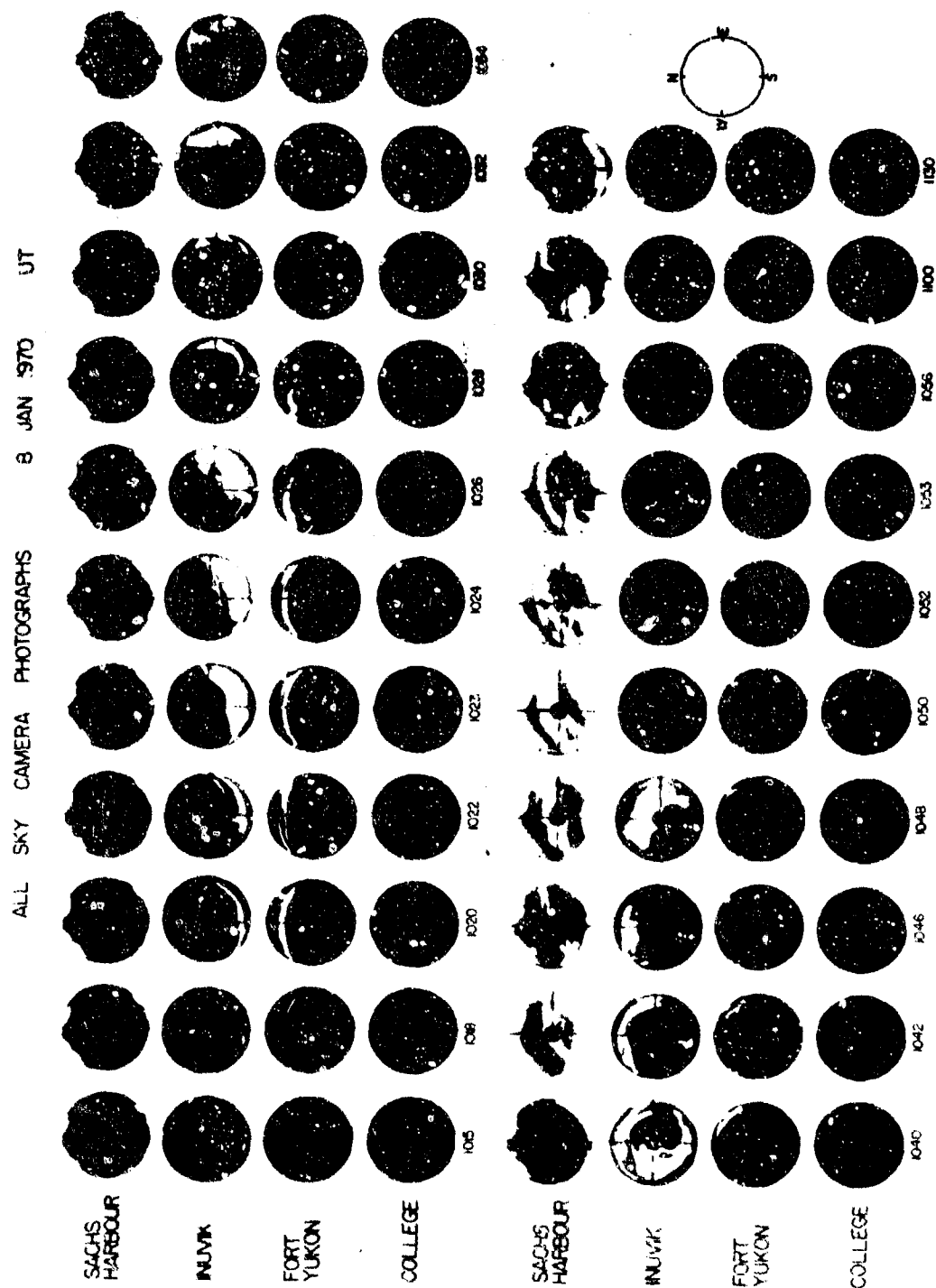


Fig. 3 ASC pictures for a meridian chain of observatories showing a poleward expansion that crossed the Inuvik zenith at 1024 from $\phi = 200^\circ$ at 1030 m/sec. Geomagnetic north is up on all the ASC pictures.

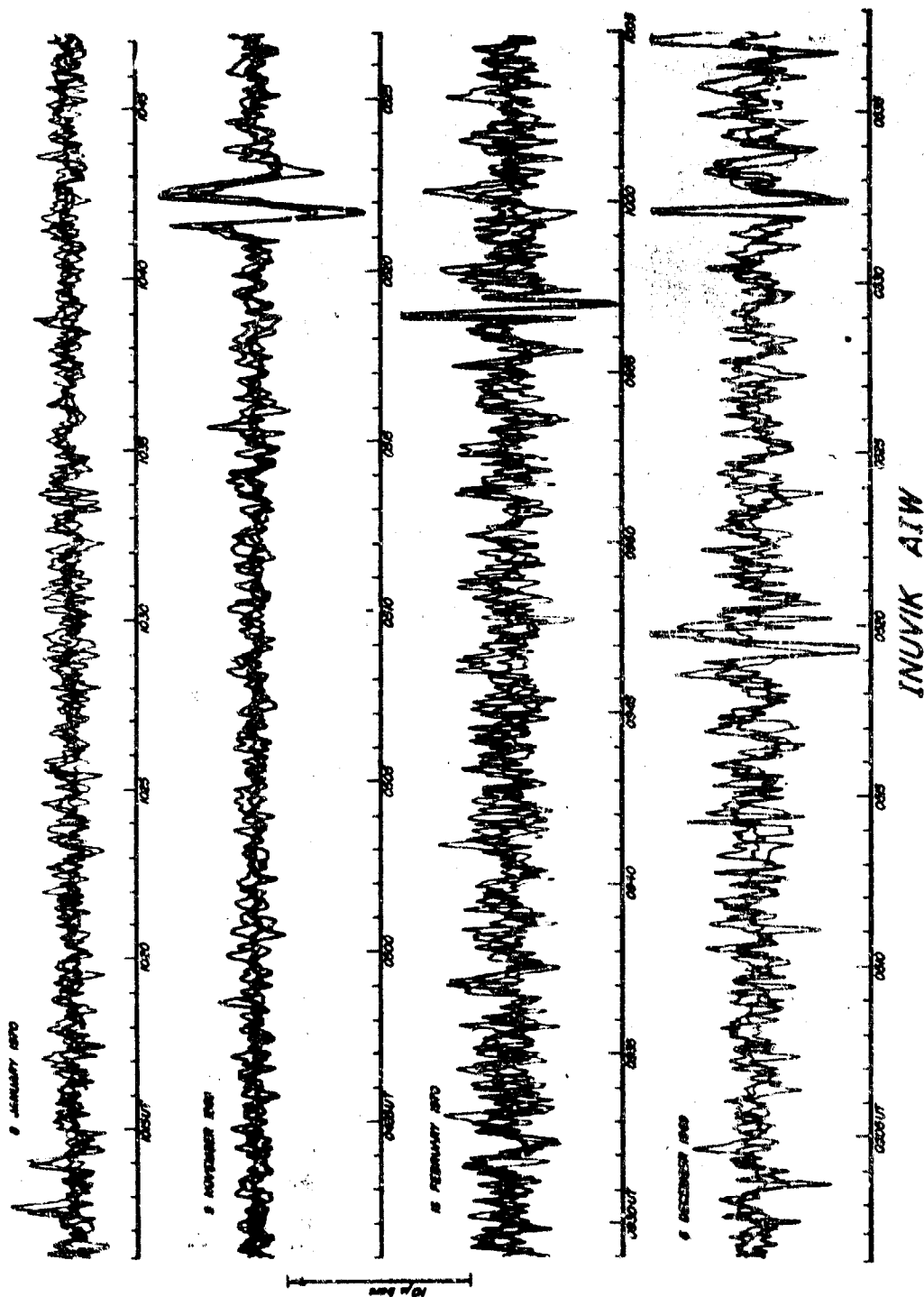


Fig.4 Infrasonic records for Inuvik during periods of poleward expansions giving pressure versus time traces from 4 microphones time shifted to show coherent AIW.

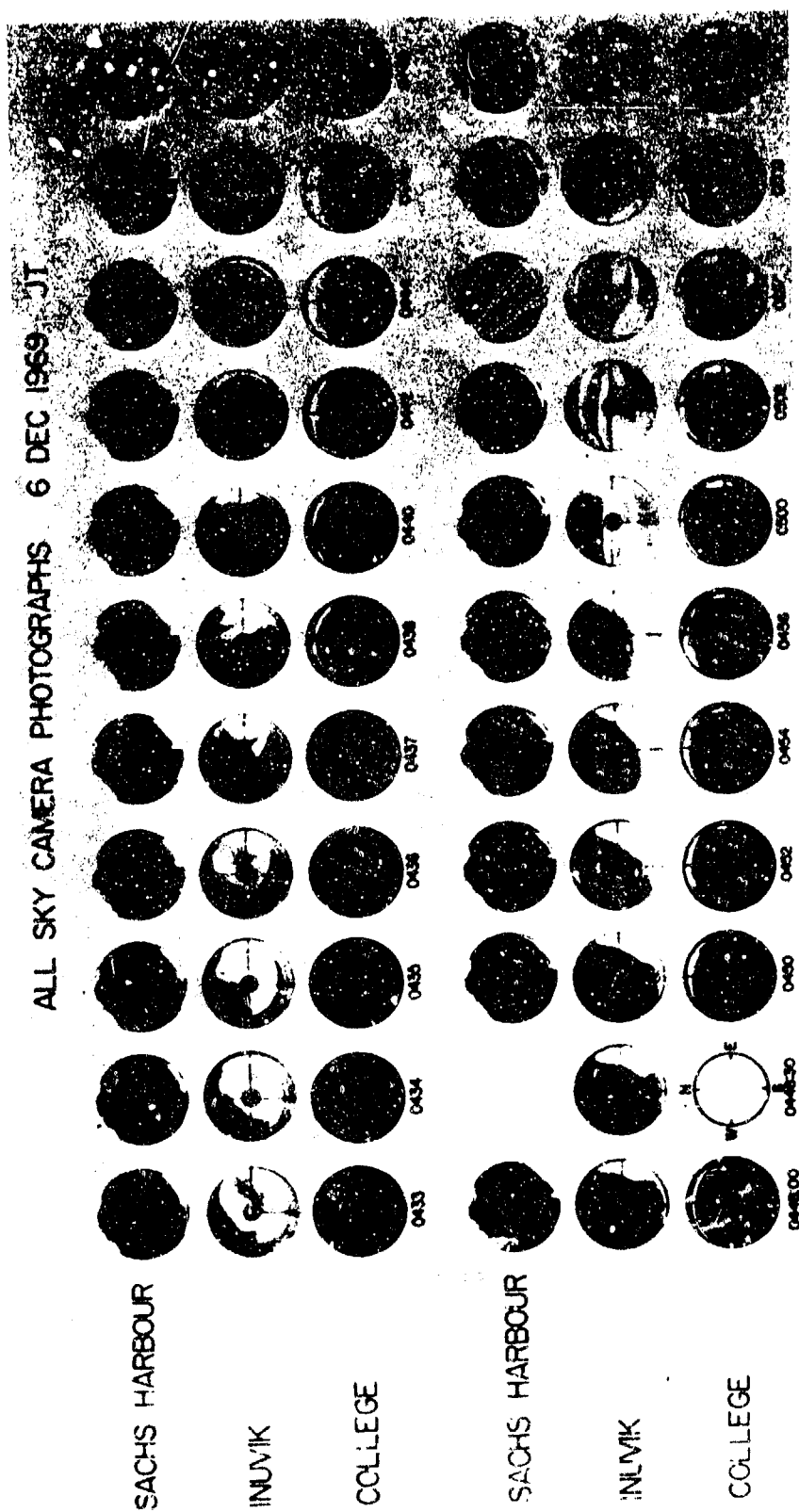
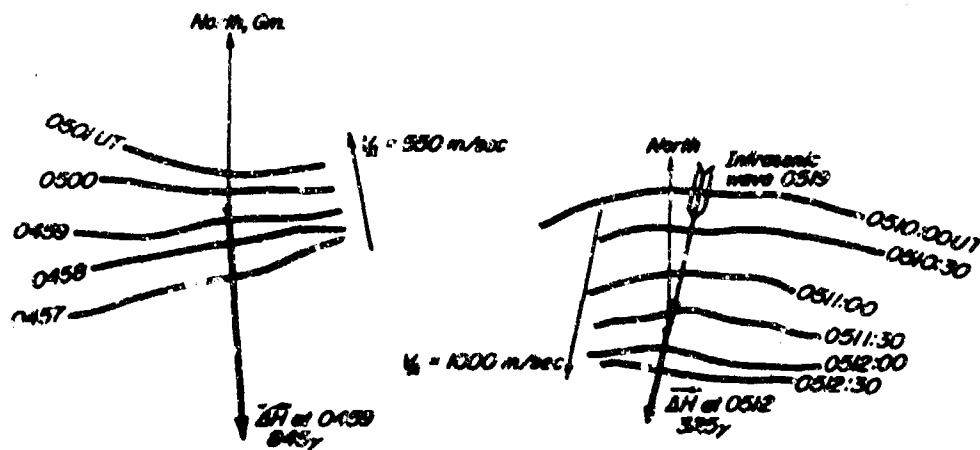
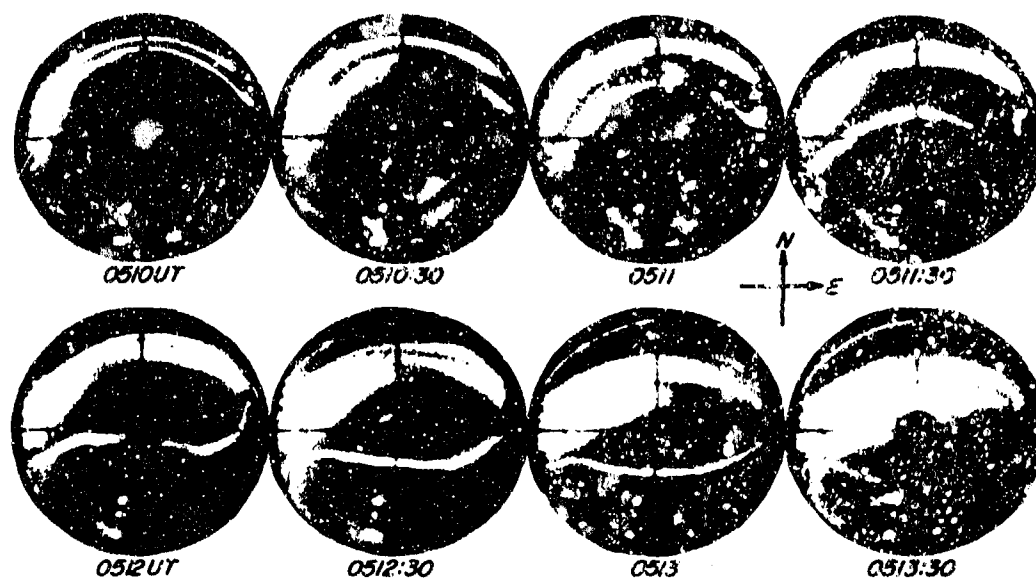


Fig 5 ASC pictures for poleward expansion of 0500 on 6 December 1969 that crossed Inuvik zenith from $\phi = 210^\circ$ with $V_n = 520$ m/sec.



INUVIK, 6 DECEMBER 1969

Fig.6 Inuvik ASC pictures of supersonic arc traveling from $\phi = 45^\circ$ at 0512. Maps of auroral arcs projected on earth's surface for minute intervals showing poleward expansion at 0500 and equatorward moving arc at 0512. ΔH (total horizontal perturbation vector) and the directions of AIW at 0519 are shown.

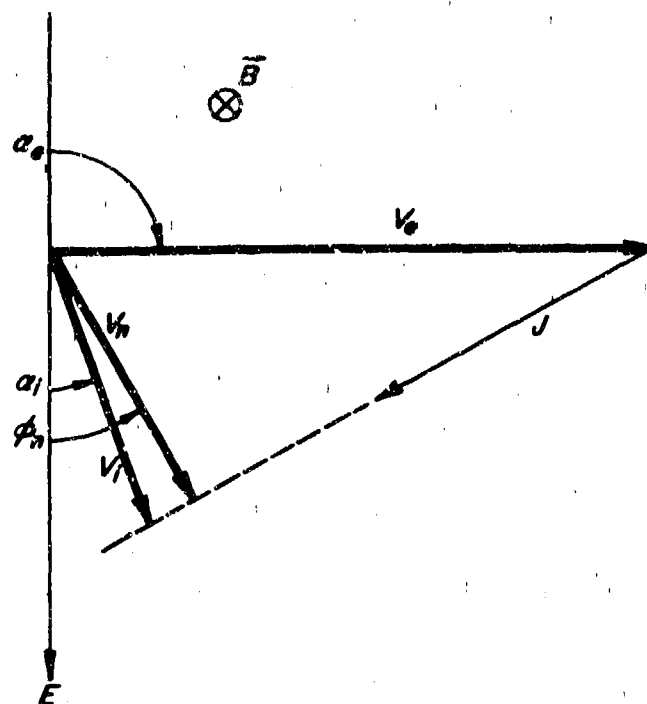


Fig.7 Plane view of the horizontal motions of the electrons \vec{V}_e and the ions \vec{V}_i and the "neutral" ionization \vec{V}_n in crossed electric and magnetic fields in the E region ionosphere. The current density \vec{J} is shown perpendicular to \vec{V}_n . \vec{B} is into the paper.

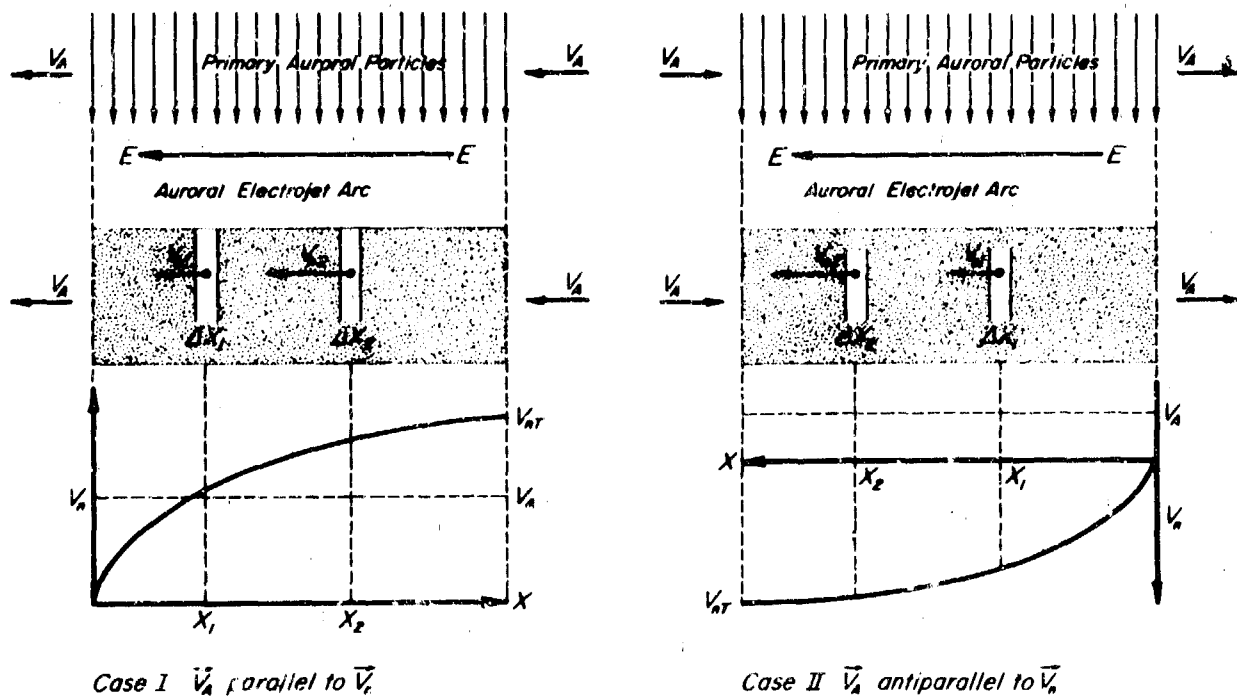


Fig.8 Relationship of \vec{V}_n , the electrodynamic drift velocity to the auroral velocity \vec{V}_A showing how a wall of neutral ionization is built up in Case I where \vec{V}_n and \vec{V}_A are parallel if $V_{nT} > V_A$. In Case II \vec{V}_n and \vec{V}_A are antiparallel and no wall of ionization is built up.

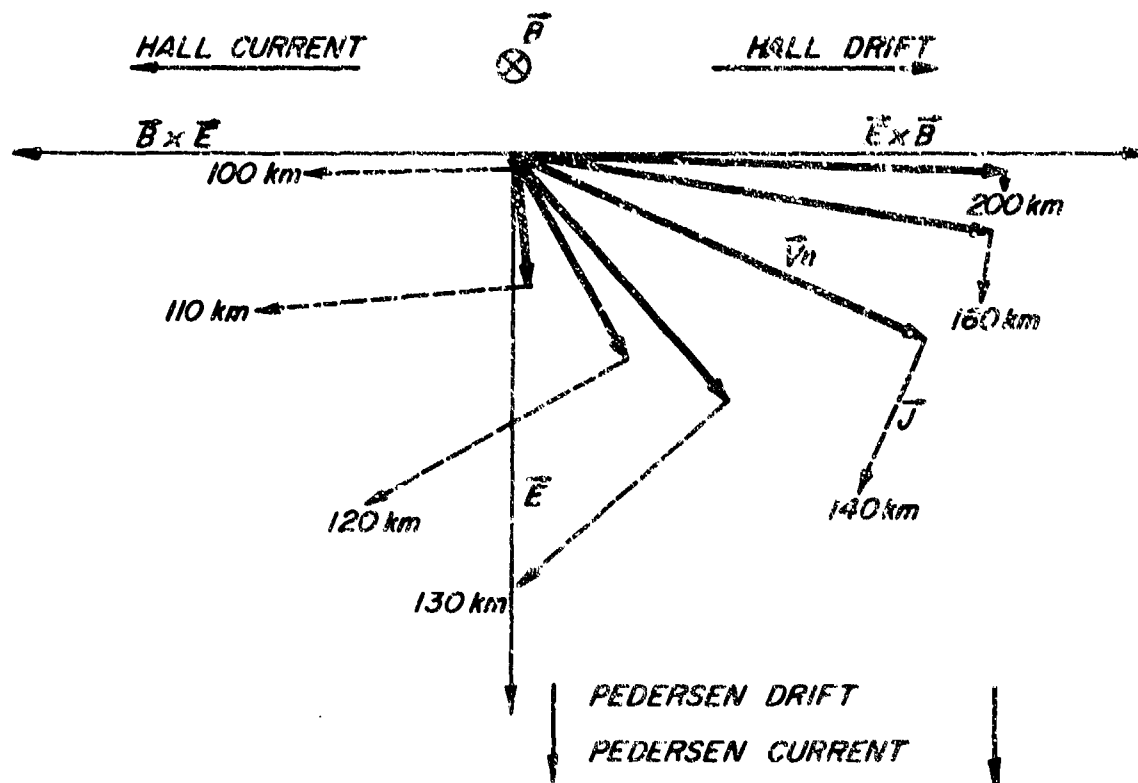


Fig.9 Neutral ionization drift \vec{V}_n and current density \vec{J} as a function of height in crossed electric and magnetic fields. \vec{B} is into the paper.

DETECTION OF 2 Hz INFRASOUND PRODUCED BY
MOVING AURORAL ELECTROJETS

by

Ludwik Liszka and Hans Westin

Kiruna Geophysical Observatory
S-981 01 Kiruna I
Sweden

DETECTION D'INFRA-SONS DE 2 HZ PRODUITS PAR LES DEPLACEMENTS DES ELECTROJETS AURORAUX

par

L. Liiska et Hans Westin

Sommaire

Au cours d'observations effectuées à Kiruna, en Suede (67,8 N, 20.0 E), à l'aide de réseaux de microphones, on a détecté des infrasons de 2 HZ produits pendant un certain nombre d'orages magnétiques majeurs. On a pu enregistrer la direction d'arrivée et la vitesse de phase horizontale, des infrasons, au moment où ils franchissaient les réseaux de microphones. Les quantités ainsi obtenues ont été comparées aux mouvements de l'électrojet auroral, déterminés à partir d'observations géomagnétiques effectuées dans cinq stations scandinaves. Cette comparaison, effectuée à l'aide d'une technique de trajectographie, a révélé qu'une partie seulement des infrasons observés peut être produite par les mouvements supersoniques des électrojets auroraux.

DETECTION OF 2 HZ INFRASOUND PRODUCED BY MOVING AURORAL ELECTROJET

Ludwik Liszka
and
Hans Westin
Kiruna Geophysical Observatory
S-981 01 Kiruna 1, Sweden

ABSTRACT

2 Hz infrasound was detected during a number of major geomagnetic storms using microphone arrays at Kiruna (67.8 N, 20.0 E), Sweden. The direction of arrival and the horizontal phase velocity of the infrasound at the microphone arrays were obtained. These quantities were compared with motions of the auroral electrojet as determined from geomagnetic observations at five Scandinavian stations. The comparison, using a ray tracing technique, has shown that only a part of the observed infrasound may be produced by supersonic motions of auroral electrojets.

1. INTRODUCTION

The existence of auroral infrasonic waves with periods in the minute range is at present well established through observations of Wilson (cf. e.g. (1)). It has been proposed (2), (3) that the waves are produced by auroral arcs and surges moving with supersonic speeds. A quantitative analysis of the production mechanisms has been given by Chimonas (4) and Chimonas and Peltier (5). First in 1970 it has been proved by Procunier (6) that the infrasound in the near infrasonic range (1-16 Hz) is associated with auroral events. He has also pointed out that this frequency range is especially suitable for detection of weak signals from a high altitude source. On average, due to the acoustic absorption the highest frequency which may be received from a source at 80 km level is 16 Hz and 1 Hz for a 110 km source. From the other side the power spectrum of atmospheric turbulence, being the effective noise, decreases with increasing frequency. A favourable signal to noise ratio may be obtained at frequencies above 1 Hz.

In the present research it has been assumed that the auroral infrasound is produced between 100 and 110 km and the frequency of detection should be located between 1 and 2 Hz. The recording equipment at Kiruna (67.8 N, 20.0 E), Sweden (for description see Liszka et al. (7)) is operated at 1.9 Hz with a bandwidth of 0.2 Hz. Horizontal phase velocities and angle of arrivals of infrasound during 4 nights in August - September 1971 has been compared with simultaneous magnetic activity. The period has been chosen with regard to favourable wind conditions in the upper atmosphere. As rocket measurements of wind and temperature were not available at that time a model atmosphere has been used between 35 and 120 km. The lowest part of the model has been adapted to simultaneous results of the geographically closest balloon soundings, i.e. from Sodankylä (67.3 N, 26.6 E), Finland. As the optical aurora can not be seen from Kiruna at this time of the year (all-sky camera recording start after September 15) the infrasound recordings have been compared with motions of auroral electrojets as deduced from magnetic observations.

2. DETERMINATION OF MOTIONS OF AURORAL ELECTROJETS

The method used here is the latitude profile method discussed by Bonnevier et al. (8). The current is assumed to be infinitely extended in the direction of the constant corrected geomagnetic latitude (9). When an auroral electrojet is located above a magnetic station the vertical Z-component is equal zero and the horizontal H-component reaches its extremum value. Having a chain of magnetic stations along the same geomagnetic meridian it is possible for a given instant to construct the latitude profile of geomagnetic field variations and thus determine the location of the electrojet.

In the present study magnetograms from five Scandinavian stations: Tromsø, Abisko, Kiruna, Sodankylä and Lycksele are used. Geographical and geomagnetic coordinates of the stations are given in Table I. The Z-component on the magnetograms has been digitized at 1 minute intervals and corrected for the Z_{sq} variation. The latitude profiles were plotted for every minute and the position of the auroral electrojet determined to be at latitude for which $Z_{corrected} = 0$. The velocity of the electrojet is then calculated from its positions at two consecutive minutes. The maximum error in the calculated velocity is estimated to be 50 m/sec. Only velocities larger than 375 m/sec are used in the comparison with recorded infrasound assuming the maximum influence of the measuring error and the sound velocity at the auroral height of 325 m/sec.

An example of determination of the electrojet position and its velocity is shown in Fig. 1 for a 8 minute period during the night August 22 - 23, 1971.

3. INFRASOUND OBSERVATIONS

During periods when supersonic motions of electrojets were obtained and coherent infrasound was recorded above the microphone array, E-W and N-S phase differences and the amplitude were scaled once every minute. Phase differences were then converted into the horizontal phase velocity and the direction of arrival. These two parameters, together with the amplitude are shown in three lowest diagrams of Figs. 2-5 where results from all four analyzed nights are presented. Three of the nights were characterized by negligible ground winds, while during one of them on August 25-26, 1971 the ground level wind of about 3 m/sec made impossible reliable amplitude measurements.

The upper two diagrams of Figs. 2-5 show the electrojet velocity and its position (plotted only at occasions of supersonic movements). Positions of the electrojet when it moves towards Kiruna have been plotted with thicker lines. It is during these motions that the recording station will be reached by the shock front. When the electrojet moves towards the South the infrasound should reach the station from the northern part of the sky and from the southern part of sky for a northward motion. The larger the translational velocity of the electrojet, the larger will be the horizontal phase velocity of the infrasound recorded on the ground and the shorter the travel between the source and the ground. The relation between the Mach number of the electrojet motion and the initial horizontal phase velocity is shown in Fig. 6 for ambient sound velocities of 300 and 330 m/sec. During the night August 22-23, 1971 a moderate jet stream (50 m/sec) was observed at 10 km height. The jet stream increases the cut-off phase velocity for infrasound arriving from the North. This may be seen by comparing Figs. 7 and 8 with results of ray tracing for a night without a jet stream (Fig. 9).

It must be also remembered that also the travel time of the infrasound between the source and the ground is a function of the direction of propagation, the horizontal phase velocity and the atmospheric conditions.

All these propagation parameters are also dependent on the direction of propagation due to influence of the atmospheric wind system. This is illustrated in Figs. 7-8 showing results of ray tracing for six different directions of motion of the electrojet and different initial horizontal phase velocities. The calculations are made using a method similar to that of Cowling et al. (10), (11) and for the wind and temperature conditions at midnight August 22-23, 1971.

Thus, a detailed comparison between the position of the auroral electrojet and the infrasound observed on the ground is only possible by applying the ray tracing technique to each one-minute scaling of the infrasound. In such a way the position of a possible source at 110 km height may be obtained. As only the meridional position of the electrojet is known, only the latitude of the estimated source position may be compared with the latitude of the electrojet. Such a detailed comparison, as extremely time-consuming, has been made only for a limited number of periods during the investigated storms. The following periods were analysed:

17 Aug. -71	2240 - 2340 UT
18 Aug. -71	0030 - 0120 UT
18 Aug. -71	0140 - 0250 UT
22 Aug. -71	1930 - 2010 UT
4 Sep. -71	2000 - 2140 UT

Results of the comparison are shown in Figs. 10-14. The geomagnetic latitude of each zero crossing of the vertical component of the geomagnetic field, interpreted as individual electrojets, is plotted once a minute as a function of time. The geomagnetic latitude of the estimated infrasound source position is indicated by empty circles. In cases when the intensity of the 1.9 Hz infrasound exceeded 6 db above the background level the position of the source has been marked by solid circles. It may be seen that the largest portion of the infrasound observed during analysed periods seems to be steadily originated between 64.5° and 65.5° geomagnetic latitude. Only during periods shown in Figs. 12 and 13 the infrasound source tends to follow the motion of the electrojet, but is not necessarily associated with supersonic motions of the electrojet. In Fig. 13, at 1945 UT on August 22, 1971, strong bursts of infrasound emission may be seen which agrees well with supersonic motions of the electrojet. On August 17, 1971 at 2250 UT and 2300 UT and on September 4, 1971 at 2005 UT and 2110 UT there are bursts of infrasound which are observed from the northern part of the sky, while the supersonic motions of the electrojet took place in the southern part of the sky. Interesting cases may be seen on August 22 after 1935 UT and on September 4 after 2050 UT where strong bursts of infrasound are apparently associated with a disappearance of two, oppositely directed, weak electrojets. There are also few cases when the infrasound was originated to the South of the station, far from any electrojet. Unfortunately, no information about the motion of auroral surges is available from the magnetic measurements. This type of motions may also produce infrasound (3) which will be easiest observed in the direction of electrojet. This could possibly be case on September 4, when the infrasound was observed from azimuths around 60° .

CONCLUSIONS

A weak, coherent infrasound has been observed at 1.9 Hz during a number of magnetic storms. The emission is rather persistent during long periods of time and is not always associated with translational supersonic motions of the auroral electrojet. In some cases when the enhanced infrasound emission coincides in time with supersonic motions of the electrojet there is a discrepancy between the direction of arrival of the infrasound and the position of the electrojet. The infrasound emission is often observed also when the electrojet as whole does not move at all. It is therefore possible that if the infrasound is produced by dynamic processes in the aurora, it may be due to motions of individual current filaments in the electrojet. Such motions may be difficult to discover on geomagnetic recordings.

ACKNOWLEDGEMENT

The present research was sponsored in part by the Research Institute of National Defence.

Table I
Coordinates of magnetic stations

	Geographic		Geomagnetic	
	Latitude	Longitude	Latitude	Longitude
Tronsb	69.67	18.95	66.3	- 1.1
Abisko	68.36	18.82	65.0	- 1.9
Kiruna	67.83	20.42	64.4	- 0.8
Sodankylä	67.37	26.65	63.4	4.2
Lycksele	64.60	18.80	61.3	- 3.7

REFERENCES

1. Wilson, C.R., "Auroral Infrasonic Waves", J. Geophys. Res. 74, 1812, 1969.
2. Wilson, C.R., "Two-Station Auroral Infrasonic Wave Observations", Planet. Space Sci. 17, 1817, 1969.
3. Wilson, C.R., "Infrasonic Waves from Moving Auroral Electrojets", Planet. Space Sci. 17, 1107, 1969.
4. Chimonas, G., "Infrasonic Waves Generated by Auroral Currents", Planet. Space Sci. 18, 591, 1970.
5. Chimonas, G. and Peltier, W.R., "The Bow Wave Generated by an Auroral Arc in Supersonic Motion", Planet. Space Sci. 18, 599, 1970.
6. Procunier, R.W., "High Frequency Acoustic Aurora", Paper presented at 1970 National Fall Meeting AGU, San Francisco, December 1970.
7. Liszka, L., Olsson, S., Englund, K. and Koskenniemi, K., "Infrasound Recording Equipment at Kiruna Geophysical Observatory", KGO Technical Report 71:105, December 1971.
8. Bonnevier, B., Boström, R. and Rostoker, G., "A Three-Dimensional Model Current System for Polar Substorms", J. Geophys. Res. 75, 107, 1970.
9. Hakura, Y., "Tables and Maps of Geomagnetic Coordinates Corrected by the Higher Order Spherical Harmonic Terms", Rept. Ionosphere Space Res., Japan 19, 121, 1965.
10. Cowling, D.H., Webb, H.D. and Yeh, K.C., "A Study of Travelling Disturbances in the Ionosphere", Tech. Rep. 38 Ionosph. Radio Lab. Univ. of Illinois, 1970.
11. Cowling, D.H., Webb, H.D. and Yeh, K.C., "Group Rays of Internal Gravity Waves in a Wind-Stratified Atmosphere", J. Geophys. Res. 76, 213, 1971.

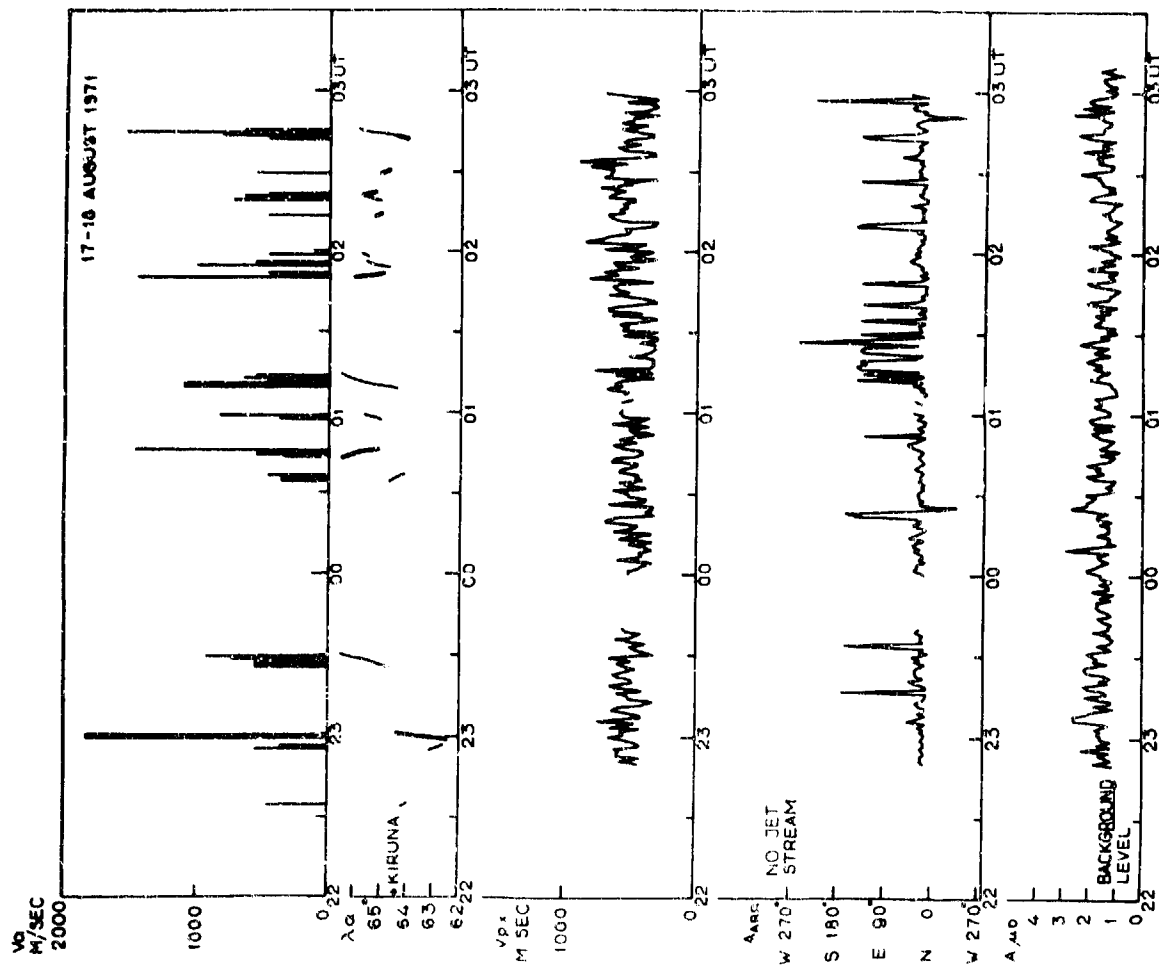


Fig.2 Supersonic velocities of the electrojet, its geomagnetic latitude together with parameters of the observed infrasound. The horizontal phase velocity, the angle of arrival and the amplitude for the night August 17-18 1971.

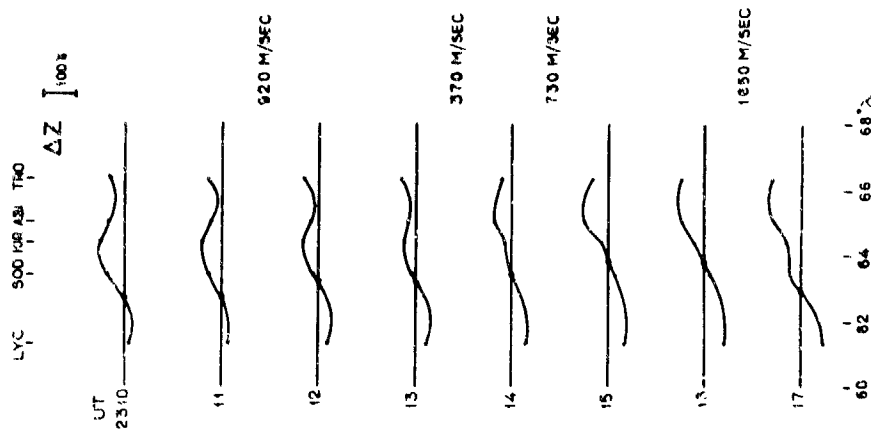


Fig.1 Latitude profiles of corrected Z-component between 2310 UT - 2317 UT on August 22, 1971 showing position of the electrojet ($Z=0$) and determined supersonic translational velocities of the electrojet.

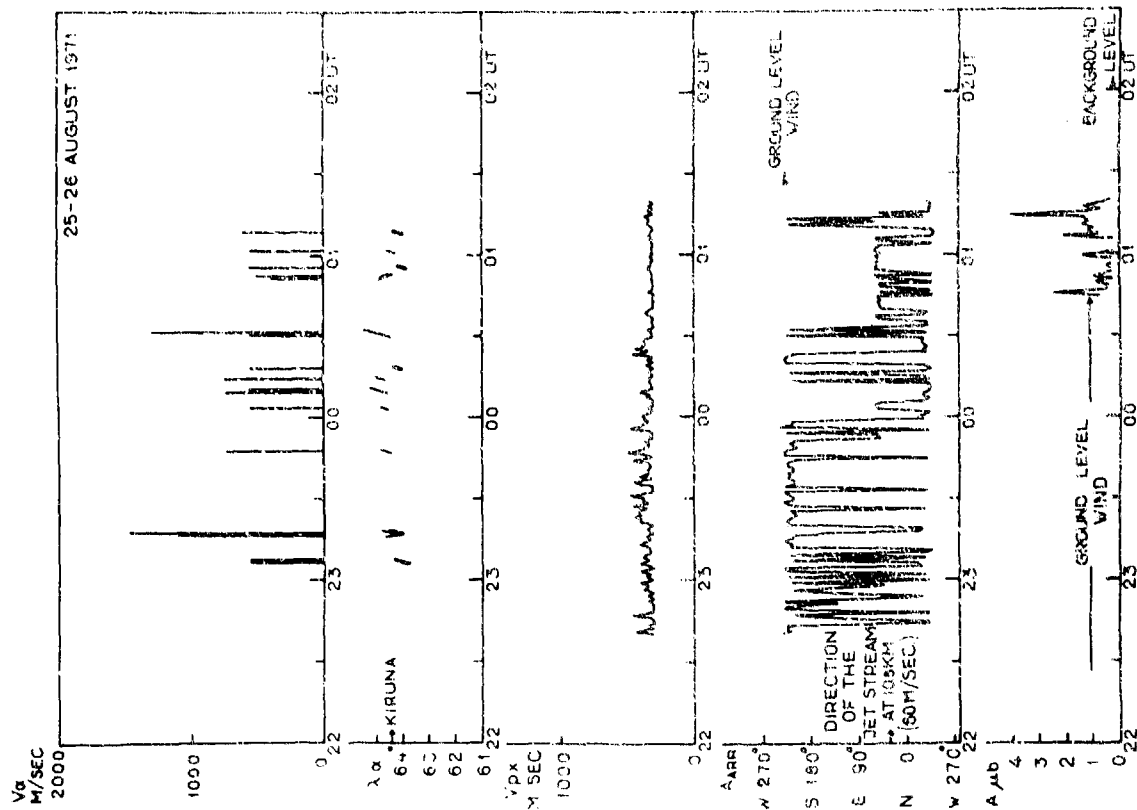


Fig. 4 The same as Fig. 2 for the night August 25-26, 1971.

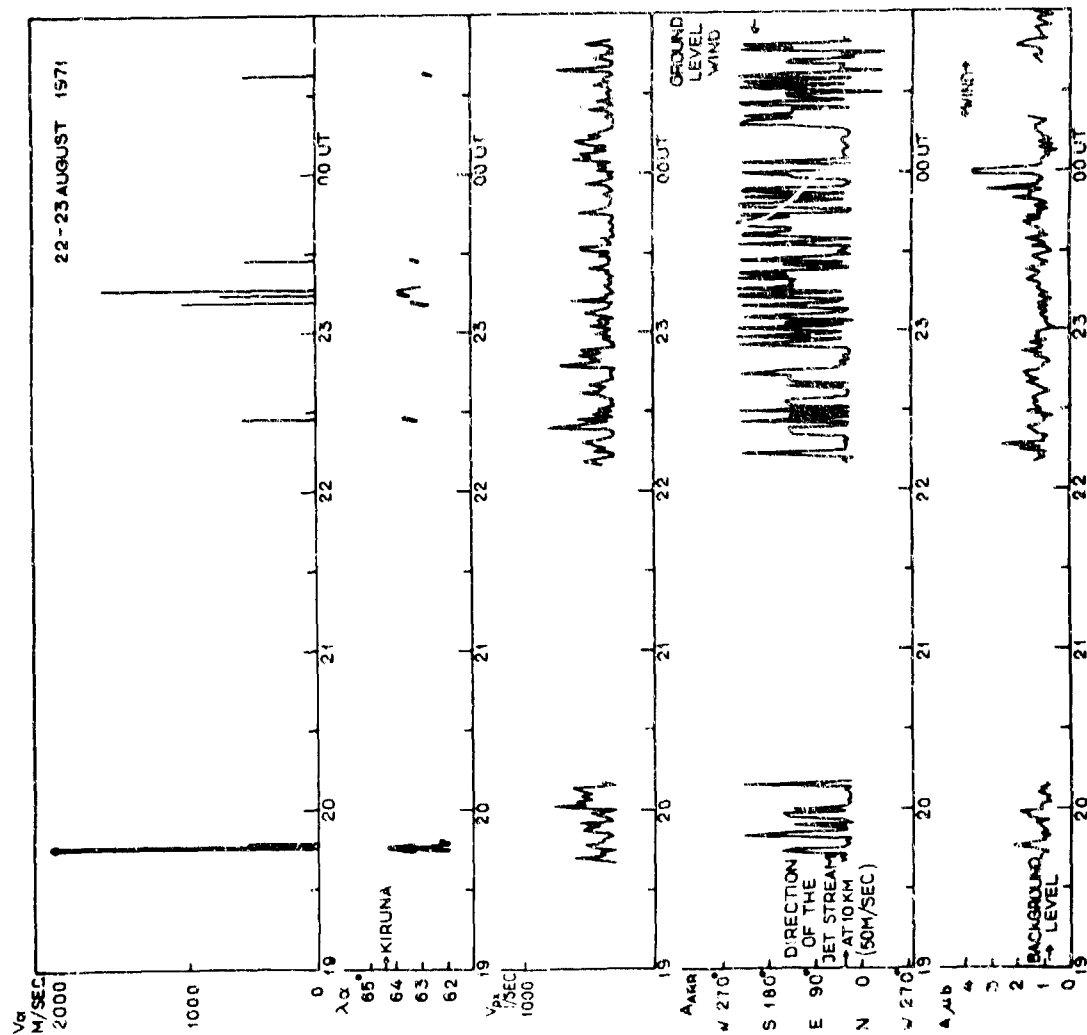


Fig. 3 The same as Fig. 2 for the night August 22-23, 1971.

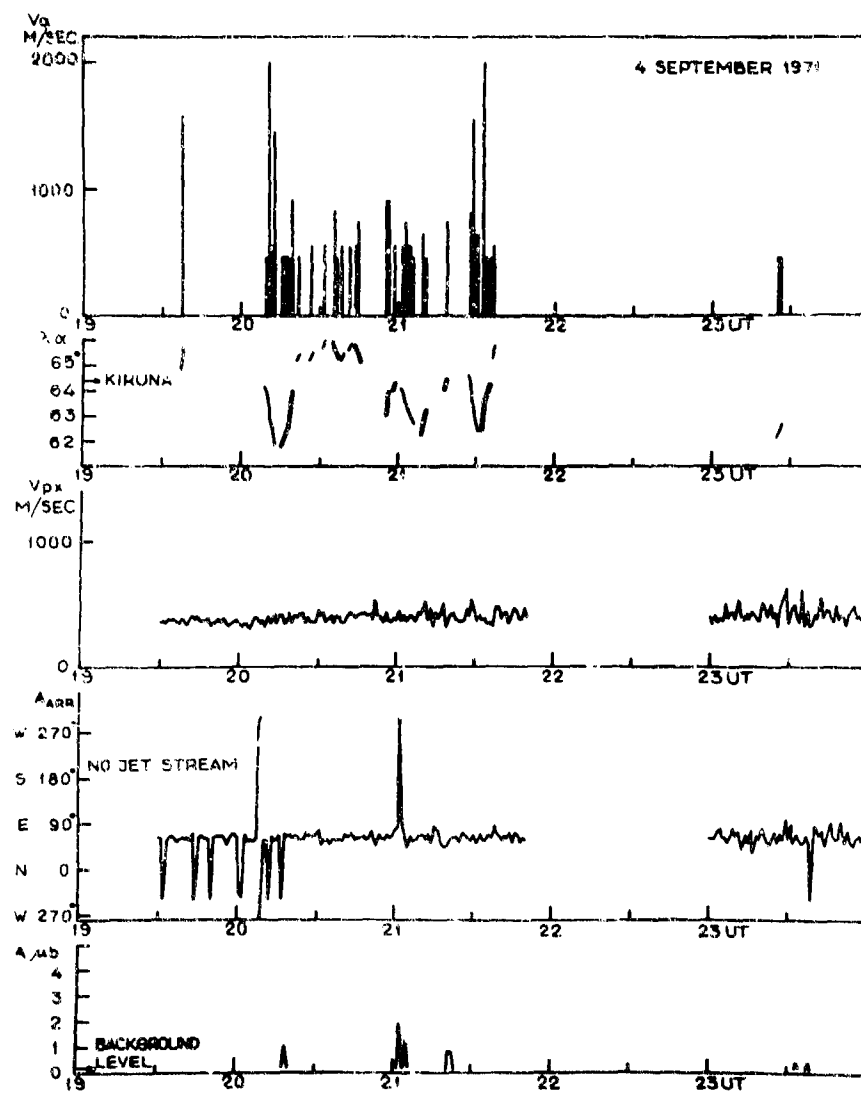


Fig.5 The same as Fig.2 for the night September 4-5, 1971.

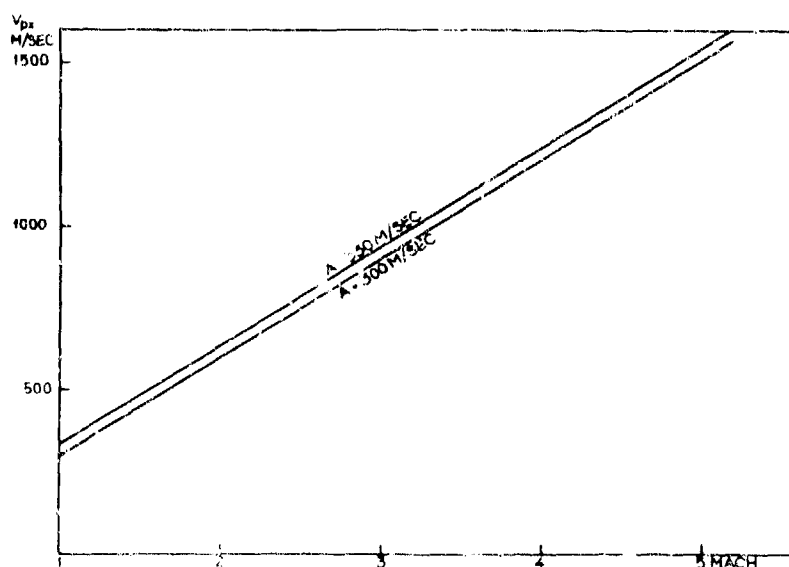


Fig.6 The relation between the Mach number of the electrojet motion and the initial horizontal phase velocity for

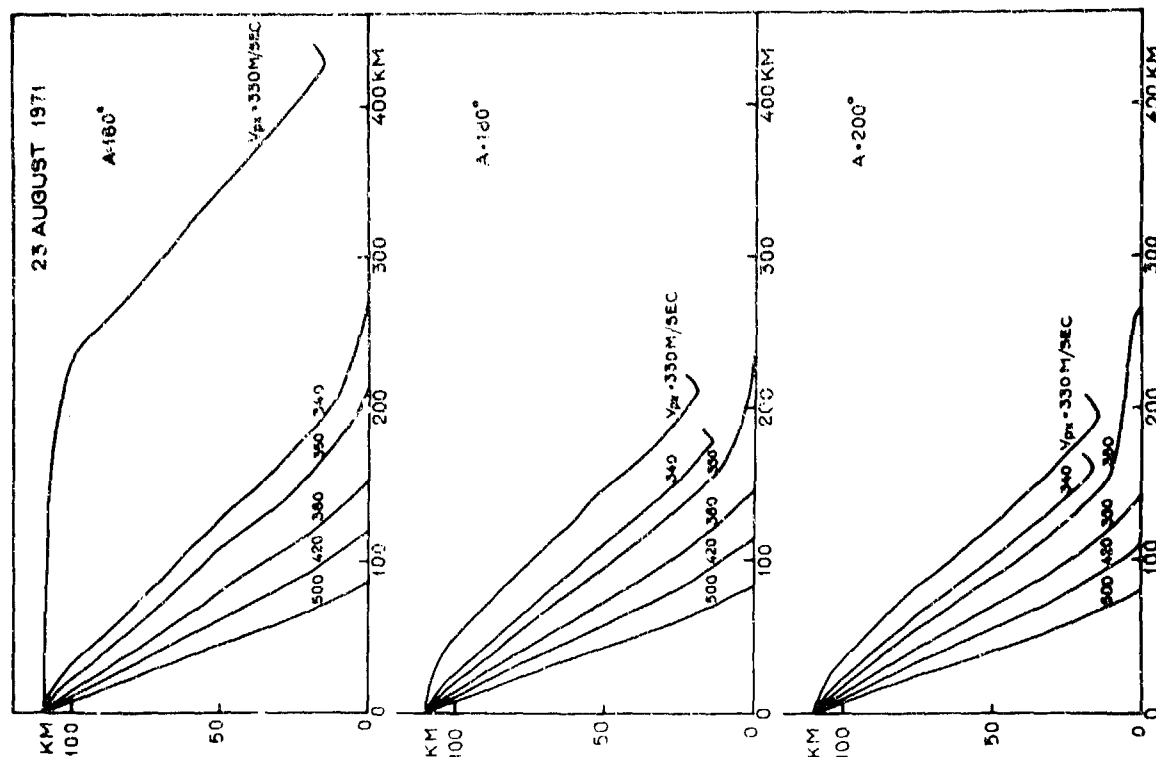


Fig. 8 Examples of ray tracing for different directions of motion of the electrojet and different initial horizontal phase velocities.

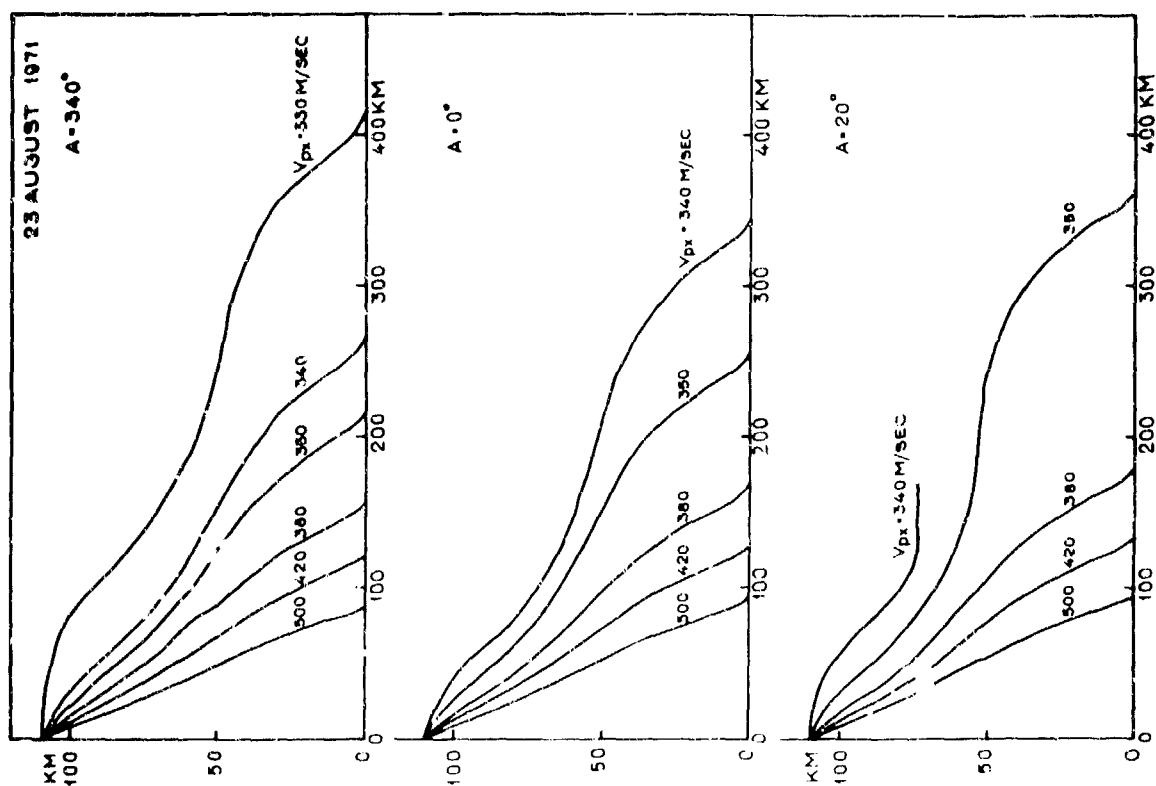


Fig. 7 Examples of ray tracing for different directions of motion of the electrojet and different initial horizontal phase velocities.

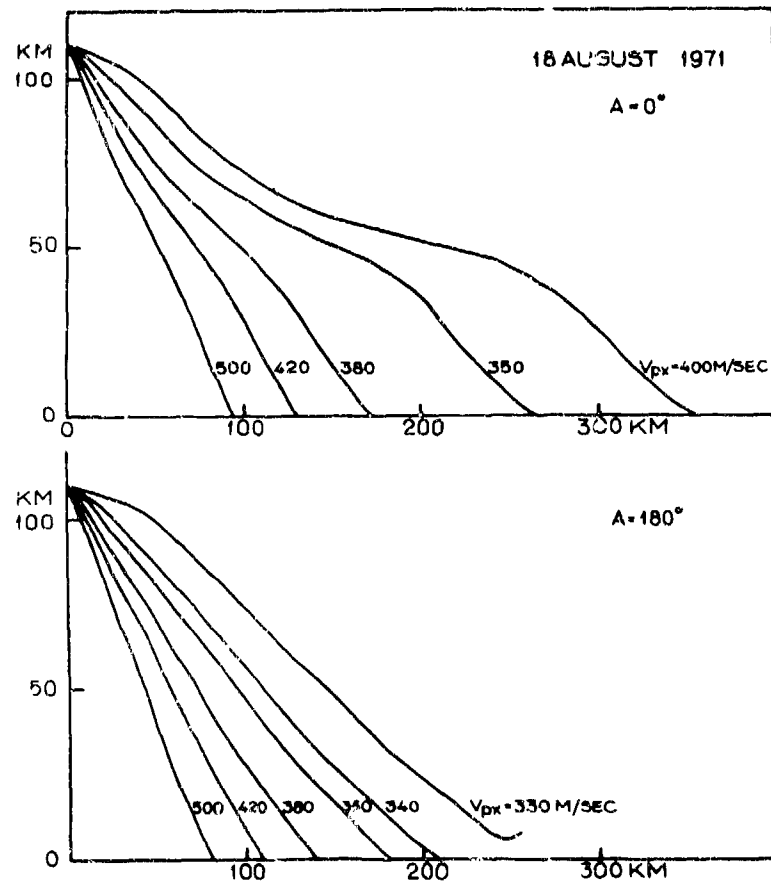


Fig.9 Examples of ray tracing for different directions of motion of the electrojet and different initial horizontal phase velocities. A night without a jet stream.

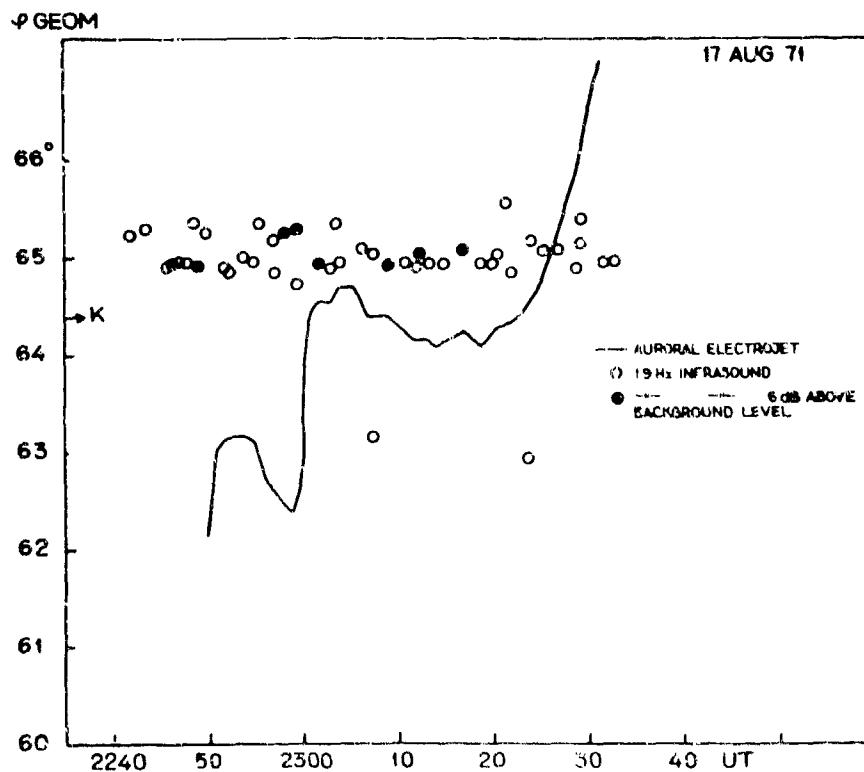


Fig.10 Detailed comparison between the electrojet latitude and the latitude of the estimated infrasound source.

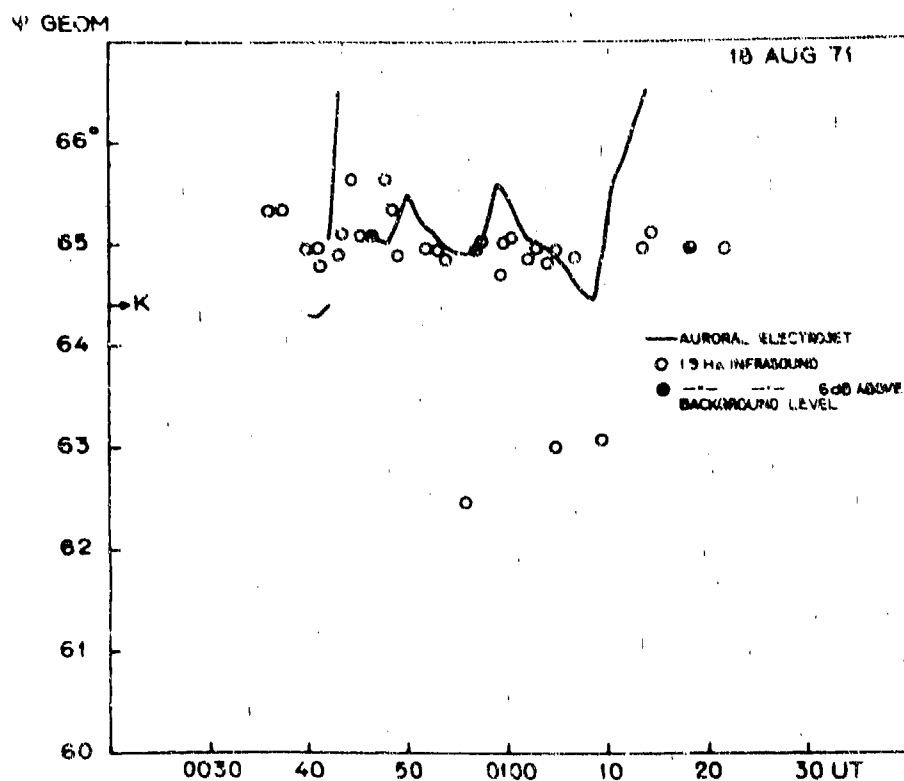


Fig.11 The same as Fig.10 for the period 0030 UT - 0120 UT on August 18, 1971.

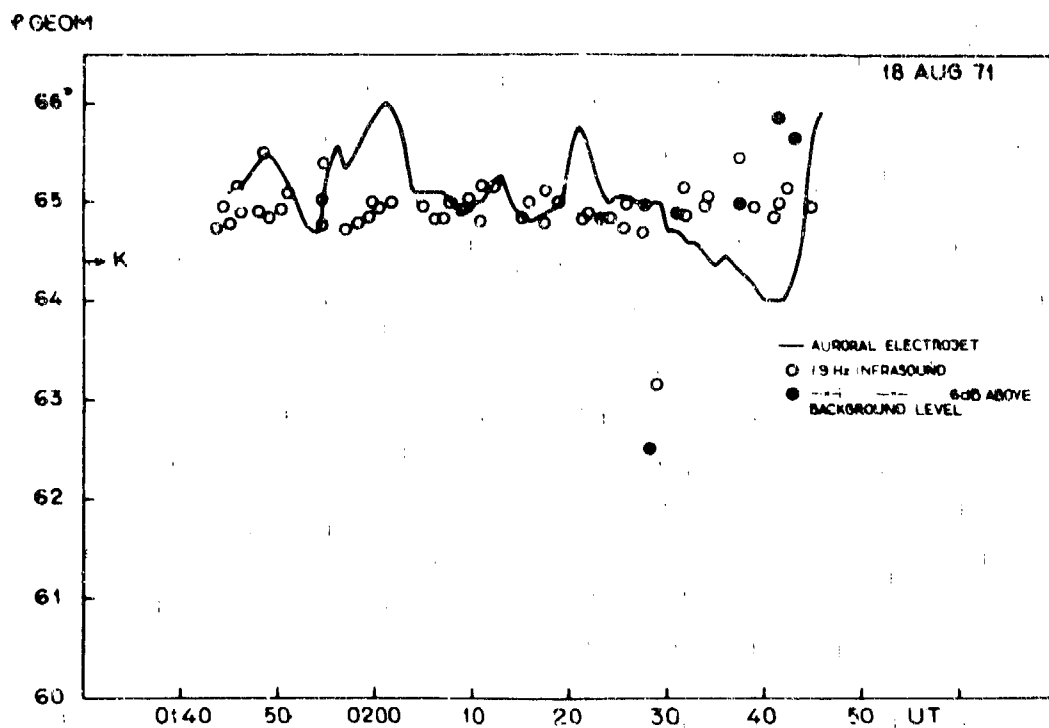


Fig.12 The same as Fig.10 for the period 0140 UT - 0250 UT on August 18, 1971.

f GEOM

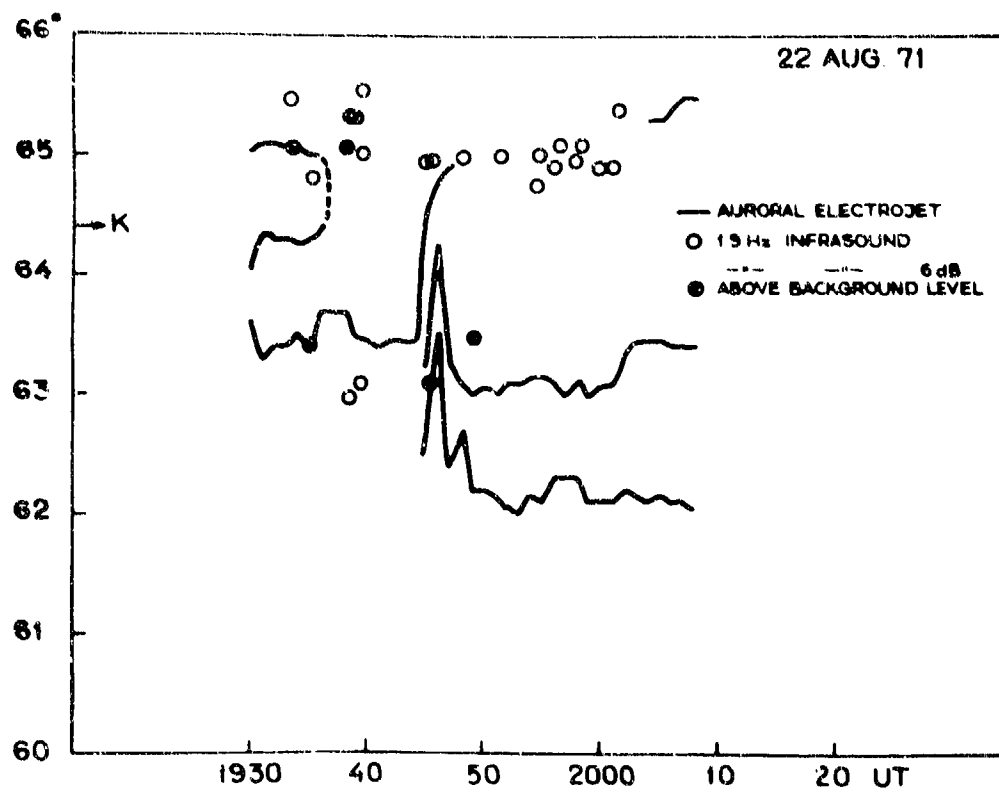


Fig.13 The same as Fig.10 for the period 1930 UT - 2010 UT on August 22, 1971.

f GEOM

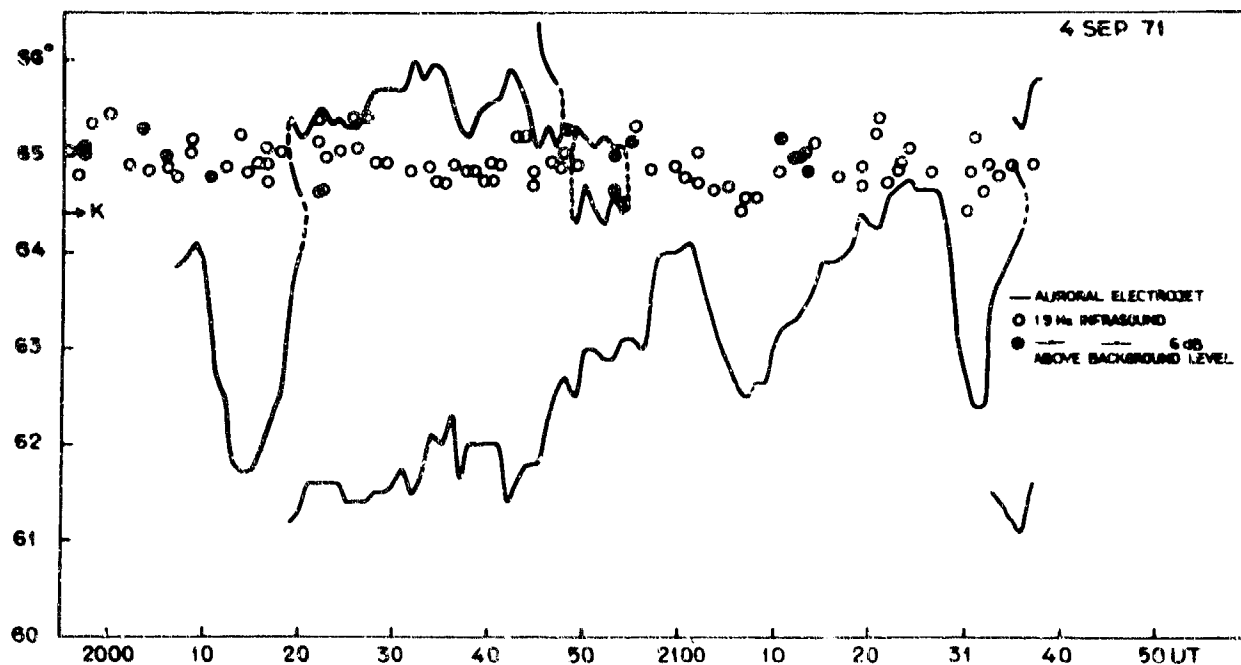


Fig.14 The same as Fig.10 for the period 2000 UT - 2140 UT on September 4, 1971

8

ON WAVES GENERATED BY STATIONARY AND TRAVELING SOURCES
IN AN ISOTHERMAL ATMOSPHERE UNDER GRAVITY

by

C.H.Liu and K.C.Yeh

Ionosphere Radio Laboratory
Department of Electrical Engineering
University of Illinois at Urbana-Champaign 61801
USA

SUR LES ONDES PRODUITES PAR DES SOURCES STATIONNAIRES ET ITINERANTES
DANS UNE ATMOSPHERE ISOTHERME SOUMISE A GRAVITE

par

C.H. Liu et K.C. Yeh

SOMMAIRE

Au cours de ces dernières années, on a accumulé les mises en évidence expérimentales qui ont montré que les ondes acoustiques et de gravité de l'atmosphère neutre peuvent être produites par diverses sources naturelles et artificielles telles que des tremblements de terre, des fronts de perturbations météorologiques, des explosions nucléaires dans l'atmosphère, des courants-jets, des déplacements supersoniques d'arcs auroraux, des sous-orages auroraux, des éclipses de soleil, des avions à réaction, des lanceurs de fusées, etc.. On peut considérer ces divers mécanismes d'excitation comme appartenant à l'un des trois types de sources suivants, ou comme représentant une combinaison de ceux-ci : production de masse, production de quantité de mouvement, et production d'énergie ; que l'on peut étudier d'une façon très générale. On considère tout d'abord le cas de sources stationnaires. La réponse transitoire et la forme générale de l'onde en un point d'observation donné dépendent d'un certain nombre de paramètres tels que l'altitude et la distance de ce point, l'instant d'observation, la dépendance spatiale et temporelle de la source, la nature de la source, etc. On fournira une étude systématique de la réponse transitoire en fonction de certains de ces paramètres, dans l'espoir que cette approche puisse se révéler de quelque utilité aux expérimentateurs pour l'identification de diverses sources.

Ensuite, l'examen est étendu aux sources itinérantes, pour les deux cas subsoniques et supersoniques. Les applications possibles de ces résultats aux problèmes d'excitation, dans lesquels interviennent des sources itinérantes, englobent : les lanceurs de fusées, les éclipses de soleil, les fronts de perturbations météorologiques, etc.,.

L'effet de sol prend de l'importance lorsque les sources sont situées au voisinage du sol. On étudie en particulier la réponse transitoire de l'atmosphère à un mouvement du sol au cours d'un séisme. On discutera le couplage entre ondes sismiques et atmosphériques.

ON WAVES GENERATED BY STATIONARY AND TRAVELING
SOURCES IN AN ISOTHERMAL ATMOSPHERE UNDER GRAVITY

C. H. Liu and K. C. Yeh
Ionosphere Radio Laboratory, Department of Electrical Engineering
University of Illinois at Urbana-Champaign 61801
U.S.A.

ABSTRACT

Experimental evidences have been accumulated in the last several years to indicate that acoustic-gravity waves in the neutral atmosphere can be generated by various natural and artificial sources such as earthquakes, severe weather fronts, nuclear detonations in the atmosphere, jet streams, supersonic displacements of auroral arcs, auroral substorms, solar eclipse, jet aircrafts, rocket launchings, etc. These various excitation mechanisms can be considered as one or a combination of the three types of sources: mass production, momentum production and energy production which can be studied in a very general fashion. We consider first the case of stationary sources. It is shown that the transient response and the overall wave form at a given observation point depend on a number of parameters such as the height and the range of the observation point, the time of observation, the spatial and temporal dependence of the source, the nature of the source, etc. A systematic study of some of these parametric dependences of the transient response will be given. It is hoped that the approach may be of some use to the experimentalists for the identification of various sources.

The investigation is next extended to traveling sources for both supersonic and subsonic cases. Possible applications of the results to excitation problems involving moving sources include rocket launching, solar eclipse, weather fronts, etc.

The ground effect becomes important when the sources are near the ground. In particular, we study the transient response of the atmosphere due to ground movement during an earthquake. Coupling between the seismic and the atmospheric waves will be discussed.

1. INTRODUCTION

One of the most important problems in the study of acoustic-gravity waves in the thermosphere is the source problem. Whether one is interested in the dynamics of the ionosphere or concerned with the effects of traveling disturbances on communication, it is essential that one knows where, when and how those waves are excited. Experimental and theoretical studies have suggested many possible generating mechanisms, such as nuclear detonation in the atmosphere (Dieminger, W. and Hohl, H., 1962; Obayashi, T., 1962; Wickersham, A. F., 1966), earthquakes (Davies, K., and Baker, D. M., 1965; Yuen, P. C., et. al., 1969), supersonic displacement of auroral arcs (Wilson, C. R., 1969), polar substorms (Davies, M. J., and da Rosa, A. V., 1969), tropospheric storms (Georges, T. M., 1968; Baker, D. M. and Davies, K., 1969), solar eclipse (Chimonas, G. and Hines, C. O., 1970) and many more. These various excitation mechanisms can be considered as one or a combination of the three types of sources: mass production, momentum production and energy production plus the effects of the boundary surface. In this paper, the transient excitation of acoustic-gravity waves in an isothermal atmosphere due to these three types of sources and the boundary effect will be studied in a very general fashion. Specific examples will be given with the emphasis on the dependence of the transient response on the various observable parameters.

In section 2 the problem is formulated in a general manner. Asymptotic techniques useful in obtaining far field expressions are reviewed briefly. The case of stationary source is treated in section 3 and some results are discussed. In section 4, the moving source problem is investigated. The ground effect and the coupling between ground movement and atmospheric waves are studied in section 5. Some conclusions are discussed in section 6.

2. GENERAL FORMULATION

Let us consider a stationary, non-rotating atmosphere made of inviscid ideal gas. The equations that govern the dynamics of this atmosphere are derived from the conservation laws and are given by

$$\begin{aligned} \partial \rho / \partial t + \nabla \cdot (\rho \vec{v}) &= q_1, \\ \rho (\partial / \partial t + \vec{v} \cdot \nabla) \vec{v} + \nabla p - \rho \vec{g} &= \vec{q}_2, \\ \rho^\gamma (\partial / \partial t + \vec{v} \cdot \nabla) (p \rho^{-\gamma}) &= (\gamma - 1) q_3, \end{aligned} \quad (1)$$

where ρ , p and \vec{v} are the density, pressure and velocity of the fluid particles respectively, γ is the ratio of specific heats and \vec{g} is the gravitational acceleration. q_1 , \vec{q}_2 and q_3 are respectively the rate of mass production per unit volume, the rate of momentum production per unit volume and the rate of heat production per unit volume. These source terms are generally functions of time and space and are assumed to be localized.

The equilibrium atmosphere is assumed to be isothermal with an exponential variation in density and pressure characterized by the scale height

$$H = T/mg = c^2/\gamma g \quad (2)$$

where T is the temperature in energy units, c is the speed of sound of this isothermal atmosphere.

To study small amplitude acoustic-gravity waves in the atmosphere, we apply the usual linearization procedure to (1) by writing

$$\rho = \rho_0 + \rho', \quad p = p_0 + p', \quad \vec{v} = 0 + \vec{v}' \quad (3)$$

where the second terms on the right hand side are the perturbed quantities. Substituting (3) into (1) and linearizing the resulting equations, a set of differential equations for the perturbed quantities are obtained. It can be expressed in matrix form

$$\mathcal{Q} \vec{F} = \vec{Q} \quad (4)$$

where the matrix operator is given by

$$\mathcal{Q} = \begin{bmatrix} \partial/\partial t & 0 & \partial/\partial x & \partial/\partial y & \partial/\partial z - 1/2H \\ 0 & \partial/\partial x & \partial/\partial t & 0 & 0 \\ 0 & \partial/\partial y & 0 & \partial/\partial t & 0 \\ g & \partial/\partial z - 1/2H & 0 & 0 & \partial/\partial t \\ -c^2\partial/\partial t & \partial/\partial t & 0 & 0 & (\gamma-1)g \end{bmatrix} \quad (5)$$

and the field vector \vec{F} and the source vector \vec{Q} are given by

$$\vec{F} = \begin{bmatrix} p'/\rho_0^{1/2} \\ p'/\rho_0^{1/2} \\ v_x/\rho_0^{1/2} \\ v_y/\rho_0^{1/2} \\ v_z/\rho_0^{1/2} \end{bmatrix} \quad \vec{Q} = \begin{bmatrix} q_1/\rho_0^{1/2} \\ q_{2x}/\rho_0^{1/2} \\ q_{2y}/\rho_0^{1/2} \\ q_{2z}/\rho_0^{1/2} \\ (\gamma-1)q_3/\rho_0^{1/2} \end{bmatrix} \quad (6)$$

Eq. (4) can be recast into the form

$$D(\nabla, \partial/\partial t) \vec{F} = \vec{S} \quad (7)$$

where $D(\nabla, \partial/\partial t)$ is a scalar operator

$$\begin{aligned} D(\nabla, \partial/\partial t) &= \det \mathcal{Q} \\ &= \partial^4/\partial t^4 - c^2(\partial^2/\partial t^2)(\nabla^2 - 1/4H^2) - \omega_b^2 c^2 \nabla_h^2 \end{aligned} \quad (8)$$

and $\nabla_h^2 = \partial^2/\partial x^2 + \partial^2/\partial y^2$ is the horizontal Laplacian,

$$\omega_b = (\gamma - 1)^{1/2} g/c \quad (9)$$

is the Brunt-Väisälä frequency.

\vec{S} in (7) is the equivalent source function given by

$$\vec{S} = \hat{\mathcal{Q}} \vec{Q} \quad (10)$$

where $\hat{\mathcal{Q}}$ is the adjoint operator of \mathcal{Q} .

The operator $D(\nabla, \partial/\partial t)$ in (8) is called the acoustic-gravity wave operator. We see that regardless of the type of source, the transient response of the isothermal atmosphere is governed by an equation of the type (7) and the boundary and radiation conditions. The transient response, therefore, depends on our ability to solve (7). Eq. (7) can be solved by the transform technique and the solution may be written formally as

$$\vec{F}(\vec{r}, t) = \frac{i}{2\pi} \int_{\Gamma} \vec{F}(\vec{r}, \omega) \exp(-i\omega t) d\omega \quad (11)$$

where

$$\vec{F}(\vec{r}, \omega) = \frac{1}{(2\pi)^3} \int \frac{\vec{S}(\vec{k}, \omega)}{D(\vec{k}, \omega)} \exp(i\vec{k} \cdot \vec{r}) d\vec{k} \quad (12)$$

and

$$D(\vec{k}, \omega) = \omega^2 (\omega^2 - \omega_a^2) - \omega^2 c^2 \{ (1 - \omega_b^2/\omega^2) (k_x^2 + k_y^2) + k_z^2 \} \quad (13)$$

$\hat{S}(\vec{k}, \omega)$ is the Fourier transform of the equivalent source function, and $\omega_a = c/2H$ is the acoustic cutoff frequency.

To satisfy the causality principle, the integration path Γ in (11) is taken parallel to the real ω -axis and above all singularities of the integrand.

Eq. (11) is the general solution for the excitation of acoustic-gravity waves in an isothermal atmosphere by arbitrary sources. The inverse transform in (11) and (12) in general are difficult and for most sources no closed form solutions are possible. In this paper, however, our main interest is the radiation field far away from the localized sources. For this case, asymptotic techniques are available to yield physically meaningful, simple and analytic expressions. In the following, several cases will be discussed.

3. STATIONARY SOURCES

We first consider the case where the sources are stationary. For this case, we can integrate (12) using the asymptotic method developed by Lighthill (1960). The technique makes use of the dispersion surface $D(\vec{k}, \omega) = 0$ in k -space. The normal to the dispersion surface indicates the direction of the group velocity (Lighthill, M. J., 1960). The asymptotic method is based on the idea that at any observation point \vec{r} far away from the source, the contribution to the radiation fields come only from those rays whose group velocity vector lie in the same direction as \vec{r} . Using this technique, a rather simple far-field expression for $\hat{f}(\vec{r}, \omega)$ in (12) can be obtained (Liu, C. H. and Yeh, K. C., 1971). Substituting this expression into (11), we are left with the ω -integration. Again, for far field, this integral can be evaluated using the saddle point technique (Felsen, L. R., 1969). The general results indicate that a high frequency spherical acoustic mode arrives at an observation point first. Some time later a cylindrical caustic at a lower frequency, say, ω_b less than ω_a arrives and then splits into two frequencies, the one with $\omega > \omega_b$ is called the buoyancy mode and the one with $\omega < \omega_b$ the internal gravity mode. From this instant on, the total response consists of all these three modes. As time increases, the frequencies of the three modes approach ω_a , ω_b and $\omega_c = \omega_b z/r$ respectively. Note that $z/r = \cos \theta$ where θ is the polar angle of the observation point in a coordinate system with the origin inside the source region. If the source is harmonic in time with frequency ω_s , then some time after the arrival of the acoustic precursor at the observation point, the main signal with frequency ω_s will arrive with the group velocity corresponding to ω_s . General expressions for the transient response at different time intervals were given by Liu and Yeh (1971). In particular, explicit expressions for the transient response due to impulsive point source were derived there (also see Cole, J. D. and Greifinger, C., 1969) and numerical computations were made for various cases. Fig. 1 shows a sample of the results. It can be seen from the figure that at any observation point, for large observation time, the total signal includes a dominant gravity mode with a smaller acoustic mode superimposed on it. Figs. 2 and 3 indicate that this is true in general. Fig. 2 shows the constant R_{GA} curves in $r - ct$ plane for $z = 300$ km, where R_{GA} is the amplitude ratio between the gravity mode and the acoustic mode. We see that for a given observation point (fixed r), the ratio R_{GA} increases as time increases. At a given time, the contribution from the acoustic mode is more important for a more distant observation point (larger r). Fig. 3 shows the same plot for R_{GB} , the amplitude ratio between gravity and buoyancy modes. The general behavior is about the same as for R_{GA} . However, we note that at a given observation point, at a given time, the amplitude of the buoyancy mode is the smallest of the three.

Therefore, at a given observation point, as time increases (for standard F-region parameters, the time corresponds to ct greater than $2r \sim 2.5r$), the gravity mode dominates the response. The frequency for this mode approaches $\omega_c = \omega_b z/r$ as t increases. Row (1967) has used this idea to interpret successfully the ionospheric traveling disturbance caused by nuclear detonation. Additionally, because of the range dependence of ω_c , it seems that certain information about the location of the source may be obtained by measuring the wave frequency at different observation points. However, great care should be exercised when one attempts to do such experiments. Since, depending on the range r and time t , the signal is at the different stages of the transient response, i.e., the frequency of the response may not coincide exactly with ω_c . Fig. 4 shows the variation of the wave frequency for gravity mode vs. the range r for $z = 300$ km and $ct = 5000$ km. The dotted curve is for $\omega = \omega_c = \omega_b z/r$. It is seen that for large r , the actual frequency may differ from ω_c by as much as 20%.

4. MOVING SOURCES

For sources that travel with constant speeds such that $\hat{S} = \hat{S}(\vec{r} - \vec{v}t, t)$, the general formula (11) can still be used. Asymptotic techniques are also available to obtain the far field response (Lighthill, M. J., 1967). In this section, however, instead of studying the general case, we shall concentrate on a traveling impulsive point source. In this case, a more direct approach is possible. This again may be thought of as the Green's function or propagator for the general case.

Consider an impulsive point source moving in the horizontal direction with a constant speed u . If the coordinate system is chosen such that the x -axis is along the trajectory of the source, then the equation for the Green's function after Fourier transform in time can be written as

$$\left\{ \frac{\partial^2}{\partial x^2} + \frac{\partial^2}{\partial y^2} + \frac{\omega^2}{\omega^2 - \omega_b^2} \frac{\partial^2}{\partial z^2} + \frac{\omega^2 (\omega^2 - \omega_a^2)}{c^2 (\omega^2 - \omega_b^2)} \right\} G = \frac{1}{uc^2} \delta(y) \delta(z) \exp(i\omega x/u) \quad (14)$$

The solution for (14) satisfying the radiation condition is given by

$$G(x, s, \omega) = \frac{i\sqrt{\omega^2 - \omega_b^2}}{4c^2 u \omega} H_0^{(1)}(\xi(\omega)s) \exp(i\omega x/u) \quad (15)$$

where $H_0^{(1)}(x)$ is the Hankel function of first kind of zeroth order. $s = (y^2 + z^2)^{1/2}$ is the radial distance from the trajectory of the source point and

$$\xi(\omega) = \frac{\sqrt{\beta^2 - 1}}{\beta c} \sqrt{\frac{(\omega^2 - \omega_a^2)(\omega^2 - \omega_c^2)}{(\omega^2 - \omega_b^2)}} \quad (16)$$

In (16), $\beta = u/c$ is the Mach number of the moving source and ω_1 is a characteristic cut-off frequency defined by

$$\omega_1 = \left(\frac{\beta^2 \omega_a^2 - \omega_b^2}{\beta^2 - 1} \right)^{1/2} \quad (17)$$

Inverse transforming (15) in ω , we obtain

$$G(x, s, t) = \frac{1}{8\pi} \frac{i}{c^2 u} \int_{\Gamma} \frac{(\omega^2 - \omega_b^2)^{1/2}}{\omega} H_0^{(1)}[\xi(\omega)s] \exp[-i\omega(t - x/u)] d\omega \quad (18)$$

This is the formal solution of the transient response due to a traveling impulsive point source. For far field such that S is large, asymptotic expression for the Hankel function can be used and the resulting integral can be evaluated by the saddle point method (Felson, L. B., 1969).

For sources traveling with supersonic speed such that $\beta > 1$, it is easy to show that the response is confined within a conical region trailing behind the source with the apex angle θ_a given by

$$\theta_a = \sin^{-1}(1/\beta) \quad (19)$$

This corresponds to the well known Cerenkov cone.

For this case, the cutoff frequency ω_1 is greater than ω_a . The transient behavior at an observation point within the cone is similar to that of the stationary case, with ω_1 playing the role of acoustic cutoff frequency. In general, three modes contribute to the signal. They are the same acoustic, buoyancy and gravity modes. As time increases, the frequencies of the modes approach ω_1 , ω_b and ω_c respectively. The asymptotic expressions for the different modes at various time intervals are rather complicated and will not be given here. Instead, we compare the amplitudes of the three modes at large times. The amplitude ratio between the gravity and the acoustic modes R_{GA} is given by

$$R_{GA} = \sqrt{(\beta^2 \omega_a^2 / \omega_b^2 - 1) / (\omega_a^2 / \omega_b^2 - 1)} (\tan \phi / \beta) \quad (20)$$

and is independent of time, where $\phi = \cos^{-1}(z/s)$.

Therefore, at a given observation height, the farther the observation point is away from the source, the smaller is the acoustic mode contribution to the total response. (We note that cases corresponding to $\phi = 0$ and $\pi/2$ are degenerate cases and should be treated separately from the beginning). For a given observation point, the ratio R_{GA} depends on the Mach number β . Fig. 5 shows the variation of $R_{GA}/\tan \phi$ as a function of β . The ratio increases as β increases and approaches a constant value $1/\sqrt{1 - \omega_b^2/\omega_a^2}$ for a large Mach number.

The variation of R_{GB} , the amplitude ratio between the gravity and buoyancy modes, is depicted in Fig. 6. Here, constant R_{GB} curves are plotted in the ct_1 - s plane, where $t_1 = t - x/u$. At a given observation point, the larger t is, the greater is the ratio R_{GB} . In general, buoyancy mode is very small as compared with the gravity mode. The ratio R_{GB} does not depend on the Mach number β .

Next, we consider the case where the source moves with a subsonic speed. For this case, $\beta < 1$ and $\omega_1 < \omega_b$. There is no Cerenkov cone. For β close to 1, only two modes (gravity and buoyancy) are present in the response. The acoustic mode is not excited. For even smaller β , there are three modes with asymptotic frequencies approaching ω_1 , ω_b and ω_c respectively. The analysis is the same as for the case $\beta > 1$. Fig. 7 shows R_{G1} as a function of β , where R_{G1} is the amplitude ratio between the gravity mode and the mode at ω_1 . We note that when the source moves very slowly, the gravity mode is by far the

most dominant component of the response.

5. THE GROUND EFFECTS

The above discussion can be extended to include the effects of the ground. The major modification will be the additional contribution from a reflected wave and a surface wave. Their transient behavior may be evaluated in the same manner as indicated above. A more interesting problem is the excitation of acoustic-gravity waves by ground movements. In the following, a simple model will be used to investigate this problem.

We start by considering (7) for the component F_z , which is related to the vertical component of the velocity. Assume that there is no source so that $S_z = 0$. The movement of the ground is taken into account as the boundary condition.

Assume that the ground moves according to the equation

$$z = z_0 \cos k_1 (x - ut) H[k_1 (ut - x)] \quad (21)$$

where $H(x)$ is the unit step function, k_1 and u are the wave number and the phase velocity of the surface wave on the ground respectively. This movement of the ground forces the atmosphere into motion and since z_0 is small in comparison with the wavelength of the acoustic-gravity wave, we can write approximately at $z = 0$.

$$v_{z0} = \left. \frac{dz}{dt} \right|_{z=0} \quad (22)$$

where z is given by (21).

This is the required boundary condition for eq. (7) for the vertical component of the velocity. The solution may be obtained by the transform technique and we have, formally,

$$v_z(\vec{r}, t) = \frac{z_0}{2\pi} \exp(z/2H) I \quad (23)$$

Here I is an integral defined by

$$I = \int_{\Gamma} \frac{\omega^2}{\omega^2 - k_1^2 u^2} \exp\{-i[\omega t_1 - \xi(\omega)z]\} d\omega \quad (24)$$

where

$$\xi(\omega) = \sqrt{(\beta^2 - 1)(\omega^2 - \omega_1^2)}/\beta c \quad (25)$$

and ω_1 is given by (17), and $t_1 = t - x/u$.

The integral (24) can be evaluated by the saddle point method. For $\beta > 1$, it can be shown by closing the contour of integration in the upper half ω -plane that signal can only be found within a certain region above the ground. For a given t , the boundary of that region in the x - z plane is defined by the straight line

$$x + \sqrt{\beta^2 - 1} z = ut \quad (26)$$

which is above the ground and trailing behind the front of the surface wave on the ground. The apex angle of this boundary is given by $\sin^{-1}(1/\beta)$.

At any observation point, a high frequency precursor arrives first. Then at the time

$$t_0 = [x + z\sqrt{\beta^2 - 1}/\sqrt{1 - \omega_1^2/k_1^2 u^2}]/u \quad (27)$$

the main signal with frequency $\omega = k_1 u$ arrives. The asymptotic expressions at each time interval can be derived from (24) but will not be given here. For $t > t_0$, the main signal dominates and is given by

$$v_z(\vec{r}, t) \sim k_1 z_0 u \exp(z/2H) \sin[\sqrt{\beta^2 - 1} \sqrt{k_1^2 u^2 - \omega_1^2} z/u + k_1 (x - ut)] \quad (28)$$

We note that for the wave to propagate upward, $k_1 u$ must be greater than ω_1 . For $\beta > 1$, we have seen that $\omega_1 > \omega_p$. This means that the excited wave is in the acoustic branch. Experimental evidence has shown that traveling ionospheric disturbances can be related to the traveling seismic waves on the surface of the earth (Yuen, P. C. et. al., 1969). As a numerical example, we consider the wave excited by a Rayleigh wave of period 25 seconds and speed 3.9 km/sec. The ground moves 5mm ($z_0 = 5\text{mm}$). For these parameters, the corresponding v_z at a height of 150 km is approximately 30m/sec.

6. CONCLUSION

We have seen in this paper that the excitation of acoustic-gravity waves in an isothermal atmosphere by various sources can be treated in a unified fashion. In our approach the atmospheric response to any source is described by the differential equation (7) with a gravity wave operator given by (8). Since the gravity wave operator is a

differential operator with constant coefficients, the problem can be formally solved by the transform technique. As is usually the case in the transform technique the inversion can be difficult and for our problem it is not possible to do it in general. However, asymptotic methods can be used if radiation fields are interested. Three examples are considered to illustrate the technique. They are: (i) localized stationary source, (ii) moving point source, and (iii) coupling with traveling seismic waves.

When the source is localized, impulsive and stationary the large-time radiation field is composed of three components: acoustic mode, buoyancy mode and gravity mode. Relative magnitudes of these three components are examined. It is shown that the largest component in the radiation zone is given by the gravity mode. As time increases the total response can be described as essentially given by the low frequency gravity component modulated by the high frequency acoustic component. The buoyancy mode is least important.

Acoustic-gravity waves can be generated when the source is in steady motion. When the source travels with a supersonic speed, the radiation is confined within a characteristic Cerenkov cone trailing behind the source. For an impulsive point source, three modes are excited, with gravity mode having the largest amplitude. Due to motion the acoustic mode has a characteristic frequency modified by the Mach number. The radiation is still possible if the source is subsonic. In this case the Cerenkov cone is absent and the acoustic mode is not excited.

The presence of solid ground introduces additional complications in the radiation problem. The ground may reflect the wave and it may also guide the wave. When the ground is forced into motion it may also excite atmospheric waves. Following an earthquake the traveling seismic waves may couple energy into the atmosphere and this energy can be carried away to the thermosphere in the form of waves. Since Rayleigh waves have periods of the order of 25 seconds, the excited waves are all in the acoustic branch. Because of the exponential growth factor with height, a small ground movement may give rise to detectable perturbations in the ionosphere. As an example, it is shown that a 5mm movement on the ground can excite a wave which has an associated air parcel velocity 30 m/sec at a height of 150 km.

It is interesting to point out that these different excitation mechanisms can excite waves with different characteristic frequencies. Therefore, experimental determination of these characteristic frequencies can yield information not only about the nature of excitation but also about certain physical parameters of interest such as distance to the source, velocity of sound, etc.

ACKNOWLEDGEMENT

This research was supported by the Atmospheric Sciences Section, National Science Foundation, NSF Grant GA13723.

REFERENCES

1. Baker, D. M. and Davies, K., 1969, "F2-Region Acoustic Waves From Severe Weather", *J. Atmos. Terr. Phys.* **31**, 1345-1352.
2. Chimonas, G. and Hines, C. O., 1970, "Atmospheric Gravity Waves Induced By A Solar Eclipse", *J. Geophys. Res.* **75**, 875.
3. Cole, J. D. and Greifinger, C., 1969, "Acoustic-Gravity Waves From An Energy Source At The Ground In An Isothermal Atmosphere", *J. Geophys. Res.* **74**, 3693-3703.
4. Davies, K. and Baker, D. M., 1965, "Ionospheric Effects Observed Around The Time of The Alaskan Earthquake Of March 28, 1964", *J. Geophys. Res.* **70**, 2251-2253.
5. Davis, M. J. and da Rosa, A. V., 1969, "Traveling Ionospheric Disturbances Originating In The Auroral Oval During Polar Substorms", *J. Geophys. Res.* **74**, 5721-5735.
6. Dieminger, W. and Hohl, H., 1962, "Effects Of Nuclear Explosions On The Ionosphere", *Nature* **193**, 963-964.
7. Felsen, L. B., 1969, "Transients In Dispersive Media", *IEEE Transactions on Antenna and Propagation*, AP-17, 191-200.
8. Georges, T. M., 1968, "HF Doppler Studies of Traveling Ionospheric Disturbances", *J. Atmos. Terr. Phys.*, **30**, 735-746.
9. Lighthill, M. J., 1960, "Studies On Magneto-hydrodynamic Waves And Other Anisotropic Wave Motions", *Phil. Trans. Roy. Soc. (London)*, ser. A., **252**, 397-430.
10. Lighthill, M. J., 1967, "On Waves Generated In Dispersive Systems By Traveling Forcing Effects, With Applications To The Dynamics Of Rotating Fluids", *J. Fluid Mech.* **27**, 725-752.
11. Liu, C. H. and Yeh, K. C., 1971, "Excitation Of Acoustic-Gravity Waves In An Isothermal Atmosphere", *Tellus*, **23**, 150-163.
12. Row, R. V., 1967, "Acoustic-gravity Waves In The Upper Atmosphere Due To A Nuclear Detonation And An Earthquake", *J. Geophys. Res.*, **72**, 1599-1610.
13. Wickersham, A. F., 1966, "Identification Of Acoustic-gravity Wave Modes From Ionospheric Range-time Observations", *J. Geophys. Res.* **71**, 4551-4555.
14. Wilson, C. R., 1969, "Infra-sonic Waves From Moving Auroral Electrojets", *Planetary And Space Science* **17**, 1107-1120.
15. Yuen, P. C., Weaver, P. F., Suzuka, R. K. and Furumoto, A. S., 1969, "Continuous, Traveling Coupling Between Seismic Waves And The Ionosphere Evident In May, 1968 Japan Earthquake Data", *J. Geophys. Res.* **74**, 2256-2264.

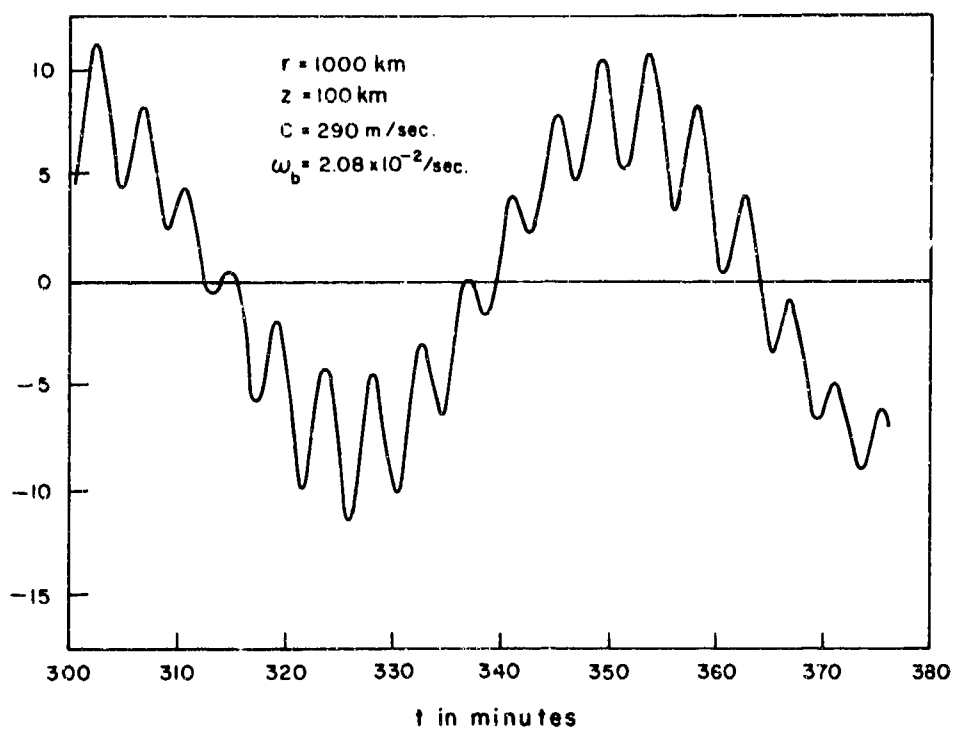


Fig.1 The response of the atmosphere due to stationary impulsive point source at large time. The total response is essentially the gravity modes modulated by the acoustic mode.

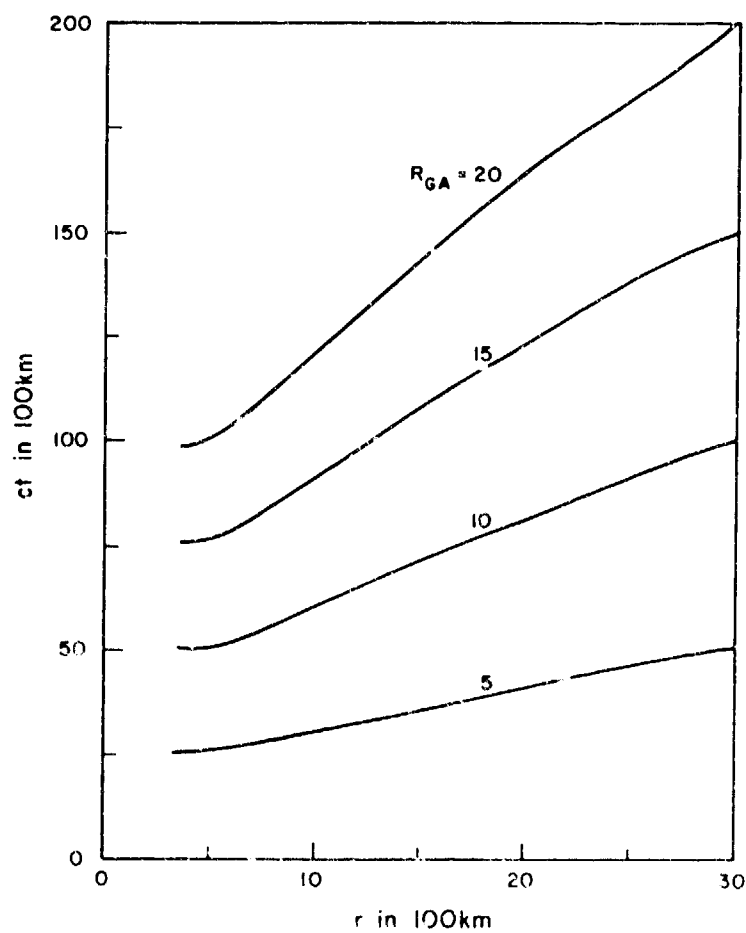


Fig.2 Amplitude ratio of gravity and acoustic modes for stationary source, $z = 300 \text{ km.}$

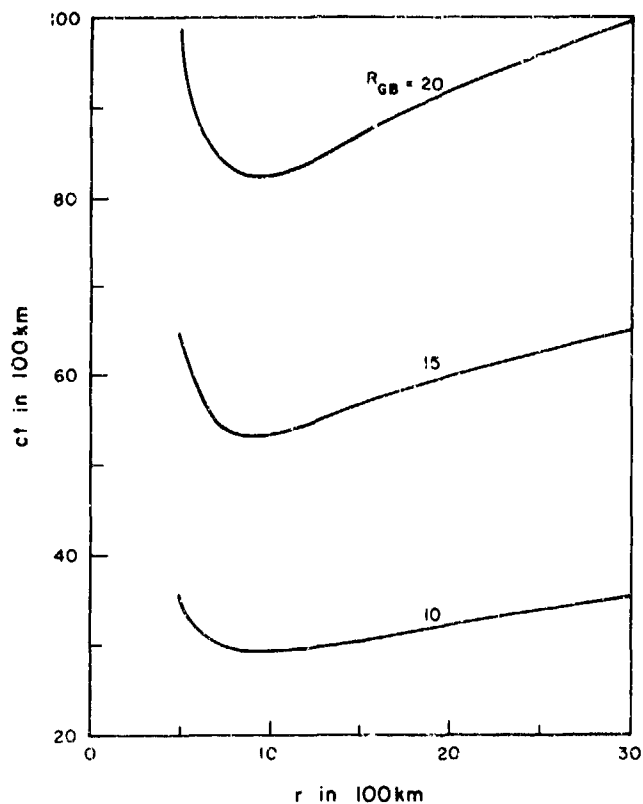


Fig.3 Amplitude ratio of gravity and buoyancy modes for stationary source for $z = 300$ km,

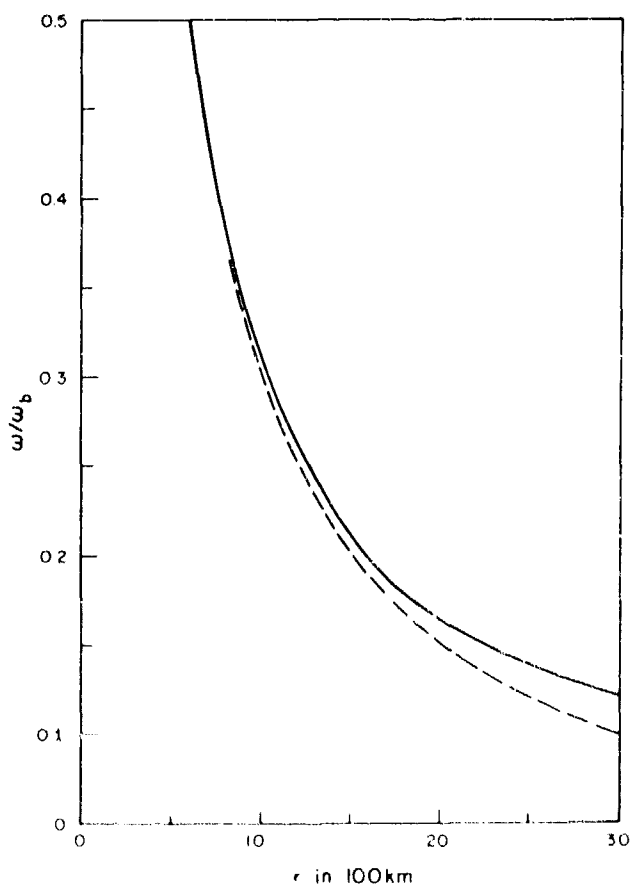


Fig.4 Frequency of the gravity mode as a function of r for stationary source for $z = 300$ km, $ct = 5000$ km.

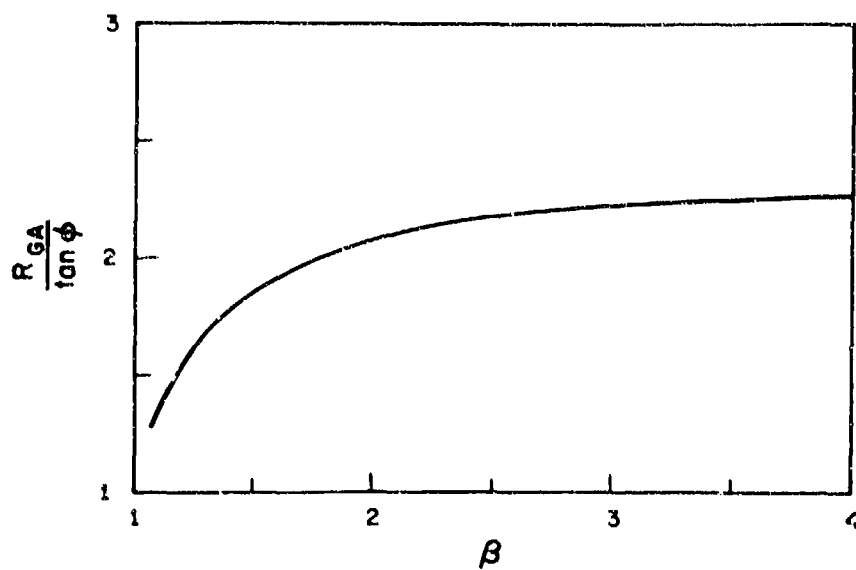


Fig.5 Variation of the amplitude ratio of gravity and acoustic modes with respect to Mach number for supersonic traveling source.

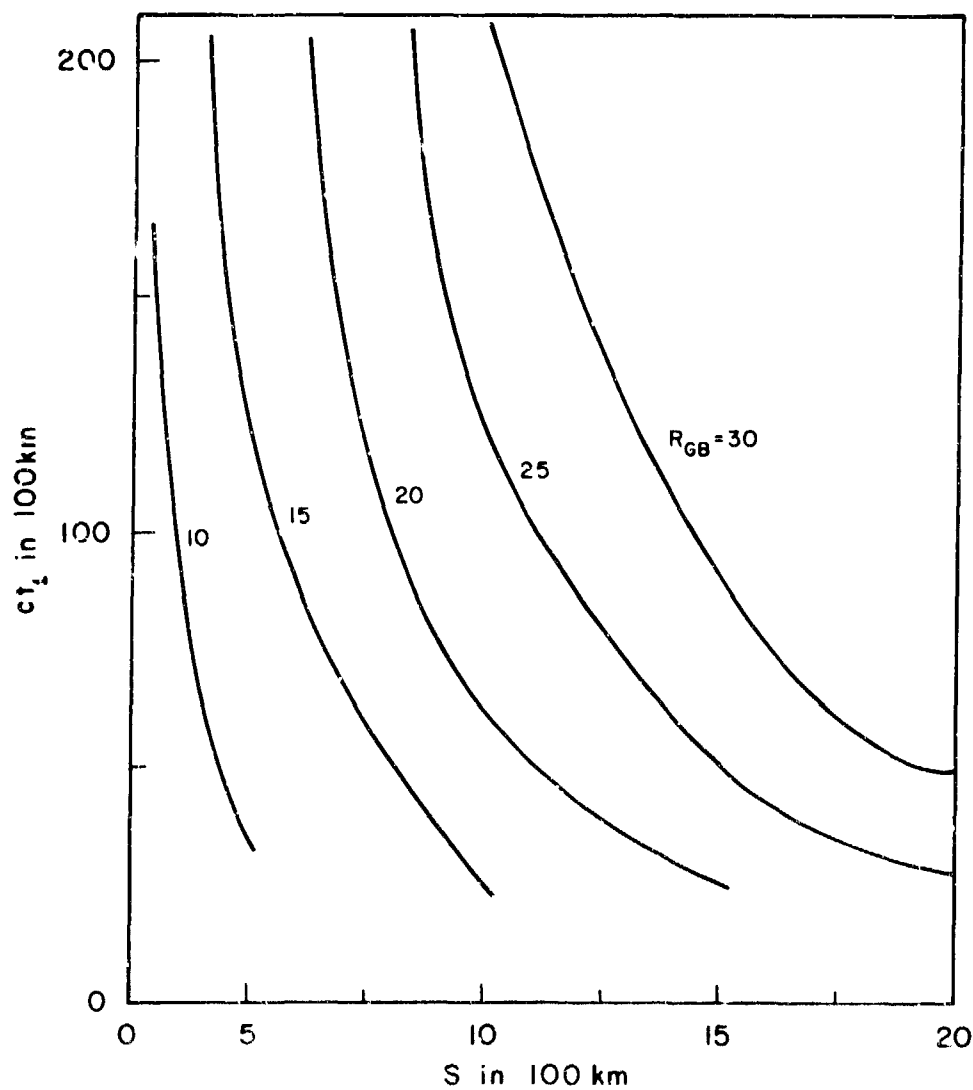


Fig.6 Amplitude ratio of gravity and buoyancy modes for traveling source, $z = 200 \text{ km}$.

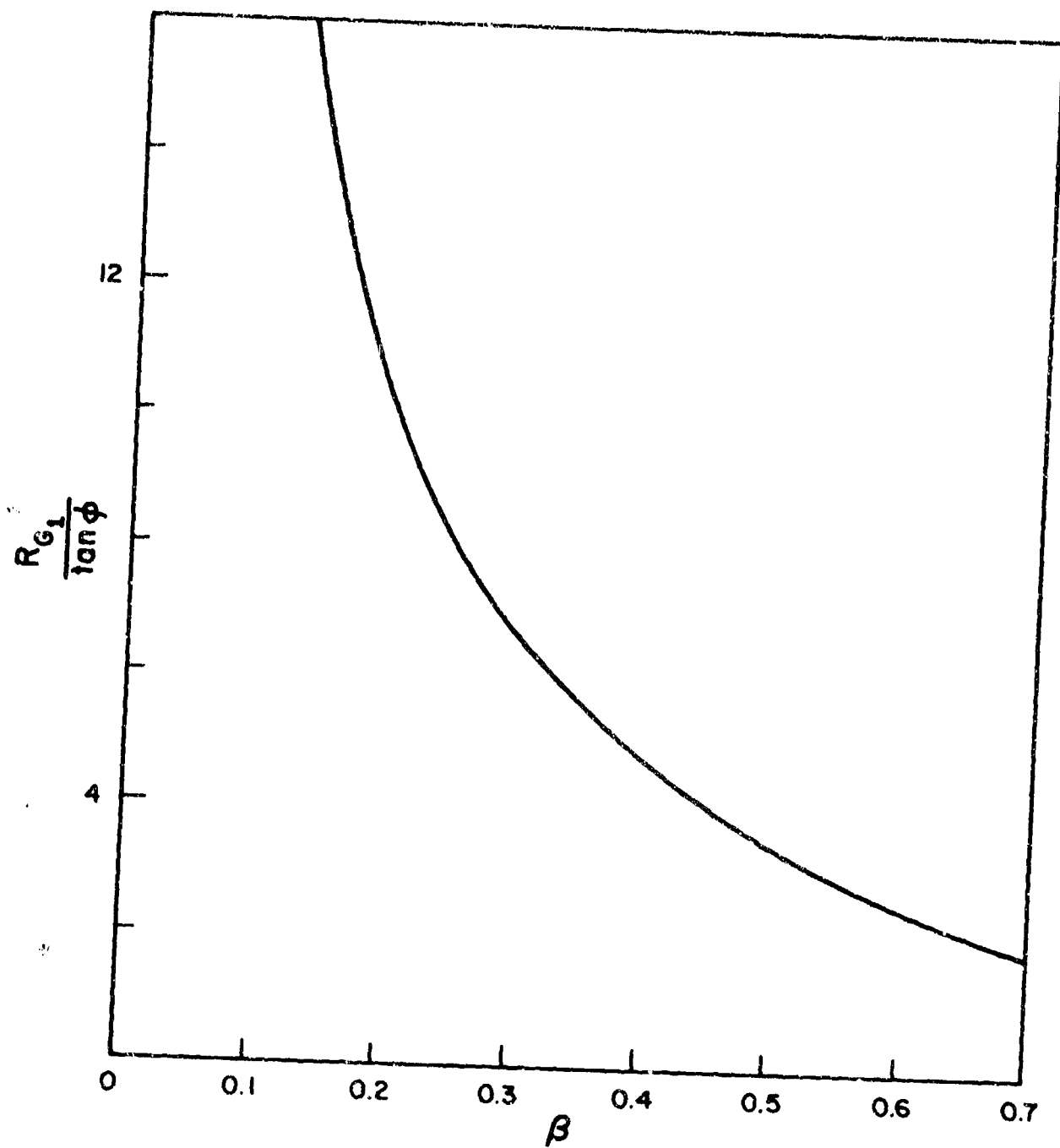


Fig.7 Variation of the amplitude ratio of gravity mode and ω_1 mode with respect to Mach number for subsonic traveling source.

DISCUSSIONS ON THE PAPERS PRESENTED IN SESSION I A
(Acoustic gravity waves in the neutral terrestrial atmosphere, Natural sources and propagation)

Discussion on paper 1 : "Some analogies between the propagation of ionospheric radio waves and acoustic-gravity waves", by K. DAVIES.

Dr. R.K. COOK : The author describes acoustical waves which occur at frequencies higher than the atmospheric resonant frequency, and acoustic-gravity waves which occur at frequencies lower than the Väisälä-Brunt frequency in an isothermal atmosphere. There is a third mode for sound propagation, the Lamb wave, which occurs at all frequencies, including those between the resonant and Väisälä-Brunt frequencies. The Lamb wave propagation is in a direction parallel to the earth's surface. Later papers in this meeting discuss its significance for the propagation of sound over global distances in the atmosphere, at infrasonic frequencies.

Dr. K. DAVIES : I was referring to internally propagating waves only.

Discussion on paper 2 : "3 D Ray tracing for acoustic-gravity waves", by T.M. GEORGES.

Dr. R.K. COOK : Ray-tracing techniques show clearly the non-reciprocal character of sound propagation in a windy atmosphere. This is true also for electromagnetic wave propagation in a moving material medium ; the reciprocal theorem does not hold. In 19th century language, the "ether" is partially dragged along by the moving medium, the relative velocity being dependent on the index of refraction of the material medium. In the windy atmosphere, the departure from reciprocity is relatively much less for electromagnetic waves than for sound waves.

Even with no wind, but with a steady magnetic field present in a material medium, the propagation of electromagnetic waves is non-reciprocal. This occurs because the component of the magnetic field which is parallel to the direction of propagation causes a rotation of the plane of polarisation (the Faraday rotation) directly proportional to the strength of the magnetic field.

Prof. A.D. PIERCE : Possible instances of cases when ray tracing techniques to predict wave amplitudes become inapplicable is at points or loci of points (caustics) where adjacent rays intersect.

Dr. T.M. GEORGES : Although pure geometrical acoustics fails at caustics, several apparently successful techniques have been developed to "patch-up" ray-tracing programs with full-wave and / or phase-integral calculations of field strength at places where flux-tube arguments break down. These techniques have potential for greatly enhancing the utility of ray techniques.

Discussion on paper 1 by K. DAVIES and paper 2 by T.M. GEORGES.

C.F. P. HALLEY : Commentaires 1. Dans les théories magnétoionique d'une part et acoustique et de gravité d'autre part, on obtient pour l'onde plane une équation de dispersion et une équation qui fournit la direction du rayon. Lorsque les milieux de propagation sont au repos, il est facile de voir, sur les équations, que les chemins sont réciproques. La non-réciprocité des chemins lorsque le milieu ionisé ou neutre est animé d'un mouvement de translation, uniforme dans chaque stratification, est assez fictive et revient à un simple changement de repères. Cet effet de non-réciprocité est pratiquement toujours négligeable pour les ondes électromagnétiques se propageant dans l'atmosphère ionisée.

2. La différence importante par les complications qu'elle crée est, semble-t-il, la suivante. Pour les ondes acoustiques ou acoustiques et de gravité, on peut considérer un modèle simple sphérique puisque le champ de gravité est homocentrique. Il en résulte des trajectoires planes et des symétries. Par contre, pour les ondes électromagnétiques, le champ magnétique terrestre qui n'est pas homocentrique complique le modèle. Les trajectoires sont gauches et dissymétriques en général. Enfin, de l'effet Faraday résulte la non-réciprocité de polarisation.

Dr. K. DAVIES : In the case of acoustic gravity waves propagating in a moving dispersive atmosphere some non-reciprocal effects may arise. Going downwind the intrinsic frequency is $\omega - k U$ where ω is the wave frequency, k the propagation number and U the wind. Upwind the intrinsic frequency is $\omega + k U$. Hence there may well be non-reciprocal propagation.

Dr. T.M. GEORGES : Ray-path reciprocity requires that a medium's refractive index everywhere remain invariant with respect to a 180° reversal of wavevector direction. Such is not the case for acoustic (and consequently acoustic-gravity) waves in a moving fluid. Therefore the acoustic ray path from point a to point b in a moving fluid differs from the path from b to a . For electromagnetic waves in a stationary magnetoplasma, refractive index does not change upon wavevector reversal ; therefore, electromagnetic ray paths in such a medium are reciprocal. Observed amplitude non-reciprocities in VLF waveguide are apparently due to anisotropy of the loss (absorption) on reflection from the upper waveguide boundary (the D region).

Discussion on paper 1 : "Generation and propagation of sound waves between the ionosphere and the lower atmosphere", by R.K. COOK.

Dr. Ch.R. WILSON : Observations of auroral infrasonic waves show that the generation mechanism is asymmetric with respect to the direction of motion of the supersonic aurora relative to the direction of the E region electric field. Therefore Lorentz force and not heat is probably the source of the pressure jump within the aurora, as described in paper 6.

Your suggestion that the upward propagating shock wave has a negative phase may explain the frequent observation of negative AIW in that the upward propagating shock would be refracted back to the ground by the thermosphere.

Prof. R.K. COOK : The analysis of this paper establishes a relationship between the strength of a heat source (an auroral discharge) moving at supersonic speed through the ionosphere, and the strength (pressure jump observed at ground level) of the weak shock produced by the source. There are certainly other mechanisms (in addition to heating) which might produce weak pressure shocks having a supersonic horizontal trace velocity as observed at ground level. Definitive data on the heating rate during an auroral discharge would, when available, lead to a good estimate for the pressure jump.

The question of the asymmetry of appearance of pressure jumps, vis-à-vis the direction of motion of supersonic auroral forms, seems to be still open in view of the observations reported by Liszka later on during this meeting.

Dr. Ch.R. WILSON : Dr. Liszka has stated that he has not observed the transient auroral bow wave type signals which are the ones that show the asymmetry described.

Dr. A.D. PIERCE : The inference in this paper is evidently that the infrasonic oscillations as observed at College, Alaska, during auroral activity may actually be small-amplitude shocks. Would such shocks be audible to someone on the ground ?

Dr. R.K. COOK : The observed values of the pressure jumps caused by auroral supersonic motions are approximately 1.0 N/m^2 . Such jumps are probably too weak to be audible to a casual observer, unattentive and in the presence of ambient noise. Since the jump ($\approx 10^{-5}$ atmosphere, a small-amplitude shock) is well-aged after propagation over distances of the order of tens of kilometers, its rise time is of the order of one second. Therefore it would be inaudible. The situation is quite different with respect to a sonic boom generated by the supersonic flight of aircraft. The pressure jump is typically 100 N/m^2 (a small-amplitude shock nonetheless), with a rise time of the order of only a few milliseconds. The boom is quite audible even to an unattentive observer, and usually startles and annoys him.

Discussion on paper 4 : "A model for acoustic gravity wave excitation by buoyantly rising and oscillating air masses" by A.D. PIERCE.

Dr. B.L. MURPHY : (1) For a supersonic fireball the fireball dimensions may be expected to be comparable with a scale height. Thus, rather than radial oscillations due to the greater than ambient pressure, venting at the top would seem more likely.

(2) $\frac{1}{2} E$ is not the available energy for wave generation : $\frac{1}{2} M V^2$ would be a better estimate where M is the fireball mass plus Darwin's virtual mass and V is the initial rise velocity. This is the order of a few times $10^{-3} E$ for megaton yields.

Prof. H. VOLLAND : What is the physical meaning of the drag force ?

Dr. A.D. PIERCE : The drag force has been inferred from experimental observations of Scover and of Turner, so its underlying physical mechanism is not well understood. My present guess is that the apparent drag arises because the flow around the bubble or fireball is not laminar. The wake and backside of a mushrooming cloud is turbulent. Perhaps the energy lost due to drag actually reappears as the kinetic energy of the turbulent wake.

Discussion on paper 2 : (Validity of WKB approx. and Ray tracing).

Prof. H. VOLLAND : Dr. Georges, can you comment on the range of validity of ray-approximation for acoustic-gravity waves ?

Dr. T.M. GEORGES : The question of the "range of validity" of ray theory vis-à-vis the WKB criterion must be answered in two parts : one has to do with the accuracy of the ray-path calculation itself, and the answer is that one can always compute the ray path (i.e., the path satisfying Fermat's Principle for some initial conditions) to any desired accuracy for any wave in any medium, even if the WKB criterion is grossly violated. This fact is apparently not widely appreciated. The second answer has to do with how one interprets ray paths ; i.e. the adequacy of the ray picture for describing real wave phenomena. This answer must be a lot more fuzzy because "adequacy" obviously depends a great deal on what wave phenomena one is interested in. Ray theory obviously fails to predict wave amplitude when significant partial reflections occur, in the vicinity of caustics or turning points, or when waves travel multiple paths (as in wave guides), even when WKB is satisfied. On the other hand, WKB seems to be much too stringent a criterion if one is interested in where wave energy goes in a gross sense, or in reflection heights of VLF radio waves or internal gravity waves in the atmosphere, for example. Simultaneous ray and full-wave calculations give very similar results in many cases in which the WKB criterion would predict a breakdown of ray theory. Clearly, then, a lot more work remains in determining when one needs to "doctor" ray-path calculations to account for purely wave-like effects. At present it seems safe to say that no one really knows exactly how to assess ray theory except by direct comparison with full-wave results. Like any other tool, it goes without saying, one has to know when to use it when not to.

Discussion on paper 5 : "Acoustic gravity waves and diffusion effects at the atmospheric boundaries", by Prof. F. WARRER.

Dr. C.M. LIX : In the discussion of critical layer, I might add one point. That is, when the wave approaches the critical layer, the phase speed approaches zero in the moving system. Here, the non linear effects in the sense of "long waves" may become important. There is a recent paper by Breeding in J. Fluid Mech. showing some numerical computed results. For some cases, non-linear effects indeed are appreciable.

Prof. F. WARRER : The non-linear terms are undoubtedly important in some cases, but here the time scale envisaged is such that these terms are not likely to be important. Theoretical results to date give an indication of the transient development of a broad banded excitation in a non linear dispersive system. Some authors suggest the existence of a cat's eye pattern in certain cases, while Breeding's results would be invalid if turbulence developed. This latter wave-breaking mechanism as in Thorpe's experiments is probably the relevant one for the real atmosphere. Thus if non linear terms are important, then the first requirement is a stability theorem e.g. a non linear Howard's Theorem.

Discussion on paper 6 : "Auroral infrasonic wave generation mechanism", by Dr. C.M. WILSON.

Dr. O. HOLT : I would like to suggest the $E \times B$ plasma instability as a possible alternative mechanism for the generation of AIW from moving auroral forms. The instability requires a strong gradient in the plasma density, of direction opposite to the electric field. During stable conditions, diffusion will act to smooth out the gradient, but for an auroral form in supersonic motion, this is not possible. The spectrum of plasma waves caused by the instability will travel along the front of the arc, and their energy might be transferred to the neutral gas. Qualitatively, this is in agreement with the asymmetry of northward and southward motion observed by Wilson. Quantitatively, I do not know.

Dr. Ch. WILSON : I am not familiar with the $E \times B$ plasma instability but can only say that any mechanism must produce a pressure pulse that is of constant phase in the moving frame of reference of the aurora. At this time I can not see how waves traveling along the arc itself could be the source of a bow wave that is traveling transverse to the arc. One should certainly explore all possible mechanisms however.

Prof. H. VOLLAND : Obviously, your excitation mechanism due to momentum coupling will work only within a small frequency range. Can you specify this spectral range ?

Dr. Ch. WILSON : The period of the bow wave is approximately equal to L/V_A where L is the width of the arc and V_A is its supersonic velocity of translation perpendicular to its long axis. If the ionisation collection process is taking place, then L will be less than the width of the arc depending on the Mach number of the arc. These considerations restrict the period range for the mechanism from about 1 sec to 100 sec.

Prof. H. VOLLAND : The meridional electric field component should become zero around local midnight within the auroral oval. Can you relate your observed reduced activity of acoustic wave energy during midnight with such behaviour ?

Dr. Ch. WILSON : Yes, there is a decrease in the auroral infrasonic wave activity around local magnetic midnight that is probably related to the decrease in the strength in E around that time.

Discussion on papers 6 and 7

Prof. H. VOLLAND : There appears to exist a discrepancy between the results of Wilson and Liska. In Wilson's results, acoustic wave propagation from the south is excluded, which Wilson explains by the excitation mechanism within the auroral electrojet. This anisotropy is not seen in Liska's results. What is the reason for this discrepancy ?

Dr. Ch. WILSON : It is not correct to say that a discrepancy in our observations exists when one does not know for certain that Liska's observations at 2 Hz and nine in the passband from 0.1 to 0.01 Hz are both due to the same mechanism. My results concerning AIW refer only to bow waves due to supersonic motions of large scale electrojet auroras. There probably are other mechanisms which produce infrasonic waves in the aurora in a different frequency region such as direct heating from auroral particles during pulsating aurora or two-stream plasma instability to produce ion-acoustic waves in auroral arcs in the high frequency region with $f > 0.1$ Hz and in the long period region with $T > \text{Bruno period}$. Joule heat loss in the electrojet probably produces internal gravity waves with a time scale the order of the substorm rise-times of say 5 to 10 minutes.

It would be incorrect to assume that the process that I propose is the only one operating throughout the entire acoustic-gravity wave spectrum. It is just as incorrect to assume that all infrasonic radiation from the aurora is due to the same excitation mechanism as it would be to say that all the electromagnetic radiation from the aurora is from the same process.

Prof. R.K. COOK : It is quite possible that Wilson (in Alaska) and Liska (in Kiruna) are measuring the same acoustical waveform, both generated by auroral motions at supersonic speeds. But the substantial differences in their graphic recordings come about from the quite different impedance functions (different filtering) of their respective electroacoustical apparatuses. The apparatus will give the correct time (to within a few seconds for Wilson's apparatus at which a transient sound pressure starts, but the subsequent recorded waveform depends strongly on the indicial admittance (associated with the impedance function) of the apparatus. The "true" waveform of the sound pressure is in principle obtainable by convolving (mathematically) the recorded waveform with the indicial admittance. When this is attempted, though, the presence of noise makes it very difficult to arrive at the true waveform of the incident sound pressure of the au-

ral infrasound.

Dr. LISZKA : There are at least two further reasons which may explain apparent differences between results of Dr. WILSON and mine :

1. It may be seen, when making ray-tracing for specific wind and temperature profiles, that the propagation of waves in the minute range (as those observed by Dr. WILSON) is quite different from that obtained for infrasound in the Hz-region. The closer the wave frequency to the acoustic-cut off, ω , the larger will be differences in propagation paths with respect to the infrasound in the Hz-range.
2. As we in Kiruna are using the phase detection technique, the sensitivity of our equipment is much larger than that of Dr. WILSON. So we are looking on signals which are at least one order of magnitude smaller than those observed by Dr. WILSON. It is therefore not surprising that there are some differences between infrasound observed in two different frequency ranges and with different thresholds of detection.

Discussion on paper 8 : "On waves generated by stationary and travelling sources in an isothermal atmosphere under gravity", by C.H. LIU and K.C. YEH.

Dr. A. PIERCE : Have you considered the possible extension of this theory to include the case when one is receiving waves at a time when one just starts to receive the gravity wave pulse ? As you know, there is a maximum group velocity for gravity waves between ω and ω_0 . The stationary phase approximation breaks down when one is receiving that frequency for which the group velocity is a maximum.

Dr. C.H. LIU : Yes, this is the point : the horizontal line $r = ck/r$ approaches the ω -curve at $\omega = \omega_0$. At this point, the ordinary method of saddle point breaks down. A modified method can be used. It is described for example in a paper by Felsen (IEEE Trans. G-AP.1969). The solution is in terms of Airy functions instead of the usual sine, cosine functions.

Dr. J. KLOTTERMEYER : Where shall mass production in the continuity equation come from ?

Dr. C. LIU : Our analysis assumes the source terms are known. The source model is not discussed here.

Prof. H. VOLLAND : Is it possible to discriminate between the various types of the excitation sources (mass, momentum or energy coupling) from a comparison between your theory and observations ?

Dr. C. H. LIU : We are beginning to look into this problem. This depends heavily on the form of the equivalent source term \tilde{S} , its spatial and temporal dependence.

Dr. N. RISHBETH : You assume that the group velocity of a wave observed at a point must be parallel to the straight line from the source to that point. This assumption must restrict your analysis to ranges much less than an earth radius, and will also fail at ranges for which waves reflected from the upper atmosphere can contribute to the observed signal.

Dr C.H. LIU : The model we used is a flat earth one. We can extend the discussion to include the curvature of the earth, the reflection, etc.. But the dispersion surface will be different. If the solution can be written formally as an inverse transform, then the asymptotic technique we discussed will still apply.

Discussion on papers 4 and 8 :

Dr. J. LOMAX : Dr. Pierce's paper shows a number of oscillations of the cloud about its stabilization altitude. Dr Liu's paper shows a transient response with sinusoidal oscillations for hundreds of minutes. As an experimentalist, I have not observed these undamped vibrations. My question is, have the authors ignored losses or damping for mathematical simplicity ?

Dr. C.H. LIU : The loss mechanisms certainly are very important. In the analysis, these loss effects may be taken into account. Also, even for the lossless case, the amplitude of the response decreases as the distance of the observation point and the observation time increase.

Dr. A. PIERCE : Loss mechanisms on acoustic-gravity wave propagation per se are generally negligible at low altitudes ; they become increasingly more important when a wave propagates at higher altitudes. The complexity they introduce into the analysis is so great that wave theorists tend to neglect them unless they believe these loss mechanisms would substantially alter their predictions. In many cases the quality of applicable data and the necessity of making many assumptions about the largely unknown ambient state of the atmosphere suggests that only a rough agreement of theory with experiment can be achieved, even were loss mechanisms incorporated into the theory. In such cases, the incorporation of loss mechanisms would seem an unnecessary refinement unless they are of major significance in interpreting the general qualitative characteristics of the data. Concerning the damping of the cloud oscillations, I believe any successful theory should incorporate wave damping. The theory presented here is still in a rudimentary state. It should be qualitatively correct if the cloud oscillates for several cycles before becoming sufficiently damped. Data concerning this seems to be largely unavailable, although laboratory scale experiments of Mc Laven and Murphy (to be published) at Mt. Auburn Research Associates suggest 2 or 3 complete cycles may be observed.

Dr. B. MURPHY : In the experiments mentioned by Dr. Pierce two main types of damping are present ; that due to lateral spreading of the cloud and that due to wave emission. The first type is treated theoretically in our paper, the second is not. Do nuclear clouds oscillate in a manner similar to the buoyant element in our laboratory ? That is a question that can only be answered by examining the nuclear test data and, unfortunately, I am unaware of any unclassified treatment of this problem.

Prof. F. WARREN : There are three further relevant comments which could be made.

- i) A uniformly stratified atmosphere might not be the appropriate model to use because of marked temperatures changes with height. A model with an inversion would be more useful in some cases.
- ii) In this latter case, theoretical attempts to solve a problem of damping by gravity waves (Stretenkii, Ursell, Warren and others) indicate that the ultimate decay of vertical motion of a solid buoyant object about the hydrostatic equilibrium level is monotonic e.g. like $(\text{time})^{-3/2}$ although oscillations do occur at earlier times.
- iii) Formulae for viscous or turbulent drag are probably unreliable for buoyant air masses because in this case no boundary layers exist.

Prof. F. WARREN : Certain comments might be made concerning certain results for lower atmospheric phenomena :

- i) Mountain lee waves can be important sources of gravity waves in the upper atmosphere.
- ii) Results concerning the effect of the Coriolis term (in the neutral atmosphere) have been considered by W. Jones and others.
- iii) Results of certain models of the fire ball problem indicate a monotonic decay.

Dr. B.L. MURPHY : (Comment iii)

I must call attention again to the question of what fireballs really do as opposed to what models do.

Dr. K. DAVIES : I agree with Dr. Warren that this has been done for the neutral atmosphere but should be verified for the combined neutral and ion gases.

ACOUSTIC-GRAVITY WAVES IN THE
NEUTRAL ATMOSPHERE AND THE IONOSPHERE

by

Nambath K. Balachandran

Lamont-Doherty Geological Observatory of Columbia University
Palisades, N.Y. 10964
USA

LES ONDES ACOUSTIQUES ET DE GRAVITE DANS L'ATMOSPHERE NEUTRE ET L'IONOSPHERE

par

N.K. Balachandran

Sommaire

On détecte les ondes acoustiques et de gravité produites par des explosions nucléaires à de grandes distances de leur point d'émission grâce à l'emploi de microbarographes sensibles, au sol, à l'emploi de la technique Doppler à hautes fréquences, aux altitudes ionosphériques, et à l'emploi des sismographes à longues périodes. On explique la dispersion des ondes acoustiques et de gravité au niveau du sol en faisant appel à la méthode du mode normal pour une atmosphère stratifiée. Dans le cas des ondes acoustiques et de gravité détectées au niveau du sol, les modes acoustiques à courte période (période inférieure à environ 2 minutes) présentent des amplitudes plus élevées que les modes de gravité à période longue (période supérieure à environ 2 minutes), lorsque les vents stratosphériques se déplacent dans la direction de propagation des ondes. Les modes de gravité ont des amplitudes plus élevées par vent de travers ou par vent vers le haut. Des enregistrements de perturbations ionosphériques effectués avec une sonde Doppler indiquent une prédominance des modes acoustiques de courte période sur les modes de gravité. Selon la théorie du mode normal, et la théorie des ondes de Lamb, la densité d'énergie, pour les ondes de période longue, décroît exponentiellement au fur et à mesure qu'on s'élève, et l'énergie est insuffisante pour provoquer des perturbations ionosphériques. Les ondes acoustiques à période courte sont dues à des modes partiellement canalisés dans la basse atmosphère, avec déperdition d'énergie vers l'ionosphère.

ACOUSTIC-GRAVITY WAVES IN THE NEUTRAL ATMOSPHERE AND THE IONOSPHERE*

Nambath K. Balachandran
Lamont-Doherty Geological Observatory of Columbia University
Palisades, N. Y. 10964
United States of America

SUMMARY

Acoustic-gravity waves from nuclear explosions are detected at large distances from the source by sensitive microbarograph on the ground, by high frequency Doppler technique at ionospheric levels and by long-period seismographs. The dispersion of acoustic gravity waves at the ground level is explained by using normal mode approach for a stratified atmosphere. For acoustic-gravity waves detected at the ground level, the short-period acoustic modes (period less than about 2 min.) have higher amplitudes than the long-period gravity modes (period more than about 2 min.) when stratospheric winds are in the direction of propagation of the waves. The gravity modes have higher amplitudes for cross-wind and up-wind propagation. Dopplersonde records of ionospheric disturbances show more predominance of shorter-period acoustic modes than the gravity modes. According to the normal mode theory and the Lamb wave theory, the energy density for long-period waves decreases exponentially with height from the ground, thus providing insufficient energy for ionospheric disturbances. The short-period acoustic waves are due to partially ducted modes in the lower atmosphere providing leakage of energy into the ionosphere.

1. INTRODUCTION

Acoustic gravity waves have been detected at ionospheric levels and at the ground level in the atmosphere. Donn and Ewing (1962a, 1962b) and Donn and Shaw (1967) have provided the records of pressure fluctuation at ground level due to acoustic gravity waves from nuclear explosions in the atmosphere. Baker (1968) and Baker and Davies (1968) have published records and studies of ionospheric disturbances produced by nuclear explosions in the atmosphere. The observations were made at Boulder, Colorado, using high frequency Doppler technique.

Acoustic gravity waves can also get coupled to the ground. Recently Savino and Rynn (1972) have reported detection of acoustic gravity waves from the Chinese nuclear test of Oct. 14, 1970, on a worldwide network of long period seismographs.

Acoustic gravity waves in the atmosphere get coupled to the ground through the mechanism of static loading. Since the amplitude of the coupled seismic wave is dependent on the wavelength of the atmospheric wave, slower moving disturbances in the atmosphere due to wind and density discontinuities have negligible amplitudes in comparison to faster moving acoustic-gravity waves. The seismic detection of acoustic gravity waves may be an effective way of filtering other atmospheric disturbances which may contaminate the microbarograph record. In this paper we will not go further into the mechanism of seismic coupling. Interested readers may refer to the recent paper by Savino et al (1972).

2. ACOUSTIC GRAVITY WAVES IN THE NEUTRAL ATMOSPHERE

In this paper we will be concerned with acoustic gravity waves whose energy is mainly channelled in the lower atmosphere (below an altitude of about 100 Km) with small amounts of energy leaking into the ionospheric heights to produce disturbances there. The stratification of atmospheric parameters causes dispersion of acoustic gravity waves and if the above argument about channelling is correct, a similar dispersion pattern should be observed both in the ground level pressure disturbance and the ionosphere disturbance produced by these waves.

Dispersion curves for observed ground level pressure disturbance due to acoustic gravity waves have been given by Donn & Ewing (1962a, b) and Donn and Shaw (1967). Extensive theoretical work has been done to explain the observed dispersion patterns. Most of the work has involved multi-layer atmospheric models and numerical solution of the perturbation equations. Theoretical barograms have been computed which agree with the observations.

The dispersion curves for observed pressure fluctuations due to acoustic gravity waves sometimes show, in addition to the most common normal dispersion when group velocity increases with increasing period, inverse dispersion when the group velocity

*Lamont-Doherty Geological Observatory of Columbia University Contribution No. 1799

decreases as the period of the waves increases. Examples of such dispersion curves are given in Fig. 1. It is not possible to explain this type of inverse dispersion if we use reasonable models of atmospheric temperature structure. But with the use of strong upper winds in the COSPAR atmospheric model it has been possible to explain the inverse dispersion. Winds of the order of 100 meters/sec in the direction of propagation of the waves, around an altitude of about 100 Km were employed. The theoretical dispersion curves along with the observed dispersion pattern for the Russian nuclear test of 5 Aug. 1962 is given in Fig. 2. As may be seen from Fig. 2, there is good agreement between the theory and observation.

A typical pressure record of acoustic gravity waves (Fig. 3) show two distinct groups of waves. The long-period group of waves (period more than about 2 min) may be classified as gravity modes and the short period group of waves (period less than about 2 min) may be classified as acoustic modes. We have found, after examining the pressure records from various nuclear tests, that the relative amplitudes of the gravity and acoustic modes show considerable variation. Pierce et al. (1971) have shown that the amplitude of the long-period waves depends only on the yield of the explosion and the distance of the recording station from the test site. The amplitude is independent of the variation of the atmospheric parameters along the path. The acoustic modes on the other hand are very sensitive to the atmospheric parameters, especially in the lower sound channel (below about 50 Km). The synthesized barograms given by Pierce et al (1971) is reproduced in Fig. 4 along with appropriate microbarograph records. According to this figure the amplitudes of the acoustic modes are much higher in the downwind direction in comparison with the amplitudes of the acoustic modes in the upwind direction. The amplitudes of the acoustic modes for cross-wind direction have intermediate values. The amplitudes of the gravity modes do not change with the change in the direction of propagation. It is concluded that when the direction of wave propagation is in the direction of the stratospheric winds, the lower sound channel is intensified thereby trapping more energy than in the case of upwind and cross-wind directions of propagation. During winter months, when strong stratospheric winds blow from the west in the middle latitudes, the acoustic modes in the pressure waves produced by nuclear tests in the Pacific and recorded at eastern United States have very high amplitudes, higher than the amplitudes of gravity modes. During summer when stratospheric winds are easterly, the acoustic modes have smaller amplitudes than the amplitudes of gravity modes. The cases for Russian nuclear tests in Novaya Zemlya can be interpreted in a similar fashion. A more complete study of this phenomenon including synthesized far-field infrasonic pressure fluctuation using actual temperature and wind data will be presented in a later paper (Donn and Balachandran, 1972). The knowledge about the variation in the amplitudes of the acoustic modes are important for ionospheric studies, because, as we will show later, the ionospheric perturbations are caused by these acoustic modes rather than by the longer period gravity modes.

3. ACOUSTIC GRAVITY WAVES IN THE IONOSPHERE

The main part of this paper will be concerned with an interpretation of the acoustic gravity waves from nuclear explosions observed at ionospheric heights. Many authors have reported about these waves, but we will be making special reference to the observations of ionospheric disturbances by high frequency continuous wave Doppler technique at Boulder, Colorado (Baker and Davies, 1968; Baker, 1968 and Baker and Cotten, 1971). Ionospheric disturbances from the Russian nuclear tests in Novaya Zemlya as well as U. S. tests in the Pacific, during 1961-62, have been reported. The arrival time of each ionospheric disturbance agrees with the appropriate group velocity for acoustic gravity waves ducted in the lower atmosphere. The authors of the paper cited above interpret the ionospheric disturbances as being caused by the energy of the acoustic gravity waves ducted in the lower atmosphere leaking into ionospheric levels. The authors have pointed out the similarities between the ground level pressure oscillations and the ionospheric disturbance; but some difficulties remain. The most prominent wave on the ground-level microbarograph record is, in general, a wave of period of about 5 minutes and the record contains waves of period from about 5 min. to about 0.5 min. The periods of waves observed in the ionospheric disturbances are in the range of about 2 min. to 0.5 min. Although one may expect the longer period waves, due to their higher wave length and thus less attenuation at higher elevations, to be present at ionospheric heights, these long-period waves are not prominent on the Doppler-sonde records. Also, there is a significant difference in the observable life-times of ionospheric and ground-level disturbances; the ground-level pressure disturbance lasting for a longer time than the ionospheric disturbance. Finally, following large nuclear tests the microbarographs have detected the wave which travelled directly from the explosion to the detector (the A1 wave), the wave which travelled to the detector along the longer route, passing through the antipode of the source (the A2 wave), the second passage of the direct wave after it has circled the globe (A3 wave), etc. But only the direct wave (A1) has been detected on the ionospheric records. We will try to answer these problems by studying the properties of the various modes which constitute the acoustic-gravity waves.

A good example of acoustic gravity waves in the neutral atmosphere and the ionosphere produced by nuclear tests is given in Fig. 5 (From Baker, 1968). As pointed

out by the author, the similarity between the waves in the ionospheric disturbance and the waves on the microbarograph records in their group velocities and frequencies are remarkable. The shorter duration of the waves on the Doppler sonde record may be noted. Also the present author believes that there are no waves on the Doppler sonde record which correspond to the first roughly four long-period waves on each of the microbarograph records. The long period waves seen on the ionospheric record prior to about 2230 UT are, according to the present author, in the background, similar to the waves seen on the record after about 2310 and that these waves are not connected with the nuclear test. Fig. 6 shows another case where waves of period about 300 sec are present on the microbarograph record but are absent on the Doppler sonde record. Both records show waves of period less than about 100 sec. Thus, although the microbarograph record contains waves with periods from about 300 to 30 seconds, the Doppler record shows only waves with periods less than about 100 sec. According to the terminology of Balachandran (1968), the microbarograph records show waves corresponding to gravity and acoustic modes for a multilayer atmosphere whereas the record of the ionospheric disturbance shows waves corresponding to the acoustic modes only. An explanation as to why gravity modes are not seen on Doppler records will be given later.

The similarity in the dispersion pattern of the microbarograph and the Doppler records is evident from Fig. 7. Fig. 7(a) shows the running spectrum analysis of the short-period part of the Poughkeepsie, N. Y. pressure record for the U. S. Nuclear test of Oct. 30, 1952. The diagram shows the variation of the spectral characteristics of the signal with time. It may be observed from the figure that the period of the waves gradually increases from about 60 sec. to about 90 sec. with time (this corresponds to inverse dispersion in group velocity) and then decreases from about 90 sec to about 50 sec (this corresponds to normal dispersion in group velocity). Fig. 7 (b) which is a running spectrum analysis for the record of ionospheric disturbance at Boulder for the same test, shows similar dispersion pattern; inverse dispersion from a period of about 60 sec to about 100 sec and normal dispersion from about 100 sec to about 60 sec.

So much for the similarities of the waves observed at ionospheric and ground levels. The absence of long-period waves on the records of ionospheric disturbance is explained below. Pfeffer and Zariwsky (1963) and Balachandran (1968) have shown that the long period waves observed at the ground level are governed by the quasi-horizontal parts of the theoretical dispersion curves for a multilayer atmosphere. The energy density for waves corresponding to these parts of the curves decreases monotonically with height from the ground. Later, Garrett (1969), Bretherton (1969) and Pierce, Posey and Illiff (1971) have shown that for acoustic gravity waves of period more than about 2 min. the properties of the waves can be explained by invoking a modified form of Lamb's edge wave theory. The energy density for these waves decreases exponentially with height from the ground and the particle motions are horizontal. According to Bretherton (1969) the energy for these waves is located mainly in the lowest 32 Km. of the atmosphere. The theory is applicable when the variation of sound speed and wind speed with height is small in comparison with the sound speed at the ground and the wavelength of the waves is sufficiently large. The theory is valid for waves with period greater than about 2 min. As the wavelength becomes smaller, the effect of the variation of temperature and wind becomes more significant and the Lamb-wave theory is not applicable for waves with period less than about 2 min. Energy for these short-period waves is concentrated in the atmospheric sound channels. Thus, according to both the normal mode theory and the Lamb wave theory the energy distribution for waves of period more than about 2 min is such that sufficient energy does not reach ionospheric levels to cause any disturbance there, which explains the absence of these long-period waves on the Doppler-sonde records. To illustrate the above reasoning a plot of the vertical variation of the amplitudes of perturbation pressure, vertical velocity and kinetic energy density for acoustic gravity waves (normal mode theory) of period 282 sec. is shown in Fig. 8. The theory and computational procedure used to obtain these curves are explained by Balachandran (1968). Appropriate temperature and wind data was used to generate the dispersion curves and the vertical profiles of wave parameters. The data used was appropriate for the waves received at Poughkeepsie, N. Y. from the nuclear test in the Pacific on October 30, 1962. The exponential decrease of kinetic energy density and pressure with height is evident from the figure. (The plots are in arbitrary units normalized with respect to the pressure at the ground). Although the amplitude of the vertical velocity shows an increase above 100 Km. the amount of kinetic energy available is not sufficient to cause any disturbance at ionospheric heights.

In the case of acoustic gravity waves with period less than about 2 min., which corresponds to the acoustic modes in the normal mode approach, the picture is quite different. Fig. 8 also shows pressure, vertical velocity and kinetic energy density profiles for waves with period 94 sec and 65 sec respectively. The data used in the computation was the same as that for the waves with the period of 282 sec. It may be noticed that rather than decreasing exponentially with height, the energy is channelled in the sound channel below about 100 km in the atmosphere. This is clear from the kinetic energy density profile in the figure. The ionospheric disturbance may be explained as being produced by the small amount of energy leaking from the duct. The profiles in Fig. 8 may not clearly show this picture because these profiles are plotted for fully ducted modes (by utilizing a semi-infinite layer, at the top of the atmospheric model, in which the energy density decreases exponentially with height) of acoustic gravity waves. But the ducting process may be explained by the diagram and

if we imagine that the duct is slightly imperfect, the picture of acoustic waves in the ionosphere becomes clear.

The reason why only the waves which travel along the shortest path on the globe are detected at ionospheric levels may be explained as follows. The short-period acoustic modes get attenuated when they travel along the longer path (A2 wave, A3 wave etc.) and only the long-period gravity modes have sufficient amplitudes to be detected by the microbarograph at the ground level. Since the gravity modes do not produce ionospheric disturbances, as we discussed earlier, no signal is detected at ionospheric levels which correspond to A2 waves, A3 waves etc. which are detected at the ground level.

To summarize, acoustic gravity waves with periods more than about 2 minutes produced by nuclear explosions are not detected at ionospheric heights, because their energy is confined to lower levels of the atmosphere. Waves with period less than about 2 min. are detected at ionospheric levels. These waves travel as partially ducted waves in the neutral atmosphere with energy leaking to ionospheric levels to cause disturbances there.

It may be pointed out that in this paper we are considering only ionospheric and neutral atmospheric waves which travel with a group velocity roughly equal to the velocity of sound near the ground and not the higher group velocity waves reported by Tolstoy and Herron (1970).

ACKNOWLEDGMENTS

This research was supported by contracts from the U. S. Army Electronics Command, Fort Monmouth (DAAB-07-69-C-0256) and the U. S. Army Research Office, Durham (DA-ARO-D-31-124-71-G90) and National Science Foundation Grant GA 17454. The author wishes to thank Mr. D. M. Baker of the NOAA Environmental Research Laboratories for providing the records of ionospheric disturbances.

REFERENCES

- Baker, D.M.: 1968: "Acoustic Waves in the Ionosphere following nuclear explosions", Acoustic-gravity waves in the atmosphere, edited by T. M. Georges, U. S. Government Printing Office, Washington, D. C.
- Baker, D.M. and K. Davies, 1968, "Waves in the Ionosphere Produced by Nuclear Explosions", J. Geophys. Res., 73, 448-451.
- Baker, D.M. and D.E. Cotten, 1971, "Interpretation of High-Frequency Doppler Observations of Waves from Nuclear and Natural Sources", J. Geophys. Res., 76, 1803-1810
- Balachandran, N.K., 1968: "Acoustic-gravity wave propagation in a Temperature and Wind Stratified Atmosphere", J. Atmos. Sci., 25, 818-826
- Bretherton, F.P., 1969: "Lamb waves in a nearly isothermal atmosphere", Quart. J. R. Met. Soc., 95, 754-757
- Donn, W.L. and M. Ewing, 1962a; "Atmospheric waves from nuclear explosions - Part I", J. Geophys. Res., 67, 1855-1866
- Donn, W.L. and M. Ewing, 1962b; "Atmospheric waves from nuclear explosions, Part II, the Soviet test of 30 Oct. 1961," J. Atmos. Sci., 19, 264-273.
- Donn, W.L., R.L. Pfeffer and M. Ewing, 1963: "Propagation of air waves from nuclear explosions", Science, 139, 307-317.
- Donn, W.L. and D.M. Shaw, 1967: "Exploring the atmosphere with nuclear explosions", Reviews of Geophysics, 5, 53-82.
- Donn, W.L. and N.K. Balachandran, 1972: "Amplitudes of Gravity and Acoustic modes in Air Waves from Nuclear Explosions". To be published.
- Garrett, C.J.R., 1969: "Atmospheric Edge Waves", Quart. J.R. Met. Soc., 95, 731-753.
- Pfeffer, R.L. and J. Zarichny, 1963: "Acoustic-gravity wave propagation in an atmosphere with two sound channels", Geofis. Pura. Appl., 55, 175-199
- Pierce, A.D., J.W. Posey and E.F. Illiff, 1971. "Variation of Nuclear Explosion Generated Acoustic-Gravity Wave Forms with Burst height and with Energy Yield", J. Geophys. Res. 76, 5025-5042.
- Savino, J.M., K. McCamy and G. Hade, 1972, "Structures in earth noise beyond 20 sec: A window for earth quakes", Bull. Seism. Soc. Am., 62, 1972
- Savino, J.M. and J.M.W. Rynn, 1972, "Quasi-Static loading of the earth by propagating Air Waves", J. Geophys. Res., 77, in press
- Tolstoy, I. and T.J. Herron, 1970; "Atmospheric Gravity Waves from Nuclear Explosions", J. Atmos. Sci., 27, 55-61.

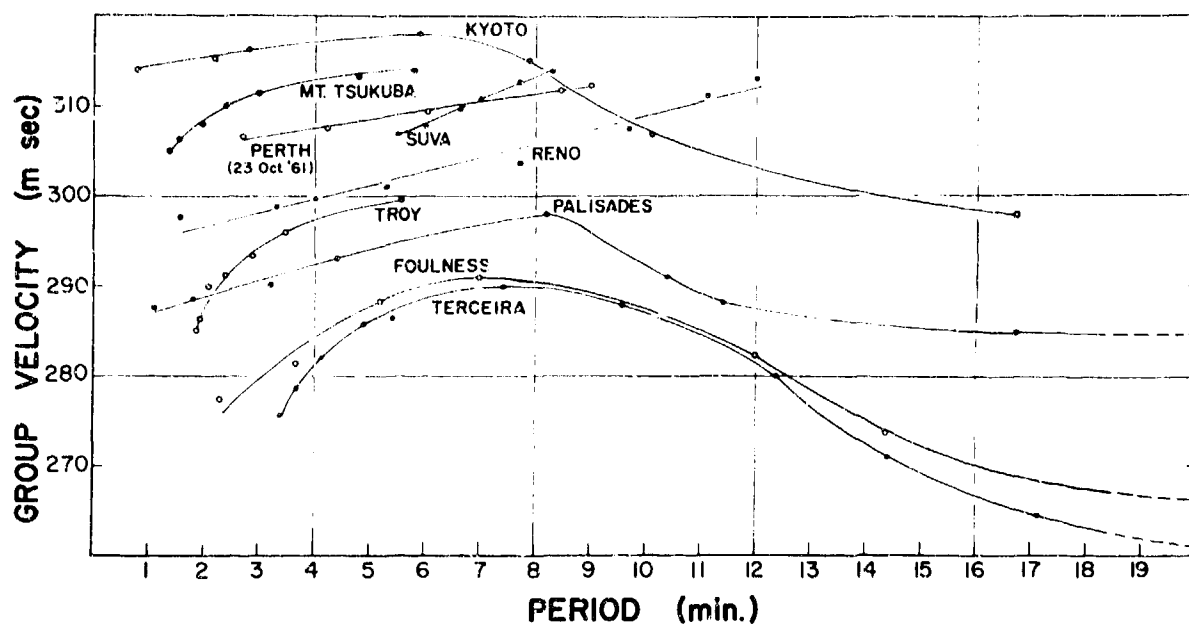


Fig. 1 Empirical dispersion curves showing normal and inverse dispersion of acoustic-gravity waves from the Soviet nuclear test of October 23, 1961, recorded at various stations around the globe (From Donn, Pfeffer and Ewing, 1963)

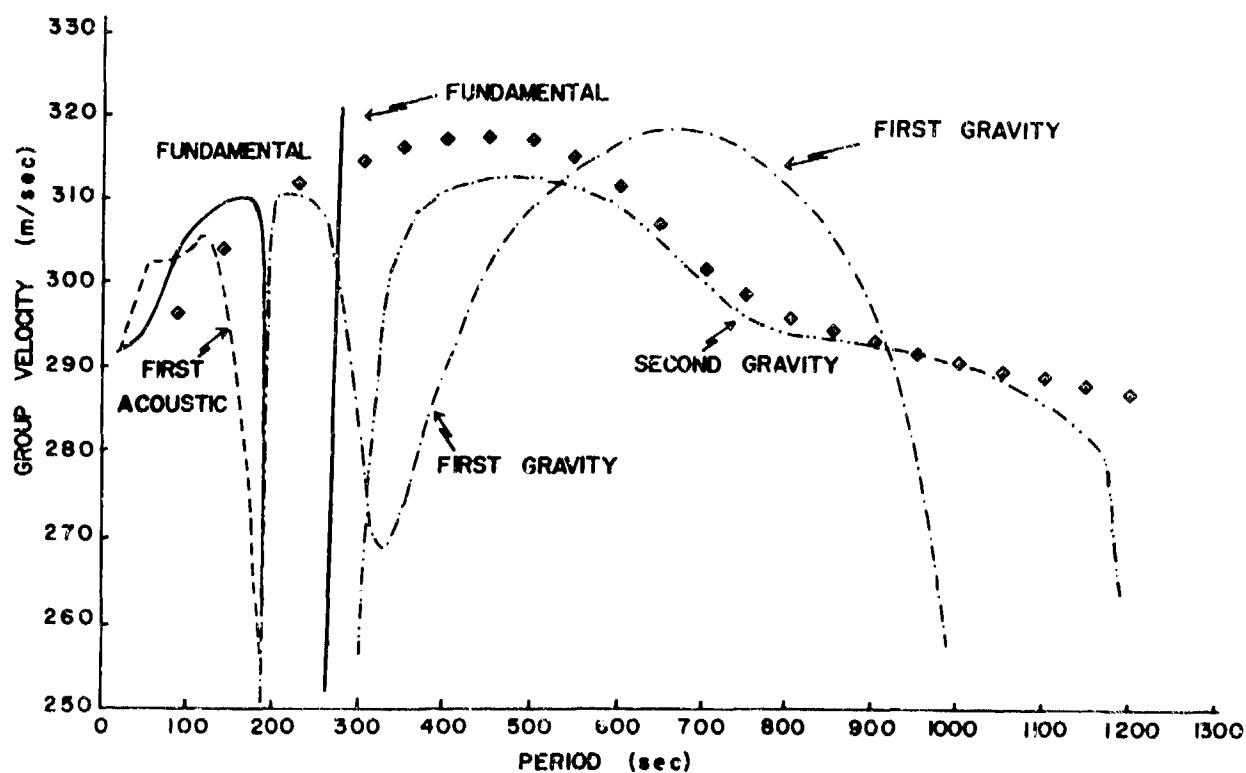


Fig. 2. Theoretical dispersion curves showing normal and inverse dispersion for a temperature and wind stratified atmosphere. The points enclosed in small squares are empirical, for the microbarogram at Palisades, N. Y. following the Soviet nuclear explosion of Aug. 5, 1962.

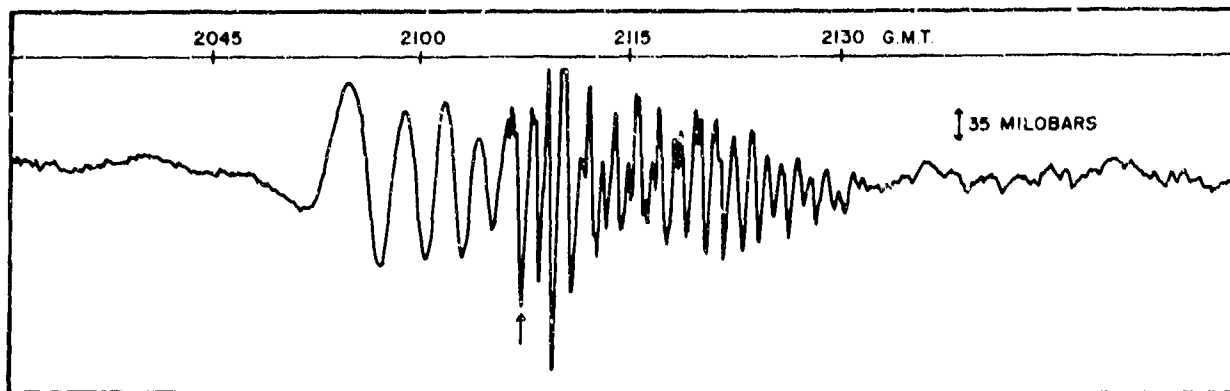


Fig. 3. Pressure fluctuations, recorded at Berkley, California due to air waves from the U. S. nuclear test in the Pacific on Oct. 30, 1962. The arrow indicates roughly the separation of shorter period acoustic modes from the gravity modes.

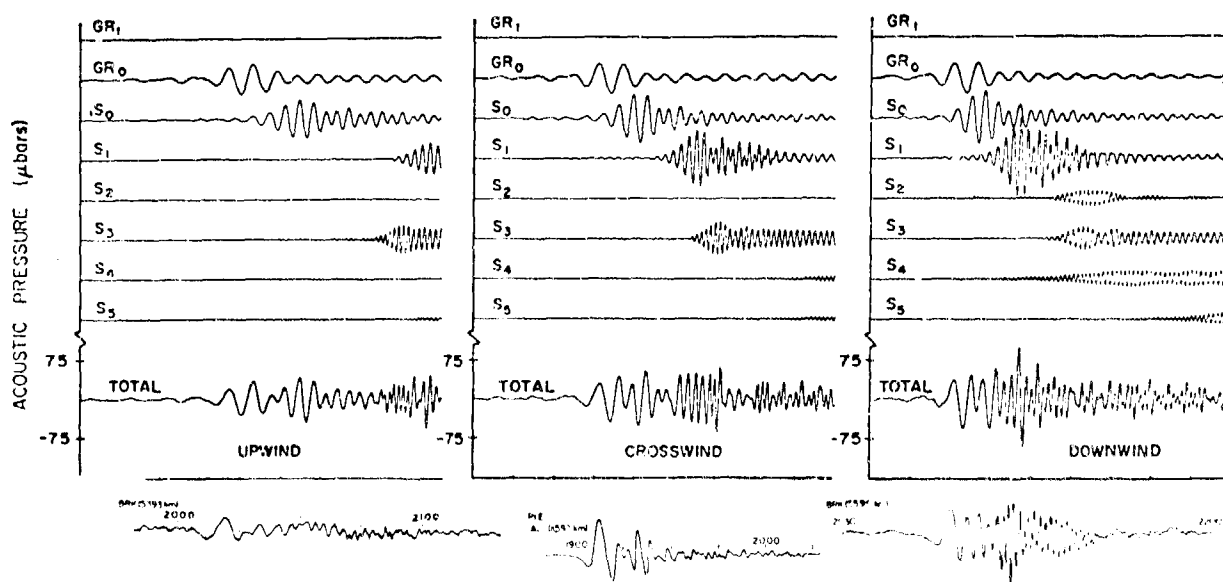


Fig. 4. Theoretical microbarograms at a distance of 10,000 km from the source in various directions with respect to the wind. (Top eight Curves, from Pierce et al., 1971). Appropriate empirical microbarograms are shown at the bottom of the figure.

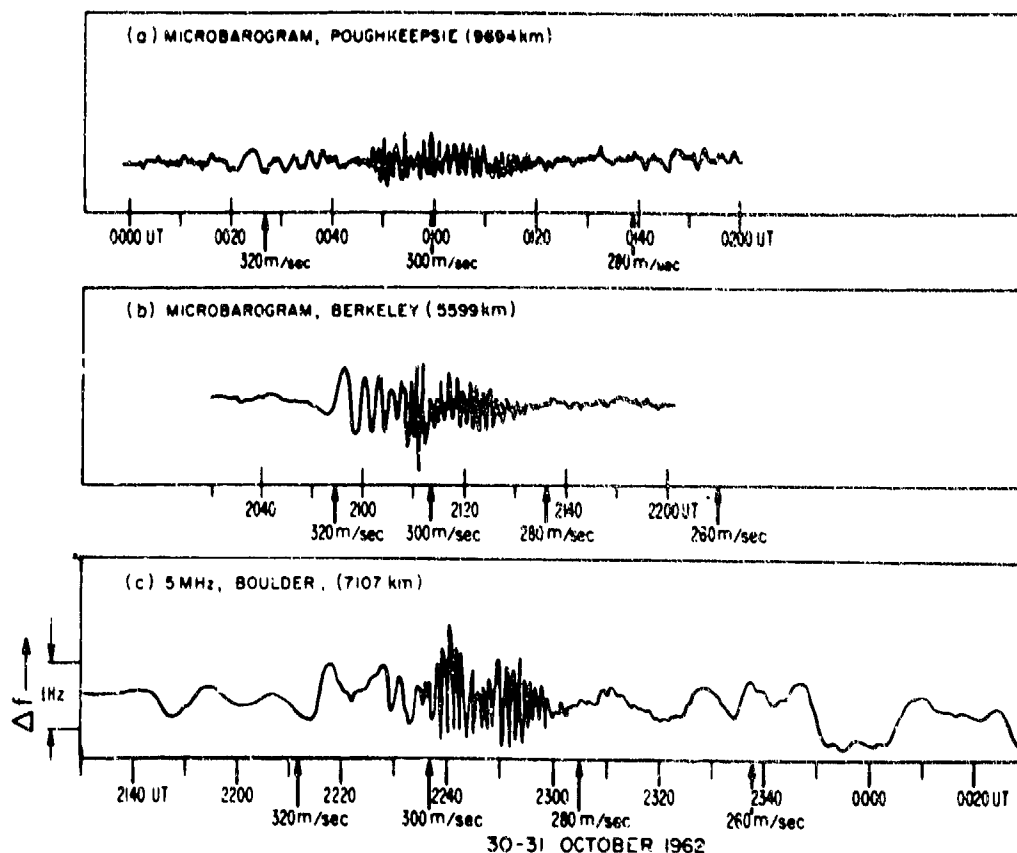


Fig. 5. Comparison of microbarograms obtained at Poughkeepsie, New York (a) and Berkeley, California (b) with ionospheric disturbance above Boulder (c) following the nuclear explosion of October 30, 1962. (From Baker, 1968)

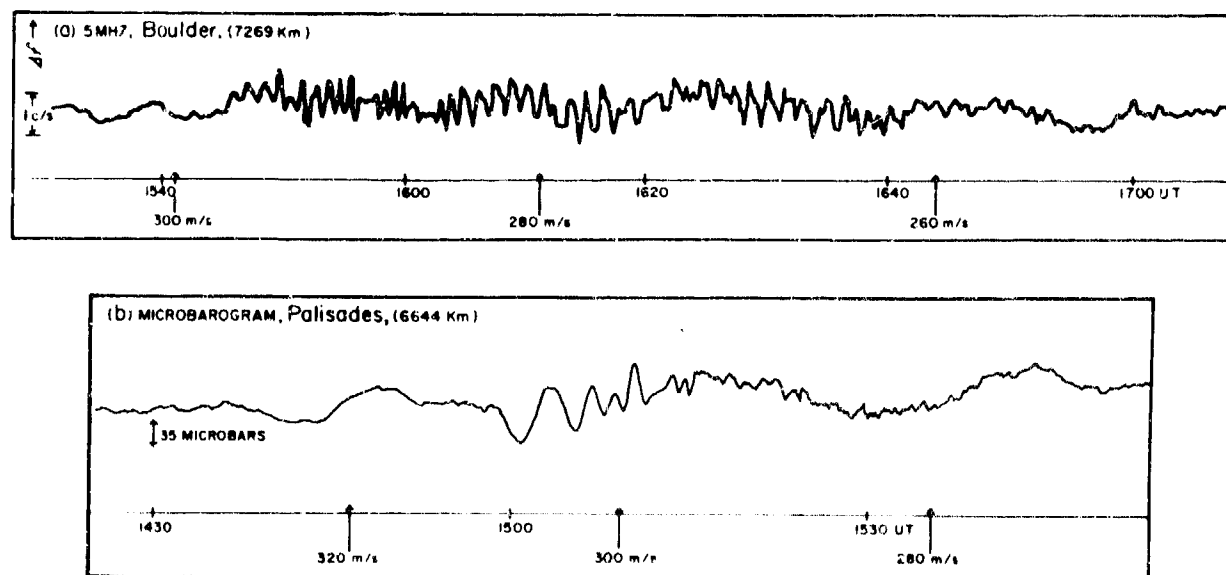


Fig. 6. Comparison of the records of ionospheric disturbance above Boulder (a) with the microbarogram at Palisades, New York (b) following the Soviet nuclear test of Sept. 10, 1961 in Novaya Zemlya. The absence of long period waves on the Doppler record may be noticed.

POUGHKEEPSIE, N.Y. OCT. 31, 1962

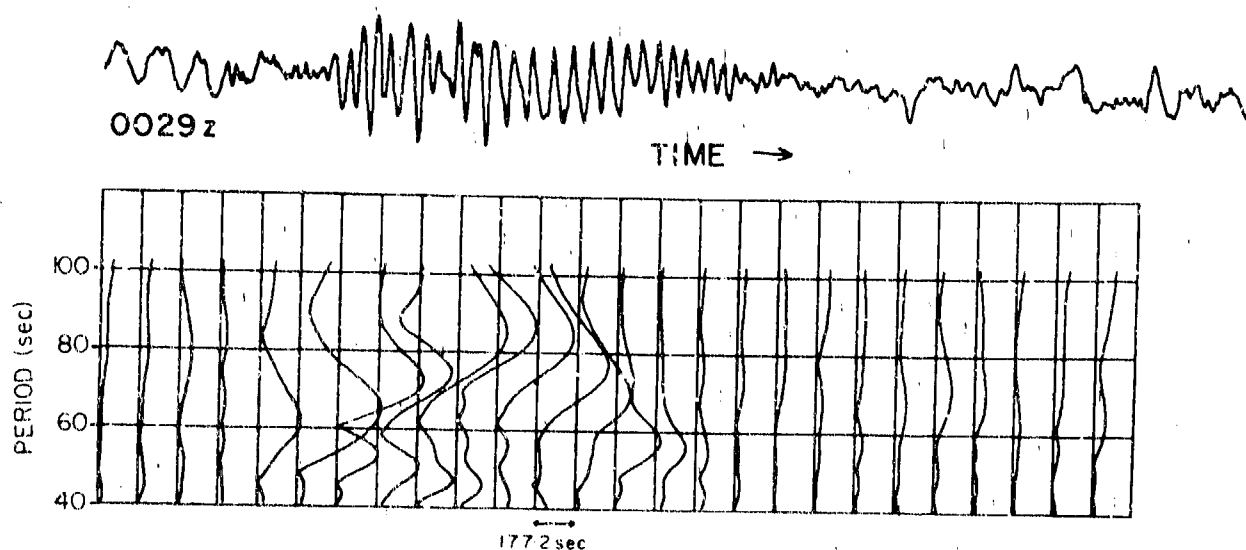


Fig. 7(a) Microbarogram recorded at Poughkeepsie, New York and its running spectrum analysis for the nuclear explosion of October 30, 1962.

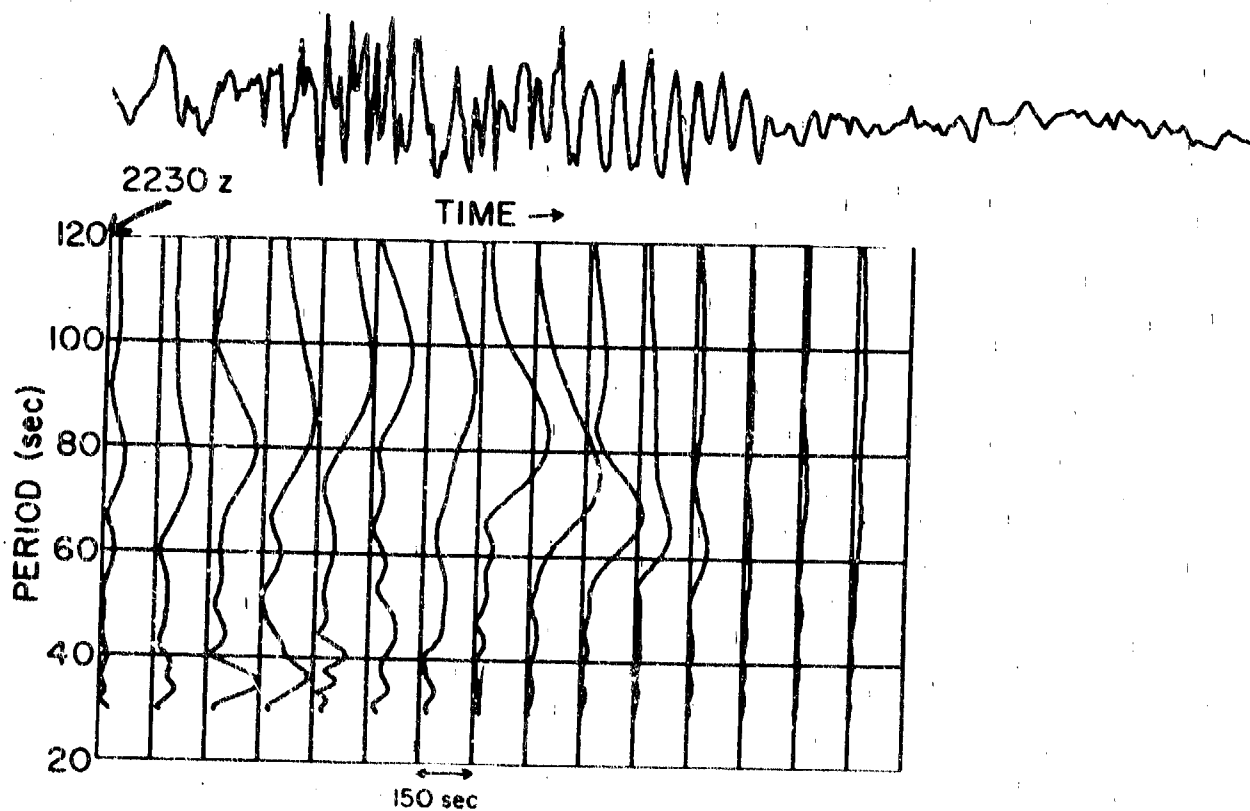


Fig. 7(b) Record of ionospheric disturbance at Boulder and the running spectrum analysis for the explosion of October 30, 1962.

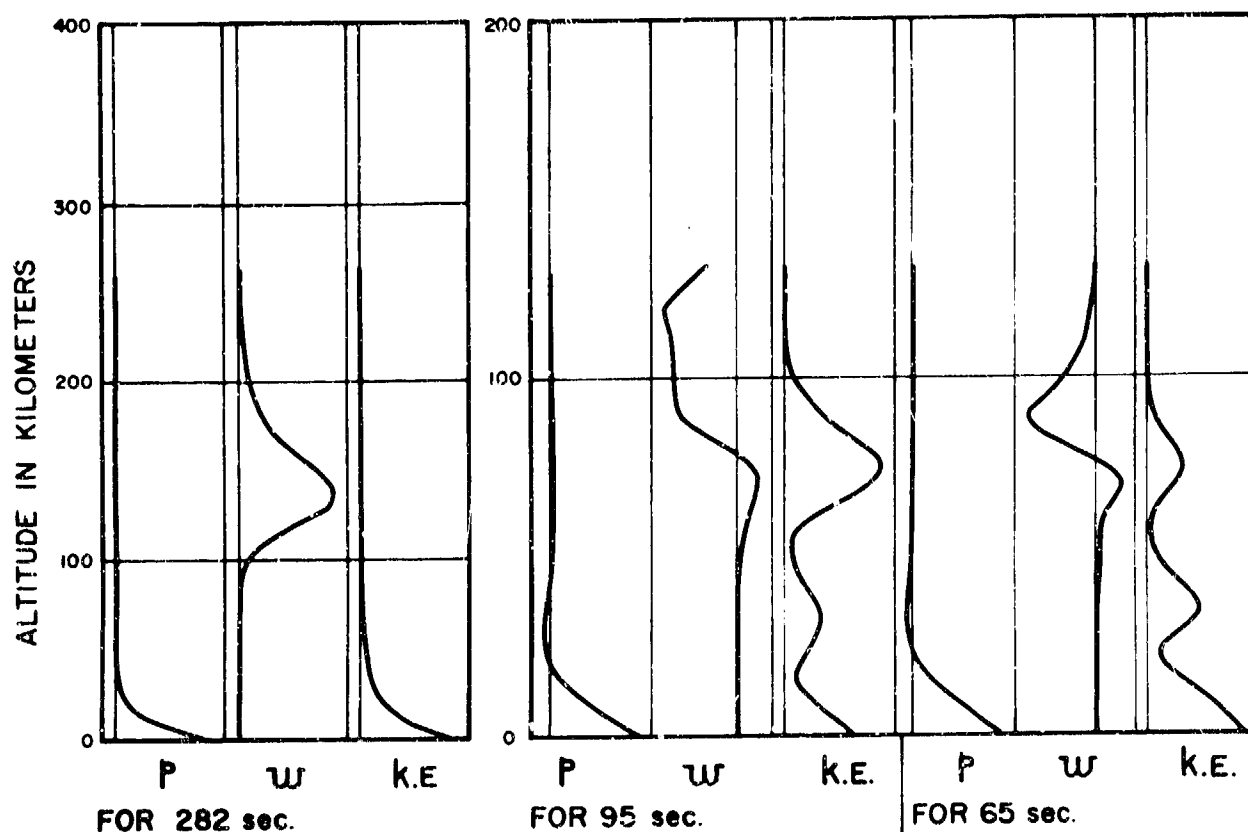


Fig. 8. Plot of perturbation pressure (p) vertical velocity (w) and kinetic energy density (K.E.) for waves with various periods. (The period in seconds is shown near each curve).

MODELING OF NUCLEAR SOURCES OF ACOUSTIC-GRAVITY WAVES

by

Brian L. Murphy and Sheldon L. Kahalas

**Mt. Auburn Research Associates, Inc.
Newton, Massachusetts
USA**

125

MISE AU POINT D'UN MODELE REPRESENTANT DES SOURCES NUCLEAIRES
GENERATRICES D'ONDES ACOUSTIQUES ET DE GRAVITE

par

B.L. Murphy et S.L. Kahalas

SOMMAIRE

Les auteurs étudient le rapport entre les mouvements hydrodynamiques créés par une explosion à faible altitude et les perturbations ionosphériques qui en résultent. Ils considèrent l'onde de choc ascendante et la boule de feu qui s'élève comme constituant toutes deux des sources hydrodynamiques. Ils montrent que l'on peut distinguer différentes parties dans le front de choc suivant la perturbation ionosphérique qu'elles créent. La partie du front de choc réfléchi par le niveau d'altitude 100 à 120 km produit des périodes de perturbation de l'ordre d'une minute pour une explosion d'une mégatonne. La partie de l'onde de choc qui se propage au-dessus de 100-120 km est responsable, par un processus non-linéaire complexe, de périodes de perturbation excédant 10 minutes. Les auteurs montrent que la boule de feu a une aptitude maximale à engendrer des ondes acoustiques et de gravité lorsqu'elle atteint son altitude de stabilisation et tend à un équilibre hydrodynamique avec l'atmosphère. La théorie et les expériences effectuées en laboratoire montrent que la boule de feu produit alors un spectre d'ondes avec des sommets correspondant à des périodes légèrement plus longues que la période ambiante de Brunt-Väisälä (≈ 5 minutes).

MODELING OF NUCLEAR SOURCES OF ACOUSTIC-GRAVITY WAVES

Brian L. Murphy and Sheldon L. Kahalas
Mt. Auburn Research Associates, Inc.
Newton, Massachusetts, U.S.A.

SUMMARY

The relationship between hydrodynamic motions caused by a low altitude explosion and subsequent ionospheric disturbances is reviewed. Both the upward going shock and the rising fireball are considered as hydrodynamic sources. It is shown that different portions of the shock front may be classified in terms of the ionospheric disturbance they create. The portion of the shock front reflected from the 100-120 km altitude level produces disturbance periods the order of a minute for a megaton detonation. The portion of the shock front which propagates above the 100-120 km level is responsible, through a complex nonlinear process, for disturbance periods in excess of 10 minutes. It is shown that the fireball is most efficient in generating acoustic-gravity waves when it reaches its stabilization altitude and approaches hydrodynamic equilibrium with the atmosphere. Theory and laboratory experiment indicate that the fireball then produces a wave spectrum peaked at periods slightly longer than the ambient Brunt-Väisälä period (≈ 5 minutes).

1. INTRODUCTION

It is known that large yield nuclear explosions result in ionospheric disturbances which can be observed by electromagnetic means at great distances from the explosion site. It is also widely recognized that these disturbances are a result of acoustic-gravity waves whose propagation is supported by the neutral fluid component of the ionosphere. A recent bibliography contains many references to observations and theory relating to detonation produced disturbances (THOMAS, J. E., et al., 1971).

Much of the previous theoretical development deals with wave propagation rather than source modeling. It is to the latter topic that this paper is devoted. In the subsequent discussion we outline how the hydrodynamic motions near a nuclear detonation result in the generation of acoustic-gravity waves and how the properties of these waves are determined by the explosion parameters. That is, how onset time, amplitude, and period of the ionospheric disturbance are related to explosion yield and height of burst.

Because we concentrate on source modeling, we will not discuss wave propagation except insofar as it is necessary to do so to relate theoretical predictions to observations. Similarly, we do not consider how the neutral fluid motions determine ionospheric electron densities and hence the ultimate electromagnetic effect. This difficult problem has been treated by a number of authors (for example, HOOKE, W. H., 1968).

Our treatment is limited to low altitude detonations where the initial energy deposition may be assumed to be local and spherically symmetric. For this type of detonation both the shock and the fireball can generate acoustic-gravity waves. The mechanisms which will be discussed are as follows:

- a. The direct effects of the shock are manifest as ionospheric signals with periods the order of a minute for a megaton detonation, the period being determined by the positive phase duration of the shock when it reaches the ionospheric level. The acoustic signal in this case undergoes multiple reflections between the ground and the base of the ionosphere. The ducting is imperfect at the upper level and energy continuously leaks into the ionosphere.
- b. In addition, the short period (order of a minute) hydrodynamic motions that characterize the shock as it enters the ionosphere above the burst evolve into long period (10 minutes and more) disturbances through a highly nonlinear process occurring at the 100-120 km altitude level. This phenomenon, which has been demonstrated by numerical calculations (GREENE, J. S., Jr. and W. A. WHITAKER, 1968), involves a refraction and folding over of the shock due to the rapid change in ambient temperature at this level. Long period wave propagation due to this mechanism commences at 10 minutes or more after the detonation. This time, which is when the effective excitation appears to have begun according to a distant observer, is the time required for the shock to reach the ionospheric level and for the long period fluid motions to become established.
- c. The fireball is most efficient in generating acoustic-gravity waves when it has reached its terminal or stabilization altitude. It then approaches hydrodynamic equilibrium with the atmosphere on a time scale comparable with the Brunt-Väisälä period, the natural oscillation period of the atmosphere. This is also approximately the time required for the fireball to reach its terminal altitude and wave generation to being. For, as will be shown, the fireball is not an efficient emitter of waves during the early portions of its rise.

Acoustic-gravity wave generation during fireball terminal phase has been modeled in the laboratory and these experimental studies will be described.

As shown below, for megaton range detonations the energy available for wave generation by the fireball is comparable to the energy available for long period wave generation by the shock. However, the dominant frequency of the waves generated by fireball stabilization is only slightly less than the Brunt-Väisälä frequency and waves of this frequency propagate at relatively steep angles to the horizontal. For this reason the fireball mechanism may only be capable of producing ionospheric disturbances in the immediate vicinity of the burst location.

These general remarks are discussed in more detail in the succeeding sections. We first discuss the shock and then the fireball mechanism. We then assess the importance of these mechanisms in terms of the resulting ionospheric effects.

2. SHOCK WAVE GENERATION OF ACOUSTIC-GRAVITY WAVES

It is useful to first consider the propagation of the shock front as it is refracted by the atmosphere. Different portions of the shock are refracted differently. This leads to a classification of different portions of the shock front in terms of the types of ionospheric disturbance that they create.

At some distance from the burst point the shock becomes weak, that is, the relative overpressure $\Delta P/P$ becomes much less than unity. ΔP is the overpressure and P is the ambient pressure. For example, for a megaton detonation $\Delta P/P = .1$ at about 9 km (LEHTO, D. L. and R. A. Larson, 1969). When the shock becomes weak the effects of atmospheric stratification and winds become important.

An example of ray tracing calculations for a realistic (but windless) atmosphere is shown in Figure 1 (BARRY, G., 1963) for a source located at the ground. The figure does not include any non-acoustic propagation effects such as those arising near the source where the shock is strong. The initial ray angles in Figure 1 start at zero degrees to the horizontal and increase in 5° increments. The ultimate behavior of different portions of the shock front is determined by the initial angle of propagation relative to the horizontal as indicated in Figure 1. As this angle is increased the different types of disturbance are:

- a. Acoustic disturbances reflected back toward the earth before reaching the ionosphere. In Figure 1 this corresponds to initial angles of less than 20° . This type of signal may undergo repeated reflections between the ground and some higher level, in Figure 1 the 40 km region of the stratosphere, where suitable temperature and wind conditions exist. When this portion of the shock front becomes weak it may be repeatedly split by winds resulting in a multipulse type of infrasonic signal (MEECHAM, W. C., 1968).
- b. The direct shock which reaches the 100-120 km level of the ionosphere before being reflected at the region of very sharp temperature increase. This signal, which corresponds to the interval from 20° to perhaps 35° in Figure 1, can be ducted between the base of the ionosphere and the ground as shown. As discussed below, leakage from the upper portion of the duct to the ionosphere is probably responsible for acoustic-wave disturbances observed in the ionosphere (BAKER, D. M. and K. Davies, 1968).
- c. A portion of the shock front which propagates into the thermosphere beyond the 100-120 km level. This corresponds to angles of more than about 35° in Figure 1. Numerical calculations of the nonlinear hydrodynamics done by Greene and Whitaker (1968), which are discussed below, show that this portion of the shock loses much of its energy in the creation of a horizontally propagating disturbance behind the front.

This disturbance is believed to be responsible for the very long period ionospheric perturbations observed at great distances following large yield explosions.

Our concern in the following is with the portion of the shock front which reaches the 100-120 km altitude level. Throughout, only the primary shock wave is considered and secondary shocks due to reflection from the fireball or the ground are neglected.

We first determine the properties of the upward going shock at the 100-120 km altitude level. We then discuss the relationship of these shock properties to the properties of short period ionospheric disturbances. Finally we discuss the nonlinear process at the 100-120 km level which results in the generation of long period ionospheric disturbances.

2.1 The Upward Going Shock

In this section we will calculate the relative overpressure and the positive phase duration of the shock at the base of the ionosphere as functions of yield and height of burst. These results are subsequently used to relate ionospheric disturbance properties to explosion parameters. To determine the properties of the upward going shock a simplified scaling law known as modified Sachs scaling is used (LUTZKY, M. and D. L. Lehto, 1968) together with weak shock theory (REED, S. G., Jr., 1959).

According to modified Sachs scaling the relative overpressure, in an inhomogeneous atmosphere, at a distance r from an explosion where the ambient pressure is $P(r)$, is just the same as if the explosion had occurred in a homogeneous atmosphere with ambient pressure $P(r)$. That is:

$$\frac{\Delta P}{P(r)} = f \left\{ r \left[\frac{P(r)}{Y} \right] \right\}^{1/3} \quad (1)$$

where Y is the explosion yield and f is the function which gives the relative overpressure in a homogeneous atmosphere. An example of the application of modified Sachs scaling is shown in Figure 2 where we compare the predictions of this scaling with the results of SAP and SHELL calculations for relative overpressure versus distance. SAP is a one dimensional Lagrangian hydrodynamic code and SHELL is a two dimensional Eulerian hydrodynamic code. These calculations are for shock propagation at 45° from the horizontal due to a 4 MT isothermal sphere at 5 km altitude (GREENE, J. S., Jr., personal communication, 1971). The modified Sachs scaling curve has been constructed using the 1962 Standard atmosphere for the ambient pressure $P(r)$ and the homogeneous atmosphere, real air, calculations of Lehto and Larson (1969) for the function f occurring in Eq. (1). Notice that the SHELL calculation consistently gives somewhat higher relative overpressures below 100 km altitude than does SAP. This is because it includes the effects of fireball rise which SAP does not. The rising fireball, particularly for large yields, prevents the shock from relieving backwards. At very small angles from the horizontal the differences between SHELL and SAP are negligible. Both SHELL and SAP show a drop in relative overpressure commencing at about 100 km altitude. The reason for this and its relation to acoustic-gravity wave generation at the ionospheric level will be discussed shortly. First we continue the discussion of modified Sachs scaling and the upward shock propagation.

It is not entirely clear why modified Sachs scaling works as well as it does. However, in this example, as well as in others not shown here, modified Sachs scaling is definitely more accurate than scaling of distance with respect to ambient pressure at the detonation altitude. Because modified Sachs scaling is expected to become more inaccurate with increasing distance, we use it only to obtain starting values near the burst point for the application of weak shock theory. In using weak shock theory to obtain scaling laws for the shock properties on entering the ionospheric level we make two simplifying assumptions: First, that the atmosphere can be approximated as exponential. Second, that in spite of refractive effects, each portion of the shock front propagates independently with its own effective radius of curvature. These assumptions are justified by the fact that we treat shock propagation in the atmosphere below 120 km altitude where the scale height is approximately constant and by the fact that we only consider the portion of the shock front which is not seriously refracted (i.e. reflected) before reaching the altitude in question.

For reasons which appear below we begin using weak shock theory at a distance r_0 where $\Delta P/P = \Delta P_0/P_0$ first equals 0.2. Assuming that the atmosphere near the burst may be approximated as exponential this value of the function f occurring in Eq. (1) corresponds to (LEHTO, D. L. and R. A. Larson, 1969):

$$r_0 e^{-r_0/3H} = .53 \left(\frac{Y}{P_b} \right)^{1/3} \text{ km}, \quad (2)$$

where Y is the yield in kilotons, and P_b is the ambient pressure at the burst point in atmospheres. H is the effective scale height in kilometers for the (upward) direction being considered.

At distances $r > r_0$ we use the weak shock equations derived by Reed (1959). These are:

$$\frac{\Delta P}{P} = \frac{\Delta P_0}{P_0} \frac{r_0}{r} \frac{t_+^0}{t_+} \sqrt{\frac{P_0}{P}} \quad (3)$$

$$\frac{t_+}{t_+^0} = \left[1 + \frac{\gamma+1}{2\gamma} \frac{\Delta P_0}{P_0} \frac{r_0}{c} \frac{1}{t_+^0} \int_{r_0}^r \sqrt{\frac{P_0}{P}} \frac{dr}{r} \right]^{1/2} \quad (4)$$

where t_+ is the positive phase duration of the shock, γ is the ratio of specific heats, and c is the speed of sound. Nonlinear (weak shock) effects are contained in Eq. (3) within the factor t_+^0/t_+ . This factor as given by Eq. (4) includes both the effects of dissipation at the shock front and positive phase lengthening due to the supersonic front velocity.

The dependence of t_+ on values of r_0 may be eliminated by taking the logarithmic derivatives of Eqs. (3) and (4) and combining to obtain:

$$t_+ = \frac{-\frac{\gamma+1}{4\gamma c} r \frac{\Delta P}{P}}{\left[1 + \frac{r}{2} \frac{\partial}{\partial r} \ln P + r \frac{\partial}{\partial r} \ln \frac{\Delta P}{P} \right]} \quad (5)$$

For an exponential atmosphere this becomes:

$$t_+ = \frac{-\frac{\gamma+1}{4\gamma c} r \frac{\Delta P}{P}}{\left[1 - \frac{r}{2H} + n \right]} \quad (6)$$

where

$$n \equiv r \frac{\partial}{\partial r} \ln \frac{\Delta P}{P} \quad (7)$$

The value of n is obtained from Eq. (1):

$$n(r) \equiv r \frac{\partial}{\partial r} \ln \frac{\Delta P}{P} = \left[1 - \frac{r}{3H} \right] \left(\frac{P_b}{Y} \right)^{1/3} r \frac{f'}{f} = \left[1 - \frac{r}{3H} \right] n_h \quad (8)$$

where f' is the derivative of f with respect to its argument and n_h is the value of n for a homogeneous atmosphere ($H \rightarrow \infty$). The quantity n_h is plotted vs. relative overpressure in Fig. 3. Note that, consistent with Figure 2, the minimum value of $\Delta P/P$ corresponding to $n = 0$ occurs at $r = 3H$, that is at an altitude 3 scale heights above the burst point.

Combining Eqs. (6) - (8) we obtain:

$$t_+ = \frac{-\frac{\gamma+1}{\gamma c} r \frac{\Delta P}{P}}{(1 + n_h) - \frac{r}{2H} (1 + \frac{2}{3} n_h)} \quad (9)$$

At $r = r_0$, $\Delta P_0/P_0 = .2$, and according to Figure 3, $n_h = -\frac{3}{2}$. Thus we obtain from Eq. (9):

$$t_+^0 = \frac{\gamma+1}{\gamma c} (.1) r_0, \quad (10)$$

which permits Eqs. (3) and (4) to be written as:

$$t_+ = \frac{\gamma+1}{\gamma c} (.1) r_0 \left\{ 1 + e^{-r_0/2H} \left[E_i \left(\frac{r}{2H} \right) - E_i \left(\frac{r_0}{2H} \right) \right] \right\}^{1/2} \quad (11)$$

$$\frac{\Delta P}{P} = \frac{.2 \frac{r_0}{r} e^{-(r_0-r)/2H}}{\left\{ 1 + e^{-r_0/2H} \left[E_i \left(\frac{r}{2H} \right) - E_i \left(\frac{r_0}{2H} \right) \right] \right\}^{1/2}}, \quad (12)$$

where r_0 is given by Eq. (2) and where the exponential integral E_i is defined as:

$$E_i(x) = \int_{-\infty}^x \frac{e^t}{t} dt. \quad (13)$$

At the base of the ionosphere (considering only low altitude detonations) the term $e^{-r_0/2H} E_i \left(\frac{r}{2H} \right)$ dominates in the radicals occurring in Eqs. (11) and (12) and furthermore may be approximated as $\frac{2H}{r} \exp \left[\frac{r-r_0}{2H} \right]$.

Making this approximation and using Eq. (2) to eliminate factors of $r_0 e^{-r_0/3H}$ we obtain from Eqs. (11) and (12):

$$t_+ = .075 \frac{\gamma+1}{\gamma c} \left(\frac{\gamma}{P_b} \right)^{1/3} e^{r_0/12H} \sqrt{\frac{H}{r}} e^{r/4H} \quad (14)$$

$$\frac{\Delta P}{P} = .075 \left(\frac{\gamma}{P_b} \right)^{1/3} e^{r_0/12H} \frac{e^{r/4H}}{\sqrt{Hr}} \quad (15)$$

The factor $e^{r_0/12H}$ may be neglected since r_0 cannot be larger than $3H$, the reason being that $\Delta P/P = .2$ must occur before the minimum at $r_0 = 3H$ if it is to occur at all. (According to Eq. (2), $\Delta P/P$ does not become as small as .2 for sea level yields in excess of 60 MT.) We set $r/H = (z-z_b)/H_s$, where z is the shock altitude, z_b is the burst altitude ($e^{-z_b/H_s} = P_b$), and H_s is the scale height in the vertical direction. Then taking $H_s = 7$ km, $\gamma = 1.4$, and $c = .31$ km/sec as representative values below 120 km altitude we obtain the final form of our expressions for the shock positive phase duration and relative overpressure:

$$t_+ = 1.1 \gamma^{1/3} P_b^{-1/12} \frac{e^{z/28}}{\sqrt{z - z_b}} \quad (16)$$

$$\frac{\Delta P}{P} = .028 \gamma^{1/3} P_b^{-1/12} \frac{\sqrt{z - z_b}}{r} e^{z/28} \quad (17)$$

For 4MT at 5 km and for shock propagation at 45° from the horizontal Eq. (17) predicts $\Delta P/P = 1.2$ at 100 km altitude. The SAP and SHELL results shown in Figure 1 both give about $\Delta P/P = 1.6$ at this altitude. That the agreement is only approximate is not surprising in view of the several assumptions made and in particular due to the fact that the weak shock theory employed becomes inaccurate when $\Delta P/P \approx 1$. For smaller yields or propagation closer to the horizontal the theoretical results should be more accurate.

The properties of the shock when it reaches the ionospheric level are given by Eqs. (16) and (17). These properties, which will be used in the subsequent discussion, are as follows:

- a. The relative overpressure and positive phase duration are both proportional to cube root of yield.
- b. Both relative overpressure and positive phase duration are insensitive to height of burst at least for low altitude detonations. Taking z to be 100 km and recalling that $P_b = e^{-z_b/H}$ where H is taken to be 7 km we find that the respective height of burst dependences are: $t_+ \sim [1 + z_b/59]$ and $\Delta P/P \sim [1 + z_b/145]$, where z_b is in kilometers.
- c. For a given altitude the positive phase duration is independent of range and the relative overpressure decreases linearly with range.
- d. A megaton detonation at sea level has a positive phase duration of about 39 seconds at 100 km.

2.2 Direct Effects of the Shock

We believe the direct effects of the shock to be the source of the many observations of ionospheric disturbances following nuclear tests with periods between 30 seconds and 10 minutes, periods of about a minute being predominant (BAKER, D. M., 1968). These disturbances were observed by a doppler technique between altitudes of 150 and 200 km and appeared to propagate at speeds of about 300 meters/sec. Typically the explosions involved were the order of a megaton.

An example is shown in Figure 4 of the disturbance observed following the United States megaton range detonation Housatonic on 30 October 1962 (GLASSTONE, S., 1964, pg. 677e). BAKER (1968) points out that a feature occurs on 4 MHz, which is reflected from 180 km, about 17 seconds earlier than a 5 MHz, which is reflected from 190 km. He finds therefore that the disturbance was propagating upward with a speed approximately equal to the local sound speed. On this basis and because of the known acoustic ducting properties of the atmosphere he hypothesizes that the acoustic signal has the bulk of its energy confined in a duct below 110-120 km altitude and that it is leakage from this duct that is responsible for the ionospheric disturbance.

The point we wish to make is that the observed periods of these ionospheric disturbances are approximately the same as the periods which the shock from a megaton range explosion would contain on reaching the ionospheric level. We say approximately because among other things it is not clear whether the periods contained in the shock are the order of $2t_+$ or some slightly larger value. In terms of Figure 1 this means that the portion of the shock which initially propagates at angles of from about 20° to 35° is responsible for these short period ionospheric disturbances.

Ionospheric disturbances with periods greater than 10 minutes, which we now discuss, are related in a complex manner to the portions of the shock which initially propagate at steeper angles to the horizontal.

2.2 Long Period Acoustic-Gravity Wave Generation by the Upward Going Shock

As previously noted, Figure 2 shows a dramatic drop in relative overpressure commencing at about the 100 km altitude level. The reason for this can be seen by examining the SHELL outputs for the detailed flow, one of which is shown in Figure 5. This Figure is a contour plot of relative pressure as a function of altitude and horizontal distance at a time of 600 seconds. The spherically expanding and upward moving shock wave is refracted at the 100-120 km altitude level where the ambient temperature begins to increase radically. Of course, the vertically propagating shock front is unrefracted. The result is the generation of a horizontally propagating disturbance in the flow behind the shock front. This disturbance drains energy from the shock which continues outward and upward.

The essential feature of the Greene-Whitaker calculation is that the effective source of the long period gravity wave disturbance is located at an altitude of 100-120 km above the burst. The effective source commences 10 minutes or more after a sea level detonation, this being the time required for the shock wave to reach the ionospheric level and for the rotating flow of Figure 3 to become established. This delay time correction to the travel time has been observed following several low altitude explosions (HERRON, T. J., 1971).

The velocity vector plots, which are not shown, indicate that the dominant motion in the disturbance depicted in Figure 5 is a rotating or vortex flow and on this basis we proceed to estimate the disturbance kinetic energy. The geometry assumed for this vortex flow is indicated in Figure 6.

The kinetic energy of the motion is:

$$E_s = \int \frac{1}{2} \rho v^2 dV, \quad (18)$$

where the volume element for the region containing the vortical flow is:

$$dV = 2\pi R (2\pi r' dr') \quad (19)$$

For the assumed flow we may define a constant vorticity within the rotating region:

$$\omega = \frac{1}{2} |\nabla \times \vec{v}| = \frac{v(r')}{2r'} \quad (20)$$

in terms of which Eq. (18) becomes:

$$E_s = 8\pi^2 \omega^2 R \int_0^r \rho(r') r'^3 dr', \quad (21)$$

and approximating $\rho(r')$ by ρ_a , the ambient density, this results in:

$$E_s = 2 \pi^2 \omega^2 r^4 R \rho_a \quad (22)$$

We estimate $R = 150$ km and $r = 30$ km based on Figure 5. This latter value is approximately the gradient scale of the temperature change responsible for the shock refraction and development of the vortical motion, i.e. $T/\nabla T = r$. We estimate the maximum flow velocity $v(r)$ as being approximately equal to the sound speed at 130 km, that is about .64 km/sec. Then for an ambient density of 7.6×10^{-9} kg/meter³ we obtain $E = 5$ KT, that is about .1% of the total 4 MT yield.

For smaller yields than our 4 MT example, the yield scaling of kinetic energy is $\frac{1}{2} \rho v^2 V$, where ρ is the density, v the fluid velocity, and V the volume over which the rotational motion takes place. For a weak shock we expect only the fluid velocity to be a function of the detonation parameters. Since this velocity is proportional to the relative overpressure we find from Eq. (17) that the energy in the horizontally propagating disturbance is proportional to $Y^{2/3}$. Thus with a proportionality constant determined by the 4MT example we may write:

$$E_s/Y = 2 \times 10^{-2} Y^{-1/3} \quad (23)$$

We will compare this estimate with the energy available in the rising fireball for wave generation, which is derived below.

3. FIREBALL GENERATION OF ACOUSTIC-GRAVITY WAVES

The fireball is a buoyant rising fluid element and as such deforms into a torus or vortex ring configuration. The flow is illustrated in Figure 7. During the initial rise period, that is, well before the stabilization time the flow around this vortex ring can be treated as the flow around an equivalent solid object. Warren (1960) has calculated the wave emission and wave drag on a sphere moving vertically in a stratified incompressible fluid. His theory predicts that gravity wave emission is negligible when

$$\frac{\Omega}{N} > 1 \quad (24)$$

where $\Omega = v/2a$, v is the sphere velocity, and a the sphere radius. The Brunt-Väisälä frequency N , is the high frequency cutoff for gravity wave propagation. The onset of wave emission at $\Omega/N = 1$ has been experimentally verified (MOWBRAY, D. E. and B. S. H. Rarity, 1967).

A buoyant sphere rises at a velocity (SCORER, R. D., 1950)

$$v = (g \beta a)^{1/2} \quad (25)$$

where g is the acceleration of gravity and $\beta = \frac{\rho - \rho'}{\rho}$ is the buoyancy defined as the difference in density between fireball and its surroundings divided by the ambient density.

Warren's criterion for significant gravity wave emission therefore gives:

$$a > g \beta \left(\frac{\tau_{BV}}{4\pi} \right)^2 \approx 5.6 \beta \text{ km}, \quad (26)$$

for a Brunt-Väisälä period τ_{BV} of 5 minutes. Because of the very high fireball temperatures involved at early times we may approximate β by unity. Then Eq. (26) states that a fireball radius of 5.6 km is required for the onset of appreciable gravity wave emission. According to the data in Glasstone (1964, p 10) this would require a yield in excess of 30 MT. We conclude that for sea level detonations only very large yields could result in gravity wave emission during the initial period of the rise.

When the fireball reaches its stabilization altitude and proceeds toward hydrodynamic equilibrium with its surroundings, conditions more favorable for gravity wave emission do occur. However, before considering the details of how this wave emission arises we conclude our discussion of the initial rise period by computing the fraction of the total yield which is contained in the kinetic energy of the rising fireball for a sea level detonation. We wish to compare this energy with our previous estimate for the energy available in the shock for long period gravity wave generation. The fireball kinetic energy is:

$$E_f = \frac{1}{2} M v^2 = \frac{1}{2} M g \beta a \quad (27)$$

where we have used Eq. (25) for v . The mass occurring in Eq. (27) is not the mass of the fireball itself but rather that of the considerably larger mass of ambient air which moves with the fireball, the so called virtual mass (DARWIN, 1953). This mass is equal to half the mass of ambient air which would occupy the fireball volume. Accordingly we write:

$$E_f = \frac{\pi}{3} a^4 \rho g \beta \quad (28)$$

According to Glasstone (1964, pp. 74-75) the terminal fireball radius is about 750 feet for a 20 KT detonation. The temperature at the time (1 sec) this radius is achieved is about 10 times ambient, and hence assuming pressure equilibrium $\beta = .9$. Assuming cube root scaling with yield we may then write, $a = 8.45 \times 10^3 Y^{1/3}$ cm, where Y is in kilotons. Eq. (28) then gives the fraction of the yield which is available as kinetic energy of fireball rise:

$$\frac{E_f}{Y} = 1.5 \times 10^{-4} Y^{1/3} \quad (29)$$

Comparing this with Eq. (23) we find that for a yield of about 1.6 MT, $E_f = E_s$. Thus for yields in excess of this value we expect the energy available in the rising fireball for long period gravity wave genera-

tion to be greater than the similar energy available in the upward going shock.

We now turn to a description of how this fireball rise energy becomes available for the generation of long period gravity waves.

3.1 Oscillating Vortex Model of Fireball Stabilization

In this section, the relation between a fireball in the terminal phase of its motion and the fluid oscillations that result as it stops rising are considered. An approximate expression for the frequency of the resulting motion is derived in terms of the final motions of the fireball and the atmospheric parameters. Our analysis of gravity wave generation by a rising fireball differs from the work of Tolstoy and Lau (1971) in that it is based on the theory of buoyant vortex ring.

We consider a ring vortex where the core radius R_0 is much smaller than the major radius R as shown in Figure 8. The substance, a spheroidal mass of air surrounding the ring, moves with the ring. The difference between the mass contained in the ring and in the substance, and an equal volume of the atmosphere is:

$$\Delta M = 2\pi \int_0^{\bar{r}} \int_{z_1(r)}^{z_2(r)} (\rho' - \rho_0) dz r dr, \quad (30)$$

where $\rho'(r, z)$ is the mass density inside the vortex, $\rho_0(z)$ is the ambient density, and $z_2(r)$, $z_1(r)$ define the boundaries of the substance.

On a contour such as 1, which contains but does not intersect the core, the circulation K is given by:

$$K = \frac{R \dot{z}}{C}, \quad (31)$$

where the dot indicates a time derivative. The quantity C depends logarithmically on the distribution of vorticity within the ring. We assume that the motion is similar and that therefore C is a constant.

The circulation along contours such as 1 and 2 changes during the rise according to the Bjerkness Eq:

$$\dot{K} = - \oint \frac{dp}{\rho}, \quad (32)$$

where p is the pressure, taken to be ambient under the assumption that equilibrium has been obtained.

On a contour such as 2 which does not contain the core, $K = 0$ at all times and hence $\dot{K} = 0$ at all times. On any contour such as 1, which contains but does not intersect the core, K must be the same. Hence at any time \dot{K} must be the same for all such contours.

Eq. (32) can be rewritten:

$$\dot{K} = - \oint \frac{dp}{\rho} = - \oint \frac{dp}{\rho_0} - \int_{z_1(r)}^{z_2(r)} \frac{dp}{\rho'} + \int_{z_1(r)}^{z_2(r)} \frac{dp}{\rho_0} = - \int_{z_1(r)}^{z_2(r)} dp \frac{(\rho_0 - \rho')}{\rho' \rho_0} \quad (33)$$

since $\oint \frac{dp}{\rho_0} = 0$. Using the hydrostatic equilibrium equation $\frac{dp}{dz} = -g\rho_0$ Eq. (33) finally becomes:

$$\dot{K} = g \int_{z_1(r)}^{z_2(r)} \frac{\rho_0 - \rho'}{\rho' \rho_0} dz \quad (34)$$

which is nonzero and independent of r for $r \leq R - R_0$ and is zero for $r \geq R + R_0$. Since the model is intended to apply to the later stages of fireball rise when the buoyancy has become small we replace ρ' in the denominator of Eq. (34) by ρ_0 . We further assume that the fireball is small enough that the integration in Eq. (34) takes place over much less than an atmospheric scale height and that the factor $1/\rho_0$ may be taken outside the integral. Then using Eq. (34) we may rewrite Eq. (30) as:

$$\Delta M = - \frac{2\pi}{g} \rho_0 \int_0^{\bar{r}} \dot{K} r dr = - \frac{\pi R^2}{g} \rho_0 \dot{K} \quad (35)$$

Conservation of mass gives:

$$\frac{d}{dt}(\rho'' V) = \rho_0 \left(\frac{dV}{dt} - \frac{dV_a}{dt} \right), \quad (36)$$

where V is the volume over which the integration in Eq. (30) is done and ρ'' is the average density within this volume. The term dV_a/dt represents the volume change due to adiabatic expansion as the vortex moves upwards:

$$\frac{dV_a}{dt} = - \frac{1}{\gamma} V \frac{1}{\rho_0} \frac{d\rho_0}{dt} \quad (37)$$

Thus Eq. (36) becomes:

$$\frac{d}{dt} V (\rho'' - \rho_0) = \frac{d\Delta M}{dt} = - V \frac{\gamma - 1}{\gamma} \frac{d\rho_0}{dt} \quad (38)$$

combining this result with Eq. (35) for ΔM we obtain

$$\ddot{K} + \dot{K} \frac{d}{dt} \ln \rho_0 R^2 - \frac{gV}{\pi R^2} \frac{\gamma - 1}{\gamma} \frac{1}{\rho_0} \frac{d\rho_0}{dt} = 0 \quad (39)$$

making use of the fact that

$$\frac{d\rho_0}{dt} = \frac{\partial \rho_0}{\partial z} \dot{z} \text{ and } \dot{z} = C \frac{K}{R} \text{ this becomes:}$$

$$\ddot{K} + \dot{K} \frac{d}{dt} \ln \rho_0 R^2 + \alpha^2 N^2 K = 0 \quad (40)$$

where $N^2 = -\frac{(\gamma - 1)}{\gamma} \frac{g}{\rho_0} \frac{\partial \rho_0}{\partial z}$ is the ambient Brunt-Väisälä frequency and $\alpha^2 = \frac{CV}{\pi R^3}$ is a constant of order unity as discussed below. Eq. (40) is most conveniently solved in terms of an auxiliary function Q :

$$K = \frac{Q}{\sqrt{\rho_0} R} \quad (41)$$

where

$$\ddot{Q} + \left[\alpha^2 N^2 - \frac{\sqrt{\rho_0} R}{\sqrt{\rho_0} R} \right] Q = 0 \quad (42)$$

and where $(\sqrt{\rho_0} R)$ represents $\frac{d^2}{dt^2} (\sqrt{\rho_0} R)$.

Assuming that the bracketed term in Eq. (42) is slowly varying we obtain the WKB solution:

$$Q \sim \frac{\exp i \int \left[\alpha^2 N^2 - \frac{(\sqrt{\rho_0} R)}{\sqrt{\rho_0} R} \right]^{1/2} dt}{\left[\alpha^2 N^2 - \frac{(\sqrt{\rho_0} R)}{\sqrt{\rho_0} R} \right]^{1/4}} \quad (43)$$

Using Eqs. (31) and (41) this gives the solution for \dot{z} :

$$\dot{z} \sim \frac{1}{\sqrt{\rho_0} R^2} \frac{\exp i \int \left[\alpha^2 N^2 - \frac{(\sqrt{\rho_0} R)}{\sqrt{\rho_0} R} \right]^{1/2} dt}{\left[\alpha^2 N^2 - \frac{(\sqrt{\rho_0} R)}{\sqrt{\rho_0} R} \right]^{1/4}} \quad (44)$$

Before discussing the physical significance of this equation it is useful to consider the quantity $\alpha = \frac{CV}{\pi R^3}$ in more detail. The volume V is approximately equal $\pi R^2 \Delta z$. Δz is the vertical distance over which the z integration in Eq. (30) is done. Alternatively Δz may be interpreted as the effective distance beneath the ring from which fluid is drawn up to the ring. Observations of laboratory releases of buoyant fluid with a spheroidal substance suggest the value $\Delta z = 3R$ (TURNER, J. S., 1960). The quantity C is about .13 for a spherical vortex (LAMB, 1932). This gives $\alpha = .62$. In general we expect α to be constant so long as C is, and to have a value somewhat less than unity.

Equation (44) applies from the time the fireball has formed a vortex ring and has entrained sufficient air that the interior density ρ' is approximately equal to the ambient value ρ_0 . Thus we are not able to describe the early stages of the rise. However, the more time consuming later stages of the rise will occur on a time scale the order of $\pi/\alpha N$, that is on the order of the Brunt-Väisälä period. For nuclear clouds which do not spread rapidly when approaching their stabilization altitude, vertical oscillations will occur at a frequency αN . According to Eq. (44), clouds which spread rapidly will undergo oscillations at a lower frequency than αN and the amplitude of the oscillations will subside as $1/R^2$ as the cloud spreads. If the cloud radius spreads sufficiently rapidly (such as exponentially on a time scale shorter than $1/\alpha N$) there will be no oscillatory motion and the approach to equilibrium will be overdamped.

In any case, for megaton range detonations where the nuclear cloud penetrates into the very stable stratosphere, a rapid growth in cloud radius ensues (GLASSTONE 1964, pp. 35-37). This would tend to reduce the amplitude of gravity waves due to vertical oscillations of the cloud. In general, for given atmospheric conditions there may be an optimum yield-height of burst combination for gravity wave generation by the stabilized fireball but it is currently unknown.

To gain further insight into the wave pattern generated by this type of buoyant oscillation, laboratory experiments have been performed at Mt. Auburn, as described below.

3.2 Laboratory Observations of Gravity Wave Generation by Buoyantly Rising Masses.

A photograph of the experimental apparatus is shown in Figure 9. The experiments were performed in a plexiglas tank 5' x 3' x 3½' deep. A linearly stratified density fluid (salt and water) was established in the tank by carefully introducing fluid layers of successively decreasing density. This stratification very closely approximates an exponential medium over the dimensions of the experimental region. The density gradient was checked by carefully weighing a 300 cc teflon rod suspended at varying depths in the fluid, and after some days it was found that the initial density discontinuities had smoothed out to form a linear density gradient. Using ethyl alcohol as the buoyant, miscible fluid, a number of buoyant releases were made from a release mechanism on the base surface of the tank. Visualization of the wave motions in the fluid was achieved using small neutrally buoyant polystyrene beads which acted as excellent scattering centers for a well collimated light beam. Thus a cross-section through the fluid motions was observed.

A 16 mm cine camera was used to record the internal wave motions and schematic drawing based on a sample frame is shown in Figure 10. For this release the buoyant fluid was dyed to be readily observable. The formation of a vortex ring structure and vertical oscillations and rapid spreading of the initially buoyant fluid as it reached its equilibrium level were clearly observed.

Typically the time required for the top of the released fluid to reach its maximum altitude was about 8 seconds, somewhat shorter than the Brunt-Väisälä period in the tank (9.8 seconds).

The wave pattern, which was more complex than anticipated, is conveniently divided into the four regions shown in Figure 10: (1) Directly above and below the source region small amplitude oscillations of the beads were observed. The period of these oscillations as nearly as could be determined was equal to the Brunt-Väisälä period. (2) The amplitude and the period of the oscillations increased with increasing angle from the vertical. The amplitude reached a maximum at an angle of about 60° where the period was about 12 seconds. (3) The amplitude then decreased slightly with increasing angle. This region existed over a relatively small angle and it was difficult to observe changes in the period within this region. (4) Finally, at very small angles to the horizontal planes of stratification, motion of the beads was observed which was not periodic, rather the beads were displaced away from the source region and did not return. This motion is clearly related to the horizontal spreading of the initially buoyant fluid as it equilibrates.

The propagation theory for acoustic-gravity waves predicts that waves of period τ whose vertical wavelength is less than a scale height should propagate at an angle θ from the vertical (HINES, C.O., 1960), where:

$$\frac{\tau_{BV}}{\tau} = |\cos \theta| \quad (45)$$

This propagation law does appear to be obeyed in the experiment since $\tau = \tau_{BV}$ at $\theta = 0, \pi$ and $\tau = \frac{2}{\sqrt{3}} \tau_{BV}$ at $\theta = \pi/3, 2\pi/3$. In theory there should be no propagating solution exactly at $\theta = 0, \pi$ where $\tau = \tau_{BV}$. However, because of the limited spatial extent of the experimental region we are unable to clearly distinguish propagating from nonpropagating disturbances.

Perhaps the most interesting aspect of the laboratory observations is the confirmation of the theoretical prediction that much of the buoyant rise energy is utilized to generate waves in the period range $1 - 2 \tau_{BV}$. Our expectation is that an analogous process of wave generation would occur for a stabilizing nuclear cloud. However, while we are able to estimate the period of the largest amplitude portion of the disturbance we have not estimated what fraction of the available energy goes into very long periods, that is periods many times the Brunt-Väisälä period. These long period waves would propagate at shallow angles to the horizontal and it may be that atmospheric refraction would prevent their reaching ionospheric levels. In this connection it is interesting to note that ionospheric disturbances of about 3 minutes period, which are associated with severe weather, are not normally observed more than 250 km horizontally from the apparent source location (GEORGES, T. M., 1968). Whether the absence of longer periods at greater horizontal distances is a result of properties of the source or of atmospheric filtering and refraction is not known.

4. CONCLUSION

In the preceding sections we have attempted to relate the different kinds of disturbance seen in the ionosphere to the hydrodynamic motions accompanying a low altitude nuclear explosion. The short period ionospheric disturbances seem to be caused by the portion of the shock front which is reflected from the 100-120 km altitude level. This identification is made because the periods contained within the shock when it reaches this altitude level are the order of the observed ionospheric periods, that is, about a minute. We expect the ionospheric periods to scale with explosion parameters in the same way as does the shock positive phase duration at the 100-120 km altitude level. The ionospheric periods should therefore be proportional to the cube root of yield and essentially independent of height of burst.

The origin of ionospheric disturbances with periods exceeding 10 minutes is a more complex problem since both the upward going shock and the rising fireball are possible hydrodynamic sources. For yields in excess of about a megaton the energy available in fireball rise for the production of long period disturbances exceeds that available in the upward going shock.

The mechanism described by Greene and Whitaker (1968) for the generation of long period ionospheric waves involves a refraction of the upward going shock at the 100-120 km altitude level. This results in a

transfer of energy from the shock to a horizontally propagating disturbance which is left behind. The Greene-Whitaker mechanism is generally operative since conditions for this shock refraction are a permanent feature of the atmosphere.

The fireball is most efficient in the generation of long period acoustic-gravity waves when it has reached its terminal altitude and is approaching hydrodynamic equilibrium with the atmosphere. It may then undergo vertical oscillations with a period somewhat larger than the Brunt-Väisälä period. The efficiency of wave generation by this mechanism is very sensitive to ambient conditions at the tropopause as well as to burst parameters. In particular nuclear clouds which undergo rapid spreading upon stabilization appear to be inefficient wave generators. In theory, and this is supported by laboratory experiments, the terminal phases of fireball rise, when the mechanism is efficient, produce a wave spectrum with amplitudes peaked at one to two times the Brunt-Väisälä period. These periods propagate at relatively steep angles to the horizontal and would primarily affect the ionosphere near the burst. Whether significant wave amplitudes could be produced at much longer periods is presently unknown as is the question of whether these long periods, which propagate at shallow angles to the horizontal, would be prevented by atmospheric refraction from reaching ionospheric levels.

ACKNOWLEDGEMENTS

Drs. T. I. McLaren and T. Fohl carried out the laboratory experiments reported in the text.

This work was sponsored by the Advanced Research Projects Agency under Air Force Office of Scientific Research Contract #F44620-71-C-0086.

REFERENCES

- BAKER, D. M., 1968, "Acoustic Waves in the Ionosphere Following Nuclear Explosions" in Acoustic-Gravity Waves in the Atmosphere, T. M. Georges, Ed., U. S. Government Printing Office, pp. 79-86.
- BAKER, D. M. and K. DAVIES, 1968, "Waves in the Ionosphere Produced by Nuclear Explosions," J. Geophys. Res. **73**, 448.
- BARRY, G., 1963, "Ray Tracings of Acoustic Waves in the Upper Atmosphere," J. Atmos. Terrest. Phys. **25**, 621.
- DARWIN, Sir Charles, 1953, "Note on Hydrodynamics," Proc. Camb. Phil. Soc. **49**, 342.
- GEORGES, T. M., 1968, "Short-Period Ionospheric Oscillations Associated with Severe Weather," in Acoustic-Gravity Waves in the Atmosphere, T. M. Georges, Ed., U. S. Government Printing Office, pp. 171-178.
- GLASSTONE, S., 1964, The Effects of Nuclear Weapons, U. S. Government Printing Office.
- GREENE, J. S., Jr. and W. A. WHITAKER, 1968, "Theoretical Calculations of Traveling Ionospheric Disturbances Generated by Low Altitude Nuclear Explosions," in Acoustic-Gravity Waves in the Atmosphere, T. M. Georges, Ed., U. S. Government Printing Office, pp. 45-64.
- HERRON, T. J., 1971, "Group Velocities of Atmospheric Gravity Waves," J. Atmos. Sci. **28**, 598.
- HINES, C. O., 1960, "Internal Atmospheric Gravity Waves at Ionospheric Heights," Can. J. Phys. **38**, 1441.
- HOOKE, W. H., 1968, "Ionospheric Irregularities Produced by Internal Atmospheric Gravity Waves," J. Atmos. Terrest. Phys. **30**, 795.
- LAMB, Sir Horace, 1932, Hydrodynamics, Cambridge University Press.
- LEHTO, D. L. and R. A. LARSON, 1969, "Long Range Propagation of Spherical Shockwaves from Explosions in Air," Technical Report: NOLTR 69-88, U. S. Naval Ordnance Laboratory, White Oak, Maryland.
- LUTZKY, M. and D. L. LEHTO, 1968, "Shock Propagation in Spherically Symmetric Exponential Atmospheres," Phys. of Fluids **11**, 1466.
- MEECHAM, W. C., 1968, "Effect of Atmospheric Wind Structure on Shorter Period, Nuclear-Generated Infrasound," J. Geophys. Res. **73**, 377.
- MOWBRAY, D. E. and B. S. H. RARITY, 1967, "The Internal Wave Pattern Produced by a Sphere Moving Vertically in a Density Stratified Liquid," J. Fluid Mech. **30**, 489.
- REED, S. G., Jr., 1959, "Note on Finite Amplitude Propagation Effects on Shock Wave Travel Times from Explosions at High Altitude," J. Acous. Soc. Am. **31**, 1265.
- SCORER, R. D., 1950, "Experiments on Convection of Isolated Masses of Buoyant Fluid," J. Fluid Mech. **2**, 583.
- THOMAS, J. E., A. D. PIERCE, E. A. FLINN and L. B. CRAINE, 1971, "Bibliography on Infrasonic Waves," Geophysical Journal of the Royal Astronomical Society **26**, Nos. 1-4.
- TOLSTOY, I., and J. LAU, 1971, "Generation of Long Internal Gravity Waves in Waveguides by Rising Buoyant Air Masses and Other Sources," Geophysical Journal of the Royal Astronomical Society **26**, Nos. 1-4.
- TURNER, J. S., 1950, "A Comparison Between Buoyant Vortex Rings and Vortex Pairs," J. Fluid Mech. **7**, 419.
- WARREN, F. W. G., 1960, "Wave Resistance to Vertical Motion in a Stratified Fluid," J. Fluid Mech. **7**, 209.

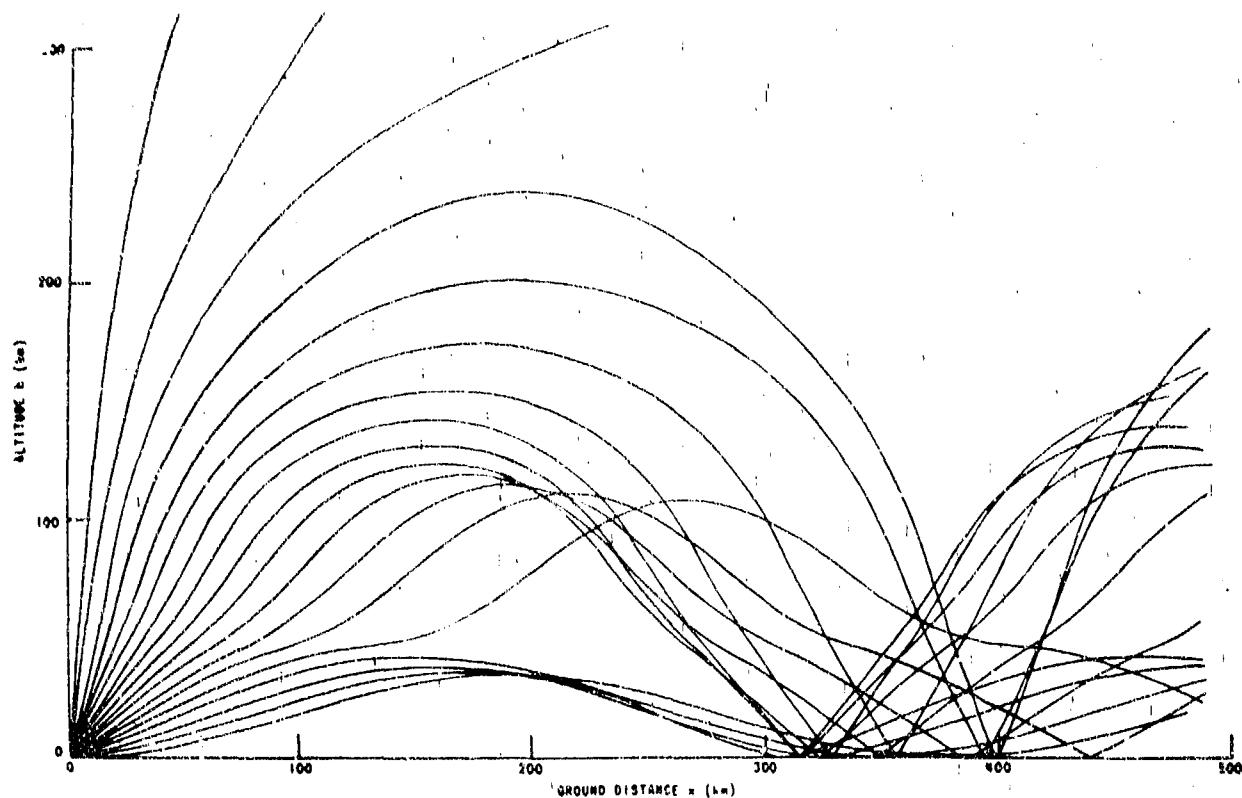


Fig.1 Acoustic ray tracing for a sea-level source. Initial ray angles begin with 0° from the horizontal and increase by 5° increments. From BARRY (1963).

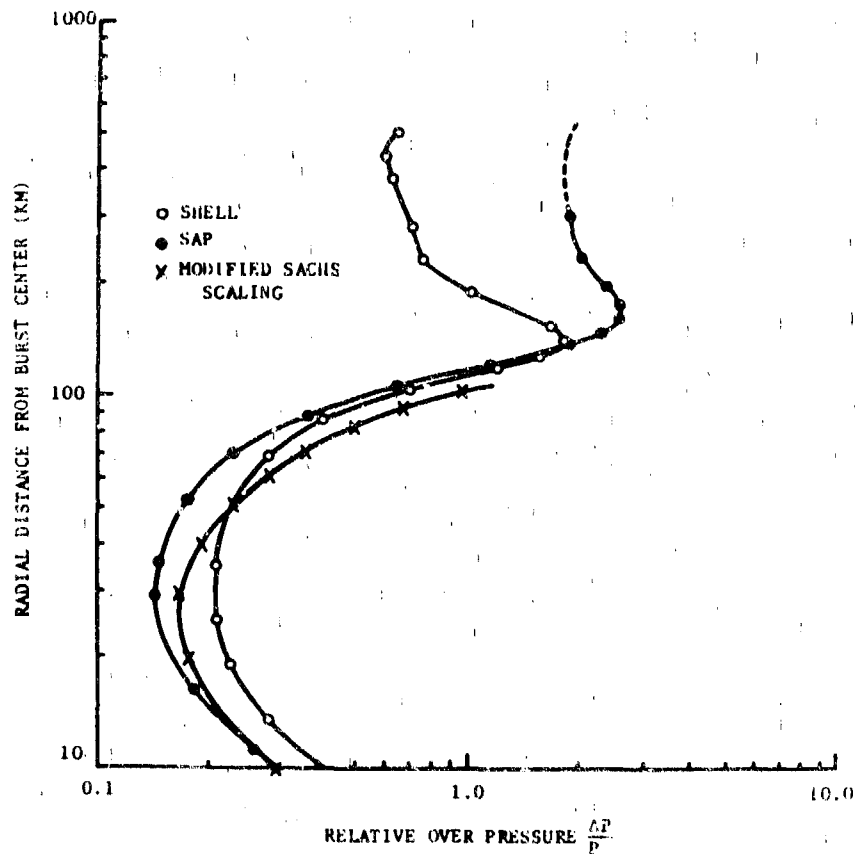


Fig.2 Comparison of SHELL and SAP Codes at 45° with modified Sachs scaling for 4 M/T at 5 km. After GREENE and WHITAKER (1968).

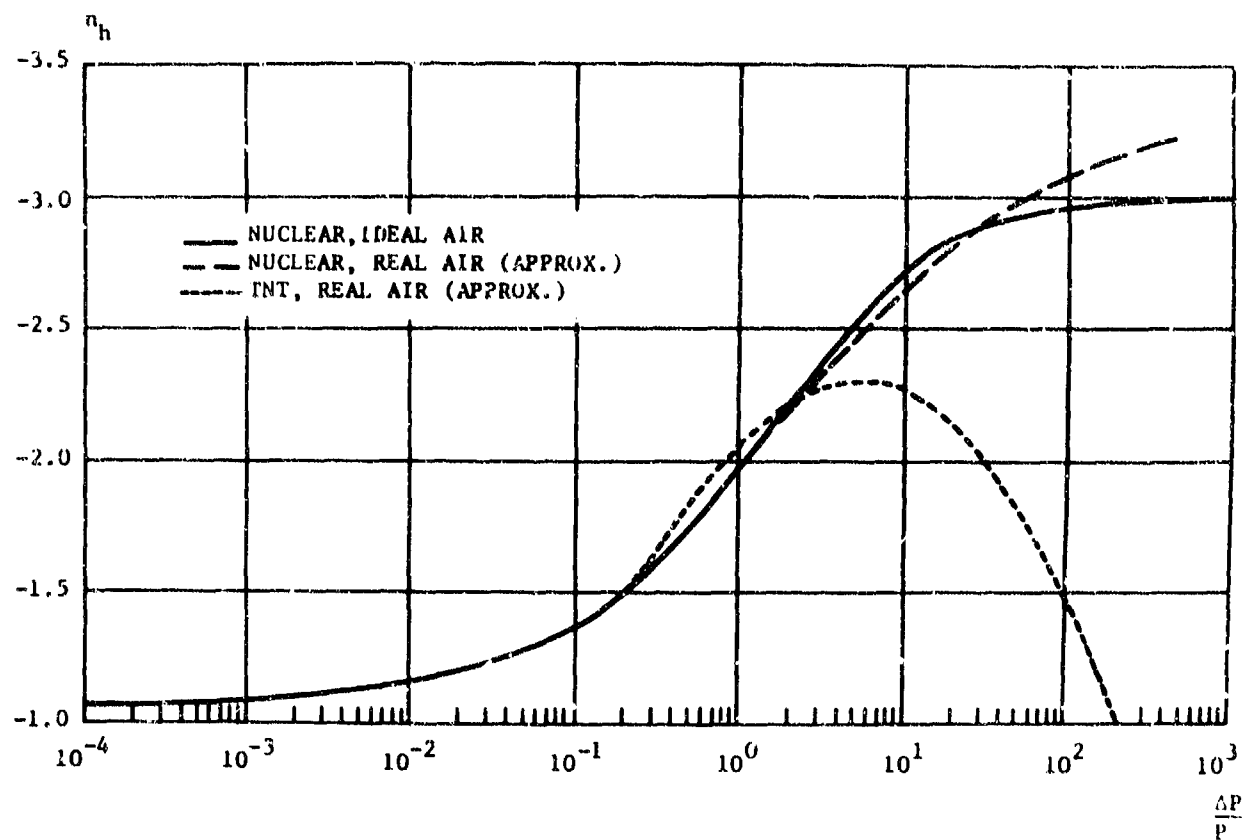


Fig.3 The Parameter n_h vs relative overpressure. From LEHTO and LARSON (1969).

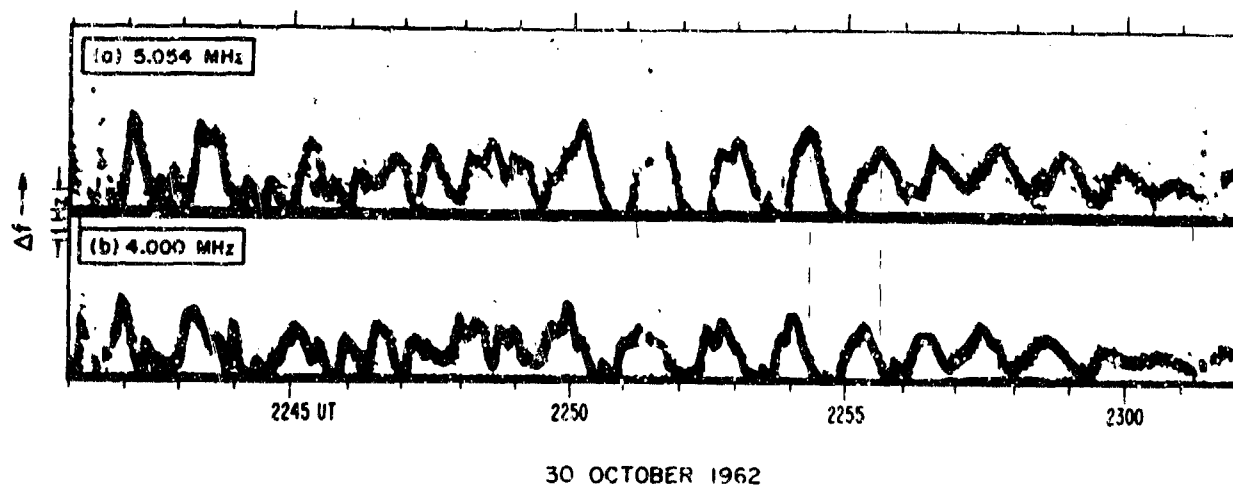


Fig.4 Detail of ionospheric disturbance above Boulder on October 30, 1962. From BAKER (1968).

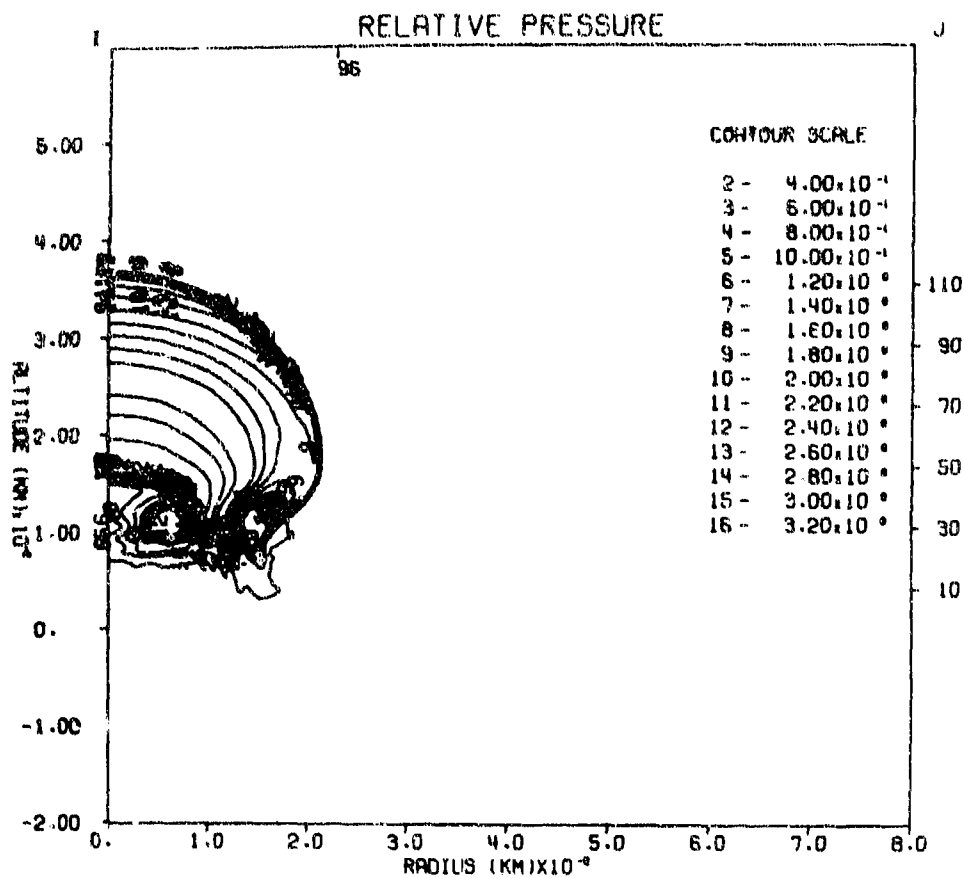


Fig.5 SHELL calculation of 4 MT isothermal sphere at a time of 600 seconds showing contours of relative pressure.
From GREENE and WHITAKER (1968).

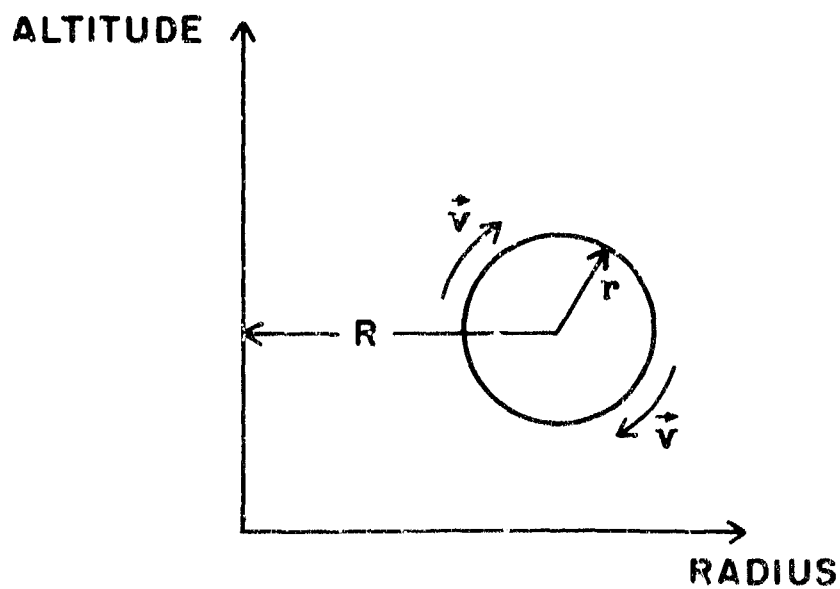


Fig.6 Assumed geometry for vortical flow due to the Greene-Whitaker mechanism.

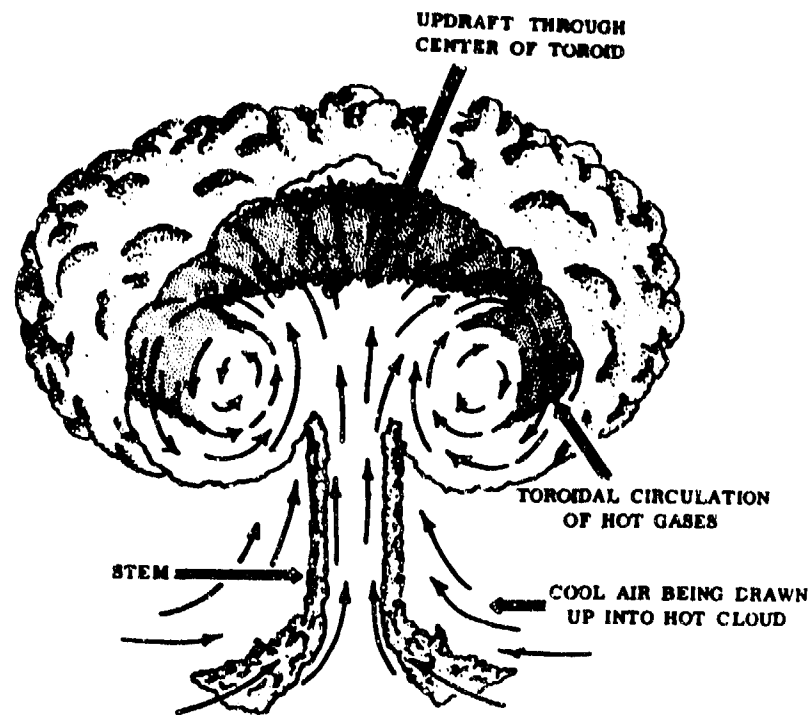


Fig. 7 Cutaway of nuclear cloud showing internal flow. From GLASSTONE (1964, p. 31).

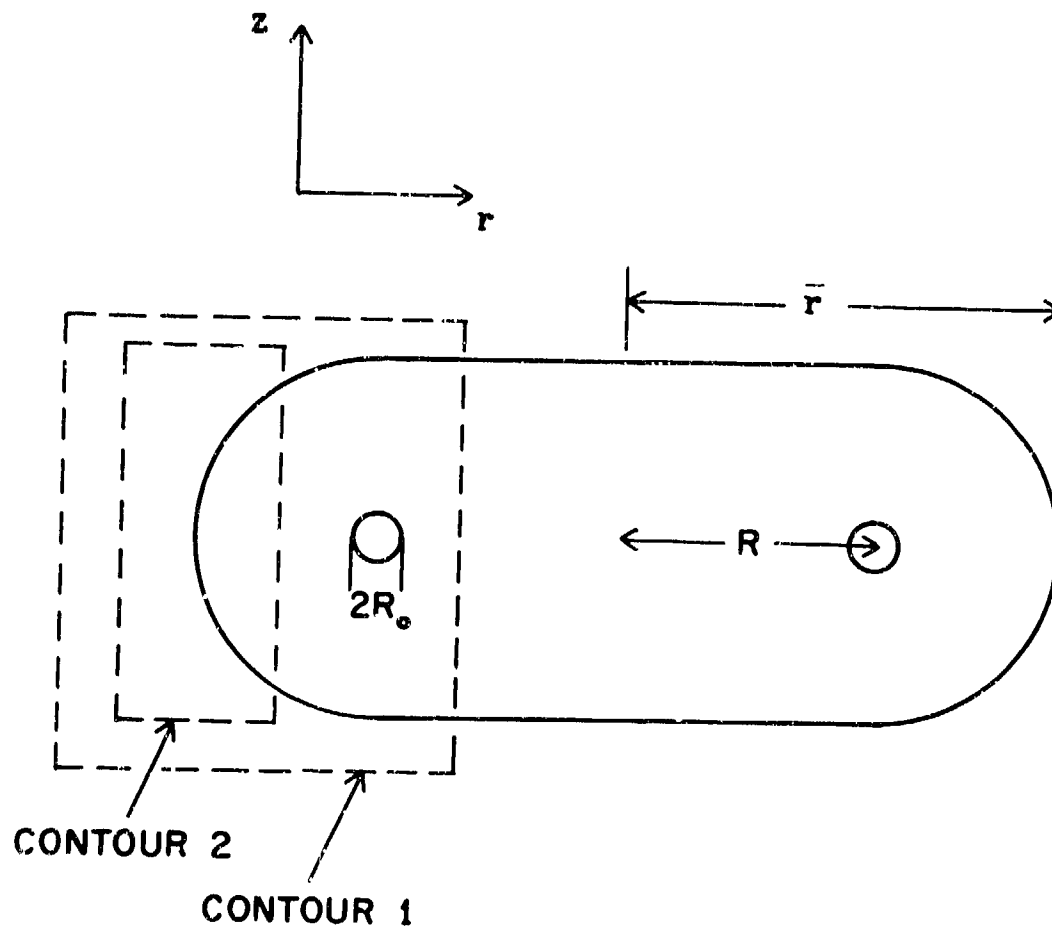


Fig. 8 Assumed vortex ring configuration with contours used to calculate vorticity.

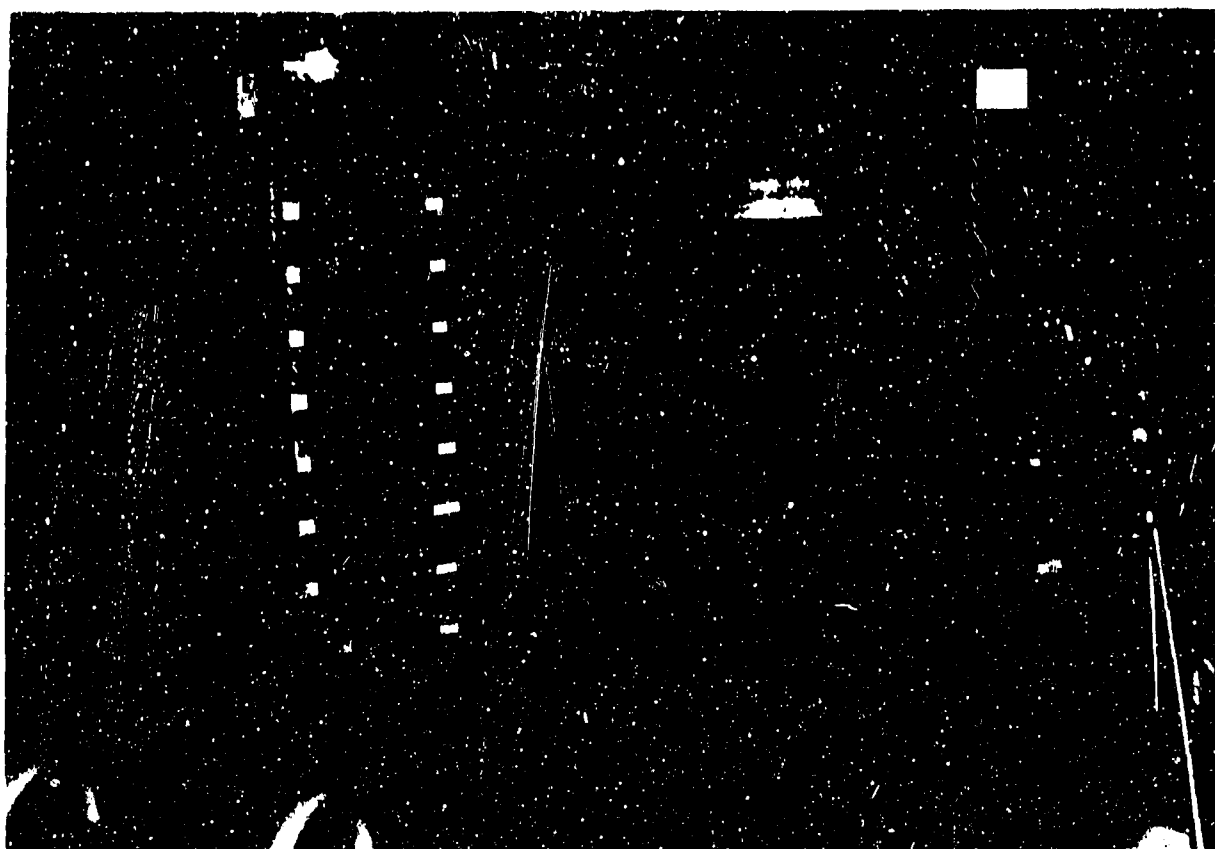


Fig.9 Experimental facility for simulation of wave generation due to buoyant rise.

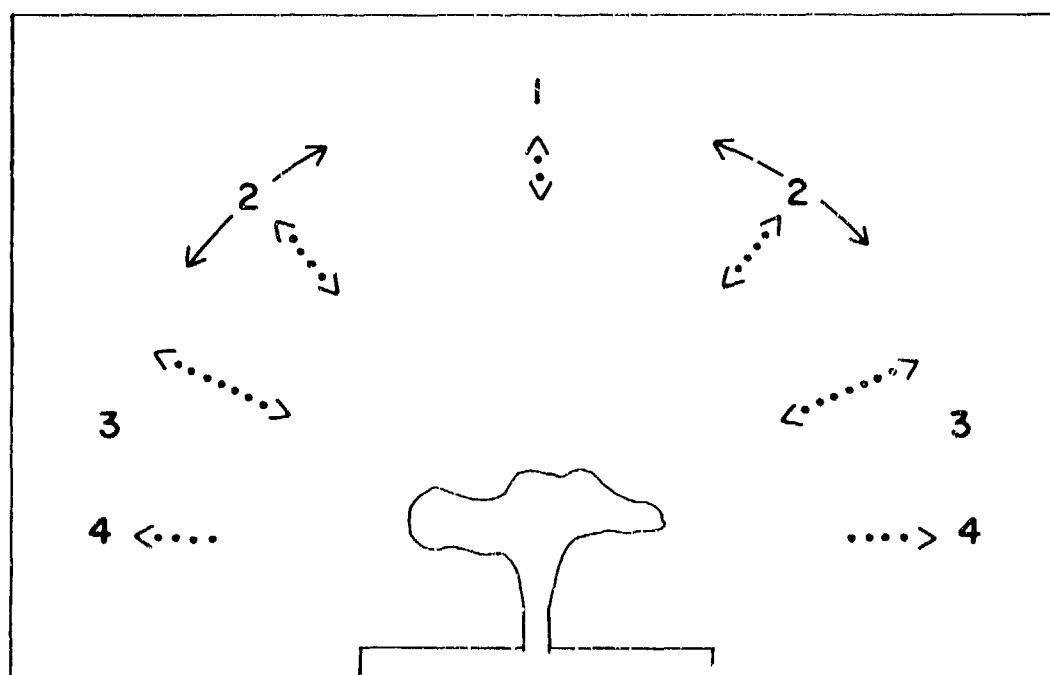


Fig.10 Observed wave pattern showing angular regions described in text.

THEORIE DE LA PROPAGATION ACOUSTIQUE ATMOSPHERIQUE

par

Ch. Berthet et Y. Rocard

Laboratoire de Physique, Ecole Normale Supérieure
Paris, France

THE THEORY OF ATMOSPHERIC ACOUSTIC PROPAGATION

by

Ch. Berthet and Y. Rocard

Abstract

Infrasonic waves generated by large explosions on the ground can be observed to propagate up to ranges of thousands of kilometers.

If an explosion is strong enough to generate gravity waves, that is exceeds a threshold of about one megaton, waves with periods near one minute travel around the earth according to a well known mechanism.

Waves of shorter period, in the range 5 to 45 seconds, are observed to propagate more efficiently than might be expected according to elementary theories of acoustic rays bending by temperature gradients and winds. However, we demonstrated a few years ago that the introduction of non linearity in the propagation of such waves resulted in the bending of acoustic rays back to the ground and that it explained most of the experimental facts.

But we also observed exceptional cases of propagation to ranges of 7 000 - 8 000 kilometers and even up to 14 000 kilometers, in fairly narrow azimuthal sectors, generally in a bearing 90 East of the explosion. The periods are in the range 30 to 60 seconds and the waves do not exhibit the characteristic dispersion of gravity waves.

In order to explain such observations, we propose the following mechanism. Waves propagating upwards away from the explosion in directions a few degrees off the vertical are bent back towards the ground at altitudes of 85 to 95 kilometers, according to the yield of the explosion. In the course of the process the various ray paths intersect along a ring centered on the vertical of the explosion and located at these altitudes, which we shall call the "Noise Ring" (Couronne de Bruit). In his Ph.D. Thesis (Paris 1969), Ch. BERTHET showed that these ray paths, besides intersecting to produce a phenomenon of geometric focusing, correspond to waves arriving roughly in phase at the noise ring which is then equivalent to a circular focus line.

The concentrating of energy at the ring produces very pronounced non linear effects and it can be shown that the ring behaves as a secondary acoustic source radiating out sonic waves in directions different from those of the rays which produced it.

Since in the range of altitudes 85 to 95 kilometers a horizontal propagation channel exists produced by the increase in temperature at higher altitudes (above 110 kilometers) and at lower altitudes (near 50 kilometers) plus an important contribution of the distribution of tidal winds, the waves radiated by the noise ring in that duct can propagate to considerable ranges.

Such an explanation is in conformity with experimental observations namely that the speed of sound waves along such paths is slightly less than the speed of sound at low altitudes. We find that it is roughly equal to the speed of sound at 80°C plus 20-25 m/s easily accounted for by non linearity in the propagation.

The purpose of the paper is to provide a comprehensive view of the phenomenon, supported by a calculation which, although elementary, demonstrates the radiating properties of the noise ring in directions other than those of the rays which formed it.

THEORIE DE LA PROPAGATION ACOUSTIQUE ATMOSPHERIQUE

Dr Ch. BERTHET^x, Prof. Y. ROCARD*

1. Equations de départ

On considère que l'atmosphère est un milieu stratifié horizontallement et on néglige la courbure terrestre. Les propriétés de cette atmosphère sont donc indépendantes de x , abscisse, et ne dépendent que de l'altitude z .

On considère en outre que l'air est un gaz parfait.

Soit une perturbation d'amplitude infiniment petite se propageant dans ce milieu avec une certaine vitesse $U(z)$, variable uniquement avec l'altitude z . Si on appelle a l'angle d'un rayon avec l'horizontale, en l'absence de vent, la propagation suivra la loi de Descartes, soit

$$\frac{U(z)}{\cos a} = \text{constante}$$

l'angle a étant également fonction de z , et les rayons auront une courbure donnée par la formule classique

$$\frac{\cos a}{U(z)} \frac{\partial U}{\partial z} = \frac{1}{R}$$

* Directeur du Laboratoire de Physique
de l'Ecole Normale Supérieure
24, rue Lhomond, Paris, 5

^x Même adresse.

2. Intervention du vent - Formules de propagation normale

On considère encore que le vent est à stratification uniquement horizontale. Le milieu n'étant plus isotrope, les rayons ne sont pas normaux aux surfaces d'onde. L'angle de ces dernières avec l'horizontale est $\pi/2 - a$. Soit θ l'angle des rayons avec l'horizontale.

Nous appellerons x la longueur de rayon, t le temps de propagation d'un front d'onde le long d'un rayon et P la pente du rayon par rapport à l'horizontale. En particulier, et dans le cas d'une atmosphère avec vent,

$$P = \operatorname{tg} \theta = \frac{dz}{dx} \neq \operatorname{tg} a$$

La vitesse de propagation de la perturbation résultera donc de la composition vectorielle des vitesses $U(z)$, déjà définie, et $v(z)$, vitesse du vent. Cette dernière vitesse est supposée toujours horizontale.

La loi de Descartes devient, exprimant que les deux rayons se réfractent en O_1 et O_2

$$v(z) + \frac{U(z)}{\cos a} = K_0 \quad (1)$$

K_0 est une constante.

D'autre part la vitesse du point M sur le rayon est donnée par les deux formules suivantes, exprimant ses composantes horizontale et verticale,

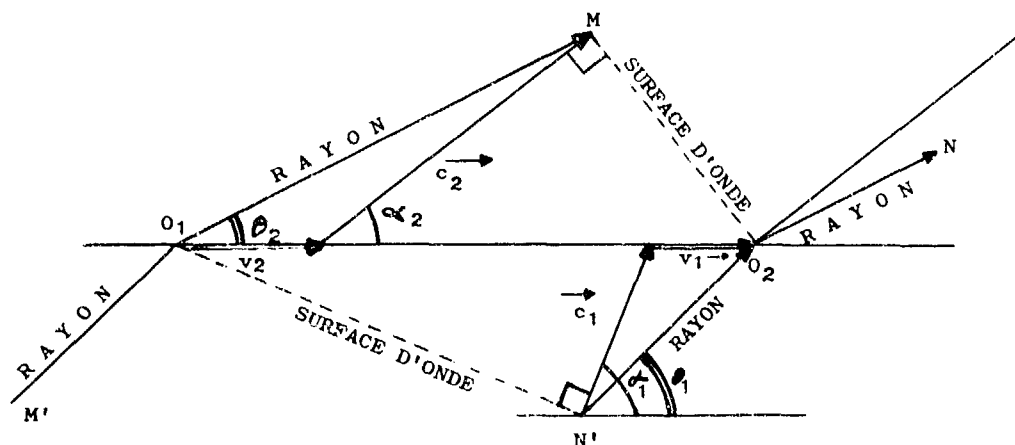


Figure classique de la réfraction avec vent.

Composition vectorielle des vitesses.

Le rayon $M'O_1$ se réfracte suivant O_1M .

c_1 et c_2 sont les vitesses du son, v_1 et v_2 les vitesses de vent.

Les rayons ne sont pas normaux aux surfaces d'onde.

$$\frac{dx}{dt} = v(z) + U(z) \cdot \cos a \quad (2)$$

$$\frac{dz}{dt} = U(z) \cdot \sin a \quad (3)$$

Eliminant a entre ces trois équations, il vient :

$$\frac{dx}{dz} = \frac{U(z)}{[(K_0 - v)^2 - U^2]^{1/2}} \cdot \frac{v (K_0 - v)}{U \cdot [(K_0 - v)^2 - U^2]^{1/2}} \quad (4)$$

On suppose qu'à l'intérieur d'une tranche d'atmosphère d'épaisseur Δz le vent est constant ($v(z) = \text{constante} = v_0$) et la vitesse $U(z)$ varie suivant la loi

$$U^2(z) = Q (z - z_0) + U^2(z_0) \quad (5)$$

Q étant une constante, variable de tranche en tranche.

On tire alors de l'équation (4) trois équations différentielles simples donnant la distance x , la longueur s et le temps t en fonction de la variable z . La constante z_0 est l'altitude inférieure de la tranche dans laquelle on effectue les calculs. On pose enfin, pour alléger les calculs,

$$G_0 = K_0 - v_0$$

On a donc :

$$dx = \frac{v_0 G_0 + U^2}{U [G_0^2 - U^2]^{\frac{1}{2}}} dz \quad (6)$$

$$ds = \left[\frac{U^2 G_0^2 + 2U^2 G_0 v_0 + G_0^2 v_0^2}{U^2 (G_0^2 - U^2)} \right]^{\frac{1}{2}} dz \quad (7)$$

$$dt = \frac{G_0}{U [G_0^2 - U^2]^{\frac{1}{2}}} dz \quad (8)$$

La pente du rayon est évidemment donnée par (6), d'autre part G_0 est une constante de la tranche, variable de tranche en tranche comme la vitesse v_0 .

On trouve ainsi, avec v_0 , s_0 et t_0 comme constantes d'intégration, les équations suivantes pour la distance horizontale, la longueur de rayon et le temps de propagation, comptés à partir du bas de la tranche dans laquelle on fait l'intégration,

$$x - x_0 = - \frac{1}{Q} \left[\left[U^2 (G_0^2 - U^2) \right]^{\frac{1}{2}} + \frac{G_0 (G_0 + 2v_0)}{2} \text{Arc sin} \frac{G_0^2 - 2U^2}{G_0^2} \right] \quad (9)$$

$$t - t_0 = - \frac{G_0}{Q} \text{Arc sin} \frac{G_0^2 - 2U^2}{G_0^2} \quad (10)$$

$$s - s_0 = - \frac{2 G_0}{Q} (G_0^2 - U^2)^{\frac{1}{2}}$$

avec évidemment $Q = (U^2 - U_0^2) / \Delta z$.

3. Calcul de la vitesse U

On sait que toute onde qui monte tend vers une onde de choc. D'autre part, on a pu constater des arrivées de signaux en forme typique d'ondes de choc.

Les formules normales de la propagation des ondes de choc permettent de déterminer la valeur de U :

$$U = \frac{\gamma + 1}{4} u + c^2 + \left(\frac{\gamma + 1}{4} u \right)^2^{\frac{1}{2}}$$

où u est la vitesse de la tranche d'air.

D'autre part, on sait également que la vitesse u est donnée par

$$u(z) = u(0) \exp(z/2H)$$

où z est l'altitude et H la hauteur réduite ($H = c^2/\gamma g$).

4. Détermination définitive de la vitesse U

H. BETHE, dès 1943, a proposé pour l'évaluation de la vitesse de l'air au sol, dans une atmosphère homogène à la pression atmosphérique,

$$u \text{ (km/s)} = \frac{0.02}{s} W^{1/3}$$

où s est la distance (en kilomètres) parcourue par l'onde et W la puissance de l'explosion qui donne naissance à cette onde, en kilotonnes équivalentes de trinitrotoluène (T.N.T.). (1 kilotonne = 10^{12} calories)

Il en résulte, en tenant compte de l'effet d'amplification en fonction de l'altitude, qu'à une altitude z on a

$$u \text{ (km/s)} = \frac{0.02}{s} W^{1/3} \exp(+z/2H)$$

Cette dernière formule, combinée à la formule donnant la valeur de U en fonction de u et de c , conduit à l'expression complète de la vitesse de propagation,

$$U \text{ (km/s)} = \frac{0.012}{s} W^{1/3} \exp(+z/2H) + \left[c^2 + \frac{0.012^2}{s^2} W^{2/3} \exp(+z/H) \right]^{1/2}$$

cette dernière formule se simplifiant et conduisant à la formule suivante, en première approximation :

$$U(-) \text{ (km/s)} = c(z) + \frac{0.012}{s} W^{1/3} \exp(+z/2H)$$

5. Propagation très lointaine par guidage en altitude

Le mode général de propagation exposé précédemment peut être considéré comme relativement stable et bien déterminé. Les distances maximales atteintes par les ondes acoustiques pour des puissances de tir inférieures à celles qui engendrent des ondes de gravité sont de l'ordre de 1500 à 2500 km environ suivant les cas, après un certain nombre de réflexions successives sur le sol ou sur la surface des océans. En effet, le coefficient de réflexion (rapport de l'amplitude réfléchie à l'amplitude incidente) est plus élevé en moyenne dans le deuxième cas que dans le premier. On peut concevoir qu'une chaîne montagneuse perturbe considérablement une réflexion au sol pour des ondes dont les périodes seraient comprises entre 20 et 30 secondes et les longueurs d'onde entre 6 et 9 kilomètres.

Les temps de propagation pour ces distances correspondent à des vitesses apparentes (en moyenne 210 m/s) très inférieures aux valeurs habituelles de la vitesse du son au sol. Ceci est évident, d'ailleurs, si on songe au trajet considérablement allongé par les arches successives que doivent parcourir les ondes infrasonores.

Or, en une certaine occasion, nous avons pu constater que des ondes infrasonores de 20 à 30 secondes de période pouvaient se propager à des distances bien plus grandes, telles que 7000 à 8000 km. Eu égard à leur période, ces ondes n'auraient pu être des ondes de gravité. Elles présentaient, sans le moindre doute, les caractéristiques des ondes acoustiques étudiées dans ce travail.

L'examen des temps de propagation de ces signaux, de l'ordre de 7 heures, fait apparaître une vitesse moyenne apparente de propagation d'environ 290 m/s, donc proche de la vitesse du son

dans une atmosphère normale à la température de 210 degrés Kelvin environ, soit encore - 63 degrés Celsius.

Cette vitesse moyenne, et pour une propagation couvrant 7400 km, est nettement supérieure à celle que l'on pourrait prévoir en extrapolant nos diagrammes de propagation. En effet, on trouverait des temps de propagation d'environ 12 à 14 heures pour cette distance et partant, des vitesses apparentes moyennes de 140 à 170 m/s.

Il est donc clair que le mécanisme exposé précédemment ne convient pas, directement, pour expliquer ce type de propagation.

Le mécanisme éventuel d'une telle propagation - à très longue distance - par le moyen des ondes de gravité ne convient pas non plus pour deux raisons: d'une part, nous l'avons déjà indiqué, les périodes des ondes considérées ici sont de l'ordre de 30 s et moins, alors que celles des ondes de gravité atteignent plutôt 1 minute et même 2 ou 3 mn. D'autre part, les vitesses de propagation les plus faibles des ondes de gravité dépassent nettement 300 m/s pour atteindre 315 m/s pour des périodes de 3 minutes. Nous allons voir que ces caractéristiques, et surtout celle, pour la vitesse, d'être plutôt de 290 m/s, confirment l'hypothèse que nous allons avancer quant au mécanisme physique de ce type particulier de propagation.

Retour sur la propagation normale proche

L'étude approfondie des propagations non-linéaires normales exposées plus haut conduit à une constatation intéressante.

- pour une propagation linéaire, donc avec une puissance W nulle, beaucoup de rayons atteignent l'altitude de 200 km et ne reviennent pas, les autres ne reviennent au sol qu'après s'être réfléchis assez haut.

- pour une propagation non-linéaire normale, par exemple avec $W = 100$ kilotonnes, on constate qu'un faisceau assez large de rayons, d'angles de site compris entre 75 degrés et 85 degrés environ, se refocalise aux alentours de 90 kilomètres d'altitude.

Cette focalisation pourrait n'être qu'apparente et géométrique, et résulter de la simple superposition des différents rayons. Or, le calcul des temps d'arrivée du front d'onde au point de convergence de ces rayons montre qu'il n'en est rien. Les ondes arrivent en même temps à cet endroit. On a donc bien là un authentique phénomène de focalisation en altitude. Par ailleurs, les surfaces d'onde convergent vers le point de focalisation pour s'y confondre elles-mêmes en un foyer, ceci étant bien entendu une vue à deux dimensions du phénomène, dans un plan vertical.

En l'absence de vent, il existe une symétrie de révolution autour de l'axe vertical et en réalité nos trajectoires se recoupent sur une focale en anneau vers 35 - 40 km de distance horizontale, rayon de la focale, et à 80 - 100 km d'altitude.

Comme nous sommes encore dans la zone de propagation proche, le vent, à moins d'être particulièrement violent, ne déforme que peu les trajectoires et on peut considérer que la focale en anneau, plus ou moins bien circulaire, existe toujours.

Il faut remarquer que seule la propagation non-linéaire donne lieu à ce phénomène de refocalisation en altitude.

En effet, dans le cas d'une propagation linéaire en atmosphère calme, quelques rayons se recoupent bien en altitude vers 125 km d'altitude et à plus de 150 km de distance, mais on n'observe pas à cet endroit de véritable phénomène de focalisation. Les temps d'arrivée au point d'intersection géométrique des rayons sont différents.

La seconde remarque importante est que les altitudes de ces différentes couronnes focales les situent à l'intérieur du guide d'onde acoustique des 90 kilomètres. En effet, la température de l'air est minimale à cette altitude (elle est de 180 degrés Kelvin environ). Si on admet que cette couronne focale se comporte comme une couronne de bruit servant de source secondaires et peut ainsi engendrer des trajectoires sonores, celles-ci pourront donc exploiter ce canal de propagation et se propager fort loin grâce au guide d'onde acoustique.

Nous voyons donc là un moyen d'expliquer le cas, cité plus haut, de propagation à très longue portée. Par ailleurs, comme nous allons le constater, les vitesses de propagation concordent.

Mais comment la focale, ou la couronne de bruit, peut-elle rayonner à l'extérieur de l'angle des rayons extrêmes du pinceau de rayons qui la forment ?

6. Analyse théorique du rayonnement par la couronne

Pour démontrer que la couronne de bruit rayonne effectivement en dehors du dièdre formé par les rayons extrêmes, il est nécessaire de faire appel, encore une fois, à des termes de non-linéarité. Nous allons montrer ceci dans un cas particulier simple, qui serait facile à généraliser.

L'équation adiabatique

$$PV^\gamma = \text{constante} \quad (1)$$

s'écrit aussi

$$\frac{P}{P_0} = \frac{1}{\left(1 + \frac{\partial}{\partial x} + \frac{\partial}{\partial z}\right)^\gamma} \quad (2)$$

si on admet par exemple une intersection des rayons sonores suivant O_x et O_z .

Dans un domaine où les ondes peuvent être considérées comme sinusoïdales, on aura

$$\left. \begin{aligned} &= A \sin \omega_1 \left(t - \frac{x}{c}\right) \\ \text{et} &= B \sin \omega_2 \left(t - \frac{z}{c}\right) \end{aligned} \right\} \quad (3)$$

Reportant ces expressions dans la formule (2), il vient évidemment

$$\frac{P}{P_0} = \frac{1}{\left[1 + \omega_1 \frac{A}{c} \cos \omega_1 \left(t - \frac{x}{c}\right) + \omega_2 \frac{B}{c} \cos \omega_2 \left(t - \frac{z}{c}\right)\right]^\gamma}$$

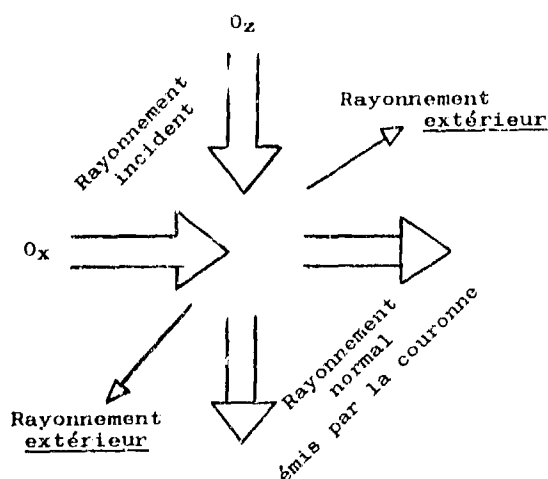
Lors du développement du dénominateur, on trouvera des termes comme

$$\omega_1 \omega_2 \frac{AB}{c^2} \cos \left[(\omega_1 + \omega_2)t - \frac{\omega_1 x + \omega_2 z}{c} \right] + \text{etc...}$$

pour lesquels on voit la possibilité d'une mise en phase dans des directions déterminées par

$$\omega_1 x + \omega_2 z = \text{constante.}$$

Ces directions sont précisément distinctes des axes O_x et O_z de propagations incidentes et sont celles d'un rayonnement extérieur, ou tout au moins d'une excitation infrasonique



au voisinage de la couronne de bruit, dans des directions extérieures au dièdre de rayonnement normal.

Cette excitation en pression avec mise en phase dans les directions indiquées est le moyen pour la "couronne de bruit" de rayonner de nouvelles ondes qui se propagent comme l'indique la figure : c'est cette possibilité qu'il s'agissait d'établir.

7. Calcul de la propagation guidée

Les calculs sont conduits suivant le mode linéaire (puissance W nulle).

On peut bien entendu calculer les temps de propagation des infrasons à l'intérieur du guide et les vitesses apparentes correspondantes. Elles sont ici toutes à peu près identiques, la propagation étant linéaire. On trouve qu'à l'intérieur même du guide d'onde, ces vitesses sont de l'ordre de 270 m/s à 310 m/s. Ceci correspond bien, du reste, aux valeurs de la vitesse normale du son à ces altitudes.

Globalement, bien entendu, les vitesses apparentes sont différentes, puisqu'il faut tenir compte du temps mis par les infrasons pour aller de la source au sol à la couronne focale: ce temps dépend évidemment de la puissance de l'explosion. En fait, sur de très grandes distances, cette différence dans le temps de propagation devient négligeable devant le temps total de propagation. En particulier, pour une distance de 7400 km, on retrouve bien un temps de propagation de 7 à 8 heures environ, en accord avec certaines constatations expérimentales.

Comment, cependant, les rayons arrivent-ils à sortir du guide et à retourner au sol ?

Il nous faut ici bien nous souvenir que les rayons filiformes que nous avons tracés n'ont pas de réalité physique. Seules les surfaces d'onde existent. Les rayons sont bien entendu un moyen commode de figurer le phénomène physique de la propagation à condition de bien vouloir considérer qu'ils s'élargissent, par le principe d'Huygens, au fur et à mesure qu'ils se

propagent. A une distance D de la source sonore et pour une longueur d'onde λ , la demi largeur du rayon, devenu un faisceau, est r , donné par $\pi r^2 = \lambda D/2$. Or, pour une longueur d'onde de 6 à 8 km, on voit que cette demi largeur atteint de 10 à 11 km à 100 km de distance.

L'épaisseur maximum du guide des 90 km étant de 25 km environ, il est clair que le guidage sera loin d'être parfait. Il en résulte que de l'énergie infrasonore va fuir vers le bas, et vers le bas seulement, le gradient positif très élevé de température qui limite supérieurement le guide empêchant les rayons de s'échapper vers le haut. Cette fuite va se produire à peu près tout au long du parcours, à partir de distances de l'ordre de, disons, 200 à 1000 kilomètres.

En effet, tout rayon frôlant l'altitude des 50 km a des chances d'être détourné, et ceci sans espoir de retour, par le gradient inverse de température existant entre 20 et 50 km.

Un piégeage dû à la seule courbure terrestre est impossible. Les rayons suivront le guide, un peu à la manière de la lumière dans les fontaines lumineuses, les ordres de grandeur du rayon de courbure terrestre (6400 km) d'une part ainsi que du guide et des longueurs d'onde d'autre part n'ayant aucun rapport.

Un facteur est déterminant, par contre, dans une propagation de ce type: le vent à l'intérieur du guide. Supposons en effet qu'il existe un vent à l'intérieur du guide, dont le profil présente un minimum ou un maximum. Il est évident que dans le premier cas ce profil de vent va contribuer à accentuer le guidage, tout en ralentissant un peu la vitesse générale de propagation. Dans le deuxième cas, l'inverse va se produire, et le vent diminuera l'efficacité du guide.

En effet, en projection horizontale, la vitesse du vent s'ajoute algébriquement à la vitesse de propagation acoustique en atmosphère calme, et un gradient positif de vitesse de vent est équivalent à un gradient positif de température. Les gradients de vitesse de vent se composent donc avec les gradients de température pour intervenir sur la propagation.

Ainsi on aura un guide "polarisé", bon conducteur du son dans un sens, mauvais conducteur dans l'autre sens.

Notons qu'il n'est pas impossible, à priori, de trouver un profil favorable (donc à minimum), mais accélérant la propagation générale. Il suffit que ce minimum soit relatif.

Si on se reporte aux calculs de propagation, on voit bien que pour un même profil de vent, à un instant donné, la propagation dans un sens "voit" des vitesses de vent d'un certain signe alors que la propagation en sens inverse les "voit" avec un signe opposé. Dans les deux cas, par contre, les gradients de température sont les mêmes.

Si on admet que le profil de vent s'inverse périodiquement en raison de la marée atmosphérique, on constate que le guide sera ouvert à la propagation des infrasons alternativement dans un sens (par exemple est-ouest) et dans l'autre sens (ouest-est).

Ainsi peut-on expliquer une propagation très lointaine du son, effectivement observée à très grande distance dans des directions étroites en azimut, et à des heures favorables : d'une part le guide nécessaire se forme, d'autre part la "couronne de bruit" fournit la source à haute altitude capable d'y rayonner. Le résultat d'ensemble est une propagation à une vitesse finalement très voisine de la vitesse du son.

EXPLOSIVE EXCITATION OF LAMB'S ATMOSPHERIC EDGE MODE

by

Joe W. Posey and Allan D. Pierce

Massachusetts Institute of Technology
Cambridge, Massachusetts
USA

160

EXCITATION PAR UNE EXPLOSION DU MODE TRANCHANT ATMOSPHERIQUE DE LAMB

par

J.W. Posey et A.D. Pierce

SOMMAIRE

Des observations antérieures ont montré que les relevés de pression effectués à grande distance et au niveau du sol, sur des ondes acoustiques et de gravité engendrées par une explosion, sont souvent dominés par le mode tranchant atmosphérique de Lamb pour le premier cycle ou les deux premiers cycles. Au cours du présent exposé, les auteurs examinent particulièrement l'excitation de ce mode par une onde de souffle provoquée par une explosion importante dans l'atmosphère. On a pu observer que la force de l'excitation dépend dans une large mesure de la queue de l'onde de souffle. Toutefois, on ne possède pas d'informations sur la forme exacte de cette queue d'onde de souffle ; par conséquent, toute représentation analytique est obligatoirement assez arbitraire.

Un développement théorique montre que, pour le mode de Lamb pur, il existe une relation analytique simple entre l'énergie de la source, d'une part, et, d'autre part, l'amplitude et la période initiales du type d'onde de pression enregistrée dans le champ éloigné. Cette relation est comparée avec certaines données empiriques, et semble bien concorder avec les estimations d'énergie basées sur des observations sismiques.

EXPLOSIVE EXCITATION OF LAMB'S ATMOSPHERIC EDGE MODE

Joe W. Posey* and Allan D. Pierce
Massachusetts Institute of Technology
Cambridge, Massachusetts
U.S.A.

ABSTRACT

It has been previously demonstrated that far-field ground-level pressure observations of explosively generated acoustic-gravity waves are often dominated by the Lamb atmospheric edge mode for the first cycle or two. In this paper, particular attention is given to the excitation of this mode by a blast wave from a large atmospheric explosion. It is found that the strength of the excitation is strongly dependent upon the tail of the blast wave. However, information on the precise form of the blast wave tail is unavailable, so that any analytical representation must be somewhat arbitrary.

A theoretical development shows that for the pure Lamb mode, a simple analytical relation exists between the energy of the source and the initial amplitude and period of the far-field pressure waveform. This relation is compared with some empirical data and appears to be in fair agreement with yield estimates based on seismic observations.

1. INTRODUCTION

Lamb [1910] found an acoustic wave propagation mode through an isothermal atmosphere above a flat, rigid ground and in the presence of gravity which contains no vertical particle motion. This mode propagates nondispersively at the speed of sound c , and has a pressure profile which decays exponentially with altitude z .

$$p(\vec{x}, z, t) = f(ct - \vec{x} \cdot \vec{e}_k) e^{-gz/c^2} \quad (1.1)$$

Here, \vec{x} is the horizontal position vector, t is time, g is the acceleration of gravity, and \vec{e}_k is the unit vector in the direction of propagation. Bretherton [1969] found the long wave speed, c_L , for the counterpart of Lamb's mode in a temperature-stratified atmosphere, and Garrett [1969a,b] determined the dispersion relation for this mode, which he called the Lamb atmospheric edge mode, in a temperature-and-wind-stratified atmosphere. Garrett's dispersion relation may be simply expressed as

$$\omega = c_E k - Dk^3 \quad (1.2)$$

where ω is frequency, c_E is the equivalent long wave speed in the direction of propagation, D is the dispersion coefficient and k is the wave number. For realistic temperature and wind velocity profiles, c_E is approximately c_L plus an average wind speed in the direction of propagation. Since the edge mode is nondispersive in an isothermal atmosphere with constant wind, it is no surprise that D increases with the rms deviations of the profiles of sound speed and wind speed. Since the Lamb mode energy decays exponentially with altitude, the appropriate weighting function for calculating profile averages decays similarly.

Pierce and Posey [1972] investigated the Lamb mode further, comparing its dispersion curve and waveform synthesis for a particular case with the corresponding curves and synthesis resulting from the multi-mode theory as detailed earlier by the same authors [Pierce and Posey, 1970]. It was demonstrated that the earliest cycle or two of observed acoustic-gravity waveforms thousands of kilometers from explosive sources are sometimes dominated by the Lamb edge mode.

In this paper, the problem of mathematically modeling a nuclear-explosion blast wave is examined, and some theoretical edge mode waveform characteristics are noted and compared with observations.

2. BLAST WAVES FROM NUCLEAR EXPLOSIONS

The basic nonlinear hydrodynamic model of a nuclear explosion [Taylor, 1950; Brode, 1955, 1968] consists of an initially isothermal sphere of very small radius in an unbounded isothermal atmosphere with negligible gravity. The initial sphere has ambient density and fluid velocity, but is assumed to have very high temperature and pressure. The total initial potential energy (the specific heat of air is assumed independent of temperature) inside the sphere is assumed a fixed fraction of the total energy Y released by the explosion. It would appear from comments in sections 1.22, 2.119 and 7.25 of Effects of Nuclear Weapons (ENW) [Glasstone, 1962] that $Y/2$ is a good approximation of this initial energy for bursts below 100,000 ft (~ 30 km) and a fair approximation at altitudes up to 350,000 (~ 100 km), although no quantitative description of this fraction is given. In any event, the results of this paper will not be invalidated by such a variation, provided energy yield is always interpreted as twice the hydrodynamic energy of the explosion.

* Present address: General Motors Research Laboratories, General Motors Technical Center, Warren, Michigan 48090

The pressure waveform in this idealized basic nonlinear model corresponds to hydrodynamic scaling; i.e., at distance R ,

$$p = p_0 F(R/cT_Y, t/T_Y) \quad (2.1)$$

where F is a universal function of two dimensionless quantities and where T_Y is a characteristic time, which may be defined as any constant times $(Y/p_0)^{1/3}/c$. For convenience T_Y is defined such that, when p_0 and c correspond to the standard reference pressure ($p_{ref} = 1 \text{ atm}$) and sound speed ($c_{ref} = 331 \text{ m/sec}$) and when Y is 1 KT ($4.2 \cdot 10^{19} \text{ ergs}$), then T_Y is equal to the time duration t_{ref} of the blast wave at a distance R_{ref} (taken here as 1 mile) from a 1 KT explosion. As explained later in this section, t_{ref} is chosen to be 0.33 sec. Thus,

$$T_Y = (p_{ref}/p_0)^{1/3} (c_{ref}/c) Y_{KT}^{1/3} t_{ref} \quad (2.2)$$

where

$$Y_{KT} = Y/(4.2 \times 10^{19} \text{ ergs}) \quad (2.3)$$

Since, in the homogeneous atmosphere currently being considered, the amplitude of F may be expected to fall off nearly inversely with R (spherical spreading in linear acoustics), Eq. (2.1) may be rewritten in the form

$$p = (\Delta p)_{ref} \frac{p_0}{p_{ref}} \frac{cT_Y}{c_{ref}t_{ref}} \frac{R_{ref}}{R} F_1 \left(\frac{t - R/c}{T_Y}, \frac{R}{cT_Y} \right) \quad (2.4)$$

where at large distances R , F_1 should be a relatively slowly varying function of its second argument. Here $(\Delta p)_{ref}$ is the shock overpressure at the reference distance R_{ref} from a 1 KT air burst in the standard atmosphere.

Brode's [1955] results indicate that Δp falls off roughly as R^{-1} at distances greater than $3\lambda_0$ where $\lambda_0 = (Y/2p_0)^{1/3}$. For the reference burst described above, $\lambda_0 \text{ ref} = 276 \text{ m}$, $R_{ref} = 5.94 \lambda_0 \text{ ref}$, $t_{ref} = 0.33 \text{ sec}$, and $(\Delta p)_{ref} = 34 \text{ mbar}$. The solid line in Fig. 1 is the approximate form of $F_1[(t - t_s)/t_{ref}, \lambda_0]$ inferred from Brode's paper. Here λ_0 is $[R_{ref}/(c_{ref}t_{ref})]$. The negative phase duration is constant at about $1.22 \lambda_0/c_0$ (1.01 sec for the reference case). Since $(\Delta p)_{ref}$ is only about 3% of p_0 , the theory of weak shocks [Whitham, 1956] should apply at R_{ref} , which implies that the duration of the positive phase T_+ will increase with distance in the following manner.

$$T_+ = t_{ref} \left[1 + \frac{Y+1}{2Y} \frac{R_{ref}(\Delta p)_{ref}}{p_{ref}c_{ref}t_{ref}} \ln \frac{R}{R_{ref}} \right]^{1/2} \\ = 0.33 [1 + 0.047 \ln(R/R_{ref})]^{1/2} \quad (2.5)$$

Thus, the shock will propagate an additional 140 km before T_+ is increased by as little as 10%. ($T_+ = 2 t_{ref}$ at a range of $\exp(63.9) \cdot R_{ref}$.) Brode gives little information on the character of the pressure history after the negative phase.

In ENW, the following analytical approximation (shown in Fig. 1 by the dashed line) is given for the form of the pressure history in the blast wave.

$$p_G/\Delta p = (1 - t/T_+)e^{-t/T_+} U(t/t_+) \quad (2.6)$$

Here t is measured from the onset of the shock. This agrees reasonably well in the positive phase with Brode's result, but there are major discrepancies in the negative phase. The ENW curve, often referred to as the Glasstone pulse, reaches a minimum of only $p/\Delta p = -0.13$ and has a negative phase of infinite duration. On the other hand, Brode's pulse has a minimum of -0.44 and goes to zero at $t/T_+ = 3.85$. These differences are of little consequence when estimating damage due to the blast wave, which was the original intent of the Glasstone pulse approximation, but they might be of considerable importance in determining the excitation of low frequency acoustic-gravity waves. Nevertheless, the Glasstone pulse has been used [Harkrider, 1964; Pierce, Posey and Iliff, 1971] in the determination of the excitation of infrasonic modes by nuclear explosions.

The Glasstone pulse may be modified to give a pressure history which more closely resembles Brode's curve.

$$p_G/\Delta p = (1 - t/T_+) [U(t/T_+) + (3 - t/T_+)U(t/T_+ - 1)]e^{-t/T_+} \quad (2.7)$$

This is shown by the dash-dot curve in Fig. 1. Notice that this approximation has a minimum value of $p/\Delta p = -0.29$, crosses the axis at $t/T_+ = 4$, reaches a maximum of 0.03 at 5.3 and then approaches zero asymptotically. [For both Eq. (2.6) and Eq. (2.7), the total pressure impulse, $\int p dt$, is zero.]

The relative excitation of low frequencies by the expressions Eq. (2.6) and Eq. (2.7) might be determined by comparing the low frequency limits of their Fourier transforms (over time). If the transform $f(\omega)$ of a function $f(t)$ is defined by

$$\hat{f}(\omega) = (2\pi)^{-1} \int_{-\infty}^{\infty} f(t) e^{i\omega t} dt$$

then

$$\hat{p}_G/\Delta p = -i\omega/[2\pi(i\omega - 1/T_+)^2] \quad (2.8a)$$

and

$$\hat{p}_G/\Delta p = \frac{-i\omega}{2\pi(i\omega - 1/T_+)^2} \left(1 + \frac{2e^{i\omega T_+} - 1}{T_+(i\omega - 1/T_+)} \right) \quad (2.8b)$$

For $\omega \ll 1$,

$$\begin{aligned} \hat{p}_G &\approx \hat{p}_G[1 - 2e^{-1}] \\ &\approx 0.26 \hat{p}_G \end{aligned} \quad (2.9)$$

Thus, the approximation Eq. (2.7), which shows better agreement with the calculated blast wave, appears to excite the frequencies of interest at only 1/4 the level of the Glasstone pulse given by Eq. (2.6). However, since the low frequency content of the pulse is governed by its tail, and since it is not known whether either of the analytic approximations is representative of the true pulse after the negative phase, the Glasstone pulse is used in the remainder of this paper to represent the blast wave because of its simplicity. An ancillary reason for this choice is that, as noted earlier in this section, the Glasstone pulse has been used previously in the synthesis of acoustic-gravity waveforms. Thus, the blast wave pressure is taken to be given by Eq. (2.4) with $F_1(t/t_{ref}, \Lambda_0)$ approximated by $[p_G(t/T_+)/\Delta p]$ as given in Eq. (2.6). That is,

$$F_1(\xi, \Lambda_0) = (1 - \xi)e^{-\xi} \quad (2.10)$$

3. FAR-FIELD PRESSURE WAVEFORMS

The theory of excitation of the Lamb mode by an explosively generated blast wave has been detailed by the present authors [Pierce and Posey, 1972]. For the purposes of the present paper, the far-field pressure waveform may be expressed by

$$p(\vec{r}, t) = G(\vec{r}_0, \vec{r}, c_L(x, y), \vec{v}_L(x, y)) \psi(t, s, \theta) \quad (3.1)$$

Here \vec{r} denotes the observation point and \vec{r}_0 the source location. The function G is an amplitude factor which contains effects of the horizontal refraction of rays, of differences in ambient conditions and ground levels at the source and receiver, and of source strength (through the factor $Y^{1/2}$). The refraction of rays occurs whenever the gradient of $c_E(x, y)$ normal to the ray path is not identically zero. The general form of G is not repeated here for the sake of brevity. The Lamb mode long wave speed c_E is determined by the temperature and wind velocity profiles, which vary with the horizontal coordinates x, y . The function ψ depends upon the source strength and the average c_E and dispersion coefficient D along the ray path from source to receiver as well as upon time t , approximate distance along the ray s and ray parameter θ . Specifically,

$$\psi(t, s, \theta) = \frac{T_Y}{\sqrt{\pi} \tau_D} \int_0^\infty \text{Ai} \left(\frac{\tau_a - t}{\tau_D} + \mu \frac{T_Y}{\tau_D} \right) M(\mu) d\mu \quad (3.2)$$

where

$$\tau_a = \int_0^s (1/c_E) ds \quad (3.3a)$$

$$\tau_D = [3 \int_0^s (D/c_E^4) ds]^{1/3} \quad (3.3b)$$

and Ai is the Airy function, defined by

$$\text{Ai}(x) = \frac{1}{\sqrt{\pi}} \int_0^\infty \cos(v^3/3 + xv) dv \quad (3.4)$$

The universal source function $M(\mu)$ is given by

$$M(\mu) = [\mu^{1/2} + (1-2\mu)e^{-\mu} \int_0^{\mu^{1/2}} e^{y^2} dy] U(\mu) \quad (3.5)$$

and may be interpreted as the characteristic time dependence for the Lamb mode pressure in the intermediate field (before dispersion has had an appreciable accumulative effect). A plot of $M(\mu)$ is given in Fig. 2. Here, $U(\mu)$ is the Heaviside step function.

Since M does not vary from case to case, the shape and amplitude of ψ are determined solely by the ratio T_Y/τ_D , with a change in τ_a resulting only in a time shift. The variation of ψ with T_Y/τ_D is illustrated in Fig. 3. One of the present authors [Posey, 1971] has synthesized Lamb mode waveforms for a number of realistic atmospheres, source strengths, and ranges. It has been noted that T_Y/τ_D has normally been in the range 0.1 to 0.3. The largest value of this ratio calculated to date is 0.4, corresponding to an observation 1666 km from a 60 MT explosion. The ratio may be shown to be roughly proportional to $(Y/R)^{1/3}$.

4. DETERMINATION OF EXPLOSION ENERGY FROM PRESSURE WAVEFORMS

Since the waveform dependence on Y has been clearly defined, and since only a limited range of T_Y/τ_D appears to be of practical interest, the inverse problem of determining Y from the shape and magnitude of observed waveforms would seem to be tenable.

A numerical study of ψ shows that $a_1/(T_Y/\tau_D)^{3/2}$ is 0.95, 0.90, 0.85 and 0.77 for (T_Y/τ_D) equal to 0.1, 0.2, 0.3 and 0.4, respectively. Here a_1 is the absolute variation of ψ from its first peak to its first trough. The following approximation is adopted.

$$a_1/(T_Y/\tau_D)^{3/2} \approx 0.9 \quad (4.1)$$

The ratios of the periods (and other calculations not shown here) to τ_D in the in the first few cycles would appear from Fig. 3 to be relatively insensitive to the value of T_Y/τ_D . One finds

$$T_{1,2} \approx 4.0 \tau_D \quad (4.2a)$$

$$T_{2,3} \approx 2.6 \tau_D \quad (4.2b)$$

where the period $T_{1,2}$ is first peak to second peak and the period $T_{2,3}$ is second peak to third peak. Eqs. (4.2a,b) imply that $T_{1,2}/T_{2,3}$ is approximately constant at 1.5 for the Lamb mode, but observations of explosively generated acoustic-gravity waves exhibit significant variations in this ratio, due perhaps to interference of other modes with the Lamb mode. As noted in sec. 1, it is the earliest portion of the observed waveforms which is apt to be dominated by the Lamb mode. Thus, τ_D is approximated here by $T_{1,2}/4$, which assumes that the edge mode is dominant at least until the second peak.

The dependence of G on atmospheric parameters along the ray path can be eliminated by ignoring horizontal refraction, and its dependence on conditions at the receiver can be eliminated by taking the observer to be at sea level and by assuming that the ratio $c_L(x_0, y_0)/c_L(x, y)$ is approximately 1.0 and that $|\vec{v}_L|$ at each of these two locations is a small fraction of c_L . Here, (x_0, y_0) are the horizontal coordinates of the source and (x, y) of the receiver. The vector \vec{v}_L is the weighted average of the wind velocity profile. Hence, G is approximated by

$$G = Y/[T_Y^{3/2} B_1 \sin^{1/2}(R/r_e) p_0^{1-1/\gamma} (\bar{c}_0)^{3/2} (\bar{c}_0)] \quad (4.3)$$

where B_1 is a dimensioned constant equal to $1.440 \text{ atm}^{(1-\gamma)/\gamma} \text{ km}^{-3/2} \mu\text{bar}^{-1} \text{ KT}$, R is the great circle distance from source to observer, r_e is the radius of the earth, p_0 is the ambient pressure, γ is the ratio of specific heats (≈ 1.4), and c is the local speed of sound.

Eqs. (3.1), (4.1), (4.2a) and (4.3) may be combined to obtain the approximate relation

$$Y = B_2 \sin^{1/2}(R/r_e) p_0^{1-1/\gamma} (\bar{c}_0) [c(\bar{c}_0) T_{1,2}]^{3/2} P_{\text{FPT}} \quad (4.4)$$

The numerical value of the constant B_2 is about $0.199 \text{ atm}^{(1-\gamma)/\gamma} \text{ km}^{-3/2} \mu\text{bar}^{-1} \text{ KT}$ with r_e taken as 6374 km. The dependence on ambient pressure at the source is fairly weak within the troposphere, since at 10 km (the approximate altitude of the tropopause) in a typical atmosphere, $p_0^{1-1/\gamma} = 0.7 \text{ atm}^{1-1/\gamma}$. The speed of sound at the source can also vary, but generally stays within 15% of 310 m sec^{-1} up to an altitude of at least 60 km.

Taking $p_0(\bar{c}_0)$ to be 1 atm. and replacing $c(\bar{c}_0)$ by 310 m sec^{-1} , one finds that Eq. (4.4) is further approximated by

$$Y = B_3 \sin^{1/2}(R/r_e) T_{1,2}^{3/2} P_{\text{FPT}} \quad (4.5)$$

The constant B_3 has a value of about $0.034 \mu\text{bar}^{-1} \text{ sec}^{-3/2} \text{ KT}$. The relation (4.5) is considered applicable for heights of burst at least up to the tropopause. Because of the nature of the assumptions outlined above, this prediction may be too large for blasts where $p_0(z_0) < 1 \text{ atm}$ or for records at long ranges from small yield explosions [i.e., $T_Y/\tau_D < 0.2$] and too small for records at short ranges from large yield sources [i.e., $T_Y/\tau_D > 0.2$].

The waveform parameters $T_{1,2}$ and P_{ppt} read from an observed microbarogram should properly be used in Eq. (4.5) only when the record prior to the second peak represents almost solely the Lamb mode pressure perturbation. In principle, this can only be the case when there is negligible background noise, when there is not yet appreciable contribution to the record from other mechanical modes, and when there is negligible phase shift due to instrument response.

In order to check the agreement between the approximate Lamb mode relation and the empirical waveforms, the quantities P_{ppt} and $T_{1,2}$ are measured on the records presented by Harkrider [1964] and by Donn and Shaw [1967]. The records used here include all of those in these two collections for which Båth [1962] gives a source yield estimate, for which the pressure scale could be determined and for which the first cycle of the signal is recognizable above the background noise. Pressure amplitudes for Harkrider's records were computed using his microbarograph response data. Pressure amplitudes for the Donn and Shaw records were determined according to the premises [W. Donn, private communication] that (a) all records recorded by Lamont type A microbarographs are to the same scale and (b) the clip to clip amplitude of off scale oscillations was 350 μ bars. The data read from these waveforms is given in Table 1. In Fig. 4, the data is compared with the approximate theoretical Lamb mode relation of Eq. (4.5). The yield Y is taken to be given in each case by Båth's estimate based on seismic data as shown in Table 1. (The validity of these yield estimates has not been established, but they are the only quantitative estimates which have been published.) Note that the plot is full logarithmic. (This comparison was originally published in a letter to Nature [Posey and Pierce, 1971].)

The scatter about the theoretical curve could be due to various causes other than interference with the Lamb mode by other modes and by noise. One possibility which seems especially likely is the variation in amplitude due to the horizontal refraction and subsequent focusing and defocusing caused by departures of the atmosphere from perfect stratification as discussed in some detail by Posey [1971]. Also, some of the scatter would not be present if data corresponding to explosions of greater than 11 MT were omitted. Above all, it should be remembered that the first part of this paper was devoted to demonstrating that the source function utilized here was chosen primarily for its mathematical simplicity. A more realistic source function might result in a very different proportionality factor in Eq. (4.5), but the form of this relation would be the same. Thus, while the amplitude agreement seen in Fig. 4 is primarily due to chance, it is heartening to see that the theoretical curve appears to have the correct slope.

5. CONCLUDING REMARKS

Two points have been made in this paper. First, the degree of excitation of acoustic-gravity waves by a blast wave is heavily dependent upon the tail of the exciting pulse, about which little has been published. Second, a simplified analysis of acoustic-gravity wave propagation in which a single ducting mechanism (Lamb mode ducting) is considered results in a simple analytical relation between source strength and initial waveform amplitude and period. It is suggested here that similar analyses for other mechanisms of ducting (sound channel ducting in particular) might be useful in deriving other relations between waveform parameters and parameters of the source and/or medium.

REFERENCES

- Bretherton, F. P., 1969, Lamb Waves in a Nearly Isothermal Atmosphere, Quart. J. Roy. Meteor. Soc., **95**, 754-757.
- Brode, H. L., 1955, Numerical Solutions of Spherical Blast Waves, J. Appl. Phys., **26**, 766-775.
- Brode, H. L., 1968, Review of Nuclear Effects, Annual Review of Nuclear Science (E. Segre, ed.), Annual Reviews, Inc., Palo Alto, 153-202.
- Donn, W. L., and D. M. Shaw, 1967, Exploring the Atmosphere with Nuclear Explosions, Rev. of Geophys., **5**, 53-82.
- Garrett, C. J. R., 1969a, The Fundamental Mode of Acoustic-Gravity Wave Propagation in the Atmosphere, Fluid Mech. Trans. Warsaw, **4**, 707-719.
- Garrett, C. J. R., 1969b, Atmospheric Edge Waves, Quart. J. Roy. Met. Soc., **95**, 731-753.
- Glasstone, S., 1962, The Effects of Nuclear Weapons (revised edition), United States Atomic Energy Commission, Wash., D.C.
- Harkrider, D. G., 1964, Theoretical and Observed Acoustic-Gravity Waves from Explosive Sources in the Atmosphere, J. Geophys. Res., **69**, 5295-5321.
- Lamb, H., 1910, On Atmospheric Oscillations, Proc. Roy. Soc. London, **A84**, 551-572.
- Pierce, A. D. and J. W. Posey, 1970, Theoretical Prediction of Acoustic-Gravity Pressure Waveforms Generated by Large Explosions in the Atmosphere, Air Force Cambridge Research Laboratories Report AFCRL-70-134.
- Pierce, A. D. and J. W. Posey, 1972, Theory of the Excitation and Propagation of Lamb's Atmospheric Edge Mode from Nuclear Explosions, Geophys. J. Roy. Astro. Soc., **26**.

- Pierce, A. D., J. W. Posey and E. P. Iliff, 1971, Variation of Nuclear Explosion Generated Acoustic-Gravity Waveforms with Burst Height and with Energy Yield, J. Geophys. Res., 76, 5025-5042.
- Posey, J. W., 1971, Application of Lamb Edge Mode Theory in the Analysis of Explosively Generated Infrasound, Ph.D. Thesis, Massachusetts Institute of Technology, Department of Mechanical Engineering.
- Posey, J. W. and A. D. Pierce, 1971, Estimation of Nuclear Explosion Energies from Microbarograph Records, Nature, 232, 253.
- Taylor, G. I., 1950, The Formulation of a Blast Wave by a Very Intense Explosion, Proc. Roy. Soc. London, A201, 159-186.
- Whitham, G. B., 1956, On the Propagation of Weak Shock Waves, J. Fluid Mech., 1, 290-318.

The research reported in this paper was supported by the Air Force Cambridge Research Laboratories, Air Force Systems Command, USAF, under Contract F19628-70-C-0008.

TABLE 1.

Observed amplitudes and periods. This data corresponds to empirical microbarographs published by Donn and Shaw (1967) and by Harkrider (1964), referred to as DS and H, respectively. (a-i, U.S.S.R. explosions; j-n, U.S. explosions).

Event	Date	Bath's Yield Estimate (MT)	R(km)	T _{1,2} (sec)	P _{FPT} (μbar)	Source of Microbarogram
a	9-10-61	10	3676	193	100	DS
			6644	280	70	DS
b	9-11-61	9	8000	229	125	H
c	9-14-61	7	6569	258	61	DS
d	10- 4-61	8	8000	220	80	H
e	10- 6-61	11	6574	300	59	DS
			8000	390	45	H
f	10-20-61	5	8000	310	21	H
g	10-23-61	25	6677	376	280	DS
h	10-30-61	58	6688	400	500	DS
			5631	540	133	DS
			8000	690	140	H
i	10-31-61	8	5717	386	25	DS
j	5- 4-62	3	5375	200	36	DS
k	6-10-62	9	2177	187	125	DS
l	6-12-62	6	2172	200	55	DS
m	6-27-62	24	2192	187	264	DS
			5393	433	83	DS
			9307	500	90	DS
			9350	467	90	DS
n	7-11-62	12	2185	200	180	DS

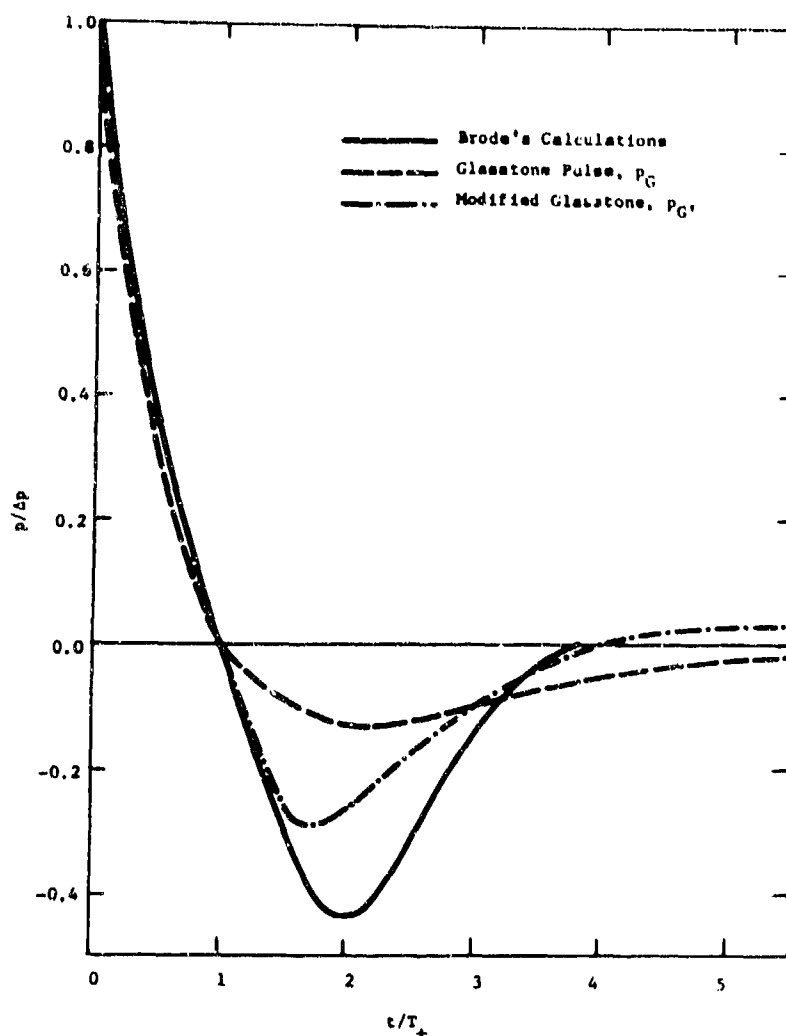


Fig.1 Blast waves from nuclear explosions. The solid line is deduced from Brode's (1955) calculations. The functions p_G and p_G' are as given by Eqs. (2.6) and (2.7), respectively.

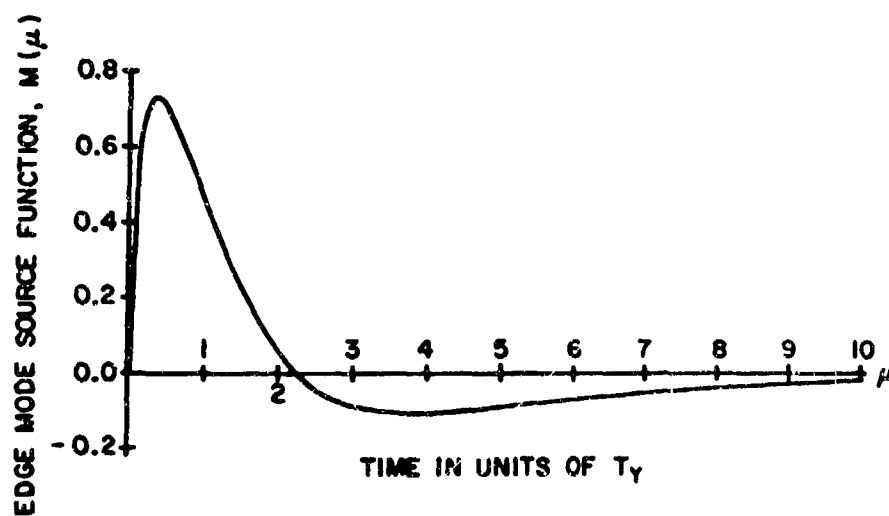


Fig.2 Universal source function, $M(\mu)$. This function, given by Eq. (3.22), describes the time variation of the effective source for edge mode excitation by nuclear explosions. Here $\mu = t/T_Y$, where T_Y is a characteristic time for the explosion.

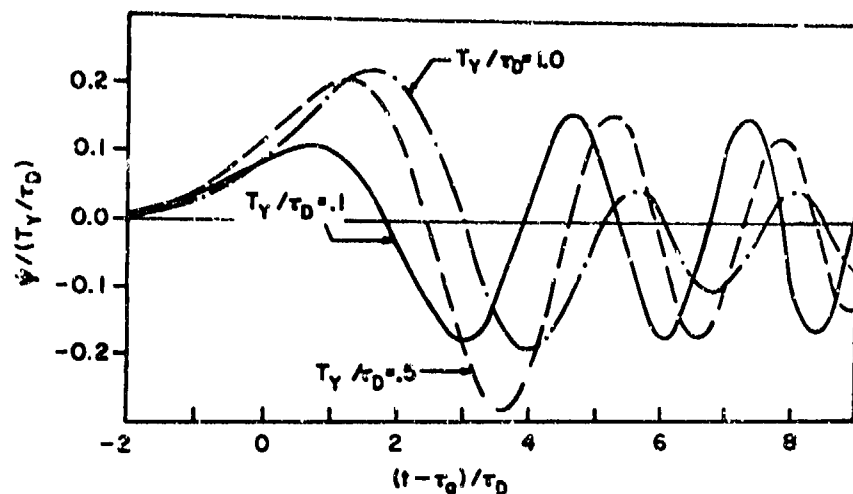


Fig.3 Variation of the waveform factor $\psi(t)$ with the parameter T_Y/τ_D . Here ψ is normalized with respect to T_Y/τ_D and the time is plotted relative to t_0 in units of τ_D .

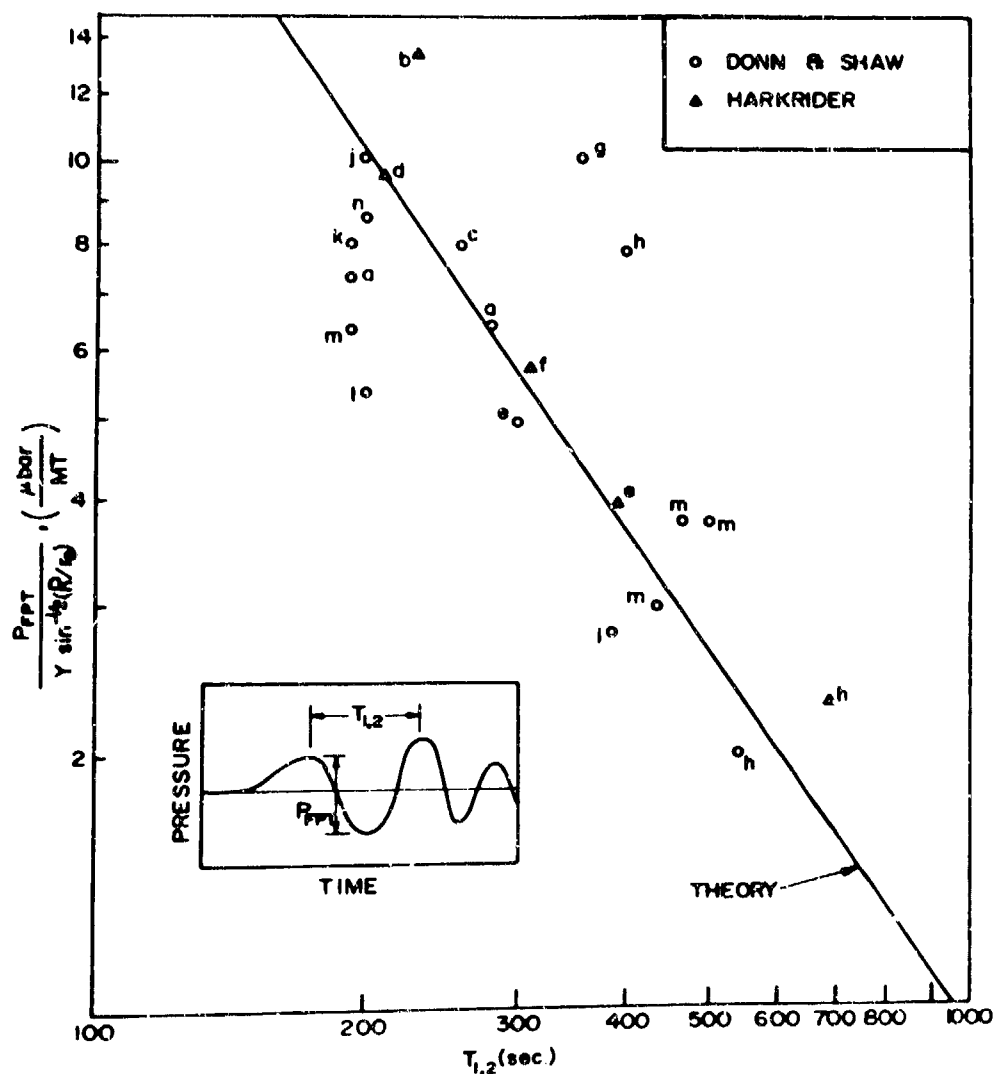


Fig.4 Comparison of Data with theoretical yield-period-amplitude relation. The data points are lettered a through n corresponding to particular events defined in Table 1. The theoretical line is that given by Eq. (4.5).

DISCUSSIONS ON THE PAPERS PRESENTED IN SESSION I B
(Acoustic gravity waves in the neutral terrestrial atmosphere - Artificial sources and propagation)

Discussion on paper 9 : "Acoustic gravity waves in the neutral atmosphere and the ionosphere",
by N.K. BALACHANDRAN.

Prof. H. VOLLAND : Did you take into account heat conduction and viscosity at thermospheric heights in your calculations ? Due to viscosity, acoustic wave energy is strongly dissipated within a frequency range increasing with altitude. Above 200 km altitude only infrasonic waves with periods between about one minute and the acoustic cut-off period are expected to exist with detectable amplitudes.

Dr. N.K. BALACHANDRAN : No, in my computations viscous effects and heat conduction were ignored. For detailed analysis of waves detected at high elevations these factors are important. For waves recorded at the ground level, the observations can be explained reasonably even if we ignore viscosity and heat conduction in the theoretical computations.

Discussion on paper 10 : "Modeling of nuclear sources of acoustic-gravity waves", by B.L. MURPHY.

C.F. P. HALLEY : Dans vos conclusions il apparaît que deux périodes sont privilégiées τ et 2τ . S'agit-il bien de la période de Brunt-Väisälä à l'altitude de l'explosion ? Dans nos observations nous trouvons plutôt τ et 2τ à l'altitude d'observation.

Dr. B.L. MURPHY : In our model the source (fireball) oscillates at a period between τ and 2τ , where τ is the Brunt-Väisälä period at the stabilization altitude (at or near the tropopause). It is tempting for me to ascribe the oscillations you observe to buoyancy oscillations of the fireball but I have no explanation as to why the period should be related to τ at the observation point.

Dr. K. DAVIES : Boulder R.F. Doppler records show that 1.1 in. waves propagate nearly vertically, so that they appear to leak from duct over Boulder which is many thousands of kilometers from nuclear burst. Can shock wave propagate over these large distances ?

Dr. B.L. MURPHY : One can show from equation (3) of our paper that after m skips between the base of the ionosphere and the ground the positive phase duration of a weak shock is increased by a factor of approximately $(1 + \frac{1}{2} \ln m)^{1/2}$ over the positive phase duration when the shock first reaches the ionosphere. Thus subsequent lengthening of the positive phase of a weak shock after the first skip would not be large enough to affect our main argument, namely that the positive phase duration of the shock at the ionosphere and the observed ionospheric periods are of the same order of magnitude. How long in fact the weak shock stays a shock (i.e. a disturbance whose front satisfies the Rankine-Hugoniot relations) I do not know.

One can imagine a variety of atmospheric phenomena which would tend to destroy a shock structure : scattering of the high frequencies at the shock front by turbulence or small scale wind gradients, spatial separation of high frequencies by frequency dependent dispersion or refraction, and alteration of pulse structure by passage through a caustic. It may be that acoustic, as opposed to weak shock, equations are applicable after only a few skips between ground and ionosphere.

Dr. N. CHANG : In regards to the $Y^{1/3}$ scaling for short period oscillations in the ionosphere, I believe that most of the Doppler observations showed periods in the range 40-90 seconds. This seems to be a contradiction of the above scaling.

Dr. B.L. MURPHY : According to Baker (1969) the periods ranged from 30 seconds to 10 minutes, periods of about a minute being predominate. Typically the yields involved were about a megaton. I do not know if a sufficient spread of yields were involved that one might check the period-yield scaling. The $(\text{yield})^{1/3}$ law is a rough estimate of what might be expected. For large yields, deviations from this law can be anticipated due to : (a) The interaction of the rising fireball with the shock. As noted by Greene and Whitaker (1968) this effect tends to compress the going shock and hence the yield exponent would tend to be less than $1/3$. (b) Other inaccuracies associated with modified Sachs scaling for large yields.

Discussion on paper 11 : "Un nouveau mécanisme pour la propagation lointaine du son dans l'atmosphère"
by Y. ROCARD and C. BERTHET.

Dr. A. PIERCE : This paper evidently gives a method of incorporating nonlinear effects into the theory of geometrical acoustics which is considerably different than that used in the analogous field of sonic booms, the theory of which was developed by Durrand, Hayes, and Whitham. In sonic boom theories, nonlinear effects are neglected in the determination of ray paths, and one dimensional weak shock theory is applied to determine shock waveforms of shocks propagating along a ray tube. An important factor there is the variation of ray tube area with focusing on defocusing rays. This factor has evidently been neglected in the present paper.

Prof. C. BERTHET : L'effet de focalisation et de défocalisation des rayons reste très secondaire devant la cause fondamentale de non-linéarité de la propagation dans l'atmosphère, liée à la diminution exponentielle de la densité avec l'altitude et sur laquelle a été basée notre approche. Naturellement, on pourrait tenir compte de la focalisation au moment où les rayons se rapprochent en une ligne focale dans la "couronne de bruit" : on trouverait alors que les effets non-linéaires sont quelque peu augmentés.

Réte des prof. Y. ROCARD et C. BERTHET :

"Le traitement de Greene et Whitaker est beaucoup plus général que les conclusions qu'en ont tiré les auteurs. Le calcul, basé sur les équations hydrodynamiques générales, n'est pas restreint au seul cas des ondes de gravité et les configurations données par exemple figures 5 et 6, qui montrent des rœuds de pression à haute altitude, ne sont autres que celles que nous avons appelées "couronne de bruit". Quand Greene et Whitaker disent que tout se passe comme si les ondes de gravité se réfléchissaient sur le fort gradient thermique de la haute atmosphère, ils pourraient étendre cette conclusion aux ondes acoustiques quelconques.

Notre approche par une acoustique de rayons assez simple a permis de mettre commodément en évidence la "couronne de bruit" et de démontrer que cette couronne était une nouvelle source rayonnant dans des directions nouvelles. La confirmation apportée par Greene et Whitaker au moyen de calculs sur ordinateurs puissants et la description plus précise qui en est résulté ont justifié notre méthode."

General discussion

J. TESTUD : En 1970, nous avons fait un calcul théorique montrant que l'électrojet auroral, qui se développe pendant un sous-orage magnétique, était capable d'engendrer des ondes atmosphériques compatibles avec les observations à moyenne latitude de perturbations ionosphériques itinérantes de grande échelle : périodes de l'ordre de deux heures, vecteur d'onde de l'ordre de 10^{-5} m^{-1} . Cependant, ce modèle théorique reposait sur des hypothèses simplificatrices qui en limitaient la validité : la hauteur d'échelle H de l'atmosphère était supposée constante, et les effets d'amortissement étaient totalement négligés.

On a récemment repris ce calcul, en essayant de lever cette limitation :

- on a utilisé un modèle réaliste pour l'échelle de hauteur H ,
- on a tenu compte de l'amortissement dû à la conduction thermique (Cet effet est la principale cause d'amortissement dans la région F de l'ionosphère.)
- on a considéré que l'approximation de l'optique géométrique était applicable aux ondes émises par la source.

Le résultat de ce calcul est le suivant :

A 2 500 km de la source et vers 300 km d'altitude (ce qui est typique d'une observation à moyenne latitude en région F) la perturbation de vitesse neutre horizontale consiste simplement en un pic de grande amplitude de largeur typique 1 heure. Ce résultat est singulièrement en contraste avec celui du précédent calcul avec lequel on obtenait des oscillations pendant environ 6 heures.

Ce résultat est important pour l'interprétation des perturbations itinérantes liées aux orages magnétiques. Il montre que la période des "ondes" observées n'est en fait que la période de répétition des sous-orages dans la zone aurorale, période de répétition dont la valeur la plus probable est d'ailleurs deux heures comme l'a montré AKASOFU.

**JUSTIFICATION FOR THE USE OF HINES' "ASYMPTOTIC RELATIONS"
FOR TRAVELING IONOSPHERIC DISTURBANCES**

by

Norman J.F.Chang

Stanford Research Institute
Menlo Park, California
USA

172

JUSTIFICATION DE L'EMPLOI DES "RELATIONS ASYMPTOTIQUES" DE HINES
POUR LES PERTURBATIONS IONOSPHERIQUES ITINERANTES

par

N.J.F. Chang

SOMMAIRE

Il est démontré que les ondes de gravité internes se propageant à des altitudes ionosphériques doivent présenter des angles de propagation proches du maximum permis. Ainsi, dans le cas des perturbations ionosphériques itinérantes (PII) l'emploi des "relations asymptotiques" de Hines est justifié par la trajectographie. On vérifie ces relations en comparant résultats théoriques et expérimentaux pour quinze PIIs. Les effets du profil de température sur les propriétés mesurables des PIIs (inclinaisons des fronts d'ondes et périodes) sont étudiés. Il est démontré que, pour les PIIs qui prennent naissance en-dessous de la mésopause, l'atmosphère se comporte comme un filtre passe-bande avec une fréquence centrale favorisant les périodes proches de 20 minutes.

JUSTIFICATION FOR THE USE OF HINES' "ASYMPTOTIC RELATIONS"
FOR TRAVELING IONOSPHERIC DISTURBANCES

Norman J. F. Chang
Stanford Research Institute
Menlo Park, California
U.S.A.

SUMMARY

It is shown that internal gravity waves propagating at ionospheric heights must have propagation angles near the maximum permitted. Thus, for traveling ionospheric disturbances (TIDs) the use of Hines' "asymptotic relations" is justified by ray tracing. Verification of these relations is made by comparison of theoretical with experimental results for fifteen TIDs. The effects of the temperature profile on the measurable properties of TIDs (wavefront tilts, and periods) are discussed. It is shown that for TIDs that originate below the mesopause, the atmosphere behaves like a bandpass filter with center frequency favoring waves with periods near 20 minutes.

1. INTRODUCTION

Following Hines' (1960) work, traveling ionospheric disturbances (TIDs) are generally interpreted as a consequence of atmospheric internal gravity waves (IGWs). Although TIDs have been observed with a variety of techniques and in widely separated locations, they appear related in terms of periods and horizontal trace speeds. For example, TIDs with periods near 20 minutes and speeds around 150 m/s seem to be most prevalent.

Observers have found that at heights of 80 to 100 km the wavelike motions of the neutral atmosphere revealed by meteor trails have horizontal scale sizes greatly in excess of the vertical scale sizes. In addition, the dominant motion observed is nearly horizontal and the periods of the dominant observed modes are much larger than the Brunt-Väisälä period of the atmosphere. The fact that such observations are in agreement with certain limiting forms of the IGW dispersion equation prompted Hines (1960) to state that "certain 'asymptotic' relations apply to the parameters that describe these waves." These limiting forms have been useful not only because they simplify the dispersion relation for internal gravity waves, but more importantly because they reduce by one the number of parameters (period, and vertical and horizontal trace velocities) necessary to describe the assumed plane wave.

This paper shows that in a temperature-stratified atmosphere, internal gravity waves at F-region heights launched from an assumed source in the lower atmosphere must have propagation angles near the maximum permitted; under these conditions the asymptotic relations are always valid. In addition, it is shown that for TIDs that originate below the mesopause the atmosphere acts like a bandpass filter favoring waves with periods of about 16 to 20 minutes. In the present discussion, validity of ray theory is assumed and the atmosphere is considered to be stationary. A comparison of the available experimental results supports the above conclusions.

2. THEORY

The propagation of plane internal gravity waves in a two-dimensional, stationary, isothermal, non-dissipative atmosphere of uniform composition throughout is governed by the following dispersion relation (Hines, 1960):

$$(\omega^2 - \omega_a^2) \omega^2 / C^2 - \omega^2 (k_x^2 + k_z^2) + \omega_g^2 k_x^2 = 0 \quad (1)$$

where $\omega_a = \gamma g / 2C$ and $\omega_g = \sqrt{\gamma - 1} g / C$ are the acoustic cut-off and Brunt-Väisälä frequencies, respectively. The angular frequency of the internal gravity wave is denoted by ω ($< \omega_g$), while C represents the sound speed, g the acceleration of gravity, γ the specific heat ratio and k_x and k_z the wave numbers in the horizontal and vertical directions, respectively. The geometry is chosen such that there is no variation in the y -direction.

The above equation, which is normally referred to as the isothermal dispersion relation, can be put in a convenient form with the transformations $k_x = k \sin \phi$ and $k_z = k \cos \phi$. The result is

$$\mu^2 = \frac{C^2 k^2}{\omega^2} = \frac{C^2}{V^2} = \frac{X - 1}{Y^2 \sin^2 \phi - 1} \quad (2)$$

where $X = (\omega_g / \omega)^2$ and $Y = \omega / \omega_a$. [For the significance of these definitions see Davies, Baker, and Chang (1969)]. The remaining parameters are the refractive index, μ , and the phase velocity, V , and its angle with the vertical, ϕ .

With the dispersion relation in the form of Eq. (2), it is apparent that the refractive index has a singularity at $\phi_c = \sin^{-1}(1/Y)$. This angle will be called the critical angle. For $\phi \leq \pi/2$, propagation is possible only when $\phi > \phi_c$. When the sources of the traveling disturbances lie in the lower atmosphere, phase propagation must be downward for an upward flow of energy. Thus,

$$\pi/2 \leq \phi \leq \phi_c = \pi - \sin^{-1}(1/Y) \quad (3)$$

where ϕ_c is now given by the right-hand side of Eq. (3).

Figure 1 shows how the refractive index varies with Y and ϕ ; its value is equal to the magnitude of the radius vector drawn from the origin to the appropriate curve. This figure shows the projection of the μ surfaces on the upper-right quadrant of the $\mu_x - \mu_z$ plane. The curves are symmetric in both axes. Note that for $Y = 2$, $\phi_c = 30^\circ$. Thus, the curve for $Y = 2$, is asymptotic to $\phi = 30^\circ$, as shown.

The path of internal gravity waves propagating in a temperature-varying atmosphere can be found by approximating the atmosphere by a series of constant-temperature layers. In each of these layers a given plane wave must satisfy both the isothermal dispersion relation [Eq. (2)], and Snell's law which can be written:

$$\frac{\omega}{k \sin \phi} = \frac{\omega}{k_x} = \frac{v_p}{\sin \phi} = \text{constant} \quad (4)$$

Subject to these restrictions, ϕ versus height has been calculated for families of IGWs propagating from a source at 10 km in the 1962 U. S. Standard Atmosphere. The results for wave periods of 10, 20, 30, and 60 minutes are presented in Figure 2. In these graphs waves with propagating angle, ϕ , between 90° and 180° propagate energy upward. This is the only type of wave that will be considered. For propagating waves, ϕ cannot exceed $\phi_c = \pi - \sin^{-1}(1/Y)$.

The feature of interest in Figure 2 is the behavior of ϕ in the thermosphere (above 100 km). Above 120 km all internal gravity waves have propagation angles within a few degrees of their critical angle, which is shown by the dashed line. For 20-minute waves launched at 10 km only those with initial propagation angles between 150° and 165° degrees will reach F-region heights. These waves will have wave-front tilts between 44° and 54° degrees from the horizontal in the height range 200 to 300 km. Waves with 30-minute periods must have initial propagation angles between 160° and 170° degrees. Their corresponding tilts are between 28° and 33° degrees over the 200-to-300-km height range. Other quantities being equal, this means that waves with 20-minute periods (since they have a larger range of allowable angles) should be detected more frequently than 30-minute waves. For waves with periods larger than 30 minutes the range of allowable ϕ 's becomes even smaller than 10° , while those with periods less than about 20 minutes are limited by the Brunt-Väisälä period of the atmosphere.

The influence of wave periods, source heights, and different atmospheres on the range of allowable ϕ is shown in Figure 3. The critical angle is calculated at the source height shown, while ϕ ($90^\circ \leq \phi \leq \phi_c$) is the largest angle at z_0 that is reflected at the mesopause. Only internal gravity waves with angles greater than this value but less than the critical angle will propagate to F-region heights. These curves show that in addition to a difference in the magnitude of $\phi - \phi_c$, the winter curve peaks at a higher period (about 2 minutes) than does the summer curve. This suggests that, on the average, waves propagating into the thermosphere during the winter should have slightly longer periods than those observed during the summer.

While the above statement should be true for waves observed at 100 to 120 km altitude, the effects of the Brunt-Väisälä period (see Figure 3) must be included for waves that propagate above 120 km and that have periods less than about 20 minutes. Since the Brunt-Väisälä period is the lower limit for propagating waves, its effect is like a lowpass filter whose cut-off period increases with increasing heights. Thus, Figure 3 shows that at 200 km only waves with periods greater than 13.5 minutes are permitted, while at 300 km the waves must have periods greater than 16 minutes. Since the wave is reflected as $\tau \rightarrow \tau_g$, ray theory probably fails in this region and it is expected that the actual lower limit is a few minutes higher than the above numbers. Hence the combined effect of the Brunt-Väisälä period and the refractive properties of the mesopause act to make the atmosphere like a bandpass filter favoring waves with periods of about 16 to 20 minutes.

3. COMPARISON WITH OBSERVATIONS, AND DISCUSSION

The most statistically meaningful observations of TIDs available are those of Munro and Heisler (Munro, 1950, 1958; Munro and Heisler, 1956). These studies in Australia revealed that the speeds of TIDs most frequently observed lie between 83 and 167 m/s. During the winter, TIDs generally travel northward with an average speed of 133 m/s and with a mean wavefront tilt of 65° degrees. During the summer they travel southward with an average speed of 117 m/s and with a mean tilt of 51° degrees. Their periods range from 10 to 60 minutes with shorter-period events being most common.

Observations have also been made in the northern hemisphere by Thomas (1959) and by Chan and Villard (1962). The former study produced results consistent with those for the southern hemisphere. Chan and Villard, however reported speeds of 400 to 765 m/s with periods from 45 to 72 minutes. Other observations

of TIDs have appeared in the literature, but the ones given above are representative. For a summary see Friedman (1966).

One problem quite evident in the literature is that, even though TIDs are generally attributable to plane internal gravity waves, the wave parameters available from measurements are insufficient to determine the wave. In spite of this it can be seen that the observations agree in principle with the conclusions of Section 2.

The Australian TIDs have periods of about 20 minutes, speeds of about 125 m/s, and tilts of about 55 degrees. The high speeds reported by Chan and Villard tend to have longer periods and thus nearly horizontal wavefronts, with a correspondingly higher horizontal trace velocity.

That TIDs do satisfy the asymptotic relations can be demonstrated more convincingly by comparison of TIDs that have the parameters necessary to describe them completely. Such events found in the literature are listed in Table 1.

The disturbances occurring during 1967 and 1968 were obtained using a CW Doppler technique as described by Davies, Watts, and Zacharisen (1962). The experiment consisted of a 5-MHz transmitter located at each apex of an approximately equilateral triangle with sides about 80 km (see Davies and Jones, 1970). The signals were all received at a site in Boulder, Colorado about 25 km east of the extreme western transmitter. A measure of the vertical trace velocity was possible with two additional transmitters of 3.3 and 4.0 MHz at one of the transmitter sites. The data obtained from this network enabled the velocity vector of a plane-wave disturbance to be found by means of the sequential time delays between observations at each pair of stations. Davies and Jones used a cross-correlation technique to find the time delays for their five events listed in Table 1. Time delays for the remaining four 1967 events in Table 1 were deduced simply by tracing the disturbance observed at one site on translucent paper and superimposing the results on the records of another site. The shift in time required to match features was the desired delay.

The TIDs obtained from the works of Georges, Klostermeyer, and Munro were all observed on sweep-frequency soundings. Velocities for these events were also determined from time delays between similar features. Further details of the measuring techniques and the methods of data reduction can be found in the respective references.

In Table 1 the parameters necessary to specify the wave are tabulated in the three columns immediately following the date of each event. The vertical and horizontal trace velocities, v_{Tz} and v_{Tx} , respectively, are related to v_p and ϕ by

$$v_p = v_{Tz} \cos \phi = v_{Tx} \sin \phi \quad (5)$$

Hence, if v_p and ϕ along with the wave period, τ , are known, the wave is also determined. Also listed are the speed of sound and the critical propagation angle of each event at the indicated height. This height is the median of the observed maximum and minimum vertical extent of the disturbance. In Davies' and Jones' observations the height represents the observed maximum.

Comparison of ϕ and ϕ_c shows that with the possible exception of the events of 12/13 February 1961, 19 July 1967, and 26 November 1967, which are marked with daggers, each of the other observations has a propagation angle within a few degrees of its critical value. For the former event the propagation angle is questionable because some of the angles averaged were less than 90 degrees, and also because of high scatter of the published values.

The periods given in Table 1 should be treated with caution. For some of the TIDs this period represents the time interval for a single cycle of a quasi-periodic event. Even when several cycles are present, the "period" associated with a disturbance may depend on which features are chosen for the measurement [e.g., Figure 3 (a) of Klostermeyer, 1969]. Thus, in addition to the problems inherent in treating a possible transient disturbance as a periodic phenomenon, some events have nonconstant periods and therefore cannot be represented by a single value.

In view of the above, a better way of deciding whether the propagation angle is near its critical value is to determine the magnitude of the refractive index μ . Figure 1 shows that whenever $\mu \geq 4$, $\phi \geq \phi_c$ regardless of the wave period. Table 1 shows that this condition is satisfied except for a single event.

Additional support for the validity of the asymptotic approximation may be found in Hines' (1967) interpretation of TIDs launched by a nuclear detonation. In that paper Hines showed that the nature of f_oF_2 perturbations observed by a number of different stations can be explained on the basis of energy flow along frequency-dependent limiting angles. This behavior is furthermore predicted from the theory of pulse propagation in a plane isothermal atmosphere (Row, 1967). The above is equivalent to the statement that plane internal gravity waves propagate with angles near their critical values.

In Table 1 no attempt was made to choose a temperature model appropriate for each event. To see how the comparison of ϕ and ϕ_c might be affected, the calculations were repeated for each of the following 1966 U. S. Standard Atmospheres: (1) summer high-temperature model, and (2) winter low-temperature model. These two models represent the two extreme temperature profiles likely to be encountered at any time. In all but three cases (Klostermeyer's events were not considered) the 1962 U. S. Standard Atmosphere (which is a mean model) was found to be the most appropriate, based on the local time of each event and its monthly averaged 10.7-cm solar flux (see CIRA 1965 for the reduction procedure). For the three exceptions, two showed better agreement between ϕ and ϕ_c .

In addition to having propagation angles near their critical values, the majority of the events listed in Table 1 have periods of about 20 minutes. Although most of these events were detected by CW Doppler technique, TID, detected by other means (Munro, 1950, 1956; Munro and Heisler, 1956; Titheridge, 1968) were also typified by periods around 20 minutes. These results are consistent with the conclusion previously stated regarding the passband of the atmosphere.

4. CONCLUSIONS

For internal gravity waves at ionospheric heights which have originated from sources below the mesopause, it has been shown that the refractive effects of the atmosphere restrict the propagation angles of the waves to values near the maximum permitted. Thus, for these waves the use of Hines' asymptotic relations is always valid. Furthermore, for these waves the atmosphere behaves like a bandpass filter with center frequency favoring waves with periods near 20 minutes. These conclusions were compared with observations and good agreement was found.

5. ACKNOWLEDGEMENT

The beginnings of this work were done while the author was with the Space Disturbance Laboratory of the Environmental Science Services Administration (now NOAA). I am grateful to Dr. Kenneth Davies for providing me with the opportunity to conduct the study there.

REFERENCES

- Chan, K. L., and O. G. Villard, Jr., 1962, "Observation of Large-Scale Traveling Ionospheric Disturbances by Spaced-Path High-Frequency Instantaneous-Frequency Measurements", J. Geophys. Res. 67, pp. 973-988.
- CIRA, International Reference Atmosphere 1965, compiled by members of Working Group IV of the Committee of Space Research, North-Holland Publishing Company, Amsterdam.
- Davies, K., D. M. Baker, and N. Chang, 1969, "Comparison Between Formulas for Ionospheric Radio Propagation and Atmospheric Wave Propagation," Radio Sci. 4, pp. 231-233.
- Davies, K., J. M. Watts, and D. H. Zacharisen, 1962, "A Study of F_2 -Layer Effects as Observed with a Doppler Technique," J. Geophys. Res. 67, pp. 601-609.
- Davies, K., and J. E. Jones, 1970, "Three-Dimensional Observations of Traveling Ionospheric Disturbances," J. Atmos. Terr. Phys. 33, pp. 39-46.
- Friedman, J. P., 1966, "Propagation of Internal Gravity Waves in a Thermally Stratified Atmosphere," J. Geophys. Res. 71, pp. 1033-1054.
- Georges, T. M., 1967, "Ionospheric Effects of Atmospheric Waves," ESSA Technical Report IER 57-ITSA 51, U. S. Government Printing Office, Washington, D. C. pp. 341.
- Hines, C. O., 1967, "On the Nature of Traveling Ionospheric Disturbances Launched by Low-Altitude Nuclear Explosions," J. Geophys. Res. 72, pp. 1877-1882.
- Hines, C. O., 1960, "Internal Atmospheric Gravity Waves at Ionospheric Heights," Can. J. Phys. 38, pp. 1441-1481.
- Klostermeyer, J., 1969, "Gravity Waves in the F-Region," J. Atmosph. Terr. Phys. 31, pp. 25-45.
- Munro, G. H., 1958, "Travelling Ionospheric Disturbances in the F-Region," Aust. J. Phys. 11, pp. 91-112.
- Munro, G. H., 1950, "Travelling Disturbances in the Ionosphere," Proc. Roy. Soc. A202, pp. 208-223.
- Munro, G. H., 1949, "Short-Period Variations in the Ionosphere," Nature 163, p. 812.
- Munro, G. H., and L. H. Heisler, 1956, "Divergence of Radio Rays in the Ionosphere," Aust. J. Phys. 9, pp. 359-372.
- Roy, R. V., 1967, "Acoustic-Gravity Waves in the Upper Atmosphere Due to a Nuclear Detonation and an Earthquake," J. Geophys. Res. 72, pp. 1599-1610.
- Thomas, L., 1958, "Some Measurements of Horizontal Movements in Region-F2 Using Widely Spaced Observing Stations," J. Atmos. Terr. Phys. 14, pp. 123-137.
- Titterton, J. F., 1968, "Periodic Disturbances in the Ionosphere," J. Geophys. Res. 73, pp. 243-252.
- U. S. Committee on Extension to the Standard Atmosphere, U. S. Standard Atmosphere 1966, Government Printing Office, Washington, D. C.
- U. S. Committee on Extension to the Standard Atmosphere, U. S. Standard Atmosphere 1962, Government Printing Office, Washington, D. C.

TABLE 1
COMPARISON OF EXPERIMENTAL OBSERVATIONS WITH THE ASYMPTOTIC
APPROXIMATION FOR 1962 U.S. STANDARD ATMOSPHERE

Reference*	Date	Tz (minute)	Tz (m s)	Tx (m s)	V (m s)	Height (km)	C (m s)	ϕ (degree)	$\frac{C}{V}$ (degree)	$\frac{C}{V_p}$
(1)	22 June 48	36	58	117	52	300	857	154	118	16.8
(2)	5 July 48	40	83	157	74	235	794	154	163	10.9
(5)	20 2 Nov 60	168	215	52	51	295	853	168	174	17.0
(5)	12 13 Feb 61	114	274	714	256	295	853	161 [†]	173	3.4
(5)	19 Oct 61	84	231	603	216	254	850	159	169	4.3
(3)	14 Dec 60	60	95	768	94	300	857	173	165	9.1
(4)	30 June 67	20	149	182	131	2.7	806	134	133	6.2
(4)	19 July 67	21	242	118	106	230	788	116 [†]	137	7.4
	26 July 67		209	182	156	271	830	126	130	5.2
	3 Aug 67	14	600	170	164	196	745	106	108	4.6
(4)	24 Sept 67	23	183	190	132	225	783	133	142	5.9
	26 Nov 67	24	178	82	74	210	765	115 [†]	140	10.3
	15 Nov 67	24	156	300	134	202	754	149	146	5.6
(4)	26 Feb 68	19	186	194	135	228	786	136	131	5.8
(4)	28 Mar 68	25	162	193	124	236	755	140	145	7.1

*References: (1) Munro (1945) (3) Georges (1967) (5) Klostermeyer (1969)

(2) Munro (1950) (4) Davies and Jones (1970)

[†]See text.

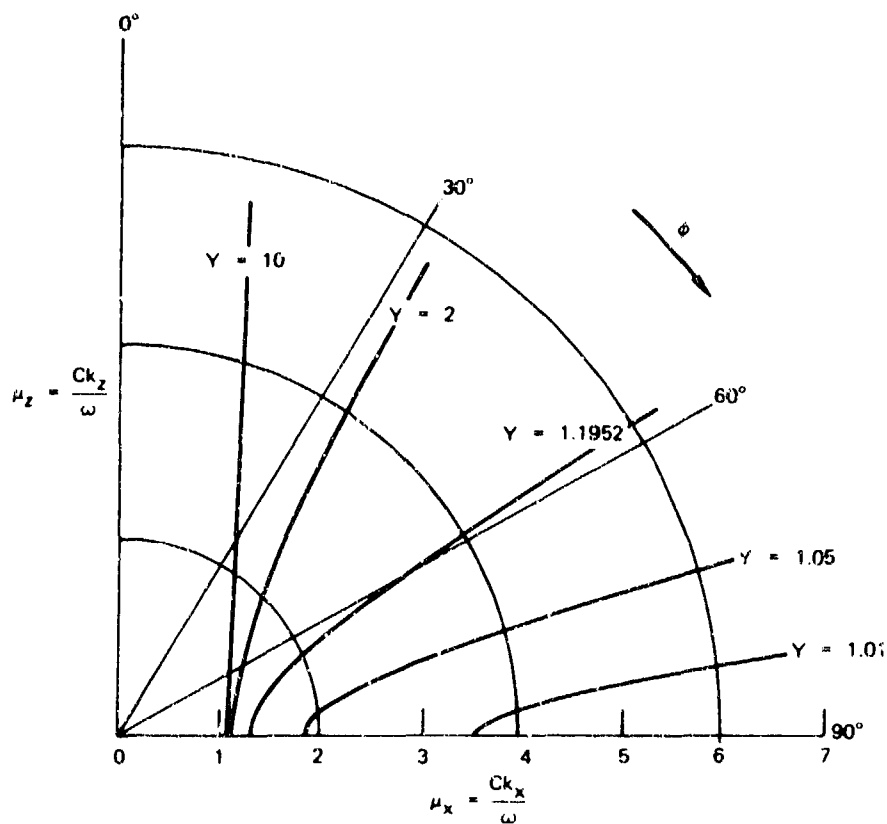


Figure 1 Refractive index surfaces for gravity waves in an isothermal atmosphere.

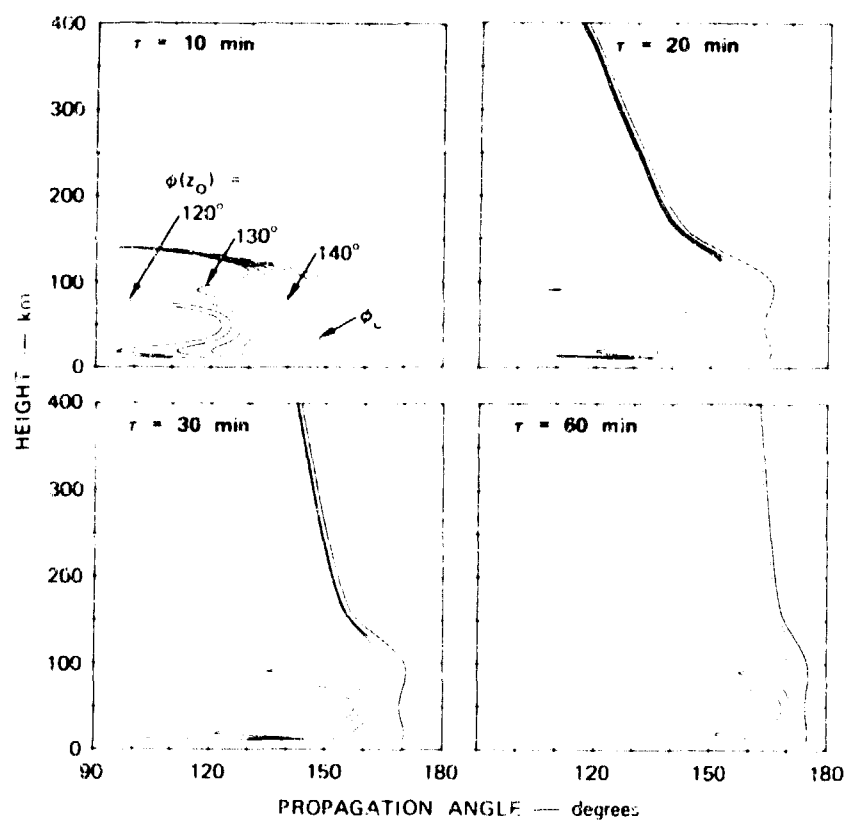


Figure 2 Height Variation of internal-gravity-wave propagation angles launched from a source at $z_0 = 10$ km in the 1962 U. S. Standard Atmosphere. The dashed line represents the critical angle, ϕ_c , for internal gravity waves of the periods shown.

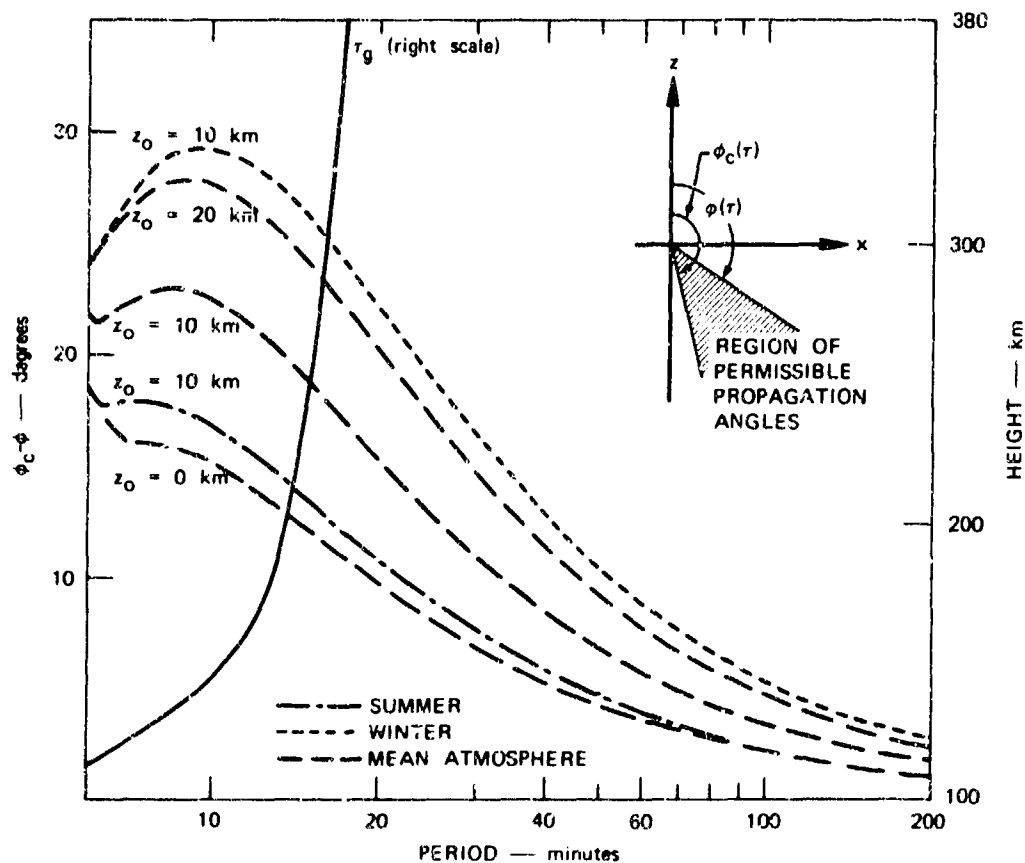


Figure 3 Range of propagation angles for sources located at 0, 10, and 20 km altitude that will launch internal gravity waves above 100 km. τ_g is the Brunt-Väisälä period.

**FULL WAVE CALCULATIONS OF ELECTRON DENSITY PERTURBATIONS
CAUSED BY ATMOSPHERIC GRAVITY WAVES IN THE F2-LAYER**

by

J.Klostermeyer

**Max-Planck-Institut für Aeronomie
Institut für Ionosphärenphysik
3411 Lindau/Harz
Germany**

182

CALCULS TOUTE ONDE DE PERTURBATIONS DE DENSITE ELECTRONIQUE
CAUSEES PAR DES ONDES DE GRAVITE ATMOSPHERIQUES DANS LA COUCHE F2

par

J. Klostermeyer

SOMMAIRE

Le système conjugué d'équations hydrodynamiques qui décrit les perturbations d'ondes de gravité dans les gaz neutre et ionisé est résolu par une méthode toute onde qui englobe les effets des températures et des vents dépendant de l'altitude, de la force de Coriolis, de la viscosité, de la conduction thermique et de la dérive des ions. Les résultats des calculs concordent bien avec les données expérimentales obtenues à partir d'ionogrammes en incidence verticale. Les résultats des calculs numériques sont en outre combinés avec les paramètres d'ondes de gravité fournis par les observations pour obtenir des profils d'amplitude et de phase des perturbations de densité électronique suivant l'altitude, en fonction de l'inclinaison magnétique et de l'azimut de propagation des ondes. Selon les calculs, la perturbation dépend dans une très large mesure de l'altitude, de l'inclinaison et de l'azimut. Son amplitude varie entre 0 et 100 % de la densité électronique non perturbée, et sa phase peut varier rapidement aux alentours du maximum de la couche F.

FULL WAVE CALCULATIONS OF ELECTRON DENSITY PERTURBATIONS
CAUSED BY ATMOSPHERIC GRAVITY WAVES IN THE F2-LAYER

J. KLOSTERMEYER

Max-Planck-Institut für Aeronomie, Institut für Ionosphärenphysik,
 3411 Lindau/Harz, Germany

SUMMARY

The coupled system of hydrodynamic equations, which describes gravity wave perturbations in the neutral and ion gases, is solved by a full wave method including the effects of height dependent temperature and winds, Coriolis force, viscosity, thermal conduction, and ion drag. Calculated results agree well with experimental data deduced from vertical incidence ionograms. The numerical calculations are further combined with observed gravity wave parameters to obtain height profiles of the amplitude and phase of the electron density perturbation as functions of the geomagnetic inclination and the azimuth of wave propagation. The calculated perturbation depends very strongly on height, inclination, and azimuth. Its amplitude varies between 0 and 100 per cent of the undisturbed electron density, and its phase may change rapidly around the F-layer maximum.

1. INTRODUCTION

During the passage of atmospheric gravity waves through the F-region the motion of the neutral gas influences the motion of the ion gas by collisions and causes corresponding changes in the motion of the electron gas as a result of Coulomb forces. If the directions of the neutral gas velocity and the geomagnetic field are different, the ion gas reacts upon the neutral gas by attenuating its motion. This interaction requires that a realistic theoretical calculation of ionization density perturbations caused by gravity waves in the F-region must be based on a simultaneous solution of a coupled system of equations describing the perturbations of the neutral and ion gases.

Theoretical descriptions of the F2-layer response to gravity waves have been published by HOOKE (1968, 1970), NELSON (1968), THOME (1968), TESTUD and FRANCOIS (1971), and CLARK, YEH and LIU (1971). These authors did not treat the problem in coupled form but introduced simplifications in order to solve it in two successive steps.

(a) They solved the equations describing the gravity wave propagation in the neutral gas or merely postulated a model for the neutral gas perturbations.

(b) The neutral gas perturbations were inserted into the continuity equation of the ion gas to calculate the ionization changes. At present the work of CLARK et al. (1971) is the last and most comprehensive one. It takes into account the effects of thermal conduction, ion drag, ion diffusion, and nonlinearity of the ion density perturbation, but neglects all terms due to neutral winds and viscosity. In order to integrate the hydrodynamic equations a WKB method is used whose validity, however, is doubtful in some cases under consideration.

It is the purpose of this paper to calculate electron density perturbations using a simultaneous full wave solution of the coupled system of equations which describe the perturbations of the neutral and ion gases. We shall also include the effects of height dependent winds and viscosity; mathematical difficulties, however, do not allow us to consider nonlinear effects in the continuity equation of the ion gas as has been done by CLARK et al. (1971). In section 2 a description of the calculations will be given. In section 3 we shall compare calculated and observed results and present height profiles of the amplitude and phase of the electron density perturbation as functions of the geomagnetic inclination and the azimuth of wave propagation.

2. DESCRIPTION OF THE CALCULATIONS

The theoretical calculation of gravity wave propagation starts from the basic hydrodynamic equations, i.e. the equations of continuity, motion, and heat conduction:

$$\frac{d\rho}{dt} = -\rho \nabla \cdot \underline{u}, \quad (1)$$

$$\frac{d\underline{u}}{dt} = \underline{f}, \quad (2)$$

$$\frac{ds}{dt} = \frac{q}{T} \quad (3)$$

with

t: time;	ρ : density;
\underline{u} : velocity;	\underline{f} : force per unit mass;
s : entropy per unit mass;	q : heat input per unit mass;
T: temperature.	

In order to solve these equations a perturbation method is used, i.e. we consider a state of the gas, in which $\rho = \rho_0 + \rho_1$, $u = u_0 + u_1$ etc. The subscript "0" denotes the unperturbed state, the subscript "1" the perturbation quantities.

We assume that the unperturbed state is already known from the solutions of the hydrodynamic equations or from experiments. Hence the model of the undisturbed atmosphere is taken from the 1966 U.S. Standard Atmosphere Supplements. The undisturbed ion number density is described by an α -Chapman layer. It has been found that observed ion density profiles at night are matched well by this approximation, whereas during daytime more serious discrepancies may occur especially in the F1-region. The horizontal neutral wind components are calculated from the results of KOHL and KING (1967); a vertical wind component is not considered.

The perturbation quantities are assumed to be small so that it is justified to neglect all terms of higher than first order. Then we have to solve the linearized form of equations (1)-(3), taking into account the effects of height dependent temperature and winds, Coriolis force, viscosity, thermal conduction, and ion drag.

Including the ion drag requires, however, that we calculate simultaneously the wave induced ion density perturbation from the continuity equation of the ion gas

$$\frac{dn_1}{dt} = -n_1 \nabla \cdot u_1 + Q - L \quad (4)$$

where

n_1 : ion number density; u_1 : ion velocity;
 Q : production rate; L : loss rate.

We introduce the following simplifications.

(a) We linearize equation (4), because we must treat it together with the neutral gas equations in coupled form:

$$\frac{\partial n_{11}}{\partial t} = -\nabla \cdot (n_{10} u_{11} + n_{11} u_{10}) + Q_1 - L_1.$$

CLARK et al. (1971) have found that this procedure may cause considerable errors especially below the F-layer maximum where the ion density perturbation may be relatively large, even if the neutral gas perturbations are small.

(b) CLARK et al. (1971) have further shown that wave induced perturbations of the ion diffusion velocity are in general unimportant in causing ion density perturbations. Also according to GERSHMAN and GRIGOR'YEV (1965) the effects of wave induced electric fields are negligible. Therefore we can take u_{11} to be the projection of u_1 along the geomagnetic field, i.e. $u_{11} = (u_1 \cdot b)b$, where b is the direction of the magnetic field.

(c) We assume that the term $n_{11} u_{10}$ can be neglected compared to $n_{10} u_{11}$. Experimental results of TESTUD (1971) indicate that $|u_{10}|$ is less than or nearly equal to $|u_{11}|$. Therefore our assumption is justified if n_{11} is small compared to n_{10} . Otherwise we obtain a further error in addition to that mentioned under (a).

(d) According to HOOKE (1968) wave induced perturbations of the production and loss rates can be neglected at F-region heights above about 250 km. Then we obtain the linearized ion continuity equation

$$\frac{\partial n_{11}}{\partial t} = -(u_1 \cdot b)(b \cdot \nabla n_{10}) - n_{10} \nabla \cdot [(u_1 \cdot b)b] \quad (5)$$

which is essentially identical with equation (48) of HOOKE (1968). The first term on the right hand side describes changes of the ion density resulting from the bodily movement of the layer, the second term describes changes of the ion density caused by compression and dilatation. Since the number densities of ions and electrons are equal, the equation also yields the electron number densities shown in the next section.

The coupled system of equations is solved numerically by a full wave method, which has been described in detail by KLOSTERMEYER (1972).

3. CALCULATED ELECTRON DENSITY PERTURBATIONS

In contrast to an analytical solution of the linearized equations of hydrodynamics, a numerical solution cannot be used for a general description of the whole gravity wave spectrum. Instead we must confine ourselves to a description of single wave modes with given periods and horizontal wavelengths. In order to get realistic electron density perturbations we shall start from a period and a horizontal wavelength which were derived from an observed large scale disturbance in the F2-layer. This procedure also allows us to compare calculated and observed results.

3.1. Comparison between calculated and observed results

During a magnetically quiet night on 19 October 1961, a travelling ionospheric disturbance was observed in the F-region by means of three vertical incidence ionosondes (KLOSTER-

MEYER, 1969). The ionosondes were spaced some 100 km apart at Lindau ($51^{\circ}39'N, 10^{\circ}08'E$), Gernern ($50^{\circ}27'N, 09^{\circ}09'E$), and Gatenland ($51^{\circ}48'N, 08^{\circ}38'E$). From a real height analysis of the ionograms the temporal electron density variation at several fixed heights can be derived. Fig. 1 shows the electron density variation at Lindau. We see the typical properties of a so-called large scale disturbance, a quasi period of 1.5h, a downward propagating phase, and electron density variations between 10 and 70 per cent. From a cross correlation analysis of the electron density variations at different stations we obtain the additional information that the disturbance had a horizontal wavelength of 3300 km and travelled from north to south.

Today it seems to be generally accepted that travelling ionospheric disturbances are caused by atmospheric gravity waves. A comparison between the observed results and numerically calculated electron density perturbations is therefore a valuable test whether the theoretical model given in the previous section represents a realistic description of gravity wave propagation in the F-region.

Fig. 2 shows the amplitude $|n_{e1}|/n_{e0}$ and the phase ϕ of the relative electron density perturbation vs. height z (n_{e1} : electron density perturbation; n_{e0} : undisturbed electron density). Strictly speaking ϕ denotes the phase delay between the relative electron density perturbations at $z = 250$ km and at other heights. Negative values of ϕ thus mean a phase advance. The continuous lines and the circles indicate calculated and observed variations respectively. Both variations agree well. This also holds true for the amplitude at lower heights although it exceeds perturbation magnitude.

Fig. 2 also shows a comparison between observed and calculated height profiles of the total electron density $n_e = n_{e0} + n_{e1}$. The height profiles are drawn for two different times which have been chosen such that the electron density at the height of the undisturbed layer maximum has its greatest value ($t = 4.00$ L.M.T.) and its smallest value ($t = 4.45$ L.M.T.) respectively. At $t = 4.00$ L.M.T. the agreement between observed and calculated data is good. At $t = 4.45$ L.M.T., however, more serious discrepancies occur. The reason is that the observed undisturbed F-layer was time dependent whereas, in the calculations, it was assumed to be constant. Nevertheless both observed and calculated profiles show qualitatively how the gravity wave affects the electron density maximum, its height, and the layer curvature during an oscillation.

3.2. Electron density perturbations as functions of geomagnetic inclination and propagation azimuth

Since a period of 1.5h and a horizontal wavelength of 3300 km seem to be representative for large scale disturbances in the F-region, these numerical values have further been used to calculate height profiles of the amplitude and phase of the electron density perturbation as functions of the geomagnetic inclination and the azimuth of wave propagation. In order to investigate the influence of both parameters, two assumptions have been made.

(a) The parameters of the undisturbed thermospheric and ionospheric models remain the same as in the calculations described in section 3.1.

(b) The amplitude and the phase of the neutral gas density perturbation at a lower boundary $z = 150$ km are assumed to have the same values as the observed wave. The choice of the neutral gas density perturbation is purely arbitrary. We could have chosen the perturbation of any other neutral gas variable, like the horizontal or vertical velocity component, temperature etc. The lower boundary has been chosen at $z = 150$ km because, at such a low height, the ion drag is small and cannot influence the gravity wave propagation.

At this point it should be mentioned that changes of the inclination include corresponding changes of the geographic latitude. Consequently the gravity wave propagation is affected not only by changes of the ion drag but also by direct changes of the Coriolis force. For a wave period of 1.5h, however, the influence of the Coriolis force is small compared to the influence of the ion drag.

Figs. 3a and 3b show height profiles of the amplitude and phase of the relative electron density perturbation as functions of the geomagnetic inclination I . Fig. 3c contains electron density profiles at two different times, which have again been chosen such that the electron density at the height of the undisturbed layer maximum has its greatest value (continuous lines) and its smallest value (dashed lines) respectively. The gravity wave is assumed to travel equatorward except for $I = 0^{\circ}$, where it may travel toward the north or south. All curves are valid for positive and negative values of I , i.e. in the northern and southern hemispheres. They can be easily interpreted by means of equation (5) taking into account that the number densities of ions and electrons are equal.

(a) At the geomagnetic poles ($I = \pm 90^{\circ}$), the term $u_1 \cdot b$ is very small, because the velocity u_1 is nearly horizontal. Therefore the amplitude $|n_{e1}|/n_{e0}$ is also very small in the whole height range, and the total electron density profiles $n_e(z)$ show no significant temporal variations.

(b) At mid-latitudes ($I = \pm 67.5^{\circ}$, $I = \pm 45^{\circ}$, $I = \pm 22.5^{\circ}$), all amplitude curves have a similar behaviour. Below the layer maximum where the gradient of the undisturbed layer, ∇n_{i0} , is very steep, the upward and downward motion of the layer as a whole yields large amplitudes which may exceed perturbation magnitude. Near the maximum where ∇n_{i0} is small, we find also relatively small amplitudes resulting mainly from layer compression and dilatation. Above the maximum the contribution of the bodily movement of the layer increases again, but the resulting amplitudes do not exceed perturbation magnitude. All phase curves at mid-latitudes show a more or less pronounced phase reversal around the layer maximum confirming that the electron density perturbations are caused mainly by an upward and downward motion of the layer as a whole while compression plays only a minor role. The total electron density profiles indicate large temporal

(c) At the geomagnetic equator ($I=0^\circ$) the term $b \cdot \nabla n_0$ is equal to zero, so that the amplitude and phase variations result only from compression and dilatation. Consequently the amplitude and phase values do not change rapidly in the whole height range. The total electron density profiles reveal only a temporal variation of the electron density at different heights, but there are no significant variations of the height of the layer maximum and of the layer curvature.

Figs. 4a-4c present height profiles of $|n_{e1}|/n_{e0}$, ϕ , and n_e as functions of the azimuth of wave propagation. The continuous and dashed lines in Fig. 4c have the same meaning as in Fig. 3c. The geomagnetic inclination is assumed to be 67.5° .

A gravity wave travelling eastward or westward causes only unimportant electron density perturbations in contrast to a wave travelling toward the equator or pole, because the term $u_1 \cdot b$ in equation (5) is very small. The amplitude curves of the equatorward and poleward propagating waves show very similar shapes; the same is true for the corresponding phase curves. However, the amplitude curves differ by a factor 2, and the phase curves are shifted against each other by about 90° . The total electron density profiles show no significant temporal variations except for equatorward propagation.

4. CONCLUDING REMARKS

In order to give a quantitative description of gravity wave induced electron density perturbations, the linearized hydrodynamic equations must be solved numerically. Consequently we cannot give a general description for the whole wave spectrum but must confine ourselves to single wave modes. Nevertheless it is possible to generalize the above mentioned results for gravity waves with long periods of the order of 1h and more.

At geomagnetic mid-latitudes the amplitude of the electron density perturbation is largest if the waves travel in the geomagnetic north-south direction. The perturbations are mainly caused by the bodily movement of the layer; compression plays a dominant role only in a small height range around the F-layer maximum. The perturbations are therefore largely determined by the undisturbed layer gradient. The typical height profile of the relative perturbation amplitude shows a minimum near the layer maximum and large values below it, which may even be greater than 1. The height profile of the perturbation phase is characterized by a phase reversal around the layer maximum.

If the purely dynamical terms in the ion continuity equation (5) are small or vanish, effects due to ion diffusion, wave induced electric fields, production and loss possibly play a dominant role in producing ionization perturbations. The results given in section 3.2 for $I = \pm 90^\circ$ and for east-west propagation may be changed by these effects. The resulting amplitudes, however, should remain small compared to the amplitudes obtained in all other cases.

Acknowledgements- The numerical calculations were performed on the UNIVAC 1108 computer of the Gesellschaft für wissenschaftliche Datenverarbeitung in Göttingen. The author thanks Dr. W. Varnum for his assistance in translating this paper into English. The paper is published by permission of the Director of the Institute.

5. REFERENCES

- CLARK, P.M., YEH, K.C. and LIU, C.H., 1971, "Interaction of internal gravity waves with the ionospheric F2-layer", J. Atmosph. Terr. Phys. **33**, 1567-1576.
- GERSHMAN, B.N. and GRIGOR'YEV, G.I., 1965, "Theory of moving ionospheric disturbances (Magnetohydrodynamic absorption)", Geomagn. Aer. **5**, 656-660.
- HOOKE, W.H., 1968, "Ionospheric irregularities produced by internal atmospheric gravity waves", J. Atmosph. Terr. Phys. **30**, 795-823.
- HOOKE, W.H., 1970, "The ionospheric response to internal gravity waves. 1. The F2 region response", J. Geophys. Res. **75**, 5535-5544.
- KLOSTERMEYER, J., 1969, "Gravity waves in the F-region", J. Atmosph. Terr. Phys. **31**, 25-45.
- KLOSTERMEYER, J., 1972, "Numerical calculation of gravity wave propagation in a realistic thermosphere", J. Atmosph. Terr. Phys., in press.
- KOHL, H. and KING, J.W., 1967, "Atmospheric winds between 100 and 700 km and their effects on the ionosphere", J. Atmosph. Terr. Phys. **29**, 1045-1062.
- NELSON, R.A., 1968, "Response of the ionosphere to the passage of neutral atmospheric waves", J. Atmosph. Terr. Phys. **30**, 825-835.
- TESTUD, J., 1971, "Gravity waves generated during magnetic substorms", J. Atmosph. Terr. Phys. **32**, 1793-1805.
- TESTUD, J. and FRANCOIS, P., 1971, "Importance of diffusion processes in the interaction between neutral waves and ionization", J. Atmosph. Terr. Phys. **33**, 765-774.

THOME, G., 1968, "Long-period waves generated in the polar ionosphere during the onset of magnetic storms", J. Geophys. Res. 73, 6319-6336.

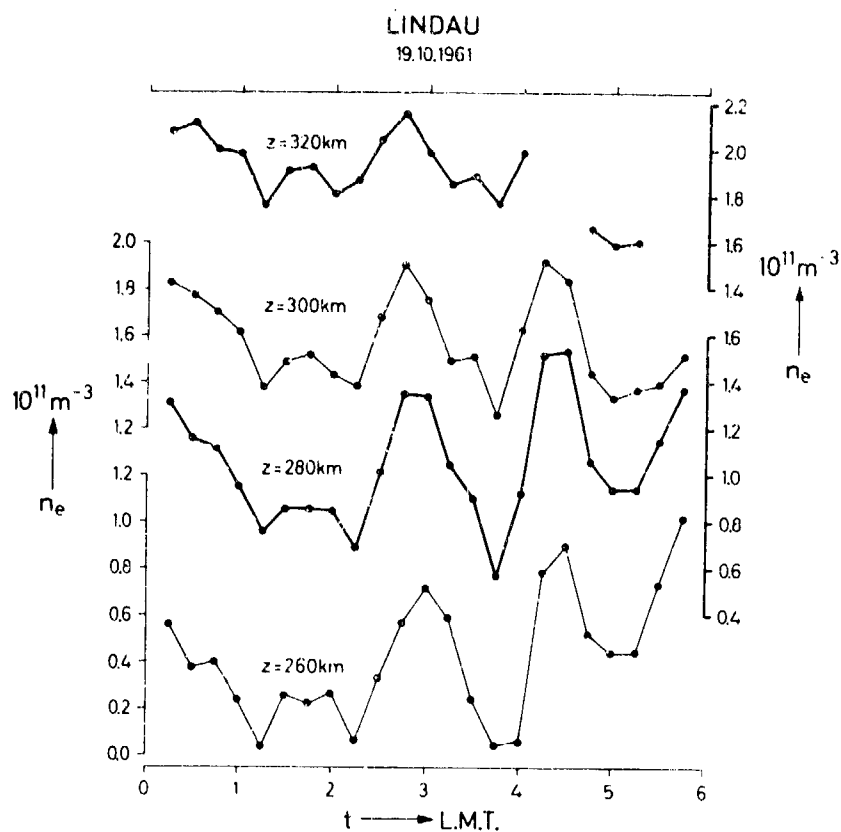


Fig. 1. Observed electron density vs. time at different heights.

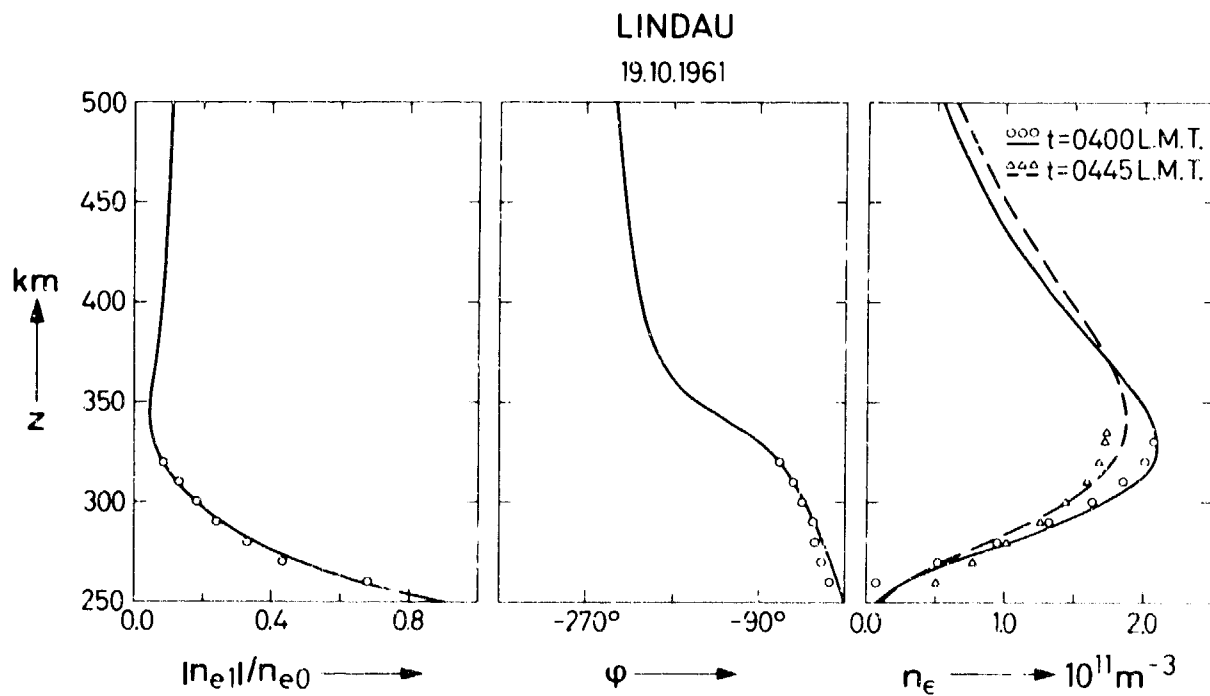


Fig. 2. Amplitude and phase of the relative electron density perturbation and total electron density vs. height.
Continuous and dashed lines: Calculated variations
Circles and triangles: Observed variations.

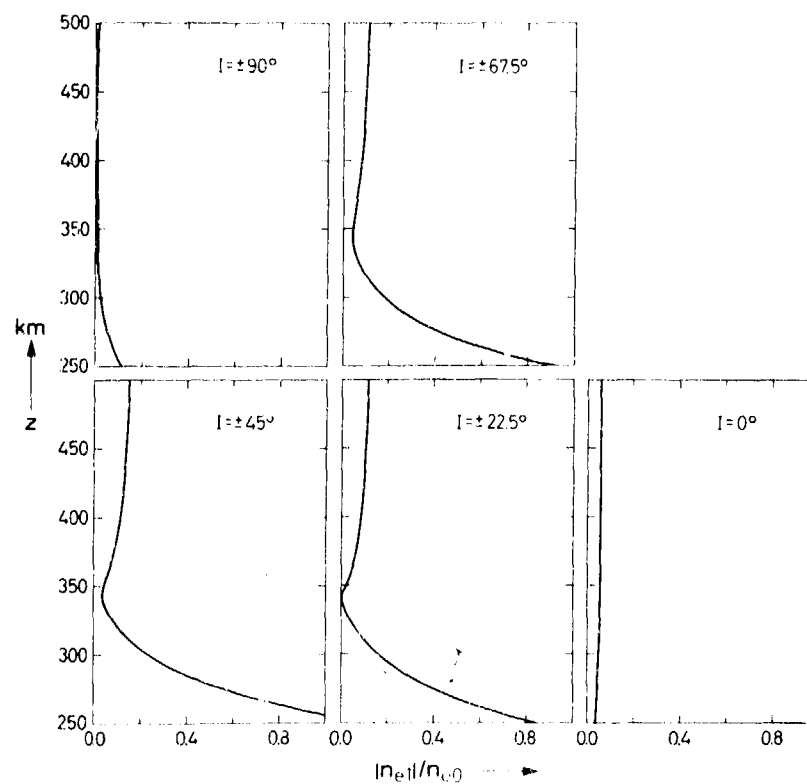


Fig. 3a. Height profiles of the amplitude of the relative electron density perturbation as functions of the geomagnetic inclination.

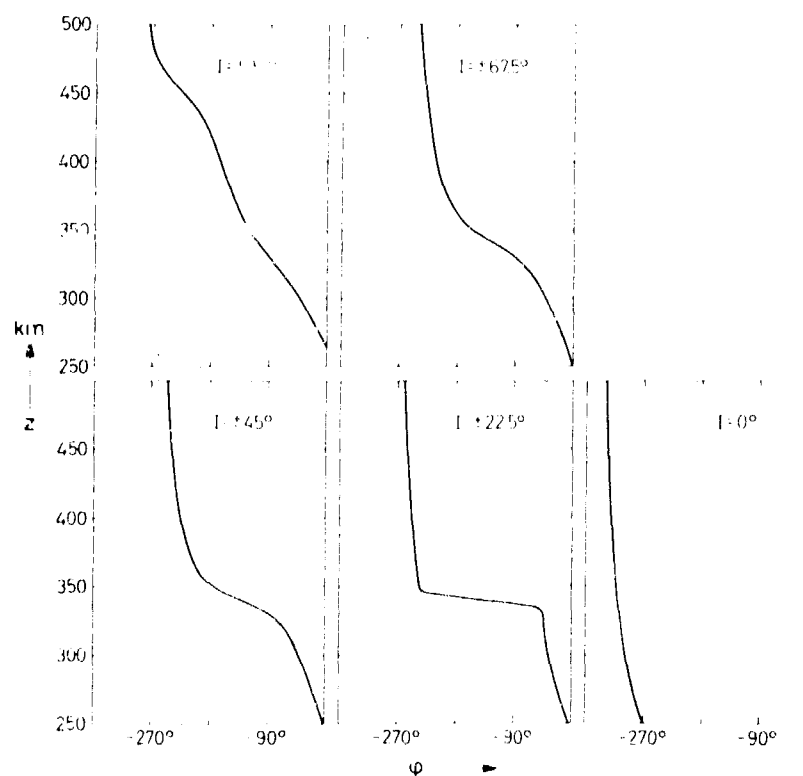


Fig. 3b. Height profiles of the phase of the relative electron density perturbation as functions of the geomagnetic inclination.

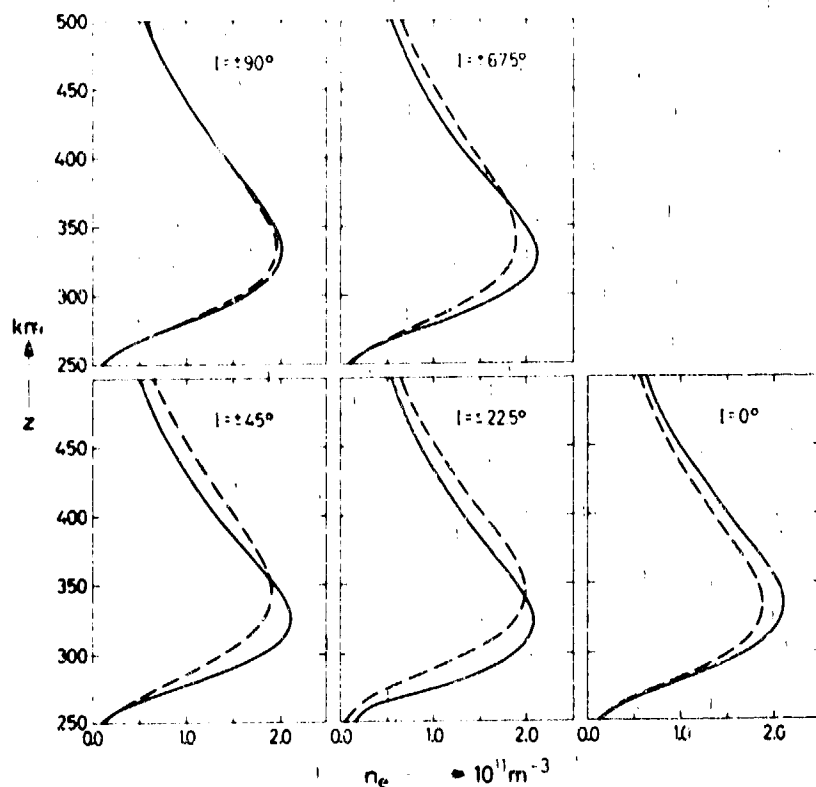


Fig. 3c. Height profiles of the total electron density as functions of the geomagnetic inclination. The continuous and dashed lines indicate two different times, which have been chosen such that the electron density at the height of the undisturbed layer maximum has its greatest and its smallest value respectively.

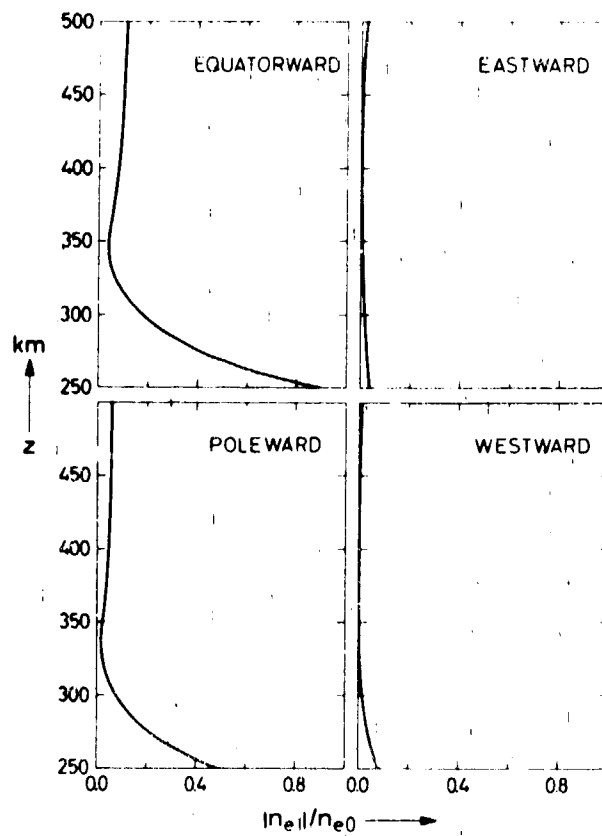


Fig. 4a. Height profiles of the amplitude of the relative electron density perturbation as functions of the propagation azimuth.

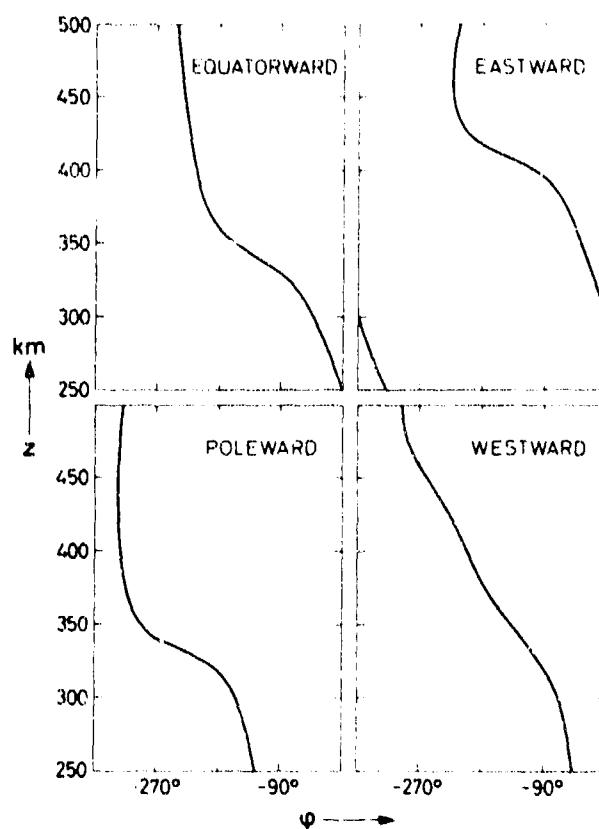


Fig. 4b. Height profiles of the phase of the relative electron density perturbation as functions of the propagation azimuth.

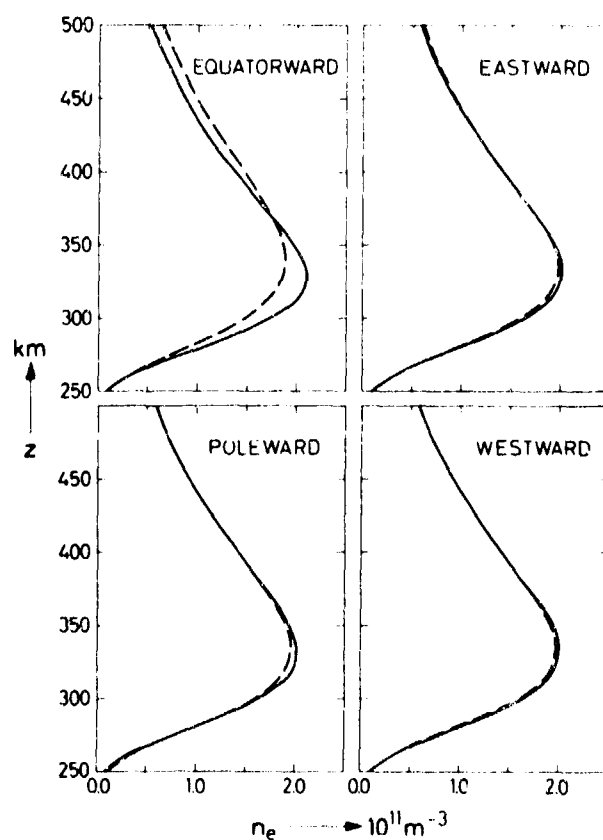


Fig. 4c. Height profiles of the total electron density as functions of the propagation azimuth. The continuous and dashed lines have the same meaning as in Fig. 3c.

**ATMOSPHERIC PRESSURE WAVES AT BRISBANE AND THEIR ASSOCIATION
WITH CERTAIN IONOSPHERIC AND SOLAR EVENTS**

by

G.G.Bowman

Department of Physics
University of Queensland
Brisbane, Q., 4067
Australia

ONDES DE PRESSION ATMOSPHERIQUE OBSERVEES A BRISBANE, ET LEUR RELATION AVEC CERTAINS PHENOMENES IONOSPHERIQUES ET SOLAIRES

par

G.G. Bowman

SUMMAIRE

Au cours de cette analyse, l'auteur étudie deux aspects des enregistrements effectués de nuit, à Brisbane, à l'aide de microbarographes de grande sensibilité. Pendant les huit années d'enregistrement, il y eut 217 nuits au cours desquelles on observa des ondes de gravité bien définies, présentant des périodes d'environ 12 minutes et des amplitudes de l'ordre de 10 μ bars. Des analyses effectuées en superposant les époques, au moyen des dates d'apparition de ces ondes considérées comme dates de contrôle, en période de minimum des taches solaires, révélèrent une apparente association entre ces dates et la présence de conditions ionosphériques à F diffus dans les régions sous-aurorales de la Terre. D'autre part, lorsqu'on effectua le relevé graphique des activités quantifiées par le nombre des taches et des activités géomagnétiques aux dates en question, on trouva, dans les répartitions, des périodicités de 27 jours. L'auteur montre que, dans certains cas, l'apparition d'ondes de gravité est liée au passage de fronts de perturbations météorologiques à Brisbane. Ce sont toutefois les autres cas qui semblent être liés à l'apparition du F diffus. L'auteur montre également que certaines données révèlent une association entre l'apparition d'ondes acoustiques atmosphériques et les activités solaires quantifiées par le nombre des taches. Ces ondes présentent des périodes d'environ 3 minutes et des amplitudes de l'ordre de 10 μ bars.

ATMOSPHERIC PRESSURE WAVES AT BRISBANE AND THEIR ASSOCIATION
WITH CERTAIN IONOSPHERIC AND SOLAR EVENTS

G.G. Bowman
 DEPARTMENT OF PHYSICS
 UNIVERSITY OF QUEENSLAND
 Brisbane, Q., 4067
 Australia

SUMMARY

This analysis investigates two aspects of the nighttime recordings, at Brisbane, of microbarographs of high sensitivity. There were 217 nights in the 8-year recording interval when the records showed well-defined gravity waves with periods around 12 minutes and amplitudes of the order of 10 μ bar. Superposed-epoch analyses using these occurrences as control dates, for a sunspot-minimum period, revealed an apparent association between the dates and the occurrence of ionospheric Spread-F conditions in sub-auroral regions of the Earth. Also, when sunspot activity and geomagnetic activity were plotted relative to these dates, there was evidence of 27-day periodicities in the distributions. Some gravity-wave occurrences are shown to be related to the passage of weather fronts at Brisbane. However, it is the remaining occurrences which appear to be associated with the occurrence of Spread-F. The paper also shows that there is some evidence for an association between the occurrence of atmospheric acoustic waves and sunspot activity. These waves have periods around 3 minutes and amplitudes of the order of 10 μ bar.

1. INTRODUCTION

1.1. The Experiment

An experiment which uses microbarographs of high sensitivity (Jones and Forbes, 1962) has been in operation at Brisbane almost continuously since June, 1963. Brisbane has a geomagnetic latitude of 36° S and is located half-way up the eastern coast of Australia. The principal reason for establishing this experiment was to search for a possible association between Spread-F conditions in the ionosphere over Brisbane and gravity waves recorded at ground level by the microbarographs. The experiment was prompted by the possibility that ionospheric Spread-F conditions are produced by the passage of gravity waves through the neutral atmosphere of the ionosphere (McNicol et al., 1956; Bowman, 1960a; Bowman, 1968a, 1968b). Although some associations have been found between ground-level pressure waves and some types of ionospheric irregularities over Brisbane (Bowman and Shrestha, 1966; Bowman and Khan, 1970; Khan, 1970; Shrestha, 1971a, 1971b), attempts to associate local Spread-F conditions with atmospheric gravity waves have not been convincing (see e.g. Figure 8 of Bowman, 1968a). In this paper atmospheric gravity waves will be abbreviated to AGWs.

1.2. Details of Observations and Methods of Analysis Used.

This paper presents evidence for an association between well-defined gravity waves at Brisbane and Spread-F conditions in regions of the Earth just equatorward of the southern and northern auroral zones. The gravity waves have an average periodicity of 12 minutes, amplitudes around 10 microbars, and exist as a series of wave trains which often persist for most of the night. Associations of the occurrence of these waves with sunspot activity and geomagnetic activity have also been investigated. In addition, the paper will discuss briefly a possible association between atmospheric acoustic waves (abbreviated here as AAWs) and sunspot activity. These acoustic waves usually take the form of an isolated burst of only a few cycles. They have amplitudes of about 10 microbars and an average periodicity of 3 minutes.

The superposed-epoch method of analysis (Chree and Stagg, 1928) is used extensively in this paper. The points in the distributions which result from this type of analysis are presented here either as displacements from the average value using the standard deviation (σ) of each distribution as a displacement of unity; or, alternatively with the average value of the displacements normalized to unity. Normal distributions are assumed for the points. Because daytime microbarograph conditions at Brisbane are often noisy, the analysis has investigated only the nighttime records. The presence of AGWs can be identified on about 30 per cent of all nights. However, the control dates used here in the analyses relate only to those particular nights when the activity was well-defined. The selection of these dates from the nights when some gravity-wave activity was detectable was somewhat subjective. It has been convenient to divide the recording interval into two periods; firstly, a sunspot-minimum period (June, 1963 to June, 1966), when there were 108 nights of well-defined AGWs, and secondly a sunspot-maximum period (July, 1966 to June, 1971) which had 109 such occasions. Also, in these sunspot-minimum and sunspot-maximum periods there were AAWs recorded on 243 and 411 occasions respectively, the second period here being extended to October, 1971. Usually when an acoustic-wave event occurred it was the only one for the night; although on some occasions several occurred on the one night.

Figure 1 shows a microbarograph record which contains well-defined AGWs. The various levels have been arranged so as to illustrate the tendency, which is seen from time to time, for the wave packets to occur at regular intervals. Here the interval is 84 minutes. Also, the record is presented with a certain overlap in time between the various levels. Figure 2 is an example of the occurrence of AAWs. Here the periodicity is 2.7 minutes. The analysis of Spread-F occurrence data presented difficulties. The marked annual and semi-annual variations (Figure 28 of Bowman 1960b) produced unwanted long-term periodicities in the distributions. In addition, if the raw data were used, periods when Spread-F activity was high had a greater influence on the calculation of any particular value in the distribution than those periods when the activity was low. These problems were overcome by dividing a normal year into

eleven 31-day periods and a 24-day period at the end. Then, before data were used in any analysis they were normalized by dividing the value of each day's activity within each period, by the average activity for that period. The Brisbane nighttime recording periods can be taken as 1800 to 0600 local time or 0800 to 2000 Universal Time. The control dates were determined from the Universal Time of the recordings.

2. SPREAD-F ASSOCIATION WITH ATMOSPHERIC GRAVITY WAVES

Daily estimates of Spread-F activity, deduced from published hourly values of ionospheric parameters, have been made for the sunspot-minimum period, for 67 ionospheric stations located throughout the world. These stations are found in one of seven regions of the Earth, the boundaries of the regions being determined by lines of constant L-shell values. Figure 3 indicates the locations of these regions in the vicinity of Australia and shows the position of Brisbane relative to them. Each L-shell region in the southern hemisphere (labelled a to g inclusive on Figure 3) has a complementary region in the northern hemisphere.

Figure 4 shows the result of a superposed-epoch analysis of Spread-F occurrence relative to the control dates for AGWs at Brisbane. In this analysis the seven regions have been grouped together in such a way that they form 3 larger regions. For regions a and b combined (Figure 4a) the high values in the distribution, which occur at the centre day and a day later, suggest an association. On the latter day the value is slightly greater than 3.5 standard deviations (σ) from the average value. Assuming a normal distribution, the significance of this value can be stated as follows. The probability of this value, or one greater than it, occurring randomly in the distribution is 1 in 4,500. In other words an association between the occurrence of Spread-F in these regions and AGWs at Brisbane seems quite probable. In the other two distributions (covering latitude regions almost up to the equator) the displacements near the centre day are not significant (see Figures 4b and 4c). Incidentally, a search for an association between AGWs and Spread-F conditions at Brisbane, by similar methods, proved negative.

The suggested association can be further tested by subdivision of the data. Figure 5 shows another superposed-epoch analysis which combines the Spread-F occurrence from regions a, b and c for 2 different time intervals (June, 1963 to December, 1964 and January, 1965 to June, 1966). It will be seen that significant peaks occur near the centre day for both distributions (namely 3.3 σ and 2.4 σ respectively). Another type of subdivision is achieved by analysing in a similar manner, each of the seven regions separately, for the total period (June, 1963 to June, 1966). Although these distributions are not shown here, the displacements for the centre day or the day after, whichever displacement is the greater, are shown plotted on Figure 6. The important feature on this figure is the highly significant values for regions a and b separately (namely 3.1 σ and 2.8 σ respectively). Thus the proposed association seems to have stood the test of these subdivisions, and so the argument for an association is further strengthened.

Spread-F stations at latitudes higher than those used here have on occasions extensive ionospheric blackout periods which make it difficult to determine the real Spread-F occurrence. For this reason these stations have been omitted from this present analysis. However, attempts to use Spread-F information from these stations could be made in future analyses.

3. ATMOSPHERIC-GRAVITY-WAVE OCCURRENCE COMPARED WITH SUNSPOT AND GEOMAGNETIC ACTIVITY

Superposed-epoch analyses have been used to examine the variation of sunspot activity and geomagnetic activity, separately, relative to the AGW control dates. Also, the sunspot-minimum period (June, 1963 to June, 1966) and the sunspot-maximum period (July, 1966 to June, 1971) are investigated separately. Figure 7(a) shows the variation of sunspot numbers relative to the control dates for the sunspot-minimum period, while Figure 7(b) is the variation for A_p indices for the sunspot-maximum period. For the sunspot numbers a 27-day periodicity can be seen particularly in the distribution for the period before the centre day. For the A_p indices a 27-day periodicity is not as obvious, although there is some evidence for it.

Figure 8 shows, by the solid lines, the results of Fourier analyses of these distributions (Figure 7) as well as two other distributions which have not been illustrated here. Figures 8a and 8c relate to the sunspot-minimum period while Figures 8b and 8d relate to the sunspot-maximum period. Three of these four diagrams show relatively large amplitudes for a period of 27.43 days (i.e. a value close to the average solar-rotation period for sunspots). The dashed lines on the diagrams show the results obtained if, instead of using the AGW control dates, an equal number of dates chosen randomly in each period, are used. There seems to be no particular tendency for these distributions to peak at 27.43 days. It is perhaps significant that the phases of the two sunspot-number distributions (Figures 8a and 8b) are such that oscillations are a maximum 2.3 and 1.9 days respectively, before the centre day. For the A_p -indices distribution showing a periodicity around 27 days (Figure 8d) the oscillation has a maximum 0.2 days after the centre day. If the gravity waves are associated with the sunspot activity by means of solar particles coming from sunspot regions, a rough estimate of the delay between the two phenomena would be 2 days. Whereas, geomagnetic activity would be expected to coincide approximately with the gravity-wave activity.

4. THE PASSAGE OF WEATHER FRONTS THROUGH BRISBANE

4.1. The Association of Fronts with AGWs

If the AGWs, which occur regularly, originate in weather systems in the vicinity of Brisbane, weather fronts are the most likely source. The occurrence of frontal passages at Brisbane (from June, 1963 to November, 1965) relative to the AGW control dates, is shown in Figure 9(a). There is a peak in the distribution of 3.9 σ which shows that there is almost certainly an association.

4.2. Spread-F and Non-frontal AGWs

This apparent association with fronts prompted the subdivision of the control dates into two groups. Figure 9(b) has used control dates which were not followed by frontal passages on either of the two days following each date. (There were 48 such occasions). This figure shows that when Spread-F occurrence from region (a) is plotted relative to these dates a peak of 2.8 σ occurs one day after the centre day.

The remaining control dates (41 in all), which presumably are associated with fronts, were used in a similar analysis using the same Spread-F data. Here (see Figure 9c) there is no significant peak near the centre day.

Thus it seems meaningful to separate the AGWs into two groups dependent on whether or not fronts are associated. This ability to isolate the AGWs, which are apparently associated with Spread-F occurrence, should prove valuable in future analyses. The gravity-wave activity at Brisbane, shown earlier as an example (Figure 1), was recorded when an extensive high-pressure weather system covered the entire Australian continent. Fine weather prevailed. A front did not pass through Brisbane until 17 days after these waves were recorded.

4.3. Spread-F and AGWs in May, 1965

Figure 10 shows the daily Spread-F occurrence for the month of May, 1965 for the same L-shell regions as were used earlier in Figure 4. Although, during this month, frontal AGWs (as defined in the previous sub-section) occurred on the 17th, 18th and 25th of the month, non-frontal AGWs were recorded on only 2 dates (namely the 11th and 13th May). Around these latter dates there was, as shown by Figure 10(c), a significant increase in the occurrence of Spread-F for regions a and b combined, while no such increase is apparent in the distributions for the lower latitudes (Figures 10a and 10b). By itself this result would not have great significance. However, taking into account the association which was suggested in section 2 by statistical analyses, it seems reasonable to assume that this particular case is a specific example of the association between Spread-F occurrence and AGWs. Figure 11 shows some of the AGWs recorded at Brisbane on 11 May, 1965.

4.4. Periodicities in AGWs

During some of the nights in 1963, 1964 and 1965 when AGWs were recorded, periodicities have been determined. On any particular night a measurement was made whenever a periodicity changed, except that individual readings were spaced at least one hour apart. Figures 12(a) and 12(b) show the distributions for non-frontal and frontal AGWs respectively. The distributions are somewhat similar to each other and show an average value of about 12 minutes for these waves. The relative response curve for the microbarograph, at the times of the measurements, is also shown on Figure 12.

5. ATMOSPHERIC ACOUSTIC WAVES AND SUNSPOT ACTIVITY

When superposed-epoch analyses followed by fourier analyses were performed in the manner already explained, no apparent 27-day periodicity in geomagnetic activity was found, when A_p indices were plotted relative to AAW control dates. A similar result was found for sunspot numbers during the sunspot-minimum period (see Figure 13a). There was however some evidence of this periodicity for sunspot activity in sunspot maximum years (Figure 13b). In Figure 13 the solid lines relate to the AAW control dates while the dashed lines relate to equivalent numbers of dates chosen randomly. This particular result is suggestive only. If the AAWs are related to sunspot numbers the association would appear to be a lot stronger than the association suggested for the AGWs (see Figure 8). Analyses similar to those described for the AGWs, have been undertaken to look for a possible association between AAWs and Spread-F. No such an association has been found.

6. SUMMARY AND CONCLUSIONS

Daily estimates of Spread-F activity have been determined in local times for each particular station. Consequently when the day-to-day variation for a region containing a number of stations is determined the distribution obtained will be slightly different from what it would be if daily Spread-F activity was determined for each station in Universal Time. However, as the average longitude of the 18 stations used in regions a and b is only 24 degrees east of the Greenwich meridian, this means that any "smoothing-out" of the true day-to-day variation of Spread-F because of the use of local times is not going to result in any significant bias. That is, activity on a particular day (Universal Time) will be spread slightly, but equally, into the day before and the day after. This means that the tendency, in the results presented here, for Spread-F to have high values not only on the centre day of the distributions but on the day after (see e.g. Figure 4a) is in all probability, significant.

From this analysis it seems likely that those gravity waves recorded at Brisbane, which are not related to frontal activity, are in some way associated with ionospheric Spread-F conditions in sub-auroral regions. The fact that there seems to be a link between the occurrence of these gravity waves and sunspot activity, and also geomagnetic activity, suggests that solar particles may be responsible for both the Spread-F and the gravity-wave phenomena. If the gravity waves travel from auroral regions they are possibly instrumental in the production of Spread-F irregularities in these regions. At least one investigation of Spread-F occurrence in auroral regions (Bowman, 1968b) suggests Spread-F structures which are consistent with their being produced by the passage of gravity waves with periodicities similar to those discussed here. One has, however, to explain the fact that in some of the distributions of this analysis Spread-F occurrence is not only high on the centre day but also on the next day. Perhaps for any event the observable Spread-F activity continues for several days whereas the AGWs associated with the onset of the event may be the only ones with sufficiently high amplitudes to be detectable at Brisbane. Auroral infrasonic waves (AIWs) have been detected for some time now (Wilson, 1971). Perhaps AGWs, and even AAWs, are produced in the high atmosphere of auroral regions by mechanisms similar to those responsible for AIWs, whatever these might be. These observations are however only speculations. It is obvious that the precise nature of any association between Spread-F and gravity waves will not be known until we have more experimental results and more analyses are performed.

Finally, this paper presents evidence for an association between acoustic waves, recorded at Brisbane, and sunspot activity for the sunspot-maximum years. This result, however, may be fortuitous, and should be treated with caution.

7. ACKNOWLEDGEMENTS

The author is grateful of assistance from Dr. K.L. Shrestha, who was closely associated with the project for the first four years. He is also grateful to Mr. G. Cooper for computer programming and Mr. S. Seers for data preparation. In its initial stages the project was supported by the Radio Research Board of CSIRO in Australia. Almost all of the Spread-F data were supplied by the World Data Centre A, Boulder, U.S.A.

8. REFERENCES

- Bowman, G.G., 1960a, "Further Studies of Spread-F at Brisbane - II, Interpretation", *Planet.Space Sci.* 2, 150.
- Bowman, G.G., 1960b, "Further Studies of Spread-F at Brisbane - I, Experimental", *Planet.Space Sci.* 2, 133.
- Bowman, G.G., and Shrestha, K.L., 1966, "Ionospheric Storms and Small Pressure Fluctuations at Ground Level", *Nature*, 210, 1032.
- Bowman, G.G., 1968a, "Movements of Ionospheric Irregularities and Gravity Waves", *J.Atmos.Terr.Phys.* 30, 721.
- Bowman, G.G., 1968b, "The Nature of Spread-F Irregularities in Antarctica", *Aust.J.Phys.* 21, 695.
- Bowman, G.G., and Khan, M.S.H., 1970, "Wave-like Structures in the Ionosphere and Related Ground-Level Pressure Oscillations", paper presented to International Conference at Toronto, "Waves in the Upper Atmosphere".
- Chree, C., and Stagg, J.M., 1928, "Recurrence Phenomena in Terrestrial Magnetism", *Phil.Trans.Roy.Soc., A*, 227, 21.
- Jones, R.V., and Forbes, S.T., 1962, "A Microbarograph", *J.Sci.Instrum.* 39, 420.
- Khan, M.S.H., 1970, "Sporadic E Structures and Pressure Oscillations at Ground Level", *Aust.J.Phys.* 23, 719.
- McNicol, R.W.E., Webster, H.C., and Bowman, G.G., 1956, "A Study of Spread-F Ionospheric Echoes at Night at Brisbane - I, Range Spreading (Experimental)", *Aust.J.Phys.* 9, 247.
- Shrestha, K.L., 1971a, "Sporadic-E and Atmospheric Pressure Waves", *J.Atmos.Terr.Phys.* 33, 205.
- Shrestha, K.L., 1971b, "Anomalous Ionospheric Absorption and Microbarometric Activity at Ground Level", *J.Atmos.Terr.Phys.* 33, 213.
- Wilson, C.R., 1971, "Auroral Infrasonic Substorms", pp.374-383, *The Radiating Atmosphere*, B.M. McCormac (ed.), D. Reidel Publishing Company, Dordrecht-Holland.

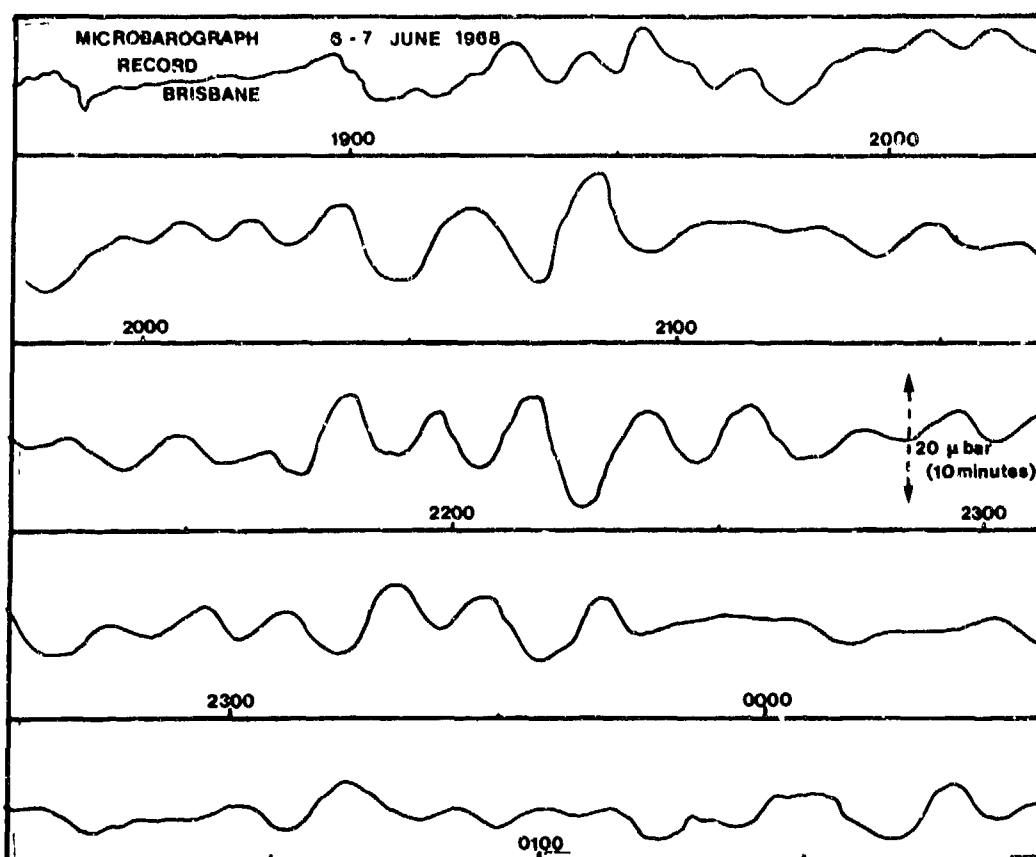


Figure 1. AGWs recorded on 6 June 1968. Local times are used.

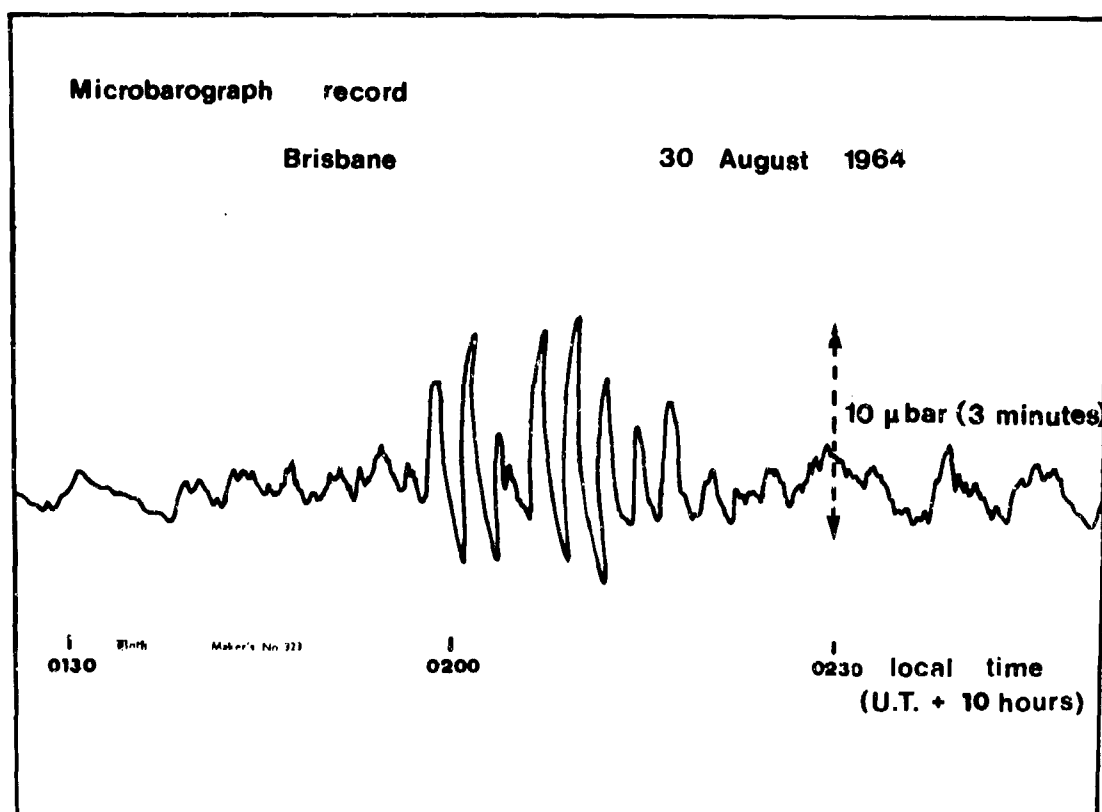


Figure 2. An example of AAWs recorded on 30 August, 1964. Local times are used.

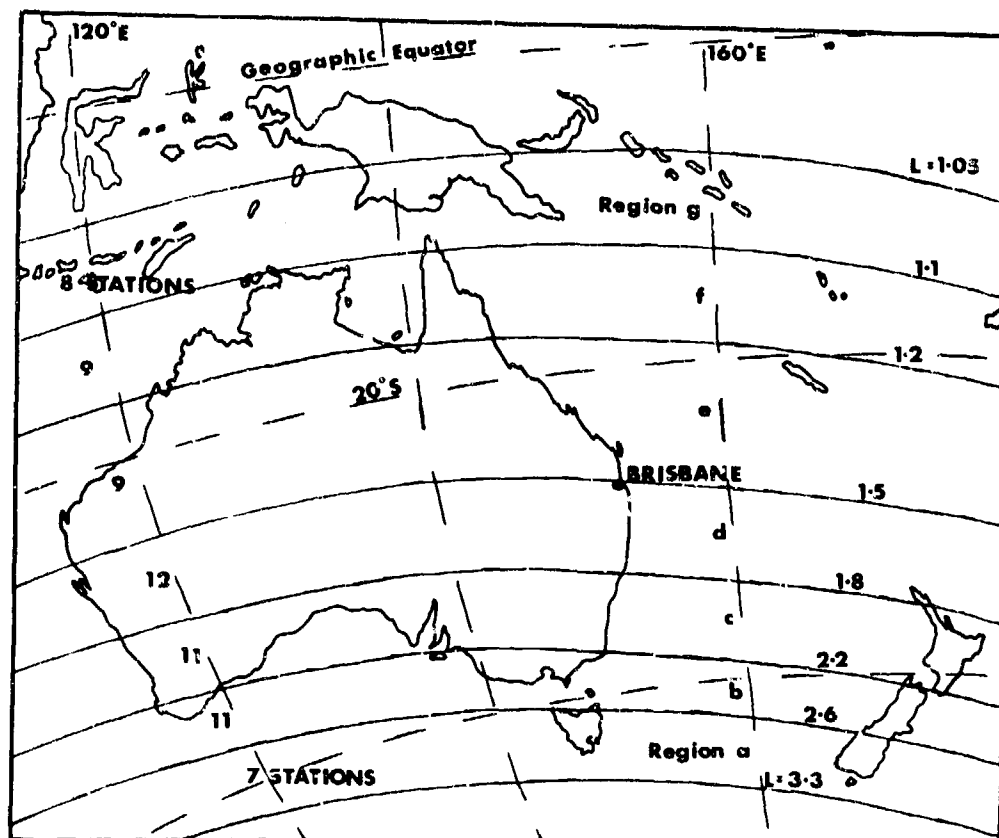


Figure 3. Map illustrating L-shell regions in the vicinity of Australia; and indicating number of stations in each region.

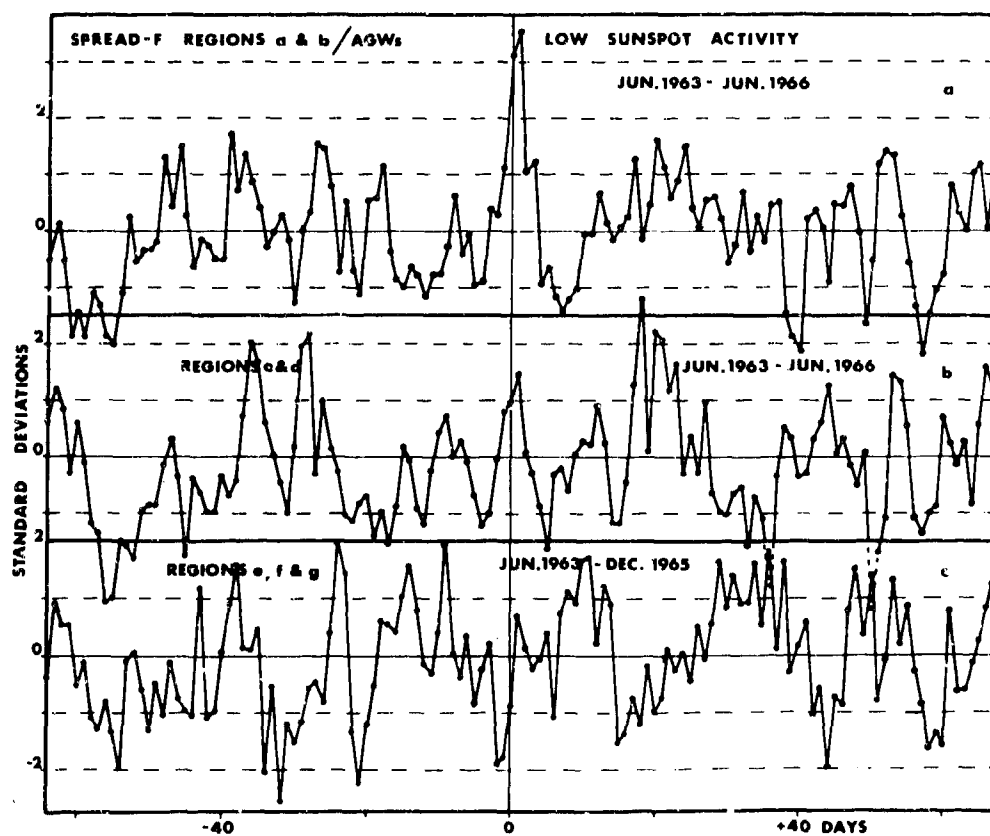


Figure 4. Spread-F activity relative to AGW control dates during a sunspot-minimum period. (a) for regions a and b; (b) for regions c and d; (c) for regions e, f and g.

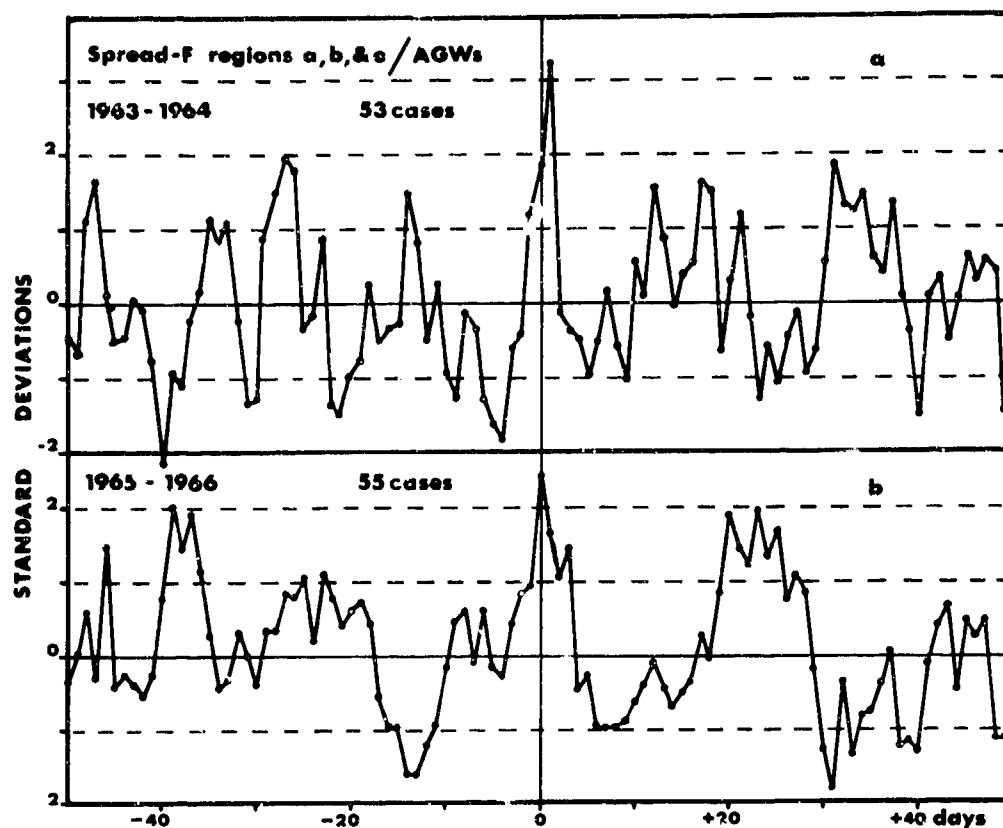


Figure 5. Spread-F activity relative to AGW control dates for regions a, b and c. (a) from June 1963 to December 1964; (b) from January 1965 to June 1966.

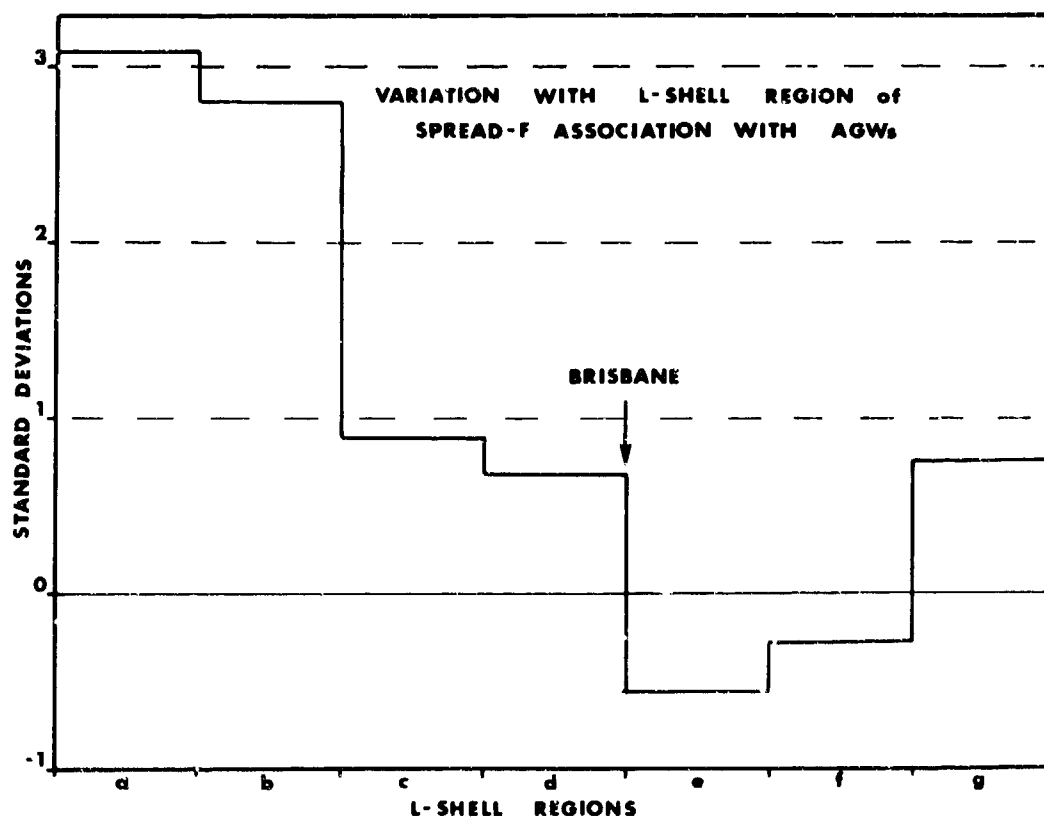


Figure 6. Maximum displacements (centre day or day later) for distributions of Spread-F activity relative to AGW control dates for 7 regions, during sunspot-minimum period.

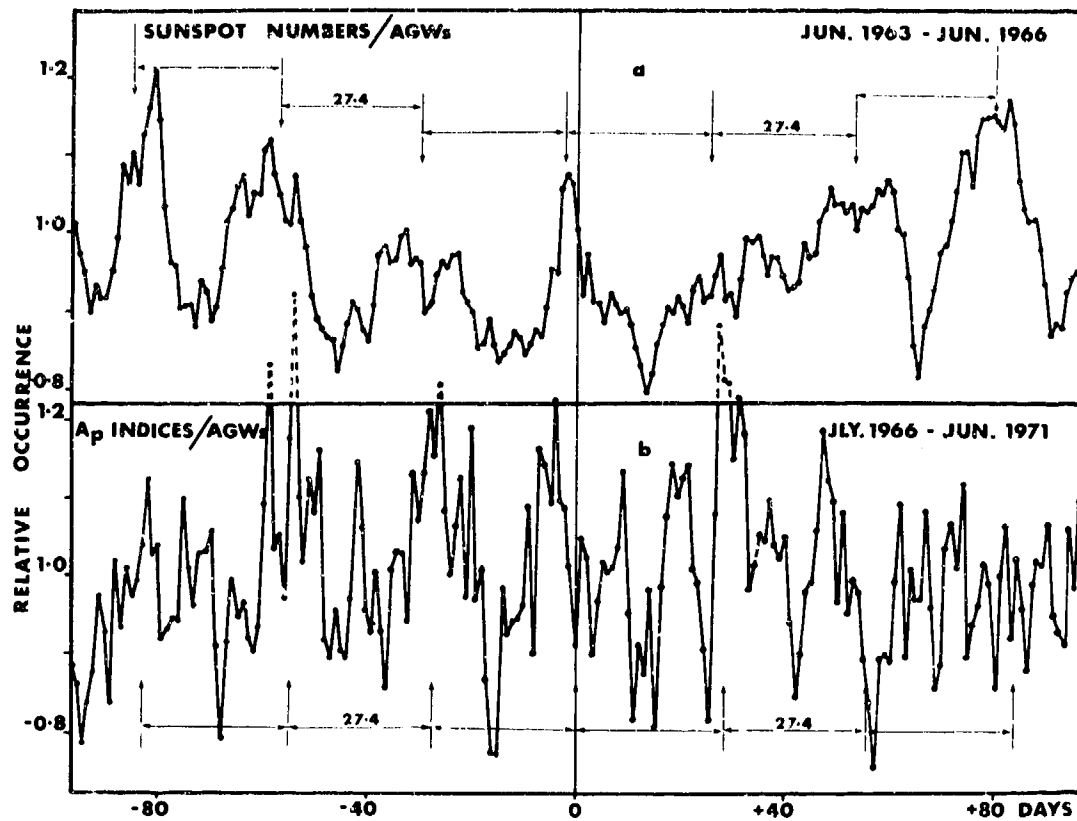


Figure 7. (a) Sunspot numbers relative to AGW control dates for a sunspot-minimum period; (b) A_p indices relative to AGW control dates for a sunspot-maximum period.

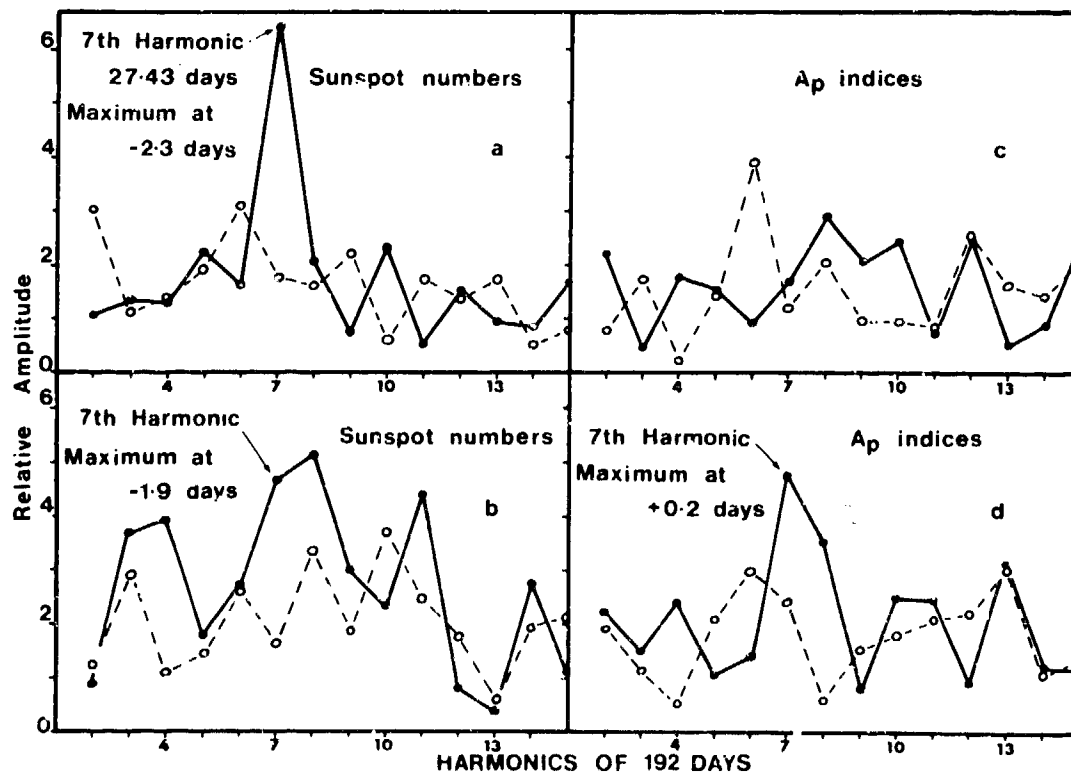


Figure 8. Fourier analyses of distributions (a) sunspot numbers (sunspot minimum); (b) sunspot numbers (sunspot maximum), (c) A_p indices (sunspot minimum); (d) A_p indices (sunspot maximum). Solid lines - relative to AGW control dates; dashed lines - relative to random dates.

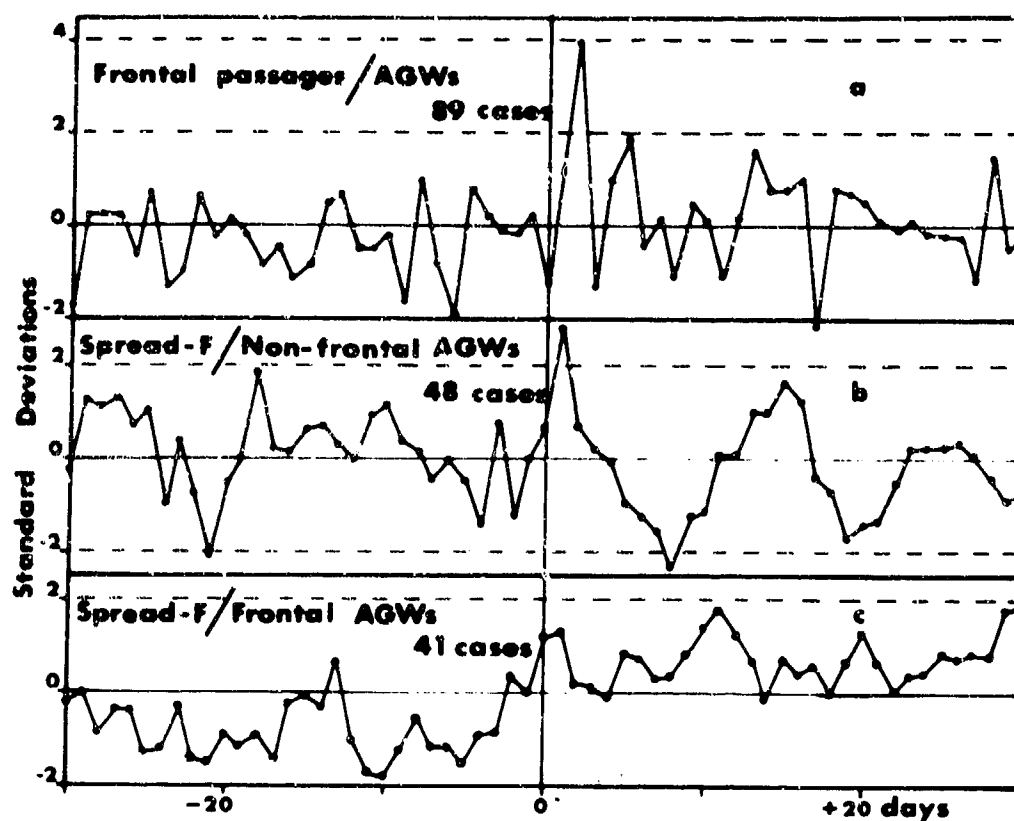


Figure 9. (a) Frontal passages relative to AGW control dates; (b) Spread-F in region a relative to non-frontal AGW control dates; (c) Spread-F in region a relative to frontal AGW control dates.

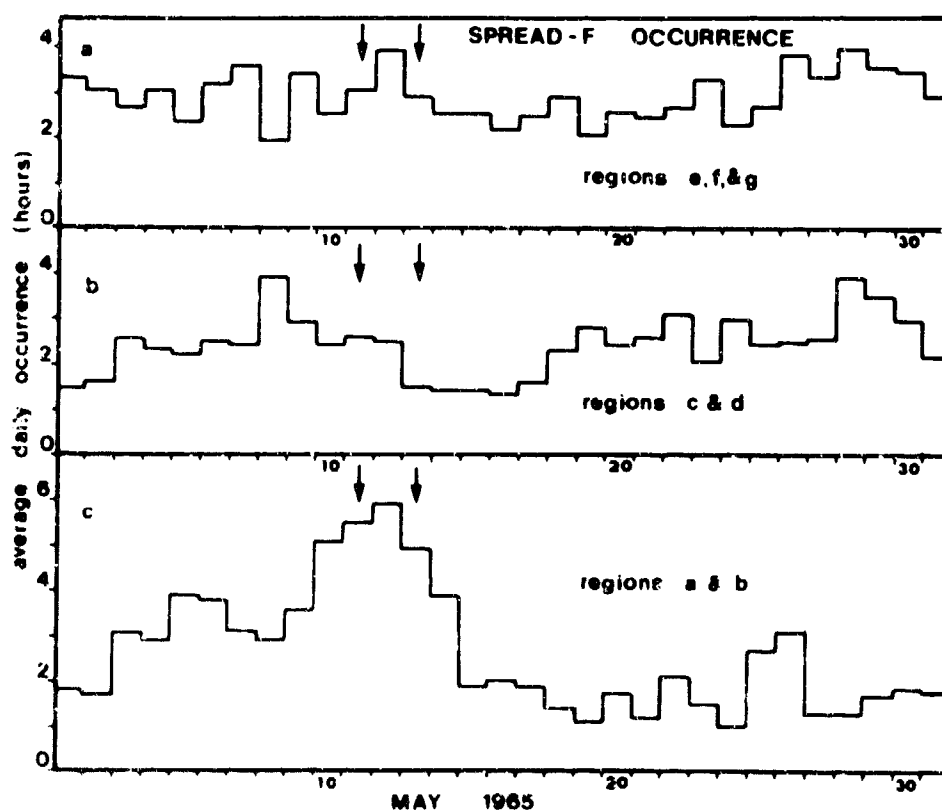


Figure 10. Average daily occurrence in May, 1965 of Spread-F for (a) regions e, f and g; (b) regions c and d; (c) regions a and b.

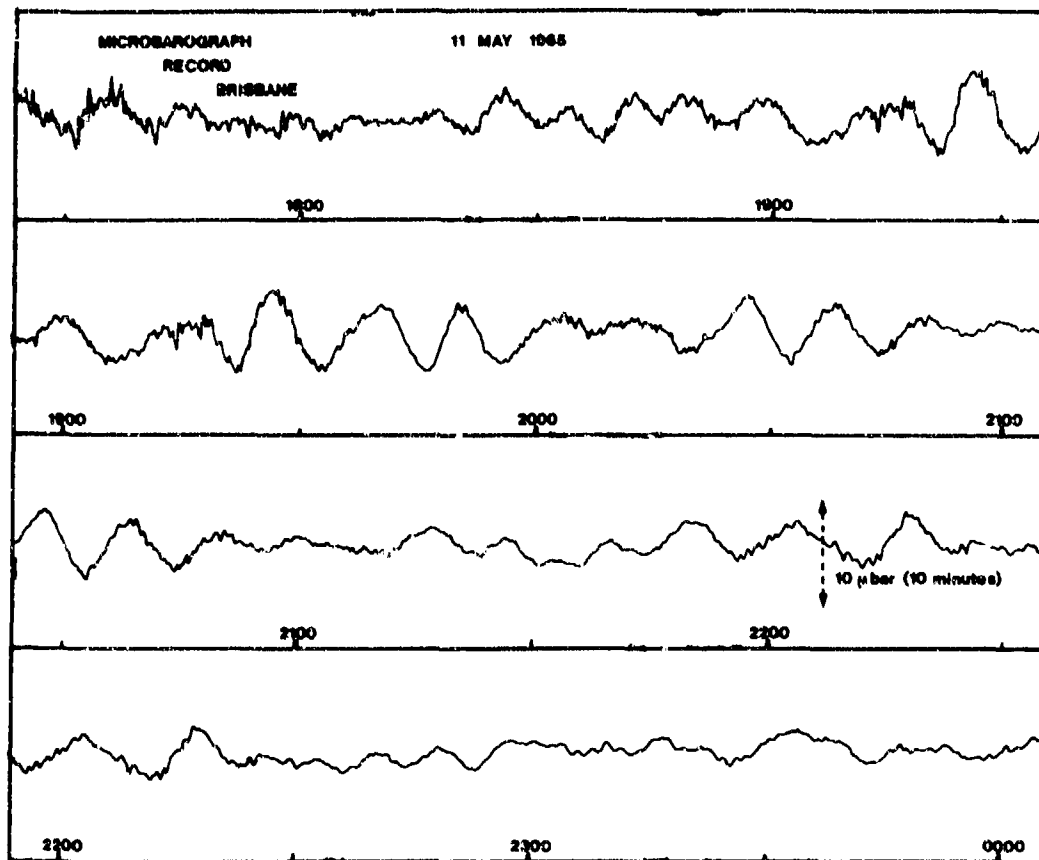


Figure 11. AGWs recorded on 11 May 1955. Local times are used.

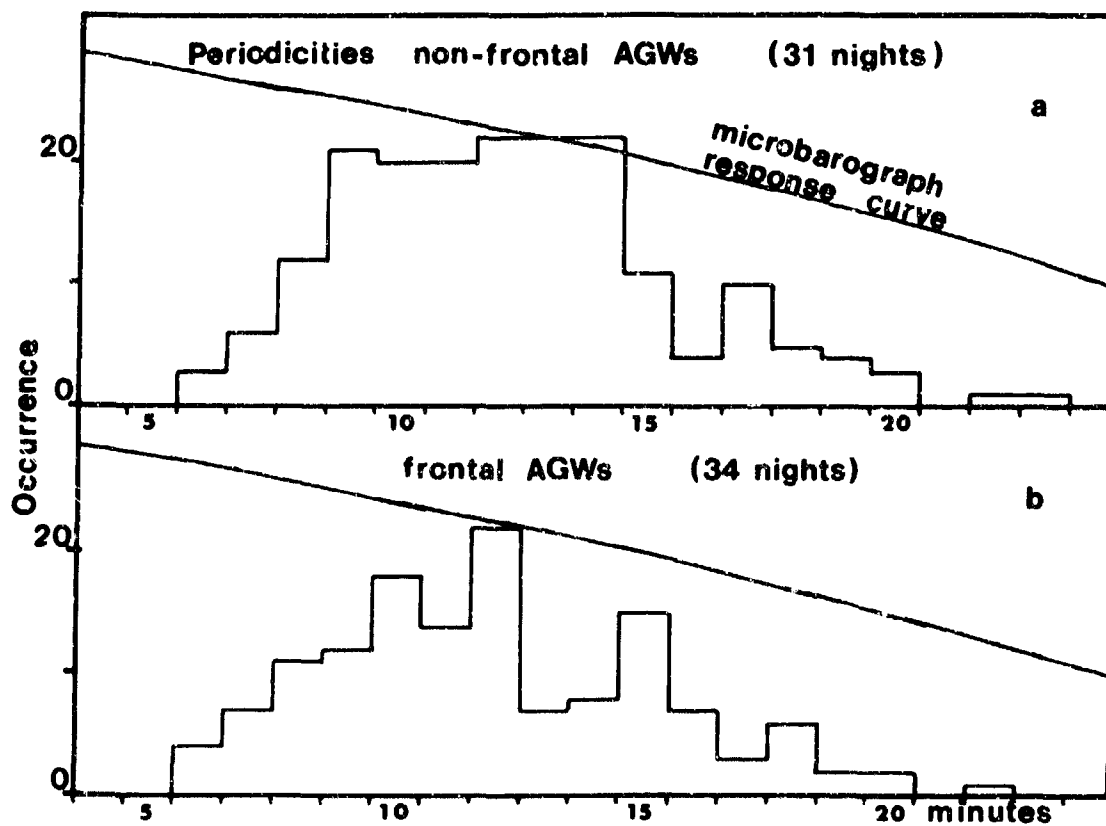


Figure 12. Distributions of occurrence of periodicities (a) for non-frontal AGWs; (b) for frontal AGWs.

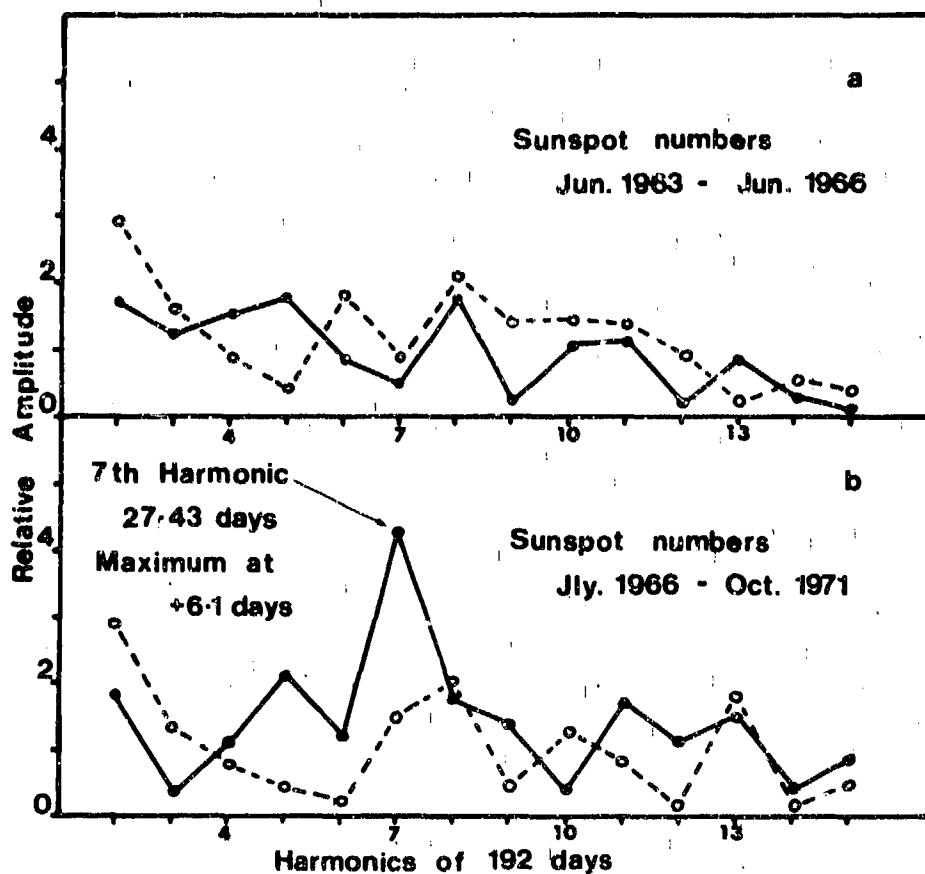


Figure 13. Fourier analyses of distributions (a) sunspot numbers (sunspot minimum); (b) sunspot numbers (sunspot maximum). Solid lines - relative to AAW control dates; dashed lines - relative to random dates.

**FURTHER REMARKS ABOUT TRAVELING IONOSPHERIC DISTURBANCES
ATTRIBUTED TO JET STREAM ACTIVITY AT MID-LATITUDE**

by

G.B.Goe

Space Environment Laboratory
NOAA Environmental Research Laboratories
Boulder, Colorado 80302
USA

206

REMARQUES COMPLEMENTAIRES SUR LES PERTURBATIONS IONOSPHERIQUES ITINERANTES
ATTRIBUES A L'ACTIVITE DU COURANT-JET AUX LATITUDES MOYENNES

par

G. B. Goe

SOMMAIRE

Des perturbations ionosphériques itinérantes d'échelle moyenne, présentant des périodes de 12 à 30 minutes sont détectées l'hiver, dans la journée, aux altitudes de la région F. Ces perturbations, dont la présence est constatée dans des conditions de calme magnétique, sont attribuées à la présence de configurations de vent "actives", liées au courant-jet à l'altitude de la tropopause. On reconnaît ces configurations actives sur les cartes de vent de la tropopause, à un cisaillement horizontal du vent lorsque la direction de l'écoulement est parallèle aux isolignes de vitesse de vent constante. L'activité diminue au fur et à mesure que le vent accélère ou décélère dans la direction de l'écoulement. On peut considérer que l'activité ionosphérique résultant de ces vents de tropopause actifs est localisée, du point de vue de la circulation globale ; par conséquent, elle n'est jamais observée ni prédite sur une base globale, ce qui est regrettable car les transmissions radio à haute fréquence sont affectées par la présence de ces perturbations ionosphériques.

FURTHER REMARKS ABOUT TRAVELING IONOSPHERIC DISTURBANCES
ATTRIBUTED TO JET STREAM ACTIVITY AT MID-LATITUDE

G. E. Goe
 Space Environment Laboratory
 NOAA Environmental Research Laboratories
 Boulder, Colorado 80302

ABSTRACT

Medium scale traveling ionospheric disturbances with periods of 12 to 30 minutes are detected during daytime winter at F-region heights. These disturbances are present when it is magnetically quiet and are attributed to the presence of 'active' wind patterns associated with the jet stream at the height of the tropopause. The active patterns on the tropopause wind analysis maps are recognized by horizontal wind shear as the direction of flow lies parallel to the isolines of constant wind speed. The activity diminishes as the wind accelerates or decelerates in the direction of flow. The ionospheric activity resulting from these active tropopause winds may be thought of as localized, in terms of global circulation and, hence, is neither observed nor predicted on a global scale. This is unfortunate as HF radio transmission is effected by the presence of such ionospheric disturbances.

1. INTRODUCTION

The medium scale traveling ionospheric disturbances known to be present at mid-latitude during daytime winter under magnetically quiet conditions are often thought to originate in the lower atmosphere. We have previously shown disturbances of 12 to 20 minute period with horizontal phase speeds of approximately 130 meters/second, for winter 1968 (sunspot maximum) at ionospheric heights near 200 km over Boulder (40° N, 105° W) to be generated by 'active' wind patterns associated with the jet stream at the height of the tropopause. In this paper we present ionospheric HF pulse data and the corresponding tropopause wind analysis maps as evidence that our criteria for the active wind patterns is equally valid for another mid-latitude location (39° N, 115° W), west and slightly south of Boulder, using a different radio technique from the earlier study.

2. BACKGROUND

The underlying theme of this paper is an investigation of medium scale traveling ionospheric disturbances thought to be generated locally at the height of the tropopause at mid-latitude during magnetically quiet conditions. The specific disturbances that concern us are observed to have periods of 12 to 30 minutes at mid-latitude ionospheric F-region heights. Since these disturbances are detected using HF radio techniques we have consistently restricted our observations to daytime when reflection conditions are optimum. Only the winter months, October through March, are considered because during those months the overhead tropopause wind patterns at mid-latitude are well-formed and persistent. In addition, during the winter months the propagation conditions from the tropopause to the ionosphere appear to be in our favor (Goe, 1971).

These medium scale mid-latitude disturbances should be contrasted with the large scale traveling disturbances also observed at ionospheric heights at mid-latitude. The large scale disturbances are thought to originate in the auroral oval during times of increased magnetic activity. A recent review of this topic is available (Evans, 1972).

Our active wind regions, as seen on the U.S. Weather Service Tropopause Wind Analysis Maps, constitute the microstructure of the ridges and troughs of planetary scale waves. A planetary wave may have a wavelength of approximately 4,500 km which is equivalent to, say, 50° in longitude (at 40° N latitude) or the width of the continental United States. This means then that our activity may be confined to, say, 20° in longitude. Because of its microscale and localized character, such "meteorological noise" is neither observed nor predicted on a global scale. This is unfortunate, in so far as HF radio propagation is concerned, because the unwanted effects on the signals, in particular the signal strength, may occur without advance warning.

In this paper we direct our attention to the source of the medium scale traveling ionospheric disturbances as detected by HF sub-microsecond pulses, while Lerbald, et. al. (1972), in a companion paper to be presented at this conference, discuss the influences of the disturbances on the pulses themselves.

As we discuss the tropopause winds we retain our simple classification for the flow patterns: active, quiet, or quasi-periodic (rapidly changing), as originally introduced (Goe, 1971). The limitations of the 'rapidly changing' classification (Goe, 1972a) soon become evident. This limitation, combined with the scarcity of tropopause maps (they are issued only every 12 hours), decreases our confidence in the interpretation of some of our wind patterns.

We remain convinced, however, that our criteria for the stability of the wind patterns and for the generation of the disturbances is as reliable for our new location, west of the Rocky Mountains, as it is for Boulder, east of the mountains. The basic difference between the two locations is that the well-developed troughs and ridges as they move in from the Pacific Northwest tend to remain north of the new location but pass directly overhead for Boulder.

3. IONOSPHERIC OBSERVATIONS

Sub-microsecond HF pulses, transmitted over an oblique (1500 km) path from Palo Alto, California to Boulder, Colorado, show ionospheric behavior appropriate for an ionospheric reflection level of approximately 200 km near the mid-point of the path (39° N, 115° W). The data are daytime data collected during the winter months, November 1969, January 1970, and February 1970.

Ionospheric motions are detected as fluctuations in the travel time for the pulses but are attributed particularly to changes in the electron density profile near the height of reflection. Such a detection of traveling ionospheric disturbances presupposes that the motions of the neutral air due to the passage of atmospheric waves are carried over to the ionized portion of the atmosphere without serious modification. That is to say, fluctuations in the electron density indicate the passage of a wavelike disturbance in the neutral atmosphere. We accept this interpretation; Davies and Jones (1971) discuss it in detail.

3.1. HF Pulse Data.

The ionospheric pulse data are shown in Figures 1, 2 and 3. The time scale, running along the bottom of the records, is marked off in half-hour intervals. These data show the periods of the rather irregular wavelike disturbances to be in the neighborhood of 15 to 30 minutes. An occasional longer period disturbance, such as the one seen on February 18, appears on the records, however. The 6-hour time interval, 1800 to 0000 hours UT, corresponds to local daytime, 1100 to 1700 hours IST.

The tick marks on the vertical time scale are spaced at 30 microsecond intervals to indicate (relative) pulse delay time. The bottom edge of the signature is the beginning of the pulse, while the length of the vertical line extending upward from this initial point represents the pulse length or, what is oft times equivalent, the pulse distortion. The transmitted signal (pulses ≈ 0.5 μ sec duration) had a frequency spectrum which peaked at 18 MHz; appreciably below the F-layer penetration frequency for this path during winter daytime.

3.2. Numerical Activity Index.

The ionospheric activity is rated on a scale from 1 to 8 according to our L/Lo numerical index (Goe, 1971). This index is assigned according to the ratio of line lengths L/Lo, where L is the measured length of the trace formed from the composite of the pulse data and Lo is the length of the base (time) line. These line lengths are shown schematically in Figure 1. We have in each case assigned the ionospheric index most appropriate for each 3-hour interval, 1800 to 2100, 2100 to 2400 hours UT. These L/Lo indices are shown as integers in the figures.

There is some ambiguity present in these numerical indices for the ionospheric activity. Nevertheless, it is clear that the activity for the November data (Figure 1) is moderately low ($L/Lo = 3$) and consistently present. Generally, an index of 2 or 3 provides assurance of low level ionospheric activity. The ambiguity becomes more apparent when $L/Lo = 4$ because then several small amplitude oscillations may contribute the same line length throughout a 3-hour interval as a few large amplitude oscillations. The index for the January data (Figure 2) is most effected by the ambiguity as $L/Lo = 4$ is observed.

As the activity increases to 5 or 6 relatively large amplitude fluctuations must persist throughout the interval and the ambiguity again tends to disappear. The data for February 18 (Figure 3) show this increased level of activity. The L/Lo index has been defined to range from 1 to 8, but the 8 is reserved for a severe magnetic storm condition (Goe, 1972b).

3.3. Remark.

With this pulse data we have been forced to abandon the spirit of our graphic period-amplitude representation used for the CW-Dopplersonde data (Goe, 1971; 1972a; 1972b). Even though such a display of ionospheric data provides a means to easily intercompare the activity for consecutive days, the pulse data are so frequently interrupted that visual scanning for trends has little purpose. Hence, only L/Lo indices shall be used in Figure 7. We discuss the data summarized in Figure 7 after we examine the flow patterns on the tropopause wind maps.

4. TROPOPAUSE WIND ANALYSIS MAPS

Tropopause Wind Analysis Maps, issued every 12 hours, 0000 and 1200 hours UT, by the United States Weather Service, are used for this study. The redrawn tropopause maps are pictured in Figures 4, 5 and 6. The wind speeds are given in knots (K, nautical miles per hour) with 100 knots equal to approximately 50 meters per second. The black dot on each map indicates the geographic location on the mid-point (39° N, 115° W) of our oblique propagation path.

4.1. Analysis of Vector Wind Field.

The wind patterns on the maps of Figures 4, 5 and 6 are represented by streamlines (solid lines), indicating the direction of flow, and isotachs (dashed lines), the isolines of constant wind speed. We confine our attention to this abstract representation of the vector wind field. Such a kinematic approach allows us to consider the stability of the wind flow without regard for the dynamic forces producing it. Even this has its limitations, however, as we allow ourselves to think only in terms of a static vector field, i.e., we assume that the streamlines represent the path of the moving air parcels. But, be that as it may, in so far as it is possible, we discuss the flow in terms of wind speed with respect to direction of flow and its consequence, the onset or disappearance of horizontal wind shear. The question of the origin of the wind field we leave to the dynamic meteorologists.

The integer index shown in the lower right hand corner of each map indicates horizontal wind shear in 0.01 meters per second per kilometer as appropriate for the mid-point of the propagation path. These numbers fail to exceed 6 (0.06 m/s/km) for the days of interest. It is common for horizontal wind shear

In passing, we take this opportunity to assure you that we have great confidence in the ionospheric absorption measurements made by Schentek at Lindau, West Germany, while the f-min data used by Deland and Friedman (1972) as an indication of ionospheric absorption are less reliable. Schentek (Labitzke and Schentek, 1968; Schentek, 1969) makes it clear that any association between ionospheric absorption and stratospheric temperature is not a straightforward one.

5.1. The problem.

Even though we likewise concern ourselves with both the upper and lower atmosphere - our disturbances originate in the tropopause and propagate into the ionosphere - we do not require a direct coupling between the two.

It was recognized earlier (Gossard, 1962; Gossard and Munk, 1974) that internal gravity waves with periods comparable to those we observe, could be generated in the troposphere and propagate into the ionosphere. Gossard outlines the general problem very well: (1) the generation of the disturbance in the lower atmosphere, (2) the propagation characteristics along the path and (3) the means of detecting the disturbances at ionospheric heights. We concentrate on the first to study the source of the disturbances; we learn nothing of the second directly but must infer everything from the characteristics of the reflected traces, and we tolerate the third as we observe the ionized rather than the neutral portion of the atmosphere.

We note, however, that Cowling, et. al. (1971), Yeh, et. al. (1972) and others contribute to (2) by discussing propagation characteristics appropriate for mid-latitude. They elaborate on their wind control theory - strong thermospheric winds acting as a directional filter for the internal gravity waves - and other atmospheric processes. Their tracing of rays from the ionosphere back to the troposphere indeed lends support to our study as they find 3 to 5 hours travel time to be realistic for our near 30 minute period waves (Yeh, 1972).

5.2. The Wave Generating Mechanism.

The tropopause Wind Analysis Maps are our primary source of observational data for the wind patterns, while Yeh (1972) and Liu and Yeh (1971) continue to provide as much guidance as possible in an effort to bring theory and practice together. At present, the best we can do is to clarify terminology in order to communicate the information we gain from the tropopause maps more effectively.

We use the kinematic approach, with streamlines and isotachs to describe the vector (wind) field. The word 'macrostructure' refers to the patterns formed by the streamlines, the ridges and troughs of the planetary-scale waves. Such a wave is shown schematically in Figure 8. A wavelength comparable to the width of the continental U.S. is usual at 40° N latitude in winter. Our stability criteria is most nearly applicable when this macrostructure is only slowly altered as the patterns meander or migrate from west to east across the United States.

The word 'microstructure' refers to the patterns formed by the isotachs about the streamlines. This microstructure is always changing with respect to the macrostructure, but the rate at which it changes is the primary interest of the wave generating mechanism. We use the term, 'quasi-periodic' to mean short term (3 to 6 hour) changes in the microstructure.

The criterium for quiet patterns is definite, the isotachs are perpendicular to the streamlines. The air parcels accelerate or decelerate in the direction of flow and there is no wind shear. The general category of an active pattern requires the presence of wind shear, the isotachs parallel to the streamlines.

As the atmosphere makes a rapid adjustment the macrostructure may change severely within 12 hours. During such times we have little confidence that the trajectory of an air parcel is represented by the streamline. Our assumption of a static vector field breaks down; we can no longer think the wind shear mechanism to have meaning.

5.3. Summary of data.

The results of the ionospheric and tropopause data are summarized in Figure 7. The days are plotted on a 24-hour time scale, with local daytime (09 - 17 hours IST) coinciding with the breaks in the heavy black lines at 16 - 24 hours UT. The ionospheric data are daytime data while the wind data are shown on a 24-hour basis.

The magnetic Kp index is shown in the first line. As was mentioned earlier, the November days follow a time of slight activity (Kp = 6⁻). Other than that, the days are magnetically quiet as would be expected since we are near winter solstice rather than equinox.

The purpose in the study was to test the validity of our criteria for the stability of the tropopause winds. We find no violation and, even though the data are meager, we feel that we have learned more about the changing (quasi-periodic) patterns. The more nearly sinusoidal wavelike disturbances appear to be associated with these changing patterns.

5.4. Overhead Winds at Mid-point.

Our last result is easily visualized by referring again to Figure 8. We note the position of the trough over the western United States. The solid line represents a deep trough, while the dashed line indicates a more usual depth. Hence, the dashed line is the usual path of the well-formed wind patterns.

By using the dashed line as the outside boundary for the wind pattern, you can see that it passes near Boulder (40° N, 105° W) but goes slightly north and east of the mid-point of the oblique path (39° N, 115° W).

C. CONCLUSION

We detect medium scale ionospheric disturbances, periods of 15 to 30 minutes. As we observe this ionospheric activity from a mid-latitude ground station located 40° N, 105° W, we see the activity come and go as the overhead tropopause wind patterns pass by. The trends in the ionospheric activity for this location are already known to be something like 3 to 5 days in duration.

When we observe the ionosphere from our new location 39° N, 115° W, the activity trends are quite different. We find, however, that the criteria of isotachs parallel to streamlines, combined with the quasi-periodic behavior, describes the active tropopause wind patterns for both mid-latitude locations.

Therefore, we conclude that the ionospheric activity is localized, in terms of global circulation, and that the observed activity depends on the characteristics of the overhead tropopause winds. Stated differently, this type of ionospheric activity is a strong function of the geographic location.

ACKNOWLEDGMENT

Helpful discussions with colleagues at the Max-Planck-Institut für Aeronomie, Lindau/Harz, in particular, H. Schwentek, Eiling and H. G. Möller, are acknowledged with pleasure. Also, I express my gratitude to G. Lerfald and W. Burkey at the NOAA Laboratories, Boulder, Colorado, for, respectively, supplying the HF pulse data and coordinating preparation of the figures. Finally, I thank Dr. William W. Kellogg, National Center for Atmospheric Research, Boulder, Colorado, for reading the manuscript and suggesting beneficial modifications.

REFERENCES

- BROWN, G. M., and D. C. Williams, 1971, Pressure variations in the stratosphere and ionosphere, *J. Atmos. Terr. Phys.*, **33**, 1321.
- COWLING, D. C., H. D. Webb and K. C. Yeh, 1971, Group rays of internal gravity waves in a wind-stratified atmosphere, *J. Geophys. Res.*, **76**, 213.
- DAVIES, Kenneth, and J. E. Jones, 1971, Three dimensional observations of traveling ionospheric disturbances, *J. Atmos. Terr. Phys.*, **33**, 39.
- DELAND, R. J., and R. M. Friedman, 1972, Correlation of ionospheric absorption and atmospheric planetary scale waves, *J. Atmos. Terr. Phys.*, **34**, (2), 295.
- EVANS, J. V., 1972, Ionospheric movements measured by incoherent scatter: A review, *J. Atmos. Terr. Phys.*, **34**, (2), 175.
- FLOHN, Herman, 1969, *Climate and Weather*, World Univ. Library McGraw Hill Book Co. (translated from German).
- GEORGES, T. M., 1968, HF Doppler studies of traveling ionospheric disturbances, *J. Atmos. Terr. Phys.*, **30**, 735.
- GOE, G. B., 1971, Jet stream activity detected as wave-like disturbances at mid-latitude ionospheric F-region heights, *J. Pure Appl. Geophys. (PAGEOPH)* in press.
- GOE, G. B., 1972a, Rapidly changing tropopause winds generate disturbances detected at ionospheric heights, *Z. Geophys.* (in preparation).
- GOE, G. B., 1972b, Medium scale traveling ionospheric disturbances attributed to mid-latitude changes in global circulation following a severe magnetic storm, *PAGEOPH* (in preparation).
- GOE, G. B., and J. A. Joselyn, 1971, Traveling ionospheric disturbances attributed to jet stream activity, presented at Spring URSI Meeting, Washington, D. C., 1971.
- GOSSARD, E. E., 1962, Vertical flux of energy into the lower ionosphere from internal gravity waves generated in the troposphere, *J. Geophys. Res.*, **67**, 745.
- GOSSARD, E. E., and W. H. Munk, 1954, On gravity waves in the atmosphere, *J. Meteor.*, **11**, 259.
- LABITZKE, K., and H. Schwentek, 1968, Midwinter warmings in the stratosphere and lower mesosphere and the behavior of ionospheric absorption, *Z. Geophys.*, **34**, 555.
- LERFALD, G. M., R. B. Jurgens, and J. A. Joselyn, 1972a, Propagation of submicrosecond HF pulses through traveling ionospheric disturbances, (in the proceedings of this conference).
- LERFALD, G. M., 1972b, A study of the oblique propagation of sub-microsecond HF pulses, (in preparation).
- LIU, C. H., and K. C. Yeh, 1971, Excitation of acoustic-gravity waves in an isothermal atmosphere, *Tellus XXIII* (2), 150.
- MACDONALD, N. J., and W. O. Roberts, 1960, Further evidence of a solar corpuscular influence on large scale circulation at 300 mb., *J. Geophys. Res.*, **65**, 529.
- SCHWENTEK, H., 1969, Similarities in the annual behavior of the stratosphere and the D- and E-layer of the ionosphere, *Space Research IX*, North Holland, Amsterdam, 405.

- SCHWENK, H., 1968, Die Lufthülle der Erde und der Weltraum, Tafel Nr. 142 02, Ernst Klett Verlag, Stuttgart.
- Shrestha, K. L., 1971, Sporadic E and atmospheric pressure waves, J. Atmos. Terr. Phys., 33, 209.
- SHRESTHA, K. L., 1971, Anomalous ionospheric absorption and microbarometric activity at ground level, J. Atmos. Terr. Phys., 33, 213.
- YEH, K. C., H. D. Webb, and D. H. Cowling, 1972, Evidence of directional filtering of traveling ionospheric disturbances, Nature (in press).
- YEH, K. C., 1972, Private correspondence, continuing November 1971 to present.

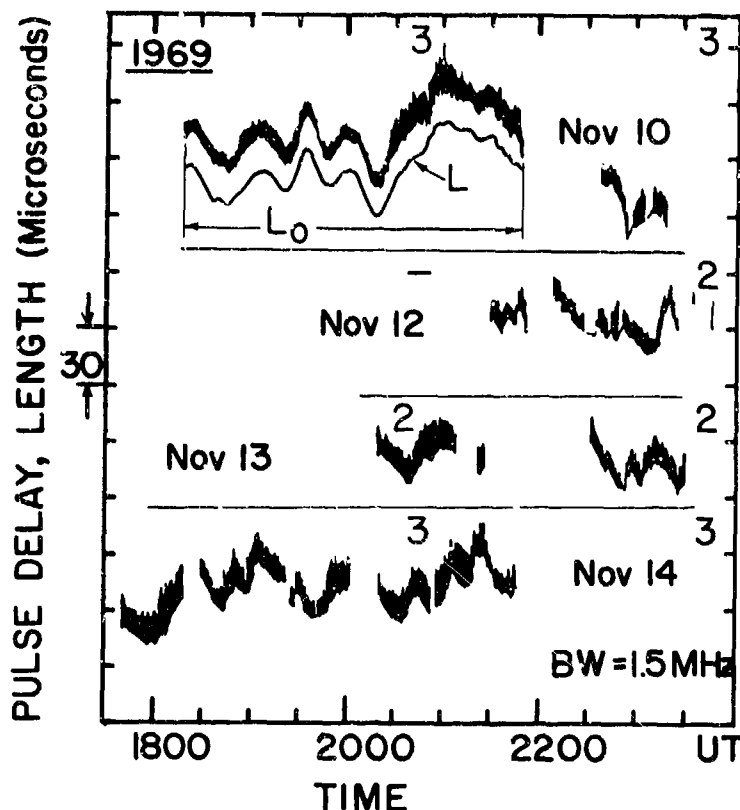


Figure 1. Ionospheric HF sub-microsecond pulse data recorded over an oblique 1500 km path from Palo Alto to Boulder. Local time is 1100 to 1700 hours (1800 to 2400 hours UT). Two integers indicate the ionospheric activity L/Lo index for each 3-hour interval, 1800 to 2100, 2100 to 2400 hours UT, for each day. Although these November data display a moderately low level ($L/Lo = 3$) of ionospheric activity, it is consistently present.

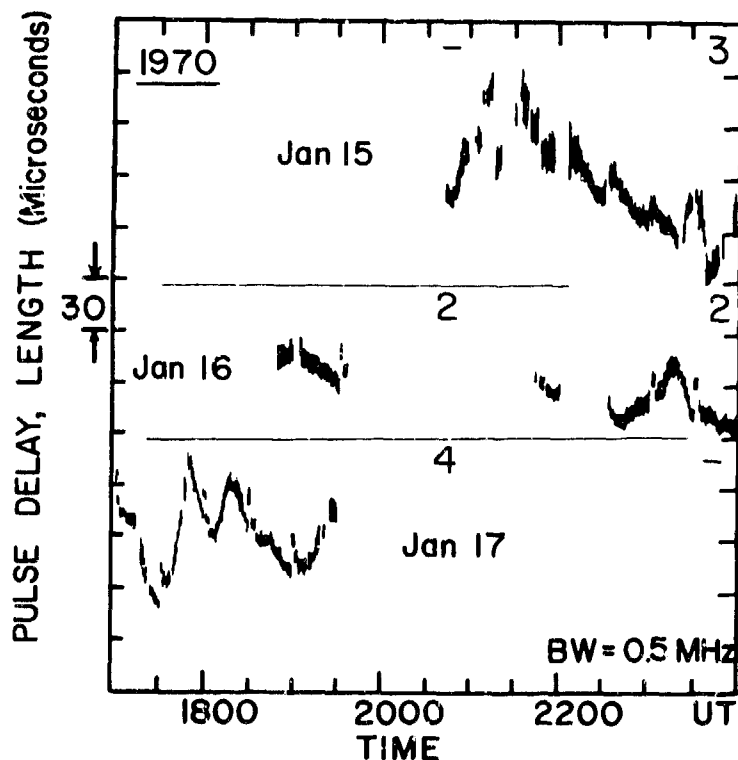


Figure 2. Ionospheric HF sub-microsecond pulse data similar to that shown in Figure 1. These January data are, unfortunately, often interrupted but show the ionospheric activity to be irregular, ranging from low ($L/Lo = 2$) to moderately active ($L/Lo = 4$).

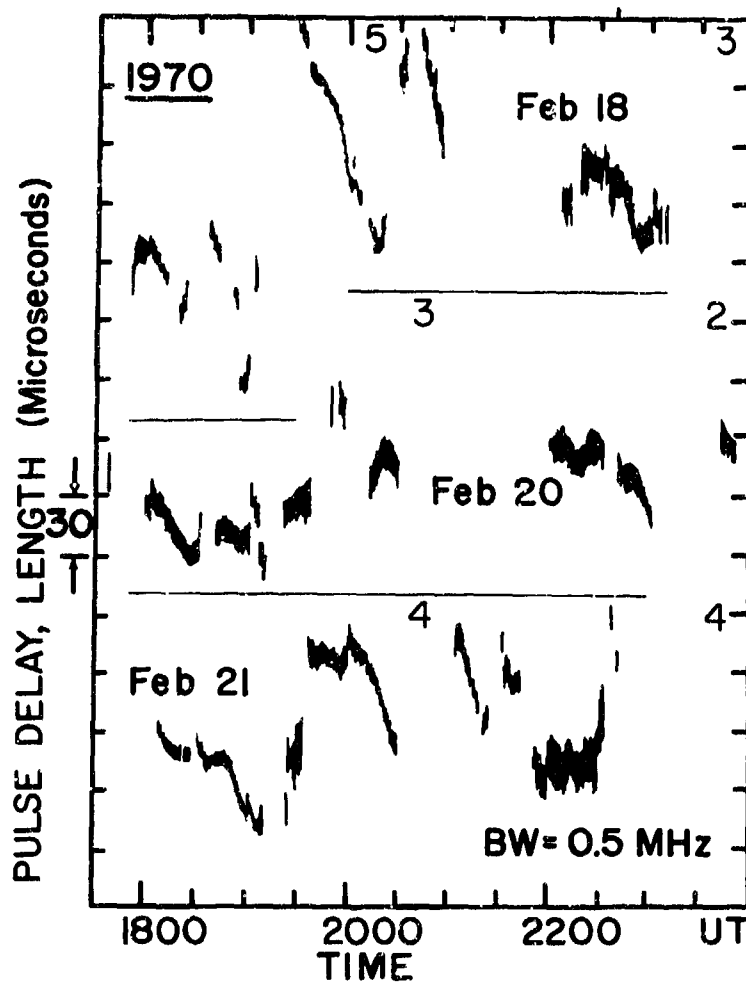


Figure 3. Ionospheric HF sub-microsecond pulse data similar to that shown in Figure 1. A high level of ionospheric activity is reached on February 18 ($L/L_o = 5$) but the disturbance probably comes from a severe vertical exchange of air in the lower atmosphere.

TROPOPAUSE WIND MAPS 1969

— STREAMLINES ---- ISOTACHS

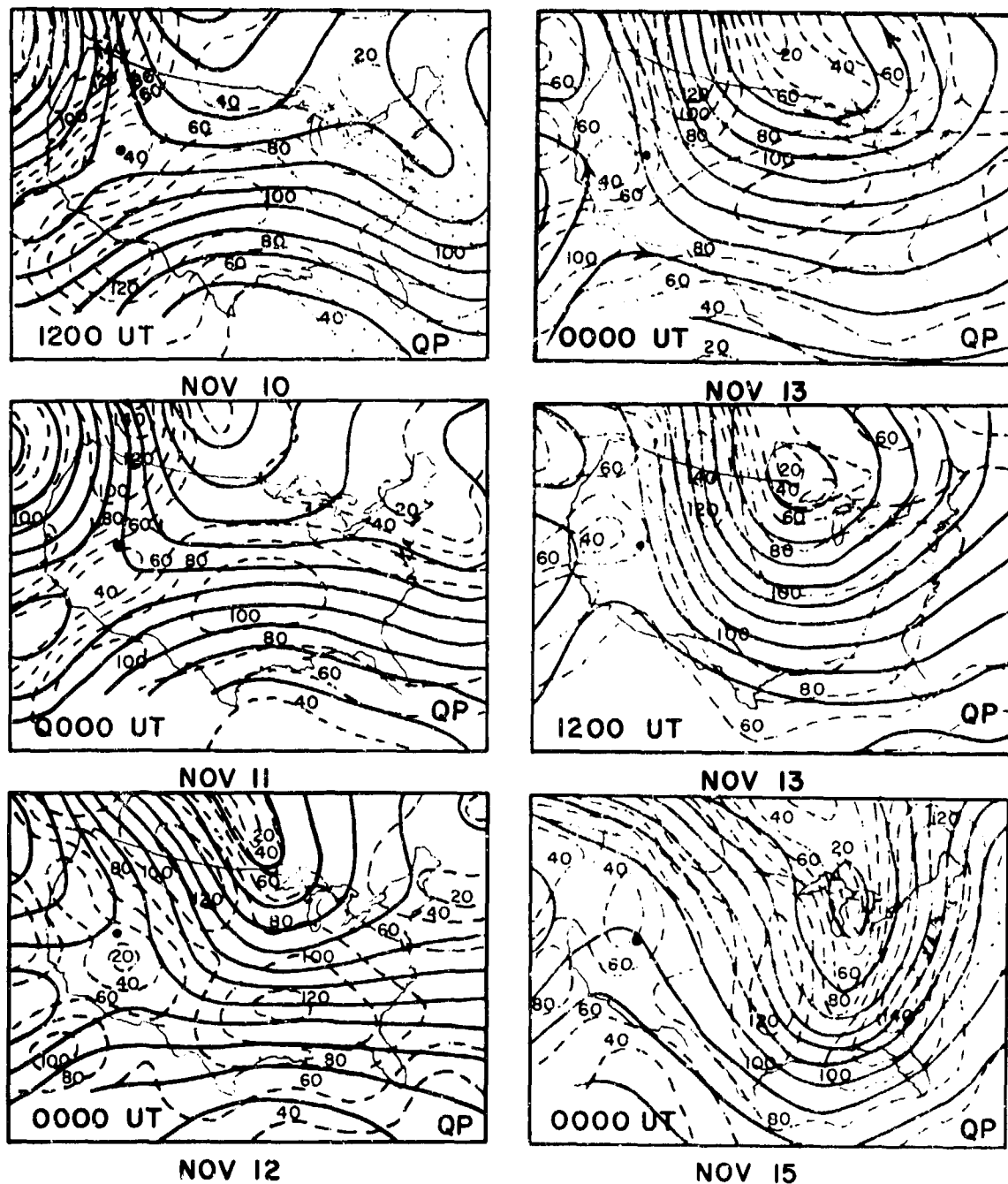


Figure 4. U.S. Weather Service: Tropopause Wind Analysis Maps. The streamlines (solid lines) indicate direction of flow, isotachs (dashed lines) represent isolines of constant wind speed. Wind speed is given in knots (nautical miles per hour), with 100 k = 5 m/s. The black dot on each map locates the mid-point of the propagation path (39° N, 115° W). These wind patterns for November 1969 are of particular interest because they follow a slight magnetic storm. The QP (quasi-periodic) classification for the flow is noted in the lower right hand corner of each map.

TROPOPAUSE WIND MAPS 1970

— STREAMLINES - - - ISOTACHS

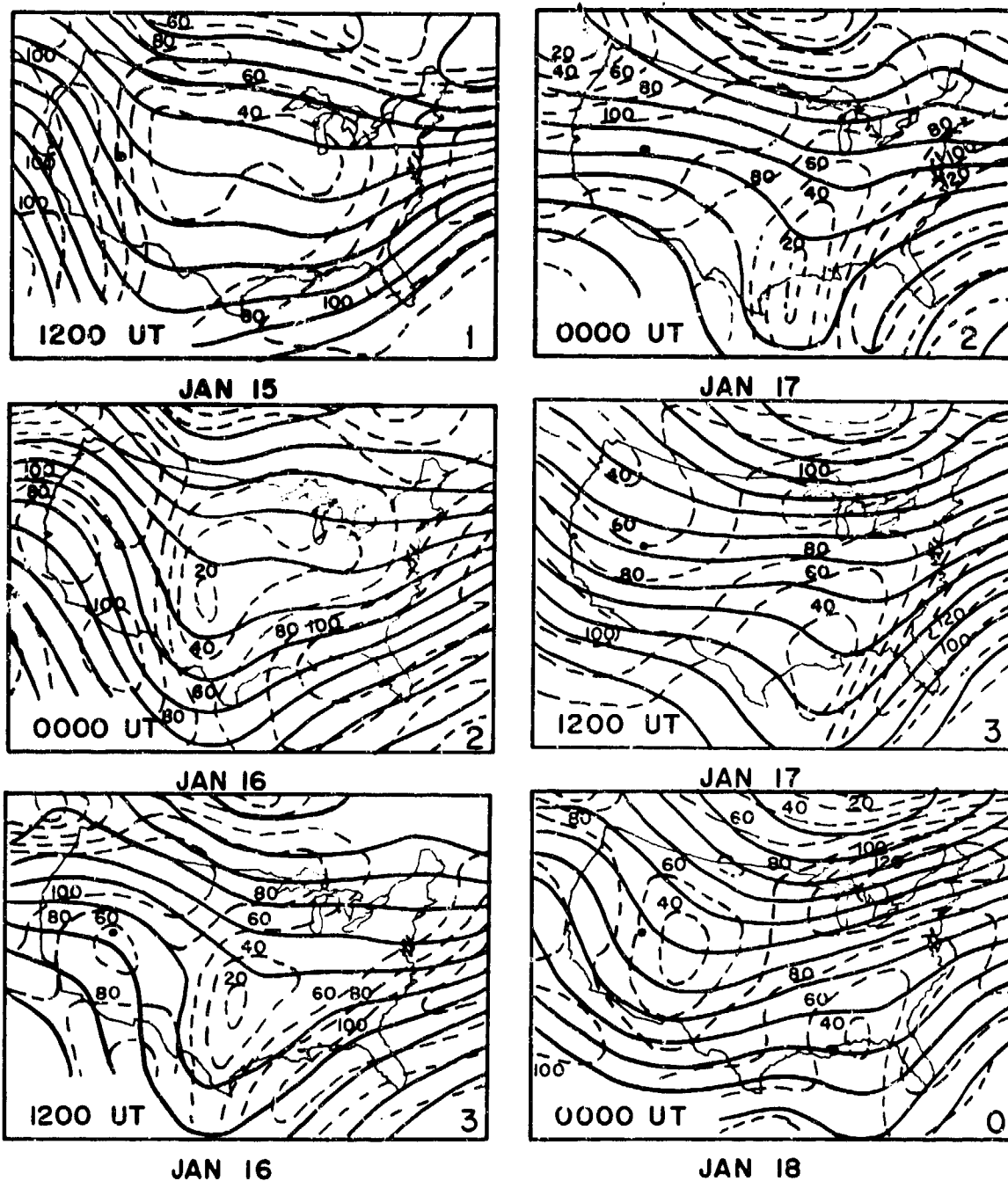
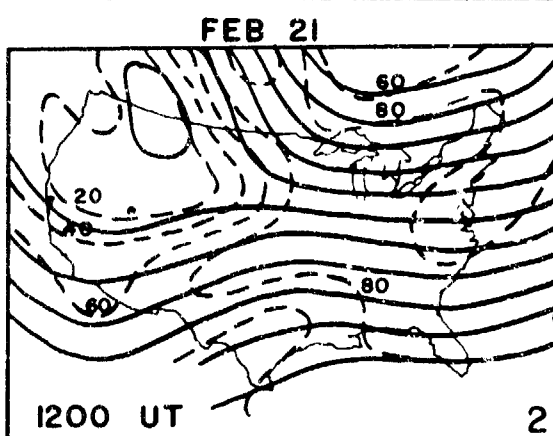
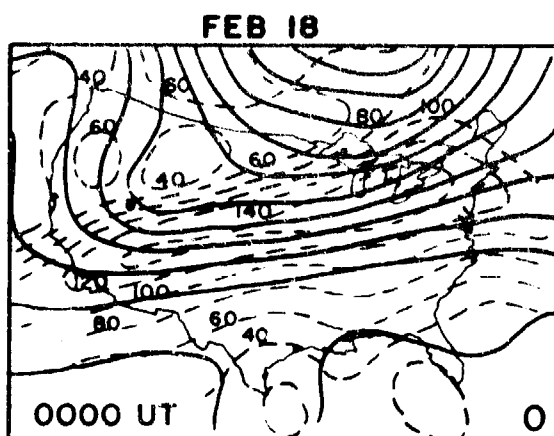
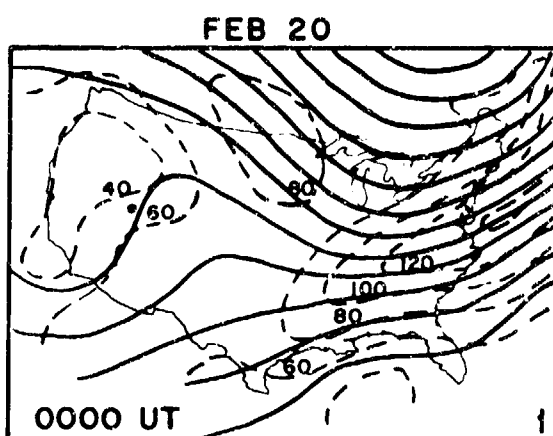
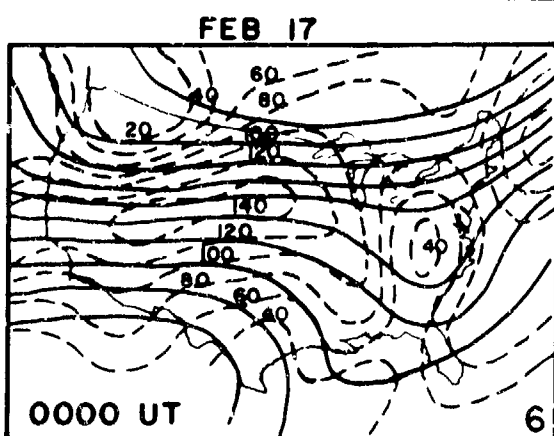
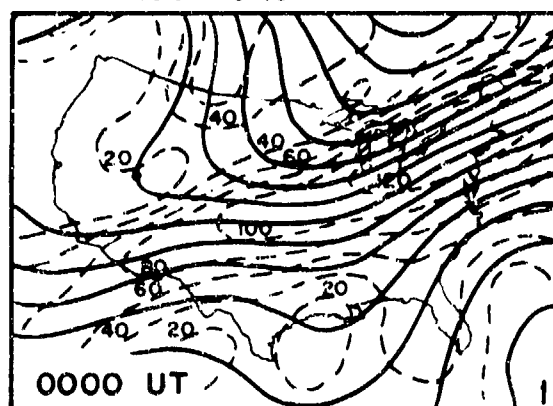
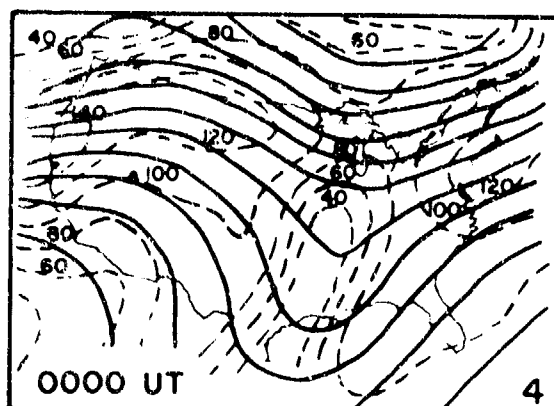


Figure 5. U.S. Weather Service: Tropopause Wind Analysis Maps. Same assignment for solid and dashed lines as given for Figure 4. The integer index seen in the lower right hand corner of each map indicates horizontal wind shear in 0.01 meters/second/km for the mid-point of the propagation path. The wind patterns for this January sequence are generally quiet.

TROPOPAUSE WIND MAPS 1970

— STREAMLINES

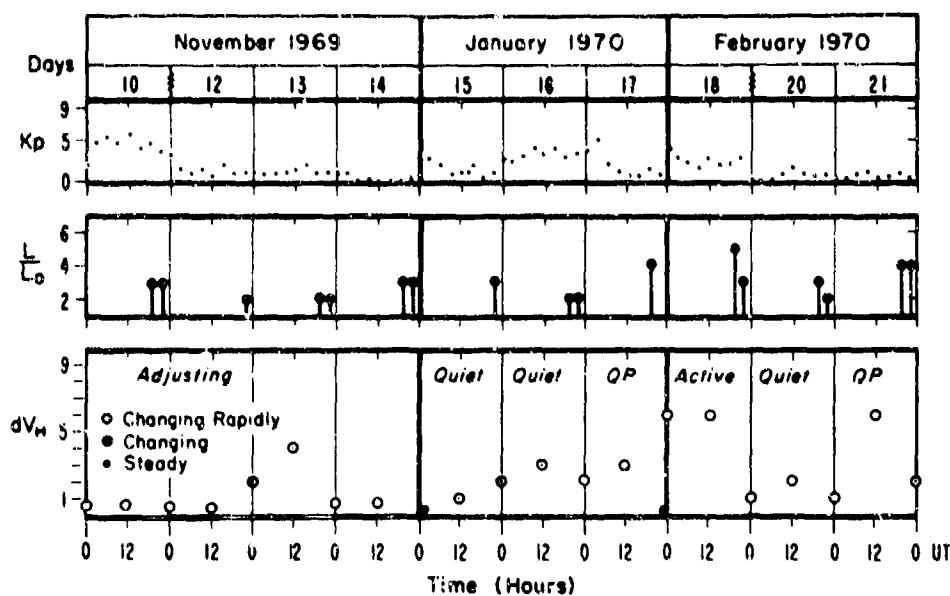
---- ISOTACHS



FEB 19

FEB 22

Figure 6. U.S. Weather Service: Tropopause Wind Analysis Maps. Same assignment for solid and dashed lines as given for Figure 4. The integer index seen in the lower right hand corner of each map indicates horizontal wind shear in 0.01 meters/second/km for the mid-point of the propagation path. There appears to be a rather severe vertical exchange of air on February 18.



IONOSPHERIC - TROPOSPHERIC ACTIVITY - (39 °N, 115 °W)

Figure 7. Comparison of magnetic, ionospheric and tropospheric data for days of interest November 1969, January 1970, and February 1970. Magnetic (Kp) indices are recorded for days of interest. The 3-hour L/Lo ionospheric activity, as deduced from the HF pulse data, is shown, as appropriate, for daytime hours. The tropopause wind patterns are classified as quiet, active or quasi-periodic (QP), changing back and forth from active and quiet.

Mid - Latitude Westerlies

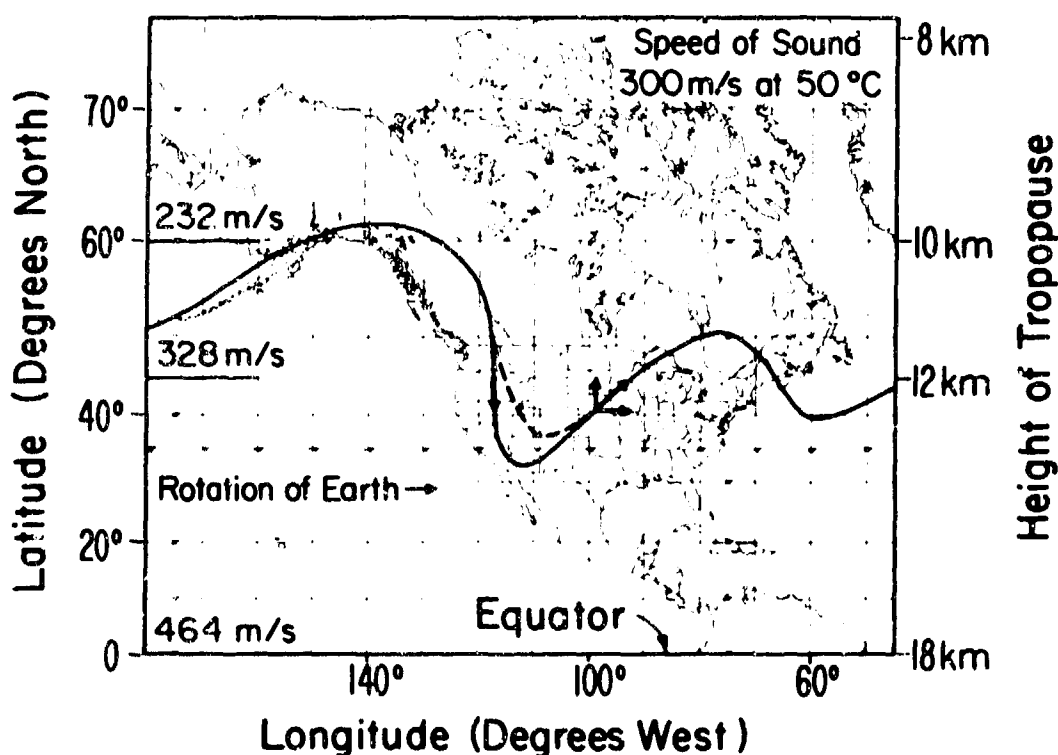


Figure 8. Planetary Wave in Lower Atmosphere, at Mid-Latitude. Wavelength extends across most of continental United States (50° in longitude) at 40° N latitude. An active wind region, the micro-structure of a ridge or trough of a planetary wave, is confined to, say, 20° in longitude at 40° N latitude. The vectors indicate a transfer of momentum causing the trough to steepen. Compare the dashed line with the solid line.

**GENERATION OF ANOMALOUS IONOSPHERIC
OSCILLATION BY THUNDERSTORMS**

by

C.A. Moo and A.D. Pierce

Massachusetts Institute of Technology
Cambridge, Massachusetts 02139
USA

219

PRODUCTION D'OSCILLATIONS IONOSPHERIQUES ANORMALES PAR LES ORAGES

par

C.A. Moo et A.D. Pierce

SOMMAIRE

De récents sondages Doppler d'ondes radio haute fréquence, effectués dans l'ionosphère, ont révélé, dans les couches atmosphériques supérieures, la présence d'oscillations pendant les périodes d'activité orageuse. Ces oscillations, qui présentent des périodes variant de 2 à 5 minutes, se prolongent fréquemment durant plusieurs heures. La cohérence de ces oscillations corrobore l'interprétation générale selon laquelle elles sont causées par le passage d'ondes infrasoniques de grande longueur. Il ne se produit apparemment pas d'oscillations distinctes semblables, avec la même gamme de période lorsqu'on observe des mouvements d'air dans la troposphère par mauvais temps. On sait toutefois que les activités de convection font naître des fluctuations et des ondes internes dont les périodes avoisinent et dépassent les périodes de Brunt-Väisälä. Les auteurs du présent exposé proposent, pour expliquer la production de ces ondes ionosphériques à périodes de 2 à 5 minutes, une théorie basée sur des principes semblables à ceux qu'utilise Lighthill pour sa théorie des sons aérodynamiques. Le fait que les périodes des oscillations ionosphériques sont considérablement inférieures aux périodes troposphériques de Brunt-Väisälä est expliqué de la façon suivante : les fréquences prédominantes émises sont la somme, obtenue par des processus non linéaires, des fréquences des champs de vitesse en interaction réciproque engendrés par les conditions météorologiques. Ces fréquences émises ne sont pas nécessairement observées dans le champ proche.

GENERATION OF ANOMALOUS IONOSPHERIC
OSCILLATION BY THUNDERSTORMS

C. A. Moo and A. D. Pierce
Massachusetts Institute of Technology
Cambridge, Massachusetts 02139
U.S.A.

SUMMARY

Recent experimental evidence, based on radio HF Doppler sounding of the ionosphere, shows oscillations of the upper atmosphere during periods of thunderstorm activity. These oscillations have periods in the range of 2 min to 5 min, frequently for many hours duration. The coherence of the oscillations is consistent with the interpretation generally given that they are caused by the passage of long wavelength infrasonic waves. There are apparently no similar distinct oscillations with the same period range associated with air motion in the troposphere during severe weather. However, convective activity is known to generate fluctuations and internal waves with periods near and above Brunt-Väisälä periods. The present paper proposes a theory for the generation of these ionospheric 2-5 min period waves, based on concepts similar to those used by Lighthill in the theory of aerodynamic sound. That the periods of the ionospheric oscillations are substantially lower than tropospheric Brunt-Väisälä periods is explained as being due to the fact that the predominant radiated frequencies are obtained as a summation, via non-linear processes, of the frequencies of the interacting velocity fields generated by the weather system. These radiated frequencies are not necessarily observed in the near field.

INTRODUCTION

In recent years, experimental evidence, based on HF radio Doppler sounding of the upper atmosphere, shows ionospheric disturbances associated with thunderstorm activity (Georges, 1968; Baker and Davies, 1966; Detert, 1969; Davies and Jones, 1971). These studies reveal that sometimes quasi-sinusoidal oscillations, with periods in the range 2-5 min, occur when thunderstorms are within a radius of 250 km of the ionospheric reflection point. The simultaneous use of multiple HF radio frequencies and of several spaced stations in a Doppler sounding system at near-vertical incidence, shows that these oscillations are coherent in the ionosphere over lateral ranges of at least the spacing of the radio reflection points and are coherent over the range of lower ionospheric HF reflection heights (Detert, 1969). This coherence is consistent with the interpretation frequently given that the observed oscillations are caused by the passage of long wavelength acoustic waves through the atmosphere. Since the principal periods (2-5 min) are somewhat smaller than the typical Brunt-Väisälä periods in the atmosphere, such waves would correspond to the acoustic branch of the acoustic-gravity wave spectrum.

A very striking feature of the HF Doppler data is the relatively narrow bandwidth of the ionospheric oscillations, sometimes with Q greater than 10 for an epoch of several hours. This is suggestive of some kind of resonant phenomenon, although there are apparently no distinct oscillations in the 2-5 min period range associated with air motion in the troposphere. However, it is well known that high convective activity generates turbulent fluctuations and generates internal gravity waves outside of the convection zones. Fig. 1 reproduces the power spectrum of atmospheric pressure given over twelve years ago in a classic paper by E. Gossard (1960). The longest solid line illustrates average conditions, but the dashed spectrum and the short solid line near it represent conditions of great excitation. Each of the latter two curves, Gossard identified as the spectrum of internal waves generated by convective activity with wave frequencies near the local Brunt-Väisälä frequency computed from radiosonde data. Brunt's period varies typically between 4 and 10 minutes in the troposphere, depending on the temperature stratification, and is the natural period of buoyancy oscillations in a stable atmosphere.

In this paper we propose a theory for the generation of the anomalous ionospheric oscillations by thunderstorms, based on the concepts successfully employed by Lighthill (1952, 1962) to explain the generation of aerodynamic sound by turbulence. In this model the ionospheric oscillations are a manifestation of acoustic waves radiated from tropospheric regions of interacting velocity fields whose frequencies are at or below the lower atmosphere Brunt-Väisälä frequencies. By means of non-linear fluctuating Reynolds' stresses, a transfer of energy is effected from the internal gravity wave regime to the acoustic wave regime of the acoustic-gravity wave spectrum. This transfer takes place with concomitant change of frequency.

Recently, Jones (1970) introduced a model to explain the ionospheric oscillations under discussion in this paper. His explanation is based on the mode theory of lower atmosphere guided acoustic-gravity wave propagation. In a typical set of multi-mode dispersion curves, there are regions where modal curves nearly 'kiss' each other, and Jones explains the phenomenon as being due to the coupling of energy between the fundamental and first gravity modes. A major objection to this explanation is that it cannot explain the ionospheric oscillations directly above the thunderstorm regions as are observed. The existence of the normal modes are really established by the extended stratification of a given atmosphere and the coupling of modes, at 'kissing', can only be achieved at horizontal ranges greater than $\pi/\Delta k$ where Δk is the wave number gap at the 'kissing' region. To explain a 280 period from Jones' curve this distance should be taken to be about 2000 km.

WAVE EQUATION AND SOURCE

The basic approach of Lighthill (1952, 1962) in the aerodynamical generation of sound is to separate the linear and non-linear terms in the equations of motion and then form an inhomogeneous wave equation for one of the variables. The linear terms are the wave propagation operator, and the non-linear terms are considered as a source function. If the wave motions are weak compared to the primary motions in the flow field, and there is negligible back reaction on the primary flow, then the inhomogeneous wave

equation can be solved for the radiation emitted in the far field. The source function is determined by the primary flow field and is limited in extent. The method is thus restricted to weak wave emission. Lighthill's procedure has been extended to wave motion in a stratified atmosphere by Moore and Spiegel (1964), Kato (1966), and Stein (1967).

For simplicity, we consider an unbounded isothermal atmosphere with undisturbed pressure p_0 and density ρ_0 , stratified with height as $\exp(-Z/H)$ with scale height

$$H = p_0 / \rho_0 g = c_0^2 / \gamma g \quad (1)$$

where c_0 is the speed of sound, and γ is the ratio of specific heats. If $\rho_1(\vec{r}, t)$, $p_1(\vec{r}, t)$ and $\vec{v}(\vec{r}, t)$ are deviations of air density, pressure and velocity from their equilibrium values, the governing equations are then (with linear terms separated on the left-hand side and the non-linear terms on the right-hand side):

$$\rho_0 \frac{\partial \vec{v}}{\partial t} + \nabla p_1 - \rho_1 \vec{g} = \vec{f} \quad , \quad (2)$$

$$\frac{\partial \rho_1}{\partial t} + \nabla \cdot (\rho_0 \vec{v}) = q \quad , \quad (3)$$

and

$$\frac{\partial p_1}{\partial t} + \rho_0 \vec{g} \cdot \vec{u} + \rho_0 c_0^2 \nabla \cdot \vec{v} = h \quad , \quad (4)$$

where

$$\vec{f} = - \frac{\partial (\rho \vec{v} \cdot \vec{v})}{\partial x_j} - \frac{\partial (\rho_1 \vec{v})}{\partial t} \quad , \quad (5)$$

$$q = -\nabla \cdot (\rho_1 \vec{v}) \quad , \quad (6)$$

and

$$h = -\gamma p_1 \nabla \cdot \vec{v} - \vec{v} \cdot \nabla p_1 \quad (7)$$

Here $\vec{g} = (0, 0, -g)$. Equations (2), (3) and (4) are the equations of momentum, mass conservation and adiabatic motion, respectively.

Eliminating ρ_1 and \vec{v} from the linear terms in equations (2), (3) and (4), and introducing the variable

$$P = p_1 / \sqrt{p_0} \quad (8)$$

in order to remove the height dependence of the perturbation amplitudes, we obtain the following inhomogeneous wave equation (Kato, 1966; Stein, 1967)

$$\left[\frac{\partial^2}{\partial t^2} - c_0^2 \nabla^2 + \omega_A^2 - \left(\frac{\partial}{\partial t} \right)^{-2} c_0^2 \omega_B^2 \frac{\partial^2}{\partial H} \right] P = S \quad , \quad (9)$$

where the source function S is given by

$$S = \frac{1}{\sqrt{p_0}} \left[\left(1 + \left(\frac{\partial}{\partial t} \right)^{-2} \omega_B^2 \right) (-\vec{v} \cdot \vec{f} + \frac{\partial q}{\partial t}) + \frac{1}{c_0^2} \left(1 + \left(\frac{\partial}{\partial t} \right)^{-2} \vec{g} \cdot \nabla \right) ((\gamma-1) \vec{g} \cdot \vec{f} - \frac{\partial}{\partial t} (c_0^2 q - h)) \right] \quad (10)$$

with

$$\nabla_H^2 = \frac{\partial^2}{\partial x^2} + \frac{\partial^2}{\partial y^2}$$

Here

$$\omega_A^2 = c_0^2 / 2H \quad (11)$$

is the acoustic cut-off frequency, while

$$\omega_B = (\sqrt{\gamma-1}/\gamma) c_0 / H \quad (12)$$

is the Brunt-Väisälä frequency of the atmosphere.

In Eq. (9) the expression in brackets is the acoustic-gravity wave operator which separates into

the acoustic branch for $\omega > \omega_A$ and into the internal gravity branch for $\omega < \omega_B$. Since we are interested in acoustic waves in the atmosphere we shall use the well-known approximation (Tolstoy, 1963) to the wave operator in the acoustic range:

$$\left[\frac{\partial^2}{\partial t^2} - c_o^2 \nabla^2 + \omega_A^2 \right] P = S \quad (13)$$

We next simplify the source function by Lighthill's procedure of treating the terms in Eq. (10) as truly known sources. This means that primary flow is only weakly coupled to the acoustic field. This is generally considered to be possible for low Mach number flow, which is tantamount to considering the primary fluid motion as almost incompressible. Although Lighthill's (1952, 1954, 1962) treatment is widely accepted, the theoretical justification for this procedure is still evolving (Crow, 1970; Lauvatad, 1968). Following in the same spirit, only terms involving \vec{f} in Eq. (10) are considered important. This follows since

$$\overline{v_{\text{acous.}}^2} \ll \overline{v_{\text{prim.}}^2} \sim M^2, \quad (14)$$

and

$$\left(\frac{1}{\rho_1^2 \text{ acous.}} \right)^{1/2} / \rho_o \ll \left(\frac{1}{\rho_o^2 \text{ prim.}} \right)^{1/2} \sim M^2, \quad (15)$$

The terms in \vec{f} become

$$-\nabla \cdot \vec{f} + \frac{\partial q}{\partial t} = \frac{\partial^2 (\rho_o v_1 v_1)}{\partial x_1 \partial x_j} \quad (16)$$

and

$$\vec{g} \cdot \vec{f} = g \frac{\partial}{\partial x_j} (\rho_o v_1 v_j \delta_{13}) \quad (17)$$

The source term $(\partial/\partial t)(c_o^2 q - h)$ represents the non-adiabatic nature of the flow field and of the stratification, and is generally negligible for low Mach numbers (Stein, 1967).

With Eqs. (16) and (17), we can then expand the source function in multipoles (Unno, 1964; Stein, 1967):

$$c_o S(\vec{x}, t) = \alpha \frac{\partial^2 (\sqrt{\rho_o} v_1 v_1)}{\partial x_1 \partial x_j} - \frac{1}{H} \beta \frac{\partial (\sqrt{\rho_o} v_1 w)}{\partial x_j} + \frac{1}{4H^2} \epsilon (\sqrt{\rho_o} w^2) \quad (18)$$

where $\vec{v} = (v_1, v_2, w)$, H is the scale height, and where

$$\alpha = 1 - \omega_B^2 \left(1 - \frac{1}{2} (\delta_{13} + \delta_{j3}) \right) \left(\frac{\partial}{\partial t} \right)^{-2} \quad (19)$$

$$\beta = \frac{1}{\gamma} - \frac{1}{2} \omega_B^2 (1 - \delta_{j3}) \left(\frac{\partial}{\partial t} \right)^{-2}$$

$$\epsilon = \frac{2-\gamma}{\gamma}$$

The three terms in Eq. (18) differ from each other in the degree of space differentiation and represent, respectively, quadrupole, dipole and monopole sources. The dipole and monopole are absent in a uniform medium, but arise because the stratification acts as a boundary surface (Curle, 1955; Unno, 1964).

RADIATION FROM THUNDERSTORMS

Equations (9) and (18) are the inhomogeneous wave equation and source function, respectively. We indicated that, because of our interest in the generation of acoustic waves of the acoustic-gravity wave spectrum, we shall use the approximation of Eq. (13) as our acoustic wave operator. We also now make simplifications on the source function Eq. (18). First, we consider that the scales of motion are small compared to the scale height H ; so that from the form of Eq. (18), only the first term, the quadrupole source term, remains. Second, with the thought in mind that the fluid motions contributing to the fluctuating Reynold's stress are near the Brunt-Väisälä frequency ω_B , and thus primarily in the vertical direction (Midgley and Liemohn, 1966), then the coefficients Eq. (19) become $\alpha = 1$, $\beta = 1/\gamma$ and $\epsilon = (2-\gamma)/\gamma$.

With the approximations indicated above our inhomogeneous wave equation becomes

$$\left[\frac{\partial^2}{\partial t^2} - c_o^2 \nabla^2 + \omega_A^2 \right] \frac{P_1}{\sqrt{\rho_o}} = \frac{1}{c_o} \frac{\partial^2 (\sqrt{\rho_o} v_1 v_1)}{\partial x_1 \partial x_j} \quad (20)$$

This equation will be the basis for most of the remaining discussion. It differs from Lighthill's equation by the dispersive term ω_A^2 and the modified independent variable $p_1/\sqrt{p_0}$, both produced by stratification.

We now introduce a time-harmonic analysis, in which

$$\frac{p}{\sqrt{p_0}} = P(\bar{x}, t) = \int_{-\infty}^{\infty} \phi(\bar{x}, \omega) e^{-i\omega t} d\omega \quad (21)$$

Thus Eq. (20) becomes

$$(\omega^2 + c_\omega^2 \nabla^2) \phi(\bar{x}, \omega) = \frac{-1}{2\pi} \frac{c_\omega^2}{c_0^3} \frac{\partial^2}{\partial x_1 \partial x_j} \int_{-\infty}^{\infty} \sqrt{\rho_0} v_1 v_j e^{-i\omega t} dt \quad (22)$$

where c_ω is the phase velocity at frequency ω , and where

$$c_\omega^2 = \frac{\omega^2}{\omega^2 - \omega_A^2} c_0^2 \quad (23)$$

Equation (22) can now be solved by standard techniques (see, e.g., Stratton, 1941). We solve for ϕ outside the source region which is in a finite volume near the ground. If \bar{y} is a point within the source region, \bar{r} the vector from this point to the observer at \bar{x} , then outside the source region we have,

$$\phi(\bar{x}, \omega) = \frac{-1}{8\pi^2 c_0^3} \int_V \frac{1}{r} e^{-i\omega r/c_\omega} \frac{\partial^2}{\partial y_1 \partial y_j} \sqrt{\rho_0} U_{ij} d^3\bar{y} \quad (24)$$

where we only consider the propagating frequencies, $\omega > \omega_A$, also

$$U_{ij}(\bar{x}, \omega) = \int_{-\infty}^{\infty} v_1 v_j e^{-i\omega t} dt \quad (25)$$

Away from the source region we can use the divergence theorem twice, so

$$\phi(\bar{x}, \omega) = \frac{1}{8\pi^2 c_0^3} \int \frac{\omega^2}{c_\omega^2} \frac{x_1 x_j}{r^2} \frac{e^{-i\omega r/c_\omega}}{r} \sqrt{\rho_0} U_{ij}(\bar{y}, \omega) d^3\bar{y} \quad (26)$$

In the far field this becomes

$$\phi(\bar{x}, \omega) \approx \frac{1}{8\pi^2 c_0^3} \frac{\omega^2}{c_\omega^2} \frac{x_1 x_j}{x^2} \int_V \frac{e^{-i\omega r/c_\omega}}{r} \sqrt{\rho_0} U_{ij} d^3\bar{y} \quad (27)$$

Now if

$$\begin{aligned} v_1 &= v_1(\bar{y}) \cos [\omega_1 t + \phi_1(\bar{y})] \\ v_j &= v_j(\bar{y}) \cos [\omega_j t + \phi_j(\bar{y})] \end{aligned} \quad (28)$$

then, from Eq. (25),

$$U_{ij} = v_1 v_j \pi \left[\delta(\omega - (\omega_1 + \omega_2)) e^{i(\phi_1 + \phi_2)} + \delta(\omega - (\omega_1 - \omega_2)) e^{i(\phi_1 - \phi_2)} \right] \quad (29)$$

If v_1 and v_j are oscillations in the internal gravity wave spectrum then

$$\omega_1, \omega_j \leq \omega_B \quad (30)$$

and since $\omega_A > \omega_B$ we require for radiation $(\omega_1 + \omega_j) > \omega_A$, and Eq. (27) becomes

$$\phi(\bar{x}, \omega) = \frac{1}{8\pi c_0^3} \frac{\omega^2}{c_\omega^2} \frac{x_1 x_j}{x^2} \int_V \frac{e^{-i\omega r/c_\omega}}{r} \sqrt{\rho_0} v_1 v_j \delta(\omega - (\omega_1 + \omega_2)) d^3\bar{y} \quad (31)$$

It is evident from this that a frequency $\omega = \omega_1 + \omega_j$ is radiated, where ω_1 and ω_j are frequencies of

internal waves.

If ω_i, ω_j are near the Brunt-Väisälä frequency ω_B then the acoustic frequency radiated would be $\omega \approx 2\omega_B$. In the troposphere, Brunt's period varies from about 4 to 10 min, so that the period of acoustic waves radiated would be from 2 to 5 min, which is the period range of ionospheric oscillation associated with thunderstorms.

Near ω_B , the fluid particles move primarily in the vertical direction so that $x_i = x_j$ and in Eq. (31) the geometrical factor is

$$\frac{x_i x_j}{x^2} = \cos^2 \theta, \quad (32)$$

where θ is measured from the vertical. We have a vertical linear quadrupole radiation pattern, with a null to the side. This null may help explain the apparent absence of the acoustic oscillations on microbarograph records during thunderstorm activity (K. Davies, private communication), because outside a cone of semiangle of about 30° the acoustic pressure would be small.

Actually, at least one of the waves v_i, v_j must have a vertical wave number component in order for the acoustic oscillation to be observed in the ionosphere above the source. This is seen if we use the representation

$$v_i \sim \int_{-\infty}^{\infty} \int \exp(i(\bar{k}_i \bar{x} - \omega_i t + \theta_i)) d\omega d^3 \bar{k} \quad (33)$$

so that

$$v_i v_j \sim \iint \exp(i(\bar{k}_i + \bar{k}_j) \bar{x} - (\omega_i + \omega_j)t + (\theta_i + \theta_j)) d\omega d^3 \bar{k} \quad (34)$$

Here $\bar{k}_{i,j} = (k_x, k_y, k_z)_{i,j}$, and $(\bar{k}_i + \bar{k}_j)$ is the acoustic wave number so that for vertical propagation $(k_{z,i} + k_{z,j}) > 0$.

CONCLUSIONS

In this paper we have developed a theory to explain the generation of 2-5 min period acoustic oscillations in the ionosphere by thunderstorms in the troposphere. Using the approach of Lighthill to explain the generation of aerodynamic sound, an inhomogeneous acoustic wave equation was developed with multipole sources, of which the quadrupole is the most important.

Thunderstorms and other convective activity are known to generate oscillations and waves in the internal gravity wave spectrum. Through the nonlinear quadratic interaction of these internal waves the multipole sources are excited, generating acoustic waves whose frequency is the sum of the frequencies of the primary internal waves. For internal wave periods near Brunt's period, this process would generate acoustic periods near one-half Brunt's period in the troposphere, i.e., periods 2-5 min for typical Brunt's periods 4-10 min.

Near Brunt's period τ_B particle motions are primarily vertical, so that for interacting internal waves with periods near τ_B , the quadrupole (and dipole) radiation pattern in the far field for acoustic waves is in the vertical direction, with a null to the side.

REFERENCES

- Baker, D.M. and K. Davies, 1969, F2-Region acoustic waves from severe weather, *J. Atmos. Terrest. Phys.* **31**, 1345-1352.
- Crow, S.C., 1970, Aerodynamic sound emission as a singular perturbation problem, *Studies. Appl. Math.* **49**, 21-44.
- Curle, N., 1955, The influence of solid boundaries upon aerodynamic sound, *Proc. Roy. Soc.* **A231**, 505-514.
- Davies, K. and J.E. Jones, 1971, Ionospheric disturbances in the F2 region originating in severe thunderstorms, *J. Atmos. Sci.* **28**, 254-262.
- Detert, D.G., Feb. 15, 1969, A study of the coupling of acoustic energy from the troposphere to the ionosphere, Avco Corp. Report to Marshall SFC, NASA, on Contract NAS8-21079.
- Georges, T.M., 1968, HF Doppler studies of traveling ionospheric disturbances, *J. Atmos. Terrest. Phys.* **30**, 735-746.
- Gossard, E.E., 1960, Spectra of atmospheric scalars, *J. Geophys. Res.* **65**, 3339-50.
- Jones, W.L., 1970, A theory for quasi-periodic oscillations observed in the ionosphere, *J. Atmos. Terrest. Phys.* **32**, 1555-1566.
- Kato, S., 1966, The response of an unbounded atmosphere to point disturbances, *Astrophys. J.* **143**, 893-903.
- Lauvstad, V.R., 1968, On non-uniform Mach number expansion of the Navier-Stokes equations and its relation to aerodynamically generated sound, *J. Sound Vib.* **7**, 90-105.
- Lighthill, M.J., 1952, On sound generated aerodynamically: I. General theory, *Proc. Roy. Soc.* **A211**, 364-387.
- Lighthill, M.J., 1962, The Bakerian Lecture, 1961. Sound generated aerodynamically, *Proc. Roy. Soc.* **A267**, 147-182.
- Midgeley, J.E. and H.B. Liemohn, 1966, Gravity waves in a realistic atmosphere, *J. Geophys. Res.* **71**,

3729-3743.

- Moore, D.W. and E.A. Spiegel, 1964, The generation and propagation of waves in a compressible atmosphere, *Astrophys. J.*, Vol. 139, 48-71.
- Stein, R.F., 1967, Generation of acoustic and gravity waves by turbulence in an isothermal stratified atmosphere, *Solar Phys.* 2, 385-432.
- Stratton, J.A., 1941, *Electromagnetic theory*, McGraw-Hill Book Co., New York.
- Tolstoy, Ivan, Jan. 1963, The theory of waves in stratified fluids including the effects of gravity and rotation, *Rev. Mod. Phys.*, Vol. 35, 207-230.
- Unno, W., 1964, Generation of acoustic noise in convection zones, *Trans. IAU*, 12 B, 555-558.

The research reported in this paper was supported by the Air Force Cambridge Research Laboratories, Air Force Systems Command, USAF, under Contract F19628 70-C-0008.

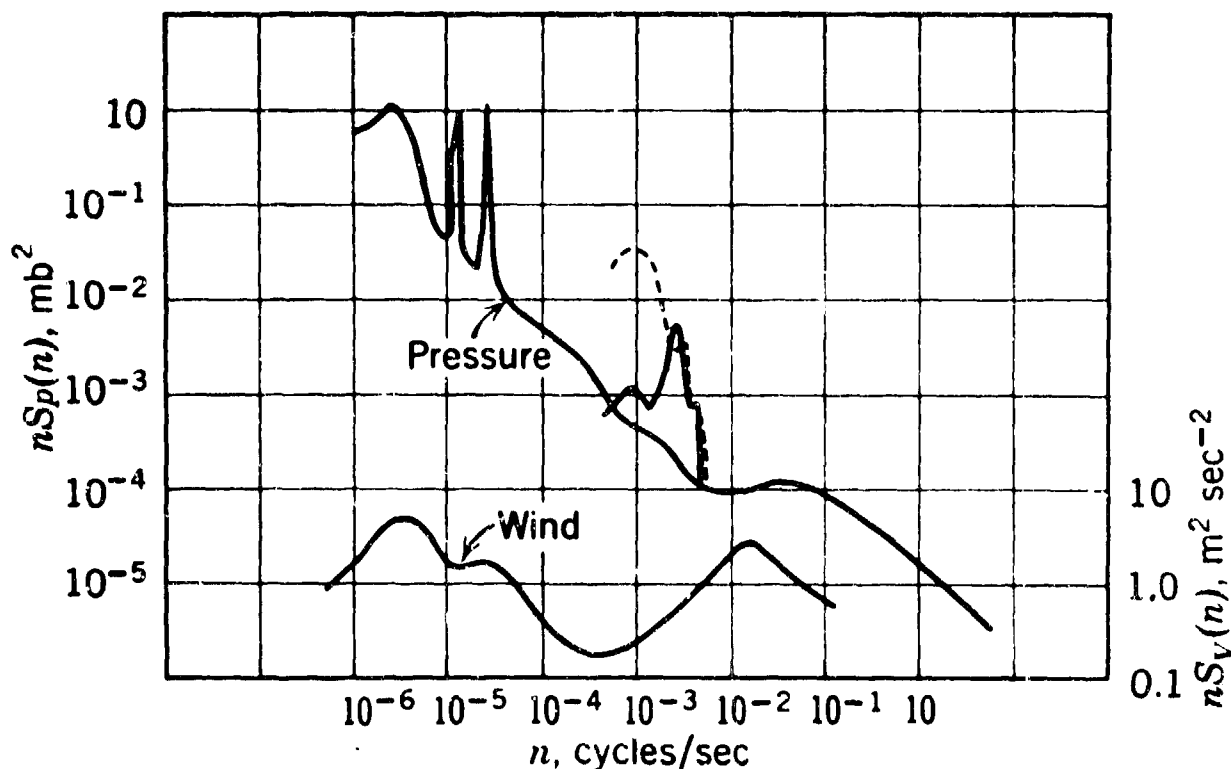


Fig. 1. Pressure power spectrum of the atmosphere, after Gossard (1960), with examples of spectra of gravity waves generated by convective activity.

**A PHENOMENOLOGICAL INVESTIGATION OF AMPLITUDES
AND SPECTRA OF GRAVITY WAVES**

by

J.P.Schödel

**Max-Planck-Institut für Aeronomie
Abteilung für Weltraumphysik
3411 Lindau/Harz
Fed. Rep. Germany**

227

ETUDE PHENOMENOLOGIQUE DES AMPLITUDES ET DES SPECTRES D'ONDES DE GRAVITE

par

J.P. Sédell

SOMMAIRE

Les observations du contenu en électrons de l'ionosphère au moyen de satellites balistiques géostationnaires révèlent très fréquemment la présence d'oscillations de forme sinusoïdale. Les enregistrements de rotation de Faraday représentent, pour ces oscillations, un bon système de contrôle. Pour étudier ces oscillations, on a filtré numériquement les enregistrements de contenu d'électrons. Le filtre numérique est brièvement décrit. Les amplitudes des effets créés par les ondes de gravité peuvent être facilement montrées après filtrage. La partie filtrée des données, représentant les fluctuations provoquées par les ondes, peut être utilisée pour calculer les spectres d'énergie. Le calcul de ces spectres d'énergie est décrit pour clarifier les résultats. A partir des spectres, on peut déduire les faits suivants : 1°) l'amplitude de l'onde décroît rapidement en même temps que diminue la longueur de la période, 2°) toutes les périodes peuvent être observées, 3°) les fréquences harmoniques ne sont pas habituellement observées. Une étude de statistique portant sur un grand nombre de jours révèle en moyenne que toutes les fréquences ont la même probabilité, bien que des périodes de 35 minutes puissent apparaître de préférence. Des jours particuliers sont étudiés.

A PHENOMENOLOGICAL INVESTIGATION OF AMPLITUDES
AND SPECTRA OF GRAVITY WAVES

J.P. Schödel

Max-Planck-Institut für Aeronomie
Abteilung für Weltraumphysik
3411 Lindau/Harz
Fed. Rep. Germany

SUMMARY

Observations of the ionospheric electron content by means of geostationary beacon satellites very often exhibit oscillations of sinusoidal form. Faraday rotation records represent a good monitoring system for these oscillations. For the investigation of the oscillations the records of the electron content were filtered numerically. The numerical filter is described briefly. The amplitudes of effects caused by gravity waves can easily be demonstrated after the filtering. The filtered part of the data - representing the wave induced fluctuations - can be used for the computation of power spectra. The computation of the power spectra is described in order to clarify the following results. From the spectra we can deduce the following facts: 1. the wave amplitude decreases rapidly with decreasing period length, 2. all periods can be observed, 3. harmonic frequencies are usually not observed. A statistical investigation for a large number of days shows on average that all frequencies have the same probability, although periods of 35 minutes may be preferred. Particular days are discussed.

1. INTRODUCTION

If linear or elliptically polarized radio signals from geostationary satellites are observed, one finds short-time periodic fluctuations in addition to the usual rotation of the plane of polarization (Faraday effect), which is due to the daily variation of the ionospheric electron content. Figure 1 presents the record of Faraday rotation for December 2, 1969. One sawtooth corresponds to a relative rotation of 180° . The satellite ATS-3 was observed in Lindau. Superimposed on the record are sinusoidal oscillations whose period is less than one hour. Continuous observations of this kind are relatively inexpensive to carry out and are obviously useful as a monitoring system. Since this measuring procedure gives the integral of the electron density along the direction of propagation of the radio signals, no conclusions can be drawn concerning height dependent parameters of the observed oscillations. When we speak of amplitudes and spectra here, we always mean those which refer to the electron content of the ionosphere.

2. PRESENTATION OF WAVE AMPLITUDES BY MEANS OF FILTERING

Presented in Figure 2 in arbitrary units are all of the observed daily variations in the electron content for the month of December 1969. We recognize that the oscillations during a day obviously occur regularly. Since the amplitudes of these oscillations are small with respect to the amplitude of the daily variation itself, we want to separate out these oscillations by means of filtering. The filter is determined from the following considerations:

- (a) atmospheric gravity waves have periods from a few minutes to a few hours
- (b) tides should be eliminated by the filter
- (c) the smoothing process associated with the filter should not in itself produce oscillations where the normal daily variation is rapid, such as in the morning hours.

Thus we want to examine only oscillations with periods from 5 to 120 minutes. The use of numerical bandpass filters is relatively costly in programming and computing time. Therefore we use a numerical high pass filter which has a pass range containing the desired frequencies (Schödel, Münch, 1972). Figure 3 shows the pass response curve $R(f)$ of the high pass filter, which consists of 27 coefficients. The response $R(f)$ is plotted versus frequency f (or equivalently period P). The filter opens for a period $P = 180$ minutes. The 3 dB point lies at $P = 135$ minutes, and the filter is fully open, i.e. $R(f) = 1$, at $P = 120$ minutes. The filter is linear and phase preserving.

Before demonstrating the results of filtering we should first describe the procedure for the determination of the spectral frequency distribution.

3. CALCULATION OF THE SPECTRAL FREQUENCY DISTRIBUTION

We have already made an important step in the direction of a spectral analysis, namely that the amplitude of the daily variation is much larger than that of the superimposed oscillations and would yield in a spectrum as described below only a line with $P = 24$ hours. It can further be determined that temporal phase jumps between oscillations of the same period occur, and therefore a harmonic analysis is excluded. The power spectrum method offers a way around this problem (Blackman, Tukey, 1958). According to Blackman and Tukey in finite time intervals one can determine an approximate autocorrelation function of a continuous function of time. One then obtains the power spectrum of the function of time through a Fourier transformation of the approximate autocorrelation function. When the data points are a fixed distance apart, an estimate of the power

spectrum can be calculated. Further details can be found in the papers of Blackman and Tukey (1958) and Schödel and Münch (1972).

4. SELECTED EXAMPLES

Out of 117 daily recordings of the electron content N_f examined, samples were selected which exhibited distinct lines in the spectrum. A preference for fall and winter appears only accidentally, since the satellite ATS-3, which was observed in Lindau, was not available for observation in the spring and summer months. Twelve daily recordings will be presented in chronological order and their characteristics described.

Figure 4 from December 19, 1968, shows a typical daily electron content curve for winter. It has a deep minimum in the morning hours, then a steep increase, and after about four hours an equally steep decrease. The curve is relatively flat during the night. This curve is in the lower left corner of the figure. The measured values are represented by a solid line. The dotted line represents the filtered curve. In the upper left corner of the figure is the high frequency part N_f^1 of the electron content. Since all periods less than or equal to 120 minutes are included, one can immediately see only a wave period of about 120 minutes. The power spectrum on the right of the figure gives information about all represented periods. The relative amplitude A is shown as a function of the period P (in minutes). The vertical line in the spectrum corresponds to the 3 dB point of the high pass filter. In the right part of the figure is given the 90 % confidence limit (Blackman and Tukey, 1958). We consider a spectral line significant only when this limit is exceeded. From the spectrum we can then read off two spectral lines, one between 127 and 76 minutes and one at about 29 minutes. A further line can be expected at a period of about 20 minutes. Consideration of the spectral lines makes the irregular appearance of the N_f^1 curve understandable. It should be pointed out again that the N_f^1 curve contains all frequencies passed by the filter. From this example we can extract a characteristic which holds for all spectra; that the relative amplitude decreases more than an order of magnitude whenever the period of oscillation decreases by a factor of 5. It is therefore to be expected that higher frequencies are, as a rule, lacking. In fact data from Lindau/Harz verifies that periods of about 5 minutes are observable on only about 0.2 % of all days. On the other hand, however, the limit for acoustic waves in the F-region of the ionosphere has been reached (Hines, 1960).

Figure 5 from December 25, 1968, shows a very clear wave development in the morning hours with a superimposed oscillation of short period. The power spectrum verifies that there are oscillations with periods of 120 and 38 minutes. The quantity N_f^1 represents approximately 3 % of the maximum electron content. In Figure 6 from August 22, 1969, the relatively sharp spectral line at $P = 54$ minutes appeared in two wave trains at about 13 and 21 hours. Figure 7 from September 17, 1969, shows a regular wave pattern for nearly 24 hours. In the ideal case the disturbance N_f^1 is directly proportional to the total electron content (Georges and Hooke, 1970). That presupposes, however, that the wave vector of the gravity wave is independent of height. The example just given shows clearly that the proportionality does not hold. Thus the wave vector should be considered height dependent in all cases. This is especially meaningful with respect to a quantitative analysis of the wave amplitudes (Schödel, 1972). A further example indicating that proportionality between the magnitude of N_f^1 and N_f is not maintained is shown in Figure 8 from September 19, 1969. The smallest value of the amplitude N_f^1 occurs when N_f is the largest. From this we can conclude that there is a time dependent source of gravity waves. The curve of electron content corresponds to the summer months. The minimum occurs appreciably earlier than in winter, and the increases and decreases are not so steep. Moreover, the difference in electron content from day to night is not as large as in winter.

The next two examples in connection with the previous examples leads one to suspect that there is no preference for a given spectral line. In Figure 9 from October 9, 1969, there are three (four) specific periods whereas in Figure 10 from November 12, 1969, there are two closely spaced spectral lines against a background of continuous spectrum. In Figure 11 from November 13, 1969, one can see a nearly harmonic frequency relation of the wave part of the electron content. Regular wave structures are only recognizable for short time intervals. As before the electron content falls sharply between 16³⁰ and 18⁰⁰, and then remains constant for about two hours. We assume the cause of this is the nightly rise of the F-region (Eisemann, 1966). Through the rise of the F-layer the electrons are moved into a region of lesser density and therefore smaller loss. Because of this there apparently arises a sinusoidal structure in the electron content which cannot be ascribed to a gravity wave. At this point a restriction of our analysis, which was pointed out in section 2, becomes clear. Filtering and spectral analysis must be carried out in such a way that changes in the electron content which are part of the "normal" daily variation do not become part of the wave structure. This applies especially for the morning hours in which the electron content can have a sharp minimum. The filtering process would in this region produce oscillations which cannot be ascribed to atmospheric gravity waves.

Up to now the largest wave amplitudes observed were on November 25, 1969 (see Figure 12). They are roughly five to seven percent of the maximum electron content. There are two distinct wave trains between 8 and 11 hours and between 12⁴⁵ and 14⁴⁵. In Figure 13 from November 30, 1969, two specific harmonic frequencies again appear whose phases are such that the minimum of the oscillation of higher frequency falls in the maximum of the oscillation of lower frequency and vice versa. The high frequency oscillation in the noon hours of December 2, 1969, (Figure 14) corresponds to the spectral line at about 35 minutes. A further line is to be expected between $P = 76$ and $P = 127$ minutes.

The examples given, with the exception of two, can be considered taken under geophysically quiet conditions. December 16, 1969 (Figure 15) belongs to the group of geophysically disturbed days as well as December 25, 1968, and November 30, 1969. The constancy of geophysical conditions led to the analysis of only 24 hours in each case. In two cases (November 2-3, 1969, and November 16-19, 1969) periods of four days were analyzed for the spectral frequency distribution. The respective spectra show 7 and 8 significant spectral lines. This is obviously a sign that no preferred frequencies exist in the ionosphere. To date 117 days have been analyzed. From the spectra

the rate of occurrence of oscillations of given period P was obtained. Figure 16 shows the results. The rate of occurrence N is plotted as a function of P . The shaded bars correspond to the significant spectral lines. If the lines are also included which lie in the neighborhood of the confidence limit, then $N(P)$ is increased by the unshaded bars.

A connection between the geomagnetic index A_p and the spectral distribution of relative amplitude $A(P)$ in the spectra could not be verified since the data for such an analysis is not sufficient.

5. CONCLUSION

Continuous observations of the electron content of the ionosphere exhibit oscillations which can be explained as atmospheric gravity waves. Gravity waves are a regular occurrence, at least in the F-region of the ionosphere. The method given encompasses the oscillation period interval from five minutes to several hours. Since the oscillations are presented in analog form, it is very easy to carry out a spectral analysis. A chain of observing stations will in the future obtain information on the horizontal wave vector, which will make a quantitative analysis possible. That is the next goal of this work.

6. REFERENCES

- Blackman, R.B.; Tukey, T.W., 1958, "The measurement of power spectra," New York 1958
 Eisemann, E. 1966. *Aleinheubacher Berichte* 11 (1966), 17
 Georges, T.M.; Hooks, W.H., 1970, *J. Geophys. Res.* 75 (1970) 6295
 Schödel, J.P.; Münch, J.W., 1972, *Zeitschrift für Geophysik*, in press
 Schödel, J.P. 1972, Thesis, to be published

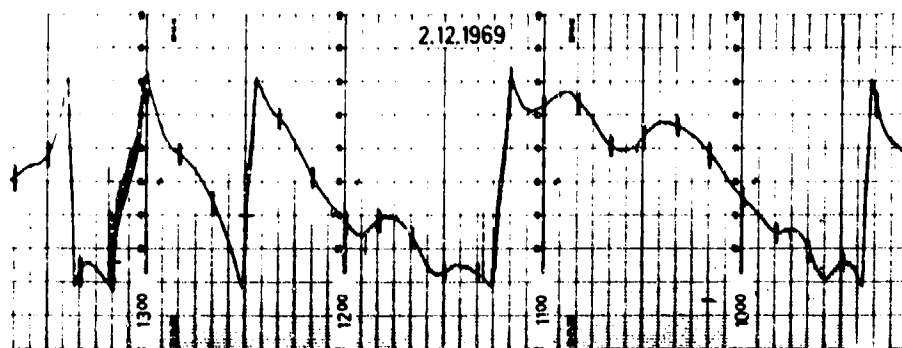


Figure 1: Faraday rotation record, December 2, 1969, Lindau/Harz. Time scale from left to right. One sawtooth is equivalent to a rotation of 180° . Superimposed are sinusoidal oscillations which are related to atmospheric gravity waves.

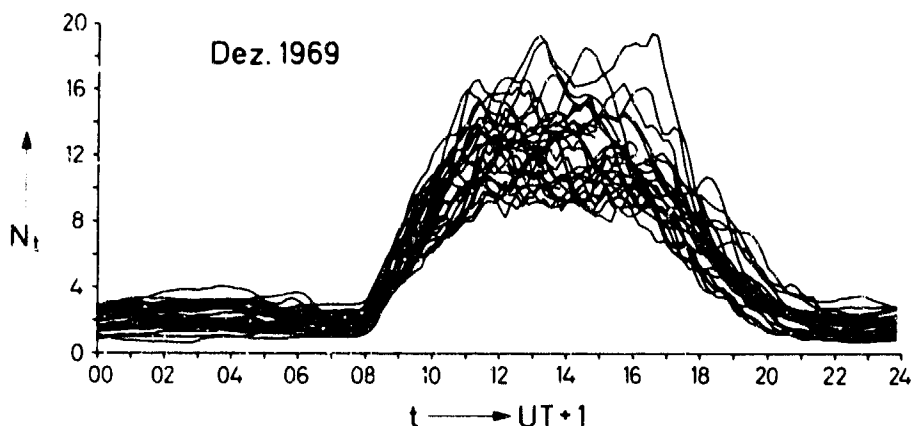


Figure 2: Total electron content N_t during December 1969. N_t in arbitrary units. Oscillations occur regularly.

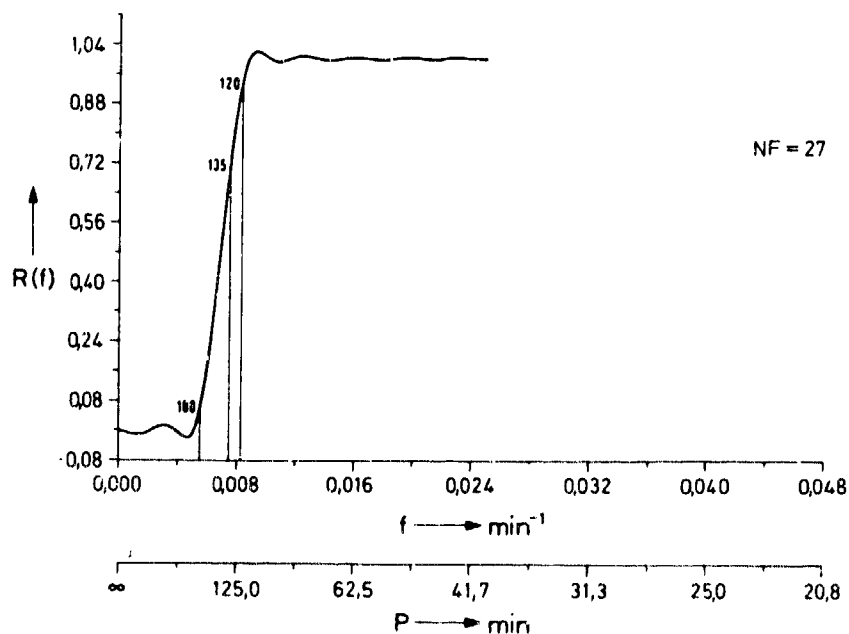


Figure 3: Numerical filter, consisting of $NF = 27$ coefficients. Response R versus frequency f and period P . The filter opens for a period $P = 180$ minutes. The 3 dB point lies at $P = 135$ minutes, and the filter is fully open, i.e. $R(f) = 1$, at $P = 120$ minutes.

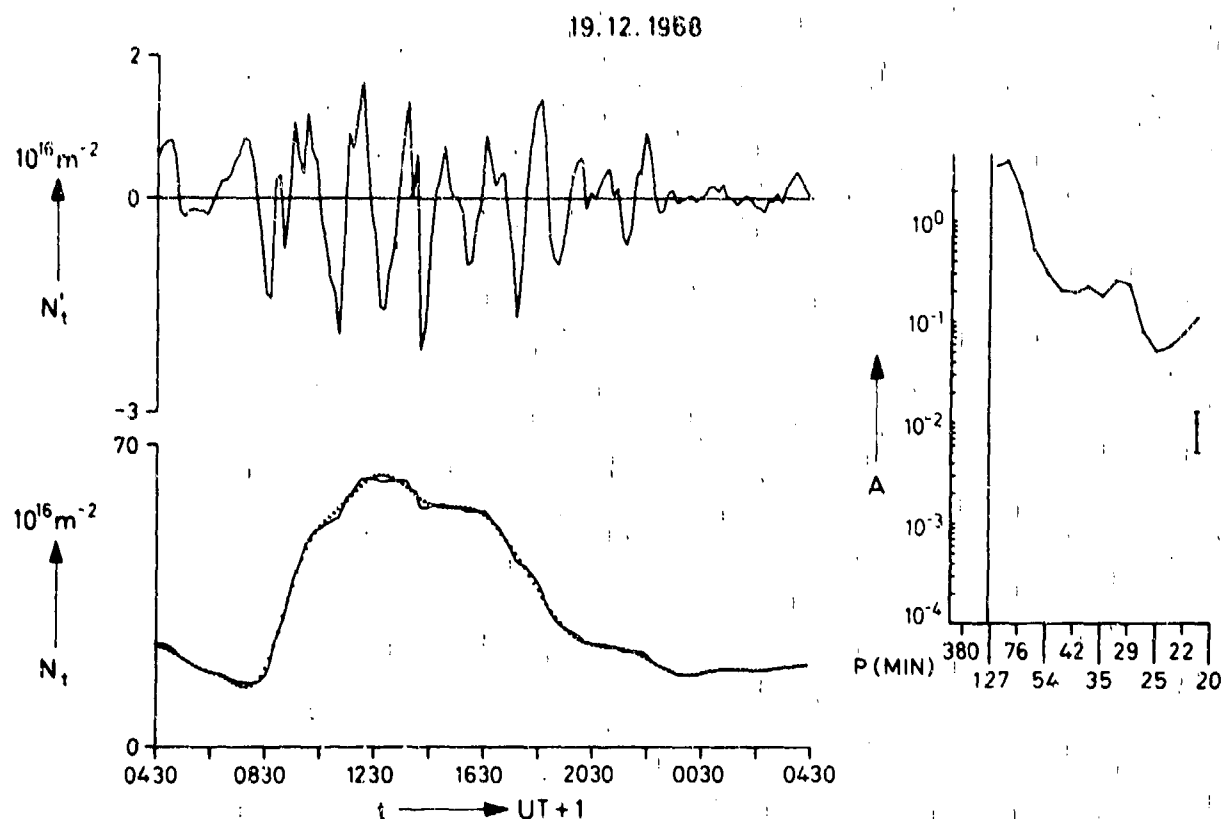


Figure 4: Data of December 19, 1968. Left hand, lower part: electron content N_t , measured curve as a solid line, smoothed curve is dotted. Left hand, upper part: high frequency part N'_t of the electron content as obtained by means of filtering. Right hand: power spectrum of N'_t . Relative amplitude A versus period P . The 90 % confidence limits are given by error bars.

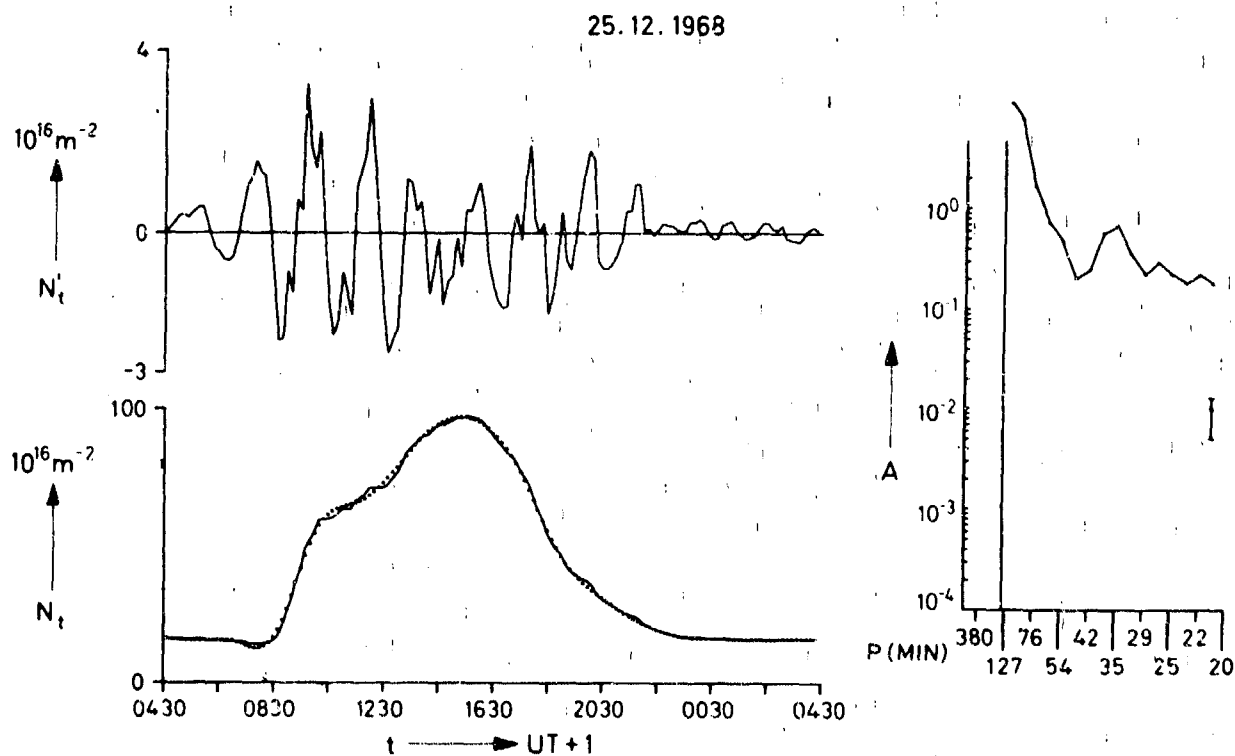


Figure 5: Data of December 25, 1968.

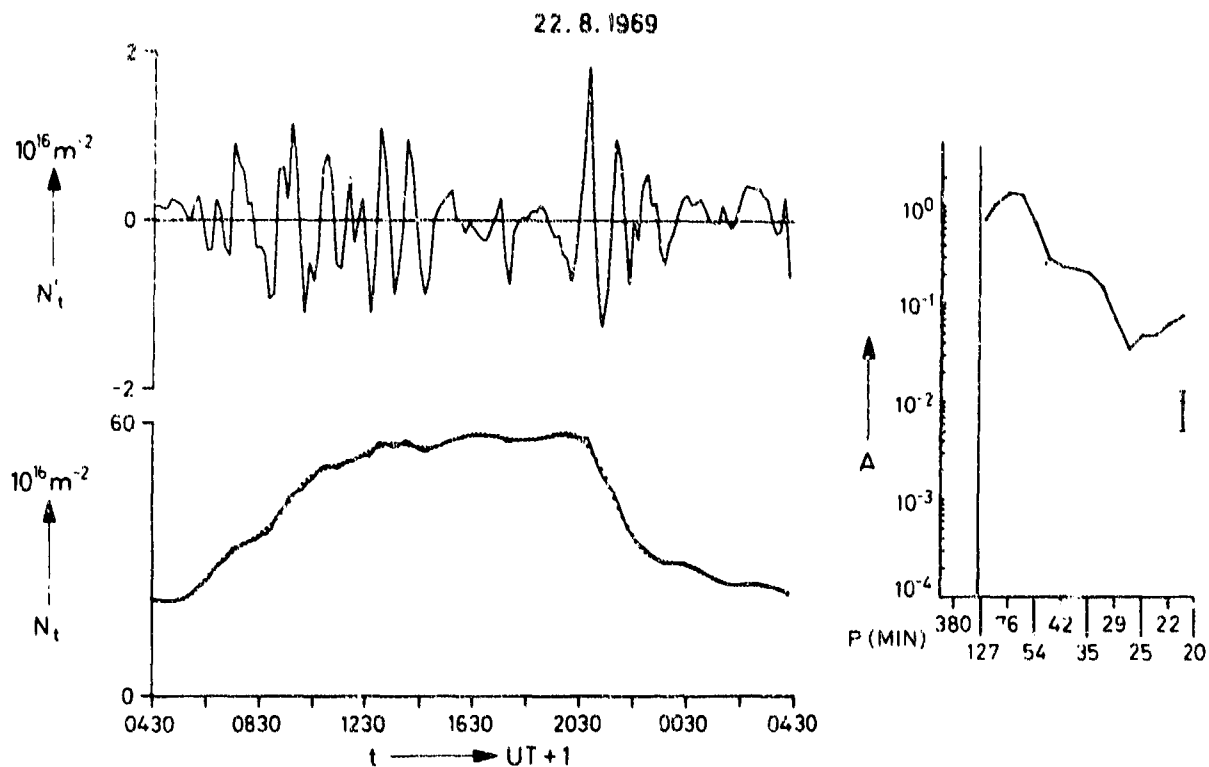


Figure 6: Data of August 8, 1969.

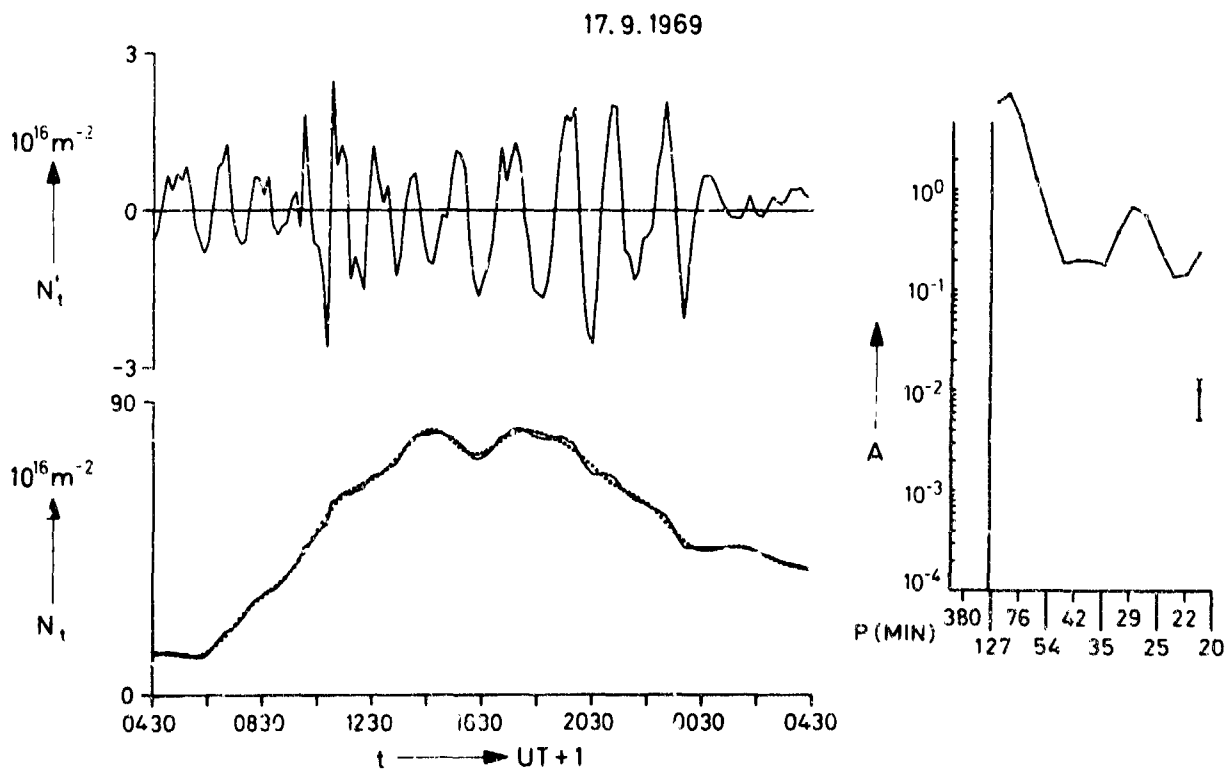


Figure 7: Data of September 17, 1969.

19.9.1969

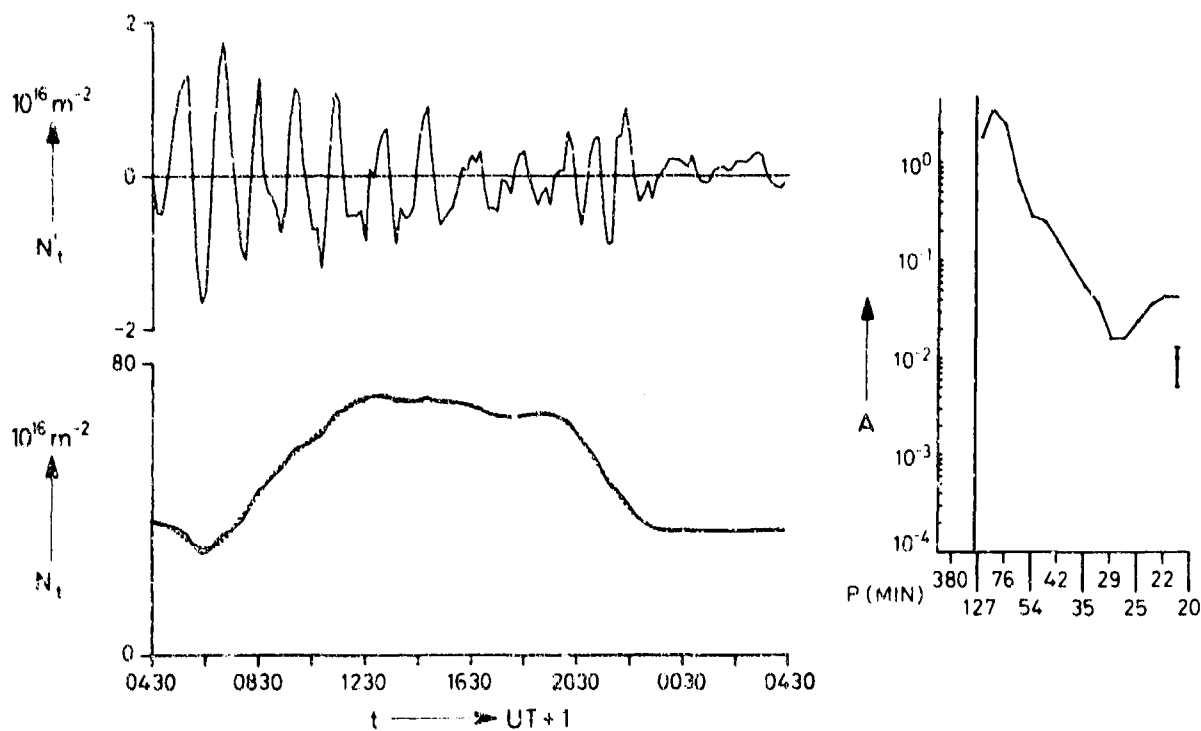


Figure 8: Data of September 19, 1969.

9.10.1969

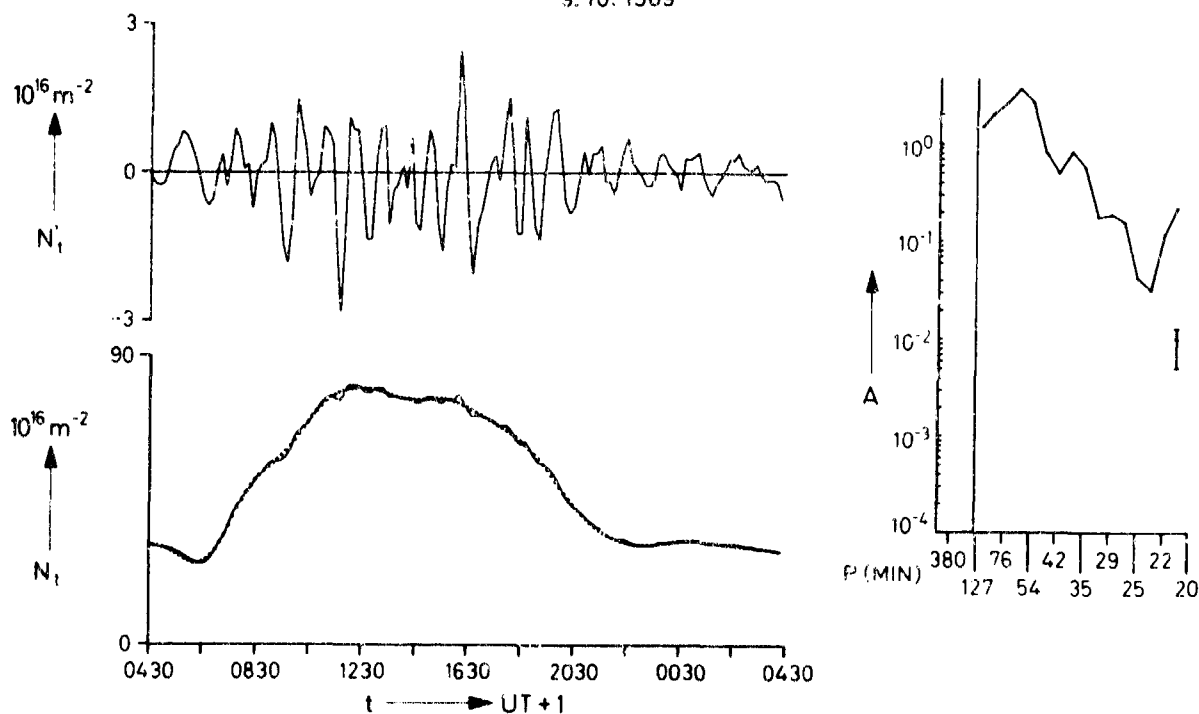


Figure 9: Data of October 9, 1969.

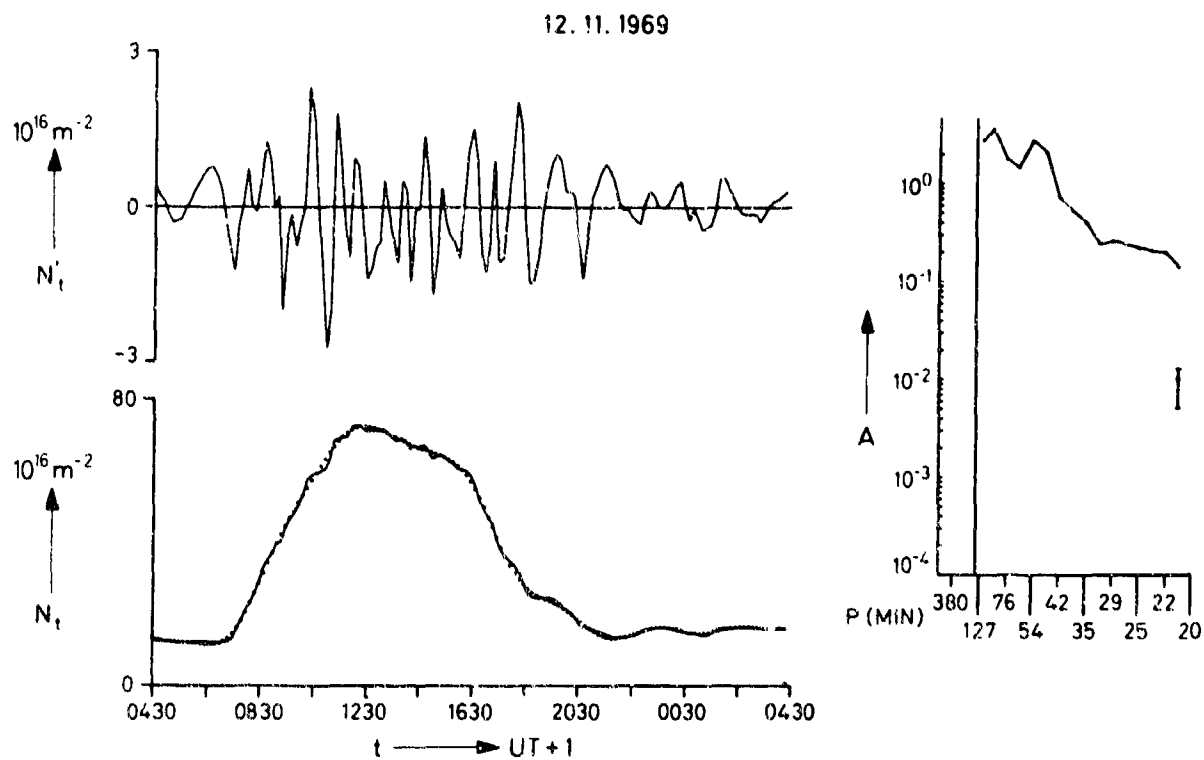


Figure 10: Data of November 12, 1969.

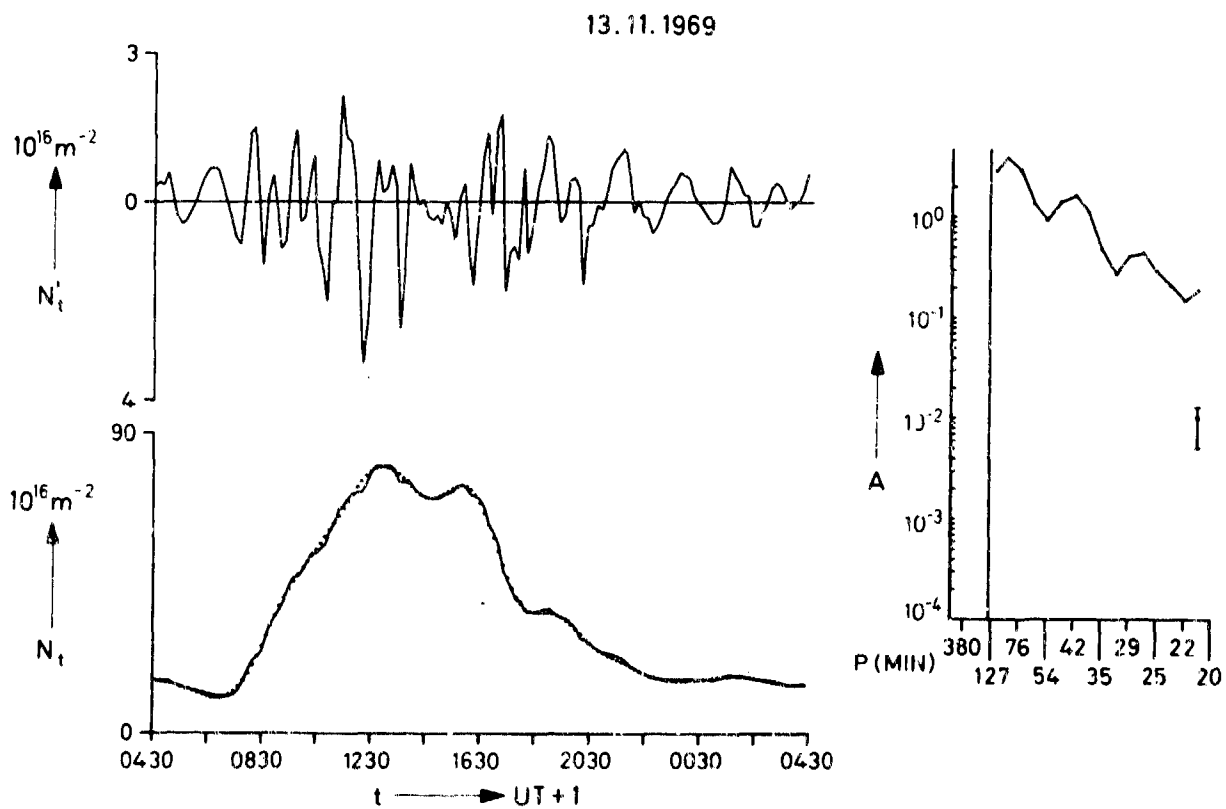


Figure 11: Data of November 13, 1969.

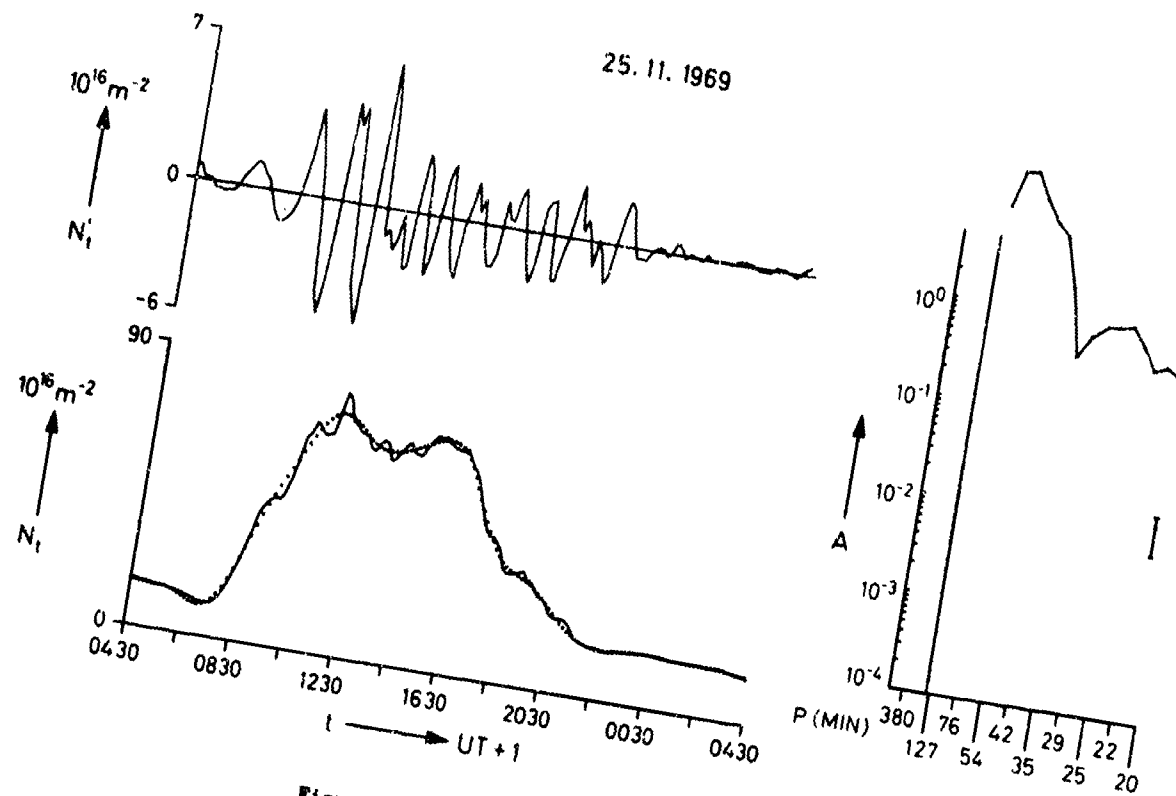


Figure 12: Data of November 25, 1969.

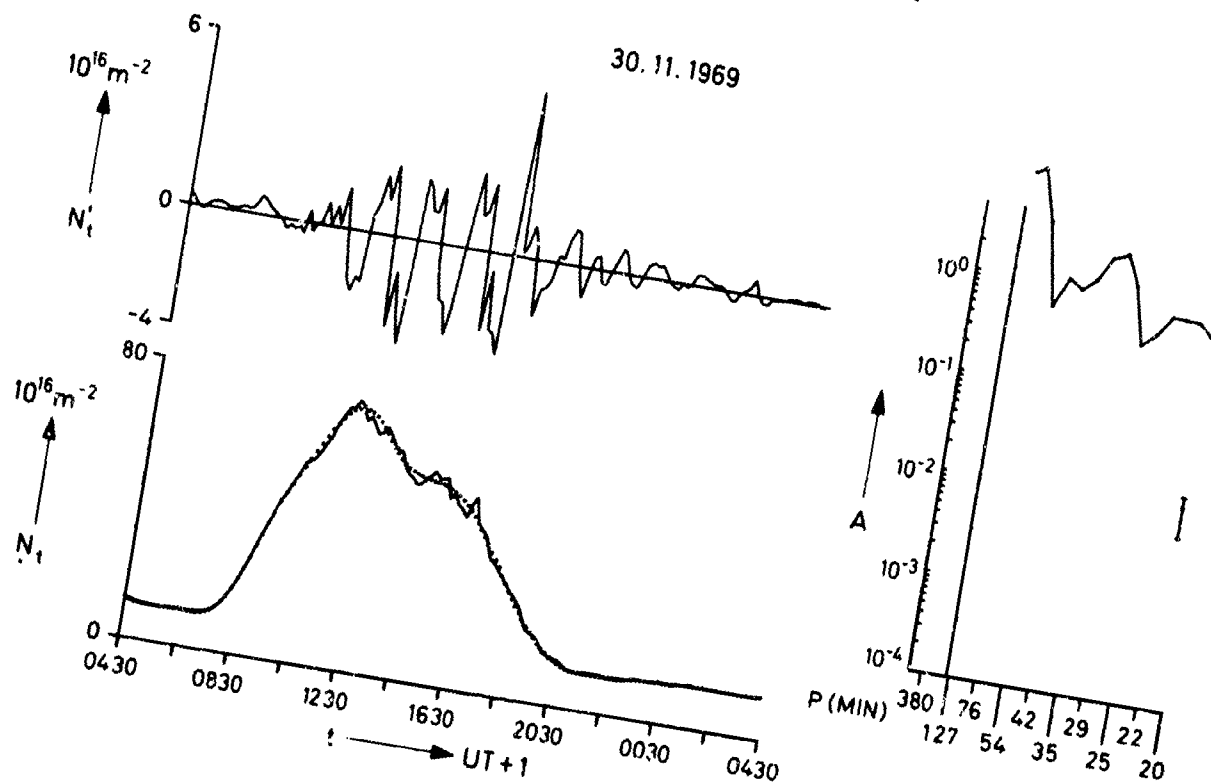


Figure 13: Data of November 30, 1969.

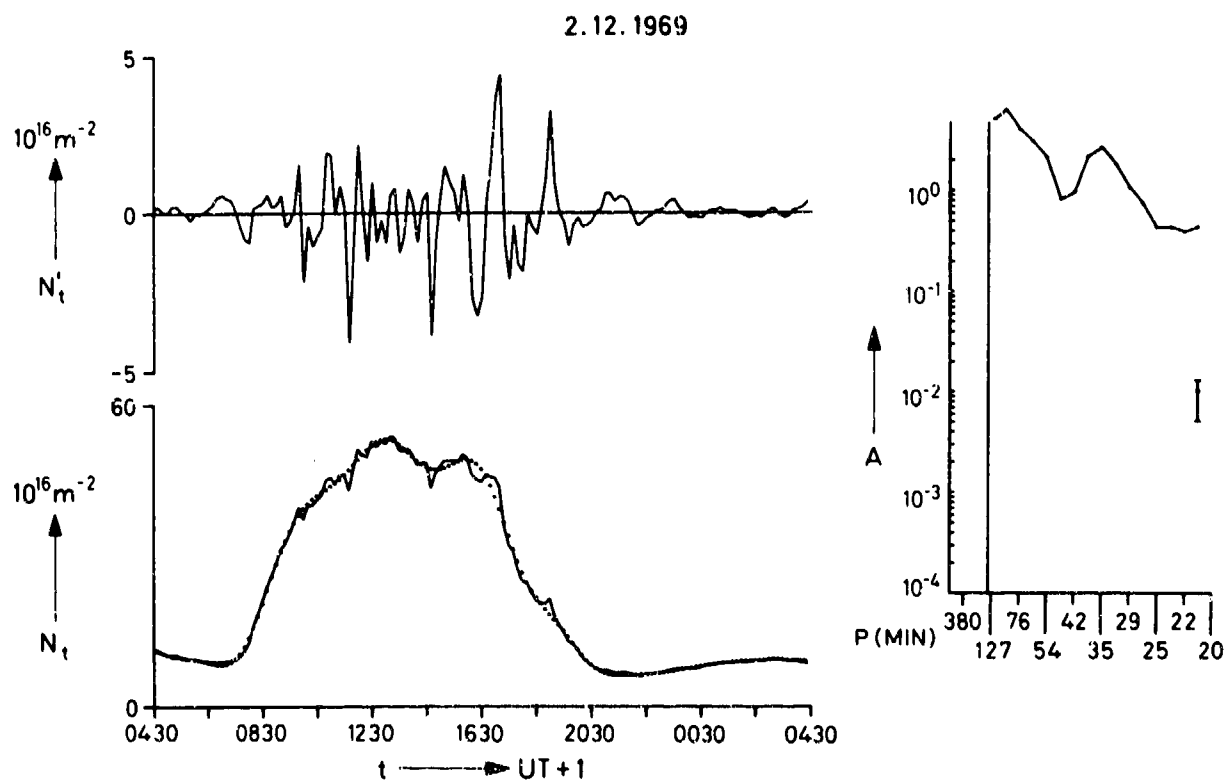


Figure 14: Data of December 2, 1969.

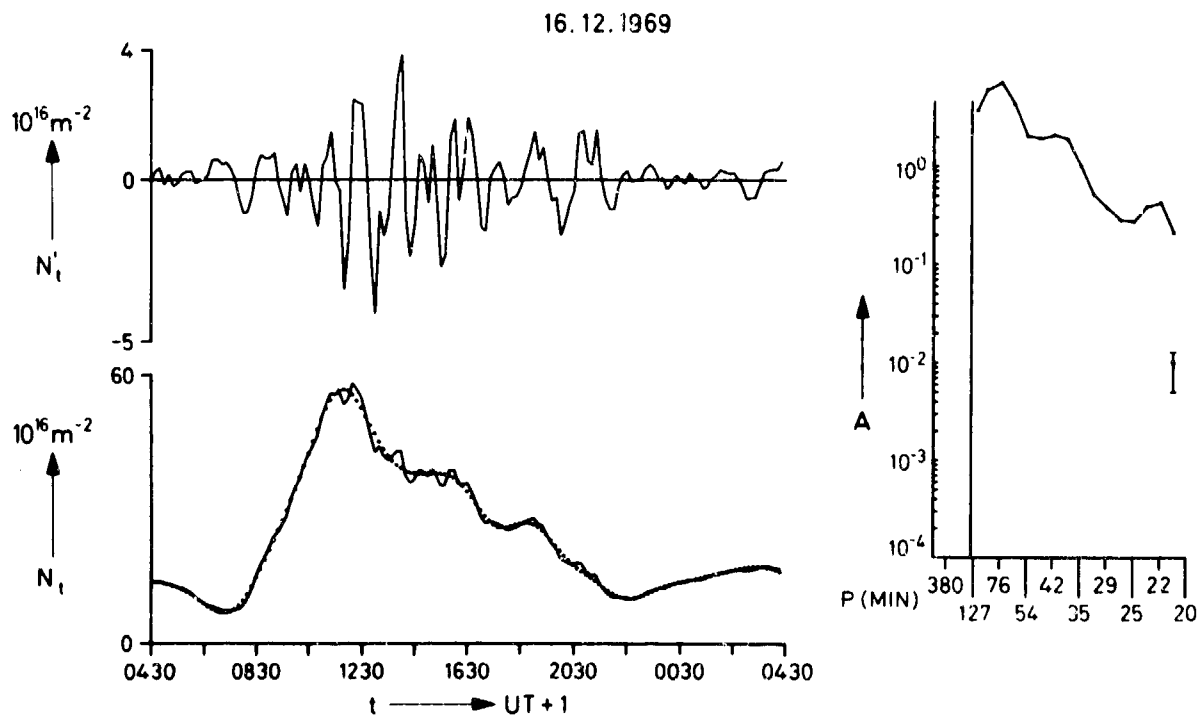


Figure 15: Data of December 16, 1969.

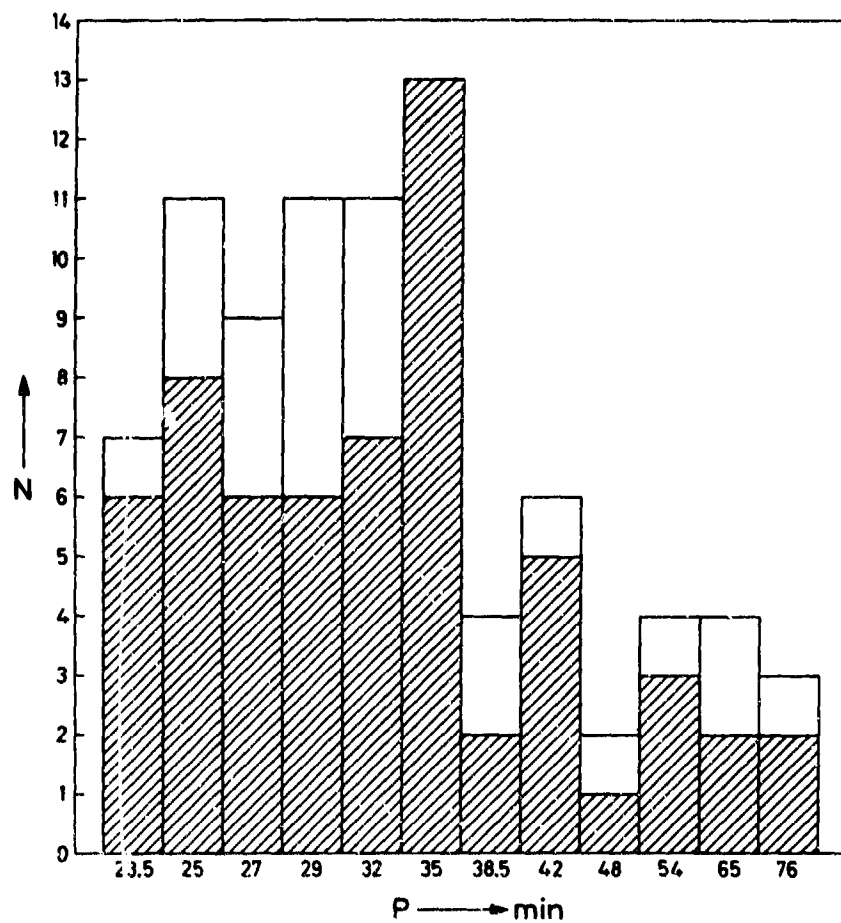


Figure 16: The rate of occurrence N of given period P as function of P . The shaded bars correspond to the significant spectral lines. If the lines are also included which lie in the neighborhood of the confidence limit, then $N(P)$ is increased by the unshaded bars.

**COMPARISON OF COMPUTED AND OBSERVED SHOCK BEHAVIOR
FROM MULTIKILOTON, NEAR-SURFACE NUCLEAR EXPLOSIONS**

by

Demetri P.Kanellakos and Raymond A.Nelson

**Radio Physics Laboratory
Stanford Research Institute
Menlo Park, California 94025
USA**

2.10

COMPARAISON DES CALCULS ET DES OBSERVATIONS PORTANT SUR LE COMPORTEMENT
DE L'ONDE DE CHOC ENGENDREE PAR DES EXPLOSIONS NUCLEAIRES DE L'ORDRE DE
PLUSIEURS KILOTONNES, PRODUITES AU VOISINAGE DU SOL.

par

D.P. Kanellakos et R.A. Nelson

SOMMAIRE

On fait des comparaisons entre les résultats de calculs hydrodynamiques numériques de la propagation, à travers l'ionosphère, de fronts de choc produits par des explosions nucléaires au voisinage du sol, et les données fournies par l'observation des perturbations ionosphériques liées à ces fronts de choc. Le but de ces comparaisons est de prouver la validité des calculs hydrodynamiques numériques aux altitudes ionosphériques.

On a pu situer l'onde de choc dans l'intervalle d'altitude compris entre 100 et 225 km grâce à une réduction à l'altitude réelle des hauteurs d'ionogrammes obtenus en incidence verticale à l'aide d'ionosondes situées à 10 km environ du lieu des explosions. Pour effectuer les calculs numériques de la propagation ascendante de l'onde de choc, on a utilisé le code hydrodynamique SHELL originellement mis au point à la "General Atomic".

Les valeurs expérimentales ont été obtenues à partir des ionogrammes correspondant aux expériences D et E de la série de tests nucléaires BUSTER-JANGLE effectuée en 1951. Les points expérimentaux et les courbes théoriques montrent clairement tous deux une accélération du front d'onde de choc au-dessus de 100 km d'altitude. Les valeurs obtenues d'une part expérimentalement, d'autre part grâce aux calculs, concordent à quelques kilomètres près pour le front d'onde de choc primaire, bien que l'on ne connaisse pas les paramètres atmosphériques exacts au moment des essais.

L'exposé sera suivi d'un petit film de 16 mm montrant les perturbations ionosphériques observées à Kusaie (sur l'équateur magnétique) à la suite d'une forte explosion nucléaire de faible altitude ayant eu lieu à 740 km au nord de ce point.

COMPARISON OF COMPUTED AND OBSERVED SHOCK BEHAVIOR FROM MULTIKILOTON, NEAR-SURFACE NUCLEAR EXPLOSIONS*

Demetri P. Kanellakos and Raymond A. Nelson
Radio Physics Laboratory
Stanford Research Institute
Menlo Park, California 94025
USA

SUMMARY

Comparisons are made between numerical hydrodynamic calculations of the propagation through the ionosphere of shock fronts arising from near-surface nuclear explosions and experimental observations of the ionospheric disturbances associated with these shock fronts. The purpose of these comparisons is to provide a test of the validity of numerical hydrodynamic calculations at ionospheric heights.

The location of the shock wave in the height range from 100 to 225 km was obtained from true-height reduction of vertical-incidence ionograms obtained by ionosondes situated about 10 km from the location of the explosions. Numerical calculations of the upward propagation of the shock wave were made using the SHELL hydrodynamic code that was originally developed at General Atomic.

Experimental values were obtained from ionograms taken for the Dog and Easy events of the 1951 BUSTER-JANGLE nuclear test series. Both the experimental points and the theoretical curves clearly show an acceleration of the shock front at altitudes above 100 km. There is agreement between experimental and calculated values to within a few km for the primary shock front in spite of a lack of knowledge of the exact atmospheric parameters at the times of the tests.

A brief 16-mm film will be presented, showing ionospheric disturbances at Kusaie (on the magnetic equator) following a large, low-altitude nuclear explosion 740 km to the north.

1. INTRODUCTION

When a nuclear detonation takes place in the earth's atmosphere, a shock wave propagates outward from the point of detonation. Initially, this shock wave weakens rapidly due to geometric spreading and dissipative processes in the shock front, but the portion of the shock wave that propagates nearly vertically upward weakens less rapidly than the rest of the wave because of the nearly exponential decrease in atmospheric density with increasing altitude. At later times, when the effect of geometric spreading is greatly reduced, the portion of the wave that propagates upward from a near-surface burst can actually increase in strength (Mach number) at ionospheric heights. The progress of this shock wave through the ionosphere can be detected by means of an ionosonde.

Calculations of the progress of this shock wave in a realistic atmosphere can be made on a high-speed computer using the SHELL code (GREENE, J. S., Jr., and WHITAKER, W. A., 1968).

Late-time effects for a number of yields and altitudes (below 30 km) have been studied, using the SHELL code. As an example of the calculations that have been made, two plots of relative pressure for a 4-MT sea-level burst are reproduced in Figure 1 (GREENE, J. S., Jr., and WHITAKER, W. A., 1968). Figure 1(a) shows that the primary shock front has reached about 133 km height directly above the explosion point 300 sec after the burst time. By 400 sec [Figure 1(b)] the primary shock has moved to about 245 km, and a secondary disturbance is clearly evident between 100 and 120 km. In addition, the primary shock front has become bell-shaped.

As a check on the validity of making such hydrodynamic calculations at ionospheric heights, comparisons are made with experimental data obtained from the BUSTER-JANGLE nuclear test series, which was conducted in Nevada during 1951 (DANIELS, F. B., and HARRIS, A. K., 1951).[†] Daniels and Harris have made observations of this type on a number of nuclear tests (DANIELS, F. B., and HARRIS, A. K., 1958; DANIELS, F. B., et al., 1960).

* The work reported in this paper was supported by the Advanced Research Projects Agency of the Department of Defense under Air Force Contracts F33657-68-C-1147 and F33657-70-C-0090.

† We wish to thank these authors for lending us their original records.

2. COMPARISON OF EXPERIMENTAL AND THEORETICAL RESULTS

2.1 DOG Event

The Dog event of the BUSTER-JANGLE nuclear test series was a multikiloton explosion that took place on 1 November 1951 at 0730 local time at an altitude of approximately 430 m. It was an air burst over Nevada where the ground elevation is approximately 1300 m above sea level. Observations of the shock-induced ionospheric disturbances were made by a vertical-incidence ionosonde located roughly 10 km south of the place of detonation.

Figure 2 presents selected ionograms for the Dog event showing the undisturbed ionosphere and the arrival and propagation of the primary shock front and a secondary disturbance. The first ionogram in this figure was taken approximately 15 min before the time of the detonation, T_0 , (at -15:00).^{*} Both ordinary- and extraordinary-ray traces are visible for the F region. The second ionogram was taken after T_0 but before the shock wave had arrived at ionospheric heights. On the remaining ionograms, arrows indicate the location and time of the disturbance produced by shock waves. Cusps in the F-layer traces (beginning with the +6:54 ionogram) are indicated by solid arrows for the primary shock and dashed arrows for the secondary disturbance; cusps in the trace for the ordinary ray are indicated by an O and cusps in the extraordinary-ray trace are indicated by an X.

At +5:31 the first evidence of the shock wave is given by the second echo from the E region, as shown in the third ionogram of Figure 2(a). The E-region disturbance broadens and moves to higher altitudes in the next two ionograms. At +6:54 the shock arrived at the F region, as indicated by a new cusp at 3 MHz. On succeeding ionograms new cusps are seen on both ordinary and extraordinary traces as the primary shock moves up through the F region. The secondary disturbance is first seen at 7:54 on the last ionogram of Figure 2(a). Both disturbances are seen to move through the F layer in the ionograms of Figure 2(b). True-height curves for selected ionograms of the Dog event are shown in Figure 3. Comparison of the data using ordinary- and extraordinary-ray cusps to obtain the plasma frequency (and thereby the true height) at the shock front are given in Table 1. It is to be noted that there is generally good agreement between the ordinary frequency, f_o , at the disturbance, and the equivalent frequency $(f_x^2 - f_x f_H)^{1/2}$ obtained from the extraordinary frequency, f_x , at the disturbance.

Table 1

COMPARISON OF IONOGRAM CUSP FREQUENCY FROM ORDINARY RAY
WITH EQUIVALENT FREQUENCY DERIVED FROM EXTRAORDINARY RAY FOR DOG EVENT

Primary Disturbance					Secondary Disturbance				
Local Time	f_o cusp (MHz)	f_x cusp (MHz)	$(f_x^2 - f_x f_H)^{1/2}$ (MHz)	$f_o - (f_x^2 - f_x f_H)^{1/2}$ (MHz)	Local Time	f_o cusp (MHz)	f_x cusp (MHz)	$(f_x^2 - f_x f_H)^{1/2}$ (MHz)	$f_o - (f_x^2 - f_x f_H)^{1/2}$ (MHz)
7:10	3.4	4.2	3.42	-0.02					
7:25	3.8	4.5	3.72	+0.08					
7:40	4.4	5.1	4.33	+0.07					
7:55	5.15	5.9	5.14	+0.01					
8:03	5.6	6.3	5.54	+0.06	8:02	3.1	3.8	3.01	+0.09
8:10	6.2	6.8	6.05	+0.15	8:08	3.2	3.9	3.11	+0.09
8:18	6.6	7.4	6.65	-0.05	8:16	3.3	4.0	3.21	+0.09
8:26	7.0	7.7	6.96	+0.04	8:24	3.5	4.2	3.42	+0.08
					8:41	3.8	4.5	3.72	+0.08
					9:03	4.5	5.2	4.43	+0.07
					9:18	5.2	5.9	5.14	+0.06
					9:35	6.0	6.6	5.85	+0.15
					9:48	6.6	7.2	6.45	+0.15

* Times are given in minutes and seconds before the detonation (-) and after the detonation (+).

Figure 4 presents a comparison of the theoretical and experimental positions of the two fronts as a function of time for the Dog event. There is rather good agreement for the primary shock, with relatively poor agreement for the secondary disturbance.

2.2 Event Easy

The Easy event of the BUSTER-JANGLE series was also a multikiloton explosion, and took place on 5 November 1951 at 0830 local time at an altitude of about 400 m.

Selected vertical-incidence ionograms taken during the Easy test are shown in Figure 5. Some of the relevant true-height-reduction curves are presented in Figure 6.

Analysis of the Easy ionograms parallels exactly the analysis of the Dog event. The first two ionograms of Figure 5(a) were taken before the primary shock wave reached the ionosphere. E-region perturbations are seen on the next two ionograms. On the remaining ionograms of Figure 5(a) the primary disturbance is observed in the F region on the ordinary-ray trace only at +6:42 and +6:50, and then on both ordinary- and extraordinary-ray traces in the remaining ionograms. Propagation upward of both the primary and secondary disturbances is observed in Figure 5(b). True-height curves for several ionograms of the Easy event are shown in Figure 6.

The frequency of the cusp caused by the shock waves in the ordinary ray is compared with the corresponding frequency derived from the cusp in the trace for extraordinary ray in Table 2. In Figure 7 a comparison is made of the theoretical and experimental positions of the primary and secondary fronts. The agreement for the primary front is not as good as for the Dog event, and there is poor agreement for the secondary front. Parametric studies indicate that the discrepancy between the observations and the calculations cannot be attributed entirely to an inadequate knowledge of the temperature profile of the atmosphere above the Event Easy, or to the cell sizes used in the numerical calculations. Perhaps the accuracy which may be attributed to the interpretation of the ionosonde data should be reconsidered.

Table 2

COMPARISON OF IONOGRAM CUSP FREQUENCY FROM ORDINARY RAY
WITH EQUIVALENT FREQUENCY DERIVED FROM EXTRAORDINARY RAY FOR EASY EVENT

Primary Disturbance					Secondary Disturbance				
Local Time	f_o cusp (MHz)	f_x cusp (MHz)	$(f_o^2 - f_x f_H)^{1/2}$ (MHz)	$f_o - (f_x^2 - f_x f_H)^{1/2}$ (MHz)	Local Time	f_o cusp (MHz)	f_x cusp (MHz)	$(f_o^2 - f_x f_H)^{1/2}$ (MHz)	$f_o - (f_x^2 - f_x f_H)^{1/2}$ (MHz)
6:57	3.8	4.5	3.72	+0.08					
7:06	4.1	4.8	4.03	+0.07					
7:21	4.6	5.2	4.43	+0.17					
7:36	5.4	6.0	5.24	+0.16					
7:51	6.4	7.1	6.35	+0.05	7:50	3.3	4.1	3.31	-0.01
					8:05	3.7	4.4	3.62	+0.08
					8:20	4.0	4.8	4.03	-0.03
					8:36	4.4	5.1	4.33	+0.07
					9:06	5.6	6.2	5.44	+0.16
					9:37	7.1	7.8	7.06	+0.04

3. CONCLUSION

It is concluded that numerical hydrodynamic calculations can provide a valid representation of shock-wave-propagation at ionospheric heights.

REFERENCES

DANIELS, F. B., and HARRIS, A. K., 1951, unpublished 3' mm film records from continuous sweep ionograms, Institute for Exploratory Research/United States Army Signal Radio Propagation Agency, Fort Monmouth, New Jersey.

DANIELS, F. B., and HARRIS, A. K., 1958, "Some Effects of Strong Blast Waves upon the Ionosphere," Fall Meeting of URSI at Pennsylvania State University.

DANIELS, F. B., et al., 1960, "Vertically Traveling Shock Waves in the Ionosphere," J. Geophys. Res., Vol. 65, pp. 1848-1850.

GREENE, J. S., Jr., and WHITAKER, W. A., 1968, "Theoretical Calculations of Travelling Ionospheric Disturbances by Low-Altitude Nuclear Explosions," Proceedings of the Symposium on Acoustic-Gravity Waves in the Atmosphere, T. M. Georges, Ed., U.S. Government Printing Office.

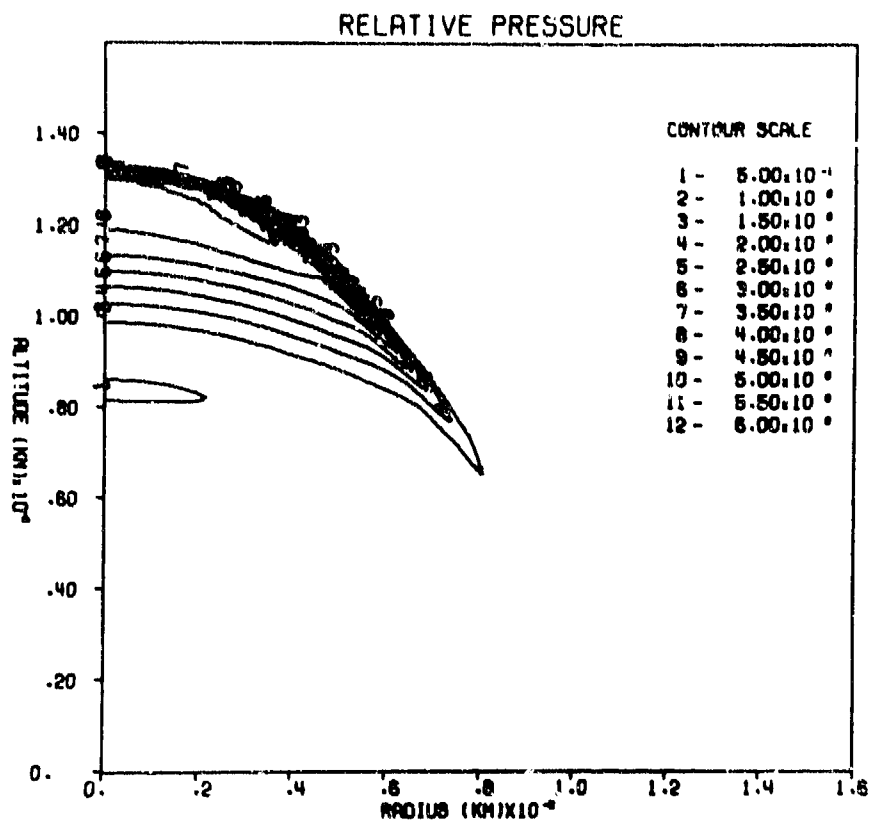


FIGURE 1(a) SHELL CODE CALCULATION OF RELATIVE PRESSURE 300 s AFTER RELEASE OF 4 MT AT SEA LEVEL

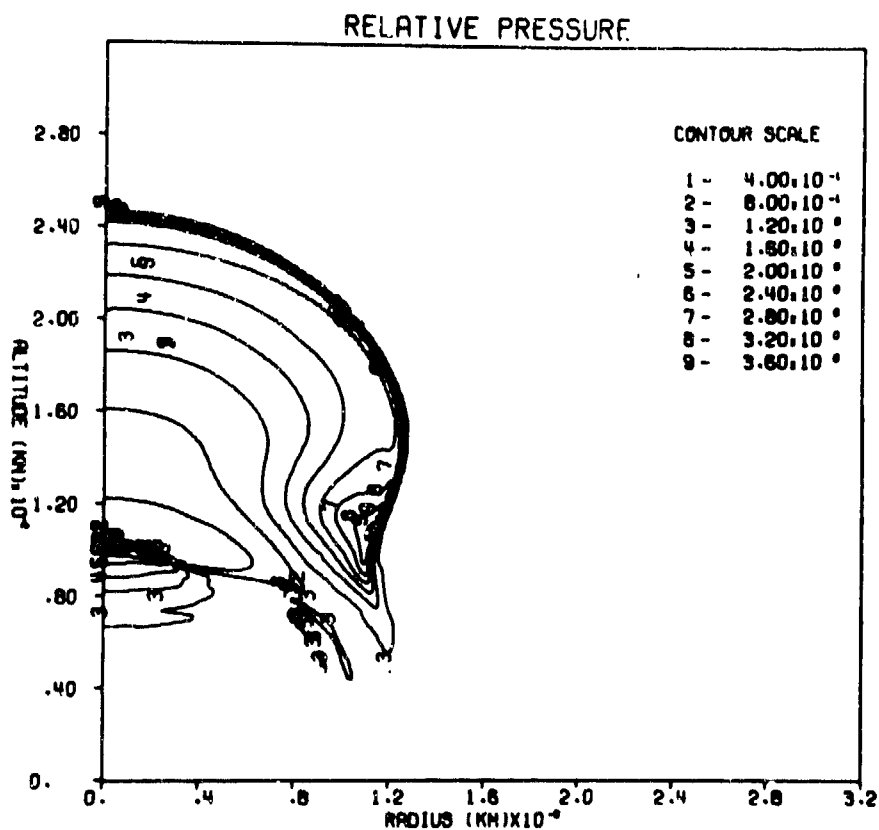


FIGURE 1(b) SHELL CODE CALCULATION OF RELATIVE PRESSURE 400 s AFTER RELEASE OF 4 MT AT SEA LEVEL

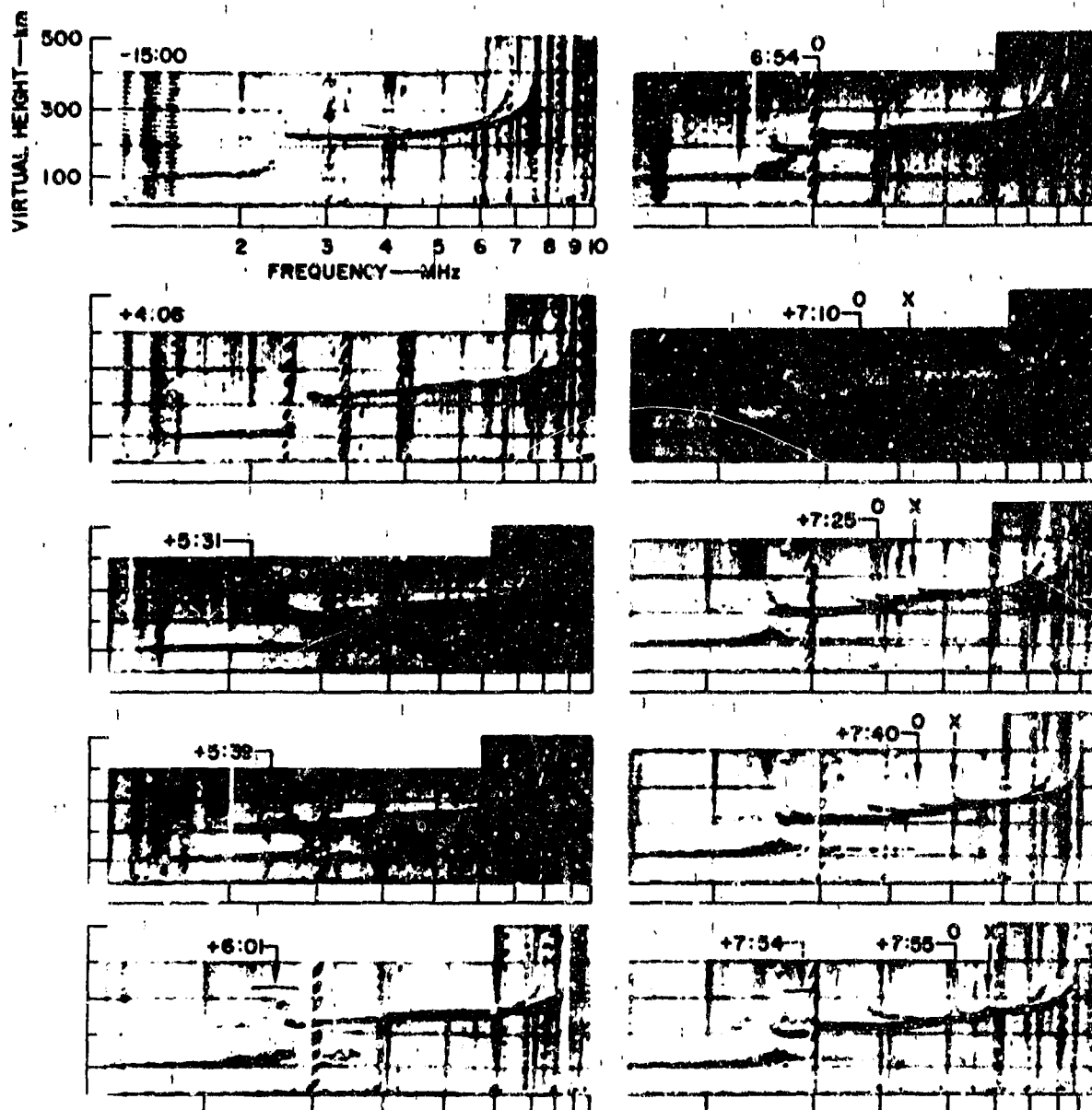


FIGURE 2(*) SELECTED IONOGRAMS FOR DOG EVENT OF BUSTER-JANGLE SERIES

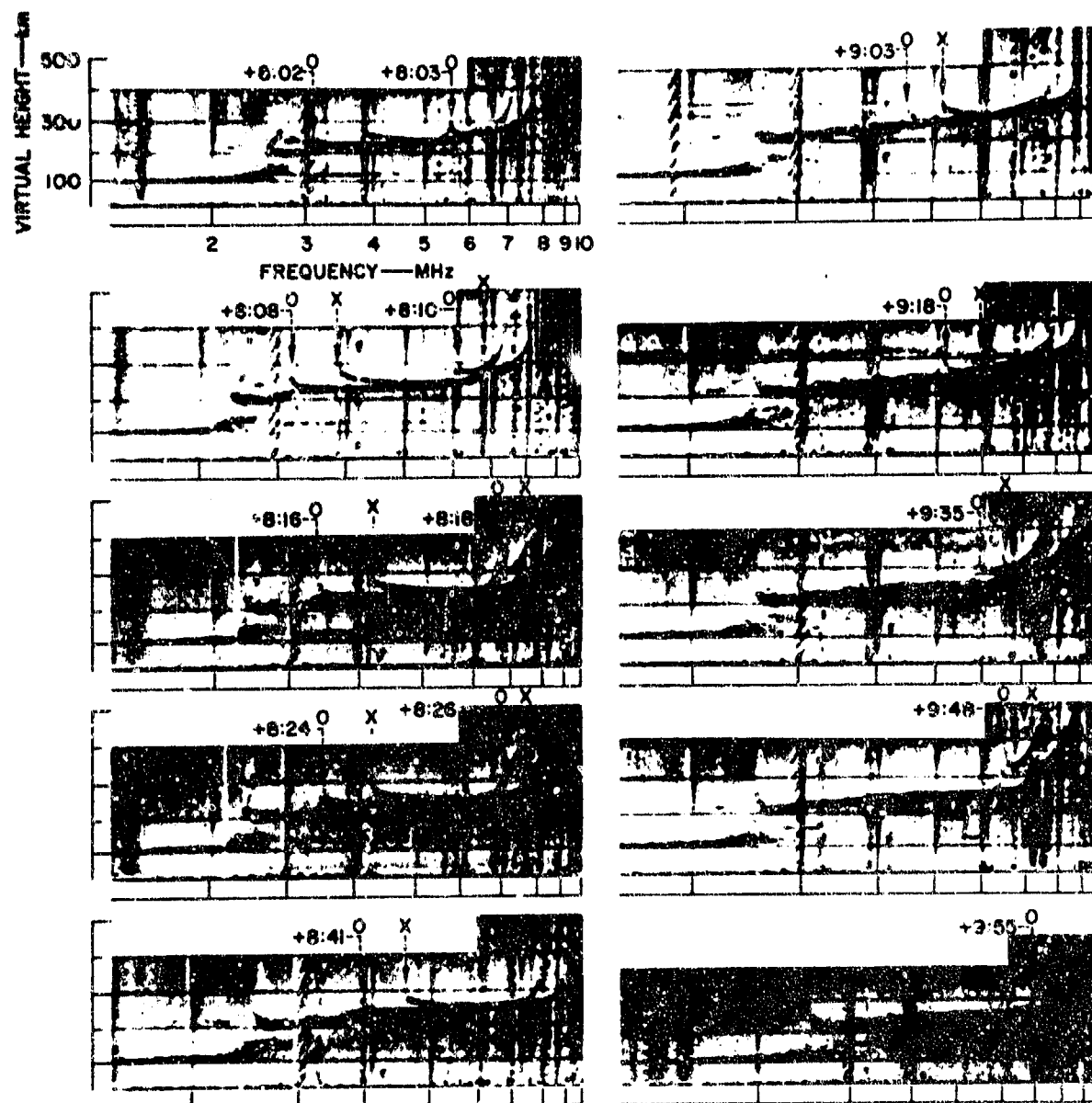


FIGURE 2(b) SELECTED IONOGRAMS FOR DOG EVENT OF BUSTER-JANGLE SERIES

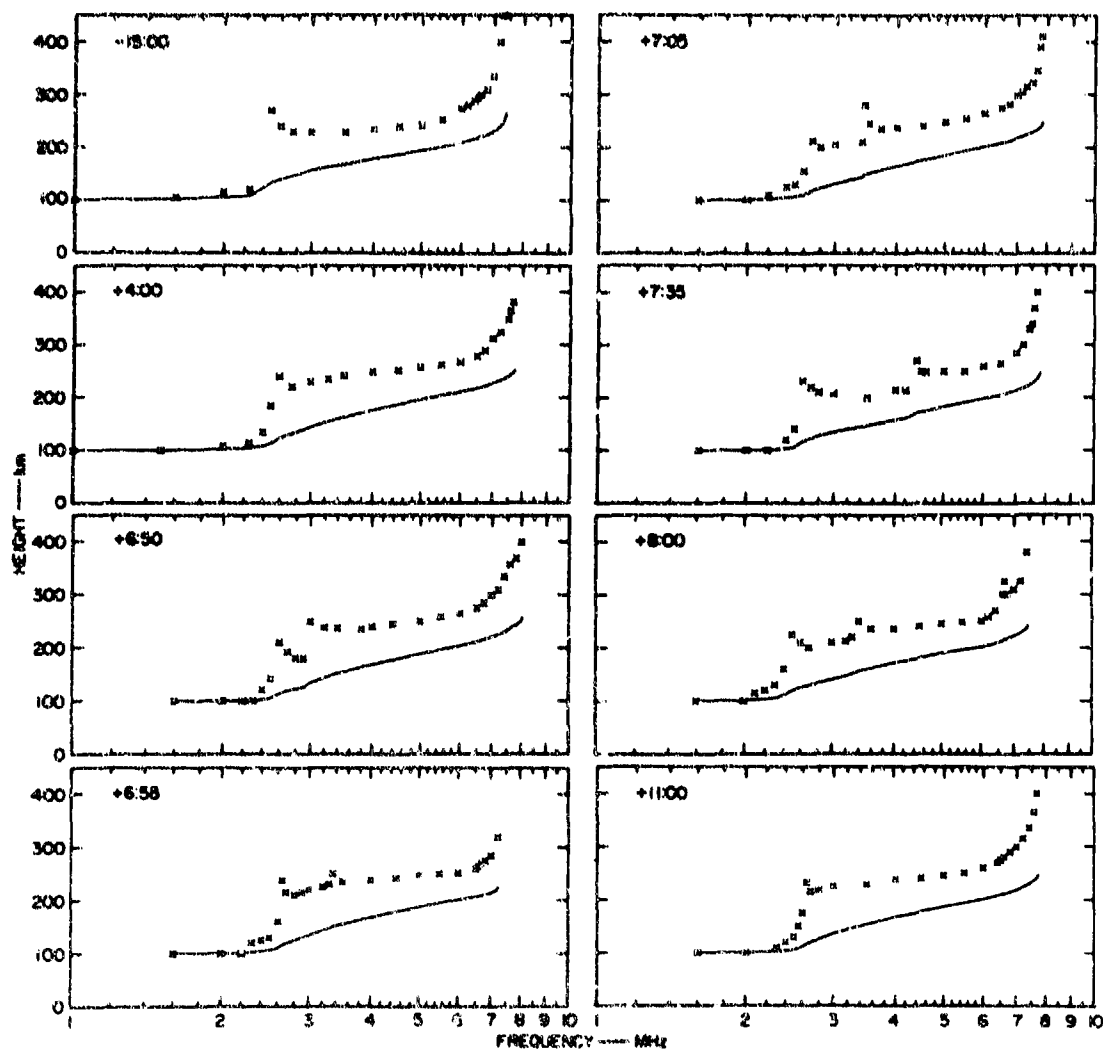


FIGURE 3 TRUE-HEIGHT REDUCTION (solid curves) FOR SELECTED IONOGRAMS (x's) FROM DOG EVENT

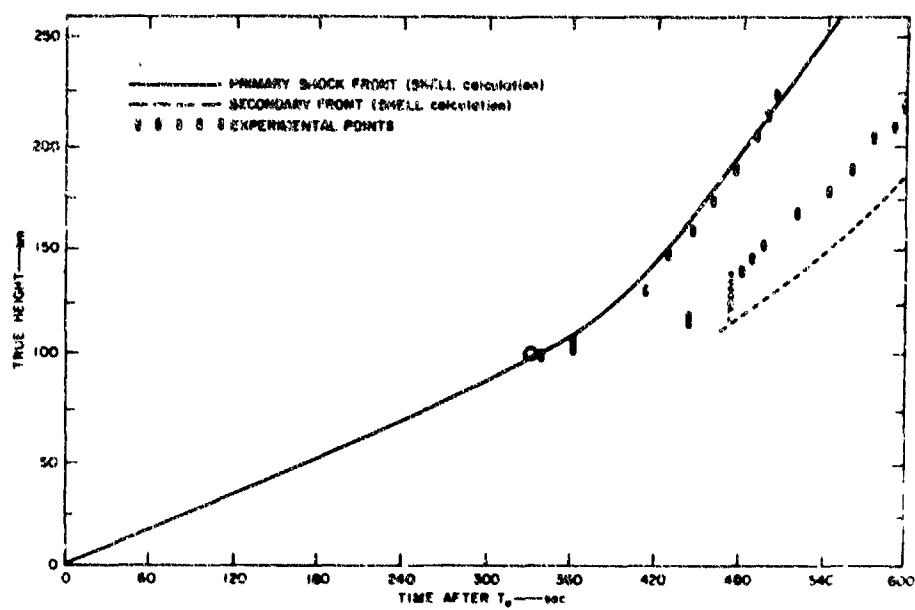


FIGURE 4 COMPARISON BETWEEN EXPERIMENTAL POINTS AND THEORETICAL CURVES FOR DOG EVENT

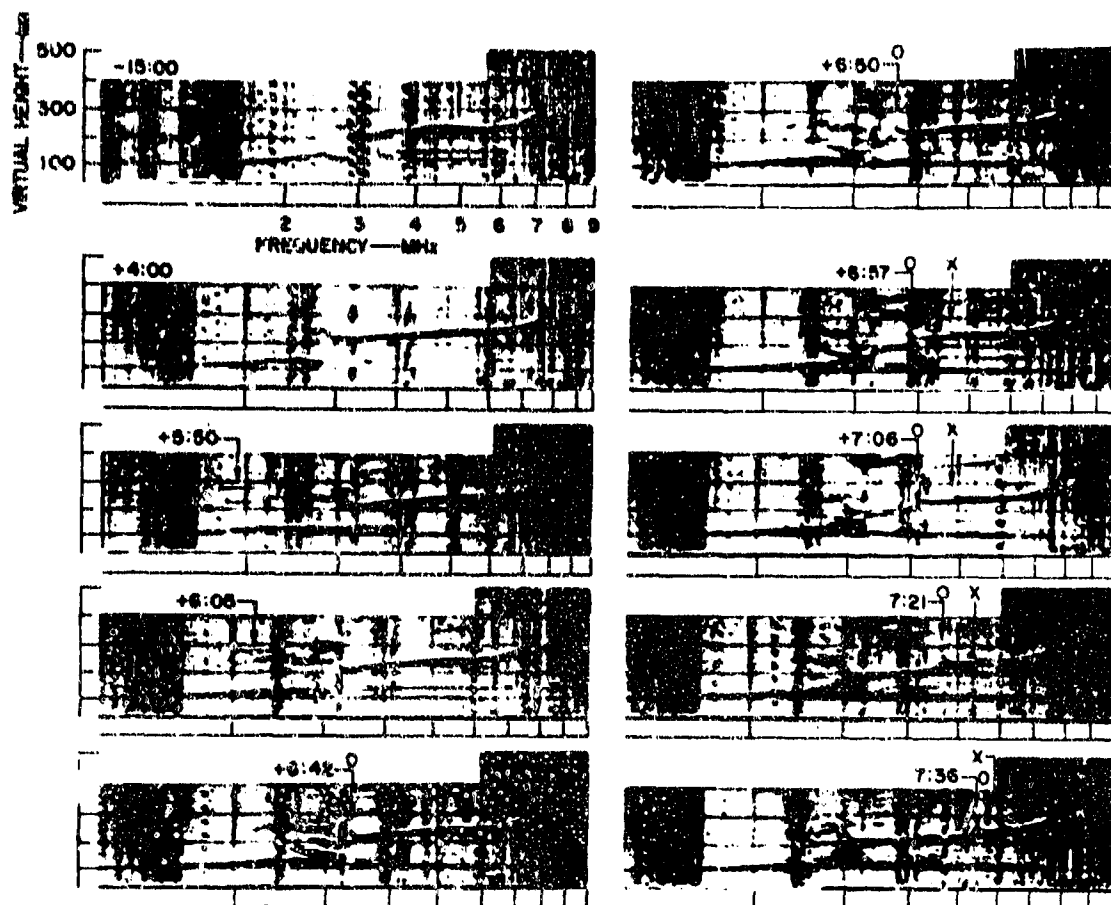


FIGURE 5(a) SELECTED IONOGRAMS FOR EASY EVENT OF BUSTER-JANGLE SERIES

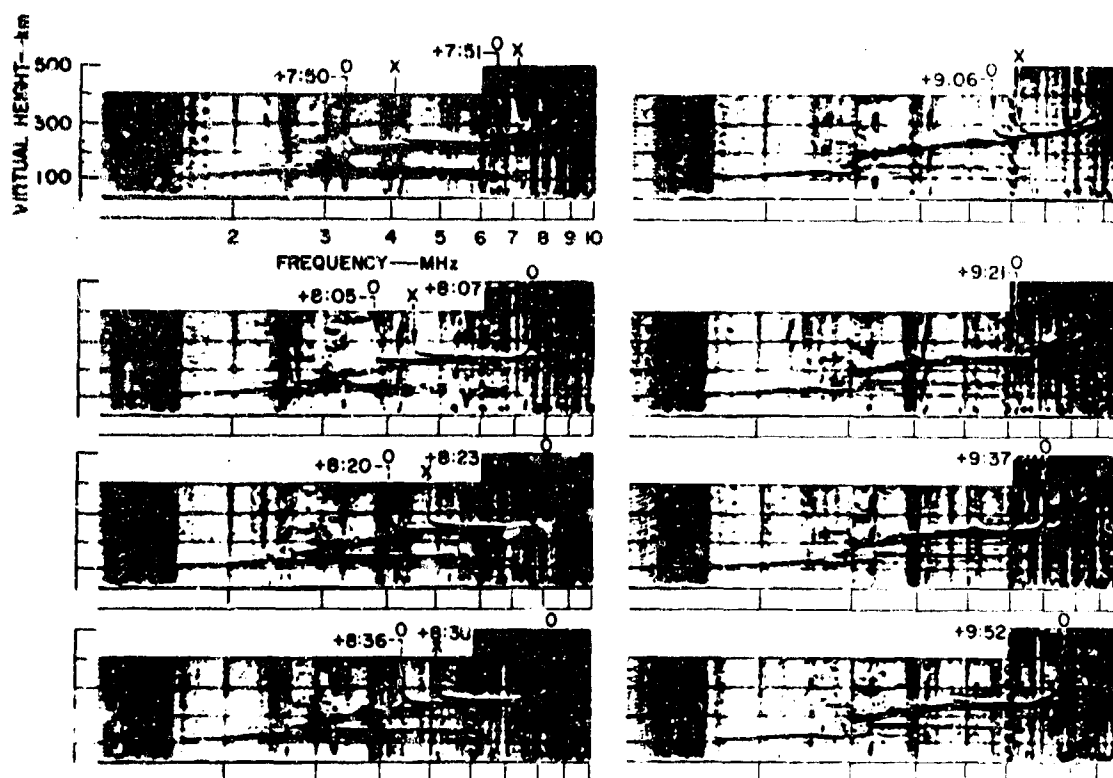


FIGURE 5(b) SELECTED IONOGRAMS FOR EASY EVENT OF BUSTER-JANGLE SERIES

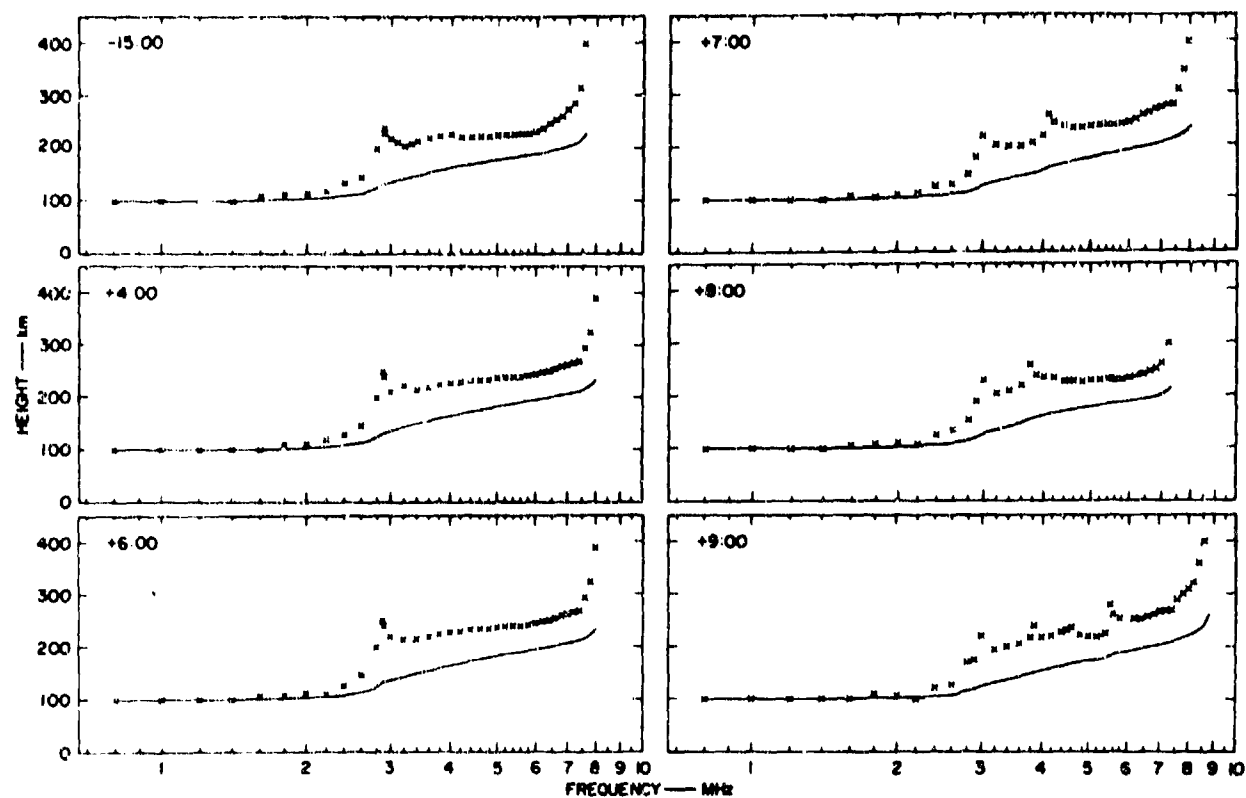


FIGURE 6 TRUE-HEIGHT REDUCTION (solid curves) FOR SELECTED IONOGRAMS (x's) FOR EASY EVENT

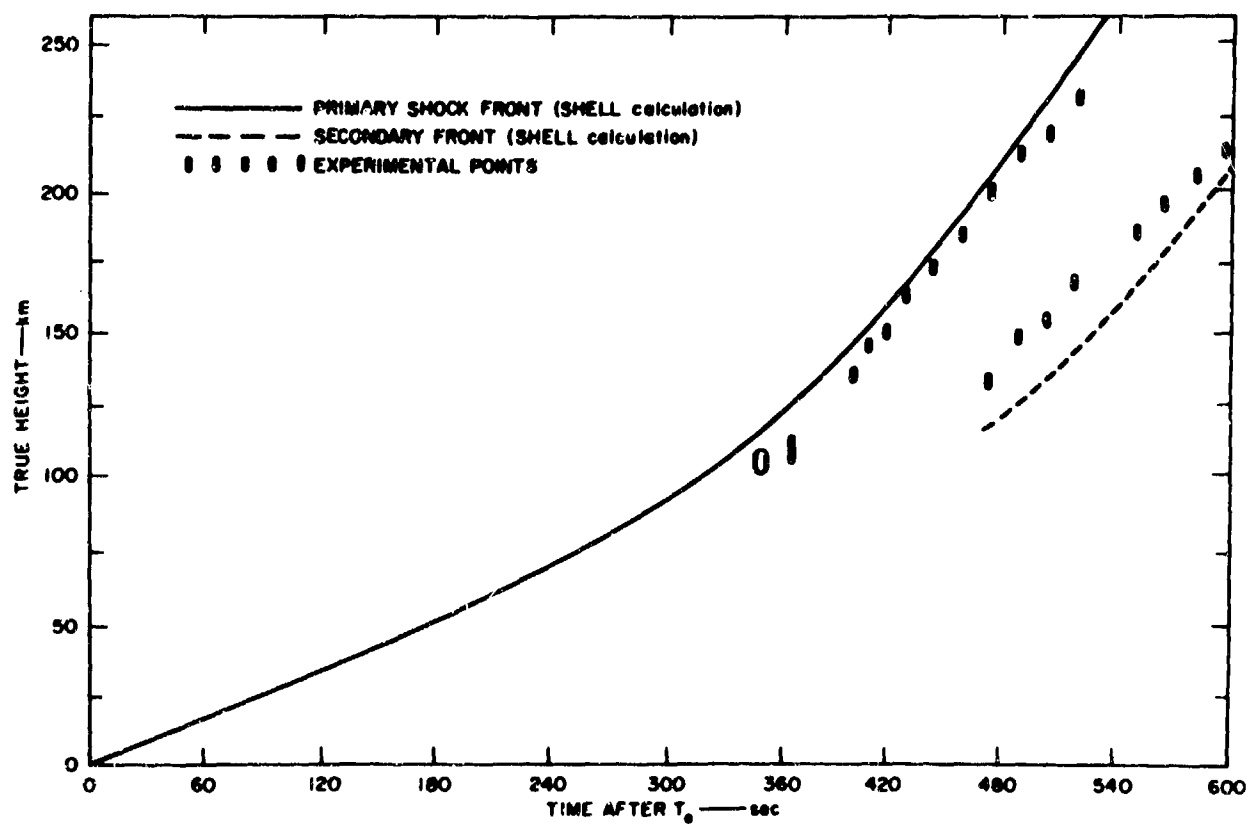


FIGURE 7 COMPARISON BETWEEN EXPERIMENTAL POINTS AND THEORETICAL CURVES FOR EASY EVENT

Discussions on the papers presented in Session II
(Coupling between the ionized atmosphere and the neutral atmosphere disturbed by acoustic gravity waves)

Discussion on paper 13 : "Justification for the use of Hines Asymptotic relations for traveling ionospheric disturbances" by N.J.F. CHANG.

Dr. C.H. LIU : Could you comment on the filtering effects of the lossy mechanism ?

Dr. N. CHANG : The technique described in my paper neglects losses of any kind, so I do not feel that I can comment on the filtering effects of losses at this time. However the predominance of internal gravity waves with 20 minute periods in agreement with that predicted by my simple analysis would lead me to believe that the neglect of losses in the current analysis is justified.

Dr. J. KLOSTERMEYER : The observational results given by Klostermeyer (1969) for 12/13 February 1961 seem to be doubtful. As has been shown by Klostermeyer (Numerical calculation of gravity wave propagation in a realistic thermosphere, JATP. 1972, in press), no agreement could be found with full wave solutions of the hydrodynamic equations.

Dr. N. CHANG : I agree with Dr. Klostermeyer's comments on the 12/13 February event. I can only add that, had this event been excluded, the last column in table 1 would indicate that every event considered had a propagation angle near the maximum permitted.

Dr. K. DAVIES : The effects of neutral winds are crucial to the propagation of gravity waves because the horizontal trace speed of the waves is comparable with the wind speed. While a uniform horizontal wind does not affect the direction of propagation, it affects the frequency as seen by an observer moving with the medium. This has the effect of altering the effective Brunt-Väisälä frequency as observed on the ground. For example, there is abundant evidence in the literature that the lowest cut-off period τ_c for gravity waves is near 5 min. For a stationary atmosphere this cut-off would be the Brunt-Väisälä period τ_B which is about 15 min. in the F. region. Taking the horizontal speed V_h as 150 m/sec we find that the maximum wind speed U is :

$$U = V_h \left(1 - \frac{\tau_c}{\tau_B} \right) = 100 \text{ m/sec.}$$

Dr. CHANG : There is no question that winds can have a major effect on the propagation of internal gravity waves and indeed if F-region wind profiles were available, winds can easily be included in my analysis. However, provided that the horizontal winds do not exceed the horizontal trace speed (Doppler shifted frequencies always non-zero and positive), my conclusion regarding the asymptotic behavior of internal gravity waves will remain unchanged even if winds are included. This follows since under the above condition winds and temperature have a similar effect on the propagation of the gravity waves. Hence, the effects of a horizontal wind field can be included in a modified temperature profile. The new temperature profile will alter the curves shown in figure 2, but the proximity of ϕ to ϕ_c in the thermosphere will remain.

Discussion on paper 14 : "Full wave calculations of electron density perturbations caused by atmospheric gravity waves in the F_2 layer" by J. KLOSTERMEYER.

J. TESTUD : Le progrès qu'apporte le calcul de Klostermeyer (sur l'interaction onde de gravité-ionisation dans la région F), consiste en ce que l'auteur tient compte de l'influence en retour des oscillations de l'ionisation sur la propagation de l'onde de gravité qui les a provoquées. Cet effet avait été négligé par les précédents auteurs. Cependant, dans sa communication Klostermeyer n'a pas présenté de comparaison entre des résultats de calcul où cet effet est pris en compte, et des résultats où cet effet est négligé ; de sorte que l'on a du mal à apprécier l'importance réelle de cet effet. Nous lui suggérons d'effectuer une telle comparaison.

Dr. KLOSTERMEYER : The coupling of gravity wave induced ion density variations to the wave propagation is determined by the wave induced perturbation of the neutral-ion collision frequency, ν_1 , which is roughly proportional to n_{i1} . The effect of this coupling can be estimated by comparing the ion drag term $\nu_1 (u_1 - u_{i1})$ being normally included into the equation of neutral gas motion with the term $\nu_1 (u_1 - u_{i1})$ which must be added in the presence of neutral background winds. The second term has the same order magnitude as the first one and may even be larger. Therefore it cannot be neglected if the effect of ion drag shall be properly taken into account. This is true especially for waves with periods of about 1 hour and more, because then ion drag is the most effective dissipative process.

Discussion on paper 15 : "Atmospheric pressure waves at Brisbane and their association with certain ionospheric and solar events", by G.G. BOWMAN.

Dr. G. SILLKE : The example (Fig. 1) of the records of AGWs in Brisbane is much like what we get in Hamburg with an array of microbarographs. Especially the "night time - fine weather" cases seem to be ducted AGWs in tropospheric low-level or ground based ducts (temperature inversions), that under such conditions nearly always are formed. I think that the AGW effect (origin and propagation) then might be confined only to the lowest atmospheric layers.

Dr. P.L. GEORGE on behalf of G. BOWMAN : I would agree that the locally observed AGW effects may be evident largely in the lower atmospheric layers, I would suggest that Dr. Bowman has presented considerable evidence for the association of local AGWs not associated with frontal activities with ionospheric effects at remote locations in the sub-auroral regions.

Dr. C. WILSON : Was an array of microphones used so that you could be sure the pressure fluctuations were due to propagating waves ?

Dr. P.L. GEORGE : I think only single microphones were used at various latitudes.

Dr. K. DAVIES : The observations of Dr. Bowman suggest that the correlation between gravity waves and spread F may be the result of ionospheric heating. Observations at Boulder show that spread F is nearly always produced by heating of the F region with a powerful transmitter (50 megawatts) on a frequency near the F2 ordinary wave critical frequency (Utlaut W.F. 1970, J.G.R. Nov.).

Discussion on paper 16 : "Medium scale travelling ionospheric disturbances attributed to unstable tropopause winds at mid latitude", by G.B. GOE.

Prof. R.K. COOK : When the jet stream blows over the eastern seaboard of the U.S.A. it appears to oscillate (vertically) and generate acoustic gravity waves having oscillation periods 300-600 sec. These waves are observable at an infrasonic station having its microphones at ground level, and have a very substantial pressure amplitude of about 10 N/m². May I suggest that the jet stream oscillations might radiate acoustic gravity waves propagating upwards toward the ionosphere, and that it would be worthwhile to look for ionospheric motions particularly when the jet stream blows in the neighborhood of the reflection area for the electromagnetic probing waves.

Dr. G. LERFALD on behalf of G. GOE : I agree wholeheartedly with your suggestion that it would be worthwhile to investigate the relationship between jet stream activity and ionospheric motions. A systematic study involving infrasonic sensors and ionospheric HF Doppler sounders is being started at Boulder and hopefully some useful data will be obtained before long.

Dr. K. DAVIES : 1.- This subject of ionospheric disturbances and weather is one that deserves to be pursued and the present paper is a step in the right direction.

2.- In looking for correlations between weather and gravity wave effects in the ionosphere it should be remembered that gravity waves do not travel vertically. Thus one should look at the ionosphere a distance of perhaps a 1 000 km. from the source.

Dr. G. LERFALD : The propagation path by which an AGW travels from the troposphere to ionospheric heights, will depend to a great extent on the vertical wind profile it encounters at intervening heights. It is no doubt possible that energy from a specific source point could arrive at the ionosphere as far as 1 000 km. away from the overhead point, but I would think a displacement of a few hundred kms. to be more typical. The localization of a plausible AGW source from tropopause wind maps also has uncertainties of the order of hundreds of kilometers and the limitations imposed by having only two maps available per day. The implication I meant to give by saying that ionospheric effects may be localized is that one might expect them to be largely caused by jet stream sources within about 500 km of the ionospheric measurement point.

Discussion on paper 17 : "Generation of anomalous ionospheric oscillations by thunderstorms", by C.A. MOO and A.D. PIERCE.

Dr. C.H. LIU : I shall make a comment on the idea of resonant wave interaction. In the acoustic-gravity wave case, the conservation of ω and the real part of k can be satisfied, but the imaginary part of k can not satisfy the resonant condition. Of course, your computation did not really use the wave-wave interaction approach.

Dr. Ch. MOO : The model here presented is concerned with the weak emission of acoustic wave by the non linear interaction of gravity wave velocity fields confined to a finite volume. The dynamical theory of wave-wave interaction as, for example, presently employed in upper ocean wave theory, is not used. There are common ideas, however, which follow from the geometrical structure of the dispersion equation.

Dr. K. DAVIES : 1.- The spectra of ionospheric disturbances generally contain two peaks. One peak has a period near 4.6 min the other around 3.5 min. The acoustic cut-off period of the tropopause over Oklahoma during 1969 and 1970 is 4.6 ± 0.1 min. Any acceptable theory must explain these two peaks.

2.- In 1970 spaced transmitter measurements in Oklahoma City were used to locate the sources. Good agreement was found between the calculated source positions and the thunderstorm positions given by weather radar records.

Dr. Ch. MOO : Using the model of generation we propose the acoustic wave frequency is the sum of two gravity wave frequencies. Generally a severe weather system has several convective cells which might generate internal waves with different frequencies, so that any acoustic waves generated by interaction of gravity wave fields would have multiple frequencies. I think calculation of source positions, by for example ray tracing, can only give the general effective source region, since usually we have only average ideas of the temperature and wind profiles, especially in the mesosphere and thermosphere, to make the calculations.

Dr. G. STILKE : We have several years of continuous records of micropressure variations in Hamburg with an array of microbarographs. With most thunderstorms we get nearly sinusoidal pressure oscillations with pe-

riods of several minutes, superimposed on the longer pressure changes.

Dr. Ch. MOO : We would very much appreciate receiving copies of the microbarograms showing the pressure oscillations in period range of minutes. In records I have seen, these oscillations are frequently suppressed by the large pressure changes of frontal activity.

Prof. H. VOLLAND : The limited bandwidth of infrasound waves with periods between about 2 and 5 min observed at F2 layer heights can be explained alternatively by the filtering effect of the thermosphere, filtering out on the one hand vertically propagating waves beyond the acoustic cut-off frequency and on the other hand high frequency waves due to dissipation effects according to molecular viscosity. This high frequency cut-off period is proportional to η/p , where η is the coefficient of viscosity and p the mean pressure. Therefore the period increases with height and has reached about 2 min at F2 layer heights. These wave periods between 2 and 5 min are expected only in that height range. (Volland, "Attenuation of acoustic-gravity waves within the thermosphere" Forschungsbericht der Astronomischen Institut der Universität Bonn, Nr. 4/69, Bonn, 1969.)

Dr. Ch. MOO : A similar suggestion of filtering was also made by Georges (1968). However, since this pass band varies with height in the ionosphere, I find it hard to believe that the relatively high Q of the ionospheric oscillations at all HF radio reflection heights is due to filtering. The quasi-monochromatic nature of the oscillations must be characteristic of the source in the troposphere.

Discussion on paper 18 : "A phenomenological investigation of amplitude and spectra of gravity waves" by P.J. SCHÖDEL.

Dr. K. DAVIES : The spectrum of gravity waves, as observed by total content measurements, is affected by the direction of the ray path with respect to the magnetic field. This has been shown by Georges and Hooke. Would you please comment on this as it affects the spectra of the Lindau measurements.

Dr. J. SCHÖDEL : Computations show that the measurements in Lindau/Harz are not affected.

General Discussion

Dr. Ch. WILSON : I would like to suggest that it is important to relate the observation of TID's to specific auroral substorms to test the ideas of C. Hines, W. Blumen and Chimonas that either Lorentz force or Joule heat loss in auroral electrojets will generate gravity waves. If auroral data are not available then the magnetic index AE should be used because this is the best magnetic indication of auroral substorm activity.

Dr. D. NIELSON : Regarding the coupling of the neutral and ionic gases during the passage of a gravity wave, there are quite definitive observations available from the 1962 U S Nuclear test series. The data are in the form of vertical and oblique incidence ionograms from equipment especially distributed for the tests. A very consistent picture of the effects on the ion gas of the neutral wave emerges from these data. While the published data from these tests does not adequately provide the detailed scaling that would make a test of theory convenient, any coupling theory or scaling relation must be consistent with the general empirical picture as presented in Ref 1 and 2. That is that equatorward-directed waves produce a decrease in layer critical frequency during the first half cycle whereas poleward waves produce an increase. The changes are at times substantial with decreases as much as a factor of two in critical frequency and increases both north of the burst and south of the equator as much as 4 or 5 times. Thus the wave effects are very clear and offer observational data on vertical, geographical, and temporal variations. More on this will be shown later.

Ref. 1 : Lomax and Nielson, J.A.T.P., vol. 30, P.P. 1033-1050 (1968).

Ref. 2 : Kanellakos, AGARD PROCEEDINGS N. 33, "Phase and Frequency Instabilities", p.p. 439-453, July 1970.

Dr. D.P. KANELLAKOS : The same situation is met during low-altitude explosions, as during the high altitude cases mentioned by Mr. NIELSON. A discussion for large yield nuclear explosions near the earth's surface at the Pacific (Johnston Island) and Novaya Zemlya is given in the paper by D.P. Kanellakos.

("Spatial and Temporal Model of the TID from a low-altitude Nuclear Explosion" pp. 439-452 in "Phase and Frequency Instabilities in Electromagnetic Waves Propagation" AGARD Conf. Proc. N. 43.)

J. TESTUD : Je suis d'accord avec la suggestion de C. WILSON pour conclure que l'activité aurorale est la source des ondes de gravité observées dans la région F à moyenne latitude, il est préférable de faire des études détaillées sur des observations spécifiques, plutôt que des études statistiques.

En France, on a analysé récemment des observations mettant en jeu :

- le sondeur à diffusion incohérente de St Santin Nançay qui permet l'étude de la structure verticale des perturbations,
- le réseau européen d'ionosondes, qui permet d'observer la propagation horizontale,
- les données de magnétogrammes auroraux provenant de nombreuses stations sur le pourtour de l'ovale auroral.

Dans plusieurs cas, on a pu relier des perturbations ionosphériques de grande amplitude observées pendant la journée à des événements auroraux se produisant du côté jour.

Dr. N. CHANG : I would like to comment on Dr. Wilson's suggestion that TID observations be related to specific substorm activity. In October and November of 1969 Stanford Research Institute operated a spaced transmitter HF CW Doppler network near Homer, Alaska for this very purpose. During the 6 week observation period a variety of signatures, some apparently unique to high latitudes, were detected. A number of TID's were also detected including 2 events which unlike mid-latitude events were characterized by long trains (3 to 4 hours) of regular fluctuations of roughly 20 minute periods. These events arrived from the north and therefore may be related to auroral activity. There were, however, TID's which did not arrive from the north and therefore do not appear to be auroral related. In general when auroral activity over Alaska was high the ionosphere was highly disturbed so, even if TID's were launched from a specific substorm, we could not detect them. In spite of the disturbed ionosphere over Alaska during active period I believe that it is possible to detect TID's launched from a specific substorm if different probing frequencies were used (the Alaskan system used frequencies of about 3.0 MHz) in addition to a longer observing period. Independent of the above, however which after all occurs over only about 30 % of the observing period, a high latitude site is valuable because one can readily separate the non-auroral events from those that are auroral related. For the latter a plot of their arrival angle versus time of day should yield a similar fractionated relation as the direction of ray, the midnight sector of the oval with respect to the observer. While the same could be done at mid latitudes the advantages of the high latitude sites are obvious.

Dr. J. LOMAX : Dr. Bowman's paper describes a significant correlation in the occurrence of gravity waves observed at Brisbane and of spread-F at locations with high dip latitude. Dr. Wilson's paper describes the generation of auroral infrasonic shock waves by motions of the auroral electrojet. These two factors recall to me a paper that I delivered at the AGARD meeting in Copenhagen. In that paper I presented observations on the onset time of spread F in the equatorial region. On nights with strong spread-F activity, the onset time appeared to be equal to the acoustic propagation time from the termination of the equatorial electrojet to the location at which spread-F onset was being observed. The inference that I am making is that acoustic gravity waves may be generated by both the auroral and the equatorial electrojets, and farther, that these waves then act as triggers of instability mechanism that result in the occurrence of spread-F at both high and low latitudes respectively.

**FM/CW RADAR STUDIES OF PRODUCTION OF TURBULENT INSTABILITY
WITHIN THERMALLY STABLE LAYERS BY INTERNAL WAVES**

by

Earl E.Gossard

**Wave Propagation Laboratory
NOAA Environmental Research Laboratories
Boulder, Colorado 80302
USA**

J.H.Richter

**Naval Electronics Laboratory Center
San Diego, California 92152
USA**

ETUDES MENEES A L'AIDE D'UN RADAR A MODULATION DE FREQUENCE
SUR LA CREATION, PAR DES ONDES INTERNES, D'INSTABILITES TURBULENTES
A L'INTERIEUR DE COUCHES THERMIQUEMENT STABLES.

par

E.E. Gossard et J.H. Richter

SOMMAIRE

Un récent développement dans le domaine du sondage radar, a rendu visible la structure de la troposphère à un degré qu'on n'avait pas précédemment approché. L'appareil de sondage par radar est un système modulation de fréquence/onde entretenue conçu et réalisé par le Dr. J.H. RICHTER (1969).

Les caractéristiques les plus marquantes qui apparaissent dans les enregistrements sont les ondes de gravité internes, certains traits rappelant les structures d'instabilité de Kelvin/Helmholtz, et les couches multiples présentant fréquemment des stratifications de quelques mètres seulement d'épaisseur, et des cellules de convection à l'intérieur de la couche marine (GOSSARD, RICHTER et ATLAS, 1970 ; GOSSARD, JENSEN et RICHTER, 1971).

On a émis des doutes considérables sur ce que le radar "voyait" réellement. Il est évident, d'après les enregistrements, que les images de retour proviennent des régions à gradient d'indice de réfraction élevé ; cependant, que l'écho de retour soit une rétrodiffusion sur une zone mince de turbulence intense de petite échelle ou bien qu'il comprenne une réflexion cohérente partielle sur des couches à fort gradient d'indice de réfraction, reste à déterminer.

Les auteurs de l'exposé présentent toute une gamme de configurations structurales atmosphériques, et les comparent à plusieurs modèles hypothétiques de structures d'ondes internes pour mieux comprendre les processus atmosphériques en action. Ils consacrent une attention particulière à la répartition du Nombre de Richardson dans les ondes de gravité piégées et non piégées. Ils concluent que les couches multiples proviennent d'ondes de gravité internes non piégées, dont le vecteur de propagation suit une direction presque verticale à l'intérieur de régions élevées très stables, et que les couches sont créées par une instabilité de Kelvin/Helmholtz résultant d'une réduction du Nombre de Richardson sous l'influence d'un accroissement du rapport amplitude/longueur d'onde au fur et à mesure que les ondes se propagent pour pénétrer dans des régions élevées thermiquement stables de l'atmosphère.

FM/CW RADAR STUDIES OF PRODUCTION OF TURBULENT INSTABILITY
WITHIN THERMALLY STABLE LAYERS BY INTERNAL WAVES

Earl E. Gossard
 Wave Propagation Laboratory
 NOAA Environmental Research Laboratories
 Boulder, Colorado, U.S.A. 80302

J. H. Richter
 Naval Electronics Laboratory Center
 San Diego, California, U.S.A. 92152

ABSTRACT

A recent development in radar sounding has made the detailed structure of the troposphere visible to a degree previously not approachable. The radar sounder is an FM/CW system designed and built by Dr. J. H. RICHTER (1969).

The most outstanding features evident in the records are internal gravity waves, features resembling Kelvin/Helmholtz instability structures, multiple layering often displaying lamina only a few meters thick, and convection cells within the marine layer (GOSSARD, RICHTER and ATLAS, 1970; GOSSARD, JENSEN and RICHTER, 1971).

Considerable doubt has existed as to just what the radar is "seeing." It is evident from the records that the returns come from regions of large refractive index gradient, but whether the return is backscatter from a thin region of intense, small scale turbulence (either "fossil" or mechanical) or whether it may include coherent partial reflection from gradient layers of refractive index remains a question.

This paper shows a variety of atmospheric structural patterns and compares them with several hypothetical models of internal wave structures to obtain more insight into the atmospheric processes at work. Special attention is given to the distribution of Richardson's Number in trapped and untrapped gravity waves. It is concluded that the multiple layers result from untrapped internal gravity waves, whose propagation vector is directed nearly vertically within very stable height regions. The layers are concluded to be caused by Kelvin/Helmholtz instability resulting from reduction in Richardson's Number due to growth of the amplitude-to-wavelength ratio as the waves propagate into thermally stable height regions of the atmosphere.

1. INTRODUCTION

Radar pictures of the structure of the clear atmosphere reveal many patterns suggestive of some kind of dynamic instability. They provide fundamental new information about the manner in which turbulence in the atmosphere is created and the role played by thermal stratification in fluid dynamics.

Correct interpretation of the radar patterns in terms of atmospheric motion and structure is necessary in order to make radar sounding an effective tool in weather forecasting. The proper interpretation of many patterns seen, and even the precise mechanism for reflection (or scattering) of the radar waves, remains in doubt. It is the purpose of this paper to extend an earlier analysis (GOSSARD, JENSEN and RICHTER, 1971) (hereafter referred to as GJR), to include effects of finite amplitude and compressibility in the medium. In the earlier analysis GJR proposed that the mechanism for generating and maintaining thin regions of intense, small scale turbulence within thermally stable layers was the propagating upwards or downwards of untrapped gravity waves. They analyzed the distribution of Richardson's Number through internal waves in terms of wave structures seen by a special high resolution radar sounder (RICHTER, 1969).

Only the case of infinitesimally small amplitude perturbations was considered by GJR in the analysis. Furthermore, it was pointed out that the perturbation wave equations are linear in the variables

$\rho(z)z$, $\rho(z)z^{1/2}(u, v, w)$ and $\rho(z)^{-1/2}p$ but they ignored the dependence of density, ρ , on height, z , when computing the distribution of Richardson's Number within the wave. In their notation u, v, w are the x, y, z components of perturbed velocity, η is amplitude of parcel displacement and p is pressure perturbation. As they stated, the neglect of the height dependence of $\rho(z)$ is permissible when the inverse scale height, $\chi = -\rho^{-1}d\rho/dz \approx g/c^2$, is negligible compared with the inverse vertical scale, or skin depth, of the wave system. In other words, their analysis was applicable to the usual wave systems seen by the radar which are confined to relatively thin height ranges in the troposphere in the neighborhood of temperature inversions.

It is the purpose of the present paper to extend the earlier analysis to the case of finite amplitude and to examine (1) the shape of the isotherms (and refractive index isopleths); (2) examine the

effect of neglecting the height dependence of $\rho(z)$ when taking the height derivatives required in the calculation of wave Richardson's Number.

Specifically, the shape of the isotherms corresponding to Frame III of Figure 3 in the GJR paper is computed in order to consider the question of whether the radar is "seeing" isopleths of perturbed refractive index within a height gradient or some passive trace constituent carried with the displaced parcel (e.g., fossil turbulence). Furthermore, the Richardson's Number within the stable layer is recalculated for a hypothetical case in which the atmospheric scale height is not large compared with the vertical scale of the wave system.

2. FINITE AMPLITUDE WAVES

One classical approach to finite amplitude theory is the method of successive approximations in which a nonlinear wave equation is made linear by substitution of a lower order solution in the nonlinear terms and solved. Equations corresponding to successively higher order solutions result. The sum of the solutions describes finite amplitude effects as long as kn is small, where k is horizontal component of wave number and n is parcel displacement. The lowest order of differential equation is linear with the usual small amplitude solution. This solution is introduced into the nonlinear, next higher order equation, etc. The method is well described and illustrated by THORPE (1968, page 579). For an incompressible fluid, the method is fairly convenient. The most practical form of the wave equation is the vorticity equation in the stream function χ and density, ρ . The form of finite amplitude solution which results from this approach will be derived here assuming an incompressible fluid and a first order wave perturbation of the form $\chi_1 = A_{\chi_1} \cos(kx + nz - \sigma t)$, $\rho_1 = \rho_0 \cos(kx + nz - \sigma t)$ for unbounded waves. The velocity perturbations, $u, w = \partial\chi/\partial z, -\partial\chi/\partial x$. The solution desired is for the displacement, δ , of the surfaces of equal density in a stably stratified fluid. For infinitesimally small amplitude, the solutions for both χ and ρ are sinusoidal in both x and z .

The vorticity equation is (see, for example, THORPE, 1968):

$$\frac{\partial}{\partial t} \nabla^2 \chi + u \frac{\partial}{\partial x} \nabla^2 \chi + w \frac{\partial}{\partial z} \nabla^2 \chi = \frac{g}{\rho_0(z)} \frac{\partial \rho}{\partial x} \quad (1)$$

and the equation of continuity for an incompressible fluid is:

$$\frac{d\rho}{dt} = \frac{\partial \rho}{\partial t} + u \frac{\partial \rho}{\partial x} + w \frac{\partial \rho}{\partial z} = 0 \quad (2)$$

Taking $\chi = \alpha \chi_1 + \alpha^2 \chi_2 + \alpha^3 \chi_3, \dots$

and $\rho = \rho_0 + \alpha \rho_1 + \alpha^2 \rho_2 + \alpha^3 \rho_3, \dots$

where the power of α is the indicator of order of perturbation, the successively higher order solutions for χ and ρ are:

$$\chi_1 = A_{\chi_1} \cos(kx + nz - \sigma t)$$

$$\chi_2 = A_{\chi_2} \cos 2(kx + nz - \sigma t)$$

$$\chi_3 = A_{\chi_3} \cos(kx + nz - \sigma t) + B_{\chi_3} \cos 3(kx + nz - \sigma t)$$

$$\rho_1 = A_{\rho_1} \frac{k}{\sigma} \frac{d\rho_0}{dz} \cos(kx + nz - \sigma t)$$

$$\rho_2 = \frac{1}{4} A_{\rho_2} \left(\frac{k}{\sigma} \right)^2 \frac{d^2 \rho_0}{dz^2} \cos 2(kx + nz - \sigma t)$$

$$- A_{\rho_2} \frac{d\rho_0}{dz} \left(\frac{k}{\sigma} \right) \cos 2(kx + nz + \text{const})$$

so

$$\chi = \chi_1 + \chi_2 + \chi_3 \dots \quad (3)$$

where

$$A_{X2} = \frac{1}{4} A_{X1}^2 \frac{\frac{d^2 \rho_0}{dz^2} \left(\frac{k}{\sigma} \right)}{4\sigma^2 \left(\frac{n^2}{k^2} + 1 \right) - N^2}$$

$$A_{X3} = \frac{1}{8} A_{X1}^3 \frac{\frac{d^4 \rho_0}{dz^4} - \frac{d^3 \rho_0}{dz^3} \frac{4 \left(\frac{\sigma}{R} \right)^2 (n^2 + k^2) - N^2}{\sigma^2 (n^2 + k^2) - k^2 N^2}}{4 \left(\frac{\sigma}{R} \right)^2 (n^2 + k^2) - N^2}$$

$$B_{X3} = \frac{1}{8} A_{X1}^3 \frac{\frac{d^4 \rho_0}{dz^4} - \frac{d^3 \rho_0}{dz^3} \frac{4 \left(\frac{\sigma}{k} \right)^2 (n^2 + k^2) - N^2}{9n^3 (n^2 + k^2) - k^2 N^2}}{4 \left(\frac{\sigma}{k} \right)^2 (n^2 + k^2) - N^2}$$

It is evident that all the higher order perturbation terms in χ are multiplied by higher order derivatives of the unperturbed density profile. Therefore, if $\rho_0(z)$ is linear with height, or perhaps exponential with a large scale depth, χ (and therefore the velocity field) is little affected by nonlinearity in the equations of motion.

Our main concern lies with the displacement of the density surfaces, because the same reasoning applies to the displacement of potential temperature and of refractive index surfaces. Expanding the density in a Taylor's series the displacement, δ , of a surface of constant density is determined by

$$\rho(z_0 + \delta) = \text{const} = \rho_0(z_0) + \delta \frac{\partial \rho}{\partial z} + \frac{1}{2} \delta^2 \frac{\partial^2 \rho}{\partial z^2} \dots \quad (4)$$

where

$$\rho(z_0) = \rho_0(z_0) + \alpha \rho_1(z_0) + \alpha^2 \rho_2(z_0) + \alpha^3 \rho_3(z_0) \dots$$

$$\delta = \alpha \delta_1 + \alpha^2 \delta_2 + \alpha^3 \delta_3 \dots$$

Since the first term in the expansion of $\rho(z_0)$ cancels $\rho_0 z_0$:

$$\begin{aligned} \alpha \rho_1 + \alpha^2 \rho_2 + \alpha^3 \rho_3 \dots \\ = -(\alpha \delta_1 + \alpha^2 \delta_2 + \alpha^3 \delta_3 \dots) \frac{\delta(\rho_0 + \alpha \rho_1 + \alpha^2 \rho_2 + \alpha^3 \rho_3 \dots)}{\partial z} \dots \end{aligned}$$

so

$$\begin{aligned} \delta_1 &= \delta_0 \cos(kx + nz - \sigma t) \\ \delta_2 &= \delta_0^2 n \cos(kx + nz - \sigma t) \sin(kx + nz - \sigma t) \\ \delta_3 &= \delta_0^3 n^2 \left[\cos(kx + nz - \sigma t) - \frac{3}{2} \cos 3(kx + nz - \sigma t) \right] \end{aligned} \quad (5)$$

and

$$\begin{aligned} \frac{\delta}{\delta_0} &= \frac{\delta_1 + \delta_2 + \delta_3}{\delta_0} = \left(1 - \frac{1}{8} (n \delta_0)^2 \right) \cos(kx + nz - \sigma t) \\ &\quad - \frac{1}{2} n \delta_0 \sin 2(kx + nz - \sigma t) - \frac{3}{8} (n \delta_0)^3 \cos 3(kx + nz - \sigma t) \dots \end{aligned}$$

plus terms which are products of $d^2\rho_0/dz^2$ or higher order. If $\rho_0(z)$ is exponential, note that $d^k\rho_0/dz^k = (N^2/g)^k$.

where

$$n = k \sqrt{\left(\frac{N}{g}\right)^2 - 1} \text{ and } \frac{k^2}{g} = \frac{1}{c_0^2} \frac{d\rho_0}{dz}$$

for an incompressible fluid (see ECKART, 1960). The above approach to the problem of nonlinear effects is laborious and the physics is obscured by the mechanical complexity, so we consider an equivalent but conceptually different approach.

Suppose we consider only equations (4) and (2). Equation (2) yields the perturbation equation of continuity as:

$$\frac{\partial \rho}{\partial t} = -w \frac{d\rho_0}{dz}$$

where ρ and w are the perturbed values of density and vertical velocity and $\rho_0(z)$ is the unperturbed density distribution. Noting that $w = \delta\eta/dt$, where η is the parcel displacement, and integrating, we have

$$\rho - \rho_0 = -\eta \frac{d\rho_0}{dz}$$

so that

$$\frac{d\rho}{dz} = \frac{d\rho_0}{dz} - \frac{\partial \eta}{\partial z} \frac{d\rho_0}{dz} = \frac{d\rho_0}{dz} \left(1 - \frac{\partial \eta}{\partial z}\right) \quad (6)$$

and

$$\frac{d^2\rho}{dz^2} = \frac{d\rho_0}{dz} \left(\frac{\partial^2 \eta}{\partial z^2}\right) \quad (7)$$

if $d^2\rho_0/dz^2$ is negligible. Also the fluctuations in density at z_0 for small wave perturbations are described by

$$\rho(z_0) - \rho_0(z_0) = \eta \frac{d\rho_0}{dz} = \frac{d\rho_0}{dz} \eta_0 \cos(kx + nz - \sigma t)$$

so that (4) gives

$$\eta_0 \cos(kx + nz - \sigma t) = -\delta \left(1 - \frac{\partial \eta}{\partial z}\right) + \frac{\delta^2}{2} \left(\frac{\partial^2 \eta}{\partial z^2}\right) + \dots \quad (8)$$

Dividing by $1/2(\partial^2 \eta / \partial z^2)$ gives an expression quadratic to this order; i.e.,

$$\delta^2 - \delta \left(\frac{1 - \frac{\partial \eta}{\partial z}}{\frac{\partial^2 \eta}{\partial z^2}} \right) - \frac{2\eta}{\frac{\partial^2 \eta}{\partial z^2}} = 0 \quad (9)$$

Expanding, using successive approximations, and assuming $\eta = \eta_0 \cos(kx + nz - \sigma t)$, we find

$$\begin{aligned} \frac{\delta}{\eta_0} = & \left(1 - \frac{1}{8} n^2 \eta_0^2\right) \cos(kx + nz - \sigma t) - \frac{1}{2} n \eta_0 \sin 2(kx + nz - \sigma t) \\ & - \frac{3}{8} (n \eta_0)^2 \cos 3(kx + nz - \sigma t) \dots \end{aligned} \quad (10)$$

This is the same as equation (5) to 3rd order, where terms in $d^2\rho_0/dz^2$ have again been ignored, if it is recognized that the 1st order isotherm displacement, δ_1 , is the same as particle displacement, η .

Two important conclusions can apparently be stated:

A. To this order, the shape of the isopycnals in an incompressible fluid are not apparently affected by nonlinearity in the equations of motion, but only by nonlinearity resulting from higher order terms in the Taylor expansion. Thus, other nonlinear effects will be quite negligible compared with the

effect on shape. The reason nonlinearity in the equations of motion is not very important can be seen when written in the form of the vorticity equation (1). The important nonlinearity is in the inertial terms, the second and third terms from the left. However, they cancel since

$$u \frac{\partial}{\partial x} (\nabla^2 \chi) + v \frac{\partial}{\partial y} (\nabla^2 \chi) = \frac{\partial \chi}{\partial z} \frac{\partial}{\partial x} (\nabla^2 \chi) - \frac{\partial \chi}{\partial x} \frac{\partial}{\partial z} (\nabla^2 \chi) = 0$$

Thus, the stream function $\chi = \chi_1 + \chi_2 + \chi_3 \dots = \chi_1$ to third order, and departures from this form depend on second and higher derivatives of $\rho_0(z)$ of z , i.e., velocity perturbations remain essentially sinusoidal.

B. If (A) is true for an incompressible fluid, it implies that the linear form of the solution for the compressible case (for which no comparable vorticity equation can be written) can be used in the Taylor expansion to achieve a valid description of the potential temperature isotherms in a compressible fluid.

The linear form of solution for displacement in a compressible fluid is

$$\eta \rho_0(z)^{1/2} = \eta_1 \rho_0(z_0)^{1/2} \cos(kx + nz - \sigma t) \quad (11)$$

for atmospheric layers in which the coefficients of the differential equations are constant; i.e., $(g/\theta)(d\theta/dz) = N^2 = \text{constant}$, $c = \text{constant}$ and $(2\rho_0)^{-1} d\rho_0/dz + g/c^2 = \Gamma = \text{constant}$. The density and displacement amplitudes are ρ_0 , η_0 , respectively, at a reference level. θ is potential temperature.

Rewriting (4) for isotherm displacement

$$\theta_0(z_0) = \theta(z_0) + \delta \frac{\partial \theta}{\partial z} + \frac{1}{2} \delta^2 \frac{\partial^2 \theta}{\partial z^2} \dots$$

where to 1st order

$$\rho_0(z_0) - \rho(z_0) = \eta \frac{d\rho_0}{dz}$$

and

$$\frac{\partial \theta}{\partial z} = \frac{d\theta_0}{dz} \left(1 - \frac{\partial \eta}{\partial z} \right), \quad \frac{\partial^2 \theta}{\partial z^2} = - \frac{d\theta_0}{dz} \frac{\partial^2 \eta}{\partial z^2} \quad (12)$$

Thus, for the compressible fluid case, an equation identical to (9) results, but $\eta(z)$ and its derivatives now include an additional dependence on z through $\rho_0(z)^{-1/2}$ according to (11).

The isotherm (or isopycnal) displacements for the two cases of incompressible and compressible fluids are shown by the black curves in Figures 1 and 2, respectively. The difference in shape is indistinguishable to the scale shown. The model for the figures is a three-layer model in which the upper and lower fluids have small stability and extend to infinity. The value for N is constant and the same in the upper and lower layers and greater in the middle layer. This model was discussed in detail by GOSSEARD, JENSEN and RICHTER (1971) and these figures correspond to their frame III, figure 3. The eigen equation for this model, plotted in Figure 3, is:

$$\tan n\Delta_1 = \frac{2n\gamma}{n^2 - \gamma^2} \quad (13)$$

where

$$n = k \sqrt{\left(\frac{N_2}{n}\right)^2 - 1} \quad \gamma_{1,3} = k \sqrt{1 - \left(\frac{N_{1,3}}{c}\right)^2}$$

Note that $n_k = i\gamma_k$ in a layer, k , in which the waves are evanescent.

The important points to note are: A) the wave troughs are sharpened and crests flattened above the center of the stable layer. B) the wave crests are sharpened and the troughs flattened below the center of the stable layer. C) at the center, both crest and trough are flattened.

For purposes of illustration, an amplitude-to-vertical wavelength ratio corresponding to $n\eta_0 = 0.75$ has been assumed in the figures. This value was chosen as not being so large as to make the approximate methods used in calculating wave shape completely invalid, while being sufficiently large that the changes in shape are visibly obvious.

In addition to the three layer model, the case of untrapped waves was computed and is shown in Figure 4. In contrast with the trapped waves in the model above, the introduction of finite amplitude now leads to an asymmetry in the wave shape that is reminiscent of some of the waves seen by the radar as shown in Figure 5. However, untrapped waves should exhibit a phase shift with height and such a phase shift is seldom seen by the radar. Therefore, the resemblance in shape of the waves in Figure 4 to the asymmetric, breaking waves seen by the radar should not be interpreted as necessarily providing the correct physical explanation of the waves.

The second mode waves for the three layer model were also computed and the isotherm displacements are shown by the thin wavy lines in Figure 6. The displacement curves display a pattern reminiscent of the figure eight or "cat's eye" patterns so often seen by the radar as shown in Figure 7. Once again, this is probably fortuitous since the patterns seen by the radar usually are associated with a breaking sequence and do not seem to be typically a steady state phenomenon.

3. RICHARDSON'S NUMBER

In addition to isotherm shape, the Richardson's Number must be considered a very important parameter in the interpretation of the radar records. The gradient Richardson's Number is defined as

$$R_i = \frac{g}{\theta} \frac{\partial \theta}{\partial z} \frac{N^2}{\left(\frac{\partial u}{\partial z}\right)^2 + \left(\frac{\partial v}{\partial z}\right)^2} \quad (14)$$

and is generally considered to be an important criterion for the onset of wave instability (breaking) or turbulence. Work by TAYLOR (1931), MILES (1961), MILES and HOWARD (1964), and CHIMONAS (1970) indicate that reduction of the Richardson's Number to less than 0.25 is a necessary condition for the development of wave instability.

GJR proposed that the propagation of untrapped gravity waves into a height region of large thermal stability can reduce R_i sufficiently to cause the onset of dynamic instability at the crests or troughs of the waves, if some shear already exists in the propagation medium. It is, therefore, argued that many of the thin, multiple layers commonly seen by the radar can be explained in terms of untrapped gravity waves propagating into a height region of great thermal stability as shown schematically in Figure 8. As the stability increases, the wave vector tilts toward the vertical so that equiphase surfaces are nearly horizontal. If the vertical energy flux is constant with height, the ratio of amplitude to vertical wavelength, $n\eta_0$, will increase, reducing the (numerator of) Richardson's Number to a level of dynamic instability at some phase of the wave. A record which may be an example of this phenomenon is shown as Figure 9.

From (12), it follows that the numerator of (14) can be written in terms of the wave induced displacement η , as

$$\frac{g}{\theta} \frac{\partial \theta}{\partial z} = \frac{g}{\theta} \frac{d\eta}{dz} \left(1 - \frac{\partial \eta}{\partial z}\right) \quad (15)$$

In order to derive the relation between u and displacement, η , needed in the denominator we require the two-dimensional equation of continuity for a compressible fluid:

$$\frac{\partial u}{\partial x} + \frac{\partial w}{\partial z} = -\frac{1}{\rho_0} \left(\frac{D\rho}{Dt} + w \frac{\partial \rho_0}{\partial z} \right) \quad (16)$$

and the 1st Law of Thermodynamics:

$$\frac{Dp}{Dt} + w \frac{\partial p_0}{\partial z} = \frac{1}{c^2} \left(\frac{D\rho}{Dt} + w \frac{\partial \rho_0}{\partial z} \right) \quad (17)$$

where D/Dt is the operator $\partial/\partial t + V \partial/\partial x$; p , ρ , w , u are the perturbed pressure, density, vertical velocity and horizontal velocity, and ρ_0 , p , c are the unperturbed density, pressure and sound velocity. V is the unperturbed horizontal wind speed.

Eliminating p and using the hydrostatic relation $\partial p/\partial z = -\rho_0 g$, (15) becomes

$$\frac{\partial u}{\partial x} + \frac{\partial w}{\partial z} - \frac{g}{c^2} w = -\frac{1}{\rho_0 c^2} \frac{Dp}{Dt} \quad (18)$$

where p is related to u by the 1st equation of motion, i.e.,

$$\frac{Eu}{Dt} = -\frac{1}{\rho_0} \frac{\partial p}{\partial x} \quad (19)$$

so

$$\frac{D^2 u}{Dt^2} = -\frac{1}{\rho_0} \frac{D}{Dt} \left(\frac{\partial p}{\partial x} \right) \quad (20)$$

Taking the partial of (18) with respect to x we get

$$\left(\frac{\sigma^2}{\partial x^2} - \frac{1}{c^2} \frac{\partial^2}{\partial t^2} \right) u = - \left(\frac{\partial}{\partial z} - \frac{g}{c^2} \right) \frac{\partial w}{\partial x}$$

For solutions of the form $F(z) \exp[i(kx - \sigma t)]$

$$(\sigma^2 - k^2 c^2) u = -ikc^2 \left(\frac{\partial}{\partial z} - \frac{g}{c^2} \right) w$$

so

$$u = \frac{i}{k \left(1 - \frac{C^2}{c^2} \right)} \left(\frac{\partial}{\partial z} - \frac{g}{c^2} \right) w \quad (21)$$

where $C = \sigma/k$. If we define $(u, w)\rho^{1/2} = U, W$, then

$$\frac{\partial W}{\partial z} = \rho_0^{-1/2} \left(\frac{\partial W}{\partial z} - \frac{1}{2\rho_0} \frac{\partial \rho_0}{\partial z} W \right)$$

If we return to (18) we get on substitution

$$U = \frac{i}{k \left(1 - \frac{C^2}{c^2} \right)} \left(\frac{\partial}{\partial z} - \Gamma \right) W$$

Equations (20) and (21) are equations used by GOSSARD, RICHTER, ATLAS (1970), and GJR. They do not include shear within the medium. Noting that $w = D\eta/Dt$ and assuming $C^2 < c^2$

$$\frac{\partial u}{\partial z} = \frac{\sigma}{k} \left(\frac{\partial}{\partial z} - \frac{g}{c^2} \right) \frac{\partial \eta}{\partial z} \quad (23)$$

So that

$$R_1 = \frac{N_0^2}{C^2} \frac{1 - \frac{\partial \eta}{\partial z}}{\left[\left(\frac{\partial}{\partial z} - \frac{g}{c^2} \right) \frac{\partial \eta}{\partial z} \right]^2} \quad (24)$$

For untrapped waves, a solution of the form $\eta = \eta_0 \cos(kx + nz - \sigma t)$ may be assumed. For the three-layer model discussed above.

$$\begin{aligned} \eta_1 &= \eta_0 \cos \left(n \frac{\Delta h}{2} \right) \exp \{ i \gamma_1 (z - \Delta h/2) \} \\ \eta_2 &= \eta_0 \cos nz \\ \eta_3 &= \eta_0 \cos \left(n \frac{\Delta h}{2} \right) \exp \{ -i \gamma_3 (z - \Delta h/2) \} \end{aligned} \quad (25)$$

where the subscripts 1, 2, 3 apply to the lower, middle and upper layers respectively, and where the origin is chosen at the middle layer. The Richardson's Numbers in Figures 1 and 2 were calculated using equations (24) and (25) assuming $[N_{1,3}/\gamma_{1,3} C]^2 = 0.25$, $n\eta_0 = 0.75$. For Figure 1 it was assumed that $g/c^2 \ll \partial/\partial z$ and the effect of the height dependence in $\rho_0(z)^{-1/2}$ on η and its derivatives was ignored (incompressibility assumption). Figure 4 shows the corresponding patterns of R_1 in untrapped waves, where R_1 is represented by sloping straight lines; and Figure 6 shows patterns of R_1 in 2nd mode trapped waves where R_1 is shown by heavy lines.

If g/c^2 is negligible the numerator and denominator of (24) go to zero together as $n\eta_0 \rightarrow 1.0$ at a limiting $R_1 = 0.5$. Further increase in $n\eta_0$ leads to negative R_1 which implies that the wave can produce super-adiabatic gradients. This is important because it means that the wave cannot reduce R_1 to the level of dynamic instability, i.e., $R_1 = 0.25$, but may, instead, produce convective instability. For the case of untrapped waves, this might argue that layers of convective instability and superadiabatic temperature gradients as proposed by ORLANSKI and BRYAN (1969) might be observed instead of dynamically unstable lamina resulting from reduced R_1 . However, our balloon soundings have failed to detect

superadiabatic temperature gradients within temperature inversion layers [RICHTER and GOSSARD, 1970], and GJR pointed out that the substructure revealed by the radar within the lamina resembles the Kelvin/Helmholtz instabilities seen at larger scales and commonly attributed to dynamic instability. When any background shear in the medium is included, it is found that the limiting $R_i = 0.5$ no longer applies and R_i decreases smoothly to $R_i = 0.25$ as $n\eta_0$ increases. We therefore propose that dynamic instability in untrapped wave systems, imbedded in a medium with some shear, is responsible for the creation of the thin layers of turbulent instability seen by the radar within temperature inversions.

4. REFERENCES

- CHIMONAS, G., 1970, "The Extension of the Miles-Howard Theorem to Compressible Fluids," J. Fluid Mech. 43, 833-836.
- ECKART, C., 1960, "Hydrodynamics of Oceans and Atmospheres," Pergamon Press, New York, p. 107.
- GOSSARD, E.E., D. R. JENSEN, and J.H. RICHTER, 1971, "An Analytical Study of Tropospheric Structure as Seen by High-Resolution Radar," J. Atmospheric Sci. 28, No. 5, 794-807.
- GOSSARD, E.E., J.H. RICHTER, and D. ATLAS, 1970, "Internal Waves in the Atmosphere from High Resolution Radar Measurements," J. Geophys. Res. 75, 903-913.
- MILES, J.W., 1961, "On the Stability of Heterogeneous Shear Flows," J. Fluid Mech. 10, 496-508.
- MILES, J.W., and L.N. HOWARD, 1964, "Note on Heterogeneous Shear Flow," J. Fluid Mech., 20, 331-336.
- ORLANSKI, I., and K. BRYAN, 1969, "Formation of the Thermocline Step Structure by Large Amplitude Internal Gravity Waves," J. Geophys. Res., 74, 6975-6983.
- RICHTER, J.H., and E.E. GOSSARD, 1970, "Lower Tropospheric Structure as Seen by a High-Resolution Radar," Naval Electronics Lab. Center Technical Report 1718, p. 26.
- RICHTER, J.H., 1969, "High Resolution Tropospheric Radar Sounding," Radio Science 4, 1261-1268.
- THORPE, S.A., 1968, "On the Shape of Progressive Internal Waves," Proc. Royal Soc. London, 263, 563-614.
- TAYLOR, G.I., 1931, "Effect of Variation in Density on the Stability of Superposed Streams of Fluid," Proc. Roy. Soc. A, 132, 499-523.

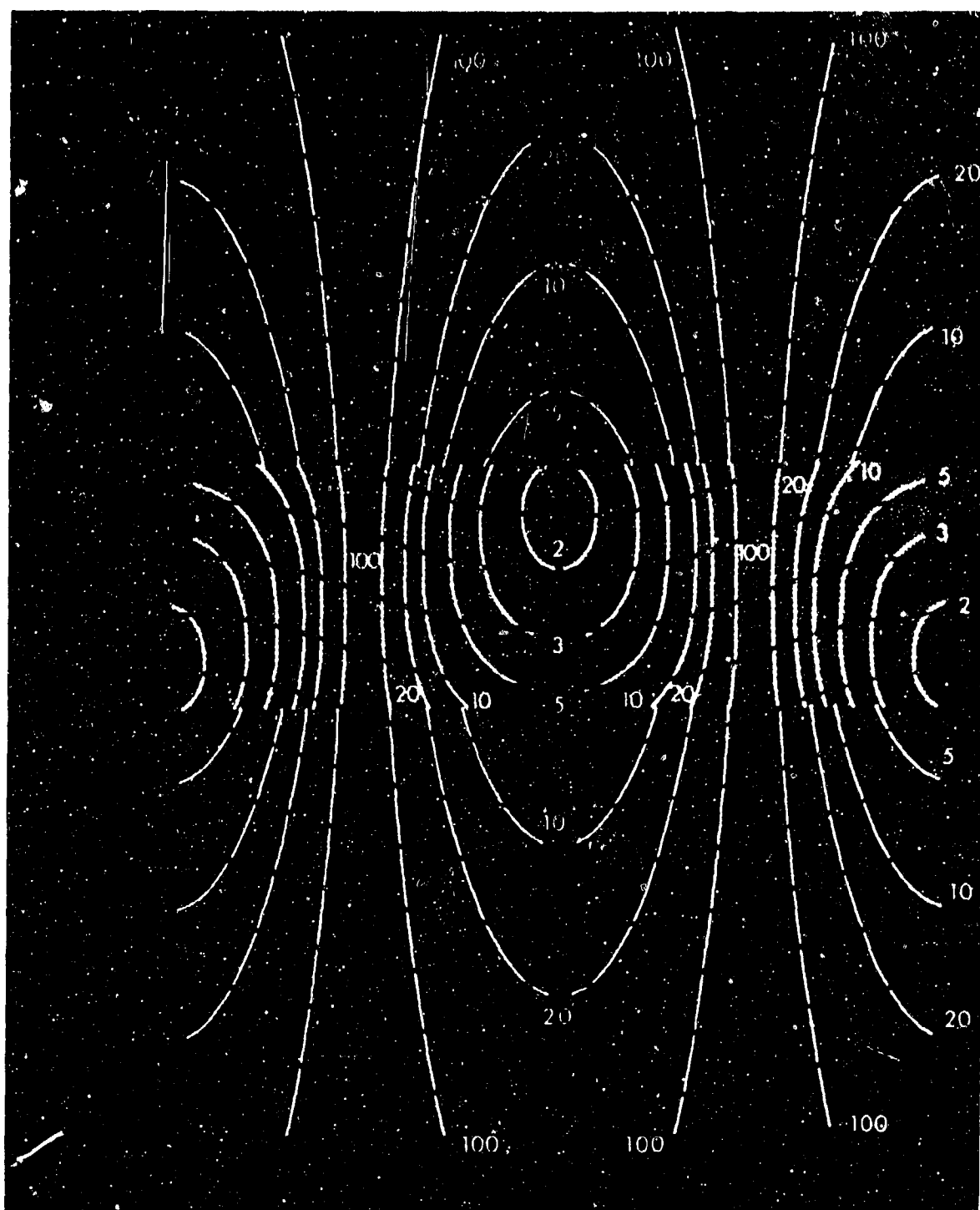


Fig.1 Plot of R_1 (white curves) and wave shape (black curves) through a three-layer model wave system. Waves evanescent above and below a stable layer in which ratio of amplitude to vertical wavelength is $0.75/2\pi$ (i.e., $n\eta_0 = 0.75$). It is assumed that $N_2/N_{1,3} = 5.5$, $n\Delta h/2 = 0.375$ and $N_{1,3} k/\omega n = 0.5$ (see text). Terms in g/c assumed negligible compared with n (i.e., incompressibility condition in which plane wave solution assumed for η). No shear.

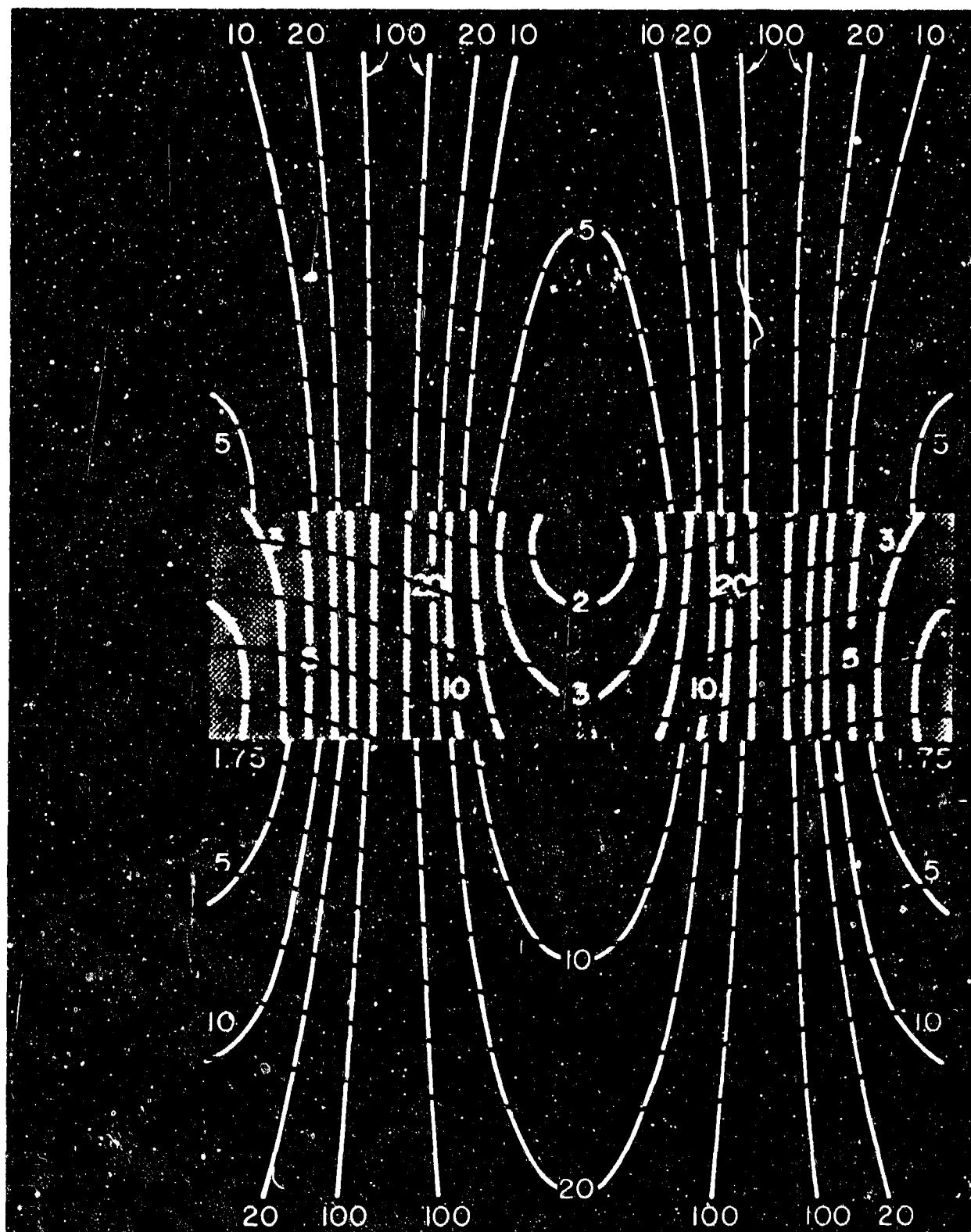


Fig. 1. Conditions same as those of Figure 1 except plane wave solution assumed for $\eta\rho_0(z)^{1/2}$ where $\rho_0^{-1}d\rho_0/dz \approx -g/c^2$ and it is assumed that $g/c^2/2n = 0.1$. Note that this inclusion of compressibility makes virtually no difference in wave shape and little difference in R_1 even for the extreme condition assumed.

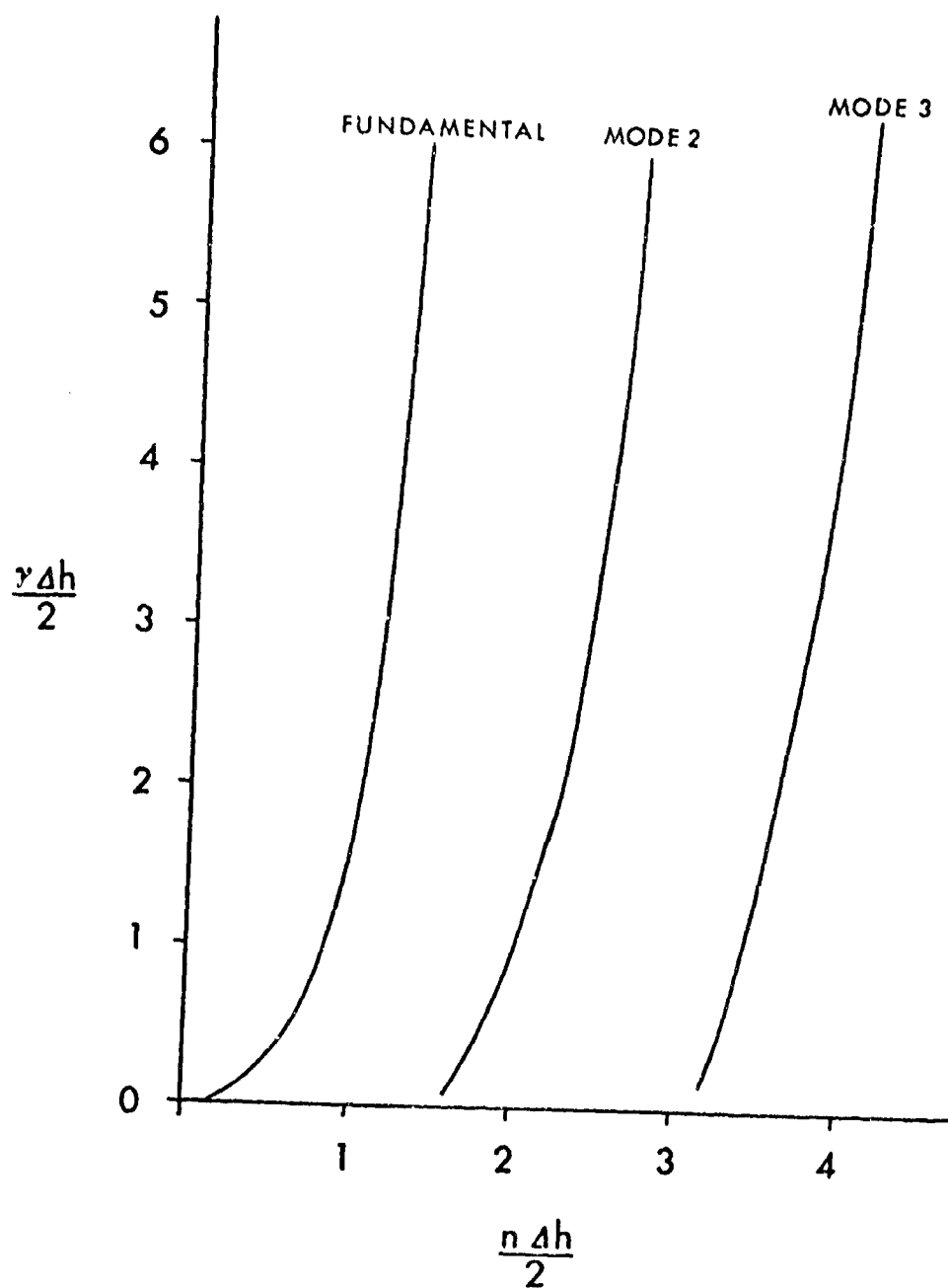


Fig.3 Plot model relation, equation (13).

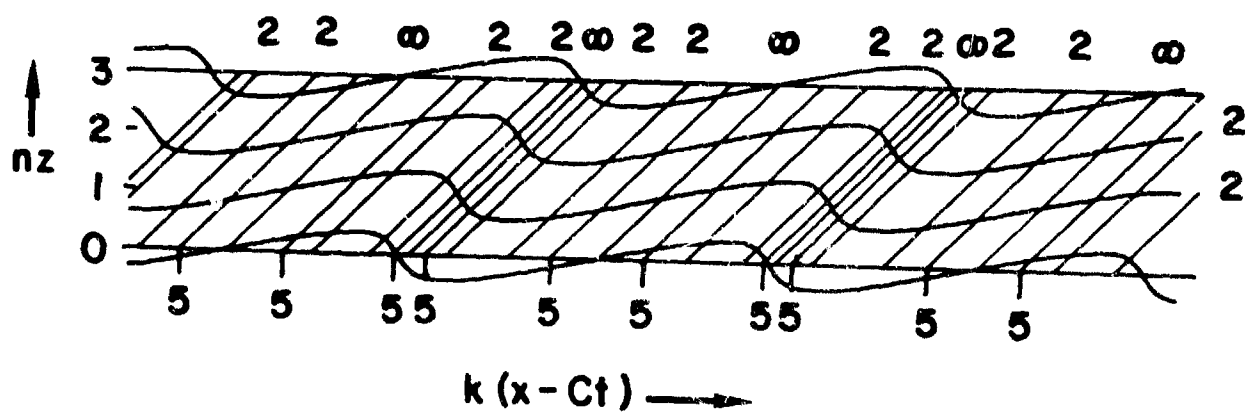


Fig.4 Wave shape and R_i for untrapped wave model assuming same conditions as in Figure 2.

13 AUG 1970

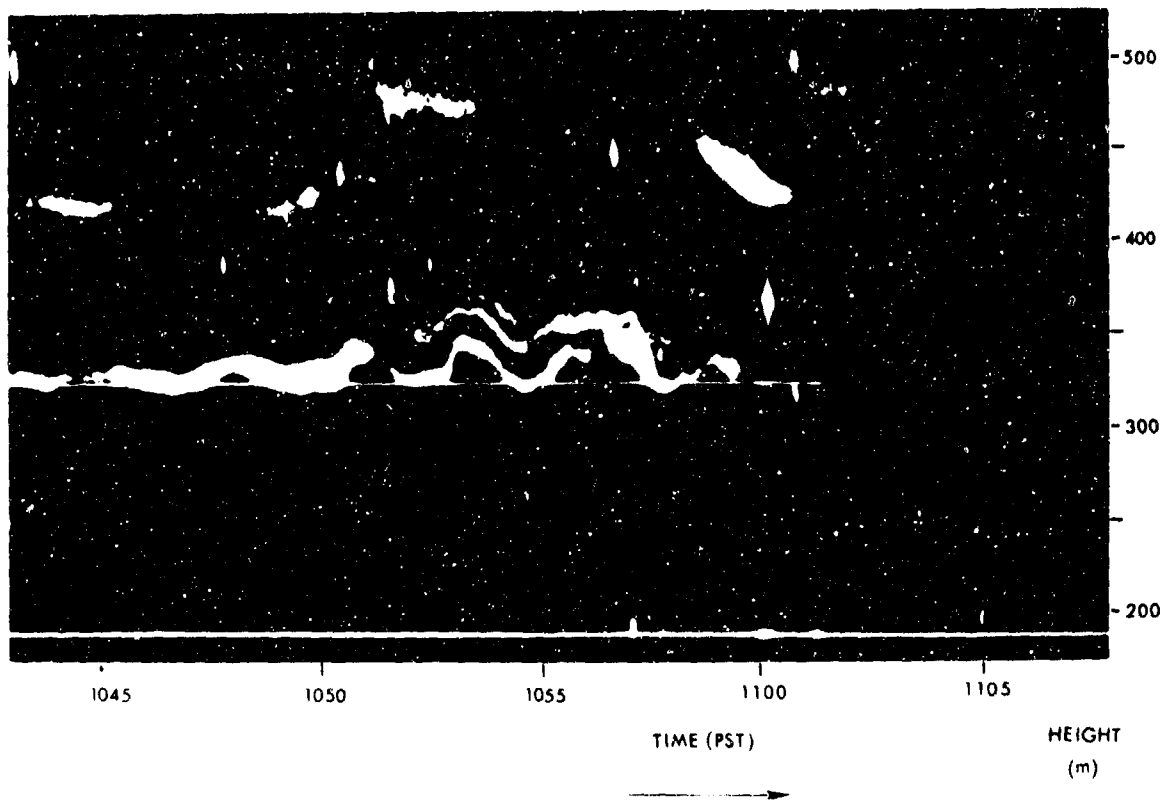
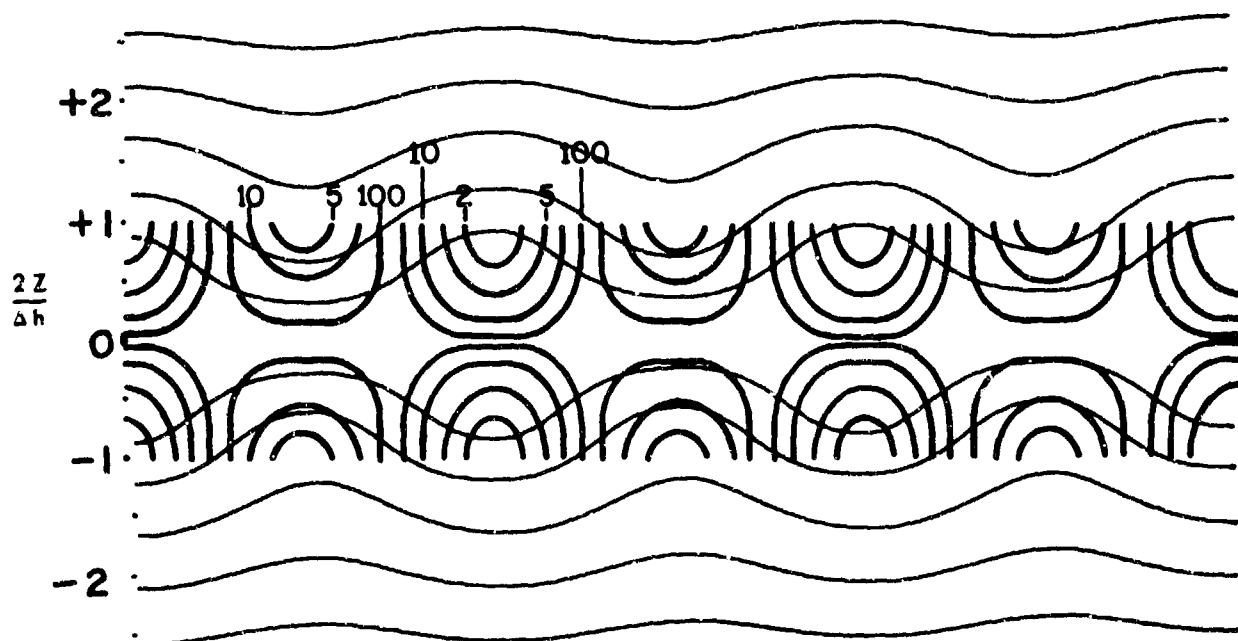


Fig.5 Example of record showing similar wave shape to that of Figure 4.

Fig.6 Wave shape and R_1 for 2nd mode assuming same model as Figure 2.

23 JUNE 1970

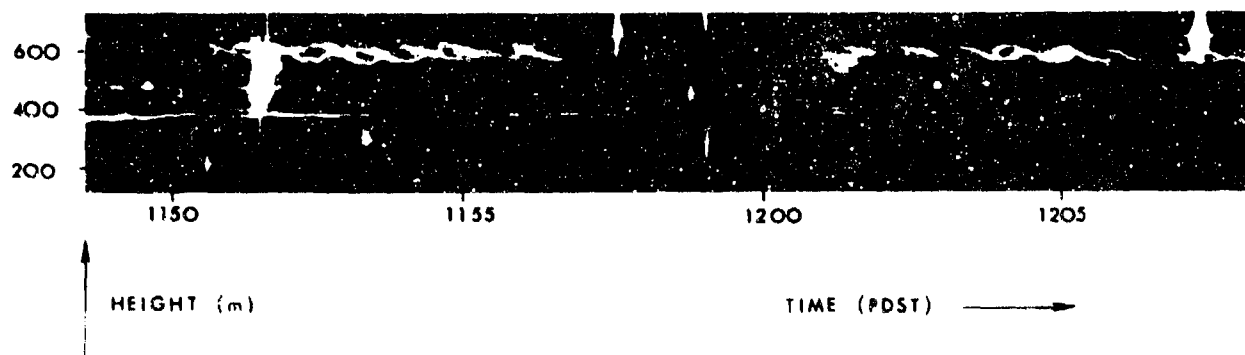


Fig.7 Example of record showing "cat's eye" pattern similar to wave shape of Figure 6.

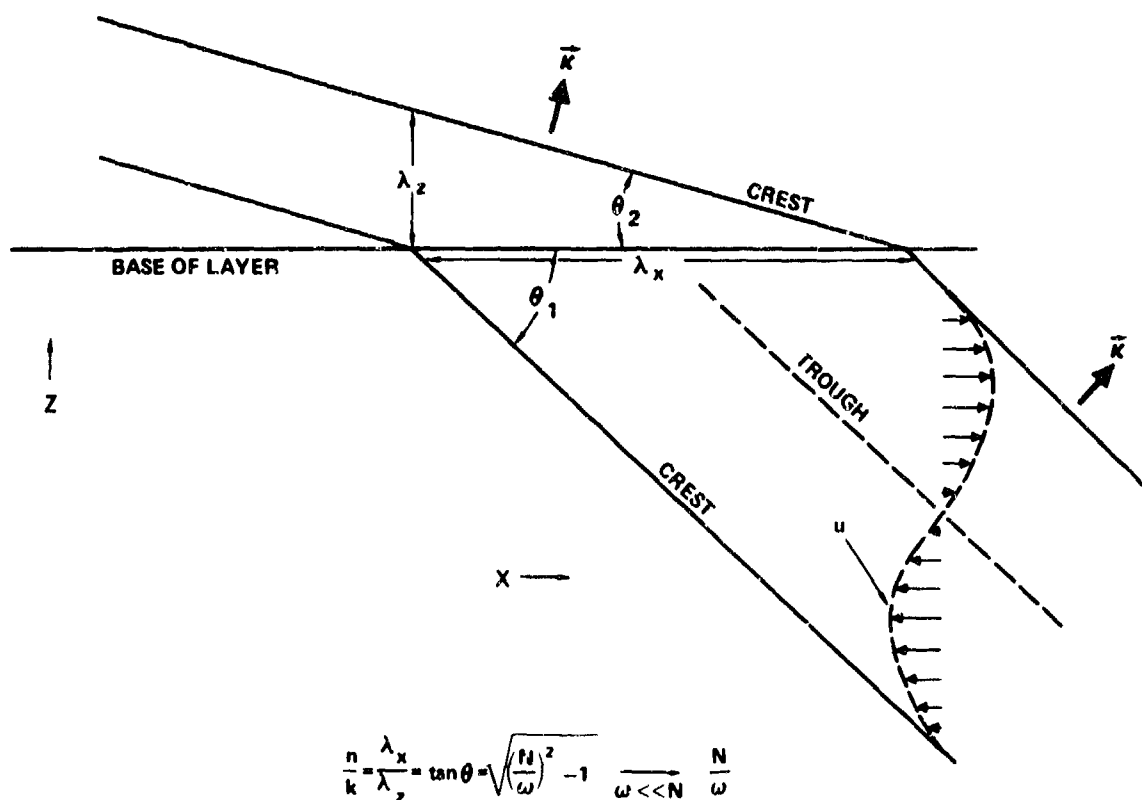


Fig.8 Schematic illustration of reduction in λ_z due to untrapped wave propagating into stable region of atmosphere.

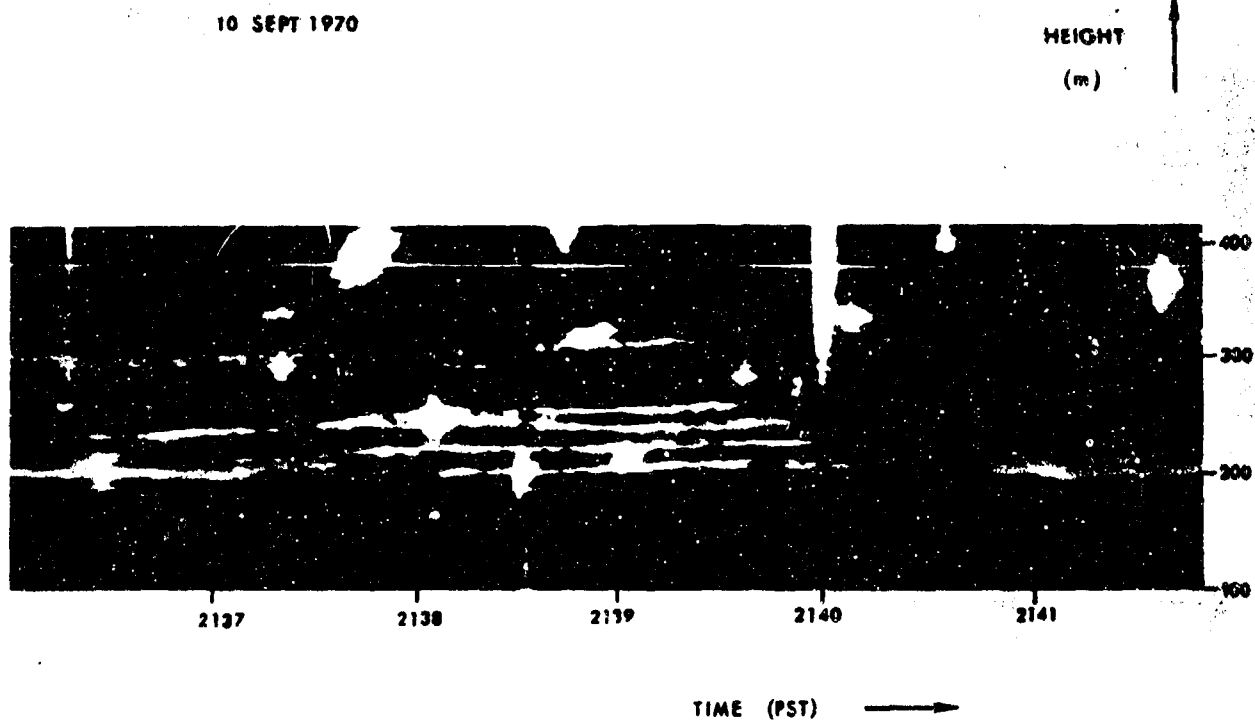


Fig.9 Example of record showing wavelike structures which illustrate regions of reduced R_i propagating in the vertical (as well as horizontal) direction with untrapped gravity waves.

THE DETECTION AND STUDY OF GRAVITY WAVES WITH MICROWAVE RADAR

by

Isadore Katz

Applied Physics Laboratory
Johns Hopkins University
Silver Spring, Md.
USA

272

DETECTION ET ETUDE D'ONDES DE GRAVITE A L'AIDE DE RADARS MICRO-ONDES

par

I. Katz

SOMMAIRE

L'emploi de radars ultra-sensibles a permis de "voir" la structure et les mouvements de l'atmosphère d'une façon qui était autrefois impossible. Ces radars ont, entre autres, détecté la présence d'ondes de gravité à la tropopause. En outre, nous avons vu, à travers toute la troposphère, de nombreux exemples de phénomènes d'ondes invariablement liés à des couches stables.

On a obtenu des preuves expérimentales qui montrent de façon incontestable que la diffusion de Bragg est la cause essentielle du phénomène de diffusion électromagnétique. On a découvert que l'intensité de signal des échos radar était une fonction linéaire de la densité spectrale (à une demi longueur d'onde radar) des fluctuations de l'indice de réfraction dans l'atmosphère.

Une étude portant sur 26 cas d'ondes de gravité détectées au cours d'autres recherches, a permis de caractériser ces ondes, à titre d'essai, en fonction de leurs dimensions, de leurs formes, de leur persistance et des conditions dans lesquelles elles apparaissent. On espère que cette caractérisation servira de base à une étude expérimentale plus complète des ondes de gravité à l'aide de détecteurs radar.

The Detection and Study of Gravity Waves With Microwave Radar

ISADORE KATZ

Applied Physics Laboratory
 Johns Hopkins University
 Silver Spring, Md., U.S.A.

1. Abstract

The use of ultra-sensitive radars has resulted in a new ability to "see" structure and motion of the atmosphere not possible before. Among other things these radars detected gravity waves at the tropopause. In addition, we have seen many examples of wave phenomena throughout the troposphere invariably associated with stable layers.

Experimental proof has been obtained which shows incontrovertible evidence that Bragg scattering is the prime cause of the electromagnetic scattering phenomenon. The signal strength of the radar echoes was found to be a linear function of the spectral density (at one-half the radar wave length) of refractive index fluctuations in the atmosphere.

A review of 26 gravity wave cases which were detected during the course of other investigations permits a tentative characterization of these waves in terms of sizes, shapes, persistence and conditions under which they occur. It is hoped that this characterization will provide a basis for a more complete experimental investigation of gravity waves with radar sensors.

2. Introduction

Radar has been used to detect discrete objects such as aircraft and birds and also has been effective in the study of precipitation. More recently high-power microwave radars, equipped with large antennas, have been used in the study of clear-air atmospheric phenomena. These ultra-sensitive radars, now in use for about 6 years, are capable of detecting the structure of convective cells, stable layers and waves, all in optically clear air. Convective activity in clear air is generally limited to the lowest 2000 m of the atmosphere. Layers, on the other hand, have been found to occur from near the surface up to the highest clear-air detection altitudes, say 15 km. These layers frequently exhibit gravity wave characteristics and it is these waves which comprise the subject of the present paper. No experiments have been directed primarily toward a study of gravity waves using radar, but in the course of carrying out other programs many cases of gravity waves have been encountered. In this paper we describe the characteristics of these gravity waves.

3. Bragg Scattering

Scattering of electromagnetic waves by turbulent media has been the subject of many scientific studies; for example: Booker and Gordon (1950), Batchelor (1955), Tatarski (1961). These theories, although different in detail, relate the scattering to fluctuations in the refractive index of the atmosphere. One finds from theory the following relationship between the normalized radar scattering cross section, η , in $\text{m}^2 \text{ per m}^3$, and the energy in the index fluctuations $F_n(k_r)$ at the radian wave number, k_r , corresponding to one-half the radar wavelength,

$$\eta = 0.65 k_r^2 F_n(k_r) \quad (1)$$

where $k_r = 4\pi/\lambda_r$. This equation says that electromagnetic energy incident on a turbulent medium is strongly affected by those irregularities or eddies in the medium whose size is about one-half the radio frequency carrier wavelength. These eddies contribute mainly to the scatter because only these sizes can provide the phase additions which produce a strong signal in the backscatter direction. This is essentially the Bragg condition for constructive interference from a grating.

Experiments have been performed which provide quantitative verification of the applicability of Eq. (1). The experiments carried out at Wallops Island, Va., involve radar tracking of a meteorologically equipped airplane, making simultaneous radar measurements and meteorological measurements. The radar tracks the airplane with one gate and, by linking a second gate to the first, measures signal returned from the clear atmosphere from a region of space just ahead of the incoming airplane. This technique provided a radar measurement from the atmosphere and an in-situ refractometer measurement from identical regions within about 10 seconds. Adjustment for the 10-second lag permitted a direct comparison between radar cross section and the appropriate portion of the refractivity spectrum. Fig. 1 shows a comparison of η versus $F_n(k_r)$. From these results one can conclude that Eq. (1) is essentially correct and that Bragg scattering is applicable to the optically clear atmosphere. Because these small irregularities in refractive index are quite often present in the atmosphere and are of sufficient intensity for detection on ultra-sensitive radars, they act as markers which move with the wind and can be used to determine atmospheric structure and motions.

4. Layers, Waves and Turbulence

Strata in the atmosphere are commonly detected with ultra-sensitive radars, especially at the lower atmospheric levels. In Fig. 2 is a photograph of a Range-Height radar indicator (RHII) showing at least 10 stratified layers below 6 km. This photograph shows height versus range at a fixed antenna azimuth. Layers like these may be as thick as 1 km or as thin as 1 to 10 m. Such layers have been the subject of much discussion in attempts to explain the mechanism for radar detection. Ottersten (1970) theorizes that these layers are stable which allows vertical wind shear to develop. As the shear increases, small-scale instabilities occur causing turbulence in thin layers. If this turbulence is insufficient to erode the shear, progressively larger instabilities break out and one finds larger-scale turbulence. Perhaps the stable layers are tilted by fronts, or waves which increases the shear even more and turbulence will occur over large vertical extents. If the above mechanism is correct then Ottersten has provided the explanation for the radar detection of the stable stratified layers.

This mechanism, then, results in the capability with ultra-sensitive radars to observe the formation of stratified atmospheric layers and their development into waves if conditions are appropriate.

At the higher altitudes radar layers have almost invariably been found to be associated with turbulence. Experiments have been carried out at Wallops Island during the winter months in which aircraft have been flown into regions containing radar layers to determine the relationship between radar layers and the occurrence of turbulence. To date, a high correlation exists between them. Most high altitude layers are found to be turbulent; Glover and Duquette (1970).

5. Wave Characteristics

The present stage is a rather early one with respect to understanding wave phenomena in the atmosphere. Since radar is yielding experimental evidence of wave formations it may be fruitful to describe the various forms these waves take and the conditions under which they occur. The following examples and discussion comes from considering a group of 26 occurrences of waves from May 1966 to August 1970 at Wallops Island. They are by no means all the wave formations seen with these radars but they are probably at least representative of all those which did occur. It is hoped that describing the wave characteristics even at this early stage will lead to more definitive experiments to shed light on these atmospheric gravity waves.

A. Waves Form Along Horizontal Interfaces

Although waves can propagate horizontally or vertically, radar has shown waves only along horizontal interfaces. Most radar detection of gravity waves at Wallops Island have been made in clear air. The signal strength from these waves are weak and are mostly limited to within a radius of 40 km. The layers, the waves and the breaking waves which occur are horizontal and are almost invariably associated with stable layers and with vertical wind shear. Fig. 3 is a good example of a horizontal wave structure which formed at an altitude of about 3.5 km to the north of Wallops Island. This wave formation lasted for over 105 minutes and could be seen on many RHI photographs over an azimuth range of about 25 degrees. Outside this azimuth range a radar layer was seen but there was no associated wave structure. Other layers and coherent targets, (birds) may also be seen in this figure.

B. Wave Shape

Some waves are sinusoidal. However, most of the wavy layers detected with radar have a "braided" appearance as illustrated in Fig. 4. Braided waves were interpreted by Hicks and Angell (1968), to be breaking gravity waves. Other mechanisms were proposed to explain the braided appearance but none provided a more satisfactory explanation than that of breaking waves. In addition, there are available optical photographs of clouds which are almost identical with the radar photographs, Colson (1954). It must be concluded that breaking waves remain the most plausible explanation for the radar-detected wave shapes.

Waves sometimes take on the appearance of a wave train. A good illustration of such a formation is shown in Fig. 5. In this figure one can see six stages of the wave within a period of 12 minutes. The radar antenna was pointed toward the west; the wind, and probably also the waves at 1.1 km altitude, were coming toward the radar from the west.

C. Altitude and Wavelength of Gravity Waves

Waves occur at all altitudes up to the maximum radar detection altitudes with no preferred altitude being apparent. A listing of the waves, their altitudes, wavelengths and amplitudes are given in Table 1. From this table one can see the wavelengths lie between 0.6 and 3.4 km with a mean of 1.7 km. Amplitudes vary between 0.2 to 1.5 km, with a mean of 0.5 km. The waves on 17 January 1969 are not included in the averages since the wave structure was uncommonly large. Reed and Hardy (1972); this case will be discussed again below.

TABLE 1

No.	Date	Altitude km	Wavelength km	Amplitude km	No.	Date	Altitude km	Wavelength km	Amplitude km
1	5-10-66	3.2	1.4	0.3	14	1-20-67	11.0	1.7	0.6
2	5-12-66	3.5	1.9	0.4	15	5-16-68	3.5	1.1	0.3
3	5-13-66	4.6	1.8	0.3	16	11-19-68	6.1	1.2	0.5
4	5-20-66	3.7	2.0	0.6	17	11-22-68	1.5	3.4	0.8
5	5-24-66	7.3	1.3	0.5	18	12-20-68	0.8	2.2	0.6
6	5-26-66	3.1	1.5	---	19	12-20-68	2.1	2.2	0.6
7	5-26-66	3.4	0.9	0.4	20	1-24-69	1.1	1.1	0.4
8	5-31-66	4.3	1.4	0.2	21	1-24-69	5.0	3.3	1.5
9	6-1-66	3.5	2.2	0.3	25	4-13-70	1.4	0.6	0.2
10	6-2-66	0.6	2.0	0.4	26	8-24-70	2.5	1.8	0.2
11	6-2-66	1.4	1.4	0.3	Mean			1.7	0.5
12	6-10-66	5.8	1.4	0.2	22	3-17-69	8.5	15-30	2.0
13	12-28-66	12.2	--	0.6	23	3-17-69	8.5	1.6	1.0
					24	3-17-69	7.6	5.0	---

D. Multi-layering

Waves sometimes appear simultaneously at different altitudes and apparently unrelated to each other. Fig. 6 is an example of a situation in which there are four distinct layers with waves in each layer. A sequence of RHI photographs over a 15 minute period showed the layers were somewhat transient with the layers .55 to 1.1 km and 1.9 to 2.4 km being the more persistent and intense. The waves at one level were seen to have little or no relationship with the waves at any other level. This observation suggests that the waves develop independently at the different altitudes and proceed with little or no coupling between the layers.

E. Wave Directions

Wave directions are difficult to obtain from the radar measurements discussed here. Most radar detections of waves were made in the course of investigating other phenomena. Thus one has, in general, only one RHI wedge through the atmosphere and with this a unique direction is not obtainable; measurements over a significant azimuth range are necessary. In the one case in which many RHI slices were made within a 25 degree azimuth range, the breaking waves were found to be aligned with the wind shear. In the study of other wave directions, necessarily coarse, there seems to be a tendency toward alignment with the shear vector, but to date a definitive statement in this regard is as yet not possible.

The Reed and Hardy observation of a large amplitude wave was also one in which waves from different directions were found to coexist. It is relatively common to observe (optically) wave structures in cirrus aligned in different directions. In fact, one of the wave structures in the Reed and Hardy paper was so irregular, Fig. 7, that one would need a Fourier analysis to resolve its spectral content. As yet no spectra have been extracted from radar measurements on waves. Some doppler spectra have been obtained in a deformation field containing a wave structure by Dobson and Meyer (1972) but the shortness of the sampled record precludes extracting a spectrum on the longer period waves.

F. Acoustic or Acoustic-Gravity Waves

A few attempts have been made to measure the phase speed of the waves with the conclusion that they travel with the wind. From this it is apparent that at least some of the radar-detected waves discussed in this paper are either stationary or move slowly with respect to the mean fluid motion. If the waves did indeed move with acoustic speeds, i.e., about 3×10^4 cm per sec, such motion relative to the wind would be readily detectable. Since their motion is slow with respect to the wind, it will require a simultaneous accurate measurement of the wind and the wave phase velocity. The most promising technique for this purpose involves doppler.

G. Seasonal Occurrence of Waves

At the lower altitudes, say up to 5 km, layers and waves occur during all seasons at Wallops Island. Moisture gradients contribute strongly to the radar backscattering; hence, the result that one finds many more strongly reflecting regions at the lower altitudes. Also, it is likely that layers and waves are more predominant during the summer although no definitive statistics are available in this regard.

At the altitudes above about 8 km, layers and waves are detected at Wallops Island only during the winter season when the tropopause is low and also when the jet stream is overhead.

H. Large Amplitude and Long Wavelength Wave

The Reed and Hardy (1972) case is noteworthy because of its obvious difference from the other waves. The large amplitude, 2 km, long wavelength, 15 to 30 km, wave had only a portion of one cycle visible. This is shown in Fig. 8. Their analysis showed the wave occurred within a frontal zone whose width was also 2 km. This outstandingly large wave, in which the Richardson number was less than the critical value of 0.25, contained moderate to severe turbulence. Cirrus clouds above the clear air gravity waves also showed the wave structure as may be seen in Fig. 9. It is interesting to note that here too the two long wavelength waves, one in clear air, the other in cirrus, are not in phase with each other. It would be instructive to postulate a mechanism for such large internal waves relatively close in altitude but yet unrelated.

6. High Resolution Radar Measurements

The previous sections in this paper have dealt with wave structures as seen with radars whose spatial resolution was of the order of 100 m. Recently a high resolution radar system was developed by Richter (1969) which has yielded a wealth of information on the fine detail of waves within the lowest km of the atmosphere.

Recordings from that radar system indicate that gravity waves are always present whenever significant stability exists, Gossard, et al. (1976). Wave periods between 7 and 20 minutes are frequently observed. Calculations of wave speed using the measured perturbations of surface pressure and wind yield values of wave periods which check the periods observed with radar. The ratios of the wave frequency to the Brunt-Vaisala frequency were less than unity. It is concluded these waves represent the fundamental mode of oscillation of gravity waves for a stable atmosphere. Phase speeds were much greater than the local wind speeds. (The measurements at Wallops Island seem to differ from these reports).

The high resolution of the Richter radar yields remarkably clear pictures of breaking gravity waves and helps shed light on the generation of turbulence. In Fig. 10 is reproduced an example from that radar of a portion of a wave train increasing in amplitude with time, obviously breaking. An important feature of this photograph lies in the fact that the structure was visible to the radar before breaking occurred. This implies turbulence at a smaller scale existed prior to the formation of the gravity wave. This is in keeping with the theory of Ottersten (1970) discussed earlier.

7. Conclusions

As a result of the radar observations at Wallops Island and elsewhere one can characterize gravity waves, some of these quite tentative at present, as they occur in the troposphere:

- (1) Waves are a common occurrence in the troposphere,
- (2) They form on horizontal stable layers,
- (3) They are acoustic-gravity waves,
- (4) They are transient or they may last up to several hours,
- (5) They may be sinusoidal in shape and appear as wave trains,
- (6) They frequently become breaking waves,
- (7) They appear at all altitudes up to the tropopause,
- (8) They have a mean wavelength of 1.7 km and range between 0.6 and 3.4 km; (some are much larger),
- (9) They have amplitudes between 0.2 and 1.5 km with a mean of 0.5 km,
- (10) They are multi-layered, sometimes as many as four waves appear at different closely spaced altitudes, each with phases and perhaps directions independent of the other,
- (11) They tend to be aligned with the shear vector,
- (12) waves from different directions can coexist at the same altitude,
- (13) They occur during all seasons.

Much excellent theoretical work has been done on the subject of gravity waves. However, the experimental results described in this paper and summarized above suggest a complex system of wave structures and motions whose ultimate description will probably require a 3-dimensional spectrum similar to that in use at present to describe the ocean surface.

It is hoped that the characterization of the waves presented here, although based on a relatively small number of cases, will lead to future experiments with high resolution radars and, hopefully, in-situ probes which will improve our total understanding of the dynamics of the atmosphere.

8. Acknowledgements

The research reported here is being sponsored by Air Force Cambridge Research Laboratories and NASA. Many of the observations on waves are credited to Jack Howard and his staff operating the Wallops Island radar systems; without their alertness and technical competence much of the progress on clear air phenomena would not have been possible.

9. Bibliography

- Batchelor, G. K., (1955), "The scattering of radio waves in the atmosphere by turbulent fluctuations in refractive index." Tech. Rept. No. 26, School of Electrical Engineering, Sept., p. 16.
- Booker, H. G., and Gordon, W. E., (1950), "Theory of radio scattering in the troposphere," Proc. IRE 38, p. 401-412.
- Colson, D., (1954), "Wave-cloud formation at Denver," Weatherwise 7, p. 34-35.
- Dobson, E. B., and Meyer, J. H., "Doppler radar investigation of a clear air layer," Applied Physics Laboratory, Memorandum BPD72U-002, 3 Jan. 72, to be submitted for publication.
- Glover, K. M. and Duquette, E. F., (1970), "A study of clear air turbulence using sensitive radars," Fourteenth Radar Meteorology Conference, Tucson, Arizona, November, p. 89-94.
- Gossard, E. E., and Richter, J. H., (1970), "The shape of internal waves of finite amplitude from high resolution radar sounding of the lower atmosphere," Journal of Atmospheric Sciences, 27, 6, September, p. 971-973.
- Hicks, J. J., and Angell, J. K., (1968), "Radar Observations of breaking gravitational waves in the visually clear atmosphere," Journal of Applied Meteorology 7, 1, February, p. 114-121.
- Ottersten, H., (1970), "Radar observations of the turbulent structure in shear zones in the clear atmosphere," Fourteenth Radar Meteorology Conference, Tucson, Arizona, November, p. 111-116.
- Reed, J. R., and Hardy, K. R., (1971), "A case of persistent, intense clear air turbulence in an upper level frontal zone," submitted for publication to the Journal of Applied Meteorology.
- Richter, J. H., (1969), "High resolution tropospheric radar sounder," Radio Science, 4.
- Tatarski, V. I., (1961), "Wave propagation in a turbulent medium," McGraw-Hill, New York, 285 p.

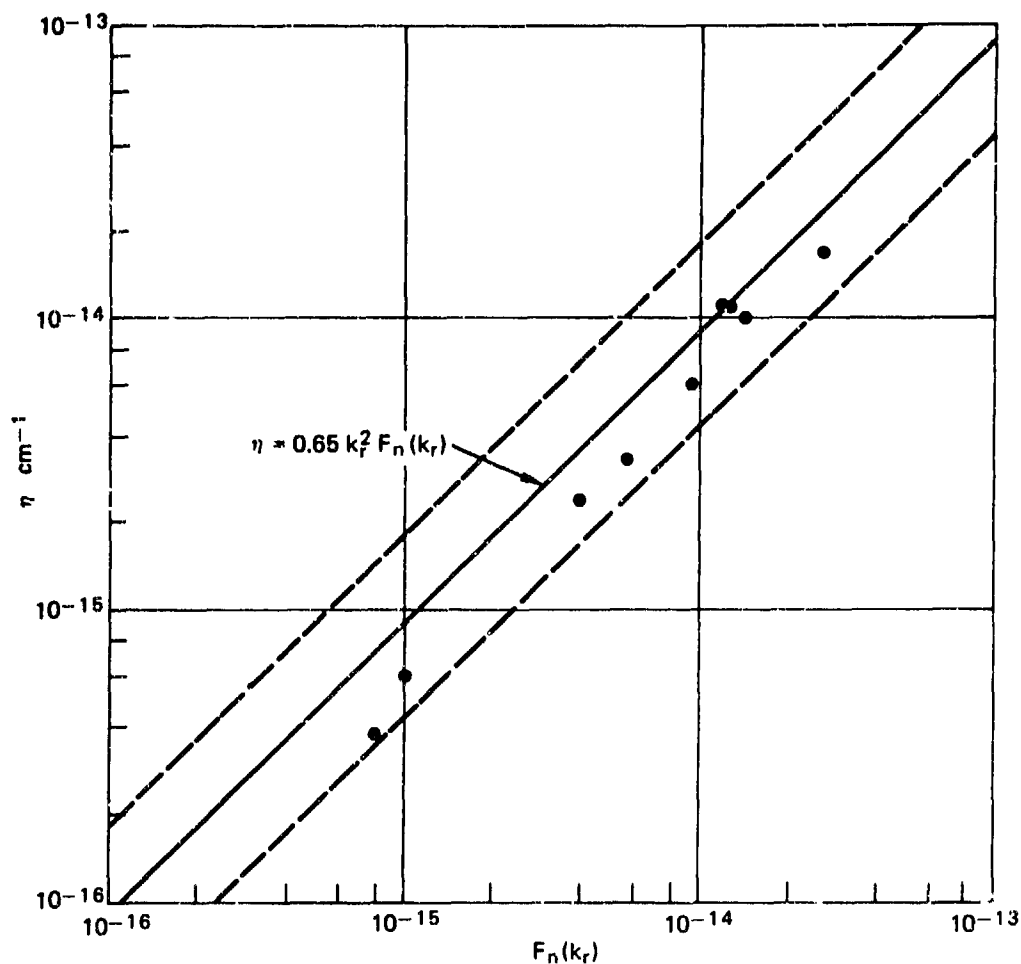


Fig.1 Experimental verification of theoretical prediction of the dependence of radar reflectivity, η , on the refractivity spectrum, $F_n(k_r)$. The solid line gives the theoretical prediction and the dotted lines are ± 3 db.

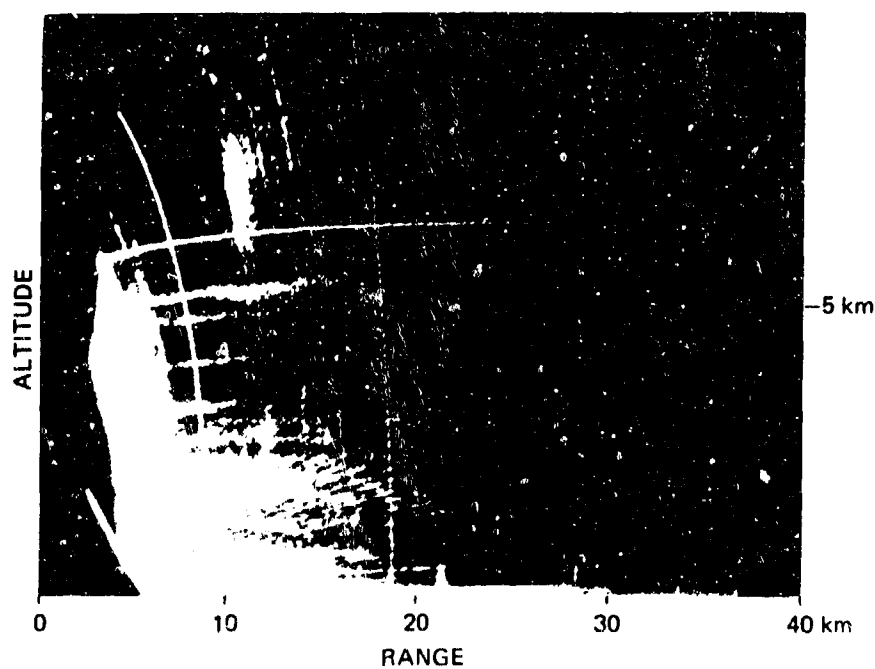


Fig.2 Range-height photograph showing many stratified layers. Azimuth is fixed at 180 degrees. Date: 19 May 66.

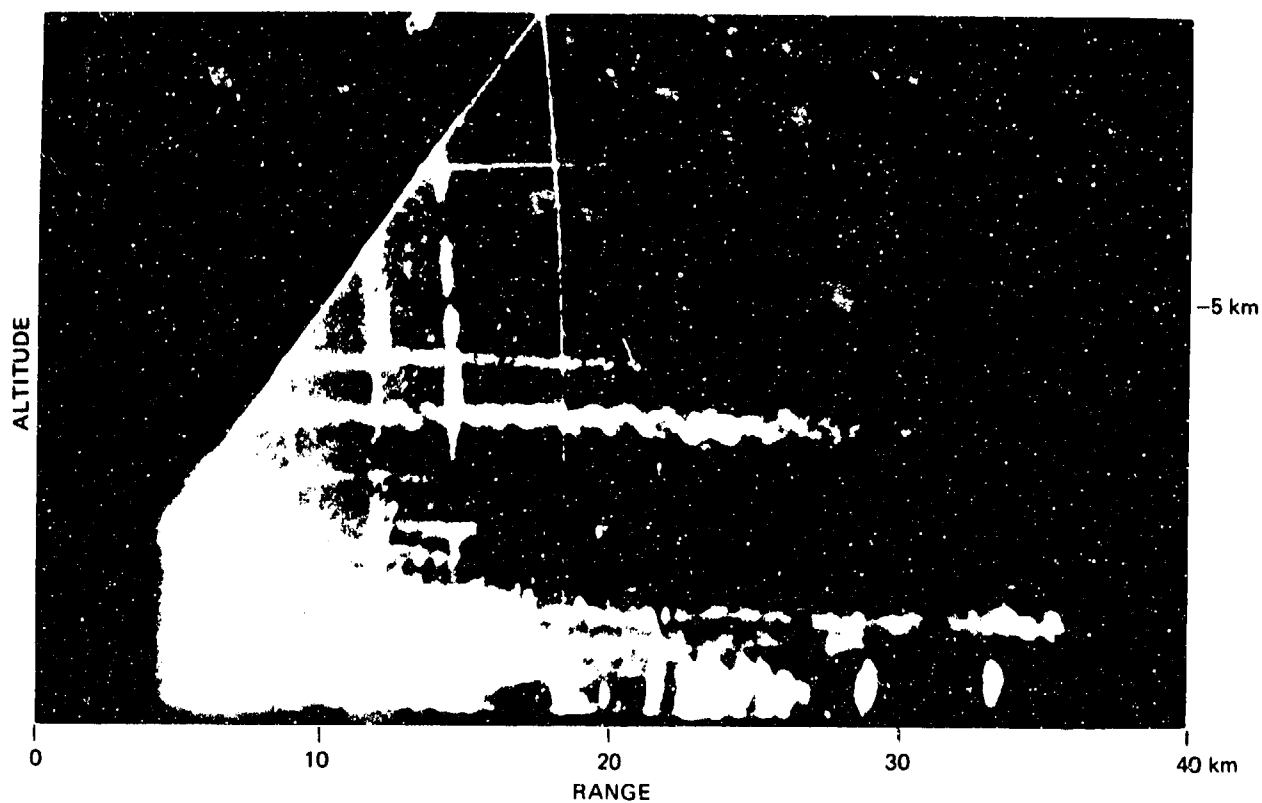


Fig.3 Horizontal wave structure at 3.5 km to the north of Wallops Island, 16 May 68. This wave extended over a 25 degree azimuthal range and lasted over 105 minutes.

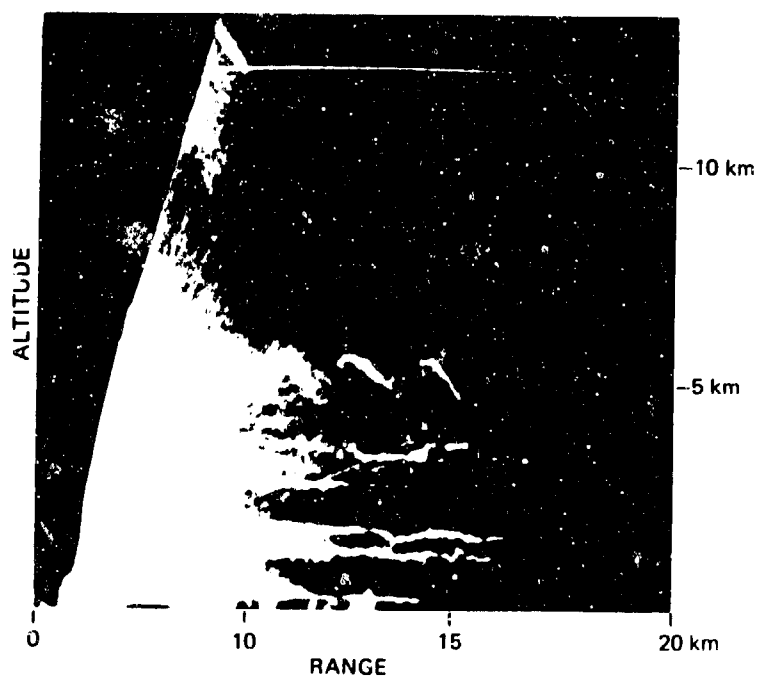


Fig.4 Braided wave structure at 5 km on 24 Jan. 69. Braided appearance is interpreted as breaking gravity wave.

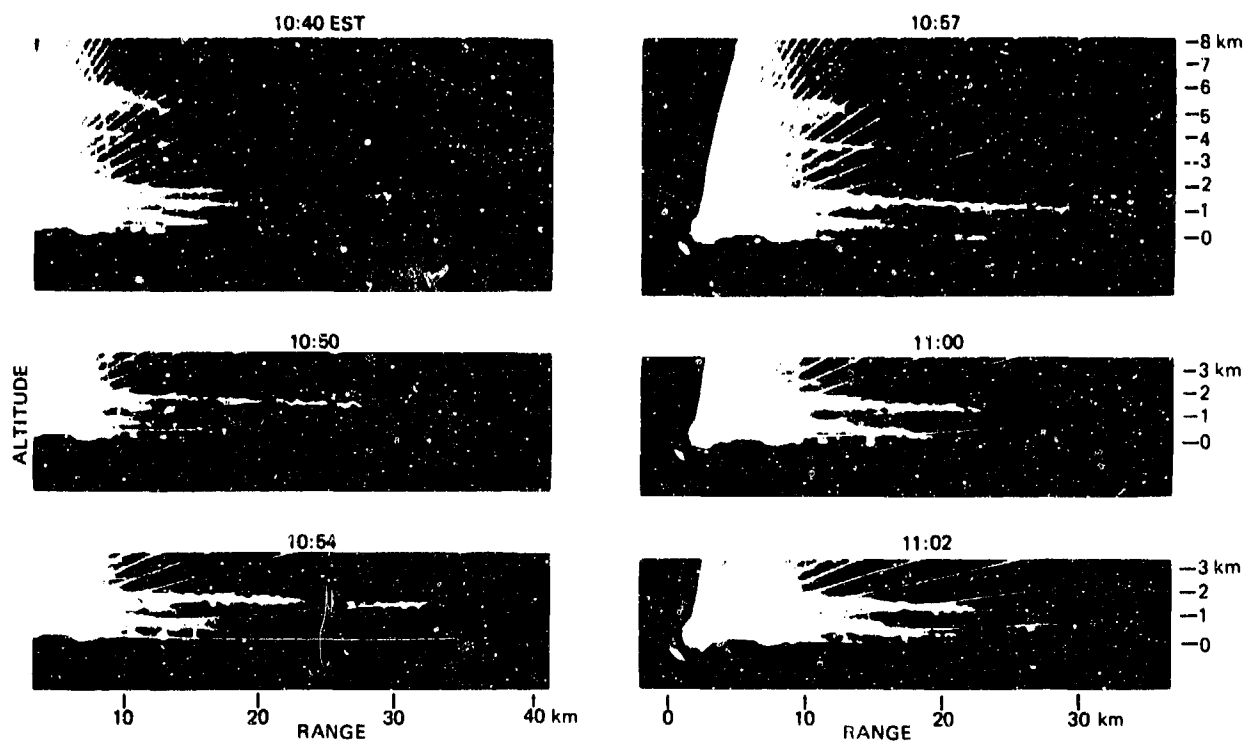


Fig.5 Six stages of a wave in a wave train formation, 24 Jan. 69. Waves are probably traveling toward the radar from the west and lasted about 12 minutes.

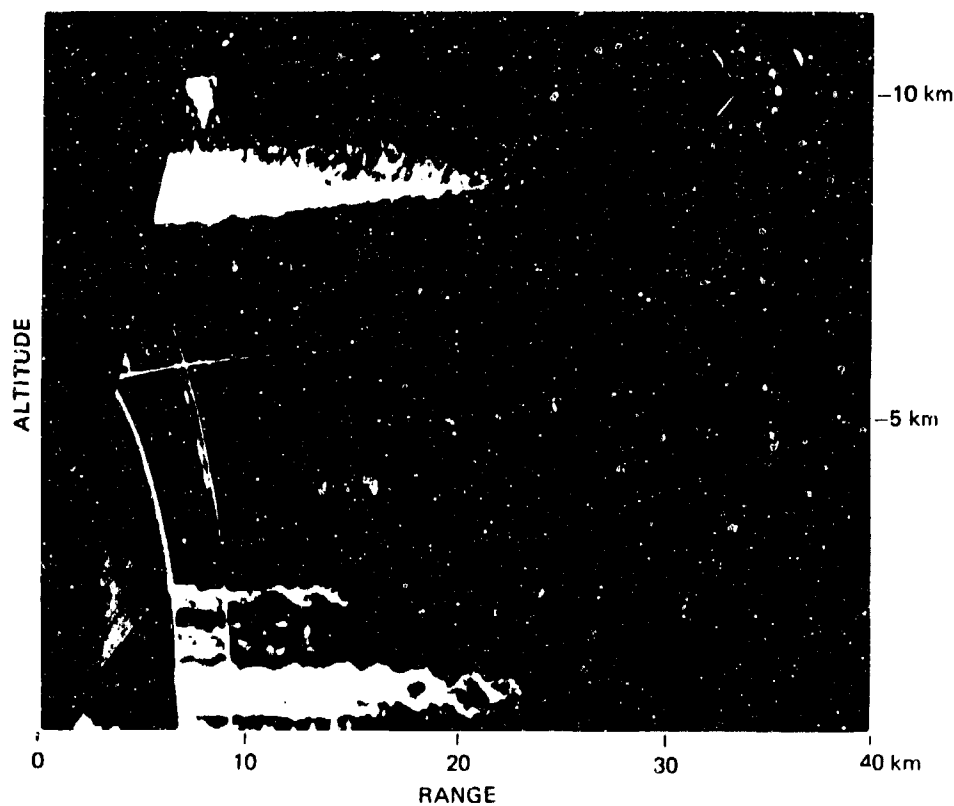


Fig.6 Waves occurring at different altitudes simultaneously with little or no apparent coupling between the layers. The layer at about 8 km is cirrus cloud.

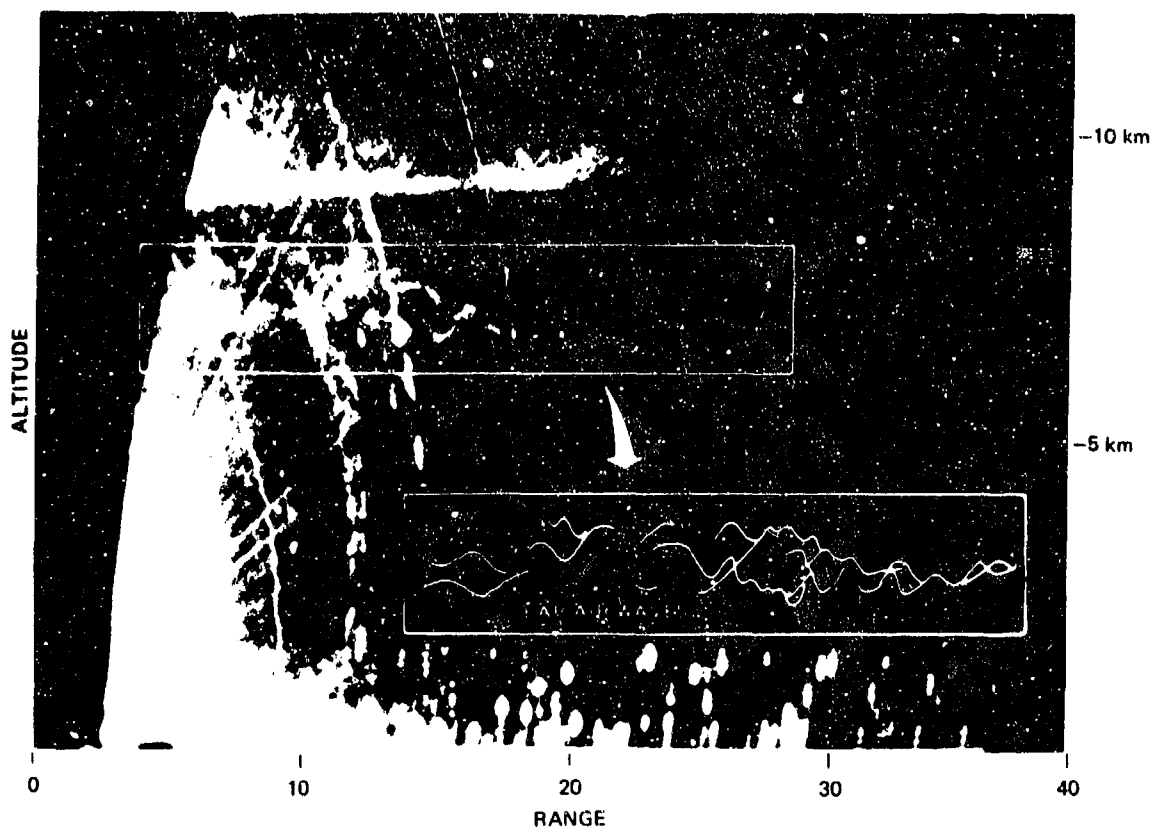


Fig.7 Complex wave structure at 7.5 km, possibly resulting from waves arriving from different directions.

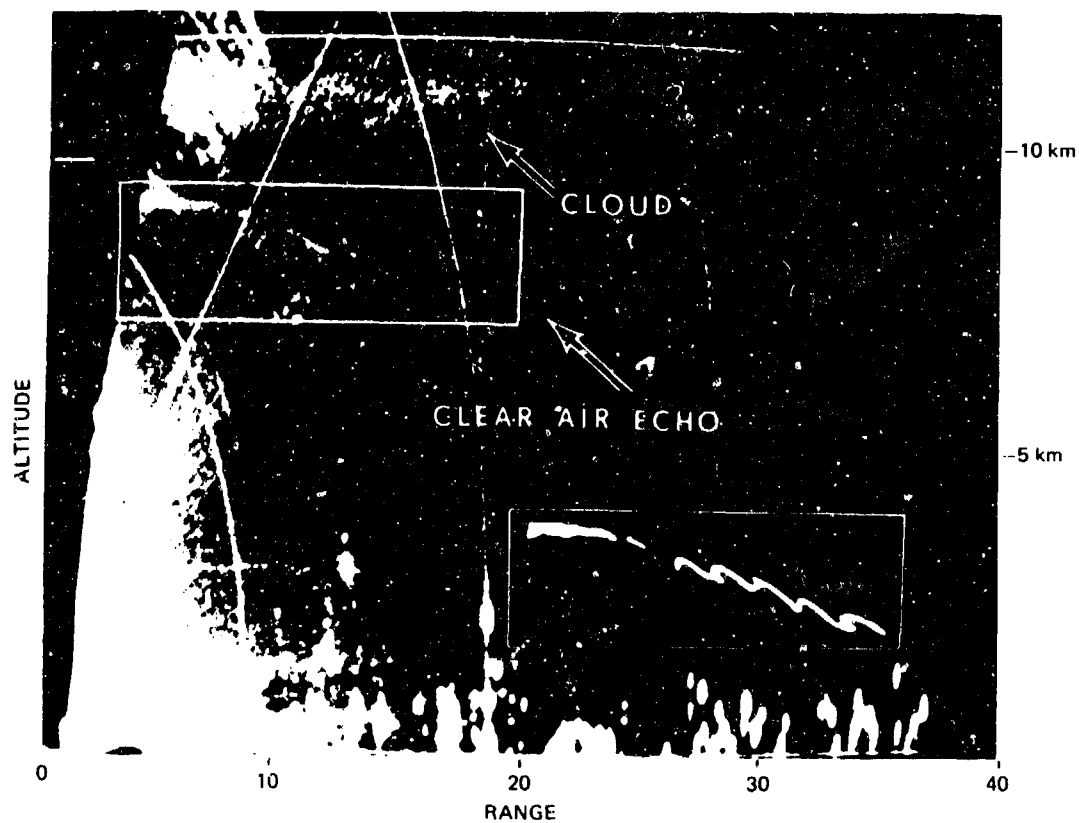


Fig.8 Very large amplitude and long wavelength wave which occurred on 17 Mar. 69. Smaller amplitude wave is riding riding on the larger wave. The larger wave was associated with high rate of wave turbulence.

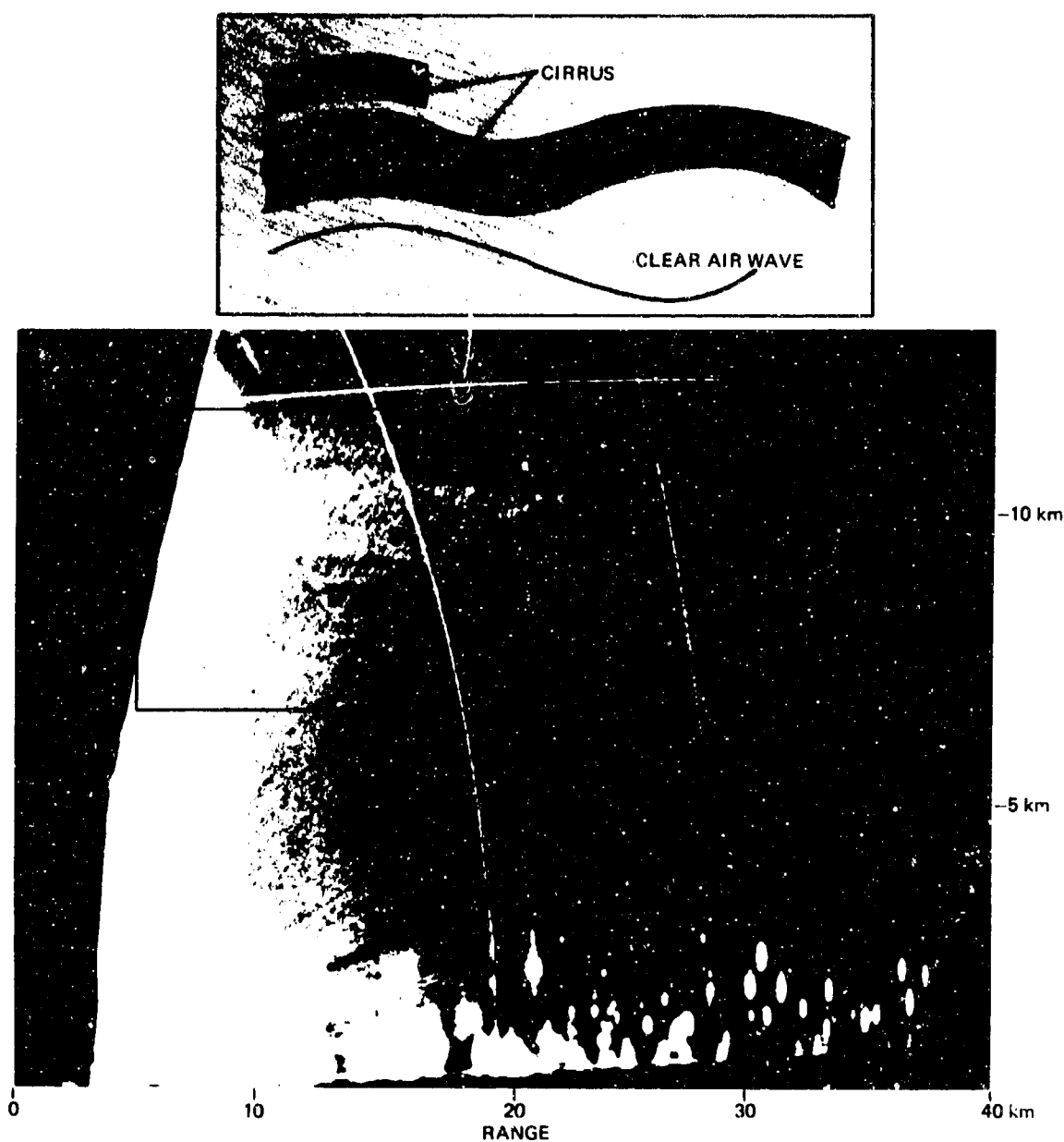


Fig.9 Another photograph of the wave structures on 17 Mar. 69. This is an example of a clear air gravity wave out of phase with the cirrus waves above it.

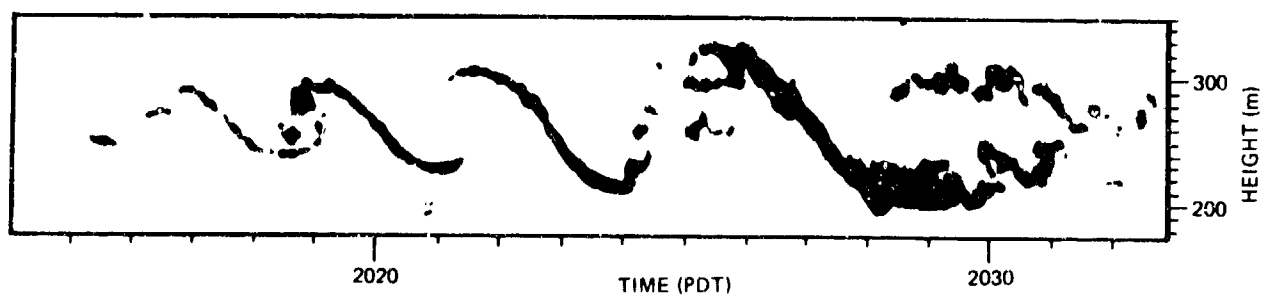


Fig.10 Portion of a breaking wave train at 250 m altitude as measured on the Richter radar. Note that the wave is visible on the radar prior to the larger scale breaking. This indicates turbulence at a small scale before the gravity wave developed.

OBSERVATIONS OF GRAVITY WAVES IN THE HEIGHT RANGE 50-70 KM

by

G.E.Perona

**Istituto di Elettronica e Telecomunicazioni
Politecnico di Torino, Italy**

L'OBSERVATION DES ONDES ACOUSTIQUES ET DE GRAVITE DANS LA ZONE SITUÉE
ENTRE 50 ET 70 KM D'ALTITUDE

par

G.E. Perona

SOMMAIRE

On peut détecter avec succès des ondes acoustiques et de gravité dans la région D de l'ionosphère, malgré les difficultés bien connues liées à l'interprétation des données de cette région. Cette possibilité est d'abord démontrée théoriquement, puis confirmée par une analyse attentive des données TBF et des données d'intermodulation portant sur la zone située entre 50 et 70 km d'altitude. Les limites relatives à l'amplitude, à la fréquence et à la longueur d'onde des ondes acoustiques et de gravité susceptibles d'être détectées à ces niveaux sont brièvement examinées.

OBSERVATIONS OF GRAVITY WAVES IN THE HEIGHT RANGE

50 - 70 KM.

G.E. PERONA

Istituto di Elettronica e Telecomunicazioni
Politecnico di Torino, Italy

SUMMARY

Acoustic-gravity waves can successfully be detected in the D region of the ionosphere in spite of all the well-known difficulties that characterize the interpretation of the data concerning that region. This possibility is demonstrated from a theoretic point of view and is successively confirmed by a careful analysis of VLF data and cross-modulation data, related to the 50-70 Km range. The limits on the amplitude, frequency and wavelength of acoustic-gravity waves that may be detected at these levels, are outlined.

1. INTRODUCTION

At present, no measurement techniques are available for continuously monitoring the atmospheric parameters in the height range 50-70 Km. Specifically, balloons are efficient up to 30 Km only; rockets are a source of great local perturbations. Besides, measurements with rockets and balloons are discontinuous. Even standard electromagnetic techniques present low efficiency. Therefore, acoustic and internal gravity waves are not monitored in the height range quoted above, where the theoretic analysis shows that many interesting phenomena take place, like ducting and reflection. Above 70 Km, lasers have recently detected long period internal gravity waves, (KENT G.S. et al., 1972), and below 50 Km high-resolution radar measurements are used to study internal waves in the atmosphere near the ground (GOSSARD and RICHTER, 1970).

Up to date, only two ground-based electromagnetic techniques have been successfully used in studying the lower D region, namely the cross-modulation experiments and the VLF propagation. The present paper will examine the possibility of detecting gravity waves in the height range 50-70 Km with these two techniques. Its first section evaluates changes in electron density produced by gravity waves in an idealized diurnal atmosphere, assumed to be isothermal, in photochemical and diffusive equilibrium, and without wind motions. The second and third sections deal respectively with gravity waves and cross-modulation, and gravity waves and VLF propagation. A few experimental results will be presented in support of the theoretic analysis.

2. GRAVITY WAVES AND REGION D

2.1 Gravity waves.

The "polarization" relations for gravity waves propagating in an isothermal atmosphere without winds, can be written as follows (HINES C.O., 1960):

$$p_1/P = \rho_1/\rho = U_x/X = U_z/Z = T_1/T = A \exp \{ i(\omega t - k_x x - K_z z) \} \quad (1),$$

where:

- p_1, ρ_1 , and T_1 are the normalized variations of pressure, density and temperature;
- U_x , and U_z are the horizontal and vertical components of the neutral air velocity;
- $\omega = 2\pi/T$ is the angular frequency;
- k_x , and $K_z = k_z + j/2H$ are the horizontal and vertical wave numbers;
- H is the scale height of the neutral atmosphere;
- P, ρ, X , and Z are functions of frequency, wave numbers and atmospheric parameters (HINES C.O., 1960); and
- $\psi = P - R$.

Other parameters that will appear later are defined here for convenience:

- c = speed of sound; $\gamma \approx 1.4$ is the adiabatic exponent; g is the gravity acceleration;
- $\omega_a = \gamma g/2c$; $\omega_a = 2\pi/T_a = (\gamma - 1)^{1/2} g/c$;

- $H[O], H[O_3], \dots$ are the scale heights in Km of the minor atmospheric constituents O, O_3, \dots ;
- $[O], [O_3], [O(^3P)], \dots$ are the number densities in cm^{-3} .

Changes induced by a gravity wave in diurnal lower D region will be analyzed in two steps: namely, changes in the relevant minor neutral constituents of the atmosphere, and changes in the electron density. The cross-modulation of radio waves with periods longer than 10 min. will be examined in detail because their

analysis is more involved and would lead to similar results, which could be obtained

out for shorter gravity waves and acoustic waves.

It is known (HINES C.D., 1960) that, under the following assumptions:

$$k_z^2 \gg \omega_a^2 / c^2, \quad \omega^2 < \omega_g^2 \quad (2),$$

the dispersion equation and the "polarization" relations for internal gravity waves become extremely simple:

$$\omega^2 k_z^2 = \omega_g^2 k_x^2 \quad (3),$$

$$U_z/U_x = -k_x/k_z = -\omega/\omega_g; \quad \rho_1/U_x = j(\gamma-1)^{1/2}/c; \quad \rho_1 = -T_1. \quad (4).$$

The horizontal and vertical displacements, respectively Δx and Δz , of the air masses moved by the gravity waves are approximately equal to: $\Delta x = -j U_x/\omega$ and $\Delta z = -j U_z/\omega$. The normalized real parts of ρ_1 , T_1 , U_x , U_z , Δx , and Δz are shown in Fig. 1. It is important to notice that the amplitudes of the sinusoids do not depend on ω within the approximations of the inequalities (2). Furthermore, T_1 and ρ_1 have the same amplitude but are of opposite phase, while U_x and U_z are in quadrature with them. This fact implies that the air masses moved by the gravity waves, pass through their equilibrium position (e.g. at $t=t_0$, where $\Delta x = \Delta z = 0$) with maximum speed and unperturbed density and temperature. The air found in $P_1(x_1, z_1)$ at $t = t_1$ has been displaced from its equilibrium position, $P_0(x_0, z_0)$, by an amount equal to $\Delta x(t_1) = x_1 - x_0$, and $\Delta z(t_1) = z_1 - z_0$. From P_0 to P_1 the gas followed an adiabatic transformation. Hence, $\bar{T}_1 = (\gamma-1)\bar{\rho}_1$, where \bar{T}_1 and $\bar{\rho}_1$ are the normalized Eulerian changes of the temperature and density of the gas. Since the atmosphere has been supposed to be initially isothermal, $\bar{T}_1 = T_1$ and, consequently $\rho_1 = -(\gamma-1)\bar{\rho}_1$. From P_0 to P_1 , the air expanded adiabatically ($\bar{\rho}_1$ is negative), but its density still remained larger than the density of the air present at the new level in equilibrium conditions ($\rho_1 > 0$).

2.2 Minor neutral constituents in the D region.

From P_0 to P_1 , the air carried along its minor neutral constituents, in particular $O(^3P)$ and O_3 . Let us suppose, for the moment, that the quantity of atomic oxygen and ozone present is constant, so that the new concentrations observed in P_1 are easily estimated as follows:

$$[O(^3P)]_{P_1, t_1} = [O(^3P)]_{P_0, t_0} \times (1 - \rho_1/(\gamma-1)) = [O(^3P)]_{P_1, t_0} \times (1 + \Delta z/H([O(^3P)]) (1 - \frac{\rho_1}{\gamma-1})) \quad (5),$$

$$[O_3]_{P_1, t_1} = [O_3]_{P_1, t_0} \times (1 + \Delta z/H([O_3]) (1 - \rho_1/(\gamma-1))) \quad (6).$$

The scale heights in the above equations have been estimated to be:

$$H([O(^3P)]) = -10 \text{ Km} \quad (\text{SHIMAZAKI and LAIRD, 1970}),$$

$$H([O_3]) = 4 \text{ Km} \quad (\text{SHIMAZAKI and LAIRD, 1970}),$$

for overhead sun, that is for the sun zenith angle, ζ , equal to zero. Therefore, the normalized change in $[O(^3P)]$ appears to be of the order of $-5.5\rho_1$, and the normalized change in $[O_3]$ is approximately $+2.5\rho_1$, provided such minor constituents have a life time longer than a quarter period of the gravity waves. The atomic oxygen $O(^3P)$ is at work in many reactions of aeronomic interest (HUNT G.B., 1966; SHIMAZAKI and LAIRD, 1970). It can be produced in various ways, but its main source is photodissociation of O_2 , with a dissociation coefficient of the order of 10^{-9} s^{-1} for overhead sun (SHIMAZAKI and LAIRD, 1970). In the height range under consideration, $[O_2] = 10^{16} - 10^{15} \text{ cm}^{-3}$ and $[O(^3P)] = 10^{10} - 10^{11} \text{ cm}^{-3}$, hence correspondingly the time constant is of the order of $10^3 - 10^5 \text{ s}$. $O(^3P)$ can also be produced either by photodissociation of NO_2 , or by ionization followed by dissociation of NO , or etc., but the corresponding time constants are much longer than 10^3 s . Another important source of atomic oxygen is the photodissociation of O_3 , with a dissociation coefficient as high as 10^{-2} sec^{-1} , for overhead sun and above 60 Km (SHIMAZAKI and LAIRD, 1970). However, $[O(^3P)]/[O_3] = 10 - 100$ in the height range 60-70 Km; hence, dissociation of O_3 cannot appreciably change the total oxygen content on a time scale shorter than 1000 s. In conclusion, when an internal gravity wave perturbs the atmosphere, the normalized change in $[O(^3P)]$ can be simply computed from eq.(5) if the quarter period of the gravity wave is substantially shorter than 1000 s.

The situation may be different for O_3 . Indeed, from eq. (6) it appears that $[O_3]_{P_1, t_1}$ should increase with respect to its equilibrium value in P_1 . However, as stated above, the time constant for photodissociation of O_3 , $\tau(O_3)$, is of the order of 100 s above 60 Km for overhead sun: this value is approximately equal to the quarter period of the shortest possible internal gravity wave. Hence, O_3 must be always in photochemical equilibrium with the other species. However, at middle and high latitudes, it will be seen that $\tau(O_3)$ substantially increases. For example, during winter, at 45° latitude, 60 Km height and noon local time ($\zeta \approx 90^\circ$) $\tau(O_3)$ can be estimated to be 10^3 s .

Consequently, even an internal gravity wave with a 20 min. period is able to displace O_3 without affecting the total O_3 content. In this case too, normalized changes in O_3 can be estimated from eq.(6).

The behavior of other minor neutral constituents will not be examined here, since they do not affect the electron balance in the height range considered. Even NO ceases to be important in this respect just below 70 Km.

2.3 Electron density.

Several detailed schemes of electrons and ions balance have been published (FENSENFELD F.C., et al., 1967; LELEVIER and BRANSOM, 1968; FITE W.L., 1969; FERGUSON E.E., 1969; REID G.C., 1970; FERGUSON E.E., 1971). For the present analysis, the simplified scheme of Fig.2 is adequate; it is very similar to the so-called two-ions model (ADAMS and MCGILL, 1967). In the height range 50-70 Km, two sub-regions characterized by different types of predominant recombination processes, are considered:

- region α , approximately above 60 Km, where negative charges are lost mainly by recombination of electrons with positive ions;
- region β , approximately below 55 Km, where negative charges are lost mainly by recombination of negative with positive ions.

The two regions will be examined separately. It will be assumed that ions and electrons do not significantly diffuse in a time comparable with one-quarter period of the gravity wave considered.

The ions are considered first. At 65 Km, in region α , the production rate is taken to be $0.05 \text{ cm}^{-3} \text{ s}^{-1}$ (VELINOV P., 1968; FRANDY R.Y., 1970), the ion density is at least 300 cm^{-3} , hence, the time constant for positive ion generation is longer than 6000 s. At 50 Km, in region β , the production rate is of the order of $0.5 \text{ cm}^{-3} \text{ s}^{-1}$, the positive and negative ion density is of the order of $3 \times 10^3 \text{ cm}^{-3}$, hence, the time constant is longer than $6 \times 10^4 \text{ s}$. (COLE and PIERCE, 1965). Therefore the ions follow the motion induced by the gravity waves without being significantly altered by generation and destruction processes, if the gravity wave quarter period is shorter than the time constants just computed.

For what concerns the electrons, both theoretic (COLE and PIERCE, 1965) and experimental (MECHTLY and SMITH, 1968) results seem to confirm that their density at, let us say, 65 Km, is of the order of 30 cm^{-3} . This implies a time constant of the order of 600 s. Consequently, when studying the changes produced in the electron density by a gravity wave with period of the order of 20 min. or less, $[e]_{P1,t1}$ can be easily evaluated as follows:

$$[e]_{P1,t1} = [e]_{P1,t0} \times (1 + \Delta z/H_e) (1 - \rho_1/(\gamma-1)) \quad (7).$$

The electron density profiles can be expressed in term of $H_e(z,t)$, the effective scale height. It is not uncommon to find $H_e \approx 5 \text{ Km}$ in region α (COLE and PIERCE, 1965; MECHTLY and SMITH, 1968; REID G.C., 1970). Hence, normalized changes in $[e]$ can be estimated from eq.(7) to be of the order of $\sim 10 \rho_1$.

In region β , the electron density is very small and the electron life time is of the order of a second. Therefore, the electrons reach their equilibrium density very quickly. For example, at 50 Km, the balance equation for electrons is (see Fig.2):

$$Q = K_{att} \times [e] \cdot [O_2] \cdot [O_2] - K_{det} \times [O_2^-] H_0(^3P) \quad (8),$$

where K_{att} and K_{det} are the attachment and detachment coefficient respectively. Each of the terms in the righthand-side of the above equation is much larger than Q , the production rate. Therefore, the equilibrium density can be computed by simply equating attachment and detachment, and its percent change $[e]_1$ comes out equal to:

$$[e]_1 = -[K_{att} I_1 - 2[O_2]_1 + [K_{det} I_1 + [O(^3P)]_1 + [O_2^-]_1] \quad (9),$$

where the parentheses indicate normalized changes of the bracketed quantities. The coefficient K_{att} is weakly dependent on temperature (PHELPS A.V., 1969); K_{det} too is probably a weak function of temperature, though a definite statement based on experimental results cannot be made (PHELPS A.V., 1969). Therefore, the temperature dependence effects of K_{att} and K_{det} on $[e]$ will be neglected. In eq.(9), $[O_2]_1$ can be assumed equal to ρ_1 , $[O(^3P)]_1$ can be estimated from eq.(5); $[O_2^-]_1$ has still to be evaluated. As it is known, O_2^- is one minor constituent of the negative-ion family, since its life time is very short due to the fast conversion to O_3^- by collision with O_3 . During the perturbations induced by a gravity wave, this ion can reach its equilibrium value, that is:

$$Q = K_{int} \cdot [O_2^-] H_0(^3P) \quad (10),$$

where K_{int} is the coefficient for charge exchange. The temperature dependence of K_{int} is unknown (FERGUSON E.E., 1969), but reaction rates for similar types of charge exchange have been shown to be

slightly dependent on temperature. Consequently, it seems reasonable to assume that $[O_2]_1 = -[O_3]_1$. Finally, after adding all the contributions in the right-hand side of eq.(9), it turns out that $[O]_1$ is approximately equal to $-10 [O_3]_1$ in region β .

At this point it can be stated that small normalized changes in the neutral air density produced by gravity waves with period of the order of 20 min. or less, cause changes in electron density that are ten times larger. This semi-theoretic result has to be accepted with caution. First of all, the present estimate of the phenomena concerns only an order of magnitude. A precise analysis would have to solve the full set of differential equations for the neutral and charged constituents. Secondly, the present estimate is highly dependent on the values assumed for the scale heights of the relevant atmospheric constituents, that can be affected by large errors. However, there is at least one experimental set of results supporting the conclusions reached in the course of the semi-theoretic analysis. Winter time measurements of VLF phase and amplitude have shown large perturbations. These phenomena were interpreted in terms of temperature changes in the neutral air that are known to be relatively large in such a season. The mechanism becomes operative through changes in the density of some minor neutral constituents, like $O(P)$ or O_3 (DOHERTY B.H., 1968).

3. THE CROSS-MODULATION MEASUREMENTS

These experiments produce changes in amplitude (FEUER J.A., 1955; SMITH et al., 1965), in phase (FERRARI et al., 1963), and in Faraday rotation (RUMI G.C., 1968) of a "wanted" wave as a result of the interaction with a "disturbing" wave. The height range is measured by the delay between the transmission of the "disturbing" pulse and the arrival of the "wanted" pulse. The height resolution is determined by the length, l , of the pulses. This implies that only acoustic-gravity waves with vertical wavelength longer than l_0 could be detected. Furthermore, a lower limit on the horizontal wavelength of the acoustic-gravity waves is placed by the dimensions of the first Fresnel zone.

The measured normalized quantity, M , is proportional to $[e] \times f(\nu) / \nu^2 T_e$, where ν is the electron-neutral collision frequency, T_e is the electron temperature assumed to be equal to the neutral air temperature and $f(\nu)$ is a complicated function, that can be written as $f(\nu) \sim \nu^\delta$, where $[e] \leq 1$. The collision frequency is proportional to $q T_e^\delta$, where q is the air density and δ is a positive number, varying from 0.5 to 1, depending on the theoretic model (COMPTON R.W. et al., 1953; COLE and PIERCE, 1965). Even different types of experimental techniques seem to give not quite consistent values for δ . Anyway q and T_e change in opposite direction, at least under the action of the internal gravity waves considered in the previous section. Therefore, ν and $\nu^2 T_e$ do not change appreciably, and changes in M are approximately proportional to the normalized variations in $[e]$. For different waves or disturbances such that q and T_e are not of opposite phase, the dependence of M on $\nu^2 T_e$ should be taken into account. Furthermore, in this case, whenever amplitude measurements are concerned, even changes in $f(\nu)$ could become quite important. Indeed, $f(\nu)$ is a rapidly varying function of ν at the height where it goes through zero, that is approximately where the operating angular frequency equals 2.2ν (RUMI G.C., 1962).

According to experimental evidence, most of the time the cross-modulation experiments are disturbed by spurious effects, of unknown origin, such as a modulation of the reference level with a period in the range of the acoustic or internal gravity waves. This suggests that such waves can indeed be detected. An example is reported in Fig.3, adapted from RUMI G.C. (1966). The parameters of the experiment were: "wanted" frequency = 3.335 MHz; disturbing frequency = 13.866 MHz; pulse length = 50 μ s; antenna beam = 15°; place of the experiment: Cornell University, Ithaca, N.Y.; height range = 54 Km. Fig.3 shows that the intensity of cross-modulation varied with a period of the order of 1 min. Only the above qualitative interpretation is offered. The quantitative analysis of the data is not attempted, since, at 54 Km height, eddies with characteristic dimension of the order of the "wanted" wavelength can be present (ROOKER H.G., 1956). It has been suggested (RUMI G.C., 1968) that these eddies can be important in determining the level of the signal. However, no theoretical analysis of their effect has been performed. It is worth mentioning that modulation periods longer than five minutes have been observed.

From the present discussion it appears that gravity waves can be detected, and, in fact, have been detected, by cross-modulation experiments. With this technique, it should be possible to measure not only the period of the wave, but also the vertical wavelength by quickly scanning in height. The horizontal wavelength could not be measured with the equipment presently in use.

4. VLF MEASUREMENTS

VLF propagation in the earth-ionosphere cavity is usually studied with the mode theory (WAIT J.R., 1962). Only under particular conditions the ray theory can be applied. Such conditions are in fact verified for the propagation of the G.R.R. - 15 KHz signal on the link Rugby-Torino, with mid-path reflection point just above Paris. At this frequency, the ionosphere can be considered sharply bounded and the reflection level, z_r , during the day is in the neighborhood of 70 Km (BRACEWELL R.N. et al., 1951). The total phase delay measured at the receiving station is the sum of three factors: a) the path length, b) the value of the refractive index below the reflection level, c) the phase, $\arg(\Gamma_R)$, of the reflection coefficient. Γ_R depends on two parameters, the angle of incidence, θ , and the quantity $2\mu\kappa$, where μ is the real part and κ is the imaginary part of the refractive index at the reflection level.

For the link Rugby-Torino, $2\mu x$ is of the order of 0.8 and $\theta_1 = 75^\circ$ (RUIT G.O., 1971). To a first approximation, it can be interpreted that a gravity wave does not affect $2\mu x$, but changes the height of reflection. In general, for what concerns θ_1 , and, consequently, $\arg(\mu R_1)$, it should be noted that θ_1 changes only if the refractive index of the layer below the reflection level changes. However, for the present case, no layer with refractive index sufficiently different from one and thickness sufficiently larger than a wavelength exists below z_1 during daytime. Furthermore when $2\mu x = 0.8$ and $\theta_1 = 75^\circ$, the phase of the reflection coefficient is almost independent on θ_1 . Therefore, a gravity wave changes the phase delay of VLF waves only by changing the geometry of the path, that is by moving the reflection level. Quantity Δz is easily evaluated since $\tan \Delta z/H = [\epsilon]$. From the geometrical configuration it appears that the phase delay introduced by a change in z_1 is equal to $2\Delta z \cdot \cos \theta_1/c$, where c is the velocity of light. A 10% decrease in $[\epsilon]$ causes a delay of the order of $1\mu s$. It is to be noted that the preceding discussion on θ_1 should be completely reviewed if the reflection level is higher than 70 Km. Indeed, in this case, the layer below z_1 may be sufficiently efficient in changing θ_1 ; furthermore, $2\mu x$ at z_1 may be larger, and, consequently, $\arg(\mu R_1)$ becomes very sensitive to changes in θ_1 .

In order to be seen on VLF phase records, gravity waves should satisfy the following conditions. Their vertical wavelength should be larger than the penetration depth of the VLF signal into the reflecting layer, estimated to be 1/4 of the VLF wavelength, that is 5 Km at 16 KHz. Their horizontal wavelength should be larger than the first Fresnel zone, that is of the order of 100 Km for the Rugby-Torino link at 16 KHz. These two conditions imply that only internal gravity waves with period longer than approximately 10 min. can be seen with this technique since internal waves with shorter period will be reflected well below 70 Km (HINES G.O., 1960). A type of possible "resonant" interaction may arise when the horizontal wavelength of the gravity waves is half the VLF wavelength. In this case too, changes on the VLF phase may be quite large. No quantitative analysis of such effects will be attempted here.

Fig.4 through 7 show records of 16 KHz phase measurements on the Rugby-Torino path. The distance between the two stations is 1040 Km., and the orientation of the path is 34° W of N. Fig.4 and 5 present wave-like structures with periods of the order of 15 min. Even if the amplitudes are small, of the order of $1 - 2\mu s$, these events are very noticeable since, during the days examined, the phase stays constant within much less than $0.5\mu s$ for many hours. Fig.6 shows an example of a phase modulation by an acoustic gravity wave with a period of the order of 2 min. Notice that the amplitude of the wave is attenuated, but 4 or 5 periods can be seen. Finally, Fig.7 shows a wave-like structure with a 30 min. period during a morning phase recovery. Records of the type presented do occur occasionally, they are not regular or frequent. Indeed, as it appears from the previous discussion, only relatively large-amplitude gravity waves may produce sensible changes in the phase delay of the signal.

5. CONCLUSIONS.

Gravity waves propagating in the lower ionosphere have been shown to cause relatively large changes in electron density in the height range 50 - 70 Km. In this way, the motion of the neutral atmosphere may be indirectly detected by electromagnetic techniques, as cross-modulation or VLF propagation. Few experimental data have been presented, supporting qualitatively the theoretic conclusions. Even if it appears difficult now to precisely deduce the parameters of the gravity waves involved, it seems useful to utilize the quoted techniques with this aim. In particular VLF phase and amplitude are available for many different links, and should give interesting informations without the need of any ad hoc equipment.

ACKNOWLEDGMENTS

The author wishes to thank Gian Carlo Rumi for many useful discussions and for supplying the cross-modulation data, and Sigfrido Leschiutta for supplying the data on VLF phase. He is grateful to the Istituto Elettrotecnico Nazionale Galileo Ferraris di Torino and the Istituto di Elettronica e Telecomunicazioni del Politecnico di Torino for supporting this study.

REFERENCES

- ADAMS G.W., L.R.MEGILL, 1967, "A Two-ion D Region Model for Polar Cap Absorption Events", Planet.Space Sci., 15, 1111-1130.
- BOOKER H.G., 1956, "Turbulence in the Ionosphere with Applications to Meteor-Trails, Radio-Star Scintillation, Auroral Radar Echoes, and Other Phenomena", J.Geophys. Res., 61, 673-705.
- BRACEWELL R.N., K.G.BUDDEN, J.A. RATCLIFFE, T.W.STRAKER, K.WEEKS, 1951, "The Ionosphere Propagation of Long and Very Long Radio Waves Over Distances Less Than 1000 Km", Proc.IEE of London, Part III, 98, 221-236.
- COLE R.K., E.T.PIERCE, 1965, "Electrification in the Earth's Atmosphere for Altitudes Between 0 and 100 Kilometers", J. Geoph. Res., 70, 2735-2749.
- CROMPTON R.W., L.G.H.HUXLEY, D.J.SUTTON, 1953, Proc.Roy.Soc., A219, 507-520.
- DOHERTY R.H., 1968, "Importance of Associative Detachment and Dissociative Attachment in the Lower Ionosphere as Shown by LF Radio Measurements", J.Geoph. Res., 73, 2129 - 2140.

- FERGENSELD F.C., A.L.SCHMELTE KOPF, H.I.SCHIFF, F.E.FERGUSON, 1967, "Laboratory Measurements of Negative Ion Reactions of Atmospheric Interest", Planet. Space Sci., 15, 373-379.
- FEJER J.A., 1955, "The Interaction of Pulsed Radio Waves in the Ionosphere", J.Atmosph.Terr.Phys., 2, 323-372.
- FERGUSON E.E., 1969, "Negative Ion-Molecule Reactions", Can.J.Chem., 47, 1815-1820.
- FERGUSON E.E., 1971, "D-Region Ion Chemistry", Rev. Geophys.Space Phys., 9, 997-1006.
- FERRARO A.J., H.S.LEE, S.WEISSBROD, 1963, "Phase Interaction: A New Tool for D Region Studies", J.Geoph.Res., 68, 1169-1171.
- FITE W.L., 1969, "Positive Ion Reactions", Can.J.Chem., 47, 1797-1807.
- FRANCEY R.J., 1970, "Electron Production in the Ionosphere D Region by Cosmic X Rays", J.Geophys.Res., 75, 4839-4862.
- GOSSARD E.E., J.H.RICHTER, 1970, "Internal Waves in the Atmosphere from High-Resolution Radar Measurements", J.of Geophys.Res., 75, 3523-3536.
- HINES G.O., 1960, "Internal Atmospheric Gravity Waves at Ionospheric Heights", Can.J.Phys., 38, 1441-1481.
- HUNT B.G., 1966, "Photochemistry of Ozone in a Moist Atmosphere", J.Geophys.Res., 71, 1385-1398.
- KENT G.S., W.KEENLSIDE, H.C.W.SANDFORD, W.H.WRIGHT, 1972, "Laser Radar Observation of Atmospheric Tides in the 70-100 Km Height", J.Atmosph.Terr.Phys., 34, 373-386.
- LELEVIER R.E., L.M.BRANSCOMB, 1968, "Ion Chemistry Governing Mesospheric Electron Concentrations", J.Geoph. Res., 73, 27-41.
- LESCHIUTTA S., 1972, "Private Communications", Istituto Elettrotecnico Nazionale Galileo Ferraris, Torino, Italy.
- MECKTLY E.A., L.G. SMITH, 1969, "Seasonal variation of the Lower Ionosphere at Wallops Island During the IQSY", J.Atmosph.Terr.Phys., 30, 1555-1561.
- PHELPS A.V., 1969, "Laboratory Studies of Electron Attachment and Detachment processes of Aeronomical Interest", Can.J.Chem., 47, 1783-1793.
- REID C.C., 1970, "Production and Loss of Electrons in the Quiet Daytime D Region of the Ionosphere" J.Geoph. Res., 75, 2551-2562.
- RUMI G.C., 1962, "Experiment Luxembourg: Cross Modulation at High Latitude, Low Height. Part.1: Theoretical Aspects", IRE Trans.Ant.Propag., 10, 594-600.
- RUMI G.C., 1966, "Probing the Magnetosphere and the Subionosphere at High Radio Frequencies", Center for Radiophysics and Space Research, CRSR 251, Cornell University, Ithaca, N.Y.
- RUMI G.C., 1968, "Probing the Magnetosphere and Subionosphere at High Radio Frequencies", Center for Radiophysics and Space Research, CRSR 302, Cornell University, Ithaca, N.Y.
- SHIMAZAKI T., A.R.LAIRD, 1970, "A Model Calculations of the Diurnal Variation in Minor Neutral Constituents in the Mesosphere and Lower Thermosphere including transport Effects", J.Geoph.Res., 75, 3221-3235.
- SMITH R.A., I.A.BOURNE, R.G.LOCH, C.S.G.K.SETTY, T.N.R.DOYNE, P.H.BARRAT, B.S.N. PRASAD, 1965, "Radio Wave Interaction Using Gyrowaves", Air Force Cambridge Res.Lab., AFCL - 65-460, Scientific Report n.3 and Final Report, 17 June, 1965.
- VELINOV P., 1968, "On Ionization in the Ionospheric D Region by Galactic and Solar Cosmic Rays", J.Atmosph. Terr.Phys., 30, 1891-1905.
- WAIT J.R., 1962, "Electromagnetic Waves in Stratified Media", Pergamon Press.

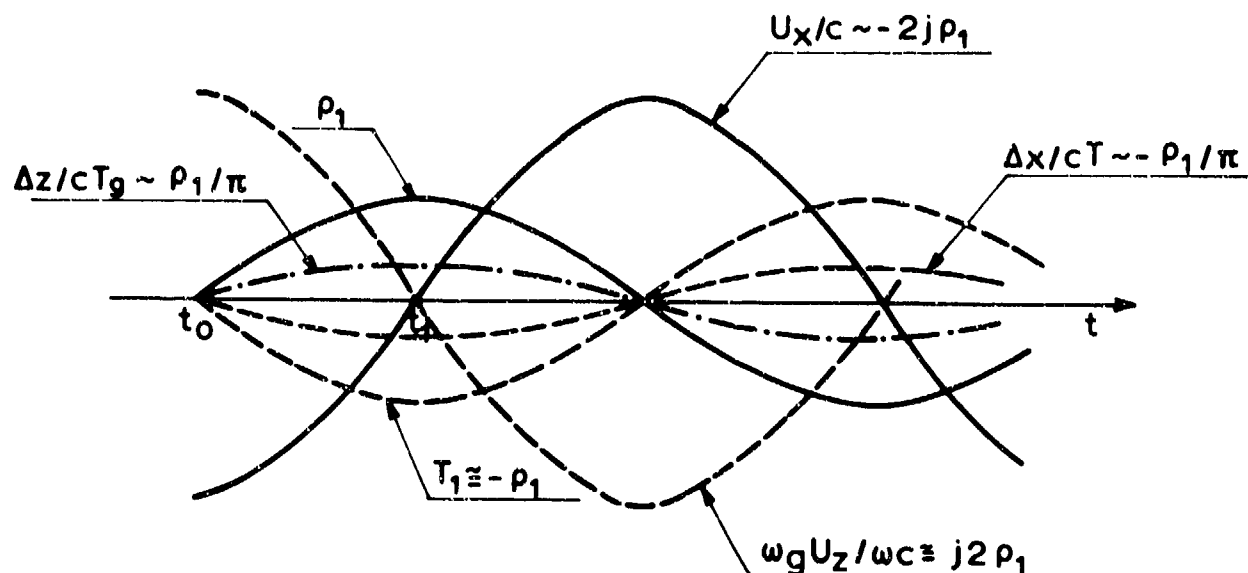


Fig.1 The normalized real parts of ρ_1 , T_1 , U_x , U_z , Δx , Δz , vs. time for internal gravity waves characterized by $k_z^2 \gg \omega_g^2/C^2$ and $\omega^2 < \omega_g^2$

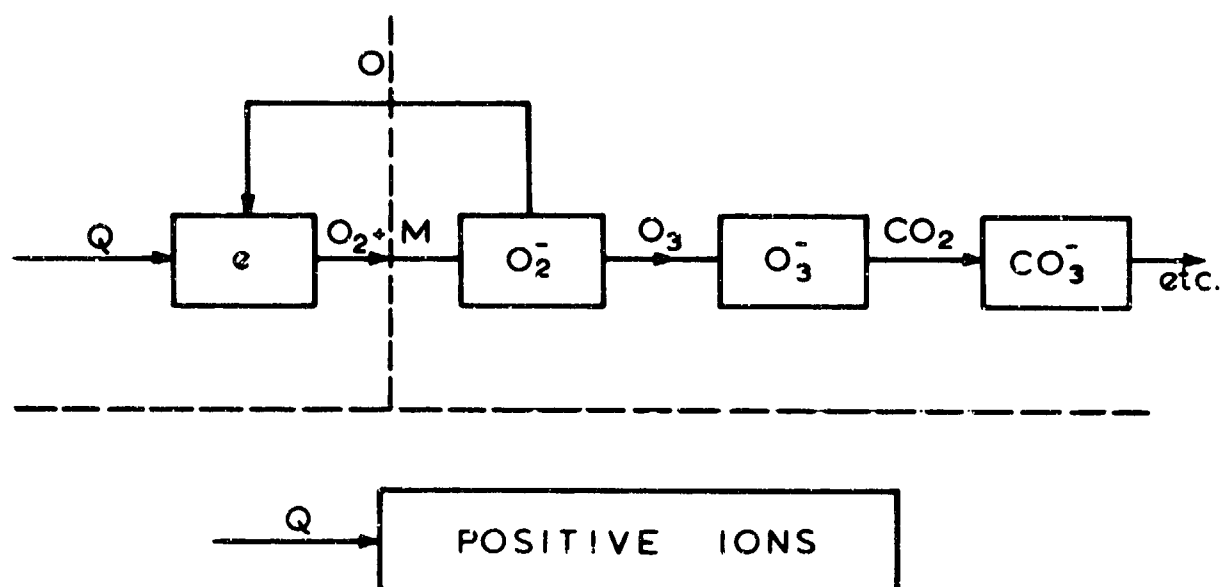


Fig.2 A simplified scheme of electron and ion reactions.

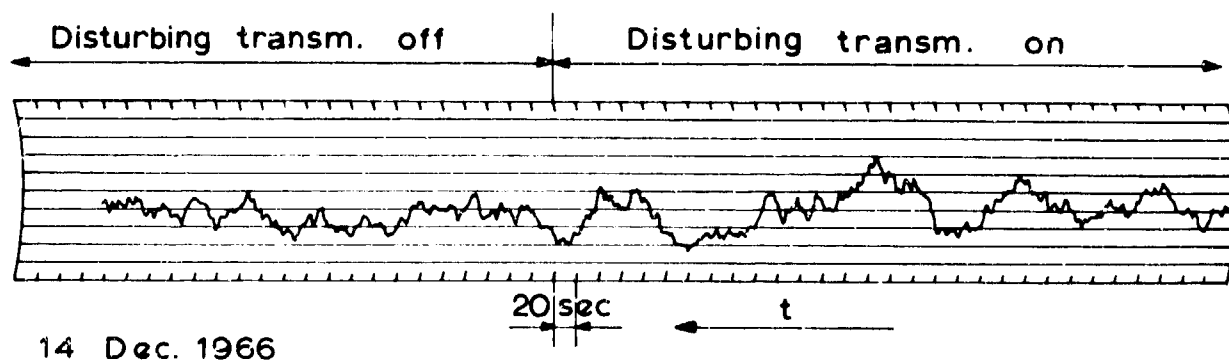


Fig.3 Cross-modulation experiment data (after RUMI G.C., 1966)

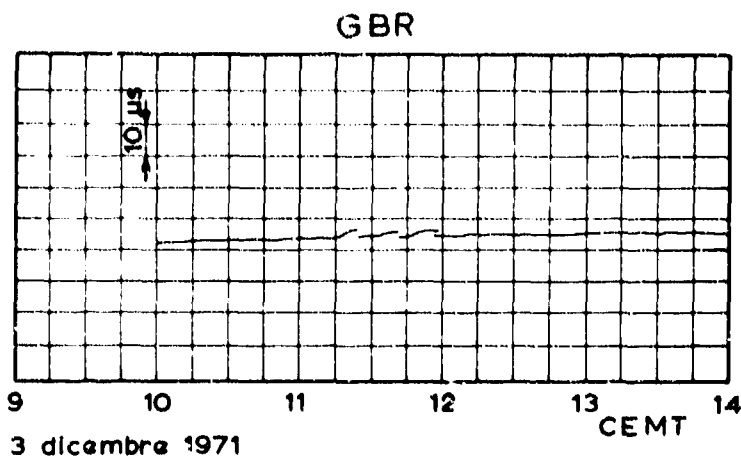


Fig.4 Phase record on 16 KHz (LESCHIUTTA S., private communication)

Fig.5 Phase record on 16 KHz (LESCHIUTTA S., private communication)

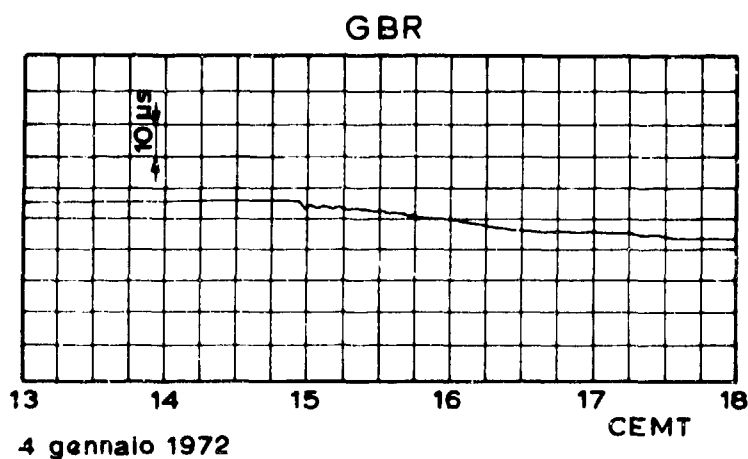
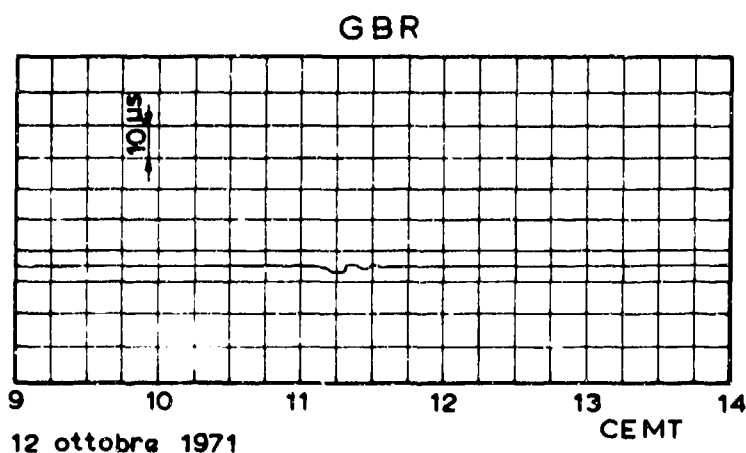
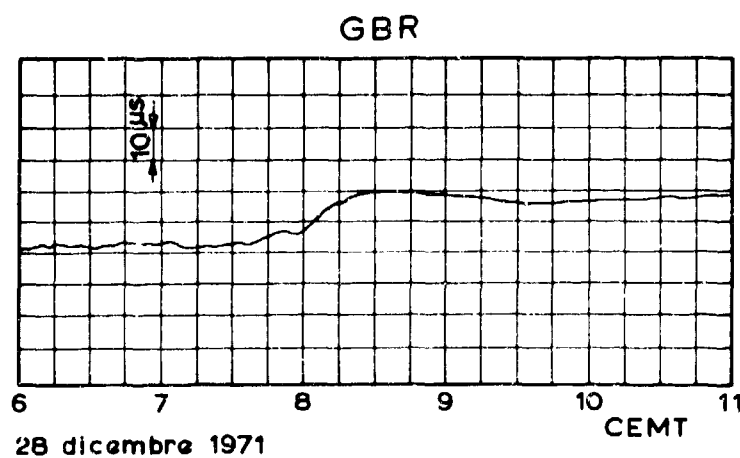


Fig.6 Phase record on 16 KHz (LESCHIUTTA S., private communication)

Fig.7 Phase record on 16 KHz (LESCHIUTTA S., private communication)



**OBSERVATION D'ONDES DE GRAVITE DANS LA HAUTE ATMOSPHERE
PAR DETECTION DES TRAINEES METEORIQUES**

par

M.Glass

Laboratoire de physique de l'Ecole Normale Supérieure
Paris, France

A.Spizzichino et I.Revah

Centre National d'Etudes des Télécommunications
38-40, rue du Général Leclerc
92131 - Issy-les-Moulineaux, France

OBSERVATIONS OF GRAVITY WAVES IN THE HIGHER ATMOSPHERE BY MEANS OF METEOR TRAIN DETECTION

by

N. Glass, A. Spizzichino and I. Revah

Abstract

Over 1000 individual values of neutral wind can be obtained daily, within the 75-105 altitude range, with the meteor radar of C.N.E.T. (National Center for Studies on Telecommunications). Data processing and harmonic analysis significantly exhibit progressive waves whose vertical propagation can be tracked owing to the accuracy in location due to the radar. The length of the measurement period (10 days) makes it possible to acquire data on the life duration of the gravity waves observed.

C.N.E.T. has installed a meteor radar at Sens-Brauven (43°N). Returns from ionized traces produced by meteorites penetrating into the higher atmosphere are obtained. The radar is extremely sensitive (0.2 μ V for a 10 dB signal/noise ratio) and therefore can detect over 1000 meteor echoes daily. Owing to a novel device for measuring the distance between the radar and the meteor echo, and to the accurate determination ($\pm 0.7^\circ$) of the elevation and azimuth of this echo, the altitude can be determined within ± 500 meters.

The motions of the East-West component of the neutral wind within the 75-105 altitude range can be deduced from the Doppler effects on these echoes. Waves are thus exhibited, whose vertical propagation can be tracked since the altitude is known. Besides tidal motions, with periods ranging from 12 to 24 hours and over, shorter period oscillations are observed which can be compared to gravity waves.

Up to 1969, measurement periods were of reduced duration (2-3 days), and only "instantaneous" gravity waves could be observed. With automatized data processing, the duration of these periods was extended to 10 days as soon as December 1969, thus permitting studies of the stability of the observed motions.

This paper surveys preliminary investigations on gravity waves observed from 20 April to 30 April 1970.

OBSERVATIONS D'ONDES DE GRAVITE DANS LA HAUTE ATMOSPHERE

PAR DETECTION DE TRAINEES METEOROLOGIQUES

Par M. GLASS*, A. SPIZZICHINO[†], I. REVAH[†]

* LABORATOIRE DE PHYSIQUE DE L'ECOLE NORMALE SUPERIEURE - PARIS FRANCE

[†] CENTRE NATIONAL D'ETUDES DES TELECOMMUNICATIONS - 3, AVENUE DE LA REPUBLIQUE
92 - ISSY-LES-MOULINEAUXRésumé

Le radar météorologique du C.N.E.T. permet d'obtenir plus de 1000 valeurs individuelles de vent neutre par jour aux altitudes comprises entre 75 et 105 km. Après traitement des données et analyse harmonique, on met en évidence de façon significative des ondes progressives dont on peut suivre la propagation verticale grâce à la précision de la localisation due au radar. La durée des mesures (10 jours) permet de déterminer quelques résultats sur la durée de vie des ondes de gravité observées.

Le Centre National d'Etudes des Télécommunications a implanté un radar météorologique à Sens-Beaujeu (43°N). Il permet d'obtenir des échos radar provenant des traces ionisées créées par les météorites pénétrant dans la haute atmosphère. Ce radar a une grande sensibilité (0,2 μ V) pour un rapport signal/bruit de 10 dB ce qui lui permet de détecter plus de 1000 échos météorologiques par jour. Un dispositif original de mesure de la distance entre le radar et l'écho météorologique ainsi que la détermination précise ($\pm 0,7^\circ$) du site et de l'azimut de cet écho permet d'obtenir une définition de l'altitude à ± 500 mètres.

En étudiant l'effet Doppler sur ces échos, on peut reconstituer les mouvements de la composante Est-Ouest du vent neutre dans la gamme d'altitude comprise entre 75 km et 105 km. On met alors en évidence des ondes dont on peut suivre la propagation verticale grâce à la connaissance de l'altitude. On constate outre la présence de mouvements de marée (période 12 heures et 24 heures) et de période supérieure à 24 heures, l'existence d'oscillations de période plus courte que peuvent être assimilées à des ondes de gravité.

Jusqu'en 1969, les campagnes de mesures avaient une durée réduite (2 à 3 jours), ce qui ne permettait que l'observation "instantanée" des ondes de gravité. [1] L'automatisation du traitement des données a permis de porter la durée des campagnes à 10 jours dès Décembre 1969, ce qui permet d'étudier la stabilité dans le temps des mouvements observés.

Cet exposé représente un travail préliminaire d'études des ondes de gravité observées du 20 Avril au 30 Avril 1970.

I - TRAITEMENT DES DONNEES

1) Le radar météorologique du C.N.E.T. fonctionne à la fréquence de 30 MHz environ et les antennes d'émission et de réception sont dirigées vers l'Est. En raison de la fréquence utilisée, ces antennes sont assez peu directives (l'ouverture du faisceau à 3 dB est de 28° en azimut et de 30° en site). Ceci signifie que l'on observe des échos météorologiques dans un volume important (30 km en altitude, 150 km dans la direction Est-Ouest, 80 km dans la direction Nord-Sud). Comme la mesure du vent se fait par effet Doppler, on obtient en réalité la valeur de la composante radiale du vent qui peut être différente de la valeur de la composante E.O : l'erreur sur celle-ci peut atteindre 10 m/s. Pour traiter les données brutes, on est donc obligé de faire certaines hypothèses.

a) On traite les données comme si elles représentaient la composante E.O. Pour éviter d'introduire des erreurs trop importantes, on est amené à éliminer les échos trop écartés de l'axe des antennes.

b) On néglige les variations horizontales du vent dans le volume étudié. Ceci signifie que les mouvements de vent d'échelle horizontale inférieure à 200 km seront ignorés par l'analyse.

c) On suppose que le vent neutre aux altitudes considérées est pratiquement horizontal. Ceci a été montré théoriquement pour les ondes de gravité de période supérieure à 1 heure et expérimentalement

d) On admet que la mesure de vitesse obtenue est égale à la vitesse de l'air neutre.

Avec ces hypothèses, on obtient une série de valeurs du vent dépendant uniquement de l'altitude et du temps.

2) Pour reconstituer les profils de vent, on veut calculer les valeurs sur un maillage régulier en temps et en altitude. En considérant que l'erreur sur l'altitude est de ± 500 mètres et que l'on se limite à l'étude des oscillations de période supérieure à 2 heures 30, on a fixé les pas du maillage respectivement à 1 km et 10 mn. Les profils de vent sont calculés par interpolation linéaire. Celle-ci est limitée aux points (t_0, z_0) tels que la valeur du vent en (t_0, z_0) ne soit pas entachée d'une erreur supérieure à 10 m/s. Cette analyse agit comme un filtre sur les oscillations de faible période (< 3 h.). La figure ci-contre montre l'atténuation $\frac{u'_0}{u_0}$ d'une onde d'amplitude u_0 et de période τ , ρ représente le nombre d'échos par heure. On voit que pour $\rho = 20$ et $\tau = 3$ heures, on a

$$\frac{u'_0}{u_0} = 0,75$$

3) On effectue alors une analyse harmonique du profil de vent ainsi obtenu à chaque altitude. On constate alors la présence d'une très forte composante de période 12 heures correspondant au phénomène de marée. Pour obtenir une précision plus grande sur les ondes de période différentes, on est amené à retrancher la composante de période 12 heures des valeurs expérimentales et à effectuer une analyse harmonique sur le signal restant.

Pour obtenir une précision plus grande sur les ondes de gravité, on pourrait avoir intérêt à effectuer l'analyse harmonique sur une durée aussi grande que possible. Cependant, on verra que la durée de vie d'une onde de gravité est limitée à 3 jours en moyenne et que de toutes façons, la phase de ces ondes est assez peu stable dans le temps. Dans ces conditions, il existe une limitation physique à la valeur de la durée de l'échantillon que l'on a fixée à 3 jours.

II - Observation d'ondes de gravité

L'analyse harmonique d'un échantillon de durée 3 jours a été effectuée à chaque altitude de z comprise entre 75 et 105 km et pour une série de valeurs équidistantes de la fréquence allant de $\frac{1}{12}$ heure⁻¹ à $\frac{1}{2,5}$ heure⁻¹ par pas égal à

$$\Delta f = \frac{1}{2T}$$

où T est la durée de l'échantillon ($T = 72$ h.). On représente chaque composante par :

$$V(t, z) = v(z) \sin(2\pi f t + \phi(z))$$

L'étude expérimentale des valeurs $v(z)$ et $\phi(z)$ du 20 au 30 Avril 1970 conduit aux résultats suivants :

Le spectre de puissance présente une série de "pics" de forte amplitude, ce qui avait déjà été observé en 1965-66 [3]

- A la fréquence correspondante, on constate fréquemment que $\phi(z)$ varie linéairement avec z . On est alors en présence d'une onde progressive de longueur d'onde

$$\lambda = -2\pi / \frac{d\phi}{dz}$$

Le plus souvent $\frac{d\phi}{dz}$ est positif (figure 1 à 4). L'onde a donc une vitesse de phase dirigée vers le bas. Plus rarement (un cas sur dix), elle semble dirigée vers le haut (fig.n°5). λ est généralement comprise entre 10 et 40 km.

Tests de validité

Pour vérifier qu'un "pic" du spectre de puissance des vents représente une onde atmosphérique de manière significative, nous avons utilisé le test proposé par SPIZZICHINO qui consiste à calculer le spectre de puissance bidimensionnel $S(f,k)$ du vent zonal $u(t,z)$

$$S(f,k) \approx \frac{1}{TZ} \left[\int_0^T \int_{z_0}^{z_0+z} u(t,z) e^{2i\pi(kz-ft)} dz dt \right]^2$$

où T est la durée de l'échantillon et Z l'épaisseur de la tranche d'altitude analysée.

A toute onde atmosphérique correspond un maximum de $S(f,k)$. Réciproquement pour s'assurer qu'un pic correspond à une onde atmosphérique, on peut :

- comparer l'amplitude de ce maximum à celle du bruit ambiant et ne considérer que les pics pour lesquels le rapport signal/bruit est supérieur à 10.

- comparer la forme de $S(f,k)$ autour du maximum à celle de $S_{th}(f,k)$ qui résulte théoriquement d'une onde pure de fréquence f_0 et de nombre d'onde k_0 .

$$S_{th} = A_{max} \left[\frac{\sin \pi T (f_0 - f)}{\pi T (f_0 - f)} \frac{\sin \pi Z (k_0 - k)}{\pi Z (k_0 - k)} \right]^2$$

Les figures 6 et 7 montrent des comparaisons entre le spectre expérimental et le spectre théorique pour deux raies spectrales observées. On voit que ces raies représentent des ondes de fréquence et de longueur d'onde stable pendant la durée de l'échantillon, c'est-à-dire pendant une durée de 3 jours.

Erreurs sur les caractéristiques d'une onde de gravité

Pour estimer les erreurs Δu , $\Delta \phi$ et Δk sur l'amplitude $u(z)$ la phase $\phi(z)$ et le nombre d'onde k d'une onde de gravité, on supposera que ϕ varie linéairement avec l'altitude aux erreurs de mesure près

$$\phi(z) = 2\pi kz + l + \Delta \phi(z)$$

k et l peuvent être déterminées par une méthode de régression linéaire, à condition de connaître la loi de variation de $\Delta \phi$ en fonction de l'altitude. Nous admettons que l'erreur a une phase aléatoire, d'où

$$\Delta \phi = \text{Arc sin} \left(\frac{\Delta u}{u} \right)$$

et que Δu est, en première approximation, indépendant de l'altitude. La méthode de régression linéaire permet de déterminer $\Delta \phi(z)$ et l'équation précédente permettra d'obtenir Δu puisqu'on connaît $u(z)$. On trouve que la valeur quadratique moyenne de Δu est

$$\Delta u = 2 \text{ à } 3 \text{ m/s}$$

On peut voir d'autre part que si un point $\phi(z)$ est très éloigné de la droite ($>90^\circ$) il correspond à une valeur $u(z)$ inférieure à 2 m/s ce qui est une preuve expérimentale de la détermination précédente.

On explique ainsi pourquoi la phase de l'onde de gravité de la figure 5 présente des fluctuations par rapport à une variation linéaire. On voit en effet que l'amplitude de cette onde est très petite.

D'autre part on sait que la variance de l'estimation de k est

$$2N \Delta k = \frac{\sigma}{\sqrt{\sum_1^N (z_1 - \bar{z})^2}}$$

où N est le nombre d'altitude z_1 considérées dans la régression linéaire, \bar{z} l'altitude moyenne et σ la variance de $\phi(z)$.

Avec $85 \text{ km} < z_1 < 105 \text{ km}$ et $\sigma = 1$ radian, on a :

$$\Delta k = \frac{1}{150} \text{ km}^{-1}$$

La variance de la longueur d'onde est donnée par

$$\Delta \lambda = \lambda^2 \Delta k$$

On voit que plus λ sera grand, moins sa détermination sera précise. En particulier une valeur de λ supérieure à 150 km ne permettra plus de savoir dans quelle direction la phase de l'onde se propage.

Autres cas observés

On constate parfois que le spectre $S(f, k)$ à la fréquence f_0 donnée n'a pas la forme théorique. Deux cas se présentent :

- Il y a deux pics distincts ; on peut interpréter le résultat obtenu comme la superposition de deux ondes de fréquences égales ou proches, mais de longueur d'onde différente (figure 8)
- On a un pic très élargi ; par rapport à la forme théorique. On peut interpréter ceci comme le résultat de la superposition d'au moins deux ondes de gravité de longueur d'onde proche. Dans ces conditions, la longueur d'onde ne pourra être déterminée qu'avec une erreur plus grande que l'erreur précédemment calculée. (figure 9).

Pouvoir séparateur

On utilise la même définition qu'en optique. On ne peut séparer deux ondes de gravité que si les maximum des spectres sont assez éloignés. La plus petite valeur Δk que l'on peut séparer est telle que lorsque la valeur du spectre est maximum pour l'onde de nombre d'onde k , elle est nulle dans le bruit pour l'onde de nombre d'onde $k + \Delta k$ (soit $\frac{1}{10}$ du maximum du spectre).

On en tire

$$\left[\frac{\sin \pi Z \Delta k}{\pi Z \Delta k} \right]^2 = \frac{1}{10}$$

$$\text{soit } \Delta k = \frac{0,75}{Z}$$

$$\text{Pour } Z = 20 \text{ km, on a } \Delta k = \frac{1}{26} \text{ km}^{-1}$$

L'erreur due à la régression linéaire était de $\frac{1}{150} \text{ km}^{-1}$ dans le cas où le spectre $S(f, k)$ était celui d'une onde pure. Lorsque ce n'est pas le cas, on sait qu'il y a plusieurs ondes de gravité, mais leur détermination pourra être entachée d'une erreur atteignant $\frac{1}{26} \text{ km}^{-1}$.

Les figures 9 et 10 montrent des exemples où l'on peut séparer les ondes de gravité et des cas où c'est impossible.

De même il existe une limite Δf telle que si la fréquence de 2 ondes de gravité est inférieure à Δf , on ne peut plus les séparer.

$$\Delta f = \frac{0,75}{T}$$

où T est la période de l'échantillon.

$$\text{Pour } T = 72 \text{ heures } \Delta f = \frac{1}{96} \text{ heure}^{-1}$$

III - Stabilité de la longueur d'onde des ondes de gravité

Pour étudier la variation des ondes de gravité au cours du temps, on a effectué une série d'analyses harmoniques sur des échantillons de durée égale à 3 jours. Chaque échantillon est décalé d'un jour par rapport au précédent. On a obtenu ainsi 9 analyses harmoniques du 20 Avril 1970 au 30 Avril 1970. Sur chacune d'elles, on a cherché à reconnaître les ondes de gravité en utilisant les critères définis au chapitre précédent. La période de ces ondes a été déterminée seulement par les maximum du spectre de puissance.

On a estimé la durée de vie d'une onde de gravité en cherchant le nombre d'échantillons sur lequel une onde d'une période donnée était présente. On en a déduit un histogramme donnant la durée de vie en fonction du nombre d'échantillons.

On voit que très peu d'ondes sont présentes plus de 3 jours, ce qui confirme qu'il est illusoire de faire des analyses harmoniques sur des périodes supérieures.

On constate dans quelques cas particuliers la présence de la même période pendant les 9 périodes étudiées dans la campagne. Pour caractériser plus précisément le phénomène observé, on a porté la longueur d'onde associée à chaque période (10h.40, 7h.20, 6h.00, 4h.50).

La barre d'erreur associée à chaque longueur d'onde a été calculée soit à partir de la régression linéaire dans le cas d'une seule onde soit à partir de la longueur du "pic" dans le cas de plusieurs ondes de gravité inséparables.

Quand on considère l'évolution de la longueur d'onde au cours du temps, on constate qu'elle présente d'importantes fluctuations (figure 12.15). Si on interprète ce fait en supposant que lorsque la longueur d'onde varie brusquement, on n'a plus affaire à la même onde de gravité, on est conduit à donner à ces ondes de gravité une durée de vie plus courte que celle donnée dans l'histogramme de la figure 11. Le tableau I donne le nombre d'échantillons de 3 jours où l'on constate la présence de la même onde. En partant de ces données, on peut construire un nouvel histogramme qui correspond à la durée de vie d'une onde de gravité du 20 au 30 Avril 1970. (figure 16).

Conclusion

Cette étude préliminaire représente la première tentative pour observer l'évolution au cours du temps des ondes de gravité à haute altitude. On a utilisé pour cela une campagne d'observations continues de 10 jours, sur les 8 campagnes semblables effectuées en 1970 ; d'autre part, on s'est limité souvent à des observations qualitatives là où une étude quantitative systématique serait à faire. Pour toutes ces raisons, les résultats décrits doivent être considérés comme provisoires.

On a cependant pu mettre en évidence une étude de vie moyenne des ondes de gravité à haute altitude, de l'ordre de 2 à 3 jours, avec plus rarement des ondes dont la durée de vie peut atteindre 6 jours. Il serait intéressant de comparer ces ordres de grandeur à la durée de vie des phénomènes météorologiques qui pourraient être une source (directe ou indirecte) des ondes de gravité observées dans la haute atmosphère.

Bibliographie

- [1] I. REVAH, Ann. Géophys., t.25, fasc 1, 1969, p.1 à 45 -
- [2] Manning et al., Proc.IRE, 38, 877 -
- [3] A.SPIZZICHINO, Thèse d'Etat, 19-11-69, Université PARIS VI -

Tableau ILongueurs d'onde des oscillations présentes du 20-4-70 au 30-4-70

Période	λ_{km}	Nombres d'échantillons consécutifs où la longueur d'onde est stable
10h.40	+ 40	3
	- 22	4
	- 16	6
7h.20	- 18	6
6h.00	+ 50	3
	- 50	4
	- 20	5
5h.40	- 13	4
	- 100	5
4h.50	- 40	5
	- 25	5

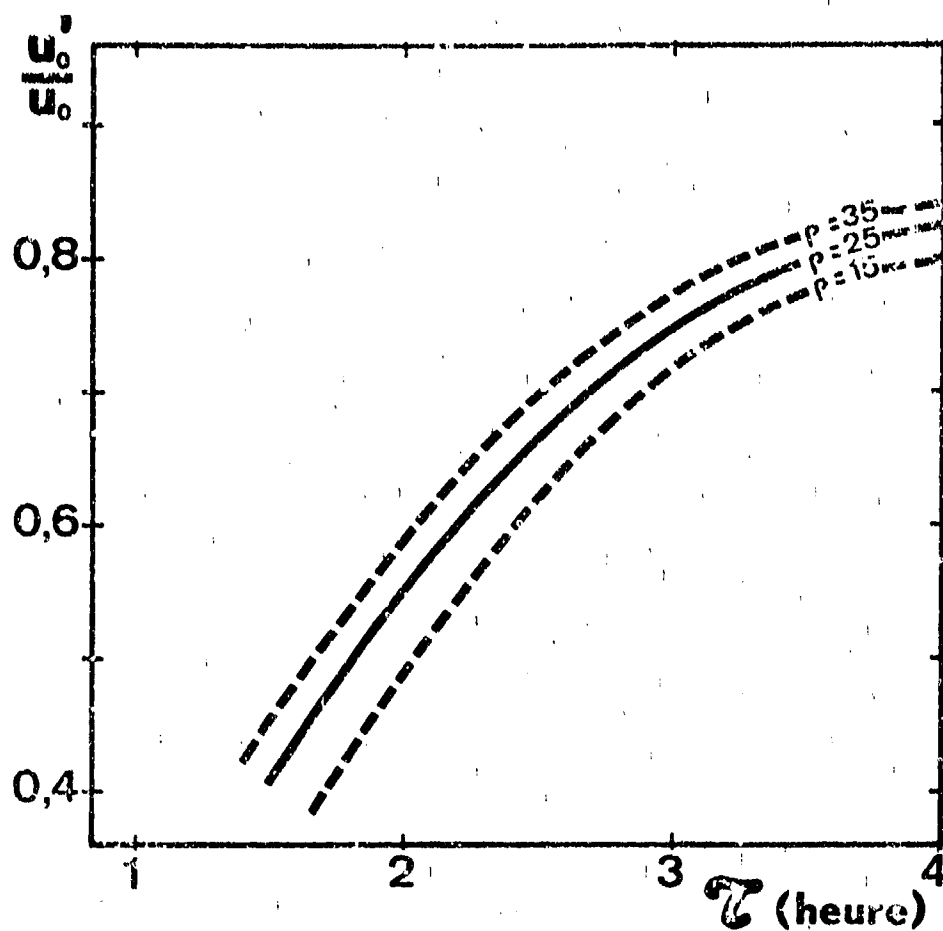


Fig.1 Erreur introduite par la méthode d'analyse utilisée. La méthode d'analyse utilisée agit à la manière d'un filtre sans distorsion de phase, mais qui transmet l'amplitude avec un affaiblissement u'_0/u_0 fonction de la période. Pour $\rho > 15$ les courbes de réponse de ce filtre varient peu autour d'une courbe moyenne.

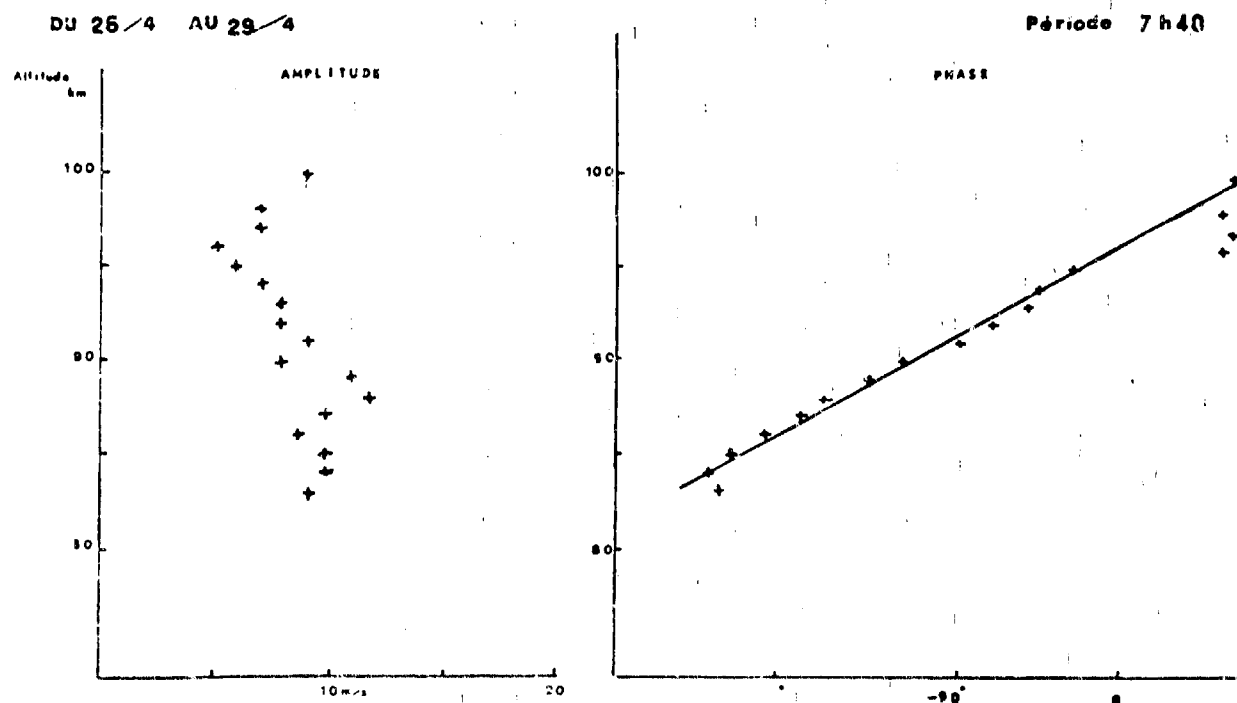


Figure 2

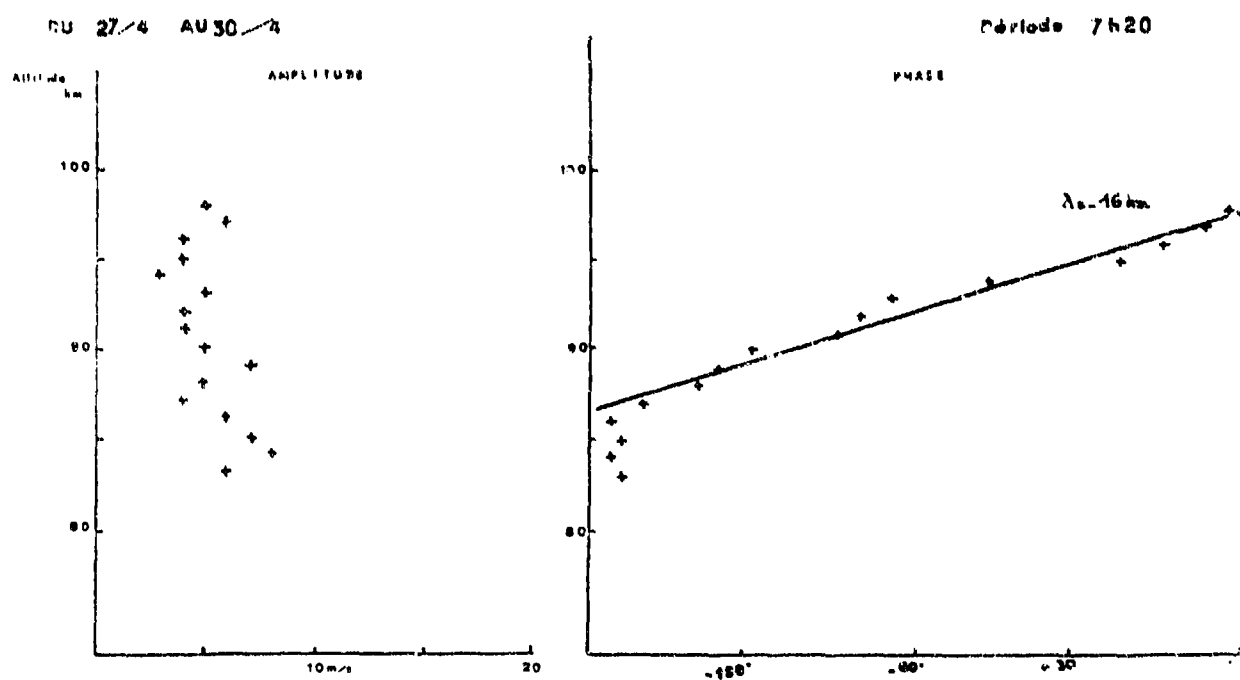


Figure 3

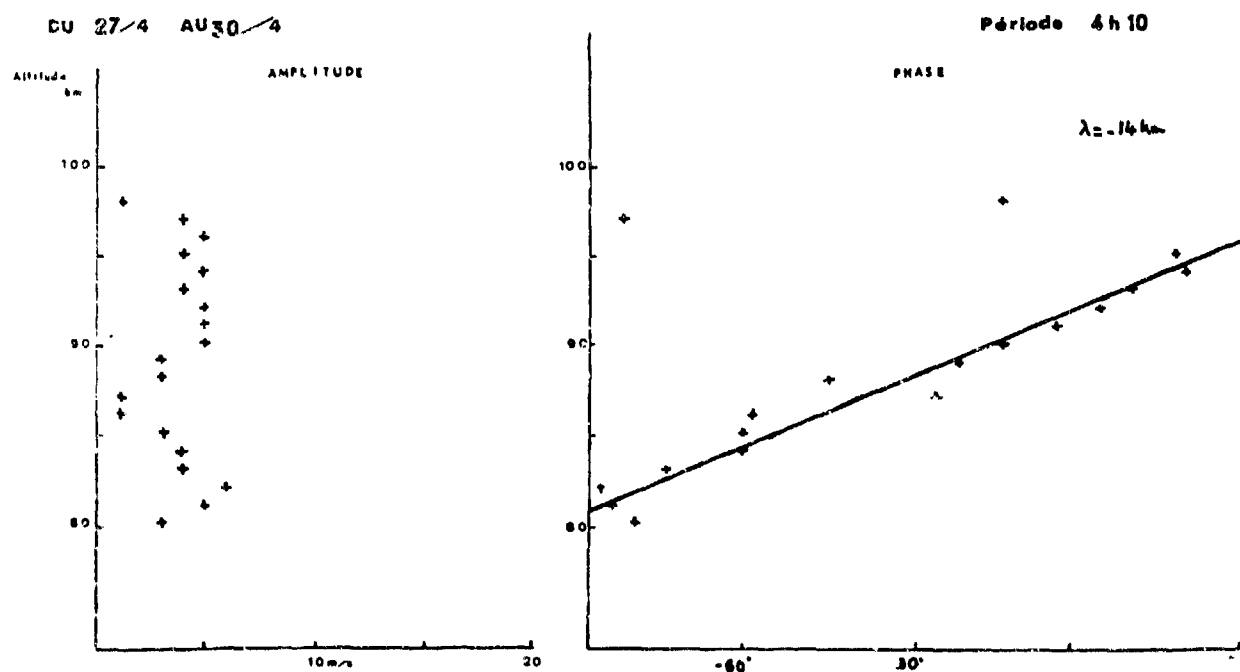


Figure 4

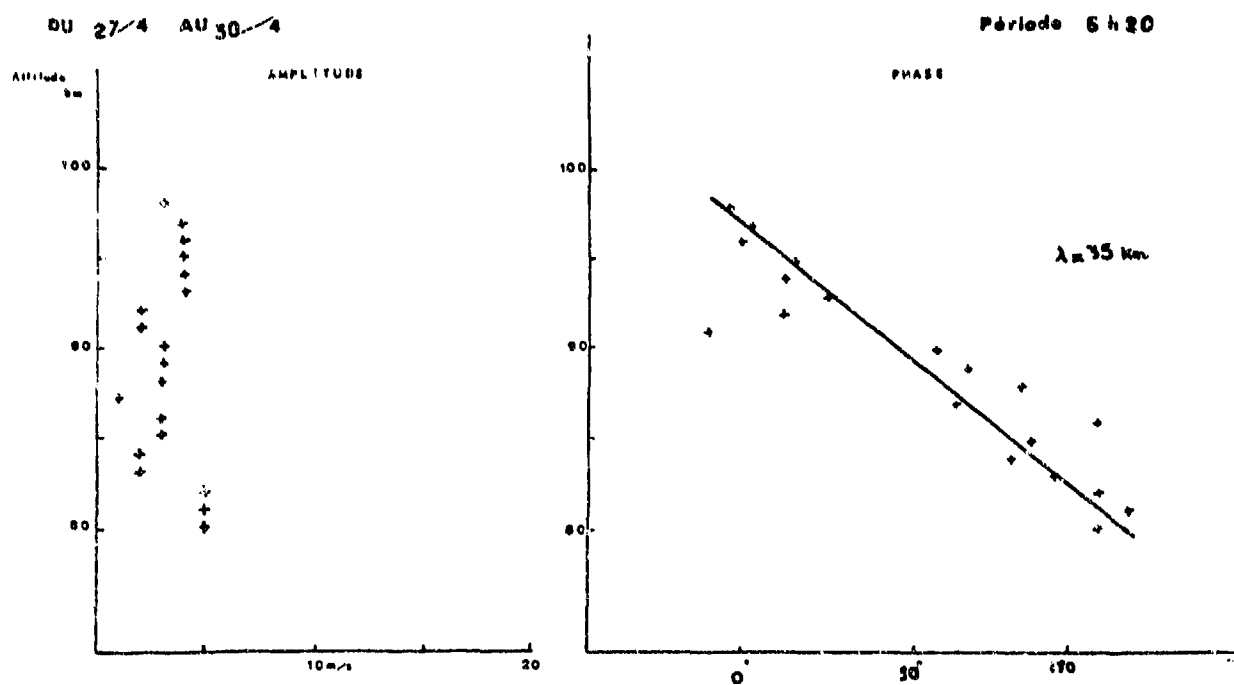


Figure 5

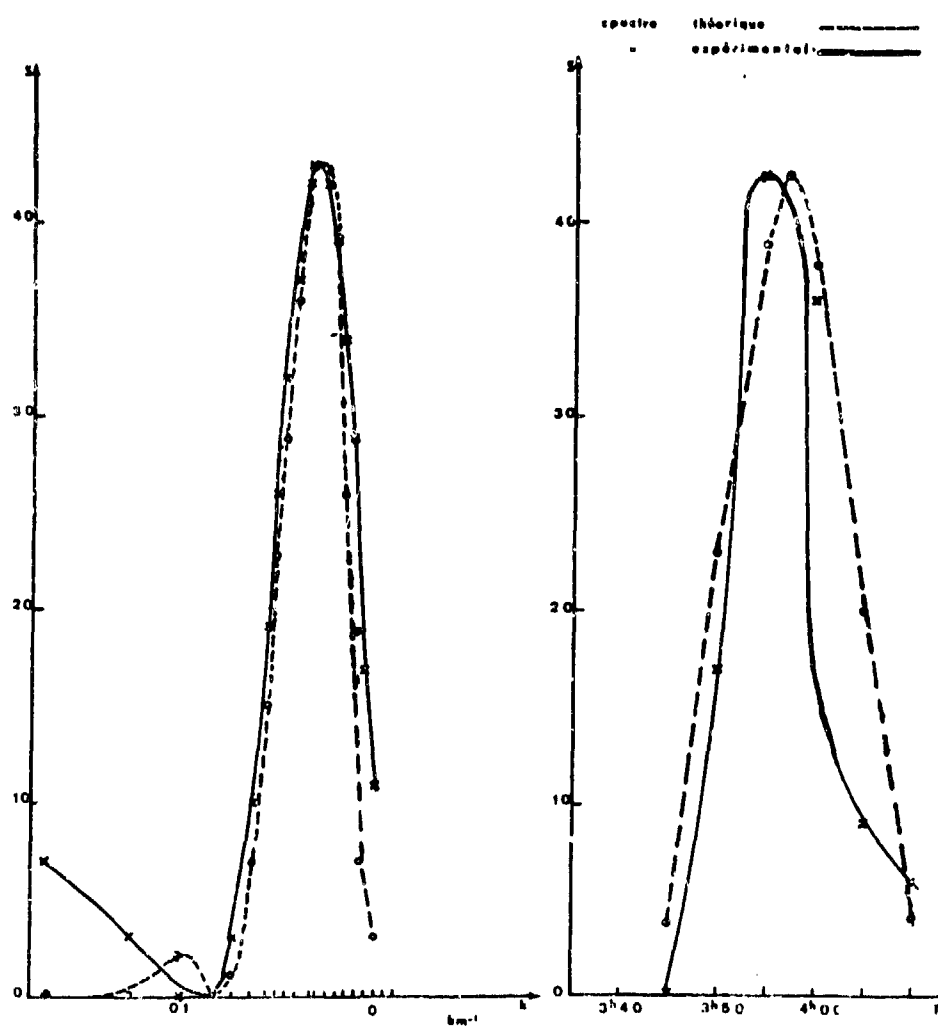


Fig.6 Spectre de puissance de l'onde de période 3h 57

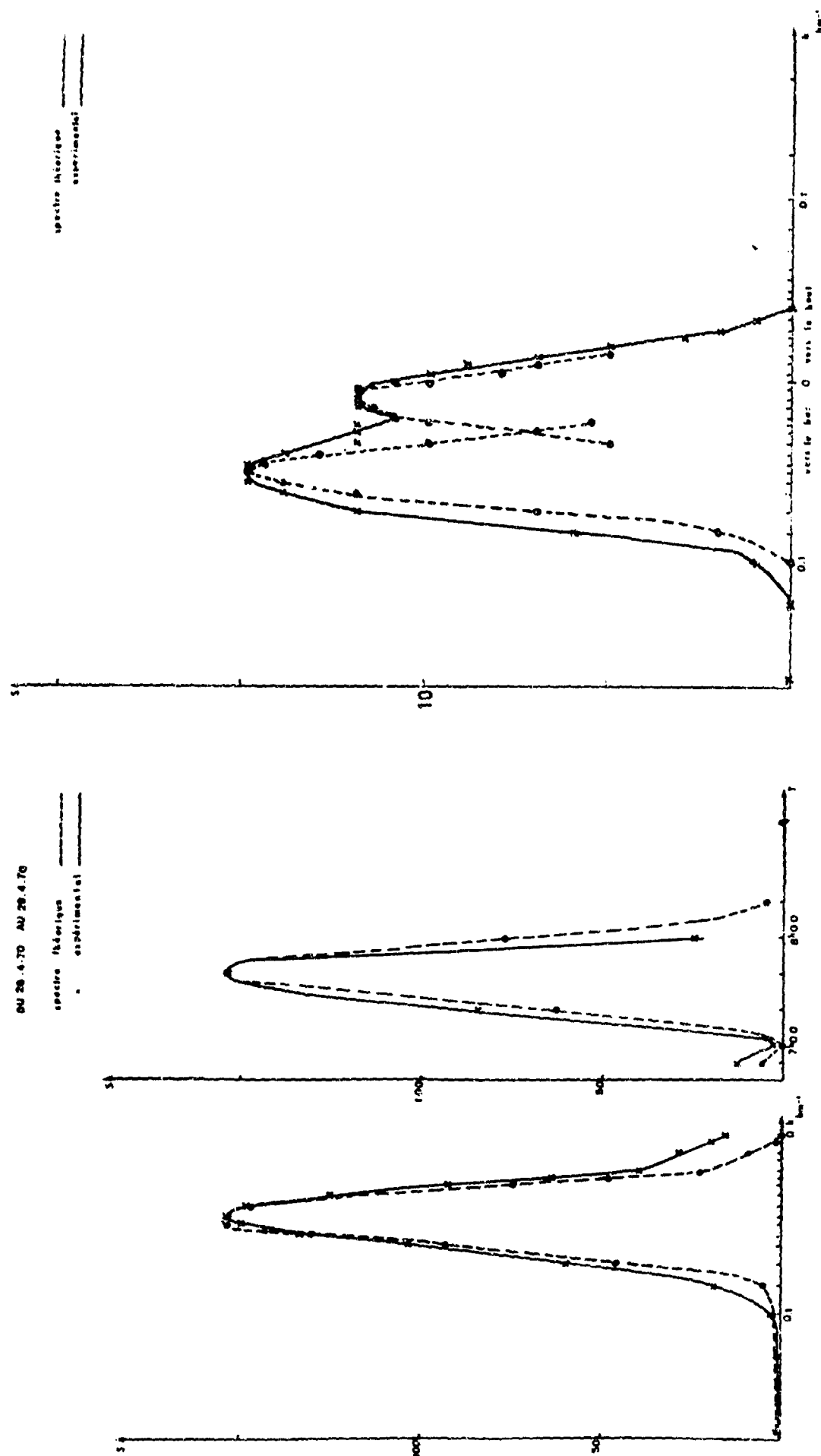


Fig.7 Spectre de puissance de l'onde de période 7h 40. Du 26.4.70 au 29.4.70

Fig.8 Spectre de puissance de la composante $T \approx 5h 55$

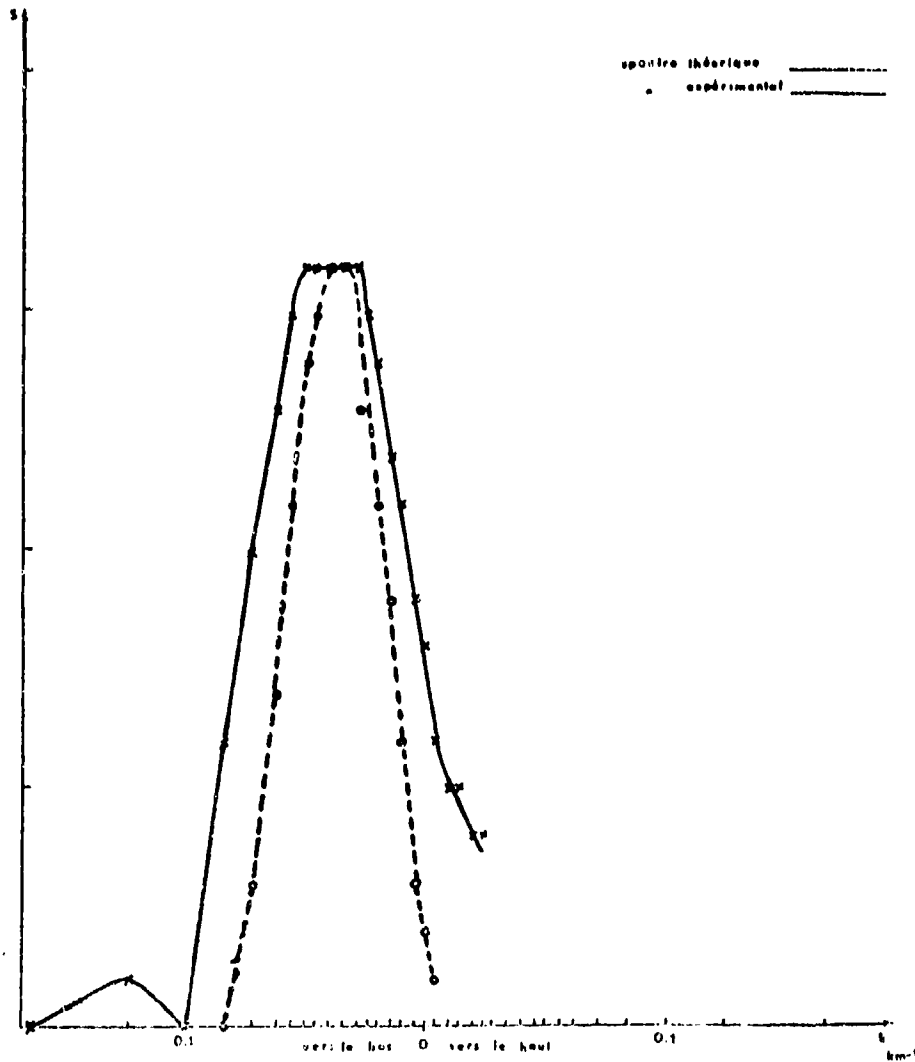


Fig.9 Spectre de puissance de la composante T = 8h 00

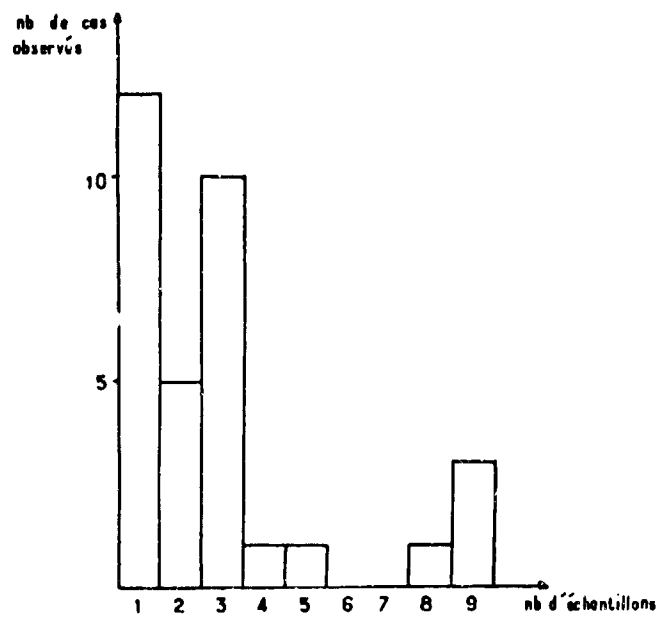


Fig.10 Durée de vie des ondes de gravité

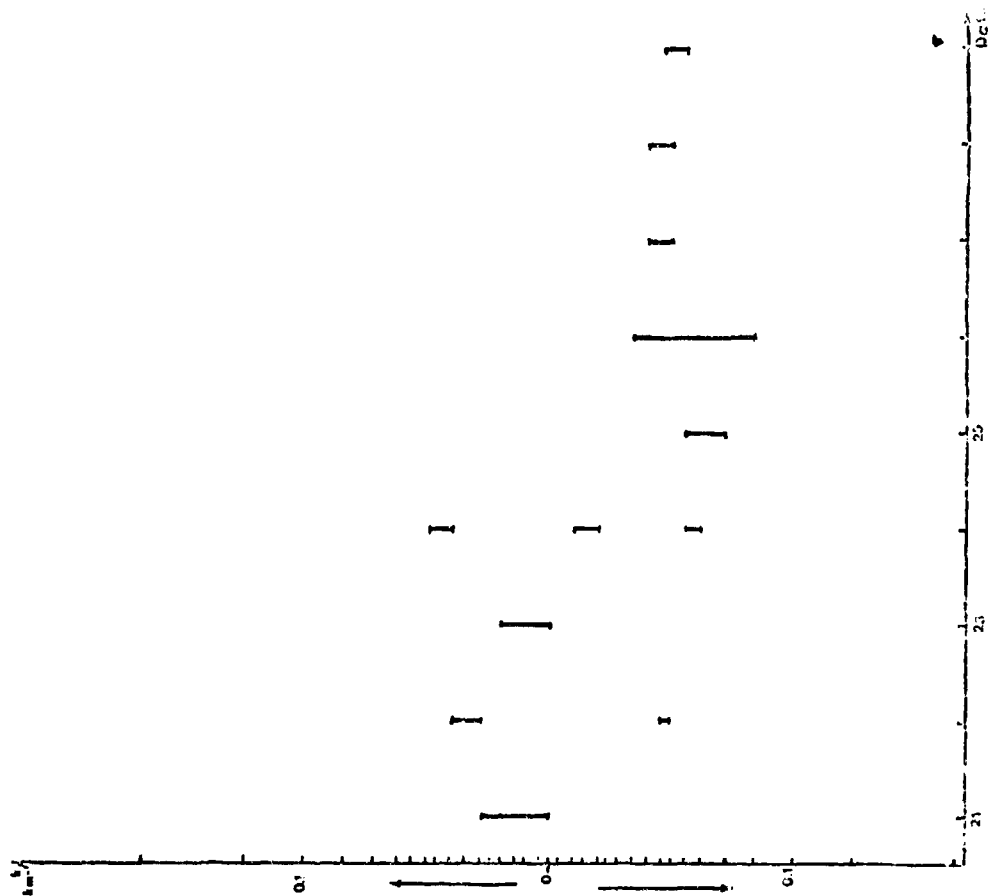


Fig.11 Variation du nombre d'onde en fonction de l'échauffement. T = 10h 40 Avril 1970

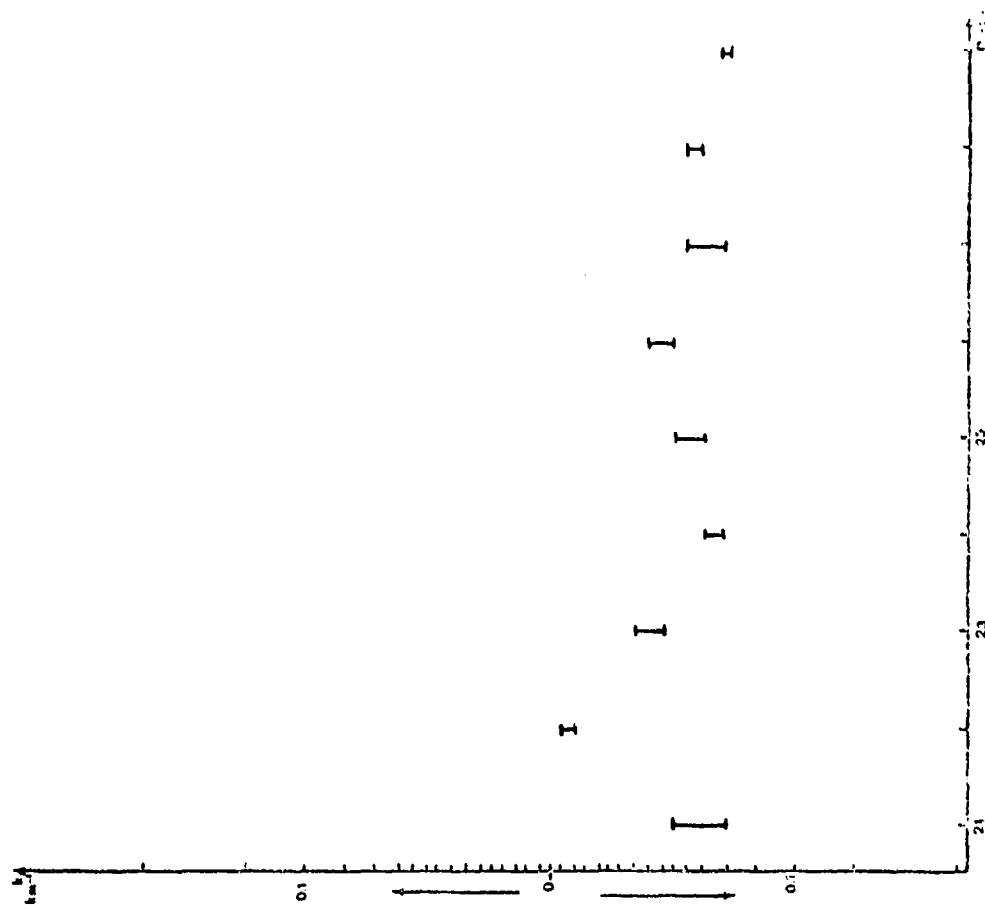


Fig.12 Variation du nombre d'onde en fonction de l'échantillon. T = 7h 20 Avril 1970

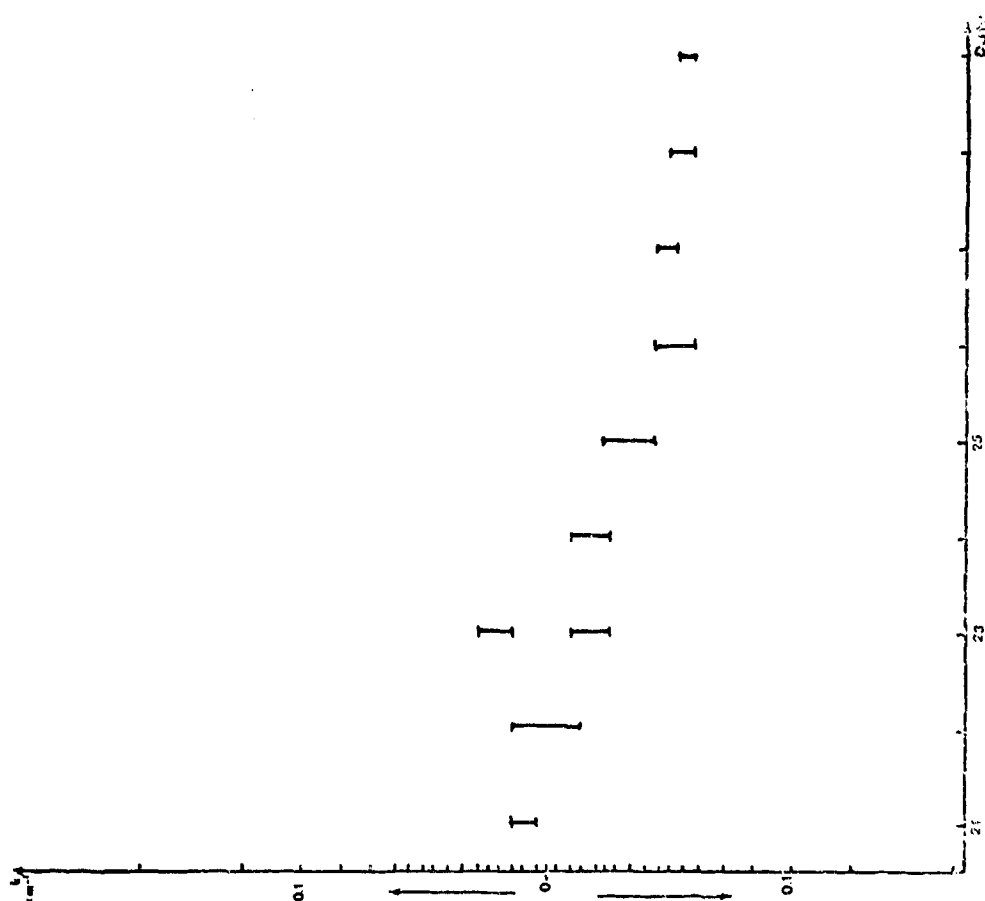


Fig.13 Variation du nombre d'onde en fonction de l'échantillon. T = 6h 00 Avril 1970

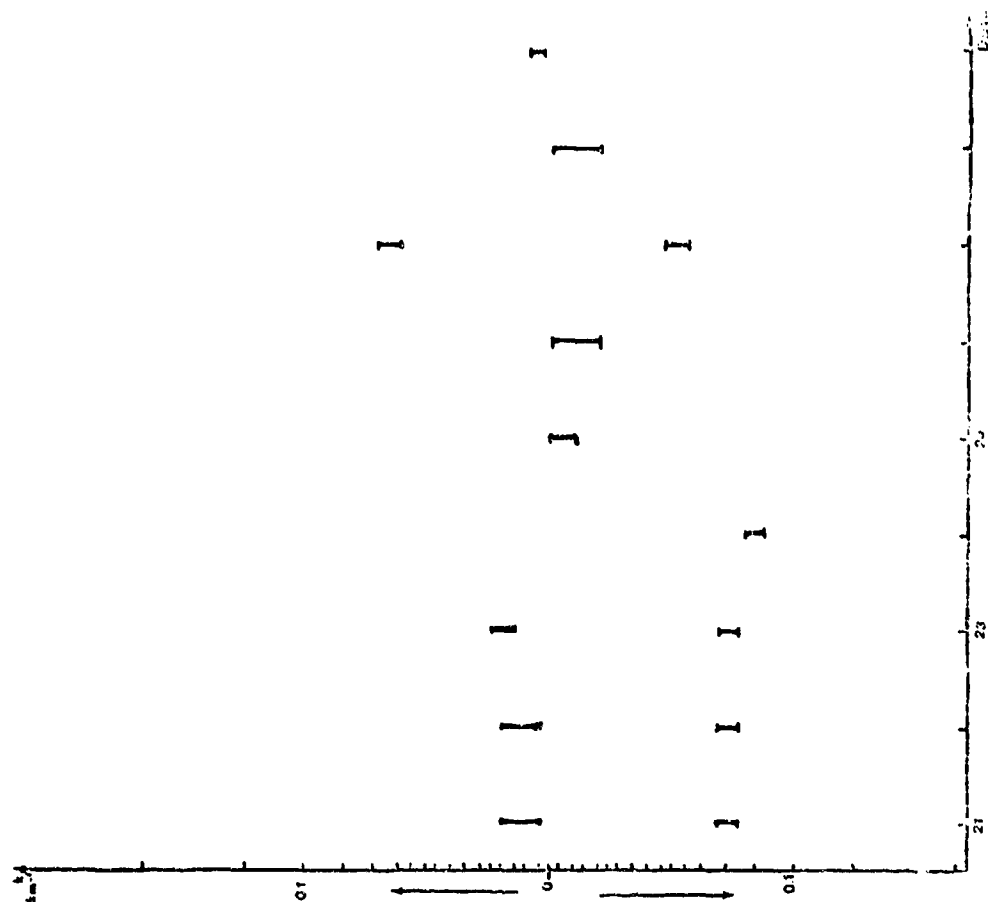


Fig.14 Variation du nombre d'onde en fonction de l'échantillon. T = 5h 40 Avril 1970

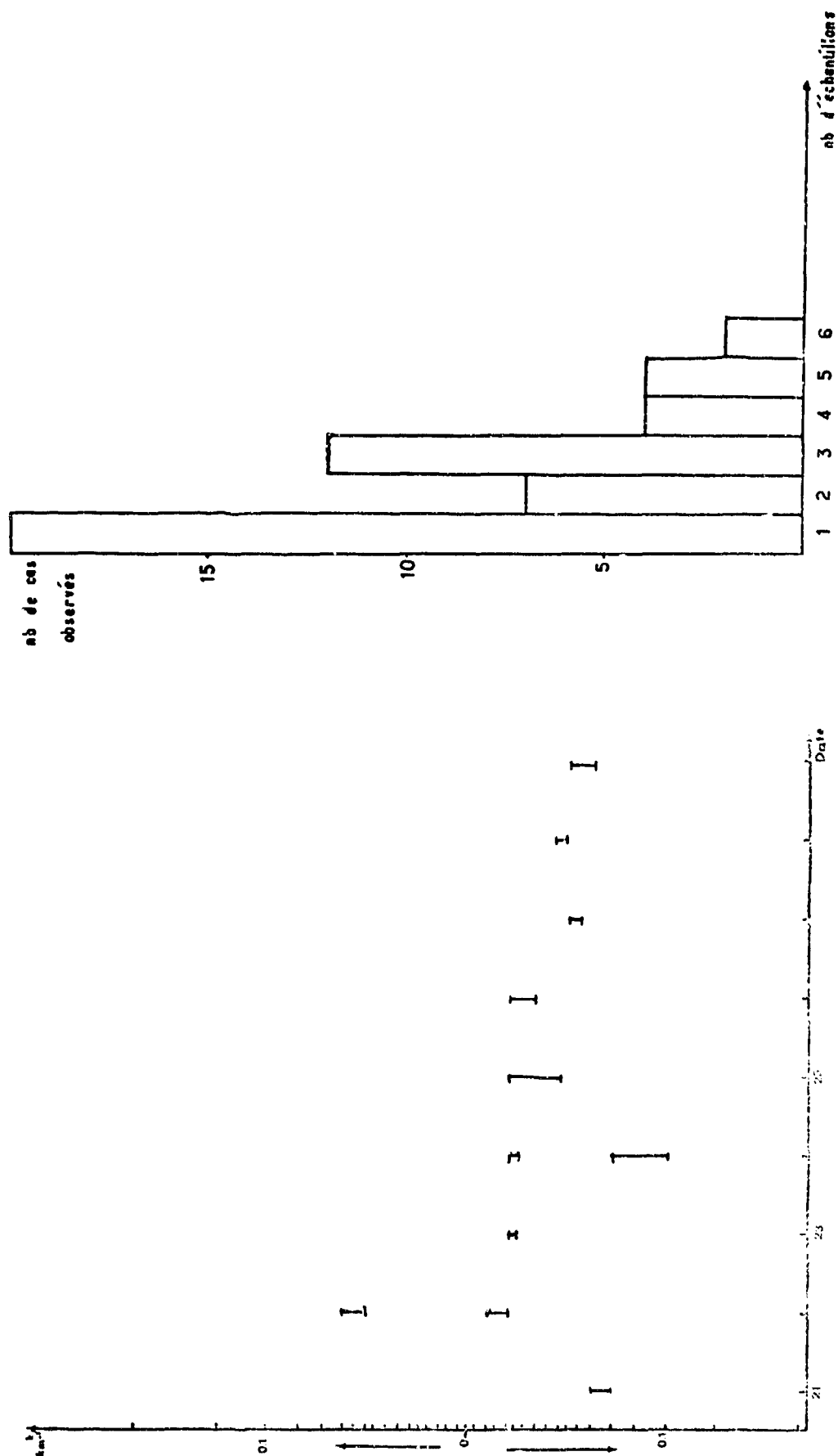


Fig.15 Variation du nombre d'onde en fonction de l'échantillon. T = 4h 50 Avril 1970

Fig.16 Durée de vie des ondes de gravité

**NARROW-BEAM HF RADAR INVESTIGATIONS OF
MIDLATITUDE IONOSPHERIC STRUCTURE AND MOTION**

by

Robert D. Hunsucker

Geophysical Institute
University of Alaska
College, Alaska 99701
U.S.A.

309

RECHERCHES SUR LA STRUCTURE ET LES MOUVEMENTS DE L'IONOSPHERE
AUX LATITUDES MOYENNES, EFFECTUEES A L'AIDE D'UN RADAR A FAISCEAU ETROIT

par

R.D. Hunsucker

SOMMAIRE

On a analysé en détail des données obtenues de 1964 à 1968 grâce à un sondeur (ou "Radar HF") par rétrodiffusion, à haute fréquence et faisceau étroit, avec balayage en site et azimuth, situé à Boulder, Colorado. Cette analyse a révélé que la "structure irrégulière" de l'ionosphère aux latitudes moyennes constitue la règle générale plutôt qu'une exception. Des irrégularités d'ampleur et de mouvement apparent variées furent observées dans environ 90 % des cas. Les "signatures" observées par ce Système Radar HF ont été classées en huit types génériques auxquels on a attribué des noms qui décrivent approximativement leur aspect sur l'enregistrement du balayage en site et azimuth. L'auteur examine la fréquence d'apparition relative de ces signatures suivant le moment du jour et la saison, ainsi que leur corrélation avec le cycle qualitatif des taches solaires et le géomagnétisme.

Un type particulier de "signature" a été analysé grâce à une trajectographie à trois dimensions, avec calculs sur ordinateur, mise au point à l'ITS ; on fit appel à des données expérimentales pour modifier un modèle de perturbation causée par une onde de gravité atmosphérique. L'"enregistrement de rétrodiffusion synthétique" s'avéra assez proche de l'enregistrement expérimental effectué grâce au Radar HF pour justifier l'utilisation de cette méthode dans l'interprétation des données de rétrodiffusion.

NARROW-BEAM HF RADAR INVESTIGATIONS OF
MIDLATITUDE IONOSPHERIC STRUCTURE AND MOTION

Robert D. Hunsucker *
Geophysical Institute
University of Alaska
College, Alaska 99701

SUMMARY

Data acquired from 1964 - 1968 with a narrow-beam azimuth and elevation scan high-frequency backscatter sounder (or "HF Radar") located at Boulder, Colorado, have been analyzed in detail. This analysis has revealed that the "irregular structure" of the midlatitude ionosphere is the rule rather than the exception. Irregularities of varying scale size and apparent motion were present in about 90% of the observations. The "signatures" observed by this HF Radar System have been categorized into eight generic types which have been labelled with names roughly describing their appearance on the range-azimuth scan record. The relative diurnal and seasonal occurrence as well as the qualitative sunspot cycle and geomagnetic correlation of these signatures are presented.

One particular type of "signature" was analyzed using a three-dimensional computer ray-tracing technique developed at ITS, utilizing experimental data to modify an atmospheric-gravity-wave disturbance model. The "synthetic backscatter record" was sufficiently similar to the experimental HF Radar record to justify this approach in the interpretation of backscatter data.

I. INTRODUCTION

Many investigators have utilized the HF backscatter technique to measure various parameters of the ionosphere, beginning in the early 1950's. Some of these investigators have been concerned with the characteristics (height, speed, direction of motion, and structure) of patches of sporadic-E ionization [Villard, et al., 1952; Clark and Peterson, 1956; Shearman and Harwood, 1958; Harwood, 1960, 1961; Bates, 1961; Dueño, 1962; Egan and Peterson, 1962; Steele, 1964; Bates, 1965]. Other investigators utilized the technique to ascertain irregularity structure in the F-region [Villard and Peterson, 1952; Silberstein, 1954; Shearman, 1956; Peterson, 1957; Wilkins and Shearman, 1957; Widdel, 1957; Stein, 1958; Valverde, 1958; Bates, 1959, 1961; Egan and Peterson, 1963; Ranzi and Dominici, 1963; Tveten, 1961; Dueño, 1963; Davis, et al., 1964; Wickersham, 1964; Gilliland, 1965; Croft, 1967; Hunsucker and Tveten, 1967; Croft, 1968].

The purpose of this paper is to present the results of observations of the midlatitude ionosphere using a narrow-beam high-frequency (HF) oblique-incidence backscatter sounder scannable in azimuth and elevation which has been developed at the Institute for Telecommunication Sciences in Boulder, Colorado. Except for the cases of direct backscatter from meteor and intense sporadic-E ionization and some F-region irregularities, the data obtained are ground backscatter (groundscatter) "signatures". It is quite important to emphasize the point that the cathode-ray-tube (CRT) photographs displayed in this paper are simply the "backscatter signatures" obtained by this particular system. In order to quantitatively describe the actual ionospheric perturbations responsible for some of the more esoteric "signatures", it is necessary to use rather sophisticated analysis techniques.

There are four or five backscatter sounding techniques which have been utilized to provide most of the observations of ionospheric phenomena reported in the literature. Each of these techniques are briefly described in Table 1.

II. EXPERIMENTAL RESULTS

The Institute for Telecommunication Sciences (ITS) scan backscatter sounder (or "HF Radar") located near Boulder, Colorado, is unique in its combination of narrow antenna beamwidths in the HF region, simultaneous azimuth and elevation scan, and the ability to be rapidly "stepped" through several frequencies during a scan period. Descriptions of some of the equipment parameters may be found in publications by FitzGerrell, et. al., [1966]; Hunsucker and Tveten [1967]; Tveten and Hunsucker [1969]; and Hunsucker [1970]. A more complete description of the entire system including airborne antenna measurements of the antenna radiation patterns was published by Hunsucker [1969]. The system produces two fan beams, one scanning in azimuth and the other simultaneously scanning in elevation. The horizontal scan fan beam is 2° - 3° between azimuthal half-power points, and the elevation scan beam is 3° - 4° between vertical half-power points for the frequencies used in this investigation.

A picture of the receiving antenna system is shown in Figure 1, and a block diagram of the receiving system basic electronics is shown in Figure 2. Table 2 lists the most important parameters of the azimuth and elevation receiving systems, and Figure 3 shows the geographical area scanned by the azimuth array as a function of operating frequency.

The backscatter film data discussed in this and following sections of this paper were obtained using the ITS Scan Backscatter Sounder during the period October, 1964, through June, 1968. Typically, the sounder was operated for 1 - 10 days per month during this period and it took two minutes to acquire each

* Formerly at the Institute for Telecommunication Sciences, Office of Telecommunication, Boulder, Colorado 80302.

Table 1. - Ionospheric Backscatter Techniques

Technique	Typical Frequency Range (MHz)	Typical Antenna Half-power Beam-widths (degrees)		Characteristics		Reference
		Azimuth	Elevation			
Range-azimuth) scan Range-elevation)	12-25	3°-1.5°	4.2°-2.1°	High angular resolution	Limited scan width	Hunsucker and Tveten (1967); Tveten and Hunsucker (1969)
Range-time	Fixed frequency (HF)	20°-30° -40°	--- ---	Good range resolution	Poor angular resolution	Tveten (1961); Kanzi and Dominici (1963);
Sweep or step frequency	3-25 4-64	-20° 105°	--- -60°	Resolution in frequency domain	Very poor angular resolution	Silberstein (1954); Bates (1966)
Rotating antenna, PPI display	Fixed frequency (HF)	-40°	-30°	Large area surveillance	Poor angular resolution	Peterson, Egan and Pratt (1959)
Rotatable fixed frequency	Fixed frequency (16 MHz)	8°	-15°	Quite good angular resolution	Long rotation time (2-3 min.)	Thomas and McNichol (1960).

data photograph. A complete azimuth and elevation scan takes 12 seconds, so each data photo is an integration of 10 scans. The occurrence statistics in this section are based on analysis of 18,330 data photographs acquired starting near the minimum phase (sunspot Number =10) and ending near the maximum phase (SSN =106) of Solar Cycle 20.

Figure 4 shows the data format for the azimuth and elevation scan backscatter data photographs and illustrates the type of "signature" that one observes on this type of backscatter data display.

An attempt has been made to categorize these signatures into eight generic types which have been given names roughly describing their appearance on the range-azimuth record. Although the signatures being described apply to the azimuth scan record, the elevation scan data are also included and both have been discussed in detail by Hunsucker [1969].

A typical signature designated as a "patch" (P) is shown in Figure 5. It generally has a roughly circular or elliptical shape, always is observed at ranges less than the "uniform" echo, and always appears to move approximately parallel to the time delay markers (left-to-right or right-to-left). Another signature is shown in Figure 6 and is called "bands" (B) because it consists of two or more echoes structured in roughly parallel bands which appear to move in a direction perpendicular to their major dimension.

Additional examples of the "signatures" observed using the ITS azimuth and elevation scan system as well as many examples of data obtained by other backscatter techniques are contained in a data atlas recently published [Hunsucker, 1970].

Occurrence statistics for the various signatures observed with the ITS backscatter sounder are presented by Hunsucker [1971 a] and summarized in Table 3. The most commonly observed signature was the (MSB) type. Examination of Table 3 reveals that only the hook (H) and patch (P) signature types are nighttime echoes while all the others show maximum occurrence during the daytime. The medium-sized-blob and fine structure types are the most common echoes and the H type is the least common. The LSB, FS and P signatures show a clear maximum during mid-summer; the B-type echo appears to be a wintertime phenomenon and the remainder of the signatures show mixed seasonal occurrence statistics. The association of signature type with sunspot activity was done on a daily basis, and the comparison with geomagnetic activity used 3-hourly Kp values. The data were of such a nature that strictly quantitative comparisons could not be made; so the last two lines in Table 3 show a plus sign (+) for a positive association, a minus sign (-) for negative association and a zero (0) for no association.

III. DISCUSSION OF RESULTS

The purpose of this section is to attempt to gain some insight into the nature of the ionospheric irregularities which produce certain "signatures" observed by this particular backscatter system. The approach used here is to analyze one of the characteristic signatures in considerable detail utilizing whatever other simultaneous geophysical data are available [Hunsucker, 1971 b].

Table 2. - System Parameters

<u>Azimuth Array (1392 ft. aperture)</u>			
Elements: Log periodic horizontally polarized transposed dipoles			
Frequency, 12-25 MHz			
Gain, 5 dB above isotropic			
Front-to-back ratio, 20 dB			
E plane beamwidth, 72°			
H plane beamwidth, 115°			
Element spacing: 17.67 m			
Element height above ground: 24.38 m			
Boresight azimuth: 114° true bearing			
Horizontal Antenna			
Frequency (MHz)	Horizontal beamwidth (deg)	Main lobe elevation (deg)	Width of sector scan (deg)
12	3.0	14.8	90
15	2.3	11.8	69
18	2.0	9.8	56
21	1.7	8.4	48
25	1.4	7.1	40
<u>Elevation Array (1000 ft. effective aperture)</u>			
Elements: Same as for azimuth array			
Element Spacing: First element 8 m above ground and remaining ones successively spaced at 16 m			
Boresight azimuth: 114° true bearing			
Vertical Antenna			
Frequency (MHz)	Vertical beamwidth (deg)	Effective Elevation sector scanned (deg)	
12	4.2	3-52	
15	3.2	2.6-39	
18	2.8	2.3-32	
21	2.4	1.9-26	
25	2.0	1.5-22	

Table 3

Occurrence Statistics	Signature Type							
	U	LSB	MSB	FS	T	H	B	P
Relative Occurrence*	.31	.33	1.0	.97	.57	.18	.34	.41
Diurnal Peak Occ.	08-11	14-15	12-14	09-16	08-16	18-24	08-16	21-24
Diurnal Min. Occ.	17-19	00-07		00-06	00-06	11-14	00-08 17-24	11-14
Seasonal Peak Occ.	April & Nov.	June July	Jan. & July	July	May	May	Feb. Dec.	July
Seasonal Min. Occ.	July Aug.	April	March April	Equinoxes	---	March April	July	March
Correlation with sunspot Number	+	-	-	-	-	0	+	-
Correlation with Geomag. Activity	0	-	-	+	+	+	+	-

* Normalized to MSB = 1.0

Figure 6 illustrates the "Bands" signature and there is considerable evidence that this type of signature is caused by traveling-ionospheric-disturbances (TIDs) which are manifestations of internal atmospheric gravity waves [Hines, 1960; Munsucker and Tveten, 1967; Georges and Stephenson, 1969]. In particular, Georges and Stephenson [1969] use an ionospheric model perturbed by a gravity wave to simulate a record with the "bands" signature. TIDs have been classified as "Very large, Medium-Scale, and Small-Scale" disturbances by Georges [1967]. He lists some of the characteristics of the "medium-scale" TID as:

1. Always travel at speeds of less than 300m/sec.
2. Have periods, $10 \text{ min} < T < 40 \text{ min}$.
3. Appear mainly in the daytime.
4. Are not well correlated with any known geophysical events.
5. Often appear as "trains".

A backscatter "band" observation at 1330 MST (2030 UT) on November 17, 1966, at a frequency of 17.4 MHz is chosen as the "signature" to be analyzed. This observation was made during a relatively undisturbed day, geomagnetically.

Vertical incidence ionospheric soundings were available during this period from stations at Ponca City, Oklahoma; Texarkana, Arkansas; and Springfield, Missouri: -- all in the scan sector of the backscatter sounder. The vertical ionograms from these stations at the time of the backscatter observation indicate that the ambient ionosphere was quite uniform over a large part of the scan sector.

A "true height analysis" was performed on each of the vertical ionograms to obtain the vertical electron density distributions and to define the heights of layer maxima (h_{max}) and the scale heights (H). The most important layer parameters are listed in Table 4, showing in a more quantitative manner that the ambient ionosphere was quite uniform over a large horizontal region of the backscatter scan sector.

Table 4.

Station	E-Layer			F-Layer		
	f_c (MHz)	h_m (km)	H (km)	f_c (MHz)	h_m (km)	H (km)
Ponca City	2.94	111.	8.70	9.93	257.	36.1
Springfield	2.86	122.	11.0	9.99	273.	35.8
Texarkana	3.05	129.	13.7	9.67	289.	42.2
Averages	2.95	121.	11.1	9.86	273.	38.1

The average values of the parameters listed in Table 2 are used to describe a double, concentric α -Chapman layer defined by

$$f_N^2 = f_{c1}^2 \exp \left[\frac{1 - z_1 - e^{-z_1}}{2} \right] + f_{c2}^2 \exp \left[\frac{1 - z_2 - e^{-z_2}}{2} \right]$$

where

- f_N = plasma frequency
- $z_1 = (h - h_{m1})/H_1$
- $z_2 = (h - h_{m2})/H_2$
- h = height above ground
- f_{c1} = critical frequency of F-layer (MHz)
- f_{c2} = critical frequency of E-layer (MHz)
- H_1 = scale height of F-layer (km)
- H_2 = scale height of E-layer (km)
- h_{m1} = height (km) of F-layer maximum ionization density
- h_{m2} = height (km) of E-layer maximum ionization density

This ambient ionosphere perturbed by the wave model discussed later is used to obtain the "3D ray-sets" in computer programs developed by Jones [1966], and Stephenson and Georges [1969].

There is considerable evidence which indicates that the "medium-scale" TIDs cannot always be observed on vertical ionograms but can be detected by other more sensitive radio techniques such as Doppler or oblique backscatter soundings. Another method of observing the medium scale TIDs is to scale the variation of ionospheric virtual height with time at selected fixed frequencies from vertical ionograms. Figure 7 shows plots of virtual height variations during the backscatter observations.

In order to determine the fixed frequencies on the vertical ionogram which pertain to the ionospheric region where the backscatter sounder indicates TIDs, the following technique was used. First, from the backscatter azimuth and elevation record at 2030 UT the delay time and elevation angle were recorded. Next, these values of elevation angle and delay time were used as input to a computer program developed at ITS to calculate secant ϕ for curved earth, parabolic ionospheric electron density distribution. Or, alternatively a nomogram described in detail by Tveten and Hunsucker [1969] was used. This secant ϕ value and the radar operating frequency were then used in the secant law to obtain the appropriate plasma frequency to be scaled on the vertical ionosonde record. The values obtained (5.5, 8.0, and 9.0 MHz) were then the plasma frequencies corresponding to the locations of the ionosondes at Ponca City, Springfield and Texarkana respectively, in relation to the radar operating frequency. The backscatter delays were measured at the appropriate azimuth angle for each ionosonde location. The vertical line in Figure 7 indicates the time of the backscatter observation and the arrow at 1720 UT shows a magnetic storm sudden commencement (SSC). Magnetograms from Dallas, Texas, were examined in detail and there was no correlation between the ionospheric and magnetic data.

Examination of the simultaneous backscatter observations and virtual height variations (Figure 7) reveals the following characteristics of this TID signature:

- The TIDs appear in "trains" (from backscatter record)
- The approximate horizontal TID separation is ≈ 225 km. (Estimated from backscatter record.)
- The periods range from ~ 15 to 30 minutes (from Fig. 7).
- The vertical wavelength is ~ 225 km (from Fig. 7).
- There is no apparent correlation with magnetograph variations.

Comparing these observations with the "medium scale TID" characteristics listed at the beginning of this section seems to justify our working hypothesis that we are, indeed, observing the medium scale TIDs.

The ambient ionosphere described earlier in this section is now perturbed with the "medium scale" gravity wave model developed by Georges and Stephenson [1969] modified by the results of the experimental backscatter and vertical incidence data obtained at 1330 MST November 17, 1966. Mathematically the complete model is described by the equations [Georges and Stephenson, 1969, p. 682]

$$N = N_0 (1 + v)$$

and

$$v = \delta \exp \left\{ - \left[\frac{(R - R_e - Z_0)}{N'} \right]^2 \right\} \cos 2\pi \left[t' - \frac{R_e n}{\lambda_x} + \frac{(R - R_e)}{\lambda_z} \right]$$

where

- R = distance from the center of the earth
- n = polar angle ($\frac{\pi}{2}$ - latitude)
- R_e = radius of the earth
- N_0 = the double Chapman layer described earlier
- Z_0 = height of maximum wave amplitude
- N' = the wave amplitude "scale height"
- δ = perturbation wave amplitude
- λ_x = horizontal wavelength
- λ_z = vertical wavelength
- t' = time in wave periods

The asterisks denote quantities determined experimentally, and the remaining quantities are obtained from the theoretical gravity wave model. The next step is to carry out a three-dimensional (3D) ray tracing through this model to obtain the "rayset" cards, which are then used in the backscatter simulation program.

Figure 8 shows the experimental azimuth scan record on the left and the synthetic backscatter record from the 3D ray tracing and simulation on the right for 1330 MST on November 17, 1966. Before attempting a detailed comparison between the two records, several features of the experimental record should be explained: (1) the vertical band near the center of the azimuth scan sector is due to strong HF interference and will not, of course, appear on the synthetic record. (2) the receiver video gain was set too high and consequently there were some saturation effects in the cathode-ray-tube and photographic recording process.

There are some strong similarities between the two records: (1) the "band" structure is at the same range of time delays in both records. (2) the orientation and curvature of the bands is very similar. (3) there are approximately the same number of bands in both records.

The strong focused echo between 8 and 10 msec delay in the experimental record does not appear in the synthetic record. From examination of several experimental azimuth and elevation scan records and evaluation of the experimental parameters, it appears that this echo is most probably a combination of a gain saturation and an antenna sidelobe (equipment) effect.

In summary, there are enough similarities between the experimental backscatter TID signature and the simulated record to suggest that this analytical approach is a valid one. However, in applying the ray-tracing simulation approach, one must always remember that the basic question of "uniqueness" remains unanswered. That is to say, will different ionospheric perturbation models produce essentially the same simulated signature?

An even more difficult problem is the attempt to ascertain the nature of the source of the internal gravity waves that produce the TIDs. The difficulty of this problem is illustrated by the following crude antenna-array-factor analogy. One may roughly consider the source of the disturbances as a radiator of energy in the internal gravity-wave mode which is then multiplied by several antenna-array factors and finally convolved with the response characteristics of the particular observing system, as shown in Figure 9.

The energy sources of internal gravity waves are thought to be numerous and to vary in their location in altitude from the surface of the earth to ionospheric heights [Georges, 1968], but relatively nothing is known about their polar diagrams, i.e. whether they radiate energy isotropically or in a multi-lobed manner. For sources located low in the atmosphere, the source polar diagram would have to be multiplied by array factor 1, which describes the atmospheric wind structure existing at the time [c.f. Hines and Reddy, 1967]. Array factor 2 represents the ionospheric response to internal gravity waves, which is highly anisotropic, as has been shown recently by Hooke [1970]. Lastly, array factor 3 represents the response characteristics of the particular radio technique used to detect the TIDs (e.g., HF backscatter sounders, spaced ionosondes, Thomson scatter radar, Faraday rotation). Each of the various radio techniques will inherently be biased in such a way as to emphasize certain characteristics of the TIDs.

The preceding discussion is only intended to portray some of the difficulties one encounters in attempting to gain information on the ultimate source of the TIDs that are observed by radio methods.

IV. CONCLUSIONS

The specific results of this investigation are:

A. Based on examination of several thousand frames of data obtained with the ITS HF Radar, it is apparent that the "irregular-structure" of the midlatitude ionosphere is the rule rather than the exception. That is to say, irregularities exhibiting a wide variation in size and lifetime are observed most of the time. The "uniform" backscatter signature mentioned in Table 3 was only observed approximately 6% of the time during an observing period of several years spanning over one-half of a sunspot cycle. This midlatitude ionosphere "irregular-structure" is largely "washed out" when one sounds the ionosphere with the wide antenna beams used in most backscatter sounding techniques.

B. In compiling an "atlas" of midlatitude backscatter "signatures" observed with the ITS/ESSA high resolution HF radar, the signatures have been categorized into eight generic types which have been labelled with names roughly describing their appearance on the range-azimuth record. Examination of several thousand frames of data has revealed that over 90% of the signatures fall into these eight classifications or their various combinations and permutations.

C. One particular type of signature, the "bands" illustrated in Figure 6 has the characteristics of the "medium-scale" TID in Georges' [1966] classification scheme. If one assumes his medium-scale gravity-wave TID model and utilizes experimental data to construct the model and define the ambient ionosphere, then perform a 3D ray-tracing and backscatter simulation computer analysis, a synthetic backscatter record is obtained. There are enough similarities between the experimental TID signature and the simulated record to justify the use of this approach in the analysis of backscatter data.

V. ACKNOWLEDGEMENTS

Many people at the Institute for Telecommunication Sciences have contributed significantly to the development of this unique and sophisticated HF Radar instrumentation system. It is impossible to acknowledge the contribution of each individual, but I would like to express sincere thanks to: Mr. Lowell H. Tveten, who directed the HF Ionospheric Radar Program for several years; to Messrs. L. L. Melanson, G. E. Wasson, A. R. Mitz, D. C. Whittaker and J. L. Valega for developing, maintaining and operating the equipment during these experiments; and to Mr. L. A. Berry, Mr. Vaughn Agy, Drs. W. F. Ullaut, W. J. Surtees, W. H. Hooke and E. K. Smith, for stimulating discussions during the course of this investigation. Research funding was provided by ITS/ESSA and various agencies of the Department of Defense. Finally, I would like to thank Mrs. Pat Brooks of the Geophysical Institute for her painstaking preparation of this manuscript.

VI. REFERENCES

- Bates, H. F. (1959), The height of F-layer irregularities in the Arctic ionosphere, J. Geophys. Res., **64**, 1257-1264. (See also correction, J. Geophys. Res. **65**(4), 1304, 1960.)
- Bates, H. F. (1961), The slant-E_s Echo -- a high frequency auroral echo, J. Geophys. Res., **66**, 447-454.
- Bates, H. F. (1961), An HF sweep frequency study of the Arctic ionosphere, Sci. Report No. 1, UAG-R115, Geophysical Institute, University of Alaska, College, Alaska.
- Bates, H. F. (1965), Some effects of dense E_s clouds on high-latitude HF backscatter observations, J. Geophys. Res., **70**, 5895-5905.
- Clark, C. and A. H. Peterson (1956), Motion of sporadic-E patches determined from high-frequency backscatter records, Nature **178**, 486-487.
- Croft, T. A. (1967), Computations of HF ground backscatter amplitude, Radio Sci. (New Series) **2**, 739-746.
- Croft, T. A. (1968), The influence of ionospheric irregularities on sweep-frequency backscatter, J. Atmospheric Terr. Phys., **30**, 1051-1063.
- Davis, J. R., W. C. Headrick, and J. L. Ahoern (1964), A HF backscatter study of solar eclipse effects on the ionosphere, J. Geophys. Res., **69**, 190-193.
- Dueño, B. (1962), Sporadic-E as observed from Mayaguez, Puerto Rico by backscatter sounder, Ionospheric Sporadic-E, ed. by E. K. Smith, Jr., and S. Matsushita, pp. 110-122, Pergamon Press.
- Dueño, B. (1963), Interpretation of some sweep-frequency backscatter echoes, J. Geophys. Res., **68**, 3603-3610.
- Egan, R. D., and A. M. Peterson (1962), Backscatter observations of sporadic-E, Ionospheric Sporadic-E, ed. by E. K. Smith, Jr., and S. Matsushita, pp. 89-109, Pergamon Press.
- Egan, R. D., and A. M. Peterson (1963), The influence of sudden ionospheric disturbances on backscatter sounding, The Effect of Disturbances of Solar Origin on Communications, ed. by G. J. Gassmann, AGARDograph **59**, pp. 155-165, Macmillan.
- FitzGerrell, R. G., L. L. Proctor and A. C. Wilson (1966), An HF antenna array electronically scanned in elevation, ESSA Tech. Rept. IER 11-ITS 11, Clearinghouse for Federal Scientific and Technical Information, Springfield, Va. 22151, Acc. No. AD 645233.
- Georges, T. M. (1967), Ionospheric effects of atmospheric waves, ESSA Tech. Rept. IER 57-ITS 54, U.S. Govt. Printing Office, Washington, D.C. 20402.
- Georges, T. M. [Editor] (1968), Acoustic-gravity waves in the atmosphere - Symposium Proceedings, pp. 1-215, 15-17, U.S. Government Printing Office, Washington, D.C. 20402.
- Georges, T. M., and Judith J. Stephenson (1969), HF radar signatures of traveling ionospheric irregularities -- 3D ray-tracing simulation, Radio Science **4** (8).
- Gilliland, C. R. (1965), Sweep-frequency backscatter with calibrated amplitude, Rep. SU-SEL-65-095, Tech. Rept. 111, Electronics Laboratories, Stanford University.
- Harwood, J. (1960), A preliminary report on observations of sporadic-E by the backscatter technique, Some Ionospheric Results obtained during the IGY, ed. by W. G. Beynon, pp. 231-238, URSI/AGI Committee Symposium, Elsevier.
- Harwood, J. (1961), Some observations of the occurrence and movement of sporadic-E ionization, J. Atmospheric Terr. Phys., **20**, 243-262.
- Hines, C. O. (1960), Internal atmospheric gravity waves at ionospheric heights, Can. J. Phys. **38**, 123-129.
- Hines, C. O. and C. A. Reddy (1967), On the propagation of atmospheric gravity waves through regions of wind shear, J. Geophys. Res., **72**, 1015-1034.
- Hook, William H. (1970), The ionospheric response to internal gravity waves, I. The F2 response, J. Geophys. Res., **75**, 5535-5544.
- Munsucker, R. D., and L. H. Tveit (1967), Large traveling disturbances observed at mid-latitude utilizing the high resolution HF backscatter technique, J. Atmospheric and Terrest. Phys., **29**, 909-916.
- Munsucker, Robert Dudley (1969), Remote sensing of the midlatitude ionosphere with a narrow-beam high-frequency radar, Ph.D. Dissertation, University of Colorado, Boulder, Colorado. (Available from University Microfilms, Ann Arbor, Mich.).
- Munsucker, Robert D. (1970), An atlas of oblique-incidence high-frequency backscatter ionograms of the midlatitude ionosphere, ESSA Tech. Rept. ERL 162-ITS-104, U.S. Govt. Printing Office, Washington, D.C. 20402.

- Hunsucker, Robert D. (1971a), Characteristic signatures of the midlatitude ionosphere observed with a narrow-beam HF backscatter sounder, Radio Science, 5, No. 5, 535-548.
- Hunsucker, Robert D. (1971b), Analysis of a backscatter signature obtained with a high-resolution HF radar system, Radio Science, 6, Nos. 8/9, 763-768.
- Jones, R. M. (1966), A three-dimensional ray tracing computer program, Tech. Rept. IER 17-ITSA 17, Clearinghouse for Federal Scientific and Technical Information, Springfield, Va., Acct. No. PB174502.
- Peterson, A. M. (1951), The mechanism of F-layer propagated backscatter echoes, J. Geophys. Res., 56, 221-237.
- Peterson, A. M., (1957), Ionospheric backscatter, in Annals of the IGY III, Part IV, pp. 361-381, Pergamon Press.
- Peterson, A. M., R. D. Egan and D. S. Pratt (1959), The IGY three-frequency backscatter sounder, Proc. IRE, 47, 300-314.
- Ranzi, I., and P. Dominici (1963), Backscatter sounding during ionosphere storms, in The Effect of Disturbances of Solar Origin on Communications, ed. by G. J. Gassmann, AGARDograph 59, pp. 143-154, Macmillan.
- Shearman, E. D. R. (1955), The technique of ionospheric investigation using ground backscatter, Proc. IEE, 103B, 210-221.
- Shearman, E. D. R., and J. Harwood (1958), Sporadic-E as observed by backscatter techniques in the United Kingdom, in Sporadic-E Ionization, ed. by B. Landmark, AGARDograph 34, pp. 111-128.
- Silberstein, R. (1954), Sweep-frequency backscatter -- some observations and deductions, IRE Trans. Ant. Prop., AP-2, 56-63.
- Steele, J. G. (1964), The effect of the ground backscatter coefficient on observations of sporadic-E over sea, land and mountains, J. Atmospheric Terr. Phys., 26, 322-324.
- Stein, S. (1958), The role of ionospheric layer tilts in long-range high frequency radio propagation, J. Geophys. Res., 63, 217-241.
- Stephenson, Judith J., and T. M. Georges (1969), Computer routines for synthesizing ground-backscatter from three-dimensional raysets, ESSA Tech. Rept. ERL 120-ITS 84, U.S. Govt. Printing Office, Washington, D.C. 20402.
- Tveten, L. H. (1961), Ionospheric motions observed with high-frequency backscatter sounders, J. of Res. NBS 65D, 115-127.
- Tveten, L. H., J. C. Blair, R. D. Hunsucker, L. L. Melanson, H. G. Muller, W. B. Schlak, Jr., W. J. Surtees and J. M. Watts (1966), Propagation studies for RFD, Vol. II, High frequency backscatter studies, Tech. Rept. No. RADC-TR-66-431.
- Tveten, Lowell H., and Robert D. Hunsucker (1969), Remote sensing of the terrestrial environment with an HF radio high-resolution azimuth and elevation scan system, Proc. IEEE, 57, No. (4), 487-493.
- Valverde, J. F. (1958), Motions of large-scale travelling disturbances determined from high-frequency backscatter and vertical incidence records, Sci. Rept. No. 1, Electronics Research Laboratories, Stanford University.
- Villard, O. G., Jr., A. M. Peterson, and L. A. Hanning (1952), A method for studying sporadic-E clouds at a distance, Proc. IRE, 40, 992-994.
- Villard, O. G., Jr., and A. M. Peterson (1952), Scatter-sounding: A technique for study of the ionosphere at a distance, IRE Trans. Ant. Propagation, PGAP-3, 186-201.
- Wickersham, A. F. Jr., (1964), Identification of ionospheric motions, detected by the high-frequency backscattering technique, J. Geophys. Res., 69, 457-463.
- Widdel, H. V. (1957), Beobachtungen an ruckgestreuten Echoes bei Kurzwellen-Fernubertragung, Arkiv der Elektrischen Übertragung, 11, 429-439.
- Wilkins, A. F., and E. D. R. Shearman (1957), Backscatter sounding: an aid to radio propagation studies, J. Brit. IEE, Instn. Radio Engrs., 17 (11), 601-616.



Fig.1 Azimuth and elevation scan receiving antenna located at ITS Table Mountain Field Site near Boulder, Colorado.

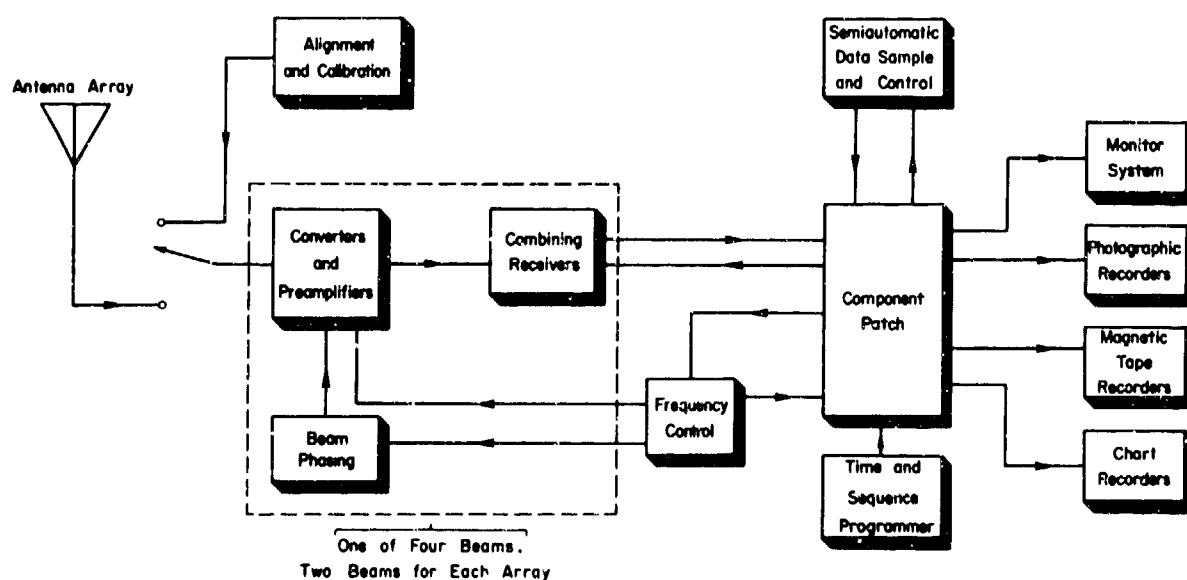


Fig.2 Simplified block diagram of receiver antenna system electronics.

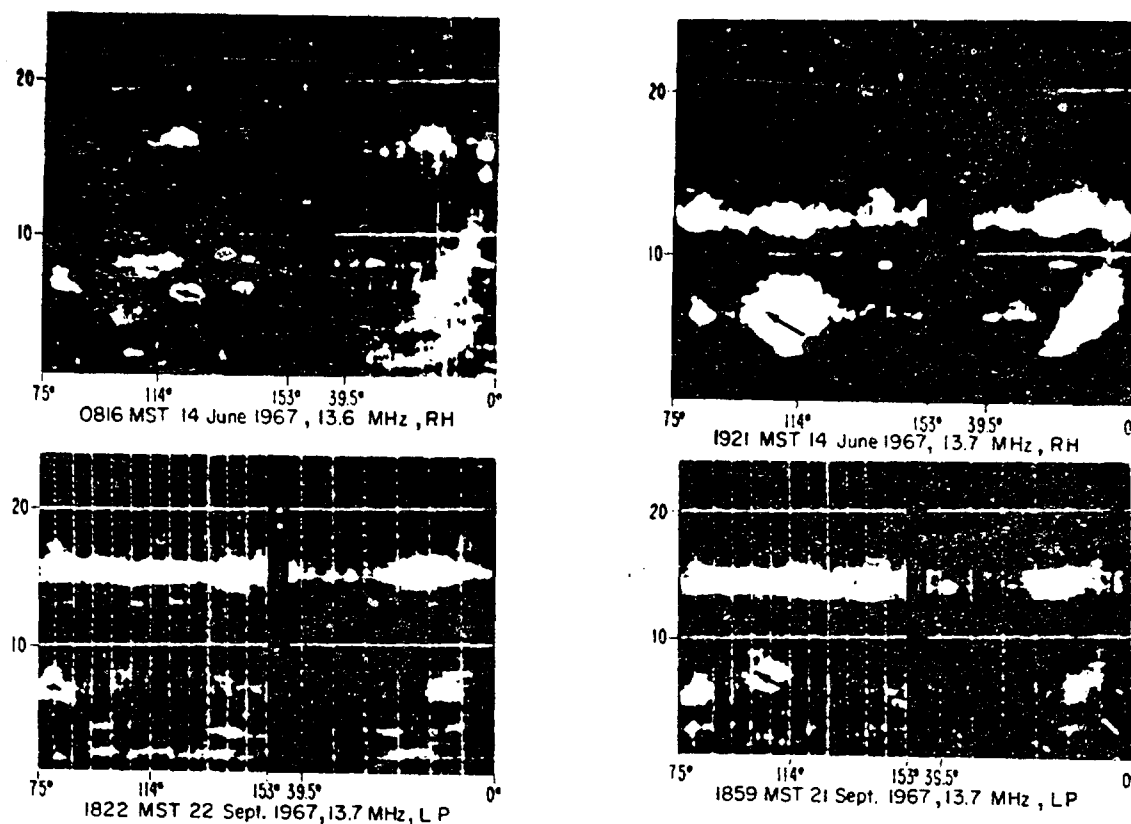


Fig.5 Examples of "Patch" (P) backscatter signature.

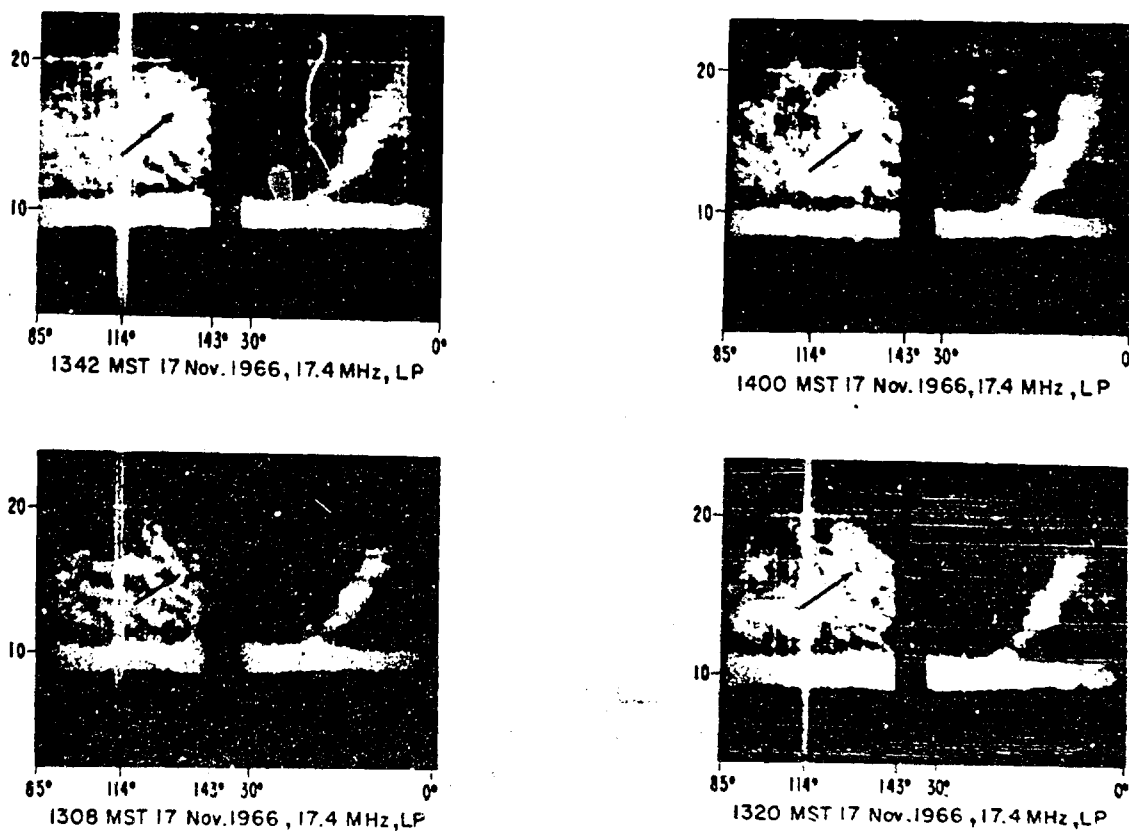


Fig.6 Examples of "Bands" (B) backscatter signature.

fig. 320

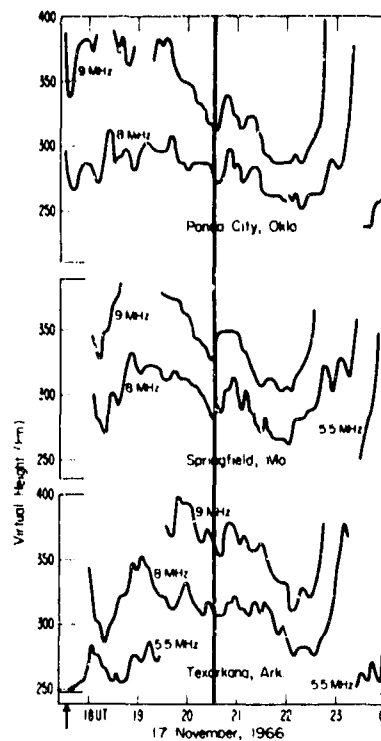


Fig.7 Plots of virtual height at fixed frequencies from the three vertical ionosondes during the backscatter observation.

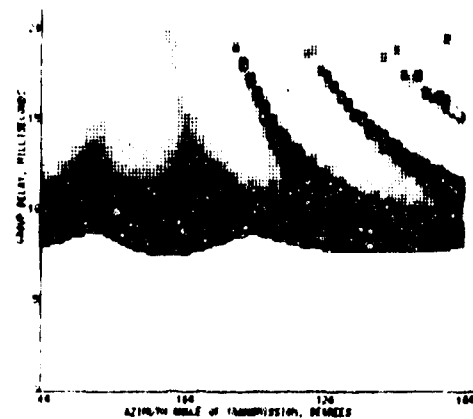
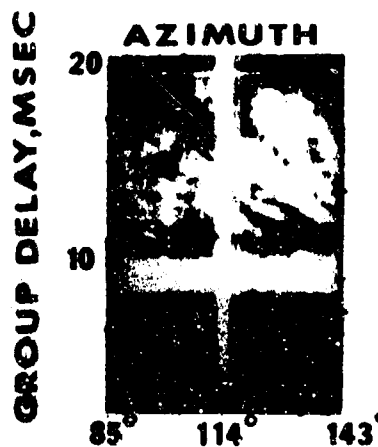


Fig.8 Experimental azimuth scan backscatter record (left) and synthetic backscatter record (right) for 1330 MST November 17, 1966.

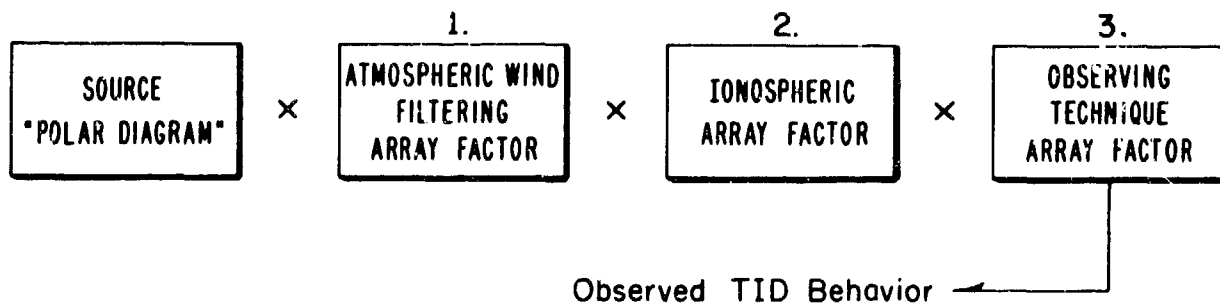


Fig.9 Antenna-array-factor analogy for determination of the nature of TID sources.

**AN IMPORTANT CHARACTERISTIC OF SOME
TRAVELING IONOSPHERIC DISTURBANCES**

by

I.Ranzi and P.Giorgi

**Centro Radioelettrico Sperimentale "G.Marconi"
V.Trastevere 189,00100-Roma-Italy**

UNE CARACTERISTIQUE IMPORTANTE DE QUELQUES PERTURBATIONS
IONOSPHERIQUES ITINERANTES

par

I. Ranzi et P. Giorgi

SOMMAIRE

L'observation des PII d'hiver de la région F2 en sondage vertical à fréquence fixe a montré que l'instant d'apparition des PII de certains groupes avançait de jour en jour.

AN IMPORTANT CHARACTERISTIC OF SOME TRAVELING IONOSPHERIC DISTURBANCES

I. Ranzi and P. Giorgi
Centro Radioelettrico Sperimentale
"G. Marconi"
V. Trastevere 189, 00100-Roma-Italy

SUMMARY

The observation of the F2 region winter TIDs, by means of vertical sounding on a fixed frequency, showed that the occurrence time of some TID groups anticipates from day to day.

1. EXPERIMENTAL RESULTS

During the last four winters, the observation of large scale traveling disturbances (TIDs) in the F2 region was carried out in the experimental station of Torrechiaruccia, near Rome (lat. 42.03° N, long. 11.84° E), by means of contemporary backscatter sounding on 18.6 MHz and vertical sounding on 6.8 MHz. Furthermore, during some months, a vertical sounding on 6.7 MHz was carried out at Pontecchio Marconi, near Bologna (lat. 44.4° N, long. 11.2° E), at a distance of 265 km from Torrechiaruccia, in the direction of 10° from North to West. The time delay between the passages of a given TID group (directed towards the equator), over the two stations presented a maximum value of about 30 minutes, which corresponds to a speed of 530 km/hr along the great circle passing through the two stations; an example is reported in Fig.1.

The vertical sounding records, taken at the main station of Torrechiaruccia, showed that, during the daily hours, the TIDs generally appear as a sequence of two or more oscillations in the virtual reflection height or a sequence of some focusing effects, which are particularly well visible in the second echoes; the period of each oscillation is of the order of one hour; furthermore, these more intense TIDs appear in groups of days, separated by days of reduced activity.

But the more interesting characteristic we observed in many cases is that the TID sequences show a day-to-day anticipation in their occurrence time; an example is reported in Fig.2. During winter 1971-1972, the periods during which such a phenomenon was observed were the following: 19,20 and 21 Nov ; 23 and 24 Nov ; 29,30 Nov and 1 Dec ; 6,7 and 8 Dec ; 20,21 and 22 Dec ; 23,24 and 25 Dec ; 27,28 and 29 Dec ; 5,6 and 7 Jan ; 12,13 and 14 Jan . A remarkable similarity of structure was showed by the TID trains occurring in the various days of a given period.

2. A TENTATIVE EXPLANATION

If the observed TIDs were due to gravity waves generated in the lower atmosphere, the propagation of these waves to the F-region should depend on the direction and the intensity of the tidal winds at the lower ionospheric levels, which produce a filtering action; in the case of a moving source of the gravity waves, the time, on which such a propagation is allowed, should show a day-to-day change (+).

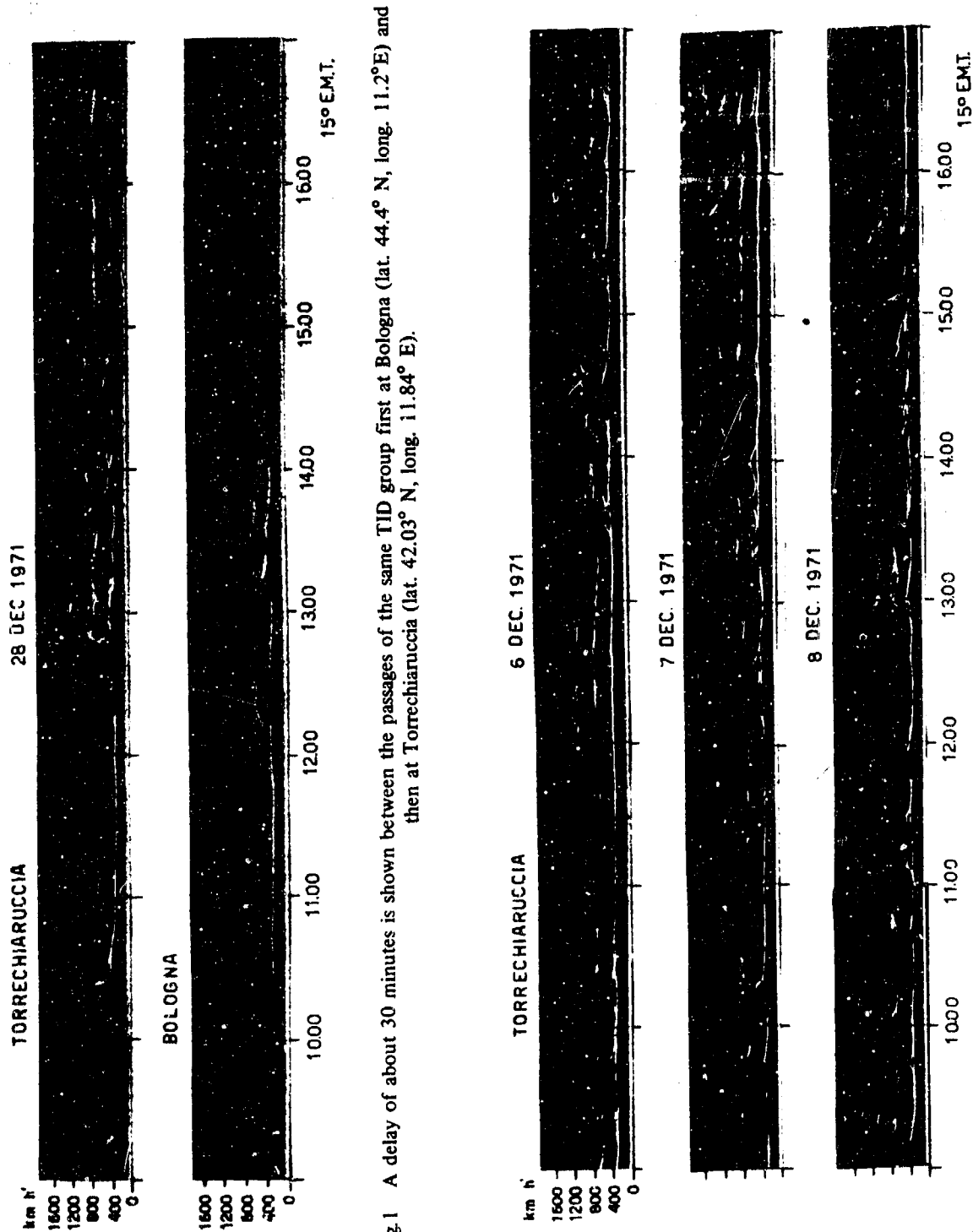


Fig. 1 A delay of about 30 minutes is shown between the passages of the same TID group first at Bologna (lat. 44.4° N, long. 11.2° E) and then at Torrechiaruccia (lat. 42.03° N, long. 11.84° E).

Fig. 2 The TID group first appearing on the afternoon of December 6, 1971, is seen earlier on the two following days.

**IONOSPHERIC DISTURBANCES CAUSED BY LONG PERIOD
SOUND WAVES GENERATED BY SATURN-APOLLO LAUNCHES**

by

Ganti L. Rao

Research Institute, University of Alabama in Huntsville
Huntsville, Alabama 35807 U.S.A.

327

PERTURBATIONS IONOSPHERIQUES CAUSEES PAR DES ONDES SONORES A PERIODE
LONGUE ENGENDREES PAR LES LANCEMENTS DE SATURNE-APOLLO

par

G.L. Rao

SOMMAIRE

Des perturbations en forme d'ondes furent observées dans l'ionosphère à la suite de plusieurs explosions nucléaires, au début des années 60. Les ondes de choc supersoniques créées dans l'atmosphère par des fusées de grandes dimensions peuvent également donner naissance à des perturbations de densité d'électrons dans l'ionosphère. A l'occasion des lancements de Saturne-Apollo 12 et 13, on a utilisé un réseau d'observation doppler de trajets de phase et enregistré des déplacements de fréquence doppler dus aux lancements des fusées. Des analyses de densité spectrale et des inter-corrélations des enregistrements de variation de fréquence doppler révélèrent les vitesses de phase d'arrivée de signaux qui provenaient du Sud du réseau, avec 700-800 m/s, et correspondaient à des périodes de l'ordre de 2 à 4 minutes. Des ionogrammes effectués toutes les 60 secondes à partir de l'île Wallops mirent clairement en évidence des perturbations ionosphériques dues aux fusées. Une analyse de hauteur réelle des ionogrammes indiqua que les ondulations affectant les densités électroniques à diverses hauteurs avaient une période de 2 à 4 minutes. On estima à 450 m/s environ les vitesses de groupe, obtenues à partir des premières perturbations visibles observées sur les enregistrements doppler en ondes entretenues et les ionogrammes, et à partir des données relatives à la trajectoire de la fusée. On peut expliquer ces arrivées de signaux comme un effet de guide d'ondes dans lequel le son est réfléchi dans sa totalité à partir de la thermosphère par la courbure des rayons, et entièrement (ou presque entièrement) réfléchi à partir de la mésosphère sous-jacente du fait des gradients de densité plus élevés, et, par conséquent, de l'augmentation de la fréquence de coupure acoustique. Ainsi, le son et, par conséquent, la perturbation, est canalisé au voisinage de la mésopause et de la basse thermosphère.

IONOSPHERIC DISTURBANCES CAUSED BY LONG PERIOD SOUND WAVES GENERATED BY SATURN-APOLLO LAUNCHES

Ganti L. Rao
Research Institute, University of Alabama in Huntsville
Huntsville, Alabama 35807 U. S. A.

SUMMARY

Wavelike disturbances were observed in the ionosphere following several nuclear explosions in early 1960's. Supersonic shock waves within the atmosphere generated by large rockets can cause ionospheric electron density perturbations. A CW phase path doppler array in the New York area was operated during the Saturn-Apollo 12 and 13 launches and recorded doppler frequency fluctuations due to rocket launchings. Cross correlation and power spectral analyses of the phase path-doppler frequency variation records showed that the phase velocities of the signal arrivals were from South of the array with $700 - 800 \text{ m. sec.}^{-1}$ corresponding to periods in the range of 2 - 4 minutes. Ionograms taken every 60 seconds from Wallops Islands showed clearly ionospheric disturbances due to rockets. True height analysis of the ionograms showed that the undulations in electron densities at various heights has a period of 2 - 4 minutes. The group velocities were estimated to be of the order of 450 m. sec.^{-1} obtained from the earliest visible disturbances seen on CW phase path doppler records and ionograms together with the rocket trajectory data. It may be possible to explain these arrivals of signals in terms of wave guide effect in which sound is totally reflected from the thermosphere by the bending back of rays, and is totally (or almost totally) reflected from the underlying mesosphere because of stronger density gradients and consequent increase in the acoustic cut off frequency. Thus, the sound and, hence, the disturbance is channeled near the mesopause and the lower thermosphere.

I. INTRODUCTION

Wave like disturbances were observed in the ionosphere following several nuclear explosions in the early 1960's. Baker (1968) detected these ionospheric disturbances due to atmospheric nuclear explosions at 150 - 200 km altitude with periods of one minute and speeds 300 m. sec.^{-1} . The periods and propagation characteristics of the ionospheric disturbances were found to be essentially the same as those observed on the ground. Baker (1968) interpreted these ionospheric disturbances as manifestations of imperfectly ducted acoustic gravity waves. Acoustic signals which can propagate long distances (in the order of thousand kilometers) from large rockets were also detected and reported (Donn *et al.*, 1968).

Supersonic shockwaves within the atmosphere generated by large rockets can cause ionospheric electron density variations. Ionospheric variations due to Saturn-Apollo launches were noticed from the ionograms taken at Grand Bahama Islands (Fehr, 1968). Disturbances on Grand Bahama Island ionograms were observed for a period of almost two hours after the launch of Saturn-Apollo rocket. These disturbances first appeared as a kink on the ionogram which appeared to have traveled downward. Disturbances such as these were also observed by Golomb *et al.* (1963) during high altitude chemical release experiments. In this paper, ionospheric perturbations caused by Saturn-Apollo rocket launchings were detected by using CW doppler array and conventional ionosonde and interpreted as long period sound waves.

II. CW DOPPLER ARRAY

Ionospheric observations were made using an array of CW doppler sounders and an ionosonde. The CW doppler system was built similar to Davies' system (Davies, 1962; Davies and Baker, 1969). A significant difference between Davies system and our system is in the presentation of data. In our system, the doppler signal was digitized and stored in digital magnetic tape, whereas in the Davies system, the signal was recorded in analog form. The digital form of recording of data allows the use of digital processing techniques such as cross correlation, digital filtering, power and cross spectral analyses. The doppler technique is very sensitive to phase path changes and the sensitivity in its present state of development is about 0.1 Hz, that is, phase path changes as small as $1/10$ of a radiowave length per second can be measured. At 4 MHz, this corresponds to $dp/dt = 7.5 \text{ m. sec.}^{-1}$. The geographic location of the CW doppler sounder system is shown in Figure 1. Two CW transmitters operating at 4.8 MHz and 6 MHz were continuously monitored by the receivers located at Catskill, Thornhurst, Lebanon and Westwood. The receiver outputs were digitized and transmitted by telephone lines to the central station, Westwood, for storage on magnetic tape. The data stored on the magnetic tape was later subjected to analysis for further study.

III. OBSERVATIONS AND RESULTS

The CW doppler array was in operation at Westwood, New Jersey, during the launches of Saturn-Apollo 12 and 13 rockets. These rocket launchings produced ionospheric perturbations which were successfully detected using our CW doppler array (Tolstoy, Montes, Rao, and Willis, 1970). Figure 2 shows the CW doppler record for Saturn-Apollo 12 launch on November 14, 1969. The CW doppler data for Lebanon and Thornhurst immediately before the signal arrival between the time windows 1100 to 1220 EST was subjected to cross spectral analysis to study the background noise coherence as shown in Figure 3. It can be seen from Figure 3 that the background noise coherence is rather poor in the entire period band and remained less than 0.2. Cross spectral analysis between several station pairs during the time of signal interval 1220-1340 EST was adopted to find the dominant periods. The results of the cross spectral analysis are presented in Figures 4, 5, and 6. It can be seen from the figures that during the time window 1220-1340 EST, there is a concentration of energy in the period band 1 to 5 minutes and in all station pairs the coherency remained over 0.75. The CW doppler data was then filtered, using a bandpass filter of 1 to 5.02 minutes and the resulting plots for Apollo 12 and 13 are shown in Figures 7 and 8.

Cross correlation analysis between station pairs was used for Apollo 12 CW doppler data to compute the phase velocities of the signal arrivals. The results of the analysis are shown in Table 1. The average phase velocity was found to be $700\text{--}800\text{ m. sec}^{-1}$ coming from south of the array. The variations in the phase velocities during the signal may be due to the nature of the source, which is a supersonic disturbance moving in both horizontal and vertical dimensions. Also, there are some inherent experimental errors due to the obliquity of the received radio waves. The apparent direction of signal arrival intersects the ground level projection of the trajectory at a point approximately 30.7°N , 72.8°W . The approximate altitude of the vehicle at this point was about 160 km. The group velocities of the signal arrival were estimated by using beginning and ending times of the recorded disturbance together with the trajectory data. This gave group velocities between 450 and 220 m. sec^{-1} .

An ionosonde was in operation at Wallops Island, Va., during Apollo 12 launch and the ionograms were taken every minute immediately after launch for a period of two hours. These ionograms were examined to detect any disturbances caused by the Saturn rocket. It was found that a kink on the ionogram near the ordinary F_2 layer critical frequency appeared which slowly moved downward and finally merged into F_2 layer ordinary trace. Several additional stratifications (traces) were also noticed all over the F_2 region indicating the disturbed nature of the ionosphere. The ionograms were then subjected to true height analysis to study the electron density fluctuations due to the Saturn rocket. Electron density variations at various heights at 10 km interval were plotted against local time and the plot is shown in Figure 9. It can be seen from the figure that the undulations in electron density at various heights has a period of 2-4 minutes. It might be of interest to note that the maximum effect on the ionosphere by the rocket was felt around 1218 hours. If the distance between Wallops Island and ground range of rockets when in F_2 region was taken approximately as 1000 km, then the group velocity of the arrival of the signal to ionospheric levels over Wallops Island was of the order of 450 m. sec^{-1} . Tolstoy et al. (1970) tried to explain the signal arrivals with group velocities 450 m. sec^{-1} corresponding to periods in the range 2-4 minutes and the horizontal phase velocities near 800 m. sec^{-1} , in terms of wave guide effect in which sound is totally reflected from the thermosphere by bending back of rays, and sound is totally (or almost totally) reflected from the underlying mesosphere because of stronger density gradients and the consequent increase in the acoustic cutoff frequency. Thus the disturbance is channeled near the mesopause and the lower thermosphere.

ACKNOWLEDGMENTS

This research was supported by NASA Marshall Space Flight Center under Contract NAS8-27088 and administered under the technical direction of the Aero-Astronautics Laboratory with Robert E. Smith as project manager.

TABLE 1

Phase velocities of the Saturn-Apollo 12 signal arrival as seen on Westwood, New Jersey CW doppler array.

<u>Time</u> (EST)	<u>Velocity</u> (m. sec. ⁻¹)	<u>Direction</u> (Degrees measured East of North)
1225 - 1235	810	185
1238 - 1248	808	178
1251 - 1301	750	176
1304 - 1314	700	177
1317 - 1327	650	140

REFERENCES

- Baker, D. M.
 "Acoustic Waves in the Ionosphere Following Nuclear Explosions"
Acoustic-Gravity Waves in the Atmosphere, edited by: T. M. Georges,
 U. S. Government Printing Office, Washington D. C.
- Davies, K.
 "Doppler Studies of the Ionosphere with Vertical Incidence"
Proc. IRE 50, 94, and Correction on 1544, 1962.
- Davies, K. and Baker, D. M.
 "F-2 Region Acoustic Waves from Severe Weather"
J. Atmosph. Terr. Phys., 31, 1345, 1969.
- Dunn, W., Posmentier, E., Fehr, U., and Balachandran, N. K.
 "Infra-Sound at Long Range from Saturn V", Science, 162, 1116, 1968.
- Fehr, U.
 "Propagating Energy in the Upper Atmosphere Including Lower Ionosphere Generated by Artificial Sources"
Acoustic-Gravity Waves in the Atmosphere, edited by: T. M. Georges, U. S. Government Printing
 Office, Washington D. C.
- Golomb, D., Rosenberg, N. W., Wright, J. W., and Barnes, R. W.
 "Formation of Electron Depleted Region in the Ionosphere by Chemical Releases"
Space Research IV, North-Holland Publishing Company, 1964.
- Tolstoy, I., Montes, H., Rao, G. L., and Willis, E.
 "Long Period Sound Waves in the Thermosphere from Apollo Launches"
J. Geophys. Res., 75, 5621, 1970.

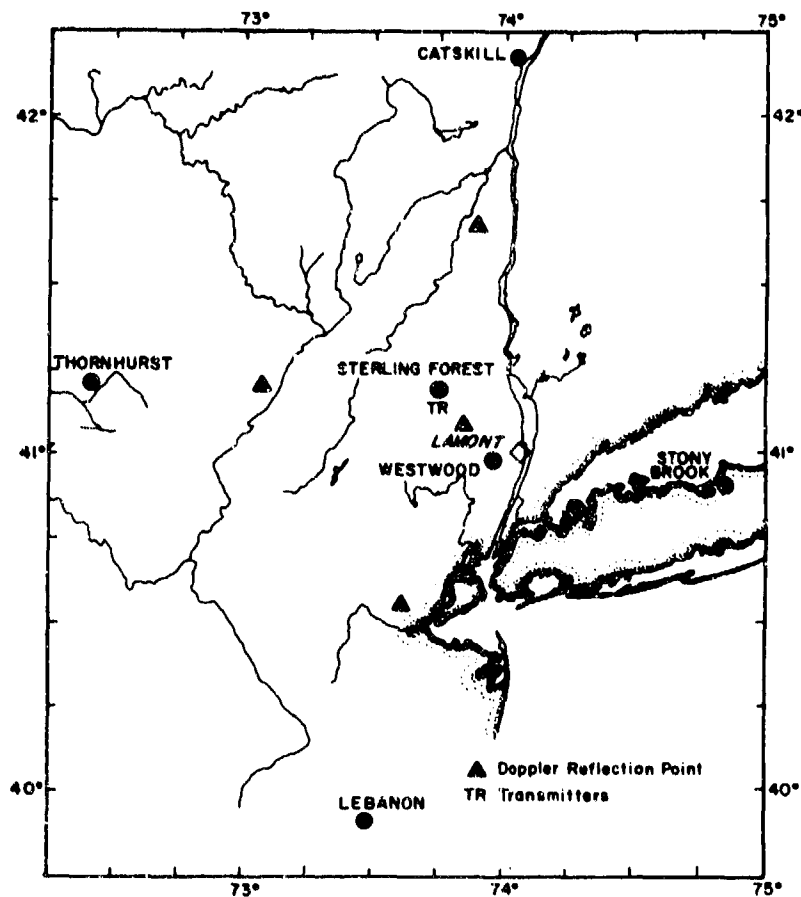


Fig.1 Geographic location of the stations of the CW doppler array.

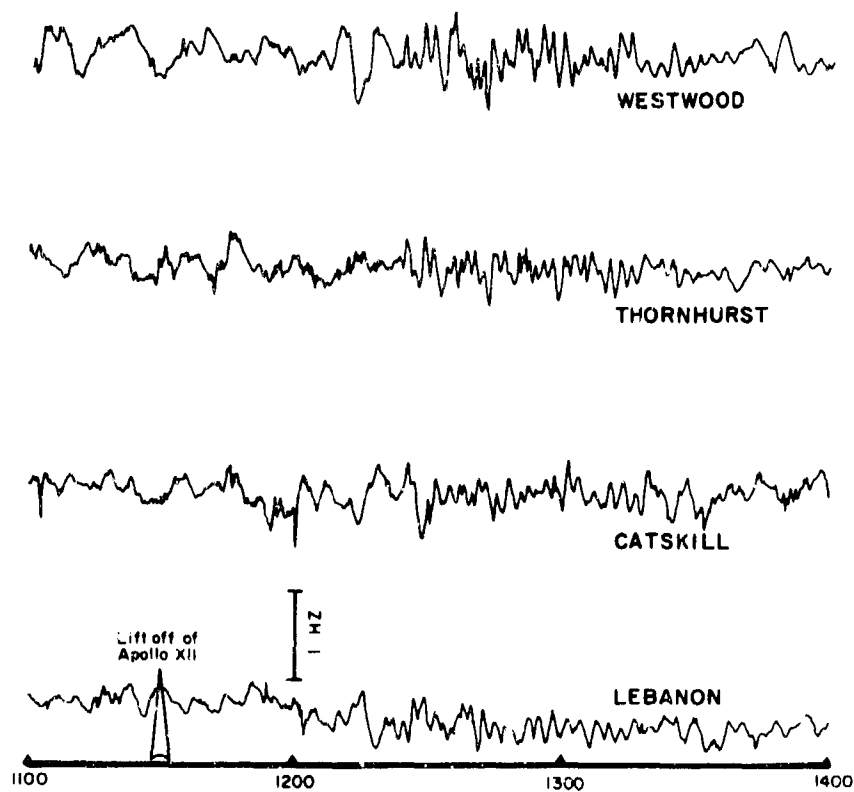
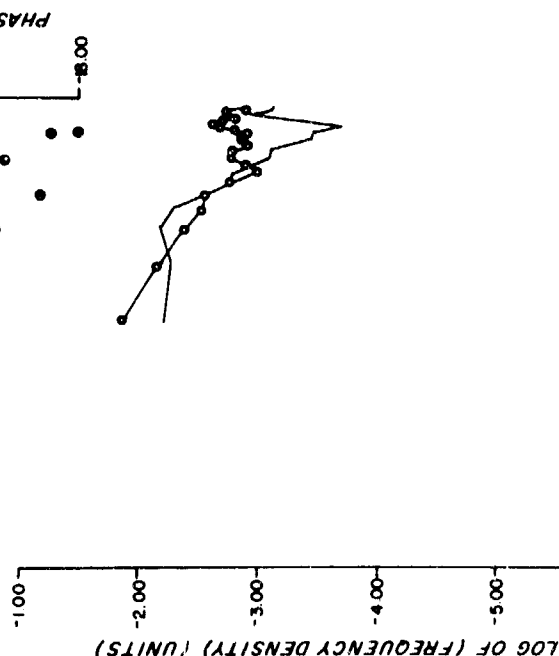
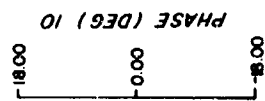
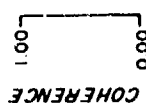


Fig.2 CW doppler record Saturn-Apollo 12 rocket signal.

DOPPLER LEB X DOPPLER THORN

NOV 14 1969 1100 TO 1220 EST

PERIOD (MIN)



DOPPLER LEB X DOPPLER WESTWOOD

NOV 14 1969 1220 TO 1340 EST

PERIOD (MIN)

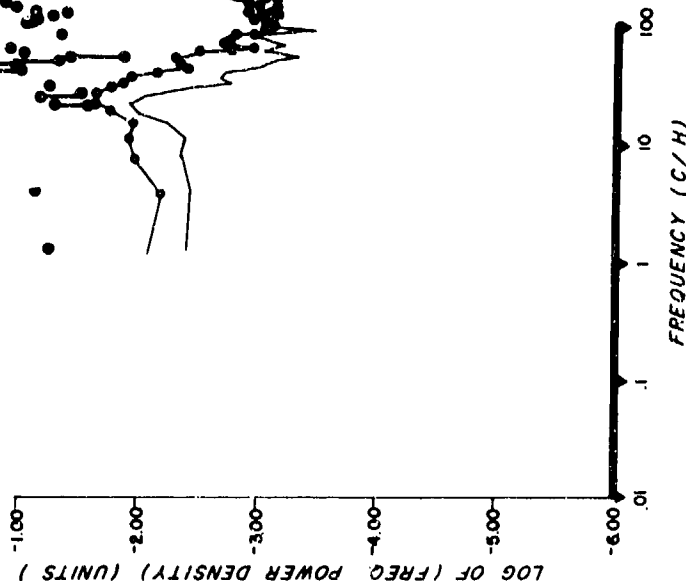
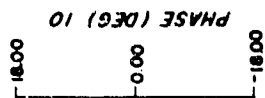


Fig.3 Cross spectral plots of CW doppler record before the Saturn-Apollo 12 signal arrival.

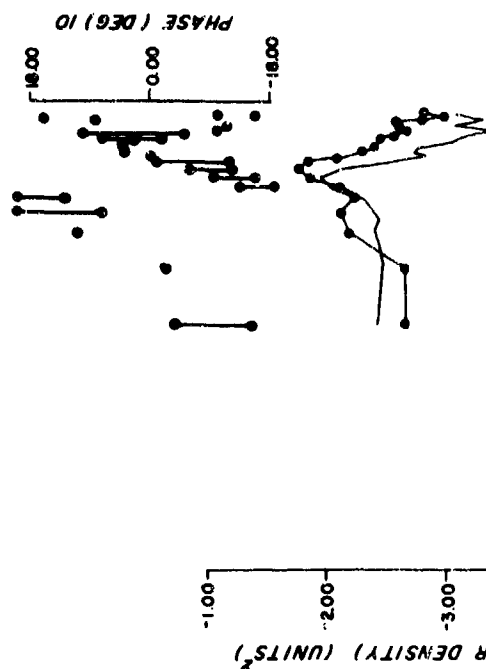
Fig.4 Cross spectral plots of CW doppler signal between Lebanon and Westwood.

DOPPLER LEB X DOPPLER THORN

NOV. 14 1969 1220 TO 1340 EST

PERIOD (MIN)
600 240 120 60 30 15 10 5 2 1

COHERENCE
1.00
0.00



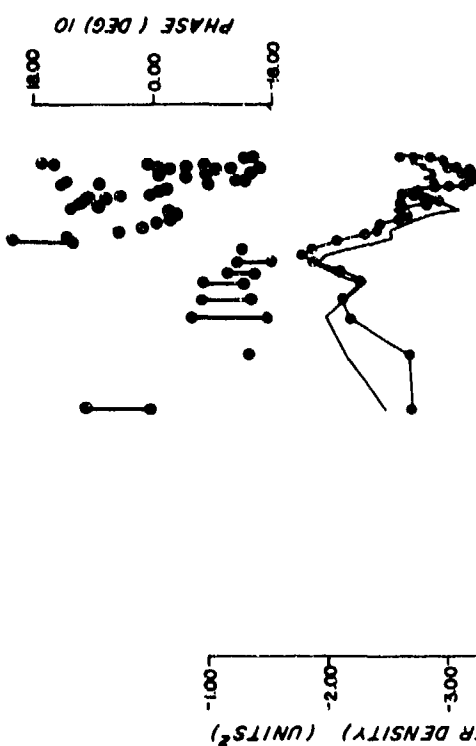
PHASE (DEG) 10
18.00
0.00
-18.00

DOPPLER CATS X DOPPLER THORN

NOV. 14 1969 1220 TO 1340 EST

PERIOD (MIN)
600 240 120 60 30 15 10 5 2 1

COHERENCE
1.00
0.00



PHASE (DEG) 10
18.00
0.00
-18.00

Fig.5 Cross spectral plots of CW doppler signal between Lebanon and Thornhurst.

Fig.6 Cross spectral plots of CW doppler signal between Catskill and Thornhurst.

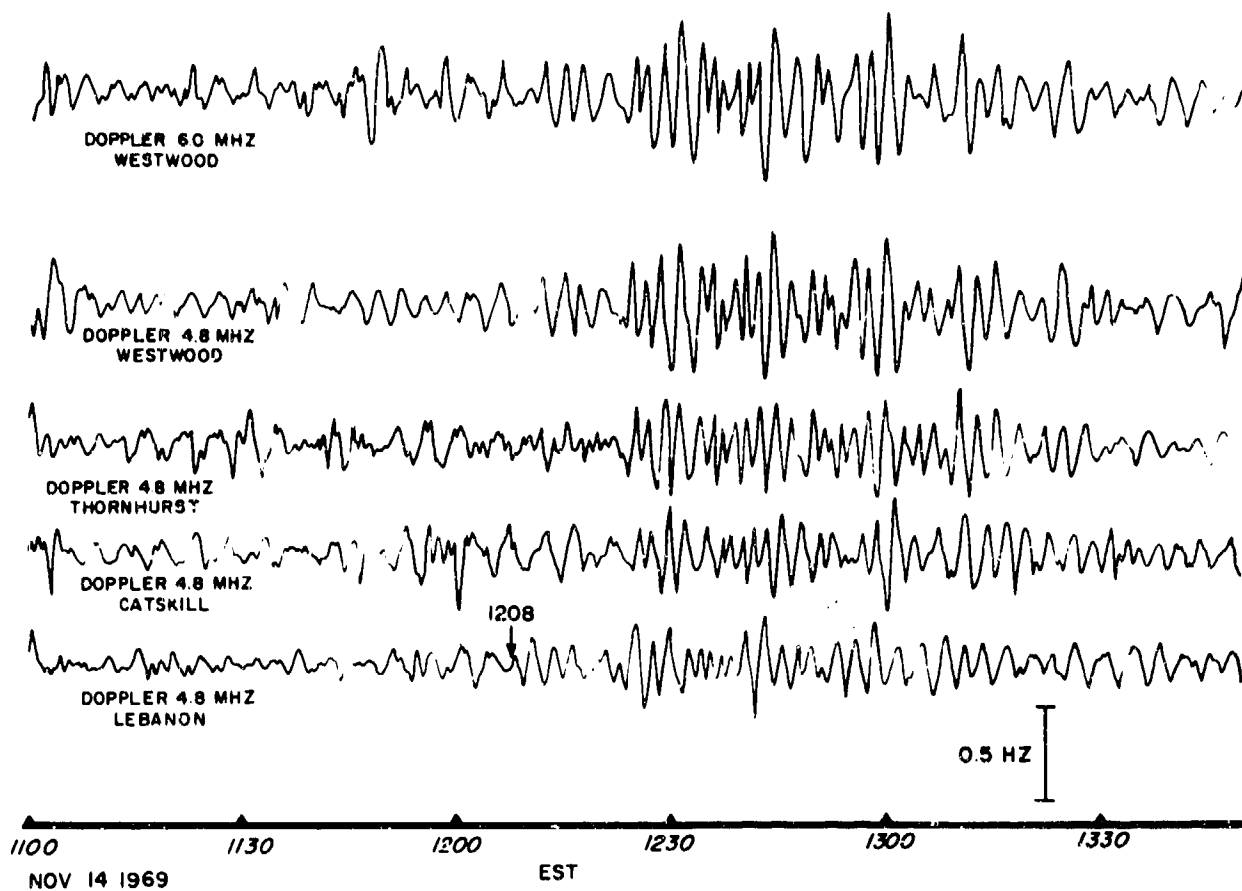


Fig.7 The 1.0 – 5.0 minute band pass filtered CW doppler record showing Saturn-Apollo 12 signal.

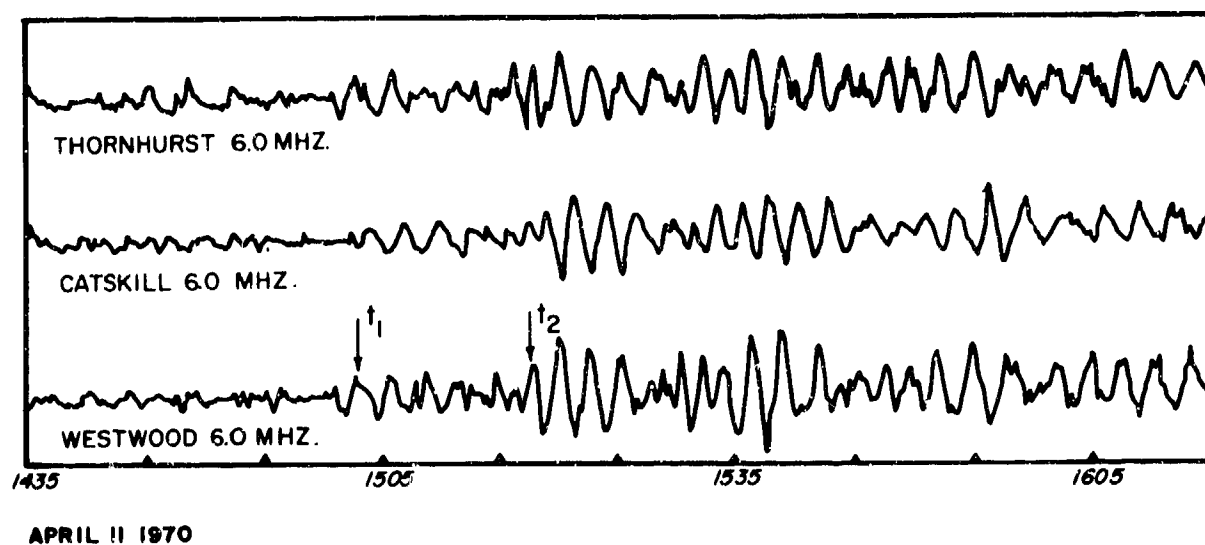


Fig.8 The 1.0 – 5.0 minute band pass filtered CW doppler record showing Saturn-Apollo 13 signal.

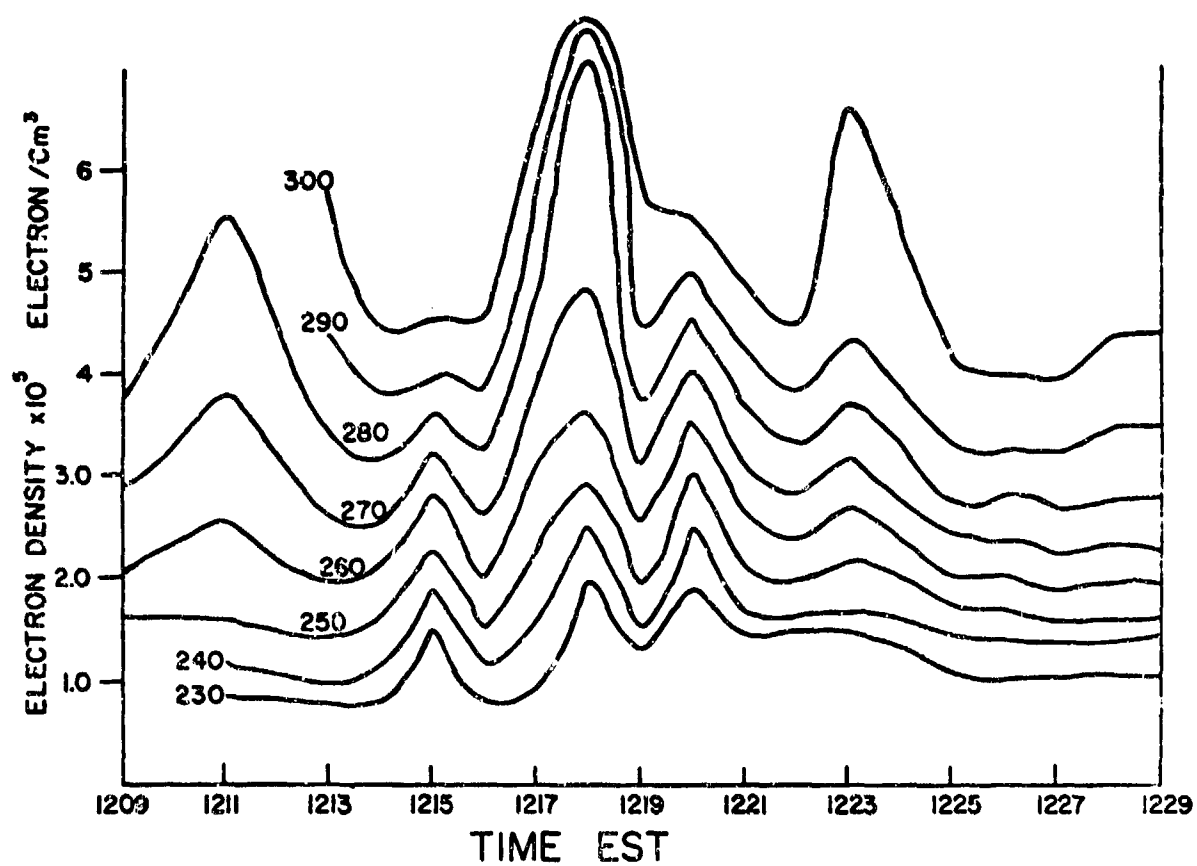


Fig.9 Electron density contours showing the effects of Saturn-Apollo 12 rocket launch.

**OBSERVATIONS OF TRAVELLING IONOSPHERIC DISTURBANCES
AT LONDON, CANADA**

by

J.Litva

**Communications Research Centre
Department of Communications
Ottawa
Canada**

338

OBSERVATIONS DE PERTURBATIONS IONOSPHERIQUES ITINERANTES EFFECTUEES A LONDRES (CANADA)

par

J. Litva

SOMMAIRE

L'auteur rend compte de certaines observations de perturbations ionosphériques itinérantes (PIIs) effectuées à Londres (Canada). Pour procéder à ces observations, on a eu recours à une nouvelle technique, décrite en détail, et qui consiste à mesurer l'angle d'arrivée et les variations d'amplitude des ondes radio se propageant à travers l'ionosphère à partir de régions localisées d'émission accrue sur le disque solaire. Un examen des observations antérieures indique un maximum de quatre cycles d'ondes dans les trains d'ondes des PIIs. Les observations dont il est rendu compte ici révèlent clairement la présence de trains d'ondes de PIIs jusqu'à quatre fois plus longs, et comportant de 15 à 18 cycles d'ondes. D'après les mesures effectuées, les déflexions angulaires de la ligne de visée solaire à 51,7 MZz varient de ± 6 à ± 20 minutes d'arc ; sur la base de ces chiffres, on calcule que les perturbations de densité d'électrons sont de l'ordre de 1 à 2 %. Les variations d'amplitude observées, correspondant aux scintillations à angle d'arrivée le plus grand, étaient d'environ 5 dB.

Les PIIs se classaient essentiellement en deux catégories : l'une dont la période était d'environ 6 minutes, l'autre dont la période atteignait 21 minutes. Les perturbations de la première catégorie se déplaçaient à une vitesse d'environ 200 km/heure, avec une longueur d'onde correspondante de 20 km. La vitesse des perturbations de la deuxième catégorie variait entre 800 et 2 000 km/heure, avec une longueur d'onde correspondante allant de 300 à 700 km ; d'autre part, elles se déplaçaient suivant une trajectoire préférentielle orientée nord-sud.

OBSERVATIONS OF TRAVELLING IONOSPHERIC DISTURBANCES AT LONDON, CANADA

J. Litva
Communications Research Centre
Department of Communications, Ottawa, Canada

SUMMARY

Some observations made at London, Canada, of travelling ionospheric disturbances (TIDs) are presented. They were obtained by way of a new technique which is described in detail; namely, measurement of angle of arrival and amplitude variations of radio waves which propagated through the ionosphere from localized regions of enhanced emission on the solar disk. A survey of past observations suggests that at most four wave cycles are observed in TID wave trains. The observations reported here show good evidence of TID wave trains up to four times as long, consisting of 15 to 18 wave cycles. The angular deflections of the solar line of sight at 51.7 MHz were measured to be between ± 6 to ± 20 minutes of arc; from which, electron number density perturbations are calculated to be of the order of 1 to 2 percent. The observed variations in amplitude corresponding to the larger angle of arrival scintillations were about 5 dB.

The TIDs were primarily of two types; one with a period of approximately 6 minutes, the other with a period of 21 minutes. The former travelled with the speed of about 200 km/hr and a corresponding wavelength of 20 km. The speed of the latter was between 800 and 2000 km/hr and the corresponding wavelength between 300 and 700 km; they also had a preferred line of travel which was orientated north-south.

1. INTRODUCTION

TIDs or travelling ionospheric disturbances are electron density irregularities in the F region which have been observed to move over horizontal distances of thousands of kilometers. The disturbance consists of a periodic change of the electron density with horizontal distance. When TIDs are represented by contours of constant electron density it is found that they tend to be tilted or displaced forward from the vertical in the direction of motion (THOME, 1964).

The velocity of TIDs has been measured at many locations by many workers using a variety of techniques. Some of the techniques employed are vertical incidence sounding (PIERCE and MINNO, 1940; WELLS, WATTS and GEORGE, 1946), doppler radar (GEORGES, 1968; CHAN and VILLARD, 1962), backscatter radar (TVETEN, 1961), in situ satellite density measurements (NEWTON et al, 1964), three station single frequency ionosondes (MUNRO, 1958), Thomson radar (THOME, 1968; VASSEUR and WALDEUFEL, 1969), faraday rotation (TITHERIDGE, 1963) and angle of arrival measurements (LAWRENCE and JESPERSEN, 1961; VITKEVICH, 1958). TIDs have wavelengths from about 50 to 2000 km and horizontal velocities from 180 to 2500 km/hr. The higher velocity TIDs tend to travel in the north-south direction and the lower velocity ones have no preferred direction of travel.

A description is given of some observations made at London, Canada, of TIDs. They were detected by measurements of deviations or scintillations in angle of arrival and amplitude of radio waves which propagated through the ionosphere. The measurements were made with radio interferometers monitoring radio waves of frequency 51.7 MHz emitted by a localized source in the sun's corona. There are times when the disturbed sun radiates meter wavelength radio waves at an enhanced level for periods of a day or more. On a number of these occasions the sun was used as a radio source and scintillations in angle of arrival of solar radio waves refracted by TIDs in the ionosphere were observed.

At VHF frequencies the angular deflection due to refraction of radar waves traversing the ionosphere is proportional to the spatial gradient, transverse to the line of sight, of the total number of electrons per square meter in the line of sight. It follows that, since gradients in total columnar electron content due to TIDs were measured, it is reasonable to assume that they were contained between the altitudes 100 and 500 km, or so. This, after all, is where most of the electrons of the ionosphere are contained.

It is assumed that for the most part TIDs perturb linear propagation of radio waves through the ionosphere because of their horizontal electron density gradients. These perturbations manifest themselves to an observer on the ground monitoring a radio signal as scintillations in the angle of arrival and amplitude of the signal. Equations will be developed relating the magnitude of the angle of arrival scintillations to both the electron density gradients and the characteristics of the interferometers used for the measurements. It will be shown that the apparent motion of the sun produces variations in both the magnitude and period of the angle of arrival scintillations. This motion and the variations induced by it are described in detail and it is shown that the line of travel and speed of the TIDs producing the scintillations can be deduced from the observed variations. Finally, equations are developed relating the magnitudes of the amplitude scintillations and angle of arrival scintillations produced by TIDs; from which the speed of the TIDs as a function of height can be deduced.

2. TECHNIQUE

Consider Fig. 27-1 where two antennas forming an interferometer are located at O and A along the baseline OY and separated by distance d. Two rays from the sun and denoted by S are shown arriving at each antenna. The total phase difference Φ of the radiation arriving from the source at the two antennas may be expressed generally as

$$\Phi = (2\pi + \phi) = \frac{2\pi d}{\lambda} \cos \theta \quad \text{Eq. 27-1}$$

where;

- ϕ = the measured phase difference in the range 0 to 2π
 n = an integer in the range $-\frac{d}{\lambda} \leq n \leq \frac{d}{\lambda}$
 λ = the wavelength of the radiation
 θ = the angle between solar ray and interferometer base line.

From the knowledge of the location of the sun the angle θ_S between a ray from the center of the solar disk and the interferometer base line can be calculated and substituted into Eq. 27-1 to solve for n . The angle θ_N of the solar radiation with respect to the interferometer's base line can then be determined from Eq. 27-1 and a measurement of ϕ_N where, ϕ_N is the phase between the solar radiation received at the two interferometer antennas. The angle θ_{SN} is defined by

$$\theta_{SN} = \theta_S - \theta_N \quad \text{Eq. 27-2}$$

Both θ_N and θ_S are always positive and measured from the line OY. θ_{SN} as defined here may be both positive or negative. It is called the angle of arrival henceforth, and the measured values reported here form the principle data base for this paper. It is augmented by the amplitude of the solar signal which also was measured and recorded.

Fig. 27-2 shows the relative location of the antennas of the compound solar interferometer used for the measurements. The antennas were linearly polarized five element yagis and were mounted to accept signals of vertical polarization. The amplitude of the incoming solar radio waves was recorded. Two phase measurements out of a possible five were also recorded. In some cases the phase difference between the waves arriving at Y_0 and Y_3 and between Y_0 and Y_2 were recorded; in other cases, the phases between Y_0 and Y_2 and between Y_0 and Y_1 were recorded. The measured phase differences were converted to angle of arrival θ_{SN} of the solar ray with respect to the interferometer base-line and the center of the sun. The various antenna pairs are denoted as follows:

- Y_0, Y_2 = wide E-W interferometer
 Y_0, Y_1 = narrow E-W interferometer
 Y_0, Y_3 = N-S interferometer

and the angle of arrival measurements presented here will be identified by these labels.

3. MOTION OF THE SOLAR LINE OF SIGHT

The loci of the intersection of the solar line of sight with various levels in the ionosphere may be determined with the aid of Fig. 27.3. In particular Fig. 27-3 (a), which shows a plane containing the solar line of sight, the observer and the center of the earth C. The intersection of the solar line of sight with an ionospheric layer whose height above the earth is D is given by R. The zenith angle of the sun is z ; B is the distance OR and δ is the angle RCO. It can be shown (HARROWER, 1963) that B is given by the following:

$$B = [(r + D)^2 - r^2 \sin^2 z]^{\frac{1}{2}} - [r^2 - r^2 \sin^2 z]^{\frac{1}{2}} \quad \text{Eq. 27-3}$$

and δ by the expression:

$$\delta = \cos^{-1} \frac{r^2 + (r + D)^2 - B^2}{2r(r + D)} \quad \text{Eq. 27-4}$$

where:

r = radius of the earth

The observer's celestial hemisphere is shown in Fig. 27-3 (b) with the observer at O, the north celestial pole at P, and the zenith at Z. The intersection of the extension of CR in Fig. 27-3 (a) with the observer's celestial sphere is given by R' and the co-latitude PZ and hour angle ZPR' of R' are given by S and t respectively.

The altitude of the sun denoted by h in Fig. 27-3 (a) is given by (SMART, 1944).

$$h = \sin^{-1} [\sin(\text{LAT}) \sin(\text{DEC}) + \cos(\text{LAT}) \cos(\text{DEC}) \cos(\text{HA})] \quad \text{Eq. 27-5}$$

where:

DEC = declination of the sun
 HA = hour angle of the sun.

The zenith angle z of the sun is given by

$$z = \frac{\pi}{2} - h \quad \text{Eq. 27-6}$$

and the azimuthal angle A_z by:

$$A_z = \sin^{-1} \left[\cos(\text{DEC}) \frac{\sin(\text{HA})}{\cos(h)} \right] \quad \text{Eq. 27-7}$$

From the spherical triangle PZR¹ in Fig. 27-3(b) it follows that

$$S = \cos^{-1} [\cos \delta \cos(\frac{\pi}{2} - \text{LAT}) + \sin \delta \sin(\frac{\pi}{2} - \text{LAT}) \cos(2\pi - A_z)] \quad \text{Eq. 27-8}$$

and,

$$t = \sin^{-1} \left[\frac{\sin \delta \sin(2\pi - A_z)}{\sin S} \right] \quad \text{Eq. 27-9}$$

The latitude and longitude of R or R' are given respectively by

$$\text{LAT}(R) = \frac{\pi}{2} - S \quad \text{Eq. 27-10}$$

$$\text{LONG}(R) = \text{LONG}(O) + t \quad \text{Eq. 27-11}$$

where:

$$\text{LONG}(O) = \text{longitude of the observer.}$$

Curves tracing out the loci of the intersection of the solar line of sight with various levels in the ionosphere, as a function of time, are given in Fig. 27-4. The paths shown were derived for values of η equal to 150, 300 and 450 km using solar parameters correct for November 12, 1969 and equations 27-8 to 27-11. The intersection of the dashed lines with the curves defines the position of the intersection point, R at the indicated times; positions at other times can be obtained by extrapolation. The co-ordinate axes shown in the insert define positive values of the velocity components V_x and V_y of the intersection point R; with positive V_x directed towards the west and positive V_y directed towards the north. These two velocity components are given by

$$V_x = (r + d) \cos[\text{LAT}(R)] \times \frac{d}{dt} [\text{LONG}(R)] \quad \text{Eq. 27-12}$$

$$V_y = (r + d) \frac{d}{dt} [\text{LAT}(R)] \quad \text{Eq. 27-13}$$

Curves for November 12, 1969 derived from Eqs. 27-12 and 27-13 giving V_x and V_y as a function of time for the altitudes 150, 300 and 450 km are given in Fig. 27-5. The component V_x , although positive throughout the interval between 1330 and 2030 UT, is seen to vary considerable and in a manner characterized by high values in the morning, relatively low ones at local noon, and high ones again in the afternoon. On the other hand V_y whose absolute value is less than V_x throughout this interval, begins with positive values, becomes zero at local noon, and assumes increasingly negative values in the afternoon.

Since the intersection point R moves through the ionosphere, it is to be expected that the period of the scintillations in angle of arrival of the solar line of sight, caused by TIDs, will be an apparent period. The apparent period will differ from the actual TID wave period by a quantity which is a function of the component of the velocity of the solar line of sight through the ionosphere parallel to the horizontal velocity of the TIDs. In the insert accompanying Fig. 27-4, let U represent the velocity of the TID and V the velocity of the intersection point R. The azimuthal angles of these vectors with respect to the negative Y axis are α_U and α_V respectively. They are both defined to be positive in the counter-clockwise direction. Their values are given by

$$\alpha_U = \tan^{-1} \frac{U_x}{U_y} \quad \text{Eq. 27-14}$$

and

$$\alpha_V = \tan^{-1} \frac{V_x}{V_y} \quad \text{Eq. 27-15}$$

The apparent period T' of the scintillations as a function of U is given by

$$\frac{1}{T'} = \frac{U}{\lambda_t} - \frac{V}{\lambda_t} \cos(\alpha_V - \alpha_U) \quad \text{Eq. 27-16}$$

where λ_t = TID wavelength.

4. MAGNITUDE OF ANGLE OF ARRIVAL SCINTILLATIONS

At VHF frequencies the refractive index, μ , of a radio wave propagating through the ionosphere is given to good approximation by

$$\mu = 1 - \frac{b}{\omega^2} N \quad \text{Eq. 27-17}$$

where

$$\begin{aligned} b &= e^2 / \epsilon_0 m = 1.6 \times 10^3 \text{ (mks)} \\ N &= \text{local number density of free electrons} \\ e &= \text{charge of an electron} \\ m &= \text{mass of an electron} \\ \epsilon_0 &= \text{permittivity of free space} \\ \omega &= \text{angular radio frequency} \end{aligned}$$

Eq. 27-17 is approximate because it neglects the effects of the earth's magnetic field and of absorption.

The total angular deflection, τ , of a radiowave from its average position (CHANDRASEKHAR, 1952) is given by

$$\tau = - \frac{b}{\omega^2} \frac{d}{du} \int_0^S N dl \quad \text{Eq. 27-18}$$

where l , is measured along the ray, and
 u , is measured along a normal to l .

Equations are now derived giving the variation, as a function of time, of the magnitude of TID induced scintillations in the solar angle of arrival measured by the E-W and N-S interferometers. Consider Fig. 27-6 with the observer at O where:

SO = solar line of sight
 OP = projection of the solar line of sight on the observer's horizon plane
 h = altitude of the sun
 \underline{U} = projection of the TID's horizontal velocity vector onto the horizon plane
 TS = azimuth of OP with respect to the OX axis
 α_U = azimuth of \underline{U} with respect to the OX axis.

In the derivations which follow it is assumed that:

- the TID's direction of travel defined by α_U remains constant
- the refraction of the solar line of sight from its average position is due, for the most part, to TID induced horizontal electron number density gradients
- the horizontal gradients are parallel to the TID's horizontal velocity.

It will be shown that since TS in Fig. 27-6 changes from positive values in the morning to negative values in the afternoon in a regular and defined fashion that the magnitude of the solar scintillations will vary in a unique manner determined by the TID's direction of travel.

It follows from the spherical triangle, ABC, in Fig. 27-1 that

$$\cos \theta = \cosh \cos A'_z$$

so that Eq. 27-1 can be written in the following form

$$\phi = \frac{2\pi d}{\lambda} \cosh \cos A'_z \quad \text{Eq. 27-19}$$

where:

$A'_z = A_z - \frac{\pi}{2}$, for the E-W interferometers and, $A'_z = \pi - A_z - 0.3098$, for the N-S interferometer.

The magnitude of the phase variations measured by the interferometers due to changes in h and TS caused by refraction of the solar line of sight may be obtained by finding the differential of Eq. 27-19 and substituting in the appropriate value for A'_z . It follows from a comparison of Figs. 27-2 and 27-6 that A'_z is equal to $\frac{\pi}{2} - TS$ and $TS - 0.3098$ radians respectively for the E-W and N-S interferometers.

The equations resulting from the substitution of A'_z into the differential of Eq. 27-19 are:

$$\Delta \phi_1 = -\beta_1 \sin(h) \sin(TS) \Delta h + \beta_1 \cos(h) \cos(TS) \Delta TS \quad \text{Eq. 27-20}$$

$$\Delta \phi_2 = -\beta_2 \sin(h) \sin(TS) \Delta h + \beta_2 \cos(h) \cos(TS) \Delta TS \quad \text{Eq. 27-21}$$

$$\Delta \phi_3 = -\beta_3 \sin(h) \cos(TS - 0.3098) \Delta h - \beta_3 \cos(h) \sin(TS - 0.3098) \Delta TS \quad \text{Eq. 27-22}$$

where:

$$\beta_1 = 2\pi (49.361)$$

$$\beta_2 = 2\pi (16.571)$$

$$\beta_3 = 2\pi (54.289)$$

In the above, Eqs. 27-20 and 27-21 give the magnitude of the phase scintillations $\Delta \phi_1$ and $\Delta \phi_2$ measured by the wide and narrow E-W interferometers respectively and Eq. 27-22 gives the magnitude of the phase scintillations $\Delta \phi_3$ measured by the N-S interferometer. The variations in the interferometer angle θ which are also equal to the variations in the angle of arrival as defined in Eq. 27-2 may be obtained by equating the differential of Eq. 27-1 to Eqs. 27-20, 27-21 and 27-22 in turn

$$\Delta \theta_{1,2} = \frac{\sin(h) \sin(TS) \Delta h}{\sin \theta} - \frac{\cos(h) \cos(TS) \Delta TS}{\sin \theta} \quad \text{Eq. 27-23}$$

$$\Delta \theta_3 = \frac{\sin(h) \cos(TS - 0.3098) \Delta h}{\sin \theta} + \frac{\cos(h) \sin(TS - 0.3098) \Delta TS}{\sin \theta} \quad \text{Eq. 27-24}$$

where:

$\Delta\theta_{1,2}$ = perturbation of angle θ for the wide and narrow E-W interferometers due to refraction of the solar ray

$\Delta\theta_3$ = perturbation of angle θ for the N-S interferometer due to refraction of the solar ray.

An expression, giving the variation of, $\Delta\theta_{1,2}$ and $\Delta\theta_3$ as a function of TS or local time may be obtained from a consideration of Fig. 27-6. The point C denotes the intersection of the solar ray with a layer in the ionosphere. The average horizontal electron number density gradient ξ is indicated and shown to be parallel to OA. Close inspection of Fig. 27-6 reveals that the component of ξ perpendicular to the solar line of sight ξ_\perp is contained in the plane defined by OS and OA. Thus the refracted solar ray whose angular deflection τ is given by Eq. 27-18 will be contained within this plane.

If a ray undergoes a deflection of τ it follows from the geometry in Fig. 27-6 that

$$\Delta h = \tau \sin \gamma \cos(TS - \alpha_U) \quad \text{Eq. 27-25}$$

where:

$$\gamma = \tan^{-1} \left[\frac{\tan(h)}{\sin(TS - \alpha_U)} \right] \quad \text{Eq. 27-26}$$

$$\Delta TS = \tau \frac{\cos \gamma}{\cos(h)} \quad \text{Eq. 27-27}$$

Substitution of Eq. 27-25 and 27-26 into 27-23 and 27-24 and dividing by τ to normalize the equations, allows one to write the following:

$$F_{1,2} = \frac{\Delta\theta_{1,2}}{\tau} = \frac{\sin(h) \sin(TS) \sin \gamma \cos(TS - \alpha_U)}{\sin \theta} - \frac{\cos(h) \cos(TS) \cos \gamma}{\sin \theta \cos(h)} \quad \text{Eq. 27-28}$$

and

$$F_3 = \frac{\Delta\theta_3}{\tau} = \frac{\sin(h) \cos(TS - 0.3098) \sin \gamma \cos(TS - \alpha_U)}{\sin \theta} + \frac{\cos(h) \sin(TS - 0.3098) \cos \gamma}{\sin \theta \cos(h)} \quad \text{Eq. 27-29}$$

where it is assumed that τ is constant with time.

The function $F_{1,2}$ and F_3 are called the 'response' of the E-W and N-S interferometers respectively. They give the efficiency of the interferometers in measuring angular deflections in the solar line of sight as a function of time and geometry. The response given by Eq. 27-28 of the E-W interferometers as a function of time is plotted in Fig. 27-7 with α_U in degrees indicated on the curves. It is seen that the shape of the curves is a function of the parameter α_U ; in particular, the local time at which, $F_{1,2}$ becomes zero is a function of α_U . This suggests that the line along which TIDs travel may be determined by the modulation imposed by the interferometers on the observed magnitude of the solar angle of arrival scintillations. In Fig. 27-8 the corresponding response F_3 of the N-S interferometer is plotted as a function of time for various values of α_U .

5. FOCUSING AND DEFOCUSING EFFECTS OF TIDS

Closely following Turnbull and Forsyth (1965) focusing and defocusing of the radio-wave energy by TIDs is now considered. Only the simplest case dealing with relatively small deviation angles or irregularities at low altitudes is considered. In this case the only effect on the ground is slight focusing and defocusing of the radio-wave energy as the solar line of sight encounters TIDs. The more complex case where rays from two or more widely separated points in the TID reach the observer, while rays from intervening regions do not, is not considered because the deep amplitude fading which would result from this type of mechanism was not experimentally observed.

The geometry is illustrated in Fig. 27-9 where the plane of the diagram is assumed to be the plane containing the solar line of sight and the TIDs' line of travel. The refracted solar line of sight will also be in this plane. Since only variations within this plane are of interest, it is convenient to consider energy densities as for a system of cylindrical symmetry. Two solar rays SPB and S'QE are shown meeting the ground at B and E. They intersect the ionosphere MN at P and Q and undergo angular deflection θ and $\theta + d\theta$ respectively. The undeflected rays make an angle ϵ with the ground. The distance r between the observer and the ionospheric intersection point of the solar ray, is given by:

$$r = H / \cos(h) \quad \text{Eq. 27-30}$$

where:

H = height of the intersection point
h = altitude of the sun

Energy falling on the element of the irregularity ds would, in the absence of the irregularity, fall on the ground spread over an element dp and in the presence of the irregularity spread over an element dx .

Since:

$$dq = rd\theta/\sin(e) \\ dp = ds$$

then:

$$dx = ds + \frac{rd\theta}{\sin(e)}$$

Eq. 27-31

If the energy density at MN is E_0 then the energy density at point x on the ground is given by

$$E_0 ds = E(x) dx \quad \text{Eq. 27-32}$$

By combining Eqs. 27-30, 27-31 and 27-32 one may write

$$\frac{d\theta}{ds} = \frac{\sin(e)\cos(h)}{H} \left[\frac{E_0}{E(x)} - 1 \right] \quad \text{Eq. 27-33}$$

The distance of separation ds of the rays may be written as

$$ds = U' dt \quad \text{Eq. 27-34}$$

where:

$U' = U - \underline{U} \cdot \underline{V} / U$
 \underline{U} = TID velocity
 \underline{V} = velocity of the point of intersection of the solar line of sight with the ionosphere.

Eqs. 27-33 and 27-34 are combined to give

$$U' = H/K \quad \text{Eq. 27-35}$$

where:

$$K = \frac{\sin(e)\cos(h)}{d\theta/dt} \left[\frac{E_0 - 1}{E(x)} \right] \quad \text{Eq. 27-36}$$

Since \underline{V} is known as a function of height and the direction of travel of the TIDs can be determined from Fig. 27-7, the apparent speed U of the TIDs can be obtained as a function of height from Eq. 27-35.

6. EXPERIMENTAL AND ANALYTICAL RESULTS

6.1 Angle of Arrival Results for East-West Moving TIDs

The angle of arrival versus time measured with the wide E-W interferometer on October 28, 1968 is given in Fig. 27-10. The curve is fairly steady between 1330 and 2030 UT; although, it does show some evidence of quasi-periodic scintillations with peak-to-peak (p-p) amplitude of 10° arc. This is the type of result one would expect for the case of a relatively undisturbed ionosphere; one in which TIDs, for example, if present possessed small amplitudes.

The angle of arrival versus time measured with the N-S interferometer on November 12, 1969 is shown in Fig. 27-11. In this case the curve shows well defined quasi-periodic scintillations between 1430 and 2000 UT, or so, with maximum p-p amplitude of 45° arc. The slow decrease and then increase of angle of arrival between 1300 and 2100 UT is not considered herein and may be due to the solar source of the radio waves not being located at the center of the solar disk. The quasi-periodic scintillations between 1430 and 2000 UT are attributed to refraction of the solar line of sight by TIDs. The solar flux density recorded by the N-S interferometer on November 12, 1969 is also given in Fig. 27-11. There are some scintillations discernible in the solar flux density; in particular, near 1515 UT. These are attributed to focusing and defocusing effects or in other words to redistribution of the radio-wave energy by refraction of the solar line of sight.

Fig. 27-12 shows a direct comparison of the wide E-W and N-S interferometer angle of arrival data recorded on November 12, 1969. The dashed curve gives the angle of arrival for the E-W interferometer and the solid curve gives the equivalent data for the N-S interferometer. It can be seen that there is a high degree of coincidence in the occurrence of the scintillation on both sets of data. The solid vertical lines indicate the times when 'peaks' or local maximum in angle of arrival occurred for both sets of data. In one case, namely at 1615 UT, a peak in the E-W curve corresponds to an inflection in the curve. The dashed vertical lines suggest possible coincidences in the peaks but are not used in the analysis since the coincidences are not well defined.

6.2 Properties of East-West Moving TIDs

The magnitude of the angle of arrival scintillations observed by the wide E-W interferometer on November 12, 1969 is given in Fig. 27-13. The average amplitude throughout the interval is approximately 6° of arc. It follows from Fig. 27-7 that the line of travel of the responsible TIDs is in the east-west direction with a possible deviation from this of $\pm 35^\circ$. Only for angles between 55° and 90° and between -55° and

90° is the response of the E-W interferometer sufficiently constant to be able to account for the observed constant average amplitude.

The apparent period of the scintillations on November 12, 1969 is given in Fig. 27-14. These values were obtained by measuring the distance between the vertical lines in Fig. 27-12. A scintillation is defined for this measurement as a local maxima in the angle of arrival that occurs on both the E-W and N-S interferometers simultaneously. The scintillations defined by the dashed lines do not meet this requirement and therefore are not used in the analysis. They are mentioned here because there is some indication that a scintillation may have occurred at these times. The peaks of the scintillations have been used here but the troughs could have been used equally well. There is a monotonic decrease of the period of the scintillations with time before local noon (1709 UT) and a monotonic increase with time after local noon. Since the east-west component of velocity of the intersection of the solar line of sight and the ionosphere varies in the same manner this behaviour is consistent with the direction of travel deduced above; namely, the east-west direction. Furthermore, since the period of the scintillation decreases towards local noon and increases afterwards, rather than the reverse, suggests that the TIDs moved towards the west. From the degree of symmetry of the pattern produced by the systematic variation of the period in Fig. 27-14 about local noon, and Eq. 27-17, one can estimate that the deviation of the line of travel from the E-W direction is at most $\pm 15^\circ$. Finally, it is to be noted that the average period of the scintillations between 1600 and 1830 UT, when the apparent speed of the sun reaches its lowest value, is approximately 13 minutes. It follows that the true TID period is somewhat less than 13 minutes.

A plot of the inverse of the apparent period of the scintillations observed on November 12, 1969 versus the E-W component of the velocity of the solar line of sight through the ionosphere is given in Fig. 27-15. The altitude of the intersection point used is 200 km. The dashed line was obtained from a least squares fit of the data. The dashed curve shown in Fig. 27-14 was derived from the straight dashed line in Fig. 27-15 and is appropriate for an intersection altitude of 200 km. Similar analyses at other values of altitude would produce curves which were indistinguishable from the one shown in Fig. 27-14. The dashed curve in Fig. 27-14 appears to explain the systematic variation of the period of the scintillations. The questionable data point at 1940 UT appears to be in agreement with the curve and the one at 1430 UT does not. Further evidence that the point at 1940 UT may be real is given by the fact that there appears to be in Fig. 27-11, a scintillation in the flux density at 1940 UT similar in duration to the corresponding angle of arrival scintillation. At 1420 UT, on the other hand, it is difficult to tell whether there is a corresponding scintillation in the flux density.

It follows from Eq. 27-16 that if, $\alpha_p = 270^\circ$, as is the case here, the slope of the straight line in Fig. 27-15 is equal to, $1/60\lambda$, and the intercept with the vertical axis at, $V_x = 0$, is, $1/T$; where T is the true TID wave period in minutes. Thus, one is able to solve for the period, wavelength, and velocity of the TIDs. The only unknown is the altitude, so that the analysis must be repeated for a number of altitudes between 100 km and 500 km, or so. The velocity of the TIDs as a function of height is indicated by the solid curve in Fig. 27-16; the period in minutes is indicated by the numbers beside the data points. The standard deviation of the period is ± 4 minutes. The period decreases with increasing height. The wavelength as a function of height is shown in Fig. 27-17.

The dashed curve in Fig. 27-16 was obtained by correlating the scintillations in angle of arrival and flux density in Fig. 27-11 between 1445 and 1505 UT. From the ratio of maximum flux density divided by average flux density and the rate of change of angle of arrival at the time of maximum flux density the apparent velocity, U' , given by Eq. 27-35 can be solved for as a function of height. Since one knows the velocity of the solar line of sight through the ionosphere as a function of height the 'true' TID velocity can be solved for as a function of height and is given by the dashed curve in Fig. 27-16. There is agreement between the two curves in the lower ionosphere. The curves appear to diverge above 300 km, or so, suggesting that the centroid of the TIDs was contained between 100 and 300 km.

6.3 Angle of Arrival Results for North-South Moving TIDs

The angle of arrival for October 27, 1968 is shown in Fig. 27-18. The solid curve gives the data recorded by the wide E-W interferometer and the dashed curve gives the data recorded by the narrow E-W interferometer. Quasi-periodic scintillations are present between 1340 and 1830 UT. The agreement between the two sets of data is excellent except between 1330 and 1420 UT; during which time the narrow E-W interferometer appears to have undergone a slow phase drift; although the agreement between the small scale structure is good. The scintillations that appear on both sets of data are attributed to refraction by TIDs. Fig. 27-19 shows the magnitude of the solar flux density on October 27, 1968. For purposes of comparison the angle of arrival for October 27, 1968 is shown once again. A comparison of the October 27, 1968 wide E-W interferometer angle of arrival data with two sinusoids; one with a period of 21 minutes and the other with a period of 13 minutes, is given in Fig. 27-20. Local noon is indicated by the dashed line at 1709 UT. The period of the scintillations is approximately 21 minutes between 1340 and 1630 UT and again between 1750 and 1840 UT. The 21 minute scintillations in the first interval are in phase with the sinusoid; whereas, the 21 minute scintillations in the last interval are approximately 180° out of phase with the sinusoid. The period of the scintillations in the time interval 1645 to 1740 UT is approximately 13 minutes.

The angle of arrival and solar flux density measured with the wide E-W interferometer on October 29, 1968 is given in Fig. 27-21. Scintillations in the angle of arrival are present between 1330 and 1700 UT. The solar radio-wave emissions on this day were sufficiently constant in amplitude to show scintillations in the measured flux density between 1330 and 1700 UT. The scintillation in flux density at 1600 UT is especially well defined and approximately 90° out of phase with the corresponding angle of arrival scintillations. The scintillations in angle of arrival are due to refraction of the solar line of sight by TIDs. The scintillations in solar flux density are attributed to focusing and defocusing associated with refraction of the solar line of sight.

6.4 Properties of North-South TIDs

The magnitude of the 21 minute scintillations measured by the E-W interferometers on October 27, 1968 is given in Fig. 27-22. It can readily be seen that after 1520 UT the amplitude decreases towards local noon and increases after local noon. In addition, as mentioned above, the phase of the 21 minute scintillations occurring after local noon is approximately 180° out of phase with those occurring before local noon. One can see by referring to the 0° curve in Fig. 27-7 that the above characteristics are just what one would expect for scintillations recorded by an east-west interferometer caused by TIDs moving along a north-south line of travel. There is a two-fold ambiguity in that one does not know whether the motion is towards the north or towards the south along this line of travel. The maximum deviation of the line of travel from the N-S direction is $(\pm 8^\circ)$. The increase in magnitude of the scintillations before 1520 UT in Fig. 27-22 is not inconsistent with the above interpretation. In all likelihood the observed TIDs consist of wave-packets, so that the increase in magnitude corresponds to the increase in magnitude one would expect at the beginning of a realistic wave-packet.

Close inspection of Fig. 27-20 shows no discernible systematic change in the period of the 21 minute scintillations between 1345 and 1630 UT. The speed of the responsible TIDs is therefore greater than 870 km/hr assuming the centroid of the TIDs was contained between 200 and 500 km, since the north-south component of the velocity of the solar line of sight changed by about 135 km/hr in this interval. The TID wavelength is greater than 300 km because the wave-period, to a good approximation, is 21 minutes.

Since the 13 minute scintillations are discernible at local noon the responsible TIDs are travelling in a predominantly E-W direction. Their magnitude is smaller and they are only discernible when the response of the E-W interferometers is low or non-existent to the larger scintillations produced by the N-S TIDs. These scintillations are similar to those produced by the E-W TIDs observed on November 12, 1969. They have similar apparent periods, amplitude, and constancy of amplitude about local noon.

The direction of travel of the TIDs which produced the scintillations shown in Fig. 27-21 is not readily discernible from the characteristics of the scintillations. Since the period of the scintillations between 1515 and 1610 UT is 21 minutes suggests that the responsible TIDs may have travelled north-south because the scintillations in Fig. 27-21, caused by north-south travelling TIDs also had a period of 21 minutes. The scintillations in flux density are again attributed to focusing and defocusing of the radio-wave energy by TIDs. If one makes no assumption concerning the direction of travel of the TID, assumes only that its height was approximately 300 km and then correlates the angle of arrival and amplitude scintillations between 1540 and 1610 UT, as before, one can deduce the speed of the TIDs responsible for bending the solar ray as being greater than 300 km/hr. The upper limit of the speed is a function of the line of travel; for a north-south line of travel, for example, it is roughly 1500 km/hr and for an east-west line of travel it is roughly 700 km/hr.

The maximum observed TID induced angular deflection was ± 20 minutes of arc, indicating, according to Eq. 27-18, a maximum gradient in columnar electron content for the TID of 3.5×10^{14} el/m² km. If one assumes that the TID which generated the scintillation was contained between 250 and 350 km the above columnar electron gradient corresponds to an electron number density perturbation of only 1 percent, or so.

There is evidence that the motion of the TIDs responsible for the scintillations on November 12, 1969 was perturbed. For example the amplitude of the scintillations recorded by the N-S interferometer in Fig. 27-23 deviates significantly from a possible average value of $8'$ arc at, 1500, 1610 and 1730 UT. The apparent period in Fig. 27-14 departs from the dashed curve at 1540, 1610 and 1720 UT. In Fig. 27-11 one can discern an enhancement in flux density at 1430, 1520, 1630 and 1730 UT. The good agreement between the above times at which these parameters were perturbed suggests that the perturbations are real and have a period of the order of an hour, or so.

7. CONCLUSION

7.1 The solar radio interferometer was shown to be a sensitive instrument for detecting TIDs in the ionosphere; capable of detecting TIDs with electron number density perturbations as low as one percent or less. The TIDs were observed as quasi-periodic scintillations in the angle of arrival of radio-waves emitted by localized disturbed regions on the solar disk. It was shown that the speed, line of travel, period and wavelength of the TIDs could be deduced from the manner in which the period and magnitude of the observed scintillations varied with time. The speed of the TIDs as a function of height was also determined by correlating the degree of amplitude fading due to defocusing and focusing effects with the maximum observed rate of change of angle of arrival.

The sun, when emitting rf energy at an enhanced level, was shown to be an effective source for detecting TIDs. In effect, it tends to select time intervals, for the observer, when there is a good likelihood of TIDs being present in the ionosphere. TIDs tend to be present when the ionosphere is disturbed and the ionosphere tends to be disturbed when the sun is disturbed. The fact that the sun radiates at an enhanced level, only at times when it is in a disturbed state, completes this cause effect relationship. On the other hand it is not an effective source for obtaining synoptic measurements because measurements are possible only on those infrequent occasions when the sun is radiating at an enhanced level.

8. GENERAL INFORMATION

8.1 References

- THOME, G.D., 1964, "Incoherent Scatter Observations of Travelling Ionospheric Disturbances", *J. Geophys. Res.*, 69(19), 4047.
- PIERCE, J.A., MINNO, H.R., 1940, "The Reception of Radio Echoes From Distant Ionospheric Irregularities", *Phys. Rev.*, 57, 95.
- WELLS, H.W., WATTS, J.M., GEORGE, D.E., 1946, "Detection of Rapidly Moving Ionospheric Clouds", *Phys. Rev.*, 69, 540.
- GEORGES, T.M., 1968, "H.F. Doppler Studies of Travelling Ionospheric Disturbances", *J. Atmosph. Terr. Phys.*, 30, 735.
- CHAN, K.L., VILLARD, O.G., 1962, "Observation of Large-Scale Travelling Ionospheric Disturbances by Spaced-Path High-Frequency Instantaneous-Frequency Measurements", *J. Geophys. Res.*, 67, 973.
- TVETEN, L.H., 1961, "Ionospheric Motions Observed with High Frequency Backscatter Sounders, *J. Res. NBS*, 65D, 115.
- NEWTON, G.P., PELZ, D.T., VOLLAND, H., 1969, "Direct in Situ Measurements of Wave Propagation in the Neutral Thermosphere", *J. Geophys. Res.*, 74(1), 183.
- MUNRO, G.H., 1958, "Travelling Ionospheric Disturbances in the F-Region" *Anst. J. Phys.*, 11, 91.
- THOME, G.D., 1968, "Long-Period Waves Generated in the Polar Ionosphere During the Onset of Magnetic Storms", *J. Geophys. Res.*, 73(19), 6319.
- VASSEUR, G., WALDTEUFEL, P., 1969, "Thomson Scatter Observations of a Gravity Wave in the Ionospheric F-Region", *J. Atmosph. Terr. Phys.*, 31, 885.
- TITHERIDGE, J.E., 1963, "Large-Scale Irregularities in the Ionosphere", *J. Geophys. Res.*, 68, 3399.
- LAWRENCE, R.S., JESPERSEN, J.L., 1961, "Refraction Effects of Large-Scale Ionospheric Irregularities Observed at Boulder, Colorado, Space Research II, Proc. 2d Intern. Space Sci. Symp., 277.
- VITKEVICH, V.V., 1958, "Measurement of Phase and Amplitude fluctuations of Radio Waves which have Traversed the Ionosphere", *Radiotekhnika, Elektronika*, 3, 478.
- HARROWER, G.A., 1963, "Theoretical Considerations in the Interpretation of Radio Star Scintillation Observations; Radio Astronomical and Satellite Studies of the Atmosphere", J. Aarons, ed., Interscience Pub. New York, 38.
- SMART, W.M., 1944, Text-book on Spherical Astronomy, Cambridge Eng., The University press, 4th ed., p.35.
- CHANDRASEKHOR, S., 1952, "A Statistical Basis for the Theory of Stellar Scintillation", M.N. of the Roy Astr. Soc., 112, 478.
- TURNBULL, R.M., FORSYTH, P.A., 1965, "Satellite Studies of Isolated Ionospheric Irregularities", *Can. J. Physics*, 43, 800.

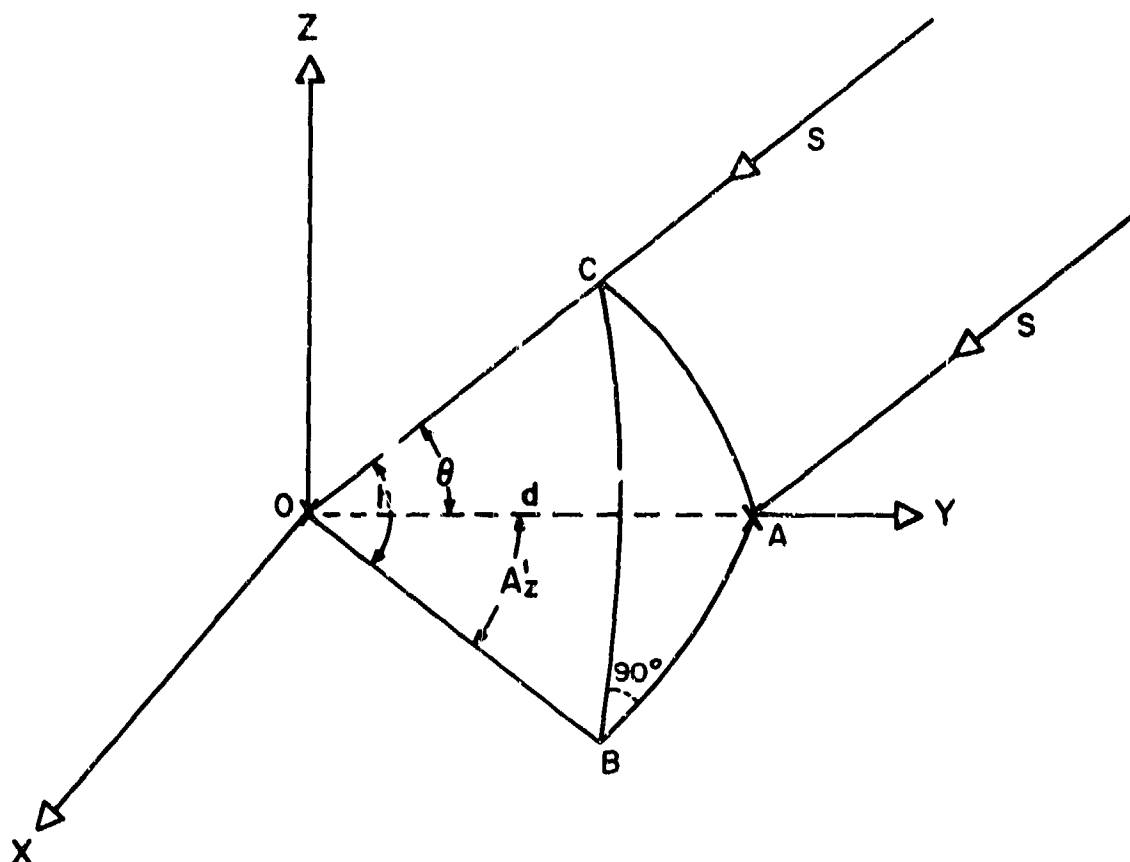


Fig. 27-1

Geometry of two rays, S, from a radio source and an interferometer with its base-line on the OY axis. The two elements of the interferometer are located at, O, and, A. The interferometer angle is, θ ; the altitude of the source is, h; and the azimuth of the source with respect OY is, A'_z

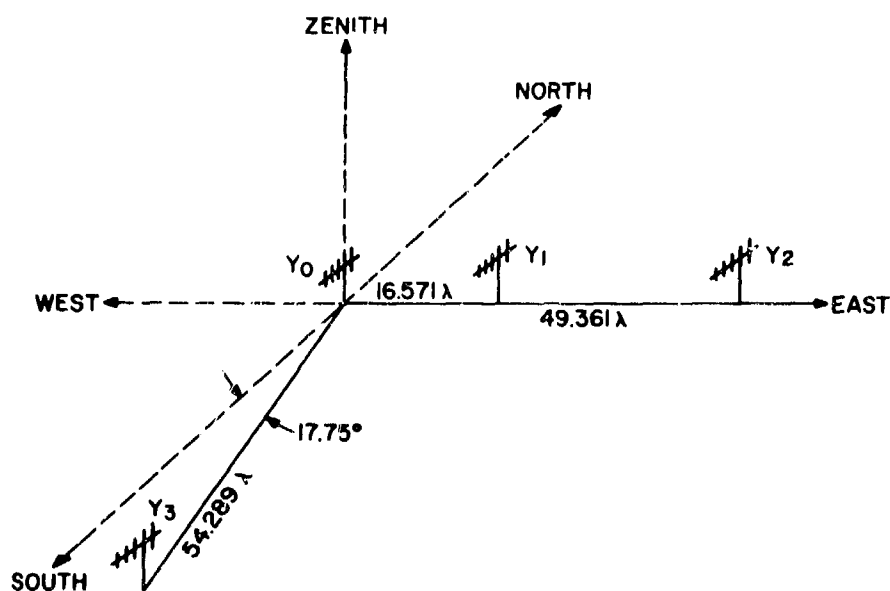


Fig. 27-2

Geometry of narrow and wide east-west interferometers and north-south interferometers; consisting of the following pairs of antennas Y_0 and Y_1 , Y_0 and Y_2 , Y_0 and Y_3 , respectively.

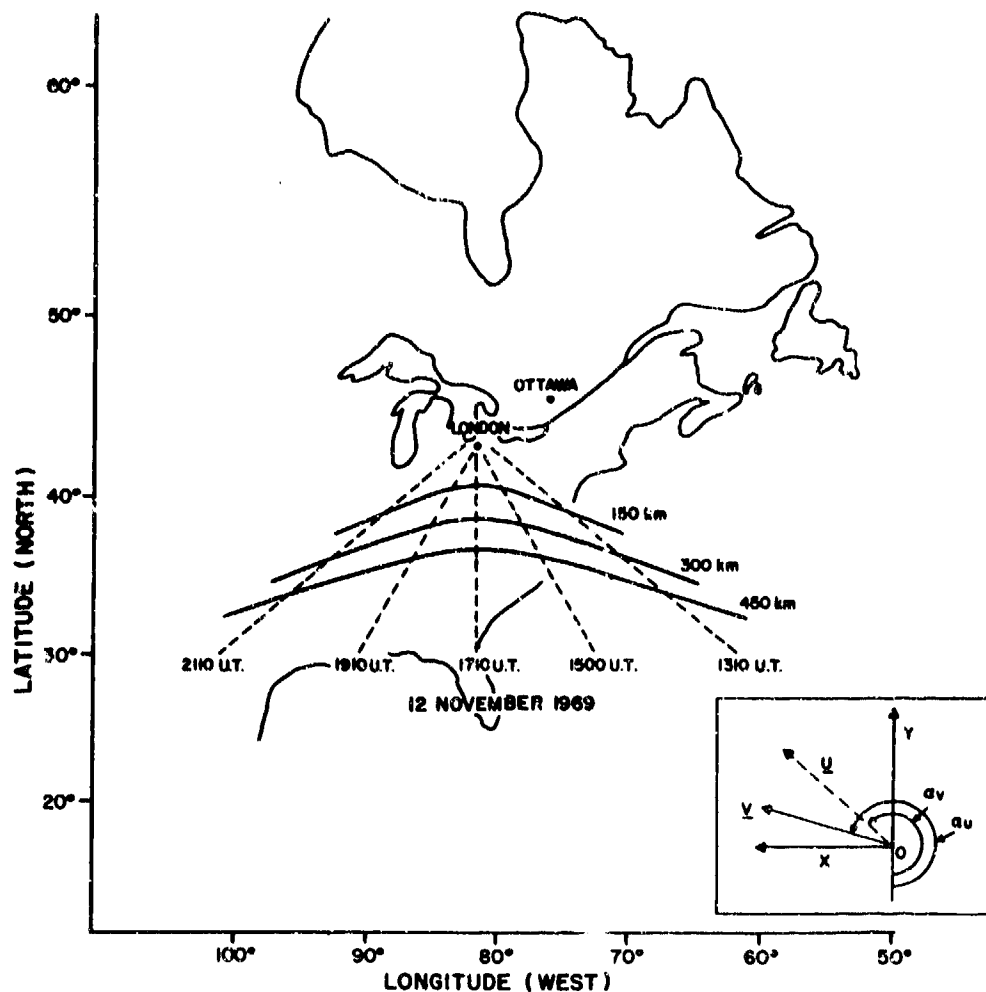


Fig. 27-4

The curves show the loci of the intersection of the solar line of sight with various levels in the ionosphere as a function of time. Co-ordinate axes shown in the insert define positive values for the two velocity components, V_x , and, V_y , of the solar line of sight through the ionosphere.

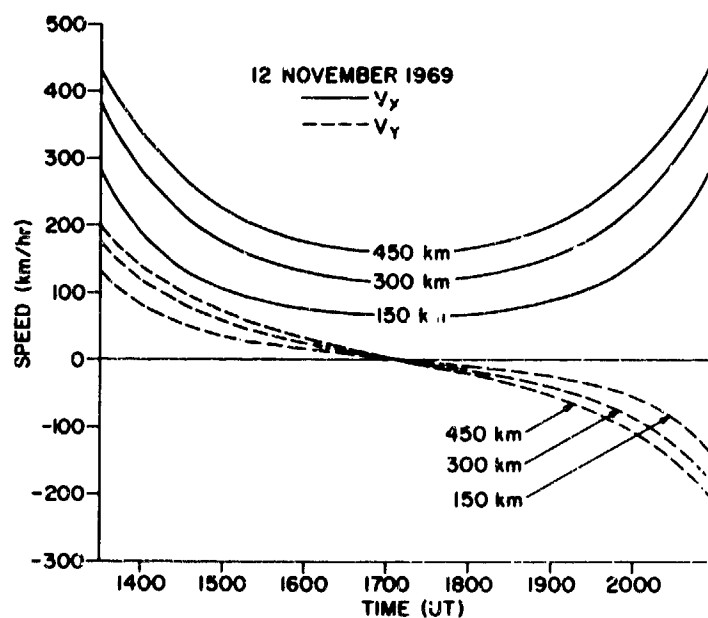


Fig. 27-5

Plot of November 12, 1969 values of, V_x , and, V_y , as a function of time for various heights.

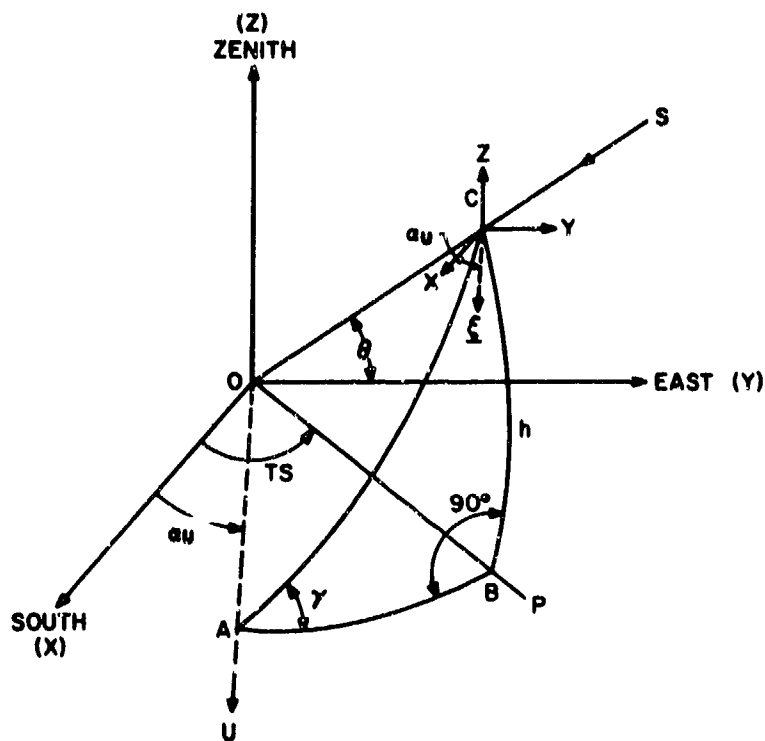


Fig. 27-6

Solar ray - interferometer geometry showing spherical triangle, ABC , which is defined by the solar line of sight, OS ; projection, OP , of the solar line of sight onto the observer's horizon plane; and the projection, U , of the TID's horizontal vector onto the observer's horizon plane.

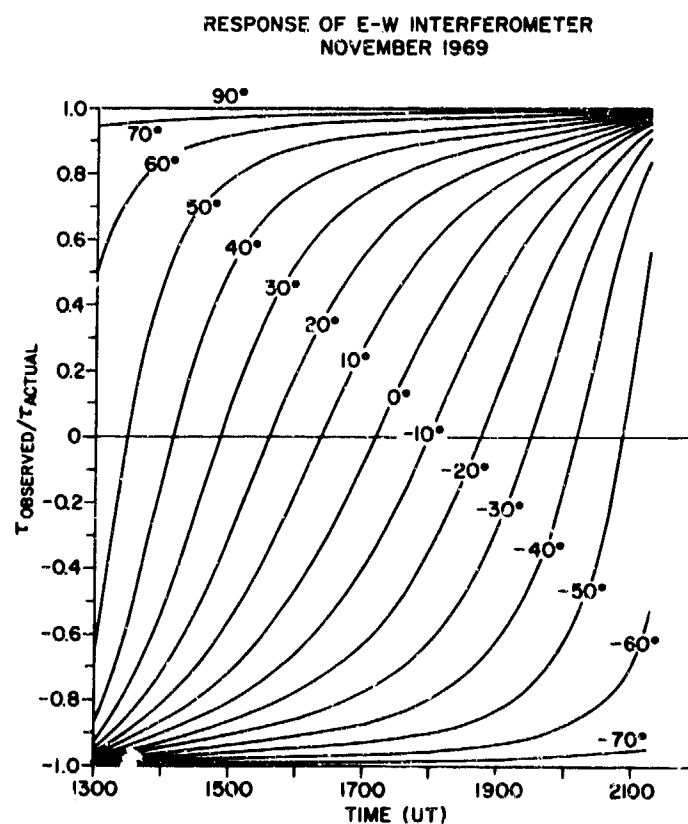


Fig. 27-7

Plot of response, $F_{1,2}$, of the E-W interferometers versus time, on November 12, 1969, to angular deflections of the solar line of sight due to refraction. The numbers on the curves give the TID's direction of travel.

RESPONSE OF N-S INTERFEROMETER 12 NOVEMBER 1969

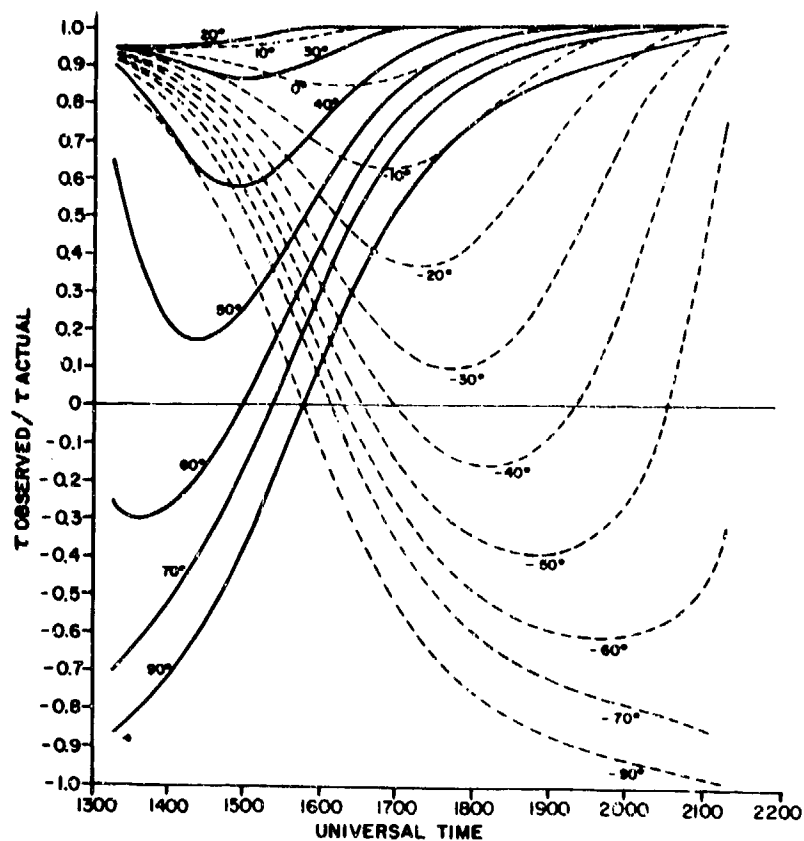


Fig. 27-8 Plot of response, F_3 , of the N-S interferometer, on November 12, 1969, to angular deflections of the solar line of sight due to refraction. The numbers on the curves give the TIDs' direction of travel.

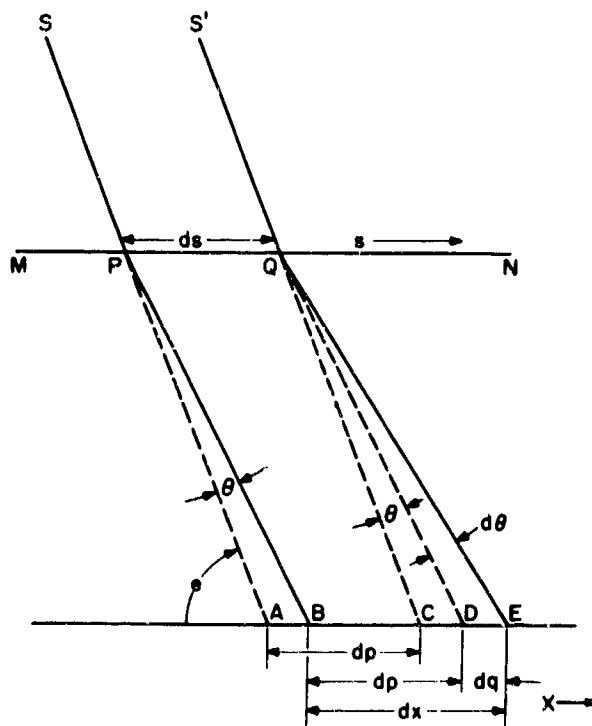


Fig. 27-9 Geometry of the refraction of two solar rays by a spatially varying horizontal electron density gradient in the ionosphere (After, Turnbull and Forsyth, 1965).

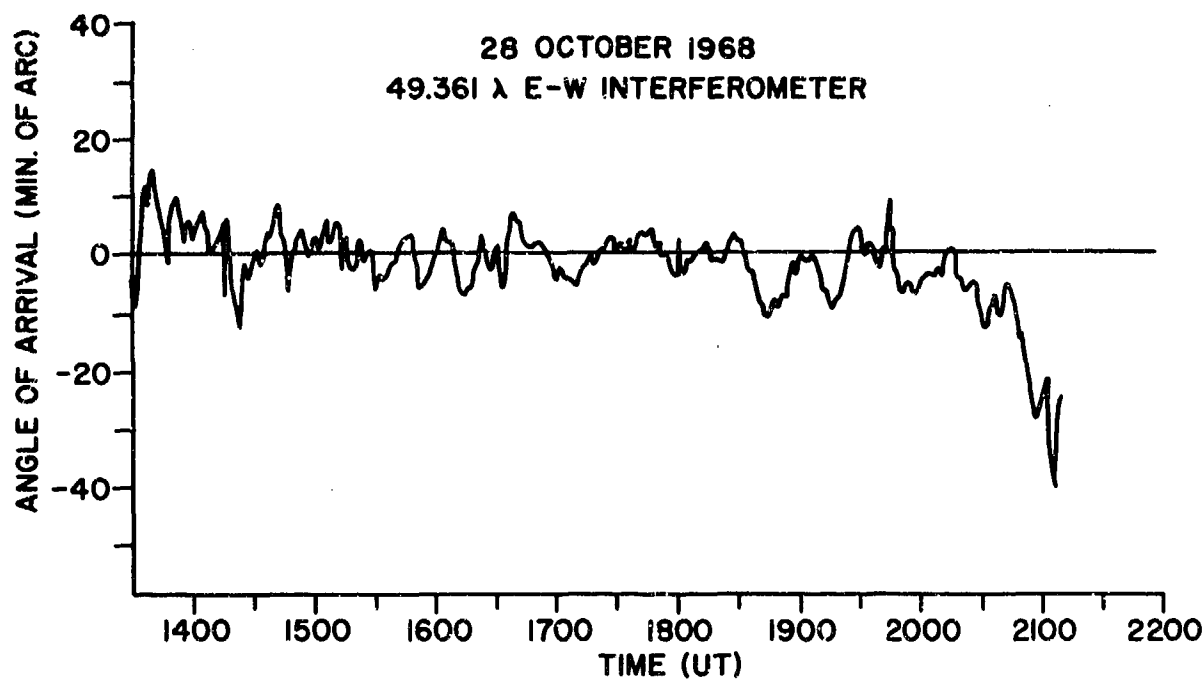


Fig. 27-10 Angle of arrival versus time measured by wide E-W interferometer on October 28, 1968. This result is consistent with a stationary solar source and a relatively undisturbed ionosphere.

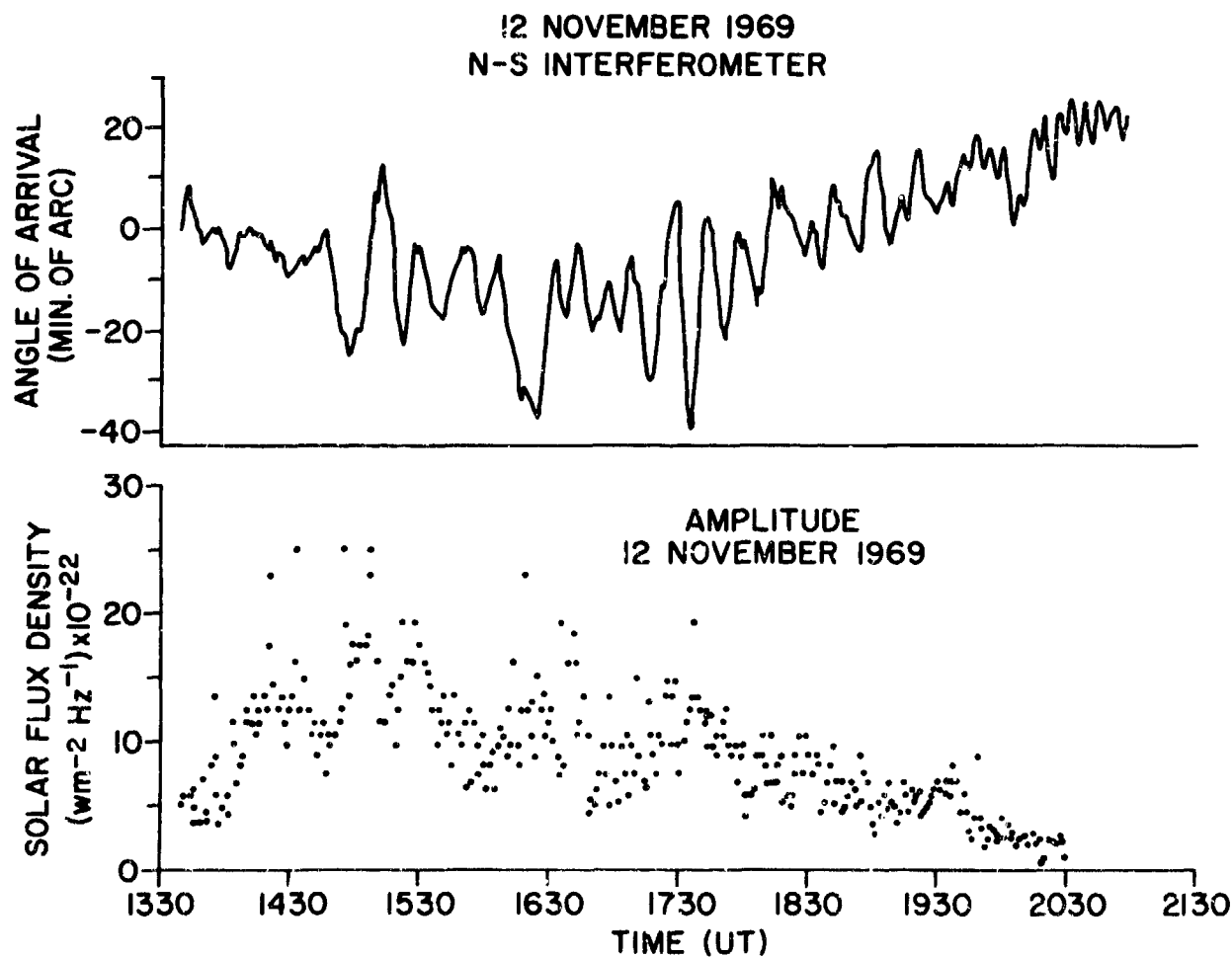


Fig. 27-11 Comparison of angle of arrival and solar flux density measured with the N-S interferometer on November 12, 1969.

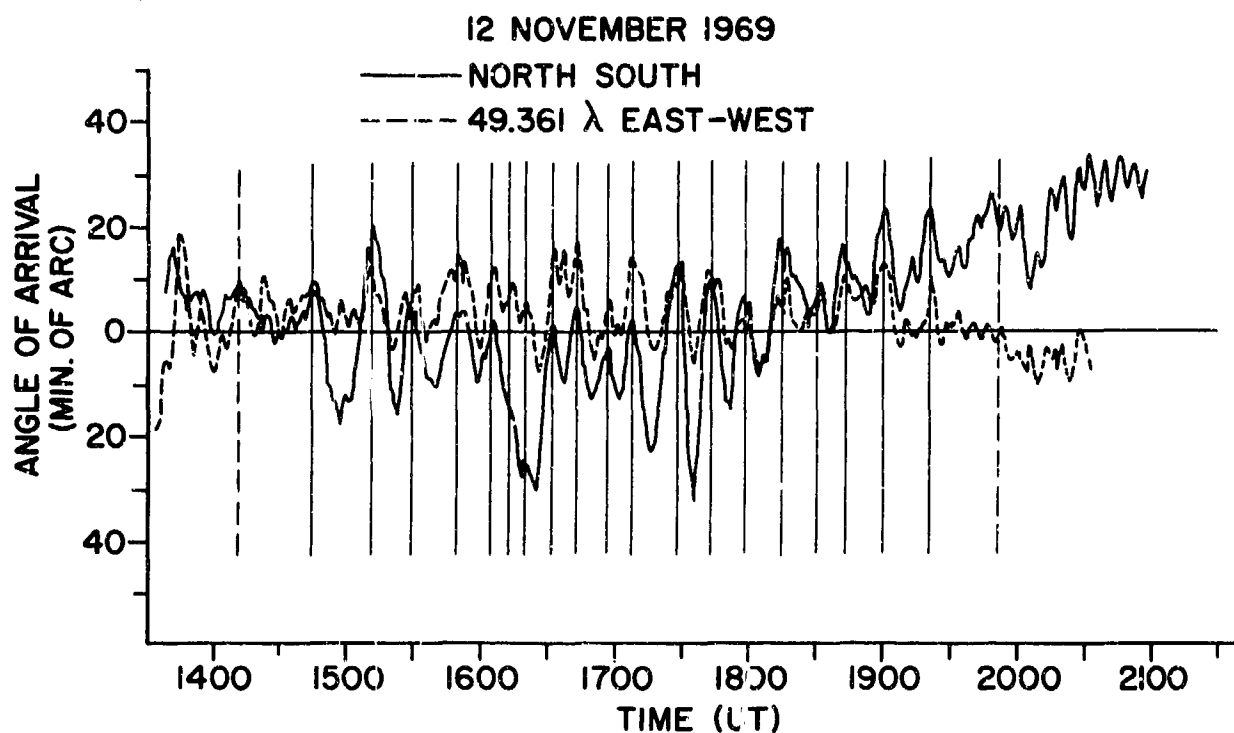


Fig. 27-12 Comparison of angle of arrival measured by both the wide E-W and the N-S interferometers on November 12, 1969.

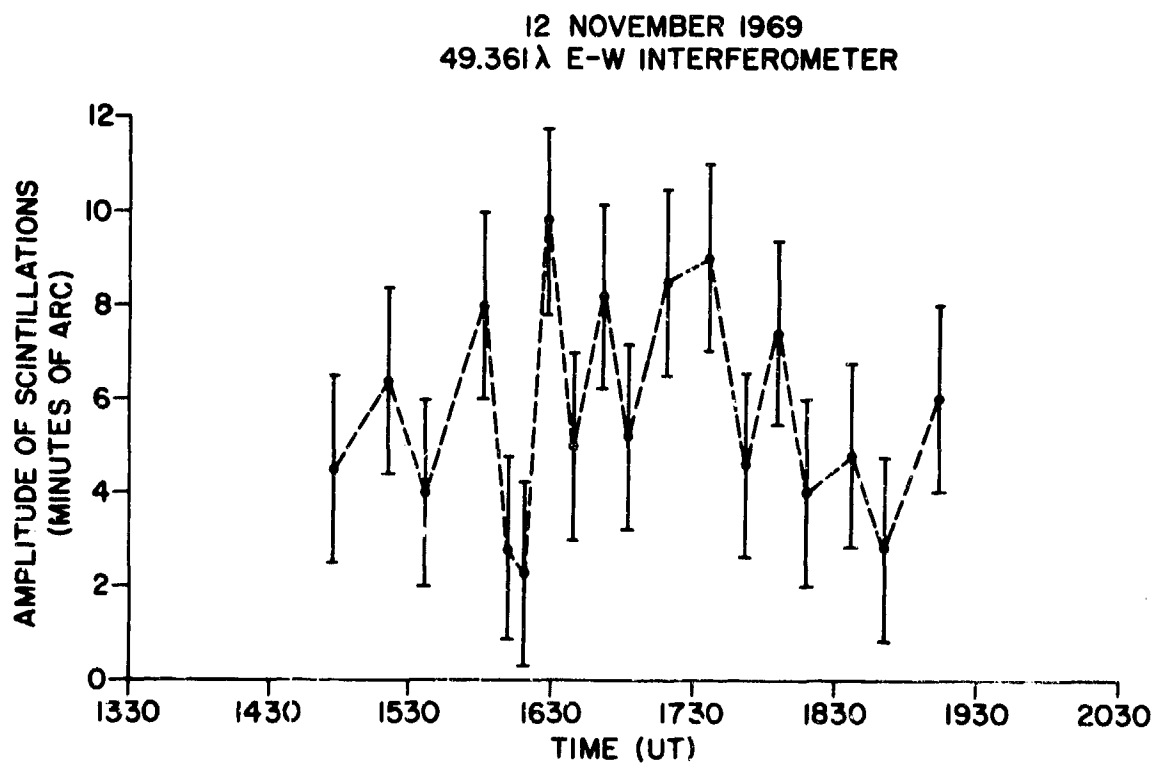


Fig. 27-13 Amplitude of scintillations measured by wide E-W interferometer on November 12, 1969 versus universal time.

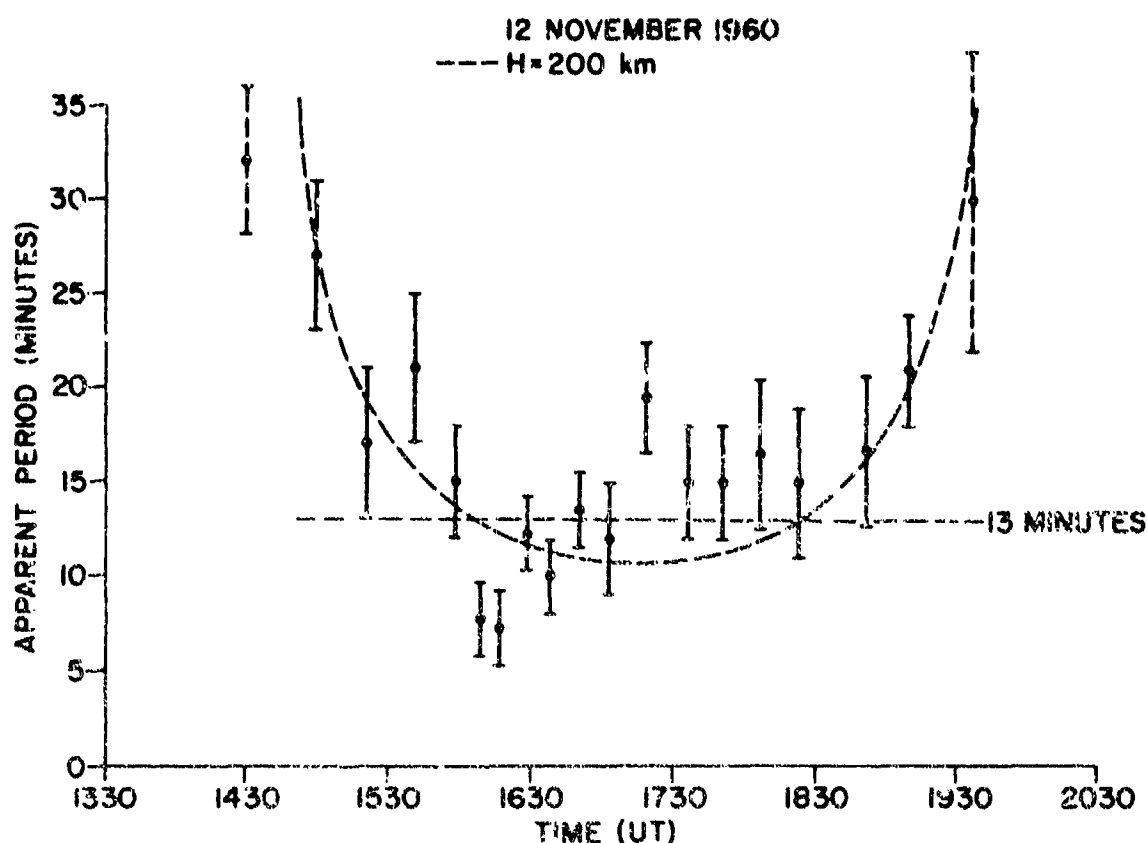


Fig. 27-14 Apparent period of scintillations observed on November 12, 1969 versus universal time.

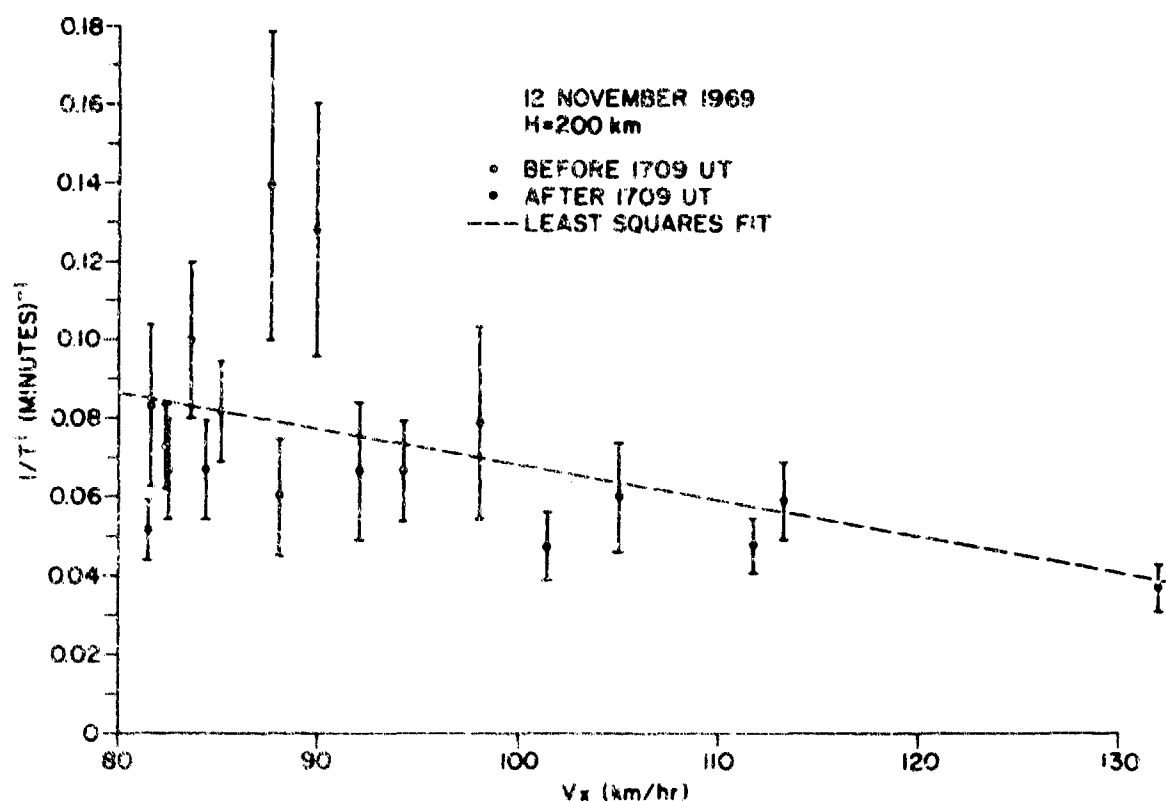


Fig. 27-15 Plot of the inverse of the apparent period of the November 12, 1969 scintillations versus the west component of the velocity of the solar line of sight through the 200 km level.

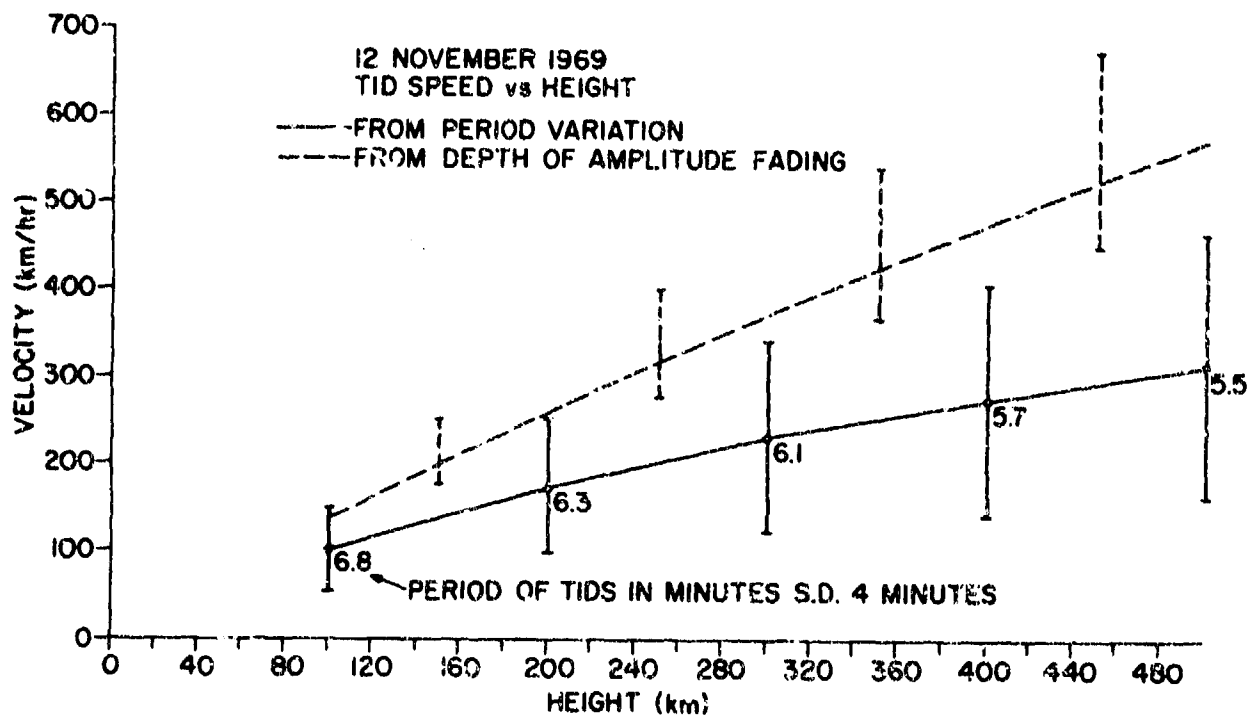


Fig. 27-16 Speed of the E-W TIDs; observed on November 12, 1969 versus altitude. Solid curve was derived from the observed long term variation in the apparent period. Numbers on the curve give the TID period in minutes. Dashed curve was obtained from a correlation of the amplitude and angle of arrival scintillation.

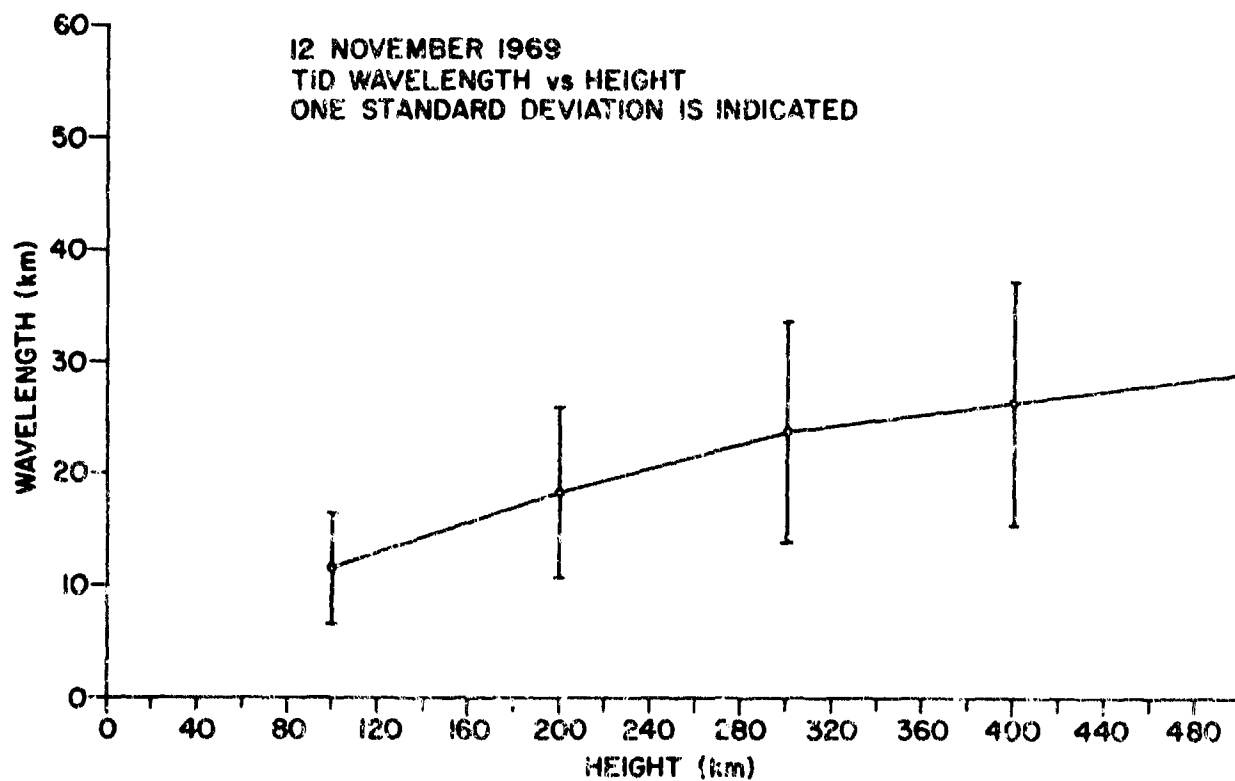


Fig. 27-17 Wavelength of E-W TIDs observed on November 12, 1969 versus altitude.

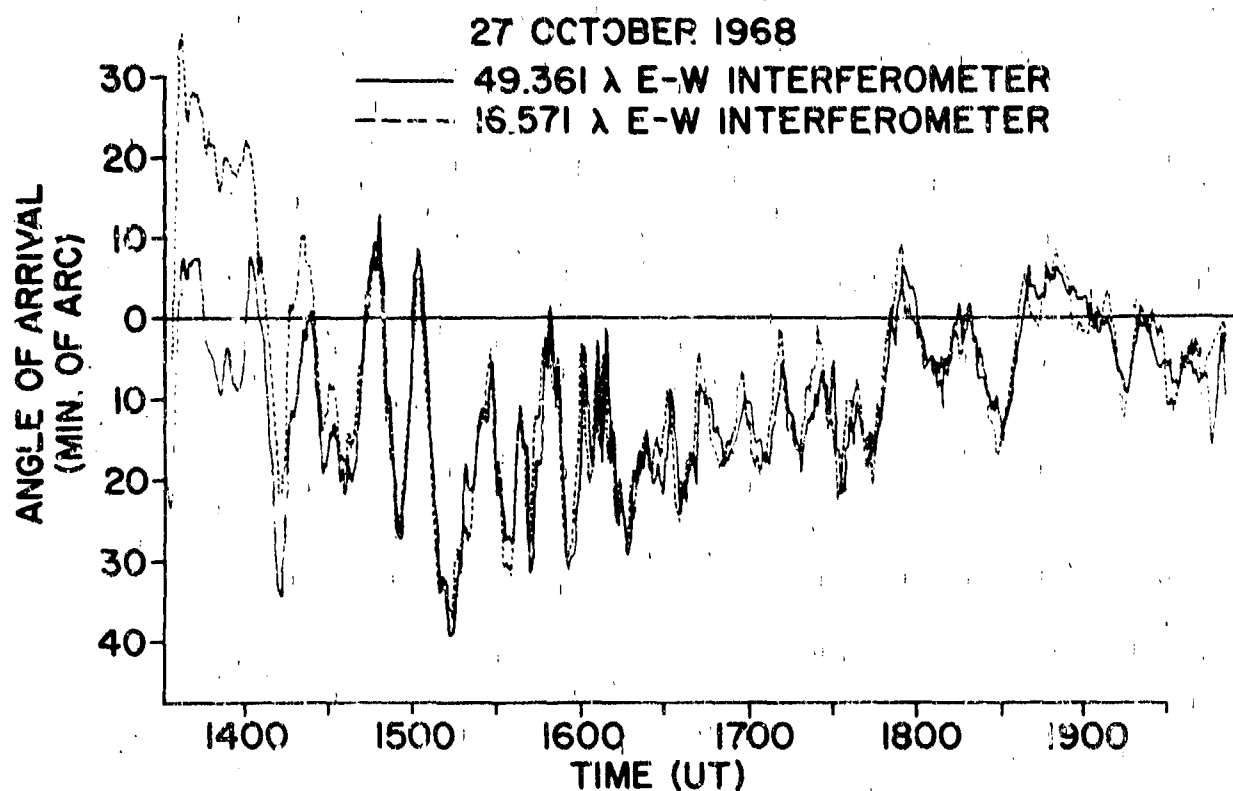


Fig. 27-18 Comparison of the angle of arrival versus time measured by the wide E-W and narrow E-W interferometers on October 27, 1968.

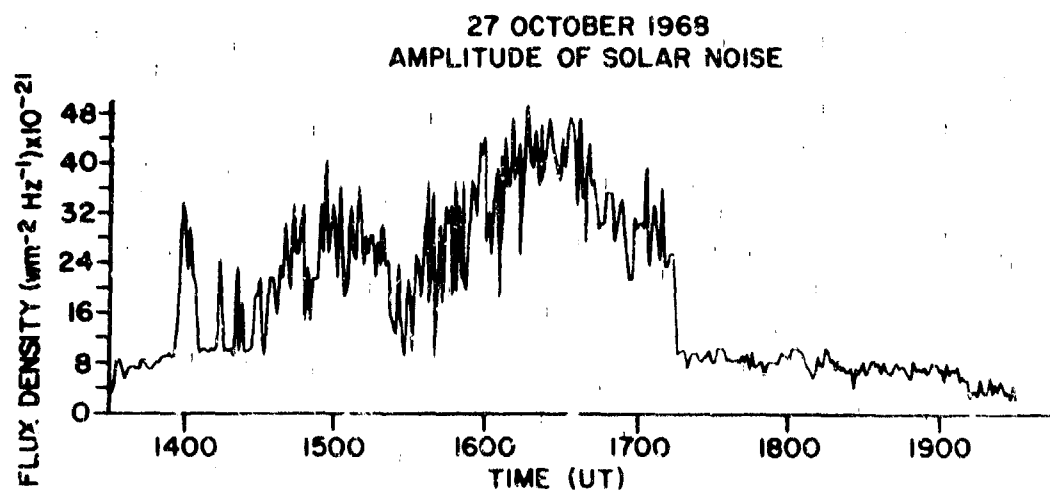
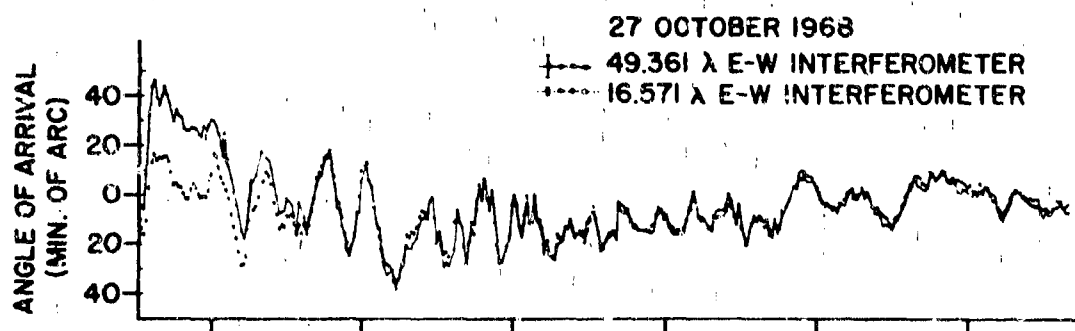


Fig. 27-19 Comparison of angle of arrival and solar flux density measured on October 27, 1968.

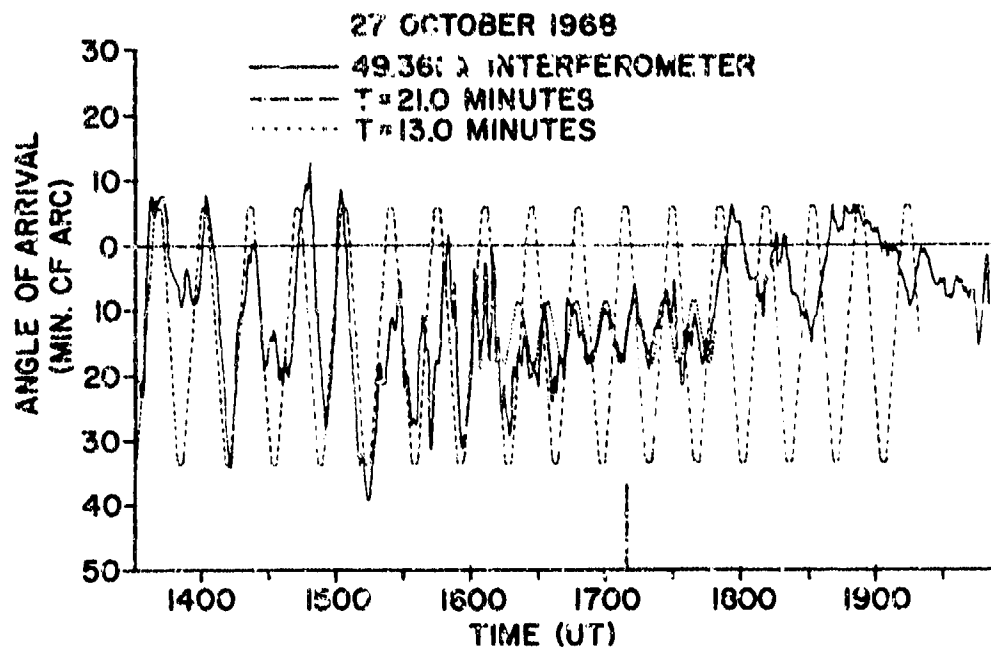


Fig. 27-20 Comparison of the angle of arrival measured with the wide E-W interferometer on October 27, 1968 with two sinusoids one with a period of 21 minutes, the other with a period of 13 minutes.

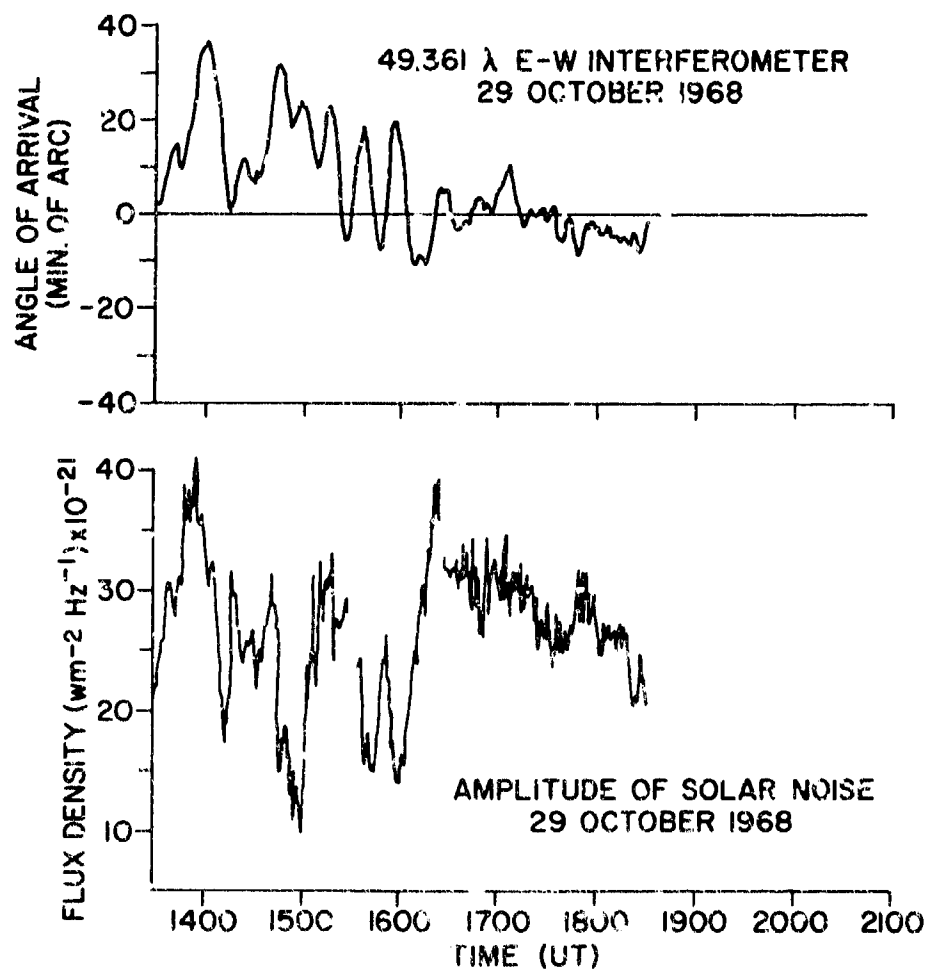


Fig. 27-21 Angle of arrival and solar flux density versus time, measured with the wide E-W interferometer on October 29, 1968.

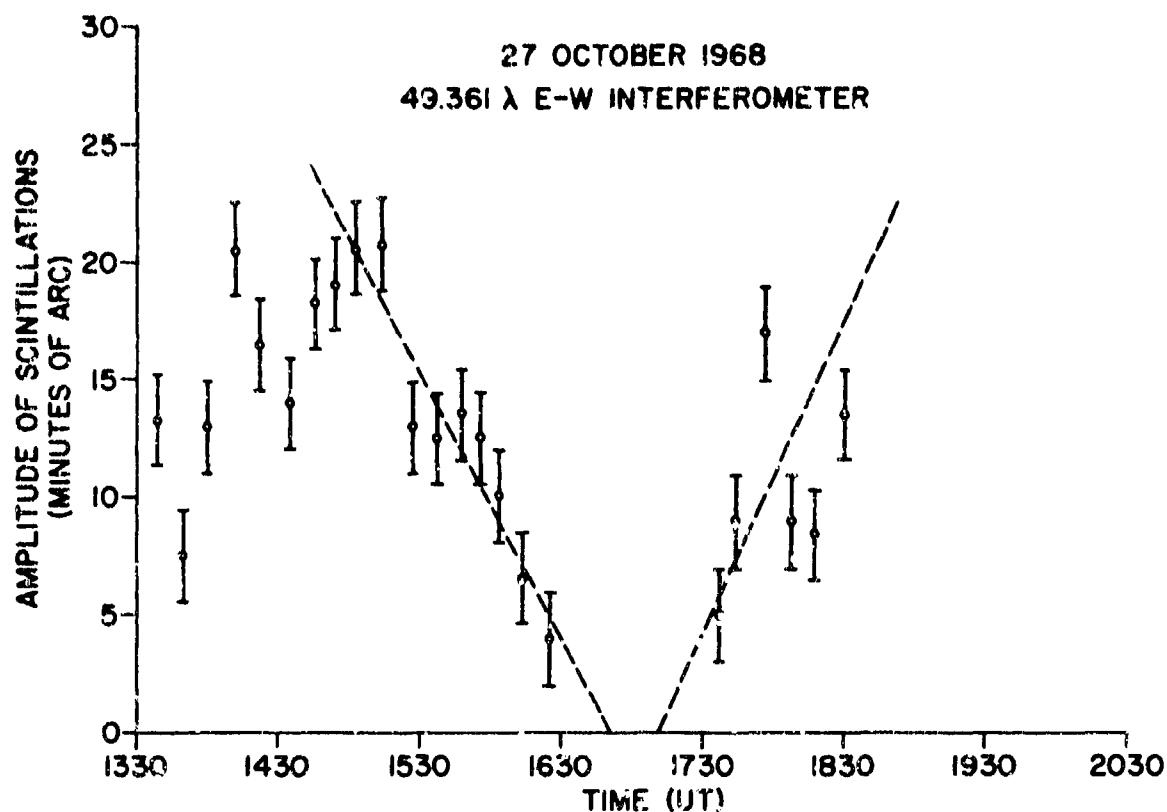


Fig. 27-22 Amplitude of scintillations measured by wide E-W interferometer on October 27, 1968, versus universal time.

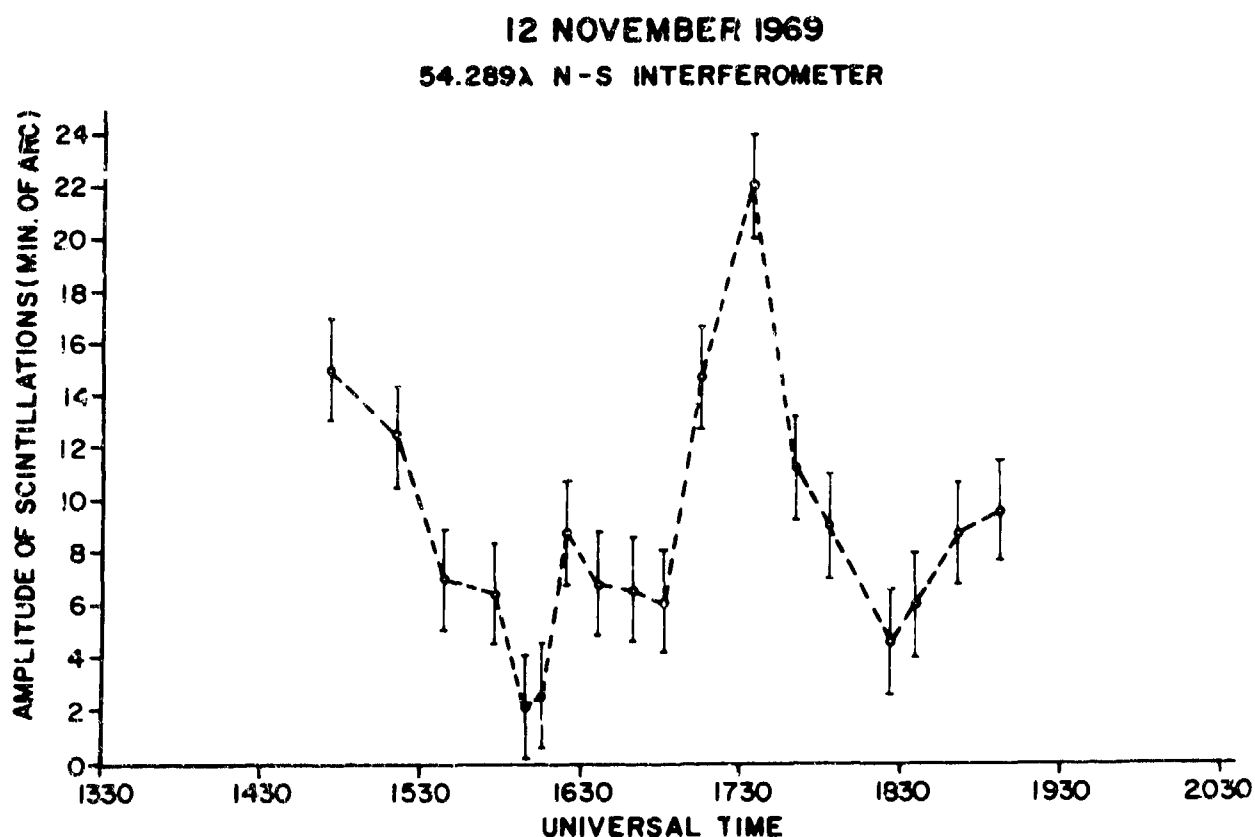


Fig. 27-23 Magnitude of the scintillations measured by the N-S interferometer on November 12, 1961 versus universal time.

**THE EFFECT OF IONOSPHERIC DISTURBANCES ON THE
BEARINGS OF INCOMING SKY WAVES**

by

A.D.Morgan

Government Communications Headquarters
Cheltenham
England

361

L'EFFET DES PERTURBATIONS IONOSPHERIQUES SUR L'AZIMUT DES ONDES
D'ESPACE INCIDENTES

par

A.D. Morgan

SOMMAIRE

On a procédé à une série d'expériences consacrées aux effets des perturbations ionosphériques itinérantes sur les mesures d'azimut. Le système d'antenne réceptrice utilisé était un ensemble à large ouverture, disposé en cercle ; les données fournies par ce dispositif étaient traitées par un système automatique de mesure d'azimut. Les résultats obtenus indiquèrent que l'azimut était affecté de fluctuations présentant des périodes de l'ordre de 20 minutes. Certains jours, une séquence continue de fluctuations apparaissait sur l'enregistrement, et d'autres jours, elles en étaient presque absentes. En supposant que l'on était en présence d'une réflexion spéculaire on voyait que l'erreur de gisement observée pour un seul saut correspondait à des pentes ionosphériques atteignant jusqu'à 9 degrés. De plus, on estimait que ces pentes pouvaient varier à raison de 1° par minute. Les résultats suggèrent également la présence, dans l'ionosphère, d'inclinaisons systématiques qui varient avec l'angle zénithal solaire. Les implications de ces résultats pour les communications radio sont examinées du point de vue pratique.

THE EFFECT OF IONOSPHERIC DISTURBANCES ON THE BEARINGS OF INCOMING SKY WAVES

A D MORGAN

Government Communications Headquarters, Cheltenham, England.

SUMMARY

A series of experiments was conducted to examine the effects of TIDs on bearing measurements. The receiving aerial used was a circularly disposed wide aperture array and the output from the array was processed by an automatic bearing measuring equipment. The results showed that the bearing fluctuated with periods of the order of 20 minutes. On some days, the bearing record showed a continuous sequence of these fluctuations whereas, on other days, the fluctuations were almost absent. On the assumption of a mirror type of reflection, the observed bearing error for a single hop path corresponded to ionospheric tilts of up to 9 degrees. Further, on this assumption, it is estimated that these tilts can change at the rate of up to one degree per minute. The results also suggest the presence of systematic tilts, in the ionosphere, which change with the diurnal change of the solar zenith angle. The implications of these results, on practical radio communication, are briefly discussed.

1. INTRODUCTION

In general, a travelling ionospheric disturbance (TID) causes deformation of the contours of constant electron density, ie, they are no longer spherical with respect to the earth's surface. Under these circumstances, the contours of constant electron density will be "tilted" and these tilts will deflect sky waves from their true great circle path (provided that the component of the tilt, transverse to the path, is not zero). This deflection can be measured by recording the bearing of the incoming sky wave. In this paper, the effects of ionospheric tilts, on bearing measurements, are examined. Ionospheric tilts can be thought of as consisting of 2 components, namely:-

(a) The systematic tilts

and (b) The random tilts.

The present paper deals with the effect of random tilts on bearing measurements.

Ross (1949) distinguished between two types of random bearing errors, namely:-

(i) Slowly changing bearing deviations

and (ii) Rapidly changing bearing deviations.

The slowly changing bearing deviations, the quasi periods of which were 10 to 30 minutes, or more, were ascribed to the tilting or wrinkling of the ionosphere. The more rapid fluctuations were attributed to wave interference effects. Later papers by Bramley and Ross (1951) and Bramley (1956) gave the periodicity of the slow fluctuations as between $1\frac{1}{2}$ and 30 minutes, or more, while the rapid fluctuations (caused by wave interference) had periods of the order of a few seconds.

The ionospheric wrinkles (or tilts) which give rise to the slowly changing bearing deviations are often referred to as the Ross tilts. The bearing deviations, caused by the Ross tilts, can be regarded as having a periodicity of the order of 20 minutes. Clearly, when bearing measurements are averaged over periods of the order of 5 to 10 minutes, the averaged effect of wave interference will tend to zero, but the effect of the Ross tilts, on the averaged bearing measurements, will not tend to zero. Thus the effect of the Ross tilts on bearing measurements is important and this paper deals with this effect.

The present series of experiments, described in this paper, differed in two ways from the earlier experiments, undertaken over 20 years ago, by Bramley and Ross. Firstly, the initial measurements of Bramley and Ross were taken manually (photographing the CRT of a twin channel CRT direction finder) whereas, in the present investigation, an automatic bearing measuring equipment was used. The second difference was that, in the present experimental investigation, an aerial array with an aperture of 1075 ft was used, as compared with an aperture of 100 metres used by Bramley and Ross.

2. EXPERIMENTAL DETAILS

2.1 Equipment

A circularly disposed wide aperture array, situated at Blakehill in S.England, was used for the experimental investigation. The elements of the array consisted of pairs of elevated feed monopoles. Each monopole was 30 ft high with the feed point located 10 ft from the base. The bottom 10 ft section was earthed and it was isolated from the upper section. Two of these elements were then combined to form a doublet. The 2 elements of the doublet were placed on a radial, of the circular array, at a separation of 16 ft. The output from the inner element (as judged from the centre of the array) was fed through a delay cable and then combined, by means of a hybrid transformer, with the output of the outer element. The output from the doublet was taken from the difference port of the hybrid transformer to give the doublet an outward looking cardioid polar diagram. The null of this cardioid pattern pointed towards the centre of the array thus giving relatively low response in the backward direction.

The complete array consisted of 96 doublets equally spaced on a circle of 1075 ft diameter. A beam was formed by combining, in a rotating goniometer, the outputs from any adjacent 32 doublets of the array. The goniometer rotated at the rate of 600 revolutions per minute, and it had the facility to provide either a sum or a difference pattern. For the sum pattern, the output from the 32 doublets were added (through suitable delay networks) to give a $\frac{\sin x}{x}$ type of distribution. For the difference pattern, the output from

the doublets were subtracted and this gave a pattern with a notch in the main beam and a shape approximately equal to the differential of the sum pattern. In general, the bearing measurements were made with the aerial used in its difference pattern mode.

The output of the goniometer was digitized and recorded on magnetic tape. The magnetic tape was processed by a computer and the bearing was computed by means of an algorithm which extracted the notch of the difference pattern. For each bearing, a second algorithm computed a 'figure of merit' and this tested the closeness with which the output from the goniometer fitted the expected polar diagram. The maximum and minimum values of the figures of merit were normalized to 100 and zero, respectively. Typically, large values of the figure of merit (greater than 90) would correspond to bearings taken under ideal conditions, for example, when there was no wave interference which would occur when the signal was being received by one mode of propagation only. On the other hand, low values of the figure of merit would generally correspond to bearings taken at times when conditions were bad, for example, when there was severe wave interference which would occur when the signal was being received, simultaneously, by several modes of propagation.

Both the bearing error and the figure of merit were plotted, as a function of time, by a computer controlled plotter. These results are described in section 3.

2.2 Choice of Transmitter

The transmitters that were chosen for monitoring had to satisfy two criteria. The first criterion was that the arriving sky wave should be a 'nominally' single hop, single mode signal. This enabled the effects of the Ross tilts, on bearing measurements, to be examined under the simplest conditions. The ESSA ionospheric predictions were used to test whether the above criterion could be met. Since these predictions only gave the 'median' conditions for a month, no account could be taken of day to day changes in the ionosphere. Further, no account was taken of magneto-ionic splitting (the arrival of the 'O' and 'X' components, simultaneously), the Pedersen ray or the occurrence of sporadic E. Thus the term 'nominal' was included in the first criterion in order to distinguish it from the case of a pure single hop, single mode signal. The only way in which a frequency could have been chosen to give a pure single mode signal, would have been to use an on-line oblique sounder. Clearly, it would have been necessary to have, for this type of experiment, exercised complete control over the transmitter. Neither an oblique sounder nor a co-operative transmitting site were available at the time of the experiments.

The second criterion that had to be met was that the transmitter had to have a frequency schedule such that suitable frequency changes could be made, over the full 24 hours, in order to satisfy the first criterion. In order that this second criterion could be met, the transmitter had to be active (even if it only transmitted its callsign on a band slip) on a number of frequencies over the 24 hours.

It was not possible to find any transmitters that could meet both of the above two criteria over the full 24 hours. However, there were 3 transmitters which met the above criteria for most of the time and those were Aran Juez, Prague and Rome. Full details concerning their callsigns and frequencies are given in Table I. The locations of the transmitters, listed in Table I, were obtained from the international Berne list.

Transmitter	Callsign	Frequency MHz	Range from the receiving array (kms)	True Bearing from the receiving array (deg)
Prague	OIW	6.820	1204	91.1
	OLH	6.958	1204	91.1
	OLG	10.125	1204	91.1
	OID/OLG	10.308	1204	91.1
	OLD	18.303	1204	91.1
Prague	OLE	3.777	1166	91.8
	OLZ	7.695	1166	91.8
Aran Juez	EAD	6.383	1295	186.8
	EAD	8.682	1295	186.8
	EAD	17.185	1295	186.8
Rome	IAR	6.410	1543	129.4
	IAR	8.670	1543	129.4
	IAR	13.015	1543	129.4
	IAR	17.233	1543	129.4
Norddeich	DAN	8.638	648	66.5
	DAM	12.763	648	66.5
	DAN	13.027	648	66.5

TABLE I - List of Transmitters and their Callsign used for the trial

For interest, the MUF curves for the 3 paths Aran Juez/Blakehill, Prague/Blakehill and Rome/Blakehill, for November 1970, are given in Figures 1A to 1C and it can be seen, from the frequency schedules, that for most of the time, a frequency could be chosen such that it was very close to the MUF.

A fourth transmitter, Norddeich, was also monitored. This transmitter was chosen simply to examine the effects of the Ross tilts, on bearings, for a relatively short path. It was expected that, for short paths, the effects of the Ross tilts, on bearing measurements, would be strengthened. The MUF curve for the Norddeich/Blakehill path is shown in Figure 1D.

2.3 Experimental Procedure

A transmitter was chosen from the list in Table I and it was monitored for a continuous period of 24 hours. At any time during the 24 hours, the choice of frequency was made by reference to the MUF curves from which it could be seen whether or not the frequency in use was close to the MUF. Bearing measurements were only taken on signals that arrived by a great circle path and no measurements were taken on signals that arrived by a side-scatter path. This criterion was checked by comparing the observed bearing with that of the true bearing of the transmitter. If the difference was greater than 20 degrees, then the signal was assumed to be arriving by a side-scatter path and a lower frequency was selected.

During the morning period, a monitor receiver was used to check the next highest frequency to that being recorded. As soon as the next highest frequency was audible, then a frequency change was made. In the afternoon period, when the MUF was dropping, the monitor receiver was used to check the next lowest frequency. In this way, frequency changes were made smoothly. Frequencies that were less than 0.7 of the predicted MUF were not generally recorded.

After recording a transmitter for a period of 24 hours then, either another transmitter was chosen for the next 24 hours, or the same transmitter was chosen for a second period of 24 hours. The tests were conducted over the period 23 November to 7 December 1970.

The bearing measurements were recorded, automatically, as described in section 2.1. The recording rate was set at one bearing every 4 seconds for morse signals and one bearing every 8 seconds for all other types of signals. The different recording rate for these signals was simply due to the fact that, for morse signals, the time interval for the 'off' positions of the morse keying was relatively long (100 msecs, or more). When the rotor of the goniometer pointed to the transmitter during an 'off' period, the automatic bearing recording equipment was not triggered and no bearing measurement was made. To compensate for this, the recording speed for morse signals was increased by a factor of two.

Only one revolution of the goniometer was used to give a bearing measurement. The goniometer rotated at a speed of 10 revolutions per second and a recording rate of one bearing every 8 seconds meant that only one revolution in every 80 was used to give a bearing measurement. A faster recording rate would have highlighted the rapid fluctuations of the bearing rather than the effects of the Ross tilts.

Another recording technique that would be worthwhile using would be to compute the bearing measurement using the information from all the goniometer revolutions that were made within a specific time interval, eg, with a recording rate of one bearing every 8 seconds, the bearing measurement could be estimated by averaging all of the 80 bearings obtained from every revolution of the goniometer. It is intended to try this recording technique (which is more sophisticated than that used in the present experiments, described here) at a later stage.

3. EXPERIMENTAL RESULTS

3.1 Presentation of the Data

Samples of the results are shown in Figures 2 to 15. In each case, the symbol used for plotting the bearing is as follows:-

- represents a bearing with a figure of merit between 81 and 100
- ◇ represents a bearing with a figure of merit between 61 and 80
- △ represents a bearing with a figure of merit equal to, or less than 60.

The exact value of the figure of merit, associated with each bearing, was plotted by the symbol 'X' on the graphs. This enabled the trend of the figure of merit, as a function of time, to be examined on each graph.

The graphs, shown in Figures 2 to 15, have been selected to illustrate various aspects. All the bearings that were more than 10 degrees in error were not considered in this report. It is obvious that these wild bearings do not affect the general patterns of bearing fluctuation (shown in the graphs). Bearings which are greater than ± 10 degrees in error are shown at the bottom of the printout.

3.2 Typical Day-time Records

Figures 2 and 3 show examples of typical day-time records. The records were both obtained for the Aran Juez/Blakehill path (range = 1295 kms, frequency = 17.185 MHz). In both records, the bearing error varied within a range of $\pm 1\frac{1}{2}$ degrees of the true bearing.

It is interesting to note that, in Figure 2, the figure of merit has relatively high values during the bearing perturbation of $\pm 1\frac{1}{2}$ degrees at about 14-30. This is shown by the circles, printed on the graph, and it suggests that, at this time, the display given by the incoming signal was very good. However, the values of the figure of merit are relatively low during the small bearing perturbation at about 15-12. This is indicated by the presence of triangles and it suggests that the display given by the incoming signal was relatively poor. The observations suggest that, at any instant, the figure of merit gives no indication of whether the bearing was influenced by the Ross tilts. Examination of all the data obtained during the exercise has shown that this result is general.

Another interesting result concerning Figure 2 is that the overall bearing error tends to be positive. This agrees with the direction of the east-west component of the systematic tilt for the afternoon period since the true bearing of Aran Juez, at Blakehill, is 186.8 degrees and this path will be mainly affected by E-W component of the ionospheric tilts.

In Figure 3, the overall bearing error is negative. Again, this is in agreement with the direction of the east-west component of the systematic tilt for the morning period.

3.3 Quiet Record

The quietest recording obtained, during the trial, was that for Rome (frequency = 17.233 MHz, range = 1543 kms), over the period from 07.00 to 12.00 (which was the end of the recording) on 30 November. A sample from this record is shown in Figure 4 and it can be seen that the bearing error never exceeds a value of +0.5 degrees. On the assumption of a single-hop (1F mode), mirror type reflection, this bearing error corresponds to an ionospheric tilt, in a direction normal to the great circle path, of about +1.3 degrees.

Over the period of the record, shown in Figure 4, the overall bearing error is virtually centred on zero. Since the true bearing of the transmitter is 129.4 degrees, then the systematic tilt for the path will, approximately, consist of an equal contribution from the N-S and E-W components of the systematic tilt. The bearing error for the former will be positive whereas the bearing error for the latter, during the morning period, will be negative. Thus, it is reasonable that the overall bearing error for Rome, during the morning period, is around zero.

3.4 Disturbed Record

An example of a disturbed record is shown in Figure 5. The values of the bearing error appear to trace a wave-like pattern with a broadband of about one degree in width. The exception to this is the bearing perturbation that occurs between 15-33 and 16-10 since, over this period, there does not appear to be any smearing of the bearing error curve. The maximum bearing error during this period is $4\frac{1}{2}$ degrees and it occurs at about 15-55. For this time of the day, the predicted MUF for the 1F and 2F modes was 11.2 and 8.0 MHz, respectively. Since the transmitter's frequency was 10.308 MHz, it seems likely (but not proved) that the 1F mode was being propagated. On the assumption of a simple mirror type of reflection, the component of the ionospheric tilt in a direction normal to the great circle path, that would correspond to a 1F mode, is of the order of 9 degrees. This observation suggests that ionospheric tilts, as large as 9 degrees, could be associated with TIDs. It is planned to conduct further experiments in which a vertical sounder will be used at the mid-point of the path. This will provide more accurate information on the state of the ionosphere so that the mode of propagation can be deduced more precisely.

During the bearing perturbation commencing at 15-33, a relatively large number of the bearings have high values of the figure of merit - as indicated by the circles. For these bearings, the display given by the incoming signal must have been relatively very good and this again emphasises the fact that, at any instant, the DF display does not give indication as to the accuracy of the bearing.

The fast fluctuations (about one degree in amplitude), superimposed on the bearing error curve, are probably caused by wave interference. This wave interference could be caused by two modes of propagation arriving at different angles of elevation or a number of waves arriving in a cone. This latter effect could be caused by the surface of the ionosphere being corrugated.

It is also interesting to note that the overall bearing error for the Prague record, shown in Figure 5, is positive. This is in agreement with the direction of the systematic tilt for an easterly path.

As a matter of interest, the observed values of h'F (minimum height of the F layer) at Lindsau have been plotted, at half-hourly intervals, for the disturbed day of 2 December and the quiet day of 30 November (see Figure 4). The ionospheric station is not exactly at the mid-point of either the Prague-Blakehill path or the Rome-Blakehill path. Nevertheless, the station was sufficiently close to the mid-points to enable some idea to be obtained of whether the ionosphere was disturbed or quiet. The graphs of h'F, for these 2 days, are shown in Figures 16 and 17. The graphs suggest that the ionosphere was more disturbed on 2 December than it was on 30 November. This agrees with the bearing records obtained on those days.

3.5 Typical Example of a Short Path

An example of a bearing error record, for a short path, is shown in Figure 6. The record was obtained for the Norddeich/Blakehill path (range = 648 kms, frequencies = 8.638 and 13.027 MHz). The bearing perturbations are considerably larger than those observed on any of the other paths and this is primarily due to the relatively short range of the path. The value of the maximum bearing error is 5.8 degrees and it occurs at 09.38. It is shown below that the mode of propagation must have been a 1F rather than a 2F mode and, for a mirror type of reflection, this bearing error would correspond to a component of the ionospheric tilt, in a direction normal to that of the great circle path, of about 6.5 degrees.

At 09.18, there is a marked decrease in the figure of merit which corresponds with a crest in the bearing fluctuation. This occurrence is exceptional. If, of course, it occurred regularly, then the figure of merit could be used to give an indication of whether the bearing measurement was influenced by the effects of the Ross tilts.

At 08-11, a frequency change was made and a higher frequency was monitored. This frequency change was made because the higher frequency became audible at this time (a monitor receiver was used to check this). However, the bearing record shows that there is no mark discontinuity in the bearing fluctuation at that time. The radio wave at a frequency of 13.027 MHz will have been reflected at a greater height than the radio wave at a frequency of 8.638 MHz. Thus, in this case, the Ross tilt had the same effect at both reflection levels although, both reflection levels were in the F region. As yet, there have not

been sufficient data collected to test if, at any instant, the bearing error due to Ross tilts would be the same for radio waves, in a range of frequencies, reflected in the same layer.

Around 08-37, there is a gap in the bearing curve which coincides with a crest of a bearing perturbation. At this time, the working frequency was above the predicted MUF, for the 1F mode, of 11 MHz. Thus, it is safe to assume that, at this time, the skip zone was close to the receiver. One possible explanation of the disappearance of the great circle bearing around 08-37 is that the disturbance, associated with the bearing perturbation, tilted the ionosphere in such a way that the skip zone moved outwards (from the transmitter) beyond the receiver. A few minutes later, when the bearing error had decreased (and the great circle path restored), the skip could well have returned by moving inwards (towards the transmitter) and, in doing so, passed over the receiver. This would account for the disappearance of the great circle bearings at a time when there was a relatively large disturbance affecting the path. In general, phenomena, such as the one just described, can only be explained with a high degree of certainty when an oblique sounder is available over the path.

Finally, the overall bearing error in Figure 6 tends to be positive. The true bearing of Norddeich, from Blakehill, is 66.5 degrees. Thus, both the east-west and north-south components of the systematic tilt will effect the overall bearing error for the path. During the morning period, the systematic bearing error for a northerly transmitter will be positive while the bearing error for an easterly transmitter will also be positive. Thus, for a north-easterly path, the components will combine to give a relatively large positive error. For the case of the Norddeich/Blakehill path, this error is again enhanced because of the relatively short distance of the path. This probably accounts for the overall large positive error observed in Figure 6.

3.6 Night Time Records

A typical example of a night time record is shown in Figure 7. In general, the record shows a broad spread of bearings compared with the wave like appearance of the day-time records. It is thought that the broad spread of bearings, observed during the night-time is due to the night-time ionosphere being turbulent. However, only further investigations will clarify this matter.

Exceptionally, wave like patterns have been observed during the night and such an example is shown in Figure 8 for Aran Juez (true bearing = 186.8 degrees). The pattern, formed by the bearing fluctuations, is not as clear as those for the day-time records. For this record, the largest bearing perturbation occurs at 04-05 with a bearing error of 3 degrees. There is a gap in the record between 04-28 and 04-50 and this was due to the transmitter going off the air during communication with shipping.

The predicted MUF for the 1F and 2F modes at 04-00 was 6.4 MHz and 4.2 MHz, respectively. Since the transmitter's frequency was 6.383 MHz, it was reasonably certain that the signal was propagated by the 1F mode. On the assumption of a simple mirror type of reflection, the component of the ionospheric tilt in a direction normal to the great circle path, that would correspond to a 1F mode is about $6\frac{1}{2}$ degrees. This again suggests that relatively large ionospheric tilts are often associated with TIDs.

The overall bearing error for the record shown in Figure 8 is around zero. For a southerly path, the systematic error, at about 04-03, would be about -0.1 degrees and this agrees reasonably well with the observed value of the overall error.

3.7 Bearing Perturbation Persisting for an Extended Period

The longest bearing perturbation that was observed is shown in Figure 9. The bearing showed a consistent error of about 2 degrees over the period 20-07 to 21-05. Over this period, the display given by the incoming signal appeared almost perfect - as indicated by the circles. The fact that the bearing perturbation does not show a zero crossing (ie, the bearing perturbation gives an error of the same sign) obviously shows that the component of the tilt, in a direction normal to the path, did not change sign. If it is assumed that the electron density contours, along a cross-section of the ionosphere disturbance, are semi-spherical, then the above results implies that the disturbance moved along the propagation path, ie, it is moving on a north-south (or south-north) path. The fact that the bearing perturbations lasted for almost an hour suggests that the disturbance took about an hour to cross over the mid-point of the path.

3.8 Fastest Rate of Bearing Change and Ship Zone Effects

The fastest rate of bearing change that was observed during the exercise is shown in Figure 10. It occurred on the Prague/Blakehill path between 11-33 and 11-41 during which the bearing error changed from $+2\frac{1}{2}$ degrees to $-2\frac{1}{2}$ degrees, and gave a rate of change of bearing of about 0.6 degrees per minute. The corresponding change of the ionospheric tilt, in a direction normal to that of the path, was from about +5 degrees to -5 degrees giving a rate of change of about 1.2 degrees per minute. This rate of change of the ionospheric tilt is based on the assumption that the mode of propagation was 1F (predicted median values of the MUF for the 1F and 2F modes were 18.0 and 12.0 MHz respectively) and that the reflection of the radio wave was similar to that of a mirror type of reflection.

The bearing perturbation between 11-33 and 11-41 has a zero cross at about 11-37. It is assumed that the shape of the contours of the ionospheric disturbance, associated with this bearing perturbation, are semi-spherical, then a bearing perturbation with a zero crossing could be explained by a disturbance moving across the propagation path. In this case, it would mean that the disturbance was moving on a north-south (or south-north) path.

The record in Figure 10 also shows a gap (or partial gap) in the pattern formed by the fluctuation of the bearing error. These gaps occur at 10-40 and 11-27. Figure 11 is a continuation of the record shown in Figure 10 and an additional gap occurs at 12-09. The gap at 11-27 is a complete gap whereas the gap at around 12-08 is a partial gap. These gaps were due to the failure of propagation along the great circle path, and not due to a discontinuous transmission. This was confirmed by the fact that the

transmitter was still audible while, at the same time, the display on the wide aperture array showed that the signal was being received by a scatter mode. The complete gaps were due to the signal on the great circle path completely 'dropping out' whereas the partial gaps were due to the signal partially dropping out.

On each occasion when the great circle path 'dropped out' (either complete or partially), the value of the figure of merit decreased. Further, at these times, the bearing record showed a cluster of bearings appearing at about ± 8 degrees off the main pattern. Since the measured polar diagram at 18 MHz also shows that the first nulls occur at about $\pm 7\frac{1}{2}$ degrees off the main null, then the cluster of bearings are probably due to side-lobe effects. At these times, the best bearing is given by the nulls of the first side-lobes rather than the main null. The reason for this is not yet understood.

Figure 12 shows the effect when the great circle bearing establishes itself as the skip zone moves over the receiver for the first time in the morning. As the signal on the great circle path strengthens, the value of the figure of merit gradually increases. This means that the display, given by the incoming signal, gradually improves. However, even when the propagation path is fully established, for this particular bearing error record, the figure of merit is relatively low. The reason for this is not known. At around 10-27, when the working frequency was virtually equal to the MUF for the path, a cluster of bearings, at ± 8 degrees off the main bearing, appear again. This is similar to that observed in Figures 10 and 11.

The overall bearing error, for each of the three records shown in Figures 10, 11 and 12, is positive. This is in agreement with the effect of the systematic tilts for an easterly path.

3.9 Break Up of Pattern During a Bearing Fluctuation

Figure 13 shows a break up of the general pattern of the bearing fluctuation. It occurs at around 11-51 on 4 December 1970 for the Aran Juez/Blakehill path. During this break up period, there are a considerable number of good bearings - as indicated by the circles on the graph. This is unlike the previous examples where a gap (or partial gap) appears in the record and the value of the figure of merit abruptly drops - this case is generally associated with skip zone effects. The case illustrated in Figure 13 could well be due to the disturbance having a corrugated surface. However, at this stage, it is not possible to offer a conclusive explanation.

3.10 Change of Characteristics

Figure 14 shows an abrupt change in the pattern at 19.15. The broad spread of bearings after 19.15 is generally associated with night time conditions (see Figure 7), whereas the pattern like structure is associated with day time conditions (see Figures 2 and 3). The change in the characteristics in Figure 15 was probably due to the onset of night which occurs at that time. This phenomenon was repeated on other records at the sunset period.

Occasionally, a change of characteristics has been observed at times when it has not been possible to associate the change with either sunrise or sunset conditions. An example is shown in Figure 15 in which, around midnight, the pattern gradually changes from a broad band of bearings to a wave like pattern. This might have been caused by the mode of propagation changing from single mode to multi mode. Another explanation is that the spread bearing record might have been caused by single mode propagation through a disturbed ionosphere, eg spread F. There is a gap in the record between 00-16 and 00-30, and this was due to the transmitter going off the air during communication with shipping.

4. PRACTICAL IMPLICATIONS

In practical radio communication, it is advantageous to use aerial arrays with narrow beams in order to improve the received signal to noise ratio. Further, the only limitation that would decide the minimum beamwidth of the array would be the bearing error caused by the effect of ionospheric tilts. The foregoing results show that, for path lengths less than about 1200 kms, the effect of ionospheric tilts can change the bearing of the incoming sky wave by up to about 4 degrees, relative to the great circle path. Thus, under these disturbed conditions, the signal to noise ratio would have been degraded if the signal was received on a fixed beam aerial where the beamwidth was less than 8 degrees (assuming that the centre of the receiving beam was pointed towards the transmitter). However, it must be pointed out that the bearing error of $4\frac{1}{2}$ degrees was the largest bearing error observed for paths greater than 1200 kms. Consequently, for paths less than 1200 kms, it is suggested that when receiving arrays, with fixed beam of less than 8 degrees beamwidth, are used, some degradation in the signal to noise ratio can be expected as a result of travelling ionospheric disturbances.

For short paths (path lengths of about 600 kms), bearing errors of up to $6\frac{1}{2}$ degrees have been observed. Thus, for these cases, a degradation in the signal to noise ratio could occur with beamwidths of as high as 13 degrees.

It must be pointed out that, in the foregoing examination of the effect of TIDs, there has been no investigation of the bearing errors, as a function of frequency, at the time of the disturbance. Thus, it is not possible to state whether a change in frequency might generally change the bearing error as a result of the sky wave being reflected in a different part of the ionosphere. It is interesting to note that Sweeney (1970) has reported that the bearing error of the low angle 1F mode was generally less than that of the high angle 1F mode. Further work on the effect of frequency changes, using the array described in section 2, is planned. It is hoped that this new work will show the effect of changing the transmitter's frequency on communication links at times when they are affected by TIDs.

5. CONCLUSIONS

This paper must be regarded as an interim report as it is proposed to conduct a considerable amount of further investigation along the above lines. Nevertheless, the results obtained clearly show that the effects of TIDs on radio communication can be important, particularly with regard to the use of fixed narrow beam aerials. The bearing records also suggest the presence of systematic tilts in the ionosphere but the bearing errors due to this source are generally less than those due to TIDs.

It is planned to conduct further experiments in order to examine the effect of frequency on the bearing error under conditions when TIDs are present. It is also planned to use a vertical sounder at the mid-point of the paths in order to deduce the mode of propagation more precisely.

6. REFERENCES

- | | | |
|------------------------|--------|--|
| BRAMLEY E N and ROSS W | (1951) | Proc. Roy. Soc. A Vol. 207 p 251 |
| BRAMLEY E N | (1956) | Proc. IEE B Vol. 103 p 295 |
| ROSS W | (1949) | "Lateral Deviation of Radio Waves Reflected at the Ionosphere" DSIR Radio Research Report No. 19 published by HMSO London |
| SWEENEY L R | (1970) | "Spatial Properties of Ionospheric Radio Propagation as Determined with Half Degree Azimuthal Resolution". Stanford Electronics Laboratories, Radioscience Laboratory, Technical Report No. 155. |

7. ACKNOWLEDGEMENTS

The work described in this report has accrued from a team effort in the building of the array, designing and assembling the electronics and programming a computer for processing the data. The author wishes to thank those colleagues without whose help the publication of this paper would have been impossible.

This paper is published with the consent of the Director, UK Government Communications Headquarters, and with the permission of the Controller of HM Stationery Office.

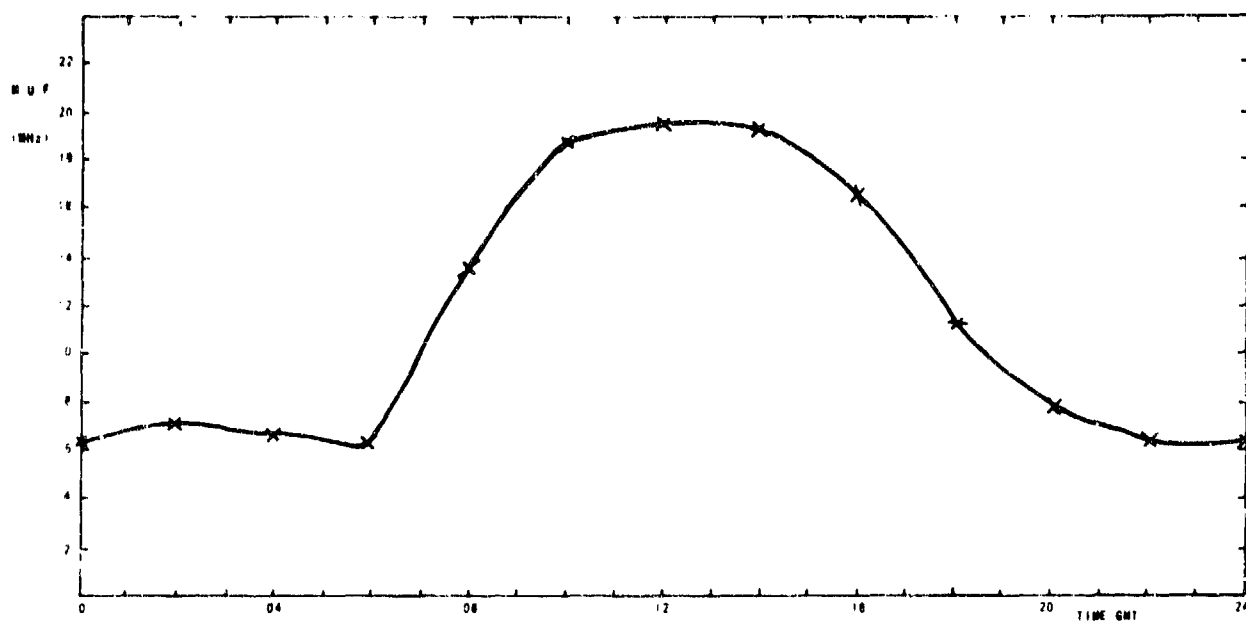


FIG 1A. MUF CURVE FOR THE ARAN JUEZ/BLAKEHILL PATH

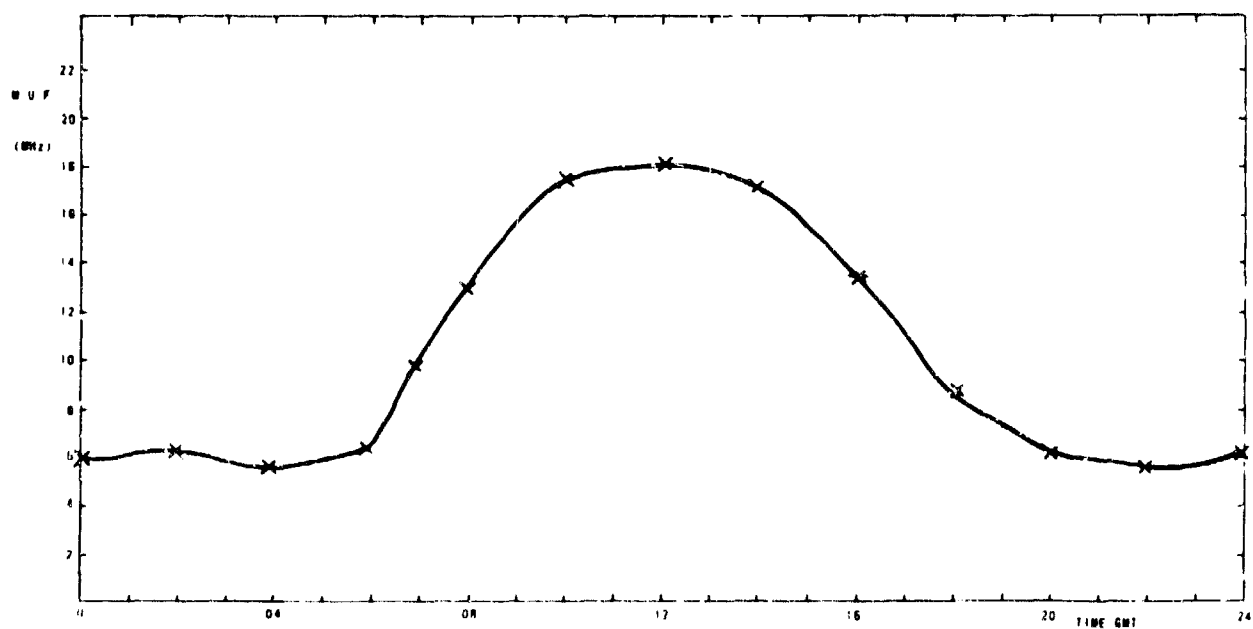


FIG 1B. MUF CURVE FOR THE PRAGUE/BLAKEHILL PATH

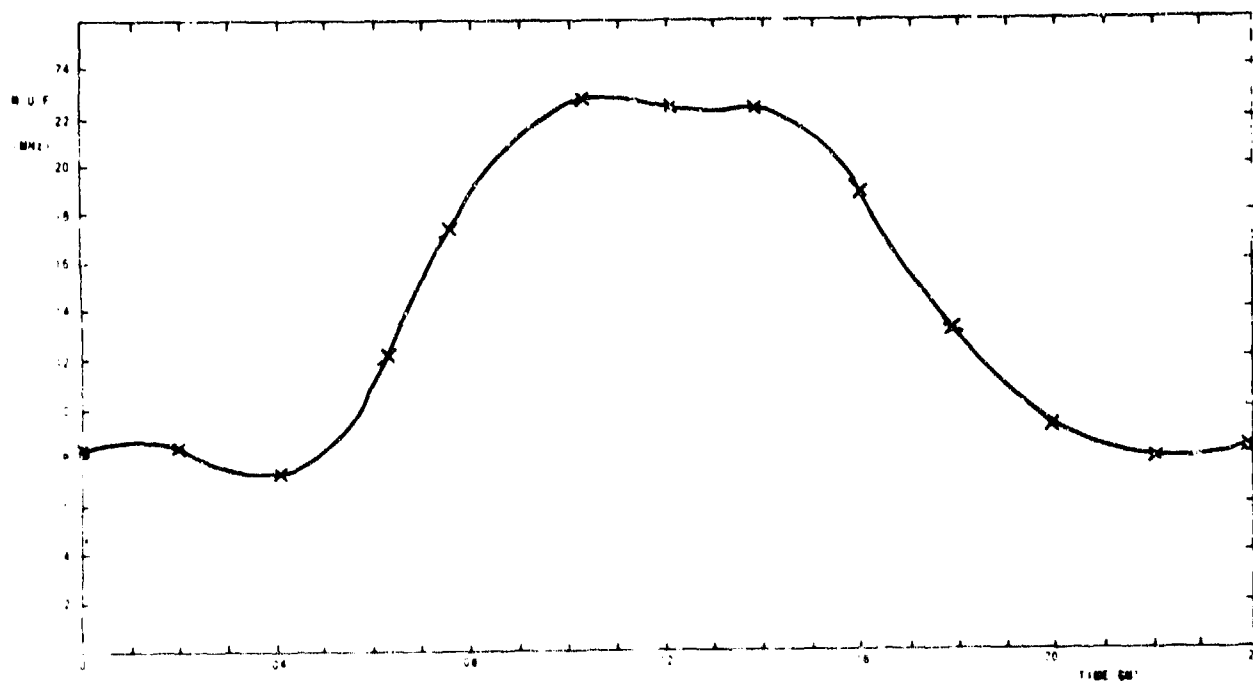
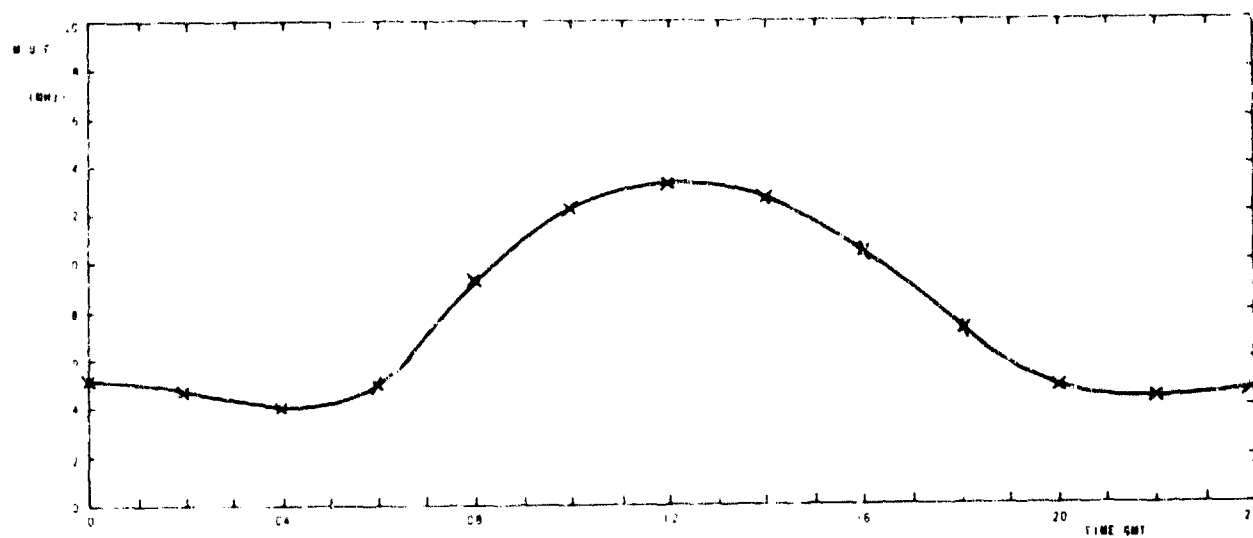


FIG 1C MUF CURVE FOR THE ROME/BLAKEHILL PATH

FIG 1D
MUF CURVE FOR THE NORDDEICH/BLAKEHILL PATH.

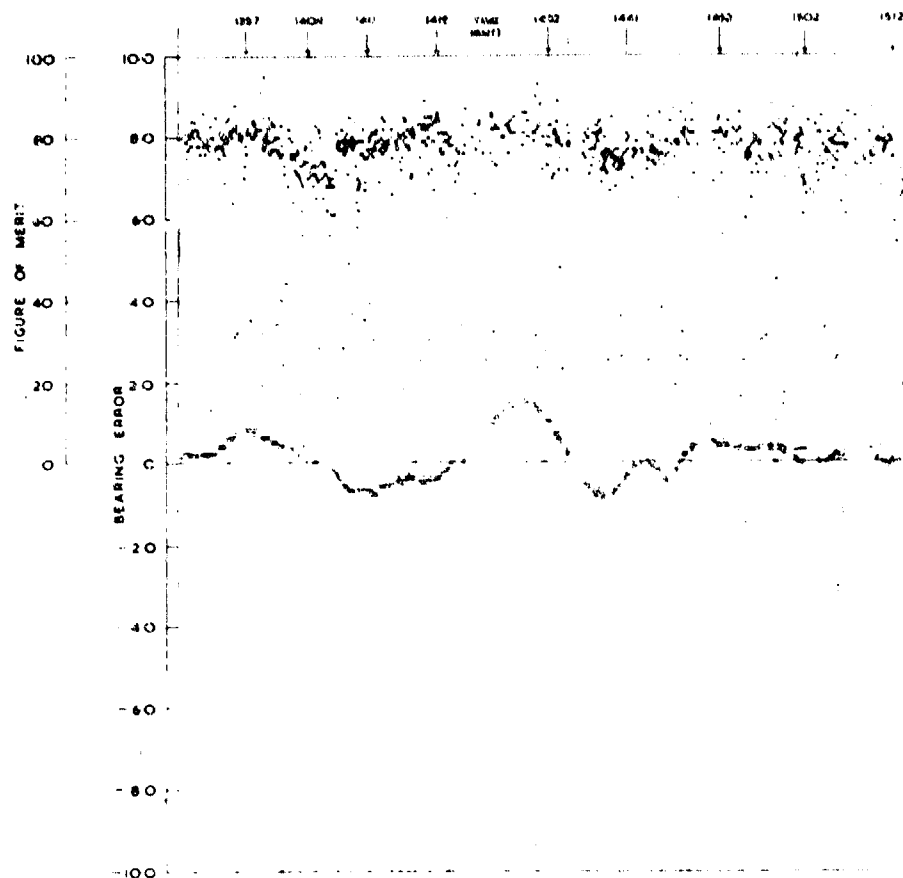


FIG 3 ARAN JUEZ DECEMBER 4th 1970

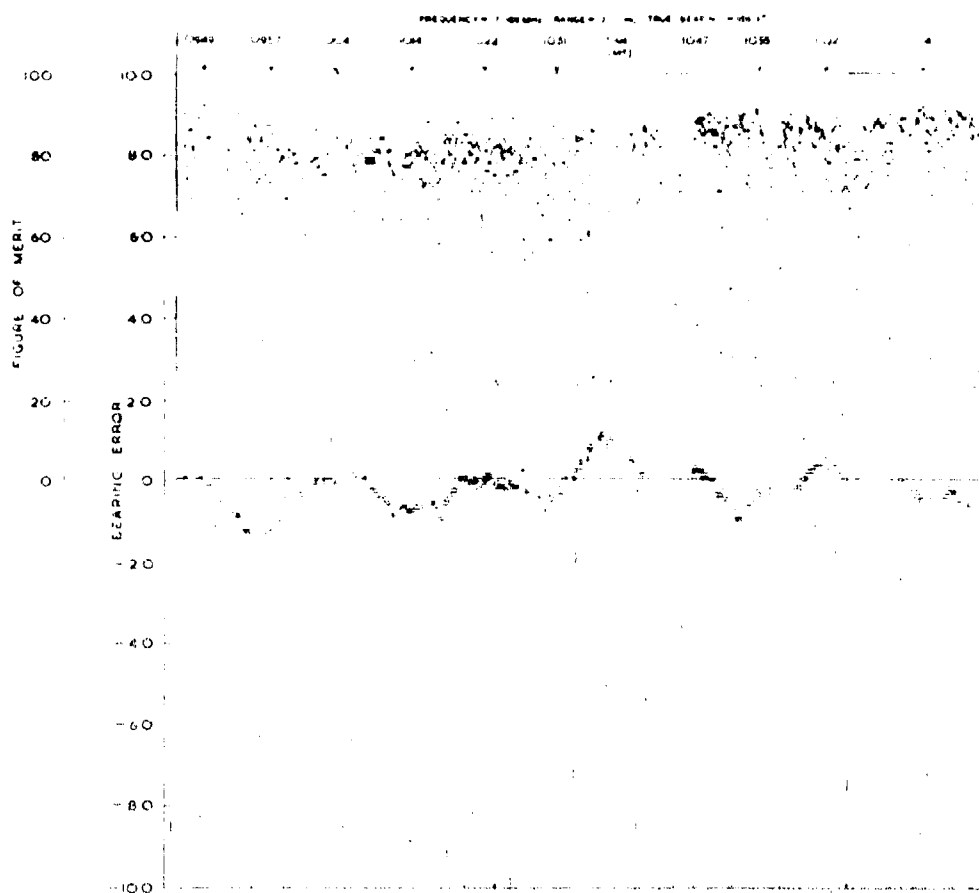


FIG. 4. ROME. NOVEMBER 30th 1970.
 FREQUENCY: 10.000 MHz. RANGE: 10000m. TRUE BEARING: 11.1°

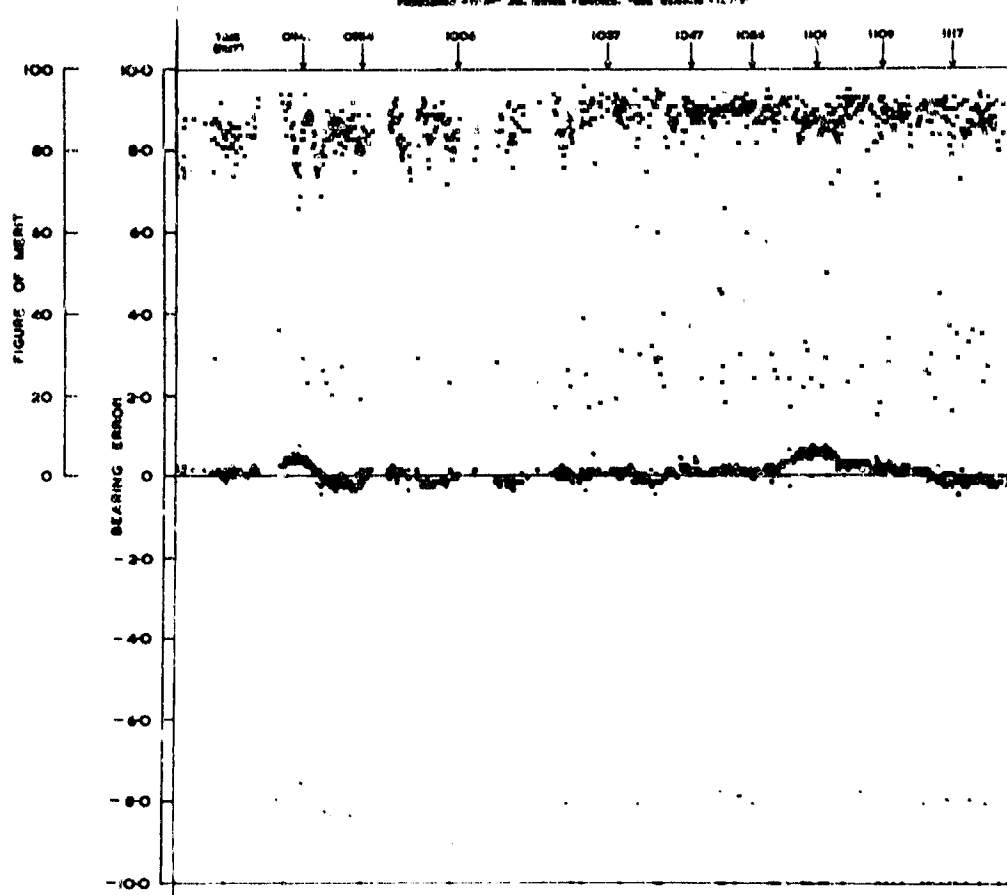
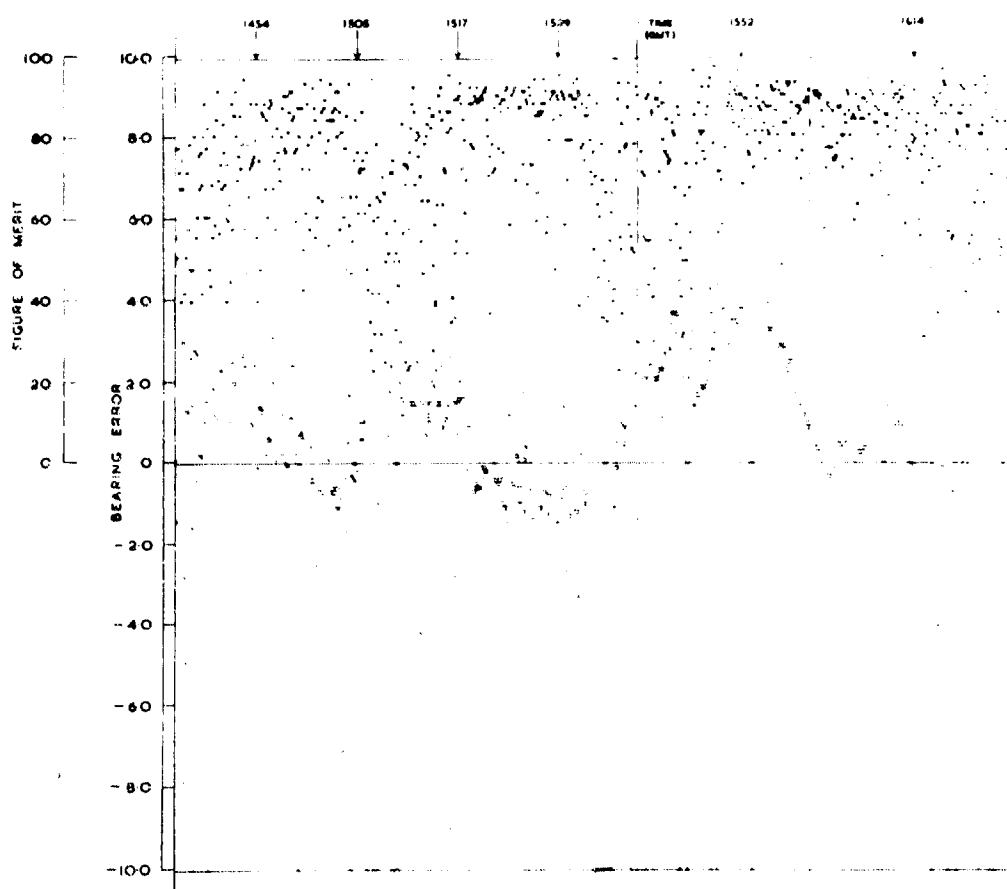


FIG. 5. PRAGUE. DECEMBER 2nd 1970.
 FREQUENCY: 10.000 MHz. RANGE: 10000m. TRUE BEARING: 11.1°



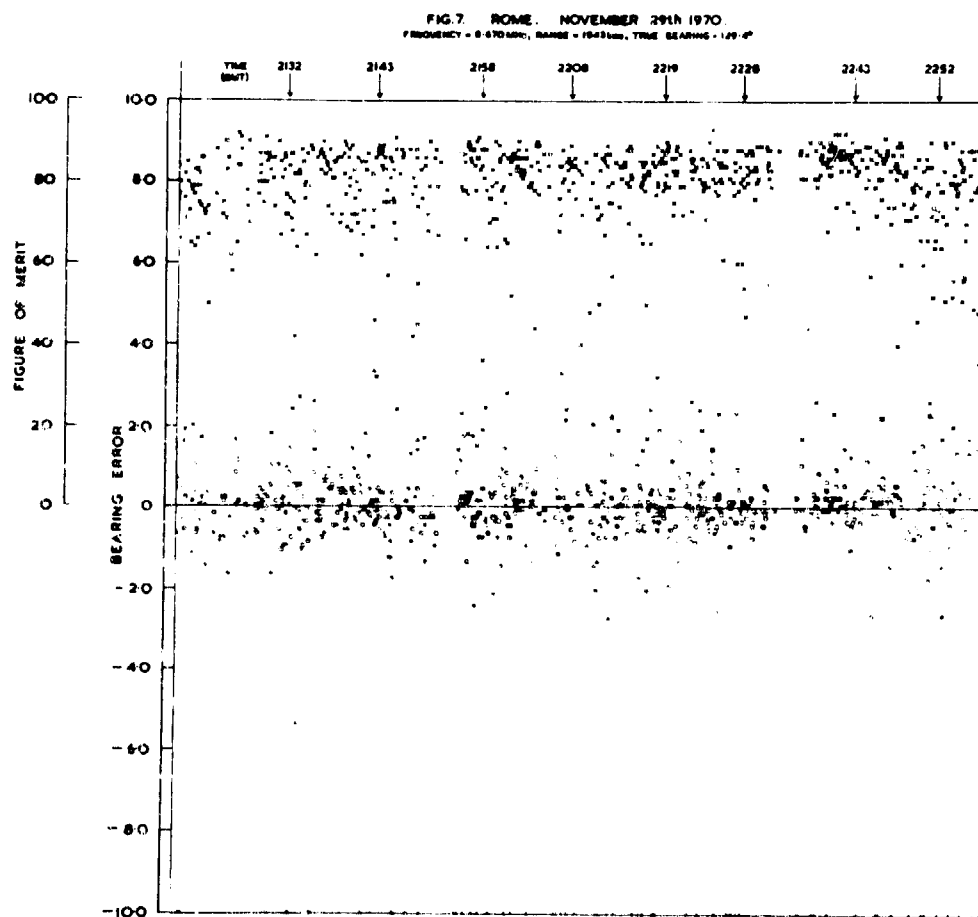
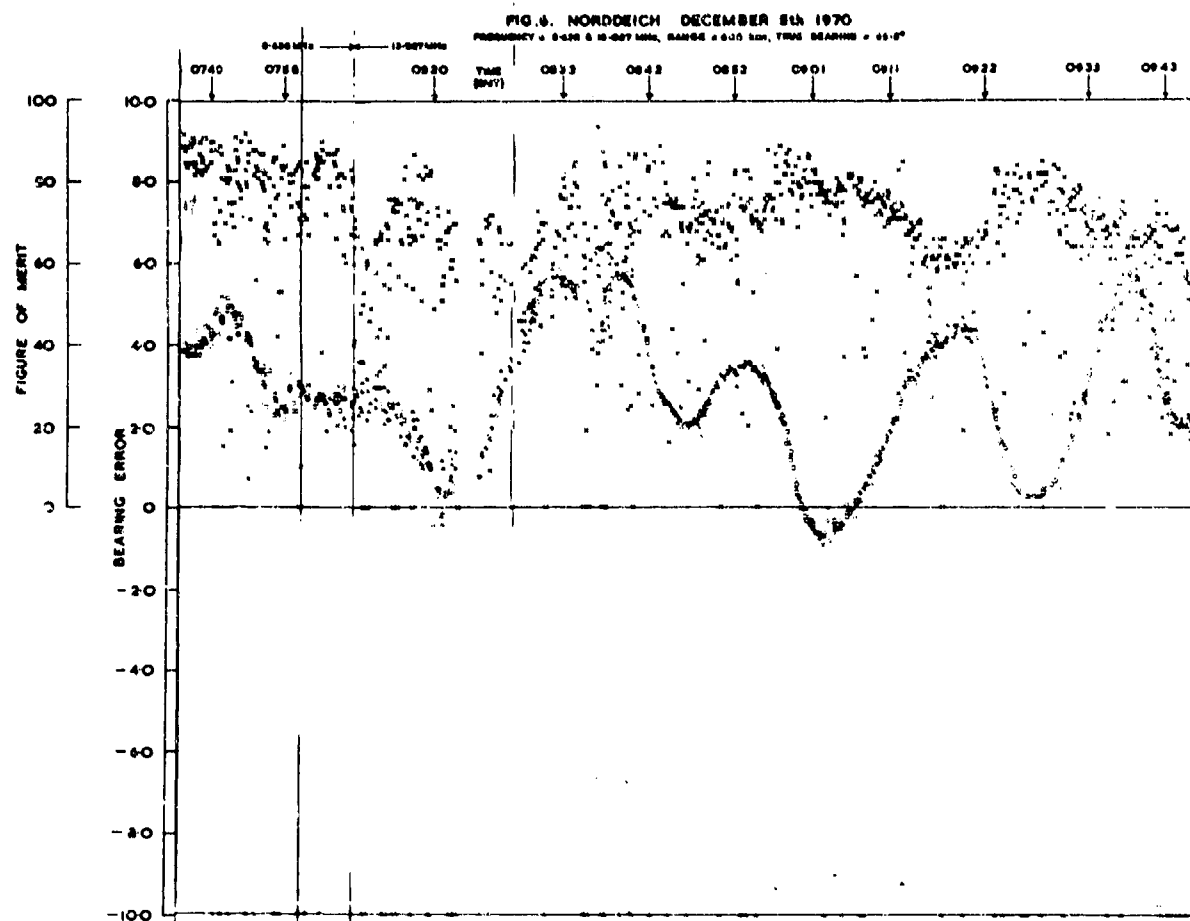


FIG. 8. ARAN JUEZ. NOVEMBER 24th 1970
 FREQUENCY = 8.32 MHz, RANGE = 1200 km, TRUE BEARING = 166.8°

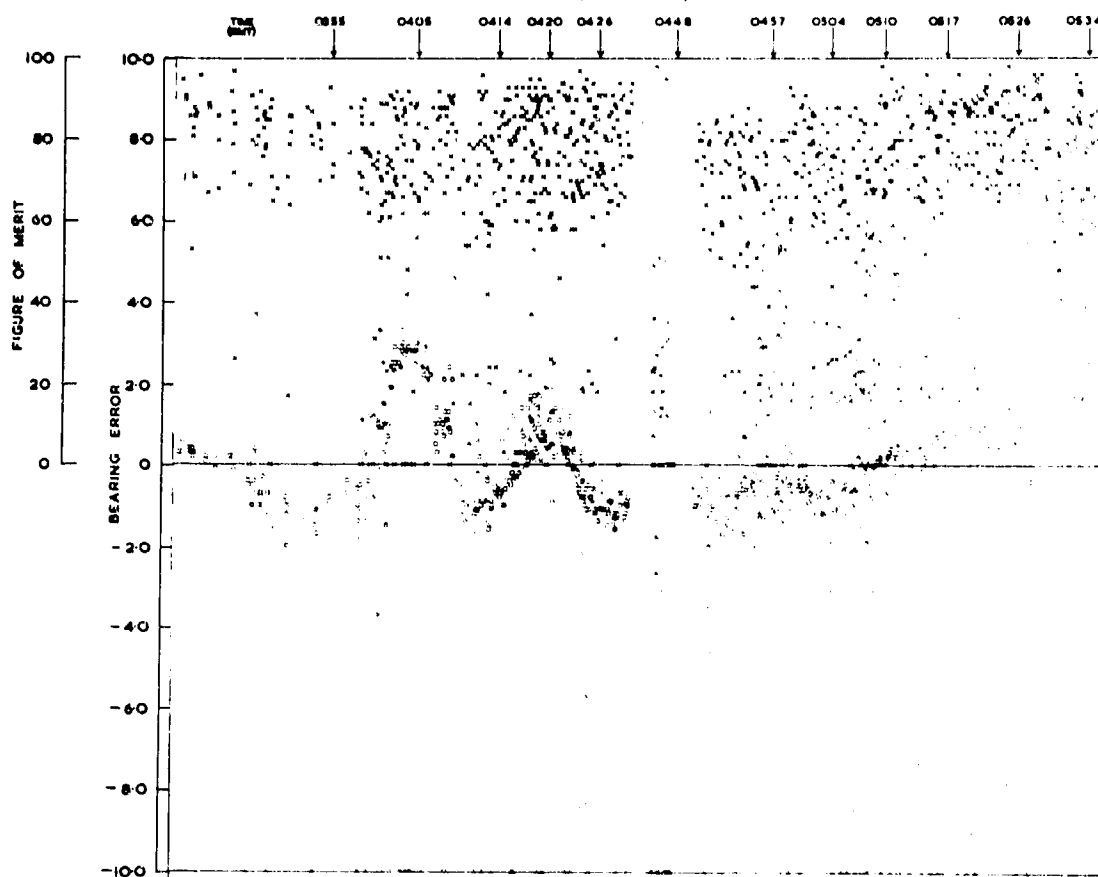


FIG. 9. ARAN JUEZ. NOVEMBER 23rd 1970
 FREQUENCY = 8.658 MHz, RANGE = 1200 km, TRUE BEARING = 166.8°

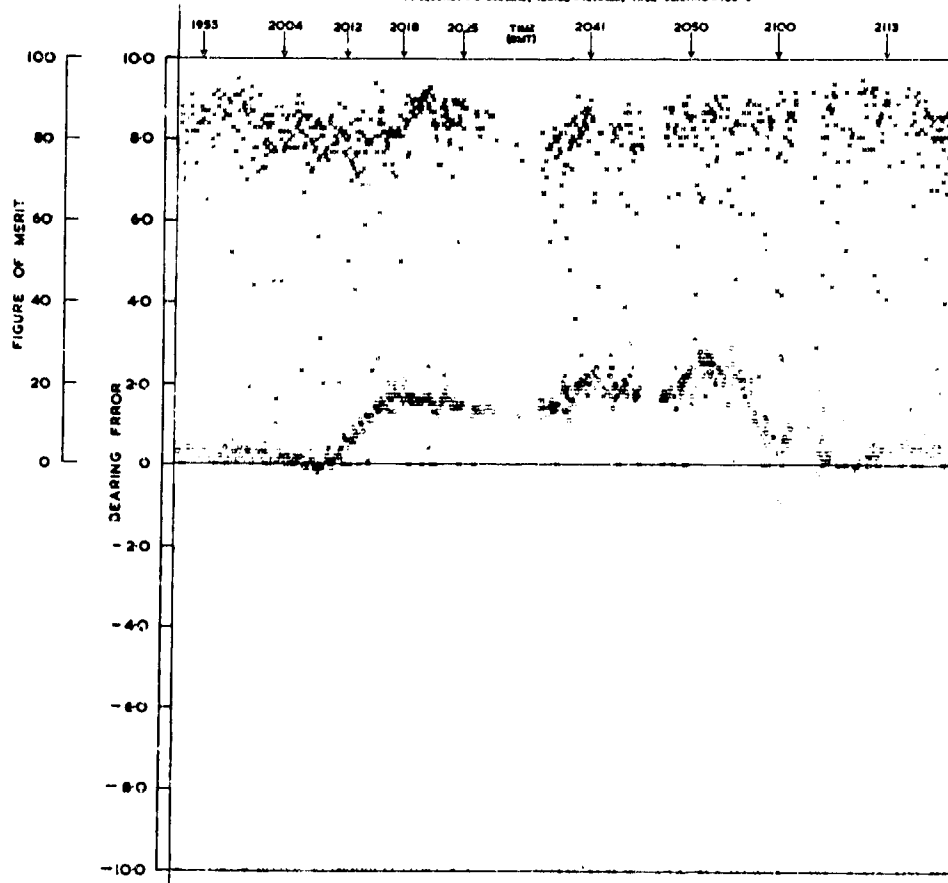


FIG.10 PRAGUE DECEMBER 3rd 1970
 FREQUENCY = 10.303 MHz RANGE = 4000 S.M. TRUE BEARING = 111.1°

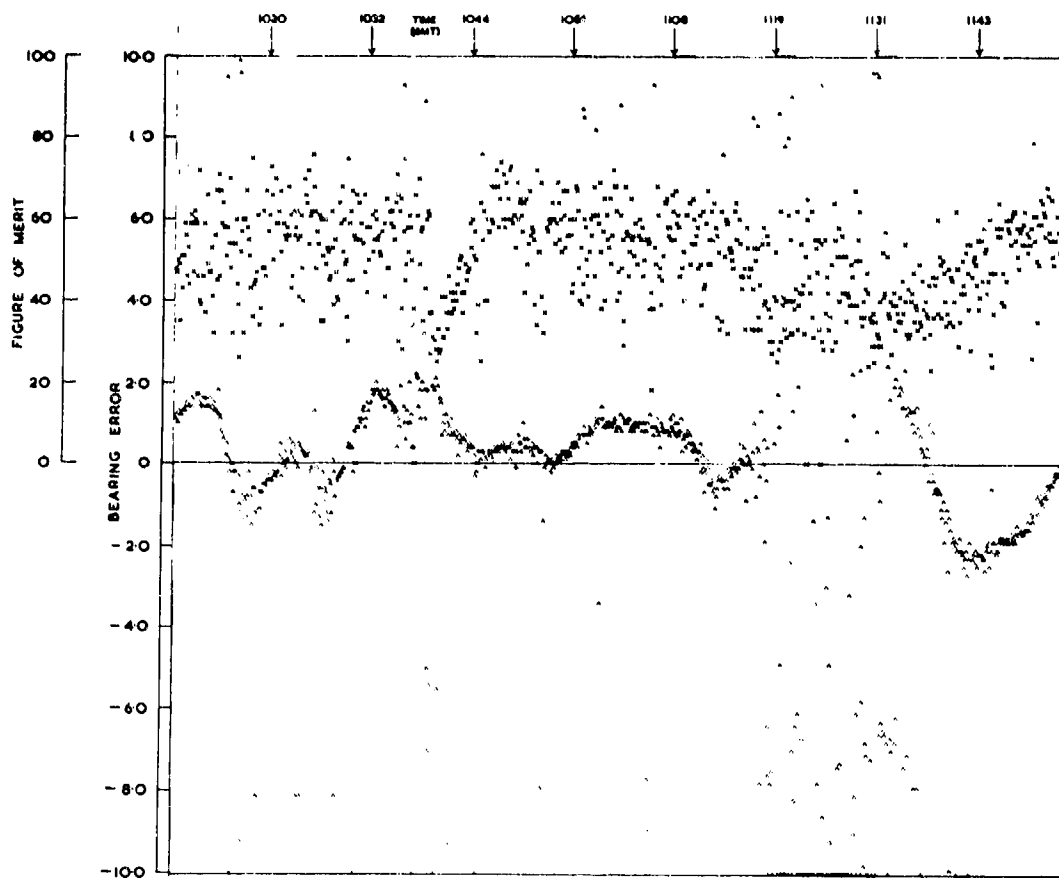


FIG.11 PRAGUE DECEMBER 3rd 1970
 FREQUENCY = 10.303 MHz RANGE = 12000 S.M. TRUE BEARING = 111.1°

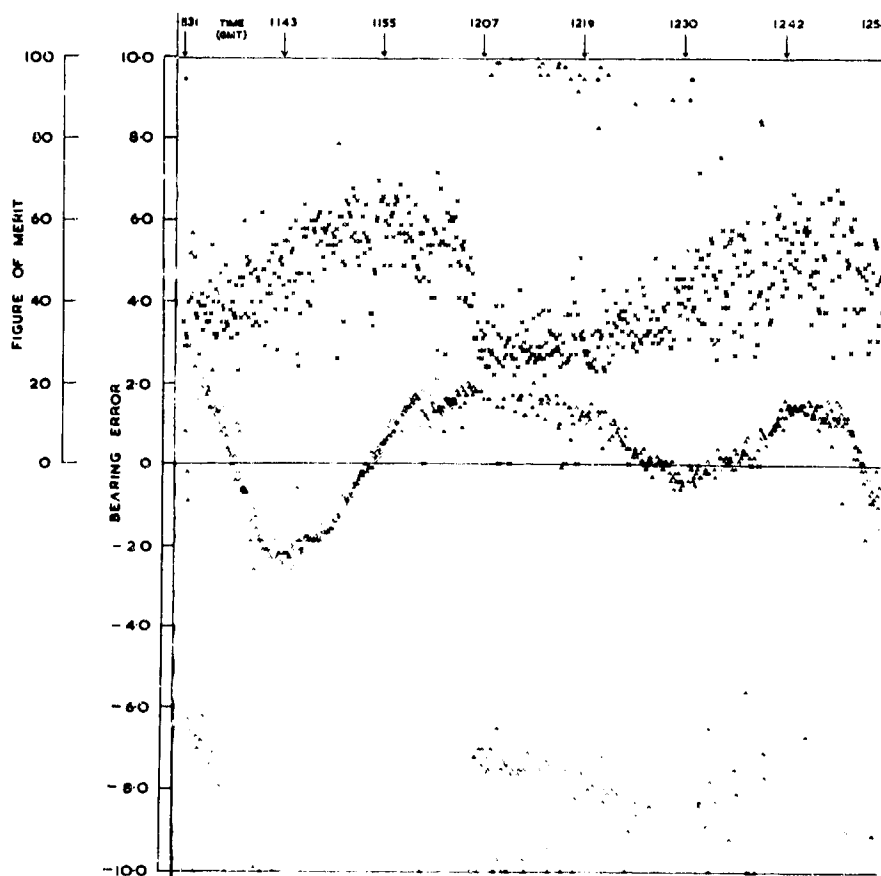


FIG. 12. PRAGUE DECEMBER 2nd 1970
 FREQUENCY = 10 000 MHz, RANGE = 1000 km, TRUE BEARING = 91°

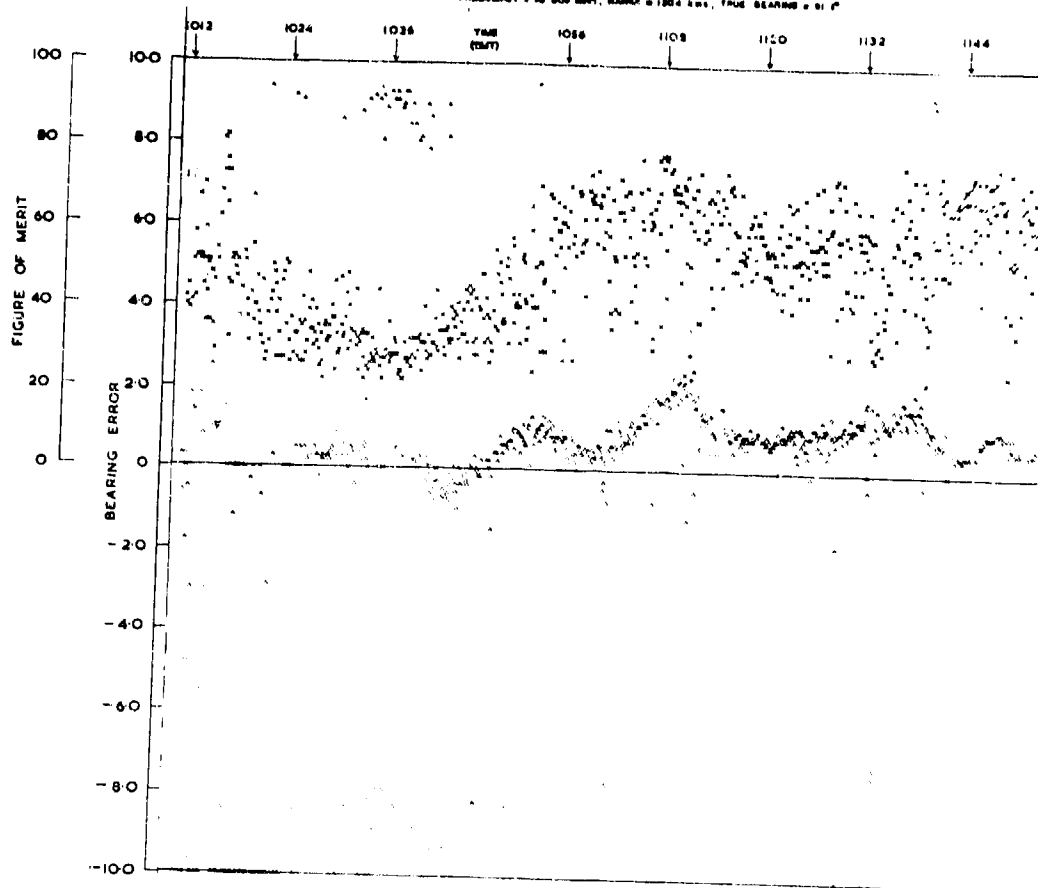


FIG. 13. ARAN JUEZ DECEMBER 4th 1970
 FREQUENCY = 17 185 MHz, RANGE = 1205 km, TRUE BEARING = 180°

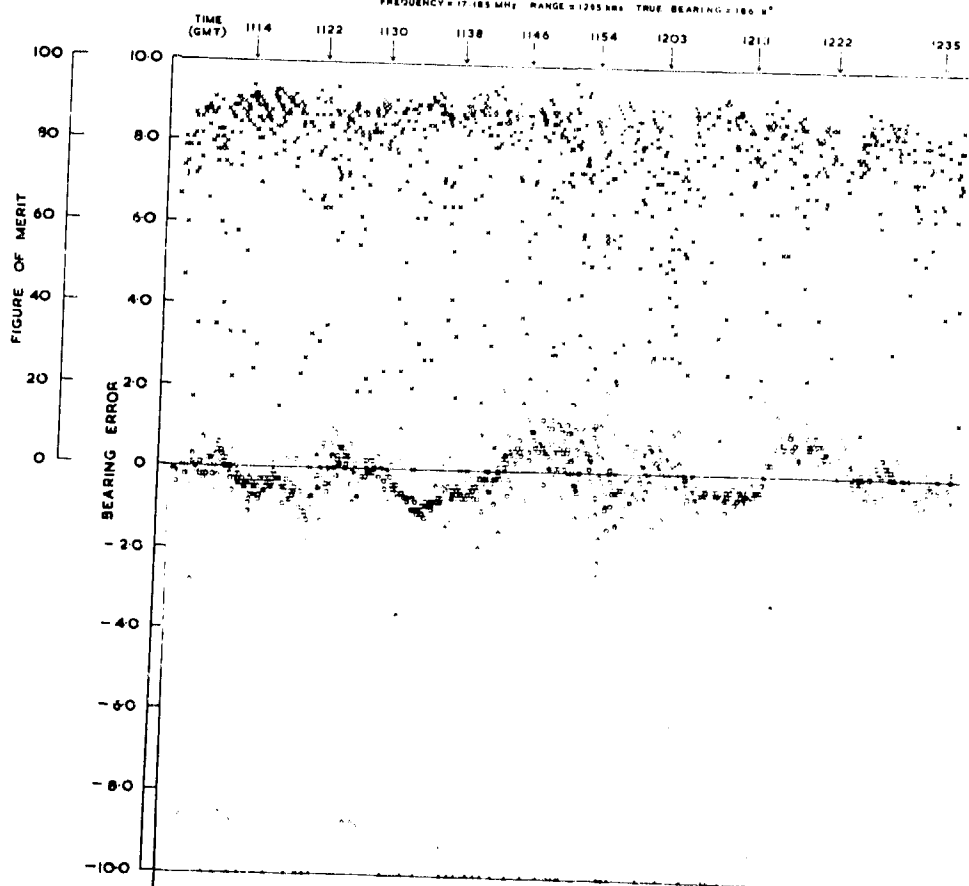


FIG. 14. ROME, NOVEMBER 24th 1970
 FREQUENCY = 6.570 MHz, RANGE = 1542 km, TRUE BEARING = 125.4°

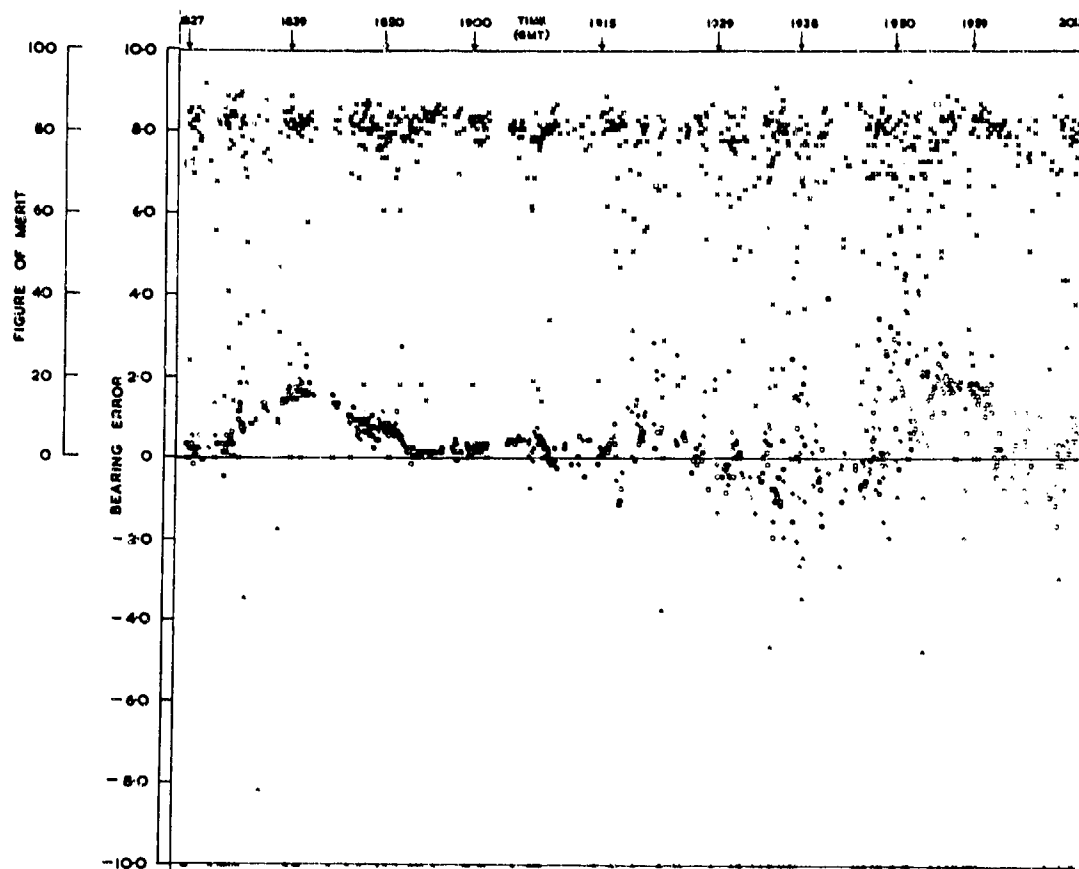
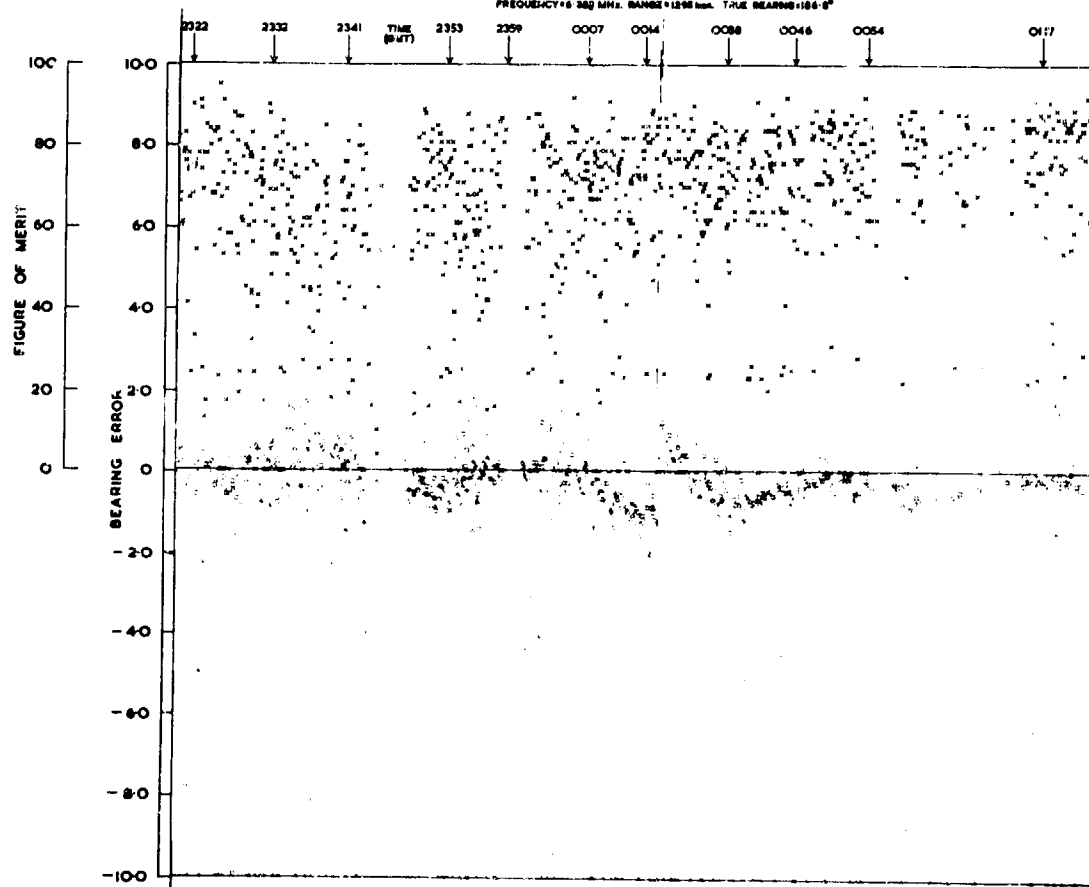


FIG. 15. ARAN JUEZ, DECEMBER 3rd/4th 1970
 FREQUENCY = 6.340 MHz, RANGE = 1248 km, TRUE BEARING = 106.8°



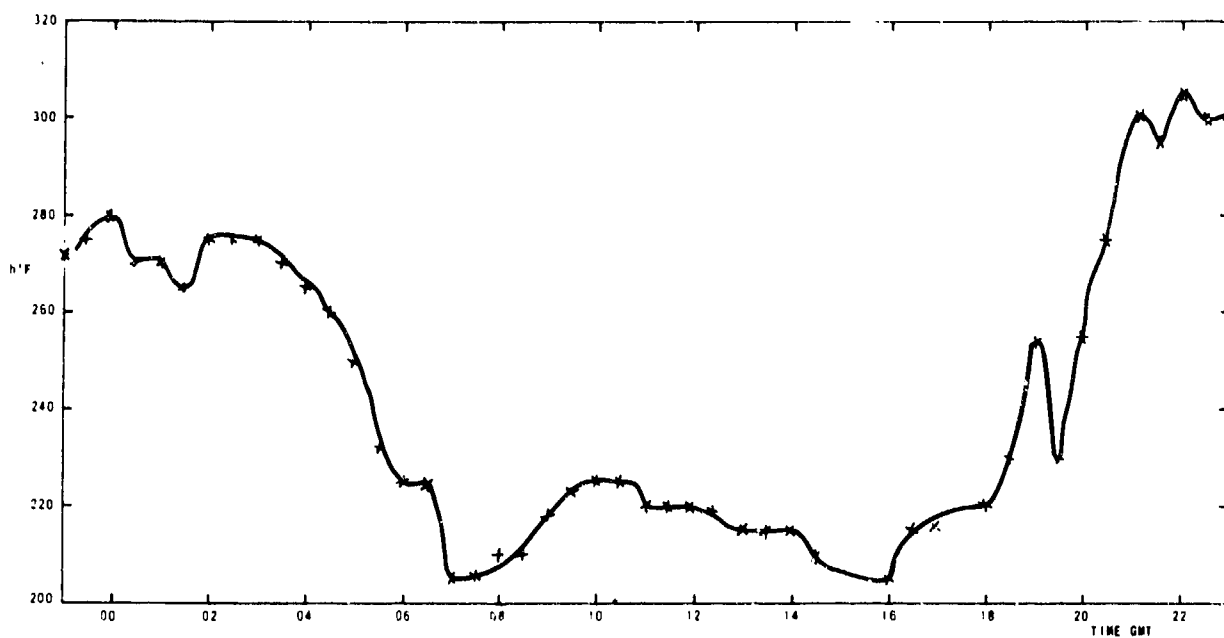


FIG.16
THE GRAPH OF $h'F$ FOR LINDAU FOR NOVEMBER 30th 1970

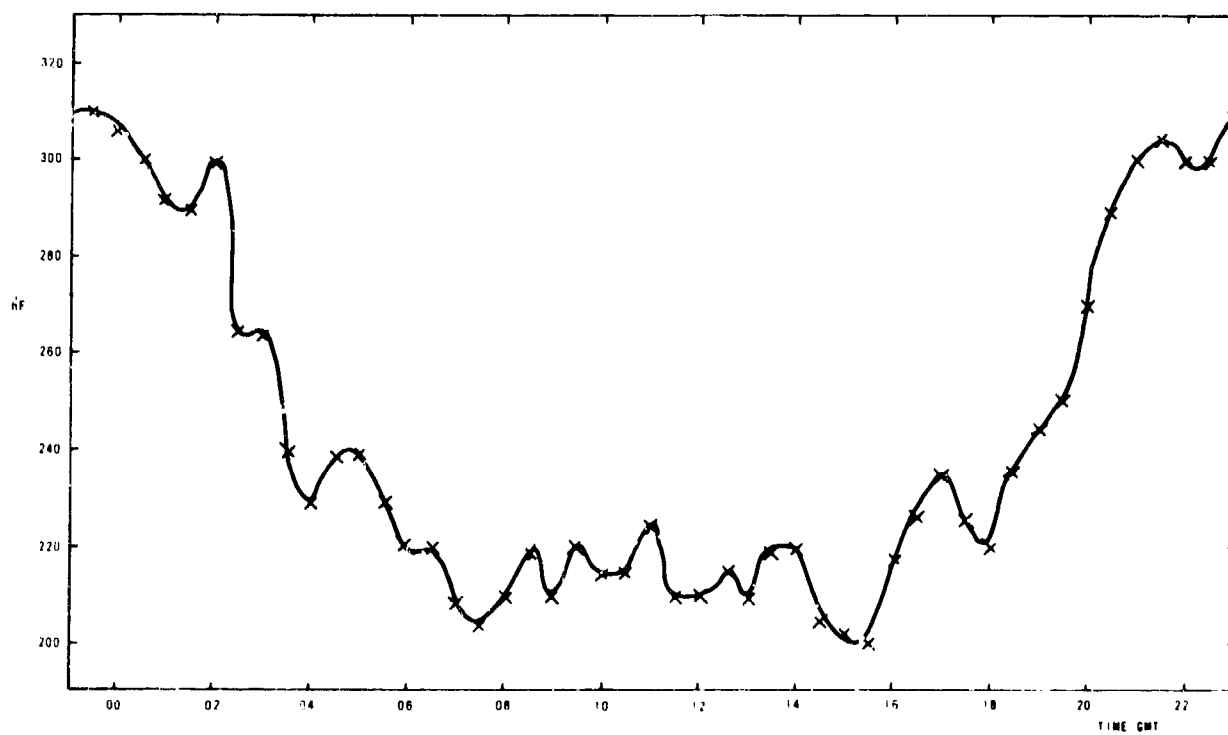


FIG.17. THE GRAPH OF $h'F$ FOR LINDAU FOR DECEMBER 2nd 1970

IONOSPHERIC TILT MEASUREMENTS NEAR THE MAGNETIC DIP EQUATOR

by

R.F.Treharne

Australian Defence Scientific Service
Weapons Research Establishment
South Australia

389

MESURE DES PENTES DE L'IONOSPHERE AU VOISINAGE DE L'EQUATEUR MAGNETIQUE

par

R.F. Treharne

SOMMAIRE

Des observations, du type Bramley et Ross, de la pente de l'ionosphère ont été effectuées au voisinage de l'équateur magnétique. De jour, ces observations étaient entravées par la présence continue d'irrégularités intenses dans la région E, mais les pentes observées semblaient plus marquées, et présentaient un aspect systématique que l'on ne voit pas aux latitudes tempérées. Elles étaient dirigées vers l'est dans la journée, et inversaient leur direction au coucher du soleil pendant les mois d'équinoxe. Le soir, si l'F diffus était absent, on pouvait observer plus clairement les pentes de la région F. Ces pentes observées le soir étaient beaucoup plus importantes, et duraient beaucoup plus longtemps qu'aux latitudes tempérées ; elles présentaient, en outre, des variations plus rapides et moins marquées, rappelant dans une certaine mesure celles de Bramley et Ross, et qui pouvaient être attribuées aux ondes de gravité. On dispose des résultats d'observations effectuées au cours de trois nuits, l'une en hiver, les deux autres en été. Dans les trois cas, la pente maximale (9 degrés) avait lieu aux environs de 21 heures (heure locale), moment où se produit habituellement l'augmentation équatoriale en h'F après le coucher du soleil ; cependant, dans le premier cas (hiver) la direction était le Nord, alors que dans le second (été), c'était l'Ouest, et dans le troisième (été également), c'était l'Est.

Au cours de ces trois nuits, on put voir les effets des variations de faible amplitude ; celles-ci présentaient les caractéristiques aléatoires habituelles, et au cours de deux de ces nuits, on put identifier les effets des ondes de gravité. Ces dernières semblent provoquer des pentes de quelques degrés d'amplitude, d'une durée de vingt minutes environ, provenant du nord en hiver et de l'ouest en été. On a pu estimer cette direction à partir des mesures directionnelles, et on a déterminé la direction de propagation à partir de l'asymétrie de la variation de pente avec le temps ; les vitesses (49 à 197 mètres par seconde), les longueurs d'onde (38 à 378 km) et les déplacements verticaux (0,13 à 2,21 km) ont été calculés à partir d'un modèle simple de perturbation ionosphérique itinérante. Les variations de faible amplitude ont été séparées des composantes plus importantes en retranchant les valeurs lissées des pentes.

IONOSPHERIC TILT MEASUREMENTS NEAR THE MAGNETIC DIP EQUATOR

R.F. Treharne
Australian Defence Scientific Service
Weapons Research Establishment
South Australia

SUMMARY

Observations of the Bramley and Ross type of ionospheric tilt have been made near the magnetic dip equator. During the daytime these observations were hindered by the continuous presence of the intense irregularities in the E region but the observed tilts appeared to be larger and to have a systematic tilt (bias) not seen in temperate latitudes; the bias was to the east during the daytime and reversed in direction at sunset during the equinoctial months. During the evening, if spread F was absent, the tilts of the F region could be observed more clearly. These evening tilts were of much greater magnitude, had a much longer time scale than in temperate latitudes, and had superposed faster variations of a smaller scale, not unlike those of Bramley and Ross, which might be attributed to gravity waves. Three nights of observations are available, one in winter, two in summer. In all three cases the maximum tilt (9 degrees) occurred near 2100 hours local time, the time normally associated with the equatorial rise in h'F after sunset, but in the first case (winter) the direction was north, whereas in the second (summer) it was west and in the third (also summer) it was east.

On all three nights the effects of small scale variations were seen; these had the usual random characteristics and on two of the nights the effects of gravity waves were identified. The latter appear to cause tilt amplitudes of a few degrees, some twenty minutes in duration, and in winter, appeared from the north whilst in summer the direction was from the west. This direction was estimated from the directional measurements and the sense of the direction of travel was determined from the asymmetry of the tilt variation with time; the velocities (49 to 197 metres per second), the wavelengths (38 to 378 kilometres) and the vertical displacements (0.13 to 2.21 km) were calculated from a simple model of the TID. The small scale variations were separated from the larger components by subtracting the smoothed tilt values.

1. INTRODUCTION

Observations were made by Bramley and Ross (1951) in Southern England of the direction of arrival of short radio waves reflected at the ionosphere at near vertical incidence; these observations were related to local (usually travelling) perturbations of the ionisation density of the ionosphere. Bramley (1952) studied the statistical properties of the perturbations in terms of time and distance variations. The apparatus consisted of spaced transmitters which emitted pulses and a three dimensional direction finder which employed phase comparison techniques (Ross et al., 1951). Observations (Treharne et al., 1965, 1969; Treharne 1969) made in South Australia in 1960 and in 1968 (using similar but somewhat improved techniques) confirmed that, as might be expected, tilts with similar characteristics were seen in southern temperate latitudes.

This paper describes some observations of this type which were made near the magnetic equator (at 3 degrees north dip angle) on a few occasions in 1969/71. During the daytime the influence of equatorial sporadic E irregularities (Cohen, 1967) dominated the observations; at night two situations may exist, when spread F is formed and a second when very slow tilts of greatly increased magnitude are observed. Measurement of the F region was made difficult during the daytime by the presence of the magnetic equatorial sporadic E (MEQES) irregularity (Treharne, 1963) through which the rays must pass to and from the F region. Even so, some measurements have been possible but it was not practicable to make continuous series of measurements of the tilt every few minutes as may be done when the MEQES irregularities are absent. At night, when spread F was absent, excellent tilt measurements were made. These evening tilts contained at least three components; a very slow, large component, medium scale components which appeared to be due to travelling ionospheric disturbances (TID), and small scale components of substantially random nature.

The daytime and sunset tilts may be related to the drifts which have been observed near the equator (Harrison, 1965); the north south components of both drifts and tilts were small, the east west components of both showed reversals at dusk and the increased variability of the tilts at dusk corresponded to the increased velocity of the drifts at this time. However, the scales of these two types of observations are different; the tilt bias may have its origin in long term ionisation gradients of a diurnal nature. Certainly the large scale components of the evening tilts appear to be associated with the post sunset rise in h'F (Treharne, 1971) again of a diurnal nature. The small scale tilts appear to be of a substantially random nature, as reported by Bramley and Ross (1951).

This paper is concerned primarily with the medium scale components of the evening tilts which appear to be caused by TID's and are therefore of some interest to this conference on gravity waves.

2. APPARATUS

The apparatus used is shown diagrammatically in figure 1. This is similar to that described elsewhere (Treharne et al., 1969; Treharne 1969). Only a brief description will be given here. A 5 kW pulse transmitter (pulse repetition rate 50 pulses/s of pulse width 100 μ s) and a 25 m vertical delta antenna whose plane was oriented at 45 degrees to the direction of the earth's magnetic field were used to illuminate the ionosphere overhead. Echoes from the ionosphere were received on a direction finder comprising four horizontal dipoles oriented in the direction of the earth's magnetic field and each located at the corners of a square of 100 m diagonal and with two sides in line with the earth's magnetic field. The four dipoles were used in pairs to form two orthogonal arms of a three dimensional interferometer; measurements were made of the phase difference of the waves with respect to each arm direction in turn.

Each dipole was connected via balancing transformers and coaxial cables of equal length to the inputs of two h.f. hybrid transformers giving sum and difference outputs for the first pair of dipoles and similar outputs for the second pair of dipoles. Solid state diode switches were used to connect the signals from each arm in turn to a twin channel receiver which converted them to an intermediate frequency of 100 kHz, maintaining phase and amplitude equality of transmission through each channel of the system. The i.f. signals were displayed on a cathode ray oscilloscope (CRO) but a fixed 90 degree phase shift network was inserted in one lead to the CRO to compensate for the fixed 90 degree phase shift introduced by the hybrids. When a simple wavefront impinged upon the antenna system the signals displayed formed a straight line of slope ϕ which was a function of direction of arrival of the normal of the wavefront with respect to the direction of the arm. Thus, for the first arm,

$$\phi_\alpha = \frac{\pi d}{\lambda} \cos \alpha \quad (1)$$

and for the second arm,

$$\phi_\beta = \frac{\pi d}{\lambda} \cos \beta \quad (2)$$

where $\phi_{\alpha, \beta}$ is the angle of the trace on the CRO

- α, β are the direction angles of the wavefront normal with respect to the first and second arms respectively
- λ is the wavelength of the radiowaves
- d is the diagonal spacing between the dipoles

The direction angles, being large for near vertical echoes, were used to obtain approximate angles from the zenith δ and δ_0 by subtraction from 90 degrees. These angles, which are measured from the zenith, may be regarded as orthogonal components of the direction of the returning rays reflected normally at the tilted ionosphere. After correction for the orientation of the arms of the antenna with respect to the true north, these angles may be plotted in cartesian coordinates.

The intensity of the CRO display was normally adjusted so that the trace was dark. Automatic circuits were used to brighten the display provided both of the following conditions were met simultaneously :

- (a) the phases of the two signals on the CRO were equal (to within a predetermined tolerance, typically 10 degrees) for a period of time corresponding to an adjustable number of i.f. cycles (typically 8 cycles); this tested the wavefront and avoided asking the simple interferometer to attempt readings when the wavefront was complex and beyond its resolving ability,
- (b) the time of observation was restricted to the 200 μ s which followed a predetermined and adjustable time delay after the transmitter pulse.

Provision was made to disconnect automatically all the feeders from the receiving dipoles for the duration of each transmitter pulse to avoid saturating the receiver.

3. OBSERVATIONS

Daytime observations, including some at sunset, were made intermittently for a few months early in 1969. With the exception of short periods immediately followed a period of normal Es which occurred sometimes in the afternoon, all the daytime and sunset observations were made with great difficulty due to the modulation of the direction of arrival of the rays from the F region by passage through the MEQES irregularities. A feature of the daytime results was a bias to the east of the order of 2 degrees which reversed, increased to 3.5 degrees to the west and became more variable towards sunset. These were spot observations, made at isolated intervals; it was not practicable to make continuous sets of observations.

During the daytime (0600 to 1730) the average tilt was 2 degrees east with a northerly scatter of up to 1 degree and southerly scatter of 1.2 degrees; on one occasion alone did the tilt move to the west (0.5 degrees). At sunset (1830 to 1930) the average tilt was 3 degrees to the west with a northerly scatter of up to 1.8 degrees and westerly scatter up to 5.3 degrees; the most easterly tilt observed during the sunset period was only 1.8 degrees (Treharne, 1971).

During the evening (1930 to 2400) observations have been made on a few occasions, viz., 26 and 28 November 1970, 20 and 21 May 1971. On the 28 November spread F was found to be present and tilt observations were not taken due to the very variable nature of the direction of the returns from the F region. However, it was noted that at 6 MHz the A-scan, although spread and varying rapidly in a manner reminiscent of the type of echoes seen from ground backscatter, did appear to have a favoured time delay for which echoes were returned strongest and most frequently. This behaviour was consistent with the ionograms associated with a rectangular equatorial spread F which has been described by Calvert and Cohen, 1961.

On the evenings of the 26 November 1970, 20 and 21 May 1971, on the other hand the spread F condition was absent but some remarkable tilts were observed; these tilts were strongly biased to the north and to a lesser extent to the east, their magnitudes were larger than observed in temperate latitudes and their period was several times greater than reported to date. The north component of tilt is shown as a function of local time in figure 2. Starting at 2000 hours (5 degrees) the tilt slowly increased, reaching a peak of 9 degrees north at 2100 hours, then slowly reduced to about one degree north at 2300 hours. The corresponding easterly tilt variation is shown also in figure 2; it has less magnitude although there is a distinct maximum easterly tilt of some 6 degrees at the same time as the peak in the northerly tilt, namely at 2100 hours. It should be noted that the general smooth shape of the northerly tilt variation of figure 2, is also found in the virtual height variations (see figure 3) and that the peak in the latter appears about 30 min earlier than the peak in tilt.

Measurements of virtual base height (h'F) and the virtual height at 6 MHz have been scaled from the ionograms and plotted in figure 4. Again there is a peak in both parameters around 2000 hours and a steady fall of the order of 100 km during the following two hours or so.

On the 20 May 1971 the peak tilt occurred at 2010 hours and had a magnitude of 6.5 degrees east with a corresponding south component of 2 degrees and a height peak (at the same time) of 345 km. On the other hand, on 21 May the peak tilt was 9 degrees to the west and had a south component of 2 degrees. Plots of the evening tilts are shown in figures 5, 6 and 7.

The evening tilts show small departures from the smoothed tilt which might be attributed to TID's. These will be examined in greater detail in section 5 below.

4. OBSERVATION OF TRAVELLING IONOSPHERIC DISTURBANCES BY THE TILT METHOD

Bramley and Ross (1951) published a good example of the observation of a TID by means of ionospheric tilt measurements: series of such measurements (made at about minute intervals at two stations about 27 km apart in an east west direction) were plotted in their figure 10. The characteristic swoop of the tilt values to a maximum, in this case in the direction 125 degrees, was seen clearly at both stations. The disturbance was seen to occur at Winkfield after Theale by a minute or two, thus confirming that the direction of travel was 125 degrees and not the reciprocal of 305 degrees (the opposite sense of direction). Thus the direction, including the sense of direction, was given by the direction of the maximum value of the tilt. It should be noted that the sense of the direction of travel of the TID may also be inferred from the shape of the variation of the component of tilt along the apparent direction of travel knowing the shape of these disturbances. The latter is illustrated in figure 8. An observer on the ground sees rays reflected at normal incidence from the rippled ionosphere; these rays are seen to move slowly from the zenith as the TID approaches, reach a maximum value of tilt, suddenly fall through zero tilt as the peak of the TID passes overhead, and then take negative values as the trailing edge of the TID passes. This behaviour can be seen in the Theale tilts by resolving them along the 125 direction as has been done in figure 9, using a solid line. The direction of travel of the TID is given by the direction of the SLOWLY changing tilt components (a) which is followed by a FAST return of the tilt value (b) in figure 9.

A theoretical shape for this curve has been described by George (1972) following his figure 8(c). This shape is illustrated by the broken line in figure 9. Clarke (1972) has used an approximation to the shape of a TID consisting of two contiguous sinewaves of different wavelength. He has shown that the horizontal phase velocity of propagation of the TID, V_{px} , is given by,

$$V_{px} = 2h (\tan \delta_1 + \tan \delta_2) / (T - 2\tau) \quad (3)$$

where h is the unperturbed reflection height

δ_1 is the modulus of the maximum tilt angle on the leading edge

δ_2 is the modulus of the maximum tilt angle on the trailing edge

T is the period of the TID

τ is the time interval between the occurrence of the maximum tilt angle on the leading and the maximum tilt angle on the trailing edges

The horizontal wavelength of the TID is

$$\lambda_x = V_{px} T \quad (4)$$

The total vertical displacement is

$$I = 2\lambda_x \tan \delta_1 \cdot \tan \delta_2 / \pi (\tan \delta_1 + \tan \delta_2) \quad (5)$$

It is possible, therefore, to measure at a single site a number of the properties of TID's by observations of the apparent ionospheric tilts caused by the passage of the TID's overhead. However in some cases the tilts produced by the TID's have superposed large tilt components due to diurnal effects; this is particularly noticeable near the magnetic equator. If the TID effects are to be studied it is necessary to remove the diurnal components by subtracting the tilt values observed from the smoothed tilts. This introduces a degree of uncertainty in the central reference of the tilt information. It is no longer practicable to measure δ_1 and δ_2 separately, only to measure their sum, Δ .

Thus,

$$\Delta = \delta_1 + \delta_2 \quad (6)$$

Then, for small values of tilt angle, equation (3) becomes:

$$V_{px} = 2h \Delta / (T - 2\tau) \quad (7)$$

The wavelength, λ_x , is given by equation (4) but the total vertical displacement, I , cannot be obtained from equation (5) due to the smoothing technique used.

For small tilt angles equation (5) may be simplified to

$$I = 2\lambda_x \delta_1 \delta_2 / \pi \Delta \quad (8)$$

Put $\kappa = \delta_2 / (\delta_1 + \delta_2)$

$$(9)$$

Then

$$I = 2\lambda_x \Delta \kappa (1 - \kappa) \quad (10)$$

where Δ is measured in radians.

The value of κ may be estimated from the data of Bramley and Ross (1951). For example,

$$\kappa = 0.36$$

Then equation (9) becomes

$$I = 2.56 \times 10^{-3} \Delta \lambda_x \quad (11)$$

where Δ is measured in degrees.

It is not clear that this value of κ seen in England is necessarily applicable to the equatorial site, however, it may give an indication of the order of magnitude of the displacement of the TID's seen.

5. MEDIUM SCALE CONSTITUENT OF TILT DUE TO TID

In addition to the large slow variation in the tilts seen near the magnetic equator smaller scale variations occur, see figure 7. These smaller and faster constituents may be separated from the total tilt by the subtraction of the smoothed constituent from the total tilt values. The slow variation has been removed and the TID component plotted in figure 10. Note that the scale of figure 7 is one tenth that of figure 10. The effects of two TID's may be seen in figure 10; both cause the pattern to be elongated in an approximately east and west direction (more precisely along 100 or 228 degrees from north).

Since it is necessary to remove the large slow component of tilt by subtracting the smoothed tilt values, the values of figure 10 have no central reference. Even so, many of the properties of the TID may still be obtained as discussed in paragraph 4 above.

At least eight TID's have been identified in the three nights for which observations are available near the magnetic equator. The characteristics of these TID's are given in summary in Table 1. This table contains the place of observation, date, season, local time, the number of TID's observed, the duration of the TID (T), the maximum tilt interval (τ), the quantity $(T - 2\tau)$, the direction of travel of the TID, the maximum tilt excursion ($\delta_1 + \delta_2 = \Delta$), the height of unperturbed reflection (h), the horizontal phase velocity V_{ph} , the wavelength of the TID (λ_{TID}), the vertical displacement (I) calculated on the basis of $\kappa = 0.36$, the sounding frequency of the radiowaves, and the geomagnetic planetary index (K_p). For comparison purposes Table 1 also has similar characteristics for TID's observed in South Australia (Treharne, et al., 1968), in England (Bramley and Ross, 1951) and in Queensland (Clarke, 1972).

6. DISCUSSION

Although the tilt data available from the region of the magnetic equator is very limited it appears that the TID's seen by Bramley and Ross (1951) and discussed by George (1972) certainly do traverse the equatorial region where they may be observed by the tilt method. In the evenings (if spread F is absent) several TID's have been observed having durations of the order 20 minutes. Their directions appear to be seasonally dependent. For this Asian site just north of the magnetic equator, the direction of travel of these TID's in local winter was from the north; in local summer the direction of travel of the TID's was from west to east. The winter observations favour the suggestion that TID's may travel from the winter pole; whereas the summer observations favour excitation by some equatorial source (Kent, 1965).

Observations of layer tilts have also been made in Canada by Burtnyk, et al (1962) and recently more observations have been made by MacDougall (1966) in England. Stirling, et al (1971) have made observations of TID's at the magnetic equator using two incoherent scatter systems spaced east and west. They observe TID's travelling in a north/south direction thereby confirming the theoretical predictions made by Hooke (1970). On this basis the west-east TID's reported near the magnetic equator (see Table I) are unexpected.

Davies (1968) has observed by a Doppler technique in equatorial Africa swoopers which he describes as asymmetric atmospheric waves propagating from west to east with velocities in the range 100 to 150 m/s. These swoopers have a period of 60 minutes, occur at night, have a wavelength of the order of 400 km, appear to be associated with the occurrence of Spread F (not its absence), and have a marked minimum in summer. It is unlikely that swoopers are the same type of disturbance as described in this paper.

The TID's seen near the magnetic equator appear to be somewhat weaker, slower and shorter than those seen by a similar technique in England, South Australia and Queensland.

7. CONCLUDING REMARKS

Observations of the direction of arrival of radio waves reflected at the ionosphere at near vertical incidence close to the magnetic equator have shown tilts having:

- a systematic bias to the east of two degrees during the day time
- a three degree systematic bias (with greater variability) to the west at sunset
- large values in the evenings containing slow components which appear to be related to the post sunset peak in h'F, medium components which appear to be caused by TID's and small components of a random nature

In this paper the characteristics of a few equatorial TID's are described by observation of the ionospheric tilts which they produce. It seems possible that the TID's seen in equatorial regions at night may have more than one origin, perhaps polar in winter and equatorial in summer. They may be of a different character; certainly the summer TID's appeared to move more slowly than the winter TID's. The latter were directed north to south whereas the summer TID's were directed west to east. These west to east TID's have not been observed near the magnetic equator by the tilt method before and current theory suggests that their probability of occurrence is low.

REFERENCES

1. Bramley, E.N. and Ross, W. 1951 "Measurement of the Direction of Arrival of Short Radiowaves Reflected at the Ionosphere" Proc. Royal Soc., London, Series A, Vol. 207, pp 251-267.
2. Bramley, E.N. 1953 "Direction-Finding Studies of Large-scale Ionospheric Irregularities". Proc. Royal Soc., London, Series A, Vol. 220, pp 39 - 61
3. Burtnyk, N. McLeist, C.W. and Wolfe J. 1962 "Ionosphere layer tilts at Ottawa, Canada." Canadian Journal of Physics, Vol. 40, pp 1614 - 1619

4. Calvert, W. and Cohen, R. 1961 "The Interpretation and Synthesis of Certain Spread F Configurations appearing on Equatorial Ionograms." Jnl. Geophys. Res., Vol. 66, No. 10, pp 3125 - 3140, October
5. Clarke, A.H. 1972 "Ground based observations of ionospheric irregularities at Brisbane." University of Queensland. Ph.D. Thesis.
6. Cohen, R. 1967 "The Equatorial Ionosphere Chapter III-4." The Physics of Geomagnetic Phenomena, Vol.1, ed. Matsushita and Campbell, Academic Press, N.Y.
7. Davis, K. and Chang, N.J.F. 1968 "Radio-Doppler observations of the ionosphere near the magnetic equator." NATO-AGARD-RPC-Symposium on Scatter Propagation of Radio Waves. Sandefjord, Norway, August
8. George, P.L. 1972 "Ray tracing of Gravity Wave Perturbed Ionospheric Profiles." NATO-AGARD-RPC Conference on Effects of Acoustic Gravity Waves on Electromagnetic Wave Propagation, Paper No. 26, Wiesbaden
9. Harrison, V.A.W. 1965 "Ionospheric drift measurements at Singapore." Report on Equatorial Aeronomy, ed. Mendonca, C.N.Pq., C.N.A.E., LAF 32, Sao Jose dos Campos Brazil, November, p290.
10. Hooke, W.H. 1970 "The ionospheric response to internal gravity waves, 1, The F2 region response." J. Geophys. Res., Space Physics, 75, 28, pp 5535-5544.
11. Kent, G.S. 1965 "Ionospheric Drifts - Review Paper." Report on Equatorial Aeronomy, ed. Mendonca, C.N.Pq., C.N.A.E., LAF 32, Sao Jose dos Campos, Brazil, November
12. Ross, W., Bramley, E.N. and Ashwell, G.E. 1951 "A Phase Comparison Method of Measuring the Direction of Arrival of Ionospheric Radio Waves." Proc. I.E.E., Vol. 98, Part III, p294, July
13. Sterling, D.L., Hooke, W.H. and Cohen, R. 1971 "Travelling Ionospheric Disturbances observed at the Magnetic Equator." Jnl. Geophys. Res., Vol. 76, No. 16, June, pp 3777-3782.
14. Treharne, R.F. 1963 "Propagation Properties of the Ionospheric E Region Near the Magnetic Equator." Proc. I.R.E.E. Australia, Vol. 26, No. 9, pp 275-283, September.
15. Treharne, R.F., McCue, C.G., Jeffrey, Z.R. and Hewett, B.S. 1965 "Some Characteristics of the Propagation of Skywaves over Short Ionospheric Paths." Proc. I.R.E.E. Australia, Vol. 26, No. 8, p 245-254, August.
16. Treharne, R.F. 1969 "The Observation of Local Ionospheric Movements Using Directional Backscatter Techniques." Symposium on Atmospheric Physics, ANZAAS, Adelaide Congress.
17. Treharne, R.F., Raymond, A.L.J., and Ellard, R.M. 1969 "Ionospheric Tilt Observations in South Australia." Abstracts of Technical Papers, 12th National Radio and Electronics Engineering Convention, Sydney, Australia, p 164.
18. Treharne, R.F. 1971 "Ionospheric tilts in the F Region in the absence of Spread F near the Magnetic Equator." Weapons Research Establishment, Technical Note A199 (NP), May. South Australia.

TABLE I

PLACE	MAGNETIC EQUATOR *			STH. AUST +	ENGLAND *	QUEENSLAND **
DATE	26 NOV 1970	20 MAY 1971	21 MAY 1971	26 JAN 1968	15 FEB 1950	8 MAY 1971
SEASON	WINTER	SUMMER	SUMMER	SUMMER	WINTER	WINTER
LOCAL TIME	2130 (2018-2243)	1940 (1941-1955)	2031 -	1243 -	1200 -	0800 -
NUMBER OF TID'S	5	2	1	1	1	1
DURATION, T, (mins)	23 (15-32)	14 (13-15)	30 -	22 -	25 -	28 -
MAX TILT INTERVAL τ (mins)	9 (5-15)	4 (4-5)	9 -	8 -	9 -	8 -
(T - 2 τ), (mins)	5 (2-6)	5 -	12 -	6 -	5 -	12 -
DIRECTION OF TRAVEL	173 (135-225)	67 (45-90)	108 -	125 -	125 -	10 -
TILT EXCURSION $\delta_1 + \delta_2 = \Delta$ (deg)	2.4 (2.2-2.7)	1.7 (1.3-2.2)	4.5 -	6.5 -	5.5 -	12.5 -
HEIGHT, h, (km)	328 (275-370)	332 (325-340)	366 -	350 -	300 -	260 -
VELOCITY, V_{px} (m/sec)	129 (87-197)	68 (49-87)	80 -	217 -	192 -	170 -
WAVELENGTH OF TID, λ_x (km)	193 (96-376)	57 (38-77)	144 -	286 -	265 -	280 -
DISPLACEMENT, I ($\kappa = 0.36$) (km)	1.18 (0.67-2.21)	0.28 (0.13-0.44)	1.65 -	4.75 -	3.73 -	9 ** -
SOUNDING FREQUENCY, MHz	5.7	5.7	5.2	6.71	6.12	4.7 **
GEOMAGNETIC PLANETARY INDEX Kp	17	10	10	-	-	22

() Numbers in brackets indicate range of values observed.

* Bromley and Ross, 1951, Theale, England.

+ 3° north magnetic dip, South East Asia.

+ Treharne, et. al., 1969, St. Kilda, South Australia.

** Clarke, 1972, Brisbane, Queensland; displacement calculated from equation 5; swept frequency system.

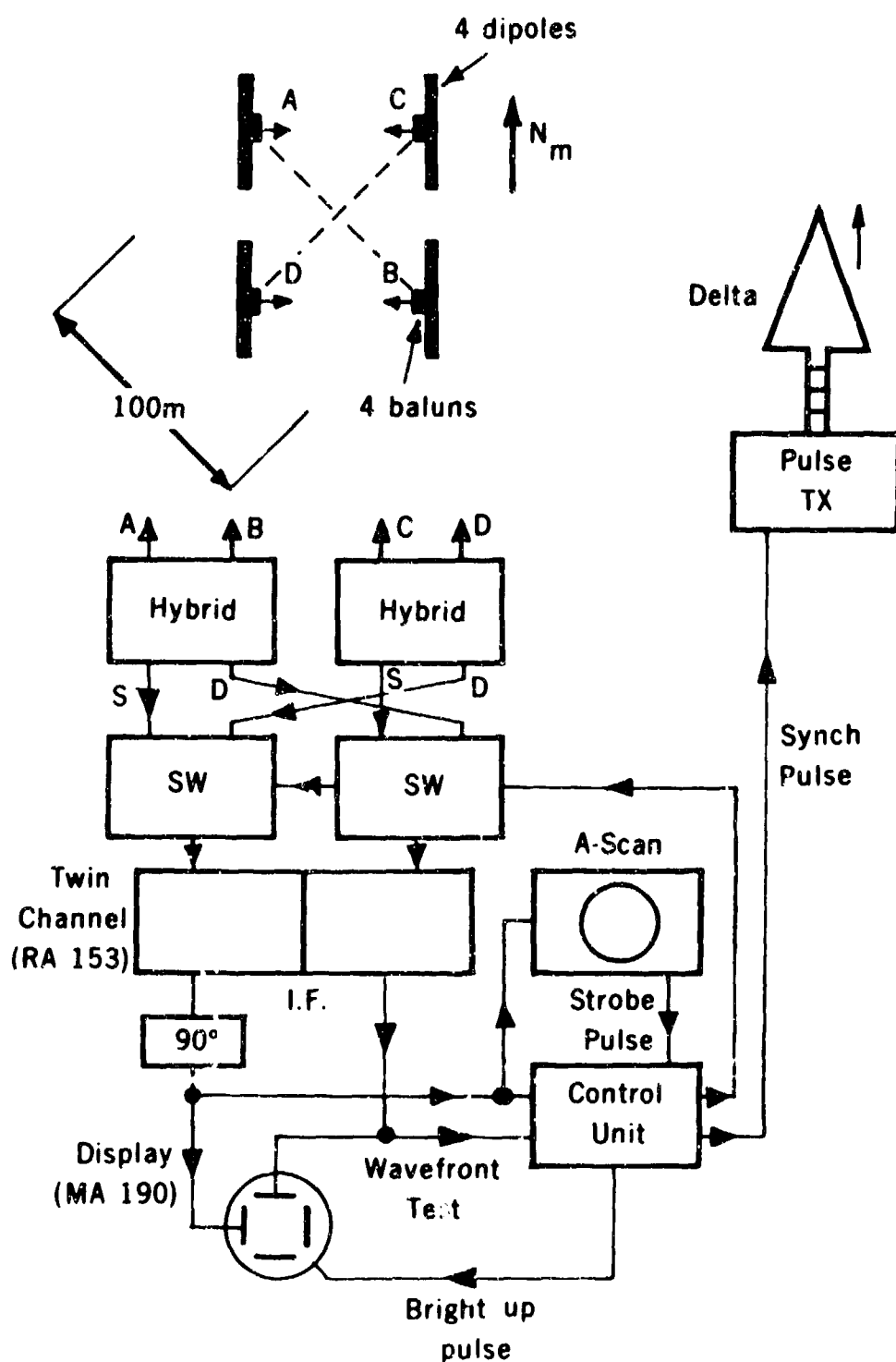


Figure 4 Block diagram of apparatus used for the observation of ionospheric tilts. The ionosphere is illuminated with pulses of radio waves by means of a pulse transmitter and delta antenna. Echoes are returned at greatest strength for rays which are "normal" to the apparent surface of the ionosphere. The direction of arrival of these echoes is measured by means of four dipole which form the two arms of an orthogonal interferometer. A wavefront test is applied automatically to select moments when the wavefront is simple and capable of resolution by the simple interferometer. A strobe is used to select the small time interval corresponding to the reflection height needed.

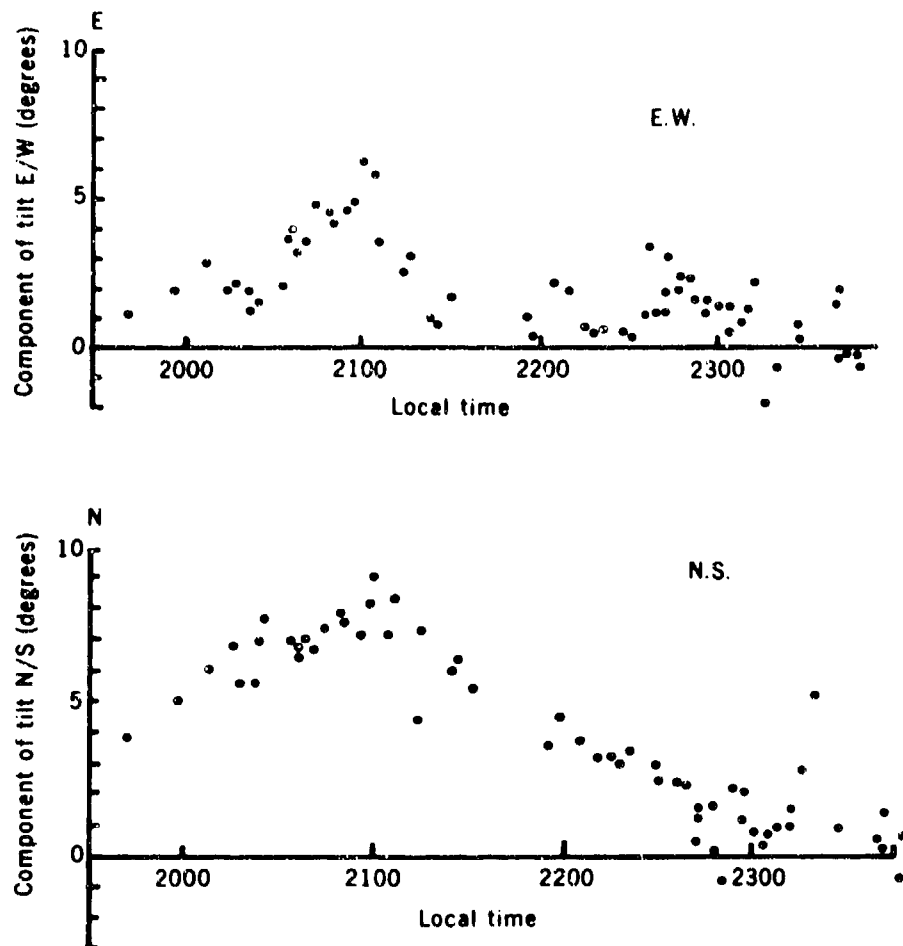


Figure 2 Individual observations of the north or south and the east or west components of the tilt as a function of local time - 26 November, 1970. Location, 3 deg. N magnetic dip, South East Asia.

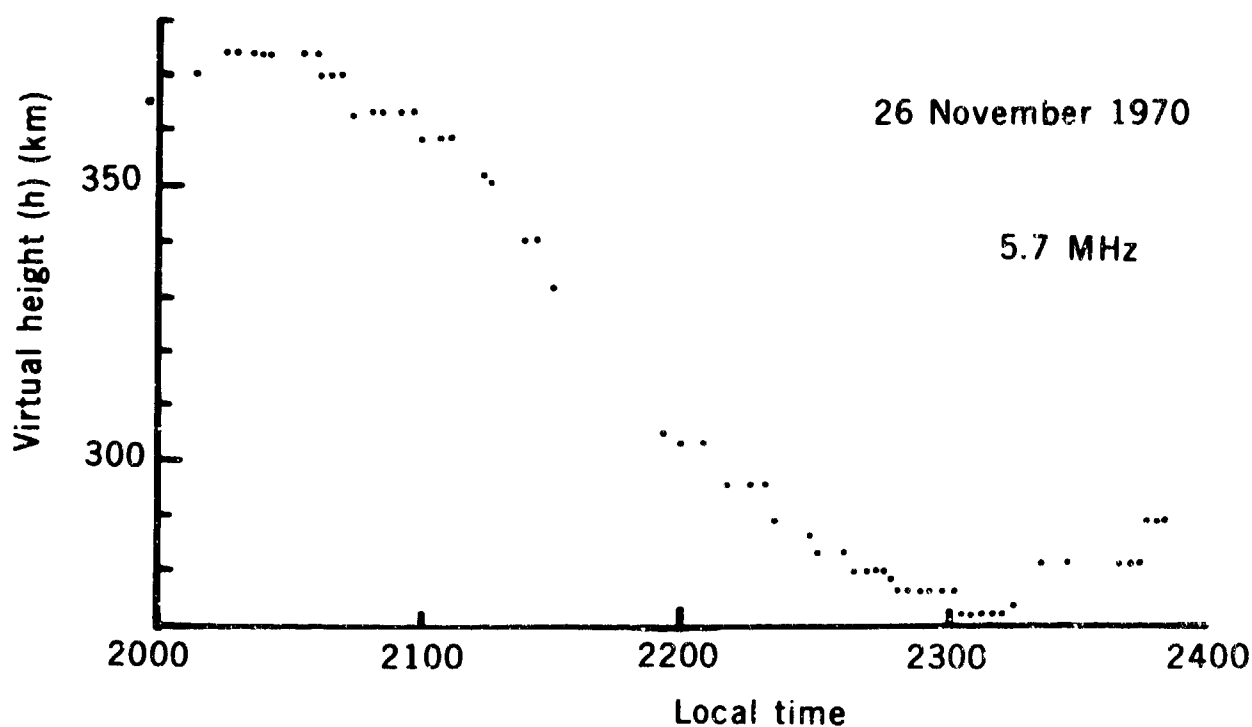


Figure 3 Individual virtual height settings used for the data collected in Figure 2.

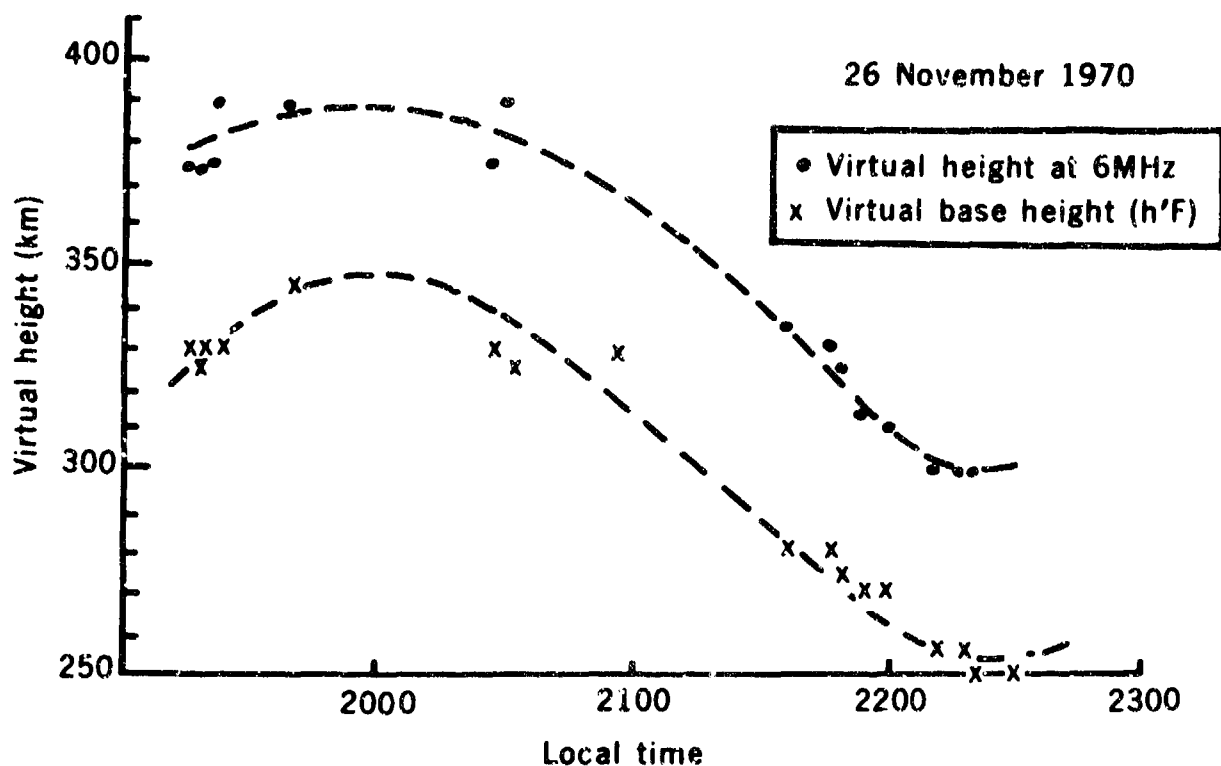


Figure 4 Ionosonde observations of the base height, $h'F$, and the virtual height at 6 MHz for the period covered by Figure 2.

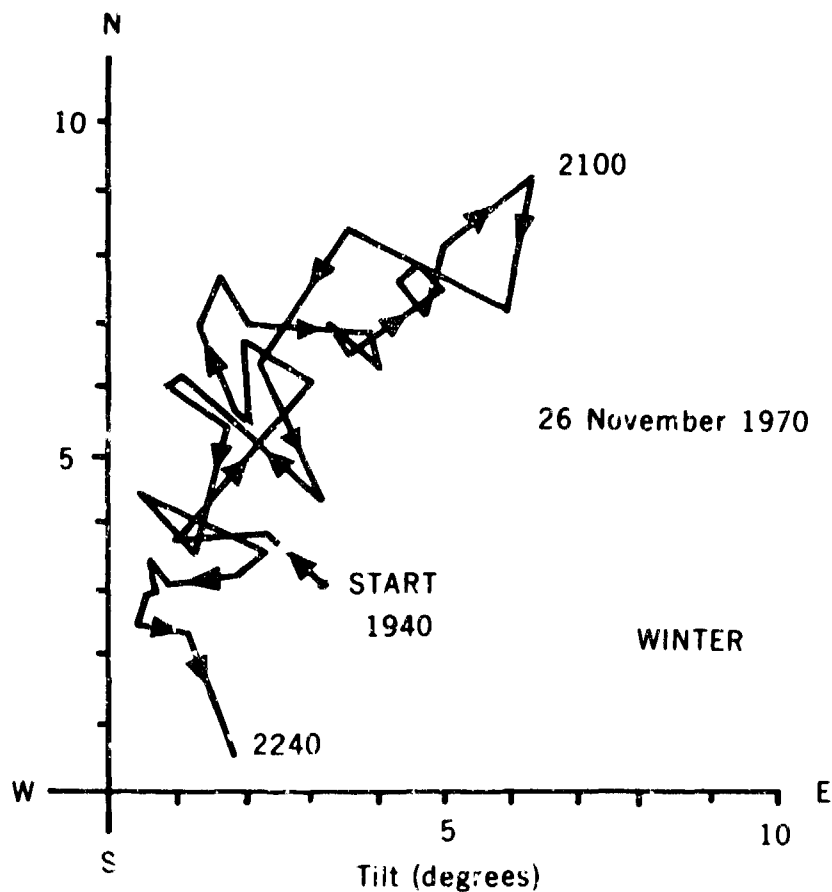


Figure 5 Plot of individual tilt observations made on 26 November, 1970. This is the same data as given in Figure 2.

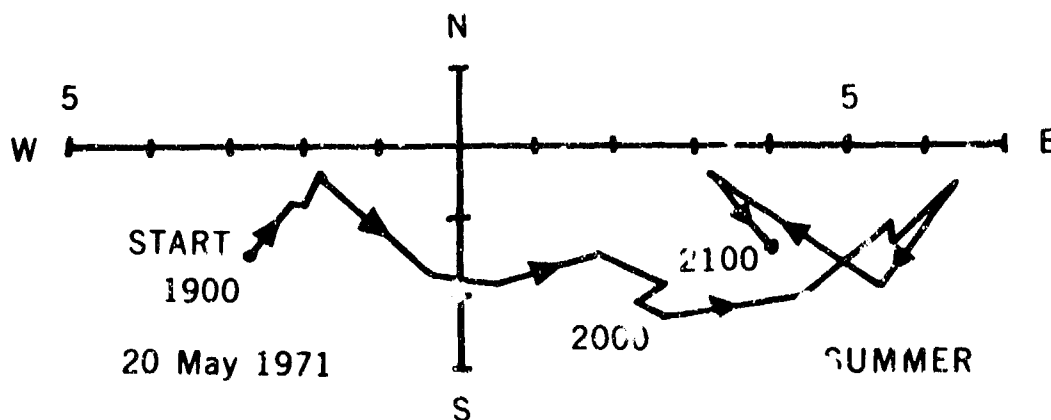


Figure 6 Plot of individual tilt observations made on 20 May, 1971. This is the same data as given in Figure 2.

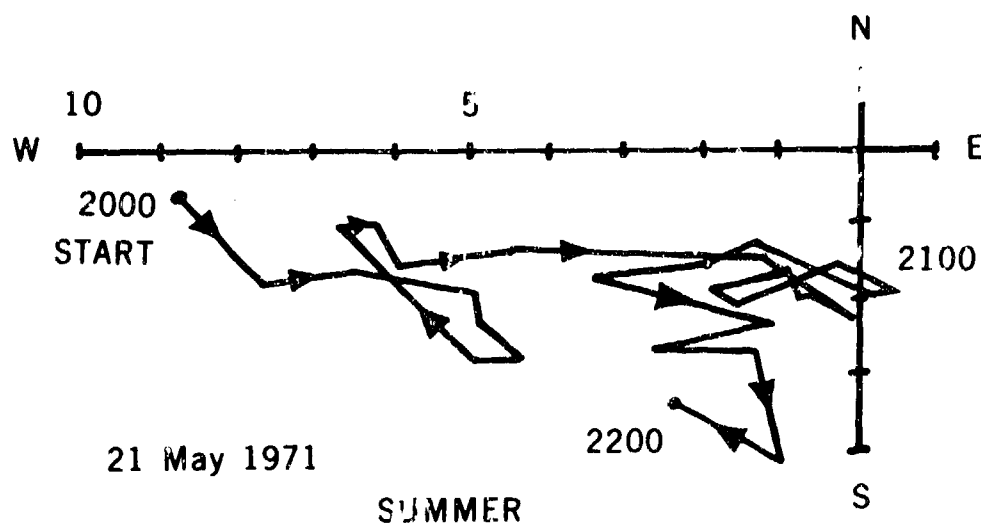


Figure 7 Plot of individual tilt observations made on 21 May, 1971. This is the same data as given in Figure 2.

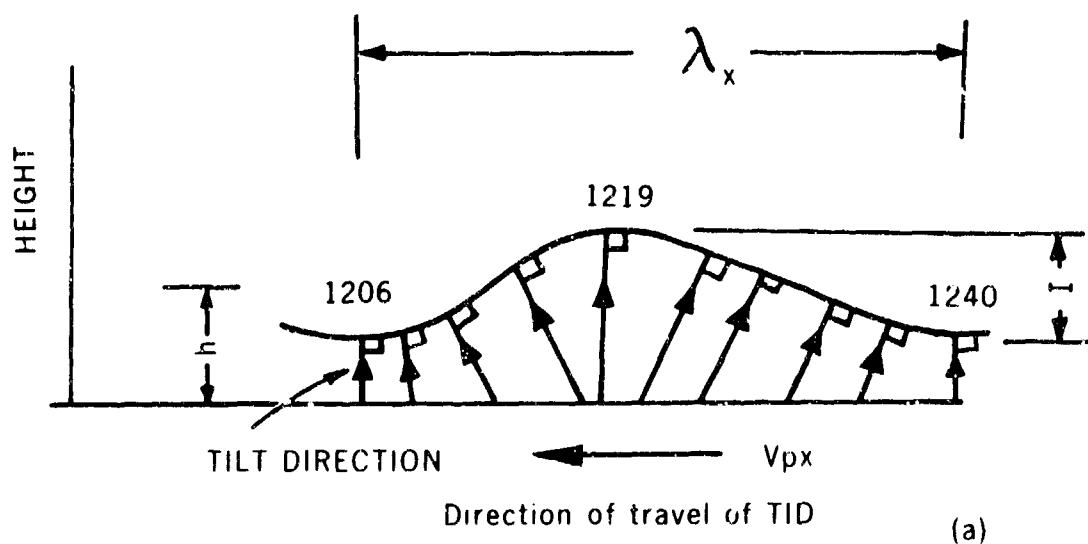


Figure 8 Representation of TID surface showing the variation of apparent tilt as the disturbance passes overhead.

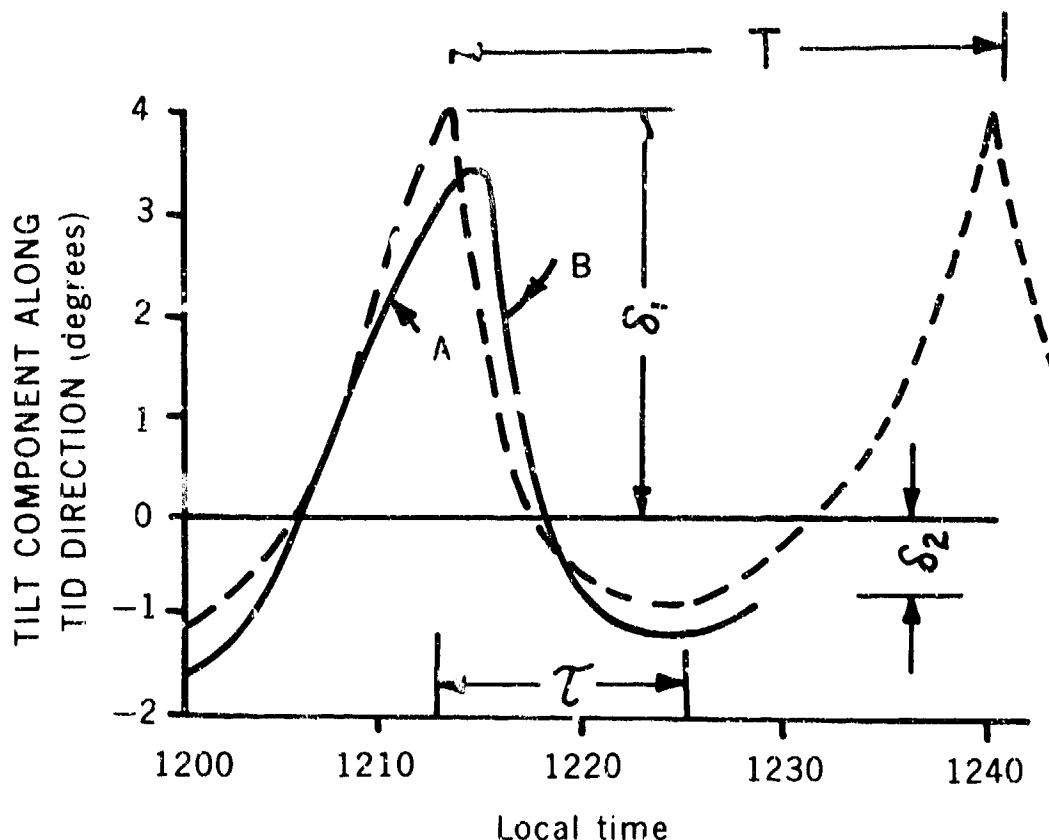


Figure 9 Variation of apparent tilt of returned echo with time. The solid line as observed at Theale by Bramley and Ross (1951). The part marked A corresponds to the slow increase in tilt as the leading edge of the TID approaches; the part B corresponds to a faster change in tilt as the leading edge of the TID approaches its crest. The broken line is an ideal representation of the shape of this characteristic.

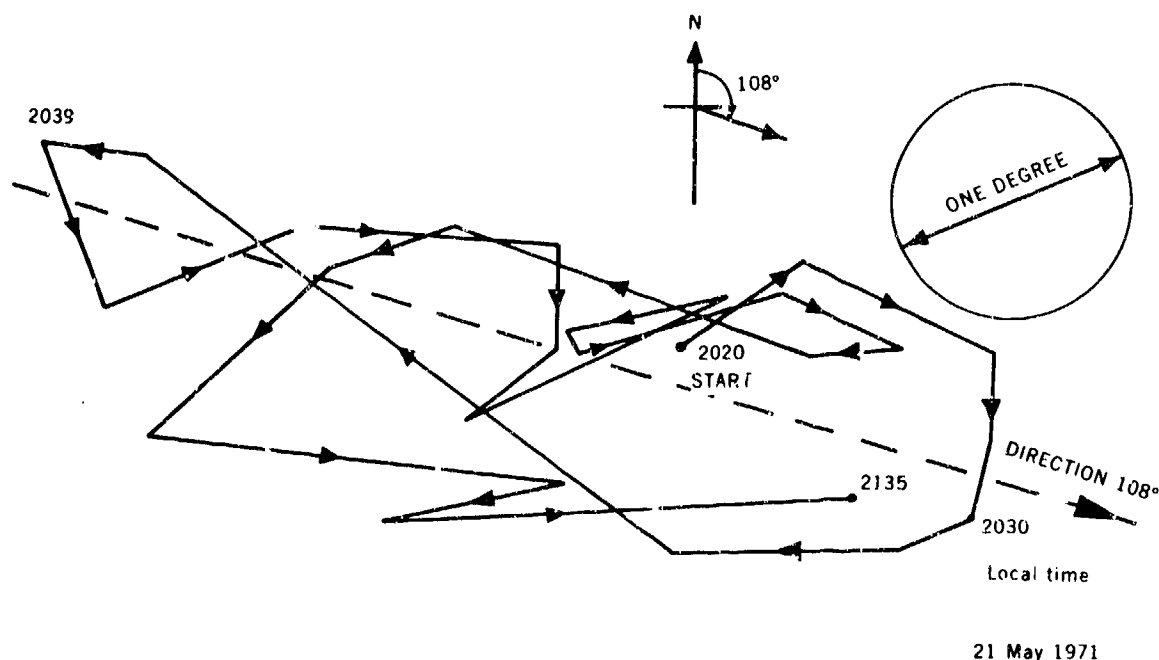


Figure 10 Plot of difference between observed tilt and smoothed tilt value. Scale is enlarged ten times that used for Figures 5 to 7. The direction 108 degrees is identified as the direction of travel of the TID system. The tilt angles are resolved along this direction of travel, the displacements at right angles to this direction are ignored. Two TID's are shown, one starting at 2020 local time and a second finishing about 2135.

ON THE GENERATION AND DETECTION OF ARTIFICIAL ATMOSPHERIC WAVES

by

Ludwik Liszka and Sixten Olsson

Kiruna Geophysical Observatory
S-981 01 Kiruna 1, Sweden

393

PRODUCTION ET DETECTION D'ONDES ATMOSPHERIQUES ARTIFICIELLES

par

L. Liszka et S. Olsson

SOMMAIRE

Les auteurs présentent les résultats préliminaires de détections d'ondes atmosphériques produites par la focalisation d'ondes de choc engendrées par des avions supersoniques. Les trajectoires de vol furent choisies de façon que les ondes acoustiques et de gravité qui suivent l'onde de choc soient focalisées au sol après réflexion par la stratosphère, ou dans la couche E. Des ondes infra-acoustiques furent détectées au sol grâce à un corrélateur infra-acoustique de 2 Hz. Dans la couche E, les ondes furent détectées au moyen d'une technique de sondage vertical modifiée. Les résultats obtenus au cours de 11 vols d'essai montrent que l'on peut faire appel avec succès à la technique de trajectographie pour prédire la propagation des ondes atmosphériques qui suivent les fronts de choc.

ON THE GENERATION AND DETECTION OF ARTIFICIAL ATMOSPHERIC WAVES

Ludwik Liszka
and
Sixten Olsson
Kiruna Geophysical Observatory
S-981 01 Kiruna 1, Sweden

ABSTRACT

Preliminary results of detection of atmospheric waves produced by focussing of shocks generated by supersonic aircraft are presented. The flight trajectories were chosen so that the acoustic gravity waves following the shock front were focussed on the ground after reflection from the stratosphere, or in the E-layer. Infra-acoustic waves were detected on the ground using a 2 Hz infra-acoustic correlator. At the E-layer, the waves were detected using a modified vertical sounding technique. Results obtained during 11 test flights have shown that the ray tracing technique may be successfully used for predicting the propagation of atmospheric waves following shock fronts.

1. INTRODUCTION

Propagation of atmospheric waves in internal gravity and acoustic gravity regions may be easily studied using the ray tracing method for the group path developed by Cowling et al. (1). The method applies to a model atmosphere with stratified winds. The method is further based on the dispersion relation for an isothermal atmosphere and for waves with small amplitudes only. If the method has to be used for location of sources of the natural infrasonic and internal gravity waves produced at high latitudes by auroral mechanisms it is necessary to find a way of verifying it.

A convenient method of testing of the method has been found by applying it to atmospheric waves produced by supersonic aircraft. It has been shown by Meyer (2) that the shock front produced by a supersonic source is in the far zone followed, at any given point in space, by a decaying oscillation. The major part of the oscillation energy is located with the uppermost frequency range of internal gravity waves and the lowest frequencies of acoustic gravity waves. The waves travelling upwards are amplified (Daniels et al. (3) due to the density stratification in the atmosphere.

The idea of influencing the ionosphere by the shocks produced by supersonic aircraft has been developed by Marcos (4). Flight trajectories of supersonic aircraft were chosen to obtain focussing of the shock at ionospheric altitudes. Effects of the shock on the ionosphere were detected by studying frequency shifts of radio waves reflected at the point where the waves were focussed.

In the present experiment, flight trajectories of Saab-35 Draken supersonic aircraft were programmed in two different ways in order to obtain:

- (i) Focussing of waves on the ground after reflection from the stratosphere at about 40 km altitude.
- (ii) Focussing of waves at the E-layer.

During the first test period, 12-15 January 1971, six flights were performed, three along each of two types of trajectories. In all three flights along the type (i) trajectory, clear ground effects were observed. During three flights with ionospheric focussing, clear effects were observed during two of them. During the second test period, 1-3 February 1971, five flights were performed. The flights were performed along the type (ii) trajectory, although the deceleration of the aircraft in the final part of the flight was programmed during 15 seconds to obtain focussing effects on the ground. During four flights rather clear effects were observed both on the ground and in the E-layer. During the flight on 1 February 1971, ground measurements of 2 Hz signals were impossible due to a strong wind and the ionospheric measurements were uncertain because the E-layer reflection was very weak and unstable. The present results indicate that the ray tracing method may be satisfactorily applied for calculation of flight trajectories for which the focussing of waves will occur.

2. CALCULATION OF FLIGHT TRAJECTORIES

It has been assumed that the direction of the group velocity of the wave packet following the shock front is normal to the shock front. The orientation of the shock front is determined by the direction of the motion (see Fig. 1) and the Mach angle. The Mach angle is defined as

$$\sin \alpha = a/v = 1/M \quad (1)$$

where a is the local sound velocity, v is the velocity of the aircraft and M is the Mach number. For a flight trajectory with elevation ϵ the slope of the normal to the upward going shock front is given by

$$\tan \theta = 90^\circ + \epsilon - \arcsin(1/M^2 - 1). \quad (2)$$

The principle for focussing of the wave packets is shown in Fig. 2 a,b for trajectories type (1) and (2), respectively. In order to obtain focussing at a point X of rays generated along the trajectory between points 1 and 2 following conditions must be fulfilled for any pair of points i, j of the trajectory part 1-2:

- 1) Ray paths from points i and j must intersect in the point X.
- 2) The travel time along the ray path, i.e. the travel time between points i and X must be equal to the sum of the travel time between j and X and the flight time between i and j .

Ray paths and travel time were calculated using the ray tracing method of Cowling et al. (1). Winds and air temperatures up to 20 km were taken from local radiosonde measurements. Temperatures above 20 km were taken from the 1966 US Standard Atmosphere adjusted to the observed 20 km value. The wind model used in the height interval 20-70 km is based on rocket measurements made in January 1970 at the rocket range ESRANGE in Norway, using a falling parachute method. In the final reduction of last three flights made on 15 January 1971, rocket measurements of the wind made on the same day at ESRANGE were used. In the height interval 70-120 km the wind profile was taken from contour map given by Mangatroyd (5) for 60°N and adjusted to observed 20 km values. Temperature profiles were converted to sound velocity profiles. Also during the test period, 1-5 February 1971, wind measurements from ESRANGE were used.

3. METHOD OF DETECTION OF FOCUSED WAVES

The atmospheric waves focused on the ground were detected only in the infra-acoustic range, at a frequency of 10 kHz using a correlator (Guska et al. (6)). The correlator measures the cross-correlation between two signals recorded at spaced piezoelectric microphones. The baseline of the correlator has been oriented in the direction perpendicular to the expected direction of arrival of focussed infra-acoustic signals.

The atmospheric waves focused in the ionosphere were detected using a modified vertical sounding method. The recently developed "first reflection recorder" (Olsson (7)) has been used to record the virtual height of vertical reflection of 3 MHz pulsed transmission. The virtual height was measured with an accuracy of 1 km. During the present experiment the height interval 85-185 km was selected on the recorder. The height of the first reflection appearing in this interval was recorded. On 15 January a weak ionospheric disturbance associated with ionospheric absorption occurred which limited the amount of radio interference at 3 MHz and ended all high-accuracy measurements of the reflection height. Also during flights on 1-5 February 1971 a strong E-layer was present which enabled measurements of reflection height.

4. RESULTS OF MEASUREMENTS

Table 1 shows parameters of all 11 flights. The first three flights were performed along the type (1) trajectory giving the ground focussing. An example of the corresponding correlator recording from 16 January 1971 is shown in Fig. 3. The vertical scale on this figure gives approximate values of the cross-correlation between two signals recorded at a distance of 60 m. The broken line along the time axis shows the approximate position of the upper end part of the flight. The solid line indicates the part of the

Table 1

Flight No.	Date	Time MIN	Trajectory type	Maximum Mach number	Infra-acoustic signals	Ionospheric effects	Remarks
1	11 Jan. 1971	09 20	1	1.14	Yes	-	
2	11 Jan. 1971	10 46	1	1.14	Yes	-	
3	14 Jan. 1971	09 22	1	1.14	Yes	-	
4	15 Jan. 1971	09 33	2	1.40	No	Yes	Variation in reflection height: +6 km.
5	15 Jan. 1971	11 14	2	1.40	No	Yes	Variation in reflection height -2 to +5 km.
6	15 Jan. 1971	11 09	2	1.45	Yes, 20 µb	Yes	Variation in reflection height -3 to +4 km.
7	1 Feb. 1971	13 40	2 (with deceleration)	1.45	No	?	Surface wind, very weak and variable E-reflection results doubtful.
8	2 Feb. 1971	09 35	2 (with deceleration)	1.45	Yes, 16 µb	Yes	Variation in reflection height -4 to +3 km. Unusual short duration E _s echo at 130 km 50 sec before the expected arrival of infraacoustic waves. Clearly audible acoustic signal on the ground.
9	2 Feb. 1971	10 02	2 (with deceleration)	1.45	Yes, 40 µb	Yes	Variation in reflection height +7 km.
10	3 Feb. 1971	09 26	2 (with deceleration)	1.45	Recorder failure	Yes	Variation in reflection height -2 to +7 km.
11	3 Feb. 1971	10 03	2 (with deceleration)	1.45	Yes, 11 µb	Yes	Variation in reflection height -2 to +6 km.

flight programmed for the focussing of infra-acoustic waves at the observing site on the ground. It may be seen that the 2 Hz signal is modulated with a low frequency. In particular, in the initial phase of the focussing a period of 2 min may be clearly observed. The solid arrow on the diagram shows the expected start of the infra-acoustic signal, calculated under assumption that the waves propagate with the velocity of sound. The duration of the 2 Hz signal is very large and cannot be simply explained. No ground wind was measured during this experiment. It must be remembered that the waves recorded on the ground travelled along a distance of the order of 200 km. No acoustic signals were heard during this experiment at the recording site.

An example of recording of ionospheric effects of shock focussing during flight No. 6 on 15 January is shown in Fig. 4. The recording gives the reflection height of 3 MHz pulses transmitted from Kiruna. The broken line along the time axis shows the approximate duration of the supersonic part of the flight. The solid line indicated the part of the flight during which the infra-acoustic waves were focussed in the E-layer. The solid arrow indicates the expected time of arrival of infra-acoustic waves (6-sec period) to the 100 km level measured from the start of focussing trajectory. The empty arrow indicates the expected time of arrival of waves with periods close to the Brunt period (2.5 min). It may be seen that the reflection height starts to oscillate much before the expected time of arrival of infra-acoustic waves. This is the case during two other flights on the same day and it is difficult to say if the flights coincided with a natural variation of the reflection height, or if it has been caused by shock waves produced at the very beginning of the supersonic trajectory. Another reason for the earlier onset of oscillations may be due to the fact that the shock front travels, in general, with a velocity V_s larger than the velocity of sound. After Friedman et al. (8) V_s is related to the pressure jump in the shock front as follows:

$$V_s = a \left[1 + \frac{\gamma + 1}{4\gamma} \delta \right]^{\frac{1}{2}} a \left[1 + 0.43\delta \right]$$

where a is the sound velocity, γ is the ratio of specific heats, and δ is the relative overpressure. As the shock travelling upwards is amplified (Daniels et al. (3)), velocities appreciably larger than the sound velocity may easily be achieved at ionospheric heights even for shocks which are weak in the lower atmosphere.

It is interesting to compare present results with those obtained during similar experiments by Marcos (4). Ionospheric effects were detected there by a phase path technique giving merely the derivative of the phase path length. His experiments have shown small phase path changes of the order of 1 Hz with durations from 20 to 50 sec. This corresponds to the resulting overpressure at E-layer of 20 per cent. Ionospheric effects observed by Marcos seem to be caused by the redistribution of the ionization during the passage of the shock front. Decaying oscillations following the shock front, which were observed in the present experiment, are too slow to be easily observed by the phase path technique.

The main result of the present experiment is that the ray-tracing technique based on the linear theory may be satisfactorily applied in studies of propagation of atmospheric waves following shock fronts. The ray-tracing technique may thus be used in studies of the source of atmospheric waves associated with the auroral activity. These waves, according to Wilson (2), are produced by auroral arcs or surges moving with supersonic velocity. Accurate ground measurements together with the ray tracing technique are planned to be used for testing the above hypothesis.

Another interesting aspect of the present experiment is that even a relatively small supersonic aircraft when accelerating in a particular manner may influence in a measureable way the E-layer.

Only direct rays have been taken into consideration in the present experiment. Rays reflected from the ground are attenuated at the reflection and by the much longer propagation path. For an aircraft flying at an altitude of 10 km at Mach 1.42 the propagation path to E-layer for reflected rays is about 28 km longer than for direct rays.

ACKNOWLEDGEMENTS

The above research was sponsored by the Swedish National Council of Natural Sciences and was only rendered possible by the invaluable contribution of the Royal Swedish Air Force in Luleå who supplied and operated the SAAB-35 aircraft. The authors are in particular indebted to Lieutenant K. Nordström who organised the flights. Radiosonde measurements of winds and temperatures up to 20 km height have been supplied by the Meteorological Service at the Kallax Airport, Luleå and wind measurements up to 70 km height have been supplied by the rocket range ESRANGE, Kiruna. The radio contact with the aircraft has been performed through the Air Traffic Control at the Kiruna Airport.

REFERENCES

1. Cowling, D.H., Webb, H.D. and Yeh, K.C., "A Study of Travelling Disturbances in the Ionosphere", Tech. Rep. 38, Ionosph. Radio Lab., Univ. of Illinois, 1970.
2. Meyer, R.E., "On the Far Field of a Body Rising through the Atmosphere", J. Geophys. Res. 67, 2361, 1962.
3. Daniels, F.B., Bauer, S.J. and Harris, A.K., "Vertically Travelling Shock Waves in the Ionosphere", J. Geophys. Res. 65, 1848, 1960.
4. Marcos, F.K., "Aircraft-Induced Ionospheric Disturbances", Airforce Surveys in Geophys. No. 175, AFRL, Bedford Mass., 1966.
5. Murgatroyd, R.J., "The Dynamics of the Stratosphere, Mesosphere and Lower Thermosphere", ESRO SP-30, September 1968.
6. Liszka, L., Olsson, S., Englund, K. and Koskenniemi, K., "Infrasound Recording Equipment at Kiruna Geophysical Observatory", KGO Technical Report 71:105, 1971.
7. Olsson, S., "Ionosonde Receiver with Automatic Noise Suppression and Digital-Analogue Recording of the First Ionospheric Reflection", J. Atmosph. Terr. Phys. (in print), 1972.
8. Friedman, M.P., Kane, E.J. and Sigalla, A., "Effects of Atmosphere and Aircraft Motion on the Location and Intensity of a Sonic Boom", AIAA Journal 1, 1327, 1963.
9. Wilson, C.R., "Two-Station Auroral Infrasonic Wave Observations", Planet. Space Sci. 17, 1817, 1969.

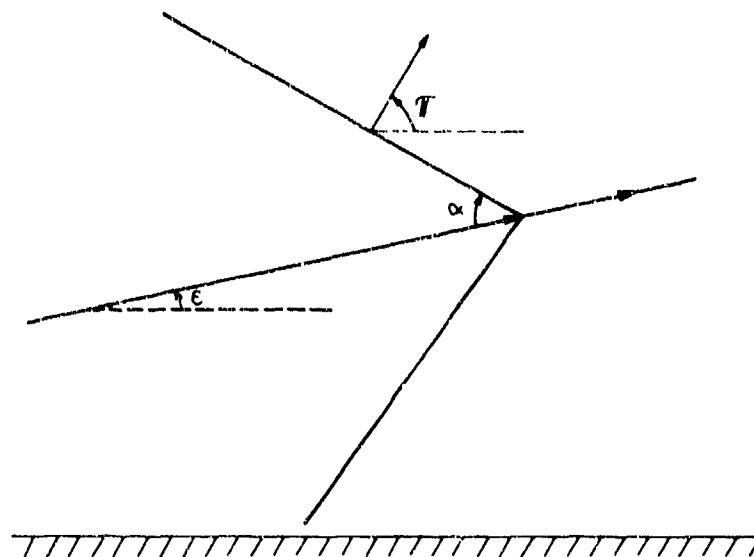


Fig.1 Orientation of the shock front

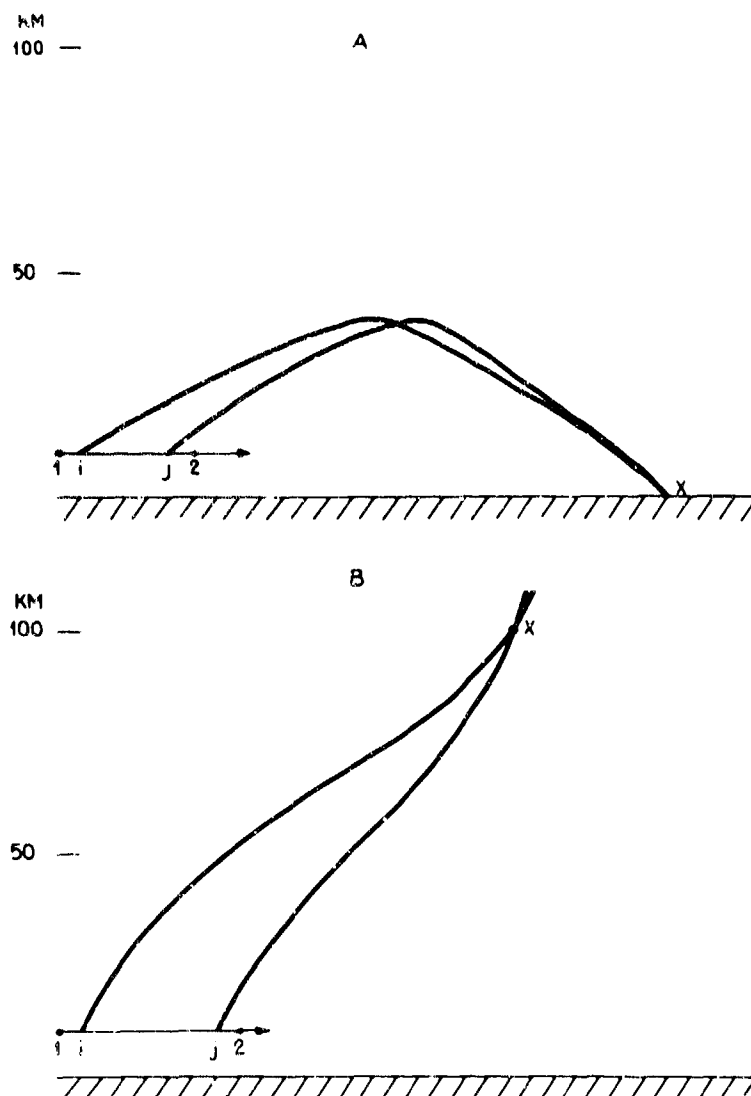


Fig.2 The principle for focussing of the wave packets: (a) focussing on the ground after reflection from the stratosphere: (b) focussing at the E-layer.

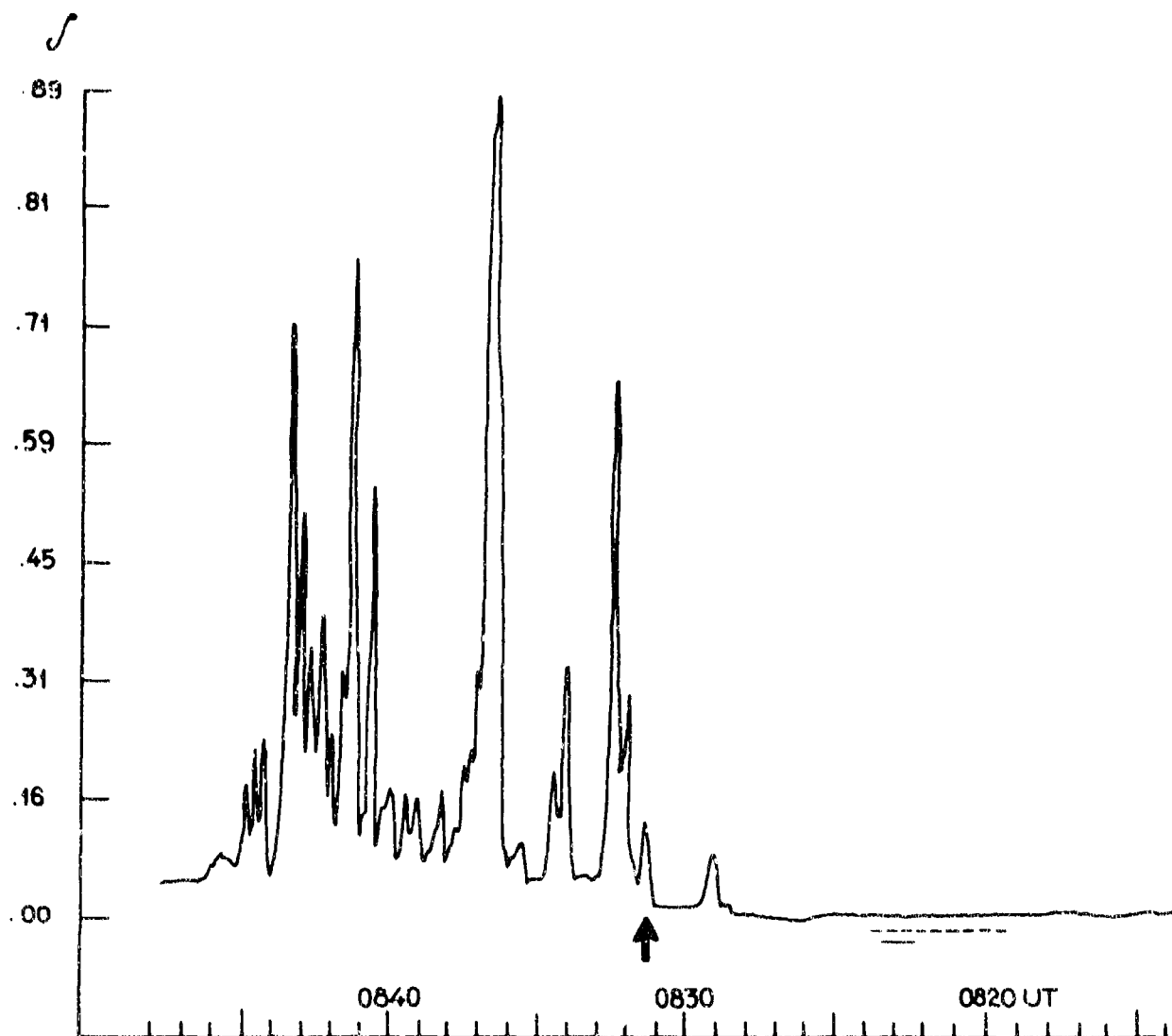


Fig.3 An example of the 2 Hz correlator recording during flight No. 3 on 14 January 1971. The broken line along time axis shows the approximate duration of the supersonic part of the flight. The solid line indicates the part of the flight programmed for the focussing of infrasonic waves at the observing site on the ground.

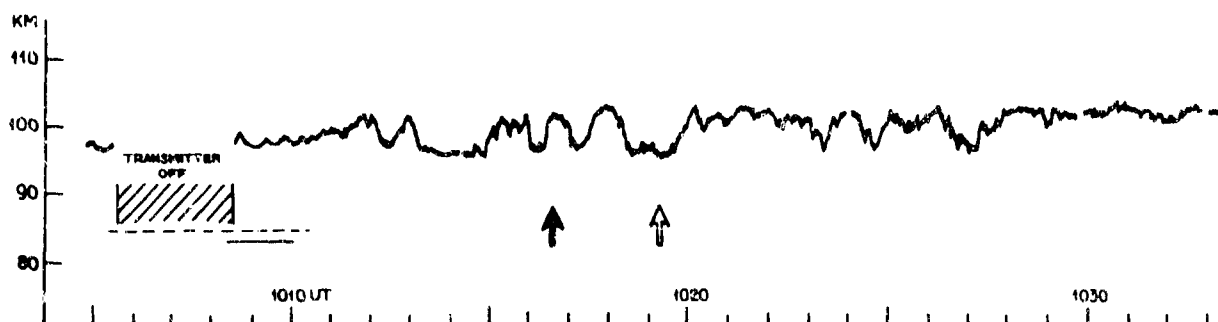


Fig.4 An example of reflection height recording during No. 6 on 15 January 1971. Duration of supersonic and focussing portions of the trajectory is shown as in Fig. 3. The solid arrow indicates the expected time of arrival of waves with the period of 6 sec; the empty arrow indicates time of arrival of waves with the period of 2.5 min.

Discussions on paper presented in Session III
(Radioelectric studies on acoustic gravity waves in the neutral and ionized atmosphere)

Discussion on paper 22 : "Observations of gravity waves in the height range 50 - 70 km", by G. PERONA.

Dr. G. LANGE - HESSE : Have you made sure that the variations in VLF amplitude and phase you have shown are not caused by mode interference ?

Dr. G. PERONA : In Turin, the ground wave is presumably very small, since Turin is just behind the Alps. The two-hops sky wave is strongly attenuated, since the reflection coefficient at the path midpoint is very small (the path midpoint is in the industrial area around Paris). Therefore the signal received in Turin is mainly due to the first-hop sky wave, and mode interference does not seem to be possible.

Discussion on paper 26 : "Ionospheric perturbations caused by long period sound waves generated by Saturn - Apollo rocket launches", by G.L. RAO.

Dr. T.M. GEORGES : 1° - How do your digital-processing techniques account for multivalued Doppler traces commonly seen on analog Doppler records and how do you determine when "mode - switching" occurs in your equipment ?

2° - Your frequency-vs time records appear very much like the 3-5 min. waves associated with severe storms, including the "beaded" appearance of the wave envelope. This suggests the presence of two closely spaced frequencies such as those shown by Davies. Does your spectral analysis reveal the presence of these two frequencies ?

Dr. G.L. RAO : 1° - This is one of the disadvantages of using digital recording of the data in our system, the stronger mode that appear at the time of digitization is usually recorded which means that there is a possibility of mode switching in our form of recording.

2° - We have not clearly noticed presence of two frequencies in our spectral analysis of the CW Doppler data for Saturn-Apollo launches.

Discussion on paper 27 : "Observations of travelling ionospheric disturbances at London, Canada", by I. LITVA.

Dr. H. RISHBETH : You observed TID's on only nine days out of a period of 1 1/2 years. Does this mean that TID's were rare, or does your equipment select only certain kinds of TID ?

Dr. J. LITVA : I suspect that my equipment, as all TID sensing equipments, is most sensitive to certain types of TIDS. The sun, during this period of time, acted as a radio source for a total of only 11 or 12 days. Therefore my equipment was a TID sensor during this time interval only when the sun was a radio source.

Dr. K. DAVIES : How does the velocity of the TID's observed by you depend on wave period ?

Dr. J. LITVA : I measured the velocity of TID's at two wave periods ; namely 21 minutes and 6 minutes. The velocity of the former was about 1 000 km/h, and that of the latter about 200 km/h ; therefore, for these two measurements the velocity of the larger period TID was greater than that of the lower period TID.

Discussion on paper 29 : "Ionospheric tilt measurements near the magnetic dip equator", by R.F. TREHARNE.

Dr. H.P. WILLIAMS : The ionospheric tilts referred to by Dr. GEORGE would presumably not include the large scale tilts caused by the transition from a sunlit to a dark region. We found in oblique soundings across the Atlantic that such large scale tilts could account for the 50 % or so extension in the MUF which occurred when the sun was near either terminal. I think it is important to bear this distinction in mind since the significance to the communicator is very different in the two cases.

Dr. P. GEORGE on behalf of Dr. TREHARNE : We would agree that the significance of large slowly varying gradients and smaller more rapidly varying tilts to the communicator will in general be rather different. The communicator is more often concerned with the relation of his operating frequency to the MUF, and the large gradients which vary more slowly in time are of significance here. Treharne's results do include these large slowly varying tilt effects and they must be removed in order to study the occurrence of TID's.

Dr. J. RÖTTGER : As I understood you cannot observe TID's during spread F conditions. Is my assumption right that TID's are not absent when spread F is evident ?

Dr. P. GEORGE : Since we cannot usually make observations of angle of arrival with this equipment when spread F is present I am unable to comment on an experimental basis on whether or not TID's are also then present. From a theoretical point of view I would think it most likely that TID's and spread F do coexist. I might even speculate that TID's are associated in the same way with the production of some forms of spread F.

Dr. G. LERFALD : If the amplitude of a TID is sufficiently great, returns may be obtained simultaneously from more than one reflection point. Can the equipment described in this paper deal with multiple reflections and, if so, are any results available ?

Dr. P. GEORGE : The equipment described in this paper is deliberately designed to make measurement of direction of arrival only when a single mode is instantaneously present, that is, it tests for plane wave front conditions. The equipment can of course be used to measure directions of arrival on 1st, 2nd or any other mode provided only that such measurements are not simultaneously possible.

Discussion on paper 30 : "On the generation and detection of artificial atmospheric waves", by L. LISZKA and S. OLSSON.

Dr. B. MURPHY : I am interested in your statement that the infrasonic signal observed on the ground is not an N wave, that the high frequencies are filtered out. Does this mean that the signal no longer begins with a steep rise or does it mean that the dominant period of the disturbance has increased (as one might expect from nonlinear, weak shock, effects) ?

Dr. L. LISZKA : As we can see it with our narrow band equipment the rise time of the N - wave does not change very much, but there is a tail of lower frequencies following the N - wave. The larger the distance from the source, the longer seems to be the tail.

Prof. R.K. COOK : The train of sound waves which follows after the N - wave of a sonic boom might have several origins. If a supersonic aircraft passes almost directly overhead, a few kilometers above an observer, he will hear the jet engine noise immediately after the sonic boom. All of the engine noise is contained within the Mach cone of the supersonic flight, and therefore is not audible until the cone has passed over the observer. When an observer is off to one side, 40 - 50 km away from the flight path, then he usually hears a low-pitched rumbling sound. This is mainly reverberation of the sonic boom energy, arising from scattering and reflection of the sonic boom by trees, buildings, etc. At the end of a very long propagation path through the atmosphere, 300 km or greater, the sonic boom energy might reverberate for a time duration of a minute or so. The reverberation observed at such locations is inaudible. The sound wave energy is concentrated at infrasonic frequencies. The reverberation arises from scattering of the sound, in transit to the observer, by atmospheric inhomogeneities rather than by dispersion in sound velocity at various frequencies.

Dr. L. LISZKA : A part of the "tail" following an N - wave may of course be due to scattering processes. However, a dispersion of sound velocity at different frequencies is a consequence of the dispersion relation for acoustic waves and should be observed also in case of sonic booms. It is a common explanation of wave trains following remote ground level explosions, where the length of the tail and its spectral content depends on the distance.

General discussion

Prof. I. RANZI : A very important application of the studies on the radioelectric effects of acoustic - gravity waves is that concerned with the over-the-horizon HF radar. This is a classified matter, but we all know what are the basic principles of this device, and we may then be able to provide data of a direct usefulness for the designers (e.g., influence of acoustic-gravity waves on azimuthal and vertical angle of arrival of the backscattered echoes, and on their delay). Perhaps, somebody in this audience may contribute to this discussion.

Dr. L. WETZEL : Prof. RANZI raised the topic of over-the-horizon radar as a possible focus of AGARD interest. Obviously, the military applications and characteristics of such devices are classified, but it should be fairly obvious that since an OTH, or HF, radar utilizes propagation in the ionosphere, such parameters as bearing accuracy, available signal bandwidth, etc., will depend critically on both the large and small-scale features of the ionosphere. For this reason the acoustic-gravity waves being discussed at this meeting will exert a significant influence on the performance capabilities and limitations of HF radars and deserve close study.

Dr. Ch. WILSON : With respect to over-the-horizon radar propagation disturbances I feel that it is important to investigate further the possibility that an ionization - collection process may be taking place in the E region of supersonic auroral arcs during the generation of auroral infrasonic waves by a "wall" of moving ionization within such arcs. Approximate calculations of the expected ion densities indicate that the ion density may increase up to values of 2×10^7 ions/cm³ within the arc. Thus the ion density gradients may be as large as two orders of magnitude within a few hundreds of meters from in front of the supersonic arcs to within the "wall" of swept-up neutral auroral ionization.

Thus the implications of recent research in auroral infrasonic wave generation is that ion densities in some auroral arcs that are in supersonic translation with a direction of motion that is parallel

to the E region ambient electric field may be one hundred times as large as that in other arcs that are, in all other respects, similar.

Dr. W. STOFFREGEN : A backscatter sounder on 16.8 at Uppsala can be operated with two transmitted pulses, the time delay between them can be varied from zero to some milliseconds. The returning reflections from both pulses are compared and a correlation analysis can be made in order to study the life-time of ionized elements in aurora and fast variations in backscatter from different sources. This double pulse method seems to give promising results.

Dr. H.G. MÖLLER : By sweep frequency groundscatter measurement it is possible to trace travelling disturbances over a wide range. Such measurements are being made at Lindau/Harz West Germany in a frequency range 2.8 - 45 MHz with rhombic antennas switched in 10 different azimuth directions.

The range-frequency dependence of the traces is in very good agreement with the ray tracing calculations made by T.M. Georges (1969) who should that looking in the direction of the movements of the travelling disturbances the slope of the traces is positive (increasing with increasing frequency). Looking in the opposite direction the slope is negative.

As the maximum range of the records is 2 500 km and focussing takes place near the apex of the path, the travelling disturbances can be traced from 1 250 km in the north to 1 250 km in the south.

Dr. K. DAVIES : My fixed frequency H.F. Doppler measurements show that on fixed frequencies, TID's appear bigger by day than by night. Your data indicate the reverse. Can you explain this ?

Dr. A.D. MORGAN : For the conditions of the experiment, namely, at frequencies near the MUF during November and December 1970, we generally observed more bearing perturbations during the day than during the night. However, some bearing perturbations were observed during the night and examples of these were shown in my presentation. As the quantity of data I presented was limited to 2 months, it was too small to enable a comparison to be made between the magnitude of the bearing perturbations between day and night. In fact, in my presentation, I gave no comparison between the size of the perturbation during the day and night periods ; I only compared the occurrence.

Dr. H.G. MÖLLER : I would like to support Mr. MORGAN.

From groundscatter observations at Lindau/Harz West-Germany made with antennas pointing to the south we know that the ionosphere is much more stable at night than at day by the following reason : At the trailing edge of the groundscatter trace magnetoionic splitting is observed quite regularly at night, except for the severely disturbed ones. On daytime records, however, magnetoionic splitting is observed only on E-layer reflected groundscatter but not on F layer reflected groundscatter.

As magnetoionic splitting can be observed only if reflecting layer is concentric homogeneous inside the azimuthal sector illuminated by the antenna or if the deviation from concentric homogeneity is very small, one can conclude from these observations that the ionosphere is much more stable at night than at day south of our backscatter site.

**AN APPROACH TO THE ANALYSIS OF COUPLING BETWEEN ACOUSTIC-GRAVITY
WAVES AND ELECTROMAGNETIC WAVES**

by

H.R.Raemer

**Northeastern University
Boston, Massachusetts
USA**

404

UN APPROCHE VERS L'ANALYSE DU COUPLAGE ENTRE ONDES ACOUSTIQUES OU DE GRAVITE
ET ONDES ELECTROMAGNETIQUES

par

H. Raemer

SOMMAIRE

Au cours de ces dernières années, l'auteur de cet exposé a travaillé à la recherche et au développement de modèles théoriques de plasmas à paramètres variables dans l'espace, et a utilisé ces modèles pour étudier, à l'aide d'ordinateurs extrêmement rapides, la propagation des ondes au sein de ces milieux. Il montre comment on peut faire appel à certains de ces modèles théoriques pour étudier les effets de premier ordre d'une perturbation en onde de basse fréquence (par exemple, une onde acoustique et de gravité d'une fraction d'Hertz) sur une onde électromagnétique à haute fréquence (de l'ordre du kilohertz ou du mégahertz) se propageant dans l'ionosphère. L'auteur décrit tout d'abord la formulation du modèle et son adaptation au problème étudié au moyen de la théorie de perturbation. Il expose ensuite, d'un point de vue général, la façon dont on peut utiliser cette théorie pour calculer les effets de premier ordre produits par l'onde acoustique et de gravité sur l'onde électromagnétique. Il achève sa conférence par une brève discussion de certaines implications de cette théorie sur les systèmes de communication.

AN APPROACH TO THE ANALYSIS OF COUPLING BETWEEN ACOUSTIC-GRAVITY WAVES AND ELECTROMAGNETIC WAVES

by

H. R. Raemer
Northeastern University
Boston, Massachusetts

ABSTRACT

During the past few years, the author has been involved in research on the development of theoretical models for plasma media whose parameters are spatially variable, and the use of these models to study wave propagation in such media with the aid of high-speed computers. It is shown in this paper how some of these theoretical models can be used to study the first-order effects of a low frequency wave disturbance (e.g. an acoustic-gravity wave at a fraction of a Hertz) on a high frequency electromagnetic wave (at kilohertz or megahertz) propagating in the ionosphere. The formulation of the model and its adaptation to the problem of interest via perturbation theory are first described, followed by a general outline of the way in which this theory could be used to calculate the first-order effects of the acoustic-gravity wave on the electromagnetic wave. Some communication systems implications of this theory are briefly discussed at the end of the paper.

1. INTRODUCTION

In recent years the author has been involved in research on the development of very general mathematical models for analysis of wave propagation in spatially inhomogeneous partially ionized gases and the computer-aided solution of the equations comprising these models (Raemer 1966, Raemer and Verma, 1966, 1970, Verma and Raemer, 1971, Raemer, 1972). Solutions based on these models contain information which could be valuable in studying coupling between acoustic-gravity waves and electromagnetic waves in the ionosphere.

In Section 3 a linearized electron-ion-neutral model (Raemer, 1966) is discussed as the basis for analyzing effects of an acoustic-gravity wave in inducing low frequency disturbances of the ionospheric plasma. The wave frequency is extremely low (a small fraction of a Hertz) and the zero-order, (known) parameters are those of the undisturbed ionosphere. An acoustic-gravity wave couples with the plasma through collisions. The first-order (unknown) parameters are the plasma perturbations due to the acoustic-gravity wave. Solution of the equations would result in approximate values of perturbed plasma density, pressure, current density and electric and magnetic fields as functions of position and time.

A linearized electron-plasma model (Raemer, 1972) accounts for vertical inhomogeneities in all ambient gas parameters including static magnetic field, and includes effects of gravity and the possibility of static electric fields. Effects of ions and neutrals, horizontal spatial inhomogeneities and slow time variations of ambient gas parameters are not accounted for rigorously, but can be included as perturbation terms if desired.

The application of this later model (Sections 4 and 5) is in the analysis of an electromagnetic wave, with wave frequencies in the kilohertz to megahertz range. Superposed on the parameters of the undisturbed ionosphere to make up the "zero-order" plasma parameters are perturbations due to the low frequency wave, which could be determined from the analysis discussed in Section 3. These are functions of horizontal position coordinates and time as well as vertical position, but because the periods and wavelengths are so long compared with those of the electromagnetic wave, then (if pressure and density departures from the ambient values are not too large) these can be considered as perturbations on the basic equations, in which only vertical inhomogeneities are accounted for. First order (unknown) quantities are the electric field components of the electromagnetic wave propagating through the region disturbed by the acoustic-gravity wave.

In this paper the above set of procedures are described in general (Sections 3 and 4) and a method of approximate solution is discussed (Section 5), wherein with suitable approximations one could obtain estimates of the magnitude of the influence of an acoustic-gravity wave on an electromagnetic wave propagating through the disturbed region.

Communications people are interested in characterization of a medium in the language of linear systems theory; i.e., the medium through which the wave propagates is considered as the equivalent of an electrical filter whose impulse response and complex frequency response function may be changing slowly with time. The results of the analysis in this paper can be cast in these terms (Section 6). Through boundary conditions at the lower edge of the ionosphere, a linear relationship between received wave fields and transmitted wave fields is described. This relationship is equivalent to consideration of the propagation medium as a linear filter whose impulse response may be time varying.

2. FORMULATION

The theoretical models referred to above are formulated with the following equations:

$$\rho_i \left(\frac{\partial}{\partial t} + \underline{u}_i \cdot \nabla \right) \underline{u}_i = - \nabla p_i + \frac{\rho_i q}{m_i} (\underline{e} + \underline{u}_i \times \underline{b}) - \underline{i}_z (\rho_i g)$$

$$- \rho_i [v_{in}(\underline{u}_i - \underline{u}_n) + v_{ie}(\underline{u}_i - \underline{u}_e)] \quad (\text{ion-motion equation}) \quad (i-1)$$

$$\rho_e \left(\frac{\partial}{\partial t} + \underline{u}_e \cdot \nabla \right) \underline{u}_e = - \nabla p_e - \frac{\rho_e q}{m_e} (\underline{e} + \underline{u}_e \times \underline{b}) - \underline{i}_z (\rho_e g)$$

$$- \rho_e [v_{en}(\underline{u}_e - \underline{u}_n) + v_{ei}(\underline{u}_e - \underline{u}_i)] \quad (\text{electron-motion equation}) \quad (e-1)$$

$$\nabla \cdot (\rho_i \underline{u}_i) + \frac{\partial \rho_i}{\partial t} = 0 \quad (\text{ion continuity equation}) \quad (i-2)$$

$$\nabla \cdot (\rho_e \underline{u}_e) + \frac{\partial \rho_e}{\partial t} = 0 \quad (\text{electron continuity equation}) \quad (e-2)$$

$$\left(\frac{\partial}{\partial t} + \underline{u}_i \cdot \nabla \right) \left(\frac{p_i}{\rho_i \gamma} \right) = 0 \quad (\text{ion adiabatic state equation}) \quad (i-3)$$

$$\left(\frac{\partial}{\partial t} + \underline{u}_e \cdot \nabla \right) \left(\frac{p_e}{\rho_e \gamma} \right) = 0 \quad (\text{electron adiabatic state equation}) \quad (e-3)$$

$$\nabla \times \underline{e} = - \frac{\partial \underline{b}}{\partial t} \quad (4)$$

$$\nabla \times \underline{b} = \mu_0 \epsilon_0 \frac{\partial \underline{e}}{\partial t} + \mu_0 q \left(\frac{\rho_i}{m_i} \underline{u}_i - \frac{\rho_e}{m_e} \underline{u}_e \right) \quad (5)$$

where

ρ_i = ion mass density

ρ_e = electron mass density

p_i = ion pressure

p_e = electron pressure

\underline{u}_i = ion velocity

\underline{u}_e = electron velocity

\underline{u}_n = neutral velocity

t = time

$\gamma = \frac{c_p}{c_v}$ = ratio of specific heats (constant pressure/constant volume)

\underline{e} = electric field

\underline{b} = magnetic induction

μ_0, ϵ_0 = constitutive parameters of free space

q = magnitude of electron charge

m_i = ion mass

m_e = electron mass

v_{in} = ion-neutral collision frequency

v_{en} = electron neutral collision frequency

v_{ei} = electron-ion collision frequency

v_{ie} = ion-electron collision frequency

g = acceleration due to gravity

Linearization of these equations is accomplished with the following assumptions (where subscripts 0 and 1 indicate "zero order" and "first order" respectively.)

$$\begin{aligned} \underline{u}_n &= \underline{u}_{n1} & \underline{u}_i &= \underline{u}_{i1} & \rho_i &= \rho_{i0} + \rho_{i1} & p_i &= p_{i0} + p_{i1} & \underline{u}_e &= \underline{u}_{e0} + \underline{u}_{e1} \\ \rho_e &= \rho_{e0} + \rho_{e1} & p_e &= p_{e0} + p_{e1} & \underline{e} &= \underline{e}_0 + \underline{e}_1 \end{aligned} \quad (6)$$

Using the forms (6), the linearized first order equations (i-1) through (5) are (where zero order quantities may, in general, be functions of time and all spatial coordinates, unlike the usual linearized model where these quantities are constant).

$$\begin{aligned} \rho_{i0} \frac{\partial \underline{u}_{i1}}{\partial t} &= - \nabla p_{i1} + \frac{q \rho_{i0}}{m_i} (\underline{e}_1 + \underline{u}_{i1} \times \underline{b}_0) + \frac{q \rho_{i1}}{m_i} \underline{e}_0 \\ &- \underline{i}_z (\rho_{i1} g) - \rho_{i0} [v_{in}(\underline{u}_{i1} - \underline{u}_{n1}) + v_{ie}(\underline{u}_{i1} - \underline{u}_{e1})] + \rho_{i1} v_{ie} \underline{u}_{e0} \end{aligned} \quad (i-1-1)$$

$$\begin{aligned}
\rho_{e0} \frac{\partial \underline{u}_{e1}}{\partial t} + \rho_{e1} \frac{\partial \underline{u}_{e0}}{\partial t} + \rho_{e0} \underline{u}_{e0} \cdot \nabla \underline{u}_{e1} + \rho_{e0} \underline{u}_{e1} \cdot \nabla \underline{u}_{e0} + \rho_{e1} \underline{u}_{e0} \cdot \nabla \underline{u}_{e0} = \\
- \nabla p_{e1} - \frac{q}{m_e} \rho_{e0} (\underline{e}_1 + \underline{u}_{e1} \times \underline{b}_0 + \underline{u}_{e0} \times \underline{b}_1) - \frac{q}{m_e} \rho_{e1} (\underline{e}_0 + \underline{u}_{e0} \times \underline{b}_0) \\
- \frac{1}{2} (\rho_{e1} g) - \rho_{e0} [v_{en} (\underline{u}_{e1} - \underline{u}_{n1}) + v_{e1} (\underline{u}_{e1} - \underline{u}_{i1})] - \rho_{e1} (v_{en} + v_{e1}) \underline{u}_{e0}
\end{aligned} \tag{e-1-1}$$

$$\nabla \cdot (\rho_{i0} \underline{u}_{i1}) + \frac{\partial \rho_{i1}}{\partial t} = 0 \tag{i-2-1}$$

$$\nabla \cdot (\rho_{e0} \underline{u}_{e1} + \rho_{e1} \underline{u}_{e0}) + \frac{\partial \rho_{e1}}{\partial t} = 0 \tag{e-2-1}$$

$$\begin{aligned}
\frac{\partial \rho_{i1}}{\partial t} - c_{s10}^2 \frac{\partial \rho_{i1}}{\partial t} + \underline{u}_{i1} \cdot \left[\nabla p_{i1} - c_{s10}^2 \nabla \rho_{i0} \right] + \rho_{i1} \left[\frac{-\gamma}{\rho_{i0}} \left(\frac{\partial \rho_{i0}}{\partial t} + \underline{u}_{i0} \cdot \nabla \rho_{i0} \right) \right] \\
+ \frac{\rho_{i1}}{\rho_{i0}} \left[-\gamma \left(\frac{\partial \rho_{i0}}{\partial t} - c_{s10}^2 \frac{\partial \rho_{i0}}{\partial t} \right) - \gamma \underline{u}_{i0} \cdot \left(\nabla p_{i0} - c_{s10}^2 \nabla \rho_{i0} \right) + c_{s10}^2 \left(\frac{\partial \rho_{i0}}{\partial t} + \underline{u}_{i0} \cdot \nabla \rho_{i0} \right) \right] = 0
\end{aligned} \tag{i-3-1}$$

$$\begin{aligned}
\frac{\partial \rho_{e1}}{\partial t} - c_{se0}^2 \frac{\partial \rho_{e1}}{\partial t} + \underline{u}_{e0} \cdot \left[\nabla p_{e1} - c_{se0}^2 \nabla \rho_{e1} \right] + \underline{u}_{e1} \cdot \left[\nabla p_{e0} - c_{se0}^2 \nabla \rho_{e0} \right] \\
+ \rho_{e1} \left[\frac{-\gamma}{\rho_{e0}} \left(\frac{\partial \rho_{e0}}{\partial t} + \underline{u}_{e0} \cdot \nabla \rho_{e0} \right) \right] + \frac{\rho_{e1}}{\rho_{e0}} \left[-\gamma \left(\frac{\partial \rho_{e0}}{\partial t} - c_{se0}^2 \frac{\partial \rho_{e0}}{\partial t} \right) - \gamma \underline{u}_{e0} \cdot \left(\nabla p_{e0} - c_{se0}^2 \nabla \rho_{e0} \right) \right] \\
+ c_{se0} \left(\frac{\partial \rho_{e0}}{\partial t} + \underline{u}_{e0} \cdot \nabla \rho_{e0} \right) = 0
\end{aligned} \tag{e-3-1}$$

$$\nabla \times \underline{e}_1 + \frac{\partial \underline{b}_1}{\partial t} = 0 \tag{4-1}$$

$$\nabla \times \underline{b}_1 - \frac{1}{c} \frac{\partial \underline{e}_1}{\partial t} - \mu_0 q \left(\frac{\rho_{i0}}{m_i} \underline{u}_{i1} - \frac{\rho_{e0}}{m_e} \underline{u}_{e1} - \frac{\rho_{e1}}{m_e} \underline{u}_{e0} \right) = 0. \tag{5-1}$$

3. MODEL FOR LOW (ACOUSTIC-GRAVITY WAVE) FREQUENCIES

In the low frequency case, both ion and electron motions should be accounted for. Vertical variation of static parameters is extremely important at those frequencies, because significant vertical variation of these parameters occurs within a wavelength or a fraction of a wavelength. Gravity effects are also important. Hence a linearized model accounting for these effects and including the ion equations is called for in attempting to analyze the effects of an acoustic-gravity wave on the electromagnetic parameters. Such a model was formulated by the author a few years ago. (Raemer, 1966). This model also included the neutral gas equations but subsequent studies with the model showed, as expected intuitively, that electron and ion disturbances do not significantly influence neutral gas motions. Hence one can consider the acoustic gravity wave as propagating in the purely neutral atmosphere, solve for the parameters of such a wave, particularly the velocity u_g , and consider the neutral velocity collision terms in the ion and electron motion equations (i-1-1) and (e-1-1) as known source-terms. In a more recent paper (Raemer and Verma, 1970) we described a method of solving for ion and electron pressures, densities, velocities and electric and magnetic fields associated with propagating waves. The method was based on postulation of a stratified layer model, numerical evaluation of the eigenvalues of the system matrix characterizing the equations in each of the layers, and an analytical evaluation of the solutions based on these eigenvalues. This method is alluded to in Section 5 of the present paper, in the context of the analysis of a high frequency wave influenced by the presence of a low frequency disturbance in the ambient ionosphere.

We will not discuss further here the analysis required to determine the low frequency electromagnetic parameters due to collision coupling with the neutral acoustic-gravity wave. We will only indicate that the solutions will yield parameters of the form

$$f(z) e^{-j(\omega_g t - k_{xg} x - k_{yg} y)},$$

where ω_g is acoustic-gravity wave frequency and where k_{xg} and k_{yg} are propagation constants associated with horizontal propagation. Using the stratified layer model referred to above, the function $f(z)$ will consist of a sum of vertical propagation modes of the form $z^{p_e j k} z^z$, where p is a positive integer that may be as high as 2 in the electron-ion case and k_{zg} will be, in general, complex, indicating both vertical propagation and damping. Assuming that only one of these modes predominates and neglecting others, low frequency perturbations of the electromagnetic parameters due to the acoustic-gravity wave are of the form

$$z^{p_e j k} e^{-j(\omega_g t - k_{xg} x - k_{yg} y - k_{zg} z)}.$$

This is used later in Sections 4 and 5 in the discussion of the theoretical model for high-frequency wave propagation in a medium permeated by a low frequency disturbance.

4. MODEL FOR HIGH (ELECTROMAGNETIC WAVE) FREQUENCIES

The assumptions for the EM wave frequency model are:

- (1) Ion and neutral motions are insignificant and can be neglected (i.e., eqs. (i-1-1), (i-2) and (i-3) are not used and $u_{i1} = 0$, $u_{n1} = 0$ in eqs. (e-1-1) and (5-1)).
- (2) Gravity term $-i_z(y\rho_{i1})$ in (e-1-1) is negligible.
- (3) The zero-order parameters are as follows:

$$\rho_{e0}(x,y,z,t) = \bar{\rho}_{e0}(z) + \zeta \hat{\rho}_e(x,y,z,t) \quad \rho_{e0}(x,y,z,t) = \bar{\rho}_{e0}(z) + \zeta \hat{\rho}_e(x,y,z,t)$$

$$u_{e0}(x,y,z,t) = \bar{u}_{e0}(z) + \zeta \hat{u}_e(x,y,z,t) \quad e_{00}(x,y,z,t) = \bar{e}_0(z) + \zeta \hat{e}_e(x,y,z,t)$$

$$b_{00}(x,y,z,t) = \bar{b}_0(z) + \zeta \hat{b}_e(x,y,z,t)$$

or generically

$$h_0(x,y,z,t) = \bar{h}_0(z) + \zeta h(x,y,z,t) = \bar{h}_0(z) + \zeta \text{Re}[\hat{h}(z)]_0 e^{-j(\omega_g t - k_{xg} x - k_{yg} y)} \quad (7)$$

where

$\bar{h}_0(z)$ = quiescent value of parameter (i.e., value in the absence of the low frequency wave),

$h(x,y,z,t)$ = perturbation in zero-order parameter due to the low frequency wave,

ζ = perturbation ordering parameter.

- (4) The high frequency wave parameters are:

$$h_1(x,y,z,t) = \sum_{n=0}^{\infty} h_1^{(n)}(x,y,z,t) \zeta^n, \quad (8)$$

where

$$h_1 = \rho_{e1}, \rho_{e1}, u_{e1}, e_1 \text{ or } b_1.$$

- (5) Using (7) and (8), we set up a new perturbation theory based on the ordering parameter ζ . This is over-and above the perturbation theory inherent in the linearization process. The equations are as follows:

Eqs. of orders $\zeta^{(0)}$ and ζ (call these sets of equations I and II respectively) are of the form:

$$\begin{aligned} \hat{\rho}_{e0} \frac{\partial \hat{u}_{e1}}{\partial t} + \hat{\rho}_{e0} \hat{u}_{e0} \cdot \nabla \hat{u}_{e1} + \hat{\rho}_{e0} \hat{u}_{e1} \cdot \nabla \hat{u}_{e0} \\ + \frac{q}{m_e} \hat{\rho}_{e0} (\hat{e}_1 + \hat{u}_{e1} \times \hat{b}_0 + \hat{u}_{e0} \times \hat{b}_1) \\ + \left[\hat{u}_{e0} \cdot \nabla \hat{u}_{e0} + \frac{\partial \hat{u}_{e0}}{\partial t} + \frac{q}{m_e} (\hat{e}_0 + \hat{u}_{e0} \times \hat{b}_0) \right] \rho_{e1} \end{aligned} \quad (e-1-1)$$

$$\begin{aligned} + \hat{\rho}_{e0} (\hat{v}_{en} + \hat{v}_{e1}) \hat{u}_{e1} + (\hat{v}_{en} + \hat{v}_{e1}) \hat{u}_{e0} \rho_{e1} = f_{e11} \\ \nabla \cdot \left(\hat{\rho}_{e0} \hat{u}_{e1} + \hat{u}_{e0} \rho_{e1} \right) + \frac{\partial \rho_{e1}}{\partial t} = f_{e21} \end{aligned} \quad (e-2-1)$$

$$\frac{\partial \rho_{e1}}{\partial t} - \hat{c}_{se0}^2 \frac{\partial \rho_{e1}}{\partial t} + \hat{u}_{e1} \cdot (\nabla \hat{p}_{e0} - \hat{c}_{se0}^2 \nabla \hat{\rho}_{e0}) = f_{e31} \quad (e-3-1)$$

$$\nabla \times \hat{e}_1 + \frac{\partial \hat{b}_1}{\partial t} = 0 \quad (4-1)$$

$$\nabla \times \hat{b}_1 - \frac{1}{c^2} \frac{\partial \hat{e}_1}{\partial t} + \mu_0 q \frac{\hat{\rho}_{e0}}{m_e} \hat{u}_{e1} + \frac{\mu_0 q}{m_e} \hat{u}_{e0} \rho_{e1} = f_{51} \quad (5-1)$$

where superscripts zero and one are understood but not explicitly indicated on quantities \hat{u}_{e1} , ρ_{e1} , \hat{p}_{e1} , etc. where f_{e11} , f_{e21} , f_{e31} and f_{51} are all zero for equations of order $\zeta^{(0)}$ and these quantities for equations of order ζ are:

$$\begin{aligned} f_{e11} &= - \hat{\rho}_e \frac{\partial \hat{u}_{e1}^{(0)}}{\partial t} - \hat{\rho}_{e0} \hat{u}_e \cdot \nabla \hat{u}_{e1}^{(0)} - \hat{\rho}_e \hat{u}_{e0} \cdot \nabla \hat{u}_{e1}^{(0)} \\ &\quad - \hat{\rho}_{e0} \hat{u}_{e1}^{(0)} \cdot \nabla \hat{u}_e - \hat{\rho}_e \hat{u}_{e1}^{(0)} \cdot \nabla \hat{u}_{e0} - \frac{q}{m_e} \hat{\rho}_e \hat{e}_1^{(0)} \\ &\quad - \frac{q}{m_e} \hat{\rho}_e \left(\hat{u}_{e1}^{(0)} \times \hat{b}_0 + \hat{u}_{e0} \times \hat{b}_1^{(0)} \right) - \frac{q}{m_e} \hat{\rho}_{e0} \left(\hat{u}_{e1}^{(0)} \times \hat{b} + \hat{u}_e \times \hat{b}_1^{(0)} \right) \\ &\quad - \left[\hat{u}_{e0} \cdot \nabla \hat{u}_e + \hat{u}_e \cdot \nabla \hat{u}_{e0} - \frac{\partial \hat{u}_e}{\partial t} + \frac{q}{m_e} (\hat{e} + \hat{u}_e \times \hat{b}_0 + \hat{u}_{e0} \times \hat{b}) \right] \rho_{e1}^{(0)} \\ &\quad - \hat{\rho}_e \hat{v}_{en} \hat{u}_{e1}^{(0)} - (\hat{v}_{en} + \hat{v}_{e1}) \hat{u}_{e0} \rho_{e1}^{(0)} \\ f_{e21} &= - \nabla \cdot \left(\hat{\rho}_e \hat{u}_{e1}^{(0)} + \hat{u}_e \rho_{e1}^{(0)} \right) \\ f_{e31} &= \hat{c}_{se0}^2 \frac{\partial \rho_{e1}^{(0)}}{\partial t} - \hat{u}_e \cdot \left(\nabla \hat{p}_{e1} - \hat{c}_{se0}^2 \nabla \hat{\rho}_{e1} \right) + \hat{u}_{e0} \cdot \hat{c}_{se0}^2 \nabla \rho_{e1}^{(0)} \\ &\quad - \hat{u}_{e1}^{(0)} \cdot \left(\nabla \hat{p}_e - \hat{c}_{se0}^2 \nabla \hat{\rho}_e - \hat{c}_{se}^2 \nabla \hat{\rho}_{e0} \right) - \frac{\hat{p}_{e1}^{(0)}}{\hat{\rho}_{e0}} - \gamma \left(\frac{\partial \hat{\rho}_e}{\partial t} + \hat{u}_{e0} \cdot \nabla \hat{\rho}_e \right. \\ &\quad \left. + \hat{u}_e \cdot \nabla \hat{\rho}_{e0} \right) + \frac{\hat{\rho}_e}{\hat{\rho}_{e0}} \left(\frac{\partial \hat{\rho}_{e0}}{\partial t} + \hat{u}_{e0} \cdot \nabla \hat{\rho}_{e0} \right) \\ &\quad - \frac{\rho_{e1}^{(0)}}{\hat{\rho}_{e0}} \left[- \gamma \left(\frac{\partial \hat{p}_e}{\partial t} - \hat{c}_{se0}^2 \frac{\partial \hat{\rho}_e}{\partial t} - \hat{c}_{se}^2 \frac{\partial \hat{\rho}_{e0}}{\partial t} \right) - \gamma \hat{u}_{e0} \cdot \left(\nabla \hat{p}_e - \hat{c}_{se0}^2 \nabla \hat{\rho}_e - \hat{c}_{se}^2 \nabla \hat{\rho}_{e0} \right) \right. \\ &\quad \left. - \gamma \hat{u}_e \cdot \left(\nabla \hat{p}_{e0} - \hat{c}_{se0}^2 \nabla \hat{\rho}_{e0} \right) + \hat{c}_{se0}^2 \left(\frac{\partial \hat{p}_e}{\partial t} + \hat{u}_e \cdot \nabla \hat{\rho}_{e0} + \hat{u}_{e0} \cdot \nabla \hat{\rho}_e \right) \right. \\ &\quad \left. + \hat{c}_{se}^2 \left(\frac{\partial \hat{p}_{e0}}{\partial t} + \hat{u}_{e0} \cdot \nabla \hat{\rho}_{e0} \right) + \frac{\hat{p}_e}{\hat{\rho}_{e0}} \gamma \left(\frac{\partial \hat{u}_{e0}}{\partial t} - \hat{c}_{se0}^2 \frac{\partial \hat{u}_{e0}}{\partial t} \right) \right] \end{aligned}$$

$$+ \gamma_{e0} \cdot \left(\nabla \bar{\rho}_{e0} - c_{se0} \nabla \bar{\rho}_{e0} \right) - c_{se0}^2 \left(\frac{\partial \bar{\rho}_{e0}}{\partial t} + \bar{u}_{e0} \cdot \nabla \bar{\rho}_{e0} \right)$$

$$f_{51} = - \frac{\mu_0 q}{m_e} \left(\bar{\rho}_{e-e1}^{(0)} + \bar{u}_{e-e1}^{(0)} \right)$$

Note that the equations of order $\epsilon^{(0)}$ are those of high frequency waves propagating in the quiescent electron plasma. The equations of order ϵ are those describing the first order effects of the low frequency (including electromagnetic and electron-acoustic) waves.

Solution of the equations of order $\epsilon^{(0)}$ (Equations I) gives us the parameters $\bar{u}_{e1}^{(0)}$, $\bar{\rho}_{e1}^{(0)}$, $\bar{p}_{e1}^{(0)}$, $\bar{e}_{e1}^{(0)}$ and $\bar{b}_{e1}^{(0)}$, those associated with waves propagating in the ambient medium undisturbed by the acoustic-gravity wave. Knowledge of those parameters allows construction of the right-hand sides of the equations of order ϵ (Equations II), whose homogeneous forms have already been solved since they are the same as Equation I. The right-hand sides of II contain first-order effects of the presence of an acoustic-gravity wave propagating in the medium. In this approach, these are contained in source terms rather than within the coefficients of the partial differential equations describing the phenomenon. This is a drastic simplification of the physics of the problem. Even with the simplified linearized equations we are using, retention of the quantities $\bar{\rho}_e(x,y,z,t)$, $\bar{u}_e(x,y,z,t)$, etc. on the left-hand sides of the equations and the treatment of these quantities as of the same order as $\bar{\rho}_{e0}(z)$, $\bar{u}_{e0}(z)$, etc. would give us a set of coupled partial differential equations in the variables x,y,z and t . The perturbation approach allows reduction of the problem to that of solution of a set of coupled ordinary differential equations in z . The mathematical simplification resulting from this is enormous, although there is a price to be paid in the sense that the information we finally obtain is less than we might like.

The solutions of Equation System I are of the form $e^{-j(\omega t - k_x x - k_y y)}$, where ω_e is the E-M wave frequency and k_{xe} and k_{ye} are the horizontal E-M wave propagation constants. From (7) we can conclude that there are two sets of terms on the right-hand-side of II. One set of terms (call it T_-) is of the form $e^{-j[(\omega_e - \omega_g)t - (k_{xe} - k_{xg})x - (k_{ye} - k_{yg})y]}$ and the other (call it T_+) of the form $e^{-j[(\omega_e + \omega_g)t - (k_{xe} + k_{xg})x - (k_{ye} + k_{yg})y]}$. If we assume solutions of II of the form $e^{-j(\omega t - k_x x - k_y y)}$, then we can consider each unknown in II as composed of two components, one a response to source terms T_- , the other to source terms T_+ . The former is of frequency $\omega = \omega_e - \omega_g$, corresponding to a "lower modulation sideband", the latter of frequency $\omega = \omega_e + \omega_g$, corresponding to an "upper modulation sideband". This low-frequency modulation of the E-M wave frequency due to the acoustic-gravity wave is one effect that can be expected qualitatively. However, if ω_e is of the order of megahertz and ω_g a small fraction of a Hertz, then the ratio of modulation bandwidth to wave frequency is less than .0001%.

5. USE OF THE ELECTRON-PLASMA WAVE MODEL

The systems of equations developed in Section 4 fit into the frame-work of a general theoretical model developed by the author to analyze wave propagation in an electron plasma with vertically variable static parameters, including a vertically variable static magnetic field. This last feature is a generalization of the author's earlier work on the three-fluid gas (Raemer, 1966) in which the magnetic field is the only static parameter not allowed to vary. The variation of the static magnetic field necessitates an electron drift velocity in source free regions in order to satisfy the zero-order Maxwell equation

$$\nabla \times \bar{b}_0 = \mu_0 \bar{j}_0 = \mu_0 q \left(\frac{\bar{u}_{i0}}{m_i} + \frac{\bar{u}_{e0}}{m_e} \right) \quad (9)$$

The postulate that \bar{u}_{i0} and \bar{u}_{e0} are zero, standard in linearized plasma theory, must be abandoned in order to satisfy (9) unless the vertical variation of \bar{b}_0 is specified as one in which $\nabla \times \bar{b}_0 = 0$. This introduces many terms into the linearized equations and complicates these equations greatly.

Work relating to the general model referred to above is contained in an as yet unpublished paper by the author (Raemer, 1972) which will soon be submitted for publication. That work will not be discussed here. But the model will be used to further discuss the problem addressed in Section 4. After Fourier-transformation of both sides with respect to x,y and t , or alternatively, choosing solutions of $e^{-j(\omega t - k_x x - k_y y)}$ the equation systems (e-1-1-0) through (5-1-0) and (e-1-1-1) through (5-1-1) have been manipulated to cast them each in the form of two matrix equations:

$$\bar{v}' = A\bar{v} + \bar{s} \quad (10-a)$$

$$\bar{w} \times C\bar{v} + \bar{d} \quad (10-b)$$

where

$$\underline{v} = \begin{bmatrix} E'_x \\ E'_y \\ E'_z \\ E_x \\ E_y \\ E_z \end{bmatrix}$$

\underline{s} is a 6-element column vector whose elements are complicated but linear functions of source terms on the right-hand sides of the original equations, A is a 6×6 matrix whose elements are functions of the static parameters of the plasma, (E_x, E_y, E_z) are normalized components of the first-order electric fields,

(e_{1x}, e_{1y}, e_{1z}) and (E'_x, E'_y, E'_z) are derivatives of these normalized components with respect to a normalized z coordinate,

$$\underline{w} = \begin{bmatrix} p_e \\ R_e \\ u_{ex} \\ u_{ey} \\ u_{ez} \\ B_x \\ B_y \\ B_z \end{bmatrix}$$

where $(p_e, R_e, u_{ex}, u_{ey}, u_{ez}, B_x, B_y, B_z)$ are normalized versions of $(p_{e1}, p_{e1}, u_{e1x}, b_{1x}, b_{1y}, b_{1z})$, C is an 8×6 matrix of functions of

the static parameters and \underline{d} is an 8-element column vector of functions of source terms. In the equations of order $\epsilon(0)$ both \underline{s} and \underline{d} are zero.

The obvious procedure in solving the system (10-a) and (10-b) is to first solve the differential equation system (10-a) for \underline{v} , then determine \underline{w} through (10-b), the latter being a trivial step. In the context of the present discussion, we are only interested in the field components $(e_{1x}, e_{1y}, e_{1z}, b_{1x}, b_{1y}, b_{1z})$ of a propagating electromagnetic wave; hence other parameters (such as p_{e1}, p_{e1} , and the derivatives of e_1) present in the solutions are of only peripheral interest.

Work is in progress on analytical (WKB-type) solutions of (10-a), but this work is not yet completed. A great deal of work has been done by the author and his co-worker Dr. Verma, some of it alluded to in previous papers, on attempts to treat this class of equations (with large A -matrices, and 6×6 qualifies as "large") by direct step-by-step integration procedures such as Runge-Kutta. These attempts led to numerical instability problems and were not successful.

As a first step in dealing with this problem, we have reverted to a standard technique of postulating a stratified medium with homogeneous layers. In a previous paper dealing with a three-fluid gas (Raemer and Verma, 1970) the method of solution was delineated and some numerical results were reported for the eigenvalue computation, which is the first and most fundamental step in the numerical evaluation of the unknown parameters.

To summarize the technique, the eigenvalues of the A -matrix of (10-a) are first found numerically. This has been done for a wide range of parameter regimes characteristic of the ionosphere. At kilohertz and megahertz frequencies, the 6 eigenvalues always come out in 3 pairs indicating "upward" and corresponding "downward" damped propagation modes. These two modes in any one of these pairs are not necessarily equal and opposite although they are more nearly so as the influence of the static magnetic field becomes less important. At low ionospheric altitudes, where the plasma is more nearly collision dominated than magnetic-field dominated (i.e., collision frequency \gg electron cyclotron frequency), the up and down modes are close to equal and opposite.

Returning to the problem of finding the solutions of II, we would first solve (10-a) with $\underline{s} = 0$, resulting in a set of 6 "fundamental solutions" $\underline{v}_i^{(f)}(z)$. Based on these fundamental solutions we would construct a "state-transition matrix" $\phi(z, z')$ and write the solution of (10-a) in the form:

$$\underline{v}(z) = \phi(z, z_0) \underline{v}(z_0) + \int_{z_0}^z dz' \phi(z, z') \underline{s}(z'). \quad (11)$$

The first term on the right-hand side of (11), i.e., $\phi(z, z_0) v(z_0)$ contains the effect of a high frequency wave propagating without the presence of the low frequency wave disturbance. It is in effect the solution of the equations I in Section 4, which in turn will be used to construct $s(z)$ for solution of the equation II. Boundary conditions for specification of $v(z_0)$ can be chosen as those of an electromagnetic wave propagating in free-space below the ionosphere.

The second term of (11) provides the response of any field component, e.g., e_{1x} , to the parameters associated with the low frequency disturbance. This is a particularly useful item of information in the context of the problem of interest. To show how the relationship comes about, we will continue the discussion along lines of determination of $\phi(z, z_0)$.

In a typical case, the eigenvalues come out as follows: $\lambda_1, -\lambda_1; \lambda_2, -\lambda_2; \lambda_3, -\lambda_3$; where $\lambda_3 = \lambda_1$, $\lambda_2 \neq \lambda_1$; i.e., two of the three pairs are identical. In this case, within one uniform stratum, $\phi(z, z_0)$ takes the form

$$\phi(z, z_0) = e^{\lambda_1(z-z_0)} \left[C_1 + C_3(z - z_0) \right] + e^{-\lambda_1(z-z_0)} \left[C_{-1} + C_{-3}(z - z_0) \right] + \left[C_2 e^{\lambda_2(z-z_0)} + C_{-2} e^{-\lambda_2(z-z_0)} \right], \quad (12)$$

where $C_1, C_{-1}, C_2, C_{-2}, C_3, C_{-3}$ are 6×6 matrices whose values depend on their corresponding eigenvalues and are determined in a tedious but straight-forward manner (Raemer and Verma, 1970).

It can be shown that s is a linear function of the quantities f_{e11}, f_{e21} , etc. and that these functions are composed of terms proportional to products of the form $\hat{\rho}_e u_{e1}^{(0)}$.

We assume that quantities like $\hat{\rho}_e$ have z -dependence containing factors $z^{jk} e^{jkzg}$ (which would be the case if the same sort of uniform stratum theory had been used to obtain these quantities, as indicated in Section 3). We also note that quantities like $u_{e1}^{(0)}$ are elements of the column vector $\phi(z, z_0) v^{(0)}(z_0)$, where $v^{(0)}(z)$ is the column vector $v(z)$ defined below eqs. (10-a) and (10-b), but applying specifically to the equations I and not to equations II. Denoting $v(z)$ for the equation system II by the symbol $v^{(1)}(z)$, (11) takes the form

$$v^{(1)}(z) = \phi(z, z_0) v^{(1)}(z_0) + \int_{z_0}^z dz' (z')^p e^{jkzg} \phi(z, z') s_0^{(0)}(z'), \quad (13)$$

where in line with the remarks above

$$s(z) = \left[z^p e^{jkzg} \right] s_0^{(0)}(z) \quad (14)$$

and where $s_0^{(0)}$ is a constant column vector. We now invoke (12) and observe that $s_0^{(0)}(z)$ must be of the form

$$s_0^{(0)}(z) = e^{\lambda_1 z} \left[C_1 + C_3 z \right] + e^{-\lambda_1 z} \left[C_{-1} + C_{-3} z \right] + e^{\lambda_2 z} C_2 + e^{-\lambda_2 z} C_{-2}, \quad (15)$$

where each C_i is a column vector independent of z whose precise form can easily be computed from the expressions for f_{e11}, f_{e21} , etc.

By carrying out the tedious but straight-forward integration indicated by (12), (13), (14), and (15) we can determine $v^{(1)}$ which will turn out to be a sum of terms with factors

$$z^q e^{\pm \lambda_1 z}, z^q e^{\pm \lambda_2 z}, z^q e^{(jkzg \pm \lambda_1) z}, z^q e^{(jkzg \pm \lambda_2) z}, \text{ etc.}$$

where q is a positive integer, zero in most cases but possibly as high as 2 or 3 in others. Each such exponential form will indicate the presence of an electromagnetic or electron-acoustic mode of propagation and the relative magnitudes of the coefficients of these terms will be a measure of the relative magnitudes of these propagation modes. Terms with factors

$$e^{(jkzg \pm \lambda_2) z}$$

indicate that the presence of the acoustic-gravity wave will introduce new modes of propagation, i.e., actually change the propagation constant and attenuation of high-frequency modes that would be present

without the low frequency disturbance. Terms with factors $e^{\pm \lambda_2 z}$, whose propagation and exponential attenuation characteristics are not affected by the low frequency disturbance, are still influenced by the disturbance in the sense that the coefficients of these terms are so influenced.

6. COMMUNICATIONS SYSTEMS IMPLICATIONS

Electromagnetic waves propagating in the ionosphere at kilohertz and megahertz frequency ranges are ordinarily associated with a communication link between two points both below the ionosphere. In this

case the item of greatest interest to engineers concerned with such links is the effective reflection coefficient of the ionosphere. Due to the earth's magnetic field, the ionosphere, if it were to be considered as a lossy medium with equivalent constitutive parameters determined from simple magnetoionic theory, would be anisotropic. Hence the reflectivity properties would be expressed through a matrix of the form (where the dependence on wave frequency is explicitly indicated)

$$R(\omega) = \begin{bmatrix} R_{vv}(\omega) & R_{hv}(\omega) \\ R_{vh}(\omega) & R_{hh}(\omega) \end{bmatrix} \quad (1b)$$

where

$$R_{vv}(\omega) = \frac{E_{vr}(\omega)}{E_{vi}(\omega)} \quad R_{hv}(\omega) = \frac{E_{hr}(\omega)}{E_{vi}(\omega)} \quad R_{vh}(\omega) = \frac{E_{vr}(\omega)}{E_{hi}(\omega)} \quad R_{hh}(\omega) = \frac{E_{hr}(\omega)}{E_{hi}(\omega)}$$

and where $E_{vi}(\omega)$ and $E_{hi}(\omega)$ are vertically and horizontally polarized components respectively of the incident wave field and $E_{vr}(\omega)$ and $E_{hr}(\omega)$ are analogous components of the reflected wave field.

Allowing both horizontal and vertical components of incident electric field, we have

$$\begin{bmatrix} E_{vr} \\ E_{hr} \end{bmatrix} = \begin{bmatrix} R_{vv} & R_{vh} \\ R_{hv} & R_{hh} \end{bmatrix} \begin{bmatrix} E_{vi} \\ E_{hi} \end{bmatrix} \quad (17)$$

If the incident wave field propagates in the x-z plane, θ_i is the angle of incidence (between the wave vector and the vertical) and θ_r is the angle of reflection, then below the ionosphere (where subscript i means incident and r means reflected), $E_{yi} = E_{hi}$, $E_{xi} = E_{vi} \cos \theta_i$, $E_{zi} = -E_{vi} \sin \theta_i$, $E_{yr} = E_{hr}$, $E_{xr} = -E_{vr} \cos \theta_r$, $E_{zr} = -E_{vr} \sin \theta_r$, $k_{xi} = k_0 \sin \theta_i$, $k_{yi} = 0$, $k_{zi} = k_0 \cos \theta_i$, $k_{xr} = k_0 \sin \theta_r$, $k_{yr} = 0$, $k_{zr} = -k_0 \cos \theta_r$.

The solution of the coupled differential equation system discussed in Sections 4 and 5, would yield the following generic type of results:

$$\begin{aligned} E_x(z) &= \phi_{41}(z, z_0) E_x'(z_0) + \phi_{42}(z, z_0) E_y'(z_0) \\ &\quad + \phi_{43}(z, z_0) E_z'(z_0) + \phi_{44}(z, z_0) E_x(z_0) \\ &\quad + \phi_{45}(z, z_0) E_y(z_0) + \phi_{46}(z, z_0) E_z(z_0), \end{aligned} \quad (18)$$

where $\phi_{lm}(z, z_0)$ is the lm component of a state-transition matrix (STM). In the case of the unperturbed ionosphere, $\phi(z, z_0)$ is the STM indicated in the first term of (13). In the case where the low-frequency disturbance is present, the STM is made up from both the first and second terms of (13) with the aid of (14) by recognizing that $s_0(0)(z)$ is itself a sum of expressions involving elements of the matrix $\phi(z, z_0) \bar{v}(z_0)$. In either case, the STM would be the end-product of an analysis like that which has been described in Sections 4 and 5.

We note that (17) gives us electric field components within the ionosphere in terms of field-components and their z-derivatives at a point z_0 , which could be a point below the lower edge of the ionosphere. In this case, the values of the indicated components at z_0 would be

$$\begin{aligned} E_x(z_0) &= (\cos \theta_i E_{vi} e^{jk_0 z_0 \cos \theta_i} - E_{vr} e^{-jk_0 z_0 \cos \theta_r} \cos \theta_r) \\ E_y(z_0) &= \left[E_{hi} e^{jk_0 z_0 \cos \theta_i} + E_{hr} e^{-jk_0 z_0 \cos \theta_r} \right] \\ E_z(z_0) &= - \left[\sin \theta_i E_{vi} e^{jk_0 z_0 \cos \theta_i} + \sin \theta_r E_{vr} e^{-jk_0 z_0 \cos \theta_r} \right] \\ E_x'(z_0) &= jk_0 \left[\cos^2 \theta_i E_{vi} e^{jk_0 z_0 \cos \theta_i} + \cos^2 \theta_r E_{vr} e^{-jk_0 z_0 \cos \theta_r} \right] \end{aligned}$$

$$\begin{aligned}
 E'_y(z_0) &= jk_0 \left[\cos \theta_i E_{hi} e^{jk_0 z_0 \cos \theta_i} + \cos \theta_r E_{hr} e^{-jk_0 z_0 \cos \theta_r} \right] \\
 E'_z(z_0) &= jk_0 \left[\cos \theta_i \sin \theta_i E_{vi} e^{jk_0 z_0 \cos \theta_i} - \cos \theta_r \sin \theta_r E_{vr} e^{-jk_0 z_0 \cos \theta_r} \right]
 \end{aligned}
 \quad (19)$$

Combining (18) and (19), we would obtain a set of 3 independent simultaneous linear algebraic equations in the variables $E_x(z)$, $E_y(z)$, $E_z(z)$, E_{vr} , E_{hr} , θ_r , E_{vi} , E_{hi} , θ_i . Differentiating (18) with respect to z and again invoking (19), we obtain another set of 3 equations in $E'_x(z)$, $E'_y(z)$ and $E'_z(z)$ in terms of E_{vr} , E_{hr} , θ_r , E_{vi} , E_{hi} , θ_i . Setting z to a value above the level where reflections occur (i.e., where we can assume a plane electromagnetic wave whose wave vector has a positive vertical component and whose field components are $E_x(t)$, $E_y(t)$, $E_z(t)$, and invoking these 6 equations obtained from equations (18) and their derivatives, we will have a set of 6 equations in the unknowns ($E_x(t)$, $E_y(t)$, $E_z(t)$, E_{vr} , E_{hr} , θ_r) in terms of the known incident wave fields E_{vi} and E_{hi} and the known angle of incidence θ_i . The elements of the reflectivity matrix $R(\omega)$ can be calculated from these equations.

Once we have determined $R(\omega)$, we have available a convenient representation of a frequency response matrix for a linear system with two possible inputs E_{vi} and E_{hi} , producing two possible outputs E_{vr} and E_{hr} . By inverse Fourier-transformation of elements of $R(\omega)$, we can obtain an impulse-response matrix for the ionosphere, which might be denoted by $r(t)$. One of the effects of the perturbation due to the low-frequency wave on $R(\omega)$ or $r(t)$, in addition to a possible significant change in the functional dependence of $R(\omega)$ and $r(t)$ on ω and t respectively, is to introduce a slow time variation (a modulation at the low frequency ω_g) into $R(\omega)$ *, in which case it should properly be represented as $R(\omega; \tau)$ where τ represents time in this context. Fourier-transforming $R(\omega; \tau)$ with respect to ω , treating τ as a fixed parameter, leads to a slowly-varying impulse response matrix $r(t; \tau)$.

7. CONCLUSIONS

The theory which has been described here has not been carried to the point of obtaining numerical results beyond the computation of eigenvalues of the system matrix. Thus a great deal of work remains to be done to assess the effectiveness of this theory in predicting quantitative effects of low frequency disturbances of the acoustic-gravity wave type on ionospheric propagation of electromagnetic waves in the kilohertz and megahertz range. It is felt that the first order effects of these disturbances should be revealed by calculations based on this model. There is a possibility, of course, that revelation of the significant effects will require a theory in which horizontal spatial dependence and time-dependence of the ambient ionospheric parameters are accounted for more rigorously. The author and one of his graduate students considered such a theory (Field, 1971), in which calculations are based on the method of characteristics and the theory was applied to a much simpler problem. However, this represents an entirely new order of complexity for the problem at hand and it would be instructive to obtain information from these simpler perturbation models before proceeding to the more rigorous theory.

8. REFERENCES**

1. Field, J.C., April, 1971, "Transient Propagation of Electromagnetic Waves in a Stratified Plasm," Radio Science, Vol.6, No.4, pp. 503-510.
2. Raemer, H.R., 1966, "A Mathematical Model for Analysis of Wave Propagation in a Linearized Vertically Nonuniform Partially Ionized Gas," Canadian Journal of Physics, Vol.44, pp. 1047-1065.
3. Raemer, H.R., 1972, unpublished work (to be completed and submitted for publication).
4. Raemer, H.R. and Verma, Y.P., December 1966, "A Model for Ionospheric Wave Propagation Studies Including Viscosity and Heat Conduction," in Digest of IEEE Symposium, Palo Alto, California, p.234.
5. Raemer, H.R. and Verma, Y.P., September 1970, "An Analytical-numerical Approach to Analysis of Ionospheric Wave Propagation," Radio Science, Vol.5, No.89, pp. 1175-1183.
6. Verma, Y.P. and Raemer, H.R., January 1971, "Coupled Electroacoustic and Electromagnetic Waves in an Inhomogeneous, Compressible and Lossy Plasma," Radio Science, Vol.6, No.1, pp. 113-129.

* As indicated in Section 5 in a typical case, this modulation effect due to the acoustic gravity wave may well be insignificantly small.

** In the bibliographies in References 3 and 4, a large number of research papers by other workers relating to this subject are cited.

H.F. RAY TRACING OF GRAVITY WAVE PERTURBED IONOSPHERIC PROFILES

by

P.L. George

**Australian Defence Scientific Service
Department of supply, Weapons Research Establishment
Salisbury, South Australia**

416

TRAJECTOGRAPHIE H.F. DANS DES PROFILS IONOSPHERIQUES
PERTURBES PAR DES ONDES DE GRAVITE

par

P.L. George

SOMMAIRE

L'auteur expose les résultats de simulations, sur ordinateur, de la direction d'arrivée de trajectoires radio ionosphériques de courte portée, en présence d'une perturbation ionosphérique itinérante d'échelle moyenne. La représentation analytique de cette perturbation est basée à la fois sur des observations réelles et sur la théorie des ondes de gravité atmosphériques internes. Les résultats des calculs portant sur la dépendance à l'égard du temps de la direction d'arrivée et du déplacement doppler, telle qu'on les observerait d'une station au sol, révèlent une bonne concordance qualitative avec les données observées. L'auteur examine, pour un point situé à une faible latitude et pour un point situé à une latitude élevée, la relation entre les variations de la direction d'arrivée, telle qu'elle est donnée par les calculs, et certaines caractéristiques du modèle de perturbation ionosphérique itinérante, qui sont responsables de ces variations.

Il évalue l'exactitude d'un modèle géométrique simple proposé pour la correction de pente de la direction apparente d'arrivée. Il montre comment l'on peut améliorer considérablement les résultats incertains obtenus à l'aide de ce modèle en tenant compte de la direction de la vitesse de propagation et de l'échelle de la perturbation ionosphérique itinérante, paramètres déduits d'une observation continue dans des stations espacées.

H.F. RAY TRACING OF GRAVITY WAVE PERTURBED

IONOSPHERIC PROFILES

P.L. George
Australian Defence Scientific Service
Weapons Research Establishment
South Australia

SUMMARY

This paper reports the results of a computer simulation of the direction of arrival of short range ionospheric radio ray paths in the presence of a medium scale travelling ionospheric disturbance (TID). The analytical representation of the TID is based both on actual observations of such disturbances and upon the theory of internal atmospheric gravity waves. Computed results of the time dependence of direction of arrival and doppler shift, such as would be observed at a ground-based station, show good qualitative agreement with observations. The relationship between the computed direction of arrival variations and certain characteristics of the TID model that produced them is examined at a low latitude and at a high latitude location.

The accuracy of a simple geometrical model that has been proposed for tilt correction of apparent direction of arrival is evaluated. It is shown how the uncertain results derived from use of this model may be substantially improved by taking into account the direction of travel, velocity and scale of the TID, these parameters being derived by continuous observation at spaced stations.

1. INTRODUCTION

Measurements of the direction of arrival of radio signals reflected from the F region by Bramley and Ross (1951) and Bramley (1953) formed one of the early methods of detecting and studying travelling ionospheric disturbances. These authors studied the direction of arrival variations on an oblique path (length ≈ 700 km) and also near vertical incidence. They found that the first order F echo typically exhibits both rapid (second to second) and slow changes of direction from a quasi-period of a few minutes to more than half an hour. They concluded that the F layer could be regarded as tilted in a random manner with an r.m.s. tilt magnitude of a few degrees.

The horizontal velocity of the disturbances was measured by the usual technique of having separated receiving sites and measuring time delays between corresponding events. The results were said to be consistent with the passage through the F region of compressional waves of a wave-length of several hundred kilometres and of a velocity of order 5 - 10 kilometres a minute. Measurements made on two days suggested that the observed slow tilts of the reflecting region were uncorrelated at points separated horizontally by about 50 km.

As far as the rapid second to second fluctuations in direction of arrival were concerned, Bramley (1955) was able to show that a layer of irregular ionisation density within the E region capable of producing a phase path variation of only 3 metres at a frequency of 5 MHz could account for the quiet F layer fast tilt component. As would be expected these fast fluctuations were found to be uncorrelated at an interval of a few seconds and observations at stations 27 km apart showed zero correlation.

Similar observations of tilt have been observed in South Australia by Treharne et. al. (1969) and also near the magnetic dip equator (Treharne 1972). During the day-time observation of equatorial tilts is made difficult by the presence of E region irregularities, however, for the daylight hours (at least during March and April) there seemed to be a systematic tendency for the tilt vector to lie towards the east. At sunset the tilt vector moved towards the west. At night, in the absence of spread F, very large scale slowly varying tilts were observed; these tilts also included medium and small scale variations.

Travelling ionospheric disturbances (TIDs) have of course been studied by many methods ranging through observations of direction of arrival, group path and critical frequency variations, long period amplitude variations, n.f. ground backscatter and phase path and frequency variations among others. Significant contributions to their study have been made by Bramley and Ross (1951), Munro (1950, 1958), Valverde (1958), Tveten (1961), Chan and Villard (1962), Georges (1967), Davis and da Rosa (1969), Davies and Jones (1970) and Sterling, Hooke and Cohen (1971) and in recent years it has been shown that there is quantitative agreement between many observed characteristics of TIDs and those expected theoretically from the interaction of the ionosphere and internal atmospheric gravity waves generated below the ionosphere by some disturbing mechanism in the lower atmosphere.

It appears that the energy from such a disturbance in the lower atmosphere can be thought of as being ducted horizontally along the mesosphere with a certain fraction of the energy leaking continually upwards. Atmospheric wave motions reaching the F region would then typically have periods between a few minutes and an hour and would couple into the ionisation by means of neutral - ion collisions thus perturbing the ionised portion of the atmosphere. In the F region the ion - neutral collision frequency is much less than the ion gyro-frequency so the bulk motion of the ions is constrained to be along the direction of the Earth's magnetic field. Coulomb forces would require corresponding changes in the electron density.

It is apparent then that the redistribution of ionisation which accompanies the passage of an internal atmospheric gravity wave is strongly influenced by the magnetic field orientation to the trajectories of the neutral particles. In particular at low latitudes Hooke (1970) has shown that most

waves observed by means of F region electron concentration perturbations can be expected to be propagating meridionally since the ionisation, which is constrained to remain along the field lines, responds very poorly to waves propagating across the field lines at these latitudes.

Since ionospheric motions impose limitations on the accuracy of radio-location systems, in the last five years or so techniques for correcting apparent direction of arrival where the ionosphere was known to be perturbed, have been developed. The limitation on accuracy is particularly severe at short ranges (100 km) where azimuthal deviations of a fixed remote transmitter can be as large as 100 degrees or more.

Proceeding from the work of Bramley and Ross (1951) a simple plane-tilted ionosphere model has been applied in such a manner that the apparent direction of arrival of a fixed transmitter can be corrected for according to both the prevailing direction and magnitude of the tilt vector normal to the overhead ionosphere and to the ionospheric height. This technique has been applied by Treharne and his colleagues in Australia in 1967 and more recently by Johnson, Martin and Green (1971). Results in general have been conflicting, being often good but sometimes very bad. Effort has been expended in automating equipment so that apparent ionospheric tilts can be measured more quickly and therefore more closely in time to the measurements made on the remote transmitter. (Unfortunately a corresponding amount of effort has not been forthcoming concerning the simple ionosphere model and its inevitable limitations.) The author is convinced that the present occasional unreliability of the tilt-correction d.f. method is largely due to inadequacies of the ionosphere model resulting directly from insufficient understanding of the nature of the ionospheric disturbances perturbing the direction of arrival measurements.

It is the purpose of this paper to present the results of a computer simulation study of the direction of arrival of short range (less than 100 km) radio ray paths in the presence of a typical medium scale travelling disturbance. We shall employ an analytical representation of a TID developed by Georges and Stephenson (1969), the representation being based on actual observations such as those of Munro (1950, 1958) and also upon the theory of internal gravity waves (Hines, 1960).

Computed results of the time dependence of direction of arrival variations and of doppler shift will be compared with ground-based observations of these quantities in order to establish the quality of the simulated TID. The relationship between direction of arrival variations and certain characteristics of the TID producing them will be examined at a low latitude and at a middle latitude site. The accuracy of the simple geometrical model that has been used for tilt correction of apparent directions of arrival will be evaluated. It will be shown how knowledge of the direction of travel, velocity and scale of the TID, such as can be acquired by measurement with spaced stations, can be used to improve the tilt correction process.

2. THE MODEL DISTURBANCE AND RAY TRACING TECHNIQUE

The F region electron concentration, N , at a given time and place, is represented by

$$N = N_0(r, \theta, \phi) \cdot (1 + \beta)$$

where $N_0(r, \theta, \phi)$ is a concentric α -Chapman layer whose parameters have been chosen to represent a daytime F layer, and where β is a perturbation to the concentric model.

The α -Chapman layer can be expressed thus:

$$f_N^2 = f_0^2 \cdot \exp \frac{1}{2} (1 - z - \exp(-z))$$

where f_N is the plasma frequency and z is the reduced scale height which is given by $(h - h_{\max})/H$. h is the height above ground, f_0 is the critical frequency of the layer and H is the scale height.

The perturbation β is given by

$$\beta = \delta \exp \left(\frac{(R - R_0 - z_0)^2}{H'^2} \right) \cos 2\pi \left(t' + \left(\frac{\pi}{2} - \theta \right) \frac{R_0}{\lambda_x} + \frac{(R - R_0)}{\lambda_z} \right)$$

where R_0 is the radius of the earth

r, θ, ϕ are the spherical (earth-centred) polar coordinates

z is the height of maximum wave amplitude

H' is the wave amplitude 'scale height'

δ is the wave perturbation amplitude

λ_x and λ_z are the horizontal and vertical wavelengths

t' is the time in wave periods

The numerical parameters chosen correspond to one of the models used previously by Georges and Stephenson (1969) and are as follows: $f_0 = 6.5$ MHz, $H = 62$ km, $h_{\max} = 300$ km, $z_0 = 250$ km, $H' = 100$ km, $\delta = 0.15$, $\lambda_x = 300$ km, $\lambda_z = 100$ km

The three-dimensional time-varying model represents a TID originating at the north geomagnetic pole and travelling towards the south. It is thus considered to be typical of TIDs observed during periods of low magnetic activity during a northern hemisphere winter and a southern hemisphere summer (see for example Munro, 1958). The perturbed plasma frequency contours are illustrated in figure 1 which shows a north-south section.

In order to ascertain the direction of arrival from a given fixed transmitter in the presence of the TID, and as a function of time as the TID passes overhead, we shall employ a three-dimensional ray-tracing program developed by Jones (1966). This program calculates ray path parameters by numerical integration of a set of differential equations which define the locus of the ray path and the components of the wave normal direction as the ray progresses through the ionosphere. The phase and group refractive indices needed for evaluating the differential equations are calculated with the Appleton-Hartree equation from the ionospheric models specified by the user.

The ray-tracing program allows inclusion of a representation of the earth's magnetic field and an earth-centred dipole model with the north pole located at 78.5°N , 291°E geographic coordinates has been used here. The effect of including collisions in the calculation of the F region ray paths has been examined and found to be negligible. The exclusion of collisions reduces the computer execution time by a factor of five for a single ray. The accuracy of the ray-trace program is known to be high (Lemanski, 1968). (The major error parameter $W42$ was set equal to 10^{-6}).

3. APPARENT DIRECTION OF ARRIVAL

Let us first examine the apparent fluctuations in position of a number of fixed short range transmitters at two geographical locations having quite different magnetic dips. We shall use the same model TID at both locations and shall simulate motion of the TID overhead by stepping the parameter t' of section 2 at intervals between 0 and 1. For each value of t' we shall compute the ray paths joining the location of a given transmitter with the point of observation. We may imagine that we are located at the point of observation and are equipped with an interferometer with which we can measure the apparent direction of arrival, both in elevation and in azimuth. We note here that these parameters, together with the frequency of the transmission, are the only quantities relevant to the remote transmission that would normally be measured at the point of observation during the process of radio direction-finding.

We can think of each downcoming ray from the F region as having undergone a specular reflection from a plane reflector situated at a height h' and parallel to the earth's surface. We can measure h' at a given instant in time and at the appropriate frequency with the aid of a vertical ionosonde located close to the interferometer. In these circumstances the apparent ground range, d , will be numerically equal to $2h'/\tan\Delta'$ where Δ' is the apparent elevation angle of arrival of the downcoming ray and where the bearing of the transmitter will be equal to the apparent bearing, ϕ' .

We give in figures 2 and 3 the apparent locations of three transmitters as a function of t' which represents the passage of the disturbance overhead. The true fixed locations of the transmitters are indicated by the cross in each case. The variation of apparent locations as a function of t' is in every case very severe but is typical of that observed experimentally. It is obvious that accurate d.f. would be impossible unless the distortion or 'tilt' of the reflecting F layer due to the passage of the TID, could be accounted for in some manner.

We wish to draw attention to one important feature common to both figures 2 and 3. In each case the bearing deviations are in a direction parallel to the direction of travel of the TID; thus in the low latitude case (figure 2) the TID looks as though it is arriving from roughly geographic north and the bearing deviations lie along the north-south direction. In the middle latitude case the receiver location is such that the TID originating at the geomagnetic pole seems to come from about 8°E of north and again the bearing deviations are parallel to this direction. (In practice the sense of direction of travel of the disturbance would need to be determined.)

3.1 Direction of overhead ionospheric tilt vector:

A simple way of determining the shape and scale of the distorted F region is to measure the direction of arrival of the return pulse from a transmitter located close to the origin. The leading edge of the first return pulse should correspond to a ray bundle arriving from a direction roughly perpendicular to the tilted layer. The tilt vector will of course vary in magnitude and direction as the disturbance passes overhead. Again the average tilt vector will lie in the direction of travel of the TID. We give in figure 4 the 'observed' magnitude of the reflecting F region tilt as a function of time and space. We arbitrarily define the tilt as being positive when the point of intersection of the tilt vector and the ground is deviated northwards of the origin and we define the tilt angle, ϵ , as the angle between the tilt vector and the zenith, that is the complement of the angle at which the tilt vector strikes the ground.

The 'observed' tilt is very similar at both locations. The spatial scale of the tilt is fixed by the assumed model as indicated but the time scale is in a sense arbitrary because we have not yet had to specify a velocity for the disturbance. If we assume that the velocity is 10 km/min , then we have a horizontal period of 30 minutes which is reasonable and approaches the upper limit of what might be termed a medium scale TID. We see from figure 4 that even with a horizontal wavelength of 300 km the rate of change of tilt with distance from the origin can be as much as one degree in 5 km . This rate of change is obviously associated with the shape and scale of the reflecting surface, that is roughly, at a fixed operating frequency, the shape of the appropriate plasma frequency contour. We indicate schematically in figure 5 the relation between the distortion of the plasma frequency contour and the observed tilt. The vertical scale of the plasma frequency contour has been exaggerated but the asymmetry evident is typical, as can be seen by inspection of figure 1.

4. COMPARISON WITH EXPERIMENT

Before proceeding to an evaluation of the simple plane tilted ionosphere model currently in use in short-range direction-finding work we wish to establish the quality of the simulation of the TID. To this end we compare observable quantities, derived synthetically by ray-tracing the TID, with typical experimental observations of these quantities.

We consider first the doppler shift associated with the passage of the disturbance overhead. Davies and Jones (1971) have conducted a series of experiments using the doppler technique to investigate medium scale TIDs. We give below an example of a simulation of their doppler records pertaining to a middle latitude site near Boulder, U.S.A. We give in figure 6 the derived doppler shift appropriate to a 55 km path at roughly 90° to the direction of travel of a disturbance, together with the derived doppler appropriate to vertical incidence. These records may be compared with a tracing of a typical doppler record observed on one 25 km leg of their spaced receiver doppler experiment. The similarity is obvious and the interested reader will find in reference 8 many other doppler records of disturbances displaying the typical features seen here.

It will be noticed that as with the tilt angle simulation the asymmetric waveform seems to be typical of these TIDs. In some circumstances this asymmetry can be used to determine the sense of direction of travel of the TID. It is perhaps not surprising that the tilt angle and doppler records display similar features since it can be shown analytically that there is a very close relationship between these two variables (Bennett, 1970).

Let us now compare the overhead tilt angle derived as a function of time from the simulated TID ray tracing with some experimental results taken from Johnson, Martin and Green (1971). We give in figure 7 their observed tilt angle plotted in polar form. Clearly the mean direction of travel of the TID is along a bearing 25° west of north. In figure 8a we plot this time series of tilt angle without regard to sign of the tilt. This manner of presentation is common but in a sense misleading, because it tends to indicate quasi-periodicities roughly one half that of the true period of the TID. The correct way to establish periodicity from tilt angle measurements is first to establish the direction of travel of the TID with respect to the origin and then to assign positive or negative signs to the observed tilts according to whether they are forward or backward of a line drawn at 90° to the TID direction of travel. Figure 8b illustrates the result of applying this procedure. The negative tilts are no longer folded back onto the positive axis and the true periodicity of the TID is apparent. Figure 8c indicates the simulated noise-free tilt observations derived from the TID ray-tracing. There are obvious similarities.

5. SIMPLE TILT CORRECTION MODEL

We wish now to consider the simple tilt correction model mentioned previously. Figure 9 illustrates the principle of the method. The ionosphere overhead at an instant in time is assumed to be tilted through an angle ϵ from the horizontal. It is further assumed that the instantaneous magnitude and direction of the normal vector to the ionosphere can be measured at the origin, C, by measuring the direction of arrival (Δ_c, θ_c) of the return pulse from a transmitter located at, or very near, C.

The tilt vector at D is assumed to be the same as that at C. For small angles the difference in height h' at C and D is considered negligible in the range - bearing calculation. The ray from the transmitter at A is assumed to undergo a specular reflection at the tilted ionosphere at height h' over, which is again essentially h' . The effect of a small difference $\Delta h'$ upon the position of a downcoming ray at C can be shown to be negligible compared to the changes in position due to the measured differences in tilt angle ϵ .

The simple geometrical solutions for range and bearing are given in Appendix 1. Note that the tilt vector and the ray path are coplanar and that the only observable quantities at C are the quantities $h', \Delta', \theta',$ and Δ_c, θ_c .

Let us consider the effect of using the synthesised tilt measurement (figure 4 gives $\epsilon(t)$, and $\theta(t) \approx 0^\circ$) to correct the apparent directions of arrival corresponding to low latitude results given in figure 2. The equations of Appendix 1 have been used to calculate the true ranges and bearings as a function of t' and these results are shown in figure 10. Note that an additional transmitter has been added at distance 45 km and bearing 10°. When similar calculations are also made for the middle latitude site it is apparent that both sites display essentially similar characteristics which are entirely consistent with practical experience:

- (a) instantaneous position estimates can be either good or very bad and are about equally distributed. Bad results are not transient in time since they can occur for up to half a period (10-15 minutes).
- (b) the range of the mean position, derived from consolidation of a series of measurements spread over one or two periods of the disturbance, always exceeds the true position. This difference is small when propagation is in the east-west direction but becomes progressively larger as the azimuth of propagation approaches the magnetic meridian.

Experience gained with ray-tracing various model disturbances makes it clear that the two effects mentioned above are directly related to two systematic errors made in application of the simple tilted ionosphere model. The first error is essentially geometrical and arises from the fact that the effective tilt at an ionospheric reflection point up to 50 km away from the origin is assumed to be the same as that measured at the origin at that instant in time. Figure 4 (or 5) shows very clearly the inadequacy of this assumption since it is clear that the spatial correlation between a tilt measured at the origin and one that is effective distance d from the origin is not in general a constant for a given distance. Thus an interferometer situated arbitrarily at $d = 150$ km (figure 4) would measure a tilt which is almost constant ($\pm 0.5^\circ$) for all distances from 80 - 160 km along the north-south direction, but which is substantially different from that between 160 and 240 km along the same direction.

The isoclinic contours associated with a travelling disturbance are corrugated along the direction of travel of the disturbance and this corrugated structure is for all practical purposes maintained for a distance greatly exceeding 100 km along a direction 90° to the direction of travel. In other words, a tilt measurement at the origin can be expected to be essentially constant with distance only along a line passing through the origin and having direction approximately 90° to the direction of travel of the TID.

In the circumstances indicated above it is obvious that all direction of arrival observations should not be treated as being of equal weight when the simple tilt correction method is applied. Greatest weight should be attached to observations whose apparent bearings lie at about 90° to the TID direction and which occur at times when the ionosphere tilt is small. Conversely least weight should be attached to observations occurring at times when large tilt angles coincide with apparent directions of arrival which lie along the TID direction because the rate of change of effective tilt with distance is then greatest.

The second systematic error which we have mentioned, namely the over-estimation of range in consolidated measurements, appears to be due to neglect of the effect of the earth's magnetic field upon

the ray path geometry. Near vertical incidence the ordinary ray path at the apogee is essentially quasi-transverse (Katoliffe, 1959) and the ray tends to make an angle of 90° with the direction of the magnetic field vector. This leads to a distortion of the ray path which in the limiting case is referred to as a 'spitae'. This ray path distortion leads to the ground range associated with a given high elevation angle being extremely azimuth dependent. In figure 12 we indicate the percentage range error associated with neglect of the Earth's magnetic field for short range ray paths having elevation angles between 80° and 90° and azimuths of transmission between 0° and 180° . We define the triangulation range, d , in a concentric ionosphere to be given by $2h'/\tan \Delta'$ and we compare this with the actual range as deduced from the oblique ray trace. As can be seen the range errors arising from neglect of the magnetic field effect can be considerable, rising to 25% at the dip equator for rays propagating along the meridian. Errors decrease rapidly with increasing dip angle but a 10% error is still possible at a dip angle of 50° . Range errors along the east-west direction are in general less than 6% at all dip angles.

6. IMPROVEMENT OF THE SIMPLE TILT CORRECTION MODEL

We now consider the way in which knowledge of the direction of travel, velocity and scale of the TID, such as can be acquired by continuous observations with spaced stations, can be used to improve the tilt correction process.

Let us begin by assuming that we have been able, by continuous observation, to measure the magnitude and direction of the overhead tilt vector at the origin. Let us suppose that while continuing to observe the tilt vector we also observe the direction of arrival of rays from an unknown remote transmitter. Our problem is firstly to determine, from the apparent azimuth and elevation angles of the unknown transmitter, the vector joining the origin and the remote reflection point. This is given simply by equation 3 in Appendix 1. Having established the direction of motion of the TID from the tilt vector measurements we then take the component of the origin-to-reflection-point vector that lies in the direction of travel of the TID, that is, we calculate the magnitude of $BC \cos(\beta_{TID} - \beta')$ where β_{TID} is the direction of travel of the TID. Since we have observed the tilt as a function of time we can construct (and continuously update) the $\epsilon(t)$ record of figure 4. Knowledge of the velocity of the TID, determined from the time displacements relating to a common event (perhaps the large negative tilt peak) observed at the 3 spaced stations, will enable the time scale to be supplemented by a distance scale. Now in order to determine the effective tilt at the remote reflection point at a given time we need only progress from the point on the distance scale corresponding to the tilt measured at the origin, a distance $BC \cos(\beta_{TID} - \beta')$ in the appropriate direction along the scale which will then indicate the required tilt.

As we have pointed out before when the apparent azimuth β' is about 90° to the direction of travel of the TID the tilt observed at the origin will be the same as that observed at the remote reflection point. When, however, β' is along the direction of travel of the TID then the tilt at the remote reflection point may be very substantially different from that at the origin. If the general concept of the simple plane tilted ionosphere model is retained but the tilt at a given remote reflection point is calculated as indicated above and this tilt is used instead of the tilt at the origin, the overall d.f. results can be shown to be considerably better than those given in figure 10. However this does not seem to be the optimum method of using the tilt information. It is clear that the ionosphere is tilted to a varying degree over the whole ionospheric path so various ways of averaging the tilt over the path in the ionosphere have been tested empirically. It has been found that the spatial average of the tilt measured at the origin and that measured at the remote reflection point gives the most consistent and most accurate answers when used in the simple model.

Thus we give in figure 12 the results of recalculating the points in figure 10 but this time using the technique outlined above. If after consolidation of a number of results extending over at least one wave period and calculation of a mean, the systematic magnetic field correction is also made, the mean consolidated answer is quite reliable, being normally within 5% of the true position. The computed bearing accuracy is particularly high, being usually within 2 degrees of the correct bearing and often very much closer than this.

When the above technique is applied at high dip latitudes exceeding 60° or so, it is occasionally found that propagation paths passing through ionospheric regions where the tilt is changing very rapidly will give highly erroneous results even when the spatial average tilt method is applied. This seems to be basically a magnetic field effect since it does not seem to occur at low dip latitudes. Perhaps the large lateral deviation near apogee of the ordinary wave has an effect comparable to the tilt effect at high dip angles. It is in fact possible at high dip latitudes to generate forbidden zones such that no ray paths can exist between a transmitter and a receiver some tens of kilometres distant. Under such conditions a range/bearing polar plot of ground landing points, corresponding to a range of elevation angles at the origin, can assume an extremely distorted appearance. It should perhaps be pointed out that for a plane parallel isotropic ionosphere the locus of ground range at a constant elevation angle is a circle centred on the origin (at least up to a 100 km or so). For moderate tilts at reasonable dip latitudes these circles degenerate into ellipses whose centre is offset from the origin as indicated in figure 13. For the high dip angles mentioned above and for extreme tilts, the range and bearing plot can have the appearance of that in figure 14. Under such conditions no simple triangulation model can be expected to give reliable d.f. results.

7. CONCLUDING REMARKS

We have presented the results of a computer simulation of the time variation of direction of arrival of short range ionospheric radio ray paths in the presence of a realistic medium-scale travelling ionospheric disturbance. The quality of the simulation has been established by comparison of simulated doppler records and records of the time variation of F region tilt angles with experimental observations of these quantities.

We have examined by simulation the apparent azimuth deviation of a number of fixed remote transmitters as the simulated TID passes overhead. This study has been carried out at a low latitude and a middle latitude site and we have noted that the locus of the azimuth deviations always lies in a direction parallel to that of the motion of the TID. We have pointed out that in such circumstances

instantaneous measurements of d.f. bearings on a remote transmitter cannot be considered to be of equal weight. In particular those bearing cuts taken when the apparent direction of arrival lies along the direction of travel of the TID are considered to be of low reliability, whereas those taken when the direction of arrival lies at about 90° to the direction of travel of the TID are considered to be of high reliability and this is particularly so if the overhead tilt is also less than 2° or so.

We have related observed time series of overhead tilt angle to the shape and scale of the TID and have shown that a common method of presentation of tilt angle results underestimates the periodicity of the TID observed by a factor of roughly two. We have indicated how this may be avoided.

The accuracy of a simple plane tilted ionosphere model has been evaluated and the synthesized results show that the uncertain d.f. results commonly seen in practice at short range are mainly due to inadequacies in the simple ionosphere model. In particular we have drawn attention to two systematic errors arising in application of this model. The first essentially geometric error arises from the assumption that the instantaneous overhead tilt is maintained for a distance of about 50 km from the origin on all azimuths. The rate of change of tilt with distance in the presence of TID's has been shown to be strongly azimuth sensitive.

The second error arises from neglect of the effect of the earth's magnetic field upon the ionospheric ray paths and it is shown that this neglect, which is most severe at low latitudes and in particular along the direction of the magnetic meridian, can lead to range errors (even in an unperturbed ionosphere) of at least 25%.

Finally we have considered the manner in which knowledge of the direction of travel, velocity and scale of a TID, such as might be obtained by continuous observation with spaced stations, can be used to improve the simple tilted ionosphere model. We have been able to demonstrate a substantial improvement in direction finding when these factors are taken into account. Nevertheless we have also pointed out that at high dip latitudes, short range propagation paths can be so distorted in the presence of a TID that for a certain fraction of the period of a TID no simple model can be expected to account for the resulting distorted range and bearing plots. An example of this circumstance has been given and no means of coping with it are yet known.

8. ACKNOWLEDGEMENTS

The author acknowledges stimulating discussion with Dr. Kenneth Davies during the course of the later stages of this work. He is also grateful to the Australian Commonwealth Public Service Board for support derived from an Overseas Postgraduate Award.

The later stages of this work were carried out at the U.S. Department of Commerce National Oceanic and Atmospheric Administration Environmental Research Laboratories and the author is grateful to the Director of those Laboratories for providing facilities for him to complete this research.

REFERENCES

1. BENNETT, J.A. 1971 "Some relations involving the angles of arrival and departure of a ray", *Aust. J. Phys.*, **24**, pp 119 - 123
2. BRAMLEY, E.N. 1953 "Direction-finding studies of large-scale ionospheric irregularities", *Proc. Roy. Soc., A*, **220**, p 39
3. BRAMLEY, E.N. 1955 "Some comparative directional measurements on short radio waves over different transmission paths", *Proc. IEE*, **102**, p 544
4. BRAMLEY, E.N. and ROSS, W. 1951 "Measurements of the direction of arrival of short radio waves reflected at the ionosphere", *Proc. Roy. Soc., London, A*, **207**, p 251
5. CHAN, K.N. and VILLARD, O.C. 1962 "Observations of large scale travelling ionospheric disturbances by spaced path h.f. instantaneous frequency measurements", *J. Geophys. Res.*, **67**, pp 973 - 988
6. DAVIES, K. and JONES, J.E. 1971 "Three-dimensional observations of travelling ionospheric disturbances", *J. Atmos. Terr. Phys.*, **33**, pp 39 - 46
7. DAVIS, M.J. and DA ROSA, A.V. 1969 "TIDs originating in the auroral oval during polar sub-storms", *J. Geophys. Res.*, **74**, pp 5721 - 5735
8. GEORGES, T.M. 1967 "Ionospheric effects of atmospheric waves", U.S. Department of Commerce, ESSA Technical Report IER 57 - ITSA 54, October 1967
9. HINKS, C.O. 1960 "Internal atmospheric gravity waves at ionospheric heights", *Can. J. Phys.*, **38**, pp 1441 - 1481
10. HOOKE, W.H. 1970 "The ionospheric response to internal gravity waves, 1, The F2 region response", *J. Geophys. Res., Space Physics*, **75**, 28, pp 5535 - 5544
11. JOHNSON, E.L., MARTIN, P.F. and GREEN, T.C. 1971 "Short time scale ionospheric tilt measurements for lateral deviation compensation", *Proc. of 4th Allerton House conference on h.f. radio direction finding and radio-location research*, 2-4th June 1971, ERL publication no. 389, Dept. of electrical engineering, University of Illinois, Urbana, Illinois 61801
12. JONES, R.M. 1966 "A three-dimensional ray-tracing computer program", U.S. Department of Commerce, ESSA technical report IER 17/ITSA - 17, U.S. Government printing office.
13. LEMANSKI, T.J. 1968 "An evaluation of the ITSA 3-D ray trace program", *Radio Sci.*, **3**, No. 1, pp 95 - 100
14. MUNRO, G.H. 1950 "Travelling disturbances in the ionosphere", *Proc. Roy. Soc. London, A*, **202**, p 208
15. RATULIFFE, J.A. 1958 "Travelling ionospheric disturbances in the F-region", *Aust. J. Phys.*, **11**, p 91
- 1959 "The magneto-ionic theory and its application to the ionosphere", Cambridge University Press

16. STERLING, D.L., 1971 "Travelling ionospheric disturbances observed at the magnetic
MOORE, W.K. and equator", J. Geophys. Res., 76, No. 16, pp 3777 - 3782
COHEN, R.
17. TREHARNE, R.F., 1969 "Ionospheric tilt observations in South Australia", I.R.E.E. (Aust)
RAYMOND, M.L.J. and 12th National Radio and Electronics Conference, Sydney, Australia,
ELLARD, R.M. p. 164
18. TREHARNE, R.F. 1972 "Ionospheric tilt observations near the magnetic dip equator", To be
presented at the NATO-AGARD conference on "The effect of atmospheric
acoustic gravity waves on electromagnetic wave propagation", to be
held at Wiesbaden, West Germany, April 1972
19. TYSTAN, L.H. 1961 "Ionospheric motions observed with high frequency backscatter
sounders", J. Res. NBS, 65 D, pp 115 - 127
20. VALVERDE, J.F. 1958 "Motions of large scale travelling disturbances determined from high
frequency backscatter and vertical incidence records", Sci. Rept.
No. 1., Stanford Electronics Laboratories

APPENDIX I

Simple plane tilted ionosphere geometry : (figure 9)

$$\begin{aligned}
 DB &= h' \sin \epsilon & (1) \\
 OC &= h' \cos \epsilon / \sin \Delta' & (2) \\
 BC &= h' \cos \epsilon / \tan \Delta' & (3) \\
 CD^2 &= DB^2 + BC^2 - 2 DB \cdot BC \cdot \cos (\theta_t - \theta') & (4) \\
 \sin Y &= BD \cdot \sin (\theta_t - \theta') / CD & (5) \\
 \text{True bearing } X &= O' - Y & (6) \\
 \cos (DCO) &= (DC^2 + OC^2 - h'^2) / 2 DC \cdot OC & (7) \\
 \sin (DOC) &= DC \cdot \sin (DCO) / h' & (8) \\
 (OAD) &= \pi - 2 (DOC) - (OCD) & (9) \\
 AD &= \sin (AOD) \cdot h' / \sin (OAD) & (10) \\
 \text{Range} &= CD + AD & (11)
 \end{aligned}$$

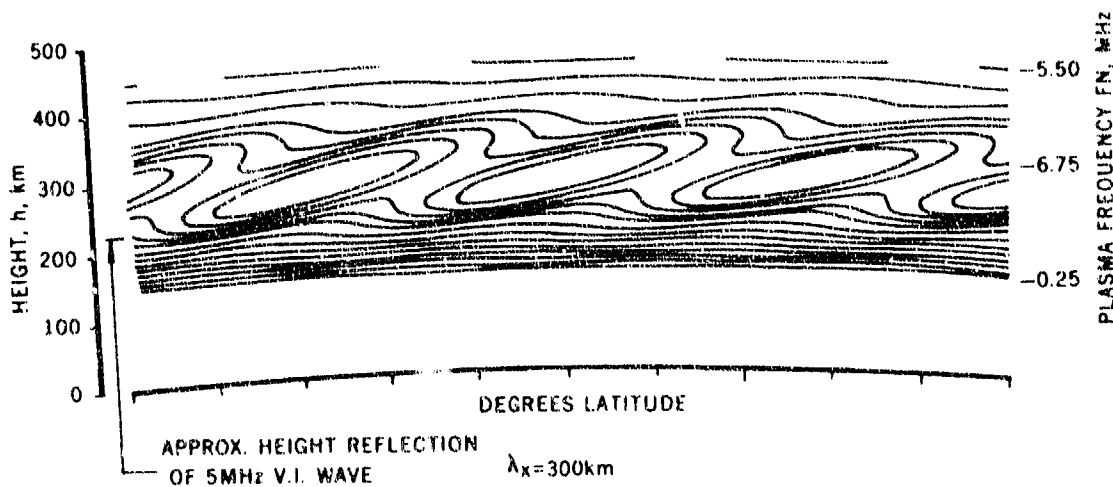


Fig. 1 This model ionosphere perturbed by a TID. Plasma frequency contours as a function of height and latitude.

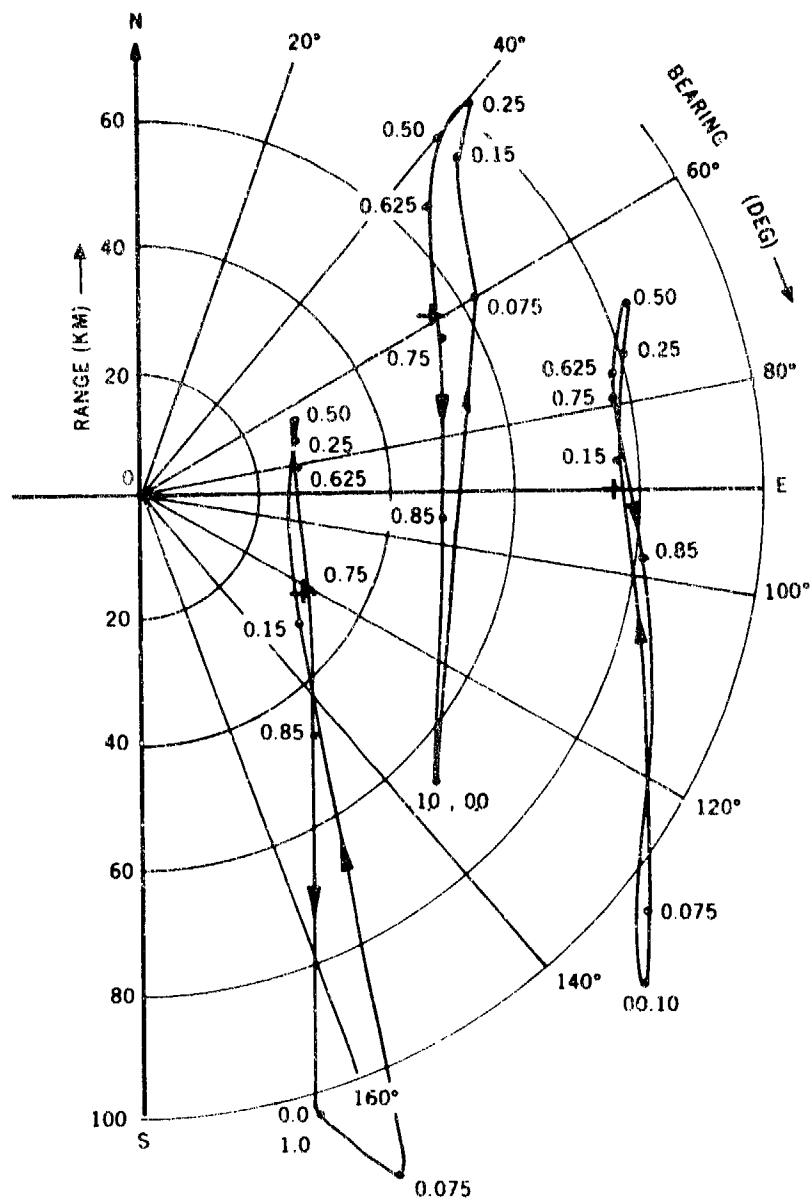


Fig. 2 The apparent position as a function of time of three hypothetical remote transmitters situated at about 10° S dip latitude.

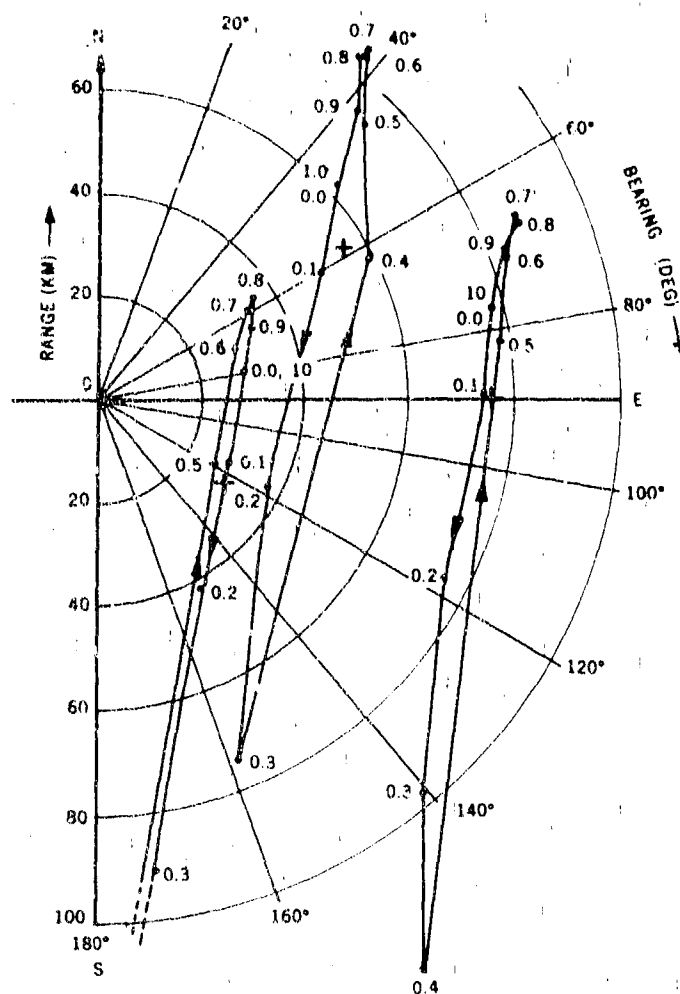


Fig. 3 The apparent position as a function of time of three hypothetical remote transmitters at about 60°N dip latitude.

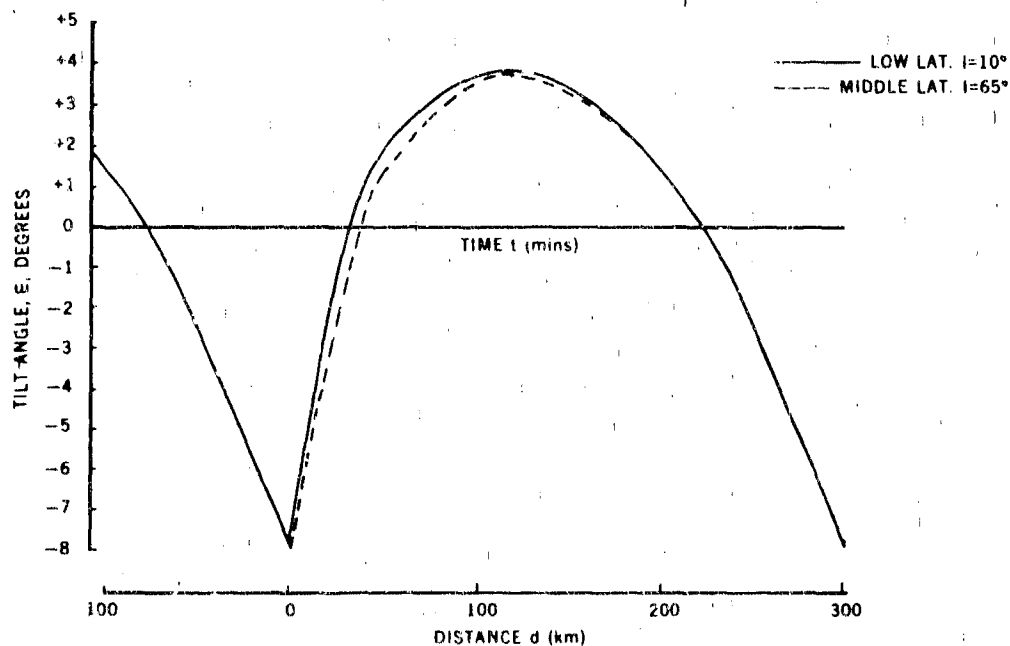


Fig. 4 The magnitude of the ionosphere tilt vector as a function of time for both the low latitude site (solid line) and the middle latitude site (broken line).

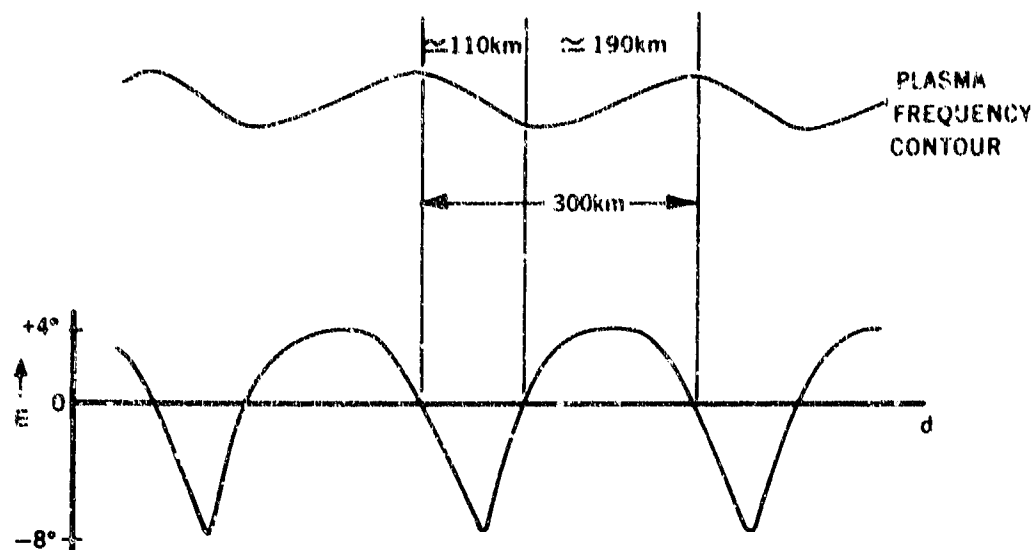


Fig. 5 The relation between the observed ionosphere tilt vector and the distorted plasma frequency contour.

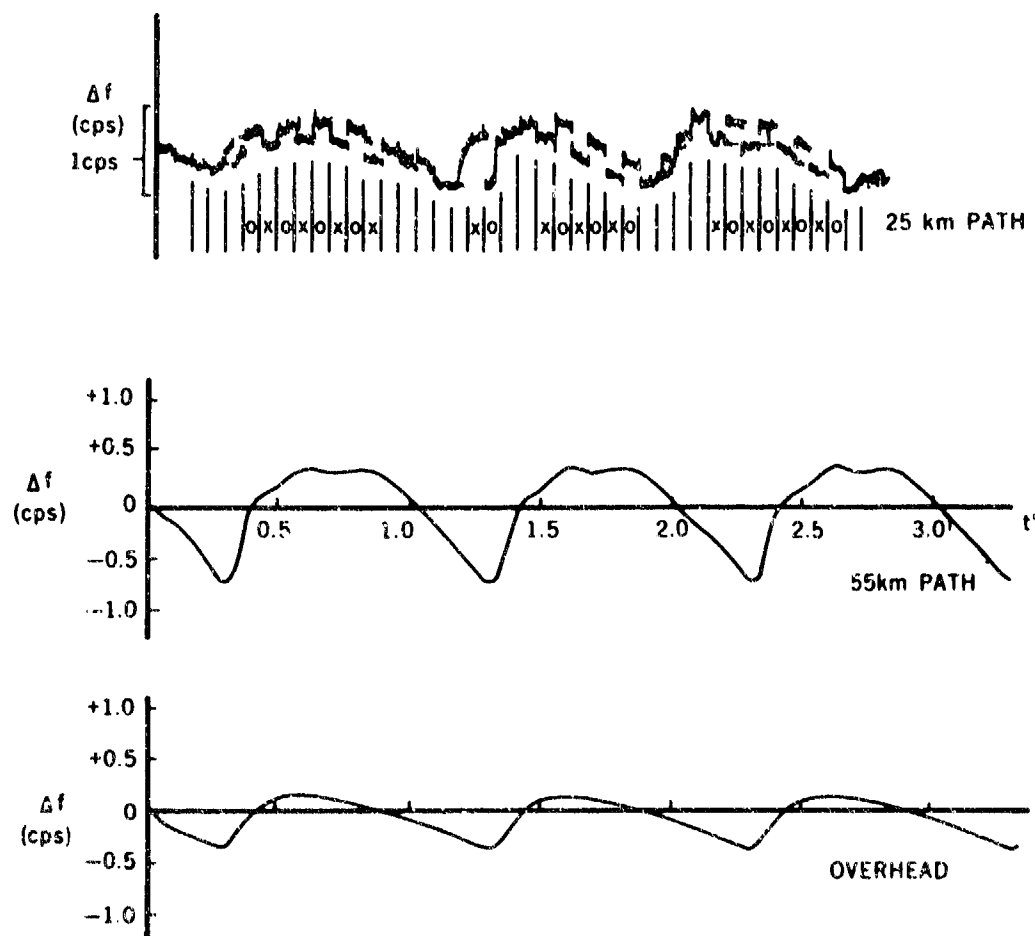


Fig. 6 Comparison of synthesized and experimental doppler shifts.
 a. experimental 25 km path
 b. synthesized 55 km path
 c. synthesized vertical incidence

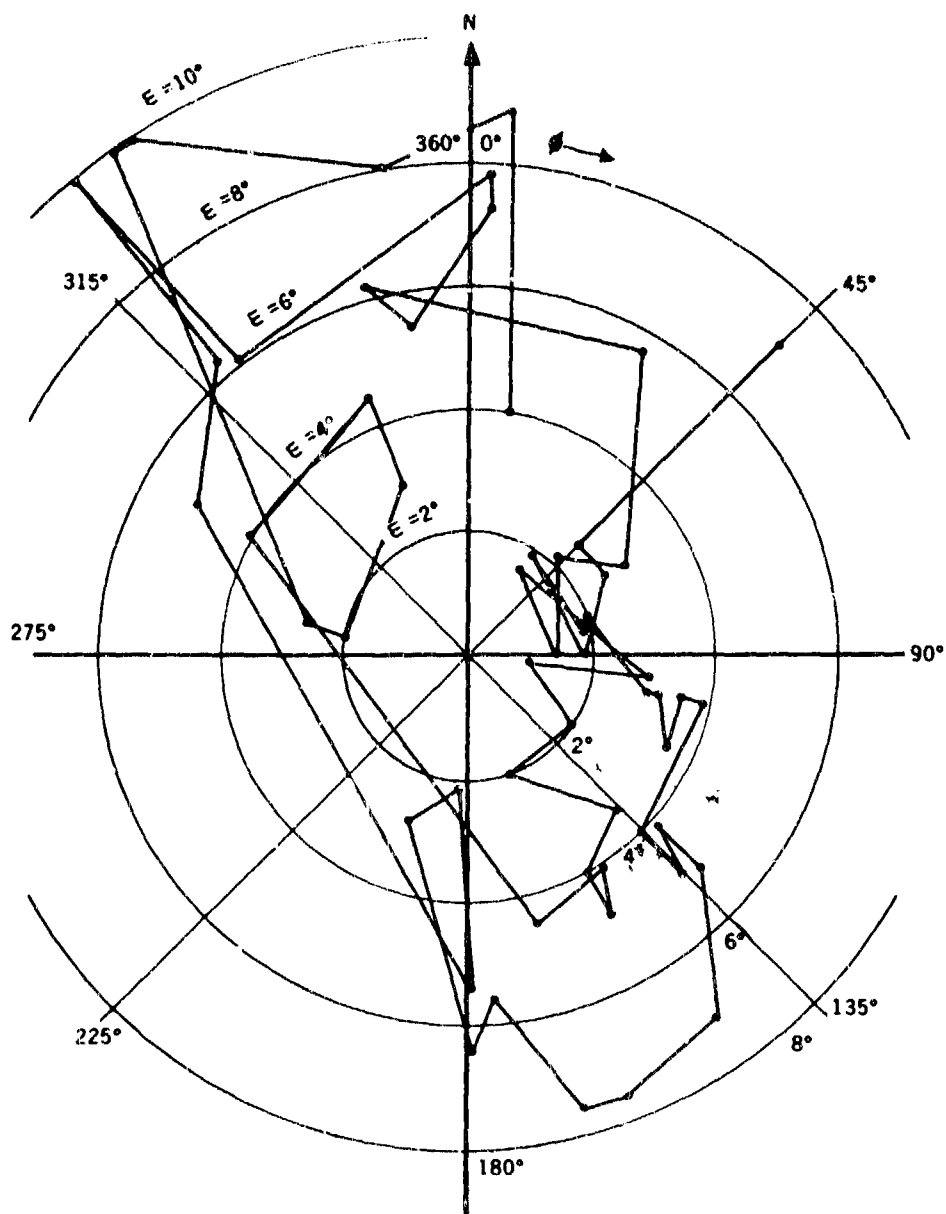


Fig. 7 The tilt observations of reference 11 in polar form.

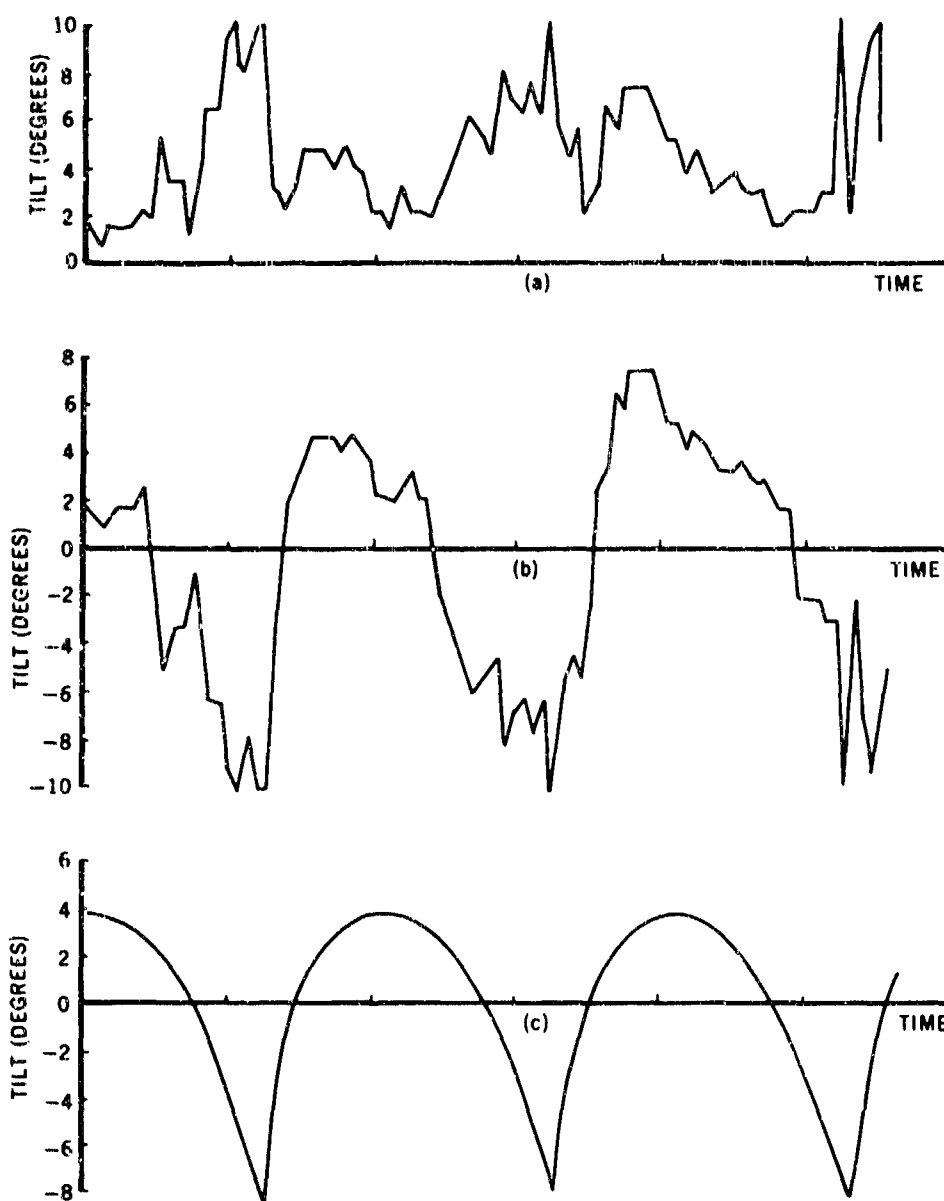


Fig. 8 The time series of tilt observations of reference 11 compared with theory.
 a. the observed magnitude of the tilt vector as a function of time
 b. the sense and magnitude of the tilt observations as a function of time
 c. the theoretical variation of tilt with time

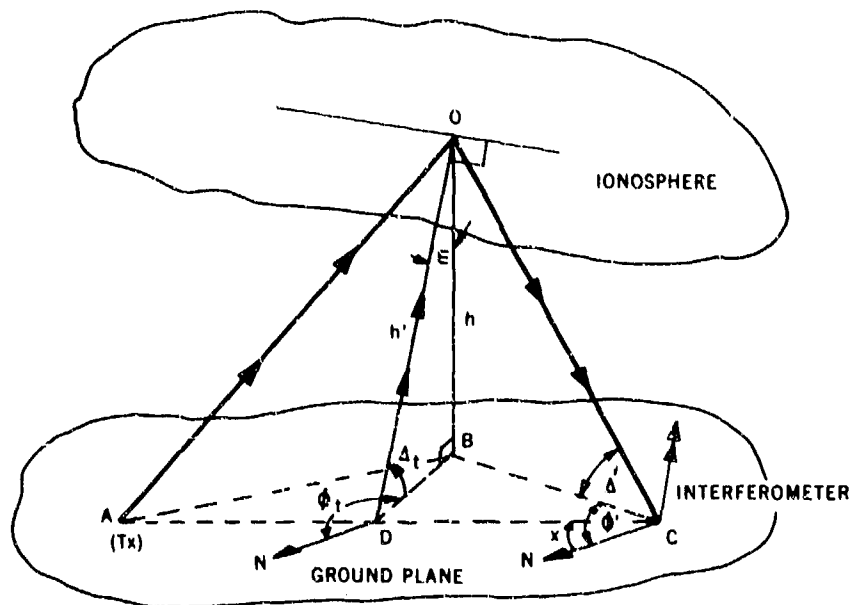


Fig. 9 The geometry of the simple plane tilted ionosphere model.

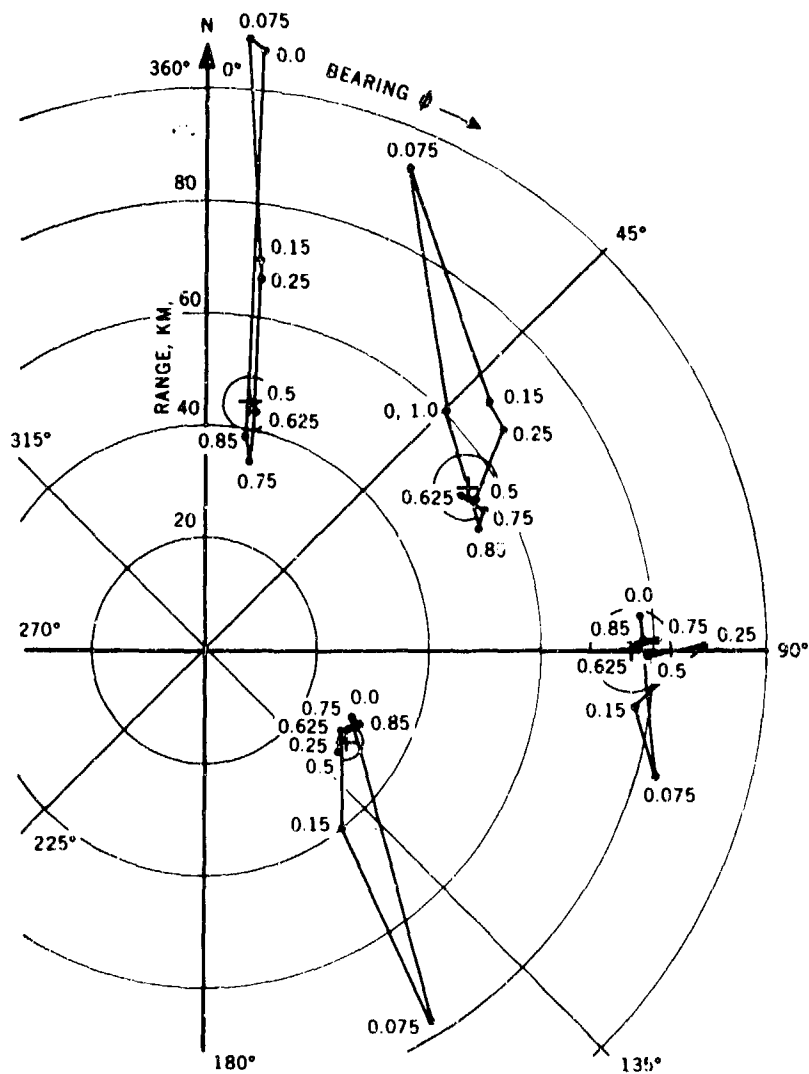


Fig. 10 Results of applying the simple tilt model to the d.f. results of figure 2.

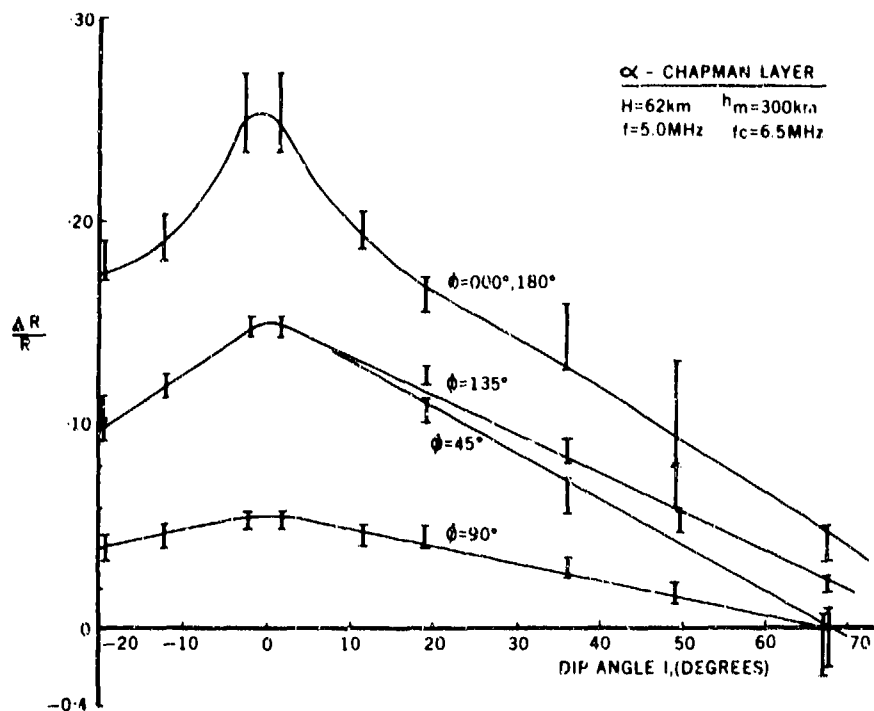


Fig. 11 The systematic error in range due to neglect of the Earth's magnetic field.

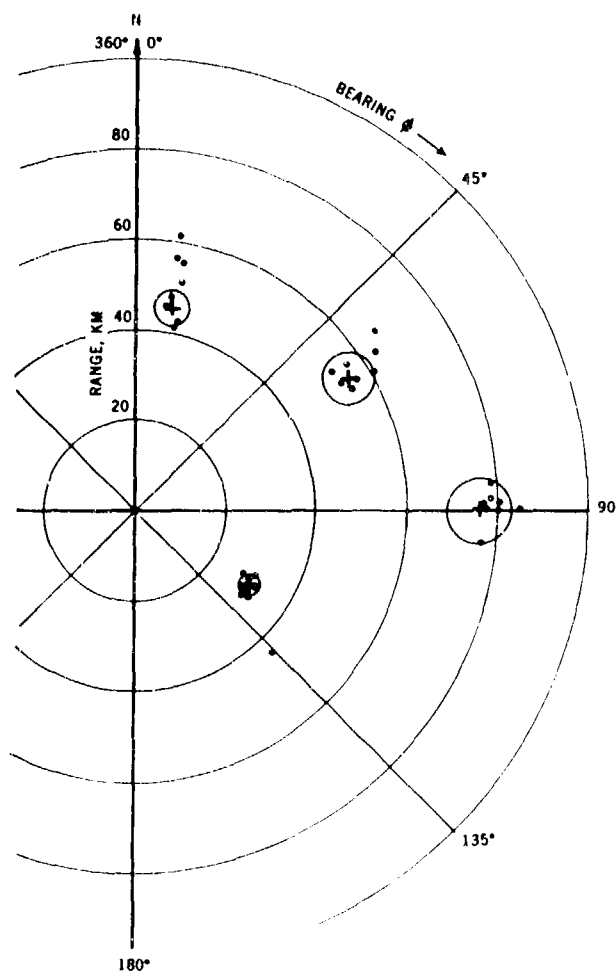


Fig. 12 Recalculation of the results of figure 10 using the spatial average tilt technique.

**SOME EFFECTS OF ATMOSPHERIC GRAVITY WAVES OBSERVED
ON A TRANSEQUATORIAL RADIO PATH**

by

J. Röttger

Max-Planck-Institute für Aeronomie
3411, Lindau/Harz
W. Germany

433

QUELQUES EFFETS DES ONDES DE GRAVITE ATMOSPHERIQUES OBSERVES SUR UNE LIAISON RADIO TRANSEQUATORIALE

par

J. Röttger

SOMMAIRE

L'auteur étudie l'influence des ondes de gravité atmosphériques sur la propagation d'ondes radio HF d'un point à un autre à travers l'ionosphère, dans deux cas particuliers : celui où les ondes de gravité se propagent parallèlement au plan du grand cercle qui joint les extrémités de la liaison, et celui où elles se propagent transversalement.

Des mesures ont été effectuées le long de la trajectoire radio HF, transéquatoriale nord-sud, reliant Lindau (Allemagne de l'Ouest) à Tsameb (Afrique du Sud-Ouest) ; ces mesures, réalisées à l'aide d'émetteurs à ondes entretenues de fréquence fixe, ont révélé des variations périodiques et nocturnes de l'amplitude du champ, que l'on suppose être dues à une focalisation provoquée par des ondes de gravité atmosphériques se propageant du nord au sud. Des calculs de trajectographie montrent qu'il peut se produire des focalisations périodiques lorsqu'on utilise des profils ionosphériques perturbés par des ondes de gravité atmosphériques. On effectue une analyse de densité d'énergie des configurations de l'amplitude du champ enregistrées, afin d'obtenir des indications sur les principales périodes de fluctuation.

On observe des déviations d'azimut allant jusqu'à 50° à l'est et à l'ouest du grand cercle passant par Lindau et Tsameb ; on peut expliquer ces déviations par la réflexion et la diffusion latérales dues à des irrégularités de l'F diffus équatorial. Les variations du temps de propagation et de l'azimut indiquent la présence de perturbations ionosphériques itinérantes se déplaçant d'ouest en est dans la zone équatoriale. La vitesse et la distance horizontale des zones où apparaît périodiquement une réflexion latérale sont comparables à celles relatives aux ondes de gravité atmosphériques.

SOME EFFECTS OF ATMOSPHERIC GRAVITY WAVES OBSERVED ON A TRANSEQUATORIAL RADIO PATH

J. Röttger
Max-Planck-Institut für Aeronomie
3411 Lindau/Harz, W.Germany

SUMMARY

The influence of atmospheric gravity waves on the point-to-point propagation of HF radio waves in the ionosphere is investigated for two cases: The gravity waves are propagating in direction of the great circle between two points, and the gravity waves are propagating transverse to the great-circle direction.

Measurements on the north-south directed transequatorial HF radio path Lindau/W.Germany - Tsumeb/South West Africa using fixed-frequency CW transmitters show periodical fieldstrength variations during night-time hours, which are assumed to be caused by focussing due to north-south propagating atmospheric gravity waves. Ray-tracing calculations prove that periodical focussing can occur when ionospheric profiles perturbed by atmospheric gravity waves are employed. A power density analysis of the recorded fieldstrength patterns is carried out in order to obtain indications about the main fading periods.

Azimuthal deviations up to 50° east and west of the great circle Lindau - Tsumeb are observed and can be explained by side reflection and side scattering due to irregularities of the equatorial spread-F. The variation in propagation time and azimuth angle is indicating traveling ionospheric disturbances moving from west to east in the equatorial zone. The velocity and the horizontal distance of periodically occurring side-reflection areas are similar to those values concerning atmospheric gravity waves.

1. INTRODUCTION

Investigations of the effect of atmospheric gravity waves on the HF radio wave propagation were carried out, concerning vertical sounding experiments (Bowman, 1960, 1968; Klostermeyer, 1965; Baker and Gledhill, 1965), and concerning oblique-incidence backscatter sounding (Tveten, 1961; Hunsucker and Tveten, 1967; Croft, 1968; Georges and Stephenson, 1969). The influence of traveling ionospheric disturbances on the point-to-point propagation of HF radio waves essentially was investigated by Davies and Chang (1968), Georges (1968), and Nielson (1969) using HF Doppler observations.

This paper outlines some results basing on point-to-point oblique-incidence pulse sounding, incidence angle, and CW fieldstrength measurements. Some examples will be given showing the influence of atmospheric gravity waves on short-wave radio propagation on the transequatorial path Lindau/W.Germany - Tsumeb/South West Africa. Two different cases will be considered:

1. The gravity waves are propagating in direction of the great circle between Lindau and Tsumeb, which is approximately the north-south direction.
2. The gravity waves are propagating transverse to the great circle, that means approximately in west-east direction.

Besides group- and phase-path variations, gravity waves concerning case 1 are effecting variations in fieldstrength of radio signals caused by focussing and defocussing. These effects can be demonstrated by using ray tracing in ionospheric profiles perturbed by atmospheric gravity waves. Measurements on the radio path Lindau - Tsumeb (fig. 1) using fixed-frequency CW transmitters often show periodical fieldstrength variations. By employing a power density analysis it is assumed that these periodical fieldstrength patterns may be caused by focussing due to atmospheric gravity waves.

The gradients of plasma frequency caused by gravity waves of case 2 are leading to a lateral deviation of the transmitted radio signal (off-great-circle propagation). Pulse transmissions on the oblique-incidence path Lindau - Tsumeb using a rotating direction finder antenna evidently show that azimuthal deviations up to 50° east and west of the great-circle direction (fig. 1) are regularly observed after sunset. This type of off-great-circle propagation is due to irregularities of the equatorial spread-F. The variation in propagation time and azimuth angle of off-great-circle paths is indicating side reflections and side scattering due to ionospheric disturbances in the equatorial ionosphere traveling from west to east. The velocity and the horizontal distance of different side-reflection areas can be deduced from these measurements. The observed values of velocity and horizontal wave length are similar to those values concerning atmospheric gravity waves.

2. ATMOSPHERIC GRAVITY WAVES PROPAGATING IN NORTH-SOUTH DIRECTION ALONG THE GREAT CIRCLE

2.1. Observations

On the path Tsumeb - Lindau CW fieldstrength measurements are carried out on 14.000 MHz and 16.996 MHz (17.413 MHz) using horizontal 4-element Yagi antennas in 10.6 m and 14.3 m height. The antenna gain is approximately 10 dB and the transmitter power is 1 kW on 14.000 MHz and 0.5 kW on 16.996 MHz (17.413 MHz). Figure 2 shows a typical fieldstrength record obtained during night. Due to the fact that the 14.0 MHz signal is below noise level during day-time hours, because of the D-layer absorption, night-time records are selected for comparison. This also omits effects of E- and F1-layer propagation. The fieldstrength record is obtained by reading the peak value of the receiver input power during a period of two minutes. Because the transmitter is switched in contrary from one frequency to the other every second minute (this is to provide a correct measurement of the signal-to-noise ratio), one fieldstrength reading is obtained every fourth minute.

The plotted signal strength of the 16.9 MHz signal is reduced to 1 kW effective transmitter power by adding 3 dB to the measured values. The field strength patterns represented by figure 2 evidently indicate periodical variations on both operating frequencies. This clearly can be seen on figure 2b which is the curve of figure 2a smoothed by digital filtering by means of the filter given in the left-hand side of figure 2b. The fading periods of up to 80 minutes and the nearly simultaneous occurring of maxima and minima on both frequencies give evidence to the assumption of focussing and defocussing due to periodical ionospheric disturbances, which are caused by atmospheric gravity waves propagating along the great circle Lindau - Tsumeb.

2.2. Ray-Tracing Calculations

The assumption of focussing by ionospheric profiles perturbed by atmospheric gravity waves can be proved by an application of ray-tracing calculations. For this purpose a two-dimensional ray-tracing program was developed. As shown by Georges and Stephenson (1969) the effect of lateral deviation of radio waves is small and can be neglected if the atmospheric gravity wave is propagating nearly along the great circle of the radio path. Considering this fact, a 2D ray-tracing is sufficient for calculation. This program, furthermore, neglects the earth's magnetic field. The signal strength calculations are basing on the spacing of adjacent ray paths. This "flux-line" approximation can be used for practical applications (Croft, 1969), in spite of the fact that it breaks down near the skip distance. Losses at ground reflection and the vertical antenna pattern are taken into account. D-layer absorption and E-layer bending of the ray can be neglected because of the intended comparison with night-time measurements. The F-layer profile is chosen to be parabolic (no F1-layer) and be perturbed by an atmospheric gravity wave. This profile can be analytically expressed by:

$$f_N^2(x, z) = f_{N1}^2(z) \cdot [1 + \delta(x, z)],$$

$$f_{N1}^2(z) = f_{01}^2 \cdot [1 - \left(\frac{z_m - z}{y_{m0}}\right)^2],$$

$$\delta(x, z) = \delta_0 \cdot \sin[2\pi \cdot \left(\frac{x}{\lambda_x} - \frac{z}{\lambda_z} - t'_S\right)],$$

where

x is the horizontal distance measured from the northern terminal of the path (Lindau),

z is the height above earth,

f_N is the plasma frequency,

f_{01} is the critical frequency of the unperturbed ionospheric profile,

y_{m0} is the semithickness of the parabolic profile,

z_0 is the height of the layer bottom,

$z_m = z_0 + y_{m0}$ is the height of the layer maximum.

The gravity wave parameters are:

δ_0 is the perturbation wave amplitude,

λ_x is the horizontal wave length,

λ_z is the vertical wave length,

t'_S is the time in wave periods.

The horizontal distance of the wave is $x_S = x - n_S \cdot \lambda_x$, where $n_S = 0, 1, 2, 3, \dots$. The normalized wave distance from the northern terminal of the path is $x'_S = \frac{x_S}{\lambda_x}$ ($\approx t'_S$). The gravity wave propagation is in the direction of x . The ionospheric profile given by these parameters is shown in figure 3. The choice of the parameters $\delta_0 = 0.1$, $\lambda_x = 600$ km and $\lambda_z = 240$ km indicates a medium-scale disturbance (Georges, 1968; Georges and Stephenson, 1969). This simplified form of an ionospheric profile, representing the influence of an atmospheric gravity wave, can clearly indicate the effects of this perturbation to oblique-incidence short-wave propagation.

The HF radio wave propagation on the 7915 km long path between Lindau and Tsumeb can only take place via multi-hop propagation. Generally, at least 3F propagation is necessary. To avoid complexity, the perturbation of the ionosphere is assumed to be limited to the ionospheric region in the northern part of the path where the first reflection takes place. The further ionospheric reflections are assumed to be in a concentric, homogeneous ionosphere with no horizontal gradients of plasma frequency.

Figure 4 shows the so-calculated range-elevation display for the two fixed frequencies 14.0 MHz and 17.0 MHz and 3F propagation, where θ is the elevation angle at the northern station Lindau, and x_D is the horizontal distance from Lindau. x'_S is the normalized wave distance. As this example evidently indicates, "ripples" are propagating to a closer distance and to higher elevation angles when the wave distance x'_S is increasing. The wave distance x'_S can be expressed by the time t'_S , which is the normalized time in wave periods. If the period of the atmospheric gravity wave is assumed to be one hour, the time $t'_S = 0.2$ ($\approx x'_S$) is standing for 12 minutes, which is the difference in time between the different divisions of figure 4. The increasing wave distance x'_S indicates increasing time.

Focussing takes place where $\frac{dx_D}{dt}$ becomes small. Regarding, for example, the case of $x'_S = 0.8$, this focussing is at the minimum 6900 km, the maximum 7800 km, and at the skip-distance minimum 5840 km. This is for the operating frequency 17.0 MHz; the focussing on 14.0 MHz is at smaller distances. Proceeding to $x'_S = 1.0$, the ripples have moved to still smaller distances. The maxima and minima at low elevation angles will lead to a focussing effect like the skip-distance focussing with a sharp decrease of field strength when the MUF is passing the operating frequency. A steady increase and decrease of field strength will be expected for increasing x'_S when only a point of inflection occurs on the range-elevation display. This point of inflection is, for example, at 5150 km on the operating frequency 14.0 MHz and $x'_S = 0.4$ (see fig. 4).

As the diagrams of figure 4 demonstrate, the focussing ripples are at different ranges x_p , considering the different frequencies 14.0 MHz and 17.0 MHz. Due to the fact, that the ripples are moving to smaller ranges with increasing wave distance x_s^* ($\approx t_s^*$), a time delay in focussing between the two frequencies will be expected when transmitting to a fixed distance $x_p = \text{const}$.

The characteristics of an oblique-incidence signal transmitted along the fixed distance of 7915 km between Lindau and Tsumeb are shown in the following figures, concerning the ionospheric model illustrated by figure 3, and using the fixed operating frequencies 14.0 MHz and 17.0 MHz. Figure 5 demonstrates the calculated elevation angles θ_1 at Lindau and θ_2 at Tsumeb for the 3F, 4F and 5F propagation as a function of the normalized wave distance x_s^* . High angle characteristics are plotted only if the fieldstrength of this propagation mode is comparable to the fieldstrength of low angle modes. This is the case only for the 4F mode on 17.0 MHz. For a specific range of x_s^* the low angle 3F mode is split into three propagation paths with different elevation angles. This effect is not so much pronounced at the steeper elevation angles of 4F propagation on 14.0 MHz. The splitting is not observed at the 5F mode on 14.0 MHz and the 4F mode on 17.0 MHz due to the fact that only inflection points exist near the skip distance, which is demonstrated by the range-elevation display of figure 4. The difference in the pattern of the elevation angles θ_1 and θ_2 (the variation in θ_1 is much greater than the variation in θ_2) is evidently caused by the tilted ionospheric model (fig. 3) used in this calculation.

Figure 6 shows the calculated group propagation time t' for the 17.0 MHz signal as a function of the wave distance x_s^* (respectively the time t_s^* in wave periods). The difference in propagation time of less than 0.06 msec concerning the split paths of the 3F mode, can hardly be measured by usual pulse-technique transmissions. The variation in propagation time of the 4F mode is exceeding 0.2 msec because the reflection level is near the layer maximum (low angle and high angle close together), where the influence of the disturbance is much more pronounced than at lower levels. The pattern of the group propagation time is periodical because the normalized wave distance

$x_s^* = \frac{x - n_g \cdot \lambda_x}{\lambda_x}$ is periodical when n_g becomes 1, 2, 3 etc. and the gravity wave is propagating through the reflection area. The same is obviously valid for the elevation angle and fieldstrength patterns. These periodical variations are accompanied by periodical variations of the received frequency (up to a few Hz) due to the variation of the phase path. Periodical variations of frequency have been observed by Georges (1960) and are explained by ionospheric perturbations by atmospheric gravity waves.

The diagrams in figure 7 demonstrate the absolute fieldstrength P_E of the split 3F mode for the frequencies 14.0 MHz and 17.0 MHz. These diagrams indicate the "skip-distance-like" focussing effects around $x_s^* = 0.1$ and $x_s^* = 0.7$. Furthermore, the time delay in focussing on these two frequencies is demonstrated: The focussing on 14.0 MHz takes place at a lower value of x_s^* than on 17.0 MHz. This is when the atmospheric gravity wave is propagating from north to south and has a tilt into the direction of propagation. Assuming a wave period of one hour, the time delay of the fieldstrength peak on 17.0 MHz (relative to 14.0 MHz) is approximately four minutes, concerning the horizontal wave length of 600 km used in this calculation.

Figures 8 and 9 show the results of fieldstrength calculations for all possible propagation modes taking into account the ground-reflection losses (relative permittivity $\epsilon_r = 7$ and conductivity $\sigma = 3 \cdot 10^{-3} \Omega^{-1} \text{ m}^{-1}$) and the vertical antenna pattern at the transmitter and receiver. Consequently, these plots are demonstrating the effective receiver input power P_A of the single modes. The 5F mode on 14.0 MHz clearly indicates the steady increase and decrease in fieldstrength due to inflection point focussing. The steady increase accompanied by a sharp decay shown on the 3F modes is due to focussing at maxima in the range-elevation display of figure 4. The rather low receiver input power of the focussed 3F modes at $x_s^* \approx 0.1$ is caused by the decrease in antenna gain at low elevation angles. The time delay in the fieldstrength maximum of the low angle 4F mode on 17.0 MHz (relative to the 14.0 MHz maximum) is approximately 15 minutes.

As all modes have to be added when CW transmission has to be considered, several maxima in the fieldstrength patterns are occurring when the atmospheric gravity wave propagates along a distance of one wave length. The interpretation of the fieldstrength pattern becomes much more complicated when the fact is regarded that at all three, four or five reflection points in the ionosphere focussing takes place. The fact that the gravity wave is propagating periodically through all reflection areas gives rise to some more complexity.

2.3. Evaluation of Measurements

As shown in the previous section, the determination of the characteristics of atmospheric gravity waves by means of fieldstrength measurements seems to be relevant only if one-hop propagation is taken into account or only one propagation mode is dominant. In spite of this fact, it seems appropriate to ask after the effect of a perturbed ionosphere on the fieldstrength pattern of a radio path. This can firstly be done by simulating the fieldstrength pattern by means of ray-tracing calculations as it is pointed out in the section before. A further possibility is to evaluate measured fieldstrength records by means of a power density analysis, which is basing on the Fourier transformation of the auto-correlation function of a time series (Taubenheim, 1969). This analysis gives evidence about the fading periods and amplitudes which are included in the measured fieldstrength patterns.

Figure 10 shows the mean power density of all night-time fieldstrength records obtained during August 1969 on 14.000 MHz and 16.996 MHz. A power density analysis was done for every night (19 - 05 UT) and the mean value of all analysed nights is plotted as a function of fading period τ , respectively fading frequency ν . The resulting diagram (fig. 10) shows that in a steady increase of the power density to longer periods slight maxima are occurring between periods of 30 minutes and 80 minutes. Three maxima are evident at the coherence plot, which is deduced from the cross-correlation function and is a measure for the similarity of both time series. The mean standard deviation of the calculated power density and coherence is not exceeding 15 % of the plotted values. The relevant maxima at approximately 45, 55 and 80 minutes indicate the dominant periods of the observed fieldstrength patterns. The best coherence between the two signals is at periods between 70 minutes

and 90 minutes. The mean phase lag Δt between the two frequencies has a standard deviation lower than ± 1 minute. In the period range of 30 minutes to 50 minutes this phase lag is negative; that means, the fading periods of the 16.9 MHz signal are occurring after the respective fading periods of the 14.0 MHz signal. This is in agreement with the calculated time delay when considering focussing due to atmospheric gravity waves (see fig. 7). The positive time delay of the periods greater than 50 minutes seems to be due to the fading-out of the 16.9 MHz signal, which sometimes occurs between 03 UT and 05 UT and takes place earlier than the fading-out of the 14.0 MHz signal.

Figure 11 indicates the occurrence frequency of fading periods observed during all nights of August 1969. It is presumable that the maximum of the occurrence frequency is within the period range of 20 minutes to 60 minutes, which is approximately the period range of atmospheric gravity waves. In spite of the fact that characteristics of atmospheric gravity waves cannot be determined from this analysis, it may be assumed that the observed long-periodic fading is caused by focussing due to atmospheric gravity waves.

3. DISTURBANCES IN THE EQUATORIAL IONOSPHERE TRAVELING TRANSVERSE TO THE GREAT CIRCLE IN WEST-EAST DIRECTION

3.1. Observations

Besides normal propagation along the great circle Lindau - Tsumeb (fig. 1) off-great-circle propagation often can be observed during evening hours. Measurements to record the great-circle deviation are carried out, using a rotating direction finder antenna which has a distinct minimum in forward direction. Pulse transmission is used to provide a correct measurement of the signal propagation time (fig. 12). The pulse repetition time is 20 msec, and the pulse duration is 200 μ sec. The pulse peak power on the fixed frequency 18.21 MHz is approximately 100 kW, and the antenna gain is about 10 dB at the transmitter and receiver site.

Figure 13 shows a typical event of this kind of off-great-circle propagation. The off-great-circle paths regularly can be observed after 17 UT east of the great circle. Between 19 UT and 20 UT propagation paths west of the great circle occur and the eastern paths disappear. On a few occasions off-great-circle propagation still is observable when the great-circle propagation has already faded out (2120 - 2200 UT). Usually normal propagation conditions without distinct off-great-circle propagation reopen during midnight hours.

The depicted effect of lateral or great-circle deviation is characterized by two different types of propagation paths: Besides a continuous background of diffuse traces (partial reflection), the spectrum of propagation time frequently indicates discrete traces (possibly due to total reflection) commencing within a few minutes and existing up to two hours. At times groups of up to ten traces with different propagation time and different azimuth angles can be detected. The propagation time of the discrete traces is increasing with time when the path is observed east of the great circle, and is decreasing with time when west of the great circle. Simultaneous with this observation a small eastbound drift of the path's azimuth is perceptible, regardless if the path has east or west deviation.

3.2. Analysis of the Observations

All the described observations point to distinct characteristics of the equatorial spread-F (Clemesha and Wright, 1966; Kelleher and Skinner, 1971). It can be shown that the observed off-great-circle paths are caused by side reflection and scattering due to spread-F irregularities near the magnetic dip equator (Röttger, 1972). If the ionospheric propagation modes on the path transmitter - equator - receiver are known and the side-reflection areas are supposed to be small compared to the length of the entire path, the position of the side-reflection areas can be calculated from the observed azimuth angles and signal propagation time (Röttger, 1971a).

The propagation on the radio path Lindau - Tsumeb during the evening hours predominantly takes place via 3F, 4F and 5F propagation. These propagation modes, concerning off-great-circle propagation, are split into the two partial modes transmitter - equator and equator - receiver. The partial modes are defined by the number of semi-hops (earth - ionosphere and v.v.). For example, the 4F mode is split into the 5-3 (5-5) mode, which indicates 5 (3) semi-hops on the path transmitter (Lindau) - equator and 3 (5) semi-hops on the path equator - receiver (Tsumeb). Using a mean ionospheric profile along the propagation path (a parabolic F-layer with $f_o = 10.0$ MHz, $z_o = 220$ km, $y_m = 0.4 z_o$), the mean position of the side-reflection areas, concerning every observed trace, can be calculated. The absolute error of the position finding of a single side-reflection area is not exceeding 1500 km in north-south direction and 150 km in west-east direction. This error is mainly caused by the statistical uncertainty in determining the ionospheric parameters along the path transmitter - equator - receiver (Röttger, 1971b).

The calculated position of side-reflection areas as a function of time t is demonstrated by figure 14. For this position determination the observed values of figure 13 are used. The relative error in the position indication as a function of time is smaller than the specified absolute error, because the variation of the ionospheric parameters during a few hours can be assumed to be normally much smaller than the variation during one month (this is used for the calculation of the absolute error). To assure the agreement between the model of figure 14 and the observations (fig. 13), the calculated propagation time t' (using this model) is compared with the observed propagation time (fig. 15). The sufficient agreement of the calculated and the observed values indicates that the model of figure 14 may be supposed to be relevant.

In figure 14 the side-reflection areas are assumed to be on the magnetic dip equator (the maximum of occurrence frequency of side reflections). The ordinates d_w and d_e are indicating the distance measured from the cross-point of the dip equator and the great circle in latitudinal direction (west-east). The west-east direction is approximately along the magnetic dip equator (see fig. 1). The ordinate λ is the corresponding geographical longitude, and α is the azimuth angle of the side-reflection areas observed at Lindau. This diagram (fig. 14) demonstrates that

the side-reflection areas are commencing after sunset at the magnetic dip equator. An eastward movement of all these areas is perceptible and the corresponding velocity is between $60 \frac{\text{m}}{\text{sec}}$ and $220 \frac{\text{m}}{\text{sec}}$. Groups of side-reflection areas can be observed, between 2040 UT and 2130 UT at least five different traces are evident. The horizontal distance in west-east direction between different traces is approximately 600 km.

The observed velocities and the horizontal distance (wave length) of the side-reflection areas give evidence to the assumption that these periodical structures in the equatorial ionosphere are caused by atmospheric gravity waves commencing after sunset in the equator region. The observed structures are evidently occurring in connection with the equatorial spread-F. As shown by Bowman (1968), a relation between atmospheric gravity waves and the occurring of spread-F can be assumed.

The hypothesis that the moving structures in the equatorial ionosphere do exhibit typical features of atmospheric gravity waves shall be supported by some more statistical data. For this purpose all data, concerning off-great-circle propagation on the path Lindau - Tsameb, obtained during March 1971 are analysed.

Figure 16 shows the analysis of the variation of propagation time t' for eastern and western deviations. The variation $\frac{dt'}{dt}$ of the signal propagation time is associated by a Doppler shift of the transmitted frequency which is indicated by the frequency variation Δf . The variation $\frac{dt'}{dt}$ is observed to be positive for eastern traces and negative for western traces. The corresponding Δf has opposite sign. This diagram, comparing the absolute values of the variations, demonstrates that the western distribution does not coincide with the respectively eastern distribution. Equality of both distributions should be expected if the variations of the propagation conditions along the path transmitter - equator - receiver are assumed to be small and similar velocities of the side-reflection areas east and west of the path are presumed. East and west deviations can be compared because the zone of equatorial spread-F (along the magnetic dip equator) where the side reflections take place is approximately symmetrical on both sides of the path Lindau - Tsameb. The observed inequality of the eastern and western distribution can be explained by a decrease of the reflection height at the dip equator. This decrease of the F-layer height is observed at equator stations after a distinct increase of layer height after sunset (GRI, 1970).

Using the observed variations of signal propagation time, the eastward velocity $\frac{dy}{dt}$ and the downward velocity $\frac{dz}{dt}$ can be derived. The measured variation of the propagation time $\frac{dt'}{dt}$ is given by:

$$\frac{dt'}{dt} = \frac{dt'}{dt} \left(\frac{dy}{dt}, \alpha \right) + \frac{dt'}{dt} \left(\frac{dz}{dt}, \alpha \right), \quad (1)$$

where the y-axis is pointing eastward, the z-axis is the vertical, and α is the azimuth angle measured at Lindau. t is the time, and t' the signal propagation time. Concerning eastward velocities, the variation $\frac{dt'}{dt}$ is positive east of the path and negative west of the path. The variation $\frac{dt'}{dt}$ is always negative for decreasing layer height, regardless if the path has eastern or western deviation. Due to this fact, both variations $\frac{dt'}{dt}$ and $\frac{dt'}{dt}$ have similar sign (minus) west of the path and have dissimilar sign east of the path. This leads to an amplification of the variation $\frac{dt'}{dt}$ at western paths and to an attenuation at the east. The variation due to eastbound velocities can be expressed by:

$$\frac{dt'}{dt} = \frac{dt'}{d\alpha} \left(\frac{dy}{dt}, \alpha \right) - \frac{d\alpha}{dt} \left(\frac{dy}{dt}, \alpha \right), \quad (2)$$

where $\frac{d\alpha}{dt}$ is a function of the eastward velocity $\frac{dy}{dt}$ and can be calculated for all expected values of $\frac{dy}{dt}$ and α . In the same manner $\frac{dt'}{d\alpha}$ can be calculated, considering the path geometry and the propagation conditions along the path. The value of $\frac{dt'}{dt}$ is determined by (1) if the value of $\frac{dt'}{dt}$ is known. Because two distributions are obtained, one for eastern paths and one for western paths, the magnitude of $\frac{dt'}{dt}$ can be obtained due to the fact that $\frac{dt'}{dt}$ has a constant sign on both sides of the path. By assimilation of the both distributions the quantity $\frac{dt'}{dt}$ and the corresponding height variation $\frac{dz}{dt}$ can be determined when searching the value of $\frac{dt'}{dt}$ which leads to the best similarity (similar median values) of both distributions. Thus, the eastward velocity is obtained from (1) and (2):

$$\frac{d\alpha}{dt} \left(\frac{dy}{dt}, \alpha \right) = \frac{d\alpha}{dt} \cdot \left(\frac{dt'}{dt} - \frac{dt'}{dt} \right),$$

where $\frac{dt'}{dt} - \frac{dt'}{dt}$ is derived from measured values. $\frac{d\alpha}{dt}$ and $\frac{d\alpha}{dt}$ are calculated, thus, the inverse function $\frac{dy}{dt} \left(\frac{d\alpha}{dt}, \alpha \right)$ leads to the wanted velocity $v_E = \frac{dy}{dt}$.

Applying the outlined method to all observed side-reflection traces, the distribution of the eastward velocity v_E is obtained from the east and west distribution of $\frac{dt'}{dt}$. This distribution is illustrated by figure 17. The corresponding mean height variation is $-24 \frac{\text{m}}{\text{sec}}$, which is in sufficient agreement with direct measurements at the equator. The measured height variation, obtained from vertical sounding ionograms of Ouagadougou (GRI, 1970) in the equator zone, is $-19 \frac{\text{m}}{\text{sec}}$ (March 1970).

The median value of the deduced velocity distribution is $\bar{v}_E = 110 \frac{\text{m}}{\text{sec}}$, the lower quart is $45 \frac{\text{m}}{\text{sec}}$, and the upper quart is $185 \frac{\text{m}}{\text{sec}}$. By measuring the horizontal distance (in west-east direction) between adjacent side-reflection areas, the distribution of the horizontal "wave length" d_{H} is obtained (fig. 17). Here the median value is 380 km, the lower quart is 210 km, and the upper quart is 650 km. These observed values of horizontal velocity and wave length are in good agreement with observations of traveling ionospheric disturbances in midlatitudes (Tveten, 1961; Hunsucker and Tveten, 1967; Georges, 1968), which are assumed to be caused by atmospheric gravity waves.

Figure 18 shows the distribution of the number of different traces observed simultaneously during a period of 15 minutes. The number of traces is indicating the number of periods of the wave propagating into eastward direction. As this diagram further demonstrates, traces west of the great circle are occurring much more frequently than traces east of the great circle. This points to an asymmetry of the periodical structure of the electron density distribution causing the side reflections. This observation is in accordance with results obtained by Davies and Chang (1968) using Doppler measurements on an equatorial radio path. As the ionospheric model of figure 5 indicates, the asymmetrical, tilted structure is an evident feature of an atmospheric gravity wave.

4. CONCLUSION

Two effects of traveling ionospheric disturbances are demonstrated in this paper. Disturbances, caused by atmospheric gravity waves, propagating along the great-circle direction of the radio path Lindau - Tsameb are producing periodical fluctuations of the received fieldstrength. It is assumed that this focussing effect may give evidence to obtain indications about some parameters of atmospheric gravity waves when analysing the fieldstrength variations on a shorter radio path.

Traveling disturbances, occurring in connection with the equatorial spread-F, are analysed. It is shown that the characteristic velocities and wave lengths are similar to observed values of midlatitude traveling ionospheric disturbances, which are assumed to be due to atmospheric gravity waves. Some more investigations seem to be necessary to understand the propagation of these disturbances, because the direction of propagation is nearly perpendicular to the direction of the earth's magnetic field.

5. REFERENCES

- Baker, D.C. and J.A. Gledhill, 1965, "An unusual traveling disturbance in the F-region of the ionosphere", JATP 27, 1223-1227.
- Bowman, G.G., 1960, "Further studies of "spread-F" at Brisbane", Planet. Space Science 2, 133-149, 150-156.
- Bowman, G.G., 1968, "Movements of ionospheric irregularities and gravity waves", JATP 30, 721-734.
- Clemesha, B.R. and R.W.H. Wright, 1966, "A survey of equatorial spread-F", AGARDograph 95, 3-27.
- Croft, T.A., 1968, "The influence of ionospheric irregularities on sweep-frequency backscatter", JATP 30, 1051-1063.
- Croft, T.A., 1969, "A review of oblique ray tracing and its applications to the calculation of signal strength", AGARD Conference Proceedings 13, 137.
- Davies, K. and N.J.F. Chang, 1968, "Radio-Doppler observations of the ionosphere near the magnetic equator", AGARD Conference Proceedings 32, 52.
- Georges, T.M., 1968, "HF Doppler studies of traveling ionospheric disturbances", JATP 20, 735-746.
- Georges, T.M. and J.J. Stephenson, 1969, "HF radar signatures of traveling ionospheric irregularities, 3D ray-tracing simulation", Radio Science 4/8, 679-696.
- GRI, 1970, "Characteristic Ouagadougou, March 1970", Groupe de Recherches Ionosphériques, Issy-les-Moulineaux, France.
- Hunsucker, R.D. and L.H. Tveten, 1967, "Large traveling-ionospheric disturbances observed at mid-latitudes utilizing the high resolution h.f. backscatter technique", JATP 29, 909-916.
- Kelleher, R.F. and N.J. Skinner, 1971, "Studies of F region irregularities at Nairobi by direct backscatter at 27.8 MHz", Ann. Géophys. 27/2, 199-200.
- Klostermeyer, J., 1965, "Fortschreitende Wellen in der F-Schicht", Kleinheubacher Berichte 10, 141-145, FTZ, Darmstadt.
- Nielson, D.L., 1969, "Long-range VHF propagation across the geomagnetic equator", Research Report, Stanford Research Institute.
- Röttger, J., 1971a, "Einflüsse des Äquatorialen Spread-F auf die Kurzwellenausbreitung", Kleinheubacher Berichte 14, 269-278, FTZ, Darmstadt.
- Röttger, J., 1971b, "An application of the Monte-Carlo-method to remote sensing systems", AGARD Conference Proceedings 20, paper 34.
- Röttger, J., 1972, "Bestimmung von Parametern des Äquatorialen Spread-F aus Schrägübertragungsmessungen auf der Strecke Lindau - Tsameb", Kleinheubacher Berichte 15, FTZ, Darmstadt (to be published).
- Taubenheim, J., 1969, "Statistische Auswertung geophysikalischer und meteorologischer Daten", 190-343, Akademische Verlagsgesellschaft, Leipzig.
- Tveten, L.H., 1961, "Ionospheric motions observed with high frequency backscatter sounders", Journal of Research of the NBS 65D2, 115-127.

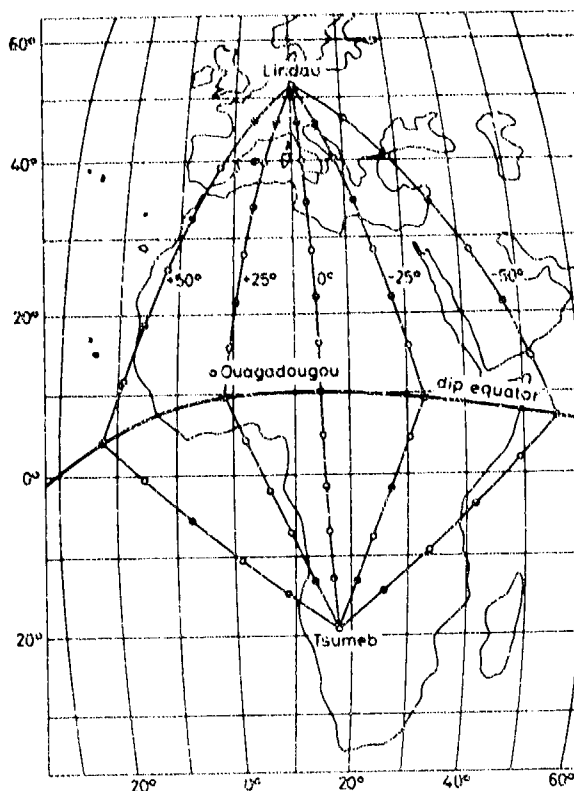


Fig. 1 Radio path Lindau/W. Germany - Tsumeb/South West Africa.
Off-great-circle propagation due to irregularities of the equatorial spread-F.

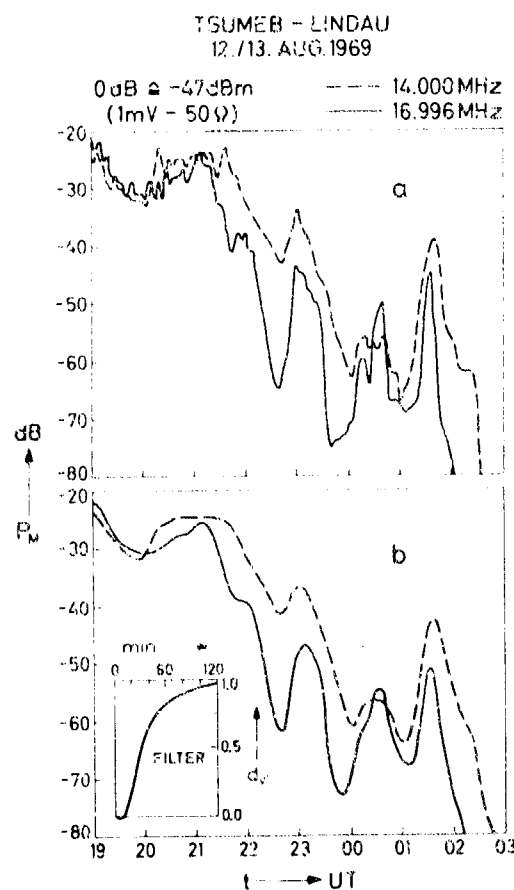


Fig. 2 CW fieldstrength record measured on the path Tsumeb - Lindau.

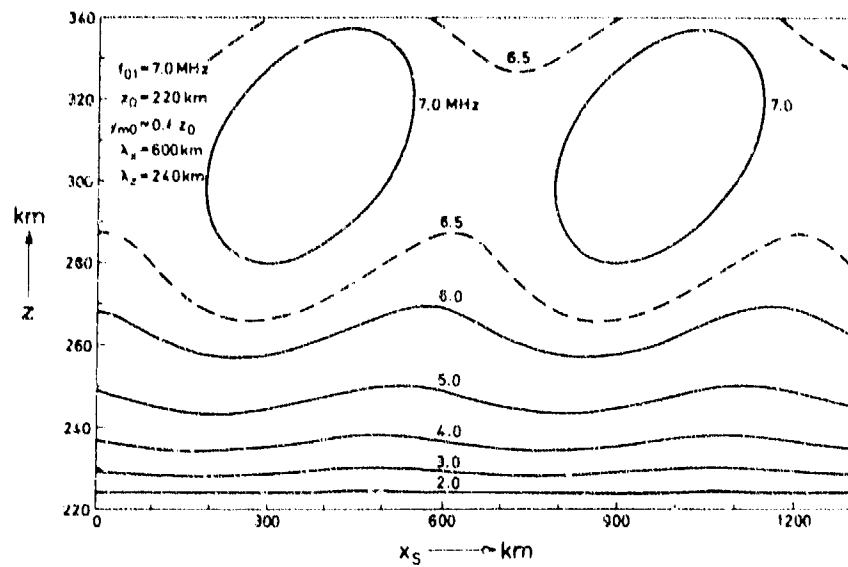


Fig. 3 Model ionosphere perturbed by atmospheric gravity wave. z is the height and x_s is the horizontal distance.

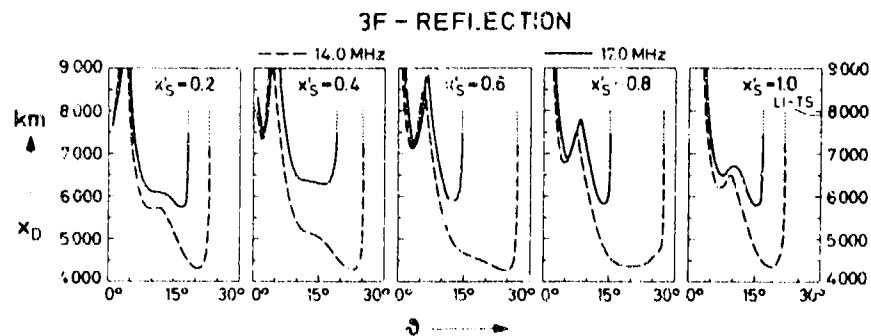


Fig. 4 Range-elevation display showing the horizontal range x_D of the downcoming radio wave, transmitted at the elevation angle θ and propagated via 3F reflections. x'_s is the normalized gravity wave distance.

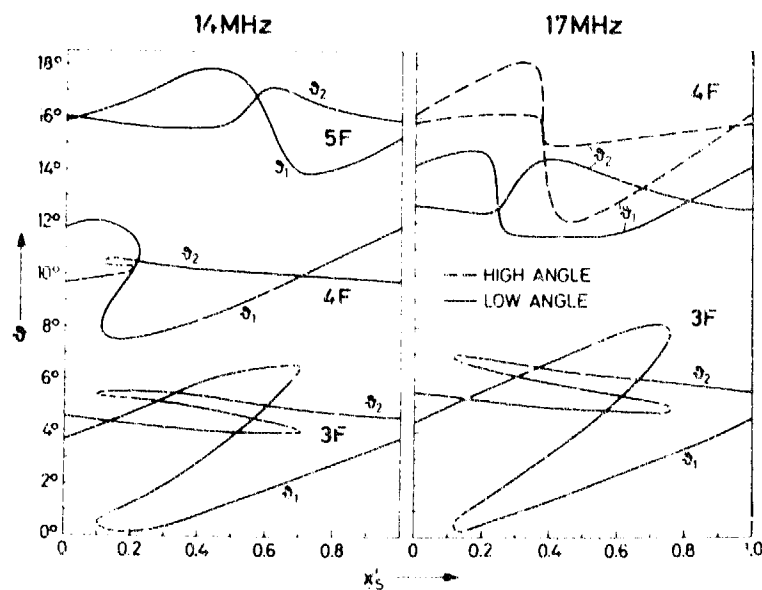


Fig. 5 Calculated elevation angle at the northern terminal (θ_1) and the southern terminal (θ_2) as a function of the normalized gravity wave distance x'_s ($x_D = 7915$ km).

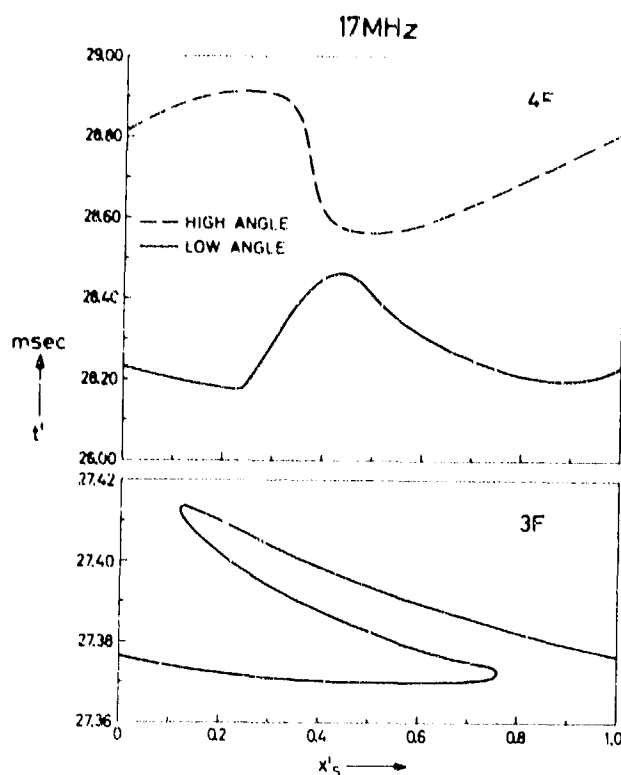


Fig. 6 Calculated group propagation time t' as a function of the normalized gravity wave distance x'_S ($x_D = 7915$ km).

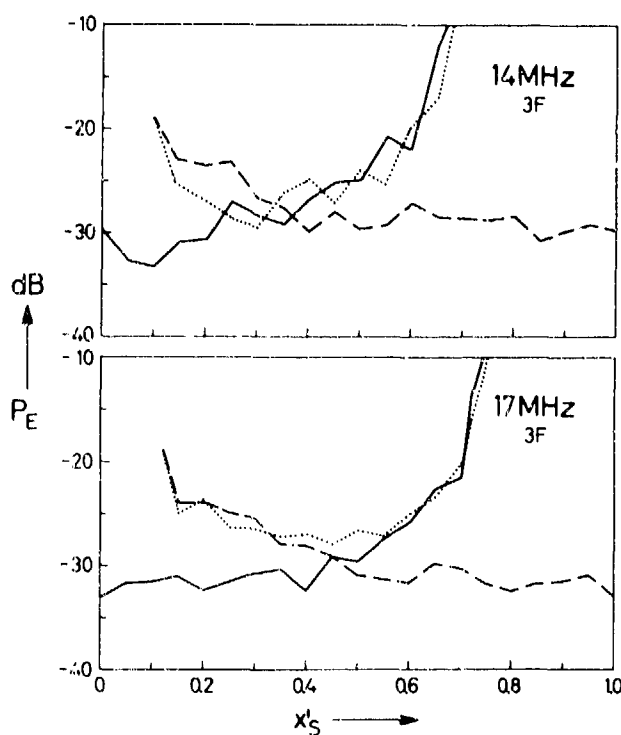


Fig. 7 Calculated absolute field strength P_E as a function of the normalized gravity wave distance x'_S ($x_D = 7915$ km).

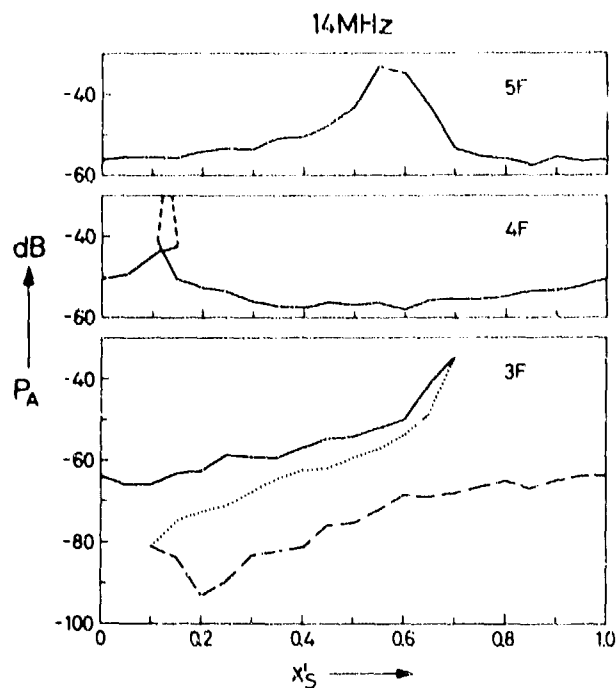


Fig. 8 Calculated relative receiver input power P_A of the 14.0 MHz signal taking into account the ground reflection losses and the vertical antenna pattern.

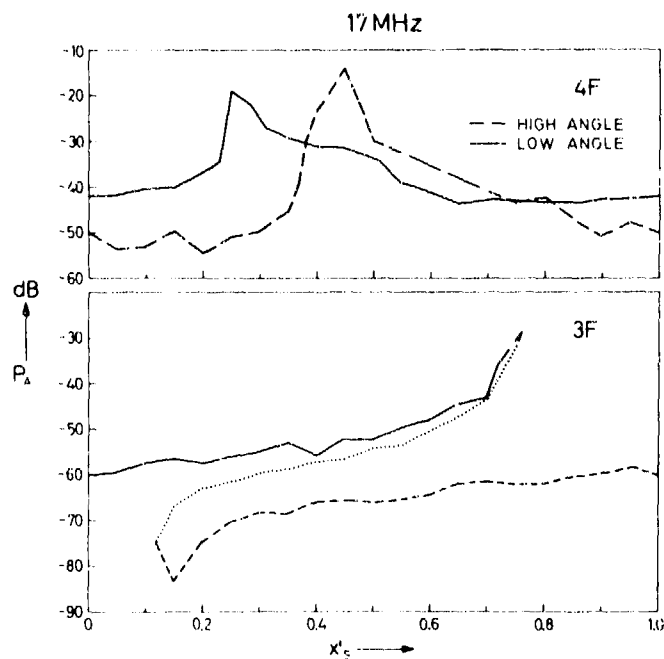


Fig. 9 Calculated relative receiver input power P_A of the 17.0 MHz signal taking into account the ground reflection losses and the vertical antenna pattern.

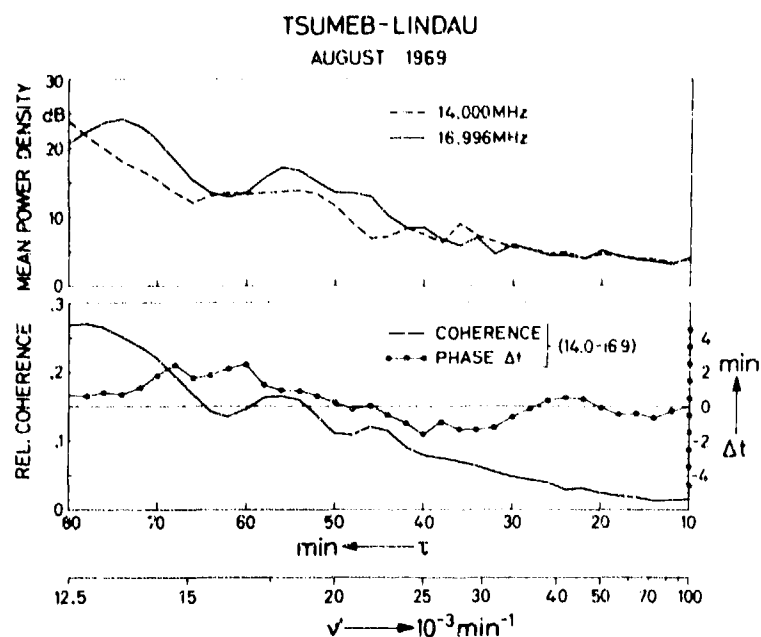


Fig. 10 Mean power density, the relative coherence, and the phase lag of the long-periodic fading measured on 14.000 MHz and 16.99 MHz.

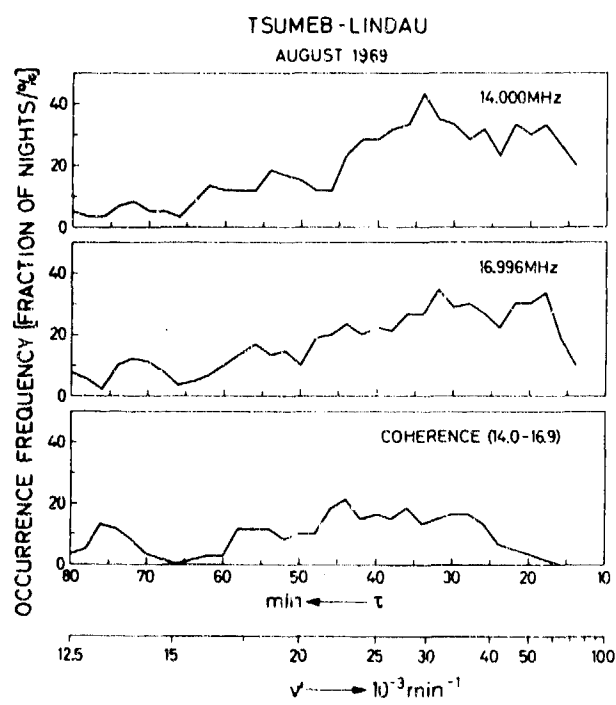
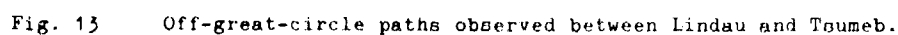
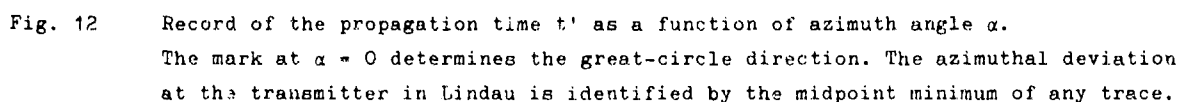


Fig. 11 Occurrence frequency of fading periods measured on 14.000 MHz and 16.996 MHz.



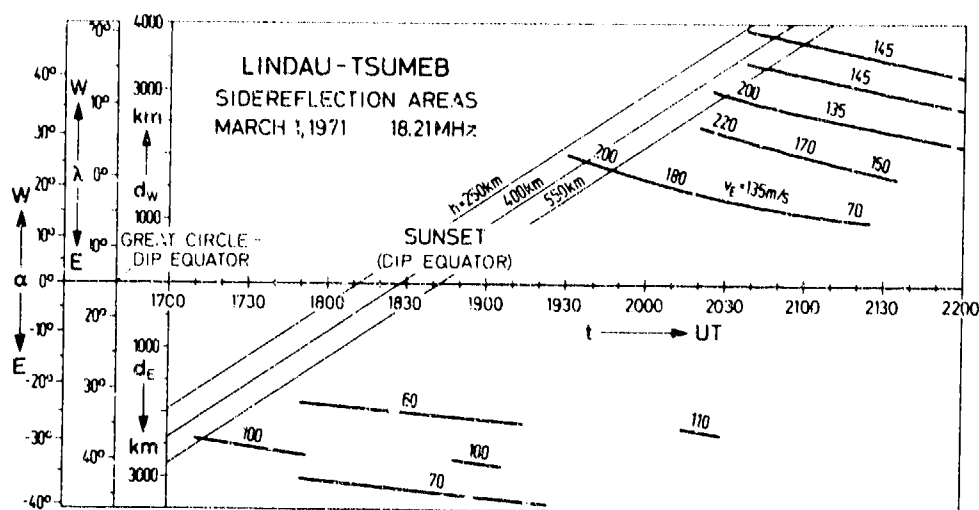


Fig. 14 Position of side-reflection areas on the magnetic dip equator. Sunset at the dip equator is in the specified heights h .

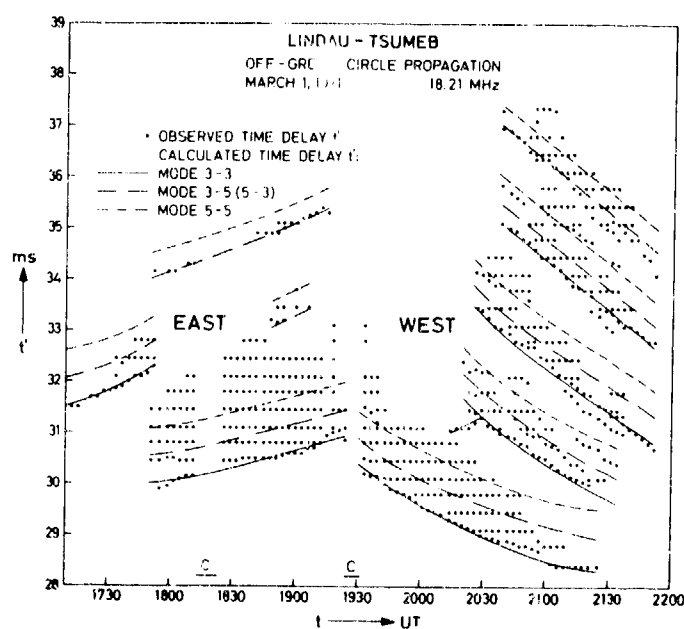


Fig. 15 Comparison of observed (fig. 13) and calculated traces, using the model of figure 14.

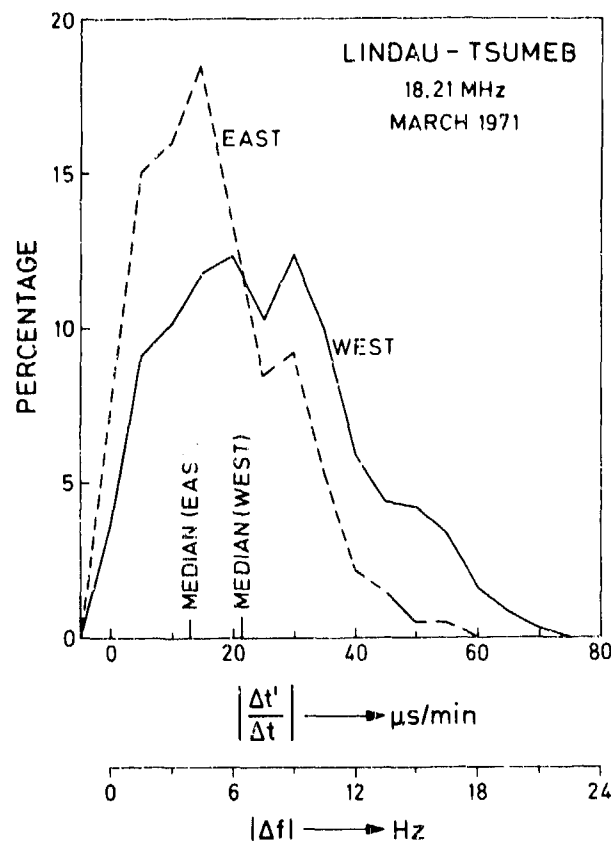


Fig. 16 Occurrence frequency of the variation of group propagation time $\frac{\Delta t'}{\Delta t}$ and frequency Δf due to eastward moving disturbances.

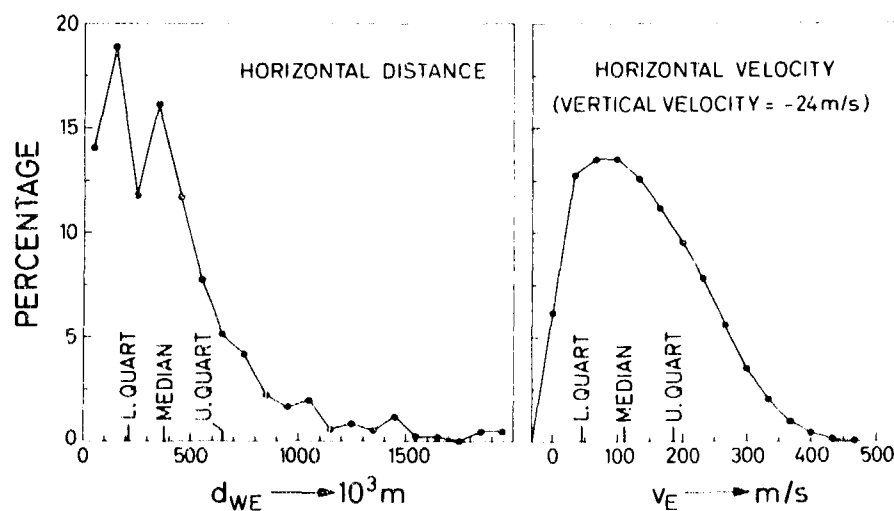


Fig. 17 Distribution of wave lengths d_{WE} and horizontal (eastbound) velocities v_E calculated from observations.

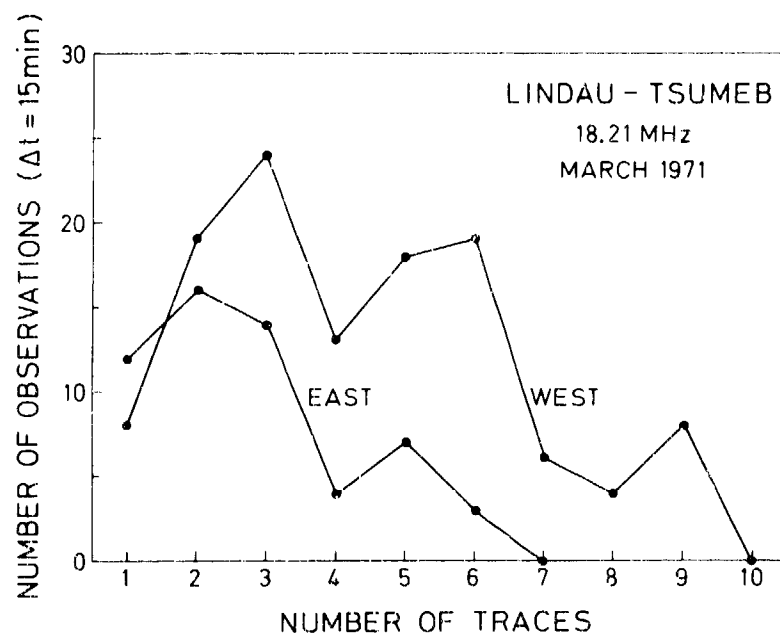


Fig. 18 Number of traces observed simultaneously within a period of 15 minutes. Observations of March 1971.

**PROPAGATION OF SUBMICROSECOND HF PULSES THROUGH TRAVELLING
IONOSPHERIC DISTURBANCES**

by

G.M. Lerbald, R.B. Jurgens and J.A. Joselyn

Space Environment Laboratory
NOAA Environmental Research Laboratories
Boulder, Colorado 80302
USA

450

PROPAGATION D'IMPULSIONS H.F. D'UNE DUREE INFÉRIEURE A LA MICROSECONDE
A TRAVERS DES PERTURBATIONS IONOSPHERIQUES ITINERANTES

par

G.M. Lørfald, R.B. Jurgens et J.A. Joselyn

SOMMAIRE

On a analysé des impulsions H.F. d'une durée inférieure à la microseconde, reçues à une distance de 1 500 km à la suite d'une seule réflexion ionosphérique par la région F, afin d'étudier les effets imposés à ces impulsions par le processus de propagation. Ces impulsions, qui étaient transmises sous forme de trains d'ondes à enveloppe quasigaussienne, avec une largeur d'environ 0,3 μ sec. entre points à demi-puissance, présentaient un spectre d'émission (d'une forme également quasi-gaussienne) d'environ 3 MHz de largeur, centré à 18 MHz. Au cours des séquences, trois impulsions étaient transmises à deux secondes d'intervalle au début de chaque minute. Des systèmes récepteurs à largeur de bande variant de 0,5 à 4 MHz étaient utilisés pour recevoir les signaux réfléchis. Les données étaient affichées sur des oscilloscopes à déclenchement et enregistrées photographiquement. Des observations diurnes furent effectuées, sur une vingtaine de journées (habituellement par séquences de 4 ou 5 jours), au cours de la période s'étendant de septembre 1969 à mars 1970.

Les impulsions enregistrées sont de forme très variée. Une des caractéristiques observées est l'allongement de l'impulsion attribuable à la dispersion ionosphérique. En général, pour un récepteur de 1 MHz, l'impulsion enregistrée dure environ 15 μ sec. Les impulsions enregistrées présentent aussi fréquemment une structure due au dédoublement de polarisation et à la réception de trains d'ondes décalés dans le temps provenant de réflexions multiples (plusieurs sauts).

Certains des résultats obtenus à partir de l'analyse statistique d'un grand nombre d'impulsions ($\sim 19\ 000$) et de l'analyse détaillée d'un petit nombre d'impulsions individuelles, sont les suivants :

1°) Les répartitions d'apparition des longueurs d'impulsion donnent les taux effectifs de dispersion ionosphérique. Cette quantité est directement liée à la capacité de transport d'information du milieu.

2°) Les tracés graphiques, par séquence temporelle, du délai d'impulsion, donnent l'amplitude et la période des changements intervenant dans les parcours équivalents de groupe. La mesure de ces changements a été effectuée avec un pouvoir séparateur d'environ 1 μ sec. à cette échelle, on peut observer, même par les journées les plus calmes, un spectre de variations dû probablement à des perturbations ionosphériques itinérantes.

3°) D'une façon générale, les caractéristiques des impulsions ne changent guère dans un intervalle de quelques secondes, mais subissent fréquemment des modifications marquées sur quelques minutes.

4°) Une analyse détaillée de certaines impulsions a montré que l'on pouvait déduire les décalages dans le temps des composantes provenant de parcours multiples, du cas le plus simple.

Les calculs, par trajectographie, des taux de dispersion et des effets de polarisation pour les modèles d'ionosphère à stratification horizontale se révèlent concorder raisonnablement avec les résultats d'observations. Les délais de temps, dans le cas des parcours multiples, que l'on obtient grâce aux calculs de trajectographie, à l'aide d'un modèle ionosphérique comportant une perturbation itinérante concordent également avec la gamme de décalage temporels observés.

PROPAGATION OF SUBMICROSECOND HF PULSES THROUGH TRAVELLING
IONOSPHERIC DISTURBANCES

G. M. Lerfeld, R. B. Jurgens, J. A. Joselyn
Space Environment Laboratory
NOAA Environmental Research Laboratories
Boulder, Colorado 80302

ABSTRACT

HF pulses of submicrosecond duration, received at a range of 1500 km after a single ionospheric reflection from the F region, have been analyzed to study the effects imposed on the pulses by the propagation process. The pulses, which were transmitted as wavetrains of quasi-Gaussian envelope, with about 0.3 μ sec. between half-power points, had a radiated spectrum (also of quasi-Gaussian shape) about 3 MHz wide centered at 18 MHz. Three pulses were transmitted at two-second intervals at the beginning of each minute during runs. Receiving systems with bandwidths ranging from 0.5 to 4 MHz were used to receive the reflected signals. The data were displayed on triggered oscilloscopes and recorded photographically. Observations were taken during daytime on about 20 days (usually in 4 or 5 day runs) during the period September 1969 to March 1970.

The recorded pulses display a wide variation in form. One pulse characteristic is the pulse stretching attributable to ionospheric dispersion. Typically, for a 1 MHz receiver, the recorded pulse has a duration of about 15 μ sec. Frequently the recorded pulses also display structure due to polarization splitting and to the reception of time-shifted wavetrains from multiple reflection points (multipath).

Some results from the statistical analysis of a large number ($\sim 19,000$) of pulses and the detailed analysis of a small number of individual pulses include:

- 1) Occurrence distributions of pulse lengths yield effective ionospheric dispersion rates. This quantity is directly related to the information carrying capacity of the medium.
- 2) Time series plots of pulse delay give the amplitude and period of changes in group path. The resolution of measuring group path length changes was about 1 μ sec. On this scale, a spectrum of variations due presumably to TIDs is observed even on the quietest days.
- 3) Pulse characteristics typically do not change much on a time scale of a few seconds but often change markedly in a few minutes.
- 4) Detailed analysis of selected pulses showed that the time shifts of multipath components could be derived for the simpler cases.

Ray tracing computations of dispersion rates and polarization effects for horizontally stratified model ionospheres gave reasonable agreement with the observations. Multipath time delays obtained from ray-tracing computations using an ionospheric model with a TID perturbation are also in agreement with the range of observed time-shifts.

1. INTRODUCTION

For several decades, the most widely used method of probing the earth's ionosphere has involved the use of pulsed radio signals in the MF and HF frequency ranges. The duration of the individual pulses used for ionospheric soundings has typically been in the range 20 to 100 μ sec. Pulse lengths of this range provide reasonably good resolution of the time required for the signal to travel to the ionosphere and back to the receiver (i.e., virtual height on a conventional ionogram) and permit the use of relatively narrow bandwidth receivers (i.e., a few tens of KHz), which in turn, result in acceptable signal-to-noise ratios (of the returned signal) for transmitted peak pulse powers of a few kilowatts. The techniques for generating such pulses and recording the returned signals in the form of a conventional ionogram have long been available.

A few years ago, workers at the Stanford Research Institute, (for a description of the system see Kanellakos, 1969), developed pulse transmitters capable of radiating electromagnetic pulses having durations of a fraction of a μ sec. and peak power of many megawatts. The frequency spectrum of these pulses typically peaks at some center frequency and is 2 to 3 MHz wide between the half-power points. The large peak power available, permits the use of wide bandwidth receivers (i.e., the returned power is sufficiently large that interference from other transmitters within the bandpass can usually be overridden). Resolution in time is given approximately by $\sqrt{2}/\gamma$, where γ is the receiver bandwidth; thus, a receiving bandwidth of 1.5 MHz will yield a time resolution of about 1 μ sec.

This paper deals with ionospheric propagation effects on such pulses over a 1500 km east-west path and the use of the received pulses as a diagnostic in the study of travelling ionospheric disturbances.

A number of workers, including Solifrey (1965), Price (1968) and Inston (1969), have developed theoretical expressions for the propagation and reception of short pulses. We will use the elegant treatment due to Wait (1969) in discussing the subject. Wait assumes a Gaussian shaped envelope for the transmitted pulse (approximately the actual shape), which implies a Gaussian shaped frequency spectral curve. In his formulation, the time function of the pulse is represented as

$$f_0(t) = F_0 e^{-\alpha^2 t^2} e^{i\omega_0 t}, \quad -\infty < t < \infty, \quad (1)$$

where Γ_0 is an amplitude factor, ω_0 is the angular carrier frequency, and α is a damping coefficient.

This leads to the expression

$$\Gamma(\omega) = \Gamma_0 (\pi^{1/2}/\alpha) \exp[-\beta^2/(4\alpha^2)], \quad (2)$$

for the frequency spectrum, where $\beta = \omega - \omega_0$. Wait goes on to assume a transfer function $P(\omega)$ for the dispersive propagation path which is approximated in the vicinity of ω_0 by

$$P(\omega) \approx |P(\omega_0)| \exp[-i\Phi(\omega)], \quad (3)$$

where

$$\Phi(\omega) = \Phi(\omega_0) + (\omega - \omega_0) \Phi'(\omega_0) + \frac{(\omega - \omega_0)^2 \Phi''(\omega_0)}{2} \quad (4)$$

The primes indicate derivatives with respect to ω evaluated at ω_0 . In expression 4, $\Phi(\omega_0) = \omega_0 \tau$, where τ is the "phase delay" of the propagation channel, $\Phi'(\omega_0) = \tau_g$ is the "group delay" and $\Phi''(\omega_0) = 1/(2W^2)$, where W is a "channel bandwidth".

To retain expressions which can be evaluated in closed form, but which are still physically realistic, a Gaussian receiver bandpass characteristic is assumed. The integral product, over all frequencies, of the spectrum of the source and the transfer functions of the propagation channel and the receiver channel, yields the detected transient signal to be expected from the receivers;

$$f(t) = \frac{K}{\alpha} \frac{e^{i\omega_0(t-\tau)}}{\left[\frac{1}{\alpha^2} + \frac{1}{\gamma^2} + \frac{1}{W^2}\right]^{1/2}} \exp\left[-\frac{(t - \tau_g)^2}{\left(\frac{1}{\alpha^2} + \frac{1}{\gamma^2} + \frac{1}{W^2}\right)}\right] \quad (5)$$

where K is the product of the constant terms and γ is the receiver bandwidth. The first part of expression 5 gives the phase delay component while the second gives the group delay effect which includes stretching of the modulation envelope of the pulse. A pulse duration is defined by setting the second exponential of expression 5 equal to

$$\exp\left[-(t - \tau_g)^2/(t_d^2)\right], \text{ where} \\ t_d^2 = \left(\frac{1}{\alpha^2} + \frac{1}{\gamma^2}\right) + \left(\frac{1}{\alpha^2} + \frac{1}{\gamma^2}\right)^{-1} \frac{1}{W^2} \quad (6)$$

The stretching of a wideband pulse can be visualized from a conventional ionogram. The change in virtual height over an appropriate frequency range, (say, 1 MHz), represents a corresponding change in group delay. Obviously, for a very short pulse, all of the frequency components are transmitted essentially simultaneously, but because they travel slightly different paths the different frequency components are separated in time as they arrive at the receiver. The treatment by Wait assumes linear dispersion, i.e., phase variations to the second order are included. The experimental data include many examples which indicate that this condition is often satisfied. Figure 1 shows a received pulse typical of quiet propagation conditions. The upper trace is a record of the RF signal received at 18 MHz while the lower trace is the output of an IF channel with center frequency at 2 MHz and bandwidth 2 MHz. The RF signal is mixed with a local oscillator offset 2 MHz from the RF center frequency and the difference frequency fed to the IF channel. The IF recording shows clearly the earlier arrival of the lower frequency components of the signal, followed by progressively higher frequencies. The oscilloscope trace lasts a total of 50 μ sec. and the pulse has a duration of about 15 μ sec.

On the other hand a sizable fraction of the data exhibit more complex behavior which indicates that the dispersion is not simple. There are two principal ways the assumption of a simple linear dispersion can be violated. One of these is when the group delay versus frequency relationship is nonlinear, and the other is when the medium exhibits multiple refringence. The best known source of birefringence is the polarization splitting of the signal into the ordinary and extraordinary modes. A second source is the presence of spatial structure which permits multiple paths for the energy to travel from the transmitter to the receiver. An analogous situation to the latter case is viewing the sun or other source of light reflected in a body of water. If the water is sufficiently calm, a single image of the light source is reflected, but if turbulence or waves are present, the image is seen as glints which spread over a larger area as the turbulence increases.

Our concern in this paper is primarily in the more complex received data which we believe often attributable to the presence of travelling ionospheric disturbances (TIDs). Analytical models of the TIDs are used to compute anticipated effects on short pulses which are then compared to the types of effects observed.

2. DESCRIPTION OF THE EXPERIMENT

During 1969 and 1970, the Space Disturbances Laboratory of the National Oceanic and Atmospheric Administration's (NOAA) Environmental Research Laboratories, and the Stanford Research Institute (SRI), conducted a cooperative experiment to study the oblique, one-hop HF path from Palo Alto, California, to Boulder, Colorado, a distance of approximately 1500 km. SRI transmitted a series of submicrosecond pulses at a center frequency of 18 MHz. The transmitted pulse was roughly Gaussian in shape with a peak power of tens of megawatts. It had a total duration of approximately .5 μ sec. and a spectrum with a fairly flat peak and fast roll-offs at about 1 MHz on either side of the center frequency (Kanellakos, 1969). According to a prearranged schedule, three pulses, spaced 2 sec apart, were sent at the beginning of each minute. The pulses were sent during daylight hours for periods of several consecutive days in September and November 1969 and January, February and March 1970.

At Boulder, Colorado, several wideband receivers and triggered oscilloscopes were synchronized with the transmissions, and the ionospherically reflected pulses were recorded on 35-mm film for later analysis. During the course of the experiment, five different bandwidths (0.5, 1, 1.5, 2, and 4 MHz) were used to receive the pulses. Data from each of these bandwidths have been scaled and analyzed, but the majority of the analysis has been done on the 0.5 MHz bandwidth data. This bandwidth was better suited to analysis because interference from strong CW signals was less of a problem than on the wider bandwidth channels.

Several antenna configurations were employed during the course of the experiment. The pulses were at first received on a sloping-V antenna. However, early in the experiment it became clear that the received pulses were often distorted due to interference between the Ordinary (O) and Extraordinary (X) modes of propagation. Two log periodic antennas were then mounted in the configuration described by Lomasney, et al. (1970) so that the incoming signals on both antennas could be summed or differenced to yield an O- or X-mode circularly polarized output signal. The effect of these antennas on a CHIRP-ionosonde signal which was propagated over the same path (Palo Alto-Boulder), is seen in figure 2. Both modes of the high (Pederson) ray are present for the linear antennas but the summed antennas effectively reflect the X-mode. Figure 3 shows the effect of antenna configuration on a pulse. In each section, the upper trace is an FM representation (the vertical scale is proportional to instantaneous frequency) of the pulse; the full width of the oscilloscope trace is again 50 μ sec. The beating due to interference between the two modes is pronounced on the linear antennas but essentially disappears for the polarized case.

The scaling procedure used for the data is illustrated in figure 4. This pulse was transmitted from Palo Alto on November 13, 1969, at 2045:00 UT, and was received at Boulder several milliseconds later with a Slope-V antenna and a 1.5 MHz bandwidth receiver centered at the transmission frequency of 18 MHz. All of the data frames, which were recorded on 35-mm film, were enlarged by 11 to 1 and printed by a zerox process for easier and more accurate scaling. Four values were scaled from each data frame; the time the pulse began and ended, the pulse amplitude, and the background interference amplitude. The scaled values, along with identification and pertinent station log information were punched onto computer cards and eventually written onto magnetic tape for ease of processing. Station time at both the transmitter and receiver sites was maintained to within a few μ sec. so the total travel time of the pulse could be measured very accurately. The relative pulse delays were obtained from the data frames by measuring the time from the beginning of the oscilloscope trace to the beginning of the pulse. Adjustments to the scope trigger were made as needed to keep the pulse centered, and these adjustments were included in the data processing procedure.

The dispersive character of the ionosphere is responsible for the lengthening of a sub- μ sec. pulse into a signal which is typically several μ sec. in duration. In figure 4, the pulse was dispersed to approximately 12 μ sec. Solving equation 6 for the "channel bandwidth" of the propagation path gives

$$W = \left\{ t_d^2 - \left(\frac{1}{\alpha^2} + \frac{1}{\gamma^2} \right) \left(\frac{1}{\alpha^2} + \frac{1}{\gamma^2} \right) \right\}^{-1/2} \quad (7)$$

For the pulse of figure 4, α is taken as 2×10^6 Hz and γ is 1.5×10^6 Hz, with the result that $W = 0.35$ MHz. A further result given by Wait yields the receiver bandwidth which will produce the shortest duration pulse;

$$\gamma_o = \left[(1/W^2) - (1/\alpha^2) \right]^{-1/2}$$

If $\alpha \gg W$, then obviously, $\gamma_o \approx W$, i.e., for a wide bandwidth source, the receiver bandwidth should equal the "channel bandwidth", if the shortest pulse possible is desired.

3. ANALYSIS AND RESULTS

There were three major data periods of 3 to 5 days each during which data were analyzed. These were November 1969, and January and February 1970. This represents 54 hours of transmission, 70 percent of which has been scaled. In all, approximately 19,000 pulses were hand-scaled and used for the following analysis. A fourth transmission period was scheduled during the March 7, 1970 eclipse. The latter data have been subjected to extensive analysis and the detailed results have been reported by Lenzfeld, et. al. (1972). These results are summarized in section 3.2.

Figure 5 summarizes the pulse-length information for the three data periods. The November data were received at 1.5 MHz, so using equation 7, a 10- μ sec. pulse length implies a "channel bandwidth" of .35 MHz. The January and February data were scaled from the 0.5 MHz bandwidth receiver and, therefore, 10 μ sec. of pulse length implies a "channel bandwidth" of .22 MHz.

Examination of the data showed that the ionosphere was reasonably stable over a few seconds of time. Therefore, the data points from the three pulses per minute were averaged, which reduced random scaling errors and allowed for simplified data display. In figure 6, the 1-min. averages of pulse delays and pulse endings have been plotted for November 10. The pulse length is represented by the vertical bar, and the vertical scale is 300 μ sec. This type of plot was made for all data scaled. Thirty μ sec. of pulse delay corresponds to a change of 10 km of virtual reflection height. Periods of missing data are due to equipment difficulties, or loss of signal.

3.1 TID EFFECTS

The variations of pulse delay on November 10, 1969 with periods of about 30 minutes seen in figure 6, are typical of travelling ionospheric disturbances (TID). Also during this time period pulse lengths began small (5-10 μ sec.), but later approached 30 μ sec. in length. Long pulses are more difficult to analyze because they generally have a great deal of internal structure and because it is more difficult to keep them on scope. (Data are not plotted when the beginning or the end of the pulse drifts off scope.)

Figure 7 shows data taken 4 days later. The characteristics are similar to the November 10 data, but with generally longer pulse lengths. For both of these days, there were no observed solar flares and no SID activity.

In Figures 8 and 9, the Boulder magnetograms for these 2 days are shown. November 10 is fairly disturbed; the K_p indices are mostly in the range 4 to 5 with a 6- from 1200 to 1400, but on November 14, the magnetic field was extremely quiet. Since the pulse data for these 2 days are very similar, there is no apparent correlation of pulse data parameters with the Boulder magnetic field for mild or moderately disturbed conditions. The largest pulse delay changes observed were recorded on February 18, 1970 and are shown in figure 10. Here, the pulse data are displayed in the same way as the November data. The added points with the connecting solid line show relative group delay at 18 MHz scaled from the CHIRP ionosonde system which ran concurrently with the pulse system on this day. The feature of interest is the excursion during which the pulses were not tracked. E-layer Doppler records from Longbranch, Illinois to Boulder, Colorado, show no similar feature on this day. Vertical ionograms from Stanford, California, Ft. Arguello, California, Boulder, Colorado, and White Sands, New Mexico, were scaled in an attempt to trace the direction and velocity of this feature, but poor time resolution (only 1 point/15 min.) limited the usefulness of this information. However, during these times, Faraday rotation data from ATS-1 were being collected by Drs. A.V. da Rosa and Michael Davis of Stanford University and Dr. Fred Smith of Colorado State University and were kindly made available to us.

These data were processed to remove diurnal trends, and are shown in Figure 11. By superimposing the pulse and satellite data, the feature was identified at the times listed in table 1. Satellite data maxima correspond to the pulse delay minimum because increasing Faraday rotations imply increasing total columnar electron content and, therefore, decreasing pulse travel times.

Assuming a plane wave front advancing uniformly, the disturbance came from the southeast (N158°E) at approximately 40 m/sec. Realistically, TID's do not propagate uniformly but are affected by local winds at the height of propagation. Also, the feature identification on the ATS-1 Ft. Collins path is not as positive as for the Stanford path. The origin of the disturbance is unknown, especially considering the lack of general magnetic activity and the apparent direction of propagation. Work to trace the origin to the troposphere was inconclusive. The basis for this effort was a paper entitled "Jetstream Activity Detected as Wave-like Disturbances at Mid-Latitude Ionospheric F-Region Heights", by G. B. Coe (1971). To our knowledge there were no major natural or unnatural catastrophic events which might have triggered this disturbance.

Table 1. Arrival Times for the TID
of February 18, 1970.

Path	Location	Time of Maximum Faraday Rotation(UT)
Stanford-Boulder pulse midpoint	39°05'N, 113°52'W	1900
ATS-1-Stanford (300 km alt.)	34°35'N, 125°W	1840
ATS-1-FT. Collins (300 km alt.)	37°26'N, 110°15'W	1700

3.2 SOLAR ECLIPSE DATA

Experimental radio sounding data collected on March 7, 1970 have been analyzed with primary interest in detecting any travelling ionospheric disturbances generated by the solar eclipse of that day, as postulated by Chimonas and Hines (1970). Data were obtained from the short pulse experiment and two oblique and four vertical incidence ionospheric sounders operating during a 6-8 hour daytime period centered on the solar eclipse. In addition to the Palo Alto-Boulder CHIRP sounder, a CHIRP system was operated by the Stanford Research Institute between Bearden, Arkansas and Los Banos, California. Geographic locations of the sounders and of the oblique path midpoints are shown in figure 12.

Relative delay times at various frequencies were scaled from the oblique ionograms at 1 minute (Palo Alto-Boulder) and 2 minute (Bearden-Los Banos) intervals. These data were then processed by a digital computer and plotted by a CRT plotter. Figure 13 is an example of these scaled CHIRP ionograms for the Bearden-Los Banos path, where relative group delay is plotted versus time for several frequencies. The extraordinary mode on vertical ionosonde data from Boulder, Colorado; White Sands, New Mexico; Point Arguello, California; and Mexico City, Mexico was similarly analysed.

Data from the short pulse experiment are presented in figure 14, which shows the variation of the starting times of the received pulses relative to time of transmission of the pulses (dashed curve) and the duration of individual pulses (solid curve) in usec. The solid curve shows several peaks in the pulse length parameter. These coincide with times when the pulse delay is tending toward a maximum and may be indicative of multipath conditions which are likely to occur when the reflection region is in the "rarefied" portion of a pressure wave travelling approximately perpendicular to the ray path. At such times, rays which leave the transmitter at azimuth angles slightly off the great circle path to the receiver, may be refracted sufficiently to cause focusing and pulse lengthening. Displacement of the peaks in pulse length with respect to the corresponding peaks in times of pulse starts is qualitatively consistent with tilts in the isoelectronic contours within a travelling disturbance.

Partial obscuration of the solar disc during the eclipse reduces the ionizing radiation flux and this will usually result in a reduction in electron concentration at any specific height. For example, at Mexico city, on 9 MHz, a 100 km virtual height increase peaks at 1755 GMT, about 25 minutes after maximum obscuration. At the northern stations, where this effect will be less, changes in reflection heights related to the eclipse shadow are masked by other disturbances.

Study of the sounder data at the several stations indicates that TIDs travelling in a generally north-to-south direction were present between 1600 and 1830 GMT. Passage of a TID is manifest on the Boulder (1614 GMT) and Point Arguello (1628 GMT) ionograms by "forked" satellite traces. The peak arrival times are consistent with a wave travelling at 400 m/sec. from an azimuth about 355 degrees (east of north).

Chionas and Hines (1970) predicted focusing of different bow wave components, from the postulated TID, near California just after 1900 GMT. Generally in our data between 1830 and 1920 GMT there are only small scale fluctuations with a gradual decay in virtual height which coincides with the uncovering of the sun. Exceptions to this statement are the oscillations in the Palo Alto to Boulder data from 1900 to 2000 GMT which might have resulted from continuation of the TIDs observed earlier. Also, at Boulder a 30 km virtual height increase at 1825 GMT does not appear elsewhere. Hence, there is no evidence of an eclipse induced TID during the 1830-1920 period.

Between 1930 and 2030 a disturbance with a generally east-to-west direction of travel was observed. The direction of arrival is $60-70^\circ$ away from that predicted for an idealized bow wave generated by the moving eclipse shadow (2140° east of north). The difference could arise from the assumptions about the propagation of the postulated disturbance from the eclipse path to the observing sites, or an eclipse-generated disturbance could suffer interference from other travelling disturbances to give a modified apparent direction of travel. Based on our data it is not possible to attribute conclusively this TID to the eclipse.

3.3 CORRELATION STUDIES

To check the dependence of pulse delay, length, amplitude, and background amplitude on each other, and on solar zenith angle, cross-correlation studies were done for six selected intervals of data encompassing approximately 16 hours of data. The data were selected to exclude periods during which the receiver gain or center frequency were changed. For every case, the two quantities being correlated were also computer plotted with one as a function of the other. After inspecting the plots for non-zero time lags and the appropriateness of linear correlation, more sophisticated correlation techniques were deemed unnecessary.

Pulse delay and the rate of change of pulse delay were shown to be uncorrelated with pulse length for the cases tried. However, one can construct specific cases for which the ionospheric dispersion is nonlinear over a small interval of frequency. Then, increasing dispersion (i.e., pulse length) and increasing path length would be correlated.

Pulse delay and pulse length were interpreted as uncorrelated with pulse and background amplitude. An apparent slightly positive mathematical result between pulse delay and background amplitude, and pulse length, pulse, and background amplitudes is attributable to a bias in the scaling procedure. If a pulse has a large signal to noise ratio the scaler is able to determine more accurately the time of pulse start and end.

The experimental conditions were such that the measurements were conducted between the hours 1700 UT (10:00 a.m., MST) and 2400 UT (5:00 p.m., MST). Therefore, the solar elevation at the path midpoint ranged from a high near 42° in February to a low near 5° in November. The correlation computations show no strong dependencies among the variables, but pulse delay was always positively correlated with solar elevation angle and pulse length was generally negatively correlated. Pulse amplitudes were uncorrelated with solar elevation, but background amplitude correlations fluctuated from case to case and showed a wide range of values. Apparently the noise sources were variable and external to experimental parameters. Figures 15 and 16 show frequencies of pulses spaced by one minute intervals in time. Pulse durations and peak amplitudes remain fairly constant in each sequence, but there is considerable complexity in the detailed structure of each pulse. We believe that the modulation seen within these pulses is the result of time-shifted wavetrains (due to multiple reflection points in the ionosphere) which interfere with one another when mixed in the receiver. From figure 15, two multipath components with group delays differing by about 3 msec. and a third component displaced in time by 12-15 msec. are implied.

These type of data tend to occur during times when other evidence indicates the passage of TIDs. Computations of expected multipath effects using ray tracing through reasonable TID models are described in the next section of this report with results that support the magnitudes of multipath time-shifts observed on the pulse data.

4. RAY-TRACE STUDIES

The purpose of this study was to investigate the temporal relationships between various homed multipath components of a monochromatic signal propagated through a travelling disturbance. For this study the ionospheric electron density model consisted of an α -Chapman layer on a curved earth with no magnetic field and no collisions, but with a perturbation consisting of a "gravity-wave" irregularity travelling from the north to the south. The electron density, N , is given by

$$N = N_0(1+\Delta)$$

$$\Delta = \alpha \left(\exp - \frac{(R-R_0-Z_0)}{H} \right)^2 * \cos 2\pi(t' + (\pi/2-\theta)R_0/\lambda_x + (R-R_0)/\lambda_z).$$

The earth's radius is R_0 ; R, θ, ϕ are earth-centered spherical coordinates, $N_0(R, \theta, \phi)$ is the α -Chapman electron density model. The perturbation, Δ , has a Gaussian amplitude distribution about height Z_0 , and vertical and horizontal wavelengths λ_z and λ_x , respectively. An example of propagation near vertical incidence into a TID with a 300 km horizontal wavelength is shown in figure 17.

Model studies for the nonhomogeneous ionosphere were based on a three-dimensional ray-tracing program developed by R. M. Jones (1966). This computer program calculated ray paths through a medium whose index of refraction varies in three dimensions. Six differential equations similar to those described by Haselgrove (1954) are numerically integrated. Additional differential equations are integrated which supply supplemental information such as a group path, phase path, absorption, and Doppler shift.

Some general properties of HF propagation through travelling disturbances are illustrated in the next two figures. Figure 18 is a ground projection of rays transmitted at a constant elevation angle and swept through a small range of azimuth angles. It shows the variations in range and final azimuth that can occur when propagating through an irregularity.

Figure 19 illustrates a number of points. In both figures the dashed line represents calculations from a concentric ionosphere and the solid curves represent calculations for a wave model with a horizontal wavelength of 100 km. Both are for a frequency of 17 MHz. The solid range-elevation curve on the left shows elevation focusing and defocusing. Focusing occurs when the rate of change of range with respect to elevation angle is small. This corresponds to reflection from concave portions of isoionic contours.

The curve on the right shows the variations in the azimuth of the landing point with respect to the transmitted azimuth for a constant elevation angle, β . Analogous to elevation focusing, azimuthal focusing takes place when rays transmitted at different azimuth angles land at the same azimuth from the transmitter.

This plot permits determination of whether or not multipath focusing is possible for any set of ray trace parameters. If the solid curve contains only inflection points and no local minima, no multipath focusing is possible. This will happen when the ray does not penetrate very far into the disturbed region or when the TID wavelength is very long. In either case the horizontal gradients in electron density at reflection heights are not great enough to permit azimuthal focusing.

Even when azimuthal focusing does exist, however, the range at which these rays land is usually different from each other. By varying the elevations we can construct a family of curves in the θ, ϕ plane as shown in figure 20. The sweep of elevation angles is made large enough to include the homing range, if it exists, at any particular landing azimuth. Since the ray tracing program does not have a homing feature, a procedure was developed to scan through a range of azimuth and elevation angles and ray path parameters such as range, group and phase path, and azimuth and elevation deviations were computed and then output onto punched cards. Using these data, homing on a given range and azimuth is accomplished using a Lagrangian interpolation scheme.

Calculations were restricted to nearly east-west propagation at 18 MHz and a homing range of 1500 km. These parameters are approximately those of the short pulse experiment. The α -Chapman model parameters used in the ray trace study were $f = 8$ MHz, $H_{max} = 250$ km, scale height = 62 km. The MUF with this model at a range of 1500 is about 22 MHz, which is near the observed MUF during midday. All TID models used had the maximum wave amplitude at a height of 250 km and a vertical wavelength of 100 km. Horizontal wavelengths of 50, 100, and 300 km have been used with 10 and 15 percent wave amplitude perturbations.

For a model TID with 50 km wavelength and 10 percent perturbation the group path variations between the different homed rays range from 4 to 18 km which corresponds to group delay variations of from 12 to over 50 microseconds. Rays were homed over elevation and azimuth ranges of 1 and 3 degrees, respectively. For the model parameters used the reflection heights are in the 160-170 km range. With the height of maximum wave amplitude at 250 km the wave perturbation at the 165 km level is around 4 percent. Even though this is large enough for multipath focusing from the 50 km TID with a 10 percent perturbation it is not the case for irregularities with horizontal wavelengths greater than about 100 km.

For a TID with a 100 km horizontal wavelength and a 15 percent perturbation amplitude we obtained multipath focusing with ranges of delay time, azimuth and elevation angles of up to 80 μ sec., 6 and 3 degrees, respectively. No multipath focusing was obtained for a TID with a 300 km horizontal wavelength and a 15 percent perturbation amplitude.

5. CONCLUSIONS

The following conclusions are drawn from the analysis and interpretation of the data described above:

- (1) The use of very short HF pulses to study ionospheric propagation provides unique information on the propagation mechanisms. The method provides a physical analog to the powerful mathematical technique of using delta function analysis of a frequency-dependent system.
- (2) At times the ionospheric response exhibits in a textbook manner the expected behavior based on magnetoionic theory. This is true for the effects of dispersion and magnetoionic splitting of the signal into the ordinary and extra-ordinary modes.
- (3) For the 1500-km range, polarized antennas can be used to reject one of the circularly polarized modes with sufficient efficiency to eliminate an appreciable fraction of the effect of magnetoionic splitting. This may not be the case for larger ranges where the signal

arrives with very small elevation angles.

- (4) During an appreciable fraction of the total observing time, the pulse signals exhibit complex behavior which is not explainable by the classical propagation effects through a smooth ionosphere. Analysis results point to spatial nonhomogeneity in the ionosphere as being responsible for small-scale multipath effects which can account for the complex behavior observed. The longest continuous period of complicated pulse structure occurred on February 13, 1970, accompanying the passage of travelling ionospheric disturbances of unusually large amplitude (virtual height changes of approximately 60 km peak to peak). However, the nonhomogeneities were not severe enough to appear as "Spread F" on the concurrent CHIPP ionograms. This is not surprising because the pulse technique is capable of detecting much smaller changes than can be resolved on an ionogram record.
- (5) Ray-tracing calculations through model ionospheres having idealized wave-like structure yield the result that the multipath delays can be accounted for by reasonable parameters of the said model.
- (6) The implication to communications which propagate through the ionosphere is that ionospheric nonhomogeneities will very likely be the limiting factor in data-bit rates and phase delays even at much higher frequencies than HF. It is, therefore, important to advance our knowledge and understanding of the irregular structure in the ionosphere and the effect such structure has on signals propagating through the medium.

6. ACKNOWLEDGEMENTS

ATS-1 satellite data was provided by A.V. da Rosa and Michael J. Davis of the Radioscience Laboratory of the Stanford Electronics Laboratories, Stanford University, California, and Fred L. Smith III of the Department of Electrical Engineering, Colorado State University, Ft. Collins, Colorado. The authors are particularly grateful to Wilma S. Burkey for many hours of accurate data analysis.

This research was supported by the Advanced Research Projects Agency of the Department of Defense under ARPA Order No. 1361.

REFERENCES

- CHIMONAS, G. and C.O. HINES, 1970, "Atmospheric Gravity Waves Induced by a Solar Eclipse", J. Geophys. Res. 75, 875.
- GOE, G.B., 1971, "Jetstream Activity Detected as Wave-like Disturbances at Mid-Latitude Ionospheric F-Region Heights", Pure Appl. Geophys. (in press).
- HASELGROVE, J., 1954, "Ray Theory and a New Method for Ray Tracing", Proc. Camb. Conf. Phys. Ionosphere (The Physical Society, London.).
- INSTON, H.H., 1969, "Dispersion of H.F. Pulses by Ionospheric Reflection", Proc. IEEE 116, No. 11, 1789-1793.
- JONES, R.M., 1966, "A Three-Dimensional Ray Tracing Computer Program", ESSA Tech. Rept. IER-17/ITSA-17.
- KANELLAKOS, DEMETRI P., 1969, "Ionospheric Propagation of Short Pulses", Semiannual Technical Report 1, Stanford Res. Inst., Stanford University, Stanford, Calif.
- LERFALD, G.M., JURGENS, VESECKY, WASHBURN, 1972, "Travelling Ionospheric Disturbances Observed Near the Time of the Solar Eclipse of March 7, 1970", J. Atmosph. Terr. Phys. 34, 733.
- LOMASNEY, J.M., and J.R. BARNUM, 1970, "An HF antenna for oblique propagation having approximately circular polarization over appreciable frequency and vertical angle intervals, Tech. Rept. No. 153, Radioscience Laboratory, Stanford Elec. Labs., Stanford Univ., Stanford, Calif.
- PRICE, G.H., 1968, "The Characteristics of Impulses Reflected From a Sech^2 Electron-Density Profile and Bandpass Filtered", Proc. IEEE 56, No. 8, 1341-1349.
- SOLLFREY, W., 1965, "Effects of Propagation on the High-Frequency Electromagnetic Radiation from Low-Altitude Nuclear Explosions", Proc. IEEE 53, No. 12, 2035-2042.
- WAIT, J.R., 1969, "On the Optimum Receiver Bandwidth for Propagated Pulsed Signals", Proc. IEEE 57, No. 10, 1784-1785.



Figure 1 Example of an HF pulse received over the Palo Alto-Boulder Propagation path.

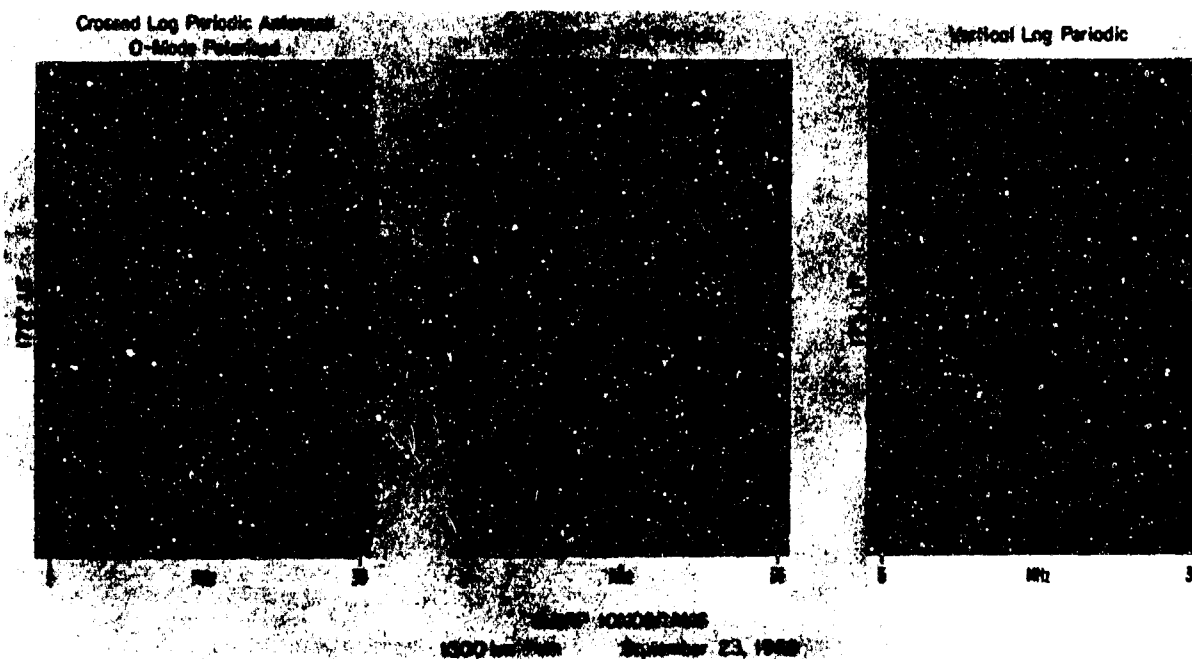


Figure 2 CHIRP ionograms, 1500-km path, Sept. 23, 1969.

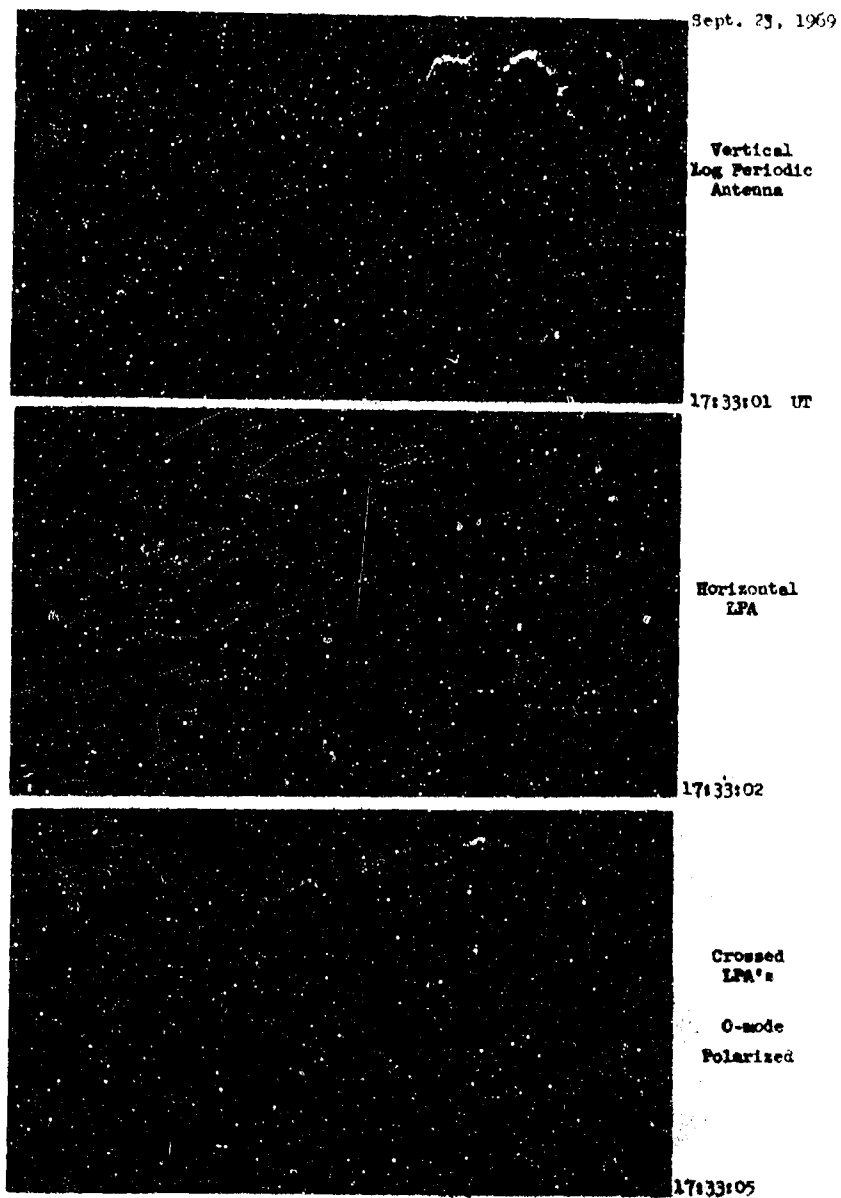


Figure 3 The effect of antenna configuration on pulses through a 2-MHz wideband receiver.

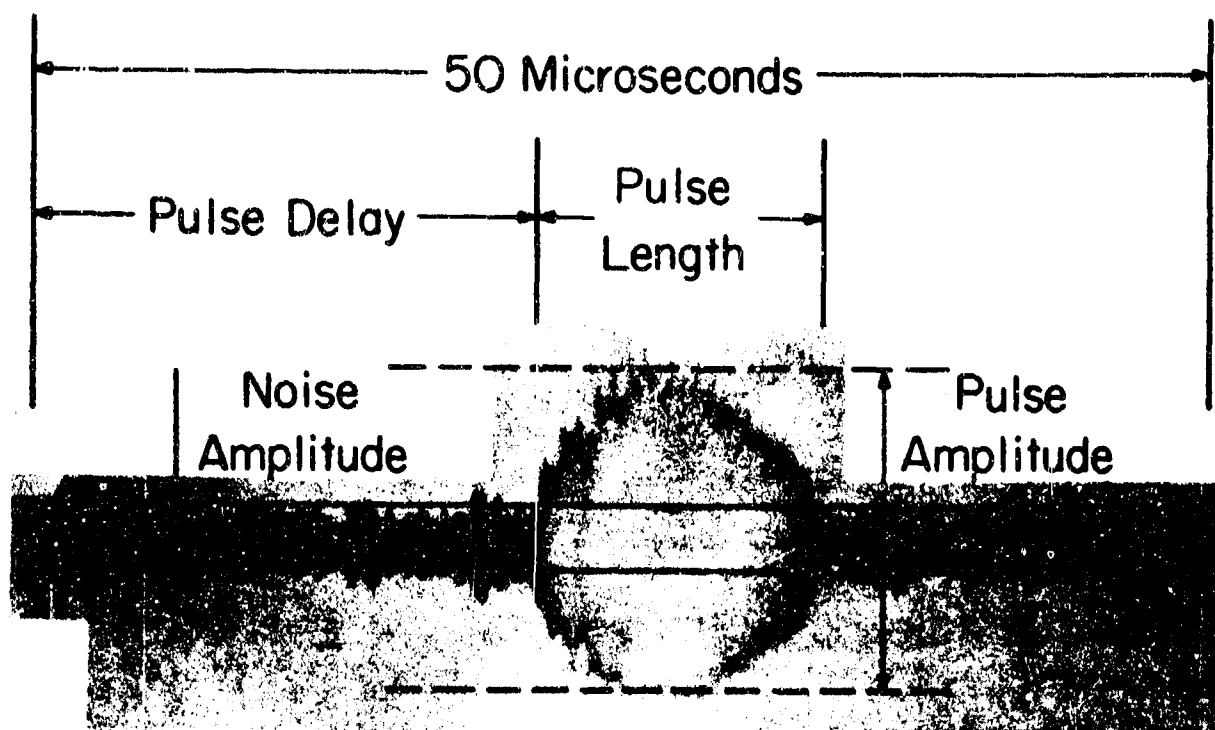


Figure 4 Example of HF pulse received at Boulder, Colo. from Palo Alto, Calif. (~ 1500 km).

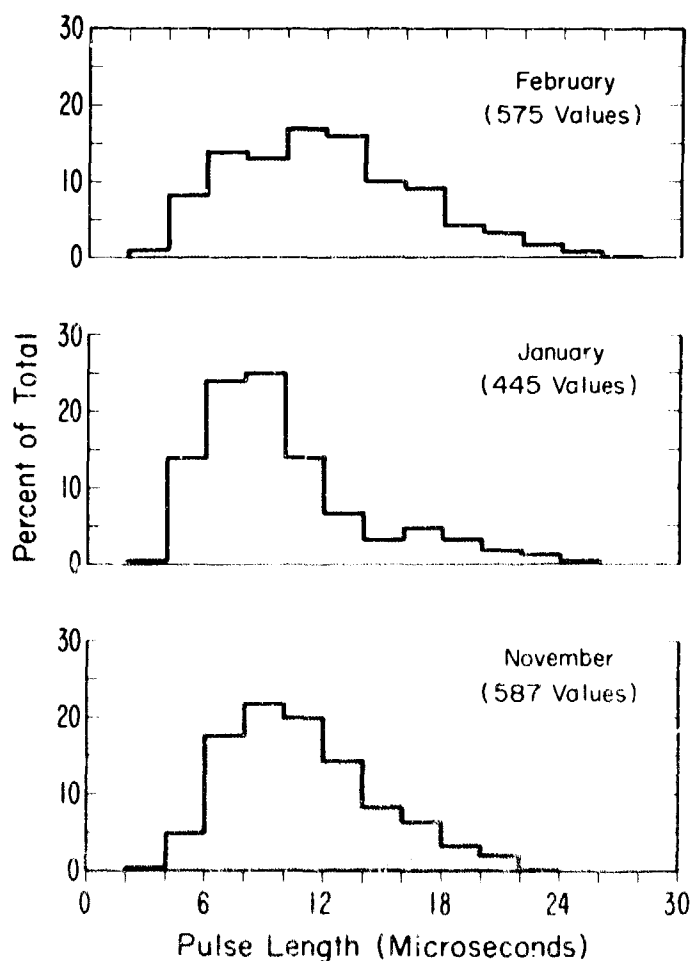


Figure 5 Histograms showing the distribution of pulse lengths for experimental data.

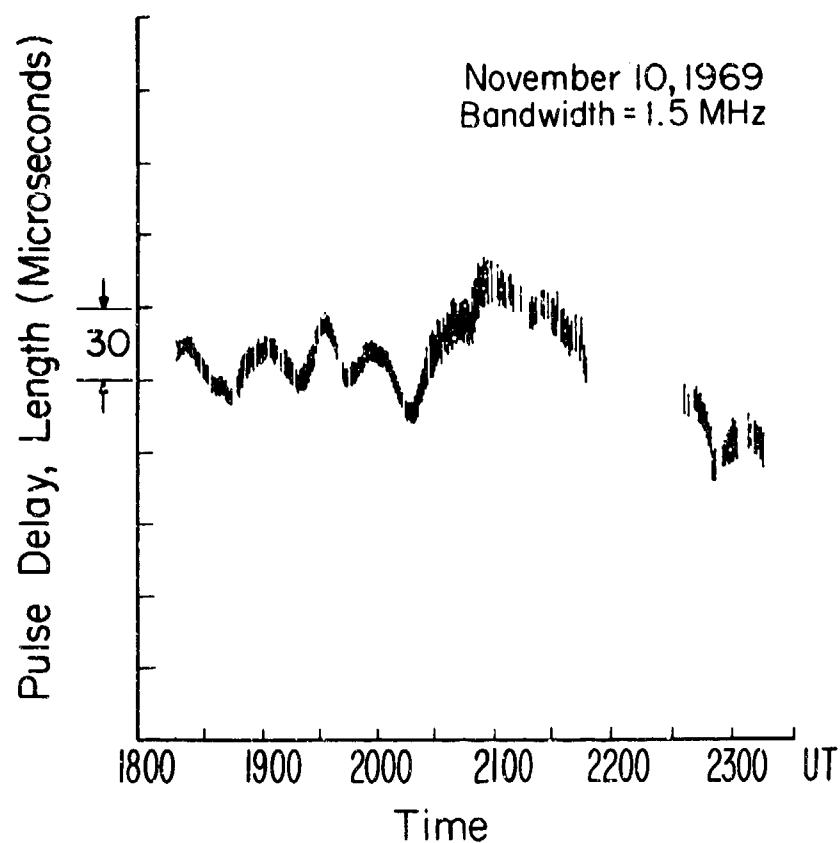


Figure 6 Pulse delay and length for November 10, 1969.

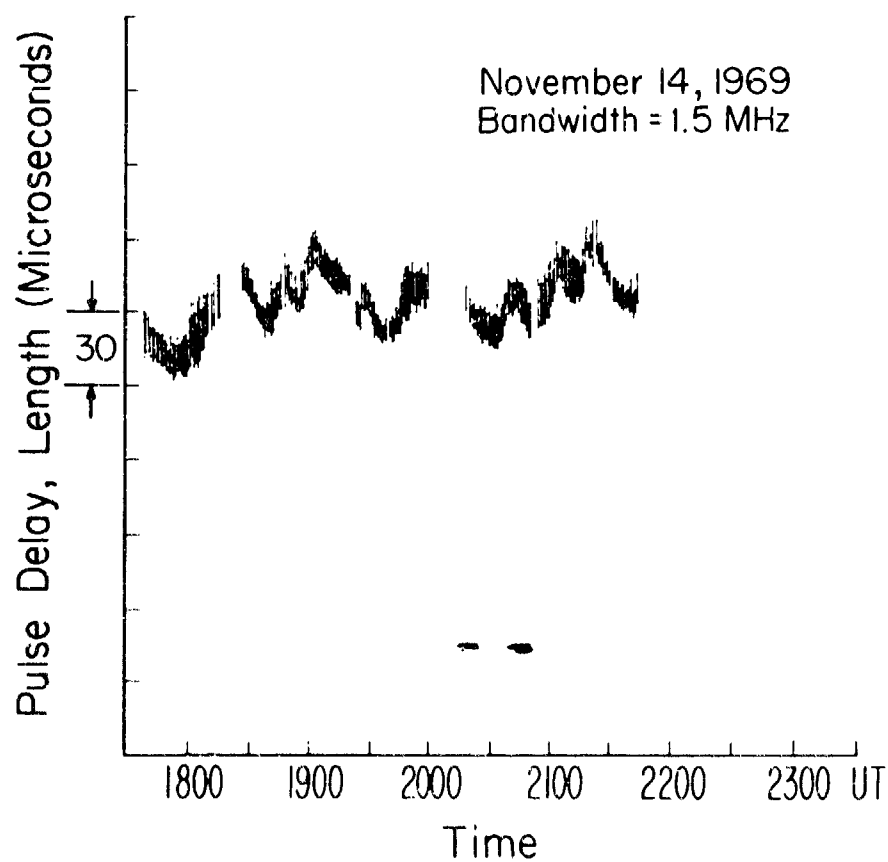


Figure 7 Pulse delay and length for November 14, 1969.

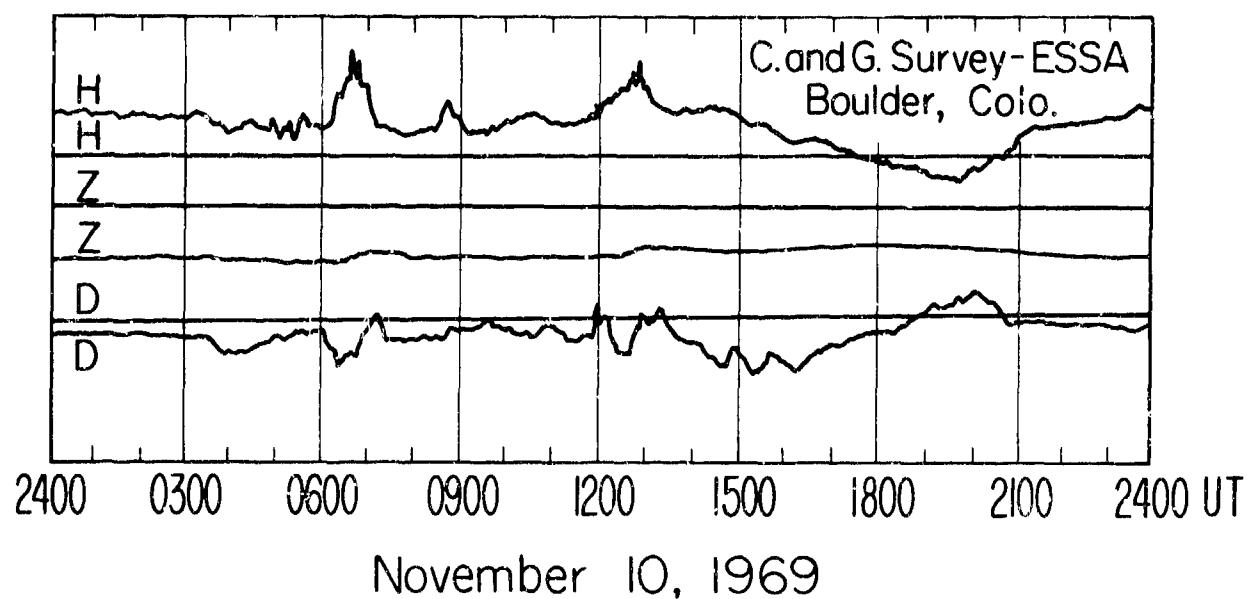


Figure 8 Boulder magnetogram for November 10, 1969.

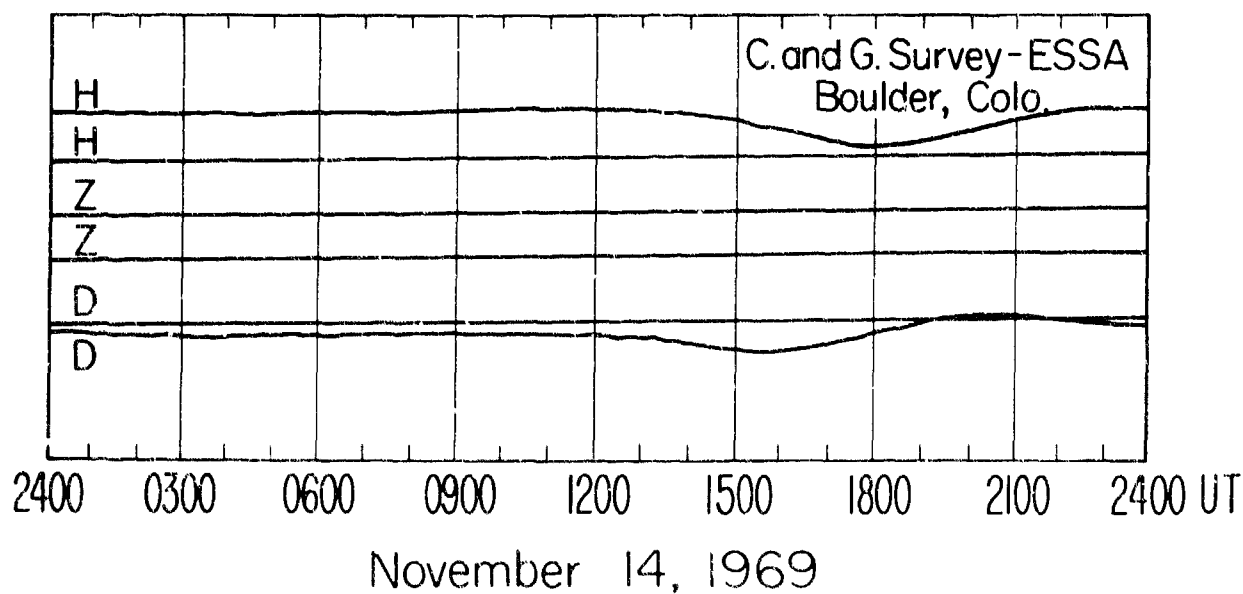


Figure 9 Boulder magnetogram for November 14, 1969.

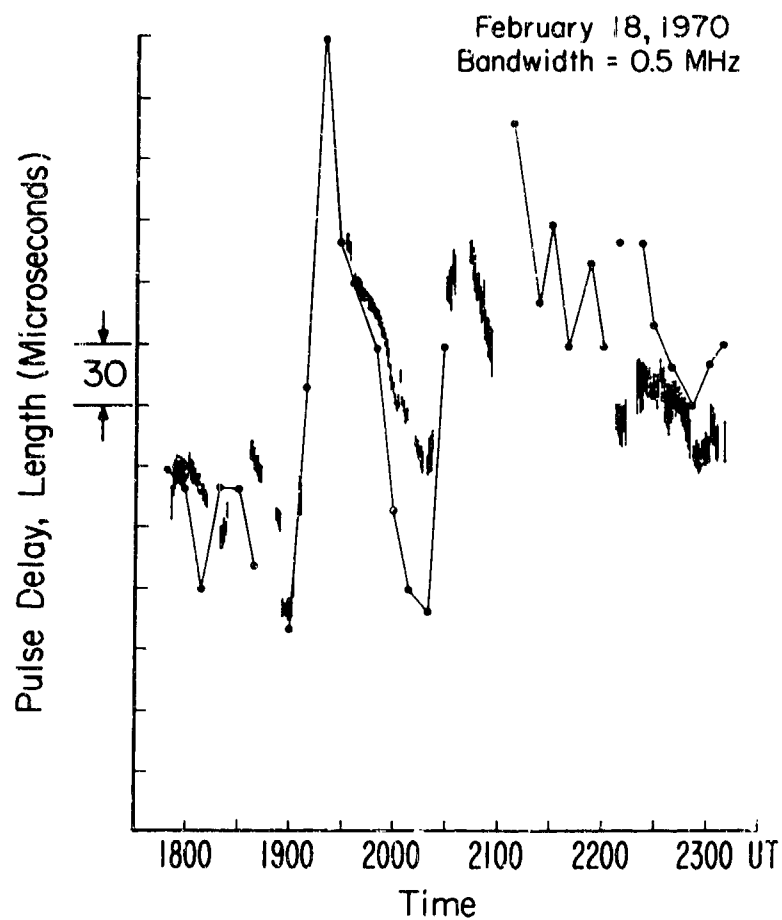


Figure 10 Pulse delay and length and CHIRP scalings for February 18, 1970.

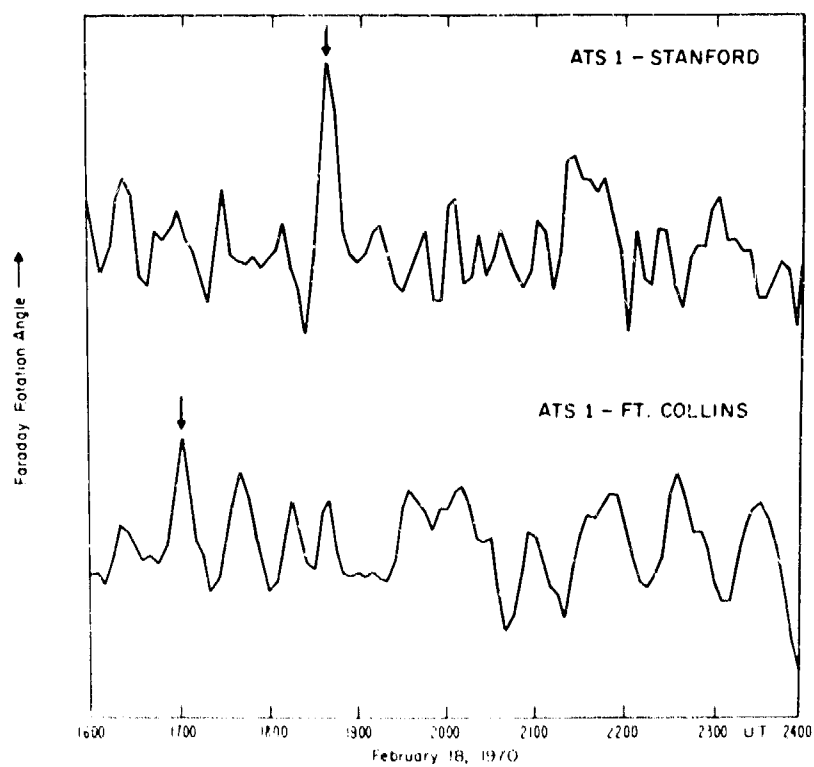


Figure 11 ATS-1 satellite Faraday rotation angles vs. time as measured at Stanford, Calif. and Ft. Collins, Colo. Arrows denote the feature of interest.

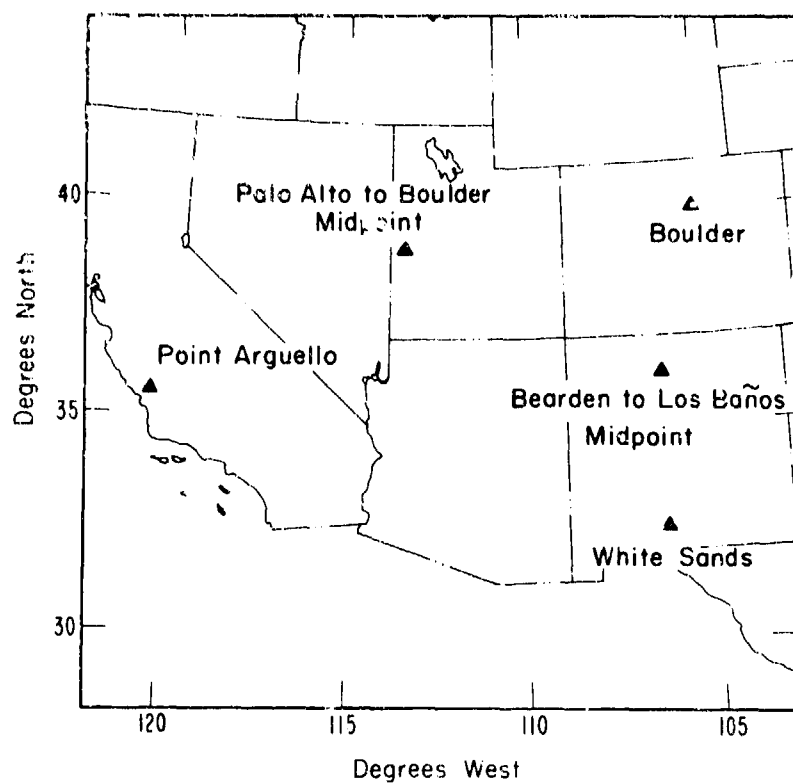
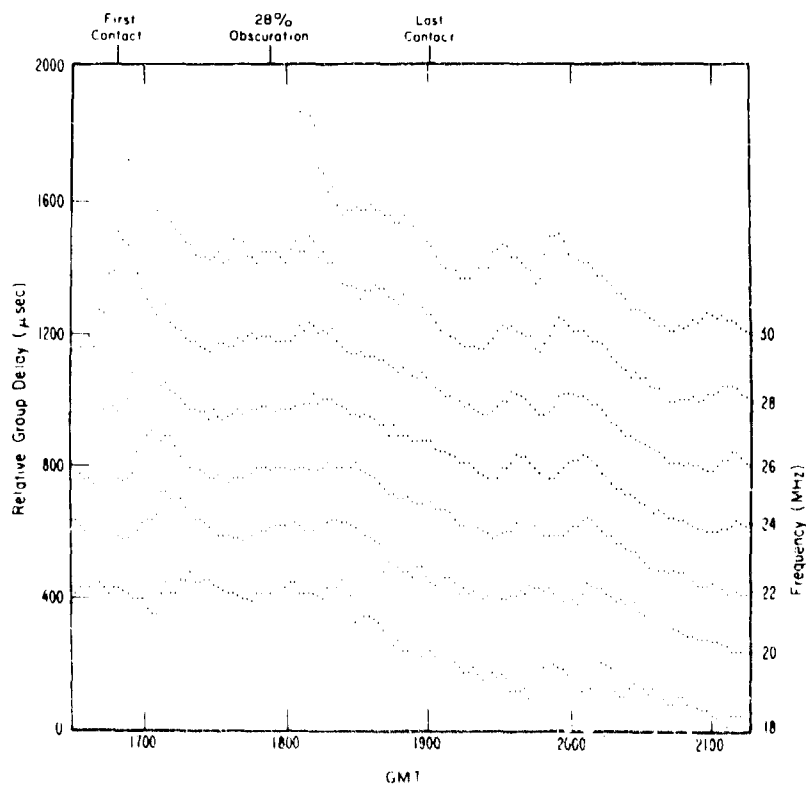


Figure 12 Location of vertical incidence sounders and oblique path midpoints in southwestern USA.



BEARDEN, ARKANSAS TO LOS BAÑOS, CALIFORNIA
CHIRP FREQUENCY SLICES
MARCH 7, 1970

Figure 13 Relative groups delay scaled from oblique ionograms between Bearden, Arkansas and Los Baños, California for probing frequencies at 2 MHz intervals.

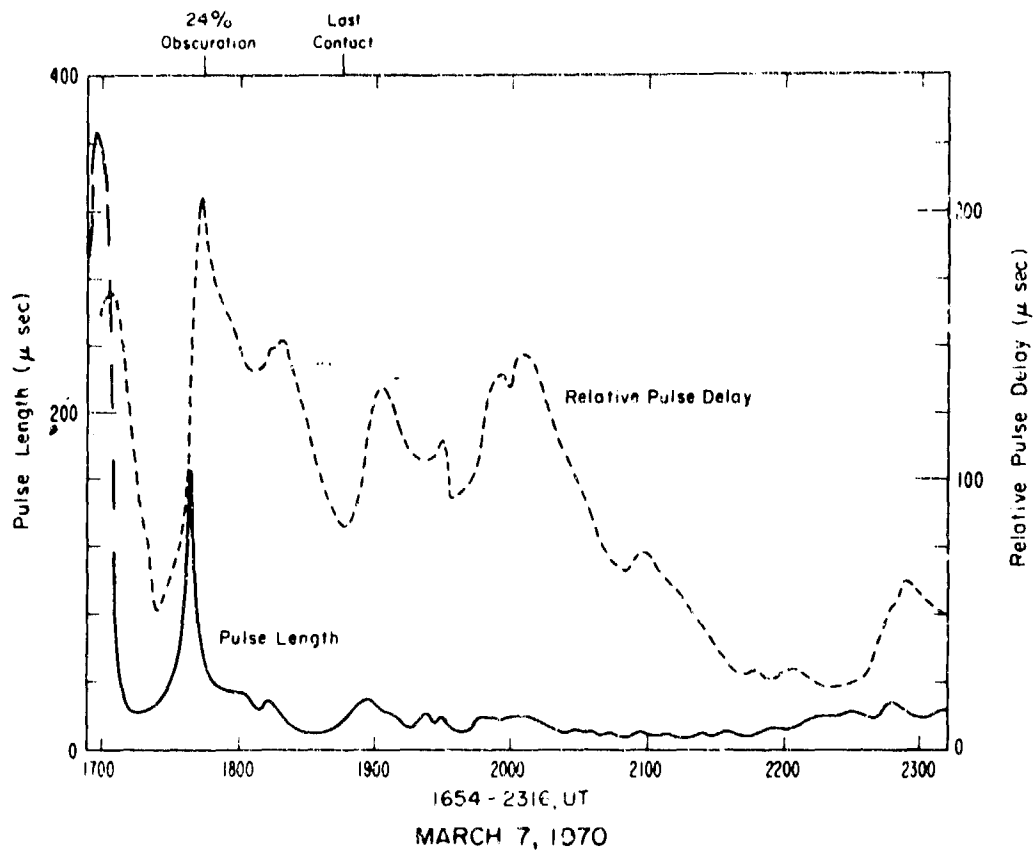
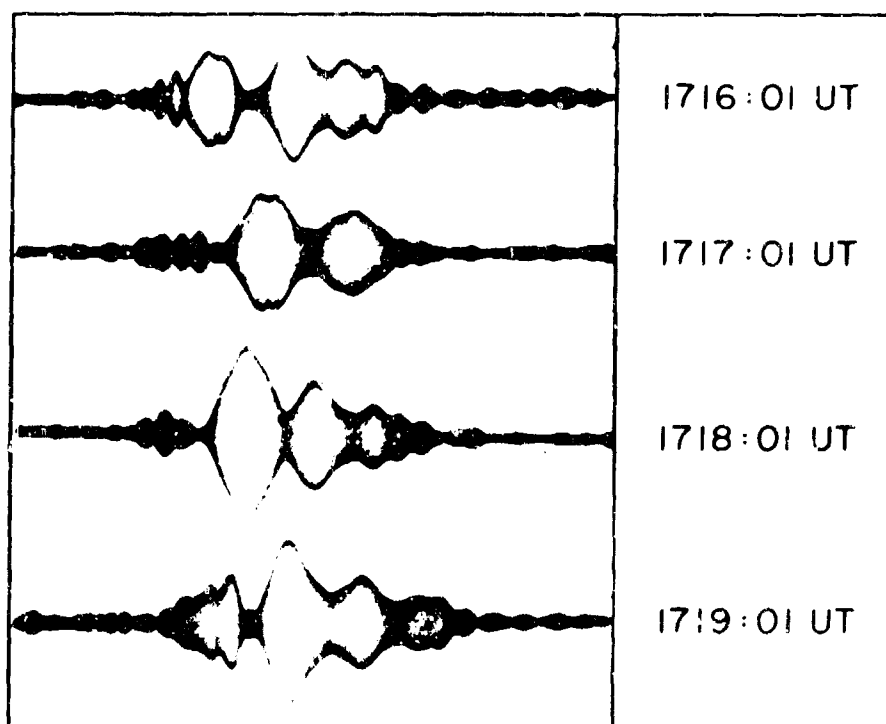
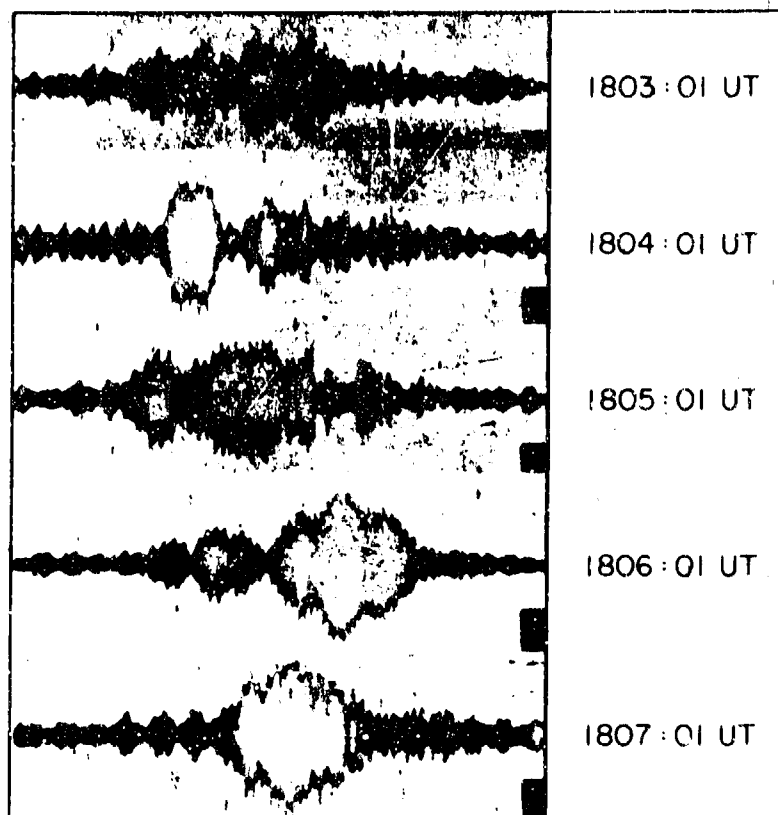


Figure 14 Palo Alto to Boulder electromagnetic pulse relative delays and pulse lengths as a function of time.



February 20, 1970

Figure 15 Example of consecutive pulses propagated through a complex ionosphere (Feb. 20, 1970).



November 14, 1969

Figure 16 Example of consecutive pulses propagated through a complex ionosphere (Nov. 14, 1969).

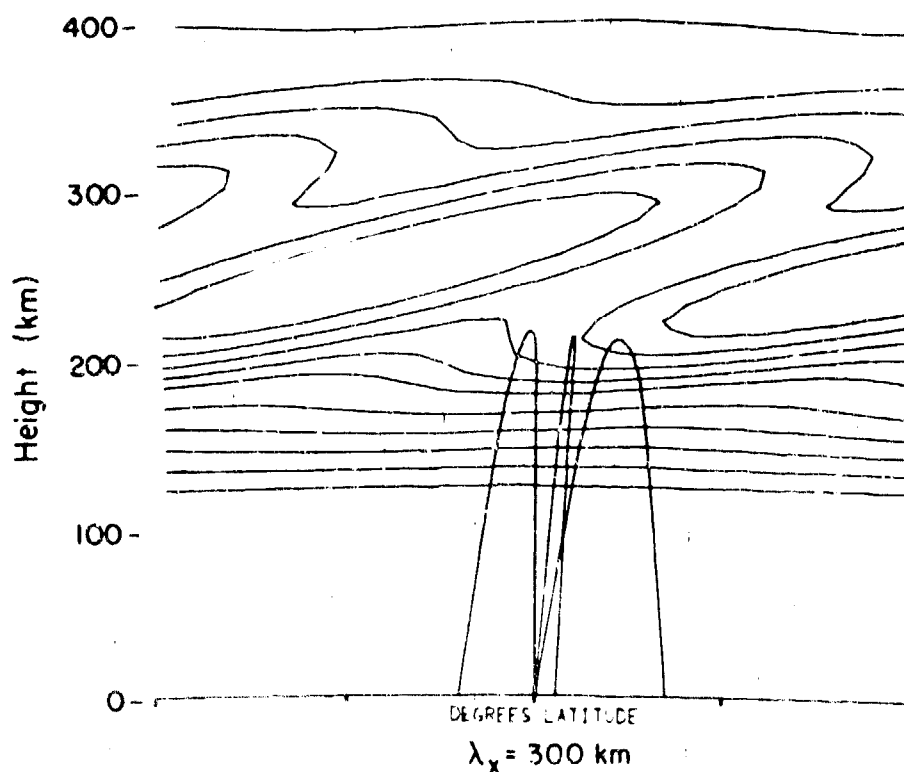


Figure 17 An example of near vertical propagation into an ionosphere with a gravity wave perturbation as described in the text.

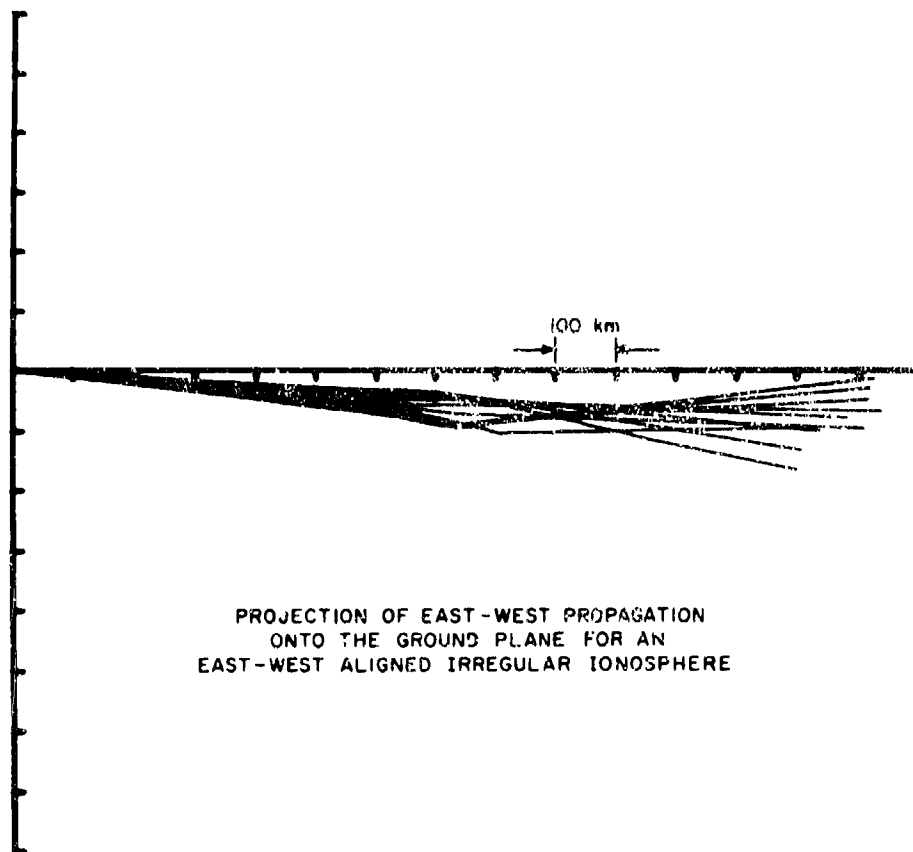


Figure 18 Projection of east-west propagation onto the ground plane for an east-west aligned irregular ionosphere.

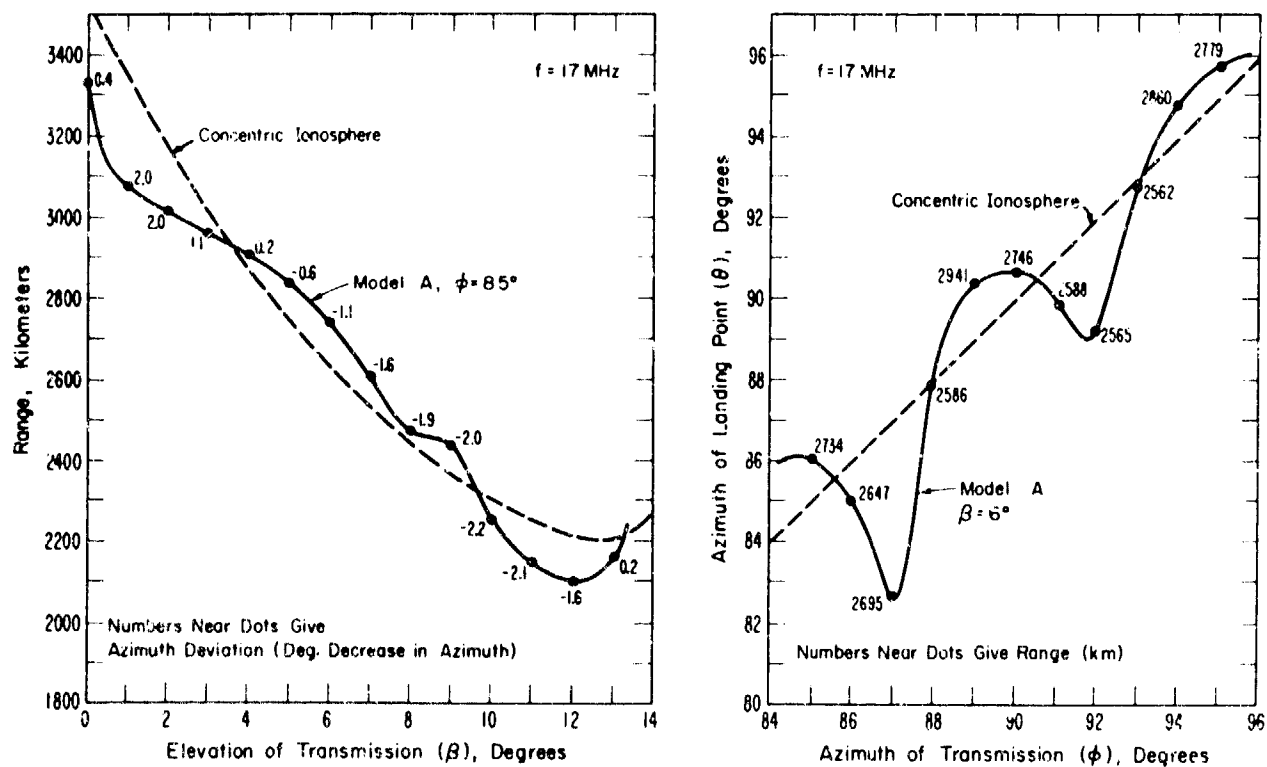


Figure 19 (Courtesy of T.M. Georges and J.J. Stephenson). Distortion of a range-elevation diagram (left) and a landing point azimuth-transmission azimuth diagram (right) in the presence of travelling disturbances.

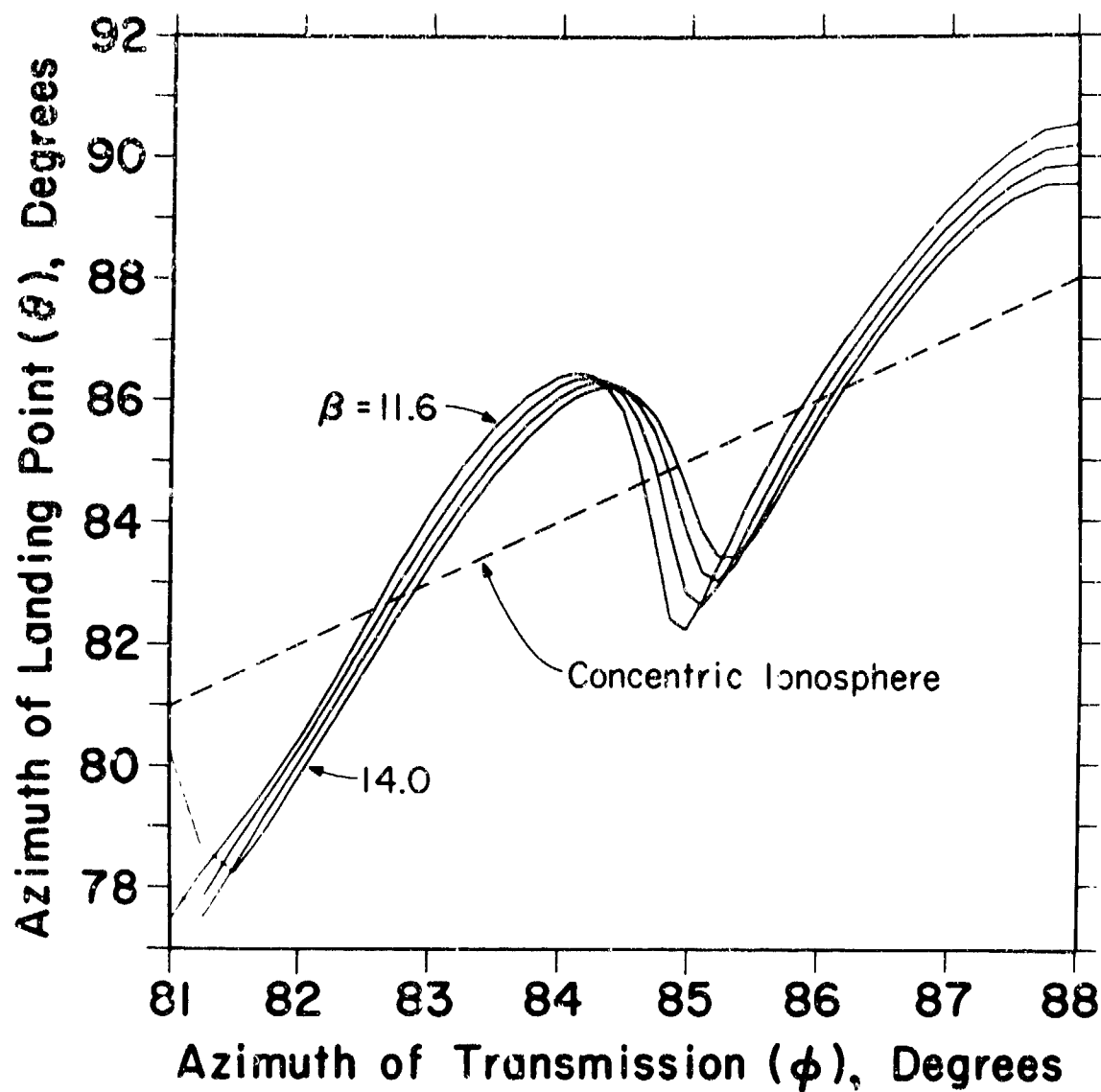


Figure 20

(θ, ϕ) diagrams parametric in elevation angle. Interpolation is made for a constant azimuth of landing point over the elevation angles to obtain a given homing range.

**TRAVELLING IONOSPHERIC DISTURBANCES INITIATED
BY LOW-ALTITUDE NUCLEAR EXPLOSIONS**

by

W.Stoffregen

Uppsala Ionospheric Observatory
S-755 90 Uppsala, Sweden

471

PERTURBATIONS IONOSPHERIQUES ITINERANTES ENGENDREES PAR DES EXPLOSIONS
NUCLEAIRES A FAIBLE ALTITUDE

par

W. Stoffregen

SOMMAIRE

A la suite de deux importantes explosions nucléaires ayant eu lieu à Novaya Zemlya, respectivement les 23 et 31 octobre 1961, on enregistra au-dessus de la Scandinavie des perturbations ionosphériques se déplaçant à une vitesse maximale de ≈ 630 m/s. Les perturbations affectant l'ionosphère étaient particulièrement marquées dans la région F, comme le révèlent les ionogrammes et les profils hauteur réelle. Lorsque la première onde arriva, on observa une augmentation spontanée de la hauteur de la couche F-2, suivie d'un fractionnement de la couche F, et d'une phase plus lente de retour à la normale. Au niveau E, une couche E sporadique apparut avec un certain délai, et l'ionisation de la région D s'accrut au cours de deux courtes périodes, avec un retard d'une heure environ par rapport à la perturbation de la couche F. On peut expliquer les délais survenant entre les perturbations aux différents niveaux de l'ionosphère grâce aux résultats d'études, par trajectographie, de la propagation des ondes acoustiques et de gravité.

TRAVELLING IONOSPHERIC DISTURBANCES INITIATED

BY LOW-ALTITUDE NUCLEAR EXPLOSIONS

W. Stoffregen
Uppsala Ionospheric Observatory
S-755 90 Uppsala, Sweden

SUMMARY

After the two large nuclear explosions at Novaya Zemlya on October 23 and 30, 1961, ionospheric disturbances travelling with a maximum velocity of ≈ 630 m/s were recorded over the Scandinavian area. The disturbances in the ionosphere were most pronounced in the F-region, as is evident from the ionograms and real-height profiles. When the first wave arrived, a spontaneous increase of the height of the F2-layer was observed, followed by splitting of the F-layer and a slower phase of recovery. At the E-level, a sporadic E-layer occurred with some delay and the D-region ionization increased during two short periods with a delay of about one hour with respect to the disturbance in the F-layer. The time delay of the disturbances at different levels of the ionosphere can be explained by the results of ray-tracing studies of the propagation of acoustic gravity waves.

1. INTRODUCTION

In the course of the series of nuclear tests at Novaya Zemlya during 1961, the influence on the ionosphere was studied at the observatories at Kiruna, Lycksele and Uppsala by making vertical ionospheric soundings. The distances between the test area and these observatories are approximately 1300 km, 1650 km and 2100 km respectively. Some interesting records were also obtained from the 16.8-MHz backscatter sounder, operating at Uppsala. The 16-mm backscatter film records are converted into diagrams which show the travelling disturbances in a concentrated manner. The results of both the vertical and the oblique soundings have been assembled in a report (STOFFREGEN, W., 1962). The aim of this paper is to summarize briefly the main results, including real-height profiles produced more recently, and to discuss the time difference between the disturbances observed at different levels in the ionosphere.

2. OBSERVATION OF IONOSPHERIC DISTURBANCES

2.1 Vertical soundings

The large nuclear explosion of October 30 at ≈ 0933 hours gave rise to violent disturbances in the ionosphere, which were observable at great distances. At Lycksele, ≈ 1650 km away from the detonation area, ionospheric records were made at 3-minute intervals. The records, assembled in Fig. 38-1, show a number of interesting details. The whole structure of the ionosphere from the D- to the F-region was changed during two successive periods. At Kiruna and at Uppsala a similar behaviour of the ionosphere was observed. The following sequences of events during the overhead passage of the waves are of special interest:

- a) The F2-layer showed a very pronounced division near 3.5 MHz at 1010. At the time the layer rapidly moved upwards. This effect is seen even better on the records at 1046-1058, when the second wave arrived at the position of Lycksele. At that time the layer was split into two levels similar to the formation of an F1- and F2-layer. Cusps going up to a virtual height of about 700 km are seen on the records between 1128-1134 and at 1246, indicating strong vertical motions. A remarkable destruction of the F-layer was observed during 1122-1207, i.e. after the passage of the first and the second waves.
- b) At the level of about 100 km, a sudden increase of the critical frequency of an Es-layer was observed at 1016. After 1046, the critical frequency of a slightly higher Es-layer increased and remained for a longer time, except for two short periods of absorption due to D-layer ionization.
- c) Increased ionization in the D-region was observed during two short periods, as is evident from the increase of f-min. The two periods appear at 1058-1110 and 1218-1231.

Real-height profiles and plots of the height of the F-layer are shown in Fig. 38-2. The two drastic changes of the profiles to higher levels at 1010 and at 1052 indicate the arrival of the wave fronts overhead. The height variations seen on the plot to the right show the steep increase at that time. The profiles further demonstrate the descent of the F2-layer to a rather low level at 1028 before the recovery to a nearly normal profile at 1034 and 1040. In the lower part of the figure to the right, the increase of ionization

in the E- and D-region is shown. The Es ionization increases about 40 minutes later than the first disturbance at the F2-height. In the D-region the corresponding delay is about 50 minutes. The phase in which the F-layer was greatly distorted is marked in the figure as "spread reflections".

2.2 Backscatter records

The backscatter sounder at Uppsala, which operates on 16.8 MHz, produces one picture each minute on 16-mm film. Travelling disturbances can easily be detected, when the ionization in the F-layer is just great enough to obtain oblique incident reflections at this frequency. During October 30, 1961, the ionization was slightly below this limit, and hence the pattern visible on the screen indicated such reflections only, which were associated with the travelling waves initiated by the explosion. To the left of Fig. 38-3, a number of the records have been redrawn. Because of the skip distance, which in this actual case was ≈ 1000 km, the pattern moves around the centre of the screen from NE. to SW. (1051-1111). The information from this film has been converted into diagrams B and C, in order to show the waves more clearly. The ionospheric conditions were more favourable during October 23. The travelling disturbances caused by the nuclear explosion at 0930 are indicated by arrows to distinguish them from other reflections. In diagrams B and C, the waves can be followed through the different sectors from N. to S. It appears also that the waves are longer to the south than at their first appearance in the northern sector. The notations a and b show that the drastic change of the height of the F-layer is still very pronounced at a distance of ≈ 3500 km from the source. Diagram C is a good example of how travelling waves observed by a backscatter sounder can easily be detected. In fact, similar waves of an other origin have been studied in this way.

3. DISCUSSION OF THE OBSERVATIONS

The large-scale disturbances in the ionosphere resulting from low-altitude nuclear detonations are interpreted as a secondary effect of the acoustic gravity waves, which are generated by the explosion. It is suggested that the coupling between these waves and the ionized medium is due to collisions. The plasma-density changes recorded by ionosondes thus give information on the periods and the velocity of the acoustic gravity waves. Of special interest is the time delay of the perturbances at lower levels in the ionosphere. These details are not yet fully understood and are still the subject of study. It seems, however, that ray-tracing of the motion of shock waves up to ionospheric heights may explain the different behaviour in the F2-, E- and D-layers. Backscatter records demonstrate the motion of the travelling waves in one preferred direction only, because of the aspect sensitivity of the reflection area. Since the waves from the source propagate in all directions, the records may include certain reflections originating from discontinuities somewhat aside from the main direction. This has to be taken into account in the analysis of the records.

4. GENERAL INFORMATION

4.1 Reference

STOFFREGEN, W., 1962, "Jonosfärstörningar observerade i samband med kärnladdningsprov vid Novaja Semlja den 23 och 30 oktober 1961", Report No. 10, Uppsala Ionospheric Observatory (in Swedish).

4. GENERAL INFORMATION

4.1 Reference

STOFFREGEN, W., 1962, "Jonosfärstörningar observerade i samband med kärnladdningsprov vid Novaja Semlja den 23 och 30 oktober 1961", Report No. 10, Uppsala Ionospheric Observatory (in Swedish).

h' f records Lycksele 30 Oct. 1961

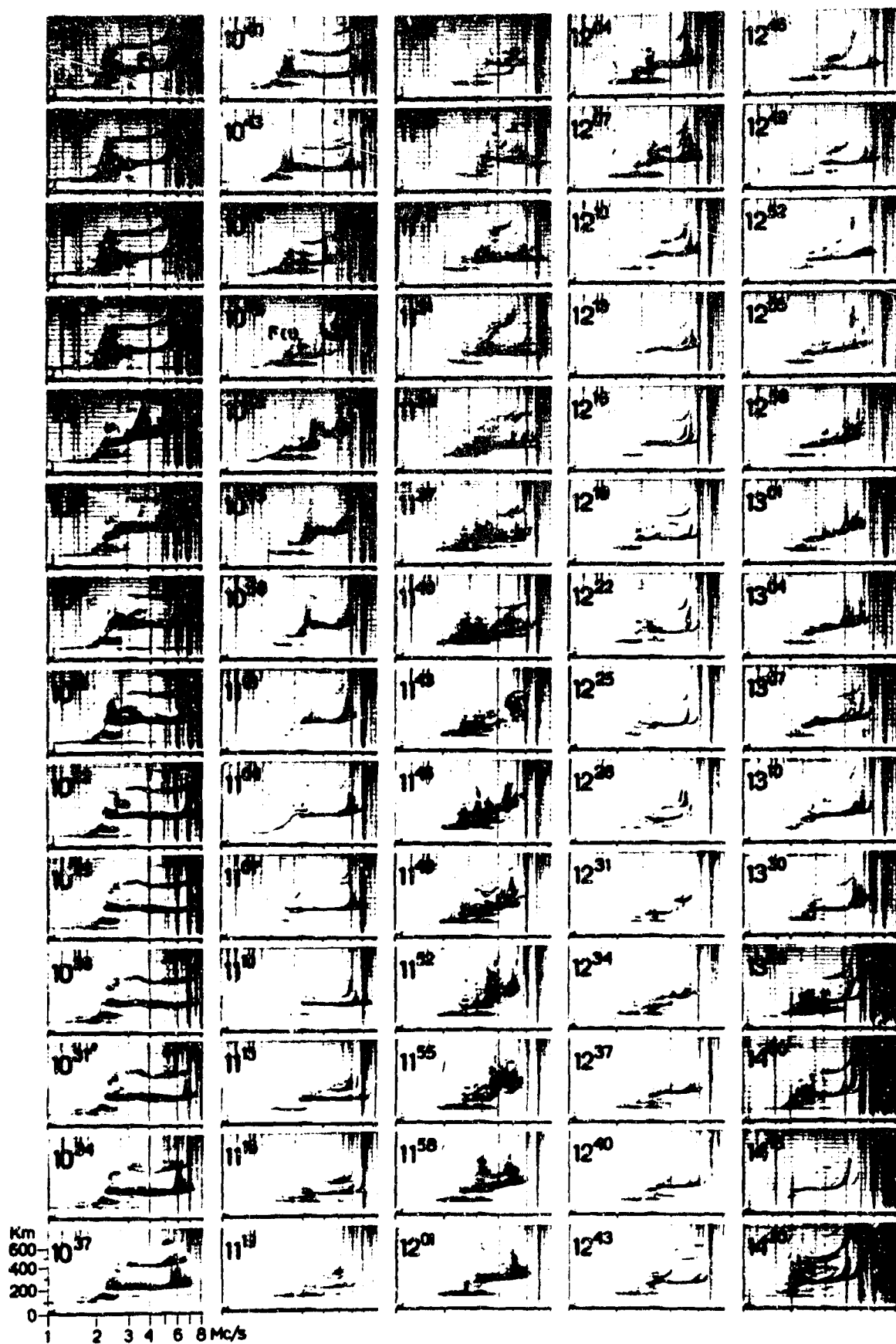


Fig.1 Ionospheric records made on October 30, 1961, showing various disturbances when the travelling waves initiated by the nuclear explosion passed overhead.

30 OCT 1961

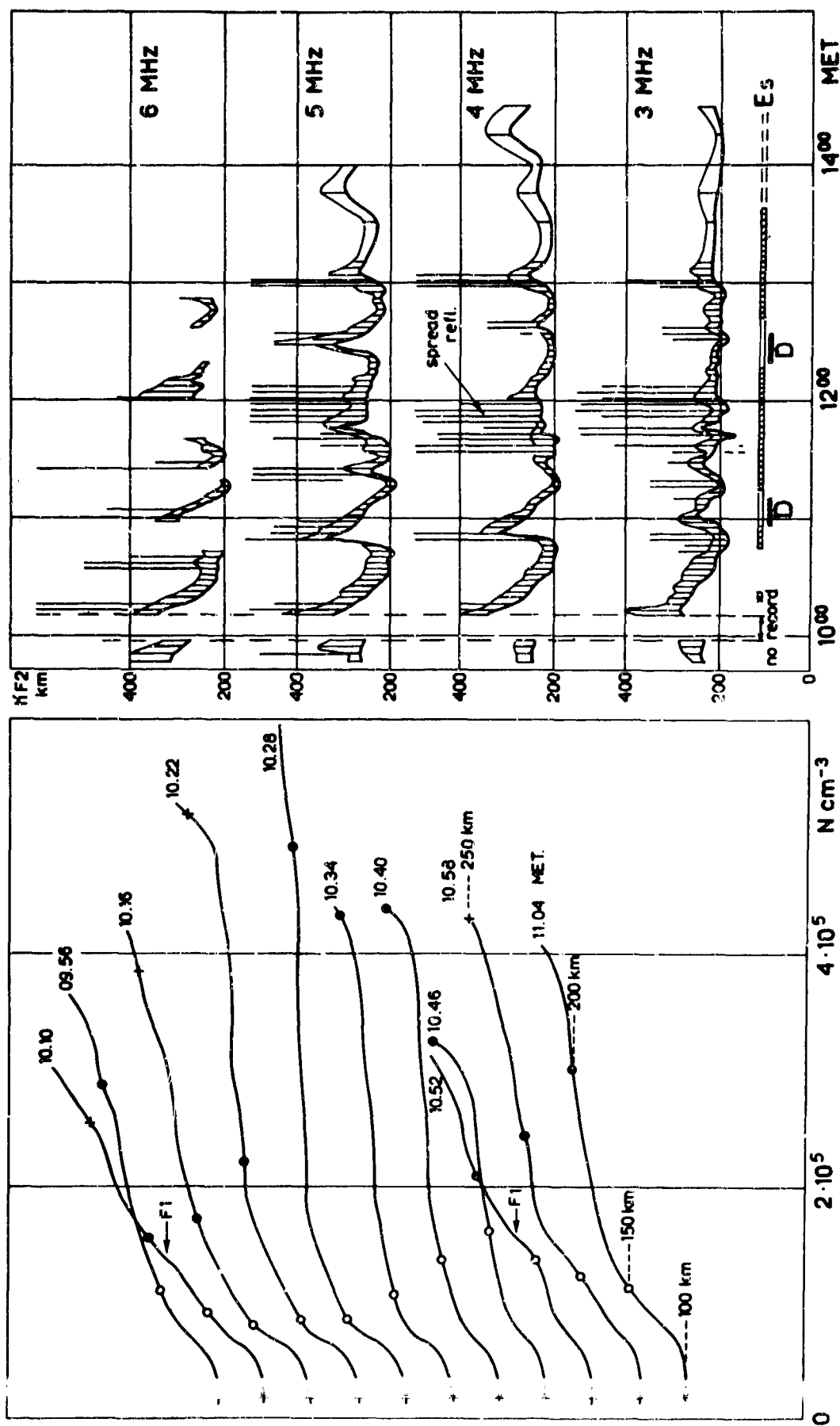


Fig. 2 To the left: real-height profiles, showing the change of electron distribution during two successive passages of acoustic gravity waves.

To the right: virtual-height variations at four different frequencies. Notation of the times, when disturbances are recorded in the Es- and D-level.

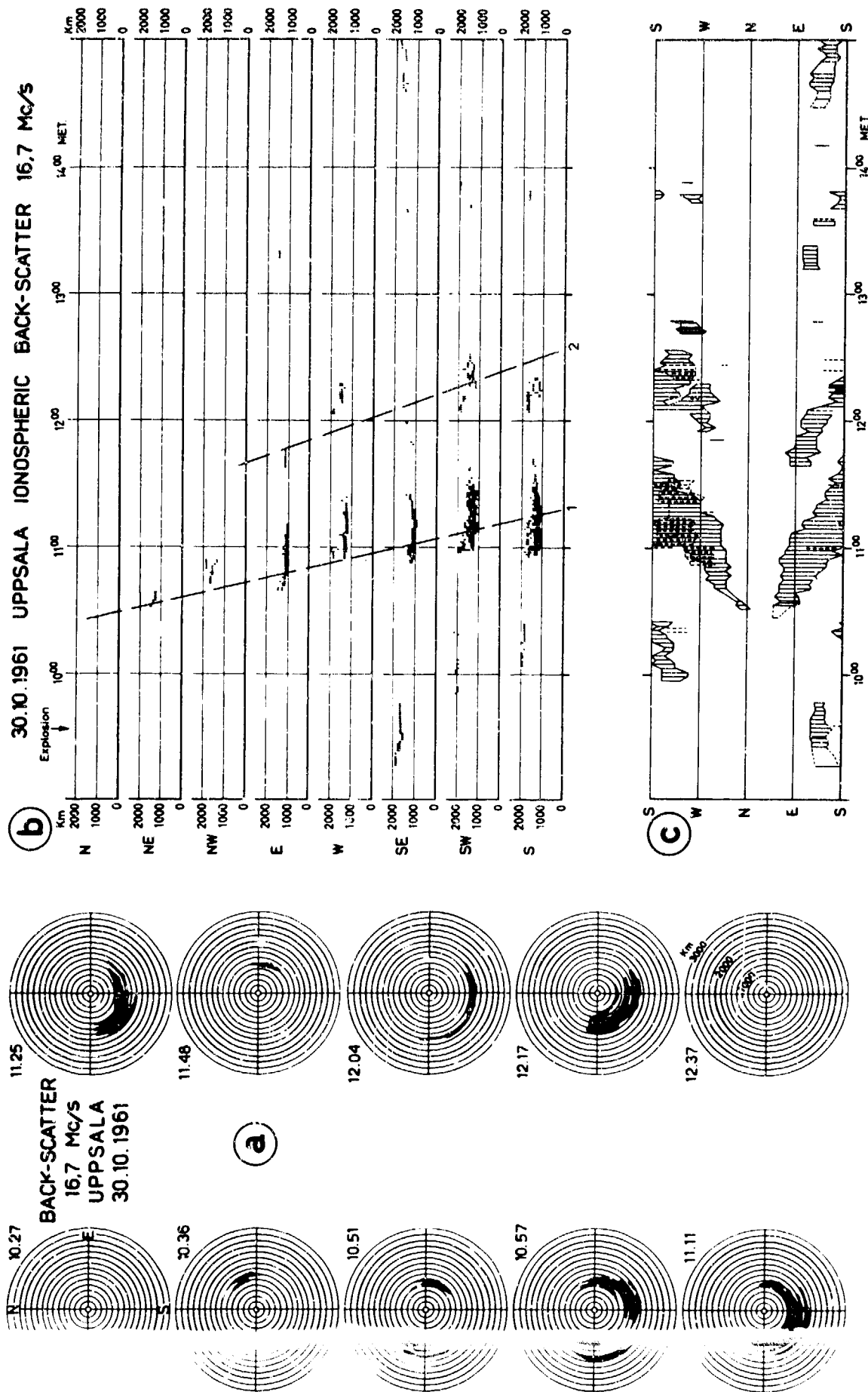


Fig.3 (a) Backscatter records of ionospheric waves, recorded on October 23, 1961.

(b) and (c) Diagrams showing the travelling disturbances in different sectors of the PPI screen.

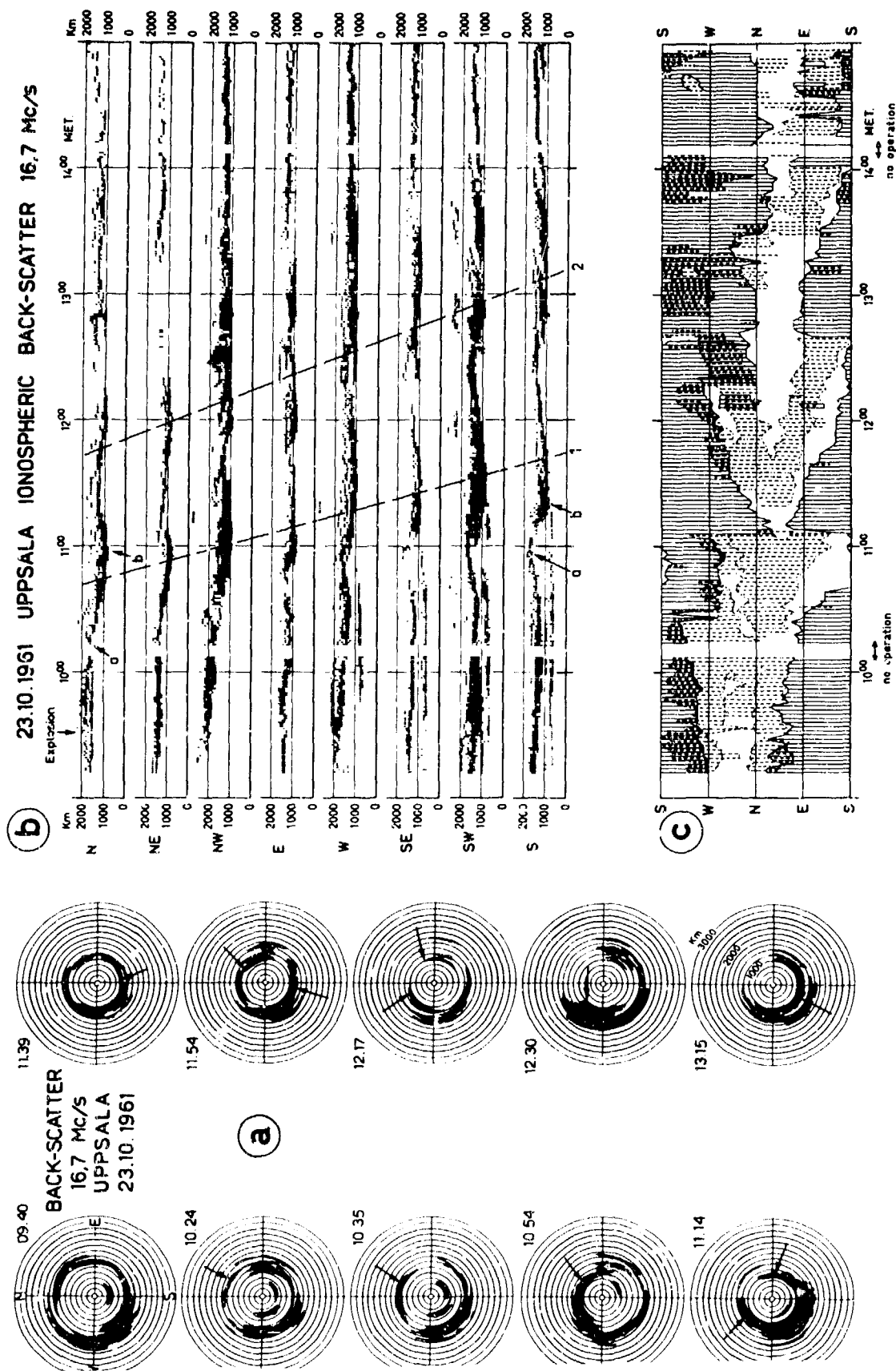


Fig. 4 (a) Backscatter records of ionospheric waves, recorded on October 30, 1961.
(b) and (c) Diagrams showing the travelling disturbances in different sectors of the PPI screen.

**LA PERTURBATION IONOSPHERIQUE DUE AUX ONDES ACOUSTIQUES ET DE
GRAVITE CREEES PAR UNE EXPLOSION NUCLEAIRE AU SOL DE 100 KT A 2000 KT
OBSERVEE ENTRE 150 ET 1000 KM DU POINT DE TIR**

par

P.Halley

Centre National d'Etudes des Télécommunications
38, 40 rue du Général Leclerc
92131, Issy-les-Moulineaux
France

480

IONOSPHERIC DISTURBANCES GENERATED BY ACOUSTIC-GRAVITY WAVES
 RESULTING FROM A 100 KT TO 2 000 KT NUCLEAR EXPLOSION ON THE GROUND,
 OBSERVED AT POINTS LOCATED BETWEEN 150 AND 1 000 KM FROM THE FIRING SITE

by

P.M. Halley

SOMMAIRE

During French nuclear experiences in Polynesia, travelling ionospheric disturbances were observed, and their impact on high frequency band propagation, essentially in the magnetic meridian plane of the firing site, was investigated.

Various recordings of Doppler effect frequency shifts, and of vertical or oblique sounding, for firing powers ranging from 100 kt to approximately 2 000 kt, are presented.

Such recordings are interpreted as exhibiting mainly two disturbance components :

- i) A rapid component which is a thermospheric wave whose instantaneous speed is approximately 720 m/s at a horizontal distance of 290 km, and then diminishes as the distance increases. This oscillation wave may appear at a very great distance, where its velocity always exceeds 400 m/s. Its frequency spectrum includes : on the one hand, an acoustic portion whose main period tends towards T_u , the upper limit imposed by atmospheric filtering ; on the other hand, an acoustic-gravity portion with a main period tending towards $T_u/\cos \theta$ and, for high energies, a period tending towards T_g , which is Brunt-Väisälä period at the point of observation.
- ii) A low component which could be a ground wave or a guided wave, whose velocity is about constant, and of the order of 305 m/s. This wave rises up to ionospheric altitudes, where it becomes superimposed on the thermospheric wave. It is essentially revealed by oblique echoes on a single and travelling flexure of the surfaces of equal density. It seems to diminish more rapidly than the thermospheric wave.

These observations are correlated with the results of the linearized theory in a non-isothermal atmosphere (numerical applications).

The impact of such a disturbance on oblique propagation and the resulting impairment of telecommunication possibilities are discussed.

An approximate representation of this disturbance in the F region, between 150 and 1 000 km around the vertical line of fire, is attempted.

**PROPAGATION NON LINEAIRE ET COUPLAGE IONOSPHERIQUE
DES ONDES ATMOSPHERIQUES ENGENDREES
PAR UNE EXPLOSION NUCLEAIRE**

par

P. Broche

Laboratoire de Physique de l'Exosphère
Faculté des Sciences de Paris,
Paris VIème
France

NON-LINEAR PROPAGATION AND IONOSPHERIC COUPLING OF ATMOSPHERIC
WAVES GENERATED BY A NUCLEAR EXPLOSION

by

P. Broche

ABSTRACT

The disturbance generated in the ionosphere by a nuclear explosion was observed at several points, using the method which consists in measuring the Doppler effect on a H.F. radio transmission. The results of such observation are described.

Two aspects of these results are stressed :

- The time delay in the occurrence of the disturbance shows that its propagation between the ground and the ionosphere is non-linear and makes it possible to define a numerical model to describe it.

- The time spectrum confirms the considerable influence of the geomagnetic field on the coupling between the motions of neutral particles and those of ionized particles.

PROPAGATION NON LINEAIRE ET COUPLAGE IONOSPHERIQUE DES ONDES
ATMOSPHERIQUES ENGENDREES PAR UNE EXPLOSION
NUCLEAIRE.

P. BROCHE (*)

Laboratoire de Physique de l'Exosphère
Faculté des Sciences de PARIS.

RESUME.

On décrit les résultats de l'observation en plusieurs points, par la méthode consistant à mesurer l'effet Doppler qui affecte une liaison radio H.F, de la perturbation engendrée dans l'ionosphère par une explosion nucléaire.

L'accent est mis sur deux aspects de ces résultats :

- le délai d'occurrence de la perturbation montre que sa propagation entre le sol et l'ionosphère est non-linéaire, et permet de définir un modèle numérique pour la décrire.
- le spectre temporel confirme l'influence importante du champ magnétique terrestre sur le couplage entre les mouvements des particules neutres et ceux des particules ionisées.

1. INTRODUCTION.

A l'occasion des campagnes d'expérimentation nucléaire françaises, on a procédé à l'étude des perturbations de l'ionosphère causées par les explosions, en utilisant la méthode qui consiste à mesurer l'effet Doppler observé sur plusieurs liaisons radio décimétriques (H.F.) bistatiques (émetteur et récepteur placés en des points différents). La Fig. 1 représente schématiquement la géographie du site d'expérience ainsi que les liaisons utilisées. Ces liaisons ont permis l'étude de la perturbation dans les régions situées au voisinage des points de réflexion sur l'ionosphère des rayons radio correspondants, c'est-à-dire à l'altitude de la couche F 2 (200-250 km) et à des distances horizontales du point d'explosion d'environ 0 (zone I), 150 (zone II), 350 km (zone III) ainsi que dans une région située à l'altitude de la couche F 1, à la verticale du point d'explosion (zone IV).

(*) Adresse actuelle : Centre Universitaire de Toulon - Chateau Saint-Michel - 83 - LA GARDE.

Il s'agit ici d'exposer les résultats spécifiquement obtenus grâce à cette diversité des points d'observation, et non d'étudier, même statistiquement, le déroulement individuel d'une perturbation.

L'effet Doppler mesuré sur une liaison donnée est essentiellement caractérisé par deux paramètres :

- son délai d'occurrence, c'est-à-dire la durée qui sépare l'instant de l'explosion du début de la manifestation de la perturbation sur la liaison. Ce temps est évidemment lié à la propagation de l'onde de choc entre la source et la région d'observation.

- sa forme, c'est-à-dire l'allure de ses variations au cours du temps, qui sont liées aux propriétés de la source et à la propagation de l'onde atmosphérique, ainsi qu'à son interaction, dans l'ionosphère, avec l'onde radioélectrique.

2. ETUDE DU DELAI D'OCCURRENCE.

En général la perturbation apparaît de façon très nette et il est possible de mesurer son temps d'apparition avec une bonne précision. Par contre, en raison de la variabilité des conditions météorologiques et ionosphériques, et de l'incertitude avec laquelle on peut définir la région perturbée, cette précision n'a en elle-même que peu de valeur lorsqu'il faut comparer entre eux les résultats relatifs à plusieurs événements différents. On peut estimer à 50% environ l'incertitude dont il faut affecter les mesures pour tenir compte de ces considérations.

Les résultats obtenus sont illustrés sur la Fig. 2, où on a représenté, en fonction de W, puissance de l'explosion, les délais d'interaction correspondant aux différentes liaisons, et sur la Fig. 3, où ces délais sont représentés, pour les différents ordres de grandeur de la puissance, en fonction de la distance de la source au point de réflexion sur l'ionosphère de la liaison radio correspondante, ce qui est une estimation de la distance parcourue par l'onde entre la source et la zone où elle est observée.

Ces résultats expérimentaux imposent deux conclusions :

a) La propagation est non linéaire.

On constate en effet que sa célérité est fonction de la puissance de la source, donc de l'amplitude de l'onde. La Fig. 3 montre en outre que cette célérité décroît au cours de la propagation (la vitesse moyenne est plus faible entre 250 et 400 km qu'elle ne l'est entre 200 et 250 km) et qu'elle a donc un comportement qualitatif analogue à celui de l'amplitude. Si c est la vitesse du son et v celle de la perturbation, l'expression la plus simple de la non-linéarité est une formule du genre

$$v = c + k A \quad (1)$$

(A = amplitude de l'onde, k constante), et, si s est une estimation de la distance parcourue, on peut écrire :

$$v = c + k' W^{1/3}/s \quad (2)$$

Une formule de ce type a déjà été proposée par BETHE (1958), et son utilisation pour des tracés de rayons acoustiques a permis à Y. ROCARD (1972) d'expliquer certains aspects de la propagation du signal acoustique à très grande distance.

b) Le calcul numérique, utilisant la formule (2), montre qu'elle conduit, dans l'interprétation de nos résultats expérimentaux, à des délais d'occurrence trop courts. La Fig. 4, où sont représentés, en fonction de W, les temps d'arrivée de la perturbation dans la région située à la verticale de la source, à environ 160 km d'altitude (zone IV), ainsi que le temps que l'on déduit de (2), illustre ce comportement.

On n'obtient un bon accord qu'en introduisant une absorption de comportement exponentiel en fonction du trajet parcouru, et dont il faut chercher l'origine dans l'action de la viscosité

atmosphérique. A partir d'une certaine altitude, variable avec la fréquence de l'onde, celle-ci introduit une diminution de l'amplitude qui, d'après (1), se traduit également par une diminution de vitesse de propagation, celle-ci étant alors donnée par une formule du type :

$$v = c + k'' W^{1/3} e^{-Bs/s} \quad (3)$$

Les résultats d'un calcul numérique utilisant (3) sont également reproduits sur la Fig. 4 (courbe b) et on constate leur bon accord avec les résultats expérimentaux.

3. ETUDE DE LA FORME DE LA PERTURBATION.

L'étude de l'effet Doppler mesuré, Δf , en fonction du temps, ou, ce qui est équivalent, du spectre temporel de Δf , montre des variations systématiques en fonction de la puissance de la source, et en fonction de la région d'observation.

Ce dernier aspect, le seul à nous intéresser ici, peut avoir deux causes :

- la dispersion et l'absorption sélective de l'atmosphère entre la source et la région d'observation. Il s'agit en première approximation d'un effet isotrope, c'est-à-dire indépendant de l'azimut de la région d'observation par rapport à la source - ne dépendant que de la distance.

- le couplage entre l'ionosphère et l'onde neutre est différent suivant l'orientation relative du champ magnétique terrestre et de la normale à l'onde, c'est un effet essentiellement anisotrope, dépendant beaucoup de la fréquence.

a) La propagation d'une onde neutre à partir d'une source explosive ponctuelle a déjà fait l'objet de nombreux travaux, dans les hypothèses très réalistes (atmosphère stratifiée, en présence de vents). L'aspect le plus important des résultats est que l'onde observée en un point à l'altitude z et à la distance R de la source ne contient que des fréquences supérieures à une limite $\omega_c = z/R \omega_B$ (ω_B = fréquence correspondant à la période de Brunt-Väisälä). Toutes choses étant égales par ailleurs, ceci signifie que la perturbation contient d'autant plus de basses fréquences que la zone d'observation est plus éloignée de la source, c'est, à titre d'exemple la Fig. 5 représente le spectre de la perturbation neutre à la verticale, et à une distance de 350 km du point d'explosion.

La viscosité atmosphérique, dont il a été déjà question au § 2 renforce cette tendance, dans la mesure où elle provoque surtout l'absorption des hautes fréquences (le coefficient d'absorption varie comme f^2), spécialement des périodes inférieures à quelques minutes.

b) Le couplage entre les neutres et les composants ionisés a également fait l'objet d'un certain nombre de travaux, du moins dans le cas d'une onde de gravité libre, c'est-à-dire pour laquelle on peut arbitrairement se fixer le vecteur d'onde \vec{k} . Dans le problème qui nous intéresse, la référence à une source ponctuelle est importante, et il en a été tenu compte dans les calculs que nous avons développés, le modèle étant le suivant :

L'atmosphère est isotherme, caractérisée par la valeur de la célérité du son c , et par la période de coupure acoustique T_a et la période de Brunt T_B . L'interaction a lieu à l'altitude de la couche F 2, de sorte que la vitesse v des ions est la projection sur la direction du champ magnétique de la vitesse u des neutres : $v = (u \cdot b) b/b^2$.

La propagation d'une onde harmonique de pulsation ω , à partir d'une source ponctuelle, est décrite par la fonction de Green $G(z, r, \omega)$ (Row, 1966) qui est donnée par :

$$G(z, r, \omega) = \alpha \frac{h}{\rho} e^{ik\rho}$$

avec

$$\rho = R(1 - \omega_c^2/\omega^2)^{1/2} \quad k = \frac{\omega}{c} \left(\frac{\omega^2 - \omega_A^2}{\omega^2 - \omega_B^2} \right)^{1/2} \quad h = 1 - \omega_B^2/\omega^2$$

la vitesse des neutres a une composante radiale u_r et une composante verticale u_z données par :

$$u_r = -\frac{1}{j\omega} \frac{\partial G}{\partial r} \quad u_z = -\frac{1}{j\omega} \left(\frac{\partial G}{\partial z} - AG \right)$$

avec $A = (\gamma/2 - 1) g/c^2$

La perturbation de densité électronique est, au premier ordre, la solution de l'équation de conservation linéarisée

$$\frac{\partial N}{\partial t} + \text{div} (N_0 \vec{v}) = 0$$

N_0 étant la densité non perturbée. Introduisant le paramètre $a = \left(\frac{1}{2H} + \frac{dN_0}{dz N_0} \right)^{-1}$, qui caractérise la hauteur d'échelle globale de la couche ionisée, cette équation, pour des mouvements harmoniques, donne :

$$|\delta N| = \frac{N_0}{\omega} \cdot \left| v_z/a + \vec{\nabla} \cdot \vec{v} \right| \quad (5)$$

On a effectué un calcul numérique utilisant ces diverses expressions, dont les résultats sont reproduits sur les Fig. 6 et 7 qui représentent, en fonction de l'azimut magnétique, la variation de $\delta N/N_0$ pour différentes périodes T ($T < T_a$ ou $T_b < T < T_c$). Le résultat important est que l'anisotropie très forte du couplage, qui est prévisible d'un simple point de vue géométrique, dépend considérablement de la période : on peut retrouver les faits essentiels de ce comportement à partir des résultats connus (HINES 1960) sur les ondes acoustico-gravitationnelles planes, en observant que l'onde qui se manifeste en M, la source étant en O, est celle dont la vitesse de groupe est dans la direction de OM (Fig. 8)

(i) lorsque la période est faible, il y a peu de dispersion, et l'onde est longitudinale : \vec{k} , \vec{u} et OM sont parallèles. Le terme essentiel dans (5) est le terme de divergence, de sorte que $\delta N/N_0$ se comporte comme :

$$\vec{k} \cdot (\vec{b} (\vec{u} \cdot \vec{b})) \quad \text{c'est-à-dire} \quad (\vec{OM} \cdot \vec{b})^2$$

(ii) lorsque la période est voisine de la valeur maxima observable en M, l'onde est transversale, et, la vitesse de groupe étant perpendiculaire à la vitesse de phase, \vec{u} et OM sont parallèles entre eux et perpendiculaires à \vec{k} . Le terme prépondérant est encore le terme de divergence, de sorte que $\delta N/N_0$ se comporte comme :

$$\vec{k} \cdot (\vec{b} (\vec{u} \cdot \vec{b})) \quad \text{c'est-à-dire} \quad (\vec{OM} \cdot \vec{b}) (\vec{k} \cdot \vec{b})$$

(iii) lorsque la période est voisine de la période de coupure acoustique, c'est le premier terme de (5) qui est le plus important. Il traduit l'influence de la stratification du milieu (le flux de particules ionisées entraînées est variable en fonction de l'altitude) et il se comporte de façon isotrope.

La dépendance importante de l'anisotropie en fonction de la période entraîne une modification de spectre de $\delta N/N_0$ suivant l'azimut magnétique du point d'observation. La Fig. 9 montre le comportement de l'excès relatif de densité électronique, rapporté à l'excès relatif de densité neutre $\delta\rho/\rho_0$, en fonction de la fréquence, pour différents azimuts, et pour une source explosive parfaite (spectre uniforme).

Deux aspects des résultats sont importants :

- Alors que les hautes fréquences (acoustiques), sont toujours affaiblies par rapport à l'amplitude de l'onde neutre, les basses fréquences (ondes de gravité), sont amplifiées,

essentiellement les périodes voisines de T_B (période de Brunt) et T_C (période maximum observable en M).

- Si l'on compare les spectres à la verticale de la source, et dans la région d'observation correspondant à une autre liaison utilisée («3ne III, D = 350 km, azimut = 60°»), on constate que la diminution de l'importance des hautes fréquences dans le spectre va dans le sens des observations expérimentales (Fig. 10).

4. CONCLUSION.

L'observation de l'onde acoustico-gravitationnelle engendrée par une source explosive et propagée dans l'ionosphère, effectuée simultanément en plusieurs points par la mesure de l'effet Doppler en H.F., permet de mettre en évidence plusieurs phénomènes physiques intéressants :

- la propagation des signaux puissants est non-linéaire, c'est-à-dire qu'elle s'effectue avec une célérité dépendant de l'amplitude.

- l'absorption, par viscosité, a, à des altitudes supérieures à 100 km environ, un rôle important sur l'évolution de l'amplitude de l'onde, donc sur sa célérité.

- la variabilité de l'allure de l'évolution temporelle de l'effet Doppler mesuré en des points différents s'explique en partie par les caractéristiques de la propagation d'une onde acoustico-gravitationnelle entre une source ponctuelle et un point quelconque, mais, certains effets anisotropes sont liés au couplage entre l'onde atmosphérique, qui affecte principalement les particules neutres, et l'ionosphère. L'effet de ce couplage est de réduire systématiquement la part des hautes fréquences acoustiques dans le spectre des variations relatives de densité électronique.

REMERCIEMENTS.

Ce travail a été accompli dans le cadre d'une Convention de la Direction des Recherches et Moyens d'Essais, et n'a pu être réalisé que grâce à l'aide du Laboratoire de Détection et de Géophysique du Commissariat à l'Energie Atomique.

REFERENCES

- | | | |
|------------|--------|---|
| BETHE H. | (1958) | Blast Waves. Los Alamos. |
| HINES C.O. | (1960) | Internal atmospheric gravity waves at ionospheric heights. Canad. Journal of Physics <u>38</u> , 1441. |
| ROCARD Y. | (1972) | Un nouveau mécanisme pour la propagation lointaine du son dans l'atmosphère. AGARD, WIESBADEN. |
| ROW R.V. | (1966) | Acoustic gravity waves in the upper atmosphere due to a nuclear detonation and earthquake J. of geophysical Research, <u>72</u> n° 5, 1599. |

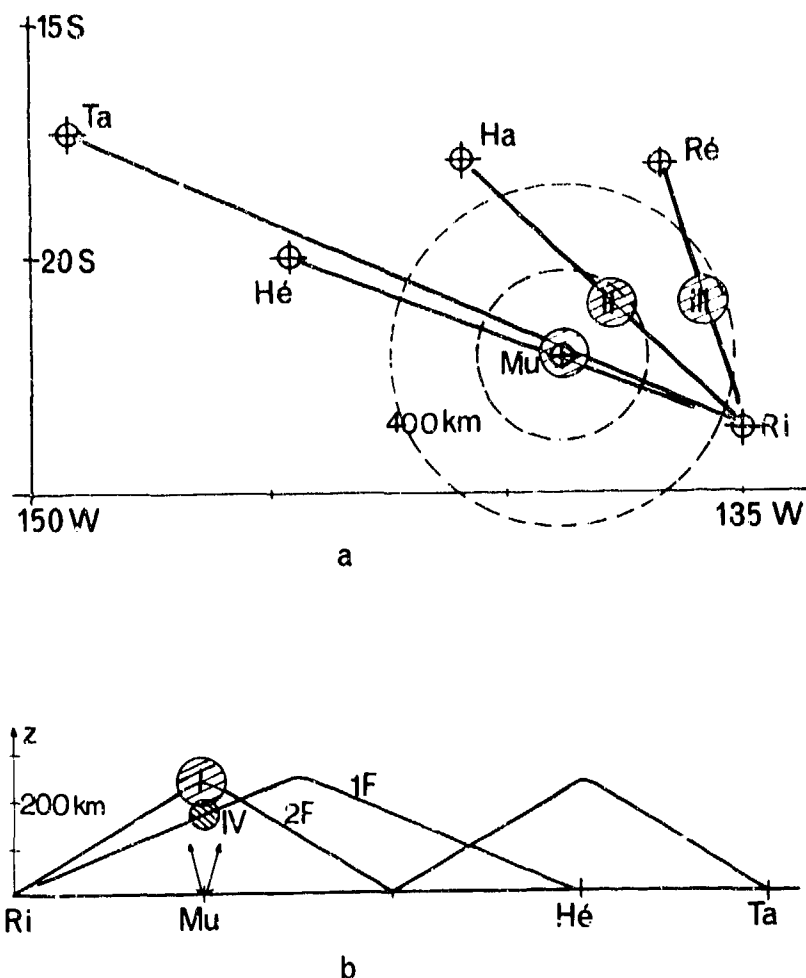


Figure 1. Représentation schématique du site d'expérience, des liaisons radio utilisées, et des zones d'observation de la perturbation ionosphérique (repérées par I, II, III, IV).

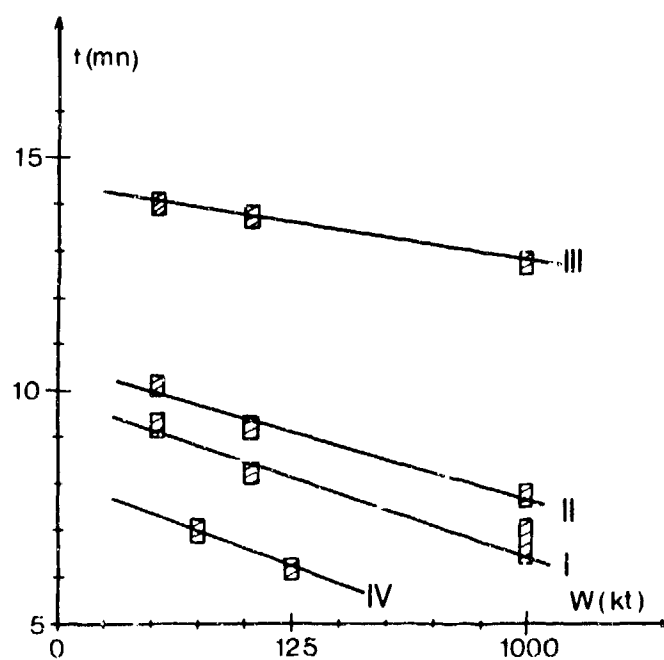


Figure 2. Variations du délai d'occurrence de la perturbation, dans les zones I, II, III, IV, en fonction de la puissance de la source.

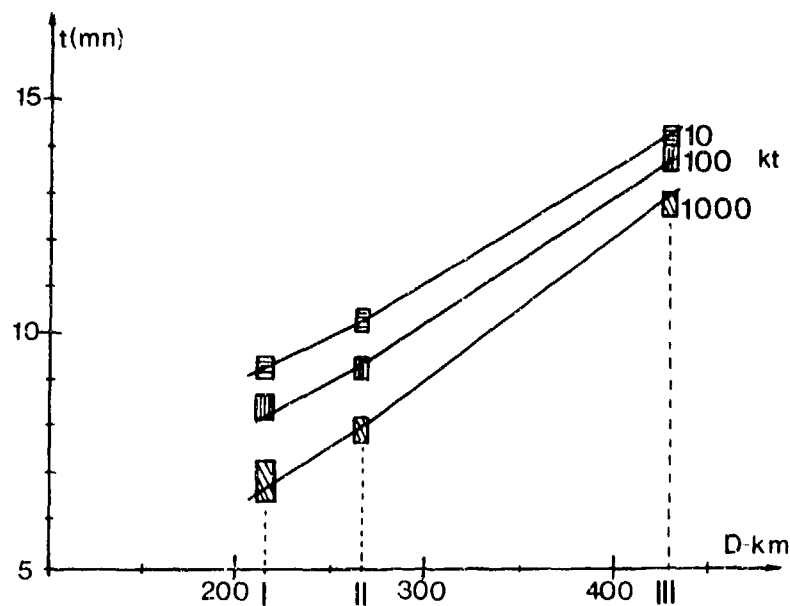


Figure 3. Variations du délai d'occurrence de la perturbation pour différentes puissances en fonction de la distance de la source à la zone d'observation.

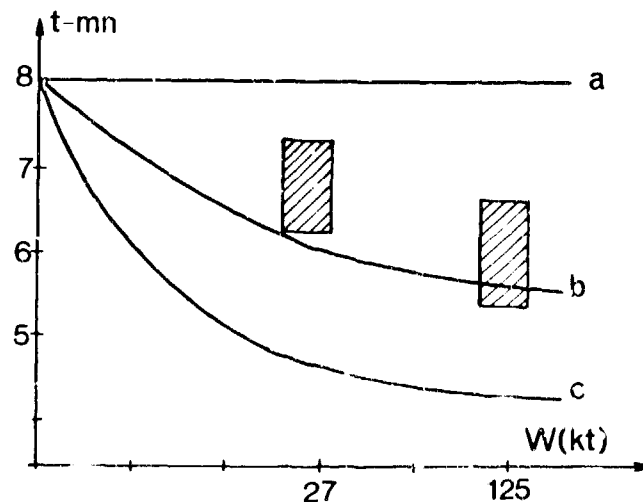


Figure 4. Délai d'occurrence de la région 4.

- (a) Calcul dans l'hypothèse d'une propagation linéaire
- (c) Calcul dans l'hypothèse d'une propagation non-linéaire, sans absorption
- (b) Calcul dans l'hypothèse d'une propagation non-linéaire, avec absorption
- ▨ Résultats expérimentaux.

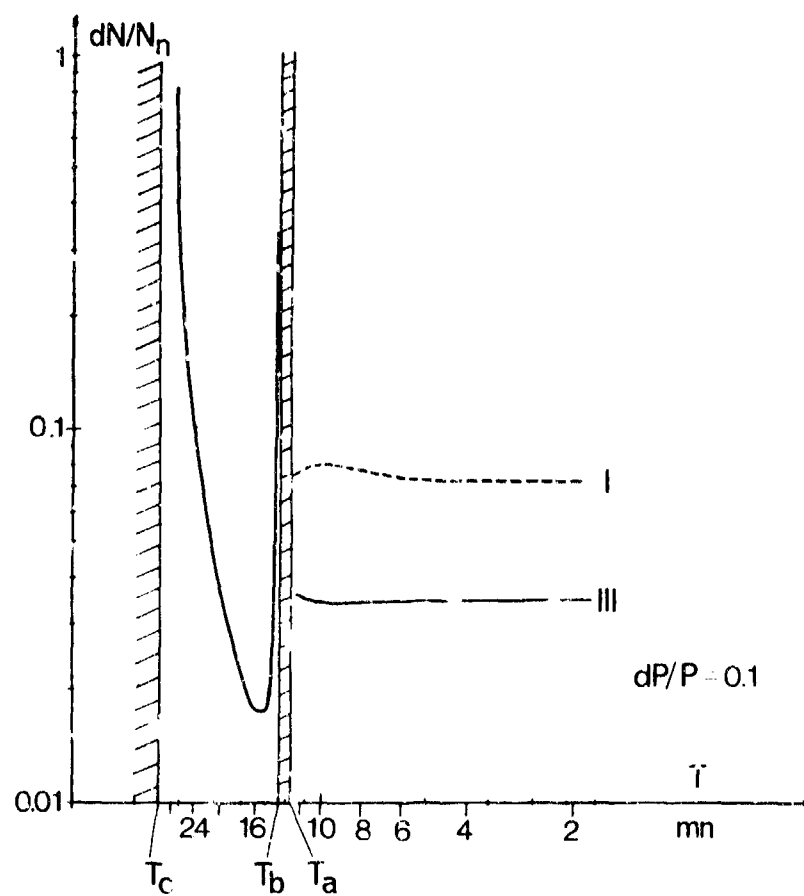
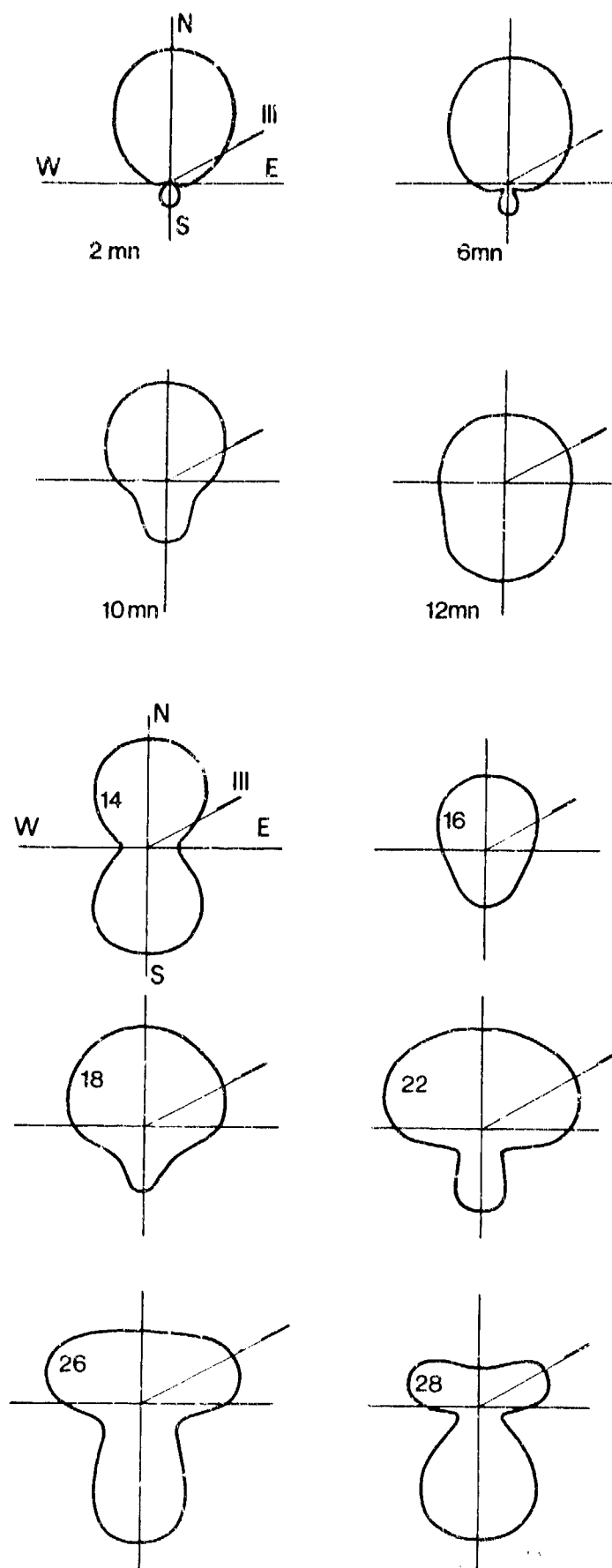


Figure 5.

Spectre de la perturbation relative de densité du gaz neutre, dans les zones I et III. (source explosive parfaite).



Figures 6 et 7.

Variations de la perturbation relative de densité électronique en fonction de l'azimut de la région d'observation, pour une distance à la source de 350 km environ, et pour différentes valeurs de la période. On a représenté également sur ces figures la direction de la zone III.

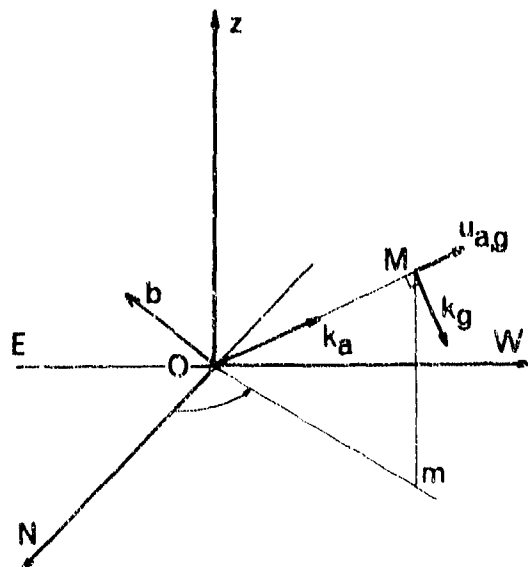


Figure 8.

Définitions géométriques

- k_a et k_g représentent la direction des vecteurs d'ondes de l'onde acoustique ($\omega + \omega$) et de gravité ($\omega + \omega_c$) issue de O et propagée en M
- u_a et u_g représentent la direction de la vitesse des neutres dans chacune de ces deux ondes
- b représente le champ magnétique terrestre.

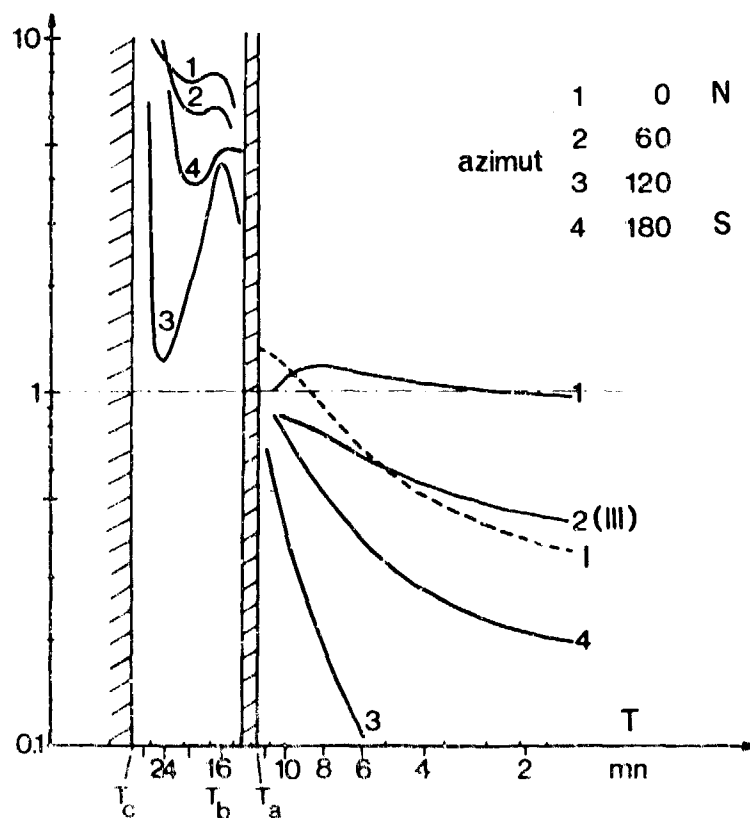


Figure 9.

Spectres de la perturbation relative de densité électronique, rapportée à la perturbation relative de densité du gaz neutre, pour différents azimuts, à la distance de 350 km de la source.

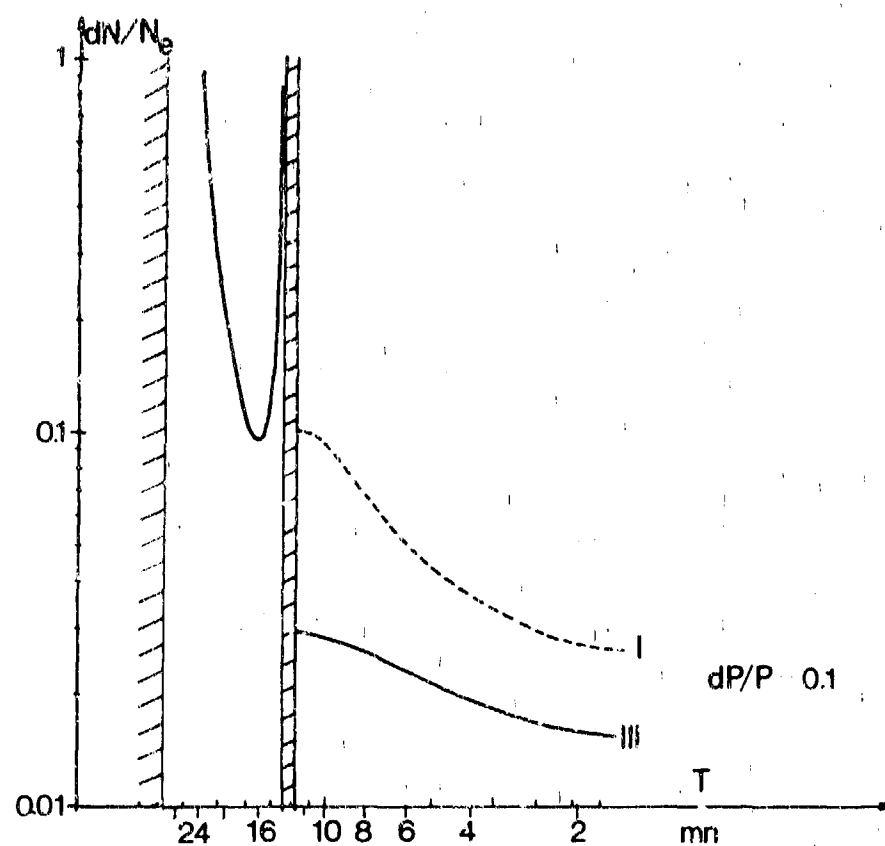


Figure 10.

Spectres de la perturbation relative de densité électronique dans les zones I et III.

NUCLEAR WEAPON EFFECTS ON THE IONOSPHERE
(F-REGION DISTURBANCES)

by

J.B.Lomax and D.L.Nielson

Stanford Research Institute
333 Ravenswood Avenue
Menlo Park, California 94025
USA

LES EFFETS DES ARMES NUCLEAIRES SUR L'IONOSPHERE (PERTURBATIONS DE LA REGION F)

par

J.B. Lomax, and D.L. Nielson

SOMMAIRE

Une explosion nucléaire en produisant à des altitudes ionosphériques est suivie d'effets multiples dans l'ionosphère et, par conséquent, sur les communications en haute fréquence. Au cours de l'été et de l'automne 1962, on a procédé au milieu du Pacifique, près de l'île Johnston, à une série d'explosions nucléaires de nuit (la série "Fish Bowl"). Dans le cadre des expériences effectuées à cette occasion, l'Institut de Recherches de Stanford a établi un réseau de sondeurs à incidence oblique, dont les parcours d'un seul saut apparaissent sur la figure 1. En tout, quatre émetteurs et huit récepteurs furent montés en multiplex pour créer un réseau de 29 parcours. Le "National Bureau of Standards" (Bureau National des Poids et Mesures), ainsi que l'Agence de l'Armée de Terre US pour la Propagation des Ondes Radio, et le Laboratoire de Recherches de l'Armée de l'Air, de Cambridge, utilisèrent dans la même région des sondeurs à incidence verticale. On verra sur la figure 2 les emplacements des sites choisis, ainsi que ceux de certaines stations internationales de sondage. En ajoutant les informations fournies par ces mesures séparées, on peut obtenir une représentation assez complète du comportement général de l'ionosphère après chaque explosion.

Les observations effectuées à partir de chacun des sites permirent de retracer l'historique de la densité électronique maximale de l'ionosphère en des endroits déterminés. L'ensemble de ces résultats a servi à établir des cartes de fréquence critique qui indiquent la variation synoptique, en fonction du temps, de la densité électronique maximale de la couche F. Ce paramètre est d'une importance extrême, tant pour l'opérateur chargé d'établir des liaisons H.F. que pour le chercheur scientifique.

Le film sonore en couleurs de 16 mm qui illustre cet exposé présente sur la carte les courbes d'égale fréquence critique montrant les variations de la densité électronique maximale de la couche F en fonction du temps et de l'espace, à la suite des trois essais nucléaires à haute altitude de l'opération "Fish Bowl". Ces cartes comprennent la région s'étendant entre 30° de latitude Nord et Sud de part et d'autre de l'équateur magnétique, et 35° de longitude Est et Ouest de part et d'autre de l'île Johnston. Les séquences commencent 60 minutes avant l'explosion et se poursuivent, par incréments de 1 à 4 minutes, jusqu'à 60 minutes après pour les essais "Star Fish" et "Check Mate", et cinq heures après pour l'essai "King Fish". Le principal effet qui se trouve illustré est la propagation radiale des ondes ionosphériques à partir du point de détonation. Le film étudie et illustre également la théorie des ondes hydrodynamiques, et présente les caractéristiques observées des ondes ionosphériques. Sa projection dure 30 minutes.

Les figures 3 à 27 représentent un choix de cartes de fréquence critique, extrait du film.

Référence : Lomax, J.B. et Nielson, D.L., 1968 "Observations of acoustic-gravity wave effects showing geomagnetic field dependence" ("Observation des effets des ondes acoustiques et de gravité montrant leur dépendance à l'égard du champ magnétique terrestre"), JATP, Vol. 30, pp. 1033-1050.

Les recherches dont il est rendu compte ici furent effectuées sous l'égide de l'Agence Nucléaire pour la Défense, dans le cadre de la sous-traitance 938/07.041, sous contrat DA 36-0395C-87197 avec le US Army Electronics Command.

NUCLEAR WEAPON EFFECTS ON THE IONOSPHERE

(F-REGION DISTURBANCES)

A 16-mm Sound/Color Movie*

J. B. Lomax and D. L. Nielson
Stanford Research Institute
333 Ravenswood Avenue
Menlo Park, California 94025
USA

SUMMARY

The detonation of a nuclear burst at ionospheric heights causes a multiplicity of effects in the ionosphere and therefore on HF communications. A series of nighttime shots, the Fish Bowl Series, was conducted in the summer and fall of 1962 near Johnston Island in the mid-Pacific. As part of the instrumentation for this series, SRI fielded a network of oblique-incidence sounders, the one-hop paths of which are shown in Figure 1. In all, four transmitters and eight receivers were time-multiplexed to create a network of 29 paths. The National Bureau of Standards operated vertical-incidence sounders in the same area, as did the U. S. Army Radio Propagation Agency and the Air Force Cambridge Research Laboratory. The locations of these sites, as well as some of the international sounder stations, are shown in Figure 2. By combining the information from these separate measurements, a fairly comprehensive picture of the gross behavior of the ionosphere after each shot can be obtained.

From each site came a time history of the maximum electron density of the ionosphere at specific locations. These were combined into critical-frequency maps which show, as a function of time, the synoptic variation of maximum F-layer electron density. This parameter is extremely important to the HF communicator as well as to the scientific investigator.

Sequences of contour maps of critical frequency are presented in this 16-mm sound/color movie, showing the variation of the F-layer maximum electron density as a function of time and space following the three-high-altitude nuclear tests in Operation Fish Bowl. The maps encompass the region 30° north and south from the magnetic equator and 35° east and west from Johnston Island. The sequences of maps start 60 minutes before the explosion and proceed, in increments of 1 to 4 minutes, to 60 minutes after the event for Star Fish and Check Mate and to five (5) hours after King Fish. The principal effect illustrated is the propagation of the ionospheric waves radially outward from the point of detonation. The theory of hydrodynamical waves is also discussed and illustrated in the film, and the observed characteristics of ionospheric waves are presented. The film has a showing time of 30 minutes.

Selected maps of critical frequency from the film are shown in Figures 3 through 27.

Reference: Lomax, J. B. and Nielson, D. L., 1968, "Observation of acoustic-gravity wave effects showing geomagnetic field dependence", JATP, Vol. 30, pp 1033-1050.

* The research reported here was sponsored by the Defense Nuclear Agency under NWER Subtask 93B/07.C41 on Contract DA 36-03980-87197 with the U. S. Army Electronics Command.

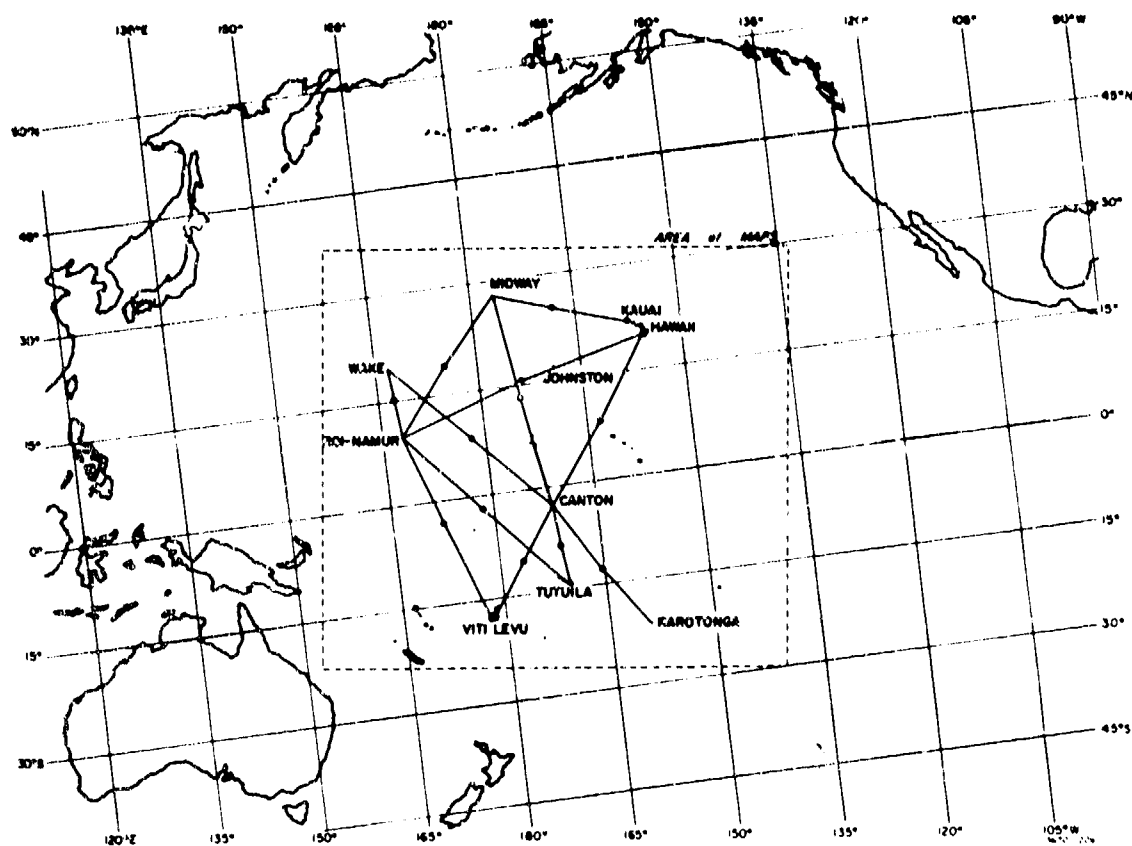


FIG. 1 MAP OF OBLIQUE IONOSONDE PATHS AND MIDPOINTS

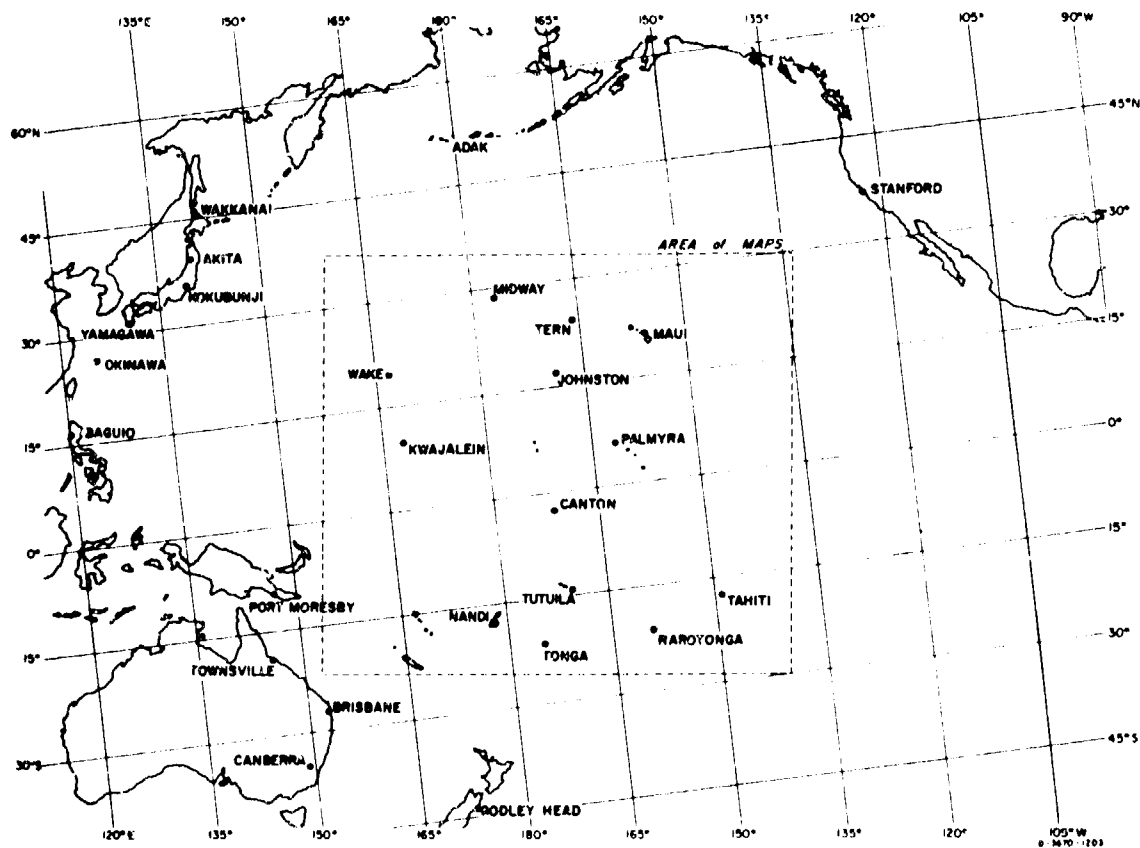


FIG. 2 MAP OF VERTICAL IONOSONDE STATIONS

Figure 3
Star Fish T - 1 min
0859 GMT, 9 July 1962

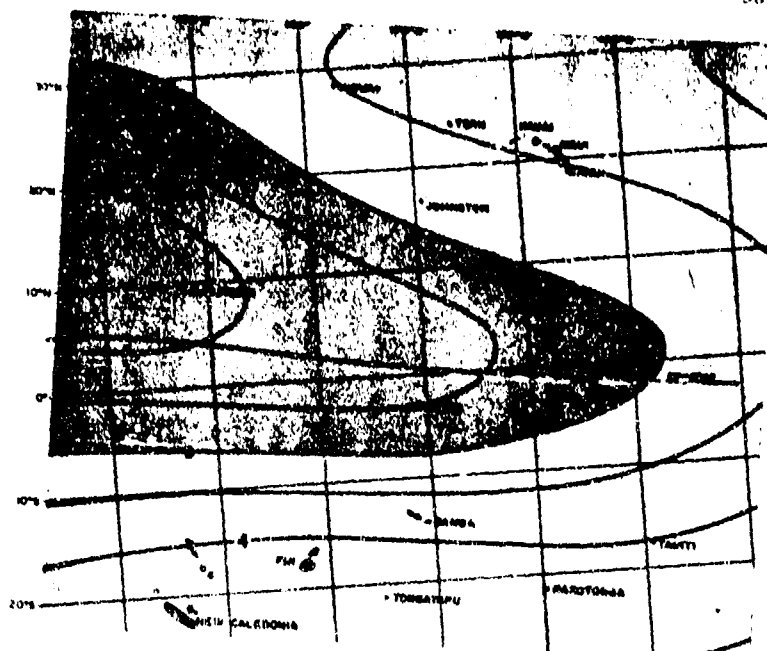


Figure 4
Star Fish T + 5 min
0905 GMT, 9 July 1962

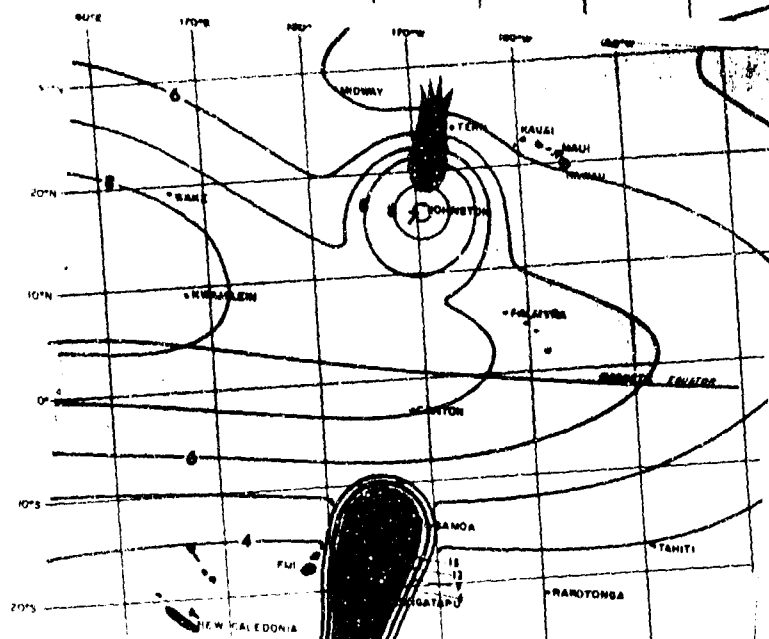
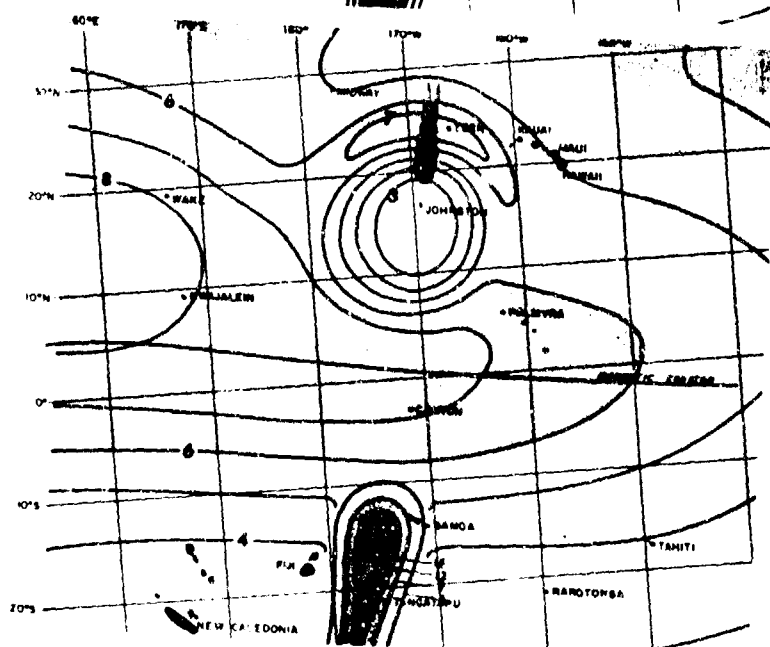


Figure 5
Star Fish T + 10 min
0910 GMT, 9 July 1962



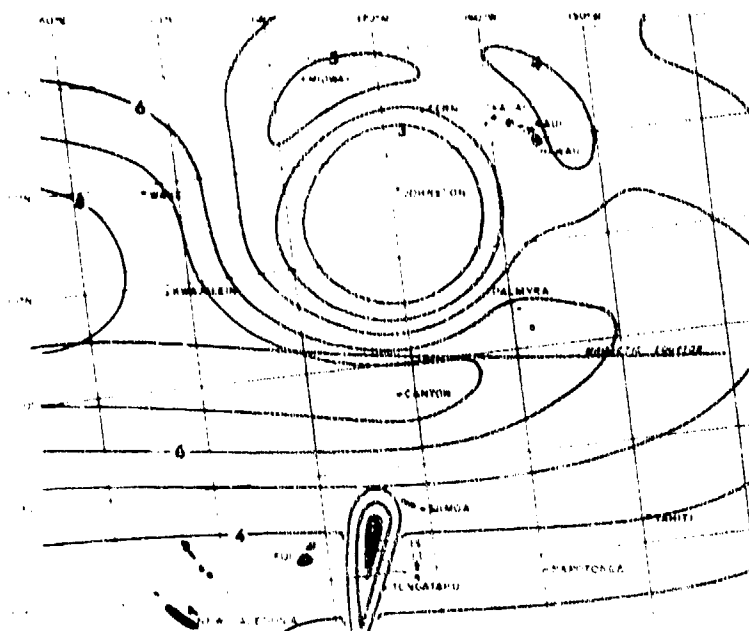


Figure 6
Star Fish T + 20 min
0920 GMT, 9 July 1962

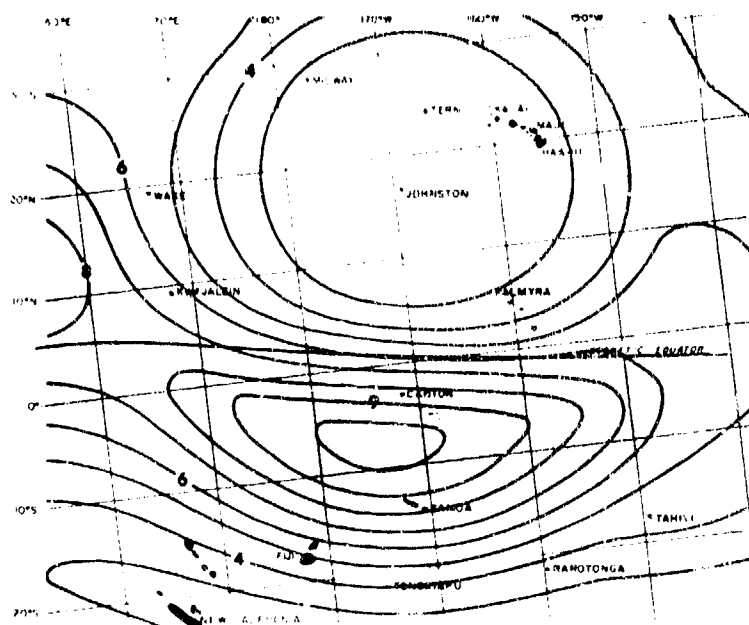


Figure 7
Star Fish T + 40 min
0940 GMT, 9 July 1962

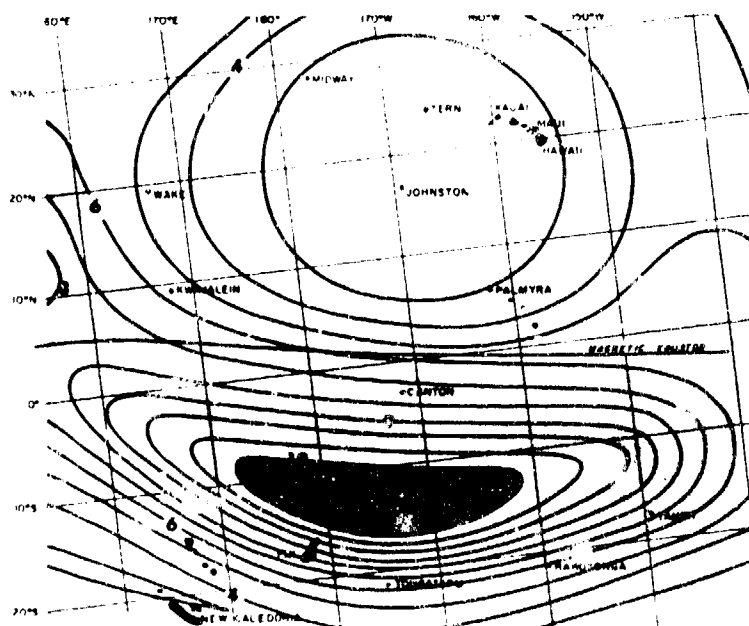


Figure 8
Star Fish T + 60 min
1000 GMT, 9 July 1962

Figure 8
Check Mate T - 1 min
0829 GMT, 20 October 1962

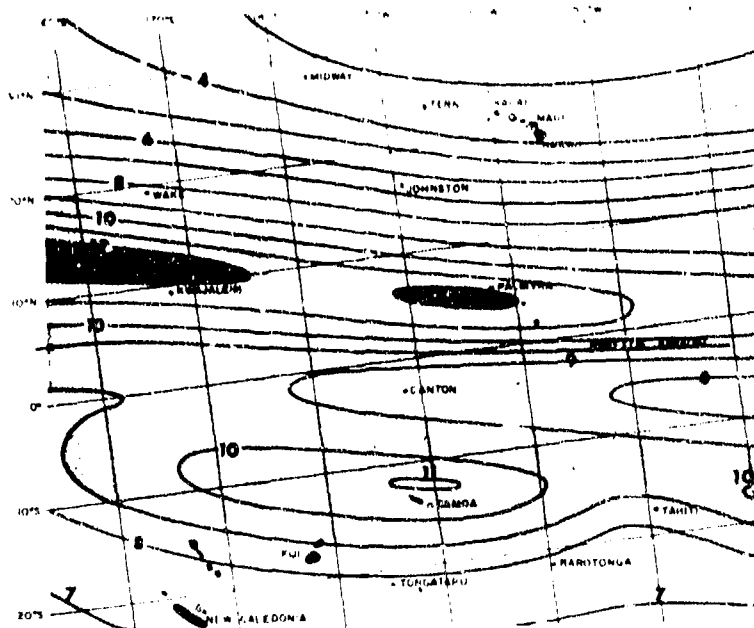


Figure 10
Check Mate T + 5 min
0835, 20 October 1962

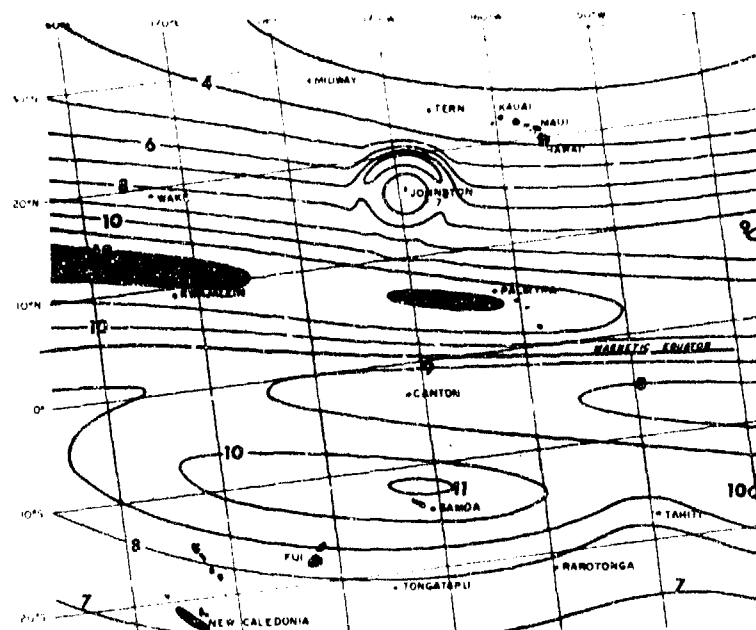
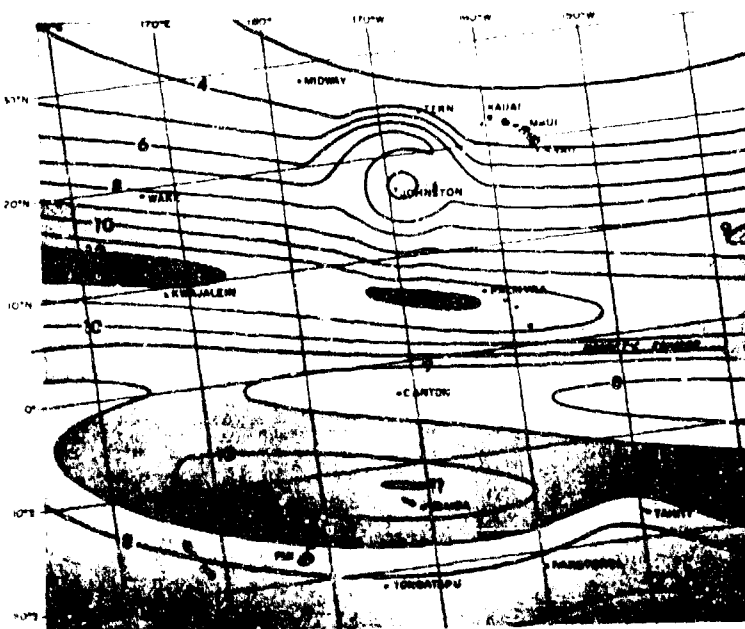


Figure 11
Check Mate T + 10 min
0840, 20 October 1962



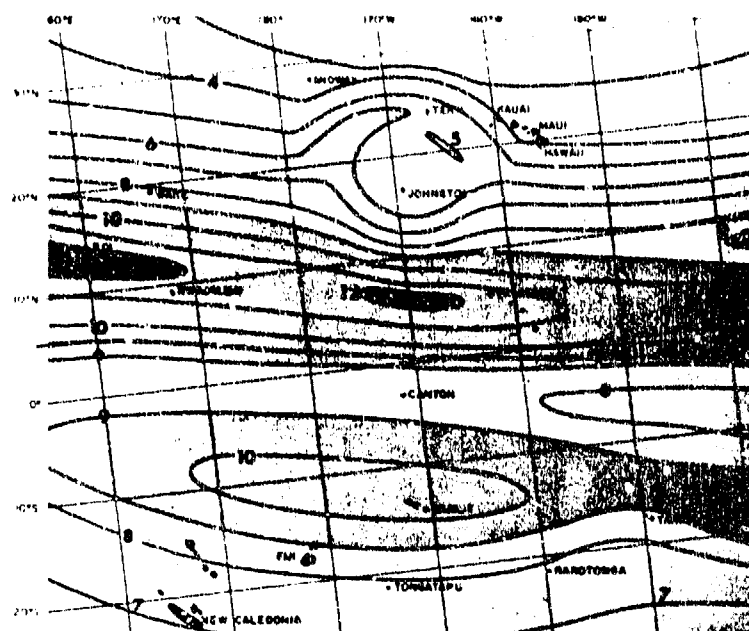


Figure 12

Check Mate T + 20 min

0850 GMT, 30 October 1962

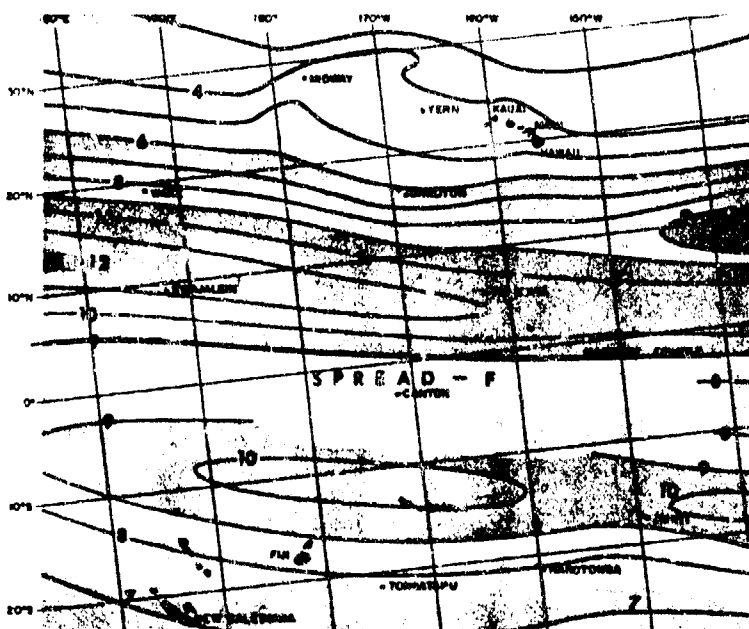


Figure 13

Check Mate T + 40 min

0910 GMT, 20 October 1962

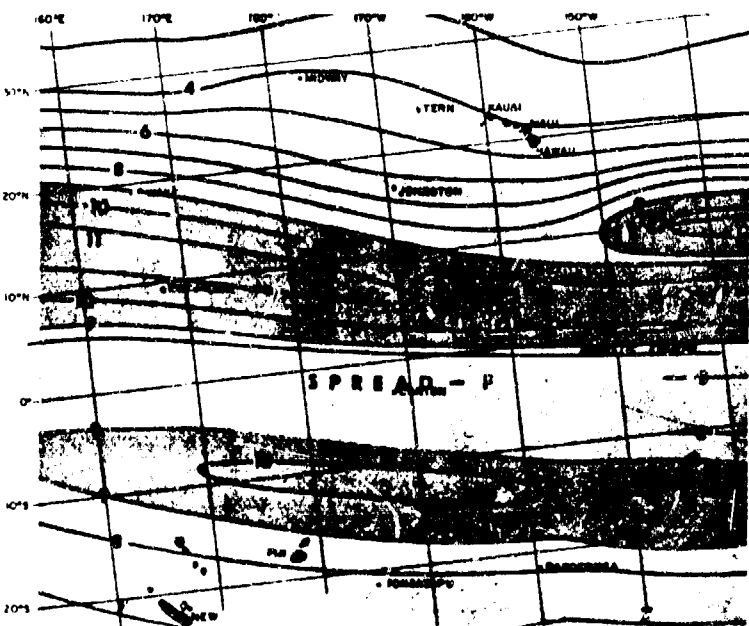


Figure 14

Check Mate T + 60 min

0930 GMT, 20 October 1962

Figure 15
King Fish T - 1 min
1209 GMT, 1 November 1962

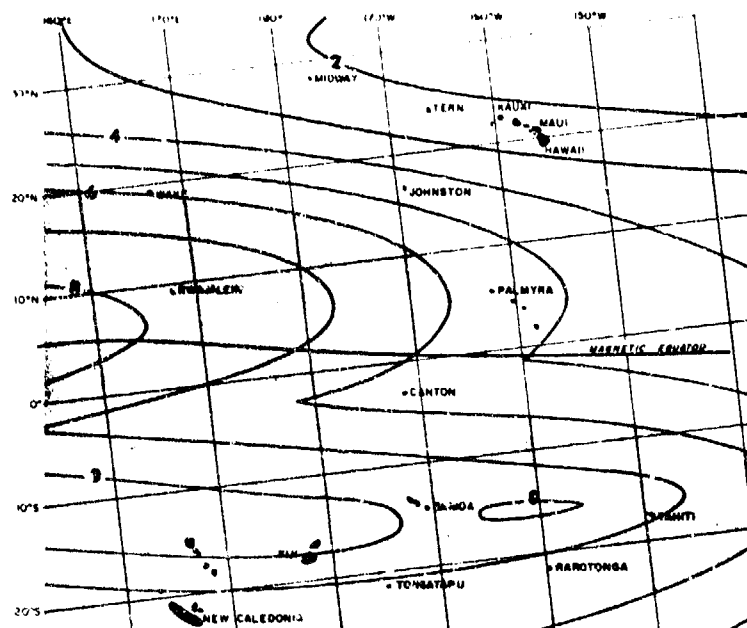


Figure 16
King Fish T + 5 min
1215 GMT, 1 November 1962

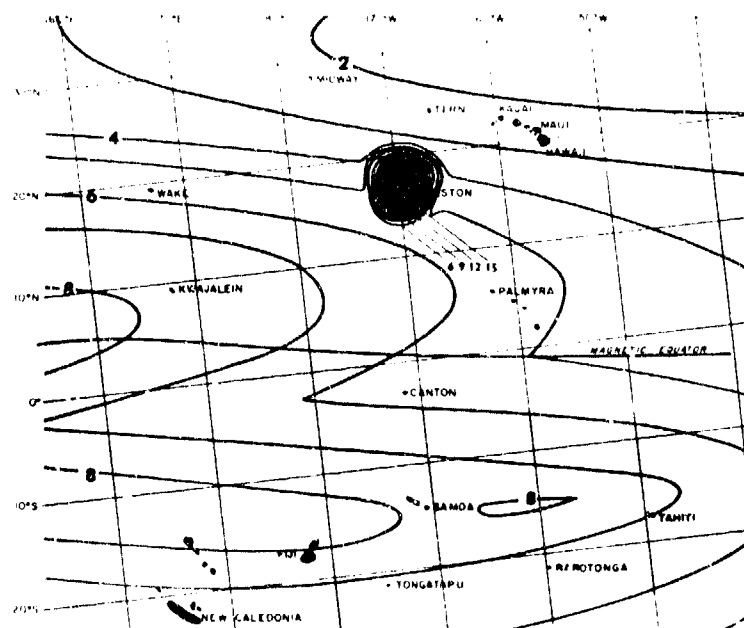
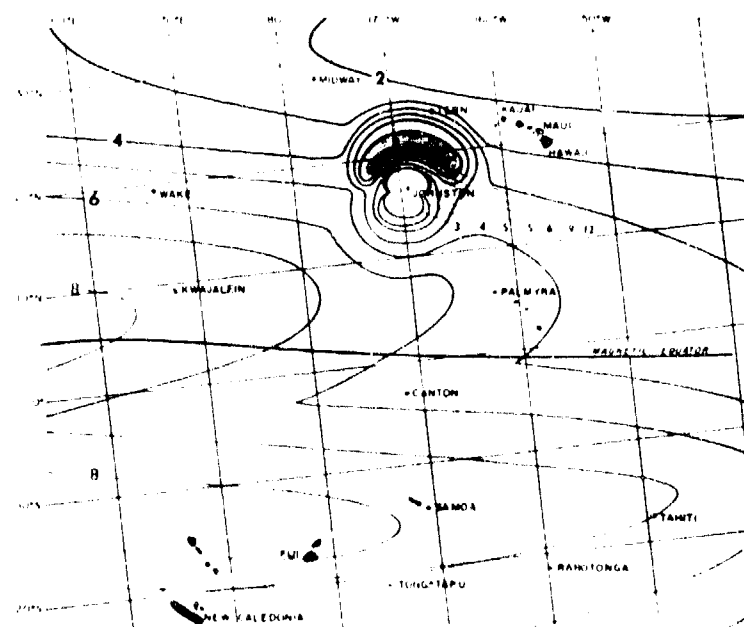


Figure 17
King Fish T + 10 min
1220 GMT, 1 November 1962



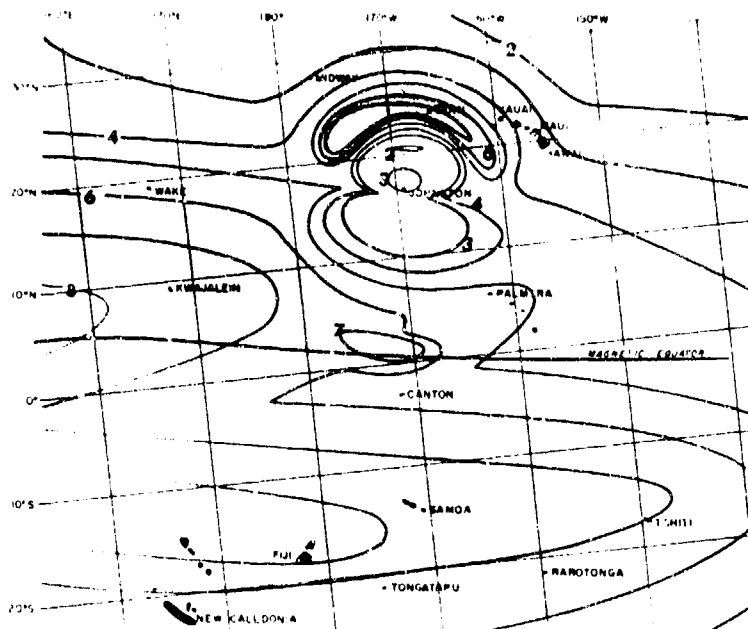


Figure 18
King Fish T + 20 min
1230 GMT, 1 November 1962

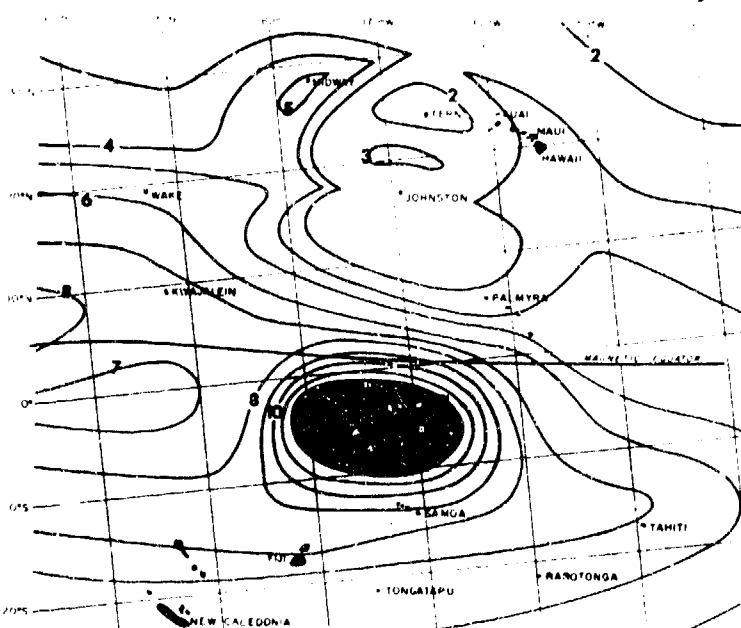


Figure 19
King Fish T + 40 min
1250 GMT, 1 November 1962

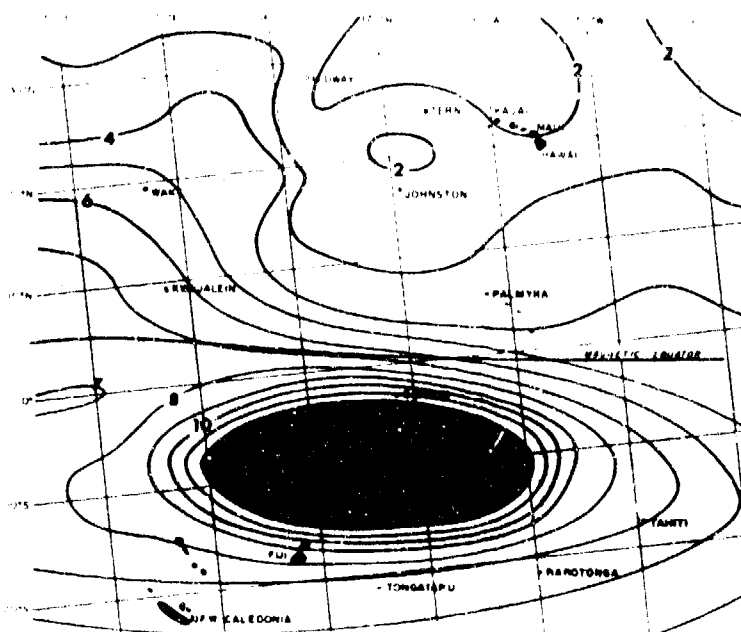


Figure 20
King Fish T + 60 min
1310 GMT, 1 November 1962

Figure 21
King Fish T + 80 min
1330 GMT, 1 November 1962

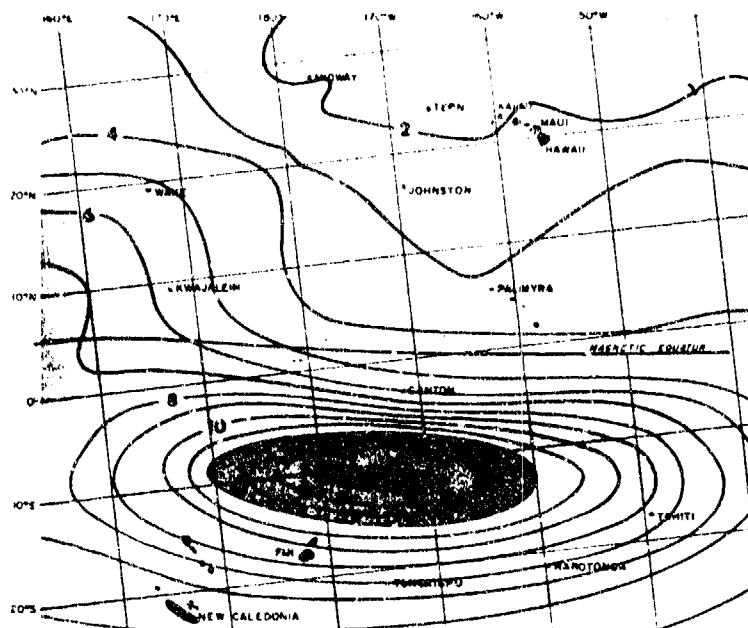


Figure 22
King Fish T + 100 min
1350 GMT, 1 November 1962

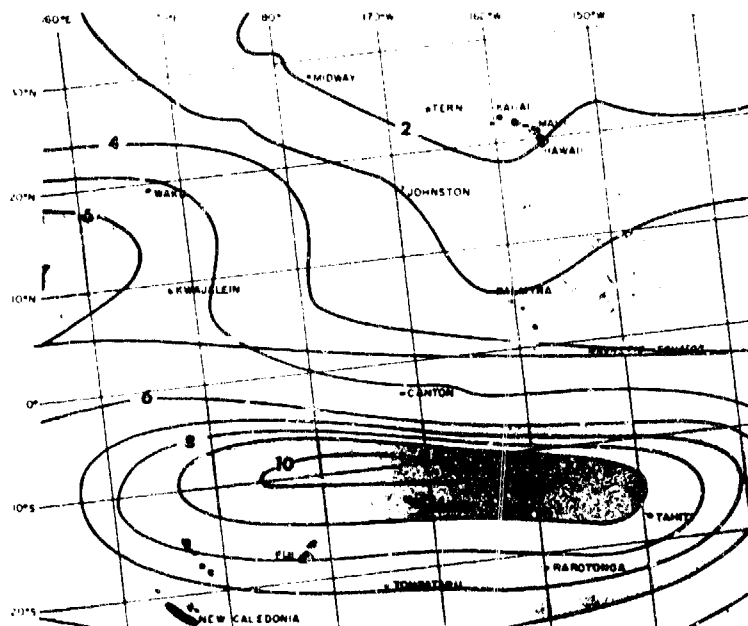
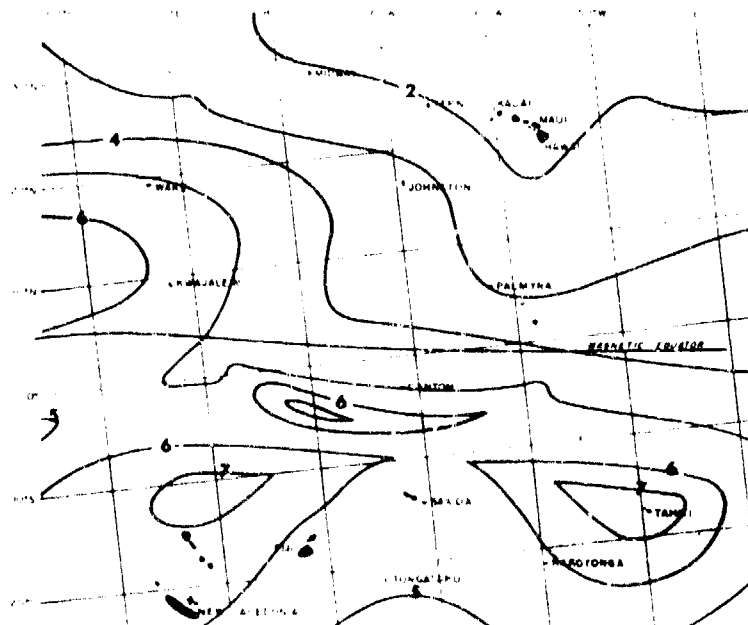


Figure 23
King Fish T + 120 min
1410 GMT, 1 November 1962



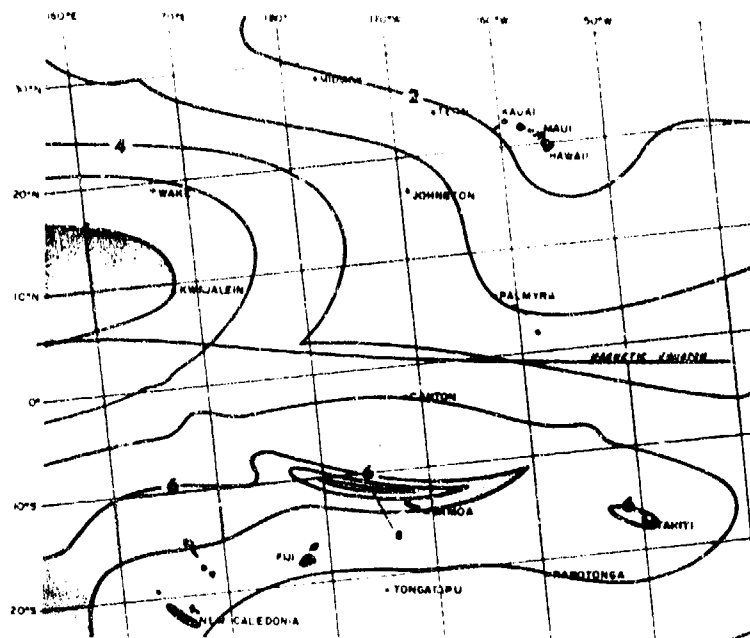


Figure 24
King Fish T + 140 min
1430 GMT, 1 November 1962

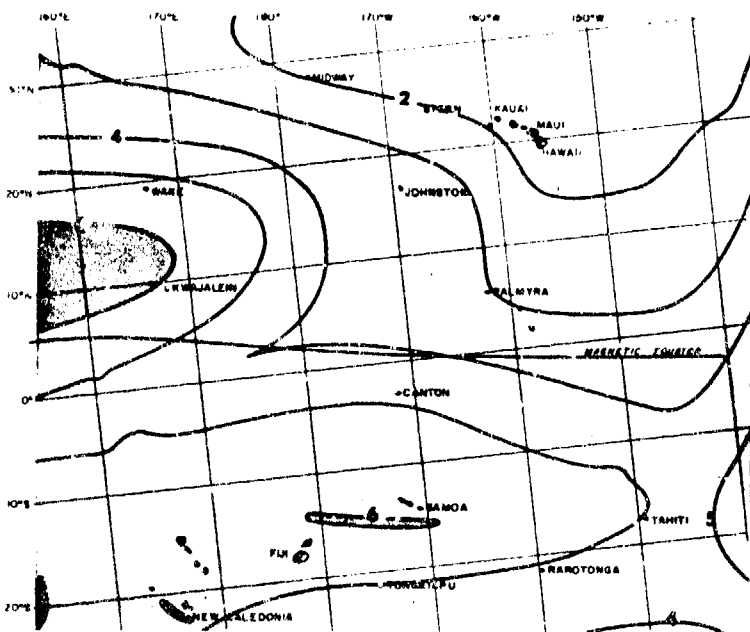


Figure 25
King Fish T + 160 min
1450 GMT, 1 November 1962

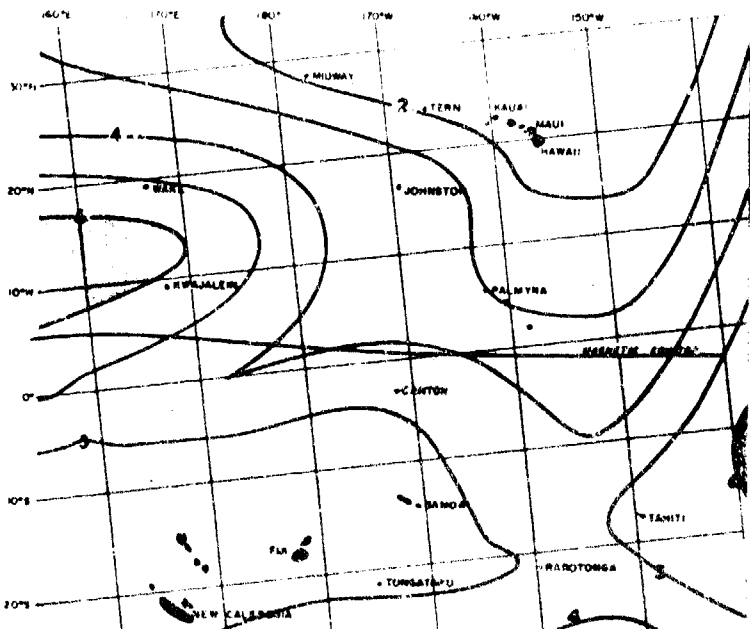


Figure 26
King Fish T + 180 min
1510 GMT, 1 November 1962

**THE EFFECTS OF NUCLEAR-BURST-PRODUCED ACOUSTIC GRAVITY
WAVES ON HF COMMUNICATION SYSTEMS**

by

D.L.Nielson

Stanford Research Institute
Menlo Park, California 94025
USA

507

LES EFFETS DES ONDES ACOUSTIQUES ET DE GRAVITE PRODUITES PAR UNE EXPLOSION NUCLEAIRE
SUR LES SYSTEMES DE COMMUNICATION A HAUTE FREQUENCE

par

D.L. Nielson

SOMMAIRE

Les ondes acoustiques et de gravité engendrées par des explosions nucléaires à haute altitude peuvent affecter momentanément les liaisons de radiocommunication en haute fréquence. Deux modifications peuvent se produire :

1) le spectre de propagation dont on dispose peut, en un certain point, diminuer de telle sorte que le circuit ne fonctionne plus à une fréquence donnée,

2) le délai dans le temps, et les distorsions de fréquence peuvent accroître la probabilité d'erreurs pour un système digital. Tous ces effets dépendent des positions relatives du trajet radio de la source, et du champ géomagnétique, ainsi que de l'état de l'ionosphère le long de ce trajet.

THE EFFECTS OF NUCLEAR-BURST-PRODUCED
ACOUSTIC GRAVITY WAVES ON HF
COMMUNICATION SYSTEMS

D. L. Nielson
Stanford Research Institute
Menlo Park, California, U.S.A.

SUMMARY

Acoustic gravity waves generated by high altitude nuclear explosions can momentarily affect the performance of HF communications. Two changes can occur: (1) the available propagation spectrum may at some point decrease such that the circuit is no longer operative at a given frequency, (2) the time-delay and frequency distortions may increase the likelihood of error in a digital system. All effects are subject to the relative orientation of the path, the source, and the geomagnetic field as well as the state of the ionosphere along the path.

1. INTRODUCTION

Through modification of the ionosphere, acoustic gravity waves (AGW) can affect the performance of HF communication systems. The extent of the effect is dependent upon path location and orientation as well as the system parameters. In this paper we will briefly examine the changes in communication system performance resulting from the passage of a wave generated by the 1962 high-altitude nuclear test King Fish. (LOMAX and NIELSON, 1968.) This test affords a good opportunity since the source is discrete and the wave is simpler than many natural occurring ones. Observations in the form of oblique-incidence ionograms are used to verify the ionospheric model from which the system performance will be estimated.

The ionospheric F-region electron density is modeled as a single parabola as far as propagation is concerned. The AGW effects are computed using quasi-empirical expressions derived by NELSON (1968) using in part these observations. Changes in all three layer parameters--height, semithickness, and critical frequency--are made as the wave proceeds along the path. The performance of two modems will be considered--an incoherent FSK system and a differentially coherent PSK(DPSK) system.

2. MODELS

The path chosen for examination is about 2500 km from the burst and running between the islands of Canton and Karotonga in the South Pacific. A constant ionospheric F-layer was used as the background propagation medium: $h_m = 385$ km, $y_m = 70$ km, and $f_o = 6.8$ MHz. These values were selected after examining ionospheric data including oblique-incidence ionograms. Since the observations are entirely at night no lower-layer ionization is considered. The propagation program used allows for linear gradients in critical frequency and layer height. The wave was modeled as in LOMAX and NIELSON (1968) with a velocity of the peak of the first half cycle of 800 m/sec.

The digital communication system models used here permit the input of both time and frequency distortions. These distortions are expressed in the form of a second central moment in time delay and Doppler shift and are thus specified as spreads in each domain. The spreads are calculated from the amplitude-weighted discrete ray paths obtained from the parabolic-layer ray-tracing propagation model. Signal-to-noise ratios are normalized to a one hertz bandwidth and only atmospheric noise is considered. A transmitted power of 3.3 watts/Hz and noise levels at the receiver from -151 dBW at 4 MHz to -171 dBW at 20 MHz resulted in about a 40 dB signal-to-noise ratio. The signaling element duration is 10 msec for both systems.

3. RESULTS

Combining the ionospheric and AGW models mentioned above we can obtain a series of calculated ionograms with which to compare against the observed records. This is done in Figures 1 and 2 for every 20 minutes during the first 100 minutes of the 2 hours for which calculations were made. While some error is apparent, the general pattern is reproduced with but two exceptions: the time-delay spreading on individual traces and the continued high frequency maintained on the one-hop trace. These effects are probably the result of the formation of irregularities in ionization during the passage of the wave. Notice that while the frequency remains high on the lowest order ray the maximum frequencies of the higher order rays decrease following the first half-cycle of the AGW (i.e., beyond 110 min.).

The spectrum available for propagation in this case incurs a pronounced change. In Figure 3 the maximum observed frequency is shown over the two-hour period. Observed values are shown only during the first quarter period. The calculated values show what might exist if the irregularities were not present. This variation in maximum frequency is not always typical but is a function of pre-wave ionization contours and the relative orientation of the wave normal of the acoustic wave and the local magnetic field (LOMAX and NIELSON, 1968), (NELSON, 1968).

The performance of a digital system is related to several factors:

- (1) the signal-to-noise ratio
- (2) the spread in time-delay and Doppler shift
- (3) the transmitted signal and other system characteristics.

Since the calculations are for nighttime conditions the signal levels are approximately constant with frequency and for the various multipath components. The number of propagating rays therefore tends to be limited by ionospheric penetration. This limiting also helps define the degree of time-delay and Doppler spread at a given frequency.

Assuming continuity in the use of a given frequency, the variation in the performance of a digital system during the passage of the wave is governed largely by the changes in time delay and Doppler shift of the individual rays. These variations for an incoherent FSK system can be seen in Figure 4 for no diversity and for uncorrelated dual diversity systems. (The dual diversity results can be plotted on the same axes only for high signal-to-noise ratios.) Similarly results for a DPSK system with no diversity are given in Figure 5. Notice that in the first 30-60 minutes or the first half-cycle the degradation of the digital system is due to increases in distortion. In the second half-cycle the distortion diminishes but in this instance the propagating spectrum is also reduced. The phase system is naturally more sensitive to Doppler spread than the incoherent FSK system. The wide and rapid excursions of error rate in Figure 5 are the result of differential Doppler shifts between various F-region rays.

If error rates of less than 10^{-3} are necessary it is apparent that some type of diversity would be required in this situation. Furthermore if the operating frequency falls below the maximum propagating frequency then a frequency change is necessary to maintain communication. This latter procedure is most important in those regions where the first half cycle causes a decrease in F-layer critical frequency. (LOMAX and NIELSON, 1968.)

4. CONCLUSIONS

This paper has attempted to show that HF communication systems may in some cases be affected by the passage of neutral atmospheric waves generated by a nuclear explosion. Degradation may come from increased distortion, a possibility only when the F-layer critical frequency is increasing, or from a loss of ionospheric support for the frequency of operation. In the latter situation the maximum propagating frequency is decreasing and because of the accompanying reduction in multipath, the distortion decreases as well. While the wave would be expected to have opposite effects in its two half cycles, observations indicate that the most significant changes occur during the first half cycle.

5. REFERENCES

LOMAX, J. B. and NIELSON, D. L., 1968, "Observation of Acoustic-gravity Wave Effects Showing Geomagnetic Field Dependence," J. of Atmos. and Terrest. Phys., Vol. 30, pp. 1033-1050.

Nelson, R. A., 1968, "Response of the Ionosphere to the Passage of Neutral Atmospheric Waves," J. of Atmos. and Terrest. Phys., Vol. 30, pp. 825-835.

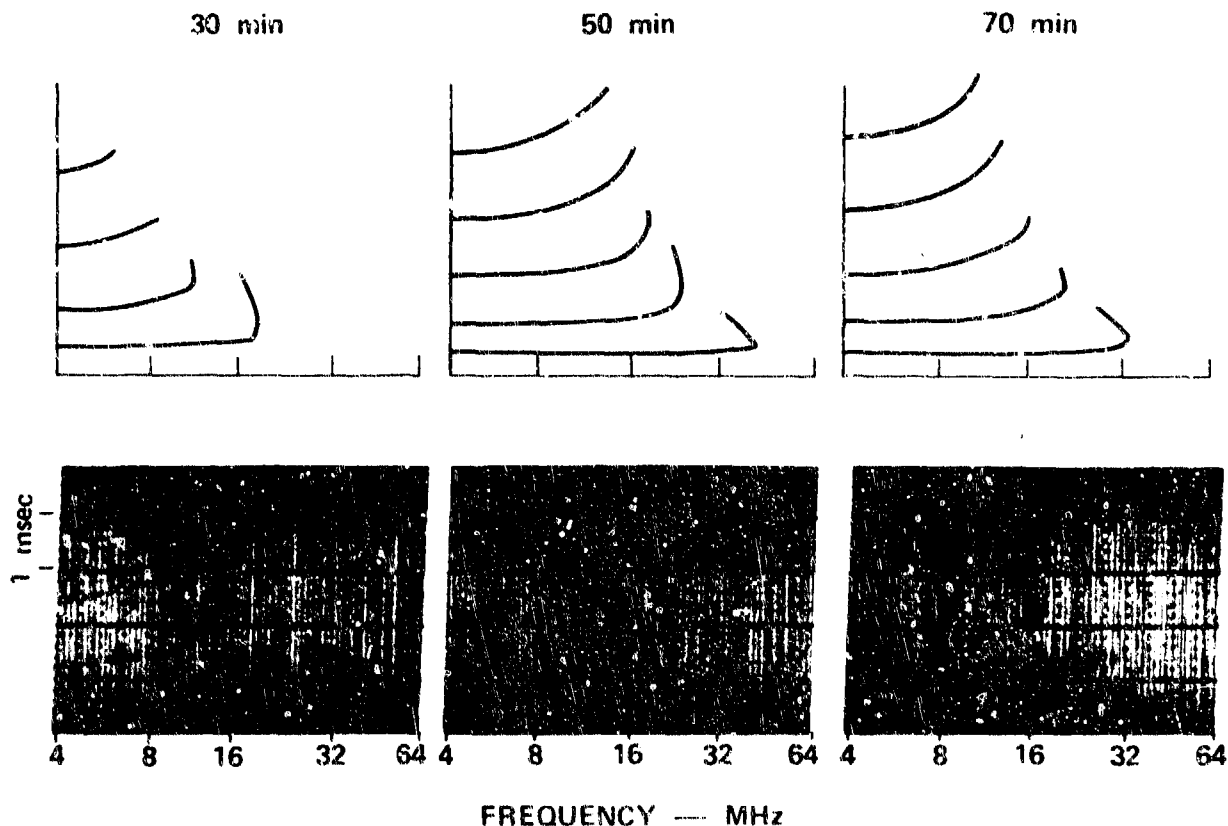


Figure 1 Comparison of Calculated and Observed Ionograms for 30, 50, and 70 Minutes after Burst

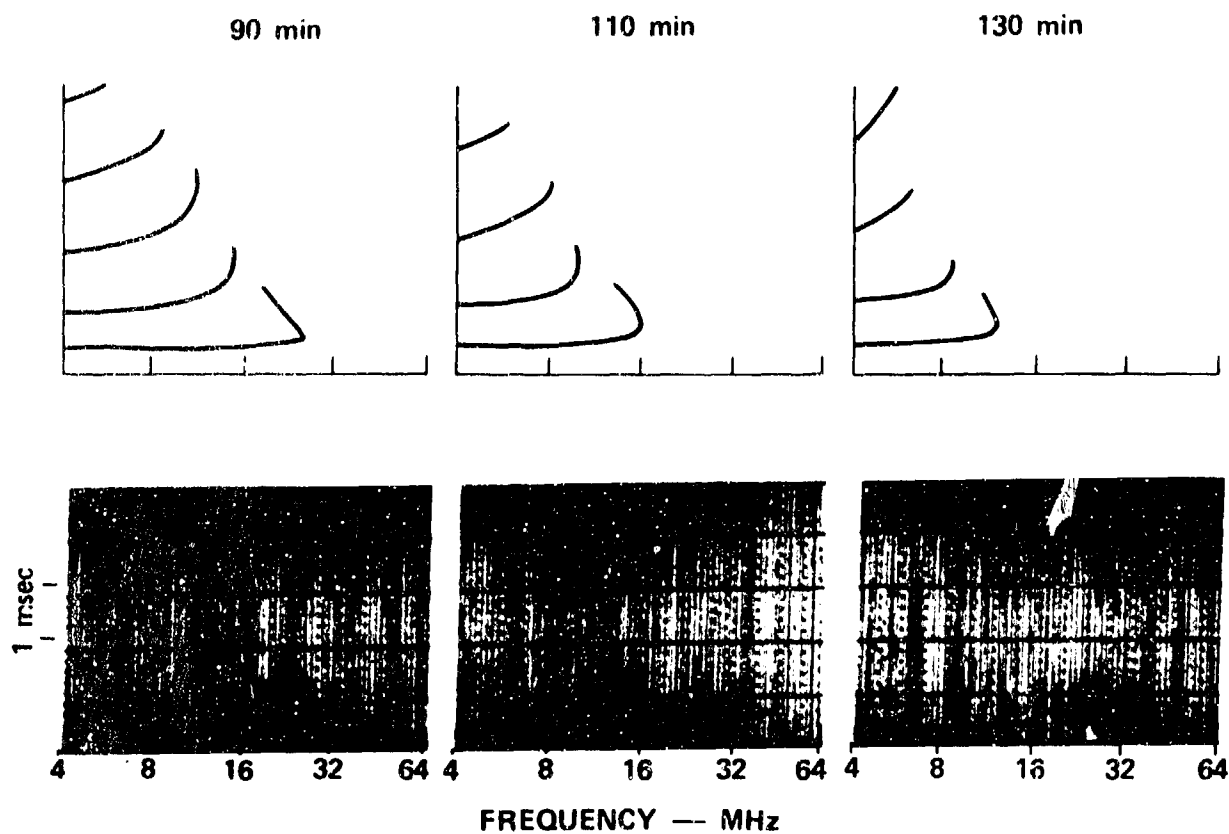


Figure 2 Comparison of Calculated and Observed Ionograms for 90, 110, and 130 Minutes after Burst

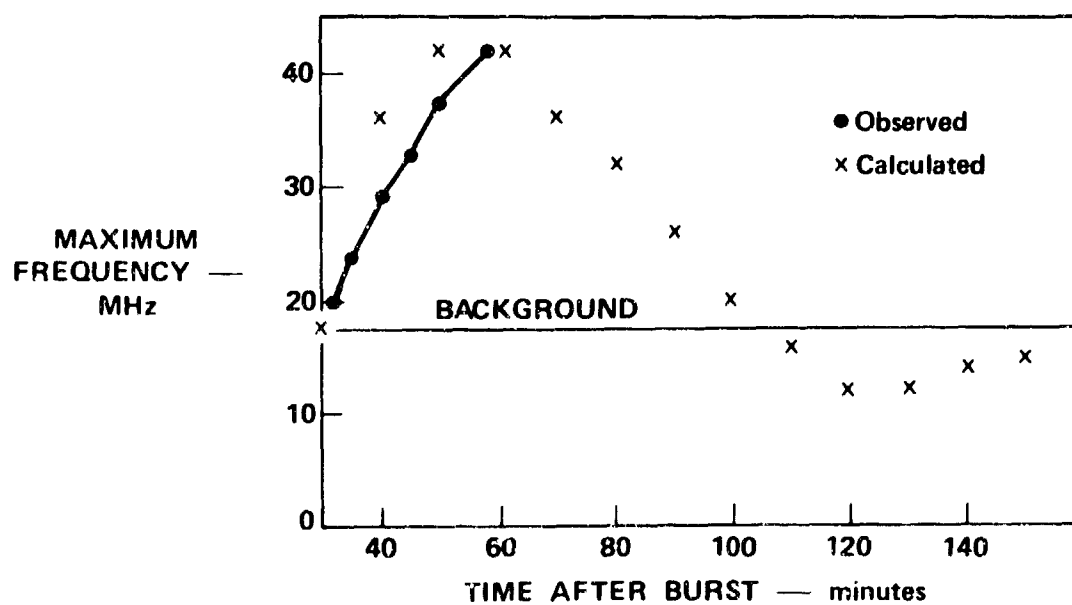


Figure 3 Calculated and Observed Variation in Maximum Frequency

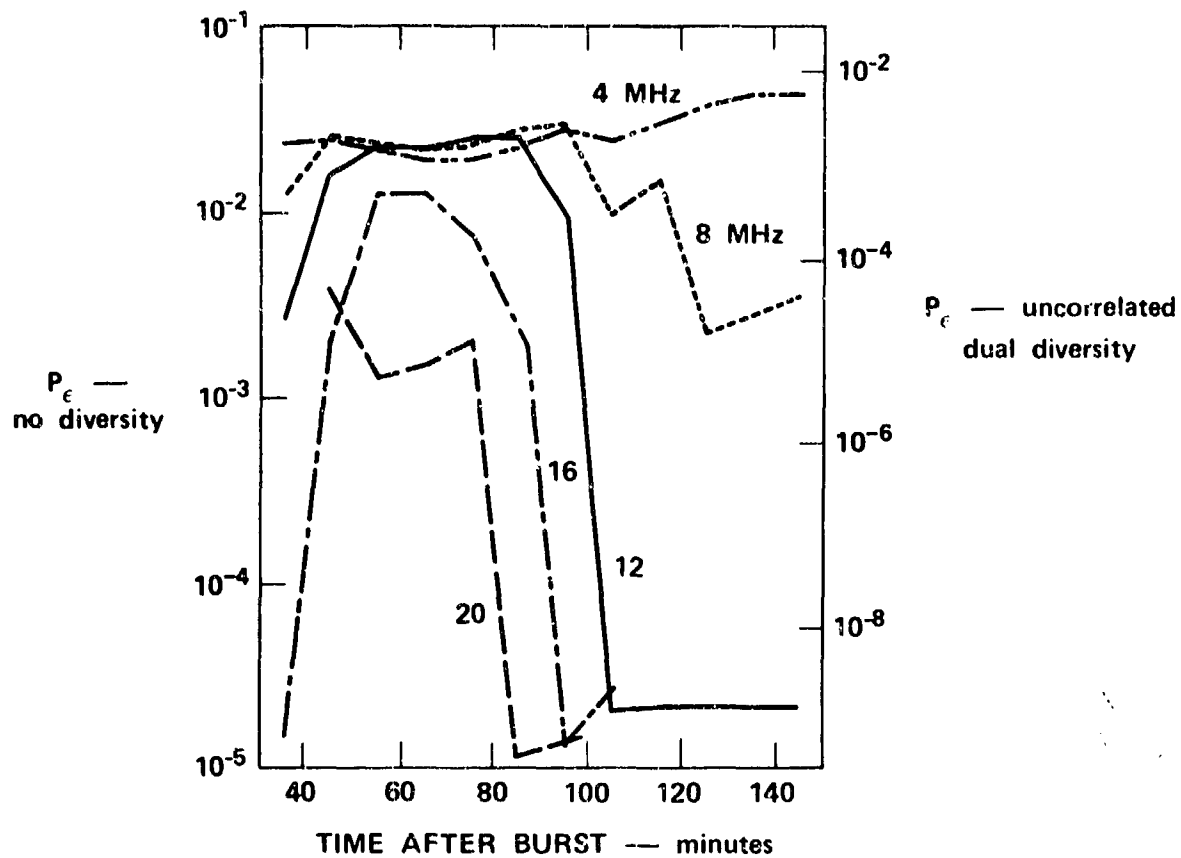


Figure 4 Probability of Error for Incoherent FSK System

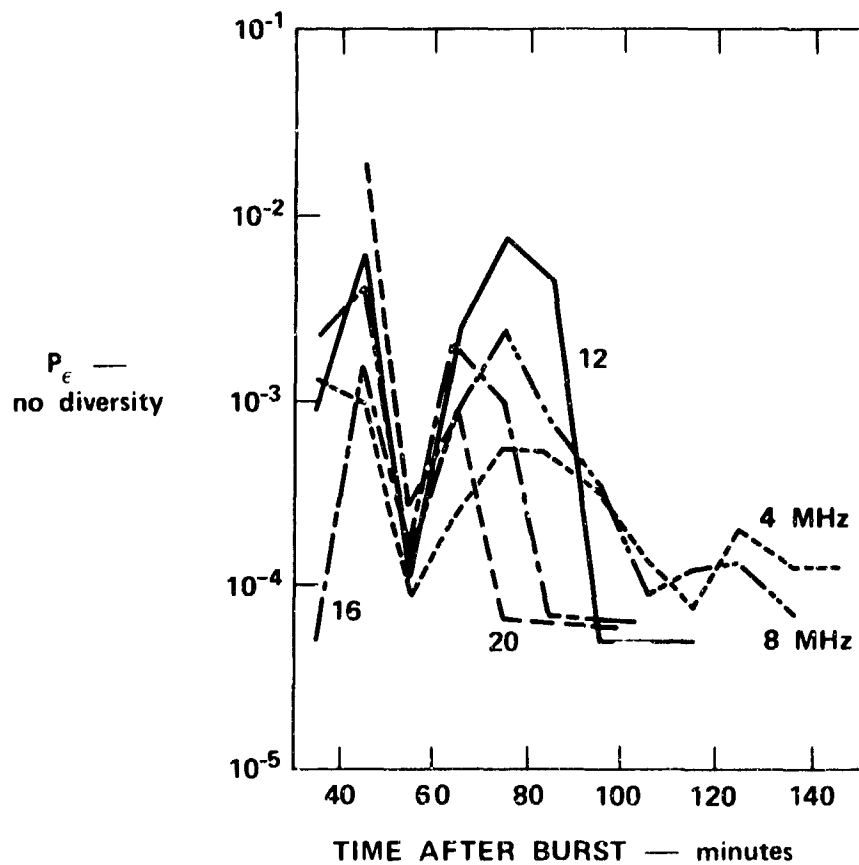


Figure 5 Probability of Error for DPSK System

Discussions on papers presented in Session IV
(Influence of acoustic gravity waves on the propagation of the electromagnetic waves)

Discussion on paper 32 : "H.F. Ray tracing of gravity wave perturbed ionospheric profiles", by P.L. George.

Dr. K. DAVIES : Mr. George's ray tracing shows that there are fundamental limitations set by the ionosphere on direction finding. Hence there should be a corresponding limit to the amount of money invested in direction finding equipment. This is a potentially valuable contribution from this meeting.

Dr. P.L. GEORGE : I think the point is that no amount of sophisticated engineering, which usually implies considerable expense, will improve radio location results if the ionospheric model is itself inadequate.

C.F. P. HALLEY : Dans le tracé de rayon électromagnétique que vous effectuez dans le milieu ionisé perturbé en présence du champ magnétique terrestre, vous calculez les trajectoires entre deux points pour une réflexion ionosphérique. Tenez-vous compte de réflexions ionosphériques multiples accompagnées d'une ou de plusieurs réflexions au sol ?

Dr. P.L. GEORGE : Multiple reflections certainly occur at near vertical incidence with TID's of some amplitudes. It is not clear that measurement of such multiple reflections will improve our ability to determine the essential characteristics of a given TID. Rather it is often the case that multiple reflections will confuse the situation. It is for this reason that the interferometer used for the type of measurements discussed in this paper is deliberately used in a manner such that measurements are accepted only when an essentially plane wave front, that is a single mode, is present.

Dr. H.P. WILLIAMS : Throughout your lecture you referred to the effects at "short distances" i.e. of the order of 50 km. In practice one is much more likely to be attempting measurements at much longer distances. In such cases I presume the gross inaccuracies due to the wavy surface would be considerably reduced. The problem would then be nearer the case of reflection at grazing incidence which, we know from the Rayleigh criterion, would come more closely the flat surface case.

Dr. P.L. GEORGE : I cannot agree that in practice one is more likely to be attempting radio location at much larger distances. It depends very much on the situation. There is a very real requirement for location at short ranges which I cannot elaborate on here. I will say however that the required accuracy is often higher than at long ranges. One must remember that at short range the frequency of operation may easily be such that penetration into the ionosphere is very great - under these circumstances the greatest tilts are seen. At long ranges however, for frequencies below the MUF, the radio ray does not penetrate deeply into the ionosphere - at distances greater than 1 000 km or so it is difficult to get more than one third of the way into the F region. - One may therefore suppose that the effective tilts seen due to TID's may be rather small.

Discussion on paper 34 : "Propagation of submicrosecond H.F. pulses through travelling ionospheric disturbances", by G.M. LERFALD, R.B. JURGENS.

Dr. L.B. WETZEL : I would like to make two comments on this paper.

1.- Taking an oblique ionogram as a plot of delay-time versus frequency over the path, one often finds that the curve is flat in places due to the presence of the underlying layers. In such regions the second term in the Taylor's expansion of the phase, being proportional to the slope of the delay-time, vanishes; at these points the surviving phase non-linearity is cubic in frequency, and the simple formula for ionospheric bandwidth based on the quadratic term is no longer valid. This formula also breaks down where the delay-time exhibits a strong curvature as when close to the MUF. (See, for example, L. Wetzel, IDA Res. Paper P-317, 1967).

2.- The question of "incoherent bandwidth" might be approached by viewing the physical locus of two paths through the ionosphere at two different frequencies. As the frequencies separate so do the paths, and the phases over the two paths become statistically decorrelated as the physical separation of the paths approaches the correlation length of the major ionospheric irregularities. These irregularities could be related to the high wave-number end of an acoustic wave spectrum, which then determines a natural limit to one's ability to do dispersion equalization.

Dr. G.M. LERFALD : 1.- I concur with these comments on the limitations of the equation given by Wait. However, in practice it seldom occurs that the delay-time versus frequency curve is truly flat over the receiver bandwidth. In this case, as for the case near the MUF, higher-order terms for the phase relationship could presumably be used, but this would probably make it impossible to solve the equations explicitly.

2.- An experiment which measured the degree of decorrelation between separated frequencies was performed with some interesting results, by Hagfors (Norwegian Defence Research Establishment, Internal Report 1962).

Discussion on paper 36 : "La perturbation ionosphérique due aux ondes acoustiques et de gravité créées par une explosion nucléaire au sol de 100 kt à 2 000 kt observée entre 150 et 1 000 km du point de tir", par P. HALLEY.

Dr. P. MURPHY : The Lamb mode which is maximized at the earth's surface has an exponentiating distance of γH with altitude, where γ is ratio of specific heats and H is the scale height. For $\gamma = 1.4$ and $H = 7$ km this means the amplitude at 100 km altitude is about 10^{-4} that at sea level. I therefore do not believe the interpretation of the 305 m/sec signal in terms of the Lamb mode can be correct. The amplitude is simply too small.

C.F. P. HALLEY : Oui, la pression de perturbation du mode de Lamb décroît exponentiellement lorsque l'altitude augmente, l'échelle de hauteur étant γH . Mais, la pression en l'absence de perturbation décroît aussi et plus vite, l'échelle de hauteur étant H . Le rapport $\frac{\Delta p}{p}$ augmente donc exponentiellement lorsque l'altitude augmente $\frac{\Delta p}{p} \sim e^{\frac{\gamma-1}{\gamma} \frac{z}{H}}$. Quoiqu'il en soit, il paraît difficile d'attribuer directement au mode de Lamb le signal qui se propage à 305 m/s.

Discussion on paper 37 : "Propagation non-linéaire et couplage ionosphérique des ondes acoustico-gravitonnelles engendrées par une explosion nucléaire", par P. BROCHE.

Dr. H. RISHBETH : You have considered the motions of F region ions parallel to geomagnetic field lines, due to neutral air motions. But in addition the air motions in the E region can possibly generate electric fields, which will be transmitted to the F region and can then move the ions across the magnetic field lines. In this case the ion motions will be more complex. You might obtain some information about electric field from magnetic data, though the problem is a complicated one.

Prof. P. BROCHE : I did not take into account these effects, my calculations were very simple, and their aim was only to show the mean features of the effect of the earth magnetic field on the coupling between the A.G.W. and the ionosphere when the A.G.W. was generated by a punctual source.

Dr. Ch. LIU : I think this non linear effect is very interesting. This is known in the theory of non linear wave in dispersive media as "amplitude-dispersion relation". Perhaps with the model you use it is possible to derive this relation and have a more exact expression for the wave velocity. Then a better check with the experimental data will be possible.

Prof. P. BROCHE : In fact the coefficient k in the expression

$$v = c + k v^{1/3} e^{3/2 H} \cdot \frac{\exp[-Bs]}{s}$$

can be approximated using the shock velocity and the coefficient B , which expresses the influence of the viscosity damping, can be calculated for a given frequency (Rayleigh expressions). The fit is obtained by choosing the convenient frequency (a few seconds to a few ten of seconds).

I agree with Dr. LIU's remark, that further theoretical work will provide better approximations for the wave velocity, and perhaps a better fit with the experimental data.

Discussion on paper 39 : "The effect of nuclear-burst produced acoustic gravity waves on H.F. communications systems", by D.L. NIELSON.

Dr. A.W. INCE : Would you please comment on the effects of high-altitude nuclear detonations on noise of terrestrial and extraterrestrial origin in HF and VHF bands, considering communications systems such as iono-scatter and meteor-burst.

Dr. D.L. NIELSON : In the face of nuclear radiations, propagated noise will of course suffer absorption just as a more useful signal does. In the initial attempts at modeling the total propagation picture in the presence of absorbing radiation, we tried to synthesize observed noise values from point source noise "transmitters". Doing so would enable us to attenuate noise as well as the signal. Unfortunately the 10 or so noise sources we felt were needed meant that all calculations were multiplied by that factor. That fact coupled with the realization that much of today's HF "noise" is interference, caused us to discontinue such calculations. Quite obviously propagated noise is directional and the attenuation picture for it may differ markedly from that for the signal. Extraterrestrial noise is much easier dealt with but must consider the E and F layer iris. We have not incorporated absorption of that noise either. Because of the location of this path with respect to radiation sources and in view of the time-after-burst, I do not expect the lack of considering noise to be of consequence in this case. Clearly there is little signal absorption.

External noise in VHF systems, being generally extraterrestrial, might be expected to attenuate more nearly as the signal-at least to the extent that the antennas are highly directive. Since signal-to-noise ratio is the quantity of interest, considering only signal absorption will yield erroneously low performance.

Dr. H. WILLIAMS : I noticed on the oblique ionograms you showed that the reflections occurred in blobs, i.e., the curve of amplitude v. frequency was modulated at short intervals. This was true even of the first ionogram which had not yet been affected by the burst. Can you tell me why you had this effect ? I met it once

myself but only in the region of a single hop. It was then probably due to polarization fading, for the time of taking the ionogram was only 20 seconds.

Dr. D.L. NIELSON : As you imply, effects such as polarization fading can occur when we use linear antennas ; however, I do not attribute most of the drop out of signal with such a cause. You will notice that in nearly all instances the signal is missing on all propagating modes. This must then relate to receiver response on that particular channel. Since these are step frequency receivers such an abrupt change is quite possible. We have never associated any propagation significance to these interruptions.

General discussion

Dr. D.L. NIELSON : I and several other attendees would like to introduce at this point the outline of an ionospheric phenomenon that has been eluded to at this meeting by Dr. Röttger and in similar reports by Crochet at the University of Paris. In his paper Dr. Röttger suggested that the postsunset disturbances that have for many years been observed in the F region near the magnetic equator may be due to acoustic gravity waves. During the next few moments I would like to neither support or contest that suggestion but to place before this group a brief outline of the phenomenon in order that those well versed in such wave motion might be able to address the likelihood of such a possibility. In order to present a consistent qualitative picture I will take some liberties about which all may not agree, I will also largely ignore the normal motion of the bulk plasma after sunset, that is, the abrupt rise and slow descent, that may be of some influence in the phenomena I describe.

The several (and the number may range from zero to perhaps 8 or 10) independent reflection surfaces that Dr. Röttger mentioned "seeing" from terminals remote from the equator are those cells or bundles or irregularities that have been common to nearly all equatorial experiments in which drift velocity could be measured. Commencing after sunset and most probably following the evening height rise, these cells form and begin to drift eastward along the dip equator. Their estimated size ranges from a few hundred to perhaps at most 1 000 km and their horizontal drift velocity from 50-150 m/sec with respect to the observer. Their lifetime over one point on the earth is typically 2 to 4 hours, so that from their initial point behind the sunset line they span perhaps as much as 30-60° degrees of longitude. Both the cells and the smaller scale irregularities associated with them drift at the same eastward rate. The magnitude and direction of the drift are compatible with electromagnetic Hall drift from downward electrostatic fields of a few millivolts per meter ; however, there is no electric field mechanism known that would produce the horizontal variations in density that define the cells. These data are evidenced at HF by means of horizontal and vertical reflections from inhomogeneities of the same scale as the cells as well as at VHF where the much smaller scale sizes are important. Nor are the observations confined to radio. Equatorial airglow records taken over large areas also indicate the presence of these cells. Since the radiance of the airglow is said to be less related to electron (ion) number density than to recombination rate (height) there is believed to be some lowering of height associated with regions of increased airglow.

From this brief outline then the following questions inquiring into the association (if any) between these cells and AGW's may be posed :

- Is the velocity (both direction and magnitude) consistent with AGW's either in or directly influencing the F-region ?
- Is the "period" or size of these cells commensurate with the velocity or AGW theory in general.
- Is the disappearance of these cells within say 30-60° longitude consistent with possible dissipation rates of AGW's.
- Could the instabilities associated with the cell be triggered or sustained by energy within such a wave.
- If the large scale irregularities have as their source changes associated with E or F region sunset, would such "wake" effects have to be stationary in the frame of reference of the sunset line.

Finally, the small scale irregularities mentioned above that are typically associated with spread-F or scintillations, are limited to those that occur prior to local midnight. This type, either because of its intensity or physical make-up is the one that is most closely associated with upper HF and VHF investigations.

Dr. J. KLOSTERMEYER : The magnitude of the horizontal drift velocity in the range 50-150 m/sec is typical for so-called medium scale ionospheric disturbances observed by various authors in the mid-latitude F-region. Today it seems to be generally accepted that these disturbances are produced by atmospheric gravity waves. The interpretation of the equatorial phenomena mentioned by Dr. Röttger and Dr. Nielson in terms of gravity waves is made more difficult by the fact that a gravity wave propagating along the magnetic west-east direction causes only relatively small ionization changes at the dip equator. However, this difficulty would not arise if the horizontal direction of wave propagation differs from the magnetic west-east direction by several degrees.

From the horizontal extent of a few hundred to 1 000 km and the horizontal velocity range we can estimate possible time scales between twenty and a few hundred minutes, which agree well with the period spectrum of gravity waves in the F-region.

The rate of energy dissipation of atmospheric gravity waves depends largely on period, wavelength, and direction of propagation. Ionospheric disturbances have often been observed to travel distances between several hundred and several thousand kilometers. The disappearance of the cells within 30-60° longitude is therefore consistent with possible dissipation rates of gravity waves.

Dr. J. ROTTGER : In addition to the interesting explanations of Dr. Nielson, I want to point out that periodical structures in the equatorial ionosphere recently have been observed by Yeboah-Amankwah and Koster in Accra ["Equatorial Faraday Rotation Measurements on the Ionosphere Using a Geostationary Satellite" published in : Planet. Space Sci. 20, 1972, pp. 395-408]. These observations indicate reasonable oscillations of the total electron content in the evening hours. The quasi-periods of these oscillations are in the range of approximately 30 min to a few hours and are assumed to be originated by a horizontal drift of plasma inhomogeneities in the ionosphere. A typical size of these inhomogeneities is about 530 km assuming a plasma drift velocity of 120 m/sec. The results obtained by oblique-incidence sounding between Lindau and Tsumeb are in sufficient agreement with these observations of Yeboah-Amankwah and Koster.

Dr. K. DAVIES : One of the difficulties concerned with the gravity wave explanation of equatorial irregularities propagation along the magnetic equator is that a gravity wave cannot move the electrons across the geomagnetic field (i.e. vertically).

Dr. J. ROTTGER : The geographical distribution of the observed side reflection areas indicates a maximum of occurrence in the west African zone between about 5° N and 20° N. In this area the magnetic declination is about 5° to 15° westerly deviation. This means that east-west propagating inhomogeneities are not propagating perpendicular to the earth's magnetic field.

In the east African area the declination is between 0° and 5° W and the perpendicularity which may restrict eastward drifts is performed earlier in this area. Irregularities east of the path Lindau-Tsumeb, located in the east African area, occur much less than irregularities west of the path. This result seems to be in agreement with the depicted difference of the declination east and west of the path.

Dr. H. RISHBETH : Concerning the irregularities in the equatorial F region at sunset,

1.- I cannot comment on the production, scale size or periodicity of the irregularities, but I think that the combination of

- a) the supersonically moving sunset,
- b) large horizontal gradients of electron density associated with sunset,
- c) crossed electric and magnetic fields might well favour instability phenomena.

2.- Once the irregularities are formed, then they can be moved across the magnetic field by an electrostatic field. The irregularities would move with the background ionization. I have a theory of how the required electric fields can be produced (indirectly by the action of thermospheric winds) though the theory is admittedly controversial.

3.- I think that, given the existence of irregularities the electron density and airglow data hang together nicely. The lifetime of the irregularities may just be similar to that of the background ionization - a few hours.

C.F. P. HALLEY : La région où l'équateur magnétique franchit et s'écarte de l'équateur géographique, au sud du Sénégal, est particulièrement irrégulière de nuit. C'est ainsi que l'on constate à partir de Dakar des difficultés de radiocommunication en H.F. vers le golfe de Guinée ou vers Madagascar. La fiabilité des communications est particulièrement mauvaise dans une certaine bande de fréquences (par exemple, entre 9 et 19 MHz) même si on utilise des antennes omni-directionnelles ou faiblement directives.

Session V

Summaries, Recommendations and future investigations

Session chairman : Prof. J. DELLOUE

Comment of Prof. H. VOLLAND reporter of sub-session I A : "Acoustic gravity waves in the neutral terrestrial atmosphere, Natural sources and propagation".

In this first sub-session, seven papers were presented dealing with the natural excitation and the propagation of acoustic-gravity waves within the lower atmosphere. Five of these papers were theoretical papers whereas two of them presented experimental work on the propagation of infrasound waves excited within the auroral zones. It appears to me that this ratio between the numbers of theoretical and experimental papers is symptomatic of the present stage of knowledge of gravity wave propagation.

Let me recall the general problem with which we are faced. Given is some natural event-earth quake, tropospheric weather disturbance auroral display etc. - which is supposed to excite acoustic-gravity waves. This source has some spatial and temporal distribution and acts like a generator transmitting a spectrum of acoustic-gravity waves into the surrounding atmosphere. The "radiation characteristic" of such disturbance can be represented by a function $g(t)$ which depends not only on time t but also on the local distribution of the source and on the radiation angle. The atmosphere on the other hand behaves like a dispersive and anisotropic wave guide which can be described by a transmission function $F(\rho, \omega)$ where ρ is the distance from the source and ω is the angular frequency of the spectral range considered. F of course depends also on the azimuth, the radiation angle and the time. At the input of a receiver we observe some fluctuation $h(\rho, t)$ resulting from the source g and deformed by the dispersive atmosphere in between.

If the observed wave structure has small amplitudes so that perturbation theory is a sufficient approximation and if the temporal variation of the atmospheric wave guide is slow compared with the periods of the waves considered we can on principle apply linear system theory and the method of the superposition of harmonic waves. Fortunately - as we saw in this meeting - this is possible in many problems of acoustic-gravity wave propagation.

It is well known from system theory that in order to relate source g and received signal h we have to transpose these functions into their frequency domains by a Fourier-transformation obtaining $g^*(\omega)$ and $h^*(\rho, \omega)$. Then the relationship

$$h^*(\rho, \omega) = g^*(\omega) F(\rho, \omega) \quad (1)$$

holds, and from a re-transformation into the time domain we get

$$h(\rho, t) = \int_{-\infty}^{\infty} g^*(\omega) F(\rho, \omega) e^{-j\omega t} d\omega \quad (2)$$

Depending on the bandwidth of our receiver we obtain at its output a signal which either approaches (1) or (2) or a value in between.

In the papers by Pierce and Warren the first step has been done to determine the source function g from some realistic natural event. Liu on the other hand studied quite generally the response of the isothermal atmosphere to an unspecified source. It means he solved F and h for some given g . Georges finally doing ray approximation obtained the transmission function F for any realistic lower atmosphere.

The theoretical papers in this sub-session therefore cover fairly well the matter outlined above. Here, the transmission function F of the lower atmosphere appears to be rather well understood. However, apart from the announced papers by Gossard and Katz who unfortunately did not attend this meeting, there was no experimental paper presented here which dealt with gravity wave propagation within the lower atmosphere. Obviously experiments of this kind are necessary to confirm or to disprove the theories and particularly to locate and identify the natural sources of gravity waves. Up to now there is indeed a nearly complete lack of knowledge about the kind and the structure of the natural source function h in the case of gravity waves.

People dealing with acoustic waves are luckier in this respect. Here the transmission function F is much simpler. Specifically, the atmosphere behaves nearly isotropic and non-dispersive with respect to acoustic waves, and ray tracing is in most cases an excellent approximation. Moreover, due to their small wave lengths, direction finding techniques for acoustic waves can be used in order to locate the sources.

Cook did calculations of the excitation and the propagation of infrasound waves, and Wilson and Liszka located infrasound waves within two different spectral ranges and identified them as caused within the auroral electro jet. Here, the paper by Wilson comes nearest to our ideal conception in (1). From the observation of h^* within a narrow spectral range he determined and located g^* assuming a known function F . Then he presented a physical explanation of the source g .

From this and the following sessions, I would like to draw the conclusion that we need simultaneous measurements of selected natural events within a wide range of frequencies and at various locations within lower and upper atmosphere, using different techniques, in order to locate and to identify the natural sources of gravity waves and to close the gap which I outlined above.

Comment of Dr. B.L. MURPHY, reporter of subsession I B : "Acoustic gravity waves in the neutral terrestrial atmosphere. Artificial sources and propagation".

I will confine my remarks to low altitude nuclear detonations as sources of acoustic-gravity waves. All the papers in Sub Session IB as well as a number in other sessions dealt with this topic in one way or another.

Consider first the various types of ionospheric disturbance which result from the detonation blast wave. A portion of the blast wave, which does not reach the ionospheric level, is responsible for exciting the Lamb mode as described by Dr. Posey and Prof. Pierce. This mode has a maximum amplitude on the ground and decreases exponentially over a distance of about 10 km. Thus the amplitude is a factor 10^{-4} less at 100 km than it is at the ground. For this reason, as noted by Dr. Balachandran, it would not seem likely that this mode is responsible for disturbances in the ionosphere. The possible exception would be when the Lamb mode can couple to some other mode which propagates at higher altitude. The main lesson to be learned from the Lamb mode analysis is simply that, in this one particular case, one may replace the usual guided modes GR_0 , GR_1 , S_0 , S_1 , etc. by a pseudomode, namely the Lamb mode, and that analysis in terms of this pseudomode is far easier than in terms of the guided modes. One need not resort to involved numerical calculations; in fact, back-of-the-envelope engineering type estimates are possible. One should definitely attempt to apply this pseudomode concept to other modes which may propagate at higher altitudes and which may produce observable ionospheric effects. These other pseudomodes are presumably related to the ducting properties of the atmosphere and ionosphere and their dispersion curves should be composed of segments of the guided mode dispersion curves.

For the portion of the shock which does reach the ionosphere Prof. Berthet has calculated the nonlinear effects on the ray paths. In a sense his analysis is the opposite of what has been done by a number of other people, for example by Whitham. Whitham includes several nonlinear effects not contained in Berthet's analysis, most notably the effects of ray tube divergence and convergence on the pulse amplitude. However, Whitham uses the ray paths of geometrical acoustics. An analysis which treats nonlinear effects on both ray paths and amplitudes in a self consistent fashion would be desirable.

Also regarding Prof. Berthet's paper, I wonder what the relation of his "ring of sound" is to the numerical results of Greene and Whitaker, some of which were shown in the paper by Dr. Kahalas and myself. The same region of space seems to be involved in both cases. In both cases it is a region of highly nonlinear hydrodynamics which acts as a secondary source of acoustic disturbance. There is a major difference in interpretation however. Prof. Berthet regards this region as a source of waves of period less than a minute. Greene and Whitaker regard their region as the source of gravity waves with periods in excess of 10 minutes. Obviously clarification and reconciliation of these points of view would be desirable.

Now, as to the short period disturbances which are observed in the ionosphere, Dr. Balachandran and Dr. Kahalas and myself both presented doppler data obtained by Baker and Davies. We both noted that these short period ionospheric disturbances are probably due to partially ducted acoustic modes beneath the ionospheric level. I made the point that the period of this disturbance was approximately equal to the period content of the shock at the base of the ionosphere and suggested a yield scaling law for the periods. It would be worthwhile to examine this doppler data or other similar data to see if any scaling laws for the period variation with yield, range, wind direction, etc. are in fact apparent in the data. Empirical scaling laws could be of great aid in formulating nuclear source and propagation models.

Finally, we come to the question of the rising fireball as a source of acoustic-gravity waves in the ionosphere. Both Prof. Pierce and Dr. Kahalas and myself have put forth gravity-wave excitation models based on buoyancy oscillations at the fireball stabilization altitude. Dr. Lomax raised the question as to whether or not real fireballs perform this type of oscillation. This question really has not been answered. A related question which may shed some light on this is: what kinds of acoustic-gravity oscillations are produced by naturally buoyant elements such as thunder clouds?

Even if fireballs do oscillate, this does not necessarily mean that they are a source of widespread ionospheric perturbation. A ray tracing program applicable to long periods, such as Dr. Georges', could be used to determine the region of the ionosphere affected by a source of waves of period comparable to the Brunt-Väisälä period and located at the tropopause. Presumably the wavelengths produced would be the order of the stabilized fireball dimensions.

Comment of Dr. K. DAVIES, reporter of session II : "Coupling between the ionized atmosphere and the neutral atmosphere perturbed by acoustic gravity waves".

There are two aspects of the meeting on which I have been asked to comment viz: (1) The theory of the interaction between atmospheric neutral motions and the motions of the ionized gas and (2) Attempts to identify specific natural sources of ionospheric wavelike disturbances. I am indebted to Drs Klostermeyer and Liu for ideas concerning the theory.

1. Theory of neutral-ion gas interactions.

Most theories on the interaction between neutrals and ions caused by the passage of gravity waves through the atmosphere have dealt with the problem in two parts. First, the motions of the neutrals are solved and second, these motions are inserted into the equations of motion of the neutral-ion gas. This approach is mathematically simple, it gives physical insight into the interactions involved and it has proved a valuable guide.

Now in practice the induced ion motion reacts and modifies the neutral motion, hence, any major advance in this area will require that the coupled hydrodynamic and ion equations of motion be solved simultaneously in a self-consistent manner. In particular, certain non-linear effects should be included because certain parameters (e.g., the diffusion coefficient) are modified by the passage of the atmospheric wave.

Also the coupling of energy between various types of waves (viscosity, heat conduction, gravity, etc.) should be included.

Inclusion of all these features will make it difficult to assess the importance of any one physical factor. Hence, in order to obtain some insight into the dominant physical processes it will be necessary to repeat the calculations many times, each time eliminating one term in the system of equations. Some of the more important terms are listed in Table 1.

One other aspect which should be encouraged is that theory and observation should advance in step.

2. Sources.

Although there is much to be elucidated in the propagation of atmospheric waves, there is a bigger void in our knowledge of the locations and characteristics of the sources of these waves. In this area there is room for both theory (source modeling) and observations. Both aspects have received some discussion in this meeting. Natural sources of acoustic-gravity waves in the ionosphere include the jet stream (Cook), auroral electrojet (Wilson), oscillation of air masses and thunderstorms (Pierce and Moo), large scale air motions near the tropopause (Goe) and the sun (Bowman).

Source modeling, in which the response of the atmosphere to different sources is calculated, would be invaluable for comparison with experimental data. This applies to both artificial as well as natural sources.

The effect of source location on the characteristics of ionospheric traveling disturbances is shown by the calculations of Chang. He shows that for gravity-wave sources in the troposphere, the ionospheric disturbance can only propagate near the asymptotic limit. This is confirmed by radio techniques. Chang also shows that the temperature profile is important in determining the periods of gravity waves penetrating to the F region. The troposphere is an important (if not the most important) source of acoustic and gravity waves in the ionosphere. Hence one must consider the entire atmosphere, between the levels of the sources and of observation, in attempting to explain the ionospheric effects.

It may be of interest to note that for acoustic waves at a given height in the upper atmosphere, the ground range to a source in the lower atmosphere is a unique function of the horizontal trace speed, i.e., for a given atmospheric model. Thus, spaced transmitter (or receiver) measurements can be used to determine the source locations of acoustic waves.

As mentioned above, we know more about the propagation of acoustic-waves than about their sources. Hence, it is appropriate to make use of observations, together with suitable atmospheric models to determine the characteristics of the sources, e.g., jet streams, aurora, solar, thunderstorms, etc. In particular, more definitive studies should be made on effects of large scale weather patterns of the type of study initiated by Mrs Goe. Bowman's data may indicate a direct relationship (cause and effect) between gravity waves and spread F. However, it is more likely that these are independent manifestations of an underlying solar influence.

The importance of winds in the propagation of gravity waves cannot be overestimated. Hence one of the most pressing needs is for realistic height profiles of neutral winds. A given wind has a much greater effect on gravity waves than on acoustic waves, because the latter have larger phase velocities. One consequence of this is that winds cause the forbidden frequency range between the acoustic cutoff frequency and the Brunt-Väisälä frequency to decrease or even disappear.

Finally, I should like to point out that the term "gravity wave" is rather unfortunate and that a more descriptive work would be "buoyancy wave". The reason for this is that in any wave propagation there must be a restoring force. In the case of gravity waves the restoring force on a parcel of gas is the difference between the weight of the parcel and that of the displaced air.

Table 1
Important terms in atmospheric neutral-ion coupling

Neutral	Ion
(1) Gravity (or buoyancy)	(a) Motion induced by neutral motion
(2) Pressure	(b) Diffusion (at great heights)
(3) Ion drag (periods \approx 1 hour)	(c) Electric fields
(4) Viscosity	(d) Production and loss (in F1 layer)
(5) Heat conduction	(e) Hydromagnetic coupling
(6) Winds and critical levels	
(7) Coriolis force when winds reduce the intrinsic frequency to near zero	

Comments on session III : "Radioelectric studies on acoustic gravity waves in the neutral and ionized atmosphere".

Prof. I. RANZI : I would like to consider the Session III contributions having some direct concern with problems of telecommunication from one hand and of radiolocation of beyond the horizon targets from the other hand.

The general problem is that of evaluating the influence of the acoustic gravity waves on the determination of the azimuthal and vertical angle of arrival of signals or of the backscattered echoes and of the distance of the backscattering target.

I must refer first to a paper which was presented at the Session IV ; that is the paper n° 33 by P. George (on ray tracing of gravity wave profiles), which very clearly shows the relationship between the structure of the ionospheric disturbance and the above indicated parameters.

On the ground of our present knowledge, it seems that, from the application point of view the more important ionospheric disturbances are those generally classified as medium-scale T.I.D.s ; but on my opinion, we should have to assume that this category does include T.I.D.s with periods up to about 60 minutes (according to the Hunsucker paper, the upper limits should be 40 minutes).

What are then the best experimental procedure which can provide useful information about the T.I.D. structure, on the ground of which to calculate the bearing and distance errors ?

The papers, which are more or less directly concerned with such problem, are the following.

The paper n° 28, presented by A.D. Morgan (on the effect of ionospheric disturbances on the bearing of incoming skywaves), not only shows that the bearing measurements may give useful information on some characteristics of T.I.D.s, but it also provides data of direct interest for ionospheric radio communication ; that is the link degradation due to the bearing deviation when use is made of highly directive arrays.

The paper n° 29, by R.F. Treharne (on ionospheric tilt measurements near the magnetic dip equator) shows that the tilt measurements in the vertical direction by means of an interferometric device may also provide important information on some T.I.D. characteristics.

We have then to consider also the methods based on the measurements of the variation of the arrival angle of signals propagating along an oblique path passing through the ionosphere ; the paper n° 27, by J. Litva is concerned with such kind of determination, which was carried out by observing the emission on 51.7 MHz from localized sources on the sun surface ; a limitation of the general validity of this method may probably derive from the fact that sometimes more than one gravity wave system are present at different ionospheric levels and with different characteristics.

The paper n° 24, by R. Hunsucker (on narrow-beam HF radar investigations of mid-latitude ionospheric structure and motion) shows that a very fine and detailed knowledge of the T.I.D. structure and movement is obtained by means of a sophisticated HF backscatter sounder, which due to the use of a very large antennae array, may simultaneously scan in azimuth and elevation, with beamwidths of 2°-3° in azimuth and of 3°-4° in elevation.

In conclusion, it seems that future work ^{should} be conveniently directed to the development of the procedure reported on paper n° 32 by P. George, by introducing new T.I.D. models as deduced by means of suitable sounding methods. These methods may have not necessarily to require such expensive and sophisticated equipment, like the narrow-beam HF radars, or incoherent backscatter sounders. It seems that a combination of some simple experimental procedures may provide very useful data i.e. a combination of bearing in an oblique or vertical path and of vertical sounding (fo H - profiles) at the ionospheric reflection zone.

To the important purpose of determining the mechanism of the acoustic-gravity wave generation and the location of the source, it appears that vertical soundings to be carried out in many places may be very useful ; this is shown by the short note presented by I. Ranzi and P. Giorgi.

Dr. H. RISHBETH : The detection of gravity waves in the lower ionosphere or mesosphere is difficult, but it is possible to use the ionization as a 'tracer' for the neutral air. Thus Glass et al. (paper 23) made use of meteoric ionization for a radar experiment which studied wave motions of 2-8 hour period, 15-30 km vertical wavelength at 75-105 km altitude. Perona (paper 22) observed VLF transmissions, reflected obliquely from heights around 70 km, and occasionally detected wavelike disturbances with periods of tens of minutes. The interpretation of these phenomena is likely to be very complex, involving both chemical and dynamical processes.

Two papers dealt with artificial sources of acoustic-gravity waves. Rao (paper 26) described how an HF doppler sounder, about 1 400 km from Cape Kennedy, detected waves in the ionosphere following the launching of Saturn-Apollo spacecraft. Liszka and Olsson (paper 30) described Swedish experiments with supersonic aircraft, whose trajectories can be chosen in such a way as to cause focussing of the shock waves. Infrasound waves (2 Hz) were observed to be reflected from about 50 km altitude, and ionospheric effects at around 100 km altitude were studied by means of an HF sounder. It was found that the disturbances travelled up to the ionosphere more rapidly than expected, and also that sporadic E patches appeared during the experiments.

Comments on Session IV : "Influence of acoustic gravity waves on the propagation of electromagnetic waves".

Dr. H. RAEMER : Adequate summaries of the contents of the papers in the first half of Session IV are covered in the abstracts. Hence, I will confine my remarks to a few very general observations as follows :

- 1) A theoretical understanding of HF radio paths in the presence of ionospheric irregularities due to AGW's can be accomplished through ray-tracing (paper by P. Georges) or approximate full-wave analysis (paper by H. Raemer). Both of these approaches can be very effective when irregularities are on a scale that is large in terms of wavelength. When the scale of these irregularities becomes comparable to a wavelength ray-tracing begins to lose its validity and valid approximations to full-wave solutions become more difficult to implement without prohibitive expenditure of computer time. It is in this domain that standard theory becomes least trustworthy in enabling prediction of effects.

There is perhaps a need for more theoretical and experimental approaches that cover this parameter regime.

- 2) The use of submicrosecond pulses to probe the ionosphere (paper by G. Larfala, R. Jurgens and J. Joselyn) provides the kind of resolution needed to determine the fine structure and movements of T.I.D.'s, from which their effects on radio propagation can be assessed. The paper by Röttger demonstrates certain interesting effects on HF propagation of T.I.D.'s both parallel and transverse to great circle paths. The paper generated a certain amount of controversy over the causes of T.I.D.'s propagating along the magnetic equator. This is discussed elsewhere in the program and will not be elaborated upon here.
- 3) The question of relevance of the work reported here to the needs of the communication engineer was raised during the question period. There seems to be no completely satisfactory answer to this question. The results obtained by ionospheric scientists cannot in every case be immediately translated into information directly useful to communications engineers. What is necessary (as remarked in another session) is to have a group of workers who bridge the gap between the study of ionospheric propagation as an end in itself and the knowledge needed by the communications engineer to design his systems. Such workers do exist, but perhaps there is need for more such liaison activity.

In analyzing and designing digital communication systems, the engineer usually needs to know such items of the propagation medium as multipath spread, coherent bandwidth, probability density functions of fading and spectrum of fading. Ideally, he would like to have a randomly time-varying impulse response of the propagation medium which contains most of the above information. The difficulty is that all of these items are "short-term" statistical in nature (i.e., they involve random processes that are roughly stationary for only a few minutes). When he looks at results obtained by ionospheric scientists, he must usually do a great deal of work relating statistics of diurnal, seasonal and possibly geographical variations, as reported in the ionospheric science literature, to the kind of short-term statistics he needs for his design work. This problem could be alleviated by the sort of liaison work alluded to above, which would be best performed by people whose interests and knowledge straddle the boundaries between ionospheric science and communications engineering.

Dr. D. NIELSON : This part of the review of Session IV will be concerned principally with the second part of the session; namely, that associated with nuclear-burst-produced waves. First one might logically ask what AGW data from nuclear bursts have to offer the general field of atmospheric wave propagation. In answer it seems apparent that at points remote from the burst where the wave is sonic, there exists a considerably simplified wave behavior as compared to many natural sources. While much of the nuclear test data on AGW's has yet to appear in the literature in an easily usable form, both general behavior (e.g., the effect on ionization profiles) and data for more detailed scalings are available. It would appear that if we fail to understand the basically simpler neutral wave from the nuclear burst, including how it couples to the ion gas, we will not understand the multiplicity of natural waves with their more complex sources and overlapping effects.

The study of nuclear-burst-produced AGW's may be classified into (1) analysis of wave mechanics or diagnosis of the medium and (2) predictive models. Considering the former we have seen in this session that the type of waves generated, that is the mode(s) into which energy is coupled, are substantially influenced by the available energy of the burst and its altitude. That a 720 m/sec principal (fast) wave from the low altitude French test appeared supersonic (decreasing velocity with distance) while an 800 m/sec wave from the U.S. high altitude test appeared linear, should not be considered contradictory. Similarly, when both low and high altitude tests generate multiple waves (in this case two) it should not be concluded that the second or slower waves have a common origin or propagation altitude. We are, of course, hampered in our analysis by proper source models without which it is difficult to stipulate the propagating ray (energy) path. This is particularly evident at higher altitudes.

It was evident from the remarks of Pr. Broche and Capitaine Halley as well as from the U.S. results, that predictive methodologies must necessarily contain empirical scaling. This empiricism reflects our incomplete understanding but nevertheless allows us to match what limited observations exist. Furthermore, calculational models that are in part empirical normally permit more rapid and economical estimates of communication effects. Quite obviously, however, limited test data and observation points do not permit scaling or extension to all possible situations. Therefore, as theory is developed which can extend the calculational model, such increased capability should be incorporated.

An effect that has not received theoretical attention at this conference but which is of critical interest in the vicinity of high altitude nighttime bursts, is the possibility of altered chemistry during the passage of a wave. Such alteration may arise either from the movement of an ion to regions of different reaction rates or by elevated pressure and temperature forming metastable ion states having substantially different capture crosssection. Whether natural waves can impart this type of non-linearity is not known.

We have seen that AGW's can affect communications in two ways : (1) altering the propagating radio spectrum between two points, and (2) changing the distortion of the communication signal. Both the French and the U.S. tests illustrated each effect. Spectrum loss on the low altitude French tests was curiously in the middle of the preshot spectrum whereas those for the high altitude tests were generally from the upper end. Distortions to the received signal in the form of Doppler and time delay spreads were seen to be of some consequence on large amplitude AGW's whereas they are of limited effect for smaller or low altitude bursts.

Finally, of general interest is the observation that AGW's may be one means of triggering and perhaps sustaining the inhomogeneities that we loosely term spread-F. This was evident both in a paper by Dr. Bowman as well as in the data from the U.S. high altitude tests. In both instances there appeared to be a requirement for an appreciable component of the earth's magnetic field to be perpendicular to the acoustic wave normal. These observations may have significance both in arbitrary AGW horizontal direction vectors at high latitude and for east-west or vertical propagation at the dip equator.

NATIONAL DISTRIBUTION CENTRES FOR UNCLASSIFIED AGARD PUBLICATIONS

Unclassified AGARD publications are distributed to NATO Member Nations through the unclassified National Distribution Centres listed below

RECEIVED

NATIONAL TECHNICAL

NOV 20 1972

INFORMATION SUPPLY

BELGIUM

Coordinateur AGARD - V.S.L.
Etat-Major Forces Aériennes
Caserne Prince Baudouin
Place Dailly, Bruxelles 3

CANADA

Director of Scientific Information Services
Defence Research Board
Department of National Defence - 'A' Building
Ottawa, Ontario

DENMARK

Danish Defence Research Board
Østerbrogades Kaserne
Copenhagen Ø

FRANCE

O.N.E.R.A. (Direction)
29, Avenue de la Division Leclerc
92, Châtillon-sous-Bagneux

GERMANY

Zentralstelle für Luftfahrtokumentation
und Information
Maria-Theresia Str. 21
8 München 27

GREECE

Hellenic Armed Forces Command
D Branch, Athens

ICELAND

Director of Aviation
c/o Flugrad
Reykjavik

ITALY

Aeronautica Militare
Ufficio del Delegato Nazionale all'AGARD
3, Piazzale Adenauer
Roma/EUR

LUXEMBOURG

Obtainable through BELGIUM

NETHERLANDS

Netherlands Delegation to AGARD
National Aerospace Laboratory, NLR
P.O. Box 126
Delft

NORWAY

Norwegian Defense Research Establishment
Main Library
P.O. Box 25
N-2007 Kjeller

PORTUGAL

Direccao do Servico de Material
da Forca Aerea
Rua de Escola Politecnica 42
Lisboa
Attn of AGARD National Delegate

TURKEY

Turkish General Staff (ARGE)
Ankara

UNITED KINGDOM

Defence Research Information Centre
Station Square House
St. Mary Cray
Orpington, Kent BR5 3RE

UNITED STATES

National Aeronautics and Space Administration (NASA)
Langley Field, Virginia 23365
Attn. Report Distribution and Storage Unit

* * *

If copies of the original publication are not available at these centres, the following may be purchased from:

Microfiche or Photocopy

National Technical
Information Service (NTIS)
5285 Port Royal Road
Springfield
Virginia 22151, USA

Microfiche

ESRO/ELDO Space
Documentation Service
European Space
Research Organization
114, Avenue Charles de Gaulle
92200, Neuilly sur Seine, France

Microfiche

Technology Reports
Centre (DTI)
Station Square House
St. Mary Cray
Orpington, Kent BR5 3RE
England

The request for microfiche or photocopy of an AGARD document should include the AGARD serial number, title, author or editor, and publication date. Requests to NTIS should include the NASA accession report number.

Full bibliographical references and abstracts of the newly issued AGARD publications are given in the following bi-monthly abstract journals with indexes:

Scientific and Technical Aerospace Reports (STAR)
published by NASA,
Scientific and Technical Information Facility,
P.O. Box 33, College Park,
Maryland 20740, USA

United States Government Research and Development
Report Index (USGDRR), published by the
Clearinghouse for Federal Scientific and Technical
Information, Springfield, Virginia 22151, USA



Printed by Technical Editing and Reproduction Ltd
Harford House, 7-9 Charlotte St, London W1P 1HD